İbrahim Dinçer · Calin Zamfirescu

Sustainable Energy Systems and Applications

Springer

Sustainable Energy Systems and Applications

İbrahim Dinçer • Calin Zamfirescu

Sustainable Energy Systems and Applications

Springer

İbrahim Dinçer
Faculty of Engineering & Applied Science
University of Ontario Institute
of Technology (UOIT)
Oshawa, ON L1H 7K4
Canada
ibrahim.dincer@uoit.ca

Calin Zamfirescu
Faculty of Engineering & Applied Science
University of Ontario Institute
of Technology (UOIT)
Oshawa, ON L1H 7K4
Canada
calin.zamfirescu@uoit.ca

ISBN 978-0-387-95860-6 e-ISBN 978-0-387-95861-3
DOI 10.1007/978-0-387-95861-3
Springer New York Dordrecht Heidelberg London

Library of Congress Control Number: 2011922501

Printed on acid-free paper

Springer is part of Springer Science+Business Media (www.springer.com)

To our parents, Fatma and Hasan Dinçer, and Verginia and Daniil Zamfirescu

and

To our children, Meliha, Miray, İbrahim Eren, Zeynep and İbrahim Emir Dinçer, and Ioana Zamfirescu, for their inspiration.

İbrahim Dinçer
Calin Zamfirescu

Preface

We have been in a fossil fuel era and ended up with such a desperate picture! The key question here is: how to cure this problem? The common consensus to tackle this problem is that we need sustainable energy solutions which cover the following six key pillars, namely, (1) better efficiency, (2) better cost-effectiveness, (3) better resources use, (4) better design and analysis, (5) better energy security, and (6) better environment. These are essentially the main pillars and what makes this book really unique as "sustainable energy systems and applications."

This book is research oriented, and therefore includes extensive practical features not found in solely academic textbooks. This book is essentially intended for use by senior undergraduate and graduate students in various disciplines ranging from mechanical to chemical engineering, and as a basic sustainable energy source on, even a handbook, for practicing energy engineers. Analyses of sustainable energy systems and their applications are undertaken throughout this comprehensive book, providing new understandings, methodologies, models, and applications, along with several illustrative examples and case studies. The coverage is extensive, and the amount of information and data presented is quite sufficient for several energy-related courses, if studied in detail. We strongly believe that this book will be of great interest to researchers, scientists, students, engineers, and energy experts, and that it provides a valuable and readable reference text for those who wish to learn more about sustainable energy systems and applications.

Chapter 1 addresses general aspects of thermodynamics to furnish the readers with background information on thermodynamic aspects, covering essentially two main laws (first and second law of thermodynamics) through energy and exergy analyses and efficiency assessment, along with some examples related to the analyses of sustainable energy systems and their applications. Chapter 2 discusses energy and environmental issues and energy sources and options and their impact of environment. Chapter 3 is a continuation of Chapter 2 by focusing primarily on global warming and climate change issues and their consequences. Chapter 4 focuses on energy conservation with some specifics on issues, measures, policies, strategies, and their assessments, and offers some illustrative examples. Chapter 5

discusses energy policies and assessment of various options for sustainable development. Chapter 6 delves into fossil-fuel alternatives and provides some examples and case studies. Chapter 7 is specifically about using ammonia as a potential substance for various options as the fuel, refrigerant, and working fluid in numerous applications and discusses ammonia as a key source of hydrogen especially for transportation vehicles. Chapter 8 provides comprehensive coverage on the nuclear energy option, addressing a broad range of topics from historical perspectives to nuclear-based hydrogen production. Chapter 9 renewable addresses comprehensive by energy systems and applications, including integrated and hybrid systems for a more sustainable future. Chapter 10 deals with district energy systems, including various subtopics from cogeneration to system analysis and offers case studies. Chapter 11 discusses energy storage options as part of sustainable energy systems and applications, and presents various examples and case studies. Chapter 12 describes integrated multigeneration systems for the production of various commodities, including power, heat, hot water, cooling, hydrogen, as well as desalination. Chapter 13 is the heart of this book as it focuses on hydrogen and fuel cell systems, covering hydrogen production, storage, transportation, distribution, and use, and fuel cell systems and their applications and analyses. Chapter 14 discusses carbon dioxide technologies and their implementation for various applications. Chapter 15 is another important chapter, focusing on life-cycle assessment for various systems and applications for better efficiency and environment. Chapter 16 provides some details on industrial ecology and its possible applications in some areas of sustainable development. Chapter 17 gives some perspectives on sectoral energy and exergy utilization to provide a comprehensive picture of economies and their activities. Chapter 18 discusses economic analysis of systems, especially sustainable energy systems.

Incorporated throughout this book are many wide-ranging, illustrative examples and case studies that provide useful information for sustainable practical applications. Conversion factors and thermophysical properties of various materials are listed in the appendices in the International System of Units (SI). Complete references and a bibliography are included in each chapter to direct the curious and interested reader to further information.

Oshawa, Canada

İbrahim Dinçer
Calin Zamfirescu

Contents

Chapter 1
Thermodynamic Fundamentals

1.1 Introduction

Sustainable energy systems exhibit a diverse nature and cover a large number of processes such as energy conversion, heating, cooling, and chemical reactions. Sustainable energy engineering is a complex subject because many disciplines such as thermodynamics, fluid mechanics, heat transfer, electromagnetics, and chemical reaction engineering are encountered in its processes and applications.

When an engineer or an engineering student undertakes the analysis of a sustainable energy conversion system and/or its application, he or she should deal with several basic issues first, depending upon the type of the problem being studied. These issues include thermodynamics, fluid mechanics, chemical reaction, heat transfer, and others. In conjunction with this, we need to introduce several definitions and concepts before moving onto sustainable systems and applications in depth. Furthermore, the units of measure are of importance in the analysis of such systems and applications. One should make sure that the units used are consistent in order to reach the correct result. This means that there are several introductory factors to be taken into consideration. While the information in some situations is limited, it is important that the reader comprehend these processes. Despite assuming that the reader, if he or she is a student, has completed necessary courses in thermodynamics, fluid mechanics, chemistry, and heat transfer, there is still a need for him or her to review, and for those who are practicing energy engineers, there is a greater need to understand the physical phenomena and practical aspects, as well as the basic laws, principles, governing equations, and related boundary conditions. In addition, this introductory chapter reviews the essentials of these principles and laws, and discusses the relationships between these aspects and provides some key examples.

We now begin with a summary of the fundamental definitions, physical quantities, and their units, dimensions, and interrelations. We then proceed to consider different fundamentals of thermodynamics, including some aspects of fluid mechanics, heat transfer, and chemical reaction.

İ. Dinçer and C. Zamfirescu, *Sustainable Energy Systems and Applications*,
DOI 10.1007/978-0-387-95861-3_1, © Springer Science+Business Media, LLC 2011

1.2 Primary Notions in Thermodynamics

For a good understanding of the operation, modeling, and design of sustainable energy systems, extensive knowledge of such topics is indispensable, especially for thermodynamics, which is the most comprehensive.

The term *thermodynamics* comes from two Greek words: *therme*, meaning "heat," and *dynamis*, meaning "power," which suggests the science of transforming heat into power. It began in the 1800s with the need for designing efficient steam engines.

One of the main concepts of thermodynamics is the *thermodynamic system*. This concept was introduced by Carnot (1824) and referred to a finite mass of water vapor that is enclosed in steam power plants and has the ability to produce *work* when *heat* is applied to it cyclically (the concepts of work and heat are formally defined in the subsequent paragraphs). In today's definition, which is a generalization of the Carnot one, a *thermodynamic system* is a part of the universe that is delimited, by a real or imaginary boundary, from the rest of the universe, which is attributed with the name *surroundings*. Following this definition, a thermodynamic system can be anything, such as a human body, a room, a building, a power plant, a heat exchanger, a piston, a terrestrial atmosphere, a planet, or the solar system.

A thermodynamic system is characterized by a volume, and therefore inside any thermodynamic system a *field* must exist, because the field is a physical quantity that is associated with each point in space and time. There is no subdomain that is void of a field observed in the known universe. Examples of fields are the electrical, magnetic, and gravitational fields. *Matter* can be enclosed in a thermodynamic system, because matter is anything that has *rest mass* and takes up space. *Mass* is defined as a quantity of matter forming a body of indefinite shape and size. The fundamental unit of mass is the kilogram (kg) in the SI (International System of Units) and its unit in the English Engineering System is the pound mass (lbm). The basic unit of time for both unit systems is the second (s). The following relationships exist between the two unit systems:

1 kg = 2.2046 lbm or
1 lbm = 0.4536 kg
1 kg/s = 7936.6 lbm/h = 2.2046 lbm/s
1 lbm/h = 0.000126 kg/s
1 lbm/s = 0.4536 kg/s

In thermodynamics the unit *mole* (mol) is commonly used and defined as a certain amount of substance containing all the components. The mole is the amount of substance of a system that contains as many elementary entities as there are atoms in 0.012 kg of carbon 12. The number of these atoms is known as the Avogadro number, $N_A = 6.023 \times 10^{23}$. The related equation is

$$n = \frac{N}{N_A} = \frac{m}{M}, \tag{1.1}$$

where N is the number of molecules (or atoms, whichever is the case). If m and M are given in grams and gram/mol, we derive n in mol. The quantity M is known as molecular mass. If the units are kilogram and kilogram/kilomol, n is in kilomol (kmol). For example, 1 mol of water, having a molecular weight of 18 (compared to 12 for carbon 12), has a mass of 0.018 kg and for 1 kmol it becomes 18 kg.

A particular thermodynamic system is a *vacuum* that is characterized by the lack of any form of matter. There are four common forms of matter, namely solid, liquid, gas, and plasma, from which any combination can be enclosed in a thermodynamic system. From a chemical point of view, any form of matter consists of atoms and molecules that interact with each other and furthermore may interact with fields throughout the system. This interaction is what it leads to movement, which can be either chaotic or organized in the form of flow. Interaction among different parts of a system assumes the existence of *forces* that drive that interaction.

A force is a kind of action that can accelerate or bring matter to rest or that changes the direction of motion (e.g., a push or a pull). The fundamental unit of force is the newton (N).

1 N = 0.22481 lbf (pound force) or
1 lbf = 4.448 N.

The four quantities as discussed above, that is, mass, time, length, and force, are interrelated by Newton's second law of motion, which states that the force acting on a body is proportional to the mass and the acceleration in the direction of the force, as given below:

$$\overrightarrow{F} = m\overrightarrow{a}. \tag{1.2}$$

Note that *acceleration* is defined as the variation of velocity in time (measured in m/s^2), while *velocity* is defined as the rate of change of position of a piece of matter in time (measured in m/s). Furthermore, changing the position in time is quantified by the length of a path. The basic unit of length is the meter (m) in the SI and the foot (ft) in the English system. The interrelations are

1 m = 3.2808 ft = 39.370 in (where "in" stands for inch)
1 ft = 0.3048 m
1 in = 2.54 cm = 0.0254 m

Equation (1.2) shows the force required to accelerate a mass of 1 kg at a rate of 1 m/s^2 as 1 N = 1 kg m/s^2.

It is important to note that the value of the earth's gravitational acceleration is 9.80665 m/s^2 in the SI system and 32.174 ft/s^2 in the English system, which indicates that a body falling freely toward the surface of the earth is subject to the action of gravity alone.

Due to its action, a force can displace matter. If this happens, one can say that the force performs *work*. The work of a force is proportional to the force magnitude and displacement. One notes that force is a vector (characterized by magnitude and

direction), while the work of a force is a scalar (characterized only by magnitude). As is known from physics, work is the scalar product of force and displacement:

$$W = \overrightarrow{F} \cdot \overrightarrow{d}. \tag{1.3}$$

The existence of a force or of a field of forces that act on a piece of matter (e.g., a body, a volume of fluid, an atom, or an atomic particle) creates the ability to do work. As is known from physics, the ability to do work quantifies *energy*.

In other words, work is the energy that is transferred by a difference in pressure or through force of any kind, and in engineering thermodynamics it can be subdivided into shaft work and flow work. Shaft work is mechanical energy used to drive a mechanism such as a pump, compressor, or turbine. Flow work is the energy transferred into a system by fluid flowing into, or out of, the system. Both forms are usually expressed in kilojoules per mass, kJ/kg. Work done by a system is considered positive and work done on a system (work input) is considered negative. The unit for power is a rate of work of 1 J/s, which is a watt (W). The relevant interconversions between the International and English unit systems are as follows:

1 W = 3.4123 Btu/h (British thermal unit per hour),
1 Btu/h = 0.2931 W,
1 Btu/s = 1055.1 W,
1 lbf ft/s = 1.3558 W,
1 hp = 745.7 W.

The concept of energy was first introduced in mechanics by Newton when he hypothesized about kinetic and potential energies. However, the emergence of energy as a unifying concept in physics was not adopted until the middle of the nineteenth century and is considered one of the major scientific achievements of that century. The concept of energy is so familiar to us today that it seems intuitively obvious to understand, yet we often have difficulty defining it precisely.

Being the expression of the ability to do work, energy is a scalar quantity that cannot be observed directly but can be recorded and evaluated by indirect measurements. The absolute value of the energy of a system is difficult to measure, whereas the energy change is relatively easy to evaluate.

Examples of energy use in our day-to-day are endless. The sun is the major source of the earth's energy. It emits a spectrum of energy that travels across space as electromagnetic radiation. Energy is also associated with the structure of matter and can be released by chemical and atomic reactions. Throughout history, the emergence of civilizations has been characterized by the discovery and effective application of energy to help meet society's needs.

Energy manifests itself in many forms, which are either internal or transient. Energy can be converted from one form to another. In thermodynamic analysis, the forms of energy can be classified into two groups: macroscopic and microscopic.

Macroscopic forms of energy are those that an overall system possesses with respect to a reference frame, for example, kinetic and potential energies. The macroscopic energy of a rising object changes with velocity and elevation.

The macroscopic energy of a system is related to motion and to the influence of external effects such as gravity, magnetism, electricity, and surface tension.

Microscopic forms of energy are those related to the molecular structure of a system and the degree of molecular activity, and are independent of outside reference frames. The sum of all the microscopic forms of energy of a system is its *internal energy*, denoted usually by U. The internal energy of a system depends on the inherent qualities, or properties, of the materials in the system, such as composition and physical form, as well as the environmental variables. Internal energy can have many forms, including mechanical, chemical, electrical, magnetic, surface, and thermal. Here are two examples:

- A spring that is compressed has a higher internal energy (mechanical energy) than a spring that is not compressed, because the compressed spring can do work on changing (expanding) to the uncompressed state.
- Two identical vessels, each containing hydrogen and oxygen, are considered to have different chemical energies. In the first, the gases are contained in the elemental form, pure hydrogen and pure oxygen, in a ratio of 2:1. The second vessel contains an identical number of atoms but in the form of water. The internal energies of these systems differ. A spark may set off a violent release of energy in the first vessel but not in the second.

The energy that a system possesses as a result of its motion relative to some reference frame is called *kinetic energy*. Kinetic energy refers to the energy of the system because of its "overall" motion, either translational or rotational. "Overall" is used here to specify that we refer to the kinetic energy of the entire system, not the kinetic energy of the molecules in the system. If the system is a gas, for example, the kinetic energy is the energy due to the macroscopic flow of the gas, not to the motion of individual molecules.

The energy that is stored in a system has the well-known name, introduced by Rankine (see Crosbie 1998), of *potential energy* because it has the potential to be used by converting it into kinetic energy or other forms (e.g., heat, electricity). There are several kinds of potential energies, namely gravitational, elastic, centrifugal, electrical, magnetic, chemical, thermal potential, and rest mass. If several kinds of forces act, the potential energy of a body is the superposition of all the individual components.

The energy that a system possesses as a result of its elevation in a gravitational field is called gravitational potential energy (or commonly just potential energy). For example, a 1-kg mass, 100 m above the ground, has a greater potential energy than the same mass on the ground. Potential energy can be converted into other forms of energy, such as kinetic energy, if the mass is allowed to fall.

Kinetic and potential energy depend on the environment in which the system exists. In particular, the gravitational potential energy of a system depends on the choice of a zero level. For example, if ground level is considered to be at zero potential energy, then the potential energy of the mass 100 m above the ground has a positive potential energy equal to the mass (1 kg) multiplied by the gravitational

constant (g = 9.807 m/s^2) and the height above the ground (100 m). Its potential energy will be 980.7 (kgm^2)/s^2 (or 980.7 Newton-meters (Nm), or 980.7 J). The datum plane for potential energy can be chosen arbitrarily. If it had been chosen at 100 m above the ground level, the potential energy of the mass would have been zero. Of course, the difference in potential energy between the mass at 100 m and the mass at ground level is independent of the datum plane.

In a more formal approach one recognizes the interdependence between *conservative forces* (or fields of conservative forces) and potential energy. The potential energy is the energy that is produced by a *conservative force*, and the conservative force has by definition the property that when it displaces matter the change in the associated potential energy does not depend on the path taken, but only on the initial and final position of the displacement. Potential energy is a function of the position of the thermodynamic system and its constituents in the field of conservative forces.

Any conservative force has an associated potential energy. Apart from gravitational energy, caused by the gravitational force, which is conservative, the following potential energies are known:

- Elastic energy, produced by elastic forces.
- Magnetic energy, produced by magnetic forces.
- Electrostatic energy, produced by Columb forces.
- Chemical potential energy, produced by Columb forces while chemical reactions occur. During chemical reactions the atoms and electrons rearrange, releasing or absorbing energy in the same time; this energy is of the electrical type in nature and is manifested among nuclei, electrons, and molecules.
- Thermal potential energy, which is a consequence of kinetic energy of molecules and the potential energy due to their relative position.
- Nuclear energy, which is caused by various nuclear forces (weak, strong).

Pressure is defined as the total force exerted per unit of surface area. Pressure is a notion coming from fluid mechanics and thus is specific to fluids, that is, liquids and gases. The mathematical definition of pressure is written as

$$P = F/A, \tag{1.4}$$

where F is the force and A is the area.

The unit for pressure in SI is the force of one Newton acting on a square meter area (so-called Pascal) as follows:

1 Pascal (Pa) = 1 N/m^2

The unit for pressure in the English system is pounds force per square foot, lbf/ft^2. Here are some pressure conversions:

1 Pa = 0.020886 lbf/ft^2 = 1.4504 $\times$ 10^{-4} lbf/in^2 = 4.015 $\times$ 10^{-3} in water = 2.953 $\times$ 10^{-4} in Hg
1 lbf/ft^2 = 47.88 Pa
1 lbf/in^2 = 1 psi = 6,894.8 Pa
1 bar = 1 $\times$ 10^5 Pa

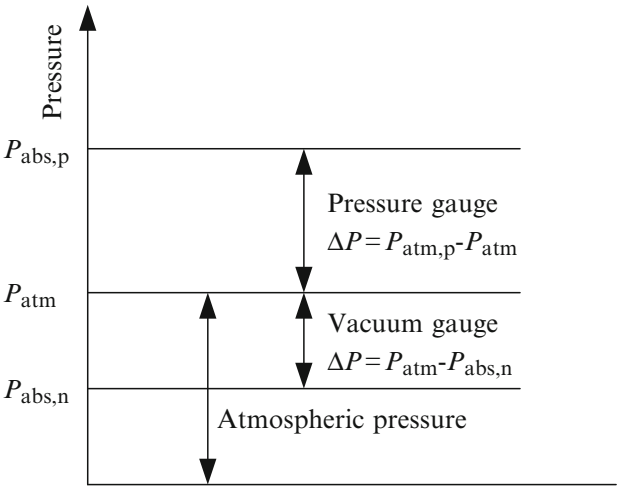

Fig. 1.1 Illustration of pressures for measurement

We now introduce the basic pressure definitions; a summary of the basic pressure measurement relationships is shown in Fig. 1.1.

Atmospheric pressure. The atmosphere that surrounds the earth can be considered a reservoir of low-pressure air. Its weight exerts a pressure that varies with temperature, humidity, and altitude. Atmospheric pressure also varies from time to time at a single location because of the movement of weather patterns. While these changes in barometric pressure are usually less than one-half inch of mercury, they need to be taken into account when precise measurements are essential.

$$\begin{aligned} 1 \text{ standard atmosphere} &= 1.0133 \text{ bar} = 1.0133 \times 10^5 \text{Pa} = 101.33 \text{ kPa} \\ &= 0.10133 \text{ MPa} = 14.7 \text{ psi} = 29.92 \text{ in Hg} \\ &= 760 \text{ mmHg} = 760 \text{ Torr}. \end{aligned}$$

Gauge pressure. The *gauge pressure* is any pressure for which the base for measurement is atmospheric pressure expressed as kPa as gauge. Atmospheric pressure serves as the reference level for other types of pressure measurements, for example gauge pressure. As is shown in Fig. 1.1, the gauge pressure is either positive or negative, depending on its level above or below the atmospheric pressure level. At the level of atmospheric pressure, the gauge pressure becomes zero.

Absolute pressure. A different reference level is utilized to obtain a value for absolute pressure. The absolute pressure can be any pressure for which the base for measurement is full vacuum, being expressed in kPa as absolute. In fact, it is composed of the sum of the gauge pressure (positive or negative) and the atmospheric pressure as follows:

$$\text{kPa(gauge)} + \text{atmospheric pressure} = \text{kPa(absolute)}. \tag{1.5}$$

For example, to obtain the absolute pressure, we simply add the value of atmospheric pressure of 101.33 kPa at sea level. The absolute pressure is the most common one used in thermodynamic calculations despite there being a pressure difference between the absolute pressure and the atmospheric pressure existing in the gauge being read by most pressure gauges and indicators.

Vacuum. A vacuum is a pressure lower than the atmospheric one that occurs only in closed systems, except in extraterrestrial space. It is also called the *negative gauge pressure*. As a matter of fact, vacuum is the pressure differential produced by evacuating air from the closed system. Vacuum is usually divided into four levels as (1) low vacuum representing pressures above one Torr absolute (a large number of mechanical pumps in industry are used for this purpose; flow is viscous), (2) medium vacuum varying between 1 and 10^{-3} Torr absolute (most pumps serving in this range are mechanical; fluid is in transition between viscous and molecular), (3) high vacuum ranging between 10^{-3} and 10^{-6} Torr absolute (nonmechanical ejector or cryogenic pumps are used; flow is molecular or newtonian), and (4) very high vacuum representing absolute pressure below 10^{-6} Torr (primarily for laboratory applications and space simulation).

A number of devices are available to measure fluid (gaseous or liquid) pressure and vacuum values in a closed system, and they require the fluid pressure to be steady for a reasonable length of time. In practice, the most common types of such gauges are as follows:

- *Absolute pressure gauge*: This is used to measure the pressure above a theoretical perfect vacuum condition and the pressure value is equal to ($P_{\text{abs,p}} - P_{\text{atm}}$) in Fig. 1.1. The most basic type of such gauges is the barometer. Another type of gauge used for vacuum measurements is the U-shaped gauge. The pressure value read is equal to ($P_{\text{atm}} - P_{\text{abs,n}}$) in Fig. 1.1.
- *Mercury U-tube manometer*: These manometers use a column of liquid to measure the difference between two pressures. If one is atmospheric pressure, the result is a direct reading of positive or negative gauge pressure.
- *Plunger gauge*: This gauge consists of a plunger connected to system pressure, a bias spring, and a calibrated indicator. An auto tire gauge would be an example.
- *Bourdon gauge*: This is the most widely utilized instrument for measuring positive pressure and vacuum. Measurements are based on the determination of an elastic element (a curved tube) by the pressure being measured. The radius of curvature increases with increasing positive pressure and decreases with increasing vacuum. The resulting deflection is indicated by a pointer on a calibrated dial through a ratchet linkage. Similar gauges may be based on the deformation of diaphragms or other flexible barriers.
- *McLeod gauge*: This is the most widely used vacuum-measuring device, particularly for extremely accurate measurements of high vacuums.

Among these devices, two principal types of measuring devices for industrial applications are manometers and Bourdon gauges. However, in many cases

manometers are not preferred due to the excessive length of tube needed, the inconvenience of using them for pressures much in excess of 1 atm, and their lesser accuracy.

There are also pressure transducers available, based on the effects of capacitance, the rates of change of strain, the voltage effects in a piezoelectric crystal, and magnetic properties (Marquand and Croft 1997). All have to be calibrated, and the only calibration possible is against a manometer under steady conditions, even though they are most likely to be used under dynamic conditions.

It is important to note at another level that the *saturation pressure* is the pressure of a liquid or vapor at saturation conditions.

1.3 Kinetic-Molecular Theory and Temperature

Kinetic-molecular theory gives a special interpretation of temperature that is worth our attention because it relates the temperature to the internal energy of a thermodynamic system. In this respect, the internal energy is a statistical mean of the energy of all molecules and is proportional to the average force that the molecules exert on the system boundary.

Let us assume a thermodynamic system formed from an *ideal gas*, which is defined as a special state of matter comprising a large number N of particles (molecules or atoms) of mass $m \neq 0$ that move freely and have randomly perfect elastic collision with the system's boundary. The number of particles with respect to the system size is small, so that the total volume of the particles is negligible and the collision among the particles is less probable than the collision of the particles with the walls. The shape of the thermodynamic system can be arbitrary, but for simplicity we assume here a cubical volume. The derivations that follow have an integrative nature and therefore are valid for a volume of any shape.

When a particle collides with the wall, say in the x direction with velocity v_x, it will be reflected back into the volume with velocity $-v_x$. Therefore, the variation of momentum is

$$\Delta p = mv_x - m(-v_x) = 2mv_x. \tag{1.6}$$

The duration of one collision is the same as the time a particle travels between two opposite walls, $\Delta t = 2l/v_x$, where l is the edge of the cube. Then according to the principle of momentum conservation, Eq. (1.6) becomes

$$F_{x,i} = \frac{\Delta p}{\Delta t} = \frac{mv_{x,i}^2}{l}, \tag{1.7}$$

where the index i indicates that the equation refers to the particle i acting on one of the two opposite walls in the direction x. It is reasonable to assume a uniform distribution of particles collisions on all three Cartesian directions, x, y, and z, which means that $N/3$ particles hit the x boundaries, that is, $i = 1 \ldots N/3$. Moreover,

the length l is equal to the volume V of the cube divided by the area of one face A_1. Therefore, Eq. (1.7) summed from $i = 1 \ldots N/3$ gives the total force acting of one cube face:

$$F_x = \sum_{i=1}^{N/3} F_{x,i} = \frac{mA_1}{V} \sum_{i=1}^{N/3} v_{x,i}^2. \tag{1.8}$$

The velocity of the particles within the system can be statistically averaged such that

$$\sum_{i=1}^{N/3} v_{x,i}^2 = \sum_{i=1}^{N/3} v_{y,i}^2 = \sum_{i=1}^{N/3} v_{z,i}^2 = N\bar{v}^2. \tag{1.9}$$

Combining Eqs. (1.4), (1.8), and (1.9), the following expression is obtained for the pressure exerted by the system on its boundary (which is the same on all faces):

$$P = \frac{F_x}{A_1} = \frac{F_y}{A_1} = \frac{F_z}{A_1} = \frac{Nm\bar{v}^2}{3V}. \tag{1.10}$$

Here, one recognizes the term Nm/V that represents the total mass divided by the system volume and is defined as the *density*, denoted with ρ and measured in kg/m^3. The inverse of the density is the specific volume v, measured in m^3/kg. Including the specific volume in Eq. (1.10), one obtains the following result for the pressure exerted by an ideal gas due to the movement of its molecules or "gas pressure":

$$P = \frac{1}{3}\frac{\bar{v}^2}{v}. \tag{1.11}$$

Note that if the gas is dense or one analyzes a vapor–liquid mixture, in addition to the pressure exerted by gas molecules, there is a gradient of density within the system due to gravitational forces. This generates a higher pressure on the bottom surface, known as hydrostatic pressure. The hydrostatic pressure represents the weight of the fluid (gas or liquid) column exerted on the surface, which is given by $P_h = \rho gZA/A = \rho gZ$, where Z is the height of the fluid column. It depends on the peculiarity of the system if the hydrostatic pressure or gas pressure must be considered or neglected. For example, in a hydroelectric power plant only the head pressure, that is the hydrostatic pressure of the water column, can be considered in the analysis. In a boiler, because its size is relatively small for gravitational effects to be considered, the hydrostatic pressure can be neglected and only the gas (vapor) pressure considered. Additional pressure components may exist if the fluid has, for example, magnetoelectric properties.

From Eq. (1.10) one can extract the average kinetic energy of a single particle:

$$K = \frac{1}{2}m\bar{v}^2 = \frac{3}{2}\frac{PV}{N}. \tag{1.12}$$

The kinetic energy corresponding to 1 mol of ideal gas results from combining Eqs. (1.1) and (1.12) and is

$$K_{\mathrm{n}} = \frac{3}{2}\frac{PV}{N}N_{\mathrm{A}} = \frac{3}{2}\frac{PV}{n}. \tag{1.13}$$

The degree of freedom (DOF) of a mono-atomic ideal gas is DOF = 3 because there are three axes of translation; since the particles are small spheres there are no rotational degrees of freedom. Therefore, the following quantity is the average kinetic energy of 1 mol of ideal gas per number of degrees of freedom:

$$\frac{K_{\mathrm{n}}}{\mathrm{DOF}} = \frac{1}{2}\frac{PV}{n}. \tag{1.14}$$

According to its definition, temperature, denoted by T, is a quantity proportional to the average energy of a single molecule (particle, atom) in the system per degree of freedom, that is, $K/\mathrm{DOF} \sim T$; for n mol of gas, this becomes $nT \sim K_{\mathrm{n}}/\mathrm{DOF}$. The constant of proportionality is known as the *universal gas constant* and is denoted by R:

$$R = \frac{2K_{\mathrm{n}}}{\mathrm{DOF} \times T} = 8314.472\,\mathrm{JK}^{-1}\,\mathrm{kmol}^{-1}. \tag{1.15}$$

Combining Eqs. (1.14) and (1.15) results in the *ideal gas equation*, namely

$$PV = nRT. \tag{1.16}$$

The universal gas constant R, divided by the molecular mass M of the gas represents the *real gas constant*, $\mathrm{R_g} = R/M$. The universal gas constant also allows expressing the average energy of a single molecule, which results by replacing PV from Eq. (1.16) into Eq. (1.12). Further, using Eq. (1.1), it results in

$$K = \frac{3}{2}\frac{R}{N_{\mathrm{A}}}T = \frac{3}{2}k_{\mathrm{B}}T, \tag{1.17}$$

which is the equation that defines the Boltzman constant k_{B}:

$$k_{\mathrm{B}} = \frac{R}{N_{\mathrm{A}}} = 1.380\,6504 \times 10^{-23}\,\mathrm{J/K}. \tag{1.18}$$

Therefore, temperature is proportional to the energy of a single molecule per number of degrees of freedom, the constant of proportionality being $2/k_{\mathrm{B}}$.

Temperature is an indication of the thermal energy stored in a substance. In other words, we can identify hotness and coldness with the concept of temperature. The temperature of a substance may be expressed in either relative or absolute units. The two most common temperature scales are the Celsius (°C) and the Fahrenheit (°F). The Celsius scale is used with the SI unit system and the Fahrenheit scale with

the English system of units. There are also two more scales, the Kelvin scale (K) and the Rankine scale (R) that are sometimes employed in thermodynamic applications; the Kelvin scale is considered an SI scale. The relations between these scales are summarized as follows:

$$T_{(^\circ\mathrm{C})} = \frac{T_{(^\circ\mathrm{F})} - 32}{1.8}, \tag{1.19}$$

$$T_{(\mathrm{K})} = T_{(^\circ\mathrm{C})} + 273.15 = \frac{T_{(\mathrm{R})}}{1.8} = \frac{T_{(^\circ\mathrm{F})} + 459.67}{1.8}, \tag{1.20}$$

$$T_{(^\circ\mathrm{F})} = 1.8T_{(^\circ\mathrm{C})} + 32 = 1.8(T_{(\mathrm{K})} - 273.15) + 32, \tag{1.21}$$

$$T_{(\mathrm{R})} = 1.8T_{(\mathrm{K})} = T_{(^\circ\mathrm{F})} + 459.67. \tag{1.22}$$

Furthermore, the temperature differences result in

1 K = 1°C = 1.8 R = 1.8°F,
1 R = 1°F = 1 K/1.8 = 1°C/1.8.

Kelvin is a unit of temperature measurement; zero Kelvin (0 K) is absolute zero and is equal to –273.15°C. The K and °C are equal increments of temperature. For instance, when the temperature of a product is decreased to −273.15°C (or 0 K), known as *absolute zero*, the substance contains no heat energy and supposedly all molecular movement stops (a detailed discussion on zero-Kelvin temperature is presented in the next section). The saturation temperature is the temperature of a liquid or vapor at saturation conditions.

Temperature can be measured in many ways by different devices. In general, the following devices are in common use:

- *Liquid-in-glass thermometers.* In these thermometers the volume of the fluid expands when subjected to heat, thereby raising its temperature. It is important to note that in practice, all thermometers, including mercury ones, only work over a certain range of temperature. For example, mercury becomes solid at −38.8°C and its properties change dramatically.
- *Resistance thermometers.* A resistance thermometer is made of resistance wire of known, repeatable, electrical characteristics so that the relationship between the temperature and electrical resistance value can be predicted precisely. The measured value of the ohmic resistance of the detector determines the value of an unknown temperature. Among metallic conductors, pure metals exhibit the greatest change of resistance with temperature. For applications requiring higher accuracy, especially where the temperature measurement is between −200°C and +800°C, platinum thermometers are used. In industry, in addition to platinum, nickel (−60°C to +180°C) and copper (−30°C to +220°C) are frequently used in resistance thermometers. Resistance thermometers can be provided with

two-, three-, or four-wire connections, and for higher accuracy at least three wires are required.

- *Averaging thermometers.* An averaging thermometer is designed to measure the average temperature of bulk stored liquids. The sheath contains a number of elements of different lengths, all starting from the bottom of the sheath. The longest element, which is fully immersed, is connected to the measuring circuit to allow a true average temperature to be obtained. There are some significant parameters, namely sheath material (stainless steel for the temperature range from −50°C to +200°C or nylon for the temperature range from −50°C to +90°C), sheath length (to suit the application), termination (flying leads or terminal box), element length, element calibration (to copper or platinum curves), and operating temperature ranges. In many applications where a multi-element thermometer is not required, such as in air ducts, cooling water, and gas outlets, a single element thermometer stretched across the duct or pipework will provide a true average temperature reading. Despite the working range from 0° to 100°C, the maximum temperature may reach 200°C. To maintain high accuracy, these units are normally supplied with three-wire connections. However, up to 10 elements can be mounted in the averaging bulb fittings, and they can be made of platinum, nickel, or copper, and fixed at any required position.
- *Thermocouples.* A thermocouple consists of two electrical conductors, of different materials connected together at one end (so-called measuring junction). The two free ends are connected to a measuring instrument, for example, an indicator, a controller, or a signal conditioner, by a reference junction (so-called cold junction). The thermoelectric voltage appearing at the indicator depends on the materials of which the thermocouple wires are made and on the temperature difference between the measuring junction and the reference junction. For accurate measurements, the temperature of the reference junction must be kept constant. Modern instruments usually incorporate a cold junction reference circuit and are supplied ready for operation in a protective sheath, to prevent damage to the thermocouple by any mechanical or chemical means. Table 1.1 lists several types of thermocouples along with their maximum absolute temperature ranges. Copper–constantan thermocouples have an accuracy of ±1°C and are often employed for control systems in practical thermal applications.

Table 1.1 Some of most common thermocouples

Type	Common names	Temperature range (°C)
T	Copper–Constantan (C/C)	−250 to 400
J	Iron–Constantan (I/C)	−200 to 850
E	Nickel Chromium–Constantan or Chromel–Constantan	−200 to 850
K	Nickel Chromium–Nickel Aluminum or Chromel–Alumel (C/A)	−180 to 1100
–	Nickel 18% Molybdenumb Nickel	0 to 1300
N	Nicrosil-Nisil	0 to 1300
S	Platinum 10% Rhodiumb Platinum	0 to 1500
R	Platinum 13% Rhodiumb Platinum	0 to 1500
B	Platinum 30% Rhodiumb Platinum 6% Rhodium	0 to 1600

The iron–constantan thermocouple with its maximum temperature of 850°C is used in applications in the plastics industry. The chromel–alumel type thermocouples, with a maximum of about 1,100°C, are suitable for combustion applications in ovens and furnaces. In addition, it is possible to reach about 1,600° or 1,700°C using platinum and rhodium–platinum thermocouples, particularly in steel manufacturing. It is worth noting that one advantage thermocouples have over most other temperature sensors is that they have a small thermal capacity and thus a prompt response to temperature changes. Furthermore, their small thermal capacity rarely affects the temperature of the body under examination.

- *Thermistors.* These devices are semiconductors and act as thermal resistors with a high (usually negative) temperature coefficient. In use, thermistors operate either self-heated or externally heated. Self-heated units employ the heating effect of the current flowing through them to raise and control their temperature and thus their resistance. This operating mode is useful in such devices as voltage regulators, microwave power meters, gas analyzers, flow meters, and automatic volume and power level controls. Externally heated thermistors are well suited for precision temperature measurement, temperature control, and temperature compensation due to large changes in resistance versus temperature. They are generally used for applications in the range −100°C to +300°C. Despite early thermistors having tolerances of ±20% or ±10%, modern precision thermistors are of higher accuracy, for example, ±0.1°C (less than ±1%).
- *Digital display thermometers.* A wide range of digital display thermometers, for example hand-held battery-powered displays and panel-mounted mains or battery units, are available on the market. Displays can be provided for use with all standard thermocouples or platinum resistance thermometers with several digits and 0.1°C resolution.

It is very important to emphasize that before temperature can be controlled, it must be sensed and measured accurately. For temperature measurement devices, there are several potential sources of error, such as sensor properties, contamination effects, lead lengths, immersion, heat transfer, and controller interfacing. In temperature control there are many sources of error that can be minimized by careful consideration of the type of sensor, its working environment, the sheath or housing, the extension leads, and the instrumentation. An awareness of potential errors is vital. Selection of temperature measurement devices is a complex task and has been discussed briefly here. It is extremely important to remember to "choose the right tool for the right task."

Internal energy U of a substance has been introduced previously as the sum of all particular energies manifesting at microscale in a particular thermodynamic system. This is an *extensive property* that depends on the size (mass) of the system. If U is divided into the mass of the system, m, then one obtains the *specific internal energy* denoted u, an *intensive property* that does not depend on the system's size, and it is measured in J/kg; mathematically $u = U/m$. Alternatively, it is used as the molar-specific energy $u = U/n$.

For a mono-atomic gas, as discussed above, the internal energy is the same with the kinetic energy of the atoms. For example, helium is a mono-atomic gas. In this case, the molar-specific internal energy is

$$u = \frac{3}{2}RT. \tag{1.23}$$

In general, through a *thermodynamic property* one denotes a physical characteristic of a substance used to describe its *state*. Any two properties usually define the state or condition of the substance, from which all other properties can be derived. Some examples are temperature, pressure, specific volume, and internal energy. Property diagrams of substances are generally presented in graphical form and summarize the main properties as listed in the thermodynamic tables.

The state of a system or substance is defined as the condition of the system or substance characterized by certain observable macroscopic values of its properties such as temperature and pressure. The term *state* is often used interchangeably with the term *phase*, for example, solid phase or gaseous phase of a substance. Each of the properties of a substance in a given state has only one definite value, regardless of how the substance reached the state. For example, when sufficient heat is added or removed, most substances undergo a state change. The temperature remains constant until the state change is complete. This can be from solid to liquid, liquid to vapor, or vice versa. Figure 1.2 shows typical examples of ice melting and water boiling.

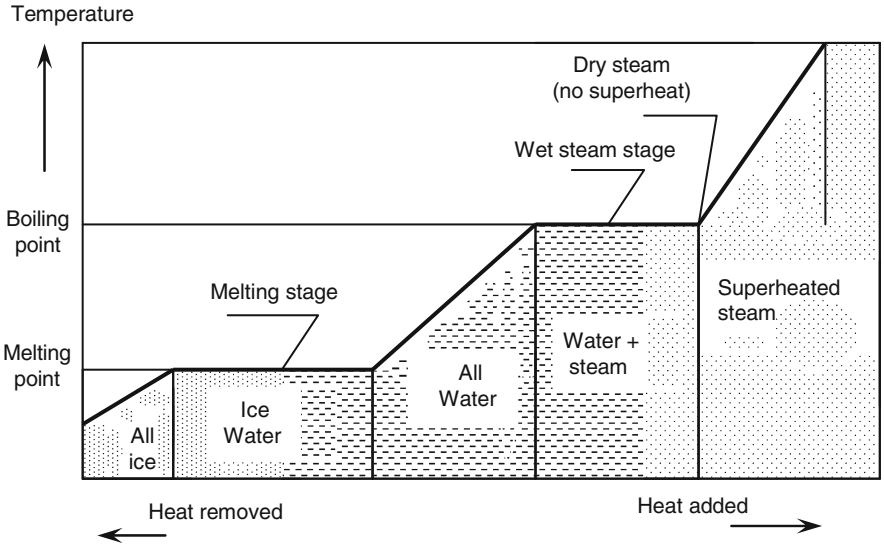

Fig. 1.2 The state-change diagram of water

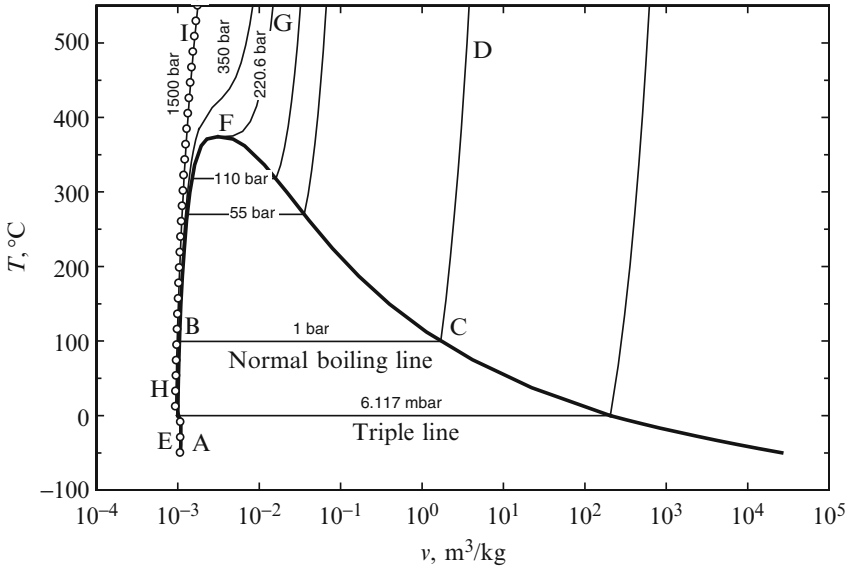

Fig. 1.3 Temperature–volume diagram for the phase change of water

A clearer presentation of solid, liquid, and vapor phases of water is exhibited on a temperature–volume (T–v) diagram in Fig. 1.3. The constant pressure line ABCD represents the states that water passes through as follows:

- *A–B*: This represents the process in which water is heated from the initial temperature to the saturation temperature (liquid) at constant pressure. At point B it is fully saturated liquid water with a quality $x = 0$, with zero quantity of water vapor.
- *B–C*: This is the constant-temperature vaporization process in which there is only phase change from saturated liquid to saturated vapor, referring to the fact that the quality varies from 0 to 100%. Within this zone, the water is a mixture of liquid water and water vapor. At point C it is completely saturated vapor and the quality is 100%.
- *C–D*: This represents the constant-pressure process in which the saturated water vapor is superheated with increasing temperature.
- *E–F–G*: In this line there is no constant-temperature vaporization process. Point F is called the *critical point* where the saturated-liquid and saturated-vapor states are identical. The thermodynamic properties at this point are called critical thermodynamic properties, such as critical temperature, critical pressure, and critical specific volume.
- *H–I*: This is a constant-pressure heating process in which there is no phase change from one phase to another (one is present only); however, there is a continuous change in density.

The other process that can occur during melting of water is *sublimation*, in which the ice directly passes from the solid phase to vapor phase. Another important point that needs to be emphasized is that the solid, liquid, and vapor phases of water may be present together in equilibrium, leading to the *triple point*.

The diagram in Fig. 1.3 presents a thermodynamic region where thermodynamic equilibrium exists between vapor and liquid. This diagram is generated with Engineering Equation Solver (EES) software (Klein 2010). A vapor is a gas at or near equilibrium with the liquid phase—a gas under the saturation curve or only slightly beyond the saturated vapor line. *Vapor quality* is theoretically assumed; that is, when vapor leaves the surface of a liquid, it is pure and saturated at the particular temperature and pressure. In actuality, tiny liquid droplets escape with the vapor. When a mixture of liquid and vapor exists, the ratio of the mass of the vapor to the total mass of the liquid and vapor mixture is called the *quality* and is expressed as a percentage or decimal fraction. *Superheated vapor* is the saturated vapor to which additional heat has been added, raising the temperature above the boiling point. Let us consider a mass (m) with a quality (x). The volume is the sum of the liquid and the vapor as defined below:

$$V = V_{\text{liq}} + V_{\text{vap}}. \tag{1.24}$$

It can also be written in terms of specific volumes as

$$mv = m_{\text{liq}} v_{\text{liq}} + m_{\text{vap}} v_{\text{vap}}. \tag{1.25}$$

Dividing all terms by the total mass results in

$$v = (1 - x) v_{\text{liq}} + x v_{\text{vap}} \tag{1.26}$$

and

$$v = v_{\text{liq}} + x v_{\text{liq,vap}}, \tag{1.27}$$

where $v_{\text{liq,vap}} = v_{\text{vap}} - v_{\text{liq}}$.

The specific internal energy of a mixture of liquid and vapor can be written in a similar form to Eqs. (1.26) and (1.27):

$$u = (1 - x) u_{\text{liq}} + x u_{\text{vap}} \tag{1.28}$$

and

$$u = u_{\text{liq}} + x u_{\text{liq,vap}}, \tag{1.29}$$

where $u_{\text{liq,vap}} = u_{\text{vap}} - u_{\text{liq}}$.

1.4 Thermodynamic Equilibrium: The Zeroth Law of Thermodynamics

Classical thermodynamics is based on the concept of equilibrium. A thermodynamic system that does not exchange matter with its surroundings is said to be a *closed thermodynamic system*. If in addition a closed thermodynamic system does not exchange energy in any form with its surroundings, then the system is said to be *insulated*. Thus no mechanical, thermal, chemical, electrical, gravitational, elastic, or other forces can act over the boundary of an insulated system.

Assume an insulated system S is divided into two imaginary volumes, forming thus two thermodynamic subsystems S_1 and S_2 that can exchange energy through their common boundary. If the boundary is elastic and permeable, the energy is exchanged in the form of work, possibly in chemical form, or even in the form of kinetic energy at microscale, that is, the energy related to temperature. By definition, the energy transfer that is caused by a difference of temperature between a thermodynamic system and its surroundings is called *heat*.

The definitive experiment that showed that heat was a form of energy convertible into other forms was carried out by the Scottish physicist James Joule. Heat is the thermal form of energy, and heat transfer takes place when a temperature difference exists within a medium or between different media. Heat always requires a difference in temperature for its transfer. Higher temperature differences provide higher heat transfer rates. The units for heat are joules or kilojoules in the International system and Btu in the English system. In thermodynamic calculations, heat transfer to a system is considered *positive*, while heat transfer from a system is *negative*. If there is no heat transfer involved in a process, it is called an *adiabatic process*. The unit for the heat transfer rate in both the International and English systems is

$$1\ \mathrm{W} = 3.4123\mathrm{Btu/h} \quad \text{or} \quad 1\ \mathrm{Btu/h} = 0.2931\mathrm{W}.$$

The unit for heat generation per unit volume is

$$1\ \mathrm{W/m^3} = 0.09665\mathrm{Btu/h\ ft^3} \quad \text{or} \quad 1\mathrm{Btu/h\ ft^3} = 10.343\mathrm{W/m^3}.$$

The unit for specific heat is

$$1\ \mathrm{J/kg\ K} = 2.3886 \times 10^{-4}\ \mathrm{Btu/lbm\ F}$$

The unit for heat flux, which is the heat per unit area, is then

$$1\mathrm{W/m^2} = 0.3171\mathrm{Btu/hft^2} \quad \text{or} \quad 1\mathrm{Btu/hft^2} = 3.1525\mathrm{W/m^2}$$

$$1\ \mathrm{kcal/h\ m^2} = 1.163\ \mathrm{W/m^2}$$
$$1\ \mathrm{cal/s\ cm^2} = 41\ 870.0\ \mathrm{W/m^2}$$
$$1\ \mathrm{Btu/lbm\ F} = 4{,}187\ \mathrm{J/kg\ K}$$

Two bodies are said to be in *thermal equilibrium* if they cannot exchange heat, or in other words, they have the same temperature. Two bodies are in *mechanical equilibrium* is they cannot exchange energy in the form of work. Two bodies are in *chemical equilibrium* if they do not change their chemical composition.

The two subsystems assumed above, being in contact with each other, will exchange mechanical, chemical, and thermal energy until the moment when no change can occur within the system. At that moment, one says that the system reached *thermodynamic equilibrium*. In a thermodynamic system in thermodynamic equilibrium, there is thermal, chemical, and mechanical energy within any of the constitutive parts.

Thermodynamics is the science of energy and entropy, and the basis of thermodynamics is the experimental observation. In thermodynamics, such observations were formed into the four basic laws of thermodynamics called the zeroth, first, second, and third laws of thermodynamics. The first and second laws of thermodynamics are the most common tools in practice, due to the fact that transfers and conversions of energy are governed by these two laws, and in this chapter we will focus on these two laws.

The zeroth law of thermodynamics can be expressed as: "If two thermodynamic systems are in thermal equilibrium with a third, they are also in thermal equilibrium with each other." A system at internal equilibrium has a uniform pressure, temperature, and chemical potential (to be defined latter) throughout its volume.

1.5 Energy Conservation: The First Law of Thermodynamics

The first law of thermodynamics (FLT) can be defined as the law of conservation of energy, and it states that in a closed system, energy can be neither created nor destroyed. A closed thermodynamic system changing its initial state 1 to a final state 2 can be formulated as follows:

$$\begin{aligned} Q_{1-2} &= (E_2 - E_1) + W_{1-2} \\ &= (U_2 - U_1) + (KE_2 - KE_1) + (PE_2 - PE_1) + W_{1-2}, \end{aligned} \tag{1.30}$$

where $(KE_2 - KE_1) = m({v_2}^2 - {v_1}^2)/2$, $(PE_2 - PE_1) = mg(Z_2 - Z_1)$.

Equation (1.28) contains kinetic and potential energies in addition to internal energy. An important consequence of the FLT is that the internal energy change resulting from some process will be independent of the thermodynamic path followed by the system, and of the paths followed by the processes, for example, heat transfer and work. In turn, the rate at which the internal energy content of the system changes is dependent only on the rates at which heat is added and work is done.

If instead of a closed system one analyzes an open system, the total energy contains an additional term that relates to the work produced by the pressure. Assume that at an inlet port of the open system, the fluid crossing the boundary

has the pressure P and the specific volume v. In this case, the work W_f that moves a volume V of fluid into the system equals the force into displacement d. If A is the cross-sectional area of the inlet port, then the volume that passes through this area is $V = Ad$. Since the force is $F = PA$ and the displacement is $d = V/A$, one concludes that the work associated with the fluid that crosses the system's boundary is $W_f = PV$; dividing this equation with the mass of fluid that enters results in $w_f = Pv$; the same is valid for any fluid that exits out of the system.

For an open thermodynamic system, Eq. (1.30) then results in the following form:

$$\dot{Q}_{in} + \dot{W}_{in} + \sum_{in} \dot{m}\left(u + Pv + \frac{v^2}{2} + gz\right) = \dot{Q}_{out} + \dot{W}_{out} + \sum_{out} \dot{m}\left(u + Pv + \frac{v^2}{2} + gz\right), \tag{1.31}$$

where in this case one uses the rates of exchange, namely the heat flux $\dot{Q}$ measured in W (watts), the work rate or mechanical power $\dot{W}$ measured also in W, and the mass flow rate $\dot{m}$ measured in kg/s. The quantity

$$h = u + Pv \tag{1.32}$$

identified in Eq. (1.31) bears the name *specific enthalpy*. The extensive enthalpy is defined by $H = U + PV$.

Since enthalpy is a state function, it is necessary to measure it relative to some reference state. The usual practice is to determine the reference values, which are called the *standard enthalpy of formation* (or the heat of formation), particularly in combustion thermodynamics. The specific enthalpy of a mixture of liquid and vapor components can be written similar to Eqs. (1.26) and (1.27) as follows:

$$h = (1 - x)h_{liq} + xh_{vap} \tag{1.33}$$

and

$$h = h_{liq} + xh_{liq,vap}, \tag{1.34}$$

where $h_{liq,vap} = h_{vap} - h_{liq}$.

If locally within the system the variation of kinetic and potential energy can be neglected, and one realizes that the work produced by the system against the environment is $dw = P\,dv$, one can deduce two equivalent formulations of the first law of thermodynamics, one based on specific internal energy and the other on specific enthalpy, as follows:

$$\left.\begin{aligned} du &= dq - P\,dv \\ dh &= dq + v\,dP \end{aligned}\right\}. \tag{1.35}$$

Both specific internal energy and specific enthalpy are thermodynamic functions depending on two independent thermodynamic variables. Internal energy is in general expressed as a function of specific volume and temperature, and enthalpy as a function of pressure and temperature. Thus, the local variation of specific internal energy and entropy is

$$\left.\begin{aligned} \mathrm{d}u &= \left(\frac{\partial u}{\partial T}\right)_v \mathrm{d}T + \left(\frac{\partial u}{\partial v}\right)_T \mathrm{d}v = \mathrm{d}q - P\,\mathrm{d}v \\ \mathrm{d}h &= \left(\frac{\partial h}{\partial T}\right)_P \mathrm{d}P + \left(\frac{\partial h}{\partial P}\right)_T \mathrm{d}P = \mathrm{d}q + v\,\mathrm{d}P \end{aligned}\right\}. \tag{1.36}$$

Equation (1.36) identifies the *specific heat* that is defined as the variation of heat per unit of temperature, namely $c = \partial q/\partial T$. The process of heat exchange of the thermodynamic system with the surroundings can evolve at constant volume or at constant pressure. From (1.36) we derive the definition of specific heat at constant volume and pressure, respectively:

$$\left.\begin{aligned} c_\mathrm{v} &= \left(\frac{\partial u}{\partial T}\right)_\mathrm{v} \\ c_\mathrm{P} &= \left(\frac{\partial h}{\partial T}\right)_\mathrm{P} \end{aligned}\right\}. \tag{1.37}$$

For an ideal gas, according to Eq. (1.23) combined with Eqs. (1.32) and (1.37),

$$\left.\begin{aligned} c_\mathrm{v} &= \frac{3}{2}R \\ c_\mathrm{P} &= \frac{5}{2}R \\ c_\mathrm{P} &= c_\mathrm{v} + R \end{aligned}\right\}, \tag{1.38}$$

where the last equation from the above set is known as Robert Mayer relation. The fraction

$$\gamma = \frac{c_\mathrm{P}}{c_\mathrm{v}} \tag{1.39}$$

is named the adiabatic exponent and has the value $\gamma = 1 + R/c_\mathrm{v} = 5/3 = 1.67$ for the ideal gas.

1.6 Equations of State

The ideal gas law is an equation of state because it interrelates pressure, specific volume, and temperature, which are intensive properties that characterize the state of matter. In the case of ideal gas, the state of matter is a rarefied (diluted) gas in

which the action of the intermolecular forces can be neglected with respect to the forces associated with the molecule–system boundary collision.

Therefore, the ideal gas law is valid in the limit of large specific volumes and low pressures. As a consequence, the specific internal energy of the ideal gas does not depend on pressure or on specific volume. The only dependence in this case is $u = u(T)$. An ideal gas with constant specific heat is referred to as *perfect gas*.

In general, the purpose of the equation for the state of a substance is to describe completely the interrelation among state variables of that substance. For example, if one specifies the pressure and temperature, one must be able to calculate the specific volume and the specific internal energy. If these last two quantities can be determined, other derived quantities (e.g., the specific enthalpy) can be calculated from them, using standard thermodynamic relations [e.g., Eq. (1.34)].

The equation connecting P, v, and T is known as the thermal equation of state, and the equation expressing internal energy as a function of, for example, pressure and temperature, is called the *caloric equation of state*. For the perfect gas these are, respectively,

$$\left.\begin{aligned} Pv &= \mathrm{R}T, \text{ where } \mathrm{R} = R/M \\ u &= c_{\mathrm{v}}T \end{aligned}\right\}. \tag{1.40}$$

In the first equation in (1.40) R is the constant associated with the considered gas of molecular mass M. The second equation is derived from Eq. (1.37) by integrating from $T = 0$ K to T with the convention that $u_{(T\,=\,0\mathrm{K})} = 0$ J/kg (see below the third principle of thermodynamics).

The perfect gas equation becomes largely inexact close to the vapor saturation line and to the critical point for two main reasons: the specific heat varies significantly with temperature and pressure, and the gas becomes less compressible than predicted by Eq. (1.40). In order to account for the compressible character of the gas, a new quantity is introduced, namely the *compressibility factor* Z defined as

$$Z = \frac{v_{\text{actual}}}{v_{\text{ideal}}} = \frac{v_{\text{actual}}}{\mathrm{R}T/P} = \frac{Pv}{\mathrm{R}T}, \quad \text{where } v = v_{\text{actual}}. \tag{1.41}$$

The order of magnitude of the compressibility factor at critical point is 0.2 for most of the thermal fluids. The compressibility chart of argon is shown in Fig. 1.4 based on calculated data with EES software (Klein 2010).

There are some special processes during which P, v, or T remains constant. At a fixed temperature, the volume of a given quantity of ideal gas varies inversely with the pressure exerted on it (in some books this is called *Boyle's law*), describing compression as

$$P_1V_1 = P_2V_2, \tag{1.42}$$

where the subscripts refer to the initial and final states.

Equation (1.42) is employed by designers in a variety of situations: when selecting an air compressor, for calculating the consumption of compressed air in

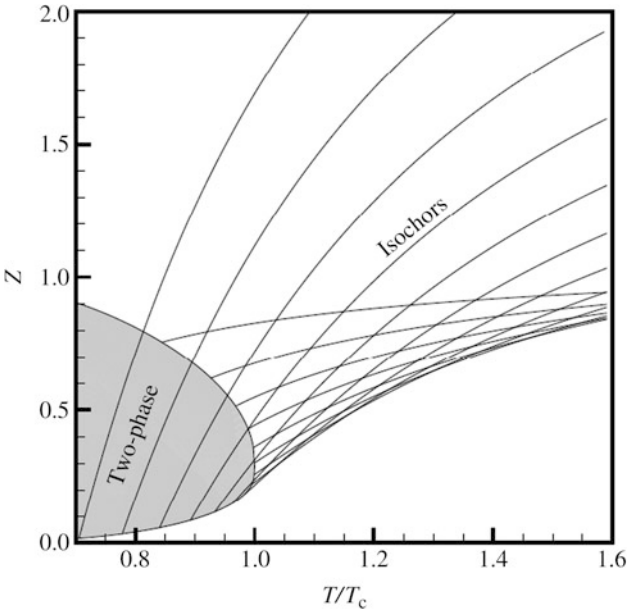

Fig. 1.4 Compressibility chart for argon

reciprocating air cylinders, and for determining the length of time required for storing air. Nevertheless, it may not always be practical due to temperature changes. If temperature increases with compression at a constant pressure, the volume of a gas varies directly with its absolute temperature in K as

$$\frac{V_1}{T_1} = \frac{V_2}{T_2}. \tag{1.43}$$

If temperature increases at a constant volume, the pressure of a gas this time varies directly with its absolute temperature in K as

$$\frac{P_1}{T_1} = \frac{P_2}{T_2} \tag{1.44}$$

Equations (1.45) and (1.46) are known as Charles's law. If both temperature and pressure change at the same time, the combined ideal gas equation can be written as follows:

$$\frac{P_1 V_1}{T_1} = \frac{P_2 V_2}{T_2} \tag{1.45}$$

As shown above, for a given mass, the internal energy of an ideal gas can be written as a function of temperature since c_{v0} is constant below

$$\mathrm{d}U = mc_{v0}\mathrm{d}T \tag{1.46}$$

and the specific internal energy becomes

$$\mathrm{d}u = c_{v0}\mathrm{d}T. \tag{1.47}$$

The enthalpy equation for an ideal gas, based on $h = u + Pv$, can be written as

$$\mathrm{d}H = mc_{p0}\mathrm{d}T \tag{1.48}$$

and the specific enthalpy then becomes

$$\mathrm{d}h = c_{p0}\mathrm{d}T. \tag{1.49}$$

For a reversible adiabatic process the ideal gas equation in terms of the initial and final states under Pv^{γ} = constant is

$$Pv^{\gamma} = P_1 v_1^{\gamma} = P_2 v_2^{\gamma}. \tag{1.50}$$

Based on Eq. (1.50) and the ideal gas equation, the following expressions can be obtained:

$$\frac{P_2}{P_1} = \left(\frac{T_2}{T_1}\right)^{\gamma/\gamma-1} = \left(\frac{v_1}{v_2}\right)^{\gamma} = \left(\frac{V_1}{V_2}\right)^{\gamma}. \tag{1.51}$$

Let us consider a closed system with ideal gas, undergoing an adiabatic reversible process with a constant specific heat. The work can be derived from the first law of thermodynamics equation as follows:

$$W_{1-2} = \frac{mR(T_2 - T_1)}{(1-k)} = \frac{(P_2V_2 - P_1V_1)}{(1-k)}, \tag{1.52}$$

which can also be derived from the general work relation, $W = P\ \mathrm{d}V$.

For a reversible polytropic process, the only difference is the polytropic exponent (n), which shows the deviation from a log$P$ and log$V$ diagram, leading to the slope. Therefore, Eqs. (1.50)–(1.52) can be rewritten with the polytropic exponent under Pv^n = constant as

$$Pv^n = P_1 v_1^n = P_2 v_2^n, \tag{1.53}$$

$$\frac{P_2}{P_1} = \left(\frac{T_2}{T_1}\right)^{n/n-1} = \left(\frac{v_1}{v_2}\right)^{n} = \left(\frac{V_1}{V_2}\right)^{n}, \tag{1.54}$$

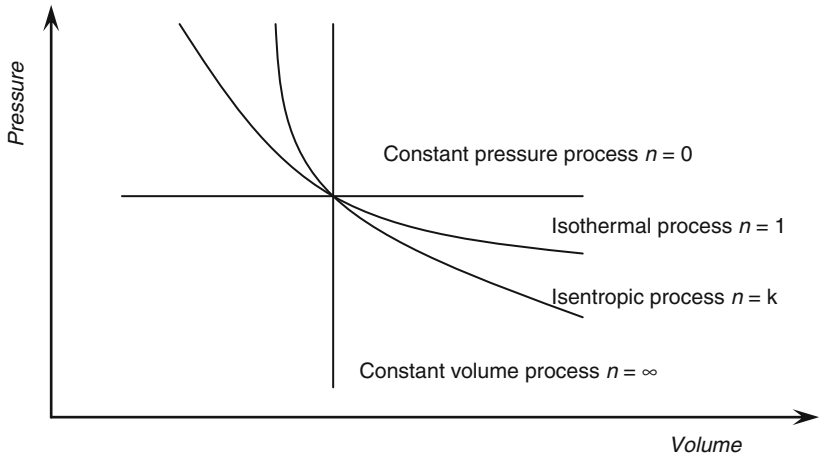

Fig. 1.5 Representation of four different polytropic processes on a pressure–volume diagram

$$W_{1-2} = \frac{mR(T_2 - T_1)}{(1-n)} = \frac{(P_2V_2 - P_1V_1)}{(1-n)}. \tag{1.55}$$

In order to give a clear idea, it is important to show the values of n for four different types of polytropic processes for ideal gases (Fig. 1.5) as follows:

- $n = 0$ for isobaric process ($P = 0$)
- $n = 1$ for iothermal process ($T = 0$)
- $n = k$ for isentropic process ($s = 0$)
- $n = \infty$ for isochoric process ($v = 0$)

As is obvious in Fig. 1.5, there are two quadrants where n varies from zero to infinity and where it has a positive value. The slope of any curve drawn is an important consideration when a reciprocating engine or compressor cycle is under consideration.

In thermodynamics, a number of problems involve mixtures of different pure substances (e.g., ideal gases). In this regard, it is of importance to understand the related aspects accordingly. Table 1.2 gives a summary of the relevant expressions and two ideal gas models: the Dalton model and the Amagat model. In the analysis it is assumed that each gas is unaffected by the presence of other gases, and each one is treated as an ideal gas. The Dalton model applies when the temperature and volume are constant, and thus it introduces the concept of partial pressure. Gases share the same volume but are at different pressure. The total pressure of the system becomes the sum of the partial pressures of all component gases. The partial pressure is given in this case by the molar concentration of the mixture component. If the temperature and pressure are the same for all mixture components, then the total volume is calculated by adding all component volumes. This is the Amagat model. With regard to entropy, it is important to note that an increase in entropy is

Table 1.2 Equations for gas and gas mixtures and relevant models

Definition	Dalton model	Amagat model
Total mass of a mixture of N components	$m_{tot} = m_1 + m_2 + \cdots + m_N = \sum m_i$	
Total number of moles of a mixture of N components	$n_{tot} = n_1 + n_2 + \cdots + n_N = \sum n_i$	
Mass fraction for each component	$c_i = m_i / m_{tot}$	
Mole fraction for each component	$y_i = n_i / n_{tot} = P_i / P_{tot} = V_i / V_{tot}$	
Molecular weight for the mixture	$M_{mixi} = m_{tot} / n_{tot} = \sum n_i M_i / n_{tot} = \sum y_i M_i$	
Internal energy for the mixture	$U_{mix} = n_1 \overline{U_1} + n_2 \overline{U_2} + \cdots + n_N \overline{U_N} = \sum n_i \overline{U_i}$	
Enthalpy for the mixture	$H_{mix} = n_1 \overline{H_1} + n_2 \overline{H_2} + \cdots + n_N \overline{H_N} = \sum n_i \overline{H_i}$	
Entropy for the mixture	$S_{mix} = n_1 \overline{S_1} + n_2 \overline{S_2} + \cdots + n_N \overline{S_N} = \sum n_i \overline{S_i}$	
Entropy difference for the mixture	$(S_2 - S_1) = -\overline{R}(n_1 \ln y_1 + n_2 \ln y_2 + \cdots + n_N \ln y_N)$	
P, V, T for the mixture	T and V are constant $P_{tot} = P = P_1 + P_2 + \cdots + P_N$	T and P are constant $V_{tot} = V = V_1 + V_2 + \cdots + V_N$
Ideal gas equation for the mixture	$PV = n\overline{R}T$	
Ideal gas equations for the components	$P_1 V = n_1 \overline{R} T$ $P_2 V = n_2 \overline{R} T$: $P_N V = n_N \overline{R} T$	$PV_1 = n_1 \overline{R} T$ $PV_2 = n_2 \overline{R} T$: $PV_N = n_N \overline{R} T$

dependent only upon the number of moles of ideal gases and is independent of its chemical composition.

Many real mixtures of gases or liquids show departures from the ideal behavior. For example, the enthalpy of the 'mixture is not the same as a weighted sum of the components' enthalpy. In this case, the term *excess enthalpy* accounts for the physical interaction between the mixture components. Two nonideal mixtures are extremely important for energy engineering, namely the lithium bromide–water mixture and the ammonia–water mixture. These mixtures are used as working fluid or refrigerants in many engineering applications such as absorption cooling or heat pumps, or special power cycles like the Kalina cycle. In the subsequent chapters of this book are several examples of using ammonia–water and lithium bromide–water mixtures in energy systems.

When the lithium bromide–water mixture is used in an absorption machine, the water plays the role of a refrigerant, while the mixture of lithium bromide with water is kept in the liquid phase and has the role of transporting water from low pressure to high pressure. The mixture has three degrees of freedom in the sense that its enthalpy (or entropy or specific energy) depends on pressure, temperature, and concentration. Appendix B presents a typical Van't Hoff chart (see Diagram B.3, p. 798) that correlates the saturation pressure of water vapor above liquid mixture (solution) with the lithium bromide concentration. In addition, the Dühring chart on the same

diagram indicates the temperature of the saturated water vapor for a given temperature of the liquid solution and a given concentration. Observe, for example, that if the temperature of the liquid is 100°C at a solution concentration of 50%, then the temperature of the water vapor is ~80°C. This proves the nonideality of the mixture, which shows always more water concentration in the vapor phase than in the liquid phase. A complication occurs at lower temperatures, where lithium bromide crystallizes and separates from the solution (see the crystallization line in the Dühring chart in Appendix B). The enthalpy of the liquid solution at various concentrations and temperatures can be read from the enthalpy plot of the lithium bromide–water system presented also in Appendix B (see Diagram B.4, p. 798).

In the ammonia–water mixture, the ammonia is considered the refrigerant. Ammonia is more volatile; thus in the vapor phase the ammonia concentration is higher than in the liquid phase. The ammonia–water solution shows high nonlinearity. Appendix B presents the enthalpy diagram of the ammonia–water solution (see Diagram B.5, p. 799). At the lower part of the diagram, the liquid isobars are shown in bold, while the isotherms are indicated with thinner lines. At the upper part of the diagram, vapor isobars are represented. For a given concentration, temperature, and pressure, one can determine the enthalpy. Also, the saturation enthalpy can be determined based on only two parameters, the pair of parameters from the following: concentration, temperature, and pressure. The dashed lines indicate the vapor–liquid equilibrium states. These lines are helpful for determining the saturated vapor and liquid concentration and enthalpies. For example, at 100°C and 10 bar on Diagram B.5 shown in Appendix B the liquid mixture concentration is ~0.3 and the enthalpy is ~250 kJ/kg. The vapor enthalpy can be found at the other end of the (dashed) vapor–liquid equilibrium line ~1,600 kJ/kg and the ammonia concentration in vapor is 0.9.

An equation of state that is more elaborated than that of the perfect gas is the Van der Waals equation. This equation is capable of predicting the vapor and liquid saturation line and the qualitatively correct fluid behavior in the vicinity of the critical point. For a polytropic Van der Waals fluid (having thus a constant specific heat) the thermal and caloric equations of state (EoS) are after Callen (1985), respectively:

$$\left.\begin{aligned} P(T,v) &= \frac{RT}{v-b} - \frac{a}{v^2} \\ u(T,v) &= c_v - \frac{a}{v} \end{aligned}\right\}, \tag{1.56}$$

where the term a/v^2 accounts for the intermolecular forces and the term b for the volume occupied by the molecules under high pressure. These terms result from imposing the requirement that the first and second derivatives of P with respect to v are nil in the critical point. Thus, using algebra,

$$\left.\begin{aligned} a &= 27\mathrm{R}^2 T_c^2/64P_c \\ b &= \mathrm{R}T_c/8P_c \end{aligned}\right\}, \tag{1.57}$$

where the subscript c indicates the critical point parameter. It is useful to express the equation of state in a dimensionless form; this offers generality to the analysis. To obtain a dimensionless format of the Van der Waals equation, one defines

$$T_r = T/T_c, P_r = P/P_c, v_r = v/v_c, u_r = u/(P_c v_c) \tag{1.58}$$

and the expressions in Eq. (1.56) become

$$\left.\begin{aligned} P_r &= 8T_r/(3v_r - 1) - 3/v_r^2 \\ u_r &= (8c_v T_r)/(3\mathrm{R}) \end{aligned}\right\}. \tag{1.59}$$

An interesting property of the polytropic Van der Waals fluids is that the compressibility factor in the critical point is constant and equal to 3/8. Another significant parameter that influences the fluid thermodynamic properties is the accentric factor, which accounts for the molecular structure of the fluid and is defined by $\omega = -\log_{10}(P''_r(T_r)) - 1$, where $T_r = T/T_c = 0.7$ is the reduced pressure of 0.7 and $P_r''(T_r) = P''(0.7 \times T_c)/P_c$ is the reduced vapor saturation pressure at the reduced temperature of 0.7. The Peng–Robinson equation of state is formulated based on the accentric factor and gives improved accuracy that is close to the critical point of many real substances. The Peng–Robinson equation of state is described by $P = \frac{RT}{v-b} - \frac{a \times \alpha}{v^2 - 2bv - b^2}$, where $a = 0.45724\, R^2 T_c^2/P_c$, $b = 0.0778\, RT_c/P_c$, R is the universal gas constant, and α is a parameter that depends on the accentric factor defined by $\alpha = [1 + (0.37464 + 1.54226\omega - 0.26992\omega^2)(1 - T_r^{0.5})]^2$. Stryjek and Vera (1986) improved even further the Peng–Robinson equation of state through a fluid-dependent empirical parameter (k_1) that allows for fitting the equation prediction to the experimental data; in this respect, the parameter (k_1) must be determined by trial and error so that the equation predicts, as accurately as possible, the vapor equilibrium data. This equation of state is defined by

$$\left.\begin{aligned} P &= \frac{RT}{v-b} - \frac{\left(0.457335 R^2 T_c^2/P_c\right)\left[1 + k\left(1 - \sqrt{T/T_c}\right)\right]^2}{v^2 + 2bv - b^2} \\ b &= 0.077796 RT_c/P_c \\ k &= k_0 + k_1\left(1 + \sqrt{T/T_c}\right)(0.7 - T/T_c) \\ k_0 &= 0.378893 + 1.4897153\omega - 0.17131848\omega^2 + 0.0196554\omega^3 \end{aligned}\right\}. \tag{1.60}$$

1.7 The Carnot Cycle and Carnot Efficiency

The Carnot cycle is a fundamental model for understanding heat-to-work energy conversion systems. As known from thermodynamics, the Carnot cycle is a model cycle for a heat engine where the addition of energy in the form of heat to the engine

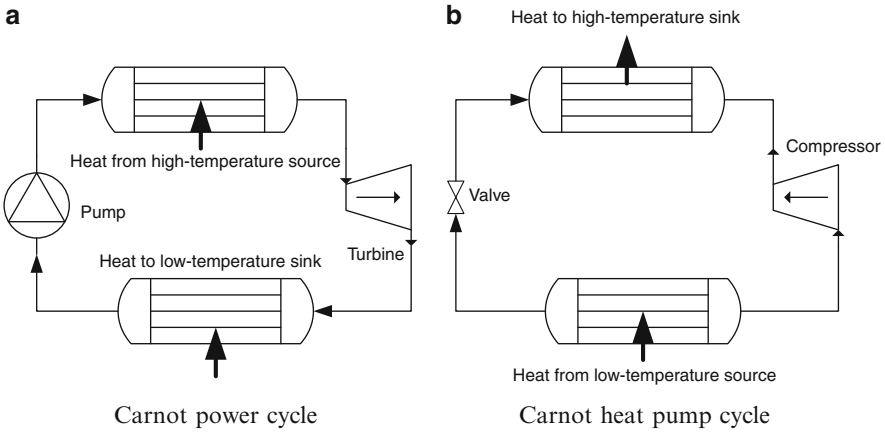

Fig. 1.6 Carnot cycle

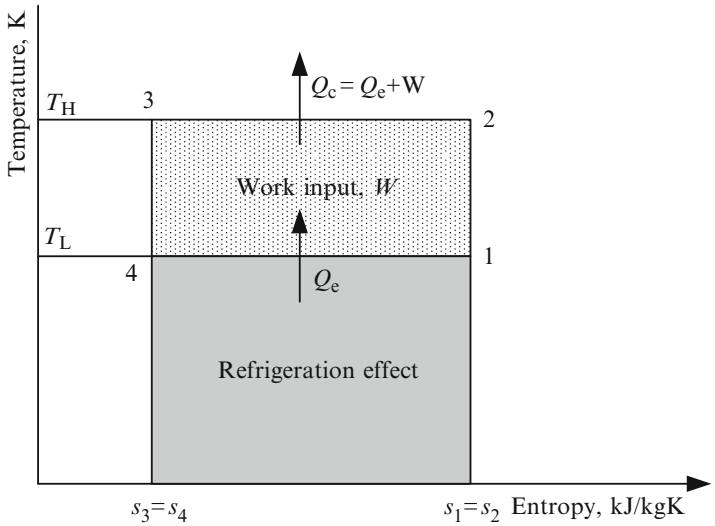

Fig. 1.7 *T-s* diagram of the Carnot heat pump cycle

produces work (Fig. 1.6a). In some applications, the Carnot heat pump cycle is known as the reverse Carnot cycle (Fig. 1.6b). The maximum theoretical performance can be calculated, establishing the criteria against which real cycles can be compared. The following processes take place in the Carnot cycle. In the case of heat pump operation, these processes are shown on a temperature-entropy diagram in Fig. 1.7:

- Line (1–2) is the ideal compression at constant entropy, and work input is required. The temperature of the refrigerant increases.

- Line (2–3) is the rejection of heat in the condenser at a constant condensation temperature, T_H.
- Line (3–4) is the ideal expansion at constant entropy. The temperature of the refrigerant decreases.
- Line (4–1) is the absorption of heat in the evaporator at a constant evaporation temperature, T_L.

For heat engine operation the process is reversed.

The specific entropy appears in the abscissa of Fig. 1.7. This is the ratio of the heat added to a substance to the absolute temperature at which it was added, and is also a measure of the molecular disorder of a substance at a given state. The specific enthalpy of a mixture of liquid and vapor components can be written as

$$s = (1 - x)s_{liq} + xs_{vap} \tag{1.61}$$

and

$$s = s_{liq} + xs_{liq,vap}, \tag{1.62}$$

where $s_{liq,vap} = s_{vap} - s_{liq}$.

From Fig. 1.7, the *coefficient of performance* (COP) can be derived as the ratio of the refrigeration effect (Q_L) to the work (W_I) required to produce the effect:

$$\text{COP} = \frac{Q_L}{W_I}. \tag{1.63}$$

The refrigeration effect is represented as the area under the process line 4–1, as follows:

$$Q_L = T_L(s_1 - s_4). \tag{1.64}$$

The theoretical work input (e.g., compressor power) for the cycle is represented as the area within the cycle line 1–2–3–4–1, as follows:

$$W_I = (T_H - T_L)(s_4 - s_1). \tag{1.65}$$

After inserting Eqs. (1.64) and (1.65) into Eq. (1.63), we find the following equation, which is dependent on the source and sink temperatures:

$$\text{COP} = \frac{T_L}{(T_H - T_L)}. \tag{1.66}$$

The theoretical COP can also be expressed in terms of the enthalpy as

$$\text{COP} = \frac{(h_1 - h_4)}{(h_2 - h_1)}. \tag{1.67}$$

For a better COP, some conclusions from the Carnot cycle are extracted, based on Eq. (1.66), as follows:

- Minimum work input is desirable.
- T_H should be as low as possible for refrigeration applications.
- T_L should be as high as possible for refrigeration applications.

Practical heat pump systems are not as efficient as the ideal models, because of the lower COP. As a result of Eq. (1.66) a smaller temperature difference between the heat sink and the heat source ($T_H - T_L$) provides greater refrigeration system efficiency.

For heat engine operation of the Carnot cycle, one defines the energy efficiency as the ratio between work output and heat input:

$$\eta = \frac{W}{Q_H} = \frac{Q_H - Q_L}{Q_H} = 1 - \frac{T_L \Delta S}{T_H \Delta S} = 1 - \frac{T_L}{T_H}, \tag{1.68}$$

which represents a fundamental result in thermodynamics indicating the factor of conversion of heat energy into mechanical work.

1.8 The Second Law of Thermodynamics

As mentioned earlier, the first law of thermodynamics (FLT) is the energy-conservation principle. The Second Law of thermodynamics (SLT) refers to the inefficiencies of practical thermodynamic systems and indicates that it is impossible to have 100% efficiency in energy conversion.

A very easy way to show the implication of both the FLT and the SLT is a desktop game that consists of several pendulums (made of metal balls) in contact with each other. When you raise the first of the balls, you give energy to the system, potential energy. Upon release, this ball gains kinetic energy at the expense of potential energy. When this ball hits the second ball, small elastic deformations transform the kinetic energy again into another form of potential energy. The energy is transferred from one ball to the other. The last one gains kinetic energy to go up again. The cycle continues but every time the energy is lower, until the balls finally stop. The FLT explains why the balls keep moving, but the SLT explains why they do not do it forever. In this game the energy is lost in sound and heat and is no longer useful in keeping the balls in motion.

The SLT also states that the entropy in the universe is always increasing. As mentioned before, entropy is the degree of disorder, and every process happening in the universe is a transformation from a lower entropy to a higher entropy. Therefore, the entropy of a state of a system is proportional to (depends on) its probability, which gives us the opportunity to define the SLT in a broader manner as "the entropy of a system increases in any heat transfer or conversion of energy within a closed system." That is why all energy transfers or conversions are irreversible.

From the entropy perspective, the basis of the SLT is the statement that the sum of the entropy changes of a system and that of its surroundings must be always positive. Recently, much effort has been spent in minimizing the entropy generation (irreversibility) in thermodynamic systems and applications.

Moran and Shapiro (1998) noted that the SLT and deductions from it are useful because they provide the means for the following:

- Predicting the direction of processes
- Establishing conditions for equilibrium
- Determining the best performance of thermodynamic systems and applications
- Evaluating quantitatively the factors that preclude the attainment of the best theoretical performance level
- Defining a temperature scale, independent of the properties of any thermometric substance
- Developing tools for evaluating some thermodynamic properties, such as internal energy and enthalpy, using the experimental data available

Consequently, the SLT is the linkage between entropy and the usefulness of energy. The SLT analysis has found applications in a large variety of disciplines, including chemistry, economics, ecology, environment, and sociology, that are far removed from engineering thermodynamics applications.

The concepts of *reversibility* and *irreversibility* are highly important to thermodynamic processes and systems. Reversibility means that both the system and its surroundings can be returned to their initial states, which is a situation never occurring in practice. Irreversibility shows the destruction of availability, and means that both the system and its surroundings cannot be returned to their initial states due to friction, heat rejection, electrical and mechanical effects, and so on. For instance, as an actual system provides an amount of work that is less than the ideal reversible work, so the difference between these two values gives the irreversibility of that system. In real applications, there are always such differences, and therefore real cycles are always irreversible. For example, the entropy of the heat given off in the condenser is always greater than that of the heat taken up in the evaporator, referring to the fact that the entropy is always increased by the operation of an actual refrigeration system.

Within the past 50 years the scientific view of nature has changed drastically. Classical science emphasized equilibrium and stability. Now we observe fluctuations, instability, and evolutionary processes on all levels from chemistry and biology to cosmology. Everywhere we observe irreversible processes in which time symmetry is broken. The distinction between reversible and irreversible processes was first introduced in thermodynamics through the concept of entropy.

The formulation of entropy is in the modern context fundamental for understanding thermodynamic aspects of self-organization and the evolution of order and life that we observe in nature. When a system is isolated, the entropy of the system continually increases due to irreversible processes and reaches the maximum possible value when the systems attains a state of thermodynamic equilibrium.

In the state of equilibrium, all irreversible processes cease. When a system begins to exchange entropy with its surroundings, then, in general, it is driven away from the equilibrium state it reached when isolated, and entropy-producing irreversible processes begin. An exchange of entropy is associated with the exchange of heat and matter. When no accumulation of entropy within a system occurs, the entropy flowing out of the system is always larger than the entropy flowing in, the difference arising due to the entropy produced by irreversible processes within the system. As we shall see in the following chapters, systems that exchange entropy with their surroundings do not simply increase the entropy of the surroundings but may undergo dramatic spontaneous transformations to self-organization. Irreversible processes that produce entropy create these organized states. Such self-organized states range from convection patterns in fluids to organized life structures. Irreversible processes are the driving force that creates this order.

Much of the internal energy of a substance is randomly distributed as kinetic energy at the molecular and submolecular levels and as energy associated with attractive or repulsive forces between molecular and submolecular entities, which can move closer together or further apart. This energy is sometimes described as being "disordered" as it is not accessible as work at the macroscopic level in the same way as is the kinetic energy or gravitational potential energy that an overall system possesses due to its velocity or position in a gravitational field. Although some energy forms represent the capacity to do work, it is not possible directly to access the minute quantities of disordered energy possessed at a given instant by the entities within a substance so as to yield mechanical shaft work on a macroscopic scale. The term *disorder* refers to the lack of information about exactly how much and what type of energy is associated at any moment with each molecular or submolecular entity within a system.

At the molecular and submolecular level there also exists "ordered energy" associated with the attractive and repulsive forces between entities that have fixed mean relative positions. Part of this energy is, in principle, accessible as work at the macroscopic level under special conditions, which are beyond the scope of this book.

Temperature is the property that reflects whether a system that is in equilibrium will experience a decrease or increase in its disordered energy if it is brought into contact with another system that is in equilibrium. If the systems have different temperatures, disordered energy will be redistributed from the system at the higher temperature to the one at the lower temperature. The process reduces the information about precisely where that energy resides, as it is now dispersed over the two systems.

Heat transfer to a system increases its disordered energy, while heat transfer from a system reduces its disordered energy. Reversible heat transfer is characterized by both the amount of energy transferred to or from the system and the temperature at which this occurs. The property entropy, whose change between states is defined as the integral of the ratio of the reversible heat transfer to the absolute temperature, is a measure of the state of disorder of the system. This state of disorder is characterized by the amount of disordered energy and its temperature.

Reversible heat transfer from one system to another requires that both systems have the same temperature and that the increase in the disorder of one be exactly matched by a decrease in disorder of the other. When reversible adiabatic work is done on or by a system, its ordered energy increases or decreases by exactly the amount of the work, and the temperature changes correspondingly, depending on the substances involved. Reversible work is characterized by the amount of energy transferred to or from the system, irrespective of the temperature of the system. Irreversible work, such as stirring work or friction work between subsystems, involves a change in the disorder of the system, such as heat transfer to a system, and has the effect of increasing the entropy.

Thermodynamic property entropy is a measure of the amount of molecular disorder within a system. A system possessing a high degree of molecular disorder (such as a high temperature gas) has a high entropy and vice versa. Values for specific entropy are commonly listed in thermodynamic tables along with other property data (e.g., specific volume, specific internal energy, specific enthalpy). The fundamental property related to the second law of thermodynamics, entropy, has the following characteristics:

- The entropy of a system is a measure of its internal molecular disorder.
- A system can only generate, not destroy, entropy.
- The entropy of a system can be increased or decreased by energy transports across the system boundary.

Heat and work are mechanisms of energy transfer. They can cause changes in the internal energy in a body as energy is transferred to or from it. Work is accomplished by a force acting through a distance. Heat requires a difference in temperature for its transfer. The definition of heat can be broadened to include the energy stored in a hot gas as the average kinetic energy of randomly moving molecules. This description helps explain the natural flow of heat from a hot to a cooler substance. The concept of random motion can be translated into the notion of order and disorder, and leads to a relation between order and disorder and probability. Energy transfers associated with a system can cause changes in its state. The natural direction of the change in state of a system is from a state of low probability to one of higher probability. Since disordered states are more probable than ordered ones, the natural direction of change of state of a system is from order to disorder. Entropy is a measure of order that helps explain the natural direction for energy transfers and conversions. The entropy of a system at a specific state depends on its probability. Thus the second law of thermodynamics can be expressed more broadly in terms of entropy as in any transfer or conversion of energy within a closed system; the entropy of the system increases.

The consequences of the second law can thus be stated as (1) the spontaneous or natural direction of energy transfer or conversion is toward increasing entropy or (2) all energy transfers or conversions are irreversible. More loosely, the FLT implies “You can’t win” because energy is conserved so you cannot get more energy out of a system than you put in, while the SLT implies “You can’t break

even" because irreversibilities during real processes do not allow you to recover the original quality of energy you put into a system.

Low-entropy energy sources are normally desired and are used to drive energy processes, since low-entropy energy is useful. Energy sources can be rated on an entropy or usefulness scale, with zero-entropy energy forms like work and kinetic and gravitational potential energy being the most useful, and high-entropy forms like heat being less useful.

This broader interpretation of the SLT suggests that real energy conservation should consider the conservation of both energy quantity and quality. For high thermodynamic efficiency, energy transfers or conversions should be arranged, all else being equal, so that the change in entropy is a minimum. This requires that energy sources be matched in entropy to energy end use.

The entropy of a system at some state is a measure of the probability of its occurrence, with states of low probability having low entropy and states of high probability having high entropy. From the previous section, it is seen that the entropy of a system must increase in any transfer or conversion of energy, because the spontaneous direction of the change of state of a closed system is from a less to a more probable state. Consequently, a simple statement of the second law is, "In any energy transfer or conversion within a closed system, the entropy of the system increases."

In open systems, energy conversions can occur that cause the entropy of part or all of a system to decrease. Charging a storage battery, freezing ice cubes, and the growth of living entities are examples. In each of these examples, the order of the system increases and the entropy decreases. If the combination of the system and its surroundings is considered, the overall net effect is always to increase disorder. To charge a battery we must provide a certain minimum amount of external energy of a certain quality to re-form the chemical combinations in the battery plates. In the case of the battery, the input energy can be in the form of electricity. Some of this low-entropy electrical energy is lost as it is converted into high-entropy heat in the current-carrying wires. In making ice cubes, we increase order by decreasing the entropy of the water in the ice cube trays through removal of heat. The removed heat is transferred into a substance that is at a lower temperature, increasing its entropy and disorder. The net change in entropy is positive. For ice cubes in a freezer, we also supply to the motor low-entropy electrical energy, which ultimately is degraded to heat. In life processes, highly ordered structures are built from simpler structures of various chemicals, but to accomplish this living entities take in relatively low-entropy energy—sunlight and chemical energy—and release high-entropy heat and other wastes. The entropy of the overall system again increases.

Figure 1.8 illustrates a heat transfer process from the entropy point of view. During the heat transfer process, the net entropy increases, with the increase in entropy of the cold body more than offsetting the decrease in entropy of the hot body. This must occur to avoid violating the SLT. More generally, processes can occur only in the direction of increased overall entropy or disorder. This implies that the entire universe is becoming more chaotic every day.

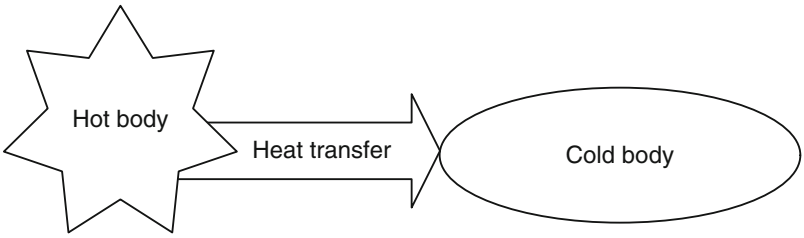

Fig. 1.8 Illustration of entropy increase and decrease for cold and hot bodies during heat transfer

Another way of explaining this consequence of the SLT is to state that all energy transfers or conversions are irreversible. Absent external energy inputs, such processes occur spontaneously in the direction of increasing entropy. In a power plant, for example, although some of the losses can be reduced, they cannot be entirely eliminated. Entropy must increase. The usual mechanisms for low-entropy energy to be converted to high-entropy heat are irreversibilities like friction or electrical resistance or leakage of high-temperature, low-entropy heat to a lower temperature region and its subsequent degradation.

Another statement of the SLT was developed more than 100 years ago. One of the most brilliant contributions was made by a young French physicist, Sadi Carnot, in the nineteenth century. Carnot, studying early steam engines, was able to deduce from the pumping pistons and spinning wheels that the conversion of heat to mechanical work requires a difference of temperature. The purpose of a heat engine, as he described it, is to take heat from a high-temperature source, convert some of it to mechanical work, and then reject the rest of the heat to a lower-temperature heat reservoir. Carnot described heat engines using a simple analogy to waterwheels. The energy available for conversion in a waterwheel is the gravitational energy contained in water as it flows from some height (behind a dam or from a mountain lake) down through the wheel. The amount of energy available depends on the difference in height—the "head" as it is called—between the source and the pool below the wheel. The energy available to a heat engine depends on the "temperature head." Just as a high dam can provide more energy than a low one, a large temperature difference can provide more energy to be converted by a heat engine than can a small temperature difference. In the example of a heat engine, the high-temperature reservoir is the hot steam produced in the power plant furnace.

For a steam turbine and condenser assembly, the low-temperature reservoir to which the device rejects the unconverted energy is the condenser cooling water. The important temperature difference is thus the difference in temperature between the incoming steam, usually about 700°C, and the water in the condenser, which is typically between environmental conditions (around 0–25°C) and the boiling temperature of water (100°C). The "temperature head" in this example would therefore be 600–700°C. Carnot's explanation of heat engines led to the second law. Once energy is in the form of heat, it cannot be converted entirely to mechanical energy. Some heat will always be exhausted.

Although a spontaneous process can proceed only in a definite direction, the FLT gives no information about direction; it merely states that when one form of energy is converted to another, the quantities of energy involved are conserved regardless of the feasibility of the process. Thus, processes can be envisioned that do not violate the FLT but do violate the SLT, for example, transfer of a certain quantity of heat from a low-temperature body to a high-temperature body, without the input of an adequate external energy form like work. However, such a process is impossible, emphasizing that the FLT is itself inadequate for explaining energy processes.

The SLT establishes the difference in the quality of different forms of energy and explains why some processes can spontaneously occur while others cannot. The SLT is usually expressed as an inequality, stating that the total entropy after a process is equal to or greater than that before. The equality only holds for ideal or reversible processes. The SLT has been confirmed experimentally.

The SLT defines the fundamental quantity entropy as a randomized energy state unavailable for direct conversion to work. It also states that all spontaneous processes, both physical and chemical, proceed to maximize entropy, that is, to become more randomized and to convert energy to a less available form. A direct consequence of fundamental importance is the implication that at thermodynamic equilibrium the entropy of a system is at a relative maximum; that is, no further increase in disorder is possible without changing the thermodynamic state of the system by some external means (such as adding heat). A corollary of the SLT is that the sum of the entropy changes of a system and that of its surroundings must always be positive. In other words, the universe (the sum of all systems and surroundings) is constrained to become forever more disordered and to proceed toward thermodynamic equilibrium with some absolute maximum value of entropy. From a biological standpoint, this is intuitively reasonable since, unless gradients in concentration and temperature are forcibly maintained by the consumption of energy, organisms proceed spontaneously toward the biological equivalent of equilibrium death.

The SLT is general. However, when intermolecular forces are long range, as in the case of particles interacting through gravitation, there are difficulties because our classification into extensive variables (proportional to size) and intensive variables (independent of size) does not apply. The total energy is no longer proportional to size. Fortunately, gravitational forces are very weak compared to short-range intermolecular forces. It is only on the astrophysical scale that this problem becomes important. The generality of the SLT provides a powerful means to understand the thermodynamic aspects of real systems through the use of ideal systems. A classic example is Planck's analysis of radiation in thermodynamic equilibrium with matter (blackbody radiation) in which Planck considered idealized simple harmonic oscillators interacting with radiation. Planck considered simple harmonic oscillators not merely because they are good approximations of molecules but because the properties of radiation in thermal equilibrium with matter are universal, regardless of the particular nature of the matter with which the radiation interacts. The conclusions one arrives at using idealized oscillators and the laws of thermodynamics must also be valid for all other forms of matter, however complex.

What makes this statement of the SLT valuable as a guide to formulating energy policy is the relationship between entropy and the usefulness of energy. Energy is most useful to us when it is available to do work or when we can get it to flow from one substance to another, for example, to warm a house. Useful energy thus must have low entropy so that the SLT will allow transfer or conversions to occur spontaneously.

The classic Kelvin-Plank statement and the Clausius statement help us formulate the SLT:

- *The Kelvin-Plank statement*: It is impossible to construct a device, operating in a cycle (e.g., heat engine), that accomplishes only the extraction of heat energy from some source and its complete conversion to work. This simply shows the impossibility of having a heat engine with a thermal efficiency of 100%.
- *The Clausius statement*: It is impossible to construct a device, operating in a cycle (e.g., refrigerator and heat pump), that transfers heat from the low-temperature side (cooler) to the high-temperature side (hotter).

The *Clausius inequality* provides a mathematical statement of the second law, which is a precursor to second law statements involving entropy. German physicist R.J.E. Clausius, one of the founders of thermodynamics, stated

$$\oint (\delta Q/T) \leq 0, \tag{1.69}$$

where the integral symbol shows the integration should be done for the entire system. The cyclic integral of $\delta Q/T$ is always less than or equal to zero. The system undergoes only reversible processes (or cycles) if the cyclic integral equals zero and irreversible processes (or cycles) if it is less than zero.

Equation (1.69) can be expressed without the inequality as

$$S_{\text{gen}} = -\oint (\delta Q/T), \tag{1.70}$$

where

$$S_{\text{gen}} = \Delta S_{\text{total}} = \Delta S_{\text{sys}} + \Delta S_{\text{surr}}.$$

The quantity S_{gen} is the entropy generation associated with a process or cycle, due to irreversibilities. The following are cases for values of S_{gen}:

- $S_{\text{gen}} = 0$ for a reversible process
- $S_{\text{gen}} > 0$ for an irreversible process
- $S_{\text{gen}} < 0$ for no process (i.e., negative values for S_{gen} are not possible)

Consequently, one can write for a reversible process

$$\Delta S_{\text{sys}} = (Q/T)_{\text{rev}} \quad \text{and} \quad \Delta S_{\text{surr}} = -(Q/T)_{\text{rev}}. \tag{1.71}$$

For an irreversible process

$$\Delta S_{\text{sys}} > (Q/T)_{\text{surr}} \tag{1.72}$$

due to entropy generation within the system as a result of internal irreversibilities. Hence, although the change in entropy of the system and its surroundings may individually increase, decrease, or remain constant, the total entropy change or the total entropy generation cannot be less than zero for any process.

It is helpful to list some common relations for a process involving a pure substance and assuming the absence of electricity, magnetism, solid distortion effects, and surface tension. The following four equations apply, subject to the noted restrictions:

- $\delta q = \mathrm{d}u + \delta w$ (a FLT statement applicable to any simple compressible closed system)
- $\delta q = \mathrm{d}u + p\mathrm{d}v$ (a FLT statement restricted to reversible processes for a closed system)
- $T\mathrm{d}s = \mathrm{d}u + \delta w$ (a combined statement of the FLT and SLT, with $T\ \mathrm{d}s = \delta q$)
- $T\mathrm{d}s = \mathrm{d}u + p\mathrm{d}v$ (a combined statement of the FLT and SLT valid for all processes between equilibrium states)

1.9 Exergy

From the thermodynamics point of view, exergy is defined as the maximum amount of work that can be produced by a stream of matter, heat, or work as it comes to equilibrium with a reference environment. In fact, it is a measure of the potential of a stream to cause change, as a consequence of not being completely stable relative to the reference environment. For exergy analysis, the state of the reference environment, or the reference state, must be specified completely. This is commonly done by specifying the temperature, pressure, and chemical composition of the reference environment. Exergy is not subject to a conservation law. Rather exergy is consumed or destroyed, due to irreversibilities in any process. Table 1.3 shows a clear comparison between energy and exergy.

Table 1.3 Comparison between energy and exergy

Energy	Exergy
It is dependent on the parameters of matter or energy flow only and independent of the environment parameters.	It is dependent both on the parameters of matter or energy flow and on the environment parameters.
It has values different from zero (which equal mc^2 in accordance with Einstein's equation).	It is equal to zero (in dead state by equilibrium with the environment).
It is guided by the FLT for all the processes.	It is guided by the FLT for reversible processes only (in irreversible processes it is destroyed partly or completely).
It is limited by the SLT for all processes (including reversible ones).	It is not limited for reversible processes owing to the SLT.
It is a measure of quantity.	It is a measure of both quantity and quality.

As pointed out by Dincer and Rosen (1999) and Dincer (2002), exergy is a measure of usefulness, quality, or potential of a stream to cause change and an effective measure of the potential of a substance to impact the environment.

Exergy analysis is a method that uses the conservation of mass and conservation of energy principles together with the SLT for the design and analysis of refrigeration systems and applications. The exergy method can be suitable for furthering the goal of more efficient energy-resource use, for it enables the locations, types, and true magnitudes of wastes and losses to be determined. Therefore, exergy analysis can reveal whether or not and by how much it is possible to design more efficient energy systems by reducing the sources of inefficiency in existing systems. In the past, exergy was called essergy, availability, and free energy. Table 1.4 gives the historical connections among essergy, availability, exergy, and free energy.

From the energy and exergy efficiency point of view, it is important to note that if a fossil fuel–based energy source were used for low-temperature thermal applications like space heating or cooling, there would be a great difference between energy and exergy efficiencies, for example, 50–70% as energy efficiency and 5% as exergy efficiency (Dincer 1998). One may ask why. Here we give the following facts:

- High-quality (or high-temperature) energy sources such as fossil fuels are being used for relatively low-temperature processes like water and space heating or cooling, etc.
- Exergy efficiency permits a better matching of energy sources and uses, leading to the fact that high-quality energy is not used for performing low-quality work.

Table 1.4 Connections among essergy, availability, exergy, and free energy

Name	Function	Remarks
Essergy	$E + P_0V - T_0S - \Sigma_i \mu_{i0} N_i$	Formulated for the special case in 1878 by Gibbs and in general in 1962, and later changed from available energy to exergy in 1963, and from exergy to essergy (i.e., essence of energy) in 1968 by Evans
Availability	$E + P_0V - T_0S - (E_0 + P_0V_0 - T_0S_0)$	Formulated by Keenan in 1941 as a special case of the essergy function
Exergy	$E + P_0V - T_0S - (E_0 + P_0V_0 - T_0S_0)$	Introduced by Darrieus in 1930 and Keenan in 1932, called the availability in steady flow by him, and exergy by Rant in 1956 as a special case of essergy
Free energy	Helmholtz: $E - TS$ Gibbs: $E + PV - TS$	Introduced by von Helmholtz and Gibbs in 1873 as the Legendre transforms of energy to yield useful alternate criteria of equilibrium, as measures of the potential work of systems representing special cases of the essergy function

Data from Szargut et al. (1988)

Some important characteristics of exergy are described and illustrated as follows:

- A system in complete equilibrium with its environment does not have any exergy. No difference appears in temperature, pressure, concentration, and so on, so there is no driving force for any process.
- The exergy of a system increases the more it deviates from the environment. For instance, a specified quantity of hot water has a higher exergy content during the winter than on a hot summer day. A block of ice carries little exergy in winter while it can have significant exergy in summer.
- When energy loses its quality, exergy is destroyed. Exergy is the part of energy that is useful and therefore has economic value and is worth managing carefully.
- Exergy by definition depends not just on the state of a system or flow but also on the state of the environment.
- Exergy efficiencies are a measure of approach to ideality (or reversibility). This is not necessarily true for energy efficiencies, which are often misleading.

Exergy can generally be considered a valuable resource. There are both energy or nonenergy resources and exergy is observed to be a measure of value for both:

- Energy forms with high exergy contents are typically more valued and useful than energy forms with low exergy. Fossil fuels, for instance, have high energy and energy contents. Waste heat at a near-environmental condition, on the other hand, has little exergy, even though it may contain much energy, and thus is of limited value. Solar energy, which is thermal radiation emitted at the temperature of the sun (approximately 5,800 K), contains much energy and exergy.
- A concentrated mineral deposit "contrasts" with the environment and thus has exergy. This contrast and exergy increase with the concentration of the mineral. When the mineral is mined the exergy content of the mineral is retained, and if it is enriched or purified the exergy content increases. A poor-quality mineral deposit contains less exergy and can accordingly be utilized only through a larger input of external exergy. Today this substitution of exergy often comes from exergy forms such as coal and oil. When a concentrated mineral is dispersed the exergy content is decreased.

An engineer designing a system makes trade-offs among competing factors. The engineer is expected to aim for the highest reasonable technical efficiency at the lowest reasonable cost under the prevailing technical, economic, and legal conditions, and also accounting for ethical, ecological, and social consequences and objectives. Exergy analysis is a tool that can facilitate this work. Exergy methods provide unique insights into the types, locations, and causes of losses and can thereby help identify possible improvements. For instance, Exergetic Life Cycle Assessment (ExLCA) is suggested as a method to better meet environmental objectives as studied in detail in Chapter 18.

Before discussing in detail linkages between energy and exergy, and the relations between exergy and both the environment and sustainable development, some

key points that highlight the importance of exergy and its utilization are provided. Specifically, exergy analysis is an effective method and tool for:

- Combining and applying the conservation of mass and conservation of energy principles together with the second law of thermodynamics for the design and analysis of energy systems.
- Improving the efficiency of energy and other resource use (by identifying efficiencies that always measure the approach to ideality as well as the locations, types, and true magnitudes of wastes and losses).
- Revealing whether or not and by how much it is possible to design more efficient systems by reducing the inefficiencies in existing systems.
- Addressing the impact on the environment of energy and other resource utilization, and reducing or mitigating that impact.
- Identifying whether a system contributes to achieving sustainable development or is unsustainable.
- Since the value of the exergy of a system or flow depends on the state of both the system or flow and a reference environment, the reference environment must be specified prior to the performance of an exergy analysis.
- The environment is often modeled as a reference environment similar to the actual environment in which a system or flow exists. This ability to tailor the reference environment to match the actual local environment is often an advantage of exergy analysis.
- Some, however, consider the need to select a reference environment a difficulty of exergy analysis. To circumvent this perceived difficulty, some suggest that a "standard environment" be defined with a specified chemical composition, temperature, and pressure. A possible chemical standard environment for global use could, for instance, be based on a standard atmosphere, a standard sea, and a layer of the earth's crust. The definition of such a reference environment is usually problematic, however, as these systems are not in equilibrium with each other.
- In accounting for local conditions, a reference environment can vary spatially and temporally. The need to account for spatial dependence is clear if one considers an air conditioning and heating system operating in the different climates across the earth. In addition, an aircraft or rocket experiences different environmental conditions as it ascends through the atmosphere. The importance of accounting for temporal dependence is highlighted by considering a technology like a seasonal thermal energy storage unit, in which heating or cooling capacity can be stored from one season where it is available in the environment to another season when it is unavailable but in demand.

Energy analysis is the traditional method of assessing the way energy is used in an operation involving the physical or chemical processing of materials and the transfer and/or conversion of energy. This usually entails performing energy balances, which are based on the FLT, and evaluating energy efficiencies. This balance is employed to determine and reduce waste exergy emissions like heat losses and sometimes to enhance waste and heat recovery.

However, an energy balance provides no information on the degradation of energy or resources during a process and does not quantify the usefulness or quality of the various energy and material streams flowing through a system and exiting as products and wastes.

The exergy method of analysis overcomes the limitations of the FLT. The concept of exergy is based on both the FLT and the SLT. Exergy analysis clearly indicates the locations of energy degradation in a process and can therefore lead to improved operation or technology. Exergy analysis can also quantify the quality of heat in a waste stream. A main aim of exergy analysis is to identify meaningful (exergy) efficiencies and the causes and true magnitudes of exergy losses.

It is important to distinguish between exergy and energy in order to avoid confusion with traditional energy-based methods of thermal system analysis and design. Energy flows into and out of a system with mass flows, heat transfers, and work interactions (e.g., work associated with shafts and piston rods). Energy is conserved, in line with the FLT. Exergy, although similar in some respects, is different. It loosely represents a quantitative measure of the usefulness or quality of an energy or material substance. More rigorously, exergy is a measure of the ability to do work (or the work potential) of the great variety of streams (mass, heat, work) that flow through a system. A key attribute of exergy is that it makes it possible to compare on a common basis interactions (inputs, outputs) that are quite different in a physical sense. Another benefit is that by accounting for all the exergy streams of the system it is possible to determine the extent to which the system destroys exergy. The destroyed exergy is proportional to the generated entropy. Exergy is always destroyed in real processes, partially or totally, in line with the SLT. The destroyed exergy, or the generated entropy, is responsible for the less-than-ideal efficiencies of systems or processes.

The *exergy efficiency* is based on the SLT. In this section, we describe the use of exergy efficiencies in assessing the utilization efficiency of energy and other resources.

Engineers make frequent use of efficiencies to gauge the performance of devices and processes. Many of these expressions are based on energy and are thus FLT-based. Also useful are measures of performance that take into account limitations imposed by the second law. Efficiencies of this type are SLT-based efficiencies.

To illustrate the idea of a performance parameter based on the SLT and to contrast it with an analogous energy-based efficiency, consider a control volume at steady state for which energy and exergy balances can be written, respectively, as

$$\text{Energy in} = \text{Energy output in product} + \text{Energy emitted with waste}. \tag{1.73}$$

$$\begin{aligned}\text{Exergy in} = {} & \text{Exergy output in product} + \text{Exergy emitted with waste} \\ & + \text{Exergy destruction}.\end{aligned} \tag{1.74}$$

In these equations, the term *product* might refer to shaft work, electricity, heat transfer, one or more particular exit streams, or some combination of these.

The latter two terms in the exergy balance Eq. (1.74) combine to constitute the exergy losses. Losses include such emissions to the surroundings as waste heat and stack gases. The exergy destruction term in the exergy balance is caused by internal irreversibilities.

From energy or exergy viewpoints, a gauge of how effectively the input is converted to the product is the ratio of product to input. That is, the energy efficiency η can be written as

$$\begin{aligned}\eta &= \text{Energy output in product/Energy input} \\ &= 1 - [\text{Energy loss/Energy input}]\end{aligned} \tag{1.75}$$

and the exergy efficiency ψ as

$$\begin{aligned}\psi &= \text{Exergy output in product/Exergy input} = 1 \\ &\quad - [\text{Exergy loss/Exergy input}] = 1 \\ &\quad - [(\text{Exergy waste emission} + \text{Exergy destruction})/\text{Exergy input}].\end{aligned} \tag{1.76}$$

The exergy efficiency ψ frequently gives a finer understanding of performance than the energy efficiency η. In evaluating η, the same weight is assigned to energy whether it is shaft work or a stream of low-temperature fluid. Also, the energy efficiency centers attention on reducing energy emissions to improve efficiency. The parameter ψ weights energy flows by accounting for each in terms of exergy. It stresses that both waste emissions (or external irreversibilities) and internal irreversibilities need to be dealt with to improve performance. In many cases, it is the irreversibilities that are more significant and more difficult to address.

Efficiency expressions each define a class of efficiencies because a judgment has to be made about what is the product, what is counted as a loss, and what is the input. Different decisions about these lead to different efficiency expressions within the class.

Other SLT-based efficiency expressions also appear in the literature. One of these is evaluated as the ratio of the sum of the exergy exiting to the sum of the exergy entering. Another class of second-law efficiencies is composed of task efficiencies.

1.10 Example: Solar Exergy and the Earth

Most energy in the thin top layer of the earth's surface, where life is found, derives from the sun. Sunlight, rich in exergy, is incident on the earth. Much is reflected by the atmosphere, while some is absorbed by atmospheric constituents or reaches the surface of the earth where it is absorbed. Most of the absorbed solar radiation is converted to thermal energy, which is emitted at the temperature of the earth's surface and atmosphere and leaves the earth as thermal radiation (heat) with no

exergy relative to the earth. Thus, while almost all the energy input to the earth with solar energy is reemitted to space as thermal energy, the exergy associated with solar radiation is delivered to the earth.

The net exergy absorbed by the earth is gradually destroyed, but during this destruction it manages to drive the earth's water and wind systems and to support life. Green plants absorb exergy from the sunlight and convert it via photosynthesis into chemical exergy. The chemical exergy then passes through different food chains in ecosystems, from microorganisms to people. There exists no material waste.

Question: A heat source (e.g., derived from concentrated solar radiation, etc.), available at 800 K loses 2,000 kJ of heat to a sink at (a) 500 K and (b) 750 K. Determine which heat transfer process is more irreversible.

Solution: A sketch of the reservoirs is shown in Fig. 1.9. Both cases involve heat transfer through a finite temperature difference and are therefore irreversible. The magnitude of the irreversibility associated with each process can be determined by calculating the total entropy change for each case. The total entropy change for a heat transfer process involving two reservoirs (a source and a sink) is the sum of the entropy changes of each reservoir since the two reservoirs form an adiabatic system.

Or do they? The problem statement gives the impression that the two reservoirs are in direct contact during the heat transfer process. But this cannot be the case since the temperature at a point can have only one value, and thus it cannot be 800 K on one side of the point of contact and 500 K on the other side. In other words, the temperature function cannot have a discontinuity. Therefore, it is reasonable to assume that the two reservoirs are separated by a partition through which the temperature drops from 800 K on one side to 500 K (or 750 K) on the other. Therefore, the entropy change of the partition should also be considered when evaluating the total entropy change for this process. However, considering that entropy is a property and the values of properties depend on the state of a system, we can argue that the entropy change of the partition is zero since the partition appears to have undergone a *steady* process and thus experienced no change in its properties at any point. We base this argument on the fact that the temperature on both sides of the partition and thus throughout remain constant during this process. Therefore, we are justified to assume that $\Delta S_{partition} = 0$ since the entropy (as well as the energy) content of the partition remains constant during the process.

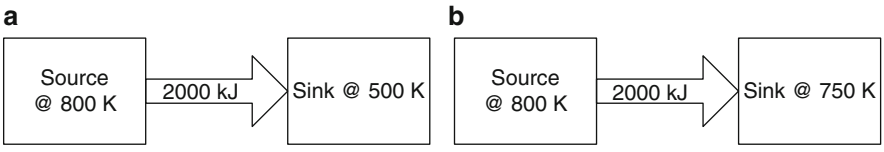

Fig. 1.9 Schematic for the example on entropy generation during heat transfer

Since each reservoir undergoes an internally reversible, isothermal process, the entropy change for each reservoir can be determined from $\Delta S = Q/T$ where T is the constant absolute temperature of the system and Q is the heat transfer for the internally reversible process.

(a) For the heat transfer process to a sink at 500 K:

$$\Delta S_{\text{source}} = Q_{\text{source}}/T_{\text{source}} = -2{,}000 \text{ kJ}/800 \text{ K} = -2.5 \text{ kJ/K},$$

$$\Delta S_{\text{sink}} = Q_{\text{sink}}/T_{\text{sink}} = 2{,}000 \text{ kJ}/500 \text{ K} = 4.0 \text{ kJ/K},$$

and

$$S_{\text{gen}} = \Delta S_{\text{total}} = \Delta S_{\text{source}} + \Delta S_{\text{sink}} = (-2.5 + 4.0) \text{ kJ/K} = 1.5 \text{ kJ/K}.$$

Therefore, 1.5 kJ/K of entropy is generated during this process. Noting that both reservoirs undergo internally reversible processes, the entire entropy generation occurs in the partition.

(b) Repeating the calculations in part (a) for a sink temperature of 750 K, we obtain

$$\Delta S_{\text{source}} = -2.5 \text{ kJ/K},$$

$$\Delta S_{\text{sink}} = 2.7 \text{ kJ/K},$$

and

$$S_{\text{gen}} = \Delta S_{\text{total}} = (-2.5 + 2.7) \text{ kJ/K} = 0.2 \text{ kJ/K}.$$

The total entropy change for the process in part (b) is smaller, and therefore it is less irreversible. This is expected since the process in (b) involves a smaller temperature difference and thus a smaller irreversibility.

Discussion: The irreversibilities associated with both processes can be eliminated by operating a Carnot heat engine between the source and the sink. For this case, it can be shown that $\Delta S_{\text{total}} = 0$.

1.11 Concluding Remarks

In this chapter, a summary of some general introductory aspects of thermodynamics was presented, and their fundamental definitions and physical quantities were given to provide sufficient thermodynamic background for a better understanding of energy and exergy analyses of sustainable energy systems and applications, and their technical details.

Nomenclature

a	Acceleration, m/s^2
A	Area, m^2
c	Specific heat, J/kg K
COP	Coefficient of performance
d	Displacement, m
DOF	Degree of freedom
E	Energy, J
F	Force, N
g	Gravitational acceleration, m/s^2
h	Specific enthalpy, J/kg
H	Enthalpy, J
k_B	Boltzmann constant, J/K
K	Kinetic energy, J
KE	Kinetic energy, J
m	Mass, kg
M	Molecular mass, kg/kmol
n	Number of moles, mol or polytropic exponent
N	Number of molecules
N_A	Number of Avogadro
p	Momentum, kg m/s
P	Pressure, Pa
PE	Potential energy, J
q	Mass specific heat, J/kg
Q	Heat, J
R	Universal gas constant, J/mol K
R_g	Real gas constant, J/kg K
s	Specific entropy, J/kg K
S	Entropy, J/K
T	Temperature, K
v	Velocity, m/s, or specific volume, m^3/kg
V	Volume, m^3
u	Specific internal energy, J/kg
U	Internal energy, J
W	Work, J
x	Vapor quality
Z	Elevation, m or compressibility factor

Greek Letters

α	Peng–Robinson parameter
γ	Adiabatic exponent

η Energy efficiency
ψ Exergy efficieny
ω Accentric factor

Subscripts

gen Generated
H High
liq Liquid
L Low
n Value corresponding to 1 mol
p Constant pressure
r Reduced value
rev Reversible
t Total
v Constant volume
vap Vapor
surr Surroundings
sys System

Superscripts

_ Average value
• Rate (per unit of time)

References

Callen H.B. 1985. Thermodynamics and an Introduction to Thermostatistics, 2nd edition. Wiley, New York.

Carnot S. 1824. Réflexions sur la Puissance Motrice du Feu et Sur les Machines Propres à Développer Cette Puissance. Bachelier, Paris.

Crosbie S. 1998. The Science of Energy—a Cultural History of Energy Physics in Victorian Britain. The University of Chicago Press, Chicago.

Dincer I. 1998. Thermodynamics, exergy and environmental impact. Proceedings of the ISTP-11, the Eleventh International Symposium on Transport Phenomena, November 29–December 3, Hsinchu, Taiwan, pp.121–125.

Dincer I. 2002. The role of exergy in energy policy making. *Energy Policy* 30:137–149.

Dincer I., Rosen M.A. 1999. The intimate connection between exergy and the environment, in Thermodynamic Optimization of Complex Energy Systems, A. Bejan and E. Mamut eds., pp. 221–230, Kluwer Academic Publishers, The Netherlands.

Klein S.A. 2010. Engineering Equation Solver (Academic Commercial v.8.629).

Marquand C., Croft D. 1997. Thermofluids—An Integrated Approach to Thermodynamics and Fluid Mechanics Principles. Wiley, New York.

Moran M.J., Shapiro H.N. 1998. Fundamentals of Engineering Thermodynamics, 3rd edition. Wiley, New York.
Stryjek R., Vera J.H. 1986. PRSV, an improved Peng-Robinson equation of state for pure compounds and mixtures. *Canadian Journal of Chemical Engineering* 64:323.
Szargut J., Morris D.R., Steward F.R. 1988. Exergy Analysis of Thermal, Chemical, and Metallurgical Processes. Hemisphere, New York.

Study Questions/Problems

1.1 Define the notions of force, momentum, and work, and explain the differences among them.
1.2 Define the following forms of energy and explain the differences among them: internal energy, work, heat.
1.3 Define the following terms: *enthalpy, entropy, free energy (Gibbs), exergy.*
1.4 Give examples of macroscopic forms of energy.
1.5 What is a conservative force?
1.6 Explain the terms *absolute, gauge*, and *vacuum pressure*.
1.7 Define the notion of temperature from the prism of kinetic theory of gases. Include relevant formulas in the explanation.
1.8 Define the universal gas constant.
1.9 Define the Boltzmann constant.
1.10 Using appropriate equations, transform the temperature of 100°C in degrees Kelvin, Rankine, and Fahrenheit.
1.11 Explain the state-change diagram of a substance.
1.12 Define the notion of vapor quality.
1.13 Define the following and explain the differences among them: closed system, open system, insulated system.
1.14 Does an exergy analysis replace an energy analysis? Describe any advantages of exergy analysis over energy analysis.
1.15 Can you perform an exergy analysis without an energy analysis? Explain.
1.16 Noting that heat transfer does not occur without a temperature difference and that heat transfer across a finite temperature difference is irreversible, is there such a thing as reversible heat transfer? Explain.
1.15 The specific heat of air is 1,005 J/kgK. Express it in kcal/lb°F. Explain the calculations.
1.16 Using the ideal gas law, derive an expression for density of atmospheric air as a function of altitude.
1.17 Argon is compressed from standard conditions up to a pressure of 5 bar. Assume polytropic compression and calculate the compression work per unit of mass. Do the same calculation for isothermal process. Explain the difference. Argon is assumed to be an ideal gas.
1.18 Water is heated from 50 to 90°C. Determine the amount of heat required to do this for 10 kg of water. Determine the relative increase in water volume.

1.19 Air at 25°C expands from 300 bar to atmospheric pressure. Determine the work generated assuming adiabatic expansion process.
1.20 Using the appropriate lithium bromide–water diagram from Appendix B, determine the temperature and pressure of the vapor when the solution temperature is 100°C and the concentration is 60%.
1.21 Calculate the enthalpy needed for unit of mass to heat lithium bromide–water solution from 30°C and 50% concentration to 100°C and 65% concentration.
1.22 Ammonia–water vapor at 25 bar and 100°C is cooled (and absorbed) in a process such that eventually it achieves 10°C and 1 bar. Calculate the amount of enthalpy extracted per kilogram.
1.23 Based on Tables B.3 and B.4 in Appendix B, calculate the chemical exergy of copper oxychloride, cupric oxide, cupric chloride, and cuprous chloride, and verify the result with the data listed in Table B.4.
1.24 Assume that superheated steam at 25 bar and 400°C expands isentropically to 6.22 bar. Determine the temperature after expansion.
1.25 Saturated ammonia vapor at −25°C is compressed isentropically to 7.62 bar. Determine the temperature after compression.
1.26 Calculate mass, energy, entropy, and exergy balances for the following devices: (a) an adiabatic steam turbine, (b) an air compressor with heat loss from the air to the surroundings, (c) an adiabatic nozzle, and (d) a diffuser with heat loss to the surroundings.
1.27 Define each of the following efficiencies for a compressor and explain under what conditions they should be used: (a) isentropic efficiency, (b) isothermal efficiency, and (c) exergy efficiency.

Chapter 2
Energy and Environment Perspectives

2.1 Introduction

The inevitable increase in population and the economic development that must necessarily occur in many countries have serious implications for the environment, because energy generation processes (e.g., generation of electricity, heating, cooling, or motive force for transportation vehicles and other uses) are polluting and harmful to the ecosystem.

Energy is considered to be a key player in the generation of wealth and also a significant component in economic development. This makes energy resources extremely significant for every country in the world. In bringing energy needs and energy availability into balance, there are two main elements: energy demand and energy supply. In this regard, every country aims to attain such a balance and hence develop policies and strategies. A number of factors are considered to be important in determining world energy consumption and production, including population growth, economic performance, consumer tastes, technological developments, government policies concerning the energy sector, and developments on world energy markets.

As stated above, there is an intimate connection between energy and the environment. A society seeking sustainable development ideally must utilize only energy resources that cause no environmental impact (e.g., that release no emissions to the environment). However, since all energy resources lead to some environmental impact, it is reasonable to suggest that some (not all) of the concerns regarding the limitations imposed on sustainable development by environmental emissions and their negative impacts can be in part overcome through increased energy efficiency. Clearly, a strong relation exists between energy efficiency and environmental impact since, for the same services or products, less resource utilization and pollution is normally associated with increased energy efficiency. Energy conservation, that is, the use of energy resources in a rational manner, represents another factor that together with energy efficiency can lead to the stabilization of the rate of growth of energy demand, which is predicted to increase rapidly in the near future due to population growth and excessive use of various commodities (e.g., cars, computers, air conditioners, household electronic

İ. Dinçer and C. Zamfirescu, *Sustainable Energy Systems and Applications*,
DOI 10.1007/978-0-387-95861-3_2,

equipment, etc.). Any reduction in the energy demand of a society leads to the extension of its available energy resources.

This chapter discusses energy resources and the environmental impact associated with their use, including global warming and acid rain. The notion of sustainable energy engineering is defined. The main kinds of energy resources are listed and characterized in terms of resource amounts, production, and consumption. To be able to project a future sustainable economy, it is important to set the context by correlating various factors, such as the present energy resources, the population growth, and the evolution of energy demand in the next 30 to 50 years. Fossil fuels and nuclear fuel are finite, while other energy resources are renewable. The term *renewable energy* suggests an energy that can be renewed, or in other words cannot be depleted. A forecast of energy resource consumption and depletion up to the year 2050 is given. Some case studies are presented at the end of the chapter, and a number of problems are proposed.

2.2 What Is Sustainable Energy Engineering?

Since historical times, humans burned wood to obtain the high-temperature heat necessary for various purposes such as melting metals, extracting chemicals, converting heat into mechanical power, as well as cooking and heating. During burning, the carbon in wood combines with O_2 to form CO_2, which is then absorbed by plants and converted back to carbon for use as a fuel again.

The Industrial Revolution started in the eighteenth century in the United Kingdom, when, essentially, manual and animal labor had been replaced with machine labor, which needed other sources of high-temperature heat in addition to coal combustion. Oil, natural gas, and coal then started to be used extensively. As a consequence, the CO_2 concentration in air increased, leading to the beginning of global warming. During the past three decades, the public has become more aware of this issue, and researchers and policy makers have focused on this and related issues by considering energy, environment, and sustainable development.

The world population is expected to double by the middle of the twenty-first century, and economic development will almost certainly continue to grow. Global demand for energy services is expected to increase by as much as one order of magnitude by 2050, while primary energy demands are expected to increase by 1.5 to 3 times. Simultaneously, energy-related environmental concerns such as acid precipitation, stratospheric ozone depletion, and global climate change (the greenhouse effect) will increase. These observations and others demonstrate that energy is one of the main factors that must be considered in discussions of sustainable development.

Several definitions of sustainable development have been put forth, including the following common one: “development that meets the needs of the present without compromising the ability of future generations to meet their own needs.” Many factors contribute to achieving sustainable development. One of the most important

is the requirement for a supply of energy resources that is fully sustainable. Increased energy efficiency is also important. The discussion in this chapter is intended to apply to both industrialized and developing countries.

While environmental issues in general have been influencing developments in the energy sector for some time, climate change poses an altogether different kind of challenge. Problems such as acid precipitation could be dealt with in part by administrative measures, such as vehicle exhaust standards or emission limits for power stations, which affect comparatively small numbers of economic factors. Technical fixes with a relatively limited scope, such as fitting flue gas cleaning equipment or catalytic converters, could contain the problem. However, emissions of greenhouse gases are so dispersed that it is not possible to take this local and relatively small approach in dealing with climate change. The nature of the problem demands a more comprehensive energy policy response that affects the actions of energy consumers and producers in all countries.

Sustainable energy engineering is a new branch of engineering with a specialty in designing, developing, and promoting sustainable energy-generation systems. This branch of engineering is interdisciplinary in nature. Advanced engineering thermodynamics (including its modern tools of analysis and design, such as exergy and constructal) stand at the base of sustainable energy engineering. Other disciplines that are important include engineering economics, environmental engineering, chemistry and biochemistry, policy, and the physical sciences. In principle, the aim of sustainable energy engineering is to develop and promote the art of using the energy resources available on earth in a manner that is sustainable, regardless of the nature of the resource. For example, fossil fuels can be combusted by paying an energy penalty. The combustion must be completely clean, with CO_2 capture and sequestration.

2.3 Fundamental Energy Sources on the Earth

Earth as a planet of the solar system draws its energy from three fundamental sources, namely, solar radiation, geothermal heat, and the planet's spinning torque combined with gravitational forces generated by the moon–earth–sun planetary system (which is sometimes called "lunar" energy). The lunar energy as a combination of planet spinning and gravitational forces generates tides that are a derived form of renewable energy, called tidal. Other forms of renewable energy can be derived from the fundamental ones. For example, geothermal energy represents a source of thermal energy originating from the earth's hot core. The geothermal energy can be either used directly as thermal energy for heating, or it can be converted into electricity by a heat engine. Solar energy is the source of many forms of renewable energies and phenomena such as wind, rain, lighting, hydro energy, crop growth and biomass, fossil fuels (which are derived from fossilized plants converted into hydrocarbons or coal), etc. In this section, we analyze the fundamental sources of energy in the following order: solar, geothermal, and tidal (lunar).

2.3.1 Solar Energy

Solar energy originates on the sun, which is a star consisting mainly of hydrogen gas and that concentrates more than 99% of the mass of the whole solar system. The average temperature of the sun is 5,500°C and the average sun–earth distance is 150 Gm. Sunlight consisting of a broad spectrum of electromagnetic radiation hits the terrestrial atmosphere after traveling more than 8 minutes through interplanetary space. The energy associated with the solar radiation drives almost all life systems on earth and the earth's climate and weather.

A general understanding of solar energy is suggested with the help of Fig. 2.1. There one sees the earth as a closed thermodynamic system having two kinds of boundary surfaces (refer to the paper by Reis and Bejan 2006). One of the boundaries is a hot surface with temperature T_H, heated by the sun, and that covers an area A_H extending from the southern to the northern polar circle and having the equator in the middle (depicted with white in Fig. 2.1). The second boundary is a cold surface of area A_L formed by the two polar zones (the South and North Pole) having the temperature T_L and cooled by the radiation heat transfer with the universe. The earth system operates as a heat engine between the temperature limits T_H and T_L. Solar and terrestrial radiations are delivered and rejected at the source and the sink, respectively, of the extraterrestrial solar–earth–universe heat engine depicted in Fig. 2.1.

The heat flux Q_H received by this heat engine at the hot surface is proportional to $A_H({T_S}^4 - {T_H}^4)$, where T_S = ~5,500 K is the temperature of the solar radiation and $T_H \ll T_S$ is the average temperature on the globe, that is, ~300 K. Neglecting T_H with respect to T_S results in $Q_H \sim A_H {T_S}^4$.

Similarly, one can estimate the heat flux Q_L lost by the earth at cold surfaces, which is proportional to $A_L({T_L}^4 - {T_\infty}^4)$, where the universe background temperature is $T_\infty \sim 3$ K (see Reis and Bejan 2006). Since $T_L \gg T_\infty$, it results that $Q_L \sim A_L {T_L}^4$. Therefore, the efficiency of the terrestrial heat engine can be estimated with

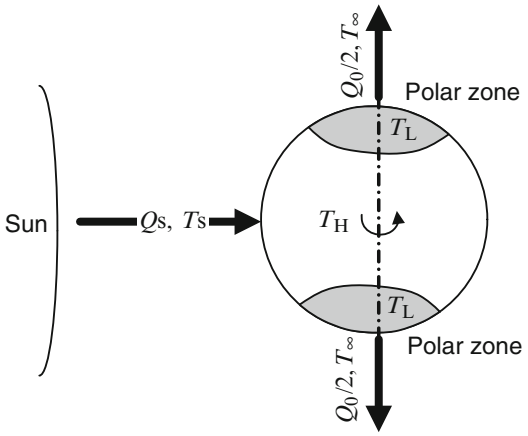

Fig. 2.1 The sun–earth–universe power plant that models solar energy conversion

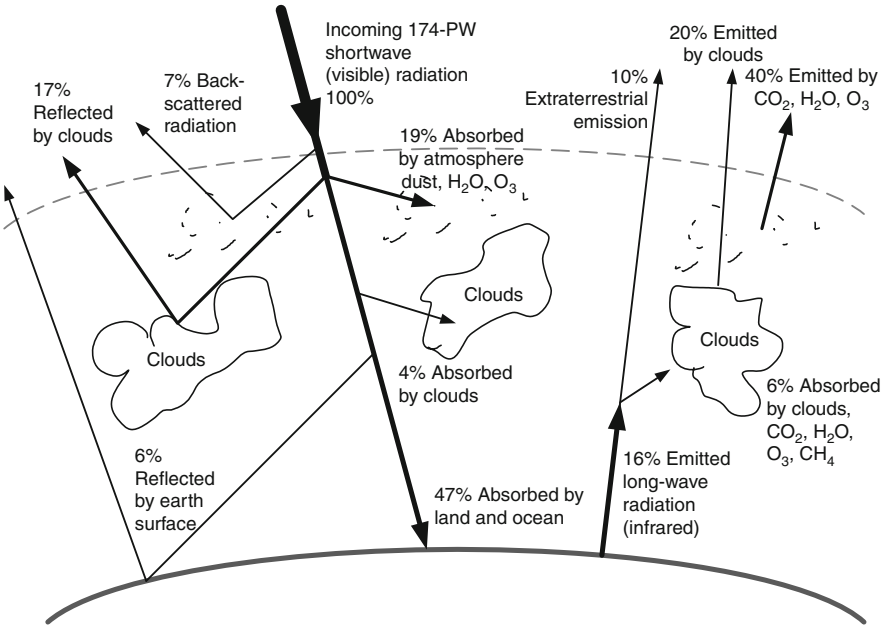

Fig. 2.2 The energy inventory of shortwave and long-wave radiation energy on the earth [data from Tiwari and Ghosal (2007)]

$\eta \sim (Q_H - Q_L)/Q_H = (1 - A_L {T_L}^4)/A_H {T_S}^4$, which is more than 0.99 and which means that due to the high temperature of the sun with respect to the temperature on the earth's surface, corroborated with the low background temperature of the universe, one may have on the earth a high efficiency of solar energy conversion into work. Nevertheless, the work generated by the sun–earth–universe heat engine is dissipated or used in various processes. The atmosphere and hydrosphere flows "consume" a significant part of this work. More exactly, winds and air movements in the atmosphere and oceanic currents in the hydrosphere are generated by solar energy.

Figure 2.2 presents the energy inventory of radiation associated with solar light as well as with terrestrial infrared emissions. All the percents shown on the figure refer to the incident solar radiation that is a flux of energy equal to about 174 PW (where 1 PW is 10^{15} W). About 30% of the incoming solar radiation is reflected back into the terrestrial atmosphere by the earth; this is called the "albedo" of the earth, which is defined as the ratio between the reflected and incident radiation and denoted by α. The reflection is caused by various phenomena, such as back-scattering (7%), reflection by clouds (17%), and reflection by the earth's surface (6%). Then, about 19% of the incoming solar radiation is absorbed by the water vapor, dust, and ozone molecules present in the atmosphere, while about 4% is absorbed by clouds. The remaining 47% is absorbed by the earth.

The earth emits radiation at a temperature that corresponds to the average surface temperature (at 300 K the emitted blackbody radiation has a 10 μm wavelength, which

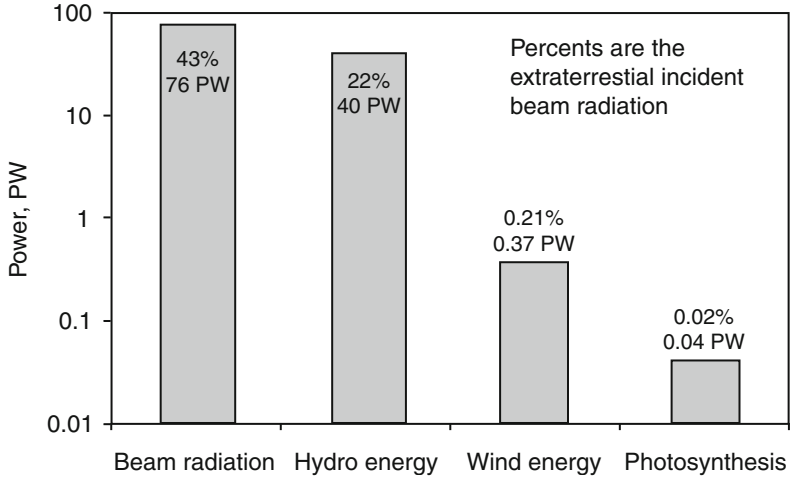

Fig. 2.3 The distribution of solar energy source absorbed by the earth [data from Tiwari and Ghosal (2007)]

is in the infrared spectrum). The radiation emitted by the land and ocean surface amounts to about 16% of the incident solar radiation. Only 10% of this quantity reaches the extraterrestrial space, the rest being absorbed by clouds and by the greenhouse gases present in the atmosphere or reflected back by the clouds. Basically, the atmosphere is heated by the earth's surface through infrared radiation, conduction, and water evaporation. The clouds emit infrared radiation in the extraterrestrial space of an amount that is 20% of the total incident radiation of 174 PW, while 40% is the infrared emission associated with atmospheric water vapor, ozone, and carbon dioxide.

Figure 2.2 shows that the amount of reflected radiation (both short- and long wave) is, from left to right (6 + 17 + 7 + 10 + 20 + 40)% = 100%, that is, the same as the incident solar radiation (of 174 PW). This fact is not in contradiction with the model introduced by Fig. 2.1. The equality of the energy fluxes that enter and leave the terrestrial system is a condition of having an average constant temperature on the earth. In any other situation, the earth's temperature will increase or decrease until an equilibrium is achieved. Figure 2.1 details the mechanism by which the earth's climate is driven by the solar and background radiations in a similar manner as a heat engine is driven by a temperature differential at the source and sink. The work generated by the heat engine presented in Fig. 2.1 is in fact completely destroyed, that is, converted back into heat, which is eventually released outside the terrestrial atmosphere. Thus, overall, the earth does not gain any energy, but it needs to keep its temperature constant.

A series of processes are driven by the incident solar energy on the earth. A breakdown of solar energy use in various natural processes is shown in Fig. 2.3. An amount of 76 PW representing 43% of the incident extraterrestrial solar radiation is the so-called beam radiation, which heats the earth's surface (the land and the ocean).

This energy can be harvested by engineered systems and used for various purposes. Here are some technologies that typically can be used for converting beam radiation into other forms of energy:

- Ocean thermal energy conversion (OTEC) uses the difference in temperature between the ocean surface and the deep waters to drive a heat engine that produces electricity or synthetic fuels (e.g., ammonia can be produced by OTEC energy using nitrogen from air and hydrogen from water).
- Solar ponds are pools of saltwater whose surface is exposed to solar radiation. A gradient of temperature is formed in the pond due to stratification; the temperature at the pool bottom reaches up to 90°C. The harvested energy can be used for either space or process heating, desalinization, or electrical power generation.
- Solar-driven heat engines can concentrate the solar radiation to obtain high-temperature sources and convert the associated heat into electricity and lower grade process or space heating, which is cogeneration.
- Photovoltaic technology transforms the incident solar radiation directly into electricity.
- Other applications such as process heating, house and space heating, water heating, cooking, steam generation, and desalinization are possible.

All these energy conversion technologies represent forms of renewable energy conversion. Supposing, for example, that all the 76 PW associated with beam radiation is converted into electricity with 20% efficiency. The result is 15 PW of electrical power; this figure can be compared with the average world energy consumption rate of 0.015 PW; that is, the direct beam radiation energy if fully harvested can generate 1,000 times more electricity than the world total energy consumption rate. This comparison gives us an idea about the abundance of solar energy, which appears to be an inexhaustible source.

Moreover, 22% of the incident extraterrestrial solar radiation, amounting to 40 PW, is consumed by the hydrological cycle. The water cycle can be regarded as a natural way of storing solar energy in the form of potential energy of water. Solar energy heats water in seas, oceans, and lakes, which results in evaporation. Solar energy also heats snow in colder regions that sublimates, forming water vapor directly. Water vapor is also generated by plants and animal transpiration and by humid soils through evaporation. The vapor rises into the air and forms clouds where the temperature is lower to allow condensation. Precipitation in the form of rain and snow is formed. Through this assembly of processes, important amounts of water are transported from the plains to the heights and thus hydro energy is formed. Dam and accumulation lakes can be constructed to generate hydroelectricity.

Other forms of solar energy are wind (0.37 PW or 0.21%) and photosynthesis (0.04 PW or 0.02%). Photosynthesis is a means of storing solar energy in the form of chemicals. For example, glucose and ATP (adenosine triphosphate) are substances synthesized by plants from photosynthesis in order to store energy. Basically, wind energy can be harvested with various kinds of wind turbines, while the energy of plants can be retrieved in the form of biomass energy. Moreover,

fossilized biomass has been converted in underground reservoirs into fossil fuels such as natural gas, coal, and petroleum of various kinds.

It is instructive to know the intensity of the incident beam radiation at the earth's surface. This value can be determined based on the solar constant, which is defined as the extraterrestrial solar radiation intensity per unit of surface and has the average value of 1,367 W/m^2. However, 30% of this radiation is reflected back into extraterrestrial space due to the albedo factor, which leaves 957 W/m^2. If one denotes the earth's radius by R, the incident radiation is the projected area of the earth's sphere, πR^2; however, the radiation distributes on average over the whole earth's surface, which is the area of the earth's sphere, $4\pi R^2$. In conclusion, the average intensity of solar beam radiation is on the order of 957/4 = 240 W/m^2.

2.3.2 Geothermal Energy

Geothermal energy manifests in the form of heat and has its source in the earth's core, where some nuclear reactions are assumed to occur. The earth's core temperature is estimated to be ~5,000 K, and due to rock conductivity the temperature at about 4 km below the earth's surface can reach ~90°C. The intensity of geothermal heat is comparatively low with respect to solar energy intensity, namely ~0.1 W/m^2 versus ~240 W/m^2 for geothermal solar, respectively (see Blackwell et al. 1991). However, at places where geysers, hot springs, hot rocks, or volcanoes exist, there is a much larger local potential for geothermal energy. The total estimated amount of geothermal energy is on the order of 10^{16} PJ (where 1 PJ is 10^{15} J). The geothermal heat flows from the earth's core to the surface at a rate of about 44 TW (where 1 TW is 10^{12} W), which is more than double the world's energy consumption rate of ~15 TW. However, since this heat is too diffuse (~0.1 W/m^2), it cannot be recovered unless a geographic location (i.e., geothermal site) shows a higher intensity geothermal resource. A simple calculation yields that at the consumption rate of 44 TW the geothermal heat will be exhausted after ~10^{12} years.

2.3.3 Tidal Energy

Tidal energy is the unique form of energy derived from the combined effect of the planet's spinning motion and the gravitational forces associated with the earth–moon and earth–sun systems. Because the most important effect is due to the gravitational forces of the moon, this kind of energy is sometimes called "lunar energy." Tidal energy is another kind of hydropower, in the sense that the energy is transmitted through water movement. However, hydro energy is originated by the hydrological cycle, while the nature of the tides is different (viz. gravitational).

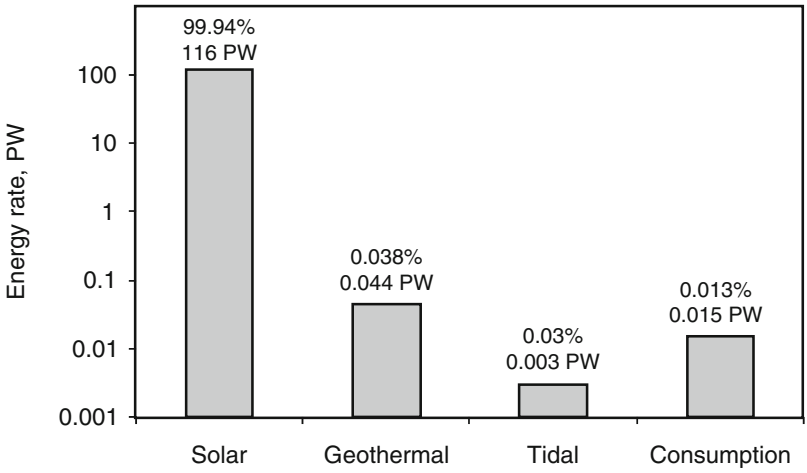

Fig. 2.4 The energy rate of the essential renewable sources and the rate of world energy consumption [data from Tiwari and Ghosal (2007)]

Figure 2.4 compares the average rate of energy consumption in the world with the rate at which the three kinds of fundamental sources may be available. The rate at which solar energy is available can be calculated from Fig. 2.3 as 76 + 40 + 0.37 + 0.04 = 116.41 PW; the rate of geothermal energy (total) available is 0.044 PW, while the rate of retrievable tidal energy is 0.003 PW. Figure 2.4 has been constructed based on these numbers and the rate of world energy consumption of 0.015 PW.

2.4 Biomass Energy

Biomass is a word derived from biological mass; thus biomass energy suggests a form of energy derived from living systems. In general, biomass energy refers to the energy embedded in materials such as wood and other crops that can be combusted or converted into synthetic fuels. The photosynthesis process can be written in a simplified manner as follows:

$$6CO_2 + 6H_2O \xrightarrow{\text{LIGHT}} C_6H_{12}O_6 + 6O_2,$$

where the products are glucose and oxygen. Some 2.8 MJ of light energy per mole of synthesized glucose is needed, and the efficiency of the photosynthesis process can be assumed to be 0.5% to 1%. On average, 1 square meter of the earth's surface is hit with incoming solar radiation of 240 W for 8 hours per day; that is, one can consider the incident radiation energy to be 2.5 kWh per day per square meter, or say 1,000 kWh per year per square meter. Assuming that 0.8% from this incident energy is transformed into glucose by plants, one gets the equivalent of 8 kWh per

Table 2.1 Energy content of biomass sources

Biomass type	GJ/kg	GJ/m^3	Biomass type	GJ/kg	GJ/m^3
Green wood	6	7	Dry dung	16	4
Dry wood	15	9	Fresh grass	4	3
Oven dry wood	18	9	Straw	15	2
Charcoal	30	9	Sugar cane	17	10
Paper	17	9	Domestic refuse	9	2

square meter per year of solar energy stored in glucose, which is the equivalent of 10 mol or 1.8 kg of glucose that can be produced per square meter per year.

The above figure is approximate, and assumes that the biomass is the same as glucose from the energy point of view. In fact, various kinds of biomass have different energy content. The energy content of the main kinds of biomass is listed in Table 2.1.

2.5 Fossil Fuels

It has been mentioned above that through photosynthesis, over long periods of time, all carbonaceous fuels including coal, petroleum, and natural gas were formed. In general, the energy of fossil fuel is used through direct combustion; therefore, this form of energy is mainly thermal. However, it is also possible to produce synthetic fuels from fossil fuels, such as hydrogen, ethanol, diesel, methane, or ammonia. There are three main kinds of fossil fuels, namely coal, petroleum, and natural gas; these will be discussed in this section.

2.5.1 Coal

Coal mainly comprises organic substances derived from plants that form sediments that also embed other mineral inclusions. There are various types of coal, each with its specific calorific heat (see, e.g., Goswami and Kreith 2008). The main component of coal is carbon. Coal plays a vital role in power generation, steam production, and steel manufacturing processes. However, it has a limited role in residential, commercial, and transportation applications. The calorific value of coal and its carbon content is presented in Table 2.2.

In Fig. 2.5, the evolution of coal production in the last three decades is presented, while in Fig. 2.6 the distribution of coal reserves in the world is shown.

2.5.2 Petroleum

Petroleum (also called crude oil) is a naturally occurring hydrocarbon-based liquid or solid (e.g., bitumen forms) found in underground rock formations. The main

Table 2.2 Parameters of various kinds of coal

Coal type	Carbon content by weight	Heat content (kJ/kg)
Lignite	~70%	<28,500
Gas coal	~83%	<35,000
Fat coal	~88%	<35,400
Forge coal	~90%	<35,400
Nonbaking coal	~91%	<35,400
Anthracite	>92%	<35,300

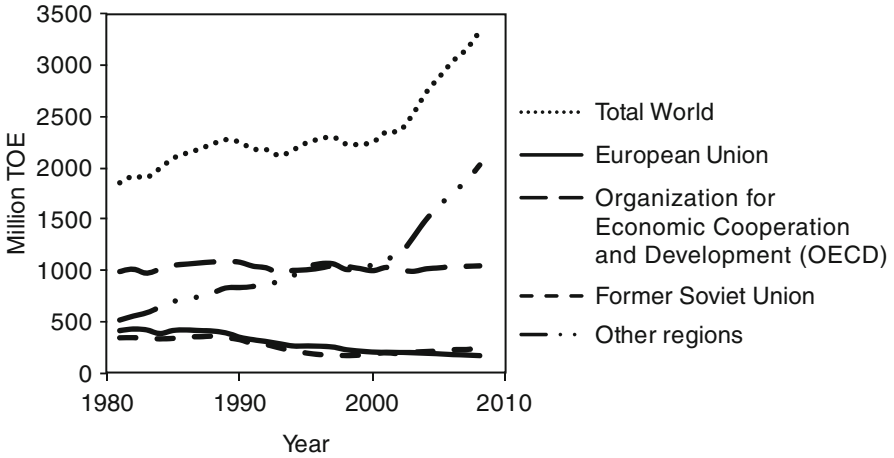

Fig. 2.5 Historical coal production in millions of tons of oil equivalent (TOE) [data from BP (2008)]

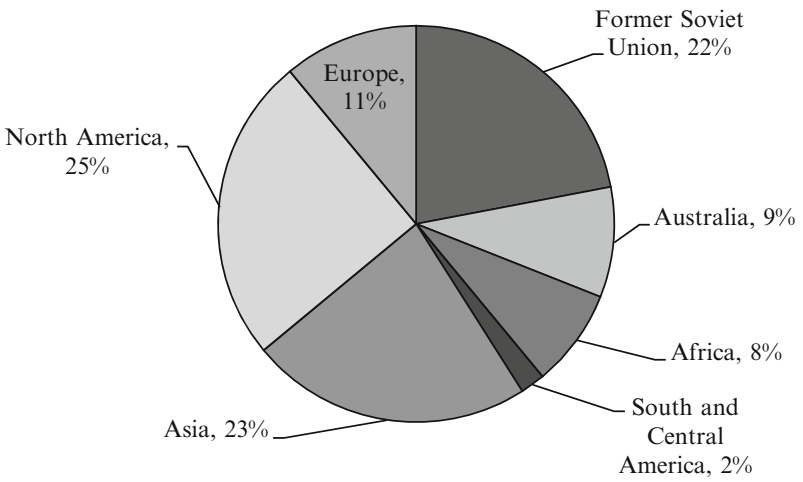

Fig. 2.6 Approximation of distribution of coal reserves in the world [data from BP (2008)]

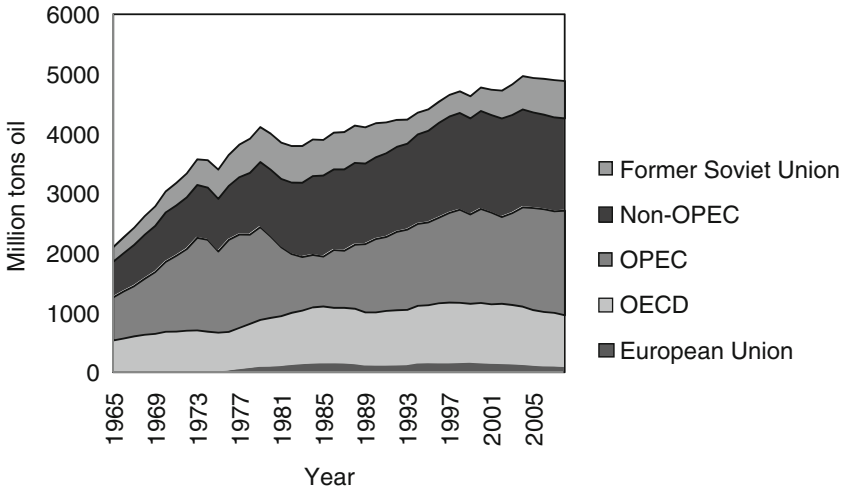

Fig. 2.7 Trend of oil production in the last 50 years [data from BP (2008)]

hydrocarbons included in petroleum are alkanes, cycloalkanes and aromatics, asphaltics, naphthalenes, and parafins. Out of the total world oil reserves, 30% is conventional oil, 15% heavy oil, and 25% extra heavy oil, and 30% of petroleum is found in the form of bitumen and oil sands. Petroleum is the number one primary source for producing transportation fuels. In Fig. 2.7, the trend of oil production for the last 50 years is shown.

2.5.3 Natural Gas

Fossil natural gas contains mainly methane and occurs naturally in oil fields, natural gas fields, and coal beds. Russia has the largest proven resource of natural gas of 47 PNm^3 (where PNm^3 stands for peta ore 10^{12} normal cubic meters). World production of natural gas accounts for 20% of world energy production, and its production is projected to double by 2025 (see, e.g., Goswami and Kreith 2008). The historical trend of natural gas production in the world is presented in Fig. 2.8.

2.6 Nuclear Energy

Nuclear energy in the form of electricity and heat is obtained through controlled nuclear fission reactions. About 15% of the world's electrical energy production originates from nuclear energy. Also, nuclear energy is used for propulsion of naval vessels. More than 400 nuclear power plants are operational worldwide at present, with an installed capacity of over 370 GWe (where GWe is giga watt electric).

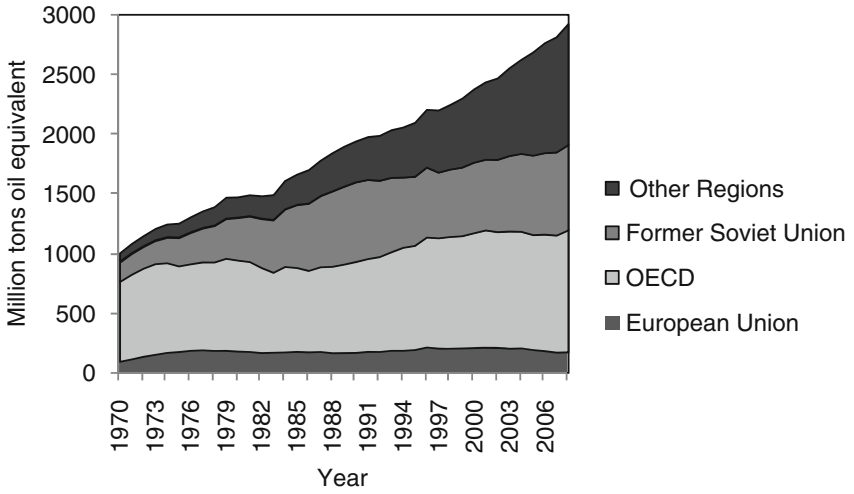

Fig. 2.8 Historical trend of natural gas production in the world [data from BP (2008)]

The conventional resource of nuclear energy is represented by uranium. The main chemical form of the uranium in the ore is U_3O_8, from which 1 ton produces 0.85 tons of uranium, which consists mainly of ^{238}U and only 0.71% ^{235}U. Therefore, one calculates that 1 ton of ore contains 5.9 kg or 1.38×10^{25} atoms of ^{235}U, which in a nuclear reactor could produce ~180 MeV of fission energy that can be converted into 40 GWh of electrical energy. The resulting fission residues are radioactive products with great potential as high specific-energy sources. For comparison purpose, one can note that 1 ton of coal produces 2.8 MWh of electrical energy, that is, 14,000 times less than the nuclear fission reaction. In Fig. 2.9, the trend of electricity production by nuclear power plants from 1965 until the present is presented.

2.7 Proven Fuel Reserves

It is recognized that fossil and nuclear fuel will be depleted, since they are finite resources. For example, the proved reserves of petroleum, natural gas, coal, and nuclear fuels are presented in Fig. 2.10. Considering this prediction and the rate of production in 2008 (BP 2008), the exploitable oil resources will last the least amount of time (about 42 years).

Regarding nuclear fuels, the total reserves were estimated based on Price and Blaise (2002) and include all conventional resources (uranium, plutonium, and thorium) plus the estimated reserves that are not possible to exploit with today's technology, comprising uranium found in phosphate-based minerals and uranium recovered from seawater.

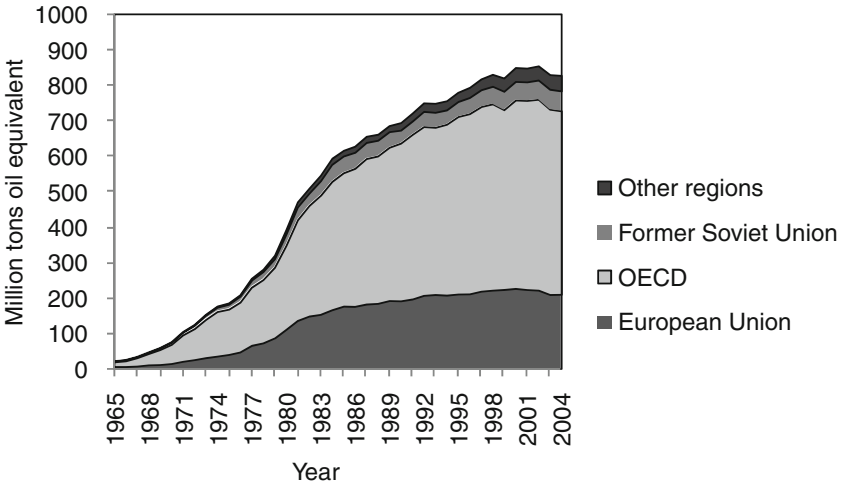

Fig. 2.9 Historical trend of nuclear electricity production [data from BP (2008)]

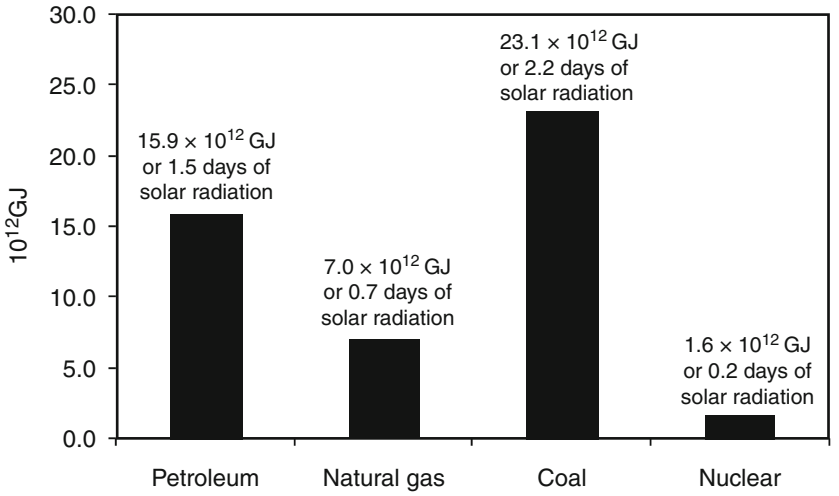

Fig. 2.10 Proved global fossil fuel reserves in year 2008 [data from BP (2008)]

An indicator denoted as R/P is introduced in Fig. 2.11 and represents the reserves versus production ratio, which is calculated by dividing the reserves remaining at the end of any year by the production in that year. The R/P ratio, measured in "years," gives an estimate of how long the respective resource will last. According to the R/P ratio in 2008, coal lasts the longest among the three main fossil fuels (133 years).

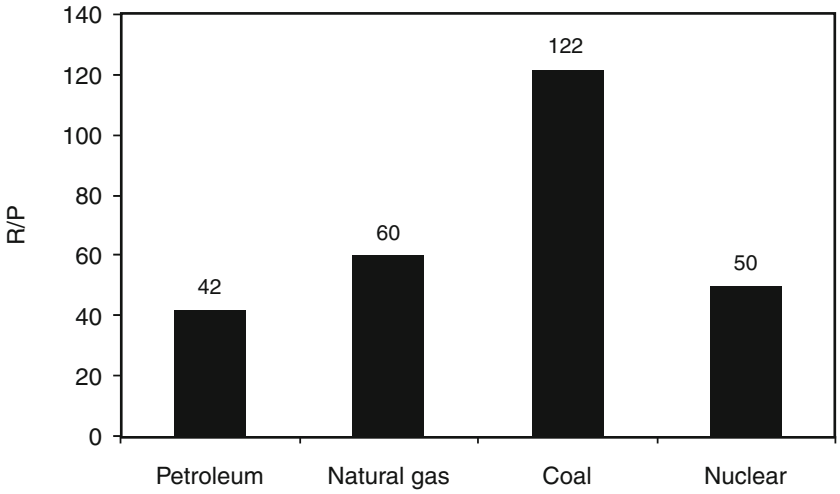

Fig. 2.11 Global fossil fuels reserves versus production ratio (R/P) in year 2008 [data from BP (2008)]

One notes that in Fig. 2.10 the resource reserves were indicated in two units: the amount of the energy resource in GJ, and the number of years needed to accumulate the equivalent energy from solar radiation incident on the earth's surface. Assuming that solar energy can be fully captured, in 2 years it will amount to the equivalent of the proven reserves of oil (see Fig. 2.10). Thus, the energy content accumulated in nearly 11 years is equivalent to that of the proved reserves of oil, natural gas, and coal combined.

Most of the world's energy supply, accounting for 86%, is currently based on fossil fuels including petroleum (36%), coal (27%), and natural gas (23%) (EIA 2008). This situation is obviously the historical consequence of the fact that, over many centuries, fossil fuels were (and still are) a profitable business.

Energy production and consumption represent important figures and are reported yearly by specialized energy agencies. These statistical data are useful for predicting the energy demand in future years. In Fig. 2.12, the world fossil energy production and consumption based on data from BP (2008) are presented. It is very interesting to note that in 2008 petroleum and coal consumption exceeded the production, meaning that reserves accumulated in previous years were used.

Other important statistics refers to the regional distribution of fossil production and consumption in a specific year. For 2008, this is shown in percents of the total corresponding figure for world production and consumption, respectively, in Figs. 2.13 to 2.15. These plots indicate the potential for export and the need for import for the respective regions. For example, Fig. 2.13 suggests that Middle East countries exported about 25% of the world's petroleum production in 2008, but they did not produce or consume coal at all.

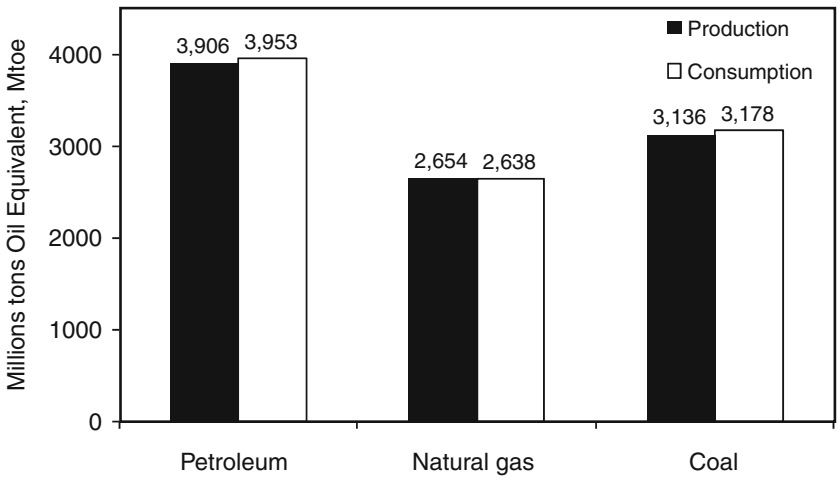

Fig. 2.12 World fossil fuel energy production and consumption in 2008 [data from BP (2008)]

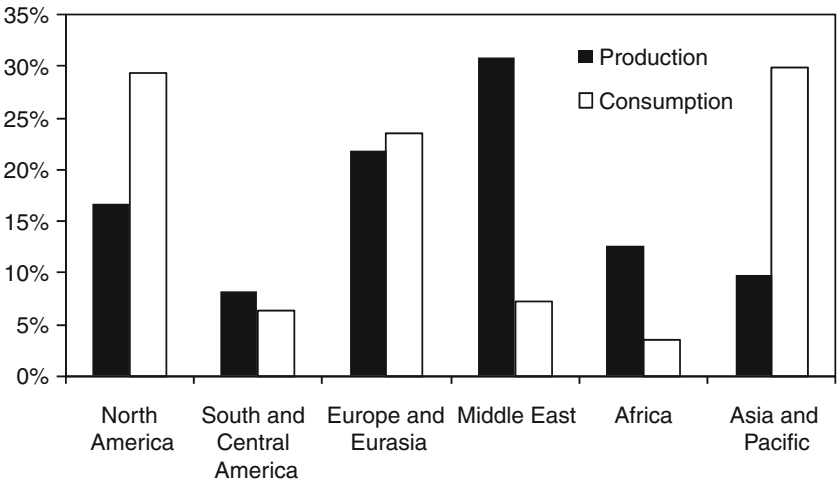

Fig. 2.13 Regional petroleum production and consumption in 2008 [data from BP (2008)]

2.8 Historical Trends and World Energy Prospects

Projections of fossil fuel and green energy consumption are important for local and global applications, and can play an important role in future energy policies, strategies, investments, and programs. It is also important to determine the transition period to a green energy economy and to plan fossil fuel or green energy budget allocations for local and industrial investments.

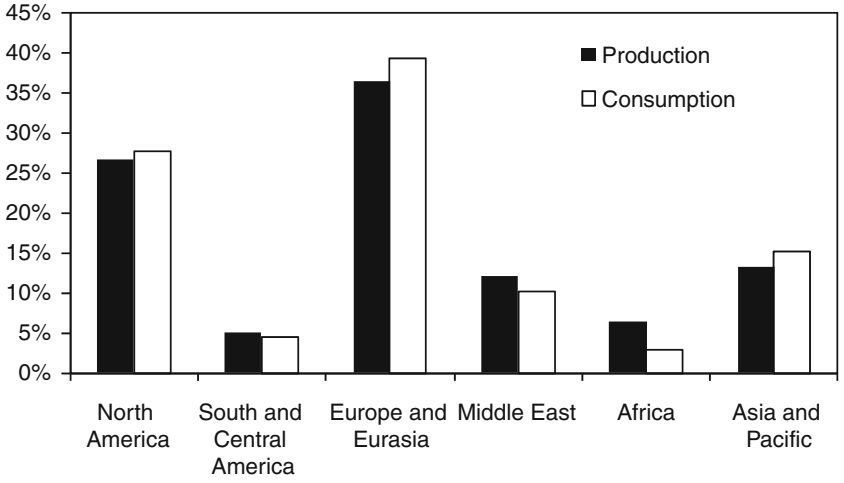

Fig. 2.14 Regional natural gas production and consumption in 2008 [data from BP (2008)]

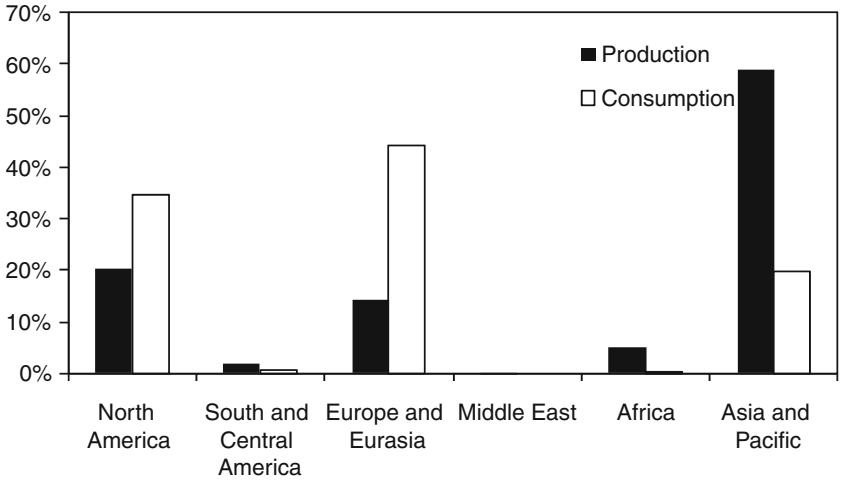

Fig. 2.15 Regional coal production and consumption in 2008 [data from BP (2008)]

Figure 2.16 illustrates the importance of predicting energy use patterns and planning. Better energy policies, strategies, and projections can facilitate the introduction of green energy–based environmental benefits in several ways. One is that energy consumption is better controlled. Also, the environmental impacts of energy sources and technologies such as greenhouse gas emissions and pollution are reduced. In addition, energy planning can contribute to innovative implementations of green energy technologies so as to achieve improved sustainability and global stability, particularly during a transition to a green energy–based economy.

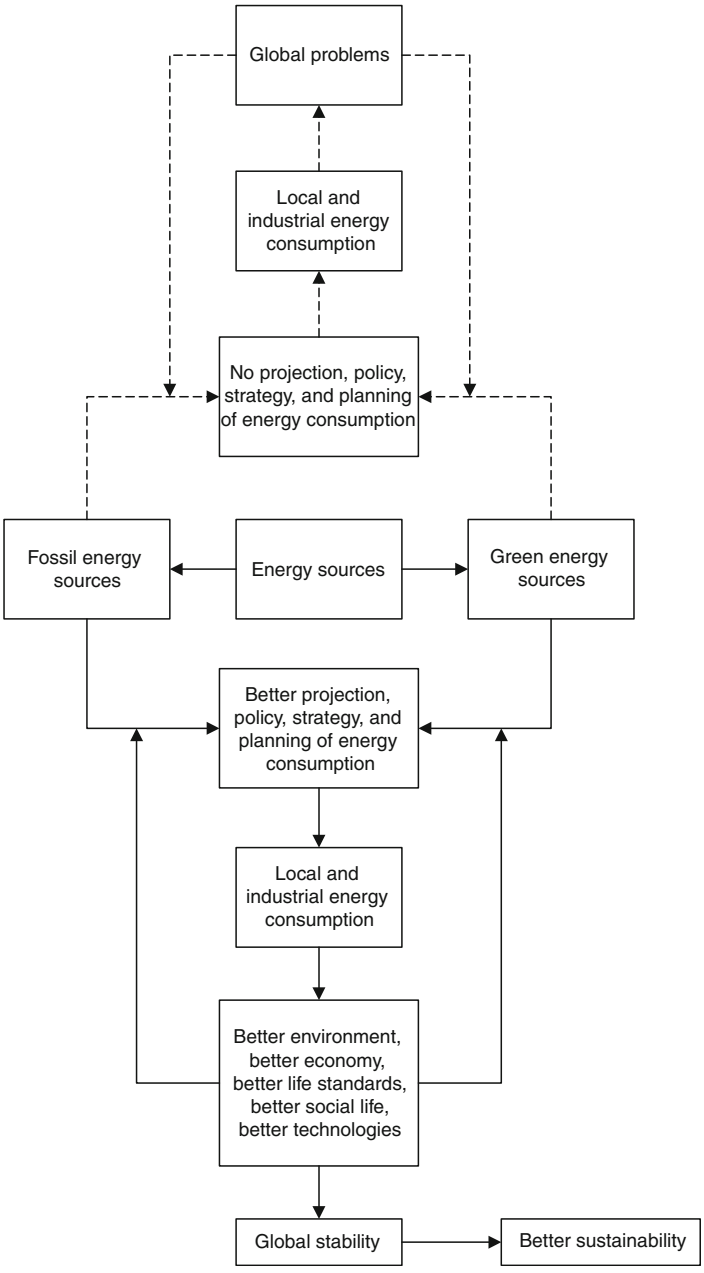

Fig. 2.16 The importance of energy forecast and planning programs. The *top half of the diagram* indicates the results of little or no planning, while the *bottom half* presents the outcomes when careful planning is applied [modified from Ermis et al. (2007)]

Predictions of the world energy consumption for the short term (couple of years) can be made based on linear or polynomial extrapolation, as first estimates. However, predictions over future decades must apply more advanced methods, because energy consumption is affected by a multitude of factors, including population growth, evolution of the gross domestic product of countries, potential conflicts, economic crises, and catastrophic events. An important method for forecasting energy consumption is artificial neural network (ANN) modeling. Although many investigations involving the ANN approach have been reported, limited studies are available in the open literature on predicting energy consumption for different applications. A review of the available studies on this subject is given by Ermis et al. (2007).

A neural network is an informatics algorithm that simulates the human brain's thinking, which can be instructed to respond to a number of events. During the instruction period, the artificial neural network algorithm adjusts and reconfigures the neurons connections. The network can be trained with past and present data, including significant historical events. The network can be validated using known data points. Here we show as an example the results by Ermis et al. (2007) regarding the predictions of world energy consumption, which includes fossil fuels and green energy for the period up to 2050. The artificial neural network used by Ermis et al. (2007) to predict the subsequent results has been trained using published statistical data for the last 40 years.

The world coal consumption curve equation derived via ANN depends on the actual and projected coal consumption data and can be expressed in EJ (exajoule, or 10^{18} J) as follows (Ermis et al. 2007):

$$E_{\text{coal}}(\text{EJ}) = 125.6667\left[1+\exp\left[-\left(\frac{Y-1{,}968.0551}{24.2314}\right)\right]\right]^{-1} \text{and } (R^2 = 0.99998), \quad (2.1)$$

where E_{coal} denotes world coal consumption in EJ and Y the year, and R is the mean square error. The results are also summarized in Fig. 2.17 and compared with linear predictions and predictions by Workbook (2005). It is expected that coal consumption will increase by 17.86% from 2005 to 2050, 11.22% from 2005 to 2025, and 5.97% from 2025 to 2050.

The world oil consumption curve equation derived via ANN depends on the actual and projected oil consumption data and can be expressed as follows (Ermis et al. 2007):

$$E_{\text{oil}}(\text{EJ}) = 184.5575\left[1+\exp\left[-\left(\frac{Y-1{,}987.7137}{10.2282}\right)\right]\right]^{-1} \text{and } (R^2 = 0.99947), \quad (2.2)$$

where E_{oil} denotes world oil consumption in EJ.

The corresponding results are also presented in Fig. 2.18. Due to rapid technological developments, transportation applications, and secondary fuel production based on oil reserves, it is expected that world oil consumption will probably increase as long as green energy sources such as solar, hydropower, wind, biomass,

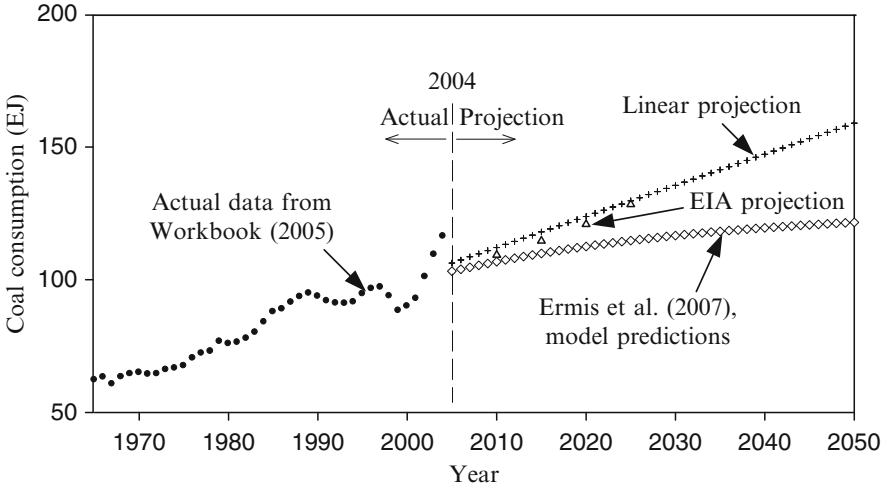

Fig. 2.17 Variation in world coal consumption with time [modified from Ermis et al. (2007)]

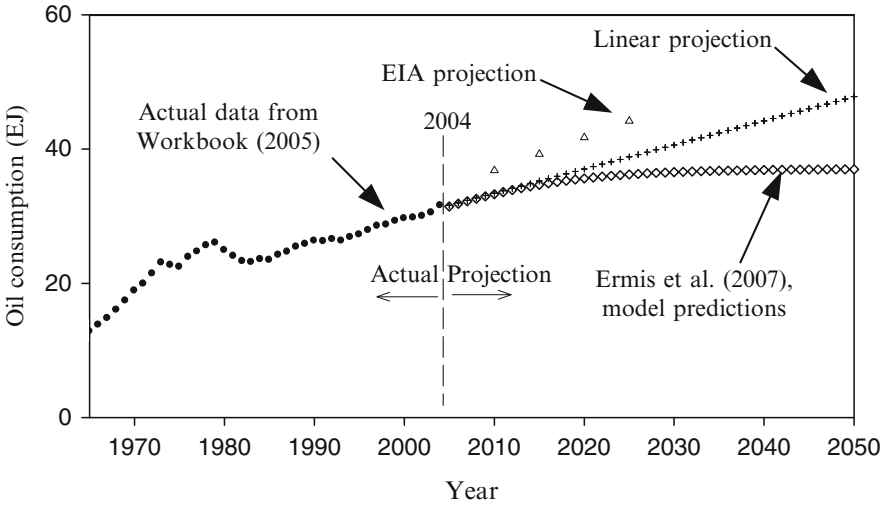

Fig. 2.18 Historical variation and future projection of world oil consumption [data from Ermis et al. (2007)]

nuclear, and hydrogen are not implemented to reduce the oil demand and consumption all over the world.

Oil consumption is expected to increase by 17.61% from 2005 to 2050, 15.14% from 2005 to 2025, and 2.14% from 2025 to 2050. After 2025, world oil consumption will probably remain stable. This stabilization in oil consumption indicates that, in the future, other green energy sources or natural gas will be mostly used to compensate for the world oil deficit.

The world natural gas consumption curve equation derived via ANN depends on the actual and projected natural gas consumption data and can be expressed as follows (Ermis et al. 2007):

$$E_{\mathrm{ng}}(\mathrm{EJ}) = 186.5923\left[1+\exp\left[-\left(\frac{Y-1,984.2525}{27.0821}\right)\right]\right]^{-1} \text{ and } (R^2 = 0.99965), \quad (2.3)$$

where E_{ng} denotes world natural gas consumption in EJ. As illustrated also in Fig. 2.19, the consumption of natural gas, which causes less greenhouse gas emissions than other fossil fuels, is expected to rise by 59.81% from 2005 to 2050, 31.89% from 2005 to 2025, and 21.16% from 2025 to 2050.

It is expected that rapid increases in technological developments, transportation applications, industrial and local energy demands, and secondary fuel production and power generation from natural gas will probably increase world natural gas consumption in the future. Thus, natural gas will probably be considered another alternate fuel for reducing greenhouse gas emissions.

Global demand for energy services is expected to increase by as much as one order of magnitude by 2050, while primary energy demands are expected to increase by 1.5 to 3 times. Trying to predict the evolution of the world energy market, policy makers studied various long- and short-term scenarios. Relevant work in this respect

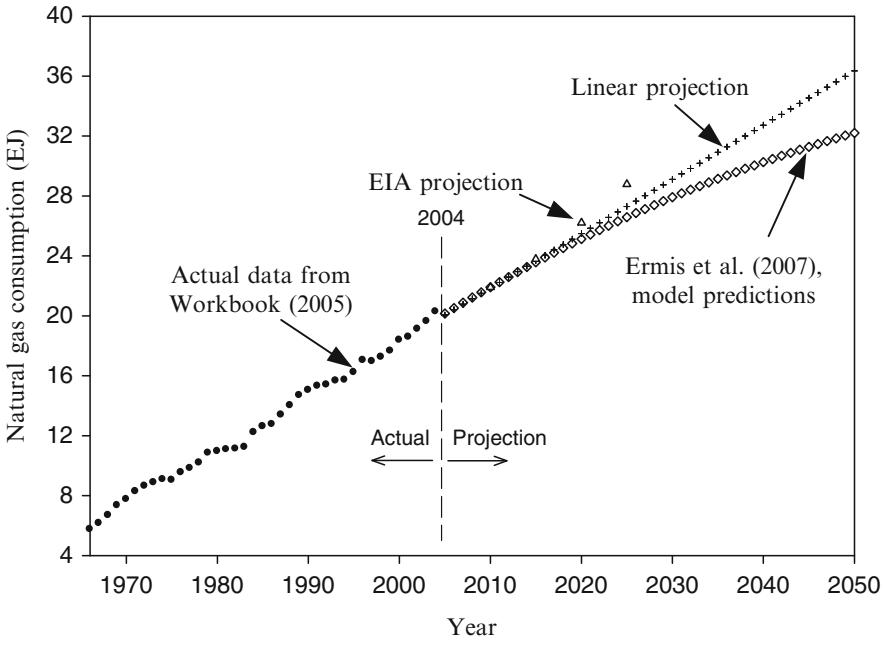

Fig. 2.19 Historical variation and future projection of world natural gas consumption [data from Ermis et al. (2007)]

has been pursued by the European Commission (EC 2006), which predicts the world energy technology outlook through 2050.

In this report, the geopolitical context, CO_2 emission profile, oil, gas, and coal production profiles, H_2-technology development, population growth, predicted energy demand, and other factors are accounted for to propose three scenarios for energy technology development up to 2050.

In the reference case (RC) scenario, a minimum degree of political initiative is assumed in all countries toward sustainable development. In the second scenario, called the carbon constraint case (CCC), severe limits in CO_2 emissions are assumed up to 2050. In the third scenario, called the H_2-case, it is assumed that a firm political decision is made in most countries toward the development of a hydrogen economy, and therefore major breakthroughs will be possible. We compiled the data from EC (2006) and give in the following paragraphs a summary, with a special focus on sustainable energy issues.

The data from Fig. 2.20 correlate the evolution of electricity consumption per capita in the three scenarios with global population growth. At present, developing countries, with a population of around four billion, represent some 77% of the world's population but use only a quarter of its global energy budget. Demographers generally predict that the total population will top eight billion by 2050. Roughly three-quarters of these people will live in developing countries. Energy service supplies for the developing world must grow considerably to meet the extra demands expected from these countries and to ensure that their economic development is not constrained. It can be seen that, while the population increases 1.4 times, the electricity consumption per capita increases ~2.6 times. In the same time, it is noted from EC (2006) that the gross domestic product (GDP) augments ~2.7 times.

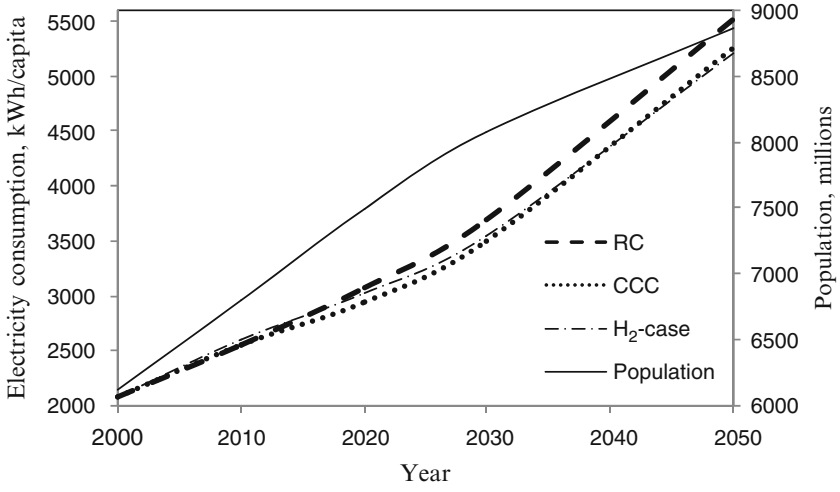

Fig. 2.20 Correlation between electricity consumption and world population for three development scenarios of energy technology (*RC* reference case; *CCC* carbon constraint case; *H_2-case* hydrogen economy case) [data from EC (2006)]

Based on Ermis et al. (2007) the world green energy consumption can be expressed as follows:

$$E_{ge}(\mathrm{EJ}) = 105.493\left[1 + \exp\left[-\left(\frac{Y - 1,999.642}{26.387}\right)\right]\right]^{-1} \text{ and } (R^2 = 0.99976), \quad (2.4)$$

where E_{ge} denotes world green energy consumption in EJ. Green energy use is projected to be the fastest growing component of world primary energy consumption according to the ANN projection by Ermis et al. (2007). This prediction is compared with other sources in Fig. 2.21.

The green energy consumption is projected to increase by 59.84% from 2005 to 2050, 32.29% from 2005 to 2025, and 20.81% from 2025 to 2050. If utilization of green energy resources and technologies is encouraged, it can be expected that countries may maximize the benefits of green energy sources and technologies, while minimizing the global unrest and other problems associated with the use of fossil fuel energy sources.

The predicted primary energy production in 2050 will increase more than two times (from 60,000 to 125,000 GJ) with respect to the year 2000. This is illustrated in Fig. 2.22 together with the respective energy shares among various kinds of energy. The share of renewables (including hydro, geothermal, biomass, wastes, wind, and solar) increases from 14% to 19% with a prominent augmentation of solar and wind production (from 0.1% in 2000 to 4.6% in 2050, respectively).

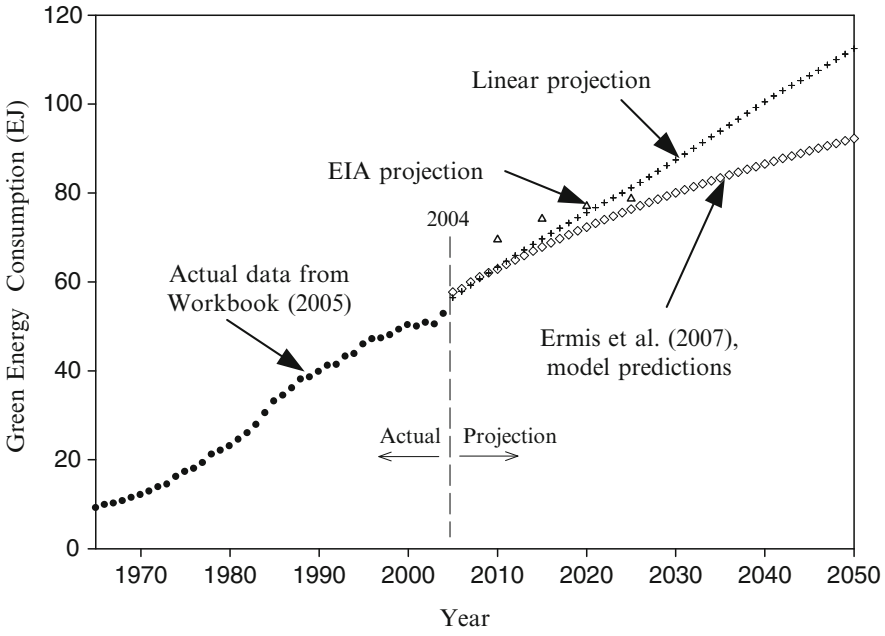

Fig. 2.21 Historical variation and future projection of green energy consumption [data from Ermis et al. (2007)]

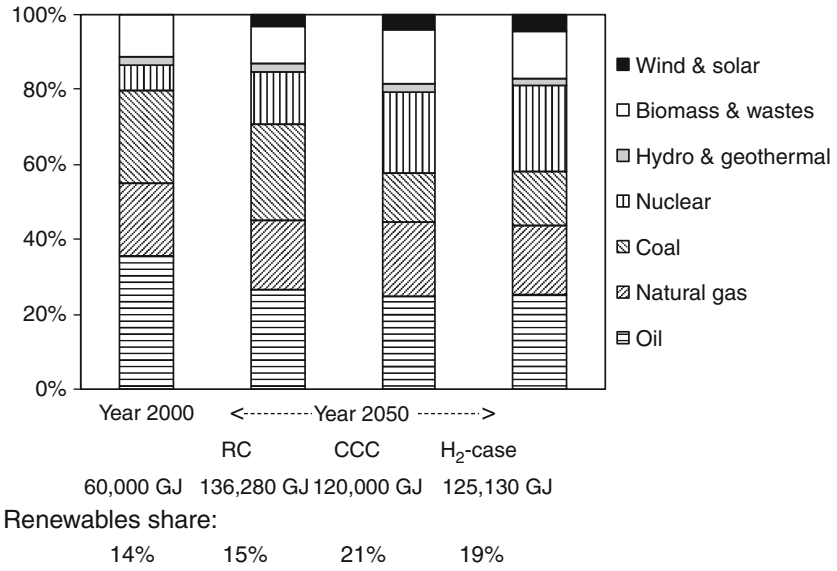

Fig. 2.22 The predicted primary energy production in the year 2050 in three scenarios in comparison with the year 2000 case (*RC* reference case; *CCC* carbon constraint case; *H_2-case* hydrogen economy case) [data from EC (2006)]

The predicted evolution of world primary energy consumption is indicated in Fig. 2.23; the associated prediction equation by Ermis et al. (2007) is as follows:

$$E_{\text{wpc}}(\text{EJ}) = 589.024\left[1 + \exp\left[-\left(\frac{Y - 1,984.253}{22.721}\right)\right]\right]^{-1} \text{and } (R^2 = 0.99965), \quad (2.5)$$

where E_{wpc} denotes world primary energy consumption in EJ.

The primary energy consumption, according to Eq. (2.5) and Fig. 2.23, has two components, namely the fossil fuel and the green energy components. The components of world primary energy consumption are also indicated in Fig. 2.23.

The fossil fuel prices are highly influenced by major political events; in fact, that complicates their prediction. For this reason, it is important to adopt a fair/realistic scenario of future political and economical events prior to any attempt to estimate oil/gas/coal price evolution. There are several serious institutions concerned with fuel price predictions for short as well as for longer terms. For example, the Natural Resources of Canada (NRC 2005) issues periodic reviews and outlooks with a range of prediction of about 15 years in the future; it is expected that the Canadian fuel price will increase by 20% in nominal value by 2020. A recent review is by the Energy Information Administration of the United States (EIA 2008) forecasting over a period up to 2030. In a so-called high-price scenario, the oil price is predicted to increase by ~60% in real value with respect to the 2008 value, while in a

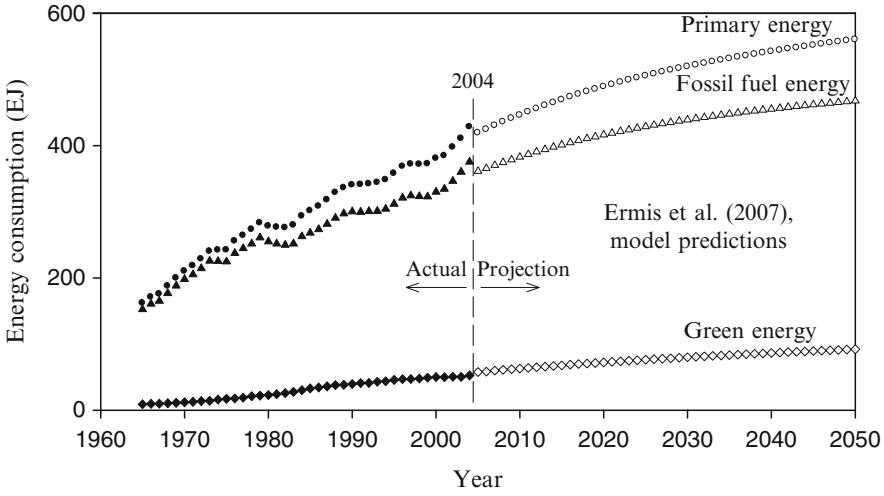

Fig. 2.23 Variation of world primary energy, fossil, and green energy consumption with time [data from Ermis et al. (2007)]

low-price scenario it might decrease by ~30%. Periodic oil market reports are prepared also by the International Energy Agency [IEA (2006, 2008)].

The World Energy Council (WEC 2007) elaborated four scenarios on world energy up to the year 2050. These scenarios account for low to high international cooperation and integration on energy policy and high and low engagements of governments in energy issues. However, the analysis does not give explicit fossil price estimations. In its report of 2006, the European Commission elaborated the world energy outlook up to 2050 and predicted the extreme limits of fuel price increases (EC 2006). The predictions are given according to the above-discussed RC and CCC scenarios.

A plot showing the past recorded prices and the future prediction of oil and natural gas prices is presented in Fig. 2.24. In order to obtain this plot, historical data from BP (2008) has been used for oil price records since 1870. For the modern era, these prices correspond to the world average, but for the 1800s and early 1900s they are the U.S. estimates. Historical natural gas annual records were obtained from the U.S. Department of Energy for the period 1930 to 2000 (EIA 2000). Recent trends in coal prices were taken from Pincock (2004) and converted into real currency, namely US$ 2008.

In Fig. 2.24, two lines for future price prediction of oil are marked; the upper line corresponds to the CCC scenario, while the lower corresponds to the RC case. For the natural gas price prediction (dashed line), the profiles for the CCC and RC scenarios cross by the year 2020. The coal price records in recent years are also indicated on the plot, to suggest that, in general, the price of coal is a little lower than that of oil and natural gas, per unit of energy content.

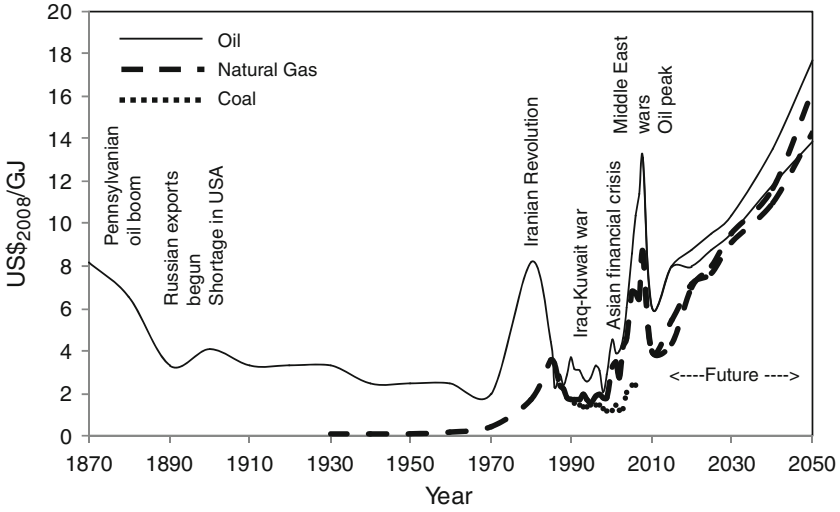

Fig. 2.24 Historical and predicted fossil fuel prices (average values for world) [data from BP (2008), EIA (2000), Pincock (2004)]

The continuous increase of fuel's real value is mainly a consequence of fuel shortage. No major political events (e.g., major wars or conflicts) are assumed in the predictions by EC (2006), even though this assumption has a certain degree of uncertainty. To observe the impact of political, economic, and social incidents on fossil fuel prices, the most influential events are added to the chart in Fig. 2.24.

One notices, for instance, the great influence of the Iranian revolution and that of the believed oil peak. The oil peak is the point in time when the maximum rate of global petroleum extraction is reached, after which the rate of production enters terminal decline. This concept has foundation in the recorded data from the oil exploitation industry and has been expressed mathematically by Hubbert (1956). The oil peak was predicted to occur by 2010.

2.9 Environmental Impact of Energy Generation and Utilization

Environmental problems associated with energy use span a spectrum of pollutant emissions, hazards, and accidents, as well as the degradation of environmental quality and natural ecosystems. Over the past few decades, energy-related environmental concerns have expanded from primarily local or regional issues, to the international and global nature of major energy-related environmental problems. Particularly in developing or newly industrialized countries, where energy consumption growth rates are typically extremely high and where environmental management has not yet been fully incorporated into the infrastructure, environmental

problems are becoming apparent or already exist. Nevertheless, industrialized countries are at present mainly responsible for air pollution, ozone depletion, and carbon emissions because of the small contribution of the developing countries.

In the 1970s, concerns about energy use mainly focused on the relationship between energy and economics. At that time, the linkage between energy and the environment did not receive much attention. An institutional structure to deal with environmental problems emerged after the 1970s in most countries. Since the late 1970s, governments have adopted a number of laws on environmental and management policies that were supposed to be the basis of central government decisions relating to economic development and environmental impact. As environmental concerns, such as pollution, ozone depletion, and global climate change, became major issues in the 1980s, interest in the link between energy utilization and the environment became more pronounced (especially in the late 1980s and early 1990s). More recently, some researchers have suggested that the impact of energy resource utilization on the environment is best addressed by considering exergy. The exergy of a quantity of energy or a substance is a measure of its usefulness or potential to cause change, and it appears to be an effective measure of the potential of a substance to impact the environment. Although many studies have been performed on energy and the environment, limited work has been reported on the link between exergy and environment concepts (Rosen and Dincer 1996).

The environmental impact of energy use is reduced by increasing the efficiency of energy-resource utilization (often referred to as energy conservation), and by substituting more environmentally benign energy resources for damaging ones.

During recent decades the environmental impact of human activities has grown dramatically because of increases in the world population, resource consumption, and industrial activity. Throughout the 1970s, most environmental analysis and legal control instruments concentrated on conventional pollutants such as SO_2, NO_x, volatile organic compounds (VOCs, which are gases emitted by various materials and which may have adverse health effects), particulates, and carbon monoxide (CO). Recently, environmental concern has extended to hazardous air pollutants, which are usually toxic chemical substances that are harmful in small doses, as well as to globally significant pollutants such as CO_2. The pollutants referred to above have a variety of effects on the biosphere (Hollander and Brown 1992).

Carbon monoxide is a significant pollutant of urban air, in which it arises mostly from the incomplete combustion of automobile fuels, and poses a human health risk on inhalation. SO_2, a corrosive gas that is hazardous to human health and harmful to the natural environment, is emitted worldwide by natural processes such as volcanoes and sea spray, and by human activities, notably combustion of sulfur-containing fuels (mainly coal and fuel oil), smelting of nonferrous metal ores, oil refining, electricity generation, and pulp and paper manufacturing. SO_2 causes respiratory difficulties, damages plant foliage, and is a precursor of acid precipitation.

Nitrogen oxides (NO_x) are produced when combustion occurs at temperatures high enough for oxygen and nitrogen (mainly in air) to react, and can lead to respiratory problems, low-level ozone formation, and the creation of acids that can damage structures and natural systems. Controlling NO_x emissions is more

Table 2.3 Essential gaseous pollutants and the impacts

Gaseous pollutant	Greenhouse effect	Stratospheric ozone depletion	Acid precipitation	Smog
Carbon monoxide (CO)				
Carbon dioxide (CO_2)	+	+/–		
Methane (CH_4)	+	+/–		
Nitric oxide (NO) and nitrogen dioxide (NO_2)		+/–	+	+
Nitrous oxide (N_2O)	+	+/–		
Sulfur dioxide (SO_2)	–	+		
Chlorofluorocarbons (CFCs)	+	+		
Ozone (O_3)	+			+

"+" stands for a positive contribution, and "–" stands for variation with conditions and chemistry, which may not be a general contributor

challenging than controlling SO_2 because SO_2 emissions come overwhelmingly from large facilities such as power plants which are relatively easy to identify and control, while NO_x sources, most of which are motor vehicles, are smaller, more mobile, and much more numerous and varied. VOCs and petroleum and solvent vapors impede the formation of ozone. Efforts to reduce VOCs emissions have resulted in a 90% reduction in tailpipe emissions of unburned fuels in the U.S. since the 1970s through the use of catalytic converters (Hollander and Brown 1992). Particles in the air (fly ash, sea salt, dust, metals, liquid droplets, soot) come from a variety of natural and human-made sources. Particulates are emitted by factories, power plants, and vehicles, and are formed in the atmosphere by condensation or chemical transformation of emitted gases including SO_x, NO_x, and VOCs. Particulates cause a variety of health and environmental effects including acid precipitation, damage to plant life and human structures, loss of visibility, toxic or mutagenic effects on people, and possibly nonaccidental deaths.

Major areas of environmental concern are described in the following subsections. For each of these items, Table 2.3 presents the pollutants and hazards involved, as well as the cause-and-effect linkage among energy activities, pollutants, and environmental effects.

2.9.1 Global Warming (Greenhouse Gas) Effect

During the past several decades, there has been growing concern over the potential dangers associated with the accumulation of greenhouse gases (i.e., infrared-absorbing gases, such as CO_2) in the atmosphere. Such gases allow solar radiation to penetrate to the earth's surface while reabsorbing infrared radiation emanating from it. In conjunction with this, this environmental problem is also called either the *greenhouse effect* or *global warming*.

The greenhouse effect, also known as the global warming effect, is potentially the most important energy-related environmental problem. The increasing

atmospheric concentration of greenhouse gases such as CO_2, CH_4, halons, N_2O, ozone, and peroxyacetylnitrate augments the atmosphere's ability to trap heat radiated from the earth's surface, thereby raising the surface temperature. The surface temperature increased about 0.6°C over the last century, and as a consequence the sea level is estimated to have risen by perhaps 20 cm. Further changes could have wide-ranging and catastrophic effects on human activities all over the world (e.g., increases in atmospheric concentrations of greenhouse gases in line with predicted fossil fuel consumption could cause the earth's temperature to increase in the next century by 2° to 4°C, causing seal levels to rise 30 to 60 cm by 2100, and such effects as flooding of coastal settlements, displacement of fertile zones for agriculture and food production toward higher latitudes, and a decreasing availability of fresh water. In Table 2.4, the role of various greenhouse gases is given.

Note that some dispute whether CO_2 levels are rising in the atmosphere, and that the quantitative linkage between atmospheric CO_2 levels and global climate change is not well understood. Since energy utilization is a major contributor to environmental degradation, decisions regarding energy policy alternatives require comprehensive environmental analysis.

A schematic representation of this global climate change problem is illustrated in Fig. 2.25. Humankind is contributing through many of its economic and other activities to the increase in the atmospheric concentrations of various greenhouse gases. For example, CO_2 releases from fossil fuel combustion, methane emissions from increased human activity, CFC releases, and deforestation all contribute to the greenhouse effect.

One of the most important aspects is thorough evaluation of the costs of reducing CO_2 emissions. From a developing-country perspective, the discussion of costs and benefits has to take into account the need for policies promoting rapid economic growth. Achieving such a balance between economic development and emissions abatement requires the adoption of domestic policies aimed at improving the efficiency of energy use and facilitating fuel switching, and the implementation of international policies enabling easier access to advanced technologies and external resources.

It is certain that atmospheric CO_2 levels will continue to increase significantly. The degree to which this occurs depends on the fixture levels of CO_2 production and

Table 2.4 Roles of different substances in the greenhouse effect

		Atmospheric concentration				
Substance	ARIRR[a]	Preindustrial (ppm)	Present (ppm)	Annual growth rate (%)	SGEHA[b] (%)	SGEIHA[c] (%)
CO_2	1	275	346	0.4	71	50 ± 5
CH_4	25	0.75	1.65	1	8	15 ± 5
N_2O	250	0.25	0.35	0.2	18	9 ± 2

Data from Aebischer et al. (1989)

[a]Ability to retain infrared radiation relative to CO_2

[b]Share in the greenhouse effect due to human activities (%)

[c]Share in the greenhouse effect increase due to human activities (%)

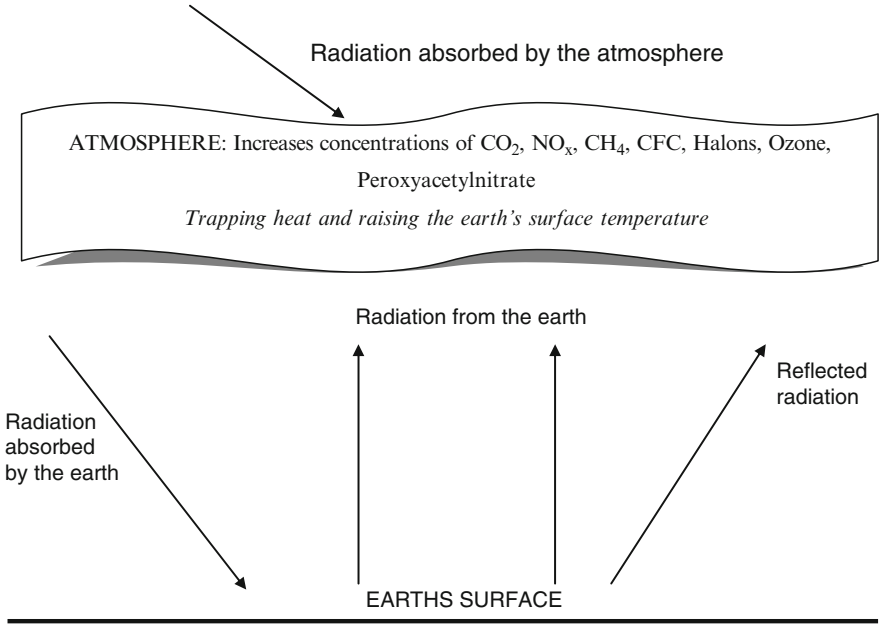

Fig. 2.25 A schematic illustration of the greenhouse effect

the fraction of that production that remains in the atmosphere. Given plausible projections of CO_2 production and a reasonable estimate that half the amount will remain in the atmosphere, indications are that sometime during the middle part of the 21st century the concentration of CO_2 will reach 600 ppm in the atmosphere (Speight 1996).

The arguments about the magnitude of the greenhouse effect have gone back and forth for some time. There are those who believe that the earth is doomed to a rise in temperature, and there are those who believe that we can go on polluting the atmosphere without consequence. Whatever the argument is, there is no doubt that the emissions are harmful and destroy the environment (Bradley et al. 1991). Of course, there are several contradictory reports and arguments published recently that make this field complicated to study. Furthermore, the environment should be considered to be an extremely limited resource, and discharge of chemicals into it should be subject to severe constraints. Nevertheless, in order to conduct a successful environmental study, we should have a clear outline and include the following significant steps:

- Definition of the main goals, both short and long term.
- Measurement or estimation of the data needed as accurately as possible.
- Evaluation of the measurements or estimations.
- Generation of new and reliable data and reporting of the results.

Many developed and developing countries, through several national and international institutes and agencies, have started taking actions to reduce (or eliminate)

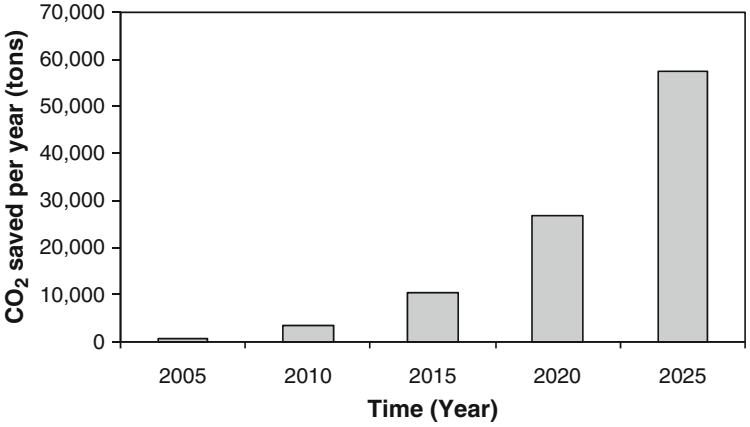

Fig. 2.26 Predicted CO_2 mitigation induced by solar power development in the world [data from Brackmann (2008)]

the pollutant emissions and to attain a sustainable supply of energy sources. In December 1997 the International Kyoto Conference on climate change came up with a list of 15 concrete proposals for curbing global greenhouse gas emissions. The list includes improving the fuel efficiency of automobiles, introducing solar power facilities, and planting forests to act as "green lungs" in densely populated areas.

It is expected that some countries will offer certain tax reductions for those businesses that promote renewable energy technologies, especially because these technologies are characterized by low or zero CO_2 emission. For example, Fig. 2.26 shows the evolution of the global CO_2 mitigation expected from the foreseen solar energy expansion. This figure is based on the data from Brackmann (2008) that predicts the trend of solar energy utilization in future years.

2.9.2 Acid Precipitation

The main sources of acid rain deposition are the emissions of SO_2 and NO_x, and such gases react with water and oxygen in the atmosphere and result in acids such as sulfuric and nitric acids (Dincer 1998) as shown in Fig. 2.27. Acids produced mainly from the combustion of fossil fuels, especially coal and oil, and the smelting of nonferrous ores can be transported long distances through the atmosphere and deposited on ecosystems.

Also, substances such as volatile organic compounds (VOCs), chlorides, ozone, and trace metals may participate in the complex set of chemical transformations in the atmosphere resulting in acid precipitation, the effects of which are as follows: acidification of lakes, streams, and ground waters, resulting in damage to fish and aquatic life; damage to forests and agricultural crops; and deterioration of materials, such as buildings, metal structures, and fabrics. A major source of acid-precipitation

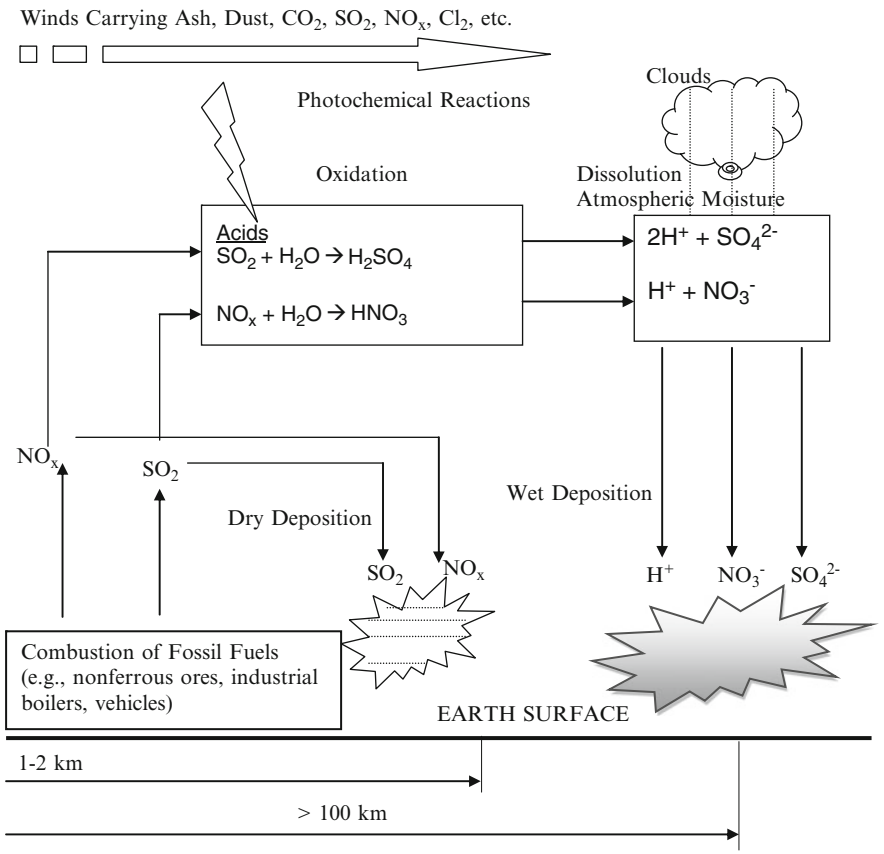

Fig. 2.27 Schematic illustration of the formation, distribution, and impact of acid rain

precursors are energy-related activities (e.g., electric power plants, residential heating, and industrial energy use account for 80% of SO_2 emissions, while road transport accounts for 48% of NO_x emissions in OECD countries).

Another source of acid precipitation is sour gas treatment, which produces H_2S that then reacts to form SO_2 when exposed to air. Road transport is also an important source of NO_x emissions. Most of the remaining NO_x emissions are due to fossil fuel combustion in stationary sources. Countries in which the energy-related activities mentioned here occur widely are likely to be significant contributors to acid precipitation (e.g., U.S., Russia, and China).

A major problem with acid rain is that its effects often occur in a different country than its source. There is a large variety of major evidence to show the damage of acid precipitation as follows:

- Acidification of lakes, streams, and ground waters
- Toxicity to plants from excessive acid concentration

- Corrosion of exposed structures
- Health hazards for fish and aquatic life
- Damage to forests and agricultural crops
- Deterioration of buildings and fabrics
- Harmful effect of sulfate aerosols on physical and optical properties of clouds

Some possible solutions include cleaning fossil fuels before combustion, burning them more cleanly by using fluidized bed technology for coal, using renewable energies, switching to a hydrogen economy, implementing thermal energy storage technologies, promoting efficient public transport, using more fuel-efficient vehicles, and so on.

2.9.3 Impact of Energy Efficiency

The implications of the limited nature of energy and other resources have led in part to significant efforts in energy-utilization efficiency improvement and resource recycling and reuse. For example, refuse and other solid wastes are now often used to supplement fuel supplies. Recycling (resource recovery) extends the lifetimes of many of the natural resources and is often profitable and usually beneficial environmentally. Energy efficiency and conservation can postpone shortages of energy resources, reduce environmental damage, and provide economic benefits. The efficient use of energy is of particular importance to developing countries, as it can forestall the need for very large capital investments.

In the early 1980s, several energy efficiency and conservation measures were applied, such as strict regulations and standards, particularly for cars and buildings; incentive schemes to stimulate energy conservation investments; energy auditing and reporting schemes, especially for energy-intensive industries; encouragement of the use of waste heat from power stations and from industries, such as the cogeneration of heat and electricity; and promotion of relevant research and development. More recently, environmental concerns have increased the usefulness of these and other measures.

Enormous potential exists through improvements in energy efficiency and conservation for decreasing total world energy consumption, and thereby the effects of energy consumption on the environment. Often, such improvements require a myriad of small changes in consumption patterns.

Despite this obstacle, energy efficiency measures can often be implemented quickly since there is a rapid stock turnover for such devices as light bulbs, cars, and refrigerators, unlike for power stations. Despite the high capital costs, many efficiency measures can result in considerable economic savings for both individual consumers and societies (e.g., the benefits of eliminating the need for a new power station through high electricity-utilization efficiency). Such savings are particularly attractive to developing countries that suffer from acute shortages of capital, since investment in new efficient technology is typically much cheaper than retrofitting

old plants. It is therefore important that the expansion of developing country economies, especially the introduction of new industries, is based on the latest technology available, bypassing the inefficient and wasteful technologies that have been used in the industrialized countries.

Increased energy efficiency reduces energy-related environmental impacts such as those discussed in Section 2.9.4 (e.g., environmental damage due to the process of extracting energy resources from the ground, and the competition for water between hydropower and such other uses as agriculture and recreational activities, and associated damage to water quality). In addition, improved efficiency enhances the reliability of future energy supplies and improves the longevity of energy supplies. The potential for energy efficiency is significant during both energy production and consumption (e.g., the 30% of oil in a reservoir that is extracted from onshore wells could be improved upon using secondary recovery techniques, such as water flooding and thermal stimulation).

2.9.4 Other Environmental Impact Aspects

Much concern is focused on the risks and consequences of major environmental accidents, such as explosions and fires at oil/gas refineries, oil rigs, tanks, and pipelines; hydroelectric dam failures, causing flooding and landslides; nuclear accidents; and explosions in mines. Population concentrations often worsen the effects of major accidents in terms of human lives lost and injured or people displaced.

Significant concern exists about the quality and quantity of available water resources including groundwater, because of its role in the supply of drinking and irrigation water. Efforts are continually made to control energy-related pollution causes, such as geothermal fluids containing toxic chemicals; acid drainage from mines; coal wastes; effluents containing hazardous chemicals from power plants and refineries; and thermal pollution from the discharges of cooling systems of power plants.

Although much public concern has concentrated on maritime pollution from large accidental oil spills, the main source of maritime-based pollution remains shipping operations. Annually 1.1 million tons of oil are discharged as a result of regular shipping, and about 400,000 tons comes from tanker accidents (EC 2006).

Economic priorities often cause land particularly suited for sustaining agriculture, housing, or natural ecosystems to be lost. In the energy sector, concern has focused on mining sites and hydroelectric reservoirs; the large land surfaces that might be needed for the large-scale exploitation of renewable energy forms, such as solar power, wind power stations, or biomass production; the sites chosen for large, complex industrial processes, such as fuel refining or electric power generation, and the disposal of solid wastes including radioactive wastes.

Hazardous wastes pose special health and environment threats, and are mainly generated by the chemicals and metal industries. Nonhazardous wastes, such as

bottom ash from power plants and air-pollution control residues, pose disposal problems regarding space and appropriate containment. The commercial use of some solid wastes as building industry products and transportation surfaces is limited by the size of the market.

About 90% of exposure to radiation is due to natural causes and 10% is human-made. Energy activities contribute about 25% of the total human-made radioactivity. Though fossil fuel combustion releases radionuclides, ongoing debate about energy-related radiation centers mainly on the nuclear fuel cycle and its various stages. Radon, which is released in uranium mining and milling, is one of the potential occupational hazards and may cause groundwater contamination. Nuclear waste disposal and facility decommissioning involve varying degrees of hazards depending on the characteristics of the wastes.

Hazardous air pollutants are usually emitted in smaller quantities than those that are the focus of ambient air quality concerns. Lead is the main hazardous air pollutant, and most of the world's lead pollution comes from the use of lead-based gasoline additives to increase octane ratings. Lead exposure may cause neurological damage. Since the 1970s many countries have taken steps to phase out these lead-based additives. Additionally, the number of suspected hazardous pollutants is very large, and knowledge of sources, emissions, and effects is still developing. The concern is both localized, effects where micropollutants are discharged, and regional for the toxic pollutants, such as cadmium, mercury, and polycyclic aromatic hydrocarbons (PAHs). Many energy-related activities emit hazardous air pollutants, such as hydrocarbons (such as benzene) emitted from oil and gas extraction and processing industries; hydrocarbon and dioxin emissions caused by the use and combustion of petrol and diesel oil for transport; small quantities of arsenic, mercury, beryllium, and radionuclides released during the combustion of coal and heavy fuel oil; and mercury, chlorinated dioxin, and furan emissions from municipal waste incinerators.

Air pollution is caused by emissions of toxic gases such as SO_x, NO_x, CO, VOCs, and particulate matter (e.g., fly ash and suspended particles). Excessive concentrations of these pollutants and of ozone have demonstrated health, welfare, and ecological effects felt locally and sometimes regionally. VOCs and NO_x are known to be responsible for photochemical smog. Air pollutants are emitted from a variety of stationary and mobile fuel consumption sources, and energy-related activities contribute significant quantities of all of these pollutants. Regulations on emissions are often used to reduce air pollution, and high chimney stacks are used to alleviate localized air pollution (i.e., transport pollutants elsewhere). Indoor air pollution is also of concern (e.g., CO, CO_2, and smoke from stoves and fireplaces; various gaseous oxides of nitrogen and sulfur from furnaces; stray natural gas and heating oil vapors; radon emitted by natural gas–burning appliances and the surrounding soil; cigarette smoke; formaldehyde from plywood and glues). Ventilation even in tightly sealed energy-efficient buildings can eliminate most indoor air quality concerns. Knowledge of indoor pollutant dose–response relationships is still incomplete.

2.10 Case Study

This example investigates the contributions to sustainable development that are possible through the provision of heat and electricity services via cogeneration, rather than via separate processes for heat production and electricity generation. Cogeneration is the more efficient of these two options for providing such services. The example is intended to be a simple yet practical and realistic illustration of one of the many ways in which increased energy efficiency can contribute to achieving sustainable development in a society.

In the example, the potential benefits are investigated of the simultaneous production of thermal and electrical energy (cogeneration) using the facilities of Ontario Hydro, the principal electrical utility in the province of Ontario, Canada. The main advantage of cogenerating thermal and electrical energy is that less input energy is consumed than would be required to produce the same products in separate processes; additional benefits of cogeneration often include reduced environmental emissions, and more economic, safe, and reliable operation.

This example is based on an investigation performed previously on the benefits of implementing cogeneration in countries and regions. Additional details to those provided here for the example are presented elsewhere (Rosen 1994; Hart and Rosen 1995). The benefits of implementing utility-based cogeneration are examined for the province, by evaluating the changes in energy consumption and environmental emissions when cogeneration is implemented, relative to a base-case year. The example considers the effects of cogeneration implementation on the electrical utility sector, the remainder of the province, and the overall province.

A high degree of cogeneration implementation is assumed. Specifically, an advanced utility-based cogeneration network supplies a large portion of these annual heat demands (i.e., 40% or 206 PJ of the heat demands of the residential, commercial, and institutional sectors, and 12% or 54 PJ of those for the industrial sector). Two main categories of heat demands are partly satisfied through cogeneration:

- Residential, commercial, and institutional processes, which require large quantities of heat at relatively low temperatures (e.g., for heating air and water). Utilization of cogenerated heat in these sectors sometimes involves district heating, where centrally supplied heat (often in the form of hot water or steam) is transported through a network of pipes to users throughout the region.
- Industrial processes, which require heat at a wide range of temperatures (e.g., for drying and boiling).

A detailed procedure described elsewhere (Rosen 1994; Hart and Rosen 1995) was used to determine the numerical values cited earlier in this subsection. Many factors relating to the usability and marketability of utility-cogenerated heat in these sectors were considered, including the following:

- The quantity, supply rate, and temperature of supplied heat must satisfy all demand requirements.

- Users and suppliers of heat must be located within a suitable distance of each other.
- Heat must be available when it is in demand, either by cogenerating when heat is demanded or storing the heat during periods between its generation and utilization.
- An overall infrastructure and all relevant technologies must exist for all cogeneration steps, including heat supply, distribution, storage, and utilization.
- The system must be able to accommodate actual variations in heat-demand parameters (quantity, temperature, etc.).
- The attitude of all parties involved (suppliers, distributors, users, etc.) must be positive.
- The economics for cogeneration options should be at least competitive with, and preferably superior to, the economics for other noncogeneration options.

Table 2.5 lists the base-case annual energy use data in the province in physical units (top section) and energy units (second section), followed by reductions in annual energy use for the example, expressed as a percentage of the corresponding base-case values. Similarly, Table 2.6 lists the base-case annual emissions to the environment for the province (top section) and percent reductions in these emissions.

Table 2.5 Base-case annual energy use in Ontario and percent reductions in base-case values for the cogeneration scenario

Base-case energy use (PJ)	Electricity	Gas and NGLs	Oil and petrol	Coal	Other	Uranium	Total
Utility sector	–	–	14	286	–	640	940
Province (excl. utility)	477	824	782	21	158	–	2,262
Province (total)	477	824	796	307	158	640	3,202
Base-case energy use (physical units)	Electricity (TWh)	Gas and NGLs (teraliters)	Oil and petrol (gigaliters)	Coal (mega-tons)	Other (kilo-tons)	Uranium (tons)	
Utility sector	–	–	0.33	10.4	–	1,040	
Province (excl. utility)	132	21.0	21.5	0.71	5,340	–	
Province (total)	132	21.0	21.8	11.1	5,340	1,040	
% Reductions in values							
Utility sector	–	–	0.0	47	–	35	82
Province (excl. Utility)	30	15	2.6	5.6	7.5	–	60.7
Province (total)	30	15	2.6	44	7.5	35	155.1

Note: Hydraulic energy use is not shown since it is free. The "other" energy category includes coke and coke oven gases, which are originally produced from coal, the energy value of uranium to be heated from fission delivered from the nuclear reactor to the power cycle. NGLs denote natural gas liquids. Total base-case annual energy use for the overall province (3,200 PJ) includes the shown primary energy forms, as well as the secondary from, electricity. PJ denotes petajoule (10^{15} J)

Table 2.6 Base-case annual emissions in Ontario and percent reductions in base-case values for the cogeneration scenario

Base-case emissions to the environment (PJ)	Pollution (10^{15} Bq)	Material emissions (kilotons)					Thermal VOC	Radiation spent	Uranium
		SO_2	No_x	CO_2	CO	Particulates			
Utility sector	321	92	32,000	4	11	0.5	1.04	591	11
Province (excl. utility)	1,060	526	132,000	3,500	837	755	–	–	–
Province (total)	1,380	618	164,000	3,504	849	775	1.04	591	11
% Reductions in values									
Utility sector	47	47	47	47	47	47	35	83	35
Province (excl. utility)	8.8	4.8	7.4	4.2	1.6	2.9	–	–	–
Province (total)	18	12	15	4.2	2.1	3	35	83	35

Note: VOCs denote volatile organic compounds. Thermal pollution is taken to be heat rejected to bodies of water, so as to cause appreciable temperature rises. Radioactive emissions from non–nuclear-energy sources, such as radioactivity in coal-station stack gases, have not been considered. PJ denotes (10^{15} J) and Bq denotes becquerel

The key points demonstrated are that energy use and environmental emissions decrease for the utility sector, the rest of the province, and the overall province; and provincial electricity generation requirements decrease. Specific implications of these findings are significant:

- Provincial annual electricity consumption decreases by as much as 30%, permitting provincial annual electrical generation to decrease correspondingly.
- For the electrical utility sector, annual coal use and coal-related emissions both decrease by up to 47%, while annual uranium use and related emissions both decrease by up to 35%.
- Excluding the electrical utility sector, the province's annual use of fossil fuels and the corresponding annual emissions both decrease by up to 15%.

This example demonstrates that the increased energy-utilization efficiency that can be achieved through cogeneration in a region or country can contribute to attaining sustainable development by doing the following:

- Reducing significantly the amounts of energy resources required to satisfy given energy demands
- Reducing significantly the environmental emissions (and related societal impacts) associated with satisfying the energy demands

It is noted that this is but one limited illustration of how increased energy efficiency can contribute to sustainable development. Numerous other areas in which increased energy efficiency can contribute exist in any society.

2.11 Concluding Remarks

In this chapter, a summary of some general introductory aspects of energy perspectives was presented. Predictions of energy consumption and population growth were correlated, and the environmental impact of energy use was discussed. One relevant case study was presented.

Nomenclature

E Energy consumption, EJ
Q Heat rate, W
R Mean square error
T Temperature, K
Y Year

Greek Letter

η Energy efficiency

Subscripts

ge	Green energy
H	Hot
L	Low
ng	Natural gas
S	Sun
wpc	World primary energy consumption

References

Aebischer B., Giovannini B., Pain D. 1989. Scientific and Technical Arguments for the Optimal Use of Energy. IEA, Geneva.

Blackwell D.B., Steele, J.L., Carter, L.S. 1991. Heat-flow patterns of the North American continent; a discussion of the geothermal map of North America. In: Neotectonics of North America, D.B. Selmons, E.R. Engdahl, M.D., Zoback, and D.B. Blackwell, eds., Vol. 1, 423–436, Geological Society of America, Boulder, CO.

BP 2008. British Petroleum Statistical Review of World Energy, June. London, UK. Internet source http://www.bp.com/centres/energy/index.asp (accessed on September 15, 2008).

Brackmann G. 2008. Concentrated solar thermal power now! Internet source http://www.greenpeace.org/raw/content/international/press/reports/Concentrated-Solar-Thermal-Power.pdf (accessed on May 26, 2008).

Bradley R.A., Watts E.C., Williams E.R. 1991. Limiting Net Greenhouse Gas Emissions in the United States. U.S. Department of Energy, Washington, DC.

Dincer I. 1998. Energy and environmental impacts: present and future perspectives. *Energy Sources* 20:427–453.

EC 2006. World Energy Technology Outlook—2050. WETO-H_2. European Commission.

EIA 2000. Historical Natural Gas Annual 1930 through 2000. Energy Information Administration, Department of Energy, report DOE/EIA-E-0110(00).

EIA 2008. International energy outlook 2008, Energy Information Administration, Report DOE/EIA-0484, June 2008.

Ermis K., Midilli A., Dincer I., Rosen M.A. 2007. Artificial neural network analysis of world green energy use. *Energy Policy* 35:1731–1743.

Goswami D.Y., Kreith F. 2008. Energy Conversion. CRC Press, Taylor and Francis Group, Boca Raton, FL.

Hart D.R., Rosen M.A. 1995. Environmental and health benefits of utility-based cogeneration in Ontario. *Energy and Environment* 5:363–368.

Hollander J.M., Brown D. 1992. Air pollution. In: The Energy-Environment Connection, J.M. Hollander, ed., Island Press, Washington, DC, pp. 15–49.

Hubbert M.K. 1956. Nuclear Energy and the Fossil Fuels 'Drilling and Production Practice'. American Petroleum Institute. Internet source http://www.hubbertpeak.com/hubbert/1956/1956.pdf (accessed on September 22, 2008).

IEA 2006. Medium Term Oil Market Report. International Energy Agency, July.

IEA 2008. Oil Market Report. International Energy Agency, September.

NRC 2005. Canadian Natural Gas, Review of 2005 and Outlook to 2020. Natural Resources of Canada, Natural Gas Division, Petroleum Resources Branch, Energy Policy Sector.

Pincock 2004. Trends in US Domestic Coal Markets. Pincock Perspectives 58.

Price R., Blaise J.R. 2002. Nuclear fuel resources: enough to last? *Nuclear Energy Agency News* 2:10–13.

Reis A.H., Bejan A. 2006. Constructal theory of global circulation and climate. *International Journal of Heat and Mass Transfer* 49:1857–1875.
Rosen M.A. 1994. Assessment of various scenarios for utility-based cogeneration in Ontario, *Energy—The International Journal* 19:1143–1149.
Rosen M.A., Dincer I. 1996. Linkages between energy and environment concepts, Proceedings of the TIEES-96 First Trabzon International Energy and Environment Symposium (T. Ayhan, I. Dincer, H. Olgun, S. Dost and B. Cuhadaroglu, eds.), pp. 1051–1057, 29–31 July, Karadeniz Technical University, Trabzon, Turkey.
Speight J.G. 1996. Environmental Technology Handbook. Taylor & Francis, Washington, DC.
Tiwari G.N., Ghosal M.K. 2007. Fundamentals of Renewable Energy Resources. Alpha Science International Ltd., Oxford, UK.
WEC 2007. Deciding the Future: Energy Policy Scenarios to 2050. World Energy Council.
Workbook 2005. Statistical Review of World Energy 2005. Internet source http://www.bp.com/statisticalreview (accessed on May 26, 2008).

Study Questions/Problems

2.1 What is the relationship among the use of renewable energy sources, environment, and sustainability?
2.2 What is the relationship among energy efficiency, environment, and sustainability?
2.3 Give a definition of sustainable energy engineering.
2.4 Enumerate and describe briefly the fundamental energy sources on earth.
2.5 Explain the nature of biomass energy.
2.6 Calculate the reaction enthalpy of glucose formation process by photosynthesis, according to the reaction $6CO_2 + 6H_2O \xrightarrow{\text{LIGHT}} C_6H_{12}O_6 + 6O_2$.
2.7 Calculate how many kilograms of green wood produce the same amount of energy as 1 kg of dry wood. Calculate how many cubic meters of green wood are equivalent in energy terms to 1 cubic meter of dry wood.
2.8 Make a prediction of world coal consumption by 2100, based on linear extrapolation of statistical data. Compare the linear prediction with that given by Eq. (2.1).
2.9 Explain the oil peak theory by Hubert.
2.10 What are the main environmental impacts of energy generation and utilization?
2.11 Explain the global warming effect.
2.12 Explain the acid precipitation formation and its environmental effect.
2.13 Comment on the energy efficiency impact on the environment.
2.14 Using the case study 2.10 as guideline, try to quantify the environmental benefit of cogeneration of power and heat within a geo-economic region.
2.15 Comment on the impact of distributed energy systems on sustainability.

Chapter 3
Global Warming and Climate Change

3.1 Introduction

The term climate refer to the average weather over a long period of time, which, based on the recommendations of the World Meteorological Organization, is 30 years. Weather is described by a set of local parameters such as the earth surface temperature, humidity, precipitation level, wind speed, and so on; nevertheless, the temperature is the most significant one. Global climate is also mainly defined by the average earth temperature, for which the currently adopted value is 15°C. The temperature of the earth is a consequence of the thermal radiation energy balance among the earth, the sun, and the extraterrestrial space.

The terrestrial atmosphere plays a major role on establishing the earth climate for two main reasons: (1) the reflection, back to extraterrestrial space, of the direct solar radiation by the clouds; and (2) the greenhouse gases (GHGs) that absorb the radiation emitted by the earth and reradiate it mostly back, toward the earth's surface. It is demonstrated and broadly accepted that the anthropogenic emissions of gases in the atmosphere, specific to the industrial era that began in the eighteenth century, affected and will further affect the global climate.

The massive carbon dioxide emissions from fossil fuel combustion produced an increase of the concentration of GHGs in the atmosphere. The effect of this fact is the creation of a radiative unbalance that tends to produce global warming. On the other hand, aerosol emissions caused by industrial activity (including fossil fuel combustion) increase the earth albedo. Aerosols are fine solid or liquid particles, in general, emitted by natural (water droplets) or anthropogenic sources (e.g., soot and smog) that rise in the air and eventually contribute to cloud formation. More aerosol emission means more cloud formation, and therefore enhanced reflection of solar radiation by the atmosphere. This effect reduces the earth's temperature. Thus, the anthropogenic GHG and aerosol emissions have the opposite effects on the climate. However, in the present global industrial setting, the planet warming effect is the dominant one.

New technologies can and will lessen damaging environmental impacts if they are employed wisely, guided by the market system and by factors such as better efficiency, better cost-effectiveness, better use of energy resources, a better

İ. Dinçer and C. Zamfirescu, *Sustainable Energy Systems and Applications*,
DOI 10.1007/978-0-387-95861-3_3, © Springer Science+Business Media, LLC 2011

environment, better energy security, and better sustainable development. Intensifying global environmental problems require internationally coordinated responses, which must balance the goals of energy security, environmental protection, and economic growth. One recent event, the Global Conference on Global Warming, held in 2008 in Istanbul, which brought together specialists from various areas, including energy technology, ecology, economy, and policy, discussed the global solutions to the global problem of earth warming and climate change (see Duffey and Dincer 2010). The adoption of a comprehensive approach to energy and environment issues and the integration of energy and environment policies have become central activities of several countries.

In this chapter, we analyze the effect of anthropogenic activity on climate change and global warming. We first discuss the thermal radiation energy balance of the planet, which is the basis for understanding and modeling the earths climate. A series of relevant concepts and notions are introduced here. Next, we quantify the effect of anthropogenic gas emissions in the atmosphere on climate change. Lastly, a number of possible ways to reduce the harmful anthropogenic effects, including novel technologies and policies, are presented and discussed.

3.2 Analysis and Modeling of the Earth's Climate

In Chapter 1we introduced all the fundamental forms of energy on the earth, among which solar radiation is the most important. We analyzed the radiation balance on the earth's atmosphere, with the purpose of deriving the amount of solar energy available on the earth. In this section, we revisit the radiation balance on the earth, this time with the purpose of explaining and quantifying the greenhouse effect of the atmospheric gases. Further, several important concepts and quantities relevant to earth climate analysis and modeling are introduced.

3.2.1 Radiation Balance of the Earth Planet

Figure 3.1 represents a simplified radiation balance of the earth's atmosphere that is essential for explaining the greenhouse effect. The earth's atmosphere comprises several layers of gases, of which the most important are the troposphere, stratosphere, and mesosphere, all three extending the earth's radius by less than 1%. That is, the layers of gases around the earth surface are extremely thin with respect to the size of the planet. However, these gases play an essential role in establishing the climate and surface temperature. This role can be summarized as follows:

- The stratospheric ozone reflects the high-energy radiation back to outer space, diminishing the radiation energy; ozone is mostly responsible for the albedo of the earth.

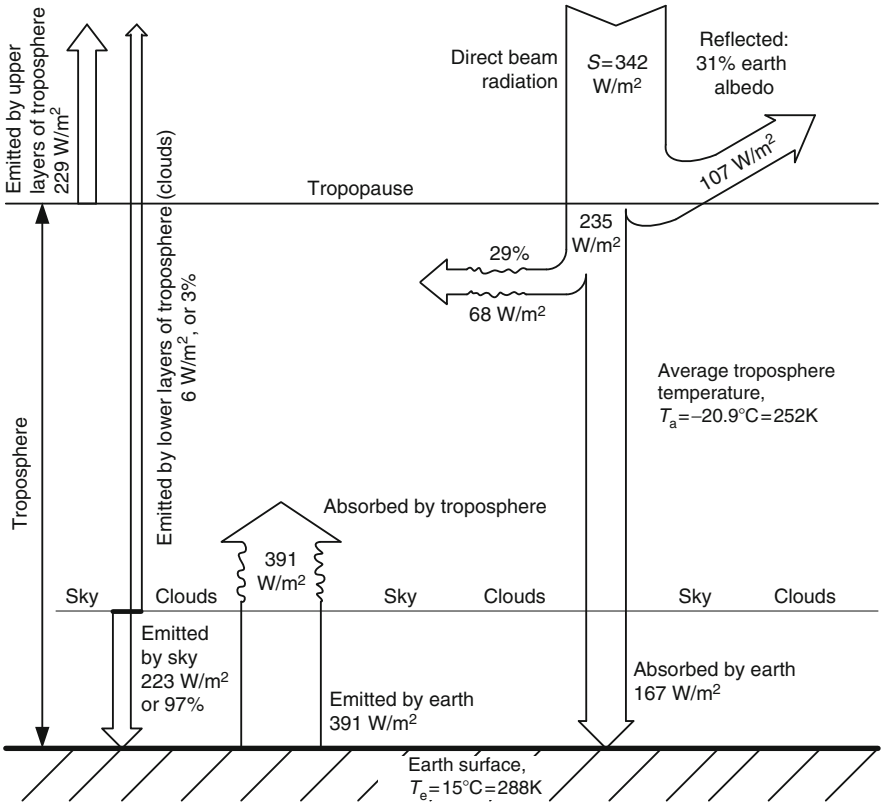

Fig. 3.1 Simplified radiation balance of the earth's atmosphere, explaining the greenhouse effect [data from Boyle (2004)]

- The troposphere, which is the layer closest to the earth's surface, absorbs a part of the incident solar radiation.
- The troposphere also absorbs an important part of the radiation emitted by the earth's surface, generating thus the greenhouse effect of the earth.

The greenhouse effect is a natural phenomenon occurring in the atmosphere that is necessary to control the average earth temperature and climate. Anthropogenic activity induced an intensification of the greenhouse effect that led to global warming.

The solar constant, discussed also in other parts of the book, can be approximated with the average value of 1,368 W/m^2. This represents the radiative power per area of the disk representing the projection of the earth on a plane normal to the direction of the sun. This disk has the area πR^2, where R is the radius of the earth. Only one hemisphere of the earth is illuminated by the sun, therefore, the incident radiation distributes at a certain moment over a hemisphere. However, considering the annual average effect of solar radiation, one can conclude that solar radiation

distributes over the whole globe's surface, which is approximated with the surface of a sphere, namely $4\pi R^2$. Therefore, the average solar radiation intensity per every square meter of outer atmosphere surface is four times smaller than the solar constant, that is $S = 1{,}368/4 = 342\ \mathrm{W/m^2}$.

Figure 3.1 shows that 31% of the solar radiation amounting to 107 $\mathrm{W/m^2}$ is reflected back to the extraterrestrial space due to the earth's albedo. The remaining radiation of 235 $\mathrm{W/m^2}$ penetrates the troposphere, where it is absorbed in a proportion of about 29% (68 $\mathrm{W/m^2}$), and the rest of the 167 $\mathrm{W/m^2}$ is absorbed by the earth. The earth emits blackbody radiation at the average earth temperature, which is 15°C; this radiation is 391 $\mathrm{W/m^2}$. The clouds emit blackbody radiation at the average temperature of the troposphere, which can be approximated as −20.9°C. Most of the radiation emitted by the clouds (97%), which can be considered as the bottom layer of the troposphere, is directed toward the earth's surface, since the clouds are mostly exposed to the earth's surface; this amounts to 224 $\mathrm{W/m^2}$. A smaller part (~5%) of the radiation emitted by the clouds crosses the troposphere and is directed toward extraterrestrial space. The outer layer of troposphere, called the tropopause, also emits radiation at the average temperature. Since this layer is at ~10 km above the earth, it is reasonable to assume that all the radiation is emitted toward extraterrestrial space; this amounts to 229 $\mathrm{W/m^2}$.

The radiative balance in the troposphere for the simplified model from Fig. 3.1 is

$$S(1-\alpha_{\mathrm{albedo}})\alpha_{\mathrm{abs}} + \sigma T_{\mathrm{e}}^4 = 2\sigma T_{\mathrm{a}}^4, \tag{3.1}$$

where α_{albedo} is the assumed albedo factor of 0.31, α_{abs} is the assumed absorption coefficient of the direct radiation in the troposphere, the term σT_{e}^4 represents the radiation emitted by the earth's surface, and the term $2\sigma T_{\mathrm{a}}^4$ represents the radiation leaving the troposphere at the lower and upper layer. Assuming the earth's surface temperature $T_{\mathrm{e}} = 15°\mathrm{C} = 288\ \mathrm{K}$, it results that $\sigma T_{\mathrm{a}}^4 = 229.5\ \mathrm{W/m^2}$ and therefore the average troposphere temperature $T_{\mathrm{a}} = -20.9°\mathrm{C} = 252\ \mathrm{K}$. This value is consistent with observations because the temperature at the tropopause is −55°C, while the mean air temperature in the vicinity of the earth's surface is 15°C, resulting in an average of −20°C.

The radiative balance at the earth's surface is

$$S(1-\alpha_{\mathrm{albedo}})(1-\alpha_{\mathrm{abs}}) + x\sigma T_{\mathrm{a}}^4 = \sigma T_{\mathrm{e}}^4, \tag{3.2}$$

where the term $S(1-\alpha_{\mathrm{albedo}})(1-\alpha_{\mathrm{abs}}) = 167\ \mathrm{W/m^2}$, which represents the direct beam radiation incident on the earth's surface, the term $x\sigma T_{\mathrm{a}}^4 = 229.5x$ is the radiation emitted by the sky in the direction of the earth's surface, and with $T_{\mathrm{e}} = 15°\mathrm{C}$ the radiation emitted by the earth becomes $\sigma T_{\mathrm{e}}^4 = 391\ \mathrm{W/m^2}$. Thus, the value of factor x is ~0.97.

As a first approximation, the influence of the greenhouse effect on the earth's and the troposphere's temperature can be determined by varying the factor x in the radiative balances in Eqs. (3.1) and (3.2). We assume that the albedo and the

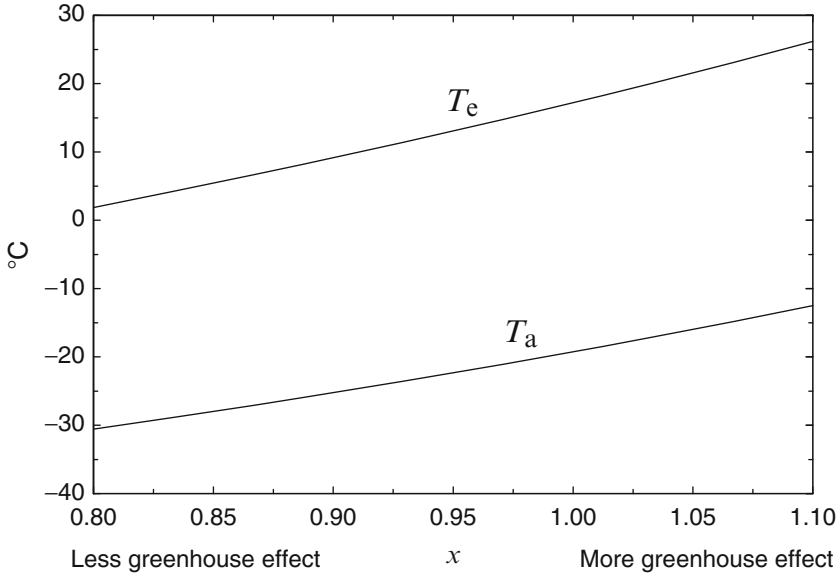

Fig. 3.2 The influence of the greenhouse effect on the earth's and the troposphere's temperatures

atmospheric absorption of direct solar radiation remain the same. There are two possibilities:

- The anthropogenic activity results in more GHG emissions. Since these gases will be more concentrated in the lower layers of the atmosphere, where human activity occurs, the troposphere reradiates more toward the earth's surface. Mathematically, this means that factor x increases.
- The GHG concentration reduces in the vicinity of the earth's surface and concentrates toward the upper layers for some unknown reason. In this case, the troposphere reradiates less toward the earth. This means a decrease in the x factor.

Figure 3.2 shows the effects of GHG concentration in the atmosphere, quantified here by the x factor on the average temperatures of the earth's surface and the troposphere. If the greenhouse effect is less, the atmosphere and the earth's surface cool down. For example, a 3% reduction in the greenhouse effect induces a temperature decrease on the earth of ~3°C. Conversely, if the GHGs concentrate and enhance the greenhouse effect, the temperature increases. Overall, one can roughly estimate that the temperature variation is of 1°C for each 1 percent of greenhouse effect intensity change.

One essential feature can be observed in connection with the model introduced in Fig. 3.1, namely, that the atmosphere absorbs more radiation from the earth than it does from the sun. In the simplified radiative balance, the absorption of solar radiation by the atmosphere is ~68 W/m^2, while the absorption of the radiation emitted by the earth is 391 W/m^2; that is, the atmosphere absorbs ~83% less radiation from the earth than from the sun. The physical explanation of this fact

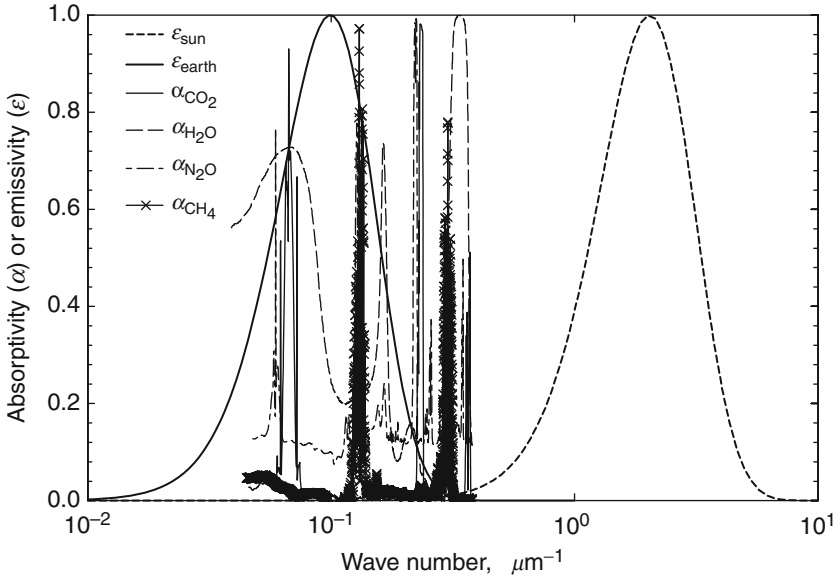

Fig. 3.3 Spectra of greenhouse gas absorption superimposed over emission spectra of earth and sun [data from NIST Chemistry Webbook (2005)]

can be contemplated in connection to Fig. 3.3, which presents the spectra of the main radiative fluxes involved in the earth's energy balance.

In Fig. 3.3, the earth and the sun are modeled as blackbodies that emit radiation corresponding to their temperature. The earth's temperature has been taken to be 288 K while the sun's temperature is 5,900 K. The emission spectra have been normalized with respect to their maximum value in order to plot the results over a scale of 0 to 1. The wave number is defined as the reciprocal of the wave length. Plotting against the wave number is a matter of choice: we choose to represent the higher energy fluxes toward the right of the horizontal scale, which appears to be more intuitive. On the same plot, we superimposed the absorption spectra of the main GHGs present in the atmosphere. These are carbon dioxide, water vapor, nitrous oxide, and methane. The data for plotting the spectra of GHGs are taken from the National Institute of Standards and Technology (NIST) Chemistry Webbook (2005). One can clearly observe that the absorption spectra of GHGs overlay the emission spectrum of the earth, which falls in the infrared region. This explains the physics behind the greenhouse effect—the selective absorption of the atmosphere, which absorbs infrared and transmits mainly visible and ultraviolet radiation.

3.2.2 Greenhouse Gases

The relevant properties of the principal GHGs except water in the atmosphere are presented in Table 3.1. Water vapor is the most important GHG. However, the

Table 3.1 The principal greenhouse gases and their approximated concentration in the atmosphere

Gas	Chemical formula	Spectral range (cm^{-1})	Atmospheric concentration		Atmospheric lifetime (years)
			Year 1750	Current	
Carbon dioxide	CO_2	550–800	280 ppm	387 ppm	50–200
Methane	CH_4	950–1,650	700 ppb	1,750 ppb	12
Nitrous oxide	N_2O	1,200–1,350	270 ppb	314 ppb	120
CFC11	$CFCl_3$	800–900	Zero	251 ppt	50
CFC12	CF_2Cl_2	875–950	Zero	538 ppt	102

ppm parts per million; *ppb* parts per billion; *ppt* parts per trillion
Data from IPCC (2007)

water vapor concentration in the atmosphere fluctuates rapidly, and water vapor absorbs radiation from the wide infrared spectrum. Therefore, water vapor as a GHG warrants a separate discussion. Three of the gases shown in the table, namely, carbon dioxide, methane, and nitrogen dioxide, are both part of the natural cycles of carbon and nitrogen and part of the anthropogenic emissions; therefore, they were present in the atmosphere prior to the industrial era, for which the year 1750 is considered as the reference. As seen, the concentration of these gases in the year 1750 is higher than zero. Two other man-made substances are shown in Table 3.1, which are examples of GHGs; these are freons.

Their concentration in the preindustrial era is nil. However, since their invention in the twentieth century, their concentration in the atmosphere started to increase. The table shows the spectral range, given in terms of wave number, for each gas and also indicates the atmospheric lifetime, which is a concept detailed in subsequent paragraphs. For now, observe that the atmospheric lifetime of freons is very high as well as that of nitrous oxide (which today is also an emission mainly from human activity). Other GHGs are a result of human activity, but they are emitted in a lower quantity and, as a result, their actual concentration in the atmosphere is low. Here is a nonexhaustive list of other gases, given in decreasing order of their influence on the greenhouse effect: 1,1,2-trichloro-1,2,2-trifluoroethane (CFC113), chlorodifluoromethane (HCFC22), CFC141b, CFC 142b, 1,1,1-trichloroethane (CH_3CCl_3), carbon tetrachloride (CCl_4), and 1,1,1,2-tetrafluoroethane (HCFC134a).

The lifetime of a mass m_0 of a gas present in the atmosphere depends on the gas reactivity with other species and its circulation as a part of one of the natural biogeochemical cycles. Methane, for example, is more reactive than CO_2, a fact that can be seen by observing the formation of enthalpies of these two substances (4.7 MJ/mol vs. 8.9 MJ/mol, respectively). The temporal decrease of the gas mass in the atmosphere, relative to the initial quantity, can be modeled with an exponential of the form

$$\frac{m}{m_0} = e^{-t/\tau}, \tag{3.3}$$

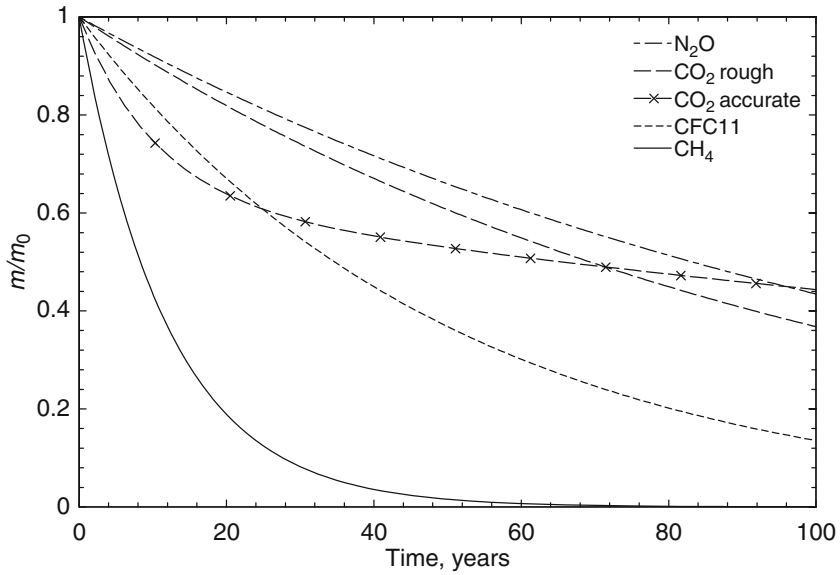

Fig. 3.4 Illustrating the concept of atmospheric lifetime of atmospheric gases

where t is the time measured from the initial moment and τ is known as the atmospheric lifetime.

The atmospheric lifetime can be estimated for each species. Based on the data from Table 3.1, the fraction of gas mass existent in the atmosphere is calculated with Eq. (3.3) and plotted in Fig. 3.4. The atmospheric lifetime is a useful parameter when modeling the concentration of atmospheric gases.

The carbon dioxide lifetime is variable, because it depends on the difference between release and uptake specific to the carbon cycle. Figure 3.4 assumes an average lifetime of CO_2 of 100 years. Enting and Newsam (1990) provide a more accurate decay equation for carbon dioxide in the form of a weighting average of two atmospheric lifetimes, namely of $\tau_1 = 10.4$ and $\tau_2 = 291.5$ years; this equation reads:

$$\frac{m_{CO_2}}{m_0} = 0.375\mathrm{e}^{-t/\tau_1} + 0.625\mathrm{e}^{-t/\tau_2}. \tag{3.4}$$

The accurate prediction of Eq. (3.4) is indicated on the same plot. The many sources and sinks of carbon flow in/out of the atmosphere, making the predictions of the rough model quite inexact. Here are the most important paths through which carbon dioxide communicates with the terrestrial atmosphere:

- Ocean absorption, ~3 Gt carbon per annum
- Anthropogenic—fuel combustion, cement production, etc., ~6 Gt carbon per annum
- Tropical deforestation, ~2 Gt carbon per annum
- Storage in the atmosphere, ~3.5 Gt carbon

3.2.3 Radiative Forcing Concept

Revisiting the radiative energy balance from Fig. 3.1, one notices that at steady state the incoming radiation crossing the tropopause in one direction $S = 342\ \mathrm{W/m^2}$ is equal to the outgoing radiation crossing in the other direction $107 + 229 + 6 = 342\ \mathrm{W/m^2}$. At this balance, the average temperature at the troposphere and the earth's surface temperature are $-20°\mathrm{C}$ and $15°\mathrm{C}$, respectively. Assume something happens that perturbs the energy balance. If more incident radiation enters than the radiation that leaves, the climate on earth, which we define for the purpose of the present explanation as the temperature of the troposphere and at the earth's surface, will also change so that the energy inventory is rebalanced. If there is a net incoming radiation, the global temperature increases, and vice versa, if there is a net outgoing energy flux, the planet cools. The following main factors can affect the net flux of radiation energy crossing the tropopause:

- A variation of the solar radiative flux; this can happen periodically for two main reasons, namely, the sun's temperature varies with a period of ~11 years, and the distance between the earth and the sun varies with a period of 1 year.
- The concentration of GHGs in the atmosphere changes; this can be caused by natural phenomena or, more recently, by anthropogenic emissions of GHGs.
- The concentration of aerosols and other particulate matter changes in the atmosphere; this is also a great proportion of the anthropogenic effect, because soot and particulate matter from fuel combustion and jet airplanes increase in the atmosphere and concentrate at higher levels than in the past, thus increasing the earth's albedo, reflecting and scattering more radiation that eventually is directed mainly toward extraterrestrial space. Natural aerosols also exist, such as water vapors and cloud formation.
- Changes in the concentration of stratospheric and tropospheric ozone; the depletion of stratospheric ozone reduces the earth's albedo, increases the net incoming flux of radiation, and produces negative radiative forcing; the tropospheric O_3 produce positive radiative forcing.

Radiative forcing is defined as the net change in radiation balance at the tropopause, produced by a specified cause. By convention, the radiative forcing is positive if it induces an increase in the planet's temperature and negative if it decreases the planet's temperature. The unit of measure of radiative forcing is the same as the unit of radiation energy rate per square meter of the earth's surface, where the earth's surface, by convention, is the area of the sphere having the average radius of the planet. The usual symbol for the radiative force is ΔF. Typical values of radiative forcing are 0 to 2 $\mathrm{W/m^2}$. It can be derived from the change in the concentration of GHGs, aerosols, and atmospheric ozone, as explained above, which induces radiative forcing. Depending on the concentration of the gas in the atmosphere, there are three regimes for producing radiative forcing: low, moderate, and high concentration.

The low-concentration regime addresses gases present in the atmosphere in parts per billion (ppb) or parts per trillion (ppt). In this case, the forcing is proportional to the concentration change, $\Delta F \sim \Delta C = C - C_0$. Freons and tropospheric ozone fall in this category. According to the Intergovernmental Panel on Climate Change (IPCC 1990, 2001), the proportionality constants are as follows: 0.25 for CFC11, 0.32 for CFC12, and 0.02 for tropospheric O_3.

In the moderate concentration regime, because the gas molecule at higher concentration absorbs considerable radiation where the absorption band is the strongest, the absorption rate for the broader range of the spectrum diminishes. For this reason, the radiative forcing is proportional to the root of the concentration, $\Delta F \sim \left(\sqrt{C} - \sqrt{C_0}\right)$. This is the case for methane and nitrous oxide molecules, for which the concentration is also of ppb, but their relative effect is higher due to a more active absorption spectrum. According to the IPCC (2001), the radiative forcing of methane and N_2O is given as follows:

$$\begin{aligned} \Delta F_{CH_4} &= 0.036\left(\sqrt{M} - \sqrt{M_0}\right) - f(M, N_0) + f(M_0, N_0), \\ \Delta F_{N_2O} &= 0.12\left(\sqrt{N} - \sqrt{N_0}\right) - f(M_0, N) + f(M_0, N_0), \end{aligned} \quad . \tag{3.5}$$

where M is the methane and N is the nitrous oxide concentrations, respectively, and index 0 refers to the initial situation. The effect of methane and nitrous oxide on radiative forcing overlap is accounted for by the following overlapping function given by IPCC (2001):

$$f(M,N) = 0.47 \ln\left[1 + 2.01 \times 10^{-5}(M \times N)^{0.75} + 5.31 \times 10^{-15} M (M \times N)^{1.52}\right]. \tag{3.6}$$

The third regime—highly concentrated gases—corresponds to carbon dioxide only, where because of the high concentration any further change produces less effect. In this situation, the radiative forcing is proportional to the variation of the natural logarithm of the concentration. The following equation is given by IPCC (2001):

$$\Delta F_{CO_2} = 5.35 \ln\left(\frac{C}{C_0}\right). \tag{3.7}$$

In Fig. 3.5, we show based on IPCC (2007) that the radiative forcing is produced from various causes. The total radiative forcing that represents the superposition of all individual anthropogenic type components is also indicated. Knowing the total radiative forcing that creates the opportunity to define an equivalent carbon dioxide concentration that is present alone in the atmosphere creates the same overall forcing. By equating $\Delta F_{CO_2^{eqv}} = \Delta F_{total}$ and using Eq. (3.7) one can obtain

$$C_{eqv} = C_0 \times \exp\left(\frac{\Delta F_{total}}{5.35}\right), \tag{3.8}$$

where C_0 is the initial concentration of carbon dioxide in the atmosphere.

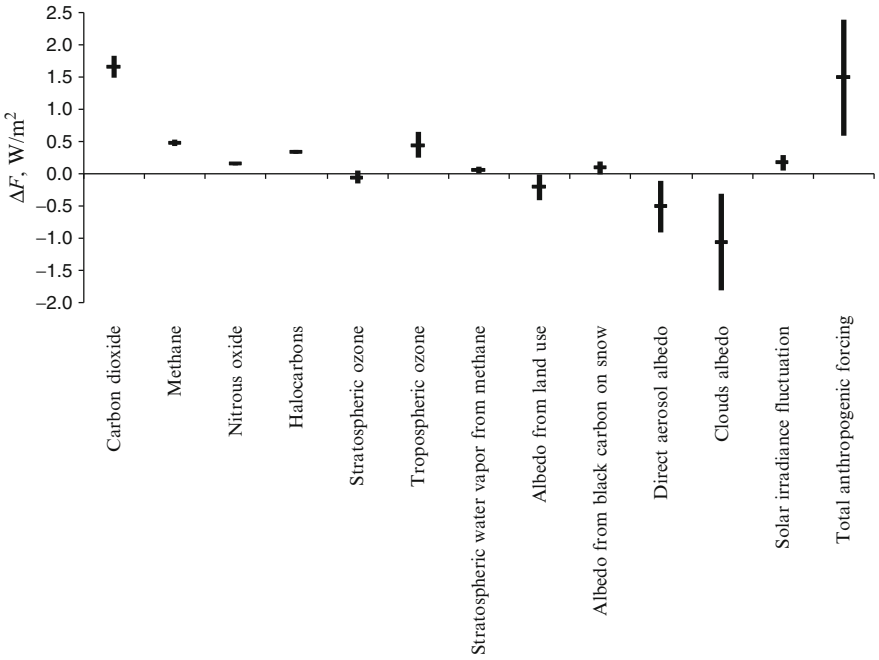

Fig. 3.5 The radiative forcing in 2005 with respect to the year 1750, due to various causes of change [data from IPCC (2001)]

Therefore, the radiative forcing can be expressed in terms of equivalent carbon dioxide concentration change, C_{eqv}/C_0. To show how this is useful for data interpretation, one can infer from Fig. 3.5 that the radiative forcing due to carbon dioxide emission in the industrial era has the average of 1.66 W/m^2. The total anthropogenic forcing is 1.6. Therefore, the relative change in carbon dioxide concentration is $\exp(1.6/5.35) = 1.35$. The equivalent carbon dioxide for this growth, based on the value of $C_0 = 280$ ppm given in Table 3.1, is $C_{eqv} = 378$ ppm. Note from Table 3.1 that the carbon dioxide concentration is currently 387 ppm, which is larger than the equivalent carbon associated with the industrial era. This situation is explained by the fact that the radiative forcing accounts for both positive and negative effects on the radiation balance of the planet.

The usefulness of radiative forcing or the equivalent carbon comes from the possibility of correlating the forcing with the global temperature change. One asks how much change in the planets temperature is produced by a given total radiative forcing. In this respect, a so-called *climate sensitivity factor* γ can be introduced as follows (see Rubin 2001):

$$\gamma = \frac{\Delta T_e}{\Delta F_{total}}, \tag{3.9}$$

where ΔT_e is the corresponding temperature variation that can be caused by ΔF_{total}.

Rubin (2001) compiles the results of two relevant studies published prior to 1979 that give constant approximations for the climate sensitivity factor in the range of 0.55 to 0.65 K m^2/W. An average value of 0.6 K m^2/W can be assumed for the first approximation calculations.

The IPCC (2007) report summarizes the results of climate change prediction based on thorough simulations that account for many relevant factors. The results of the IPCC are presented in the form of temperature increases due to doubling of the CO_2 concentration. It is estimated that the radiative forcing caused by doubling the carbon dioxide concentration with respect to the year 1992 is 4.37 W/m^2 and that the induced global temperature increase is 2.5 K; thus the probable value for the climate sensitivity factor is 0.57 K m^2/W.

Nevertheless, there must be a time lag between the moment when radiative forcing occurs and the future moment when—potentially—the radiative balance is established again and the global temperature reaches a new equilibrium. One expects that the time to reach a new equilibrium is long because the thermal inertia of the planets surface is high (it is composed of water in a large amount, ice, biomass, rocks, and land, all having high specific or latent heats).

3.2.4 Global Warming Potential

Quantifying the effect of a given atmospheric gas on climate is a multivariable problem. On one side, the radiative forcing induced by the respective gas is an indication of the direction in which the presence of the respective gas can affect the climate. If, for example, the gas absorbs more infrared spectrum, its greenhouse effect is accentuated, that is, it is associated with a positive radiative forcing. However, another parameter is also important, that is, the atmospheric lifetime. It is important how long the gas is active in the atmosphere with respect to radiative balance control.

The radiative forcing produced by introducing $m_0 = 1$ kg of CO_2 in the atmosphere is indicated by ΔF_{CO_2}. At a future moment, one can approximate the mass of carbon dioxide remaining in the atmosphere with Eq. (3.4). At time t, the fraction of the mass existent in the atmosphere is $m_0\left(0.375e^{-(t/\tau_1)} + 0.625e^{-(t/\tau_2)}\right) = m_0 f_{CO_2}(t)$, where we use the notation $f_{CO_2}(t)$ to emphasize that the fraction of gas mass existent in the atmosphere is a function of time. Since $m_0 = 1$ kg was taken, it can be omitted from the equation. Therefore, the net forcing produced during an infinitesimal time interval is given by the product $\Delta F_{CO_2}(t) \times f_{CO_2}(t) \times \mathrm{d}t$. One can integrate the former quantity over a time horizon (TH) to obtain the total forcing produced by the respective amount of CO_2. If another kind of GHG other than carbon dioxide is considered, its integrated forcing over the time horizon can be normalized with the integrated forcing of CO_2. From this reasoning comes the following definition:

$$GWP = \frac{\int_0^{\mathrm{TH}} \Delta F_{\mathrm{GHG}}(t) f_{\mathrm{GHG}}(t)\mathrm{d}t}{\int_0^{\mathrm{TH}} \Delta F_{CO_2}(t) f_{CO_2}(t)\mathrm{d}t}, \tag{3.10}$$

Table 3.2 The global warming potential (GWP) of principal greenhouse gases

Substance	Time horizon (years)			Substance	Time horizon (years)		
	20	100	500		20	100	500
Carbon dioxide	1	1	1	HCFC22	5,160	1,810	549
Methane	72	25	7.6	Carbon tetrachloride	2,700	1,400	465
Nitrous oxide	289	298	153	HFC134a	3,830	1,430	435
CFC11	6,730	4,750	1,620	Sulfur hexafluoride	16,300	22,800	32,600
CFC12	11,000	10,900	5,200	Nitrogen trifluoride	12,300	17,200	20,700

Data from IPCC (2007)

which is the global warming potential (GWP) of the GHG. It results from the definition Eq. (3.10) that the GWP of carbon dioxide is 1. Table 3.2 gives the GWP of the main GHGs for three time horizons, based on IPCC (2007).

3.3 Anthropogenic Effect on Climate

Uncontrolled human activities since the Industrial Revolution have brought the planet to a point that the amount of emissions and the magnitude of global environmental impact are incalculable. The planet has the symptoms of inadvertently catching a disease. The symptoms have slowly become more apparent due to a slight increase in the global atmospheric temperature. There is no agreement on the cause or the consequence. Some ascribe this rise to an addiction to uncontrolled energy use, carbon-based energy, and the emissions of infrared-absorbing gases. The emission of gases in the atmosphere, specific to the industrial era, will affect the radiative balance of the planet, and therefore affect the earth's climate. Figure 3.6 presents the distribution of anthropogenic GHG emissions per sector of activity (left) and per type of major GHG (right).

Experimental evidence proves that the massive emissions of industrial gases expelled in the atmosphere in the last century are related to the global temperature increase, which reflects the global warming phenomenon. In order to sustain this point, we give in Fig. 3.7, from Brohan et al. (2006), the global temperature anomaly since 1860. In correspondence with the global temperature increase, Fig. 3.8 gives the latest size variation in the Arctic sea ice, which exhibits a steady average decline (dashed line) since measurements were available.

The initial and preliminary diagnosis of the planet's disease is simple: emissions that are man-made and come from our industrial and transportation activity cause the increase. Not everyone agrees, nor do they need to, since we can now seek a second opinion from other specialists, which is natural if we are suffering from a potentially deadly or poorly diagnosed, controversial malady.

The global value of carbon emission can be evaluated based on the value of carbon energy's ability to provide economic growth. After all, this is how improvement in modern industrial society is measured and reported. The purely economic value of the carbon emissions and power source is reflected in producing financial wealth for

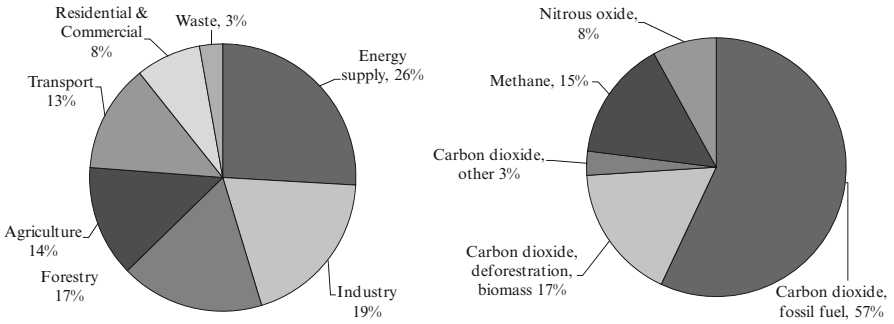

Fig. 3.6 Anthropogenic GHG emissions by sectors (*left*) and major gas type (*right*) [data from IPCC (2007)]

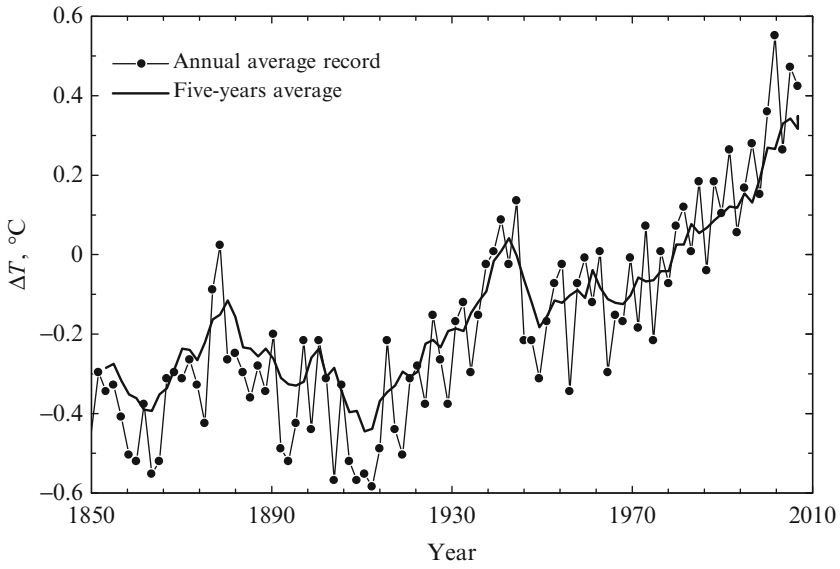

Fig. 3.7 Record of the global temperature anomaly [data from Brohan et al. (2006)]

every country (such as the national GDP) using carbon energy. Energy is greatest in developed (rich) nations, and we observe a correlation between the growth in GDP and the growth in carbon energy use. Table 3.3 shows the typical life cycle emissions for power generation from different sources (g/kWh). This relationship also holds true at the global level. Hence, the global growth in GHG concentration in the atmosphere over the last 30 years (measured as ppm CO_2 at Mauna Loa, Hawaii, where 1 ppm CO_2 ~ 9.1012 tCO_2, where t is a metric tonne) is directly and linearly correlated with the GWP (measured in terra dollars, $1,012 US). To reduce the effect of the year-to-year noise in the atmospheric CO_2 concentrations, 5-year averages for

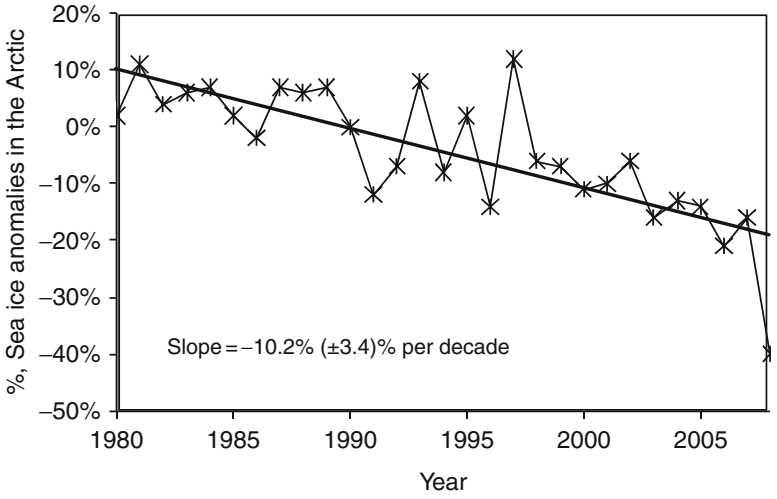

Fig. 3.8 The latest size variation in sea ice in the Arctic [data from NASA (2008)]

Table 3.3 Typical life cycle emissions for power generation from different sources (g/kWh)

Electric energy generation source	Switzerland 2000	Canada 2000	IAEA 2000	France (production only)
Natural gas	605	N/A	696	500
Coal	1,071	974	978	N/A
Solar panels	114–189	N/A	97	N/A
Nuclear	16	3–15	21	0
Oil	856	778	811	701
Wind	36	N/A	36	N/A
Hydro	4	15	16–23	N/A

IAEA International Atomic Energy Agency
Data from EIA (2008)

GWP were plotted against the change in CO_2 measured over those 5 years. Rather than plotting ppm values of CO_2, the change was converted to billions of tons (Gt) of CO_2 released based on the 7.9 Gt of CO_2 required to cause a 1-ppm increase in the atmosphere accompanied by an equal release being absorbed in the oceans. So, 1 ppm was taken to be the equivalent of a total of 15.8 Gt of CO_2 released. It is reasonable to use 1950 as the base year since the CO_2 buildup prior to about 1950 was small.

3.4 Controlling the Anthropogenic Effects on Climate

In the current circumstances, what we need is the appropriate effective cure. If one looks in the dictionary, the short definition for "cure" is "successful remedial treatment." In our search for a cure, we must distinguish between real cures and false claims.

Table 3.4 A summary of symptoms as identified by the IPCC (2007)

Symptoms	Prior (1600 a.d.) symptoms	Human causation	Future (twenty-first century) prognosis
Warmer and fewer cold days and nights over most land areas	Very likely	Likely	Virtually certain
Warmer and more frequent hot days and nights over most land areas	Very likely	Likely	Virtually certain
Warm spells/heat weaves (with an increasing frequency in most land areas)	Likely	More likely than not	Very likely
Heavy precipitation events (with an increasing frequency in most land areas)	Likely	More likely than not	Very likely
Increased droughts affecting land areas	Likely in many regions since 1970	More likely than not	Likely
Increased tropical cyclone activities	Likely in some regions since 1970	More likely than not	Likely
Increased incidence of extreme high sea level (with no tsunamis)	Likely	More likely than not	Likely

Data from IPCC (2007)

We need to find the right doctor to get the right prescription for the cure, and the right implementation of the prescription will cure the problem. Nowadays, specialists and their tests can also often delicately distinguish genetic or in-built traits from acquired trends, the mental from the physical, the curable from the treatable, and what might be a successful or unsuccessful and ineffective treatment. In our case, this specialist role is performed by the United Nation's Intergovernmental Panel on Climate Change (IPCC), which is a body of specialists armed with the latest models, data, experience, and records that are globally available. The IPCC has produced extensive compendia, diagnoses, studies, and predictions. For example, in a recent report (IPCC 2007), seven major measures are described that reflect actual changes in climate other than temperature, from warm spells to droughts to sea levels.

The IPCC went further in its consultation, ascribing whether the symptoms were likely or not, whether human in cause, and giving a glimpse of the future prognosis. This summary of the latest IPCC is shown in Table 3.4. The analysis is typical of a critical standard whereby no symptom is conclusive, but whether or not multiple factors are likely present may become more convincing. These factors are described as likely, and also likely to be human caused, where likely is about a 90% certainty, or an odds ratio of 10–1 holds true in a bet. This does not mean infallibility or that

certainty is achieved; that can only be achieved from data that we know may never be fully available (i.e., only from a postmortem can we truly give the cause of death). We find not just one but many treatment options. The prescription may be as long as the following:

- Changing lifestyle and habits
- Making systems and applications more efficient, cost efficient, and environmentally benign
- Developing cleaner technologies
- Using renewable and green energy
- Implementing hydrogen and fuel cell technologies
- Conserving energy
- Diversifying energy options
- Purchasing more efficient appliances
- Giving priority to local energy systems and cogeneration
- Providing proper education and training
- Using more cost-effective energy systems and applications
- Seeking alternative energy sources for transportation
- Using sustainable fuels
- Increasing public awareness
- Taking necessary energy security measures
- Monitoring and evaluating energy indicators
- Implementing the right energy strategies and policies (avoid side effects!)

And many more changes are necessary to achieve some of the following goals (as mentioned also at the beginning of this book):

- Better efficiency
- Better cost-effectiveness
- Better resources use
- Better design and analysis
- Better environment
- Better sustainability
- Better energy security

We share the human desire to look for a "quick fix" solution, so as a result we have a confusing menu of short-term panaceas and ineffective painkillers that treat symptoms:

- The Kyoto protocol aimed to reduce carbon pricing mechanisms, which has actually not decreased emissions worldwide.
- Seeking alternative energy sources, such as windmills, biofuels, and efficiency improvement, which are good ideas even if they do not necessarily work well.
- Denial of the problem and putting off real treatment until major surgery is required, which is an effective means to avoid unpleasant truths.

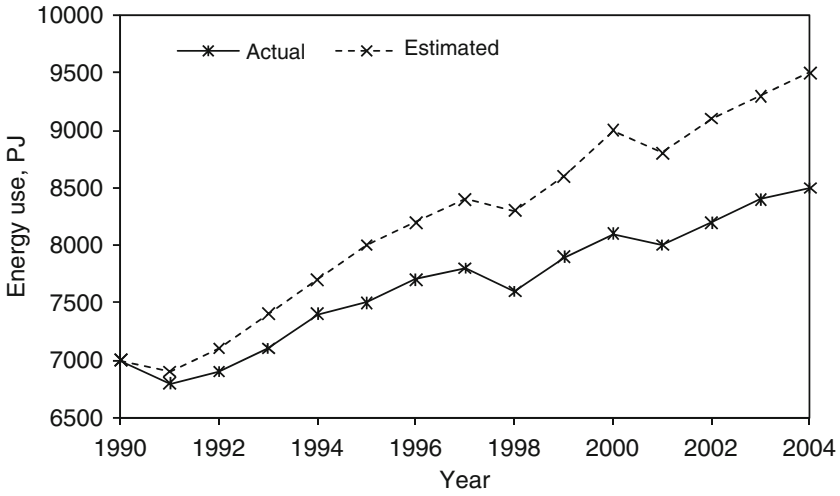

Fig. 3.9 Impact of energy efficiency improvements in Canada [data from NRCan (2008)]

- Need for "lifestyle" and feel-good cures, such as unqualified "offsets," "carbon neutral," and "allowances" that allow the energy rich to feel good about their unsustainable lifestyle.
- Shortage of key/real specialists who are living in an era with information about the pollution in the world of unqualified knowledge and with many unqualified specialists; we turn to instant judgments and views of self-anointed witch doctors who have almost magical insights.
- Long waiting times and insufficient funding for real cures means that long-term treatment is hard to find even after waiting in line for emergency help.
- Unbalanced coverage in the media, which are looking for headlines, social issues, celebrities, and awards, providing the sensational but not the solution.
- Business opportunities; out of such a complex disease, there is money to be made from peddling cures in the rush to profit from the ailments of the masses.

It should be intuitively obvious that if we improve the efficiency of energy use—do more with less—then that should reduce our demand and need for energy. If that were also economic, then that would be another incentive.

However, globally and especially nationally this has the opposite effect, in a perverse example of the law of unintended consequences. To illustrate this, we show the data for Canada in Fig. 3.9 for the energy actually used compared with that estimated to be used without efficiency improvements. The rate of increase of energy use declines, but there is no real decrease in the total amount used! The reasons are simple and rather disturbing.

First, and fundamentally, by making products cheaper by using less energy, more units are sold. So there is no incentive to actually reduce production commercially, but to make more for the same or less energy costs since manufacturers want to sell more, not less.

Second, the energy not used in the particular manufacturing process is now available for use by others, in other factories, businesses, and plants, and other countries, since a reduced demand has made that unused energy available in the marketplace, so the energy use simply moves elsewhere.

Third, in free market economies like Canada's, business wants and needs to increase its market share, turnover, shareholder returns, and profits. So economic growth is king! No business wants to actually sell less, so the pressure is to make and sell more at lower prices. Market efficiency and competitive pressures dominate and total consumption grows, and manufacturing facilities move to the location of lowest energy and labor costs (the classic example is the 50-year migration of manufacturing to foreign locations for essential items such as knives and forks).

The measure of energy efficiency is the energy intensity or the amount used per unit produced. This can also be used as a social measure, as the amount used per person in any country. Reducing intensity sounds like a good idea; after all, the so-called rich, industrialized nations have a high energy intensity and the energy-poor ones have a lower value. If one reduces the energy intensity, nationally or at factories, we should help achieve efficiency, equity, and economy at one fell swoop. But, as we should have come to expect, of course, this naive hope is not the case either.

The EIA (2008) states that the reduction in energy intensity improves the economy by nearly 30%. Energy use meanwhile has risen and will rise by over 50%. So for every percent of improvement in intensity, we have nearly 2% growth in energy use. It is working backward again, such that efficiency improvement is overwhelmed by economic improvements. Needless to say, the emissions in the United States rose in lockstep with the energy use increase. Furthermore, the EIA clearly states that improved efficiency (technology) was responsible for about 60% of the observed decline in energy intensity, while it is now declining and more expensive to introduce. As a result of the continued improvements in the efficiency of end-use and electricity generation technologies, total energy intensity in the reference case is projected to decline at an average annual rate of 1.6% between 1999 and 2020. The projected decline in energy intensity (1.6%) is considerably less than that experienced during the 1970s and early 1980s, when the energy intensity declined, on average, by 2.3% per year. Approximately 40% of that decline can be attributed to structural shifts in the economy—shifts to service industries and other less energy-intensive industries; however, the rest resulted from the use of more energy-efficient equipment. Although more advanced technologies may reduce energy consumption, in general, they are more expensive when initially introduced. In order to penetrate the market, advanced technologies must be purchased by consumers; however, many potential purchasers may not be willing to buy more expensive equipment that has a long period for recovering the additional cost through energy savings, and many may value other attributes over energy efficiency. In order to encourage more rapid penetration of new and clean technologies for reducing energy consumption and carbon dioxide emissions, it is really important to have the right market policies and the appropriate standards.

Table 3.5 Potential for energy intensity reduction for New Zealand 2007 (New Zealand Ministry of Education)

Sector	2030			
	Energy intensity reduction		Emission intensity reduction	
	Realizable potential (%)	Per year (%)	Realizable potential (%)	Per year (%)
Homes	29	1.1	19	0.8
Commercial buildings	25	1.0	17	0.7
Light industry	17	0.7	12	0.5
Heavy industry	35	1.4	33	1.3
Total nontransport energy	28	1.1	22	0.9

Let us look at an example from New Zealand on energy intensity reduction targets (Table 3.5). The Ministry of Economic Development (MED 2008) in New Zealand indicates that there is substantial potential for the energy intensity and emissions intensity of the economy to reduce over time, although it varies by sector. A reduction in energy may reflect a change in the underlying composition of a sector (e.g., some types of business are by their nature more energy intensive) or an improvement in the energy efficiency within the sector. The most significant energy efficiency opportunities are when assets are replaced or upgraded.

All these initiatives aim to achieve reducing environmental impact (through reducing GHG emissions), saving energy and using it more efficiently, employing renewable energy, increasing the business activities (e.g., job creation), and playing a key role and leadership in the international arena. Of course, it will take some time to see the outcomes of these initiatives. Dincer (2003) listed the following steps for implementing an efficient energy utilization strategy plan:

1. Defining the main goals: It is a systematic way to identify clear goals, leading to a simple goal-setting process. It is one of the crucial concerns and follows an organized framework to define goals, decide priorities, and identify the resources to meet these goals.
2. Identifying the community goals: It is a significant step to identify priorities and links among energy, energy conservation, environment, and other primary local issues. It is also important to identify the institutional and financial instruments.
3. Environmental scan: The main objective here is to develop a clear picture of the community to identify the critical energy-use areas, the size and shape of the resource-related problems facing the city and electrical and gas utilities, and the organizational mechanisms and the base data for evaluating the plan's progress.
4. Increase public awareness: Governments can increase public awareness and acceptance of energy conservation programs by entering into performance contracts for government activities. They can also publicize the results of these programs and projects. In this regard, international workshops to share

experiences would help to overcome the initial barrier of unfamiliarity in countries.

5. Information analysis: It carries out a wide range of telephone and fax interviews with local and international financial institutions, project developers, bilateral aid agencies to capture new initiatives, and lessons learned and viewpoints on problems and potential solutions.
6. Building community support: It covers the participation and support of local industries and public communities, and the understanding of the nature of conflicts and barriers between given goals and local actors; improving information flows; activating education and advice surfaces; identifying institutional barriers; and involving a broad spectrum of citizen and government agencies, referring to participation and support of local industrial and public communities.
7. Analyzing information: It includes defining available options and comparing the possible options against factors such as activity/plan implementation costs, funding availability, utility capital deferral, potential for energy efficiency, compatibility with community goals, environmental benefits, and so on.
8. Adopting policies and strategies: Priority projects need to be identified through a number of approaches, such as what is best for the community. The decision process should evaluate the cost of the options in terms of savings in energy cost, generation of businesses and tax revenues, and the number of jobs created, as well as their contribution to energy sustainability and their benefit to other community and environmental goals.
9. Developing the plan: Once a draft plan is adopted, it is important for the community to review it and comment upon it. The public consultation process may vary, but a high level of agreement should be the goal.
10. Implementing new action programs: It is important to decide which programs to concentrate on, with long-term aims being preferred over short-term aims. The option that has the greatest impact should be focused on, and all details defined, no matter how difficult it seems. Financial resources need to be identified to implement the plans/programs.
11. Evaluating the success: It is the final stage for evaluating and assessing how well the plan performed, which helps to detect its strength and weaknesses and to determine who is benefiting from it.

These are self-evident steps in attaining self-help, removing denial, defining the problem, getting expert advice, fighting the disease, taking the right medicine in the right doses, and at the same time attacking the root source of the addiction and illness, and measuring progress.

There are two dimensions of global warming and climate change: natural cycling and human activities. The outcome of human activities is at a much higher level than the level that can be neutralized by natural cycling. As a result, while one region of the world experiences drought, another region may be suffering from flood. Within this framework, the following set of precautions and conclusions was drawn by Dincer (2009) from the Global Conference on Global Warming, which was held in Istanbul, Turkey, on July 6–9, 2009:

1. Existing natural resources should be identified, and short-, medium-, and long-term road maps should be prepared. In this regard, special working groups or task forces should be formed to work on these issues.
2. Several research, development, and innovation strategies should be put into action for combating global warming.
3. Resources such as energy and water should be conserved.
4. Current systems should be improved and used more efficiently and effectively.
5. Priority should be given to renewable energy resources and related technologies.
6. Strategic steps should be taken for a smooth transition to a hydrogen economy.
7. In developing appropriate energy, environment, economic, social, and sustainable development policies, the particulars of localities should be taken into consideration when devising treatments, strategies, and policies. Therefore, societies should develop models and policies that best suit their local conditions and situation.
8. Incentive programs necessary for the dissemination and widespread use of environmentally friendly energy technologies should be put into effect.
9. Intermediary solutions for transitioning from fossil fuels to alternative energy options should urgently be developed.
10. Municipalities should develop the necessary strategies for waste management and put them in action.
11. Recycling should be done at its source according to the type of waste, not at the final collection points. Reuse options should also be developed.
12. Units and action groups of governmental and private organizations should be formed for combating global warming.
13. Incentive packages should immediately be developed and put in place to combat global warming.
14. Necessary steps should be taken for increasing green areas and preventing the warped excesses of urbanization and deforestation.
15. The concept of "global warming diet" should be developed to curb the personal and societal habits and addictions as well as activities causing global warming.
16. The concept of "global warming label" should be initiated and put into immediate effect.
17. The concept of "global warming tax" should be initiated and put into immediate effect.
18. Necessary economic, social, technical, scientific, cultural, and educational actions and measures should immediately be taken for a quick transition to the zero carbon economy.
19. Individual and social responsibilities should be joined together in combating global warming.
20. Special working groups and task forces should be formed to work harmoniously at the national and international levels to combat global warming.
21. Strategies for combating global warming should be developed at the local level and should be put in practice for each locality.

22. To overcome the economic burdens due to combating global warming, an emergency action plan should be devised and put into action.
23. The concept of "global quality standard" should be developed and put into use to minimize global warming's impact.
24. By partnering with countries that are in the process of regulating carbon trading, the necessary infrastructure for global carbon trading should be developed and put into action.
25. Trade associations and professional societies should urgently prepare their action plans for global warming.
26. Courses and educational programs should be developed on global warming and combating it.
27. The following goals should be essential in every action plan:
    (a) Better efficiency
    (b) Better cost-effectiveness
    (c) Better resource use
    (d) Better environment
    (e) Better sustainability
    (f) Better energy security
28. For the immediate action plans listed above, either a Ministry of Combating Global Warming or a State Ministry or Commission under the Prime Ministry should be established.
29. An Istanbul Protocol on combating global warming will jointly be prepared by collaborating with the Global Warming and Climate Change Watch Committee.

3.5 Concluding Remarks

The problem of climate change and global warming is real and faces humanity, which, according to the principle of sustainable development, has to be concerned with the needs of today without jeopardizing the chances of future generations. Although the early warning symptoms of climate change and global warming are present, they are not conclusive as to the diagnosis of the cause. Nevertheless, the scientific evidence shows that the anthropogenic pollution affects the climate. In this case, finding a cure for the planet's disease is necessary. Some proposed cures are rejected, and some people think the evidence is all questionable; opinions are varied even among trusted consultants and specialists.

We know now, based on data and reality, that on their own the efficiency improvements, the energy conservation, the alternate energy sources, the renewable and nuclear energy, the carbon dioxide capture and sequestration, the carbon pricing or "cap and trade" schemes, the portfolio standards, the use of more natural gas, the switching to hybrid cars without green electricity, and the hydrogen power will not work, except as part of a full-spectrum, truly multivitamin energy pill.

Nomenclature

C	Concentration, ppm
F	Radiative forcing, W/m^2
GWP	Global warming potential
m	Mass, kg
S	Average solar radiation intensity, W/m^2
t	Time, s
T	Temperature, K

Greek Letters

α	Absorption
γ	Climate sensitivity factor
τ	Time constant, s
σ	Stefan-Boltzmann constant, 5.67×10^{-8} W/m^2K^4

Subscripts

0	Initial
a	Troposphere
abs	Absorption coefficient
albedo	Albedo factor
e	Emitted
eqv	Equivalent

References

Boyle G. 2004. Renewable Energy, 2nd edition. Oxford University Press, UK.

Brohan P., Kennedy J.J., Haris I., Tett S.F.B., Jones P.D. 2006. Uncertainty estimates in regional and global observed temperature changes: a new dataset from 1850. *Journal of Geophysical Research* 111:D12106.

Dincer I. 2003. On energy conservation policies and implementation practices. *International Journal of Energy Research* 27:687–702.

Dincer I. 2009. Global Warming: Engineering Solutions. Edited book of the Global Conference on Global Warming, Istanbul, July 2008.

Duffey R.B., Dincer I. 2010. Global warming—where is the cure? In: Global Warming. Engineering Solutions, Dincer I., Midilli A., Hepbasli A., Katakoc T.H. eds., Springer, New York.
EIA 2008. Energy Information Administration, U.S. Government. Internet source http://www.eia.doe.gov/ (accessed on May 26, 2009).
Enting N.G., Newsam G.N. 1990. Atmospheric constituent inversion problems: Implication for baseline monitoring. *Atmospheric Chemistry* 11:69–87.
IPCC 1990. Climate Change: The IPCC Scientific Assessment. Houghton, J.T., Jenkins G.J., Ephraums J.J. eds., Cambridge University Press, Cambridge, MA.
IPCC 2001. Climate Change 2001: The Scientific Basis. Intergovernmental Panel on Climate Change, Houghton J.T. et al., eds., Cambridge University Press, Cambridge, UK.
IPCC 2007. Climate Change 2007: Synthesis Report. Intergovernmental Panel on Climate Change. Plenary XXVII, Valencia, Spain.
MED 2008. Using Energy More Efficiently. Draft New Zealand Energy Strategy to 2050, Ministry of Economic Development. Internet source http://www.med.govt.nz/templates/MultipageDocumentPage25256.aspx (accessed on June 15, 2009).
NASA 2008. Arctic 'Melt Season' Is Growing Longer, New Research Demonstrates. Internet source http://www.nasa.gov/topics/earth/features/longer-melt-season.html (accessed on May 26, 2009).
NIST Chemistry Webbook 2005. NIST standard reference database Number 69, Linstrom P.J., Mallard W.G. eds., National Institute of Standards and Technology, Gaithersburg, MD.
NRCan 2008. Climate Change Impacts and Adaptation Program, Natural Resources of Canada. Internet source http://www.nrcan-rncan.gc.ca/com/subsuj/envenv-eng.php (accessed on June 30, 2009).
Rubin E.S. 2001. Introduction to Engineering and the Environment. McGraw-Hill Higher Education, New York.

Study Questions/Problems

3.1 Explain the process of global warming.
3.2 Define the term *albedo* and explain the features of the earth's albedo. Refer to Eqs. (3.1) and (3.2).
3.3 In what wavelength range is the greenhouse gas absorption in the atmosphere at the maximum.
3.4 List the principal four greenhouse gases.
3.5 Using Eq. (3.4), calculate the reduction ratio m/m_0 of carbon dioxide in the atmosphere after 100 years.
3.6 Define the radiative forcing concept.
3.7 Define the climate sensitivity factor.
3.8 Define the global warming potential and the method of calculating it.
3.9 Explain the anthropogenic influence on climate and comment on the impact of the main sectors of activity.
3.10 By using linear extrapolation, predict the earth's temperature increase in 2020, using the data from years 1980 to 2000 (you can refer to Fig. 3.7).
3.11 How can one control the anthropogenic effects on climate?
3.12 Using literature data, calculate the radiative forcing effects caused by greenhouse gas emissions by passenger aircrafts.

Chapter 4
Energy Conservation

4.1 Introduction

Energy is considered to be a key catalyst in the generation of wealth and also a significant component in social, industrial, technological, economic, and sustainable development. This makes energy resources and their use extremely significant for every country in the world. In fact, abundant and affordable energy is one of the great boons of modern industrial civilization and the basis of our living standard. It makes people's lives brighter, safer, more comfortable, and more mobile, depending on their energy demand and consumption. However, in recent years, energy use and associated greenhouse gas emissions and their potential effects on the global climate change have been of worldwide concern.

Problems with energy utilization are related not only to global warming, but also to such environmental concerns as air pollution, acid rain, and stratospheric ozone depletion. These issues must be taken into consideration simultaneously if humanity is to achieve a bright energy future with minimal environmental impact. Since all energy resources lead to some environmental impact, it is reasonable to suggest that some (not all) of these concerns can be in part overcome through *energy conservation* efforts.

Energy conservation is the practice of rational energy generation and use at all levels. This practice is based on a number of factors such as better energy efficiency, best technical-economical choice among options, adequate policy, proper energy management, recycling and energy recovery, and education to reinforce behaviors toward energy savings. Energy efficiency is a matter of better design, but at the same time a matter of economics. A highly efficient energy system involves higher investment costs. Systems with low-energy efficiency use more primary energy resources (fuel) for the same useful effect; thus the lifetime cycle costs are high. Hence, for any particular energy system, one may determine the efficiency that minimizes the life-cycle cost or maximizes the life-cycle savings.

The energy-saving result of efficiency improvements is often called "energy conservation." The terms *efficiency* and *conservation* contrast with *curtailment*, which decreases output (e.g., turning down the thermostat) or services (e.g., driving less) to curb energy use. That is, energy curtailment occurs when saving energy

İ. Dinçer and C. Zamfirescu, *Sustainable Energy Systems and Applications*,
DOI 10.1007/978-0-387-95861-3_4,

causes a reduction in services or a sacrifice of comfort. Curtailment is often employed as an emergency measure. Energy efficiency is increased when an energy conversion device, such as a household appliance, automobile engine, or steam turbine, undergoes a technical change that enables it to provide the same service (lighting, heating, and motor drive) while using less energy. Energy efficiency is often viewed as a resource option like coal, oil, or natural gas. In contrast to supply options, however, the downward pressure on energy prices created by energy efficiency comes from demand reductions instead of increased supply. As a result, energy efficiency can reduce resource use and environmental impacts.

From an economic as well as an environmental perspective, energy conservation holds even greater promise than renewable energy, at least in the near-term future. Energy conservation is indisputably beneficial to the environment, as a unit of energy not consumed equates to a unit of resources saved and a unit of pollution not generated.

The choice of the system is important, and here exergy analysis is a helpful tool. For example, it is not worth while to "destroy" electrical energy to heat water, but rather we should use a heat pump that matches the temperature profiles of cold and hot streams for the best exergy efficiency.

By saving energy, the practice of using heat pumps instead of electrical heating contributes to pollution reduction at power generation, and thus contributes to a better environment. Among the two options, one has to choose the heat pumps from the technical point of view, but again the economic "climate" may discourage investment. Therefore, an adequate regulation policy must intervene to adjust the life-cycle cost through various economic factors (e.g., incentives, bonds, taxes, etc.) to encourage the right choices.

Policy has the leading role in promoting energy conservation in any society because not only can it generate an adequate economic environment that eventually leads to savings, but it may also impose regulations for proper energy management, encourage recycling and energy recovery, and promote appropriate education of the society.

To understand the role of education one can contemplate the evolution of energy use throughout history (see also Dincer and Midilli 2007). Civilization began when people discovered how to use fire. They burned wood and obtained sufficiently high temperatures for melting metals, extracting chemicals, and converting heat into mechanical power, as well as for cooking and heating. During burning, the carbon in wood combines with O_2 to form CO_2, which is then absorbed by plants and converted back to carbon for use as a fuel again.

Since wood was unable to meet the fuel demand, the Industrial Revolution began with the use of fossil fuels, such as oil, coal, and gas. Using fossil fuels has increased the CO_2 concentration in the air, leading to the beginning of global warming. Despite several warnings in the past about the risks of greenhouse gas emissions, significant actions to reduce environmental pollution were not taken, and now many researchers have concluded that global warming is occurring.

During the past three decades, the public has became more aware and researchers and policy makers have focused on this and related issues by considering

energy, environment, and sustainable development. Energy conservation is a key element of energy policy and appears to be one of the most effective ways to improve end-use energy efficiency, and to reduce energy consumption and greenhouse gas emissions in various sectors, such as industrial, residential, transportation, etc.

This is why many countries have recently started developing aggressive energy conservation programs to reduce the energy intensity of the country's infrastructure, to make businesses more competitive, and to allow consumers to save money and to live more comfortably. In general, energy conservation programs aim to reduce the need for the new generation or transmission capacity, to save energy, and to improve the environment. Furthermore, energy conservation is vital for sustainable development and should be implemented by all possible means, despite the fact that it has its own limitations. This is not only required today but also for the next generation as well.

Considering these important contributions, the energy conservation phenomenon should be discussed in a comprehensive perspective. Therefore, the main objective of this chapter is to present and discuss some practical energy conservation aspects, research and development in energy conservation, energy conservation and sustainable development, an energy conservation implementation plan, energy conservation measurements, and life-cycle costing as an excellent tool in energy conservation. In this regard, this chapter aims to:

- Help understand the main concepts and issues about energy conservation
- Develop the relation between energy conservation and sustainability
- Encourage energy conservation strategies and policies
- Provide energy conservation methodologies
- Discuss the relation between energy conservation and environmental impact
- Present some illustrative examples of the importance of energy conservation and its practical benefits

This chapter highlights the current environmental issues and potential solutions to these issues, identifies the main steps for implementing energy conservation programs and the main barriers to such implementations, and provides assessments for energy conservation potentials for different countries, as well as various practical and environmental aspects of energy conservation.

4.2 Energy Conservation and Sustainable Development

Energy conservation is vital for sustainable development, and for the best benefit of the present and future generations it should be implemented by all possible means. A secure supply of energy resources is generally agreed to be a necessary but not sufficient requirement for development within a society. Furthermore, sustainable development demands a sustainable supply of energy resources that, in the long term, is readily and sustainably available at reasonable cost and can be utilized for

all required tasks without causing negative societal impacts. Supplies of such energy resources as fossil fuels (coal, oil, and natural gas) and uranium are generally acknowledged to be finite; other energy sources such as sunlight, wind, and falling water are generally considered renewable and therefore sustainable over the relatively long term.

Wastes (convertible to useful energy forms through, for example, waste-to-energy incineration facilities) and biomass fuels are also usually viewed as sustainable energy sources. In general, the implications of these statements are numerous and depend on how the term *sustainable* is defined (Dincer and Rosen 1998).

Here, we look at the renewable energy resources and a comparison with energy conservation. While not all renewable energy resources are inherently clean, there is such a diversity of choices that a shift to renewables carried out in the context of sustainable development could provide a far cleaner system than would be feasible by tightening controls on conventional energy. Furthermore, being by nature site-specific, they favor power system decentralization and locally applicable solutions more or less independent of the national network. It enables consumers to perceive the positive and negative externalities of energy consumption. Consequently, the small scale of the equipment often shortens the time required from initial design to operation, providing greater adaptability in responding to unpredictable growth and/or changes in energy demand.

The exploitation of renewable energy resources and technologies is a key component of sustainable development (Dincer 2003). There are three significant reasons for it:

- Renewable energy resources have much less environmental impact compared to other sources of energy, but there are no any energy sources with zero environmental impact. There are a variety of choices available in practice so that a shift to renewables can provide a far cleaner energy system than would be feasible by tightening controls on conventional energy.
- Renewable energy resources cannot be depleted, unlike fossil fuel and uranium resources. If used wisely in appropriate and efficient applications, they can provide reliable and sustainable supply energy almost indefinitely. In contrast, fossil fuel and uranium resources are finite and are diminished by extraction and consumption.
- Renewable energy resources favor power system decentralization and locally applicable solutions more or less independent of the national network, thus enhancing the flexibility of the system and the economic power supply to small local settlements. That is why many different renewable energy technologies are potentially available for use in urban areas.

Taking into consideration these important reasons, the relation between energy conservation and sustainability is presented in Fig. 4.1. As suggested in Fig. 4.1, energy resources and their utilization are intimately related to sustainable development. For societies to attain or try to attain sustainable development, much effort must be devoted not only to discovering sustainable energy resources, but also to increasing the energy efficiencies of processes utilizing these resources.

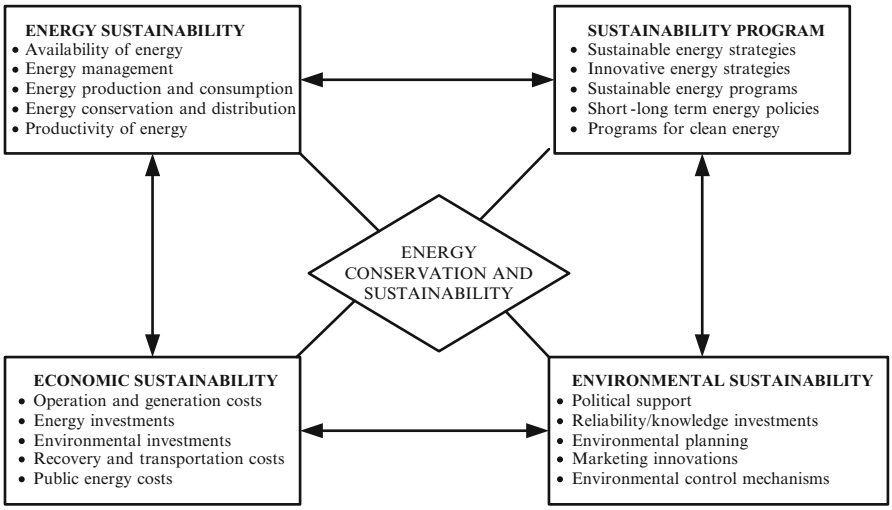

Fig. 4.1 Linkages between energy conservation and sustainable development

Under these circumstances, increasing the efficiency of energy-utilizing devices is important. Due to increased awareness of the benefits of efficiency improvements, many institutes and agencies have started working along these lines.

Many energy conservation and efficiency improvement programs have been and are being developed to reduce the present levels of energy consumption. To implement these programs in a beneficial manner, an understanding is required of the patterns of "energy carrier" consumption, such as the type of energy carrier used, factors that influence consumption, and types of end-uses (Painuly and Reddy 1996).

Environmental concerns are an important factor in sustainable development. For a variety of reasons, activities that continually degrade the environment are not sustainable over time; the cumulative impact on the environment of such activities often leads over time to a variety of health, ecological, and other problems. A large portion of the environmental impact in a society is associated with its utilization of energy resources.

Ideally, a society seeking sustainable development utilizes only energy resources that cause no environmental impact. Energy efficiency can help overcome some of the damaging effects of environmental pollution. It is clear that there is a strong relation exists between energy efficiency and environmental impact; increased energy efficiency is reflected in less resource utilization and pollution for the same services or products.

The share of energy of research and development (R&D) expenditures going into energy conservation grew greatly since 1976, from 5.1% to 40.1% in 1990 and to 68.5% in 2002 (Dincer 2003). This indicates that within energy R&D, research on energy conservation is increasing in importance. When R&D expenditures on

energy conservation are compared with expenditures for research leading to protection of the environment in the 2000s, the largest share was spent on environmental research. In fact, it is not easy to interpret the current trends in R&D expenditures since energy conservation is now part of every discipline from engineering to economics. A marked trend was observed since the mid-1970s, in that expenditures for energy conservation research grew significantly both in absolute terms and as a share of total energy R&D. They also grew more rapidly than environmental protection research, surpassing it in the early 1980s. Therefore, if R&D expenditures reflect long-term concern, there seems to be relatively more importance attached to energy conservation as compared to environmental protection. In addition to the general trends discussed above, consider the industrial sector and how it has tackled energy conservation.

The private sector clearly has an important role to play in providing finance that could be used for energy efficiency investments. In fact, governments can adjust their spending priorities in aid plans and through official support provided to their exporters, and can only indirectly influence the vast potential pool of private sector finance. Many of the most important measures to attract foreign investors include reforming macroeconomic policy frameworks, reforming energy market structures and pricing, banking reform, debt recovery programs, strengthening the commercial and legal framework for investment, and setting up judicial institutions and enforcement mechanisms. These are difficult tasks that often involve lengthy political processes.

Thus, Fig. 4.2 presents a series of important factors as proposed by Dincer and Midilli (2007), which are adapted from a workbook (Nolden et al. 1998) that can contribute to improvement of the energy conservation in real life.

Although there are a large number of practical solutions to environmental problems, three potential solutions are given priority (Dincer 2003):

- Energy conservation technologies (efficient energy utilization)
- Renewable energy technologies
- Cleaner technologies

In these technologies, we pay special attention to energy conservation technologies and their practical aspects and environmental impacts. Each of these technologies is of great importance and requires careful treatment and program development. Considering the above priorities to environmental solutions, the relevant technologies are summarized in Fig. 4.3.

4.3 Energy Conservation Measures

The ways and measures to be taken for energy conservation are determined by the adopted approach applicability, cost range, maintenance issues, and additional factors. Energy conservation involves efficiency improvements, formulation of pricing policies, good “housekeeping practices,” and load management strategies, among other measures. A significant reduction in consumer energy costs can occur

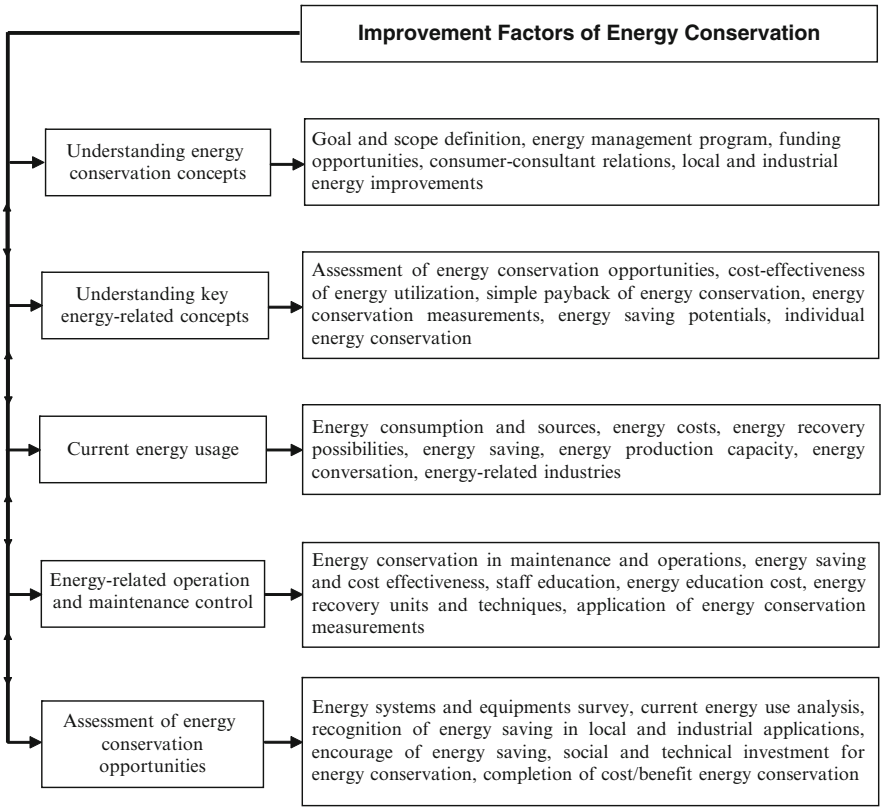

Fig. 4.2 Improvement factors of energy conservation

if conservation measures are adopted appropriately. The payback period for many conservation programs is less than 2 years.

In spite of the potentially significant benefits of such programs to the economy and their proven successes in several countries, conservation programs have not yet been undertaken on a significant scale in many developed and developing countries. Some reasons for this lack of energy conservation programs relate to the following factors:

- Technical (e.g., lack of availability, reliability, and knowledge of efficient technologies)
- Institutional (e.g., lack of appropriate technical input, financial support, and proper program design and monitoring expertise)
- Financial (e.g., lack of explicit financing mechanisms)
- Managerial (e.g., inappropriate program management practices and staff training)
- Pricing policy (e.g., inappropriate pricing of electricity and other energy commodities)
- Information diffusion (e.g., lack of appropriate information)

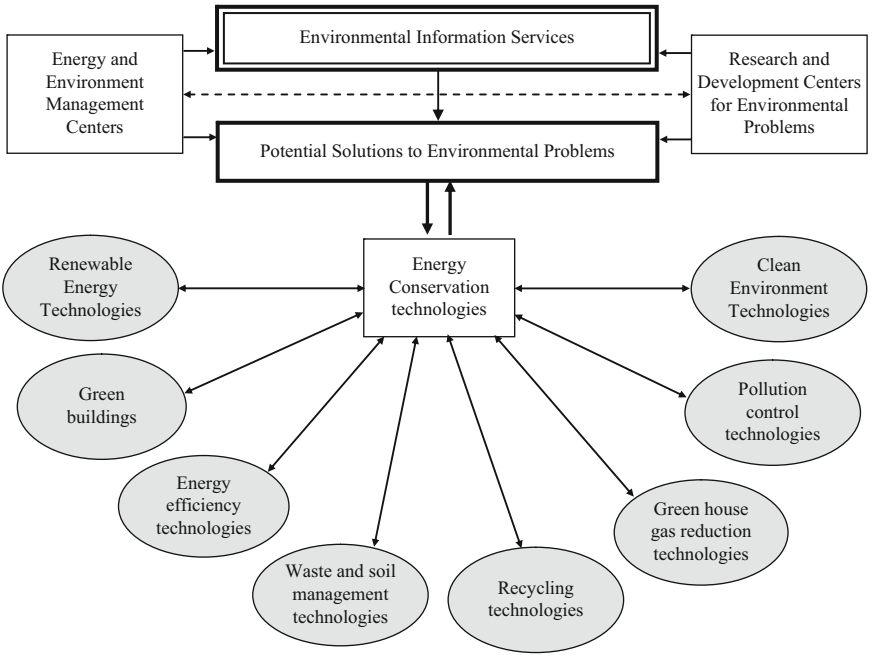

Fig. 4.3 Linkages between possible environmental and energy conservation technologies

Reduced energy consumption through conservation programs can benefit not only consumers and utilities, but also society as well. In particular, reduced energy consumption generally leads to reduced emissions of greenhouse gases and other pollutants into the environment.

Accelerated gains in energy efficiency in energy production and use, including the transportation sector, can help reduce emissions and promote energy security. While there is a large technical potential for increased energy efficiency, there exist significant social and economic barriers to its achievement. Priority should be given to market forces in effecting efficiency gains. However, reliance on market forces alone is unlikely to overcome these barriers. For this reason, innovative and bold approaches are required by governments, in cooperation with industry, to realize the opportunities for energy efficiency improvements and to accelerate the deployment of new and more efficient technologies.

Some efficiency measures, may be identified in any sector of activity. Here are some measures for buildings:

- Efficient buildings
  - Building placement is important because trees, other buildings, and landscape can provide shade and block wind.
  - South-facing windows promote passive solar heating in cold climates.
  - Light-colored roofs reduce the cooling for air conditioning in hot climate regions.
  - Window and door sealing and wall insulation reduce heat losses up to 25% to 50%.

- Efficient lighting
  - About one-fourth of electrical energy consumed by residential and commercial buildings is used for lighting; therefore, using efficient lighting is essential.
  - Effective use of daylight is essential.
- Appliances
  - Promote the use of heat pumps.
  - Use local cogeneration from natural gas instead of only heating.
  - Promote floor heating or ceiling cooling for better comfort and savings.
  - Use natural gas instead of electrical ovens and cooktops.
  - Enhance insulation of freezers.

Here, we can look at the energy conservation measures that may be classified into six categories:

- Sectorial measures
- Energy conservation through systematic use of unused energy
- Energy conservation by changing social behavior
- International cooperation to promote energy conservation to counteract global warming
- Enhancing international and government-industry-university cooperation in developing technologies for energy conservation
- Promoting diffusion of information through publicity and education

The main emphasis is given to sectorial energy conservation, and Table 4.1 presents some examples of such sectorial energy conservation measures. After determining which energy conservation measures are applicable, you should then read through the description of each of the applicable energy conservation measures. Information about the savings that can be expected from the measure, maintenance issues related to the measure, and other factors to consider are provided for each energy conservation measure. In order to evaluate the energy conservation measures, the following parameters should be taken into consideration (e.g., Nolden et al. 1998).

Cost estimation: The first step is to estimate the cost of purchasing and installing the energy conservation measure. Cost estimates should be made for the entire development rather than for a single piece of equipment (e.g., obtain the cost for installing storm windows for an entire development or building, rather than the cost of one storm window). If you are planning to implement the energy conservation measure without the help of an outside contractor, cost estimates can be obtained by calling a vendor or distributor of the product. If, on the other hand, you will be using a contractor to install or implement the energy conservation measure, the contractor should provide estimates that include all labor costs and contract margins.

Data survey: In this step, the questions can be considered on fuel consumption and cost and should list more than one possible fuel type. The appropriate data for fuel should be selected and provided for analysis and calculation.

Energy saving: The amount of energy or fuel used should be estimated.

Table 4.1 Sectorial energy conservation measures

Sector	Measures
Industrial	Strengthening of financial and tax measures to enhance adoption and improvement of energy-saving technologies through energy conservation equipment investments
	Reuse of waste energy in factories and/or in surrounding areas
	Enhancing recycling that reduces primary energy inputs such are iron scraps and used paper, and devising measures to facilitate recycling of manufactured products
	Retraining of energy managers and diffusion of new energy-saving technologies through them
	Creating databases on energy conservation technologies to facilitate diffusion of information
Residential and commercial	Revising insulation standards provided in the energy conservation law, and introducing financial measures to enhance adoption of better insulation
	Developing better insulation materials and techniques
	Developing "energy conservation" model homes and total energy use systems for homes
	Revising or adopting energy conservation standards for home and office appliances
	Developing more energy-saving appliances
	Revising guidelines for managing energy use in buildings, and strengthening advisory services to improve energy management in buildings
Transportation	Since 80% of energy consumption of this sector is by automobiles, further improvement in reducing fuel consumption by automobiles is necessary, together with improvement in transportation systems to facilitate and reduce traffic flow
	Diffusion of information about energy-efficient driving
	Adopting financial measures to enhance the use of energy-saving transportation equipment such as wind-powered boats

Data from Dincer and Midilli (2007)

Cost saving: This step is considered to determine the level of savings.

Payback period: The last step on each of the cost/benefit ratios is to estimate the simple payback period. The payback period is found by dividing the cost of the measure by the annual cost savings.

Some technical limitations on energy conservation are associated with the laws of physics and thermodynamics. Other technical limitations are imposed by practical technical constraints related to the real-world devices that are used. For example, the minimum amount of fuel theoretically needed to produce a specified quantity of electricity could be determined by considering a Carnot (ideal) heat engine. However, more than this, a theoretical minimum fuel may be needed due to practical technical matters such as the maximum temperatures and pressures that structures and materials in the power plant can withstand.

As environmental concerns such as pollution, ozone depletion, and global climate change became major issues in the 1980s, interest developed in the link between energy utilization and the environment. Since then, there has been increasing attention to this linkage. Many scientists and engineers suggest that the impact

of energy-resource utilization on the environment is best addressed by considering exergy. The exergy of a quantity of energy or a substance is a measure of the usefulness or quality of the energy or substance, or a measure of its potential to cause change. Exergy appears to be an effective measure of the potential of a substance to impact the environment. In practice, the authors feels that a thorough understanding of exergy and how exergy analysis can provide insights into the efficiency and performance of energy systems are required for the engineer or scientist working in the area of energy systems and the environment (for details, see Rosen and Dincer 1997). Considering the above explanations, the general aspects of energy conservation can be summarized as in Fig. 4.4.

A pivotal aspect to energy conservation is life-cycle cost analysis. From the energy conservation point of view, life-cycle costing appears to be a potential tool in deciding which system or product is more cost effective and more energy efficient. It can provide information about how to evaluate the options concerning design, sites, materials, and so on; how to select the best energy conservation

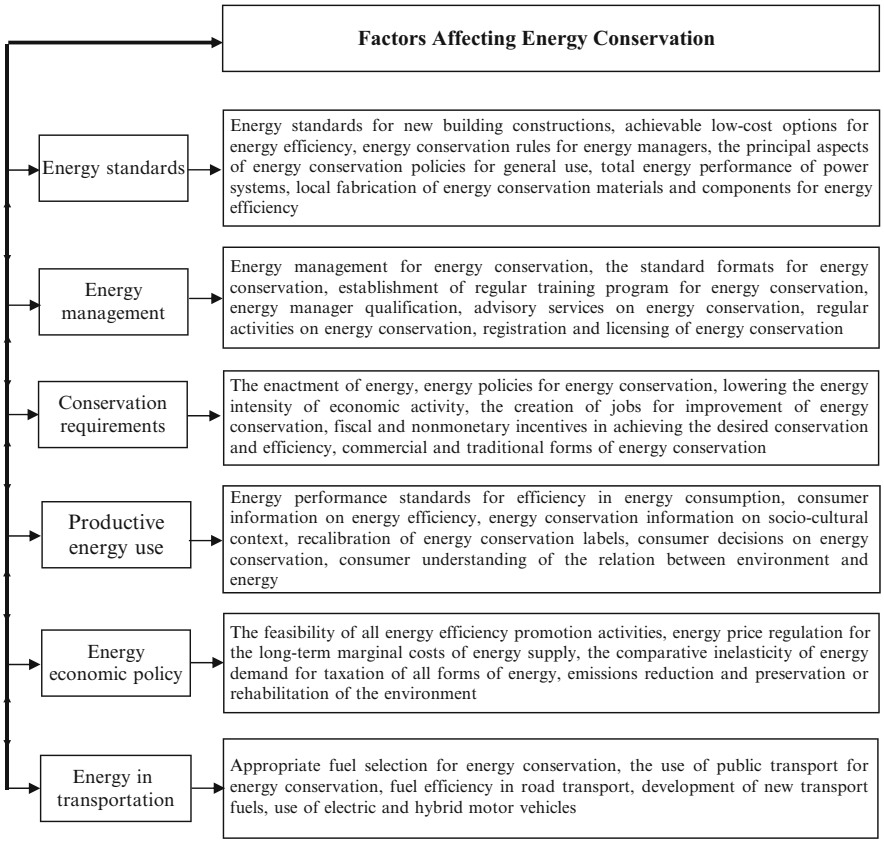

Fig. 4.4 A flow chart presenting factors affecting energy conservation

feature among various options; how much investment should be made in a single energy conservation feature; and which is the most desirable combination of various energy conservation features.

A choice can be made among various options of the energy conservation measure that produces maximum savings in the form of reduction in the life-cycle costs. For instance, a choice can be made between double-glazed and triple-glazed windows. Similarly, a life-cycle cost comparison can be made between a solar heating system and a conventional heating system. The one that maximizes the life-cycle costs of providing a given level of comfort should be chosen. This kind of application of such techniques to energy conservation is related to determining the optimum level of the chosen energy conservation measure. Sometimes energy conservation measures involve the combination of several features. The best combination can be determined by evaluating the net life-cycle costing effects associated with successively increasing amounts of other energy conservation measures. The best combination is found by substituting among the choices until each is used to the level at which its additional contribution to energy cost reduction per additional dollar is just equal to that for all the other options.

The following basic steps are the key points in implementing an energy conservation strategy plan (Dincer 2003):

1. *Defining the main goals*: It is a systematic way to identify clear goals, leading to a simple goal-setting process. It is one of the crucial concerns and follows an organized framework to define goals, decide priorities, and identify the resources to meet those goals.
2. *Identifying the community goals*: It is significant step to identify priorities and links among energy, energy conservation, environment, and other primary local issues. Here, it is also important to identify the institutional and financial instruments.
3. *Environmental scan*: The main objective in this step is to develop a clear picture of the community to identify the critical energy-use areas, the size and shape of the resource-related problems facing the city and electric and gas utilities, the organizational mechanisms, and the base data for evaluating the program's progress.
4. *Increase public awareness*: Governments can increase consumers' awareness and acceptance of energy conservation programs by entering into performance contracts for government activities. They can also publicize the results of these programs and projects. In this regard, international workshops to share experiences on the operation would help to overcome the initial barrier of unfamiliarity in countries.
5. *Information analysis*: It carries out a wide range of telephone, fax, e-mail, and Internet interviews with local and international financial institutions, project developers, bilateral aid agencies to capture new initiatives, and lessons learned and viewpoints on problems and potential solutions.
6. *Building community support*: It covers the participation and support of local industries and public communities, and understanding the nature of conflicts

and barriers between given goals and local actors; improving information flows; activating education and advice resources; identifying institutional barriers; involving a broad spectrum of citizen and government agencies; referring to participation and support of local industrial and public communities.

7. *Analyzing information*: It includes defining available options and comparing the possible options, such as program implementation costs, funding availability, utility capital deferral, potential for energy efficiency, compatibility with community goals, environmental benefits, and so on.
8. *Adopting policies and strategies*: Priority projects need to be identified through a number of approaches. Which are the best projects for the community? The decision process should evaluate the cost of the options in terms of savings in energy cost, generation of business and tax revenues, and the number of jobs created, as well as their contribution to energy sustainability and their benefit to other community and environmental goals.
9. *Developing the plan*: Once the draft plan has been adopted, it is important for the community to review it and comment upon it. The public consultation process may vary, but a high level of agreement should be the goal.
10. *Implementing new action programs*: It decides which programs to concentrate on, with long-term aims being preferred over short-term aims. The option that has the greatest impact should be focused on, and all details defined, no matter how difficult it seems. Financial resources need to be identified to implement the programs.
11. *Evaluating the success*: It is the final stage for evaluating and assessing how well the plan performed, identifying its strength and weaknesses, and determining who is benefiting from it.

In summary, this section provides an overview of those ways/approaches that implement energy conservation through energy management, policy, efficiency, and economics. Some general peculiarities for each relevant sector are mentioned, as in Table 4.1.

In the next section, we focus on policy and its impact on energy conservation. In order to illustrate the influence of policy, several illustrative cases are presented.

4.4 Energy Conservation Policies: Illustrative Examples

Policy has a key role in promoting energy conservation and influencing the behavior of the society as a whole. It is instructive to give here some concrete examples of actions that can be taken through policy measures in favor of energy conservation practices. Detailed information on these illustrative examples is available in OECD (1995).

Example 4.1: Public Awareness Campaigns

In this example, the significance of the public awareness campaigns is highlighted. One such energy conservation campaign was conducted in a developing country, Hungary. During the 1990s, three nationwide energy-saving campaigns have been

conducted in Hungary. One of them was a PHARE energy-saving campaign undertaken in 1993 by the Ministry of Industry and Trades and coordinated by the Hungary-EC Energy Centre (PHARE is the "Poland and Hungary: Assistance for Restructuring their Economies" programme and EC is "European Commission"). A media campaign using television, cinema, and newspaper advertising was the central element of the campaign.

Television was used extensively to maximize the reach and frequency of the message. In the first part of the television campaign, a 60-second advertisement was broadcast 16 times as an initial attention-grabbing message. In the second phase, a 30-second advertisement was broadcast 40 times as a reminder of the message. The slogan of the campaign was "You pay twice," that is, once for wasted energy and once for the environmental damage. A public-relations campaign for the program began and ended with a press conference attended by radio, television, and newspaper journalists. A weekly press release was issued, each with a different theme, such as "energy saving at home" and "how to save energy when cooking."

A leaflet giving simple low- or no-cost energy-saving tips for householders was prepared and distributed with the cooperation of electricity distribution companies. A school program was also implemented for children aged 10 to 14 years. The school programs included a competition asking questions about energy use and energy savings, with prizes of T-shirts and mugs with the logo and slogan of the campaign. There are both positive and negative lessons from this project:

- Publicity campaigns can succeed in changing even deeply held attitudes.
- Accurate targeting of the message and creative advertising with strong impact are important.
- Television advertising was the most effective medium to influence attitudes, and press advertising was a useful support to television advertising, but cinema advertising appeared to be ineffective.

Further information on the energy conservation policies in Hungary can be found in UNFCCC (1994).

Example 4.2: Initiating a Municipal Board for Energy and Its Conservation

Here, the importance of energy conservation is pointed out by the following example, in which the Ontario Municipal Energy Collaborative (OMEC) was conceived by the International Council for Local Environmental Initiatives (ICLEI) in 1993, in partnership with the Ontario Ministry of Environment and Energy and 11 municipalities in Ontario. The major objectives of the OMEC were to stimulate private-sector investment in aggregated municipal energy-efficiency projects, to overcome traditional barriers to energy efficiency including moving local government away from an incremental approach, and to provide efficient energy utilization in buildings, as well as developing CO_2 emission reduction technologies. The OMEC contributes to the local environment in the following ways:

- By providing a strategic approach to managing energy-efficiency resources within municipality buildings and facilities. Energy supply curve analyses and intercity comparison techniques are applied to evaluate the overall energy intensities and energy management practices.

- By stimulating local jobs and expertise.
- By enhancing the quality of working environments (i.e., indoor air quality, lighting, etc).
- By demonstrating local government leadership and sound asset management through significant energy savings.
- By increasing awareness of energy-efficiency potentials among local politicians and the general public.

In terms of the global environment, the OMEC contributes in several ways, as follows:

- By providing a model for implementing wide-scale energy-efficiency endeavors that can be replicated in other cities. The OMEC, as potentially the first aggregated demand side management for carbon abatement project, could help set the framework for incorporating CO_2 abatement into energy-efficiency schemes.
- By creating pressure on the national government to emulate local government performance in energy efficiency.
- By contributing to lower opportunity costs that other countries can benefit from, including more efficient technologies and verification procedures.
- By encouraging long-term, rather than short-term, energy-efficiency policies, which result in greater energy and environment savings and more local jobs.

The project was initiated in March 1993 and within 2 years it provided the following:

- A 37% saving on municipal energy and water costs, based on a 7-year payback period for the OMEC cities.
- A 20-MW reduction of electricity demand, primarily calculated on marginal intensity.
- A 500,000-tonne reduction in CO_2 emissions per year.

Example 4.3: Influential Activity of a Professional Association

In this example, the case study details progress made in pursuit of energy efficiency in Stockholm, Sweden, which was run from 1974 to 1984 (although some of the activities still continue to date), by the Association of Swedish Energy Advisors (ASEA). The main aims were:

- To introduce energy-efficiency programs and renewable energy technologies.
- To promote education and information concerning energy efficiency in buildings.
- To reduce the dependence on oil from 70% to 35%.
- To reduce CO_2 emissions through taxation and fees on CO_2 and SO_2.

First, the government established voluntary programs to offer advice and inspection services at the local level, to provide services for tuning boilers and burners and services for insulation and draft proofing, and to measure domestic hot water consumption. The emphasis was on energy conservation for reducing losses, lowering indoor temperatures, and similar goals.

The type of advice provided included measures to:

- Reduce indoor space temperatures and hot water temperatures
- Tune boilers
- Change furnishings
- Install draft-proof windows and doors
- Add thermal insulation
- Install heat pumps

The ASEA knew that to achieve the greatest benefit, the above measures needed to be implemented as a package, rather than individually. With increasing awareness of the threat of climate change, energy became part of the wider environmental strategy. Therefore, the focus was then on improving efficiency and environmental quality.

Consequently, after some successful implementation policy, the energy initiatives have resulted in a 15% decrease in energy consumption, showing that the energy advice program has achieved its goals.

These two case study examples indicate that such programs can lead to a reduction in ambient pollution, a decrease in emissions, a decrease in wastes sent to final disposal, a reduction in energy consumption, and a reduction in the use of raw materials.

Example 4.4: Encouraging Vehicle Fuel Savings Through Policy

In recent years, the United States government has tried to encourage through various policy measures energy savings for vehicles. One component of these measures envisages better fuel efficiency. In this respect, taxpayers have been eligible for income tax credits for purchasing hybrid vehicles. Another component envisages reduction of fuel consumption by encouraging commuting. To do this, carpooling and subsidized public transportation were encouraged by many municipalities; moreover, high-occupancy vehicle lanes and lower tolls for cars with multiple passengers were designated. Drivers are intentionally encouraged to drive at economical speed by placing signs indicating recommended car speed, which is 45 to 55 mph.

Example 4.5: Net Zero Energy Buildings Initiative

In the U.S. and the European Union, buildings use about 40% of the total energy consumption. An sample energy distribution of a household is illustrated in Fig. 4.5. This plot shows that a major contributor to energy consumption in buildings comes from space heating and air conditioning, followed by water heating.

Hence, for energy conservation, this “sources of consumption” must be diminished. Thus, better building insolation is suggested. In this direction, in many countries (e.g., U.S., Canada, Germany, U.K., France, Netherlands, and others), programs called “zero energy building” or “net zero energy building” or “ultra-low energy house” were initiated.

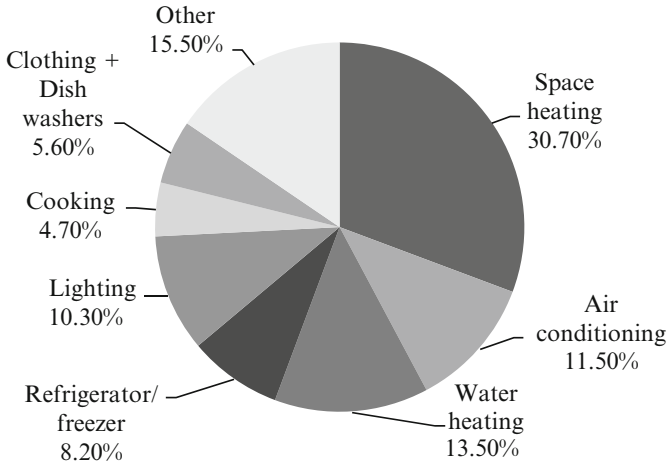

Fig. 4.5 Household energy use [data from DOE (2008)]

The term *net zero energy building* does not mean that within the building there is no energy consumption, but rather that the needed energy is generated locally from renewable resources, especially wind and solar. There are a variety of concepts here:

- Net zero site energy use, meaning that the amount of renewable energy generated locally is balanced by the energy used within the building.
- Net zero source energy use, meaning that more energy is generated locally than in a "net zero site energy use" building to compensate for the losses in electrical lines.
- Net zero energy emissions, also known as zero carbon building, compensate the used energy sources from fossil fuel (that generate CO_2) with the renewable energy production on-site.
- Net zero cost building compensates the cost for purchasing energy with the revenue from selling locally generated energy from renewables.
- Net off-site zero energy use refers to buildings that do not generate energy locally but purchase energy that is 100% from renewable sources.
- Off-the-grid building generates locally renewable energy and uses energy storage techniques to satisfy all local needs, without being connected to the grid.

Any kind of zero energy building includes complex energy conservation features, and therefore the investment is comparatively high. Therefore, subsidies are essential in promoting such technology. Some examples illustrating the involvement of energy policy in promoting zero energy buildings are summarized here:

- In California, there are important subsidies for purchasing photovoltaic (PV) panels and reducing household consumption, as a first step to zero energy buildings (see Clarum 2003). California provides $3.2 billion subsidies for residential and commercial net zero energy buildings (see Go Solar 2008).

- The Chinese government offers economic support to finance a 71-story building in Guangzhou that use a distribution system supplied with wind and solar energy (see Skidmore 2008).
- In Canada, the "Now House Project" is sponsored by the Canada Mortgage and Housing Corporation to build 12 near zero energy buildings across the country (see Equilibrium Housing Competition 2008).
- The U.K. plans to grant exemption from the stamp duty land tax lasting until 2012 for all zero carbon emission homes up to GBP 500,000 in value (see U.K. Budget 2008).

Example 4.6: Material Recycling in Ontario

One possible path to energy conservation is by recycling expensive materials that otherwise must be mined and processed with the expense of higher energy. Moreover, by recycling materials that are often toxic (e.g., mercury), one may reduce the environment pollution through waste. The Recycling Council of Ontario implemented a program called "take back the light," which is the first comprehensive fluorescent bulb recycling program in Ontario (RCO 2008). The program addresses businesses in the commercial and industrial sector and aims to recover 30 million fluorescent bulbs a year. Participants in the program also benefit from unique branding opportunities and ongoing promotion of this program in the Ontario marketplace. This program is a consequence of Ontario's commitment to electricity conservation by setting the goal of reducing the province's consumption by 6.3 GW by 2015. The benefits of this program are as follows:

- Avoids disposal of fluorescent bulbs in landfills and thus contamination of the environment with mercury (mercury can contaminate air, water, and soil).
- Recovers about 312 kg of mercury a year.
- Each bulb collected is recycled, with 98% recovery of glass, aluminum, phosphorus, and mercury, and these materials are used for new products; energy is saved in this way.
- Promotes economic growth by lowering the price of bulbs for the participants in the recycling program; as the number of participants increase, the prices decrease.
- The participants are contacted through the governmental Web site.

4.5 Energy Management and Audit

In any production process, energy is one of the inputs, which among labor, capital investment, and materials accounts for 5% to 10% of the total cost of the production (Kreith and Goswami 2008). Since production processes involve management of the resources, energy, as one of the inputs, must be the object of thorough management. In a restrained sense, energy management refers to monitoring of the expenditures of fuels or electricity. In a larger sense, energy management involves monitoring all energy fluxes, energy audits, and planning, all with the aim of achieving improved energy efficiency, increased savings, and reduced costs.

Let us review the types and procedures of energy audits, which are the first step in designing an energy management scheme. Four types of audits can be distinguished:

- Walk-through audit provides immediate measures for energy and operating cost savings by identifying low-cost actions to be taken (e.g., retrofitting the thermal insulation of the balance of plant).
- Cost analysis evaluates the operating and energy cost history over several years to identify peak and seasonal demands and potential paths for energy savings.
- Standard energy audit is a comprehensive energy analysis that includes the development of a baseline for the energy use, evaluation of energy savings, possible energy conservation measures, and cost-effectiveness.
- Detailed energy audit involves using an energy management system, which is an electronic assembly of sensors and software for monitoring all energy fluxes; this audit can recommend energy retrofits.

The specific tasks to follow when performing standard or detailed energy audits are as follows (see Kreith and Goswami 2008):

- Data analysis is done in general for data collected for 3 years or more, for the purpose of evaluating the characteristics of energy systems and energy use within the system. A particular aspect is to determine the effect of ambient temperature on exergy efficiency and fuel consumption. The building signature, in terms of thermal inertia, can be also determined.
- Walk-through survey identifies the potential energy-saving measures. The current operating and maintenance procedures are critically analyzed, and the existing operating conditions of major equipment are examined.
- Baseline for building energy use – develops a base case model that represents the operating conditions and energy fluxes of the system. It involves the review of process and instrumentation diagrams, inspection, and testing equipment for determining efficiency parameters and reliability.
- Evaluation of energy-saving measures implies elaborating several strategies for energy conservation using technical methods for energy savings and economic analysis tools.

Examples of energy conservation measures in a building that can result from an audit are upgrading the building thermal insulation, reducing the air infiltrations or leakages, replacing windows to enhance the daylight inside the building, and thus reducing the lighting.

It is not possible to manage any activity without proper monitoring and control. Energy management systems are computer-aided tools comprising pieces of equipment, distributed sensors and actuators, and software that are essential in energy monitoring, management, and audit. Their informatics system is known as SCADA (supervisory control and data acquisition) and it collects all measurements from the system and makes decisions regarding system regulation for best performance under energy conservation constraints. An energy management system is employed to:

Table 4.2 Energy management issues in industrial processes

Process	Energy management issues
Process heating	Maintain sufficient heating and adequate temperature through monitoring and regulation Avoid often shutting down the process because this leads to energy losses
Process cooling	Keep chillers properly loaded for maximum efficiency by managing the cooling charge Minimize the time of process exposure to the ambient conditions
Melting and fusion	Avoid overheating through proper control Monitor energy consumption to identify heat leakages or deteriorations
Chemical reactions	Proper management of feedstock and catalysis Assess the system for proper timing and correct balance for high efficiency
Distillation and fractionation	Manage overall operation timing, and run only when producing efficiently Monitor pinch analysis for feed and effluent streams
Drying	Proper adjustment of air flow through the dryer according to the charge Manage the charge and storage times for maximum efficiency
Mechanical processes	Follow the maintenance plan for mechanical equipment that consumes oil for lubrications and actuations, needs replacement of belt transmission systems, etc. Manage system and equipment run times
Electrical processes	Assure that voltage and current levels are appropriate by monitoring Check regularly for electromagnetic interferences, hysteresis, power factor, phase balance, grounding, and proper insulation
Combustion systems	Proper control of combustion and flame stabilization Fuel management
Pumps, fans, compressors	Good control of the circulation rate Follow maintenance scheme

- Record and compare energy usage by the day, week, month, season, and year
- Monitor all utility services (electricity, gas, water, steam, etc.)
- Evaluate and optimize energy storage strategies (e.g., load shaving)
- Detect and identify problems with nonefficient subsystems

Note that an effective energy management system within an industrial facility can reduce the energy cost by 2% to 3%, which in many practical situations justifies the investment in it. In Table 4.2, some key energy management measures relevant to various industrial processes are listed, which may lead to energy conservation improvement.

4.6 Selection of More Efficient Energy Options

Meeting the energy needs by increasing conversion (and distribution) efficiency rather than consumption of primary sources is a beneficial approach to energy conservation. Energy efficiency leads to economic growth because it lowers the cost of goods and services as a consequence of providing cheaper energy.

Therefore, implementing energy efficiency methods do not necessarily mean that energy consumption in a society is reduced; on the contrary, it may increase as a result of economic growth.

Promotion of efficient energy systems means rationally choosing among options, so that better designs can be obtained by analyzing alternatives and picking the most suitable one. It also means encouraging the most efficient solution through adequate policy (recall the example above with recycling fluorescent bulbs from Ontario).

In what follows we give some illustrative examples to show how efficiency plays a major role in energy conservation in any society. One of the relevant measures that quantify efficiency is exergy (a parameter extensively used within this book—see definition in Chapter 1). Through exergy efficiency, it is possible to identify the rational choice. A system that is efficient from the exergetic point of view is also energy efficient. However, if the system is optimized for energy efficiency only, that is, considering in the analysis only the energy fluxes and ignoring their associated exergy, the system/design choice is not necessarily a good one.

Example 4.7: Using Compact Fluorescent Bulbs

In this illustrative example, simple life-cycle costing analysis is applied for lighting in the case of both incandescent bulbs and compact fluorescent bulbs and comparing their life-cycle costs as detailed in Table 4.3. We know that incandescent bulbs are less expensive but less efficient (95% of the energy goes to heat and 5% to usable light), and compact fluorescent bulbs are more expensive but much more energy efficient.

So, the question here is which type of lighting comes out on top in an LCC analysis? This example, according to Table 4.3, clearly shows how life-cycle costing analysis helps in energy conservation and that we should make it part of our daily life.

Example 4.8: Is the Most Efficient the Best Choice?

This example illustrates that the most efficient available system will not be the best choice. The key point is that from a class of systems (e.g., water heater), the most efficient one has the higher price. Therefore, the investment cost is high, while,

Table 4.3 An example of life-cycle costing analysis

Cost of purchasing bulbs	Incandescent	Compact fluorescent
Life time of one bulb (h)	1,000	10,000
Bulb price ($)	0.5	6.0
Number of bulbs for lighting 10,000 h	10	1
Cost for bulbs ($)	$10 \times 05 = 5.0$	$1 \times 6 = 6$
Energy cost		
Equivalent wattage (W)	75	12
Watt-hours (Wh) required for lighting for 10,000 h	$75 \times 10{,}000 = 750{,}000$ Wh $= 750$ kWh	$12 \times 10{,}000 = 120{,}000$ Wh ≥ 120 kWh
Cost at 0.05 per kWh	750 kWh $\times$ \$0.05 = *\$37.5*	120 kWh $\times$ \$ 0.05 = *\$6*
Total cost ($)	*5 + 37.5 = 42.5*	*6 + 6 = 12*

Data from Dincer and Midilli (2007)

because of the high efficiency, the operating cost during the lifetime is low. The simplified cost formula is

$$C_t = C_i + C_o, \tag{4.1}$$

where C_t is the life-cycle cost, C_i is the investment cost, and C_o is the operating cost during the lifetime.

If the system is less efficient, in contrast, the investment cost is low while the operating cost is high. Hence, the two extreme situations lead to a high life-cycle cost. The optimum efficiency that minimizes the cost is somewhere in between. This reasoning is valid also for systems that save energy by harvesting from renewable sources (solar, wind, etc.).

Let us assume a PV panel. In this case, the life-cycle cost can be simply modeled as the difference between the investment cost and the energy saved during life cycle S. If one denotes the harvested energy during the lifetime by E, the unit cost of electrical energy by c_e, and the conversion efficiency by η, then $S = \eta E c_e$ and life-cycle cost is

$$C_t = C_i(\eta) - \eta E c_e. \tag{4.2}$$

Assume in this example that during the life cycle, the cost of harvested (but not converted) energy is $E \times c_e = \$10{,}000$ per square meter of solar panel (this is the cost of the incident radiation). Then, the cost of saved energy is $S = 10{,}000 \times \eta$. It is given also that the investment cost in solar panels varies with the efficiency according to the quadratic relationship $C_i = 31{,}809\eta^2 - 2{,}382.5\eta + 862.67$, measured in \$/m^2. The two curves $C_i(\eta)$ and $S(\eta)$ are illustrated in Fig. 4.6.

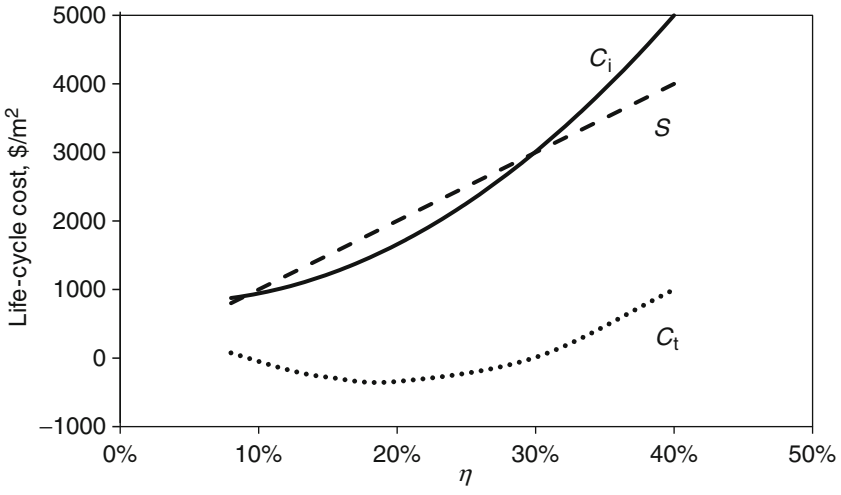

Fig. 4.6 Example of choosing the efficiency that minimizes the life-cycle cost

Their difference representing the total cost $C_t(\eta)$ has a minimum for $\eta = 19.5\%$ and a negative for $C_t = -\$342.4/m^2$. The minus sign indicates that there are life-cycle savings. Thus, an investment in panels with 20% efficiency is the right choice.

Example 4.9: Heat Pumps vs. Electric Heating

Heat pumps convert mechanical energy into high-temperature heat while at the same time recover heat from a low-temperature source. Therefore, they are more efficient than electrical heaters. In many countries, household water is heated in electrical water heaters with accumulation. A thermostat is used to stabilize the temperature in the range of 40°C to 50°C. The exergy efficiency of electrical heaters can be easily calculated if one knows the water temperature T:

$$\psi_E = \frac{Q(1 - T_0/T)}{E} = 1 - \frac{T_0}{T}, \tag{4.3}$$

where E is the electrical energy input and Q is the amount of heat. In an electrical heater, the electrical energy is integrally converted into heat, therefore $Q = E$. The temperature T_0 in Eq. (4.3) represents the reference (ambient) temperature. Since $T_0 = 300$ K and $T = 350$ K, the exergy efficiency of a household water heater is about 14%.

If a heat pump is used instead, its coefficient of performance (COP) is in the range of 2 to 5. Therefore, the exergy efficiency of a heat pump water heater is

$$\psi_P = \frac{Q(1 - T_0/T)}{E_P} = \mathrm{COP}\left(1 - \frac{T_0}{T}\right) = \mathrm{COP}\psi_E \tag{4.4}$$

or in other words, the exergy efficiency of the heat pump is from two to five times higher than that of an electrical heater. This means that much better energy utilization is obtained and conservation is obtained by promoting heat pumps.

Assume that a homeowner wants to invest in a heat pump to replace his water heater. During the lifetime of the product, he must pay price C_P for the electrical energy consumed by the heat pump, E_P. This price is lower than C, which would be paid for an electrical heater consuming the energy E during the lifetime (one assumes the same lifetime for both systems). The ratio between C_P and C is

$$\frac{C_P}{C} = \frac{E_P}{E} = \frac{Q/\mathrm{COP}}{Q} = \frac{1}{\mathrm{COP}}, \tag{4.5}$$

where one assumes that the same useful heat Q is produced by both systems to be compared.

Therefore, the savings during the lifetime, which result from consuming less energy, are

$$S = C - C_P = C \times \frac{\mathrm{COP} - 1}{\mathrm{COP}}. \tag{4.6}$$

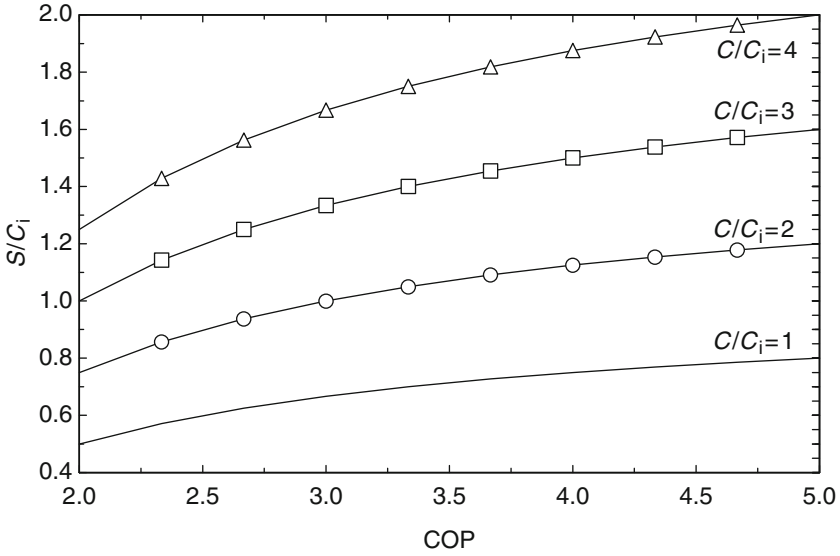

Fig. 4.7 The life-cycle savings per unit of investment cost by replacing an electrical water heater with heat pumps

If the savings are larger than the capital investment in the heat pump, C_i, then the investment is economically justifiable; otherwise it is not. To study this aspect further, we plot the ratio S/C_i for a range of COP and several values of C/C_i as indicated in Fig. 4.7.

From this plot we see that the cost of energy consumed for electrical heating during the lifetime vs. the investment cost in the heat pump is more than double, and using heat pumps becomes economically attractive because the savings are higher than the investment. Also we see that if C/C_i doubles, then S/C_i doubles, meaning that the payback period reduces by half.

The picture can be made even more favorable to heat pump implementation through an appropriate taxation policy. With proper tax credits, the heat pumps can be made economically attractive even for $C/C_i < 1$, enforcing thus their proliferation in society.

4.7 Concluding Remarks

Energy conservation is a key element in sectorial (e.g., residential, industrial, commercial, etc.) energy utilization and is vital for sustainable development. It should be implemented by all possible means, despite the fact that it sometimes has its own limitations. This is not only required for today but also for the next generation as well. A secure supply of energy resources is generally agreed to be a necessary but not sufficient requirement for development within a society.

An enhanced understanding of the environmental problems relating to energy conservation presents a high-priority need and urgent challenge, both to allow the problems to be addressed and to ensure the solutions are beneficial for the economy and the energy systems.

All policies should be sound and make sense in global terms, that is, become an integral part of the international process of energy system adaptation that will recognize the very strong linkage existing between energy requirements and emissions of pollutants (environmental impact).

This study highlights the current environmental issues and potential solutions to these issues, identifies the main steps for implementing energy conservation programs and the main barriers to such implementations, and provides assessments for energy conservation potentials for countries, as well as various practical and environmental aspects of energy conservation.

Nomenclature

c	Unit cost, currency/J
C	Cost, any currency
COP	Coefficient of performance
E	Harvested energy, J
Q	Heat, J
S	Saved energy, J
T	Temperature, K

Greek Letters

η	Conversion efficiency
ψ	Exergy efficiency

Subscripts

0	Reference state
e	Electrical
E	Electric heater
i	Investment
o	Operation
P	Heat pump
t	Total

References

Clarum 2003. Clarum Homes press release: Clarum unveils California's first zero energy building community. Palo Alto, April 1. Internet source http://clarum.com/PR.

Dincer I. 2003. On energy conservation policies and implementation practices. *International Journal of Energy Research* 27:687–702.

Dincer I., Midilli A. 2007. Energy conservation. In: Encyclopedia of Energy Engineering and Technology, Capehart B.L. ed, Chapter 57, CRC Press, New York.

Dincer I., Rosen M.A. 1998. A worldwide perspective on energy, environment and sustainable development. *International Journal of Energy Research* 22:1305–1321.

DOE 2008. Buildings Energy Data Book. Department of Energy. Internet source http://buildings-databook.eren.doe.gov (accessed on December 12, 2008).

Equilibrium Housing Competition 2008. Internet source http://www.cmhc.ca/en/en_001.cfm (accessed on December 12, 2008).

Go Solar 2008. Go Solar California Web Site. Internet source http://www.gosolarcalifornia.ca.gov (accessed on January 15, 2009).

Kreith F., Goswami D.Y. 2008. Energy Management and Conservation Handbook. CRC Press, New York.

Nolden S.D., Morse D., Hebert S. 1998. Energy Conservation for Housing—A Workbook. Contract-DU100C000018374. Abt Associates Inc., Cambridge, MA.

OECD 1995. Urban Energy Handbook. OECD, Paris.

Painuly J.P., Reddy B.S. 1996. Electricity conservation programs: Barriers to their implications. *Energy Sources* 8:257–267.

RCO 2008. Take back the light. A program of the Recycling Council of Ontario. Internet source http://www.takebackthelight.ca (accessed on December 12, 2008).

Rosen M.A., Dincer I. 1997. On Exergy and environmental impact. *International Journal of Energy Research* 21:643–654.

Skidmore 2008. Skidmore, Owings and Merrill Pearl River Tower. Internet source http://usa.autodesk.com/company/sustainability-center/articles/skidmore-owings-merrill-pearl-river-tower (accessed on December 12, 2008).

UK Budget 2008. Internet source http://www.hm-treasury.gov.uk/ (accessed on May 10, 2009).

UNFCCC 1994. *Hungary*: Stabilisation of the Greenhouse Gas Emissions. National Communication on the Implementation of Commitments under the UNFCCC. Technical Report.

Study Questions/Problems

4.1 What do you understand about energy conservation?
4.2 List and comment on the main factors affecting energy conservation.
4.3 What is the role of policy in promoting energy conservation?
4.4 Explain the link between sustainable development and energy conservation.
4.5 List and comment on improvement factors of energy conservation.
4.6 Explain and comment on the linkages between possible environmental and energy conservation technologies.
4.7 What kind of measures one can be taken for sectorial energy conservation?
4.8 Find a real example from the media of a public awareness campaign regarding energy conservation, and comment on it.
4.9 Identify from the media or other sources one professional association that has influential activity in energy conservation.

4.10 Describe the net zero energy building initiative.
4.11 Try to quantify the benefit of material recycling for a region (country, county, municipality).
4.12 What is the role of energy management and audits?
4.13 Find an example of "selecting a more efficient option" based on the example given in Section 4.6.
4.14 Repeat the analysis from Example 4.8 but this time use a solar thermal collector. You can study various kinds (like vacuum tube collectors, or glassed panels, or phase change materials). Try to develop a curve as in Fig. 4.6 and decide the optimum efficiency of the panel.
4.15 Develop further the analysis from Example 4.9 by considering and comparing various kinds of heat pumps with real data from manufacturers.
4.16 Conduct a parametric study to compare heating a house with a natural gas furnace and heating and electricity generation locally using a power cycle driven by natural gas combustion. The power cycle rejects heat at about 80°C that is used for space heating (and possible water heating); the produced electricity is delivered to the grid or immediately consumed. To model the power cycle, assume energy efficiency in the range of 15% to 30%. Moreover, assume that some heat is lost at the sink though insulation leakages and this represents 5% to 15%.
4.17 Electrical vehicles use electromagnetic brakes for energy recovery. When the vehicle brakes, the electrical drive is switched into a generator over a battery or condenser. Assume a reasonable range for the braking system efficiency and determine the overall efficiency improvement.
4.18 Repeat the analysis from 4.17 in the case when the mechanical energy recovered during braking is stored in compressed air. At the acceleration phase, the compressed air is released over a turbine and helps reduce the gas consumption.

Chapter 5
Sustainable Development and Energy Policies

5.1 Introduction

We live in a period characterized by accentuated transition efforts from a fossil fuel–based economy toward a projected economy based on sustainable energy. The development of a global society passed through the fossil fuel era when most primary energy had been obtained by combustion of coal, petroleum, and natural gas. In the present period, there is larger panoply of primary energy sources that include nuclear power and hydroelectricity; in addition, other forms of renewable energy have gained terrain such as wind, solar, biomass combustion, and biofuels for transportation. Therefore, the development of a hydrogen-fuel infrastructure for transportation is projected. Most likely in the future the combustion of fossil fuels will be performed cleanly so that zero emission power generation will be achieved at an attractive cost.

Figure 5.1 suggests that the march toward a global sustainable society is importantly influenced by policy and decision makers. Behind any policy and decision there must be a rationale that constrains the decision spectrum. Apart from various ideologies, the status of technological development and the existent theoretical assessment and prediction tools play a major role in influencing policy making and high-level decisions. This chapter discusses theoretical assessment tools and indices for sustainable development and their impact in shaping energy policies and strategies that ultimately influence the progress of society toward better and better sustainability.

Exergy analysis is of major importance in the assessment of sustainability, because exergy-based efficiency of systems and processes represents a true measure of imperfections; it also indicates the possible ways to improve energy systems and to design better ones. Destruction of exergy must be reduced as much as possible. Assessment of exergy destruction offers the opportunity to quantify the environmental impact and the sustainability of any energy system. We introduce the sustainability index and explain its influence in quantitative sustainability assessment and shaping energy policies. Other sustainability assessment indicators will be introduced as well. Some examples of energy policies and strategies include encouraging the expansion of energy and exergy efficient systems, expanding the use of renewable energy, and expanding clean fossil fuel combustion technologies.

İ. Dinçer and C. Zamfirescu, *Sustainable Energy Systems and Applications*,
DOI 10.1007/978-0-387-95861-3_5,

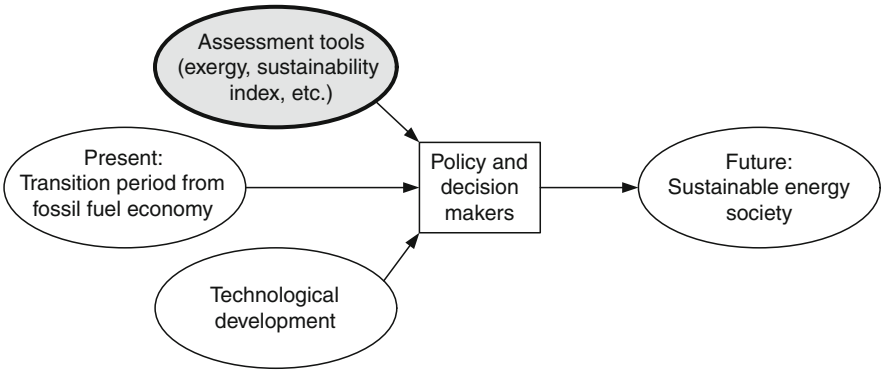

Fig. 5.1 The role of assessment tools and indicators in shaping the future sustainable society

5.2 Sustainable Energy Strategies and Policies

When shaping sustainable energy policies and strategies, it is important to understand the benefit of clean energy technologies on the one hand and the effects of fossil fuel–based systems on the other hand. The kinds of energy technologies with zero or minimum negative environmental impact (e.g., through associated pollution)—those that are more environmentally benign and more sustainable—are in general called *green energy*. Considering the benefits of green energy, sustainability of green energy supply and progress is assumed to be a key element in the interactions between nature and society. An essential increase in the scale and pace of policy instruments and their effectiveness is required to change course toward a sustainable path. It is important to possess theoretical tools to quantitatively assess green energy development and to do the following:

- Help elaborate rational strategies and policies
- Help understand green energy and sustainability issues, concepts, policies, etc.
- Identify and implement the connection between green energy use and sustainability
- Encourage the use of green energy sources
- Provide the methods for implementing energy security and green energy
- Motivate the implementation of green energy strategies for a better energy supply
- Provide solutions to reduce the negative environmental impact by proposing practical green energy strategies
- Develop the right platforms to discuss and implement green energy strategies for sectorial activities

The need for policy is justified by the fact that free markets must be enforced to meet the needs of vulnerable groups, reduce environmental pollution, and ensure energy security. At the highest level, strategies are needed, that is, plans or

methods toward a goal (in our discussion "the goal" means progress toward a global society based on sustainable energy). Once a strategy is established, the policy, which represents the course of actions to implement the strategy, must be elaborated. Any policy will specify "policy instruments," which represent specific measures taken to implement a policy. Examples of policy instruments are as follows:

- Imposing efficiency standards
- Setting public procurement policies
- Imposing appliance labeling norms
- Imposing an obligation to buy or supply energy from renewable sources
- Supporting research and development in demonstration projects

Midilli et al. (2006) provided a chart showing some key expectations from the implementation of the green energy strategies and policies for a sustainable future (Fig. 5.2). The figure suggests the crucial importance of adopting the right strategies and policies. Some examples of promising policies are given here from Jefferson (2000):

- Phasing out subsidies for fossil fuel–based energy
- Restructuring the energy sector
- Supporting energy sector innovation
- Promoting energy efficiency
- Financing rural energy
- Providing decentralized options
- Improving access to modern, efficient cooking fuel

Other factors that influence the elaboration of green energy strategies and policies (Jefferson 2000) can be summarized as follows:

- Competition among sustainable energy technologies may be hampered by market distortions that give advantages to some players.
- Improving energy efficiency requires less investment than does new generation.
- Financing large energy projects discourages smaller renewable energy projects.
- Commercialization of green energy technologies is not occurring quickly enough to meet the challenges of sustainability.
- For significant sustainable progress a critical mass of public support is needed.
- It is important to liberalize the energy markets in order to offer an opportunity to change.

In a recent study, Dincer and Rosen (2005) outlined the essential factors impacting sustainable development and their interdependencies. They referred to sustainable development as the confluence of energy and resources sustainability, economic sustainability, environmental sustainability, and social sustainability, and discussed their interrelations, as shown in Fig. 5.3. Dincer and Rosen's work is taken as the main basis of this analysis and model development.

Green energy resources and technologies are a key component of sustainable development for three main reasons (Dincer and Rosen 2005):

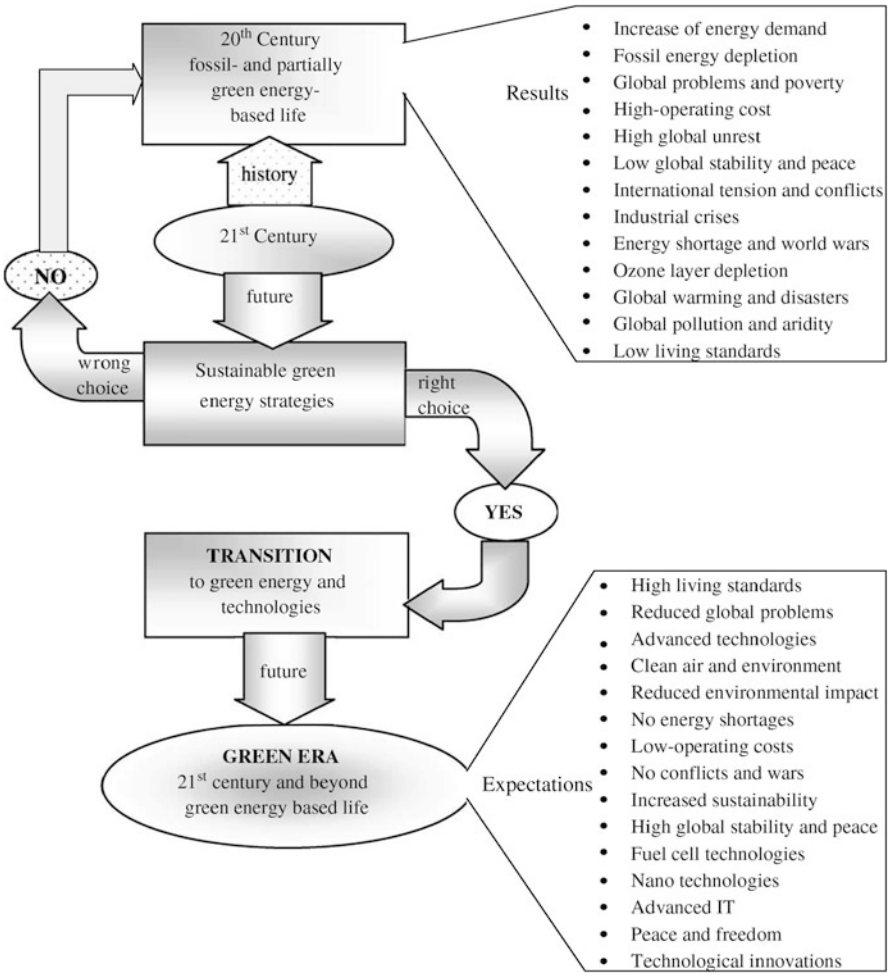

Fig. 5.2 Key expectations from implementation of green energy strategies and policies [modified from Midilli et al. (2006)]

- They generally cause less environmental impact than other energy sources. The variety of green energy resources provides a flexible array of options for their use.
- They are reliable and cannot be depleted. If used carefully in appropriate applications, green energy resources can provide a reliable and sustainable supply of energy almost indefinitely.
- They favor system decentralization and local solutions that are somewhat independent of the national network, thus enhancing the flexibility of the system and providing economic benefits to small isolated populations. Also, the small-scale equipment often reduces the time required from initial design to operation, providing greater adaptability in responding to unpredictable growth and/or changes in energy demand.

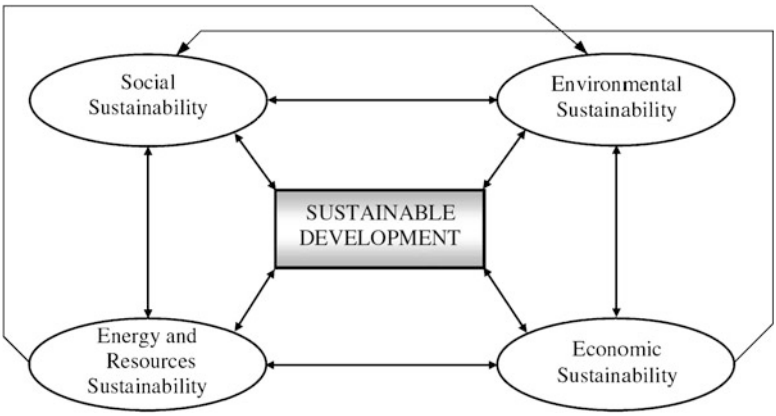

Fig. 5.3 Interdependence of the factors affecting sustainable development [modified from Dincer and Rosen (2005)]

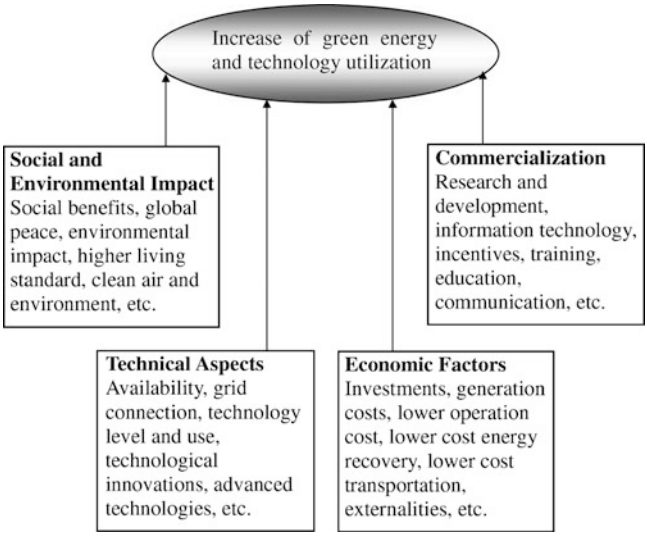

Fig. 5.4 Considerations involved in development of green energy technologies [modified from Dincer and Rosen (2005)]

The major considerations involved in the development of green energy technologies are illustrated in Fig. 5.4 and include, according to Dincer and Rosen (2005), social and environmental impact, commercialization, technical aspects, and economic factors. Apart from these considerations one can identify a number of parameters (factors) that are important in establishing green energy strategies and policies. They include public information, environmental education, innovation stimulation, promotion of technologies, financing, and very important elaborating evaluations tools and techniques. Based on Midilli et al. (2006), Fig. 5.5 shows the

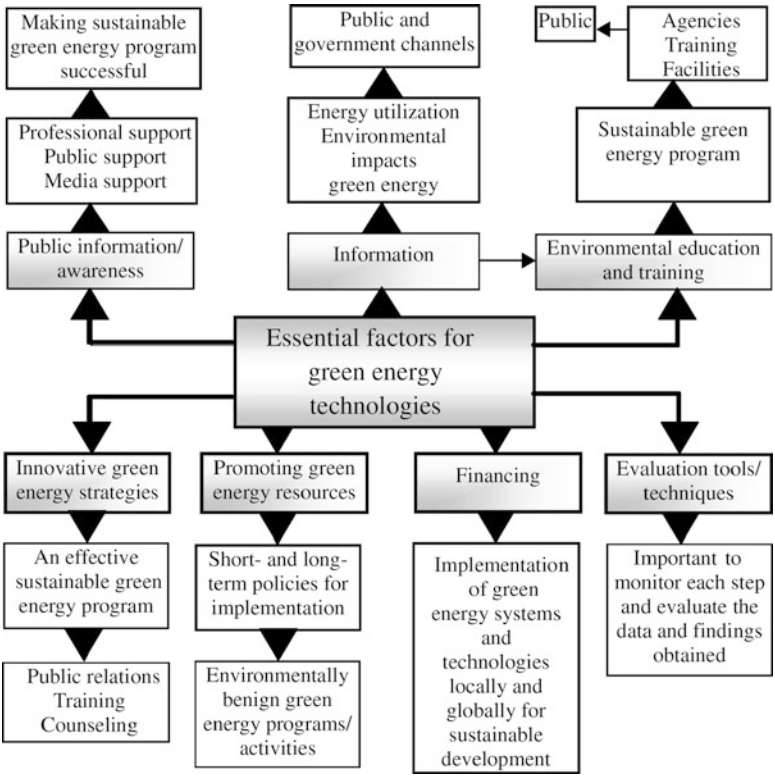

Fig. 5.5 The main factors affecting sustainable energy strategies and policies [modified from Midilli et al. (2006)]

main factors that affect the elaboration of sustainable energy policies and strategies. Green energy technologies are largely shaped by broad and powerful trends that have their roots in basic human needs. In conjunction with this, the increasing world population requires the definition and successful implementation of green energy technologies. Briefly, the important parameters and their interrelations as outlined in Fig. 5.5 are definitely required to carry out the best green energy program and select the most appropriate green energy technologies for sustainable development.

Green energy technologies are considered to play a crucial role in sustainable energy policies and their implementation for a carbon-free society in the future. The foremost factor that will determine the specific role of green energy and technologies will likely be energy demand. Therefore, green energy from renewable energy sources such as hydro, solar, wind, geothermal, wave, and biomass must be used to satisfy the demand. If so, green energy technologies can be utilized for many application fields as shown in Fig. 5.6. Thus, it appears that green energy and technologies can help do the following:

- Provide a more environmentally benign and sustainable society
- Increase energy security

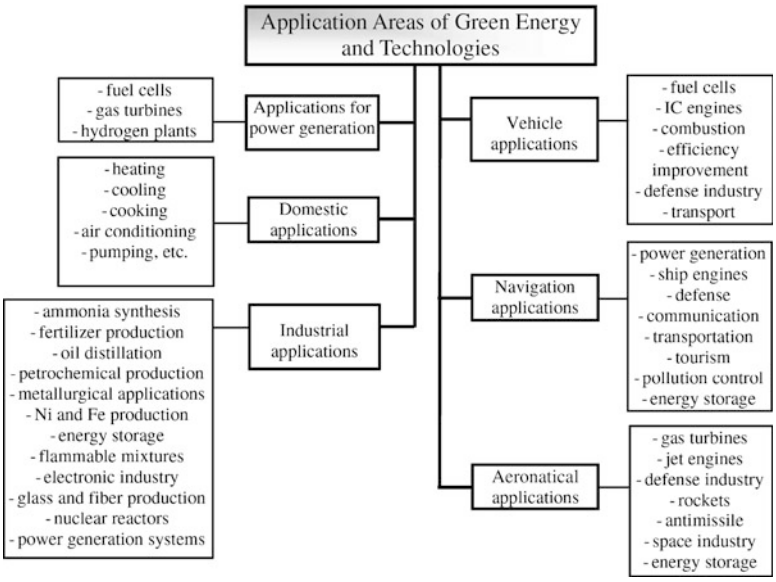

Fig. 5.6 Applications of green energy technologies [modified from Midilli et al. 2006]

- Facilitate the development of clean technologies
- Reduce air, water, and soil pollution and deforestation
- Reduce pollution-related health issues
- Contribute to a peaceful world by stopping conflicts among countries due to energy related issues

As can be understood from the above discussion, green energy and related technologies represent the unique modality through which it is possible to reduce the harmful effects of fossil fuels combustion. Therefore, the development strategies must consider elaborating policies for transition toward a green energy economy. The developed countries should play the role of drivers toward implementing such policies by increasing the investments in green and sustainable energy technologies.

The following primary green energy strategies to reduce energy-, environment-, and economy-related issues in various sectors should be taken into account (see Midilli et al. 2006) for promoting the development of sustainable energy technologies:

- Sectorial support for transition to green energy technologies
- Development of the road maps and policies for green energy sources
- Governmental and public support for green energy economy
- Production, consumption, distribution, conversion, management, and marketing of green energy technologies and options
- Research, development, and application of sustainable green energy technologies

- Availability, productivity, and reliability of green energy and technologies
- Design and fabrication of green energy–based environmental and ecological applications

5.3 Modeling Instruments for Sustainable Energy Development and Policies

The main methods and tools for elaborating sustainable development policies and strategies can be classified into four categories (see Dincer and Rosen 2005):

- Environmental tools, including performance indicators, impact assessment, and ecological footprints
- Thermodynamic tools, including exergy analysis and material flux analysis
- Sustainability tools, including life-cycle assessment and sustainable process index (as introduced above)
- Risk assessment

Environmental impact assessment (EIA) is an environmental tool used in assessing the potential environmental impact of a proposed activity. EIA can assist in making a decision on whether or not the proposed activity will pose any adverse environmental impacts. The EIA process assesses the level of impact and provides recommendations to minimize such impact on the environment.

Ecological footprint (EF) analysis is an accounting tool enabling the estimation of resource consumption and waste assimilation requirements of a defined human population or economy in terms of corresponding productive land use.

Sustainable process index (SPI) is a means of measuring the sustainability of a process producing goods. The unit of measure is square meter (m^2) of land. It is calculated from the total land area required to provide raw materials, process energy (solar derived), infrastructure (including energy generation production facilities), and waste disposal.

Material flux analysis (MFA) is a materials accounting tool that can be used to track the movement of elements of concern through a specified system boundary. The tool can be adapted further to perform a comparative study of alternatives for achieving environmentally sound options.

Risk assessment (RA) can estimate the likelihood of potential impacts and the associated degree of uncertainty in both the impact and the likelihood it will occur. The risk assessment helps in decision making.

There are a number of parameters proposed in the literature (see Dincer 2000, 2002, Dincer and Rosen 1999, 2005, Rosen et al. 2008) for the quantitative assessment of a sustainable energy impact on the society and for elaborating

adequate policies and strategies. Some relevant modeling parameters are introduced in this section, as taken from Midilli et al. (2006).

Sectorial impact ratio (R_{si}) is based on the provided financial support of public, private, and media sectors for transition to green energy–based technologies, and depends on the total green energy financial budget as a reference parameter. Mathematically,

$$R_{si} = \frac{C_{p,si}}{C_{geb}}; \quad C_{p,si} < C_{geb}, \tag{5.1}$$

where $C_{p,si}$ defines the provided financial support of the public, private, and media sectors for transition to green energy–based technologies, and C_{geb} defines the total green energy financial budget in a country. The sectorial impact ratio ranges from 0 to 1/3.

Technological impact ratio (R_{ti}): This parameter quantifies the provided financial support for research and development, security, and analysis of green energy–based technologies. This parameter depends on the total green energy financial budget as a reference parameter. The technological impact ratio is defined mathematically as

$$R_{ti} = \frac{C_{p,ti}}{C_{geb}}; \quad C_{p,ti} < C_{geb}, \tag{5.2}$$

where $C_{p,ti}$ represents the provided financial supports for research and development, security, and analysis of green energy–based technologies. The technological impact ratio ranges from 0 to 1/3 (see Midilli et al. 2006).

Practical application impact ratio (R_{pai}): This parameter quantifies the provided financial support for design, production, conversion, marketing, distribution, management, and consumption of green fuel from green energy sources and also depends on the total green energy financial budget:

$$R_{pai} = \frac{C_{p,pai}}{C_{geb}}; \quad C_{p,pai} < C_{geb}, \tag{5.3}$$

where $C_{p,pai}$ represents the provided financial supports for design, production, conversion, marketing, distribution, management, and consumption of green fuel from green energy sources.

The proportional effects of the above-defined parameters (sectorial, technological, and practical application impact ratios) on the green energy financial budget in a country can be quantified by a newly introduced parameter called the *green energy impact ratio*.

Green energy impact ratio (R_{gei}) is defined based upon Eqs. (5.1) to (5.3) as the summation of sectorial, technological, and practical application impact ratios as follows:

$$R_{gei} = R_{si} + R_{ti} + R_{pai}. \tag{5.4}$$

Green energy–based sustainability ratio (R_{ges}) is defined as the product of the green energy utilization ratio (R_{geu}) and green energy impact ratio (R_{gei}). This parameter can be written mathematically as

$$R_{\text{ges}} = R_{\text{gei}} \times R_{\text{geu}}. \tag{5.5}$$

Fossil fuel utilization ratio (R_{ffu}) quantifies the fossil fuel utilization with respect to utilization of all kinds of energies. The kinds of energies utilized by the entity subjected to analysis (a sector, a country, a continent, all countries, etc.) are categorized into two types: fossil fuel energy, and green energy (one generally considers nuclear energy as a green energy provided that all associated processes are pursued in a sustainable manner). By definition,

$$R_{\text{ffu}} = 1 - R_{\text{geu}}. \tag{5.6}$$

From the definition of fossil fuel utilization, we get

$$R_{\text{ffu}} = \frac{\sum ffc}{\sum pec}, \tag{5.7}$$

where $\sum ffc$ is the total fossil fuel consumption and $\sum pec$ is the total primary energy consumption. Therefore, from Eqs. (5.6) and (5.7) the green energy utilization ratio can be written as

$$R_{\text{geu}} = \frac{\sum pec - \sum ffc}{\sum pec}. \tag{5.8}$$

On the other hand, based on Eqs. (5.4) and (5.5) the green energy–based sustainability ratio is

$$R_{\text{ges}} = \left(R_{\text{si}} + R_{\text{ti}} + R_{\text{pai}}\right) \times R_{\text{geu}}. \tag{5.9}$$

Hence, substituting Eqs. (5.1) to (5.3) and (5.8) into Eq. (5.9), one obtains

$$R_{\text{ges}} = \left(\frac{C_{\text{p,si}}}{C_{\text{geb}}} + \frac{C_{\text{p,ti}}}{C_{\text{geb}}} + \frac{C_{\text{p,pai}}}{C_{\text{geb}}}\right) \times \frac{\sum pec - \sum ffc}{\sum pec}. \tag{5.10}$$

The following assumptions can be made for analyzing parametrically the green energy impact ratio and green energy–based sustainability ratio:

- The weights of the technological, sectorial, and practical application impact ratios split equally (one third of the total green energy financial budget). Notice that the sum of the above three parameters should equal to 1, because it is

considered that the total green energy financial budget is prepared in accordance with the activities involved in the parameters.
- The assumed values of technological, sectorial, and practical application impact ratios are selected at specified values, such as 20%, 60%, and 100%, respectively.
- The total primary energy consumption, total fossil fuel consumption, and total green energy consumption can be taken as reference points.

Bejan (1994) studied the application of entropy generation minimization principles to formulate energy policy. The primary purpose of Bejan's work was threefold: (1) to employ the art of entropy generation minimization at a level as yet unexplored; (2) in the process, to present a unified framework with a sound theoretical basis for making and analyzing energy policy proposals; and (3) to demonstrate the potential benefits of a dialogue among different disciplines, academic or professional, by presenting the results of an ongoing dialogue between an accountant and an engineer.

Exergy may be, or provide the basis for, an effective measure of the potential of a substance or energy form to impact the environment. It is important to mention that in practice a thorough understanding of exergy and the insights it can provide into the efficiency, environmental impact, and sustainability of energy systems are required for the engineer or scientist working in the area of energy systems and the environment. Further, as energy policies increasingly play an important role in addressing sustainability issues and a broad range of local, regional, and global environmental concerns, policy makers also need to appreciate the exergy concept and its ties to these concerns. The need to understand the linkages between exergy and energy and the environmental impact has become increasingly significant.

Connelly and Koshland (1997) suggest that exergy can be used to define the efficiency of fossil fuel consumption through a depletion number as follows:

$$D_{\mathrm{p}} = \frac{\mathrm{Ex_D}}{\mathrm{Ex_{in}}}, \tag{5.11}$$

which represents the relationship between the exergy destruction ($\mathrm{Ex_D}$) and the exergy input ($\mathrm{Ex_{in}}$) by fuel consumption. The relationship between the depletion factor and the exergy efficiency is

$$\psi = 1 - D_{\mathrm{p}}. \tag{5.12}$$

We express the sustainability of the fuel resource by a *sustainability index* (SI), which has been introduced by Rosen et al. (2008) as the inverse of the depletion number:

$$\mathrm{SI} = 1/D_{\mathrm{p}}. \tag{5.13}$$

5.4 Case Studies

5.4.1 Sustainability Assessment of Solar Energy

The sustainability index and green energy utilization index can be estimated for a situation in which solar thermal energy replaces (partially or totally) the combustion of fossil fuels. Zamfirescu et al. (2008) report such a study, which considers solar heating and power cogeneration.

Figure 5.7b shows the solar energy sustainability ratio over a period of time for three financial scenarios (similar to those proposed in Dincer and Rosen 2005), namely 20%, 60%, and 100% of the green energy financial investment for future years is affecting the sustainability of solar technology development and implementation. As expected, the utilization of fossil fuels decreases in favor of solar energy. Furthermore, the sustainability of solar (and renewable systems) increases with investment input. An increased sustainability of energy systems translates to a reduced impact on global warming.

5.4.2 Sustainability Assessment of Fossil Fuel Combustion

Rosen et al. (2008) considered a power plant using natural gas as the fuel (for modeling purposes, the natural gas has been assimilated to pure methane, CH_4). One expresses the environmental impact in terms of the amount of carbon dioxide emission. A balanced chemical combustion equation of methane shows that for each kilogram of methane burned, 2.75 kg of carbon dioxide (CO_2) is released. The specific chemical exergy of methane is 51,840 kJ/kg. The amount of carbon dioxide emitted and the sustainability index as a function of the exergy efficiency for 1 kWh of power production are plotted in Fig. 5.8.

The figure shows a quantitative illustration of the relation between the CO_2, SO_2, or NO_x emissions and sustainability index (SI) of a process and its exergy efficiency. Carbon dioxide emission is calculated for power generation where the fuel is methane and the results are for 1 kWh of power output. SO_2 and NO_x emissions are calculated for an air conditioner with electricity as the work input and the results are for 1 kWh of cooling load. The absolute values represented by the emissions axis are not shown. At an exergy efficiency of 50%, the CO_2 emission is 0.38 kg while the SO_2 emission is 0.43 kg and the NO_x emission is 0.25 g.

5.4.3 Assessment of Green Energy Strategies and Policies

Midilli et al. (2006) illustrate the use of sustainability parameters in assessing sustainability strategies and elaborating meaningful policies. The following three

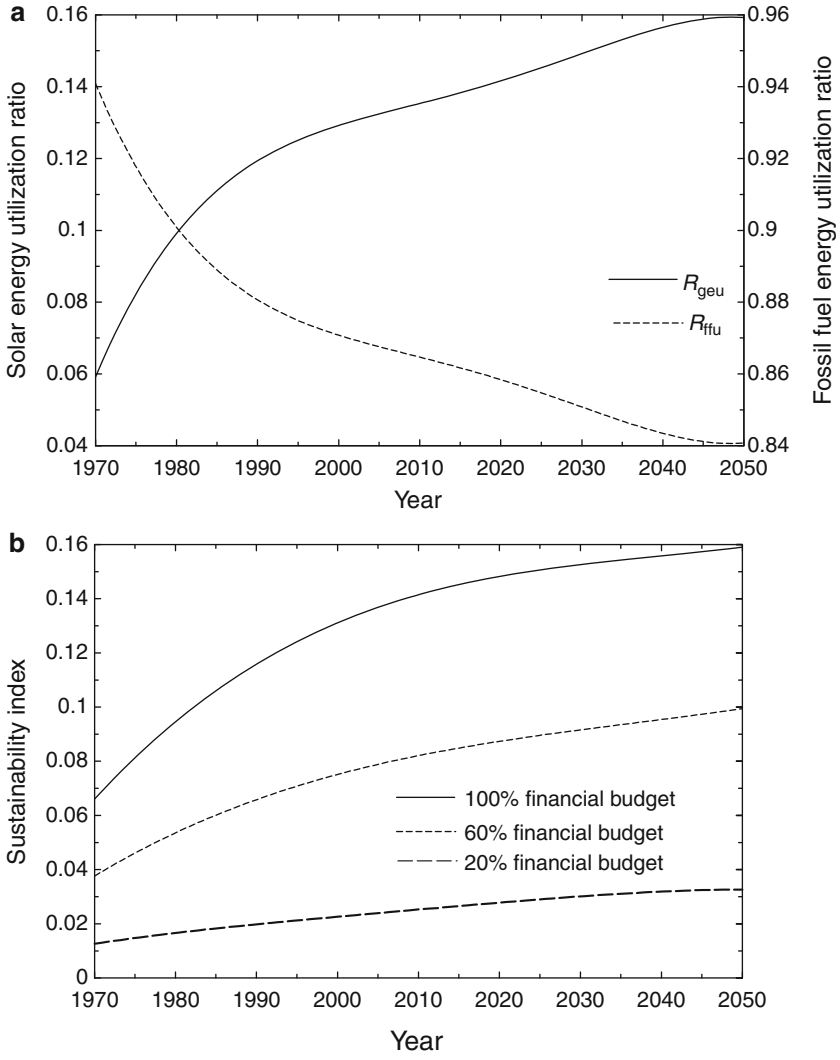

Fig. 5.7 (**a**) Energy utilization ratio comparison and (**b**) solar sustainability index [modified from Zamfirescu et al. (2008)]

cases including technological, sectorial, and practical application impact ratios are considered:

- Case 1—assumes one variable and two constant parameters. Since the maximum value of each individual parameter is 1/3, in this case the sum of the constant parameters is bounded by the value 2/3.
- Case 2—assumes two variables and one constant parameter. Thus, this time the maximum value of the variable parameters is 2/3.
- Case 3—assumes all three parameters as variables.

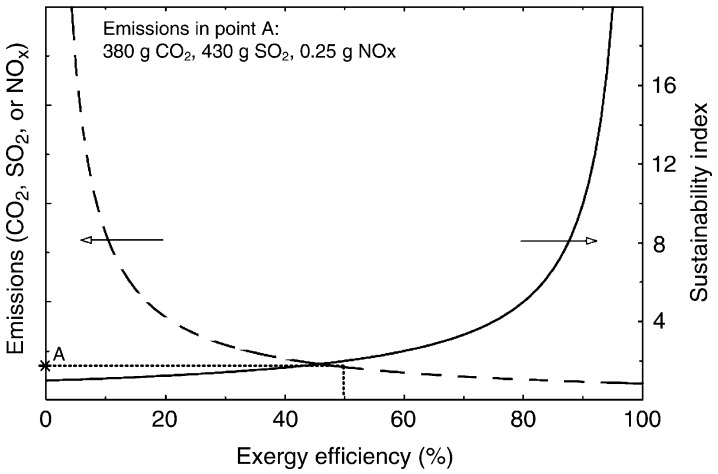

Fig. 5.8 Correlating the sustainability index with the exergy efficiency of the combustion process [modified from Rosen et al. (2008)]

The calculations presented here is based on statistical data of fossil fuel and green energy utilization and extrapolation of these data up to year 2050. The input data used in the study by Midilli et al. (2006) are given in giga tonne oil equivalent (Gtoe) in Fig. 5.9.

Figure 5.10 presents the variation of the fossil fuel and green energy utilization ratios as a function of year, and Fig. 5.11 correlates the variations of the fossil fuel utilization ratio as a function of green energy utilization ratio.

As it is clearly seen, the fossil fuel utilization ratio decreases year by year while the green energy utilization ratio increases. For example, in 1965 the green energy utilization ratio was 5.59% while the fossil fuel utilization ratio was 94.41%.

In 2004 the green energy utilization ratio reached 12.31% while the fossil fuel utilization ratio decreased to 87.69%. The projections from this study show that the green energy utilization ratio will reach almost 16.33% and the fossil fuel utilization ratio will decrease to almost 83.67% in 2050. In conclusion, through this example it is demonstrated that, in order to reduce the harmful effects resulting from fossil fuel consumption, green energy strategies should be put into practice for sustainable development.

The sensitivity analysis aims to study the effect of the sectorial, technological, and practical application impact ratios on the green energy utilization. In order to conduct the analysis, one or two of these parameters can be selected as a constant. In order to quantify the variable parameter(s), a dummy variable x is introduced, where x takes a value from 0 to 1. The results are shown in Table 5.1. When case 1 is considered, it is found that the green energy impact ratio changes between 0.733 and 1.00 depending on the percentages of the variable parameter. In case 2, it is found that the green energy impact ratio varies between 0.467 and 1.00. In case 3, it is found that the green energy impact ratio varies from 0.20 to 1.00 depending on the percentages of three variable parameters.

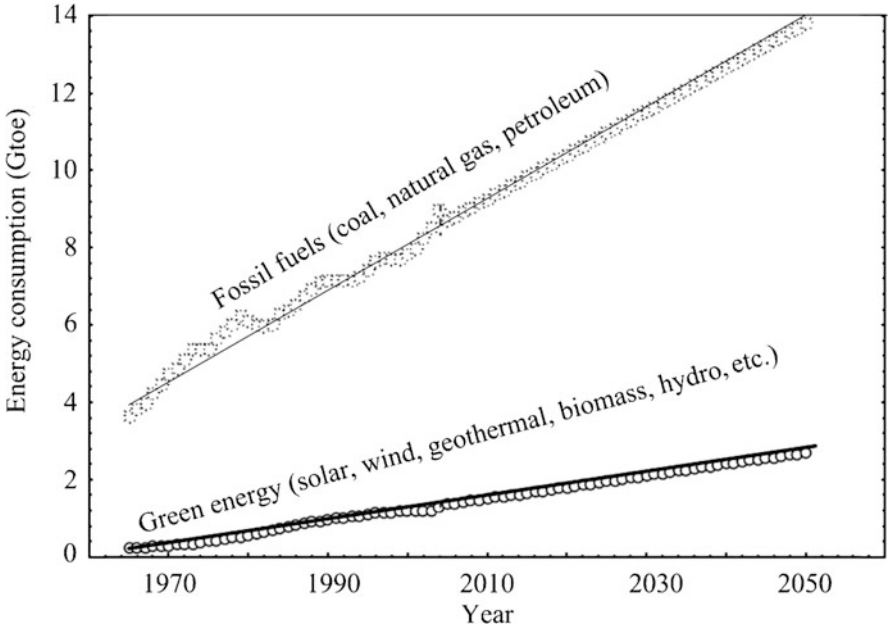

Fig. 5.9 Fossil fuel and green energy utilization history and forecast [modified from Midilli et al. (2006)]

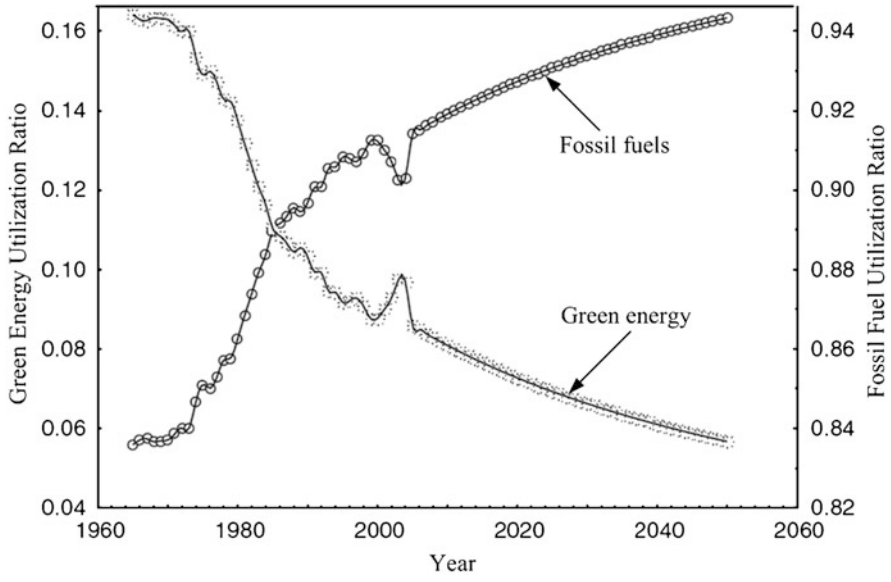

Fig. 5.10 Evolution of green energy and fossil fuel utilization ratios [modified from Midilli et al. (2006)]

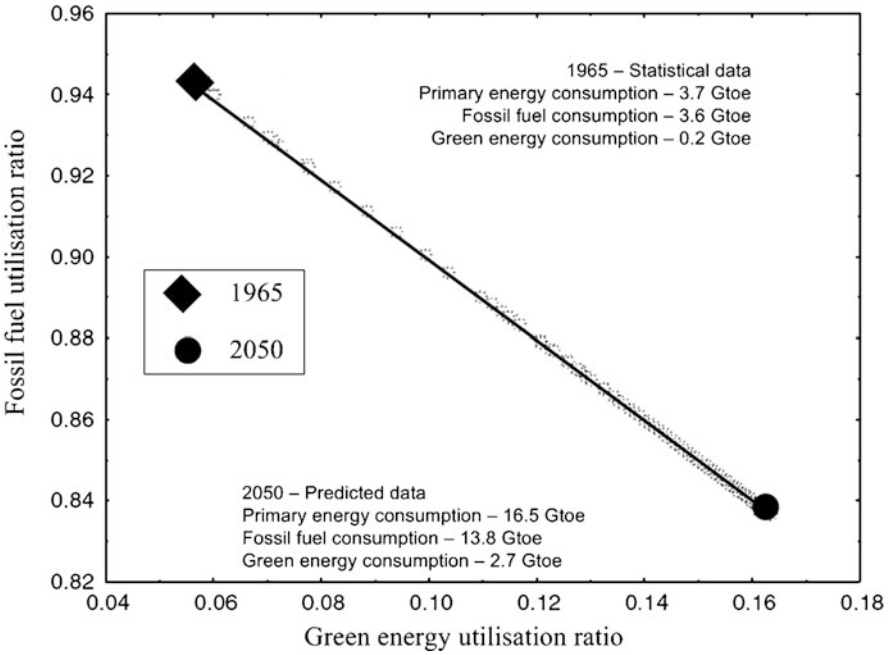

Fig. 5.11 Correlating fossil fuel with green energy utilization ratios [modified from Midilli et al. (2006)]

Table 5.1 Calculated green energy impact ratios for cases 1 to 3

			Variable parameter, a				
			20%	40%	60%	80%	100%
Case	Description	Parameter f	Green energy impact ratio				
1	2 constants 1 variable	2/3 $1 \times (1/3) \times \varepsilon$	0.733	0.800	0.867	0.933	1.000
2	1 constant 2 variables	1/3 $2 \times (1/3) \times \varepsilon$	0.467	0.600	0.733	0.867	1.000
3	3 variables	$3 \times (1/3) \times \varepsilon$	0.200	0.400	0.600	0.800	1.000

Data from Midilli et al. (2006)
Note: Parameter f represents the percent of total budget invested for green energy development

Observe that the highest values of green energy impact ratio are found in case 1. Case 3 gives the lowest green energy impact ratios. Thus, case 1 represents the rational selection to increase the green energy impact ratio and green energy–based sustainability ratio.

Figures 5.12 to 5.14 show yearly variation of the green energy–based sustainability ratio (R_{ges}) as a function of the percentages of the green energy financial

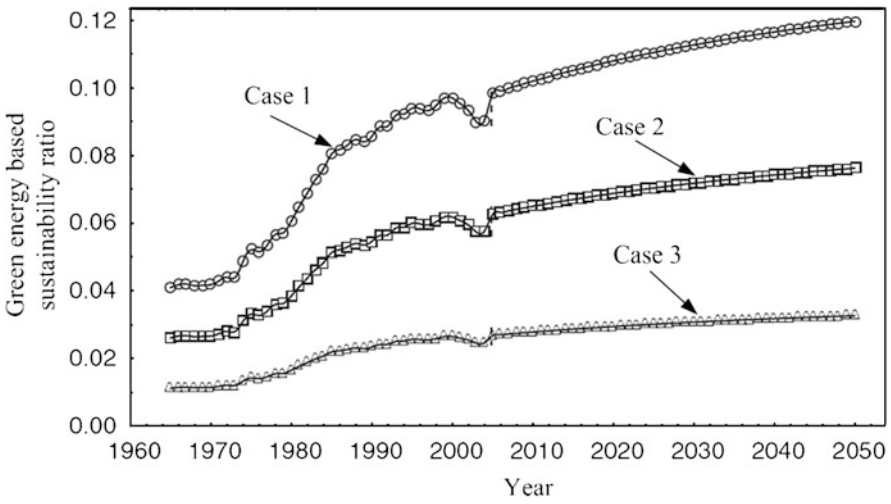

Fig. 5.12 Green energy–based sustainability ratio for a 20% green energy budget [modified from Midilli et al. (2006)]

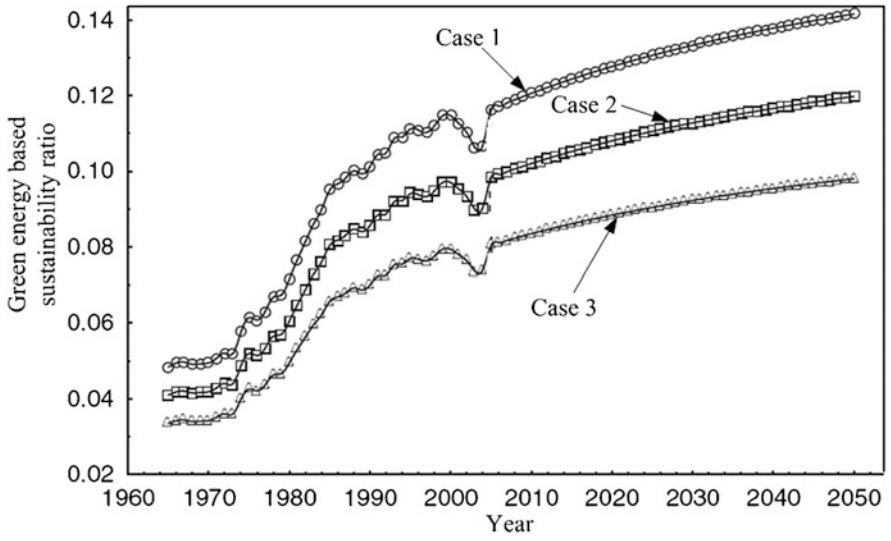

Fig. 5.13 Green energy–based sustainability ratio for a 60% green energy budget [modified from Midilli et al. (2006)]

budget, which is taken as 20%, 60%, and 100%, respectively. The values of green energy–based sustainability ratios were calculated using Eq. (5.10). As shown in these figures, the values of R_{ges} increase with time. The highest values of R_{ges} are obtained when case 1 is applied (see Figs. 5.12–5.14). For example, the green energy–based sustainability ratios are estimated at 9.8% in 2005 and 11.9% in 2050

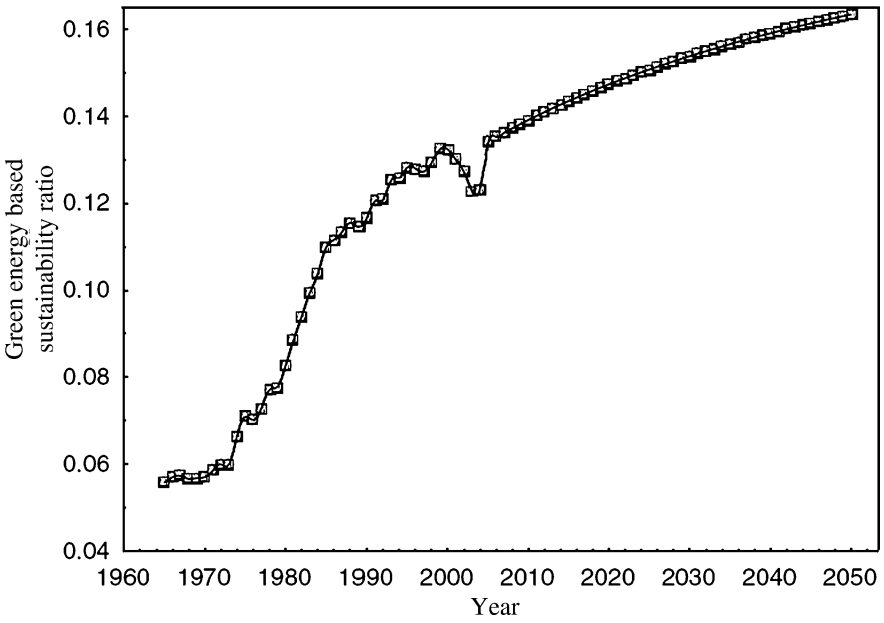

Fig. 5.14 Green energy–based sustainability ratio for a 20% green energy budget [modified from Midilli et al. (2006)]

for the case of a 20% green energy financial budget. In the case of a 60% green energy financial budget they are 11.6% in 2005 and 14.2% in 2050. In the case of a 100% green energy financial budget they are 13.4% in 2005 and 16.3% in 2050.

The importance of implementing green energy strategies through green energy systems and applications for sustainable future appears obvious. If green energy strategies are implemented, the green energy–based sustainability ratio increases, and green energy is more easily supplied, and therefore green technologies are more preferred and applied. Consequently, the negative effects stemming from fossil fuel combustion will decrease, and thus the green energy–based sustainability ratio will increase.

As mentioned in Midilli et al. (2006), by 2050 fossil fuel consumption and green energy consumption are expected to reach 13807.2 and 2694.9 Mtoe (mega tonnes oil equivalent), respectively. This increase indicates that we will still be dependent on fossil fuels. For 2004 the estimation of the green energy utilization ratio is 12.31%, while the fossil fuel utilization ratio is 87.69%. By 2050 it is expected that the green energy utilization ratio will reach almost 16.33% and the fossil fuel utilization ratio will decrease to almost 83.67%.

This analysis indicates that if the increase of fossil fuel consumption continues to increase, the associated pollution effects will be felt globally and dramatically. Such a scenario may result in increasing global unrest. It is thus suggested that the utilization of fossil fuels should be reduced, and fossil-based technologies should be gradually converted to green energy–based technologies.

The highest green energy impact ratio is found between 73.3% and 100% in case 1. This means that the highest percentage (e.g., 100%) of the variable parameter in case 1 should be selected. Moreover, the scenario from case 1 gives the best results of the green energy–based sustainability ratio.

In conclusion, sustainable green energy strategies are definitely required to ensure better environment and global stability by reducing the harmful effects of the fossil-based energy consumption and unlink society from dependence on fossil fuels. It is also important to shape transition strategies to a green energy–based economy. Developed countries, in particular, should increase investments in green energy technologies.

Progress of green energy and technologies is definitely influenced by the sustainable green energy strategies for future green energy scenarios. The most important factor influencing the specific role of green energy and technologies appears to be energy demand. The balance of energy demand and supply and sustainable green energy sources and technologies should be taken seriously into consideration.

In order to develop and implement green energy technologies and applications in any country, green energy strategies appear to be essential. It is clear that green energy strategies are becoming increasingly important for society with regard to solving global environmental problems, energy security, and supply issues.

5.5 Concluding Remarks

In this chapter the interdependence between sustainable development and energy policy was discussed. The role of green energy strategies for sustainable development was emphasized. Considering sustainable green energy strategies, it can be concluded that the most important scenario to encourage transition to green energy technologies is to facilitate interactions among countries, scientists, researchers, societies, and others. Investment in green energy supply should be encouraged by governments and other authoritative bodies for the interest of having a green alternative to fossil fuels.

Assessments of the sustainability of processes and systems, and efforts to improve sustainability, should be based in part upon thermodynamic principles and especially the insights revealed through exergy analysis. The development of a sustainability index or a ratio of energy utilization (per kind) is very important in establishing reasonable strategies and policies for sustainable energy development.

Nomenclature

a	Variable parameter (Table 5.1)
C	Financial support any currency

D_p Depletion factor
Ex Exergy (kJ)
f Percent of green energy budget
ffc Total fossil fuel consumption
pec Total primary energy consumption
R Ratio
SI Sustainability index

Greek Letter

ψ Exergy efficiency

Subscripts

D Destroyed
ffu Fossil fuel utilization
geb Green energy financial budget
gei Green energy impact
ges Green energy–based sustainability
in Input
p Provided
pai Practical implementation impact
si Sectorial impact
ti Technological impact

References

Bejan M. 1994. Energy policy. In: Entropy Generation Through Heat and Fluid Flow, Bejan A., ed. Wiley, New York.

Connelly L., Koshland C.P. 1997. Two aspects of consumption: using an exergy-based measure of degradation to advance the theory and implementation of industrial ecology. *Resources, Conservation and Recycling* 19:199–217.

Dincer I. 2000. Renewable energy and sustainable development: a crucial review. *Renewable and Sustainable Energy Reviews* 4:157–175.

Dincer I. 2002. The role of exergy in energy policy making. *Energy Policy* 30:137–149.

Dincer I., Rosen M.A. 1999. Energy, environment and sustainable development. *Applied Energy* 64:427–440.

Dincer I., Rosen M.A. 2005. Thermodynamic aspects of renewable and sustainable development. *Renewable and Sustainable Energy Reviews* 9:169–189.

Jefferson M. 2000. Energy policies for sustainable development. In: World Energy Assessment: Energy and the Challenge of Sustainability. United Nations Development Program.

Midilli A., Dincer I., Ay M. 2006. Green energy strategies for sustainable development. *Energy Policy* 34:3623–3633.

Rosen M.A., Dincer I., Kanoglu M. 2008. Role of exergy in increasing efficiency and sustainability and reducing environmental impact. *Energy Policy* 36:128–137.

Zamfirescu C., Dincer I., Verrelli T., Wagar W.R. 2008. Residential solar power generation systems for better environment. Proceedings of the Global Conference on Global Warming, Istanbul, July 6–10, Paper #805.

Study Questions/Problems

5.1 What one can understand through energy policy and what is its role in sustainable development?
5.2 Comment on the key expectations from the implementation of green energy strategies and policies.
5.3 Identify and explain the interdependence of the factors affecting sustainable development.
5.4 What considerations are involved in the development of green energy technologies?
5.5 Identify and explain the main factors affecting sustainable energy strategies and policies.
5.6 What are the applications of green energy technologies?
5.7 Explain the method of environmental impact assessment.
5.8 What is ecological footprints analysis?
5.9 Define and give examples of a sustainable process index.
5.10 Explain the material flux analysis method.
5.11 What can one understand through risk assessment?
5.12 List and define some key parameters quantifying sustainablility and sectorial impact of green technologies.
5.13 Based on a literature study determine the sustainability of concentrated solar power systems.
5.14 Determine the sustainability of applying carbon capture and sequestration at coal combustion for power generation.

Chapter 6
Fossil Fuels and Alternative Fuels

6.1 Introduction

A "fuel" is generally defined as any material that can be altered to release energy in a controlled manner in the form of heat and/or work. Fuels can be solids, liquids, or gases. *Conventional fuels* are of two types: fossil fuels and nuclear fuels. The word "altered" in the above definition signifies a chemical or physical process to which the fuel is subjected to release energy. Nuclear fuels, such as fissionable uranium, are "altered" through a chained nuclear reaction of fission to generate useful energy in the form of high temperature heat. Fossil fuels represent fossilized biomass, which stores carbon out of the natural carbon cycle in sediments for a long time. When combusted, fossil fuels release the carbon into the atmosphere in the form of carbon dioxide, thus contributing to global warming. Biomass also emits carbon dioxide when combusted; however, the emitted carbon is only returned in the global carbon cycle in this way; thus, biomass is considered a renewable energy resource. Biomass represents biological material of recently living organisms, which is regarded both as an alternative fuel and as a source of materials for synthetic fuels production.

Alternative fuels are nonconventional fuels that can be obtained from biomass (in which case they are called *biofuels*) or from fossil fuels (in which case they are called synthetic fossil–based fuels). Blends of fossil-derived fuels and biofuels are also considered alternative fuels (e.g., gasoline + bioethanol blends). The classification of fuels is represented graphically in Fig. 6.1.

Sustainable energy development requires alternative fuels, which are viewed as a cleaner means of chemical energy storage with respect to fossil fuels. In this chapter, fossil fuels and alternative fuels are introduced and compared in terms of energy and exergy per stored mass and volume and associated environmental impact.

6.2 Fossil Fuels

There are three types of fossil fuels: coal (solid), petroleum (liquid), and natural gas (gaseous).

İ. Dinçer and C. Zamfirescu, *Sustainable Energy Systems and Applications*,
DOI 10.1007/978-0-387-95861-3_6,

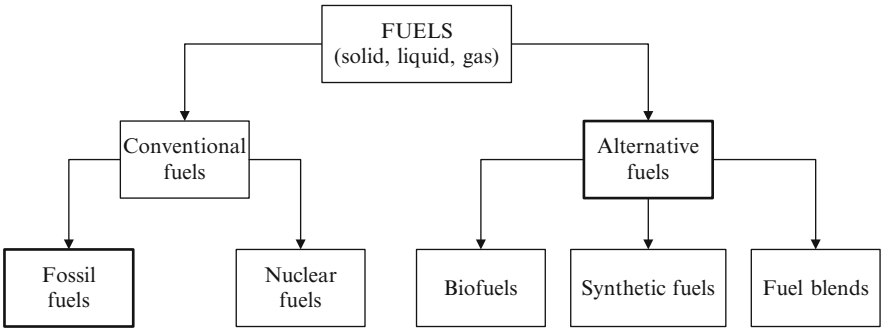

Fig. 6.1 Classification of fuels

All fossil fuels are natural hydrocarbons with a density in increasing order, starting from natural gas to the light and heavy oils, to bitumen, kerogen, sapropels, and humic coals. While the density increases, the ratio between hydrogen and carbon atoms (H/C) for 1 mol of substance decreases from about 4 for natural gas (comprising mainly methane) to 0.7 specific to coal. In a hydrocarbon, the H/C ratio indicates the *aromaticity*, which is the capability of the molecule to form aromatic rings of covalent bonds. Because of higher aromaticity, the molecules of heavier hydrocarbons are more stable and thus more difficult to crack. We discuss in this section the main features of coal, petroleum, and natural gas.

6.2.1 Coal

Coal is a sedimentary rock obtained by exposure to high pressure and temperature of fossilized organic matter and comprises primarily carbon and some smaller quantities of hydrogen, sulfur, oxygen, and nitrogen. The variety of coal rock is large with respect to composition, moisture content, and calorific value. Three of the chemical elements containing coal generate heat when combusted. These are carbon, hydrogen, and sulfur. The formation enthalpy of the oxidation products of these elements, listed in Table 6.1, is the factor contributing to the calorific value of coal. Therefore, the concentration of carbon, hydrogen, and sulfur in coal plays the major role with respect to coal value from an energy point of view.

Coal is of four main types according to the *coal rank*. The coal rank represents a conventional measure to characterize the heating value of coal in correspondence to its fixed carbon and volatile matter content and caking properties. The types of coals in the standard classification, listed from higher to lower rank, are as follows: anthracite, bituminous, subbituminous, and lignite; their characteristics are summarized in Table 6.2.

The presence of water in coal is explained by the process of its geological formation, where humid biomass was squeezed under the pressure of sediment layers. Water is both chemically and physically bound in the coal structure and is

Table 6.1 Formation enthalpy and chemical reactions of the main oxidation products of coal

Element	Symbol	Chemical reaction	Formation enthalpy, kJ/mol
Carbon	C	$C + 0.5O_2 \rightarrow CO_2$	−393,486
Hydrogen	H	$H_2 + 0.5O_2 \rightarrow HO_2$	−241,811
Sulfur	S	$S + O_2 \rightarrow SO_2$	−296,792

Note: Data calculated with Engineering Equation Solver Software (Klein 2010)

commonly denoted with the term *moisture content*. Table 6.2 shows that the moisture content in coal varies from 2% to 45% by weight. When coal is combusted, a part of the combustion heat is consumed by water evaporation; the drier it is, the higher the calorific content of coal.

Ash represents the residue that remains after the complete combustion of coal and comprises various sulfates and oxides and other inorganic chemicals. Coal embeds two types of mineral matter that ultimately led to the formation of ash by combustion: extraneous mineral matter (gypsum, shale, sand, pyrite, clay, marcasite, calcium, magnesium) and inherent mineral matter (some of the constituents of the biomass from which coal was formed).

Volatile matter is the percentage of products that are volatile—that is, they can be released as gases during pyrolysis process. Volatile matter refers to all other components, except the water vapor, which result from mixture evaporation. The loss of carbon dioxide from mineral embedded in coal structure is an example of volatile matter; other examples are hydrogen emanated by chloride minerals or sulfur from pyrite.

If the mass of volatiles, ash, and moisture is extracted from the mass of coal, the remaining quantity is known as *fixed carbon*. For anthracite, the fixed carbon is 75% to 85% by weight, while for bituminous, subbituminous, and lignite coal, it is 50% to 70%, 30% to 57%, and 25% to 30%, respectively (see Speight 2005).

The calorific value of solid fuels is usually given in two forms: gross (GCV) and net (NCV) calorific values. Note that for liquid and gaseous fuels the terms used for GCV and NCV are higher heating value (HHV) and lower heating value (LHV), respectively. The calorific values are defined as follows:

- GCV or HHV represents the heat of combustion in the case when all products are brought to the reactants' (fuel and oxidant) temperature and condensing all water vapor.
- NCV or LHV is determined by subtracting the heat of evaporation of water from GCV (HHV) and corresponds to the case when all products are brought to the reactants' temperature, but water remains in the vapor phase.

The estimation of the gross calorific value of coal can be made with Mason and Gandhi's (1983) formula, which is given as a function of the weight percentages of the main coal components:

$$\begin{aligned} \mathrm{GCV} = 2.326 \times [&0.198(\%\,\mathrm{C}) + 0.6203(\%\,\mathrm{H}) + 0.0809(\%\,\mathrm{S}) \\ &+ 0.04495(\%\,\mathrm{A}) - 5.153], \end{aligned} \tag{6.1}$$

Table 6.2 Classification of coal by rank

Rank	Description	Composition[a]							GCV, MJ/kg[b]	Density, kg/ dm^3
		C, %	H, %	O, %	S, %	N, %	Ash, %	Moisture, %		
Anthracite	Brittle, hard, black lustrous	75–85	1.5–3.5	5.5–9.0	0.5–2.5	0.5–1.0	4.0–15.0	3.0–6.0	27.9–31.4	1.35–1.70
Bituminous	Black to dark brown, dense	65–80	4.5–6.0	4.5–10.0	0.5–6.0	0.5–2.5	4.0–15.0	2.0–15.0	27.9–33.7	1.28–1.35
Subbituminous	Dark brown to bright black, dull	55–70	5.5–6.5	15.0–30.0	0.3–1.5	0.8–1.5	3.0–10.0	10.0–25.0	17.4–23.3	1.35–1.40
Lignite	Brownish black with high moisture	35–45	6.0–7.5	38.0–48.0	0.3–2.5	0.6–1.0	3.0–15.0	25.0–45.0	13.0–17.4	1.40–1.45

[a]Percent by weight
[b]Ash-free basis

given in MJ/kg. It is useful to express the NCV on a wet basis; this can be done with the equation presented in Van Loo and Koopejan (2008):

$$\mathrm{NCV} = \mathrm{GCV}(1 - w_\mathrm{w}) - 2.444\, w_\mathrm{w} - 21.839\, w_\mathrm{H}(1 - w_\mathrm{w}), \tag{6.2}$$

where w_w is the moisture content by weight.

The estimation of coal entropy and chemical exergy is of utmost importance for the second law analysis of energy systems involving coal combustion. For specific exergy content of dry and moisture-free coal, Eiserman et al. (1980) give the following regression formula, based on the concentration of main elements expressed in kmol per kg dry and ash-free coal (where c, h, o, n, and s are the concentrations of carbon, hydrogen, oxygen, nitrogen, and sulfur, respectively):

$$\begin{aligned} s_\mathrm{DAF} = c\Bigg[&37.1653 - 31.4767\exp\left(-0.564682\left(\frac{h}{c+n}\right)\right) + 20.1145\left(\frac{o}{c+n}\right) \\ &+54.3111\left(\frac{n}{c+n}\right) + 44.6712\left(\frac{s}{c+n}\right)\Bigg], \end{aligned} \tag{6.3}$$

where index DAF stands for *dry coal and ash-free* basis, and the entropy results are in kJ/kg K.

The chemical exergy of coal, dry and ash-free basis, can be calculated with the formula obtained by Kaygusuz (2009), which reads

$$\begin{aligned} ex^\mathrm{ch}_\mathrm{DAF} = \mathrm{GCV} - T_0\Bigg[&s_\mathrm{DAF} + \left(c + \left(\frac{1}{4}h\right) + s - \left(\frac{1}{2}o\right)\right)s_{\mathrm{O}_2} - c \times s_{\mathrm{CO}_2} \\ &- \left(\frac{1}{2}h\right) \times s_{\mathrm{H_2O}} - s \times s_{\mathrm{SO}_2} - \left(\frac{1}{2}n\right) \times s_{\mathrm{N}_2}\Bigg] + c \times ex^\mathrm{ch}_{\mathrm{CO}_2} \\ &+ \left(\frac{1}{2}h\right) \times ex^\mathrm{ch}_{\mathrm{H_2O}} + s \times ex^\mathrm{ch}_{\mathrm{SO}_2} + \left(\frac{1}{2}n\right) \times ex^\mathrm{ch}_{\mathrm{N}_2} \\ &- \left(c + \left(\frac{1}{4}h\right) + s - \left(\frac{1}{2}o\right)\right)ex^\mathrm{ch}_{\mathrm{O}_2}, \end{aligned} \tag{6.4}$$

where the exergy value results are in $\mathrm{MJ/kg_{DAF}}$. The chemical exergy of good-quality coals varies between 7 and 8.2 MJ per kg dry ash-free basis. The contribution of ash to chemical exergy is negligible; therefore, the specific chemical exergy of coal, wet basis, can be estimated with

$$ex^\mathrm{ch} = (\%\mathrm{coal_{DAF}}) \times ex^\mathrm{ch}_\mathrm{DAF} + \frac{(\%\mathrm{H_2O})}{M_{\mathrm{H_2O}}} \times ex^\mathrm{ch}_{\mathrm{H_2O}}, \tag{6.5}$$

where $(\%\mathrm{coal_{DAF}})$ is the percent of dry coal and $(\%\mathrm{H_2O})$ is the percent of water, both by weight.

For every 12 g of carbon, there is 1 mol of carbon content in coal, which by complete combustion is converted into 1 mol of CO_2 weighing 44 g. Therefore, if (%C) is the percent of carbon per weight on a dry basis, and w_w is the moisture content by a wet basis, the carbon dioxide emission for 1 kg of coal by a wet basis is

$$\mathcal{M}_{CO_2} = \frac{44}{12}[\%C] \times (1 - w_w), \frac{\text{kg CO}_2}{\text{kg wet}}, \tag{6.6}$$

where [%C] is the carbon fraction given in kg carbon per dry coal ash-free; thus, the carbon dioxide emission per unit of NCV wet basis is

$$\mathcal{M}_{CO_2,NCV} = \frac{\mathcal{M}_{CO_2}}{NCV}, \frac{\text{kg CO}_2}{\text{MJ wet}}. \tag{6.7}$$

Figure 6.2 shows the amounts of carbon dioxide emissions per unit of energy in MJ corresponding to the net calorific value of coal. The moisture content is considered according to the typical ranges. The ranks with more carbon content emit more CO_2 even if high ranks have a better calorific value. Equations (6.6) and (6.7) and data from Table 6.2 were used to draw Fig. 6.2.

6.2.2 Petroleum

The term *Petroleum* comes from the Latin terms *petra* meaning rock and *oleum* meaning oil. Petroleum is extracted from sediments in an oil well in liquid form. Several kinds of fossilized biological matter containing mostly lipids, amino acids, carbohydrates, and lignins contribute to the formation of petroleum currently existing in oil wells. Petroleum is a mixture of hydrocarbons that range from light ones (carbon number lower than 5) to heavier ones such as paraffins dissolved in liquid. Petroleum is toxic and flammable, and apart from carbon (83–87%) and hydrogen (10–14%), it comprises sulfur (0.5–6%) and some metals. The range of hydrocarbons that constitute petroleum (or crude oil) are as follows:

- Naphthas, with 5 to 7 carbon atoms in the molecule (used mainly as solvents).
- Gasoline, with 8 to 11 carbon atoms, which is the basis of gasoline fuel for autos.
- Kerosene, with 12 to 15 carbon atoms, from which diesel fuel is extracted.
- Lubricating oils, with 16 to 19 carbon atoms; they have a high normal boiling point.
- Solid hydrocarbons, with over 20 carbon atoms; they have melting point at higher values than the ambient temperature and are classified, in order of increased molecular weight, as paraffins, wax, tar, and asphaltic bitumen.

Petroleum is not used in practice in the form in which it is extracted (crude oil); rather, it is subjected to a distillation process in refineries. Table 6.3 summarizes the fuels derived from petroleum. Regarding jet fuels, there are currently two main

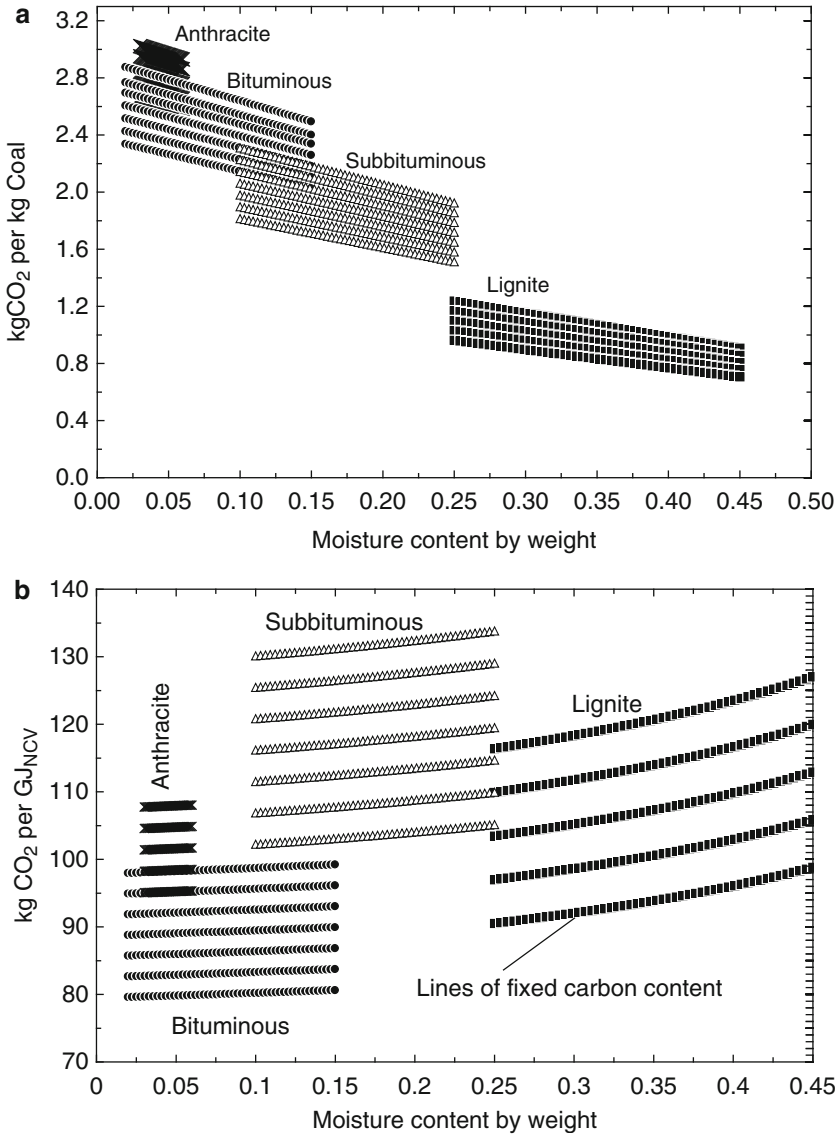

Fig. 6.2 Carbon dioxide emissions per kg and per GJ (NCV) for coal by rank

grades: jet A-1 and jet A, which are both kerosene-type fuels. There is another grade of jet fuel, jet B, which is a wide-cut kerosene (a mix of gasoline and kerosene), but it is rarely used, except in very cold climates. Jet A is a kerosene-based type of fuel, produced to an ASTM (American Society for Testing and Materials) specification and normally only available in North America. It has the same flash point as jet A-1, but a higher freeze point maximum (−40°C). Jet B is a distillate covering the

Table 6.3 Petroleum-derived fuels and their properties

Fuel name	Boiling point, °C	Molec. weight, kg/kmol	Density, kg/m^3	Carbon, wt%	LHV, MJ/kg	HHV, MJ/kg	Chemical exergy, MJ/kg	$\mathcal{M}_{CO_2}$, kg_{CO_2}/GJ_{LHV}
Light naphtha	0–150	100–150	~750	83.7	44.9	48.1	44.5	68.2
Gasoline	35–200	114	~745	85.1	43.5	46.5	47.5	71.9
Heavy naphtha	150–205	150–215	~850	85.4	43.0	46.1	49.0	64.2
Diesel fuel	150–370	233	~747	85.6	42.8	45.8	44.2	73.3
LPG	–43	44	~580	81.8	46.0	52.0	54.9	65.3
Kerosene	205–260	170	~795	84.7	43.1	46.2	49.1	71.9
Jet fuels	156–293	185	800	76.0	43.2	46.9	45.3	63.4
Fuel oil	260–425	>200	~990	85.4	40.1	42.9	41.4	78.1

LPG liquefied petroleum gas (assimilated as propane)

naphtha and kerosene fractions. It can be used as an alternative to jet A-1. Because it is more difficult to handle (higher flammability), there is significant demand only in very cold climates, where its better cold weather performance becomes important. In Table 6.3, the row for jet fuels lists the average properties of jet A and B fuels. On average, jet fuels can be approximated with the chemical formula $C_{12}H_{23}$; see Nojoumi et al. (2009).

The chemical exergy of liquid fuels can be determined, as illustrated, for example, in Szargut (2005) and Al-Najem and Diab (1992), based on the chemical composition of the fuel, expressed with respect to the molar carbon in the molecule, namely,

$$ex_{\text{fuel}} = \text{LHV}\left[1.0374 + 0.0159\left(\frac{\text{H}}{\text{C}}\right) + 0.0567\left(\frac{\text{O}}{\text{C}}\right) + 0.5985\left(\frac{\text{S}}{\text{C}}\right)\left(1 - 0.1737\left(\frac{\text{H}}{\text{C}}\right)\right)\right], \tag{6.8}$$

where H, O, S, C represent the number of atoms of hydrogen, oxygen, sulfur, and carbon, respectively.

The fuel that is used mostly in road transportation is gasoline, which is a blend of aliphatic and aromatic chemicals obtained by distillation of petroleum in refineries. Diesel fuel is also very common for road transport—especially for large capacity vehicles—and marine ships and rail locomotives. Processing of petroleum to obtain diesel fuel is simpler with respect to that of gasoline. The important aspect in diesel processing is the reduction of the sulfur content. The liquid petroleum gas (LPG) is based mainly on propane but often is mixed with butane in a 60/40 proportion. The gases that compound LPG are all extracted from petroleum in the refinery processes. The density of LPG is about the average of that of liquid propane and liquid butane at 25°C. Alcohol-based fuels, such as ethanol and methanol, can be

Table 6.4 Typical composition ranges of fossil natural gas

Component	Methane	Ethane	Propane	Butane	Pentane	Hexane	CO_2	O_2	H_2
Concentration	87.1–96.0	1.5–5.1	0.1–1.5	0.02–0.06	<0.18	<0.06	0.1–1.0	0.01–0.1	<0.02

Table 6.5 Principal properties of natural gas

Parameter	Unrefined	Refined
Molecular mass, g/mol	20	16
Density, kg/m^3	1.832	0.733
Normal boiling point, °C	N/A	−162
Autoignition temperature, °C	540	560
Octane number	120	130
LHV, MJ/kg	18.2	50.7
HHV, MJ/kg	20.2	56.2
ex^{ch}, MJ/kg	18.8	52.4
% C by weight	73	75
% CO_2 by weight[a]	2.68	2.75
CO_2, kg/MJ_{LHV}	147.2	54.2

[a]Assumed complete combustion

produced using petroleum as a fossil fuel source. However, these fuels are mostly produced from biomass through fermentation, and they are categorized here as alternative fuels.

6.2.3 Natural Gas

Fossil natural gas consisting mainly of methane is a natural resource found mainly either in natural gas fields or in oil well fields (where it is in association with oil). Other important sources of natural gas are coal-bed methane and in the form of hydrate sediments present under permafrost regions. The typical composition of natural gas is listed in Table 6.4. The existence of noncombustible components such as carbon dioxide, nitrogen, and oxygen in natural gas detracts from its heating value. One practical aspect is that natural gas is less inflammable than other hydrocarbon-based fuels, even though methane, its principal constituent, is highly flammable. When confined, natural gas presents explosion danger. Methane is a chemical with a high greenhouse effect, having 72 times higher potential than that of carbon dioxide for a time horizon of 20 years. Its lifetime in the atmosphere is 12 years.

Refining natural gas involves several processes aimed to remove humidity (water), sulfur, carbon dioxide, helium, solid particle, and liquid hydrocarbons existing in the gas. Through refining, the carbon content and the associated heating value are increased. Table 6.5 compiles the main physical properties of natural gas in unrefined and refined form.

6.3 Alternative Fuels

The classification introduced in Fig. 6.1 shows three alternative fuels to fossil fuels, namely, biofuels, fuel blends, and synthetic fuels. The need for alternative fuels is explained by two reasons: (1) fossil-based fuels deplete, thus new fuel sources must be discovered; (2) high carbon dioxide emissions are associated with fossil fuel combustion, and it is desired to limit these in order to have a better environment and avoid the danger of global warming. The three kinds of alternative fuels can be briefly described as follows:

- Biofuels are fuels derived from biomass though various physical and/or chemical (biochemical) processes. They can be solids, liquids, or gases.
- Synthetic fuels can be produced using either renewable or nonrenewable sources starting from materials such as water, air, and carbon dioxide, or starting from fossil fuels. For example, electrolysis of water can be used to obtain hydrogen, or the Fischer–Tropsch process can be used to obtain synthetic diesel fuel from coal or biomass.
- Fuel blends are blends of conventional and synthetic fuels or biofuels that are very attractive as a transition solution toward a cleaner transportation sector. A typical example is gasoline–ethanol blend, which is used in many countries. Blends help in reducing CO_2 emissions.

6.3.1 Biofuels

Biologic matter, such as wood, crops, manure, and wastes, is generally called biomass. Any fuel derived from biomass can be called a biofuel. A more exact definition of biofuel, taken from Speight (2008), is any biomass-derived fuel with at least 80% content by volume being materials sourced from living organisms harvested within 10 years preceding the manufacture. If the fuel is a gas, the common term is *biogas*. If the fuel is a solid (e.g., wood) the term *biomass* is customarily used. If the fuel is a liquid, the common term is *biofuel* (e.g., biodiesel). We discuss in this section the main types of biomass-derived fuels, their characteristics and properties, and the main methods for their synthesis. Using biofuels creates the opportunity to mitigate carbon dioxide emissions. It is important to assess the carbon mitigation potential for each specific case when a biofuel is used.

Since living species rely ultimately on solar energy for life, it appears that biomass is a true renewable energy resource. The most common way to use biomass energy is through direct incineration to generate heat. The thermal energy obtained can then be converted into electricity with the help of heat engines (viz., Rankine cycle). There are other ways to use biomass energy, including gasification, fermentation to produce biogas or alcohols, and so on. Other uses of biomass, besides the energy (heat or power) production, are in the chemical and pharmaceutical

industries, and even in civil engineering works as construction material. Examples of biomass are as follows:

- Wood: trees, tree stumps, dead trees, branches, and wood residuals from forestry and wood-processing industries.
- Agricultural residues: straw, sugarcane fiber, rice hulls, animal wastes, and dried dung.
- Biodegradable wastes from municipal and industrial sources.
- Vegetable oils: palm oil, corn oil, peanut oil, soy oil, and canola oil.
- Energy crops: *Miscanthus*, *Sorghum*, switchgrass, hemp, sugarcane, corn, poplar, eucalyptus, willow, and aquatic plants.

Because it has lower sulfur content and ash-forming components, biomass combustion is cleaner than fossil fuel combustion. Plants absorb carbon dioxide from the atmosphere and convert it into carbohydrates and fiber through photosynthesis. By combusting biomass, the same carbon dioxide is released back to the atmosphere. Consequently, biomass is a CO_2-free renewable source. The general chemical model of biomass is $C_{X_C}H_{X_H}O_{X_O}N_{X_N}S_{X_S}ash_{X_{ash}}(H_2O)_{X_w}$; X_i is number of constituents of species i. Dry biomass has the chemical formula $C_{X_C}H_{X_H}O_{X_O}N_{X_N}S_{X_S}ash_{X_{ash}}$. Molecular mass of dry biomass can be calculated as follows:

$$M = 12 \times X_C + X_H + 16 \times X_O + 14 \times X_N + 32 \times X_S + M_{ash}X_{ash}. \tag{6.9}$$

Dry basis percent by weight of each component (C, carbon; H, hydrogen; O, oxygen; N, nitrogen; S, sulfur) is

$$w_C = 12 \times \frac{X_C}{M}; w_H = \frac{X_H}{M}; w_O = 16 \times \frac{X_O}{M}; w_N = 14 \times \frac{X_N}{M}; w_S = 32 \times \frac{X_S}{M}; w_{ash} = M_{ash} \times \frac{X_{ash}}{M},$$

where typically $w_{ash} = 0.5$–12% dry basis. The moisture content is $w_w = 0$–50% wet basis and the molecular mass of wet biomass becomes

$$M_{wet} = M + X_w \times 18. \tag{6.10}$$

Thus, the correlation between moisture content by weight and molar is

$$w_w = \frac{18X_w}{M + X_w \times 18}, \tag{6.11}$$

or

$$X_w = \frac{w_w M}{18(1 - w_w)}. \tag{6.12}$$

The gross calorific value (GCV) on dry basis is, according to Speight (2008),

$$\begin{aligned} \mathrm{GCV} = {} & 34.91\, w_{\mathrm{C}} + 117.83\, w_{\mathrm{H}} + 10.05\, w_{\mathrm{S}} - 1.51\, w_{\mathrm{N}} - 1.034\, w_{\mathrm{O}} \\ & - 2.11\, w_{\mathrm{ash}}. \end{aligned} \tag{6.13}$$

Net calorific value (NCV) is calculated based on GCV using the same equation as for coal (6.2). According to Szargut (2005), the chemical exergy of biomass (the contribution of the sulfur is negligible) is

$$ex^{\mathrm{ch}}_{\mathrm{Bmass}} = NCV \times \left(1.0347 + 0.014\frac{X_{\mathrm{H}}}{X_{\mathrm{C}}} + 0.0968\frac{X_{\mathrm{O}}}{X_{\mathrm{C}}} + 0.0493\frac{X_{\mathrm{N}}}{X_{\mathrm{C}}}\right). \tag{6.14}$$

The complete biomass combustion with stoichiometric oxygen is written as follows:

$$\begin{aligned} & \mathrm{C}_{X_{\mathrm{C}}}\mathrm{H}_{X_{\mathrm{H}}}\mathrm{O}_{X_{\mathrm{O}}}\mathrm{N}_{X_{\mathrm{N}}}\mathrm{S}_{X_{\mathrm{S}}}\mathrm{ash}_{X_{\mathrm{ash}}}(\mathrm{H_2O})_{X_{\mathrm{w}}} + X_{\mathrm{O_2}}\mathrm{O_2} \\ & \quad \rightarrow X_{\mathrm{C}}\mathrm{CO_2} + X_{\mathrm{H_2O}}\mathrm{H_2O} + X_{\mathrm{N}}/2\mathrm{N_2} + X_{\mathrm{S}}\mathrm{SO_2} + X_{\mathrm{ash}}\mathrm{ash}, \end{aligned} \tag{6.15}$$

where

$$X_{\mathrm{O_2}} = 2X_{\mathrm{C}} + X_{\mathrm{H}}/2 + 2X_{\mathrm{S}} - X_{\mathrm{O}};\ X_{\mathrm{H_2O}} = X_{\mathrm{H}}/2 + X_{\mathrm{w}}.$$

Table 6.6 compiles the calorific properties of main biomass types. Combustion is the most direct method to convert biomass energy into useful thermal energy (and if it is the case, subsequently, thermal energy conversion into electricity). The additional advantage of direct combustion is the possibility to completely use the fuel.

Other methods such as gasification involve incomplete combustion—that is, partial oxidation—and production of a gaseous fuel comprising methane, hydrogen, and carbon monoxide. The conventional gasification is used as an old technology, in which biomass is heated at high temperatures to disengage combustible gas. Optimal gasification conditions were found to be about 500°C, atmospheric

Table 6.6 Calorific properties of the main biomass types

			NCV	
Biomass	GCV, MJ/kg (d.b)	Moisture, w% (w.b.)	MJ/kg (w.b.)	MJ/dm^3 (w.b.)
Wood pellets	19.8	10	16.4	9.8
Wood chips	19.8	30–50	8.0–12.2	2.8–3.9
Grass	18.4	18	13.7	2.7
Cereals	18.7	15	14.5	2.5
Bark	20.2	50	8.2	2.6
Sawdust	19.8	50	8.0	1.9
Straw	18.7	15	14.5	1.7
Oilve	22.0	58	7.3	6.3

Data from Van Loo and Koopejan (2008)
Note: *w%* percent by weight; *d.b.* dry basis; *w.b.* wet basis

pressure, and a steam/biomass ratio equal to 10:1. In the presence of a nickel catalyst, hydrogen at 65% (volume) was produced under these conditions. At temperatures from 800°C to 900°C, biomass is converted completely to CO and H_2, although in practice some CO_2, water, and other hydrocarbons including methane remain in the output stream. The char compositions produced by the fast pyrolysis of biomass can be gasified with gasifying agents. Air, oxygen, and steam are widely used gasifying agents. There are three typical gasification reactions:

- *Oxygen gasification*: It yields a better quality gas of heating value of 10 to 15 MJ/Nm^3. In this process, temperatures between 1,000°C and 1,400°C are achieved. O_2 supply may bring a simultaneous problem of cost and safety.
- *Air gasification*: It is the most widely used technology, as it is cheap, it forms a single product at high efficiency, and it does not require oxygen. A low heating value gas is produced containing up to 60% N_2 having a typical heating value of 4 to 6 MJ/Nm^3 with by-products such as water, CO_2, hydrocarbons, tar, and nitrogen gas. Reactor temperatures between 900°C and 1,100°C have been achieved.
- *Steam gasification*: Biomass steam gasification converts carbonaceous material into permanent gases (H_2, CO, CO_2, CH_4, and light hydrocarbons), char, and tar. This method has some problems such as corrosion, poisoning of catalysts, and minimizing tar components.

In addition, another method for gasification is supercritical water gasification (SCWG), which uses the property that water is miscible with organic substances above the critical point. This method is preferred especially for high-moisture biomass. One of the key works on supercritical gasification of wood is by Modell et al. (1978); a patent was issued for their work in 1978. They reported the effect of temperature and concentration on the gasification of glucose and maple sawdust in water in the vicinity of its critical state (374°C and 22 MPa). No solid residue or char was produced. Hydrogen gaseous concentrations up to 18% were observed.

When used for power generation, the synthetic biogas (biosyngas) produced by the gasification process needs a good amount of excess air for achieving satisfactory fuel utilization. Biosyngas can be used further for hydrogen production. The available methods for producing hydrogen from biomass are reviewed in Kalinci et al. (2009).

Another method for biomass conversion is pyrolysis, which implies heating in the absence of oxygen. Pyrolysis allows the release of volatile matter that is recovered as gas, char, and tar. Pyrolysis is an important process for obtaining energy from biomass. Valuable hydrogen-rich gas can also be generated by pyrolysis. As reviewed in Kalinci et al. (2009), there are three methods for producing hydrogen-rich gas. First, hydrogen can be produced by steam reforming of the pyrolysis liquid obtained from the pyrolysis of biomass. Second, the pyrolysis process is carried out at around 700°C, including the removal of the tar content of the gas and improving the quality of the product gas. In the second stage, catalysts, normally dolomites and Ni, high temperatures, steam, and oxygen could be used. In the third option, the pyrolysis occurs at a lower temperature (<750°C), and a catalyst is incorporated into the same

reactor where the pyrolysis of biomass occurs. Catalytic pyrolysis/gasification is one of the promising options for tar elimination from the product gas. Fast pyrolysis of plant material, such as wood or nutshells, at temperatures between 800°C and 900°C leaves as little as 10% of the material as solid char and converts some 60% into a gas rich in hydrogen and carbon monoxide. This makes fast pyrolysis a competitor of conventional gasification methods. Pyrolysis may be defined as an incomplete thermal degradation of carbonaceous materials into char, condensable liquids (tar, oils, or bio-oils), and noncondensable gases in the absence of air or oxygen. Fast pyrolysis is a thermal or thermocatalytic conversion process that can be characterized by rapid heating rates, quick quenching, and exclusion of oxygen from the reaction zone. It yields valuable chemical intermediates as well as synthesis gas from biomass. Fast pyrolysis is interesting, as a liquid is produced that offers advantages in storage and transport and versatility in applications, although it is still at a relatively early stage of development. Typical properties and characteristics of wood-derived crude bio-oil have been investigated. Water comes from moisture in the feed and reaction water and cannot be separated. The values can range from 15% to 35%. Bio-oil has an HHV of about 18 MJ/kg, as it is produced with about 25 wt% water that cannot be separated.

The main methods to convert biomass into useful forms of energy are presented schematically in Fig. 6.3. Apart from combustion (which generates thermal energy and/or power), gasification, and pyrolysis processes, as discussed above, additional methods are the biophotolysis process that uses bacteria (e.g., genetically modified cyanobacteria) to generate methane or hydrogen, and fermentation processes. Gasification, pyrolysis, and biophotolysis all produce mixtures of combustible gaseous fuels. The fermentation process results in liquid fuels of the alcoholic type or in biogas. The major content of biogas is methane (55–65% by volume),

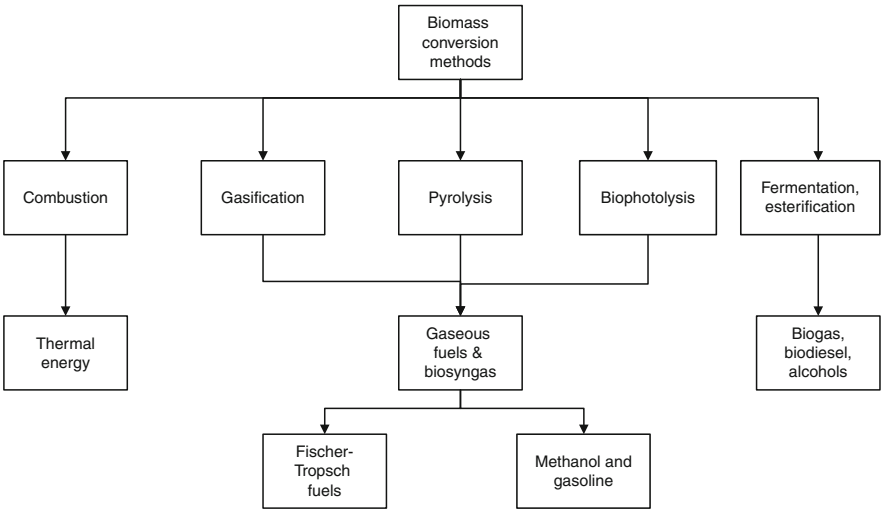

Fig. 6.3 Biomass conversion methods

while the rest is mainly carbon dioxide (35–45% by volume) and other gases (hydrogen, nitrogen, oxygen, and ammonia). Biophotolysis, fermentation, and other methods such as artificial photosynthesis and the biological water-gas shift process can be classified as biological methods for biomass conversion.

Fermentative methods can be produced using anaerobic organisms and/or photofermentation. Also, many phototropic organisms can produce hydrogen with the aid of solar energy, which is called photosynthesis conversion. Furthermore, some bacteria may easily perform water-gas shift reactions. Berberoglu et al. (2008) reported a factor 5.5 increase in hydrogen production by *Anabaena* variables ATCC 29413 using the Allen–Arnon medium compared with BG-11 and BG-110 media. The results were obtained with a flat panel photobioreactor made of acrylic and operated in two stages at 30°C. Dark as well as photoheterotrophic (light fermentation) microorganisms can convert carbohydrate-rich biomass into combustible fuels such as hydrogen or biogas. The primary source for biogas in biohydrogen generation is animal manure, which delivers the necessary microorganisms for anaerobic digestion. Energy crops are also used for biogas production, such as maize, sunflower, and grasses. Landfills are deposits of solid wastes with high content in organic materials and represent a major source of biogas. The first step is the acid or enzymatic hydrolysis of biomass into a highly concentrated sugar solution, which is further fermented by anaerobic organisms to produce volatile fatty acids (VFAs), methane or hydrogen, and CO_2. The organic acids are further fermented by the photoheterotrophic bacteria (*Rhodobacter* sp.) to produce CO_2 and methane or hydrogen, which is known as light fermentation. Combined utilization of dark and photofermentations was reported to improve the yield of hydrogen formation from carbohydrates. Many phototropic organisms, such as purple bacteria, green bacteria, cyanobacteria, and several algae can be used to produce hydrogen with the aid of solar energy. Microalgae, such as green algae and cyanobacteria, absorb light energy and generate electrons. The electrons are then transferred to ferredoxin (FD) using the solar energy absorbed by the photosystem. The mechanism varies from organism to organism, but the main steps are similar.

Other types of fuels from biomass are those based on vegetable oils. They have a different structure than petroleum-based fuels. It appears that some vegetable oils can be used in diesel fuel replacement from both an ecological and economical point of view (see Demirbas 1997). Common vegetable oils and their main properties are listed in Table 6.7.

It can be observed from Table 6.7 that the HHV of all vegetable oil fuels is at about the same value, which is ~39 MJ/kg. The saponification value of oil represents the number of milligrams of sodium or potassium hydroxide required to saponify 1 g of oil, which is a measure of the molecular weight of the fatty acids that compose the oil. The iodine number gives the number of grams of iodine in 100 g of oil. Demirbas (1997) correlated the HHV of vegetable oils with saponification and iodine values:

$$\mathrm{HHV} = 49.43 - 0.041\,\mathrm{SV} - 0.015\,\mathrm{IV}, \tag{6.16}$$

Table 6.7 Technical parameters of main vegetable oil fuels

Oil	Saponification value, mg KOH/g oil	Iodine value, g I/100 g oil	HHV, MJ/kg
Ailanthus	206.34	107.18	39.38
Beech	202.16	105.15	39.59
Castor	202.71	88.72	37.41
Corn	194.14	119.41	39.64
Hazelnut kernel	197.63	98.62	39.83
Laurel	220.78	69.82	39.32
Linseed	188.71	156.74	39.33
Peanut	199.80	119.35	39.45
Poppy seed	196.82	116.83	39.59
Rapeseed	197.07	108.05	39.73
Sesame	210.34	91.76	39.42
Soybean	194.61	120.52	39.63
Spruce	207.09	96.08	39.44
Sunflower seed	191.70	132.32	39.57
Walnut kernel	190.82	135.24	39.56

Data from Demirbas (1997)

where SV and IV represent the saponification and iodine values, respectively; HHV is given in MJ/kg.

Alcohols are probably the most common liquid fuels derived from biomass. Practically, all alcohols can be combusted to generate heat, but only a few are suitable for common motor vehicles: ethanol (C_2H_5OH), methanol (CH_3OH), butanol (C_4H_9OH), and propanol (C_3H_7OH). Ethanol has qualities that makes it a competitor of gasoline in spark ignition engines because it allows for a higher compression ratio, higher flame speed, and leaner operation despite the fact that the energy density of ethanol is lower than that of gasoline and it is more toxic. The general equation for oxidation of alcohol is

$$C_xH_{2x+2}O + 1.5xO_2 \rightarrow xCO_2 + (x+1)H_2O. \tag{6.17}$$

Alcohols can be produced from biomass mainly via fermentation processes. However, it is also possible to synthesize methanol from syngas. Simply, methanol can be produced by hydrogenation of carbon monoxide over a suitable catalyst, usually copper or zinc oxides:

$$CO + 2H_2 \rightarrow CH_3OH, \tag{6.18}$$

which is an exothermic reaction favored by high pressure and low temperature.

Biodiesel is obtained by esterification of vegetable oils; the resulting fuel is clean of sulfur and can be used directly in diesel engines. An alternative route for biodiesel fabrication starts from biosyngas and uses the Fischer–Tropsch method for conversion to diesel fuel. Biodiesel can be used in blends with petroleum diesel to reduce the carbon and sulfur emissions. Also, alcohols such as ethanol can be used to manufacture substitute diesel fuels. As is shown in the next section, ethanol blends can fuel diesel engines.

6.3.2 Other Synthetic Fuels and Fuel Blends

We described in the previous section the most common fuels synthesized from biomass. The focus in this section is on additional fuels that can be derived from conventional fossil fuels, and from other fossil fuels such as oil shale, oil sands, or from biomass. Such fuels include urea, ammonia, dimethyl ether, and others. Among possible synthesis methods, the Fischer–Tropsch method, methanol to gasoline conversion, and coal liquefaction can be used to produce synthetic fuels. Nonconventional fossil fuel sources include the following:

- Tar sand bitumen (also called oil sand or bituminous sand) is a sandstone mineral impregnated with heavy bitumen. Special conversion techniques must be applied to extract hydrocarbons from tar sand, as opposed to petroleum and natural gas, which are natural reservoirs of hydrocarbons.
- Oil shale is a sedimentary rock containing a large amount of kerogen (there is no specific chemical formula of kerogen). Petroleum can be produced from kerogen.
- Gas hydrates (mentioned briefly above) are crystalline solids in which methane is trapped in ice lattice.

Synthetic fuels can be produced by general methods, described also in Fig. 6.3 for biomass conversion. In addition, some specific methods are considered in the extraction phase, such as conversion of kerogen into petroleum, extracting bitumen from oil sands, and extracting methane from gas hydrates. These specific processes are not discussed here; rather, we mention a number of important synthetic fuels and fuel blends: hydrogen, ammonia, urea, dimethyl ether, and others.

The use of hydrogen as a synthetic fuel is believed to be a key solution for the future economy. As a transition period, various paths of producing hydrogen from fossil fuel, biomass, renewable resources, and a combination of these are considered. Hydrogen may be produced from many fossil-based sources including coal, natural gas, and hydrocarbons. As shown by Midilli and Dincer (2008), hydrogen is a sustainable solution for reducing fossil fuel consumption. Ammonia and its use as a fuel and hydrogen source are discussed in Chapter 7. Another synthetic fuel is urea, which can act as a hydrogen source. In the case study presented at the end of this chapter, the use of urea as a hydrogen source for cofueling vehicles is analyzed. Dimethyl ether (DME), having the chemical formula CH_3OCH_3, can be used as a fuel in diesel engines, or as a component of fuel blends for gasoline engine. One such fuel blend is formed by combining 30% DME and 70% LPG. Dimethyl ether can be produced from coal, biomass, or natural gas through various methods. The LHV of DME is 28.9 MJ/kg.

One of the known fuel blends is M85, which comprises 85% methanol and 15% gasoline. Because methanol can be derived from biomass sources, M85 can achieve 85% reduction of carbon dioxide reduction with respect to gasoline-only fuel. Pure methanol can be used as a fuel instead of gasoline, in which case it is called M100. Similarly, ethanol E85 fuel blend consisting of 85% ethanol and 15% gasoline is on

the market. Since ethanol is derived from biomass, the wheel-to-wheel carbon dioxide reduction is at least 80%. Ethanol also can be used in diesel engines in the form of an ED95 blend, containing 95% ethanol and 5% ignition agent.

6.4 Case Study: Urea for Cofueling Vehicles

Biofuels, being derived from biomass, are considered CO_2-free fuels; thus, in a mixture with gasoline or diesel the carbon dioxide emissions can be reduced. In this case study, we investigate the use of urea as hydrogen source onboard vehicles, where hydrogen is employed as an additive to the primary fuel (gasoline or diesel) to enhance the engine efficiency and to reduce the carbon emissions. The study is based on a previous contribution by Zamfirescu and Dincer (2010). Urea can be synthesized from biomass or other renewable energy sources such that it results in a CO_2-free fuel. Urea, with the chemical formula $CO(NH_2)_2$, is massively produced in industry and is used as a fertilizer. It is considered a nontoxic substance, and several car manufacturers use it on their passenger vehicles for NO_x exhaust reduction. Currently, urea is synthesized from natural gas or petroleum, which is then reformed to produce hydrogen. The hydrogen is therefore combined with nitrogen (taken from air) to obtain ammonia, which will eventually be combined with CO_2 to produce urea. It is simple to produce urea starting only from biomass sources. Another path to synthesize urea is via hydrogen production from renewable sources (e.g., water electrolysis, thermochemical or photocatalytic water splitting, etc.), which is then combined with nitrogen to generate ammonia and with CO_2 to produce urea. The carbon dioxide can originate from various sources: recovered from the cement factories or power plants, taken from biomass combustion, extracted from atmospheric air. In any of these cases, the produced urea will be either a zero-carbon or a low-carbon hydrogen source. H_2 extraction from urea is relatively straightforward, and the following section discusses the involved processes in detail.

Urea is a particulate material delivered in small-size prills. It can be combusted, having a low calorific value comparable to that of wood, that is, about 10 MJ/kg. The average price of urea is $0.3 per kg. In what follows, we introduce the general model regarding the use of urea as a hydrogen source on vehicles to enhance gasoline and diesel fuel efficiency, and analyze the benefits of the method with respect to gasoline and diesel reference cases.

6.4.1 Analysis

Pyrolysis and hydrolysis of urea and ammonia cracking are the key processes for hydrogen generation from urea. All these processes are well studied, but their

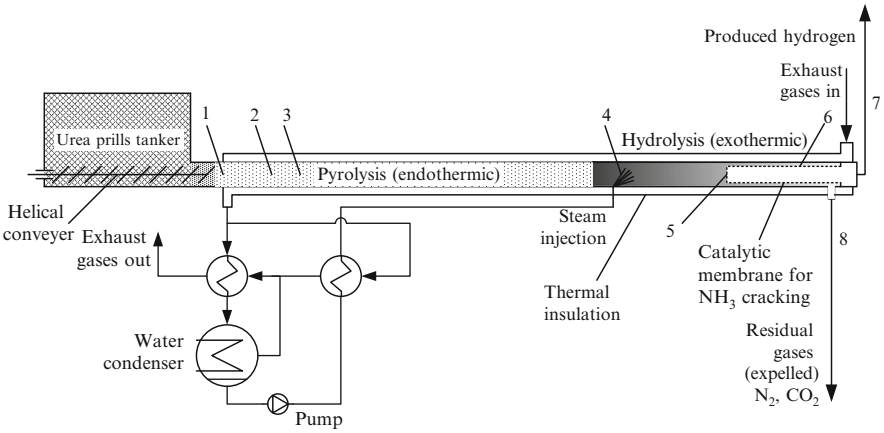

Fig. 6.4 General system layout for hydrogen generation from urea [modified from Zamfirescu and Dincer (2010)]

Table 6.8 Relevant parameters of the fuels included in the case study

Parameter	Urea	Gasoline	Diesel	Hydrogen
Chemical formula	$CO(NH_2)_2$	C_8H_{18}[a]	$C_{12}H_{23}$[a]	H_2
Molecular mass, g/mol	60.5	114.23	167	2
Heating value, MJ/dm^3	14	32	38	10.1[b]
Heating value, MJ/kg	10.5	44	45	142
Heating value, MJ/kmol	635.3	5026	7515	284
Density, kg/dm^3	1.323	0.72	0.85	0.071[b]
Specific cost, $/kmol	18	158	196	10[b]
CO_2 emitted,[c] mol_{CO_2}/mol_{fuel}	1	8	12	0

[a]Common chemical formula
[b]Cryogenic hydrogen at 20 K
[c]Assumed complete combustion

coupling with the aim to produce hydrogen received limited or no attention. Figure 6.4 introduces the overall system for generating hydrogen from urea.

Pure urea particles are kept in a tank and fed with a helical conveyer in a tubular pyrolysis reactor. The pyrolysis involves heating urea without the presence of oxygen. The general thermodynamic properties of urea and other involved substances are summarized in Table 6.8. Urea melts at 133°C, and after further heating it starts to decompose into ammonia and isocyanic acid according to the reaction (see Schaber et al. 2004)

$$CO(NH_2)_2(l) \rightarrow NH_3(g) + HNCO(g), \tag{6.19}$$

where HNCO(g) is isocyanic acid in gas phase. In a flow pyrolysis reactor, as the one indicated in Fig. 6.4, Eq. (6.19) would occur for the temperature range between 133°C and about 200°C.

After completing the pyrolysis, the hydrolysis of isocyanic acid is initiated by steam injection. This reaction is exothermic and evolves according to this formula:

$$HNCO(g) + H_2O(g) \rightarrow NH_3(g) + CO_2(g). \tag{6.20}$$

Several other intermediate compounds occur during the hydrolysis of isocyanic acid in the presence of urea, and these are mainly ammelide, ammeline, cyanuric acid, and biuret. All the intermediary products decompose if the temperature becomes high, so that at about 500°C the only products that exist include ammonia and carbon dioxide, according to the complete urea decomposition reaction as follows:

$$CO(NH_2)_2(l) + H_2O(g) \rightarrow 2NH_3(g) + CO_2(g). \tag{6.21}$$

The kinetics of Eqs. (6.19) to (6.21) has been comprehensively studied by Zanoelo (2009), who shows that reactor volumes would result at reasonable sizes for the reaction to be implemented on regular vehicles.

The reaction heat of isocyanic acid hydrolysis covers partially the necessary thermal energy for ammonia cracking, which is conducted in the last reactor shown in Fig. 6.4. This reactor is a catalytic membrane kind possessing a hydrogen-selective membrane impregnated with a ruthenium catalyst, which augments the rate of ammonia decomposition according to the reaction

$$2NH_3(g) \rightarrow N_2(g) + 3H_2(g). \tag{6.22}$$

The inner side of the membrane reactor is depressurized, thus allowing for hydrogen diffusion and separation. The residual gases comprising mainly carbon dioxide and nitrogen are expelled with possible heat recovery. The use of ammonia as a hydrogen source for transportation vehicles, according to Eq. (6.22), is discussed in detail in Chapter 7, which is dedicated to ammonia as a fuel, H_2 source, refrigerant, working fluid, and NO_x reduction agent.

The exhaust gases from the engine are used to drive the process of hydrogen production. After delivering heat to the pyrolysis reactor, the exhaust gases are cooled down to condense and separate the water. Once the water is separated, it is heated up and boiled to produce steam, which is injected into the hydrolysis reactor. The modeling assumes that all metallic parts including exhaust pipes and ducts, catalytic bed, and membranes are already at high temperature and that all processes occur at a steady state. The process of hydrogen generation from urea has various steps, explained next with reference to Fig. 6.4.

- State 1: granular urea at ambient temperature is forced into the pyrolysis reactor
- Process 1–2: urea is preheated up to its melting point, which is 133°C
- State 2: the melting temperature is achieved, and the melting process just starts
- Process 2–3: urea melting at quasi-constant temperature

- State 3: all urea is in liquid phase
- Process 3–4: urea pyrolysis according to Eq. (6.19); temperature increases
- State 4: temperature reached ~200°C and mostly ammonia and isocyanic acid remain in the stream (small concentrations of other products are also present)
- Process 4–5: hydrolysis of isocyanic acid (steam is injected); temperature increases
- State 5: temperature reaches 500°C, and Eq. (6.20) is assumed to be completed
- Process 5–6: thermocatalytic ammonia cracking according to Eq. (6.22)
- State 6: ammonia is cracked with a high yield
- State 7: hydrogen is separated through the membrane
- State 8: nitrogen and carbon dioxide remain in the main product stream

Under the assumption that the temperature of the environment is $T_0 = 298.15$ K, the enthalpy in state 1—for 1 mol of urea—is the same as the formation enthalpy; the formation enthalpy of urea is 333.1 kJ/mol. The enthalpy in state 2 is calculated based on urea's specific heat taken from the work by Andersson et al. (1993). On a molar basis,

$$h_2 = h_1 + c_p(T_2 - T_1). \tag{6.23}$$

where $T_1 = T_0$ and $T_2 = 133$°C and the specific heat is assumed constant. The energy balance per mole of urea during the melting process is

$$h_3 = h_2 + \Delta h_m. \tag{6.24}$$

where $\Delta h_m = 13.9$ kJ/mol.

At the end of the pyrolysis process it is assumed that the only chemicals present in the stream are isocyanic acid and ammonia; all products are in the gaseous phase. Therefore, the enthalpy at state 4, per mole of urea, is

$$h_4 = h_{NH_3(g)} + h_{HNCO(g)}. \tag{6.25}$$

The enthalpies of all chemicals are referenced to the enthalpies of elements at 298.15 K.

At state 5, the urea decomposition is finalized, and the only considered products are 1 mol of carbon dioxide and 2 mol of ammonia; it results in

$$h_5 = 2h_{NH_3(g)} + h_{CO_2(g)}. \tag{6.26}$$

At state 6, one retrieves the decomposition products of 2 mol of ammonia and thus the enthalpy is

$$h_6 = 3h_{H_2(g)} + h_{N_2(g)} + h_{CO_2(g)}. \tag{6.27}$$

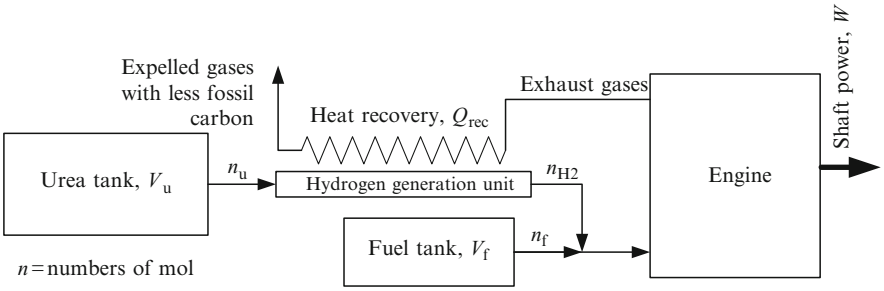

Fig. 6.5 Fueling system for combined urea–conventional fuel engine [modified from Zamfirescu and Dincer (2010)]

The energy balance on the pyrolysis reactor (endothermic) allows for the calculation of the necessary thermal energy input:

$$h_3 + Q_{\text{pyr}} = h_4. \tag{6.28}$$

The heat generated during the hydrolysis reaction (exothermic) results from the energy balance:

$$h_4 + h_{\text{H}_2\text{O(g)}@T_4} = h_5 + Q_{\text{hyd}}. \tag{6.29}$$

The necessary heat input to crack the ammonia is given by the balance (written for a mole of urea):

$$h_5 + Q_{\text{crack}} = h_6. \tag{6.30}$$

The overall energy balance on the hydrogen production system, for 1 mol of urea, gives the necessary heat input in the system as

$$h_1 + h_{\text{H}_2\text{O(g)}@T_4} + Q_{\text{input}} = h_6. \tag{6.31}$$

According to the system diagram shown in Fig. 6.4, it is assumed that steam is obtained from the exhaust gases by using heat recovery; the exhaust gases are cooled until steam condenses, then the needed quantity of water is extracted from the system and the remaining gases and water vapor are expelled into the environment.

Figure 6.5 shows the fueling system with combined urea–conventional fuel (gasoline or diesel) for an engine delivering exhaust gases at a high temperature (600–800°C). The considered engines may be of the internal combustion kind (conventional gasoline or diesel engine). During the running time, heat is recovered from the exhaust gases (Q_{rec}) and used to generate hydrogen from urea

(as explained above). The fuel used to supply the engine is a combination of hydrogen and gasoline or hydrogen and diesel. During the start-up period, when the engine is cold, only gasoline is used as a fuel. Recall that one assumes that urea is synthesized from renewable sources and thus is considered a CO_2-free fuel. Since the running time represents at least 90% of the operation time of an engine, overall the carbon emissions should be smaller with respect to the reference gasoline or diesel cases.

We write c as the concentration of hydrogen in the fuel stream, as given below:

$$c = \frac{n_{H_2}}{n_{H_2} + n_f}, \tag{6.32}$$

where n_{H_2}, n_f represents the number of moles of hydrogen and conventional fuel, respectively, that form the fuel blend delivered to the engine. The HHV of the fuel blend becomes

$$\text{HHV} = [c \times \text{HHV}_{H2} + (1 - c) \times \text{HHV}_f] \times (n_{H_2} + n_f). \tag{6.33}$$

The engine delivers shaft power (W) with efficiency, η; therefore,

$$W = \eta \times \text{HHV}, \tag{6.34}$$

and rejects heat amounting to HHV $- W$; a part $\zeta = 0 - 1$ of the rejected heat is recovered and can be used for hydrogen production from urea. The recovered heat is expressed by

$$Q_{rec} = \zeta(1 - \eta) \times \text{HHV}. \tag{6.35}$$

The number of moles of produced hydrogen is proportional to the recovered heat, namely,

$$n_{H_2} = \frac{Q_{rec}}{\Delta H_{gen}}, \tag{6.36}$$

where ΔH_{gen} represents the thermal energy to generate 1 mol of hydrogen. From the stoichiometry, the number of moles of urea is

$$n_u = \frac{n_{H_2}}{3}. \tag{6.37}$$

The above Eqs. (6.19) to (6.37) form a thermodynamic model of the fueling system (Fig. 6.5), which can be exploited to study the feasibility of the solution with respect to energy and cost consumed per unit of power produced.

Table 6.9 State points of the hydrogen generation system from urea (enthalpy given per 1 mol of urea)

State	h, J/mol	T, K	Stream composition
1	−333,100	298.2	1 mol urea granules (compacted)
2	−322,300	406.2	1 mol urea solid at melting point
3	−308,400	406.2	1 mol of liquid urea at melting point
4	−148,563	473.2	1 mol of ammonia + 1 mol of isocyanic acid (both gases)
5	−408,570	773.2	2 mol ammonia + 1 mol carbon dioxide (both gases)
6	−268,381	773.2	3 mol hydrogen + 1 mol nitrogen + 1 mol CO_2 (gases)
7	66,211	773.2	3 mol hydrogen gas at low pressure
8	−334,591	773.2	1 mol nitrogen + 1 mol CO_2 (gases)

6.4.2 Results

The heat input necessary to decompose 1 mol of solid urea has been calculated according to the procedure introduced above. The results, including stream enthalpies, temperatures, and stream composition, are listed in Table 6.9. The associated reaction heats are calculated as follows:

- Pyrolysis heat input $Q_{\text{pyr}} = 160$ kJ/mol of urea.
- Hydrolysis heat output $Q_{\text{hyd}} = 34$ kJ/mol of urea.
- Ammonia cracking heat input $Q_{\text{crack}} = 140$ kJ/mol of urea.
- Total heat input $Q_{\text{input}} = 290$ kJ per mol of urea or ~100 kJ/mol of produced H_2.

In order to compare the novel fueling solution with the conventional ones in terms of energy and cost, it is important to determine the amount of shaft power generated per mole of conventional fuel consumed, denoted here with

$$W_{\text{f}} = W/n_{\text{f}}. \tag{6.38}$$

We introduce the dimensionless ratio of fuels molar content in the fuel blend as

$$\tilde{n} = n_{\text{u}}/n_{\text{f}}, \tag{6.39}$$

representing the number of moles of urea versus the number of moles of conventional fuel. Equation (6.33) becomes

$$\text{HHV} = (3\tilde{n}\,\text{HHV}_{\text{H}_2} + \text{HHV}_{\text{f}})n_{\text{f}}. \tag{6.40}$$

Also Eqs. (6.32), (6.36), and (6.37) result in

$$\text{HHV} = 3\frac{\Delta H_{\text{gen}}}{\zeta(1-\eta)}\tilde{n}n_{\text{f}}. \tag{6.41}$$

For any η and ζ as the parameters, Eqs. (6.40) and (6.41) can be solved simultaneously for $\tilde{n}$ and HHV. The resulting analytical expression for $\tilde{n}$ is

$$\tilde{n} = \left[\frac{1}{\zeta(1-\eta)} \times \frac{\Delta H_{\text{gen}}}{\text{HHV}_{\text{f}}} - \frac{\text{HHV}_{\text{H}_2}}{\text{HHV}_{\text{f}}}\right]^{-1}. \tag{6.42}$$

Assuming in Eq. (6.41) that the number of moles of hydrogen in the fuel blend is $n_{\text{H}_2} > 0$, the solution is feasible only if the recovered heat needed for urea processing is high enough such that

$$\Delta H_{\text{gen}} > \zeta(1-\eta)\,\text{HHV}_{\text{H}_2}. \tag{6.43}$$

The maximum practical value for $\zeta(1-\eta)$ can be estimated for the worst scenario at $0.5 \times (1 - 0.25) = 0.35$; thus, Eq. (6.43) is satisfied: 100 kJ/mol $> 0.35 \times 284 \cong 99$ kJ/mol. Based on Eqs. (6.34), (6.38), (6.41), and (6.42), the specific shaft power (per mole of fuel consumed) is

$$W_{\text{f}} = 3\frac{\eta}{\zeta(1-\eta)}\Delta H_{\text{gen}}\left[\frac{1}{\zeta(1-\eta)} \times \frac{\Delta H_{\text{gen}}}{\text{HHV}_{\text{f}}} - \frac{\text{HHV}_{\text{H}_2}}{\text{HHV}_{\text{f}}}\right]^{-1}. \tag{6.44}$$

Carbon dioxide emitted by the system originates only from the combustion of the conventional fuel and can be estimated based on W_{f} and the number of moles of CO_2 generated per mole of fuel combusted, $\tilde{n}_{\text{CO}_2}$; the mass of emitted carbon dioxide per unit of shaft energy is

$$m_{\text{CO}_2,\text{w}} = \frac{\tilde{n}_{\text{CO}_2}}{W_{\text{f}}}. \tag{6.45}$$

The total cost of fuel and urea per unit of shaft energy is

$$c_{\text{w}} = \frac{c_{\text{f}} + \tilde{n}c_{\text{H}_2}}{W_{\text{f}}}. \tag{6.46}$$

The total mass of fuel and urea per unit of shaft energy is given by

$$m_{\text{w}} = \frac{\tilde{n}M_{\text{u}} + M_{\text{f}}}{W_{\text{f}}}, \tag{6.47}$$

where M_{u}, M_{f} represents the molecular mass of urea and fuel, respectively.

The total volume of fuel and urea per unit of shaft energy is given by

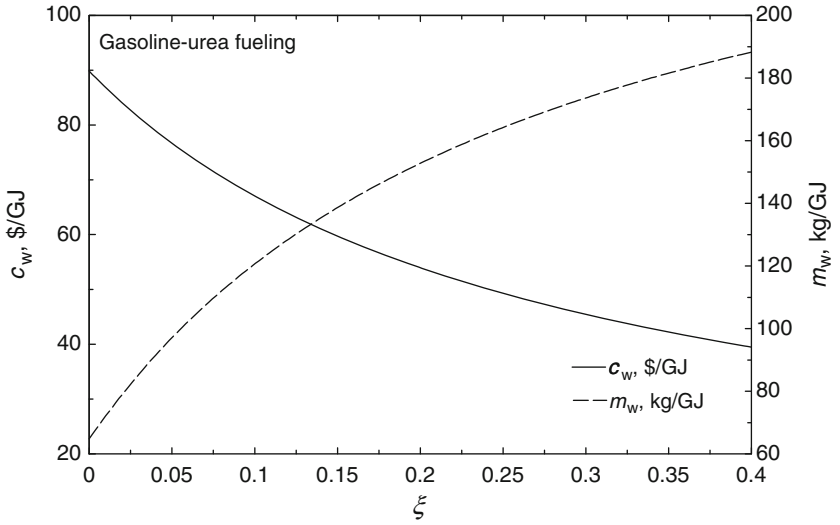

Fig. 6.6 Specific cost and total mass of gasoline + urea fuel per unit of shaft energy [data from Zamfirescu and Dincer (2010)]

$$v_w = \left(\frac{\tilde{n} M_u}{\rho_u} + \frac{M_f}{\rho_f}\right) W_f. \tag{6.48}$$

The mass fraction of urea with respect to conventional fuel $\tilde{m} = m_u/m_f$ is

$$\tilde{m} = \left(\frac{M_u}{M_f}\right) \tilde{m}, \tag{6.49}$$

whereas the volume fraction of urea versus fuel becomes

$$\tilde{v} = \left(\frac{\rho_f}{\rho_u}\right) \tilde{m}. \tag{6.50}$$

The results are presented graphically in Figs. 6.6 through 6.11 as a function of the proportion of heat recovery from the total heat recovered by the engine parameter ζ. We assumed that up to 40% of the rejected heat can be used for hydrogen production from urea, while the rest of the generated heat is lost. Moreover, the typical efficiency of a gasoline engine can be assumed to be 25%, while that of a diesel engine can go to 50%. One can assume, therefore, that the practical achievable efficiency of the engine used for this study is on average 35%.

It is noted that the urea–conventional fuel solution can be regarded as economically and ecologically attractive for specific applications. Figure 6.12 indicates the changes in specific cost, carbon dioxide emission, tank mass, and volume for

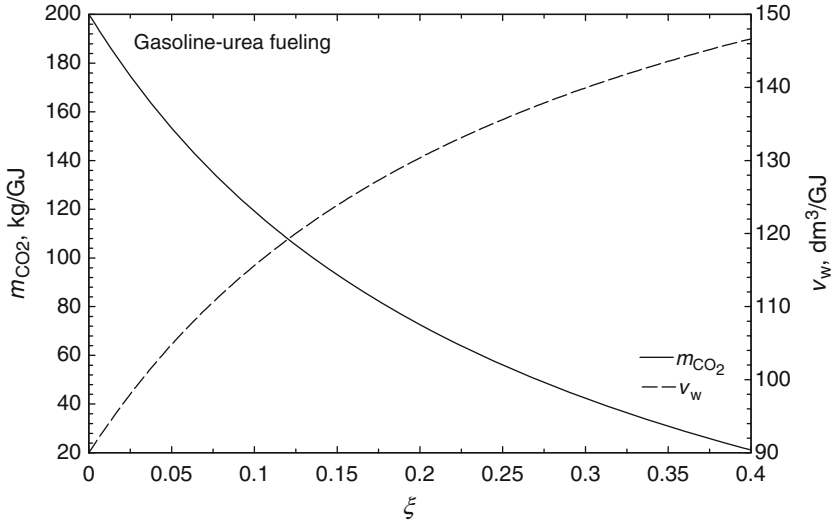

Fig. 6.7 Specific CO_2 emission and volume of gasoline + urea fuel per unit of shaft energy [data from Zamfirescu and Dincer (2010)]

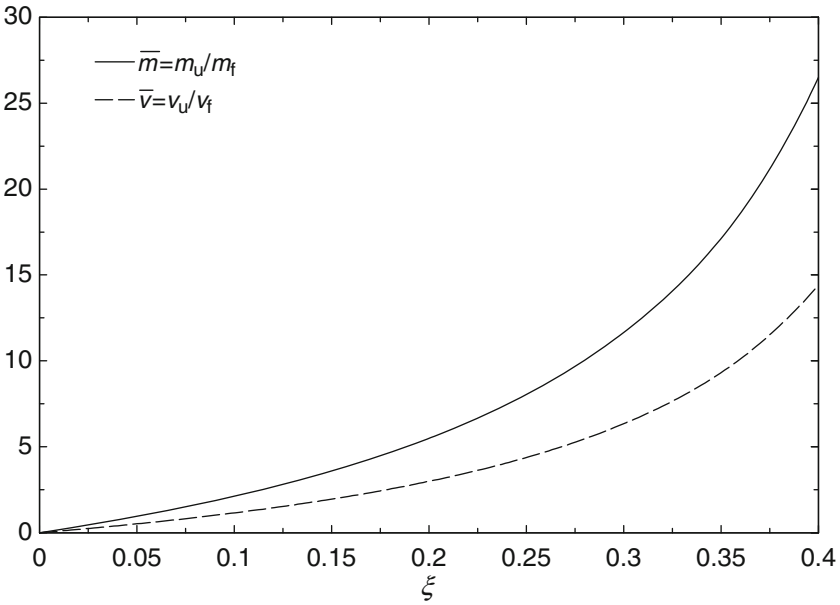

Fig. 6.8 Mass and volume ratio of urea vs. gasoline fuel as functions of the heat recovery factor [data from Zamfirescu and Dincer (2010)]

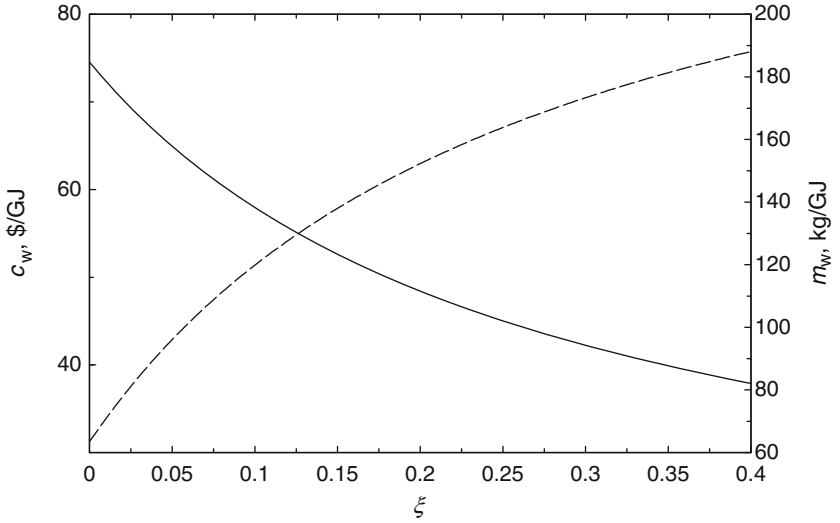

Fig. 6.9 Specific cost and total mass of diesel + urea fuel per unit of shaft energy [data from Zamfirescu and Dincer (2010)]

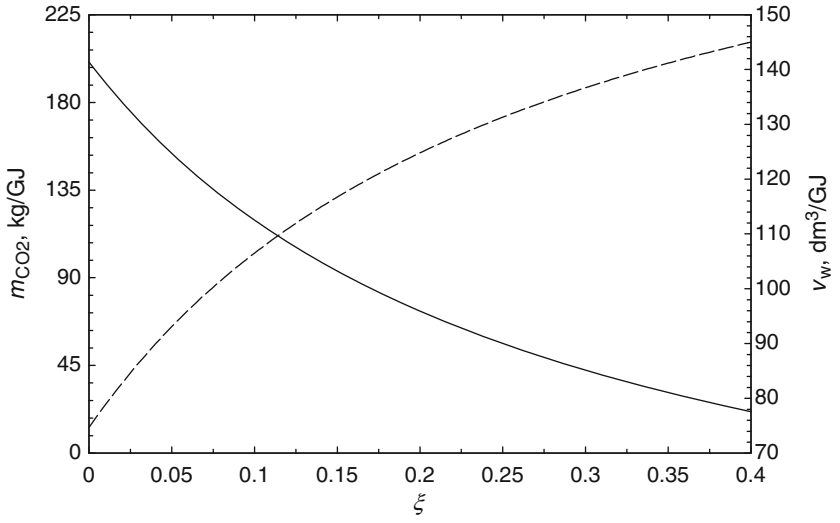

Fig. 6.10 Specific CO_2 emission and total volume of diesel + urea fuel per unit of shaft energy [data from Zamfirescu and Dincer (2010)]

the urea–conventional fuel case with respect to the reference conventional fuel case under the assumption that 10% of the total heat rejected by the engine is recovered and used for hydrogen generation from urea. The percentages in Fig. 6.12 are expressed in relative increments or decrements with respect to the

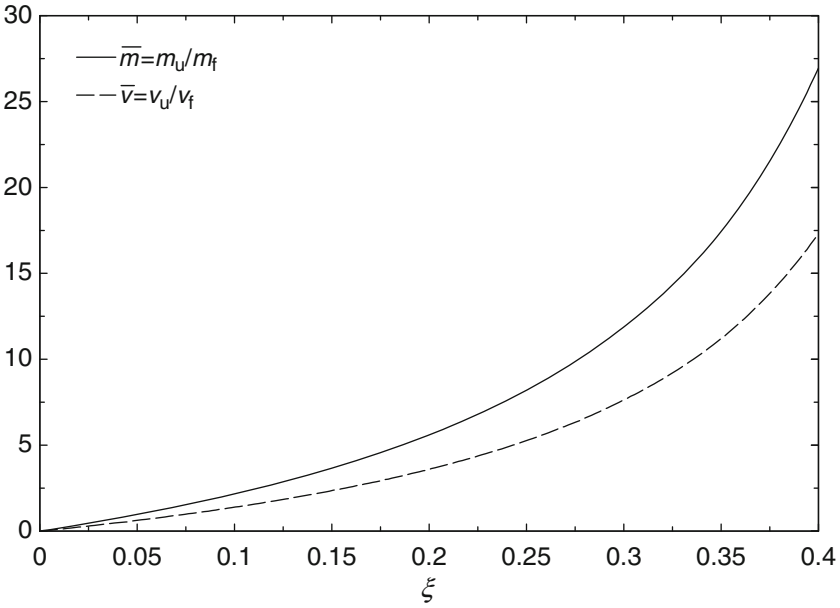

Fig. 6.11 Mass and volume ratio of urea vs. diesel fuel as functions of the heat recovery factor [data from Zamfirescu and Dincer (2010)]

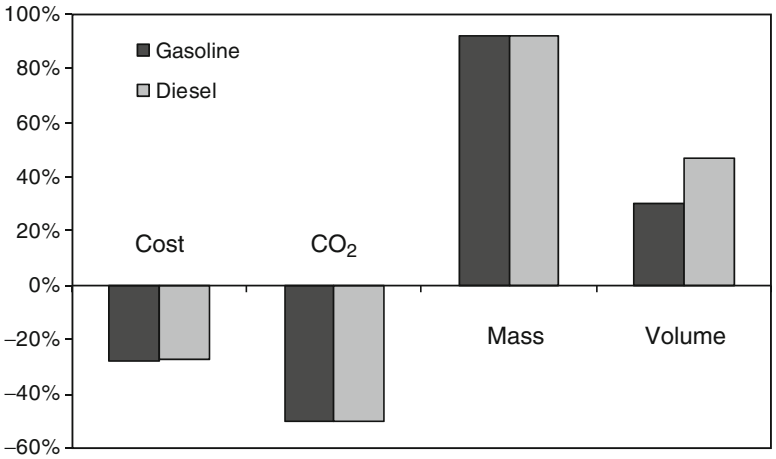

Fig. 6.12 Changes in specific cost, carbon dioxide emission, tank mass, and volume for the urea–conventional fuel case with respect to the reference conventional fuel case [data from Zamfirescu and Dincer (2010)]

reference case, namely, $(x - x_{\text{ref}})/x_{\text{ref}}$, where x represents specific cost, specific carbon dioxide emission, and specific fuel tank mass and volume; the term *specific* here means with respect to produced shaft power energy; the index *ref* represents the reference gasoline or diesel case. It is noted that the cost reduction, carbon mitigation, and mass tank increase for both cases are about the same, namely, 20%, 50%, and 90%, respectively. However, the tank volume increase for gasoline fuel case is about 20% less than in the case of diesel fuel tank, which may represent an advantage.

6.5 Concluding Remarks

Society is in a transition period from fossil fuel–based transportation toward a sustainable transportation sector. In the last century, the sources for transportation fuels and fuels for heating were mainly fossil-based: coal, petroleum, and natural gas. Presently, other fuel sources are considered, with the general aim to achieve cleaner combustion and reduced carbon dioxide emissions. New alternatives to conventional fossil fuels are those including oil sands, oil shale, and carbon hydrates. These fuel sources are considered special in conjunction with the production of synthetic fuels with reduced carbon. Such fuels may be hydrogen, ammonia, urea, methanol, or ethanol. It may be contemplated that carbon dioxide sequestration places can be installed at the extraction sites, where also the synthetic fuel production facility may be placed. Another alternative consists of promoting fuel blends of fossil-based fuel and biofuels. Such blends already exist in the form of ethanol–gasoline, methanol–gasoline, and biodiesel combined with petrodiesel. In this chapter, the fuel sources and the fuel properties, including lower HHV plus fuel's chemical exergy, were discussed in detail. Knowing the chemical exergy of a fuel is of major importance in thermodynamic analysis of processes that use the respective fuel, or in the manufacturing process itself of any specific fuel. Thus, chemical exergy values and formulas were given in the text for the main fuels. Using biofuels is of major importance because this is a real means to reducing carbon dioxide pollution and promoting cleaner options for transportation and energy sector. Many power generation systems—based on fuel combustion—eject heat into the environment. Recovering this heat for local hydrogen generation or cofueling purposes is a way of achieving improved fuel efficiency. The case study in this chapter illustrated the use of urea as a cofuel for diesel and gasoline engines. The advantages of cofueling are extremely relevant, for both mobile and stationary applications. It offers the opportunity to recover heat rejected by engines and upgrade the fuel value and thus improve the overall efficiency. Regarding the results of the case study, it may be shown that for urea + conventional fuel road vehicles, while the onboard fuel storage becomes about 50% larger and 100% heavier than for the conventional vehicle ones, the driving cost is reduced by about 30% and the carbon emissions by about 50%. These figures may be considered attractive enough to encourage further research on this topic.

Nomenclature

c	Molar concentration
ex	Specific exergy, kJ/mol
GCV	Gross calorific value, MJ/mol
h	Specific enthalpy, kJ/mol
H	Total enthalpy, kJ
IV	Iodine value
m	Mass ratio
M	Molecular mass, kg/kmol
$\mathcal{M}$	Specific CO_2 emission, kg/kg or kg/GJ
n	Number of moles
NCV	Net calorific value, MJ/mol
Q	Heat, kJ
s	Specific entropy
SV	Saponification value
T	Temperature, K
w	Moisture content, kg/kg
W	Work, kJ
X	Molar fraction

Greek Letters

η	Efficiency
v	Specific volume, kg/kmol
ρ	Density, kg/m^3
ζ	Heat recovery factor

Subscripts

0	Reference state
DAF	Dry and ash-free
f	Fuel
gen	Generated
rec	Recovery
w	Water

Superscripts

ch	Chemical
$(\sim)$	Dimensionless value

References

Al-Najem N.M., Diab J.M. 1992. Energy-exergy analysis of a diesel engine. *Heat Recovery Systems & CHP* 12:525–529.

Andersson O., Matsuo T., Suga H., Ferloni P. 1993. Low-temperature heat capacity of urea. *International Journal of Thermophysics* 14:149–158.

Berberoglu H., Jay J., Pilon L. 2008. Effect of nutrient media on photobiological hydrogen production by Anabaena variabilis ATCC 29413. *International Journal of Hydrogen Energy* 33:1172–84.

Demirbas A. 1997. Fuel properties and calculation of higher heating values of vegetable oils. *Fuel* 77:1117–1120.

Eiserman W., Johnson, P., Conger, W.I. 1980. Estimating thermodynamic properties of coal, char, tar, and ash. *Fuel Processing Technology* 3:39–53.

Kalinci Y., Hepbasli A., Dincer I. 2009. Biomass-based hydrogen production: A review and analysis. *International Journal of Hydrogen Energy* 34:8799–8817.

Kaygusuz K. 2009. Chemical exergies of some coals in Turkey. *Energy Sources, Part A: Recovery, Utilization, and Environmental Effects* 31:299–307.

Klein S.A. 2010. Engineering equation solver software. F-Chart software. McGraw-Hill Higher Education.

Mason D.M., Gandhi K.N. 1983. Formulas for calculating the calorific value of coal and coal chars: developments, tests, and uses. *Fuel Processing Technology* 7:11–22.

Midilli A., Dincer I. 2008. Hydrogen as a renewable and sustainable solution in reducing global fossil fuel consumption. *International Journal of Hydrogen Energy* 33:4209–4222.

Modell M., Reid R.C., Amin S. 1978. Gasification Process. U.S. Patent 4,113,446.

Nojoumi H., Dincer I., Naterer G.F. 2009. Greenhouse gas emissions assessment of hydrogen and kerosene-fueled aircraft propulsion. *International Journal of Hydrogen Energy* 34:1363–1369.

Schaber P.M., Colson J., Higgins S., Thielen D., Anspach B., Brauer J. 2004. Thermal decomposition (pyrolysis) of urea in an open reaction vessel. *Thermochimica Acta* 424:131–142.

Speight J.G. 2005. Handbook of Coal Analysis. John Wiley and Sons, Hoboken, NJ.

Speight J.G. 2008. Synthetic Fuels Handbook. McGraw-Hill, New York.

Szargut J. 2005. Exergy Method. Technical and Ecological Applications. WIT Press, Boston.

Van Loo S., Koopejan J. 2008. The Handbook of Biomass Combustion and Co-Firing. Earthscan, Sterling, VA.

Zamfirescu C., Dincer I. 2010. Hydrogen Production from Urea for Enhanced Fuel Efficiency of Vehicles. International Conference on Hydrogen Production, Istanbul, June 16–18.

Zanoelo E.F. 2009. A lumped model for thermal decomposition of urea. Uncertainties analysis and selective non-catalytic reduction of NO. *Chemical Engineering Science* 64:1075–1084.

Study Questions/Problems

6.1 Explain the difference between conventional fuels and alternative fuels.
6.2 Can sulfur be considered a fuel?
6.3 What is the best kind of coal with respect to emission per unit of energy embedded?
6.4 Explain the process of pyrolysis.
6.5 Based on Eq. (6.1) and Table 6.2, calculate the range of gross calorific values for anthracite.

6.6 Determine the range of carbon dioxide emission from lignite and compare your results with those shown in Fig. 6.2.
6.7 From which petroleum-derived fuel can one expect the minimum carbon dioxide emission per energy generated by combustion?
6.8 Describe the main features of biofuels.
6.9 Compare wood and olive kernels from the point of view of combustion energy and carbon dioxide emissions.
6.10 Comment on the main routes of biomass energy conversion methods.
6.11 It is given for one kind of vegetable oil fuel a saponification value of 190 mg KOH/g oil and an iodine value of 90 g I/100 g oil. Calculate the higher heating value.
6.12 Perform a case study similar to the one presented in Section 6.4 for the case of ammonia–gasoline cofueling.

Chapter 7
Ammonia as a Potential Substance

7.1 Introduction

Ammonia is a substance formed from hydrogen, the most abundant chemical element of the universe, and nitrogen, the major component of the terrestrial atmosphere (79%). It is interesting to note that the second major component of the terrestrial atmosphere, oxygen (21%) in combination with hydrogen forms water. Similarly to water, ammonia plays a major role in the global ecosystem: it represents a nitrogen source for all living species. At the same time, ammonia can play a major role in the sustainable development of mankind since it is a hydrogen source that packs 1.5 mol of hydrogen per mol of NH_3 at a density as high as 106 kg H_2/m^3. Moreover, ammonia is produced industrially in large quantities as artificial fertilizer for agriculture. With respect to sustainable development, it is of major importance to find and promote cleaner and more efficient technologies of ammonia production, since NH_3 is produced currently from fossil fuels, and its synthesis process leads to major greenhouse gas emissions on a global scale and consumes a significant amount of the world's energy budget. Recently, ammonia has been proposed as a hydrogen source because hydrogen can be generated from ammonia at a relatively low energy expense. That is, ammonia is an attractive medium to store hydrogen through chemical bonding. Storing hydrogen in the form of ammonia (detailed in this chapter) is one of the most promising and least expensive long-term storage methods. Last but not least, ammonia is an excellent refrigerant, a working fluid in power cycles, and an NO_x reducing agent.

In brief, ammonia is a special substance that can potentially play a major role in sustainable development because of its unique qualities. We will analyze in this chapter various aspects regarding the use of ammonia in advanced/sustainable energy systems, and the possible paths for the clean and efficient synthesis of ammonia.

İ. Dinçer and C. Zamfirescu, *Sustainable Energy Systems and Applications*,
DOI 10.1007/978-0-387-95861-3_7,

7.2 Ammonia Synthesis

An ammonia molecule can be formed by reacting nitrogen with hydrogen according to the following exothermic reaction:

$$1.5\,H_2 + 0.5\,N_2 \rightarrow NH_3 - 45.2\,\text{kJ/mol} \cdot NH_3. \tag{7.1}$$

However, the activation energy of this reaction, which is equivalent to that needed for breaking the triple covalent bond of nitrogen molecule ($N \equiv N \rightarrow 2\,N^{3+} + 6e^-$), namely, 460 kJ/mol, appears to be insurmountable (note that this is higher than that of CO_2 and water formation, −393.5 kJ/mol and −241.82 kJ/mol, respectively).

The Haber–Bosch process was invented at the beginning of the twentieth century to combine hydrogen and nitrogen thermo-catalytically according to the reaction in Eq. (7.1). The principle of this process is based on increasing the temperature of the reactants such that the nitrogen molecule receives enough energy to be cracked. The catalyst breaks the nitrogen bonds at the surface. If the temperature is not high enough, nitrogen atoms remain strongly bound at the surface and inhibit the catalyst from performing a new catalytic cycle. However, because in the reaction in Eq. (7.1) 2 mol of reactants produces 1 mol of products, the forward reaction is facilitated by low temperatures and high pressures. Since the reaction temperature cannot be set low (because of catalyst poisoning), the operating pressure must be extremely high. Typically, the operating temperature and pressure are 600°C and 100 to 250 bar, respectively, for 25% to 35% conversion (see Appl 1999).

A commonly used conversion loop is shown in Fig. 7.1 and operates as follows. Make-up gas consisting of hydrogen and nitrogen is provided as input and compressed up to an intermediate pressure. The make-up gas is combined with unreacted gases returned from the loop and compressed further up to the conversion pressure. The feed is directed toward the catalytic converter, which contains mainly iron-based catalysts. The resultant gases containing converted ammonia product enter the ammonia separator that operates at the intermediate pressure. There, ammonia is separated by condensation and collected as liquid from the bottom of the separator. A refrigeration plant based on ammonia is used to cool, condensate, and separate the product. The remaining gases, containing mainly unreacted nitrogen and hydrogen, are partly recycled (recompressed together with the make-up gas) and partly used in a combustor to produce process heat. Additional fuel may also be fed into the combustor. The flue gases and the heat of the exothermic ammonia reaction are used to generate steam in a Rankine cycle that drives a turbine.

For better efficiency, the pump and the compressors are mounted on the same shaft with the turbine. Pressure is the parameter that controls the ammonia conversion. For a typical case at 200 bar, ammonia conversion is ~15% and increases up to 25% at 400 bar. Two types of catalytic ammonia converters are commonly used. The first is cooled internally with a coil running through the catalyst bed, and the

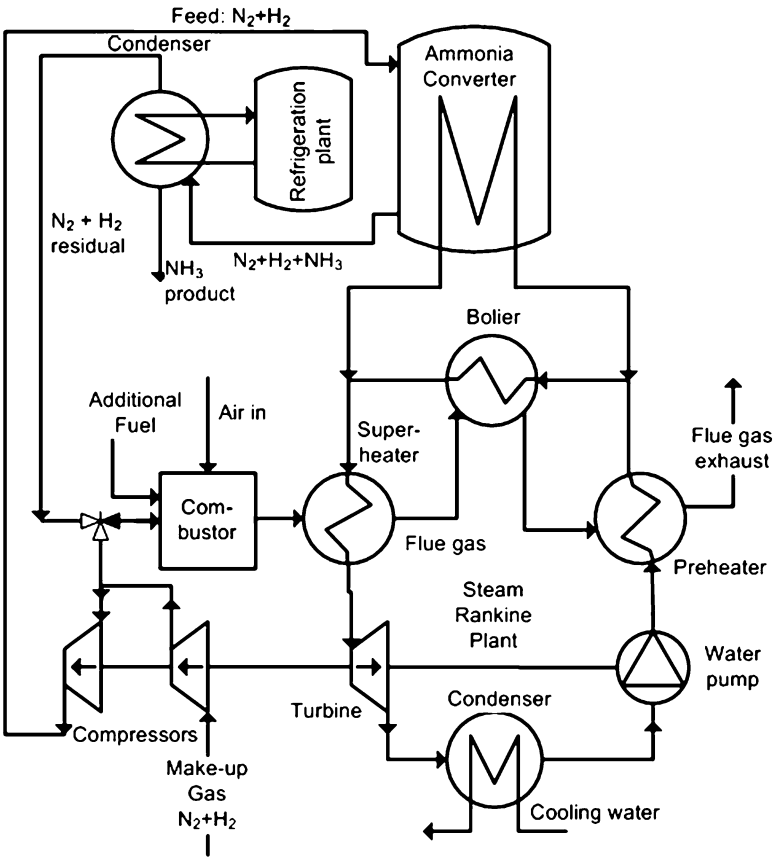

Fig. 7.1 Possible configuration of a Haber–Bosch ammonia plant with energy recovery [modified from Zamfirescu and Dincer (2009b)]

second divides the chemical reactor into modules, and after each module the products are cooled in separate heat exchangers.

Due to important heat generated during ammonia synthesis (i.e., 2.7 GJ/ton of ammonia), great emphasis is put on heat recovery. High-pressure steam further expanded in turbines (as explained above) has been found to be the most beneficial solution for heat recovery. In principle, high pressure steam at ~125 bar can be generated. According to Appl (1999), an advanced ammonia plant produces ~1.5 ton of high pressure steam per ton of ammonia, representing 90% recovery of ammonia formation enthalpy. Other gas-handling operations (e.g., hydrogen separation from returning stream, purge gas management, nitrogen separation, and hydrogen production) consume some amount of primary energy and degrade the synthesis loop efficiency. According to Rafiqul et al. (2005), ammonia production efficiency from a primary thermal energy source, through the Haber–Bosch process, varies between 37% and 65%. If hydrogen is derived from a sustainable

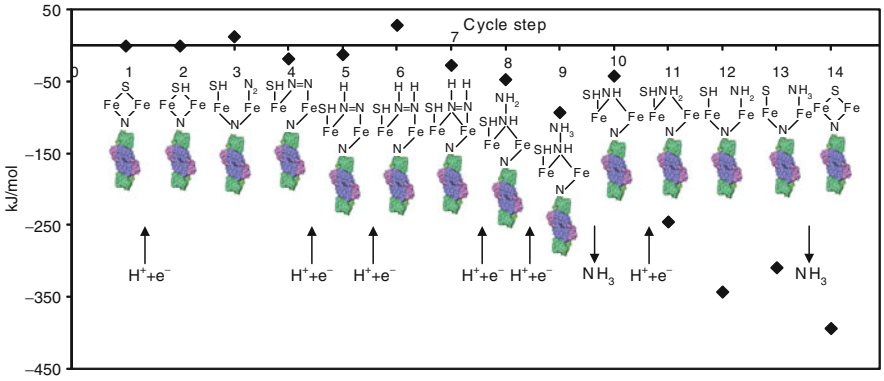

Fig. 7.2 The 14-step nitrogenase cycle for ammonia synthesis (*upward-pointed arrows* represent proton–electron inputs, *downward-pointed arrows* represent ammonia outputs, and diamonds represent the energy level) [modified from Zamfirescu and Dincer (2009b)]

source (meaning that no CO_2 emission could be associated with the hydrogen production), then the greenhouse gases (GHGs) equivalent to the energy needed to run the plants are of the order of 0.4 tCO_2/tNH_3, see Rafiqul et al. (2005). Typical CO_2 emissions are 2.2 tCO_2/tNH_3 if hydrogen is produced from natural gas, and 16.2 tCO_2/tNH_3 if coal is the primary source; the minimum possible value for GHG emission with today's technology is 1.6 tCO_2/tNH_3. In recent years, ammonia prices fluctuated between \$150/t and \$700/t.

In biological systems, nitrogenase enzyme is used to break the nitrogen molecule and to bond nitrogen to protons to form ammonia. Nitrogenase, which is one of the most complex enzymes, performs ammonia synthesis in a very "intelligent" way, by not breaking dinitrogen directly, but rather bond by bond. Nitrogenase consists of two protein clusters: (1) one that has an electron-acceptor active site based on iron (Fe) and molybdenum (Mo) having the stoichiometry $MoFe_7S_9N$ (in some alternative versions of nitrogenase, the active center is based on Fe and V), and (2) one that has an iron-sulfur center that hydrolyzes adenosine triphosphate (ATP) to obtain energy and provide electrons to the active site of the first cluster. During the ATP hydrolysis (ATP → ADP + Pi), adenosine diphosphate (ADP) and inorganic phosphate (Pi, standing for HPO_4^{2-}) are produced. The ATP comes from glucose oxidation and is the basic compound that biological systems use to store and release chemical energy. Nitrogenase uses gaseous nitrogen (N_2) directly, which is "captured" from the atmosphere by organisms by specific respiration mechanisms. Hydrogen is not used by nitrogenase in a molecular form; rather it is used in the form of protons produced by H_2 ionization at the electron-acceptor active site, and electrons provided by the electron-donor active site. Intensive efforts were dedicated in recent years to clarifying the ammonia production cycle by nitrogenase. The main findings are summarized in papers by Hinnemann and Nørskov (2006) and Kästner and Blöchl (2007). The synthesis process at the active site is presented in Fig. 7.2. Ammonia synthesis consists of 14 steps in which various intermediate

compounds are formed at the active site. All intermediates are recycled, and globally, from one nitrogen molecule and six hydrogen molecules, two NH_3 molecules are produced per cycle. Figure 7.2 presents the reactions at the active site as derived from the work by Kästner and Blöchl (2007).

The required energy for producing 1 mol of ammonia is 395 kJ, and the higher heating value (HHV) of NH_3 is 382 kJ/mol; therefore, the efficiency of the reaction itself appears to be ~96%. There are, however, possible variations in the reaction steps and in their number as the nitrogenase adapts to the substrate (i.e., the organic matter encountered for processing). Therefore, the energy per production cycle may vary. One source of irreversibilities at ammonia synthesis by nitrogenase (see Fig. 7.2) is due to the competition of ammonia formation and hydrogen formation. In this process, some protons and electrons can be lost. In any situation, nitrogenase synthesizes small quantities of hydrogen during the ammonia production. Hydrogen is mainly used for energy recovery through oxidation (see Mousdale 2008).

Nitrogenase is produced by a number of microbes that live in symbiosis with root nodules of legumes and plants such alfalfa, clover, or peas. There are also free-living microbes that produce nitrogenase, most of them being anaerobic (e.g., clostridium, *Klebsiella pneumoniae*, *Bacillus polymyxa*, *Bacillus macerans*, *Escherichia intermedia*, *Rhodobacter sphaeroides*, *Rhodopseudomonas palustris*, *Rhodobacter capsulatus*) and others being aerobic (e.g., *Azotobacter vinelandii*, *Anabaena cylindrical*, and *Nostoc commune*).

7.3 Ammonia Storage

Because of the major interest in industrial ammonia as a fertilizer, large-capacity seasonal storage tanks were developed. Ammonia demand peaks during the summer when it must be spread on agricultural fields. Ammonia is produced throughout the year, and the winter's production is stored for the summer season. Tanks with a capacity of 15,000 to 60,000 m^3 were constructed before the 1970s (Walter and Lesicki 1998). Ammonia is stored in the refrigerated state at ambient pressure and at its normal boiling point, which is $-33°C$. The tanks are cylindrical with a 38- to 52-m inner diameter and 18 to 32 m of useful height. In order to compensate for the heat penetrations, the whole construction is well insulated (a double-wall technology is used) and compressors are employed to remove the heat by simulating a refrigeration plant for which the tank plays the role of an evaporator. Basically, ammonia vapors existent above the liquid are aspired by the compressors and delivered at high pressure where the vapors are condensed and the liquid is returned back to the tank. In this way, the temperature and the pressure in the tank are kept constant.

Figure 7.3 presents a typical seasonal ammonia storage system. Cold vapors in state 1 are aspired and compressed with a two-stage compression station up to state 2 that corresponds to a condensation temperature for winter season. The liquid condensate at ambient temperature in state 3 is throttled and returned as a cold

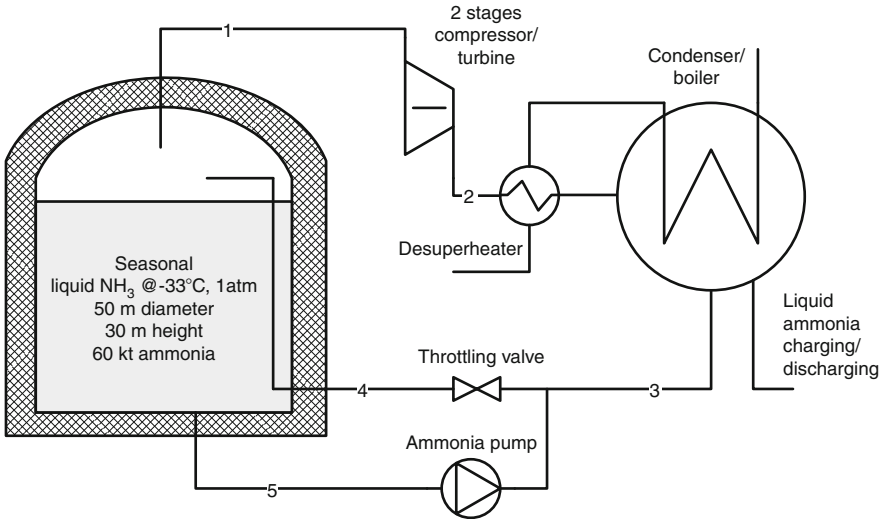

Fig. 7.3 Seasonal ammonia storage system [modified from Zamfirescu and Dincer (2009b)]

two-phase vapor–liquid mixture into the tank. The circulated ammonia flow rate must be such that it compensates for the effect of heat penetration from outside and the associated ammonia evaporation. In practice, according to Bartles (2008), 0.1% of ammonia from stored liquid evaporates per day. The latent heat of ammonia at 1 bar is 1370 kJ/kg; thus about 1.4 kJ of cooling must be provided per kg of liquid ammonia, each day. In the wintertime, ammonia refrigeration plants operating at $-33°C$ evaporation and $+15°C$ condensation temperature can achieve COP = 2.5; therefore, the corresponding compressor shaft energy is 0.6 kJ/kg every day, or 110 kJ/kg per 6 months of storage. The total energy required for running a 60-kt tank is, therefore, 6.6 GJ per storage season (the season is the 6-month winter-to-summer storage period).

Charging of ammonia into a tank is normally done by using liquid at high pressure, that is, at the condenser level. During charging, the liquid is expanded to 1 bar and, therefore, the cooling demand compensates only for the fraction of generated vapors that must be condensed. Vapor fraction in winter conditions during ammonia filling is ~15%; therefore, about 9 kt of vapors must be condensed for the 60-kt tank, or 4.9 GJ shaft energy must be provided for complete filling. In total, the shaft energy needed to drive refrigeration is ~11.5 GJ per season.

Note that cold-stored ammonia has a high exergy content, which, in principle, can be converted back into power. The specific exergy of refrigerated ammonia with reference to summer ambient temperature (e.g., 25°C) is given by

$$ex = (h - h_0) - T_0(s - s_0), \tag{7.2}$$

where h and s are specific enthalpy and entropy of liquid in the tank, respectively, and h_0 and s_0 represent the enthalpy of saturated liquid at ambient temperature.

The liquid in the tank is subcooled because it is subjected to a hydrostatic overpressure $\Delta P = \rho g \Delta z$, where Δz is the mean height of the liquid. The overpressure is estimated in these conditions to be about 1 bar, and the estimated specific exergy is 19 kJ/kg or 1.1 GJ/60 kt. In principle, 50% of this exergy can be recovered through a heat engine operating between the ambient and the low temperature of the cold storage; the recovered exergy represents ~5% of the energy spent to fill the tank and keep it refrigerated for the whole season.

Tank emptying with work recovery can be imagined as follows (see the diagram in Fig. 7.3): cold liquid is extracted at point 5 from the tank bottom, and pumped to high pressure at point 3; a part of the liquid is extracted from the tank at the discharge port from the bottom of the condenser/boiler heat exchanger; the other part of the subcooled liquid is heated, boiled, and superheated up to state 2. The superheated vapors are expanded over a turbine and expanded back into the tank. The process is repeated until all liquid is eliminated.

Ammonia is stored in smaller quantities in tanks made from regular carbon steel, designed for ~20 bar operating pressure where ammonia is kept in a liquid state at ambient temperature. A rule of thumb according to Appl (1999) is that at least 3 tons of ammonia can be stored per ton of steel. Therefore, the tank weight is about one fourth of the ammonia mass. Various sizes of cylinders are available in the industry. The size of ammonia pressurized tanks is limited for practical reasons to about 300 tons.

There is considerable experience with ammonia distribution using trucks, barges, ships, and rail. In road transport, the typical cisterns have 45-kl capacity, while rail cars have ~130-kl capacity. Ocean ships transport ammonia in low-temperature storage tanks of up to 50-kton capacity. Regarding pipeline transportation, following Bartles (2008), the distribution energy efficiency is 93% with respect to HHV at an energy density of 14 GJ/m^3.

Ammonia can be stored onboard a vehicle in pressurized cylinders in an anhydrous form or in some chemical form such as metal amines or ammonia boranes, which are produced using recently developed physical–chemical reversible methods; see Heldebrant et al. (2008) and Christensen et al. (2005). In this technology, ammonia is adsorbed on a porous metal–amine complex, for example, hexaamine-magnesium chloride, $Mg(NH_3)_6Cl_2$; to do this, NH_3 is passed over an anhydrous magnesium chloride ($MgCl_2$) powder at room temperature. The absorption and desorption of ammonia in and from $MgCl_2$ are completely reversible. The metal amine can be shaped in the desired form and can store 0.09 kgH_2/kg and 100 kgH_2/m^3.

7.4 Ammonia Use in Power Generation Systems

The use of ammonia in power generation and energy conversion applications presents unique opportunities. Ammonia can play multiple roles simultaneously: it can be used as a fuel, a hydrogen source, a working fluid, a refrigerant, and an

NO_x-reducing agent. In this and the next sections, we analyze all these roles and the relevant ammonia system for power generation and energy conversion based on the work of Zamfirescu and Dincer (2008a, b, c, 2009a, b).

Regarding the role of ammonia as an NO_x-reducing agent, the reaction of NO_x with ammonia over catalysts produces only steam and nitrogen. An average car needs only ~30 ml of NH_3 per 100 km to neutralize any NO_x emissions. Reduction of the NO_x formed during fuel combustion in many kinds of engines and furnaces is done according to the following reactions, conducted catalytically over zeolites:

$$\begin{cases} 4\,NO + 4\,NH_3 + O_2 \rightarrow 4\,N_2 + 6\,H_2O \\ 6\,NO_2 + 8\,NH_3 \rightarrow 7\,N_2 + 12\,H_2O. \end{cases} \tag{7.3}$$

When ammonia is used as a fuel in any combustion system or a fuel cell, the desired chemical reaction is the complete oxidation that produces only steam and nitrogen and some considerable amount of heat, according to the equation given below:

$$2NH_3(g) + 1.5O_2(g) \rightarrow N_2(g) + 3H_2O(g) - 634\,kJ. \tag{7.4}$$

However, in most of the practical situations, the reaction kinetics is favorable to nitric oxide formation. Thus, the partial oxidation of ammonia occurs normally as

$$2\,NH_3 + 2.5\,O_2 \rightarrow 2\,NO + 3\,H_2O - 454\,kJ. \tag{7.5}$$

The reaction heats in Eqs. (7.4) and (7.5) are indicated only for order of magnitude estimation in standard conditions (25°C, 1 atm). Considering the operating temperature range of high-temperature fuel cells and of internal combustion engines (ICEs), that is, 500°C to 1,000°C, the reaction heat for partial and complete oxidation cases is calculated using the equations, correlations, and data given in NIST (2010). The results obtained in terms of reaction heat versus process temperature are shown in Fig. 7.4. From Fig. 7.4, it can be inferred that the partial oxidation of ammonia reduces the useful reaction heat by 33%, and moreover, the reaction heat dependence on temperature is more profound than that in the case of complete oxidation. Therefore, it potentially causes problems with process control. One way to minimize partial ammonia oxidation is to crack (decompose) ammonia first, according to the endothermic reaction $2NH_3 \rightarrow N_2 + 3H_2 + 94$ kJ, thus producing hydrogen, which is used further as a fuel.

Solid oxide fuel cell (SOFC) or intermediate temperature fuel cells and ICEs present an advantage in this respect due to their high operating temperatures at which ammonia can be decomposed thermally over catalysts. Keeping this aspect in mind, let us consider some possible power systems with NH_3. As shown in Fig. 7.5, two main approaches are applicable to ammonia-fueled power generation in transportation vehicles: ICEs and fuel cell systems.

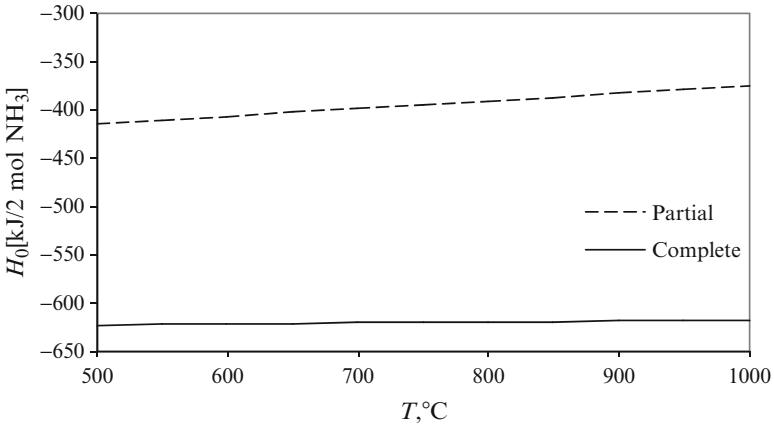

Fig. 7.4 Partial oxidation vs. complete oxidation during the anodic reaction [modified from Zamfirescu and Dincer (2008a)]

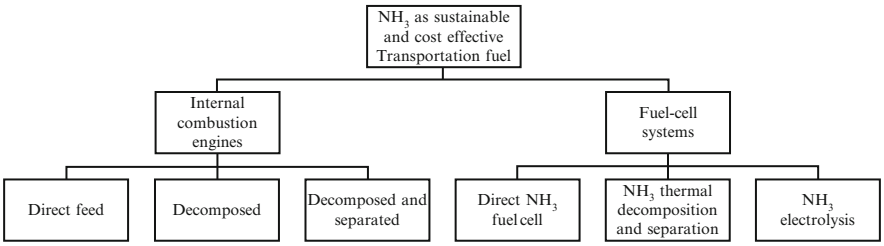

Fig. 7.5 Possible power systems fueled with ammonia

7.5 Hydrogen from Ammonia Route

The common approach to hydrogen economy is illustrated in Fig. 7.6 and consists of the following steps: production of hydrogen from primary energy sources at some locations, hydrogen distribution (infrastructure not yet developed), and hydrogen delivery on vehicles to plants where it is used for power generation/propulsion. Our aim here is to assess the total cost of hydrogen per unit mass at the utilization point (i.e., in the vehicle) for two alternative layouts of the hydrogen transportation economy. The first layout was introduced above and is illustrated in Fig. 7.6. The second layout refers to the production of hydrogen from ammonia and will be described later. For a preliminary analysis, let us assume that hydrogen is produced from liquid water, either by electrolysis or by thermo-chemical splitting. The corresponding chemical reaction is given below with the heat generated:

$$H_2O(l) \rightarrow H_2 + \frac{1}{2}O_2 + 286\,\text{MJ}. \tag{7.6}$$

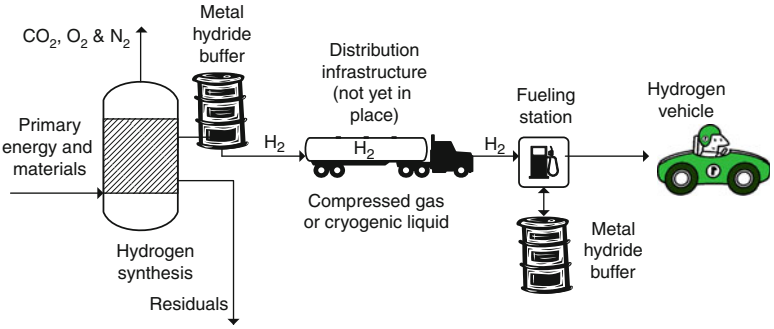

Fig. 7.6 The layout of hydrogen economy for transportation

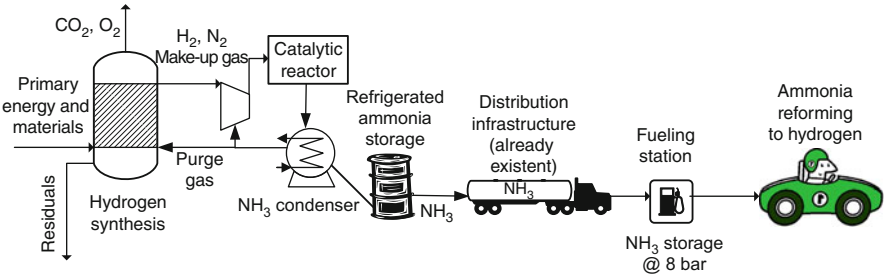

Fig. 7.7 The layout of hydrogen-from-ammonia economy for transportation

Here, in the ideal situation, for every kmol of hydrogen produced, one needs $\Delta H_{H_2O} = 286\,\text{MJ/kmol} \cdot H_2$ of energy to split the water molecule. Obviously, the practical energy needed to drive this process is larger than the theoretical one due to the imperfections. The produced hydrogen has to be stored in buffers at the production place, and then charged on vehicles specialized for pressurized or cryogenic hydrogen transport. It is then distributed to fueling stations and finally delivered to the consumers' vehicles. Along this complex chain, the cost of hydrogen will increase by amounts proportional to the energy utilization specific to each phase. We will later study the distribution costs and discuss the total cost of hydrogen delivery.

We will now study the second alternative where, instead of hydrogen, ammonia is produced at a synthesis plant, buffered locally, distributed to fueling stations, and then charged on vehicles where it is reformed to hydrogen by thermal cracking of the ammonia molecule. This scenario is illustrated in Fig. 7.7. Only ~12% from ammonia's HHV is needed for reforming. There is enough heat onboard a vehicle; the most advanced H_2ICEs have an efficiency of 50% to 60% and that of the most advanced fuel cell systems is 60% to 70%; the rest of the hydrogen energy is dissipated as heat. Thus, the onboard reforming process is "for free." An exception is the proton exchange membrane (PEM) fuel cell system in which heat is rejected at a low temperature, making it unsuitable for ammonia cracking. In this case,

which is not analyzed in this chapter, a small part of the produced hydrogen can be combusted for generating the reformation heat.

Ammonia is industrially produced from hydrogen and nitrogen via the well-established Haber–Bosch process. Hydrogen can be obtained from water (by thermochemical water splitting or electrolysis) according to the reaction in Eq. (7.6), while the nitrogen comes from atmospheric air. In order to obtain an ammonia quantity corresponding to 1 mol of hydrogen, the following reactions have to be considered (ideal case):

$$\begin{cases} H_2O \rightarrow H_2 + \frac{1}{2}O_2 + 286\,\text{MJ} \\ H_2 + \frac{1}{3}N_2 \rightarrow \frac{2}{3}NH_3 - 30.7\,\text{MJ}. \end{cases} \tag{7.7}$$

Thus the energy needed to produce 1 mol of hydrogen embedded in ammonia is 286 − 30.7 MJ, which is $\Delta H_{NH_3} = 255.3\,\text{MJ/kmol} \cdot H_2$. Therefore, on a mass basis, the cost of NH_3 over the cost of H_2 can be estimated to be proportional to the energy required for their synthesis as

$$\frac{c_{NH_3}}{c_{H_2}} = \frac{3}{\mu_{NH_3}} \frac{\Delta H_{NH_3}}{\Delta H_{H_2O}} = 0.157. \tag{7.8}$$

According to Eq. (7.8), the ideal cost of ammonia is less than 16% the cost of hydrogen per unit mass. From the stoichiometry, it can be determined that 1 kg of ammonia contains 3/17 = 0.176 kg of hydrogen. As mentioned above, this quantity of hydrogen can be released by NH_3 cracking at no cost onboard vehicles, using the heat generated locally. Therefore, producing hydrogen from ammonia becomes attractive if

$$\frac{c_{NH_3}}{c_{H_2}} < 0.176. \tag{7.9}$$

Note that from Eqs. (7.8) and (7.9), it appears that, on an ideal basis, producing hydrogen locally from ammonia is more efficient than producing pure hydrogen and then using it onboard vehicles. Up to this moment, the irreversibilities of the chemical reactions and the fuel production and distribution costs were not considered in the analysis. For a detailed analysis, the price of hydrogen, and ammonia production and distribution, respectively, must be accounted for.

Hydrogen, as stated above, is the most difficult to store in a compact form. Therefore, the distribution- and storage-related costs will impact mostly on the total costs. Depending on the production method, hydrogen cost varies from ~$1/kg at coal gasification to ~$9.50/kg using solar energy for electricity generation, which in turn is used for water electrolysis. After production, hydrogen is stored at the manufacturer's location for a certain period prior to delivery. Hydrogen storage is costly, because the hydrogen molecule is small and leakage cannot be avoided.

The best option to store hydrogen at the production facility location (and at the distribution pump) is in metal hydrides. Metal hydride tanks may operate at pressures of 15 to 20 bar and store up to 25 to 30 kg H_2/m^3. In order to release hydrogen from the tank completely, some amount of heat is needed. It must be noted that metal hydrides do not appear as a feasible solution for transportation of hydrogen. For 1 kg of hydrogen, a metal hydride tank weighing about 160 kg is required.

For transportation, hydrogen must be either compressed to extremely high pressures (~300–800 bar) or cooled for liquefaction at cryogenic temperatures. Liquefaction adds at least 30% to the hydrogen price per kilogram, and in addition to this, one must add the cost of the energy consumed to keep the storage tank at cryogenic temperatures during the storage time. If the transportation takes 1 to 3 days, the minimum cost penalty for hydrogen storage on a transport vehicle is CN \$0.3/kg for compressed H_2 and CN \$0.7/kg for liquefied H_2.

If one assumes, for example, that the hydrogen transport is made in pressurized containers at 345 bar, the transported energy content is 8 GJ/m^3, that is, four times smaller than that for the transport of gasoline (32 GJ/m^3). If a pipeline is to be developed to distribute hydrogen at such high pressure, the tube's thickness must be more than 50% thicker than that of natural gas pipes.

At distribution points (fuel stations), hydrogen may be stored in metal hydrides also. Additional costs are associated with leakages during hydrogen delivery to consumers. The high explosion risk of hydrogen will raise the price even more because of the safety measures employed. Due to these factors, the estimated minimum cost of hydrogen distribution is more than \$1/kg H_2. Furthermore, one must realize that storage of hydrogen on vehicles (either as compressed gas or as cryogenic liquid) implies additional costs due to leakages, or continuous running of the cryogenic plant to maintain the hydrogen in liquid phase.

Thus, if one considers the production, storage, and distribution costs, the minimum expected hydrogen price at delivery point should be more than CN \$2.5/kg if produced from coal, and, respectively, ~CN \$11/kg if produced from electrolysis driven by solar energy. The U.S. Department of Energy goal for 2015 is to achieve the delivery for \$2 to \$3/kg H_2, untaxed and regardless of the production method. As a matter of fact, the North American selling price of hydrogen in 2002 varied from \$7.4 to \$11.3/kg.

Ammonia is easy to store and has a distribution network on roads, rail, ships, and pipeline already in place. The production of ammonia from fossil fuels has a common route with hydrogen production, because it involves gasification to produce syngas, gas cleaning, and CO_2 removal. In addition, the following steps are necessary for ammonia synthesis: compression of the reactants, catalytic conversion, and ammonia separation through condensation.

A highly energy-consuming component of the ammonia production process is represented by the make-up gas compression that is needed to facilitate the synthesis. This apparent drawback is compensated by a very efficient synthesis process that is possible at high pressure. Moreover, ammonia synthesis is an exothermic process, and modern technologies use work and heat recovery to reduce the production costs.

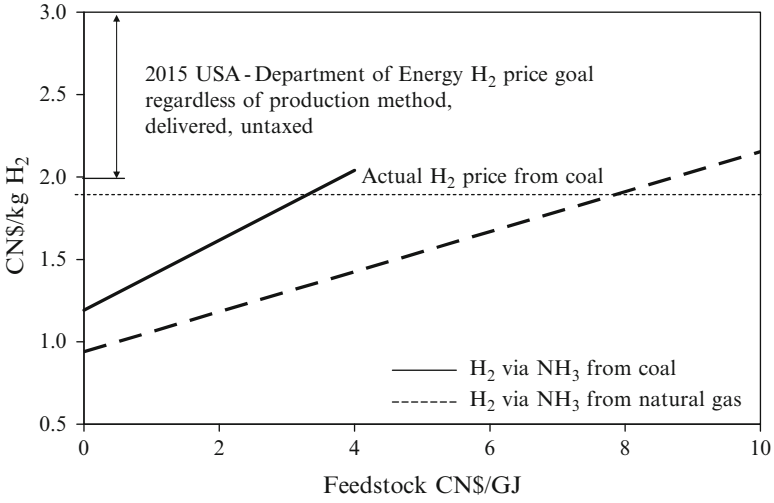

Fig. 7.8 Cost correlation for hydrogen obtained from ammonia at distribution points [modified from Zamfirescu and Dincer (2008b)]

The minimum cost for ammonia production per unit of energy is obtained with natural gas as the feedstock; the technical limit is 28 GJ natural gas for the production of 22.5 GJ of ammonia. The maximum energy cost is obtained with coal as the feedstock: ~65 GJ coal per 22.5 GJ of ammonia product. For other methods of production except those using solar energy, the cost falls in between the two extremes. The actual cost of North American coal is on average ~CN $1.5/GJ and that of natural gas is ~CN $10/GJ. These figures give an estimate of the ammonia price range at the production place, which is CN $5.25 to $20.0/GJ, or about CN $0.10 to $0.38/$NH_3$ kg.

The North African price is currently the lowest at $0.15/kg; other costs are $0.2/kg in Trinidad Tobago (based on $9/GJ natural gas feedstock), $0.25/kg in the Ukraine, and $0.3/kg in the United States. The cost of ammonia at Terra Industries in 2007 was $0.35/kg. The ammonia price in the U.S. in 2007 varied between $0.2 and $0.4/kg.

A correlation of the ammonia production price with the feedstock price in $/GJ from Zamfirescu and Dincer (2008b) is reproduced in Fig. 7.8. The cost of ammonia has been upgraded with the transportation costs. Since infrastructure development is not needed for ammonia distribution (e.g., a large pipeline network exists in the U.S. to transport ammonia at a cost of $0.1 hydrogen equivalent per 1,000 km), the ammonia transportation costs were combined with the costs of gasoline. Finally, the cost of ammonia, including that for transportation, has been multiplied by $17/3 = 5.67$ to obtain the cost per kilogram of hydrogen stored in ammonia, as shown in Fig. 7.8. Figure 7.8 shows that if ammonia is produced from coal (currently at about ~$1/GJ), hydrogen from ammonia is cost competitive with hydrogen transported in the pure state. Furthermore, if ammonia is produced from

natural gas, the hydrogen obtained from ammonia remains economically viable up to natural gas prices of $8/GJ. It should be kept in mind that as the feedstock cost increases, the hydrogen production costs also increase.

Since ammonia is produced from hydrogen, it is interesting to estimate and compare the amount of CO_2 emission at NH_3 and H_2 production, respectively. We assume natural gas as the feedstock here. Modern ammonia synthesis systems that use extensive heat recovery need ~30 GJ equivalent natural gas to produce 1 ton of NH_3. Through stoichiometry, one may deduce that ~1.32 kg of CO_2 is generated in order to produce 1 kg of NH_3; this is equivalent to ~8 kg of CO_2 generated for 1 kg of H_2 in the form of NH_3, which is similar to the amount of CO_2 released during H_2 production from natural gas. This figure demonstrates the technical, economical, and ecological value of NH_3 as a hydrogen source.

Moreover, ammonia can be synthesized at any location of the oil or natural gas extraction wells, and the resulting CO_2 re-injected back into the ground for sequestration. Ammonia can then be easily transported via pipelines, auto-cisterns, railway cars, and ships, and delivered to consumption points where it can be used as a hydrogen source, chemical, fertilizer, refrigerant, and so on.

7.6 Thermo-Catalytic NH_3 Decomposition and Hydrogen Separation

Ammonia can be cracked thermo-catalytically to obtain hydrogen according to the following endothermic reaction:

$$\frac{2}{3}\mathrm{NH_3} + 30.1\ \mathrm{kJ/mol} \cdot \mathrm{H_2} \rightarrow \mathrm{H_2} + \frac{1}{3}\mathrm{N_2}. \tag{7.10}$$

Here, the required enthalpy represents 10.6% of HHV or 12.5% of the lower heating value (LHV) of the produced hydrogen. The ammonia cracking reaction does not need catalysis to be performed at high temperatures (e.g., over 1,000 K); however, at lower temperatures, the reaction rate is too low for practical applications such as hydrogen generation for energy conversion. Nevertheless, at 400°C, the equilibrium conversion of NH_3 is very high at 99.1% (Yin et al. 2004) and at about 430°C, almost all ammonia is converted to hydrogen at equilibrium, under atmospheric pressure conditions (Hacker and Kordesch 2003).

There is a large panoply of catalysts applicable to ammonia decomposition (e.g., Fe, Ni, Pt, Ir, Pd, and Rh), but ruthenium (Ru) appears to be the best one when supported on carbon nanotubes, generating hydrogen at more than 60 kW equivalent power per kilogram of catalyst (Yin et al. 2004). Over ruthenium catalysts, at temperatures lower than ~300°C, recombination of nitrogen atoms is rate limiting, while at temperatures higher than 550°C, the cleavage of ammonia's N–H bond is rate limiting. However, the activation energy is higher at lower temperatures (180 kJ/mol) and lower at higher temperatures (21 kJ/mol). The best temperature

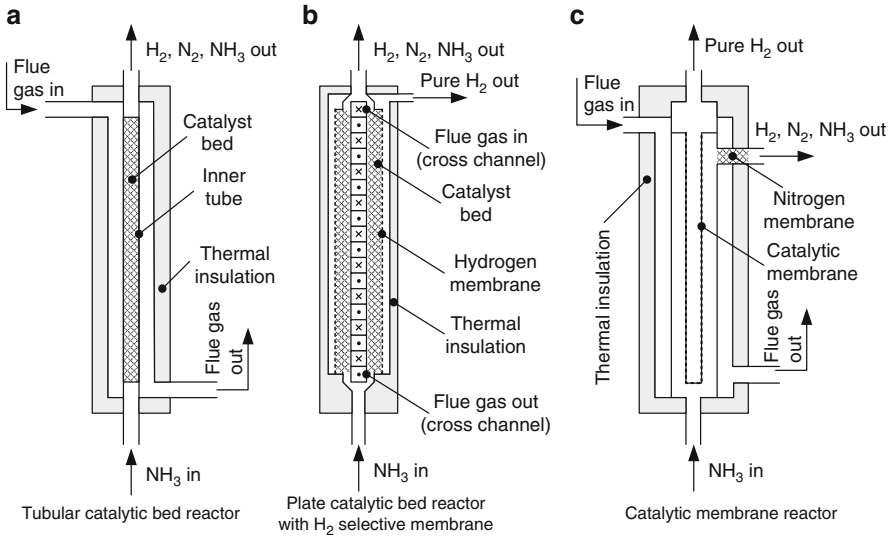

Fig. 7.9 Possible options for thermo-catalytic ammonia decomposition reactors

range for ammonia decomposition over ruthenium catalysts may be 350°C to 525°C, which suggests that flue gases from hydrogen ICEs, other hot exhausts from combustion processes, or electrochemical power conversion in high-temperature fuel cells can be used to drive ammonia decomposition.

Figure 7.9 presents three possible reactor configurations for ammonia decomposition. The direct products of decomposition consist of hydrogen and nitrogen and traces of unreacted ammonia. For pure hydrogen generation, membrane technology can be applied either in the same reactor or separately. The reactor shown in Fig. 7.9a is the simplest one and does not separate the products in the output stream. It consists of a simple tube (which can be coiled) filled with the catalytic bed and heated from the outside with flue gases. The reaction occurs at the surface and cannot go beyond the chemical equilibrium conversion at the temperature of operation. Some old trials reported by Grimes (1966) to produce this kind of reactor were based on iron catalysis and achieved, for operation at 900°C, a production of 1.3 kW power equivalent of hydrogen (with respect to HHV) for 1 l of reactor plus auxiliary heat exchangers. More recent work by Hacker and Kordesch (2003) describes a tubular reactor based on a Ni–Ru catalyst, which produced a hydrogen equivalent (HHV) with 60 kW at 600°C and 240 kW at 800°C/l of reactor.

Figure 7.9b represents the construction of a plate-type catalytic reactor with integrated hydrogen-selective membrane. The reactor is heated with flue gases circulated in cross-flow with the reactants–products streams. Ammonia is fed at the bottom and passes over the catalytic bed where the disassociation reaction occurs. The catalytic bed is surrounded by a hydrogen-selective membrane that allows only pure hydrogen to pass through. Palladium-based membranes are the most efficient known for hydrogen separation. The reactor produces a pure stream

of hydrogen and a stream of residuals, containing mainly nitrogen and traces of hydrogen and ammonia. Reactors of this kind were described by several researchers and tested with the present data in the laboratory. Garcia-Garcia et al. (2008) used Ru-based catalysis and a Pd membrane, and obtained ~20% conversion enhancement with respect to conventional (tubular) catalytic reactor; the conversion obtained at 350°C was 95%. Ganley et al. (2004) showed that hydrogen production up to 170 kW H_2 HHV equivalent is possible with 1 l of reactor.

The third decomposition reactor, shown in Fig. 7.9c, comprises a catalytic membrane and has been proposed by Skodras et al. (2006). The catalysts used were based on Ni on an alumina support. In this approach, the hydrogen-selective membrane is doped with ammonia cracking catalysts to form a catalytic membrane. The testing conditions were 500°C to 800°C, 2 to 10 bar, and 0.5 to 1 second of residence time, which are consistent with the situations specific to vehicle propulsion. At 550°C, the conversion was 85% at 2 bar pressure and 30% at 10 bar. In Fig. 7.9c, it is suggested that better product separation could be achieved if a nitrogen-selective membrane is placed at the outlet port of unreacted gases. Separating the nitrogen and hydrogen products simultaneously represents a way to shift the reaction equilibrium toward the right. By extracting nitrogen from the reactor, the recombinative nitrogen effect can be avoided and higher reaction rates could be achieved.

7.7 Simultaneous Ammonia Use as Fuel and Working Fluid

Once ammonia is decomposed (partially or totally) to produce hydrogen, the resulting gas—either pure hydrogen or a mixture of ammonia, nitrogen, and hydrogen—is used for power generation in fuel cells or ICEs. Alkaline fuel cells are tolerable to ammonia (Hacker and Kordesch 2003); therefore, there is no need to produce pure hydrogen from ammonia. A plug-flow catalytic bed reactor similar to alkaline fuel cells illustrated in Fig. 7.9a can be used. PEM fuel cells do not tolerate ammonia; in this case, membrane separation reactors such as those shown in Fig. 7.9b,c can be used. In addition, because the temperature in PEM fuel cell systems is not sufficient, some of the produced ammonia and the uncombusted fuel are burned to provide the necessary heat for ammonia decomposition. One such system is proposed by Sørensen et al. (2005) and comprises an ammonia fuel tank, a PEM fuel cell, an ammonia decomposition unit heated by a catalytic burner, and an ammonia absorber.

A possible power generation technique is presented in Fig. 7.10. The ammonia tank is thermally insulated in order to recover the cooling effect that manifests when liquid is drawn out, together with its associated enthalpy. This cooling may be used by the system (e.g., to cool gaseous streams prior to compression) or may serve some specific need (e.g., air cooling). Ammonia drawn out of the tank is pumped at high pressure and then expanded in two stages with intermediate reheating. The heat of exhaust gases is recovered by this method; if this is not possible (e.g., as in the case of a PEM fuel cell system that operates at low temperature), then a small part of the generated hydrogen must be combusted to deliver the heat necessary for ammonia

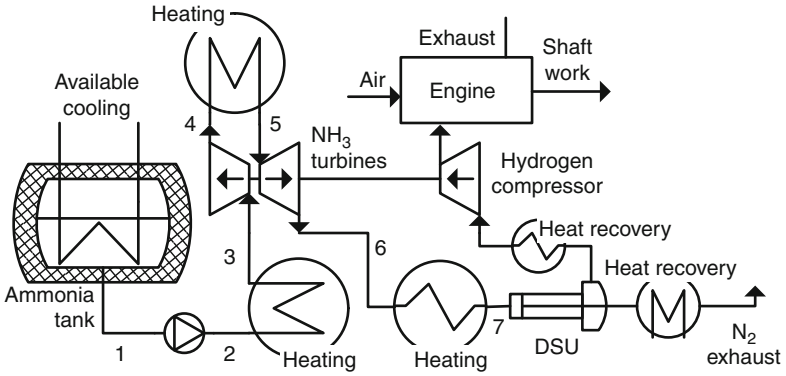

Fig. 7.10 Power generation system using hydrogen from ammonia [modified from Zamfirescu and Dincer (2009b)]

decomposition. After heating to elevated temperatures, ammonia is decomposed in the decomposition and separation unit (DSU) shown on the figure. Pure hydrogen is generated and compressed using the work recovered from the turbines. Prior to compression, the hydrogen stream is cooled with heat recovery. The resultant nitrogen stream is cooled with heat recovery and exhausted into the atmosphere.

Regarding power generation with ammonia as the hydrogen source, we are interested here in determining a practical upper bound for it. In order to do this, consider the energy conversion model introduced above in association with Fig. 7.10. We assume that the engine is either an ICE or a fuel cell operating at intermediate temperature such that the necessary quantity of thermal energy and the temperature level are satisfactory for at least 99% ammonia decomposition and generation of pure hydrogen. The aim is to maximize the power generation efficiency by generating some additional power from ammonia used as a working fluid prior to its decomposition.

The temperature per second (T-s) diagram of ammonia representing the heating process prior to decomposition is presented in Fig. 7.11. Heating of the ammonia fuel is done in three steps with two interlaced expansion processes, namely, 3–4 and 5–6. The work generated by these expansions is sufficient to drive the pump and the compressor for hydrogen. A simple calculation has been performed for the process 1–2–3–4–5–6–7 using the FluidProp software developed by Colonna and Van der Stelt (2004).

In this process, state 6 in a vacuum at 0.5 bar is chosen in order to facilitate the decomposition and separation process. Pure hydrogen produced by the DSU (Fig. 7.10) is then compressed up to 8 bar, a pressure sufficient for direct injection into the engine cylinder (if the engine is a fuel cell, the hydrogen pressure may be set at 2–3 bar). Prior to compression, the hydrogen stream is cooled with heat recovery down to 25°C for reducing the compression work. Nitrogen and the remaining unreacted gases are compressed separately after cooling with heat recovery down to 25°C; the chosen compression pressure is 1.2 bar, which is sufficient for expelling

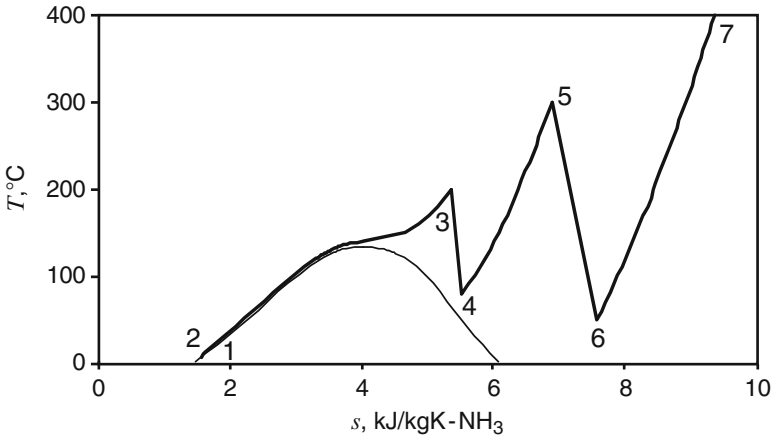

Fig. 7.11 Heating process and work recovery from the ammonia fuel stream (the state points are correlated with the system diagram in Fig. 7.10) [data from Zamfirescu and Dincer (2009b)]

the gas stream into the atmosphere after a second cooling to 25°C. Exhaust gas heat drives the process including ammonia heating and provides thermal energy for decomposition. We assumed that the decomposition unit efficiency is 80%, defined in terms of ideal decomposition heat over the actual one.

The cooling effect obtained from the ammonia tank represents, with the assumptions made, 6% from ammonia's HHV or 1% from that of hydrogen. The shaft work produced by the expander, which upgrades the engine power, was found to be 2% from the hydrogen's HHV, while the heat recovered from the exhaust gases was also 2% from the HHV. Note that this heat is mainly used for decomposition; for heating the ammonia stream prior to decomposition, most of the heat is retrieved from cooling the produced hydrogen and nitrogen streams prior to and after compression.

Figure 7.12 compares the energy balance of a hydrogen-fueled engine with that of the same engine modified according to the diagram in Fig. 7.10 and that is to be fueled with hydrogen generated by ammonia decomposition and separation. Because of internal heat recovery and heat-to-work conversion, the "hydrogen-from-ammonia" engine is 2% more efficient. This fact is felt to be of great importance in the fuel economy and greenhouse gases (GHG) mitigation.

7.8 Simultaneous Use of Ammonia as Fuel and Refrigerant

The cooling effect of ammonia is equivalent to the heat needed to raise its temperature and, if it applies, the heat needed to decompose it (partially or totally) prior to using it as fuel. Expressed in terms of enthalpy, this heat is

$$\Delta h_{c,NH_3}(T) = h(T) - h'(T_0) + x_d \eta_d \Delta h_d(T), \tag{7.11}$$

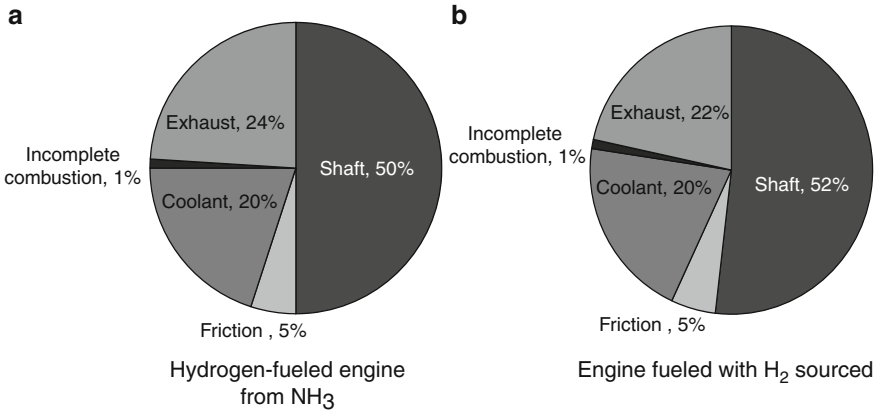

Fig. 7.12 Energy balance on two types of hydrogen-fueled engines [data from Zamfirescu and Dincer (2009b)]

where T represents the temperature at which NH_3 is used as fuel (either in an ICE or a fuel cell); x_d represents the fraction in which the ammonia stream is dissociated into H_2 and N_2 (if this applies); η_d is the efficiency of the decomposition unit, which is assumed here to be 0.9; and Δh_d represents the dissociation heat at T. In order to quantify the cooling effect of ammonia in relative terms, we use cooling effectiveness, defined through the dissociation heat given by Eq. (7.11) and the LHV of ammonia as

$$\varepsilon_{c,NH_3}(T) = \Delta h_{c,NH_3}(T)/\text{LHV}. \tag{7.12}$$

The results of applying Eq. (7.12) for a range of ammonia reforming temperatures and various decomposition fractions are presented in Fig. 7.13. The thermodynamic data for plotting Fig. 7.13 are calculated using the FluidProp software developed by Colonna and Van der Stelt (2004). The case $x_d = 0\%$ represents the hypothetical situation when ammonia is only preheated prior to oxidation, and one assumes that no decomposition occurs. This case is illustrated for reference, because in reality, at temperatures over 300°C, some ammonia decomposes spontaneously, even without the presence of catalysts. The case for which $x_d = 5\%$ is applicable in ICEs, where, as discussed above, a small fraction of ammonia is usually decomposed to produce hydrogen that boosts the combustion process. The extreme situation when $x_d = 100\%$ is applicable to some fuel cell systems that are supplied with hydrogen produced from ammonia.

The results show that the maximum achievable engine cooling with ammonia represents slightly over 20% from the LHV. Thus, in ammonia-fueled ICEs, the usual water cooling system may be downsized by up to 20%. Optionally, a part of this cooling may satisfy some air-conditioning needs of the vehicle. A second observation is that the ε_r profile for complete decomposition is flat (i.e., it is not influenced by the temperature). If the decomposition is incomplete, the temperature

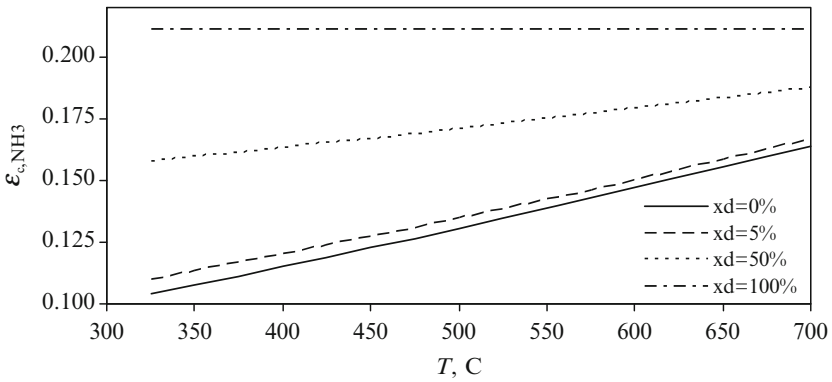

Fig. 7.13 The cooling effect of ammonia when it is consumed as fuel as a function of the decomposition temperature and for several decomposition fractions [modified from Zamfirescu and Dincer (2009a)]

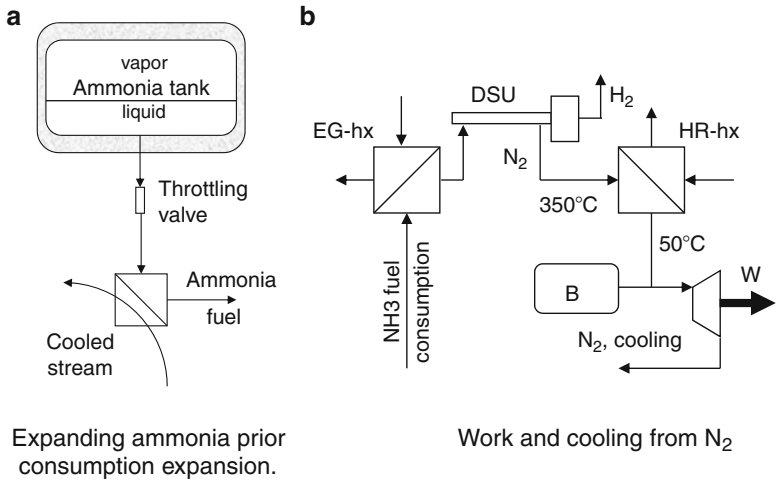

Fig. 7.14 Ways of exploiting the cooling effect of NH_3 onboard (*DSU* decomposition and separation unit, *HX* heat exchangers, *HR-hx* heat-recovery heat exchanger, *B* buffer, *W* work recovery)

profile is linear with a positive slope. This fact is explained by variations in the decomposition heat, which decreases with the decrease in temperature.

Two complementary arrangements to exploit the refrigeration effect of ammonia while it is supplied as fuel to the power plant are suggested in Fig. 7.14. With reference to Fig. 7.14a, one assumes that the saturated liquid is extracted from the thermally insulated fuel tank. The liquid stream can be throttled such that the fuel evaporation is conducted at the desired temperature (e.g., 5–10°C will suffice either for engine cooling or for obtaining some air-conditioning). After throttling, the fluid

passes through a heat-recovery heat exchanger (HR-hx) where the engine coolant is cooled with ammonia. If air-conditioning is desired, the heat recovery will have two steps: first the air and subsequently the engine's coolant are cooled with ammonia.

To give an example, let us assume that the temperature in the fuel tank is 25°C, the evaporation temperature is 5°C, and the ammonia temperature at the evaporator is 15°C (superheated vapor). With these figures, the cooling effect is quantified as 6.3% from the LHV of ammonia. This means that for a medium-sized car equipped with a 70-kW engine, while the engine runs on ammonia fuel at full load, the obtained refrigeration effect to be used in the form of air-conditioning amounts to ~4.4 kW. In addition, up to 15% of LHV, meaning 10.3 kW, is available for the purpose of engine cooling. Alternatively, ~15 kW can be made available for engine cooling only.

Note that the engine effectiveness can be further improved if the refrigeration effect of ammonia is used while it is consumed as fuel. The improvement can be quantified based on the typical coefficient of performance (COP) of the vehicular cooling systems. The gain in work at the engine shaft due to the available cooling from ammonia (i.e., which comes from fan, pump, and compressor power savings) is

$$w_{\mathrm{NH_3}} = \frac{\Delta h_{\mathrm{c,NH_3}}}{\mathrm{COP}}, \tag{7.13}$$

and induces an engine performance improvement that can be quantified by the effectiveness:

$$\varepsilon_{\mathrm{r,NH_3}} = \frac{w_{\mathrm{NH_3}}}{\mathrm{LHV}} = \frac{\varepsilon_{\mathrm{c,NH_3}}}{\mathrm{COP}}. \tag{7.14}$$

For an assumed (typical) COP of 2 (COP of the engine cooling system and the air-conditioning system at the average), the maximum gain in efficiency is about 10%.

Some additional work and cooling can be recovered if ammonia is fully decomposed according to the arrangement illustrated in Fig. 7.14b. Preheated ammonia fuel is directed toward the DSU that produces the hydrogen and nitrogen as two separate streams. While the hydrogen is directed toward the consumption point (ICE or fuel cell), the hot stream of nitrogen is cooled in the HR-hx at a temperature close to ambient, say 50°C, and it can in principle be buffered at high pressure in a small tank (B). When needed, the nitrogen is expanded in a turbine for work recovery. The resultant cold stream of nitrogen can be used for some low-temperature cooling needs before being exhausted to the atmosphere.

Calculation of the additional cooling and the corresponding work recovery can be made by assuming an isentropic efficiency of the turbine, η_{S}, and computing the actual expansion enthalpy, $h_{\mathrm{a,N_2}}$, as a function of the N_2 inlet enthalpy, h_{i}:

$$h_{\mathrm{a,N_2}} = h_{\mathrm{s,N_2}} + \eta_{\mathrm{s}}\left(h_{\mathrm{s,N_2}} - h_{\mathrm{i}}\right), \tag{7.15}$$

where h_i is evaluated at the decomposition temperature and pressure (upstream turbine), and the isentropic discharge temperature, h_{s,N_2}, is calculated with the upstream entropy and discharge pressure.

It is useful to report the recovered work in terms of energy per kilogram of consumed ammonia fuel as follows (this can be done by taking into account that the number $\lambda = 0.5\,\mathrm{kmol_{N_2}/kmol_{NH_3}}$ resulting from the NH_3 decomposition equation $NH_3 \rightarrow 1.5\,H_2 + \lambda N_2$):

$$\Delta h_{w,N_2} = \lambda \frac{\mu_{N_2}}{\mu_{NH_3}} \left(h_{a,N_2} - h_i\right). \tag{7.16}$$

The additional low-temperature cooling effect of N_2 can be quantified by considering reheating of the nitrogen stream from its low temperature T_{a,N_2} to a temperature close to ambient, T_0, featuring the flow enthalpy h_{0,N_2}:

$$\Delta h_{c,N_2} = \lambda \frac{\mu_{N_2}}{\mu_{NH_3}} \left(h_{0,N_2} - h_{a,N_2}\right). \tag{7.17}$$

Apart from ε_{c,NH_3}, one may define two additional kinds of system effectiveness, that is, one with respect to recovered work from nitrogen expansion as

$$\varepsilon_{w,N_2} = \frac{\Delta h_{w,N_2}}{\mathrm{LHV}}, \tag{7.18}$$

and one accounting for the low-temperature cooling effect of nitrogen:

$$\varepsilon_{c,N_2} = \frac{\Delta h_{c,N_2}}{\mathrm{LHV}}. \tag{7.19}$$

Therefore, the engine performance improvement due to nitrogen expansion can be quantified by

$$\varepsilon_{r,N_2} = \varepsilon_{w,N_2} + \frac{\varepsilon_{c,N_2}}{\mathrm{COP}}. \tag{7.20}$$

For example, for the arrangement illustrated in Fig. 7.14b, if one assumes a turbine efficiency of 80%, $\varepsilon_{r,N_2} = 1.1\%$ or a total of 11.1% recovered power is obtained due to combined ammonia and nitrogen expansion. For a 70-kW engine, this is equivalent to 7.8 kW of saved power.

It is to be noted that the simplicity of this cooling system (which consists only of one or two heat exchangers and one throttling valve) lowers both the initial operation and maintenance costs by eliminating or downsizing the conventional mechanical cooling system (which comprises a compressor, condenser, water pump, fan, and radiator).

7.9 Performance Analysis of Ammonia-Fueled Systems

Let us investigate the impact of using ammonia as a fuel on the performance of a vehicle. Recall that, according to what has been mentioned above, there are two main approaches for using ammonia as a fuel: ICEs and fuel cells.

In an adopted power system (either an ICE or a fuel cell), for the estimation of engine performance, the cooling effect should be taken into account. In order to derive a system effectiveness that includes the cooling effect, let us consider η as the system efficiency. The system effectiveness including refrigeration and work recovery effects is

$$\varepsilon_r = \eta + \varepsilon_{r,NH_3} + \varepsilon_{r,N_2}. \tag{7.21}$$

It is obvious that the power system efficiency depends on the system, but a range of η can be estimated based on the common literature. For hydrogen fuel cells, the typical efficiency is 40% to 65%; for hydrogen ICE, efficiency of 40% to 55% was obtained; for direct ammonia fuel cell systems, the typical efficiency ranges from 30% to 45%; and for ICEs, efficiencies range from 25% to 55%. The overall range for η is from 30% to 65% (maximum values correspond to hydrogen systems, where hydrogen is supplied by onboard decomposition of ammonia). Thus, the expected range for ammonia vehicle effectiveness ε_r is 0.35 to 0.75.

It is interesting to investigate the driving range as a function of system effectiveness. In this respect, we assume a system effectiveness and a performance indicator of the power train given in terms of shaft torque energy for each kilometer of driving range. We consider here a reasonable range for this indicator from 0.5 to 1.5 MJ/km and take three illustrative values for ε_r. The results shown in Fig. 7.15

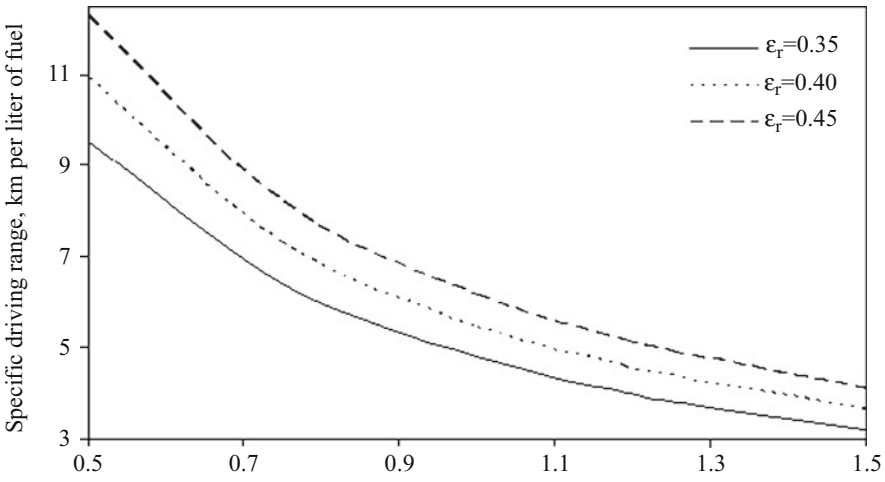

Fig. 7.15 Driving range with 1 l of fuel as a function of the shaft torque energy for 1 km driving range [modified from Zamfirescu and Dincer (2009a)]

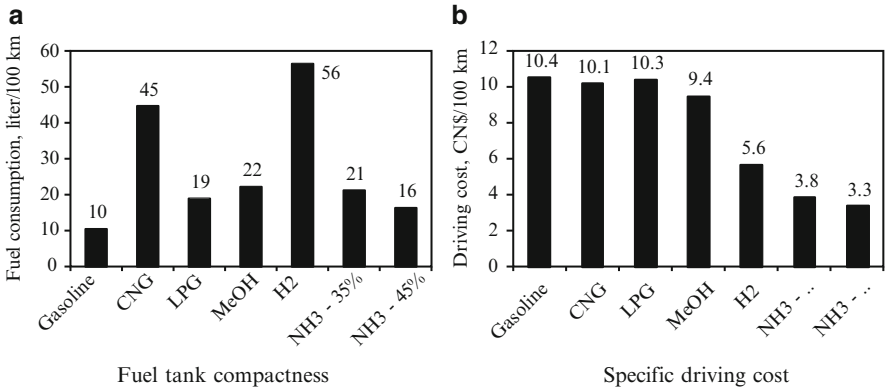

Fig. 7.16 Comparative performance analysis of several power systems for vehicles [modified from Zamfirescu and Dincer (2009a)]

indicate, for instance, that with 1.0 MJ/km, the driving range may reach 7 km/l, that is, over 500 km with a 75-l NH_3 fuel tank.

Figure 7.16 compares some performance indicators for ammonia, hydrogen, and more conventional vehicles. To calculate the data shown in Fig. 7.16, it is assumed that gasoline, compressed natural gas (CNG), and liquefied petroleum gas (LPG) vehicles run with 28% efficiency. For methanol, we assumed a fuel cell system with 40% efficiency. For hydrogen, a PEM fuel cell system with hydrogen stored in metal hydride tanks has been considered, with an efficiency of 50%. For an ammonia vehicle, a liquid storage tank is assumed and the power system is not specified; thus we only considered two efficiencies (35% and 45%) that are specific for both ammonia fuel cell systems and ICEs. All efficiencies considered herein are within the current technological capabilities. Also, the parameter τ is assumed to be 1 MJ/km. The fuel costs are as listed in Table 7.1.

The results show that the driving range of gasoline vehicles is the longest, but the associated cost is the highest among all options considered here. Therefore, the gasoline tank is the most compact. The hydrogen tank is the least compact; however, the driving cost of a hydrogen vehicle is half of that of all common fuels. Regarding ammonia, the fuel tank is reasonably compact (about two times larger than the gasoline tank), and the specific driving cost is the lowest. If the considered specific cost of ammonia is 25% higher, that is, CN $0.4/kg, still the driving cost of an ammonia vehicle at 35% is lower than that of a hydrogen vehicle at 50%.

Several automakers have developed the prototypes of hydrogen-fueled vehicles in recent years. Here, for analysis purposes, we select a Ford Focus H_2ICE prototype. In Table 7.2, we list the performance parameters of the actual prototype and some calculation results for the same prototype converted to use NH_3 fuel. For the calculation, it has been assumed that the cost of ammonia is $0.30/kg. The efficiency of the ammonia engine is assumed to be the same as that of the

Table 7.1 Comparison of ammonia with other fuels including hydrogen

Fuel/storage	P [bar]	ρ, Density [kg/m^3]	HHV [MJ/kg]	HHV$'''$ [GJ/m^3]	e''' [GJ/m^3]	c [CN $/kg]	C''' [CN $/m^3]	c/HHV [CN $/GJ]
Gasoline, C_8H_{18}/liquid	1	736	46.7	34.4	34.4	1.36	1,000	29.1
CNG, CH_4/integrated storage	250	188	42.5	10.4	7.8	1.20	226	28.2
LPG, C_3H_8/pressurized tank	14	388	48.9	19.0	11.7	1.41	548	28.8
Methanol, CH_3OH/liquid	1	786	14.3	11.2	9.6	0.54	421	37.5
Hydrogen, H_2/metal hydrides	14	25	142	3.6	3.0	4.00	100	28.2
Ammonia, NH_3/pressurized tank	10	603	22.5	13.6	11.9	0.30	181	13.3
Ammonia, NH_3/metal amines	1	610	17.1	10.4	8.5	0.30	183	17.5

Data from Zamfirescu and Dincer (2009a)

Table 7.2 Conversion of a Ford Focus H_2ICE to NH_3 fuel

Parameter	Unit	H_2	NH_3
Storage tank volume	Liter	217	76
Storage pressure	Bar	345	10
Energy onboard	MJ	710	1,025
Cost of full tank	CN $	25	14
Driving range	Km	298	430
Driving cost	CN$/100 km	8.4	3.2
Tank compactness	Liter/100 km	73	18

Data from Zamfirescu and Dincer (2009a)

hydrogen engine. In fact, ammonia can be decomposed onboard at no additional cost (using only the heat rejected by the ICE) and the engine fueled with pure hydrogen. As can be observed, the driving range of the NH_3 vehicle is much longer and hence more economical with a driving cost of $3.2/100 km compared to $8.4/100 km for the H_2ICE. Moreover, the tank compactness of the ammonia car is about four times better.

It is of interest to know the energy at the shaft with respect to the energy stored in the fuel tank. This is presented in Fig. 7.17, which shows the energy at the shaft per unit of fuel volume and fuel mass stored in the fuel tank. Note that because of the assumed higher efficiency at power conversion when hydrogen is generated from ammonia, the energy at the shaft per volume is the highest.

In Fig. 7.17, the situation when ammonia is used directly as a fuel (possibly with partial (3% per volume) decomposition) is also included. Fueling an ICE is a proved

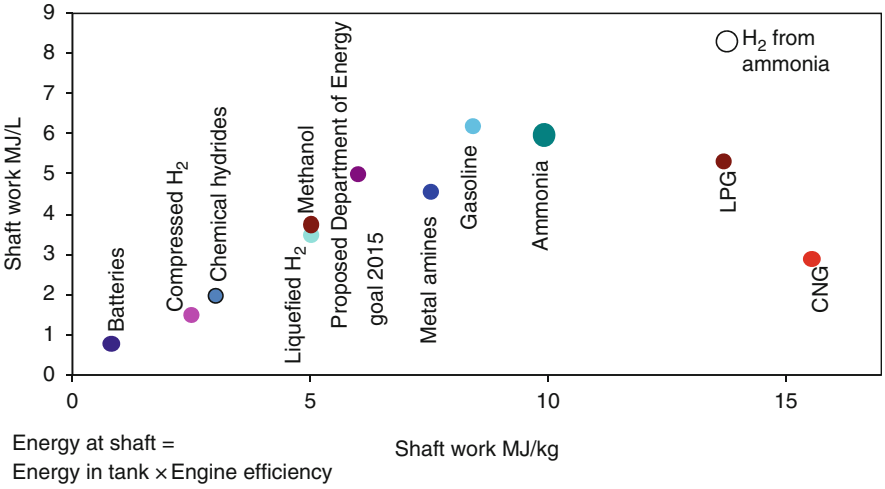

Fig. 7.17 Energy at the shaft with respect to the energy stored in the fuel tank [modified from Zamfirescu and Dincer (2009b)]

practice because an ammonia–hydrogen mixture has comparable combustion characteristics with gasoline (see Zamfirescu and Dincer 2008a,b,c). The energy developed at the shaft per unit of fuel volume is about the same for ammonia and gasoline engines, while the shaft energy developed per unit of fuel mass is in favor of ammonia. If hydrogen is produced from ammonia and work recovery is applied for improving the efficiency (as discussed above), high power conversion is achieved and this provides very promising values: ~8 MJ/l and ~14 MJ/kg shaft power.

Results regarding the life-cycle efficiency of vehicles driven with various fuels and with ammonia, and the corresponding CO_2 mitigation and cost are summarized in Fig. 7.18, which is taken from the study by Zamfirescu and Dincer (2009b). Six cases are compared in the figure:

- Reference vehicle fueled with gasoline
- Vehicle driven with hydrogen produced through sustainable methods
- Hydrogen derived from fossil fuels
- Ammonia produced by artificial biological methods (using enzymes)
- Ammonia produced from sustainable energy sources
- Ammonia produced from fossil fuels

The life-cycle efficiency includes all phases starting with primary materials and energy sources, including ammonia synthesis, storage, distribution, and power generation at remote (stationary or mobile) locations. For the reference gasoline case, the mitigation of GHG is negative, meaning that there is no mitigation in this case. When ammonia is derived from biological synthesis, the GHG mitigation is the maximum. Regarding the economics, the cheapest cost per unit of energy derived at the shaft corresponds to ammonia derived from fossil fuels.

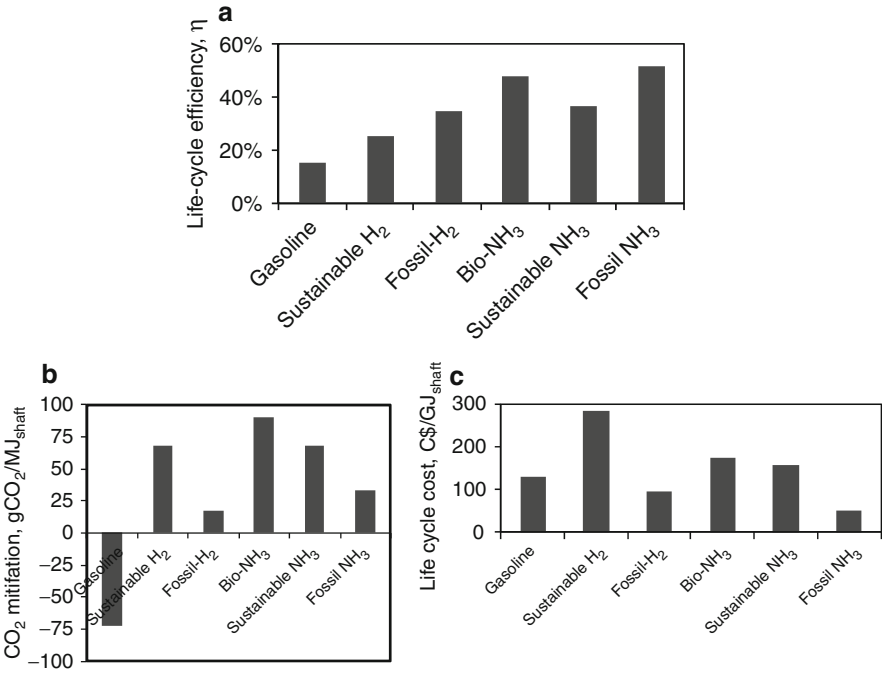

Fig. 7.18 Summary of life-cycle assessment results: (**a**), CO_2 mitigation (**b**), and unitary cost (**c**) [modified from Zamfirescu and Dincer (2009b)]

7.10 Concluding Remarks

In this chapter, it was shown that ammonia is a potential substance for sustainable energy systems because it uniquely offers the opportunity to store hydrogen at high density; it produces power when used as fuel, hydrogen source, and working fluid, and is simultaneously used as a refrigerant and an NO_x-reducing agent. Some specific conclusions from this chapter are as follows:

- Thermo-catalytic membrane reactors are the most promising devices for H_2 generation from NH_3.
- If ammonia is used simultaneously as a working fluid and a fuel, the efficiency increases by $>2\%$.
- NH_3 can be stored seasonally as opposed to H_2, which must be consumed within a few days after production.
- Ammonia delivered and converted into shaft energy is cheaper than hydrogen, although in the production phase ammonia could be up to ~25% more expensive than hydrogen from which it is synthesized.
- The energy generated at the shaft is 25% higher in hydrogen-from-ammonia cases; with respect to gasoline, per unit of fuel volume, and per unit of mass, it is 30% higher.

- Some additional advantages of ammonia are commercial availability and viability, global distribution network, and easy handling experience, while its toxicity may be seen as a challenge. This can easily be overcome with the current control and storage technologies.

Nomenclature

c	Specific cost, currency per mass
ex	Specific exergy, kJ/kg
g	Gravitational acceleration, m/s^2
h	Specific enthalpy, kJ/kg
H	Formation enthalpy, J/mol
LHV	Lower heating value, MJ/kg
P	Pressure, Pa
s	Specific entropy, KJ/kg K
T	Temperature, K
w	Mass specific work, J/kg
x_{d}	Dissociation fraction
z	Elevation, m

Greek Letters

ε	Effectiveness
η	Efficiency
μ	Molar mass, kg/kmol
ρ	Density, kg/m^3

Subscripts

0	Reference state
c	Cooling effect
d	Dissociation
i	Inlet
r	Refrigeration
S	Isentropic
w	Expansion

Superscript

$( )'''$ Per unit of volume

References

Appl M. 1999. *Ammonia — principles and industrial practice*. Wiley-VCH, New York.

Bartles J.R. 2008. A feasibility study of implementing an ammonia economy. MSc Thesis, Iowa State University, Ames, Iowa.

Christensen C.H., Sørensen R.Z., Johannessen T., Quaade U.J., Honkala K., Elmøe T.D., Køhlera R., Nørskov J.K. 2005. Metal ammine complexes for hydrogen storage. *Journal of Materials Chemistry* 15:4106–4108.

Colonna P., Van der Stelt T.P. 2004. FluidProp: A Program for the Estimation of Thermophysical Properties of Fluids. Energy Technology Section, Delft University of Technology, The Netherlands.

Ganley J.C., Seebauer E.G., Masel R.I. 2004. Development of a microreactor for production of hydrogen from ammonia. *Journal of Power Sources* 137:53–61.

Garcia-Garcia F.R., Ma Y.H., Rodrigues-Ramos I., Guerrero-Ruiz A. 2008. High purity hydrogen production by low temperature catalytic ammonia decomposition in a multifunctional membrane reactor. *Catalysis Communications* 9:482–486.

Grimes P.G. 1966. Energy deport fuel and utilization. *Transaction of the Society of Automotive Engineers*, paper #650051.

Hacker V., Kordesch K. 2003. Ammonia crackers. In: Handbook of Fuel Cells—Fundamentals, Technology and Applications. John Wiley and Sons, Chichester, England.

Heldebrant D.J., Karkamkar A., Linehan J.C., Autrey T. 2008. Synthesis of ammonia borane for hydrogen storage applications. *Energy and Environmental Science* 1:156–160.

Hinnemann B., Nørskov J.K. 2006. Catalysis by enzymes: the biological ammonia synthesis. *Topics in Catalysis* 37:55–70.

Kästner J., Blöchl P.E. 2007. Ammonia production at the FeMo cofactor of nitrogenise: results from density functional theory. *Journal of the American Chemical Society* 129:2998–3006.

Mousdale D.M. 2008. Biofuels—Biotechnology, Chemistry, and Sustainable Development. CRC Press, Boca Raton, FL.

NIST 2010. NIST Chemistry WebBook. NIST Standard Reference Database Number 69. Linstrom P.J., Mallard W.G. eds., NIST, Washington, DC.

Rafiqul I., Weber C., Lehmann B., Voss A. 2005. Energy efficiency improvements in ammonia production perspectives and uncertainties. *Energy* 30:2487–2504.

Skodras G., Kaldis S., Topis S., Koutsonikolas D., Grammelis P., Sakellaropoulos G. 2006. NH3 decomposition and simultaneous H_2 separation with a commercial Pd-Cu-Ag/V membrane. Proceedings of the Second International Green Energy Conference. June 25–29, Oshawa, ON, Paper #IGEC2-141.

Sørensen R.Z., Nielsen L.J.E., Jensen S., Hansen O., Johannessen T., Quaade U., Christensen C.H. 2005. Catalytic ammonia decomposition: miniaturized production of COx-free hydrogen for fuel cells. *Catalysis Communications* 6:229–232.

Walter M., Lesicki R. 1998. Measures taken to ensure safe operation of an ammonia storage tank. *Process Safety Progress* 17:288–296.

Yin S.F., Xu B.Q., Zhou X.P., Au C.T. 2004. A mini-review on ammonia decomposition catalysts for on-site generation of hydrogen for fuel cell applications. *Applied Catalysis: A, General* 277:1–9.

Zamfirescu C., Dincer I. 2008a. Using ammonia as a sustainable fuel, *Journal of Power Sources* 185:459–465.

Zamfirescu C., Dincer I. 2008b. Environmentally-benign hydrogen production from ammonia for vehicles. Proceedings of Global Conference on Global Warming. July 6–10, Istanbul, paper #626.

Zamfirescu C., Dincer I. 2008c. Ammonia as a green fuel for transportation. Proceedings of ASME, Energy Sustainability Conference. August 10–14, Jacksonville, FL, paper #54329.
Zamfirescu C., Dincer I. 2009a. Ammonia as a green fuel and hydrogen source for vehicular applications. *Fuel Processing Technology* 90:729–737.
Zamfirescu C., Dincer I. 2009b. Environmental impact and cost analyses of ammonia as a hydrogen source. Proceeding of Global Conference on Global Warming. July 5–9, Istanbul, paper #535.

Study Questions/Problems

7.1 How much hydrogen is embedded in 1 mol of ammonia, 1 m^3 of ammonia, and 1 kg of ammonia?
7.2 Determine the quantity of hydrogen present in a 1-m^3 ammonia tank containing 20% per volume of ammonia vapor, and ammonia liquid. Consider that the tank is kept at (a) standard temperature, (b) negative 40°C, and (c) positive 45°C.
7.3 Consider the system presented in Fig. 7.1 for ammonia synthesis. Using energy and mass balance equations and appropriate assumption, determine the ammonia production efficiency according to the first and second law of thermodynamics.
7.4 According to Fig. 7.2, determine the amount of energy needed to synthesize one molecule of ammonia using nitrogenase enzyme.
7.5 Consider the ammonia storage system presented in Fig. 7.3. Make reasonable assumptions and determine the efficiency and the cost of storage for a period of 6 months.
7.6 Calculate the reaction heat associated with NO_x decomposition on zeolites using ammonia, according to Eq. (7.3), for two cases: (a) cold start at ambient temperature, and (b) steady operation at 300°C.
7.7 Demonstrate through calculation of the cost the advantage of the "hydrogen from ammonia route" compared with the "hydrogen-only route." Use the diagram in Fig. 7.8 for the calculations.
7.8 Determine the reaction heat of an ammonia decomposition reaction for a reasonable range of temperatures and pressures.
7.9 By minimizing Gibbs energy, determine the equilibrium concentration of the ammonia decomposition reaction for pressures of 0.1 bar, 1 bar, 10 bar, and 100 bar and temperatures in the range of −40°C to 1,000°C.
7.10 Make reasonable assumptions and determine the efficiency of the power-generation system presented in Fig. 7.10.
7.11 Consider the system in Fig. 7.14a and determine the refrigeration effect associated with a 100-kW engine.
7.12 Redo through your own calculation the plot in Fig. 7.17.
7.13 Based on a literature study, determine the energy density per mass and volume of ammonia borane and compare it with that of an ammonia-only system.
7.14 Calculate the life-cycle carbon dioxide emissions when ammonia is produced from coal and then used as fuel for motor engines.

Chapter 8
Nuclear Energy

8.1 Introduction

Nuclear energy technology was developed and reached maturity in the second half of the twentieth century. It was founded on the discoveries and contributions of many renowned scientists such as Thompson, Roentgen, Becquerel, Curie, Bohr, Rutherford, Einstein, and others, which led to the formation (over a period of about 75 years, between 1875 and 1950) of new areas of physics such as nuclear physics and quantum mechanics. On the one hand, nuclear and quantum physics provided a thorough understanding of the laws of matter, and on the other hand they supported the development of various engineering applications, among which production of controlled nuclear heat in nuclear reactors appears to be the most important. Nowadays, nuclear energy is used to produce heat, which powers electricity generation plants and generates power for marine vessels propulsion or extraterrestrial spacecrafts. Nuclear energy, synonymous with atomic energy, is the energy produced by fission or fusion of atomic nuclei. Among all energy sources, nuclear energy is the most compact. Figure 8.1 compares in a simple manner the density of nuclear energy embedded in a uranium fuel pellet with other conventional sources. In the future, the implementation of nuclear hydrogen generation facilities is envisaged. Fulfillment of nuclear energy systems implies putting in place a complicated fuel cycle that must be thoroughly and securely monitored from extraction to nuclear waste deposition.

Nuclear energy is arguably considered a component of sustainable development. In this chapter, we introduce the physics of nuclear energy and associated heat generation, analyze the principal types of nuclear reactors, and discuss typical applications. Examples of systems analysis are illustrated with some case studies.

8.2 Historical Perspective

The eighteenth century was abundant in scientific discoveries in many fields, among which one of the most important was radioactivity. The term *radioactivity* was proposed by Marie Curie, who received two Nobel prizes for her discoveries in

İ. Dinçer and C. Zamfirescu, *Sustainable Energy Systems and Applications*,
DOI 10.1007/978-0-387-95861-3_8,

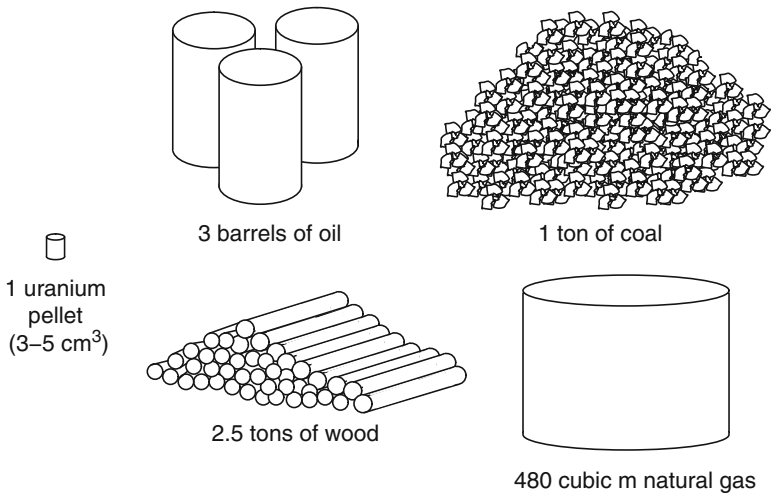

Fig. 8.1 Energy equivalents for 1 pellet of uranium fuel

physics and chemistry. The radioactive element polonium that she discovered in 1898 was named for her native country, Poland. By definition, radioactivity is the phenomenon of spontaneous emission of nuclear radiation (alpha, beta, and gamma rays, neutron particles, etc.), which is generated either directly by unstable atomic nuclei or indirectly by a nuclear reaction. Some of these kinds of radiation, such as beta and gamma rays were known from previous discoveries such as that of Roentgen, who first generated X-rays. The gamma rays and X-rays have the same nature, being a form of high-energy electromagnetic radiation. Gamma rays are produced by radioactive decay of some nuclei (which will be explained in this chapter), while X-rays are in general produced by special electronic equipment. Radioactivity can occur spontaneously by disintegration of some radioactive nuclei existent in nature. Natural radioactivity was discovered by Henri Becquerel in 1986. The process of radioactivity also can be induced, which is called artificial radioactivity. Generation of artificial radioactivity was first studied by Marie Curie's group at the University of Paris in the 1920s with a significant contribution by the Curie scholar Stefania Maracineanu, who demonstrated the first laboratory experiment proving the possibility to produce artificial nuclear radiation. In her Ph.D. thesis, completed in 1924, Maracineanu did experiments with lead and polonium and showed that lead, being activated with radioactive polonium, starts emitting radiation. This first laboratory proof was investigated for 10 more years by Frederic and Irene Joliot-Curie which formulated a theoretical model for artificial radioactivity in aluminum bombarded with alpha particles. The two savants received the Nobel Prize for chemistry in 1935 and acknowledged the initial discovery of Maracineanu in an article published in *Neues Wiener Journal* (June 5, 1934). Generating nuclear radiation in a controlled manner was of the utmost

importance for the progress of nuclear energy engineering. As pointed out by Ernest Rutherford in 1911, the heat generated by radioactive decay is enormous as compared to that generated by any chemical reaction. Another major step in explaining the process of radioactivity is attributed to James Chadwick in 1932, which was followed by relevant experiments conducted by Enrico Fermi, who succeeded in producing nuclear reactions induced by neutron radiation. Fermi demonstrated the first nuclear reactor, in which he conducted the chained fission reaction of uranium in 1942 in Chicago. Later, a nuclear reactor of 1 MW was built and tested at Oak Ridge laboratories, and the first full-size nuclear reactor of 200 MW installed capacity, called the B reactor, began to operate near Richland, Washington.

Intensive research work was pursued in the 1940s in the countries engaged in World War II—the United States, Germany, the United Kingdom, and the Russia—to develop nuclear power for both peaceful and military applications. The first nuclear power plant to produce electricity of 100 kW was commissioned in Idaho in 1951. In Russia, the first nuclear power plant of 5 MW connected to a grid was constructed. Atomic Energy Canada Ltd. (AECL) was established in 1944 in Chalk River, Ontario, with the aim of developing nuclear energy in Canada. In 1945, the AECL tested the first nuclear reactor and some years later developed the CANDU (CANadian Deuterium Uranium) nuclear power plant technology.

During the last 40 years, many kinds of nuclear reactors were developed for the purpose of electric power production and marine and space mission applications (where nuclear energy can be used for propulsion, power generation, heating, cooling, and many other needs). In recent years, the idea of hydrogen production with nuclear energy attracted considerable interest. Other novel applications of nuclear energy are in desalination, petroleum extraction from oil sands, and generation of sustainable process heat.

8.3 Basic Elements of Nuclear Power

Nuclear reactions stand at the base of nuclear energy. In current engineering applications, nuclear energy is produced in a controlled manner in nuclear reactors. Inside the reactor, the nuclear energy that manifests in the form of radiation is converted into thermal energy and transferred out with the help of a heat transfer fluid (reactor coolant). By a rough definition, a nuclear reaction is a process in which two or several nuclei or nuclear particles interact to produce some other nuclear particles or nuclei. Nuclear reactions occur at the subatomic level as opposed to chemical reactions that take place at the atomic or molecular level. In this section, the basic elements of nuclear power, which include mainly atomic structure, nuclear reactions (e.g., fission, fusion), nuclear radiation, radiation, and matter interaction to generate heat, are presented.

8.3.1 Atomic Structure

It is known from physics that matter is constituted of elements called atoms, and it is known from chemistry that the number of kinds of atoms—chemical elements—is relatively small in the universe. The term *chemical element* refers to a substance that cannot be decomposed into simpler substances by chemical means. The periodic table of elements currently contains 118 elements, which through their possible combination give rise to a very large number of chemical compounds. Any chemical element can be called an "atom," because the smallest recognized division of a quantity of a chemical element is an atom.

The atom has a complicated structure including many kinds of particles in its nucleus. For the purpose of nuclear energy engineering, the atom can be treated in a simplified manner, by considering it as consisting of a nucleus and a cloud of electrons orbiting around the nucleus on orbits approximated to be spherical in their average radius, as suggested in Fig. 8.2. The radius of an atom is of the order of 1 Å (where 1 Ångström is 10^{-10} m) while the mass ranges from about $10^{-27}$to 10^{-25} kg. The nucleus consists in a number of particles called nuclides. The nuclides are of two kinds: protons (particles having electrical charge) and neutrons (particles that do not have electrical charge). The common notation regarding the atom components is as follows:

- p^+= symbol for proton (sign "+" indicates a positive electrical charge)
- Z = the number of protons in the nucleus
- n = symbol for neutrons
- N = number of neutrons
- $A = Z + N$, representing the total number of nuclides known as atomic mass
- e^-= symbol for electron indicating that it has a negative electrical charge
- $e = -1.602176487(40) \times 10^{-19}$ C is the electrical charge of one electron in coulombs

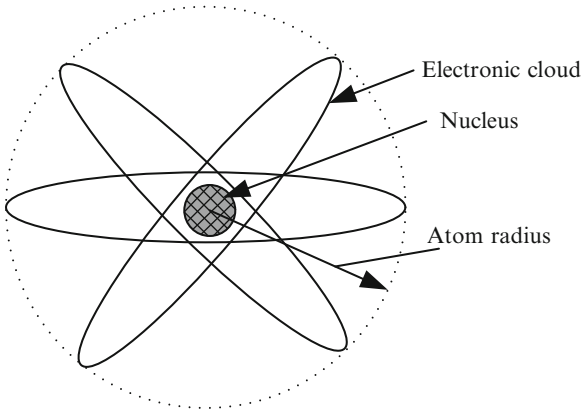

Fig. 8.2 Structural representation of an atom

Table 8.1 Main characteristics of the fundamental subatomic particles

Name	Neutron	Proton	Electron
Symbol	n	p^+	e^-
Mass (kg)	$1.674927212 \times 10^{-27}$	$1.672621638 \times 10^{-27}$	$9.10938215 \times 10^{-31}$
Mass (AMU)	1.008664916566	1.00727646661	0.0005486
Electric charge	None	+1e	−1e

Basically, the entire mass of an atom is concentrated in its nucleus. Due to the presence of the protons, the nucleus has a positive electrical charge of + *Z*e. The atom is neutral from the electrical point of view. Therefore, the electronic cloud comprises *Z* electrons, totaling an electrical charge of –*Z*e. The mass of the three elementary nuclear particles as well as their main characteristics are given in Table 8.1. The mass of particles is shown in kg and in AMU (atomic mass unit). The AMU is the standard unit for measuring the mass of atomic or subatomic particles and is defined relative to the mass of carbon 12. An atom of carbon 12 comprises $Z = 6$ protons and $N = 6$ neutrons and has a mass of 1.992×10^{-26} kg. Carbon 12 is the most abundant isotope of carbon in the universe, the abundance being 98.89%. This means that among all atoms of carbon in the universe, the ones that have a nuclear structure comprising 6 protons and 6 neutrons can be found with a probability of 98.99%. According to the definition, the mass of one atom of carbon 12 has 12 AMU. The mass of 1 AMU can be calculated easily as follows: $1\,\text{AMU} = 1.992 \times 10^{-26}/12 = 1.660538782 \times 10^{-27}$ kg.

A chemical element is constituted by atoms each having same number of electrons and protons. However, the number of neutrons in the nucleus can differ, which means that the atomic mass of a chemical element can vary in a specific range. Any variation of a chemical element, with a different number of neutrons in its nucleus, is called an *isotope*. There are about 116 known chemical elements. Many of them have several isotopes, but some (e.g., beryllium, fluorine, phosphorus) have only one isotope. All atoms having 6 protons are called the chemical element "carbon," or all atoms having 92 protons are called the chemical element "uranium." Carbon has three isotopes: one with 6, one with 7, and one with 8 neutrons.

The standard notation of a chemical element includes the symbol of the element (E), the indication of the number of protons *Z* and the indication of the atomic mass *A*; the general form of the notation is ${}^{A}_{Z}\text{E}$; for example, the isotopes of carbon (symbol C) are ${}^{12}_{6}\text{C}, {}^{13}_{6}\text{C}, {}^{14}_{6}\text{C}$, and the isotopes of uranium are six in number, from which only three occur in nature, namely ${}^{234}_{92}\text{U}, {}^{235}_{92}\text{U}, {}^{238}_{92}\text{U}$. A short notation of chemical elements that indicates only the isotope's atomic mass and its symbol is also used and has the form ${}^{A}\text{E}$. The isotopes of a chemical element are of two types: stable or radioactive. The isotopes that are stable maintain over time their nuclear structure. The radioactive isotopes have an unstable nuclear structure. Therefore, they disintegrate over time by changing their nuclear structure toward more stable arrangements. It is important to know how fast the radioactive elements disintegrate. The rate of radioactive disintegration is measured by the "half-life time," a

Table 8.2 Chemical elements relevant to nuclear energy technology and their main features

Symbol	Name	Abundance	Atomic mass (AMU)	Half-life time	Binding energy (MeV)
$^{1}_{1}H$	Hydrogen	>99%	1.00727646661	Stable	0
$^{2}_{1}H$	Deuterium	<1%	2.0141078	Stable	1.808; 1.7079937
$^{3}_{1}H$	Tritium	Traces	3.0160492	12.32 years	8.016;7.9700827
$^{3}_{2}He$	Helium 3	<0.0002%	3.0160293	Stable	6.695415271
$^{4}_{2}He$	Helium 4	>99.999%	4.002602	Stable	27.27210578
$^{11}_{6}C$	Carbon 11	Traces	11.002035	28.38 min	79.120923541
$^{12}_{6}C$	Carbon	98.9%	12.0000	Stable	89.08683
$^{13}_{6}C$	Carbon 13	1.1%	13.00335	Stable	94.03713903
$^{14}_{6}C$	Carbon 14	Traces	14.003241	5,730 years	102.20916492
$^{234}_{92}U$	Uranium 234	0.0054%	234.035265	245,500 years	1,736.67733817
$^{235}_{92}U$	Uranium 235	0.7204%	235.0439299	7.038×10^{8}years	1,736.6773536
$^{238}_{92}U$	Uranium 238	99.2742%	238.0507826	4.468×10^{9}years	1,754.506258689

Data from Haynes (2011), Kruger (2006), and Murray (2009)

parameter that is defined rigorously in the subsequent paragraphs. Basically, at half-life a quantity of a radioactive element becomes half of the initial quantity. The half-life time and other important parameters of those chemical elements and their isotopes that are relevant to nuclear energy technology are summarized in Table 8.2.

8.3.2 Nuclear Reactions: Fission and Fusion

Unstable isotopes disintegrate spontaneously through a process called radioactive decay. Radioactive decay is explained by the existence of excess energy in the nucleus. The cause of the excess energy can be an improper balance between the number of neutrons and electrons, or it can be due to other factors that lead to the establishment of a metastable state of the nucleus. Radioactive decay can be described by the following general equation:

$$R \rightarrow S + P + E, \tag{8.1}$$

where the symbols represent in order the radioactive isotope (R), the stable isotope (S), emitted particles (P), and emitted energy (E).

The equation states that when a radioactive isotope decays, it will transform into a stable isotope (possibly the isotope of a different chemical element than that of R), and it will emit some nuclear particles and radiation energy. But what is the nature of the nuclear energy and where does it come from? In order to answer this

question, one needs to introduce the notion of binding energy. In analogy with chemistry, where any chemical compound has associated an enthalpy of formation, in nuclear science one can associate a binding energy with any isotope.

At least two kinds of forces interact to maintain the nuclear structure, namely the coulomb repulsion forces and the nuclear attraction forces (known as Yukawa potential forces after the scientist who postulated their existence in 1935). The Yukawa forces explain the existence of the several protons in the nucleus. Protons have positive charge. Therefore, as they approach they reject each other. If only coulomb forces, which are associated with the electric field, would be active, then the protons can never stay together in the nucleus. The attraction nuclear forces of the Yukawa kind act at a smaller distance than the coulumb forces, between any kind of nucleons (protons or neutrons) regardless of the presence or the absence of electric charges. In other words, two protons attract each other if the distance between them is sufficiently small. A consequence of the fact that at the nucleus level two opposite effects manifest, that is, the attraction of nucleons due to nuclear (Yukawa) forces and the repulsion of protons due to electrostatic (coulomb) forces, is that the size (radius) of the nucleus establishes itself such that equilibrium exists between repulsion and attraction actions.

Figure 8.3 shows an approximation of the energy associated with coulomb and Yukawa forces between two approaching protons. It can be seen that the coulomb repulsion forces are stronger than the attraction forces for distances larger than ~3.5 fm (femtometer). For more attraction between protons, the nuclear forces overcome

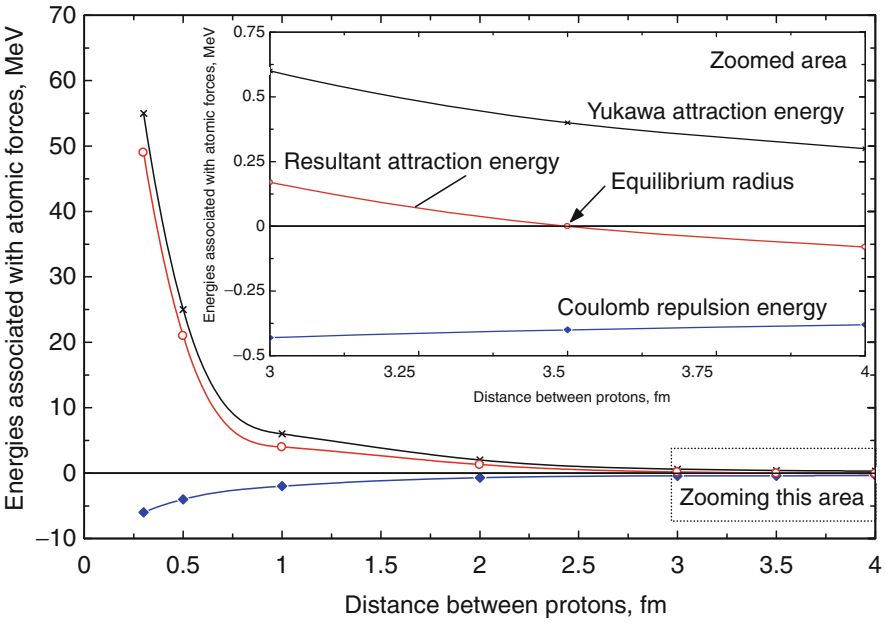

Fig. 8.3 Energies associated with coulomb and Yukawa force

repulsion forces; therefore, the protons tend to get closer. It is also known that at distances smaller than ~0.3 fm strong repulsive atomic forces other than Yukawa forces occur.

The equilibrium between attractive and repulsive nuclear forces can be stable, unstable, or metastable depending on the exact situation. If the equilibrium in the nucleus is stable, then the isotope is stable; if the nuclear equilibrium is unstable or metastable, then the isotope is radioactive, that is, it will spontaneously disintegrate to form a system with stable equilibrium. Assume that the number of nucleus constituents (protons and neutrons) is small. In this case, the element has a small atomic number (by atomic number one denotes the atomic mass measured in AMU). Consequently, the radius of the nucleus is relatively small; therefore, the particles are closer to each other, and the nuclear forces dominate. Because nuclear forces are high, a tendency of the low atomic mass elements to undergo fusion with each other exists and to form heavier atoms. In the opposite case, if the nucleus has a large number of constituents, its radius is large. In this extreme the electrostatic forces dominate the nuclear ones. Therefore, the tendency of the heavy elements is to dissociate and form smaller elements.

One can define the density of the atomic nucleus as a mass of matter (A) expressed in AMU over the volume of the nucleus (V_N), assumed spherically, $V_N = 4/3\pi R_N^3$. The nucleus density of the elements comprised in the periodic table varies from about 16,350 AMU/cm^3 to 17,270 AMU/cm^3 with an average of 16,800 AMU/cm^3. The nucleus radius can be approximated by

$$R_N = \sqrt[3]{\frac{3A}{4\pi\rho_N}} \quad \text{or} \quad R_N = 0.013A^{1/3}, \text{fm(femtometer)}. \tag{8.2}$$

During any nuclear reaction the nucleus can lose mass or gain mass, or reconfigure its structure without changing mass. Any mass variation or system reconfiguration at the nuclear level occurs together with a radiation emission or absorption. The general formula relating mass variation with energy exchange has been derived by Einstein and it is known as $E = mc^2$, which for the case of a nuclear reaction is better written in the following form:

$$\Delta E_b = -(\Delta m)c^2, \tag{8.3}$$

where Δm represents the mass variation during the reaction expressed in kg and c is the speed of light in vacuum expressed in m/s. The minus sign indicates that if the mass of the atoms that resulted after the reaction is complete is smaller than the mass of the atoms entering the reaction, then the system emits energy; if it is larger, the system absorbs energy, resulting in this equation:

$${}^{A}_{Z}\mathrm{E} \rightarrow Z\mathrm{p}^{+} + (A - Z)\mathrm{n} + \Delta E_b, \tag{8.4}$$

which states that the nucleus of element E disintegrates in its constitutive nucleons; the mass variation can be written as $\Delta m = Z \times m_{p^+} + (A - Z)m_n - m\left({}^{A}_{Z}\mathrm{E}\right)$. Equation (8.3) introduces the binding energy of the nucleus, which becomes

$$\Delta E_b = -\left[Z \times m_{p^+} + (A - Z)m_n - m\left({}^{A}_{Z}\mathrm{E}\right)\right]c^2. \tag{8.5}$$

For a mass variation of 1 AMU the corresponding binding energy is $\Delta E_{b1} = 931.4\text{MeV}$; therefore, the binding energy equation becomes

$$\Delta E_b = -(\Delta m)E_{b1}, \tag{8.6}$$

where Δm is expressed in AMU. Table 8.1gives also the binding energy of the listed elements.

Example: Calculation of the Binding Energy of Tritium

We will calculate first the mass variation associated with binding energy, according to Eq. (8.5). This is for tritium with $A = 3, Z = 1,\ \Delta m = m_{p^+} + 2m_n - m\left({}^{3}_{1}\mathrm{H}\right) = 0.0085571$ AMU; the associated binding energy is $\Delta E_b = -931.4 \times 0.0085571 = 7.9700827$ MeV.

A factor that quantifies the nuclear stability of an isotope is given by the ratio of binding energy to the atomic mass, $\Delta E_b/A$. Figure 8.4 shows the variation of the nuclear stability factor and the variation of the binding energy with the atomic mass of the element. Only the most abundant isotopes of the elements are considered in the plot. One can observe that ^{56}Fe has about the maximum binding energy per nucleon (the peak is very close to ^{56}Fe and corresponds to less abundant isotopes of ^{62}Ni followed by ^{58}Fe). The nucleus of helium 4 is also very stable, showing a peak with respect to its neighbors (hydrogen and lithium). This high stability is the

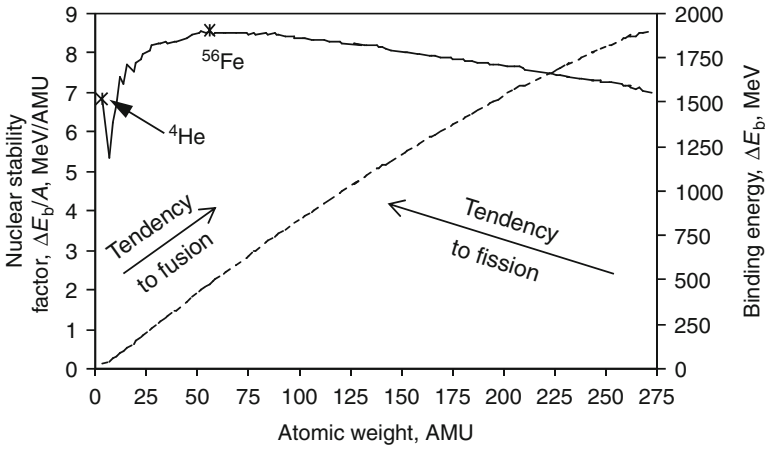

Fig. 8.4 Nuclear stability factor and the binding energy of the chemical elements [data from Kruger (2006)]

reason why this isotope results from many nuclear reactions including fusion that is believed to occur in the sun's core, where hydrogen is converted into ^{4}He or the so-called alpha decay where a fast moving nucleus of ^{4}He is generated. The nuclei that have a small atomic mass (smaller than that of magnesium) tend to associate and form heavier nuclei through nuclear fusion kinds of reactions. Elements with atomic mass in the range between magnesium ($A = 24$) and xenon, ($A = 131$) are relatively stable since the stability factor is relatively flat. For elements heavier than xenon, the nucleus size becomes large, a fact that affects the balance of forces: attractive forces become weaker and the repulsive forces stronger. Therefore, heavy elements have the tendency to disintegrate into lighter elements through a nuclear fission reaction.

Commonly, the nucleus of a radioactive isotope is called a radionuclide. The decay law states that the number of radionuclides at a given time $N(t)$ is given by

$$N(t) = N_0 \left(\frac{1}{2}\right)^{\frac{t}{t_h}}, \tag{8.7}$$

where $N_0 = N(t = 0)$ represents the number of radionuclides at the initial moment and t_h is called the half-time period. The half-time of some common radionuclides is listed in Table 8.2. Figure 8.5 correlates the decay time with the decay ratio $N(t)/N_0 = (1/2)^{t/t_h}$ for some radionuclides.

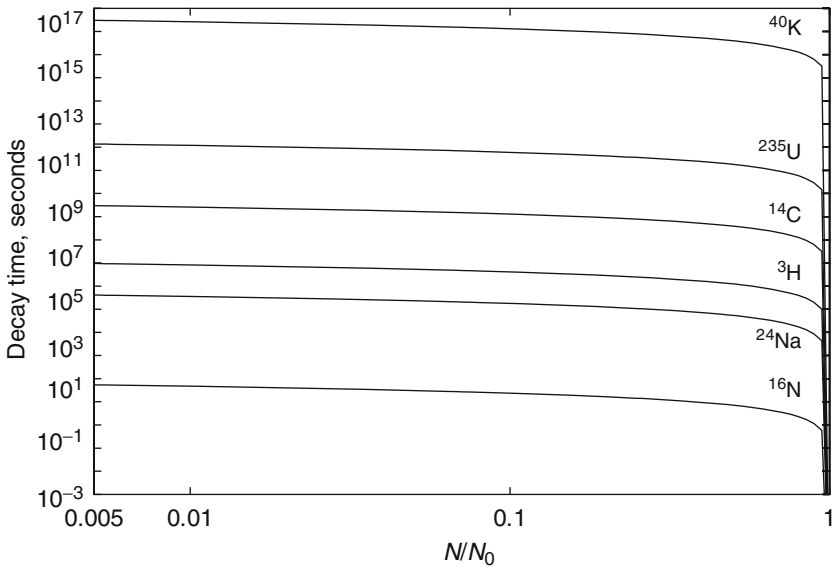

Fig. 8.5 Decay time of some radionuclides as a function of the decay ratio (N/N_0)

8.3.3 Nuclear Radiations and Decay Reactions

Radioactive decay and other nuclear reactions result in the emission of fast particles and their associated radiative energy. There are a series of subatomic particles that are important because they count in the energy balance of many nuclear reactions of practical importance. All such particles are in general not stable; they either disintegrate or dissipate in various ways. In addition to particles, nuclear reactions may emit gamma radiation. Here is some general information about common particles and radiation that occur during nuclear reactions:

- *Gamma ray*: This is electromagnetic radiation in the spectrum of pm (picometers) with associated energies of hundreds or thousands of keW. The common notation is γ.
- *Alpha particle*: This is a fast-moving particle whose composition is the same as that of the nucleus of ^{4}He. This particle therefore has an electric charge of +2e. The common notation is α or $^4He^{2+}$. The associated maximum energy is 5 MeV.
- *Positron particle*: This particle is similar in mass to an electron, but it has the opposite (positive) charge. Often it is called an antielectron. The positron eventually slows down and collides with an electron, generating thus two photons.
- *Beta radiation*: This is either a fast-moving electron or a fast-moving positron emitted by some nuclear reaction. If the electron is emitted, the associated radiation has an electrical charge of –e; the common symbol is β^-. If a positron is emitted, the symbol for the radiation is β^+.
- *Neutron radiation*: This radiation consists of beams of free neutrons. This radiation is therefore nonionized. The neutron radiation can be categorized as slow (or thermal) or fast. The common notation of this radiation is *n*.
- *Neutrino particle*: This particle has zero electric charge and nonzero mass. It is smaller than the electron and travels with a speed close to that of light. The symbol is *v*.
- *Antineutrino particle*: This is the antimatter correspondent of a neutrino. The symbol is $\bar{v}$.
- *Photon particle*: This particle is the quantum of the electromagnetic radiation. It is a particle with no resting mass. In general, the notation is either *hf* or *hv*, where *h* represents the Planck's constant, and *f* or *v* is the frequency of the electromagnetic radiation.

There are three kinds of radioactive decays, namely alpha, beta, and gamma. In alpha decay a heavy radioactive element ($Z > 83$) reduces its atomic mass by releasing two protons and two neutrons; these form immediately a ^{4}He kind of nucleus, which is the alpha particle. The general alpha decay equation is

$$ {}^{A}_{Z}\mathrm{E}_1 \rightarrow {}^{A-4}_{Z-2}\mathrm{E}_2 + {}^{4}\mathrm{He}^{2+} + Q, \tag{8.8} $$

where Q represent the generated radiative energy (that eventually transforms into heat).

Beta decay represents a means to balance the number of neutrons and protons in the nucleus such that the element becomes stable. If the number of neutrons is too high, a neutron can be converted into proton with release of energy. In the opposite situation, if the number of protons is too high, energy is absorbed to convert a proton into neutron. The beta decay reaction in the two cases can be written as

$$\begin{cases} n \rightarrow \mathrm{p}^{+} + \beta^{-} + \bar{\nu} + 0.782\,\mathrm{MeV} \\ \mathrm{p}^{+} + \text{energy} \rightarrow \mathrm{n} + \beta^{+} + \nu. \end{cases} \tag{8.9}$$

For the two cases expressed by Eq. (8.9) the following beta decay reactions correspond in order:

$$\begin{cases} {}^{A}_{Z}\mathrm{E}_1 \rightarrow {}^{A}_{Z+1}\mathrm{E}_2 + \beta^{-} + \bar{\nu} + Q \\ {}^{A}_{Z}\mathrm{E}_1 \rightarrow {}^{A}_{Z-1}\mathrm{E}_2 + \beta^{+} + \nu + Q. \end{cases} \tag{8.10}$$

In the first case of Eq. (8.10) the element E_1transforms into E_2, which has one more protons; the beta electron slows down and becomes an ordinary electron. In the second case, the produced element will have one less proton and the emitted radiation is of the positron kind. The positron eventually slows down and annihilates an electron, a process in which two photons of 0.51 MeV each are generated. Therefore, the released energy by β^{+}decay is in any case higher than 1.02 MeV.

Gamma decay represents a mechanism of rearrangement of nucleons inside the nucleus that occurs in order to achieve a stable equilibrium. In this case, the number of neutrons and protons of the nucleus is well balanced, but their relative position is energetically in an exited state. The general equation for gamma decay is

$${}^{A\mathrm{m}}_{Z}E \rightarrow {}^{A}_{Z}E + \gamma\,(\mathrm{MeV}), \tag{8.11}$$

where *A*m indicates the metastable (excited) state of the nucleus. In Table 8.3 some relevant decay reactions are compiled for better illustration.

8.3.4 Available Energy from Uranium Fuel

Probably the most important nuclear reaction, from the energy generation point of view is the reaction of fission. In the fission reaction a heavy nucleus is "bombarded" with a "slow" neutron. By capturing a neutron, the nucleus enters into a metastable state. In order to reach equilibrium, the nucleus splits into two parts of about half the weight and generates neutron radiation and energy. The only known naturally occurring fissionable isotope is ${}^{235}_{92}\mathrm{U}$. However, this isotope is the least abundant with a weight percentage of 0.7%. Only two other fissionable isotopes are known, both of them being produced artificially: one is the uranium isotope ${}^{235}_{92}\mathrm{U}$

Table 8.3 Nuclear decay reactions

Decay type	Reaction
Alpha decay	$^{226}_{88}\mathrm{Ra} \rightarrow {}^{222}_{86}\mathrm{Rn} + {}^{4}_{2}\mathrm{He}^{2+} + 4.87\,\mathrm{MeV}$
	$^{214}_{90}\mathrm{Th} \rightarrow {}^{210}_{88}\mathrm{Ra} + {}^{4}_{2}\mathrm{He}^{2+} + 7.825\,\mathrm{MeV}$
	$^{235}_{92}\mathrm{U} \rightarrow {}^{231}_{90}\mathrm{Th} + {}^{4}_{2}\mathrm{He}^{2+} + 4.6793\,\mathrm{MeV}$
	$^{238}_{92}\mathrm{U} \rightarrow {}^{234}_{90}\mathrm{Th} + {}^{4}_{2}\mathrm{He}^{2+} + 4.04\,\mathrm{MeV}$
	$^{236}_{94}\mathrm{Pu} \rightarrow {}^{232}_{92}\mathrm{U} + {}^{4}_{2}\mathrm{He}^{2+} + 5.867\,\mathrm{MeV}$
Negative beta decay	$^{3}_{1}\mathrm{H} \rightarrow {}^{3}_{2}\mathrm{He} + \beta^{-} + \bar{\nu} + 0.01859\,\mathrm{MeV}$
	$^{14}_{6}\mathrm{C} \rightarrow {}^{14}_{7}\mathrm{N} + \beta^{-} + \bar{\nu} + 0.15648\,\mathrm{MeV}$
	$^{131}_{53}\mathrm{I} \rightarrow {}^{131}_{54}\mathrm{Xe} + \beta^{-} + \bar{\nu} + 0.971\,\mathrm{MeV}$
	$^{234}_{90}\mathrm{Th} \rightarrow {}^{234}_{91}\mathrm{Pa} + \beta^{-} + \bar{\nu} + 0.273\,\mathrm{MeV}$
Positive beta decay	$^{22}_{11}\mathrm{Na} \rightarrow {}^{22}_{10}\mathrm{Ne} + \beta^{+} + \nu + 2.84\,\mathrm{MeV}$
	$^{37}_{19}\mathrm{K} \rightarrow {}^{37}_{18}\mathrm{Ar} + \beta^{+} + \nu + 6.149\,\mathrm{MeV}$
	$^{137}_{60}\mathrm{Nd} \rightarrow {}^{137}_{59}\mathrm{Pr} + \beta^{+} + \nu + 3.69\,\mathrm{MeV}$
Gamma decay	$^{60\mathrm{m}}_{27}\mathrm{Co} \rightarrow {}^{60}_{27}\mathrm{Co} + \gamma + 0.0586\,\mathrm{MeV}$
	$^{82\mathrm{m}}_{35}\mathrm{Br} \rightarrow {}^{82}_{35}\mathrm{Br} + \gamma + 0.046\,\mathrm{MeV}$
	$^{99\mathrm{m}}_{43}\mathrm{Tc} \rightarrow {}^{99}_{43}\mathrm{Tc} + \gamma + 0.14\,\mathrm{MeV}$
	$^{130\mathrm{m}}_{56}\mathrm{Ba} \rightarrow {}^{130}_{56}\mathrm{Ba} + \gamma + 0.08\,\mathrm{MeV}$
	$^{132\mathrm{m}}_{58}\mathrm{Ce} \rightarrow {}^{132}_{58}\mathrm{Ce} + \gamma + 0.3255\,\mathrm{MeV}$

and the other is the plutonium isotope $^{239}_{94}\mathrm{Pu}$. Both these isotopes can be produced starting from more abundant resources through neutron bombardment. Plutonium is obtained from $^{238}_{92}\mathrm{U}$ (~99.3% natural occurrence) through the following overall reaction $^{238}_{92}\mathrm{U} + \mathrm{n} \rightarrow {}^{239}_{94}\mathrm{Pu} + 2\beta^{-}$. The artificial fissionable uranium isotope is produced from thorium-232 (abundance ~100%) through the overall reaction $^{232}_{90}\mathrm{Th} + \mathrm{n} \rightarrow {}^{233}_{92}\mathrm{U} + 2\beta^{-}$.

The fission reaction of $^{235}_{92}\mathrm{U}$ is a chain reaction having the following general form:

$$^{235}_{92}\mathrm{U} + \mathrm{n_{th}} \rightarrow {}^{236\mathrm{m}}_{92}\mathrm{U} \rightarrow {}^{A_1}_{Z_1}\mathrm{E}_1 + {}^{236-\kappa-A_1}_{92-Z_1}E_2 + \kappa n + Q, \tag{8.12}$$

where $\mathrm{n_{th}}$ denotes a slow (thermal) neutron, and κn denotes κ fast propagating neutrons.

The first step of the reaction is the bombardment of a nucleus of $^{235}_{92}\mathrm{U}$ with one thermal neutron. As a consequence, the metastable $^{236\mathrm{m}}_{92}\mathrm{U}$ is formed, which further splits into two lighter nuclei, namely $^{A_1}_{Z_1}\mathrm{E}_1$ and $^{236-\kappa-A_1}_{92-Z_1}E_2$ and emits κneutrons. The atomic number A_1 of the first element can be found in the range of 75 to 160 with a higher occurrence between 92 and 144. The resulting elements E_1 and E_2 can have metastable nuclei, and therefore they will break apart by emitting gamma rays. The general energy breakthrough of uranium 235 fission is shown in Fig. 8.6, based on data from Murray (2009).

8.3.5 Available Energy from Nuclear Fusion

Another important nuclear reaction is the thermonuclear fusion. In this case two light nuclei are made to collide, aiming to form a heavier nucleus. The basic

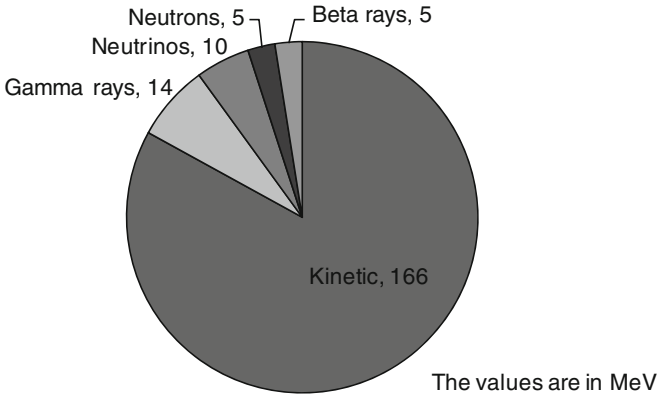

Fig. 8.6 Energy breakthrough of uranium 235 fission [data from Murray (2009)]

reaction of this kind is fusion of deuterium, which is believed to occur in the sun and other stars:

$$ {}_1^2\mathrm{H} + {}_1^2\mathrm{H} \rightarrow {}_2^4\mathrm{He} + Q, \tag{8.13} $$

where Q is the emitted radiation, which is basically of the γ kind. The most difficult problem with this reaction consists of making the two deuterium nuclei (called deuterons) collide. This can be done in a controlled way, in principle, in a particle accelerator. In this case, the two deuterons, which are positively charged particles, can be accelerated to a very high speed in opposite directions to produce the collision. When the particles approach each other, the coulomb rejection forces become extremely high. Typically, the energy needed to overcome coulomb forces is ~20 keV per collision. The energy that is released from the reaction can be calculated in a similar way as one calculates the binding energy, namely, through variation of mass. In this case $\Delta m = 0.0377$ AMU and the corresponding energy is $c^2\Delta m = 28.3$ MeV. Therefore, the theoretical gain from the reaction (28.28 MeV) is very attractive. However, the energy consumed to accelerate the particles in a particle accelerator is very much higher than 20 keV.

A second way to accelerate deuterons is by raising the temperature to extremely high values. A fusion reaction that is initiated by raising the temperature of the fuel is called a thermonuclear reaction. Based on the kinetic theory of ideal gases, the energy associated with a particle is $e = 3/2kT$, where $k = 1.38 \times 10^{-23}$ J/K is the Boltzmann constant. For 20 keV, one calculates that the temperature is 144×10^6 K, which looks impossible to be achieved on earth.

Another thermonuclear reaction that can be initiated on earth is the one that was obtained in the hydrogen bomb, namely the fusion of deuteron with triton (triton is the name for the tritium nucleus, ${}_1^3\mathrm{H}$):

$$ {}_1^2\mathrm{H} + {}_1^3\mathrm{H} \rightarrow {}_2^4\mathrm{He} + n + 17.6\,\mathrm{MeV}. \tag{8.14} $$

Table 8.4 Key terms definitions

Term	Definition
Nuclear energy	Energy produced by fission or fusion of atomic nuclei.
Atom	Smallest recognizable constituent of a chemical element. It is made up of three main parts: protons, neutrons, and electrons. The protons and neutrons make up the center of the atom while the electrons orbit around the center.
Chemical element	A substance that cannot be decomposed into simpler substances by chemical means.
Atomic number	The number of protons in an element, which identifies it.
Isotope	Occurs when an atom has a different number of neutrons and protons. Isotopes, measured by their total weight, called "mass number," are the sum of the neutrons and protons. Some isotopes are unstable and will decay to reach a stable state; these elements are considered radioactive.
Binding energy	The energy required to disassemble a nucleus into the free unbound neutrons and protons it is composed of, in such a way that the particles are distant enough from each other so that particles do not interact.
Fission	Occurs when an atom's nucleus splits apart to form two or more different atoms. The most easily fissionable elements are the isotopes uranium 235 and plutonium 239. Fissionable elements are flooded with neutrons causing the elements to split. When these radioactive isotopes split, they form new radioactive chemicals and release extra neutrons that create a chain reaction if other fissionable material is present. While uranium, atomic number 92, is the heaviest naturally occurring element, many other elements can be made by adding protons and neutrons with particle accelerators or nuclear reactors. In general, the fission process uses higher numbered elements.
Fusion	The combination of one or more atoms, usually isotopes of hydrogen, which are deuterium and tritium. Atoms naturally repel each other so fusion is easiest with these lightest atoms. To force the atoms together takes extreme pressure and temperature, which can be produced by a fission reaction.

This reaction requires ~10 keV for initiation, and in the nuclear bomb implementation, the associated temperature of 77×10^6 K was obtained by initiating an explosive fission reaction of uranium 235. The process duration in a thermonuclear bomb is of about $1\mu s$. There is a considerable research effort throughout the world to devise a reactor that performs reaction (8.14) in a controlled manner. Possible options are to use magnetic fields to keep the reaction in a confined space at high temperature, or to use of inertial confinement through shock waves thermally induced by heating with laser beams.

Definitions of some key terms introduced in Section 8.3 are listed in Table 8.4.

8.4 Controlled Generation of Nuclear Heat

Production of a fission reaction according to Eq. (8.12) implies the existence of a thermal neutron that is able to initiate the process. Once it is performed, the reaction

produces κ fast neutrons that, in principle, can be slowed down and further used to initiate new fission reactions. This observation suggests that it is possible to obtain a self-sustaining nuclear fission reaction (chain reaction).

One can ask the question: What kind of arrangement must be set in order to obtain a chain reaction? Nuclear reactors were developed starting in 1942 to produce controlled nuclear heat, which in general has been used either for electricity production or for submarine propulsion. The setting involves placing a certain amount of uranium fuel in a special vessel that is surrounded by a coolant and a moderator, which have the role of heat transfer and neutron deceleration, respectively. The relevant parameters for the design of nuclear reactors are the atomic cross-section and its size, shape, and arrangement. Note that "cross-section" is a parameter quantifying the probability that radiation interacts with the surrounding medium. The stable operation of the reactor depends on the balance of neutrons generated by the reaction versus neutrons absorbed by the surrounding medium.

Let us assume that a quantity m of uranium fuel is bombarded with neutrons. A number of uranium atoms (not all) will be hit by the neutron and it undergoes fission, generating many other neutrons. The newly generated neutrons scatter. Some of them hit other fuel atoms and generate new fission reactions. Most likely many of them escape out of the reactor because the produced neutrons are fast. One can define k, the number of neutrons producing a new fission per neutron that initiates the reaction, as given below:

$$k \begin{cases} >1, \text{ supercritical,} \\ = 1, \text{ critical,} \\ <1, \text{ subcritical,} \end{cases} \tag{8.15}$$

where in the case of $k = 1$the reaction proceeds at a steady rate; in this situation the reactor operates at the exact critical parameters. In the case of $k>1$the reaction rate amplifies, therefore, the reactor becomes a violent explosive bomb; this operation is known as supercritical. If $k<1$, the reactor is subcritical, which means that the reaction tends to cease.

If the quantity of fuel for which the reactor operates at the critical state, and therefore the reaction, is steady and self-sustained, it is called critical mass; its associated volume of fuel is known as critical volume. For uranium 235, the critical mass is around 50 kg.

The conceptual configuration of a nuclear reactor is shown in Fig. 8.7, which also illustrates the temperature levels throughout the volume. In the core, uranium fuel is prepared in the form of a cartridge (in general cylindrical) that can be of a metallic material (uranium), or as an alloy (e.g., with aluminum), or as uranium dioxide (UO_2) or uranium carbide (UC). The fuel cartridges are placed in tubular pipes constructed, for example, of zircaloy (an alloy of 2.5% niobium and 97.5% zirconium, which is highly penetrative by neutrons). The tubes are cooled by different kinds of fluids, depending on the implementation (light water, carbon dioxide, helium, liquid sodium). In a typical case, the uranium fuel reaches a

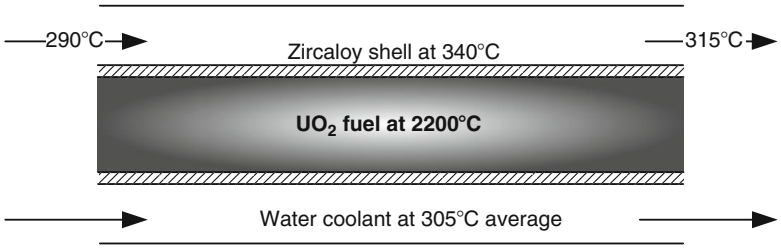

Fig. 8.7 Typical temperature levels in a water-cooled fission reactor

maximum of 2,200°C in the cartridge's core. The heat is transferred out through heat conduction at high heat density, commonly of 500 kW/m^2 of fuel rod surface. Due to intensive cooling, the average temperature of the fuel rod is kept at a temperature 200°C to 300°C higher than that of the coolant.

The generation efficiency of nuclear heat can be defined in energy or exergy terms in the following manner:

$$\begin{cases} \eta = \dfrac{q_{\text{out}}}{e_{\text{in}}} \\ \psi = \dfrac{q_{\text{out}}\left(1 - \dfrac{T_0}{T_{\text{out}}}\right)}{e_{\text{x,in}}}, \end{cases} \tag{8.16}$$

where q_{out} is the useful heat generated by the reactor (delivered at the primary or secondary loop, depending on the reactor design) per 1 kg of fuel; e_{in} represents the energy embedded in 1 kg of fuel; $e_{\text{x,in}}$ represents the exergy embedded in 1 kg of fuel; T_{out} is the maximum temperature at which the heat q_{out} is delivered; and T_0 is the temperature of the environment (or that of the sink).

It is interesting to note that the temperature of the fuel is inherently high. Therefore, the Carnot factor associated with this high temperature is very close to 1; consequently, the exergy of nuclear heat is the same as the deployed energy. The mean energy developed by 1 mol of fissionable nuclear fuel (any of $^{235}_{92}\text{U}, ^{233}_{92}\text{U}, ^{239}_{94}\text{Pu}$) is $e_{\text{in}} = 200\,\text{MeV} = 19.3 \times 10^{12}\,\text{J}$; therefore, the specific exergy of pure fuel can be calculated with $e_{\text{x,in}} = e_{\text{in}} = 19.3 \times 10^{12}/\text{M}$, where M is the molecular mass. With this, one calculates 82.13 TJ/kg of $^{235}_{92}\text{U}$, 82.83 TJ/kg of $^{233}_{92}\text{U}$, and 80.75 TJ/kg of $^{239}_{94}\text{Pu}$. For natural uranium fuel accounting for the occurrence of 0.7%, the associated exergy is of 584 GJ/kg.

Of major importance in fission reactor design is the evaluation of the heat generation rate per unit of volume, q'''. This parameter varies across the reactor core volume and is influenced primarily by the intensity of the neutron and gamma radiations produced by the nuclear reaction. In turn, the radiation intensity is influenced by the following:

- The flux density energy spectrum
- The density of various atomic constituents

- The atomic cross sections
- The kinetic energy of the resulting charged particle emissions

The nuclear reaction can be controlled (and maintained stable) in two ways, corresponding to two different reactor technologies: (1) by slowing the thermal neutrons as in "thermal reactor" technology, and (2) by enriching the fissile material in a proper proportion as in "fast neutron reactor" technology.

The cross-section parameter plays the most important role in design for both options. Thermal reactors use a so-called neutron moderator that contains a material that slows down the fast neutrons that result from each individual fission reaction. The kinetic energy of the slow neutron, which is called the thermal neutron, is of the order of magnitude of the surrounding medium. Being slow, the thermal neutrons have a higher cross section than the fast neutrons; in other words, the probability of colliding with fissionable material is higher.

The fast neutron reactors use nuclear fuel with enriched fissile material. The enrichment is made such that the probability of fast neutrons to collide with fissile atoms becomes high enough to maintain the chain reaction. These reactors do not need any moderator.

In the design process of the reactor the heat conduction equation must be solved in a region around the fissionable fuel where heat is generated. The medium is nonhomogeneous; therefore, the general equation reads as follows:

$$-\nabla \cdot (k\nabla T) + \rho c_{\mathrm{p}} \partial T/\partial t = \dot{q}''', \tag{8.17}$$

where $\dot{q}''' = \dot{q}'''(r,t)$ is the volumetric heat generation rate, which varies in time and space. Due to symmetry the problem can be treated as one-dimensional axial-symmetric. The calculation of the heat generation rate $\dot{q}'''(r,t)$ is done by considering the energy transfer at the interaction of the radiation field with the atomic constituents surrounding the reaction core. The heat generation rate can be determined with the help of the parameter ε defined as the average energy dissipated by a single interaction. Therefore, one can have

$$\dot{q}''' = \left[\frac{\text{energy}}{\text{time} \times \text{volume}}\right] = \varepsilon \left[\frac{\text{energy}}{\text{interaction}}\right] \times \left[\frac{\text{interactions}}{\text{time} \times \text{volume}}\right], \tag{8.18}$$

where the number of interactions per time and volume is proportional with the number of atoms per unit of volume, N; thus,

$$\left[\frac{\text{interactions}}{\text{time} \times \text{volume}}\right] = N \left[\frac{\text{atoms}}{\text{volume}}\right] \times \left[\frac{\text{interactions}}{\text{time} \times \text{atom}}\right]. \tag{8.19}$$

The number of interaction per unit of time and atom can be calculated based on the atomic cross section σ (discussed above and known also as the atomic

interaction coefficient), which is expressed in area normal to the radiation beam per number of radiation particles and surroundings atoms. Therefore, one gets

$$\left[\frac{\text{interactions}}{\text{time} \times \text{atom}}\right] = \sigma \left[\text{area} \times \frac{\text{interactions}}{\text{particle} \times \text{atom}}\right] \times \phi \left[\frac{\text{particles}}{\text{time} \times \text{area}}\right]. \tag{8.20}$$

Equation (8.20) introduces also the particle flux of the radiation ϕ expressed in terms of number of particles per time and cross-sectional area of the radiation beam. By observing Eqs. (8.18) to (8.20) one can easily obtain the final expression of the volumetric heat generation rate:

$$\dot{q}''' = \sigma \phi N \varepsilon. \tag{8.21}$$

The calculation of the local heat generation rate using Eq. (8.21) is a complicated matter because all parameters—the average energy dissipated, the cross section, the particle flux, and the numbers of atoms per unit of volume—vary spatially and temporarily. Moreover, the nature of the radiation varies and secondary effects can occur (e.g., scattering, low-energy X-ray emission, ionization, photon emission, beta emission, Compton scattering, etc.).

Additional complication occurs at integration of the heat transfer equation (8.17) because the thermal conductivity of both fuel and the zircaloy shell vary with temperature. The average thermal conductivity of UO_2 is about 6 W/mK. Also it is possible in certain operating conditions that the fuel melts; the UO_2 melting point is 2,800°C. In an example of reactor core configuration, fuel rods have a diameter of 5 mm and generate a linear heat flux of 15 kW/m at a temperature difference between the core and the rod surface of about 2,000°C.

Calculation of the generated nuclear heat must consider not only the variation of temperature in the cross section of rods (maximum in the center/minimum at rod's surface), but also it must account for the variation of the heat generation rate across the reactor section. As will be discussed in more detail in the next subsection, a nuclear reactor comprises a bundle of fuel assemblies, each of them being composed of a number of rods, which are in general of cylindrical shape. The coolant and the applicable moderator interact thermally with the fuel assemblies. In general, the temperature is highest at the axis of the reactor and lowest at the exterior. There is also a temperature variation along the rods and therefore along the reactor height. For preliminary design calculation purpose, it is customary to assume that the fuel assemblies are cylindrical R_f and the height h; they are also assumed to be uniformly distributed in the cross section of the reactor. Then the heat generated by a fuel assembly located at the radius r in the reactor cross section is given by

$$\dot{q}(r) = \pi R_f^2 \int_0^h \dot{q}'''(r, z) \mathrm{d}z, \tag{8.22}$$

where z indicates the vertical coordinate. Lamarsh and Baratta (2001) give the following equation to calculate the heat rate generated by a fuel assembly located at radius r from the center:

$$\dot{q}(r) = 2.32\frac{\dot{Q}_{\text{out}}}{n} \times \frac{e_{\text{g}}}{e_{\text{in}}} \times J_0\left(2.405\frac{r}{R_{\text{r}}}\right), \tag{8.23}$$

where $\dot{Q}_{\text{out}}$ is the heat rate delivered to the heat transfer fluid (coolant), n is the number of fuel assemblies, $e_{\text{in}} = 200\,\text{MeV}$ is the energy generated per mol of fissionable material (see above), $e_{\text{g}} < e_{\text{in}}$ is the average energy actually dissipated by the rods, R_r is the reactor radius, r is the radial distance from the center of the reactor to the center of the rod, and J_0 is the Bessel function of the first kind and order zero.

Example

A reactor comprises $n = 60{,}000$ cylindrical fuel assembly distributed over a circular cross section of the reactor with the radius of $R_r = 1.85\,\text{m}$. The average energy generated per mol of fissionable material in this configuration is $e_{\text{g}} = 180\,\text{MeV}$. The generated heat is 2 GW. By applying Eq. (8.23) one obtains $q(r) = \frac{2.32\times 2{,}000\times 180}{60{,}000\times 200} \times J_0\left(\frac{2.405}{1.85} \times r\right) = 0.096 \times J_0(1.3r)$; the result is in MW. It can be observed that the maximum heat flux generation occurs in the reactor's center where $J_0(0) = 1$ and has the value $\dot{q}_{\max} = 96\,\text{kW}$.

Equation (8.23) can be rewritten in terms of normalized heat flux value $\hat{q} = \dot{q}(r)/\dot{q}_{\max}$ against the normalized radius defined by $\hat{r} = r/R_{\text{r}}$. The variation is the same as that of the Bessel function $\hat{q} = J_0(\hat{r})$, where

$$\dot{q}_{\max} = 2.32\frac{\dot{Q}_{\text{out}}}{n} \times \frac{e_{\text{g}}}{e_{\text{in}}}. \tag{8.24}$$

The maximum volumetric heat generation that occurs in the reactor axis is given by the following formula from Lamarsh and Baratta (2001):

$$\dot{q}'''_{\max} = \frac{\dot{q}(0)}{2hR_{\text{f}}^2}, \tag{8.25}$$

where R_{f} is the radius of the fuel rod.

Example

Assuming that the fuel rod radius in the example above is $R_{\text{f}} = 5\,\text{mm}$ and is clad with a Zircaloy shell of $t = 0.5\,\text{mm}$ thickness and the rod height is $h = 4\,\text{m}$, one can calculate the heat flux and the temperature of the cladding outer surface provided that the temperature in the core is given; assume that the core temperature is

$T_c = 2{,}200°C$. First one can calculate the volumetric heat generation in the axis with Eq. (8.25) and one obtains $\dot{q}'''_{max} = \frac{96}{2\times4\times\left(5\times10^{-3}\right)^2} = 480\,MW/m^3$. The energy balance over the fuel rod is written as $\dot{q} = \dot{q}'''_{max} \times \pi R_f^2 h = \dot{q}'' \times 2\pi(R_f + t)h$, where the LHS represents the heat generated in the rod and the RHS represents the heat flux exiting the lateral rod surface; $\dot{q}''$ is the heat flux at the outer cladding and its value is $\dot{q}'' = 109\,W/cm^2$. The thermal conductivity of the fuel is given as $k_f = 2\,W/mK$ and that of the cladding $k_c = 20\,W/mK$. If one denotes $T_{f,s}$ the temperature at the fuel rod surface and $\Delta T_f = T_c - T_{f,s}$ the difference of temperature between the rod core and the rod surface, then, from the equation of heat transfer by conduction for cylinders, one can easily obtain $\dot{q}'''_{max} \times \pi R_f^2 h = 4\pi h k_f \Delta T_f$, which results in $\Delta T_f = 1{,}500°C$. On the other hand, the heat transfer equation through the cladding shell is $\dot{q}'''_{max} \times \pi R_f^2 h = 2\pi h k_c \Delta T_c / \ln(1 + t/R_f)$; from it one obtains $\Delta T_c = 300°C$. From these results it follows that $T_{f,s} = 2{,}200 - 1{,}500 = 700°C$ and the temperature at the cladding surface is $T_{c,s} = 400°C$. Therefore, the temperature at which the heat transfer fluid is delivered by the nuclear reactor is estimated as $T_{out} = 350°C$. Assuming that the reactor is of the thermal type, 5% to 10% of the nuclear heat is transmitted to the moderator and is considered to be lost. Therefore, the energy efficiency based on Eq. (8.16) is $\eta = 90\% - 95\%$. The Carnot factor in this example is calculated as $1 - T_0/T_{out} = 1 - 300/650 = 0.54$. The exergy efficiency of the reactor is, according to Eq. (8.16), $\psi = \eta \times (1 - T_0/T_{out}) = 0.54\eta = 49 - 51\%$.

A brief comparison of nuclear heat with other thermal energy sources is presented in Table 8.5. The nuclear heat generators produce the most thermal power per unit of hardware volume. Coal and biomass combustion facilities are massive because they must include fuel handling facilities and large stacks; this decreases the thermal power generation per unit of hardware volume (or power density). The Carnot factor, and therefore the exergy associated with thermal sources produced by combustion and with concentrated solar radiation, are the highest; however, among them, only solar and biomass combustion are sustainable sources. Moreover, solar radiation is the sole source of thermal energy available at any location of the terrestrial surface. In contrast, geothermal energy is available at a limited number of geographic locations.

8.5 Nuclear Power Reactors

A number of nuclear reactors have been developed so far; we analyze here the most important of them. The CANDU (CANadian Deuterium Uranium) reactor uses natural uranium (UO_2) as the fuel and heavy water as the moderator and coolant, while the cladding is made of zircaloy. The heavy water absorbs fewer neutrons than light water, leaving enough of them to initiate novel reactions in the fuel bundles with natural (un-enriched) uranium. The principle of the CANDU reactor is presented in Fig. 8.8. The fuel is placed in tubes through which pressurized heavy

Table 8.5 Comparison of various thermal energy sources

Thermal source	Temperature (°C)	Carnot factor	Heat transfer medium	Greenhouse gas (GHG) emissions	Remarks
Nuclear heat	300–500	0.5–0.6	Liquid	Indirect: associated with reactor construction	Including all current technologies except gas-cooled reactors. Temperature is that of the heat transfer fluid. 50–60 MW/m^3.
	700–950	0.7–0.75	Gas		Gas cooled reactors (limited use: Japan and China). 2–14 MW/m^3.
Fossil fuel combustion	1,000–1,500	0.76–0.83	Flue gas	CO_2in flue gas; about	Thermal energy is recovered from flue gas to drive process heating or steam generation with possible electric power production in setting with or without cogeneration. Coal and biomass combustion facilities are the most massive among all.
Biomass combustion	500–1,500	0.62–0.83	Flue gas	0.5–1 tCO_2 emitted per kWh thermal	
Waste incineration	1,000–1,800	0.76–0.86	Flue gas		
Solar radiation	80–1,500	0.21–0.83	Fluid	GHG amounts associated with hardware manufacture	Include thermal solar panels for water heating and concentrated solar collectors.
Geothermal	80–300	0.21–0.5	Brine		Available only at some geographic locations.
Industrial waste heat	80–400	0.21–0.57	Fluid		Many industries reject heat in the form of hot fluids or steam that can be recovered and utilized.

water coolant is flown. The coolant transfers the nuclear heat to a heat exchanger, which is typically a steam generator; the produced heat comes at about 350°C.

Outside the pressure tubes there is the moderator consisting of a heavy water bath in which the tubes are submerged. The pressure in the moderator is around 1 bar. The moderator is continuously cooled and the heat is ejected at about 80°C. The fuel rods can be replaced or extracted independently at any time through some special mechanisms. In the moderator bath there are placed a series of graphite rods (not shown) with the role of attenuating the neutron flux, to control the reaction rate and criticality.

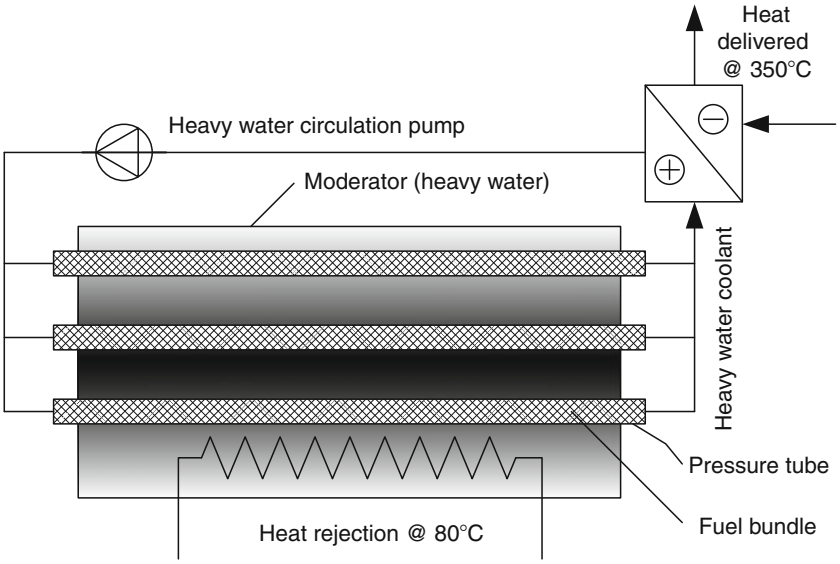

Fig. 8.8 The principle of operation of the CANDU reactor

The most used in reactor in the United States is the pressurized water reactor (PWR), which found application to power generation and propulsion of marine vessels like submarines, aircraft carriers, and ice breakers. A simplified diagram of the PWR is illustrated in Fig. 8.9 and comprises the fuel bundles, the moderator vessel, the pressurized vessel, the heat exchanger (steam generator), and the coolant pump.

The PWR uses slightly enriched uranium in the form of UO_2 containing about 3% $^{235}_{92}U$ and placed in tubes of zircaloy and sunk in light water, which plays the role of moderator. The fuel and the moderator are kept in a pressurized vessel designed to operate at about 155 bar, the pressure at which water boils at 344°C. However, in the reactor (pressure) vessel water is heated from 275° to 315°C and always remains in a liquid state. In fact, in order to enhance the heat transfer between the fuel rods and the water, the flow is set such that subcooled nucleate boiling occurs at the surface of the rods; the small vapor bubbles formed are immediately absorbed into the subcooled liquid water. Overall, the operation is very stable. The light water is an excellent moderator. In order to control the reaction rate, additional moderators are used in the form of movable bars made from boron carbide or Ag–In–Cd.

The pressure is maintained through a pressure vessel equipped with submerged electric heaters meant to maintain a vapor pressure of 155 bar; the vapor is located at the top of the pressurizer, while its bottom is always full of subcooled liquid. A heat exchanger is used to deliver the nuclear heat from the primary circuit to a secondary circuit, which may be a steam generator that runs a turbine that commonly turns a generator or propels a marine vehicle. The generated steam has typically a temperature of 275°C and a pressure of 60 bar.

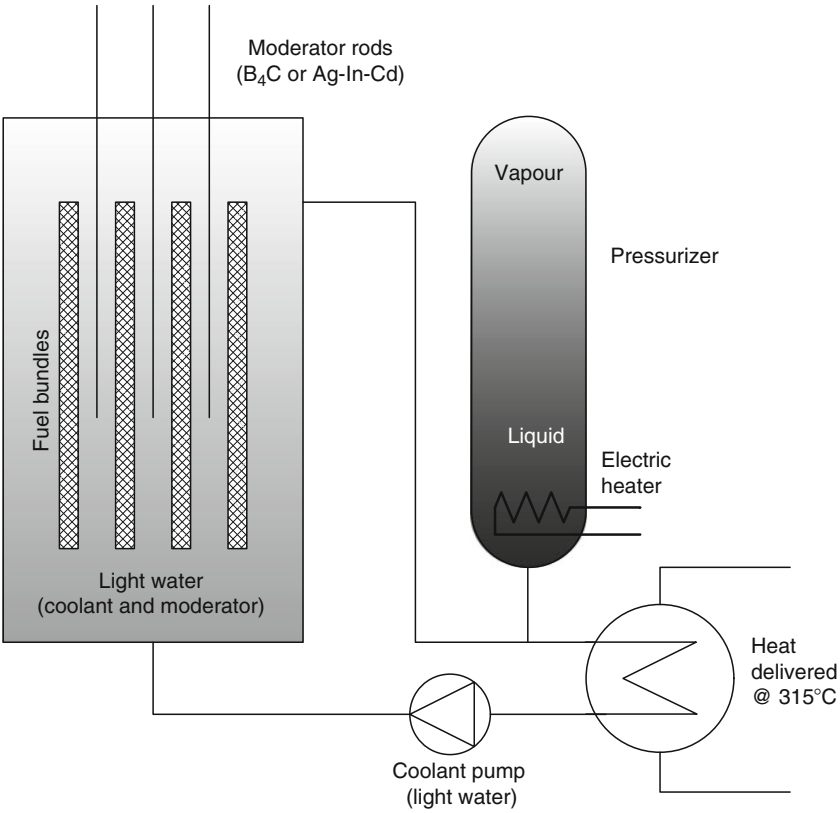

Fig. 8.9 Simplified diagram of the pressurized water nuclear reactor

Similar to the PWR, the boiling water reactor (BWR) uses water as the moderator and coolant at the same time, with the difference being that the reactor produces saturated steam. There are no primary and secondary circuits as for the PWR; simply, subcooled water enters the reactor where it is preheated and boiled to saturation. Typically, the pressure in the BWR is of 75 bar and the corresponding temperatures 285°C. The reactor has a special construction that allows for a stable boiling process. When water enters in the reactor, it is first guided into a downcomer where it is preheated. It rises thereafter and flows around the vertical fuel rods though the reactor core region. The resulting two-phase flow, having ~15% vapor quality, is directed toward a cyclone separator and steam dryer at the top of the reactor, where the saturated steam is collected. In general layout, the reactor is kept in a containment structure, while the steam turbine, the condenser, and the pumps are placed at the exterior.

Figure 8.10 presents the concept of a very high temperature gas-cooled reactor (VHTR). Running processes at temperatures as high as 1,000°C imposes important

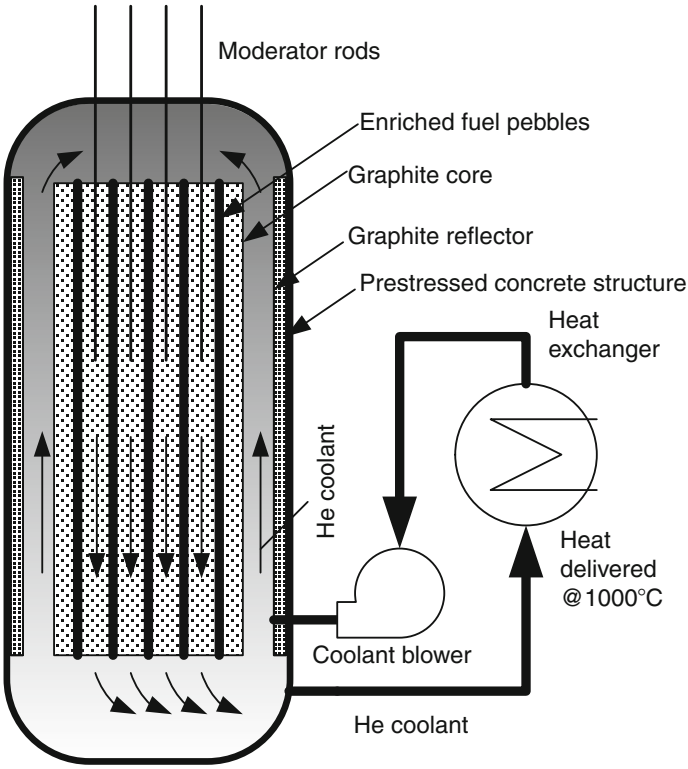

Fig. 8.10 Very high temperature gas-cooled reactor concept

safety requirements on the materials. A way to reduce mechanical stress on the construction materials is by limiting the operating pressure. The VHTR operates at a pressure close to the ambient. The coolant used is helium, which has a very stable molecule. Moreover, helium does not become radioactive when exposed to neutron radiation, because the helium nucleus is very stable.

The fuel used by VHTR consists of uranium 235 highly enriched up to ~93% and is formed as spherical pebbles of either uranium dioxide or uranium carbide. The moderator is in the form of a graphite block and the control rods are made of boron carbide (B_4C). The reactor vessel is made of prestressed concrete. The nuclear heat carried by the coolant is made available for use at 1,000°C. High-temperature reactors were tested and used in limited scale; their concept is presently reconsidered as part of the future generation IV reactors, which include a set of theoretical designs of reactors currently in the process of research and development. It is expected that the generation IV reactor will reach the commercialization phase in 2020 to 2030.

Breeder reactors use either thorium 232 or natural uranium as the primary fuel; as discussed above, these fuels are called "fertile" materials. When bombarded with neutrons, the fertile materials transform into fissionable fuel through subsequent beta decay reactions. Uranium 238 can be made fissile in about 2.5 days, while the thorium can be made fissile after about 3 weeks. The process of transforming fertile materials into fissile fuels is known as breeding. As mentioned above, it is noted that natural uranium is suitable for fast breeding; special reactors—called fast breeding reactors (FBR)—were designed for such a process. In an FBR, about 2.7 neutrons are generated per neutron absorbed in the fuel to produce fission. The difference, that is, 1.7 neutrons, is used for breeding. On the other extreme, the thorium breeding is slower; this process is called thermal breeding.

The neutrons must be slowed down for better use for breeding of thorium. In a thermal breeding reactor, 2.3 neutrons are generated per neutron producing fission; thus, 1.3 neutrons are meant for breeding. The typical fast breeding reactor design uses liquid sodium as a coolant and is of two types: pool design or loop design. The pool design has the primary heat exchanger immersed in the reactor vessel. The fuel of FBR is a mixture of about 80% natural uranium dioxide and 20% plutonium dioxide. No moderator is needed in the FBR. The advanced heavy water reactor (AWHR) is a design of generation IV of the thermal breeding kind of reactor. This reactor, being thermal, must be moderated; its moderation is made through heavy water in which vertical pressure tubes are immersed. The coolant is light water circulated through a thermo-siphon arrangement that includes a large reservoir of water placed above the reactor. The moderator system includes carbon rods for reaction control.

8.6 Nuclear Fuels and Reserves

Uranium fuel is extracted from uranium ore—uranite—which may contain up to 0.3% uranium oxide. Most of the resources of uranite are found in Australia, with 23% of global share. The map shown in Fig. 8.11 has been drawn based on the statistical data published recently by the World Nuclear Association (WNA 2010) concerning the distribution of the world's nuclear resources by country. After Australia, Kazakhstan follows with 15%, Russia with 10%, South Africa and Canada with 8%, the U.S. with 6%, Brazil, Namibia, and Niger with 5%, Ukraine with 4%, Jordan and Uzbekistan with 2%, and India with 1%.

Chapter 2 discussed the general outlook of the world's energy resource, among which the nuclear resource was included. Apart from uranite, thorium mineral can be used to produce fissionable uranium, as explained in the Section 8.3.4. Thorium is more abundant on the earth as uranium. The most thorium resources are in Australia with 25% of global share followed by India with 24%, Norway with 14%, the U.S. with 13%, Canada with 8%, and other countries with 16%. The thorium-based fissionable fuel cycle and the associated reactors are technologies currently in development.

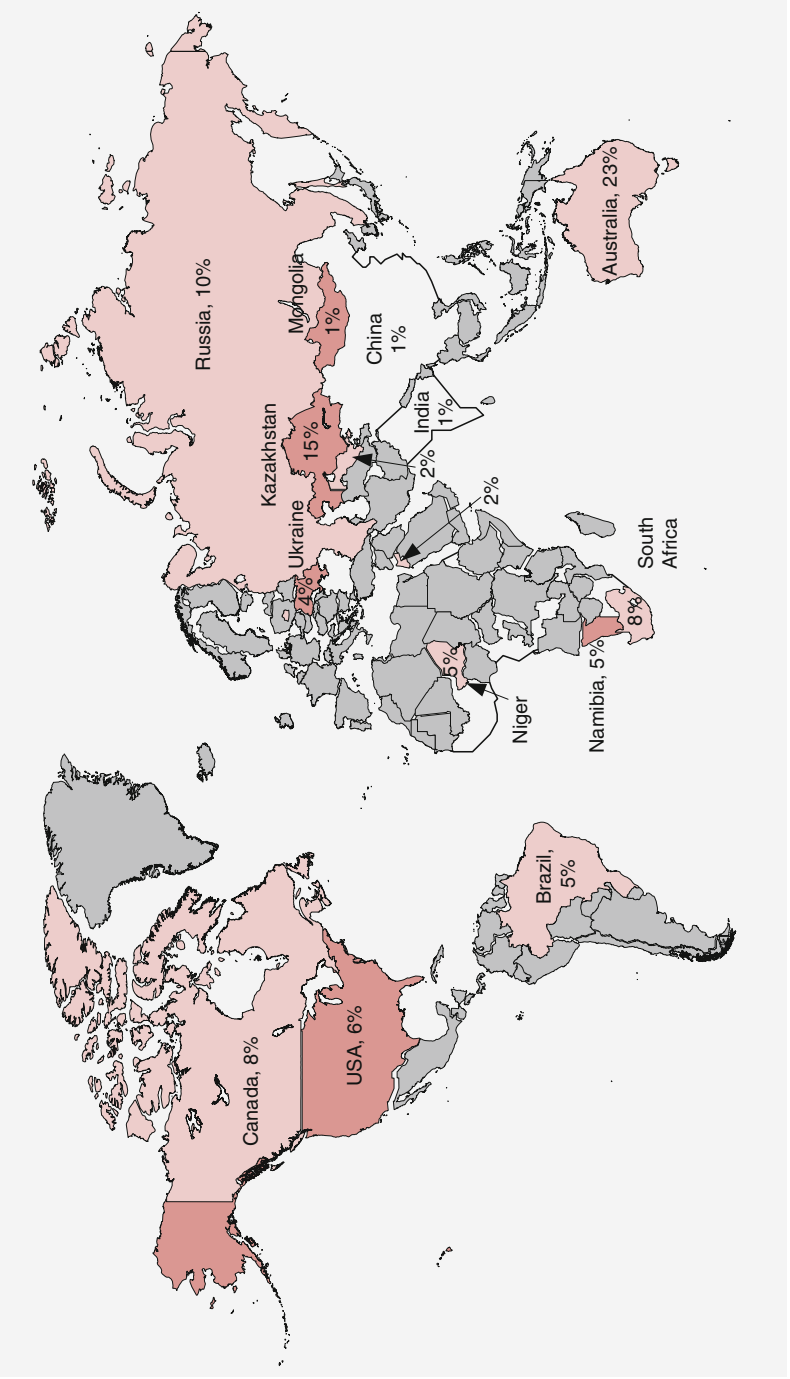

Fig. 8.11 Distribution of uranium ore resources throughout the world [data from WNA (2010)]

8.7 Nuclear Fuel Cycle and Enrichment Process

Processing and use of nuclear materials covers a number of steps, usually known as the fuel cycle. The general layout of the fuel cycle is presented in Fig. 8.12 as adapted from Bodansky (2004). The first step is mining, which refers to the extraction of the ore. Practically all primary nuclear material used throughout the world is uranium, even though some limited applications may use thorium; for the future, thorium is foreseen as the principal material to be extracted by mining. We will discuss here the uranium cycle only.

The processing steps of the uranium ore include milling and uranium extraction by chemical leaching, and results in uranium cake, which is the rough commercialized form of uranium fuel containing triuranium octaoxide (U_3O_8). The further production depends on the kind of nuclear reactor to which uranium is addressed. If enrichment is needed, then the triuranium octaoxide is converted into uranium hexafluoride, which further can be processed to increase the amount of uranium 235. If enrichment is not needed (e.g., as for CANDU reactors), the triuranium octaoxide is converted into uranium dioxide (UO_2), which can be fed directly to CANDU reactors. For reactors such as light water reactors the uranium 235 present in UF_6 is enriched up to 3.5% through isotope separation.

In some special cases, more enrichment is necessary. To enrich uranium it must be in the gas form of UF_6. This is called conversion. First, the yellow cake is converted into uranium dioxide through a heating process. Then, anhydrous hydrofluoric acid is used to make UF_4. Next, the UF_4 is mixed with fluorine gas to make uranium hexafluoride. This liquid is stored in steel drums and crystallized. These conversion steps are illustrated graphically in Fig. 8.13.

Further processing includes molding the uranium fuel into pellet form. After the fuel is used, it is discharged from the reactor and stored in interim locations. Further, the used uranium is transported to disposal places for permanent storage, or reused, depending on the case. For breeding reactors, the uranium fuel is always recycled. In such cases, the fuel is reprocessed to extract the fertile and the fissionable isotopes, which then are transported to production places to obtain new fuel pellets. The materials remaining after reprocessing can be processed even more by recovering valuable isotopes for other uses.

8.8 Nuclear Safety and Waste Disposal

So far there have been no observed human health hazards caused by nuclear wastes, but the potential for radioactive contamination does exist. In nuclear waste, there are many radioactive isotopes and transuranic elements that have an extremely long half-time. Some of these elements are neptunium, plutonium, tectenium, and iodine. Keeping such elements for a long time implies vitrification or calcination,

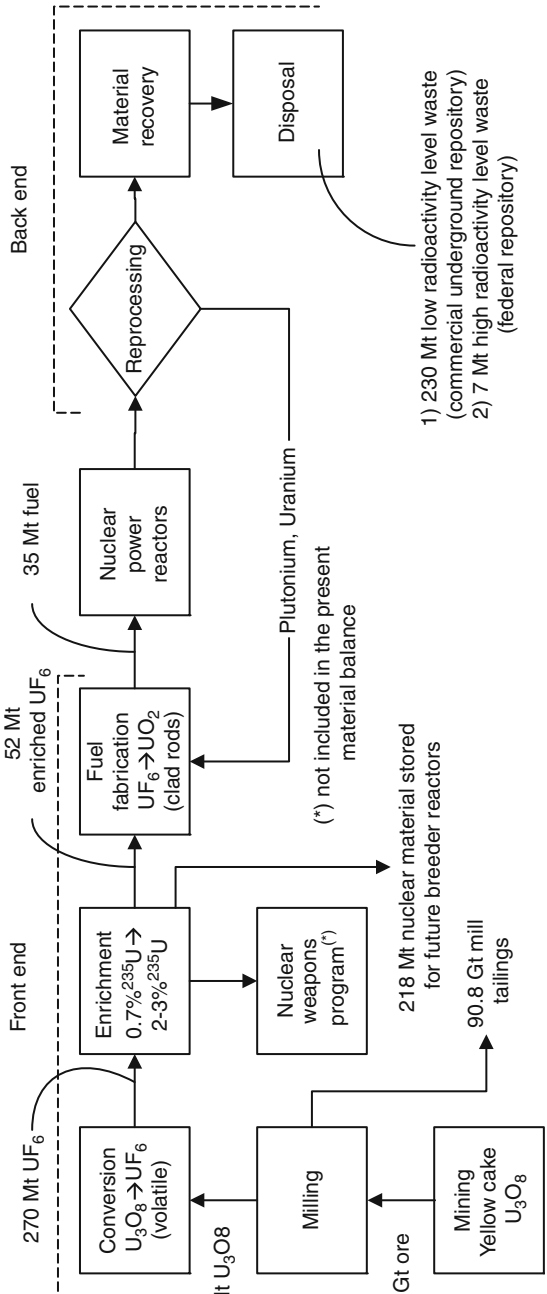

Fig. 8.12 Nuclear fuel cycle [modified from Bodansky (2004)]

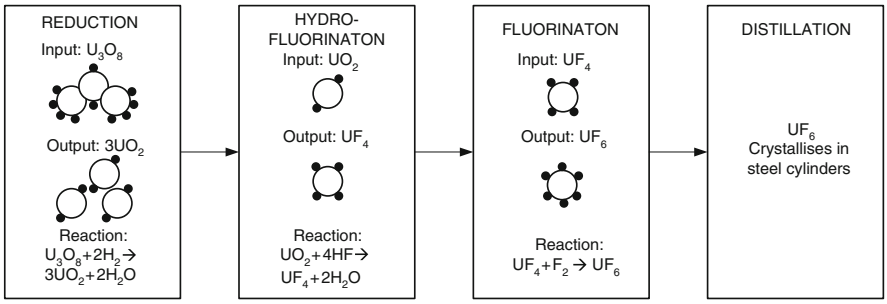

Fig. 8.13 The process of "conversion" to produce enriched uranium fuel

which embeds them in an amorphous matter with which they do not react for a long period of time. After packing well, the waste is deposited in long-term geological storage locations excavated in the form of tunnels in pits at more than 1,000 m below the earth's surface. Nuclear wastes can be categorized into three classes:

- Low-level waste comprises the residual radioactive material from medical and industrial facilities that use radionuclides for various processes involving, for example, gamma or X-ray generation. Some of the radioactive material disposed by other nuclear facilities is also a low-level waste.
- High-level waste is generated during the nuclear fuel cycle and consists of solid and liquid material that is highly radioactive.
- Transuranic waste comprises radioactive materials with decay times longer than 20 years that emit alpha particles with low intensity.

For all three categories, the safe disposal of high-level waste is the most important. These wastes are stored in underground repositories build in several places throughout the world, one of them being in Yucca Mountain, Colorado, which is planned to accommodate 70 kt of nuclear waste. The countries that have national plans for nuclear waste repositories are the following:

- United States—planned to be completed in 2010, storing the waste in tuff host rock in Yucca Mountain
- Finland—to be completed in 2020, storing the waste in granite host rock at Olkiluoto
- Germany—to be completed in 2020, with storage in salt, at Gorleben
- France—to be completed by 2020, with storage in clay and granite
- Canada—to be competed in 2025, with storage in granite
- Japan—to be competed by 2030, with storage in sedimentary rock and granite
- Switzerland—with a opening target of 2050, with storage in granite and clay
- Sweden—with a target of 2020, with storage in granite host rock

An interesting aspect is that the radiation emitted by nuclear waste generates heat. For example, the spent fuel from PWR reactors generates about 1.5 kW per ton of uranium in 10 years. This heat, in principle, can be used either to generate power with low-temperature differential heat engines or for heating applications.

However, there is a lack of confidence regarding the safety of using waste cooling systems as heat sources, and such a solution has not been implemented.

There are various safety measures that must be taken to avoid direct exposure of humans and the environment to radiation emitted by nuclear waste. Shielding is applied wherever possible. Also, the spent fuel assemblies are placed in cooling pools and transferred into shielded protective canisters. The hazard that possibly can be created by the nuclear waste is the dose that can be received through inhalation of escaped radionuclides. The maximum dose rate that a person can take is 20 to 50 millisieverts (mSv) per annum, which is the equivalent dose to tissue calculated based on the absorbed radiation dose and factors dependent on the radiation type and other relevant parameters, such that the quantity represents a quantitative measure of radiation effects; note that $1\ \mathrm{Sv} = 1\ \mathrm{m^2 s^{-2}}$.

Safety issues associated with nuclear activity were treated with major importance since the early years when proper techniques for manipulating radioactive materials in laboratories were developed. Many minor laboratory and a few major nuclear reactor accidents (viz. Chernobyl) helped in gaining experience with nuclear safety. Several safety standards are currently in practice.

The hazards from a reactor accident are of two kinds, namely core damage and large radiation release. The former can be caused by core melting and the latter by the failure of the radiation shields that are normally placed around the reactor's pressure vessel. Note that the potential reactor accidents fall also in two categories, namely criticality accidents (when the chain reaction builds up in an uncontrolled manner and can lead to explosions), and loss-of-coolant accidents (when the chain reaction is stopped but there is heat generated by the reactivity in the reactor core, which, if coolant is not circulated, leads to a temperature increase and fuel melting followed by structural damages and the possible escape of radioactive materials). With appropriate design these two kinds of accidents can be avoided.

There are many technical mechanisms designed to avoid criticality and loss-of-coolant accidents, including the so-called fuel temperature feedback through Doppler effect radiation broadening, in which the thermal neutron production rate is diminished, controlling the void fraction in boiling water reactors, using emergency core cooling systems, advanced containment structures for impeding the radionuclide escaping, and using pools of water or spraying systems to condense radionuclides in air. Reactor safety also includes sophisticated probability analysis methods for fault detection and risk assessment based on fault and event-tree methodologies. Various risks are considered in the analyses including seismic risk, core damage risk, and early containment failure risk.

8.9 Radiation Issues

Radiation exposure of human and biological species can produce serious damage that on the one hand can be lethal and on the other hand can produce very long-term effects, including genetic mutations and severe diseases. Radioactivity is a natural

phenomenon and all species are adapted to it. When the radiation dose absorbed by living systems overtakes a certain threshold, various negative effects occur. As briefly introduced in the above section, the radiation harm produced on a living tissue that absorbs radiation is measured in sieverts. The radiation quality factor used to calculate the equivalent dose in sieverts is 1 for X-rays and β-rays, 5 to 20 for neutron radiation, and 20 for alpha particle radiation. These figures indicate that neutron and alpha particle radiations are much more damaging than electromagnetic radiation associated with X-rays and β-rays. The most active radionuclide with respect to health issues is ^{239}Pu and the least ^{40}K. However, plutonium is practically nonexistent in the environment as compared with potassium 40, which appears to be the most abundant one.

The world average exposures to radionuclides expressed in dose equivalents in mSv per annum are as follows: 2.4 from natural sources, 0.43 from medical diagnostics, and 0.008 from all other sources including nuclear power reactors and nuclear weapons. Potassium 40 makes the largest contribution to the radiation dose in the human body. As can be deduced from these facts, the average contribution of radiation from nuclear power facilities is negligible to the general public compared with that originating from natural sources. However, in cases of nuclear accidents, the local radiation dose can be very high; nevertheless, from the recorded cases such contribution is not significant globally. For example, the Chernobyl accident translated to a global radiation increase of 0.002 mSv per annum. The situation is different in the case of some occupational exposures to radiation. In some activities, intensive exposure to radiation can occur regularly or incidentally. People who work in medical facilities, research laboratories, some industries, uranium mining, and fuel processing or at nuclear reactors are much more exposed than the general public. The typical exposure for these workers is, for example, about 6 mSv at nuclear power plants, 1.7 for airplane flight crews, and 1.9 for medical personal.

8.10 Applications of Nuclear Energy

There are mainly three applications of nuclear energy, namely electricity generation, marine vessel propulsion, and process heat generation. Electricity generation is the most representative application of nuclear energy. Using nuclear energy for process heat generation is presently a technology in the phase of research and development. In general, nuclear-generated heat can be used for hydrogen production or desalination, and many other uses are possible (e.g., petroleum extraction from oil sands).

Regarding electricity and hydrogen production, currently the generation VI nuclear reactors are in development that will be characterized by better fuel economy, better safety, and higher efficiency. In this generation of reactors, six models (three thermal and three fast reactors) are being promoted:

- Fast breeding reactors
  - Gas-cooled reactor, operating with helium as the coolant and thorium as the primary fuel, with a temperature of the delivered heat of over 850°C
  - Sodium-cooled reactor, operating at 550°C
  - Lead-cooled reactor, operating at temperatures up to 800°C
- Thermal reactors
  - Very high temperature reactor that uses helium as the coolant and can reach a temperature of 1,000°C
  - Supercritical water-cooled reactor, operating at about 600°C
  - Molten salt reactor that uses fluorine-based salts as the coolant and operates at 700° to 800°C

Many kinds of nuclear reactors are used for vehicle propulsion. In this case, the nuclear heat is converted into work with the help of a turbine that propels the vehicle. Using nuclear engines on submarines has essential advantages: the propulsion system does not require oxygen, but rather can be produced through sea water desalination and electrolysis; therefore, the crews reserves of oxygen and water are assured for the long term; moreover, the submarine can run at high speed for a long time without the need for refueling. Another application of nuclear propulsion is for an extraterrestrial spaceship. Several space missions used nuclear power to generate on-board electricity and help propulsion at the same time. One example is Pioneer 10, which was launched in 1972 to explore the planet Jupiter and that has operated since then.

8.10.1 Nuclear Power Production

Electric power generation with nuclear reactor is explained with the help of Fig. 8.14, which presents a simplified layout of a CANDU nuclear power plant. It consists of a nuclear reactor that generates heat that is used for steam generation in a Rankine power plant. In an actual implementation, the steam power plant is of the multistage kind, having several stages of expansion, multiple pumps, and heat exchangers. The high transfer fluid delivers heat at 300° to 330°C and is circulated at a high flow rate, typically about 11 t/s; on the other hand, steam is produced at a rate of 1 t/s. The cooling water that normally sources from a lake is circulated at 30 t/s.

The breakthrough of nuclear energy and exergy utilization—for a typical case in the CANDU nuclear power plants—is presented in Fig. 8.15. From the energy diagram Fig. 8.15a, it can be seen that from 100% energy input only 31% is converted into useful power. Regarding the exergy analysis, one can see from Fig. 8.15b that exergy efficiency is 61% and the most exergy losses occur in the turbine (15%) and steam generator (11%). Other exergy losses are 8% in feed water heaters, 3% in cooling water, and 2% in the condenser.

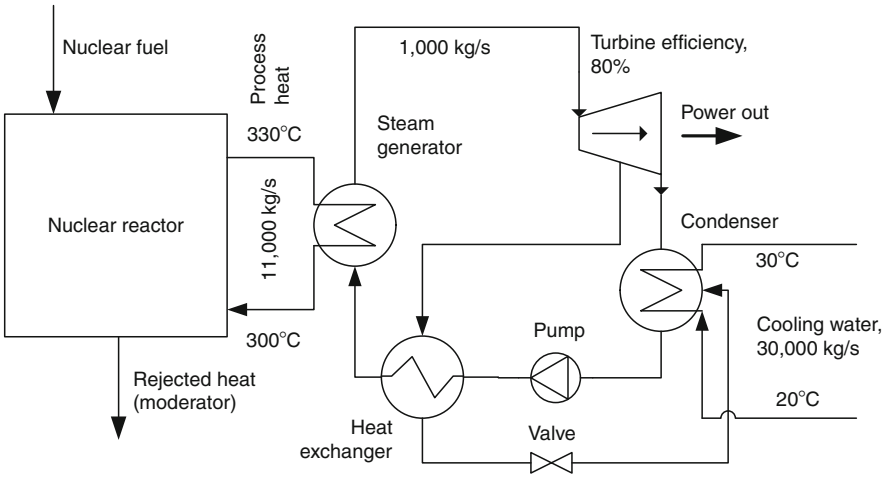

Fig. 8.14 Simplified layout of a CANDU power generation plant

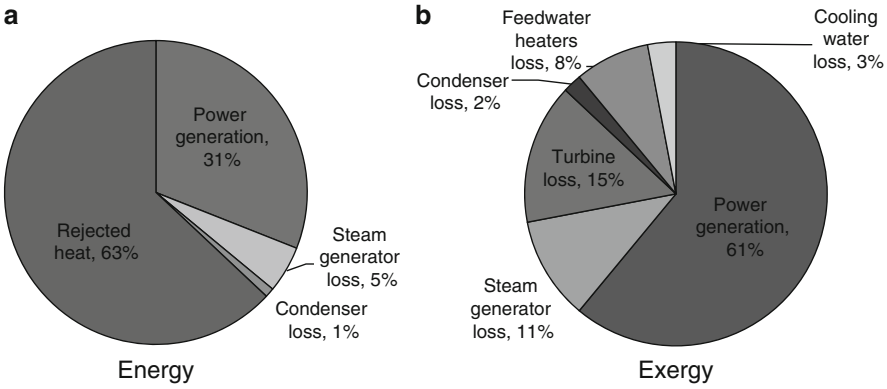

Fig. 8.15 Breakthrough of nuclear energy and exergy utilization in CANDU power plants [data from Rosen (1986)]

8.10.2 Nuclear Hydrogen Production

Converting nuclear energy to hydrogen fuel and oxygen by thermochemical water splitting is a promising sustainable alternative for the near future. In this respect, thermochemical cycles can be used. In these cycles, some chemical reactions and intermediate chemical compounds are manipulated to decompose the water molecule. As highlighted in some recent work—Zamfirescu et al. (2009a), Naterer et al. (2009), Orhan et al. (2010)—the Sandia National Laboratory and Japan Atomic Energy Agency have focused on the development of the sulfur–iodine water

splitting cycle, which requires about 900°C temperature heat input. Such a high temperature provokes some concerns about the safety of nuclear reactors.

Some novel inorganic separation membranes can be used to lower the temperature to 700°C and make the cycle more adaptable to various types of nuclear reactors. These include conventional light water reactors, high-temperature gas-cooled reactors, liquid metal–cooled fast reactors, the very high temperature reactor (VHTR), and the generation IV reactor design of Atomic Energy of Canada Ltd. (Torgerson et al. 2006), as well as the advanced high-temperature reactor (AHTR).

Another design option for generation of high-temperature heat is to couple nuclear reactors of the current generation with specially designed heat pumps that upgrade the source temperature. Solutions are discussed in a number of recent papers: Marmier and Füterer (2008), Zamfirescu et al. (2009a, b, 2010), and Granowskii et al. (2008). In principle, two kinds of heat pumps can be applied: thermomechanical and chemical. In thermomechanical heat pumps the temperature is raised by compression. After delivering the useful high-temperature heat, the pressurized working fluid of the heat pump can be expanded in a turbine that recovers a part of the work consumed for the compressor. The nuclear heat is used as a source for the heat pump. In the case of chemical heat pumps, a reversible chemical reaction is conducted. The direction of the reaction is changed by using the pressure swing. When the reaction is endothermic, it captures heat from the nuclear reactor. By reversing the reaction it becomes exothermic and is made to deliver heat at a higher temperature. An example of a chemical heat pump driven by nuclear reactors is that proposed by Granowskii et al. (2008) and is based by the reversible steam-methane reaction. The system is designed for the future generation of reactors such as the SCW-CANDU (supercritical water CANDU), which delivers steam at 600°C. Production of hydrogen by using nuclear energy is discussed in detail in Chapter 13.

8.11 Case Studies

8.11.1 Upgrading Nuclear Heat from Current Reactors to Generate Hydrogen

This case study analyzes the hydrogen/oxygen production efficiency and associated reduction of CO_2 emissions by coupling of current nuclear reactors with a copper–chlorine (Cu–Cl) thermochemical water splitting cycle. The study is based on thermodynamic analysis and considers that the water splitting plant is coupled with the nuclear reactor by using a heat pump. The type of the heat pump is not specified. Also, two possibilities of thermal coupling of the reactor and heat pump are studied: (1) the heat rejected at the moderator is recovered and used as the heat source for the heat pump, and (2) the reactor coolant delivers the heat to the heat pump. The Cu–Cl cycle has been selected here because the level of temperature it

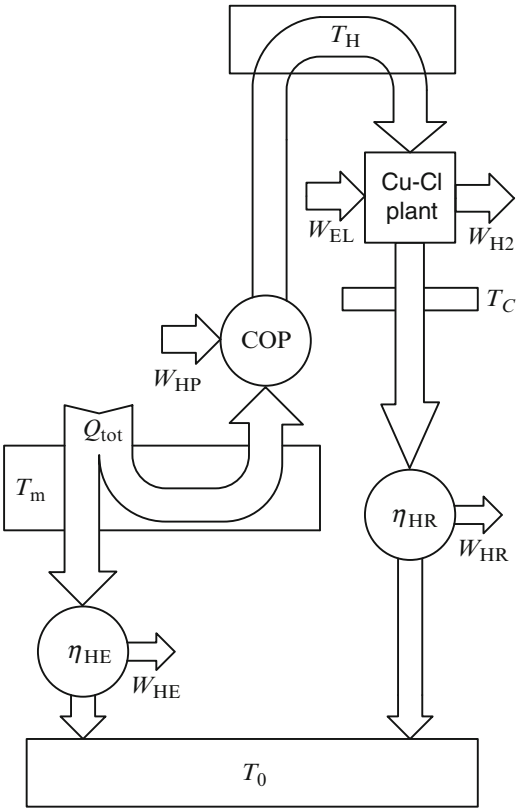

Fig. 8.16 Thermodynamic layout for hydrogen production with the Cu–Cl cycle coupled to a sustainable heat source (modified from Zamfirescu et al. 2009b)

requires is acceptably low with respect to other thermochemical water splitting cycles (~550°C).

A thermodynamic model for coupling the Cu–Cl cycle to a sustainable heat source is proposed in Fig. 8.16. This model comprises four components, namely the Cu–Cl plant, a heat pump COP (coefficient of performance), and two heat engines η_{HE} and η_{HR}. Also, the model assumes four temperature reservoirs as follows:

- Ambient temperature reservoir at T_0
- Sustainable heat source reservoir at $T_m > T_0$
- High-temperature reservoir that delivers useful heat to the Cu–Cl cycle at $T_H > T_m$
- Cooler temperature reservoir at which the Cu–Cl cycle ejects heat at T_C, with $T_H > T_C > T_0$

In a real setting, the temperatures T_H and T_C are not constant. However, to find the temperature for this analysis, which aims at determining the thermodynamic limits of the system, we introduce, as in Zamfirescu et al. (2009b) on which this case study is based, constant equivalent temperatures as $T_H = 430°C$ (source) and

$T_C = 320°C$ (sink). If T_m and T_0 are specified, one can calculate the COP and efficiency of the system components as follows:

$$\left.\begin{aligned} \text{COP} &= 1 + \varphi \frac{T_m}{T_H - T_m} \\ \eta_{HE} &= \varphi(1 - T_0/T_m) \\ \eta_{HR} &= \varphi(1 - T_0/T_C) \end{aligned}\right\}, \tag{8.26}$$

where temperatures are in Kelvin units and φ is a parameter ranging from 0 to 1 that expresses the abatement of the COP/efficiency from the Carnot value. For $\varphi = 0$, the COP takes its minimal value of 1, for $\varphi = 1$ the COP and the efficiency are maximum and equal to the Carnot limit.

Figure 8.16 shows the work requirements and the work produced by the various components of the system. The notation W_{HE} stands for the work produced by the heat engine that operates between the heat source and the environment, while the notation W_{HR} refers to the work obtained by conversion of the heat recovered from the Cu–Cl cycle. The work inputs are the heat pump W_{HP} and the electrical power W_{EL}. Among the work inputs and outputs indicated in the model from Fig. 8.11, the following relationship exists:

$$W_{HE} + W_{HR} = W_{HP} + W_{EL}. \tag{8.27}$$

The useful product of the system is found (in energy terms) in the form of the higher heating value of H_2, which is denoted in Fig. 8.11 with W_{H2}, $W_{H2} = \text{HHV}_{H2}$. Moreover, the output of the system can be expressed as follows:

$$E_{out} = E_{H2} + 0.5E_{O2}, \tag{8.28}$$

where the exergy E_{out} is given in kJ/mol H_2. The exergy of the products, in a molar ratio 1:2 (1 mol of hydrogen and a half mol of oxygen) are 236.12 kJ/mol H_2 and 3.92 kJ/mol O_2, yielding $E_{out} = 239$ kJ/mol H_2 (see Zamfirescu et al. 2009b for details).

The total heat required by the Cu–Cl cycle is as follows: $Q_H = 458\,\text{kJ/mol H}_2$, while the heat output is $Q_C = 294\,\text{kJ/mol H}_2$. The energy balance at the level of the sustainable heat reservoir is

$$Q_{tot} = \frac{W_{HE}}{\eta_{HE}} + Q_H - W_{HP}. \tag{8.29}$$

One also notes that the heat pump and heat-recovery heat engine work are given by

$$\left.\begin{aligned} W_{HP} &= Q_H/\text{COP} \\ W_{HR} &= Q_C \eta_{HR} \end{aligned}\right. . \tag{8.30}$$

Equations (8.26) to (8.30) form a closed system that allows for the determination of Q_{tot} for a given set of parameters including T_0, T_{m}, and φ. Also note that φ may have different values for the two heat engines and the heat pump. However, in the present analysis, we assume an average value for φ, and the same for the heat engines and heat pump. The determination of Q_{tot} makes possible the calculation of the energy (η) and exergy (ψ) efficiencies of the water-splitting process shown in Fig. 8.16, and it is defined as follows:

$$\left.\begin{aligned} \eta &= W_{\text{H2}}/Q_{\text{tot}} \\ \psi &= E_{\text{out}}/[Q_{\text{tot}}(1 - T_0/T_{\text{m}})] \end{aligned}\right\}. \tag{8.31}$$

The last aspect of the analysis regards the determination of greenhouse gas mitigation by hydrogen and oxygen production from water, using sustainable thermal energy as input. The energy efficiency given by Eq. (8.31) is useful in this regard because it indicates the amount of thermal energy input to split 1 mol of water.

Assume that for the production of 1 kg of hydrogen in industry, 10 kg of CO_2 are emitted into the atmosphere (this figure is the case for natural gas reforming, which is the lowest among all emissions). For producing 1 kg of oxygen, 86 g of CO_2 are emitted into the atmosphere. Using these figures, at least $\zeta = 70.7\,\text{kg}\,CO_2$ are released by industry into the atmosphere to produce hydrogen and oxygen equivalent to 1 GJ of energy content. The ζ is given in $\text{kg}\,CO_2/\text{GJ}_{\text{H2}}$ in the following equation:

$$\mathcal{M}_{\text{CO2}} = \zeta\eta, \left[\text{kg}CO_2/\text{GJ}_{\text{thermal}}^{\text{sustainable}}\right] \tag{8.32}$$

which can be derived for CO_2 mitigation, obtained if conventional industrial processes to produce hydrogen, and oxygen is replaced by systems such as that proposed in Fig. 8.16.

Consider now the ideal case of $\varphi = 1$, which is the same as considering that all machines involved in the water splitting system (the heat pump, and heat engines HE and HR) have maximum (Carnot) COP and efficiency, respectively. The heat sink temperature has been assumed as 20°C, which corresponds approximately to the average annual temperature of a lake. The temperature of the sustainable thermal energy source T_{m} has been varied between two limits, namely 40° and 350°C. The minimum value corresponds to the coupling of the Cu–Cl plant to the moderator temperature of a CANDU power plant. The upper bound corresponds to the case when a high-temperature source is the steam generated by an actual CANDU reactor.

These results are presented in Fig. 8.17 and show that the upper bound of energy efficiency of the overall process is over 60%, provided that the hot source temperature is at its highest value. For a fair evaluation of the Cu–Cl water splitting technology, its efficiency is compared on the same figure to that of water splitting through electrolysis. In this respect, one assumes the same heat reservoir at a temperature T_{m} and the same efficiency of the heat engine η_{HE} as that of a Cu–Cl system. In this case, the heat engine is used to produce electricity needed to drive the electrolysis process only.

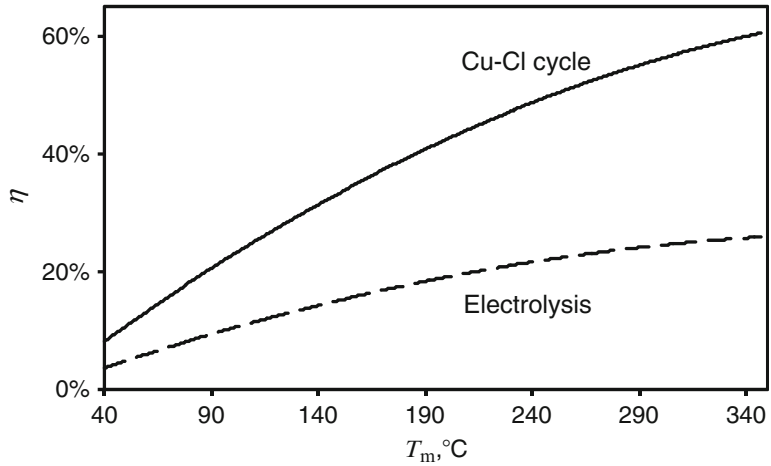

Fig. 8.17 Ideal hydrogen production efficiency from a sustainable thermal energy source with temperature T_m [modified from Zamfirescu et al. (2009b)]

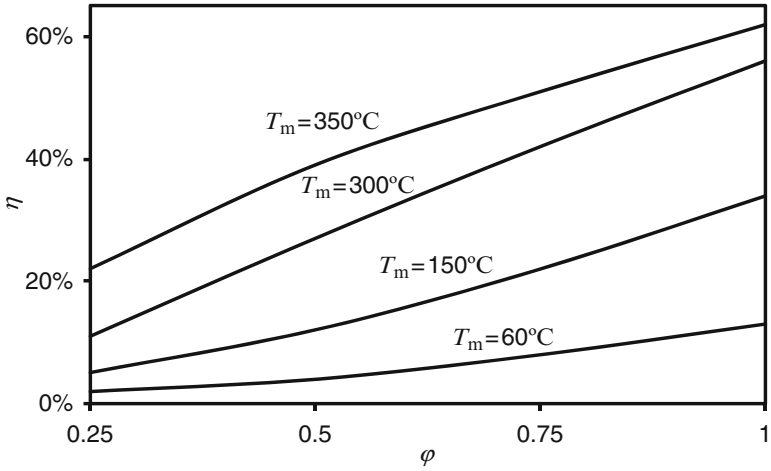

Fig. 8.18 Efficiency of the water splitting system in Fig. 8.16 with the abatement ϕ from the Carnot efficiency [modified from Zamfirescu et al. (2009b)]

From the heat engine efficiency, and assuming an electrolyzer efficiency of 50%, one obtains Fig. 8.17. This reveals that the efficiency of the Cu–Cl-based water splitting system is ideally 2 to 2.5 times higher than that of the electrolyzer driven by the same source of sustainable thermal energy.

If the parameter ϕ introduced in Eq. (8.26) is now included in the analysis, one obtains the plot presented in Fig. 8.18. This plot shows the variation of hydrogen production efficiency of the Cu–Cl cycle, with idealized constant temperature heat reservoirs, as a function of the abatement of heat engines/pump from the Carnot efficiency. For all cases, the efficiency of the system based on water electrolysis is

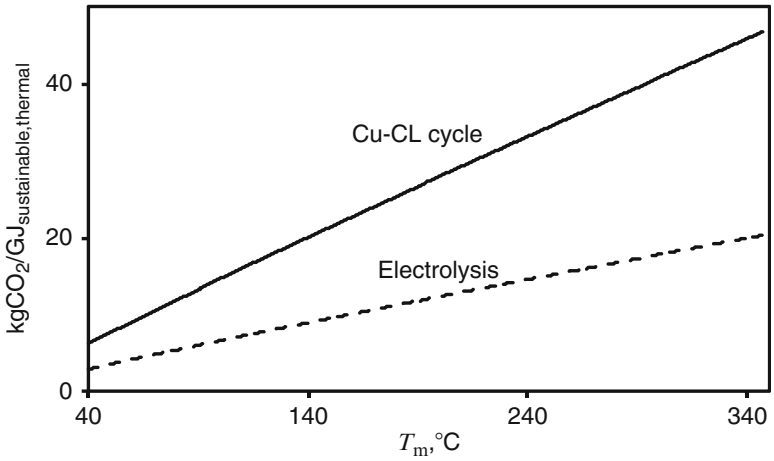

Fig. 8.19 Ideal maximum CO_2 mitigation of hydrogen and oxygen production by two benign technologies [modified from Zamfirescu et al. 2009b)]

2 to 2.5 times lower. For 50% abatement, one can expect a hydrogen production efficiency range from 4% to 39% if the temperature of the sustainable energy source varies from 60° to 350°C.

Next, by applying Eq. (8.32), one transposes the results from Fig. 8.17 in terms of CO_2 mitigation by the Cu–Cl and electrolyzer technologies, respectively. The profiles in Fig. 8.19 illustrate this result. The CO_2 mitigation potential ranges between 8 and ~45 kg CO_2 per GJ of sustainable thermal energy used in the process. This figure is 2.5 to 3 times higher than that obtained if electrolysis is applied. If a nuclear sustainable source is used to produce electricity at highest efficiency and electrolyze the water, the whole input energy-to-hydrogen efficiency is ~15%, and hence the CO_2 mitigation is ~11 kg CO_2/GJ. The same value is obtained by the Cu–Cl–based system if the thermal energy source is available at 70°C, which corresponds to coupling the cycle to the moderator of CANDU power plants. Regarding the electrolysis approach, the heat source must be available to at least 150°C in order to obtain the same mitigation. Assuming the abatement $\varphi = 50\%$, the corresponding CO_2 mitigation by the Cu–Cl–based system lies in the range of 3 to 27 $\mathrm{kg\,CO_2/GJ_{thermal}^{sustainable}}$.

8.11.2 Nuclear Heat for Desalination and Water Splitting

In this study, which is based on the work by Orhan et al. (2010), we analyze a coupling of the Cu–Cl cycle with a desalination plant for hydrogen production from nuclear energy and seawater. The supply of fresh water and energy carriers such as hydrogen raise societal concerns. To produce hydrogen by splitting the water molecule, one needs to supply fresh water to the hydrogen production facility.

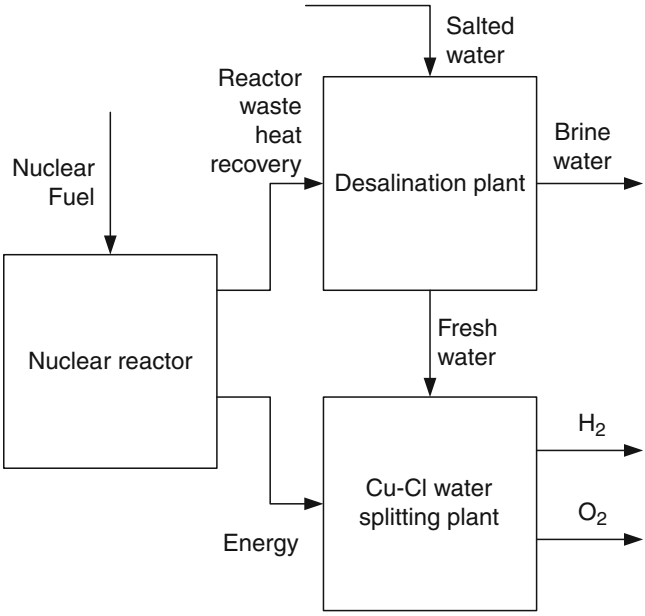

Fig. 8.20 Using waste energy from a nuclear reactor for the desalination process [modified from Orhan et al. (2010)]

Thus, to avoid causing one problem while solving another problem, hydrogen could be produced from seawater rather than limited fresh water sources. Nuclear energy is used to drive the process. Here we consider five configurations, in hopes of determining or helping to determine an optimum option to couple the Cu–Cl cycle with a desalination plant.

Configuration 1: This configuration couples the Cu–Cl cycle and a desalination plant using nuclear energy, as shown in Fig. 8.20. Salty water is input to the desalination plant, and salt is removed from the water using waste energy from the nuclear reactor moderator at 70° to 80°C. Fresh water supplied by the desalination plant is decomposed into hydrogen and oxygen by the Cu–Cl cycle driven by nuclear energy. Humidification–dehumidification (HD) technology is used for desalination.

Configuration 2: The thermal energy recovered from the Cu–Cl cycle is transferred to the desalination plant to remove salt from fresh water. As illustrated in Fig. 8.21, the desalination plant operates as a subsystem of the Cu–Cl cycle. Considering the overall system, only process/waste energy from the nuclear reactor and salty water enter the system. Hydrogen is produced, and oxygen and salt are by-products. A drawback to this configuration is the efficiency decrease (~3–5%) incurred by the Cu–Cl cycle since the recovered energy is used for the desalination process rather than within the cycle itself. But the Cu–Cu cycle is a subsection of the plant and, when the desalination plant and the Cu–Cl cycle are considered as a combined system, the efficiency is not affected significantly since the recovered energy is

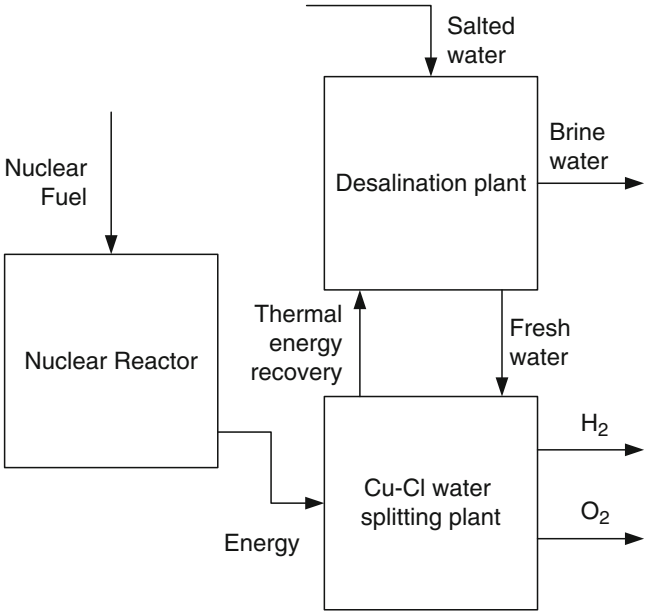

Fig. 8.21 Using recovered energy from the Cu–Cl plant [modified from Orhan et al. (2010)]

used within the overall system. The efficiency of the combined system (desalination plant and copper chlorine cycle) is about 0.4. Multiple effect desalination (MED) technology is used.

Configuration 3: The nuclear thermal energy is used directly in the desalination plant and to drive the hydrogen plant as indicated in Fig. 8.22. The thermal energy recovered in the Cu–Cl cycle is used within that cycle. A desalination method with high capacity and low production cost is used since high-grade energy is available. The multistage flash (MSF) desalination method is used.

Configuration 4: In addition to nuclear thermal energy, solar energy is used to complete the energy requirement for the process. The solar energy drives directly and completely the desalination plant, which supplies the hydrogen production plant with fresh water. Process and waste energy from a nuclear plant is used in the Cu–Cl cycle as indicated in Fig. 8.23. Vapor compression (VC) desalination technology is applied.

A drawback of this configuration is its dependence on the availability of solar energy, which is intermittent. Since the capacity of the desalination plant and hence the Cu–Cl cycle determines the required capacity of the solar collectors, the site for the Cu–Cl cycle and desalination plant are chosen carefully. However, since constraints likely exist regarding the setting of the nuclear reactor, this configuration is likely advantageous if the nuclear reactor is located in an area with high solar insolation. Otherwise, a desalination process with low-capacity and low inlet energy requirements is used. Reverse osmosis (RO) technology is applied.

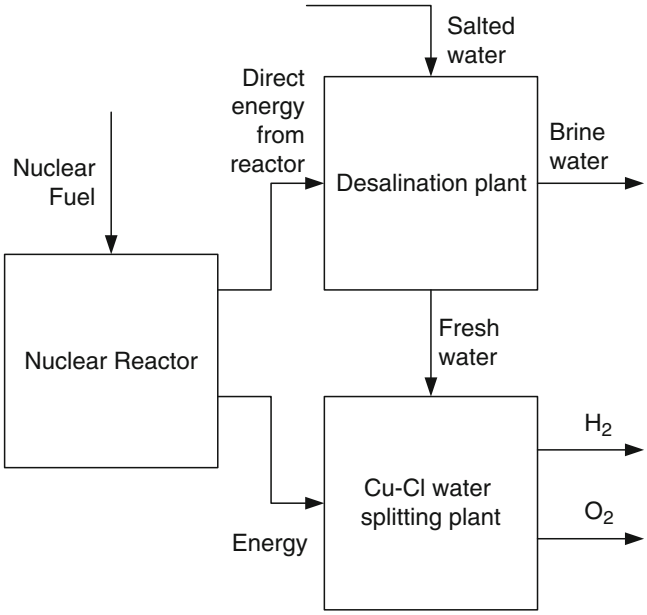

Fig. 8.22 Direct use of energy generated by the nuclear reactor for the desalination process [modified from Orhan et al. (2010)]

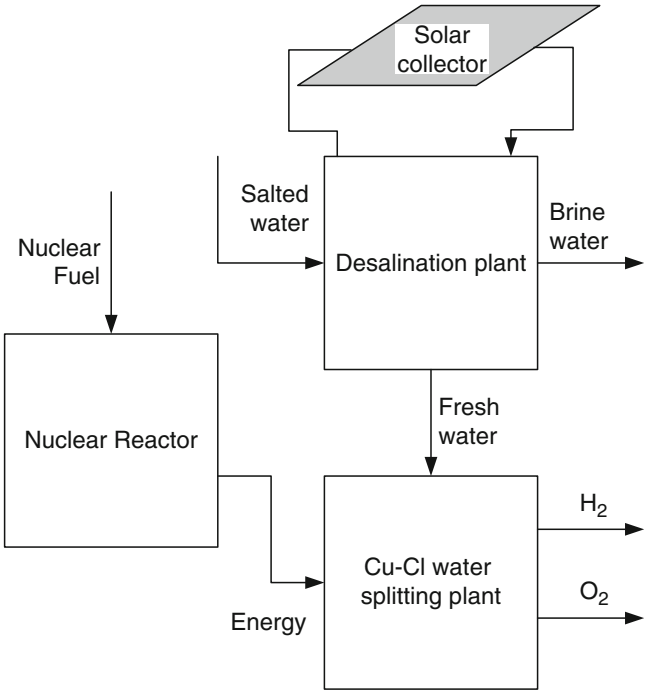

Fig. 8.23 Using solar energy for the desalination process [modified from Orhan et al. (2010)]

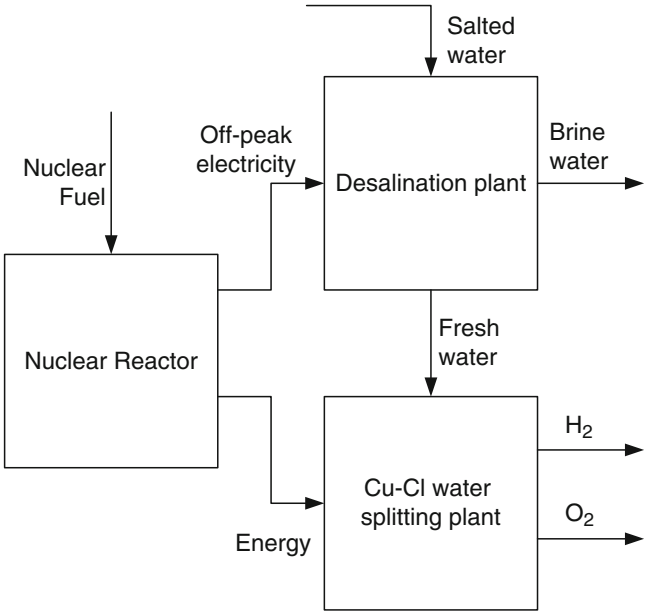

Fig. 8.24 Using off-peak electricity for the desalination process [modified from Orhan et al. (2010)]

Configuration 5: Off-peak electricity from a nuclear reactor is used to operate the desalination plant. When off-peak electricity is available, it is usually less expensive than peak electricity and thus is used by many industrial processes. Off-peak electricity can also be used to desalinate seawater and to produce hydrogen, and could be beneficial for the same reason. This configuration includes a Cu–Cl cycle coupled with a desalination plant driven by off-electricity (as in Fig. 8.24). In this case, efficient membrane processes are used since electrical energy is supplied.

The overall energy efficiency of the coupled system, η_{overall}, represents the fraction of energy supplied to produce hydrogen from salted water that is recovered in the energy content of H_2based on its lower heating value. The total energy required to produce hydrogen from salty water can be written as

$$Q_{\text{in,total}} = Q_{\text{in,Cu-Cl}} + Q_{\text{in,Desalination}} \tag{8.33}$$

and the overall efficiency is

$$\eta_{\text{overall}} = \text{LHV}/Q_{\text{in,total}}, \tag{8.34}$$

where LHVis the lower heating value of hydrogen.

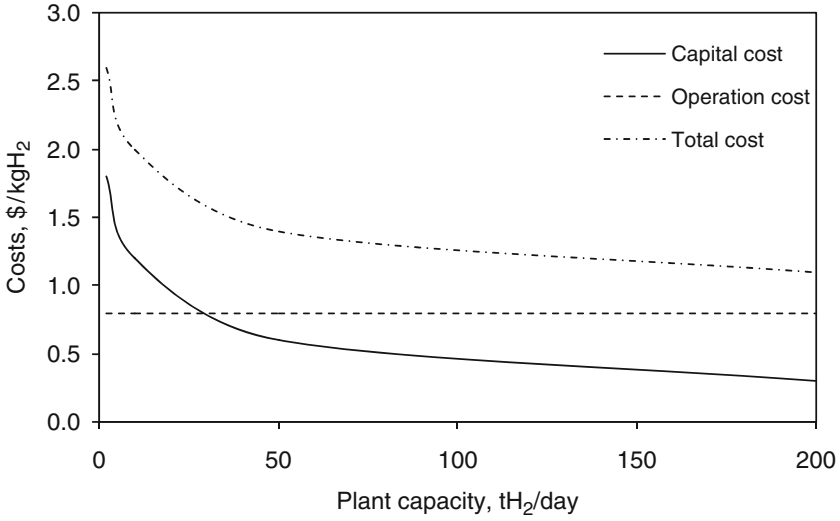

Fig. 8.25 Variation of costs with hydrogen production capacity of a Cu–Cl thermochemical water decomposition plant using fresh water [data from Orhan et al. (2010)]

The variation of costs with hydrogen production capacity of a Cu–Cl thermochemical plant is shown in Fig. 8.25. These costs are based on producing hydrogen from fresh water and do not include costs associated with desalination. As can be observed, the capital cost of the Cu–Cl cycle varies from \$0.3 to \$1.8/kg H_2 based on the capacity of the cycle. The capital cost of the cycle per unit hydrogen output is less for a larger capacity plant while the production cost (energy cost) remains constant at around 0.9 \$/kg H_2, mainly because the reaction energy (per unit hydrogen produced) of any chemical or physical reaction occurring in the Cu–Cl cycle does not change based on plant capacity. The total cost of hydrogen production is the sum of the capital cost, energy cost, and also some additional costs such as operating, storage, and distributions costs. In Fig. 8.25, two main cost items (capital and energy costs) are given along with the total cost to build a pilot plant of the Cu–Cl cycle, presumably at the commercialization stage of the cycle. The total cost varies from \$2 to \$3.5/kg H_2 in an inversely proportional relationship with plant capacity.

The total cost of the desalination plant is shown in Fig. 8.26. The least expensive desalination method is humidification–dehumidification (HD) at \$7.5/(kg H_2/day), which is considered in configuration 1, and the technology with the highest initial cost (\$11.9/(kg H_2/day)) is multistage flash desalination, which is used in configuration 3. The total costs of vapor compression (VC) and reverse osmosis (RO) appear to be the same at \$9.62/(kg H_2/day), while the capital cost of multiple effect desalination is \$11.7/(kg H_2/day).

The energy efficiencies of the Cu–Cl cycle, the desalination plant, and the overall system, including the Cu–Cl cycle and the desalination plant, are shown in Fig. 8.27.

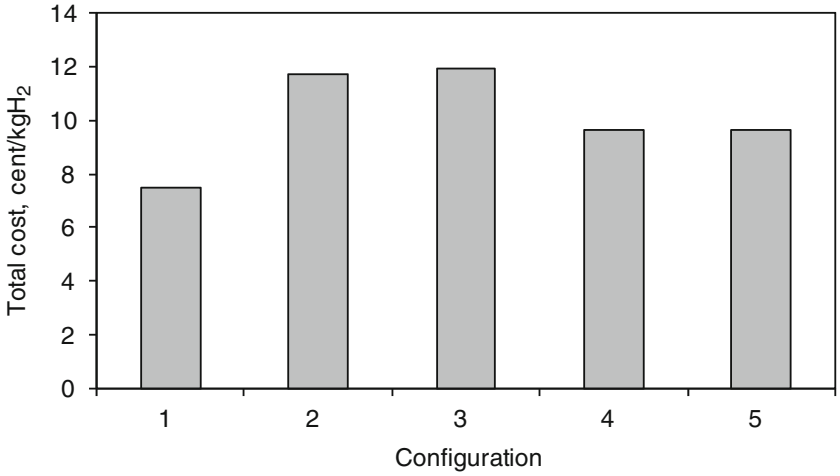

Fig. 8.26 Total cost of desalination [data from Orhan et al. (2010)]

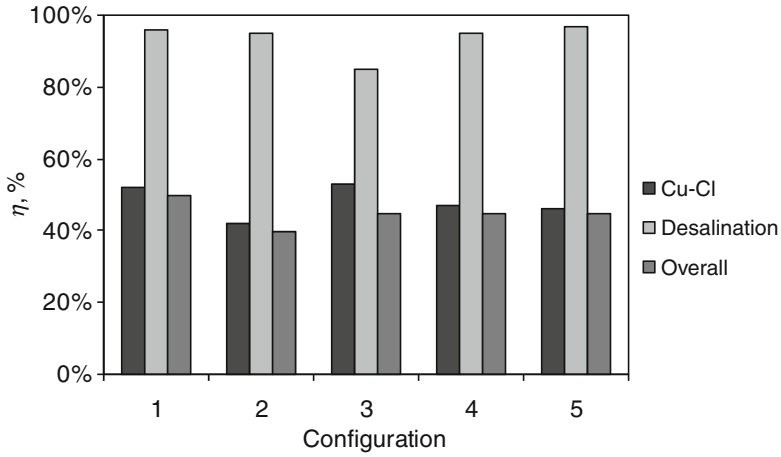

Fig. 8.27 Efficiency of nuclear driven hydrogen production and water desalination [data from Orhan et al. (2010)]

The effect of the Cu–Cl cycle on the overall system is dominant, as the desalination plant uses much less energy than the Cu–Cl cycle. Thus, the efficiency of the Cu–Cl cycle and the overall system are very similar for each case. Configuration 1 exhibits a higher efficiency, since waste heat from the nuclear reactor (which is assumed to be "free") is utilized in this option. In configuration 2, recovered heat from the Cu–Cl cycle is used for desalination instead of internally, within the cycle. Thus, the Cu–Cl cycle and the overall system operate at lower efficiencies, since the effect of the cycle is very important on the overall system.

8.12 Concluding Remarks

In this chapter, we discussed nuclear-based power and hydrogen generation options. The way of producing nuclear heat was explained in detail and as well as the possibility of quantifying the efficiency of nuclear heat generation on energy and on an exergy basis. Several technical aspects of nuclear reactors and their various applications were also discussed. Some examples demonstrated briefly the calculation of nuclear reactor heat generation and their efficiency in terms of useful heat delivered over the primary nuclear energy used. Both energy and exergy efficiency were introduced. Apart from the most common use of nuclear energy—for electric power production—there is major interest in nuclear energy as a source of process heat. The nuclear process heat can be used for hydrogen production, desalination, or other processes. It is also attractive to upgrade the temperature level of nuclear heat by using heat pumps. For safety reasons, the level of temperatures in the nuclear reactors are limited by material constraints. In order to generate a high-temperature process heat, it is reasonable to upgrade the temperature level of nuclear heat by using heat pumps. Two illustrative examples were also presented.

Nomenclature

A	Atomic mass (AMU)
c	Speed of light (m/s)
COP	Coefficient of performance
e	Specific energy (J/kg)
e_x	Specific energy (J/kg)
E	Energy (J)
ΔE_b	Binding energy (MeV)
h	Height (m)
HHV	Higher heating value (kJ/mol)
k	Thermal conductivity (W/mK)
LHV	Lower heating value (kJ/mol)
m	Mass (kg)
n	Number of elements
N	Number of atoms or particle density
q	Heat amount per unit of mass (J/kg)
r	Radial coordinate (m)
R	Radius (m)
t	Time (s)
T	Temperature (K)

Greek Letters

η Energy efficiency
ε Dissipation parameter
ψ Exergy efficiency
σ Cross section (cm^2)
ϕ Radiation particle flux
φ Carnot abatement

Subscripts

0 Initial or environment
c Cladding
EL Electric
f Fuel
H High
HE Heat engine
HP Heat pump
HR Heat recovery
in Input
L Low
m Medium
out Output

Superscripts

$\dot{()}$ Per unit of time (rate)
$()''$ Per unit of surface
$()'''$ Per unit of volume
$\hat{()}$ Dimensionless value

References

Bodansky D. 2004. Nuclear Energy: Principles, Practices and Prospects, 2nd ed. Springer, New York.

Granowskii M., Dincer I., Rosen M.A., Pioro I. 2008. Performance assessment of a combined system to link a supercritical water-cooled nuclear reactor and a thermochemical water splitting cycle for hydrogen production. *Energy Conversion and Management* 49:1873–1881.

Haynes W.M., ed. 2011. CRC Handbook of Chemistry and Physics, 91st ed. (Internet Version 2011). CRC Press/Taylor and Francis, Boca Raton, FL.

Kruger P. 2006. Alternative Energy Resources: The Quest for Sustainable Energy. John Wiley and Sons, Hoboken, NJ.
Lamarsh J.R., Baratta A.J. 2001. Introduction to Nuclear Engineering, 3rd ed. Prentice Hall, Upper Saddle River, NJ.
Marmier A., Füterer M.A. 2008. Nuclear powered heat pumps for near-term process heat applications. *Nuclear Engineering and Design* 238:2272–2284.
Murray R.L. 2009. Nuclear Energy: An Introduction to the Concepts, Systems and Applications of Nuclear Processes, 6th ed. Butterworth-Heinemann/Elsevier, Burlington, MA.
Naterer G., Suppiah S., Lewis M., Gabriel K., Rizvi G., Rosen M.A., Fowler M., Ikeda B.M., Kaye M.H., Lu L., Pioro I., Spekkens P., Tremaine P., Mostaghimi J., Avsec J., Jiang J., Easton E.B., Dincer I. 2009. Recent Canadian advances in nuclear-based hydrogen production and the thermochemical Cu-Cl cycle. *International Journal of Hydrogen Energy* 34:2901–2917.
Orhan M.F., Dincer I., Naterer G.F., Rosen M.A. 2010. Coupling of copper-chloride hybrid thermochemical water splitting cycle with a desalination plant for hydrogen production from nuclear energy. *International Journal of Hydrogen Energy* 35:1560–1574.
Rosen M.A. 1986. First and second law analyses of the Pickering Nuclear Generating Station. Proceedings of the Canadian Nuclear Association/Canadian Society Student Conference, Fredericton, New Brunswick.
Torgerson D.F., Shalby B.A., Pang P. 2006. CANDU technology for generation III+ and IV reactors. *Nuclear Engineering Design* 236:1565–1572.
WNA 2010. Australia's uranium. World Nuclear Association. Internet source http://www.world-nuclear.org/info/inf48.html (accessed on August 24, 2010).
Zamfirescu C., Dincer I., Naterer G.F. 2009a. Performance evaluation of organic and titanium based working fluids for high-temperature heat pumps. *Thermochimica Acta* 496:18–25.
Zamfirescu C., Naterer G.F., Dincer I. 2009b. Reducing greenhouse gas emissions by a copper-chlorine water splitting cycle driven by sustainable energy sources for hydrogen production. Global Conference on Global Warming. Istanbul July 5–9, paper #537.
Zamfirescu C., Naterer G.F., Dincer I. 2010. Novel CuCl vapor compression heat pump integrated with a water splitting plant. *Thermochimica Acta* 512:40–48.

Study Questions/Problems

8.1 Compare nuclear energy with other sources in terms of energy stored per unit of volume and per unit of mass.
8.2 Explain the magnitude of the nucleus radius from the perspective of coulomb and Yukawa forces.
8.3 An element has the atomic mass of 50 AMU. Determine the nucleus radius.
8.4 Define and explain binding energy.
8.5 Calculate the binding energy of uranium isotopes.
8.6 Determine the decay time of carbon 14 if $N/N_0 = 0.1$.
8.7 Explain the main types of decay reactions.
8.8 How is the available energy from uranium fuel determined?
8.9 How can one estimate the available energy from nuclear fusion?
8.10 Explain how a nuclear reaction can be controlled.
8.11 Define the energy and exergy efficiency of nuclear thermal energy generation.
8.12 Define the term *cross section*.

8.13 A reactor comprises $n = 45{,}000$ cylindrical fuel assemblies distributed over a circular cross section of the reactor with the radius of $R_r = 2\,m$. The average energy generated per mol of fissionable material in this configuration is $e_g = 200\,MeV$. The generated heat is 3 GW. Calculate the heat generation at a distance r from the fuel rod axis and the maximum heat flux.

8.14 The fuel rod radius in the example above is $R_f = 7\,mm$and is clad with a zircaloy shell of $t = 0.7$ mm thickness and the rod height is $h = 4.7\,m$. Assume the core temperature is $T_c = 2{,}500°C$. Calculate the heat flux and the temperature of the cladding outer surface.

8.15 Describe the principle of pressurized water reactor and that of boiling water reactor and state the differences between them.

8.16 Describe the CANDU reactor and explain the role of heavy water.

8.17 List the three top countries having uranium fuel reserves.

8.18 What do you understand about the process of conversion?

8.19 Comment on nuclear safety and waste disposal.

8.20 Define the unit of measure "sievert."

8.21 Consider the simplified diagram of a CANDU power reactor as in Fig. 8.14. Make reasonable assumptions and calculate the power cycle and determine the energy and exergy efficiency of nuclear power production.

8.22 What is the advantage of nuclear hydrogen production?

8.23 Consider the diagram from Fig. 8.16. Calculate the energy and exergy efficiency of hydrogen production if the Carnot abatement of the heat engines is 50% and that of the heat pump is 25%. Follow the reasoning from case study 8.11.1.

8.24 Take one of the configurations considered in case study 8.11.2 and make your own calculations to determine the system efficiency.

Chapter 9
Renewable Energies

9.1 Introduction

As mentioned in Chapter 2, there are a number of fundamental sources of energy on earth, such as solar radiation, geothermal heat, and earth spinning combined with gravitational forces of the moon–Earth–sun planetary system. These kinds of energy sources are said to be renewable in the sense that they are never depleted. In contrast, other energy resources, such as fossil fuels (coal, natural gas, petroleum) and nuclear fuels (uranium, thorium), are nonrenewable and thus limited. Among the fundamental energy sources, solar energy is the only one that manifests in a multitude of direct and indirect forms on earth. The indirect forms of solar energy also have the attribute of being renewable; they are wind, waves, hydro energy, ocean thermal energy, and biomass energy. Figure 9.1 classifies the renewable energies.

Common to all renewable energies are these features: they are intermittent, fluctuant in intensity, and regionally or globally available. For example, solar energy is globally available (at every point of the earth's surface), but intermittent—it manifests during daytime between sunrise and sunset; geothermal energy is available locally, that is only in some regions of the earth, such as close to a volcano or to places with more intensive tectonic activity. Wind energy is mostly available over plains or open waters such as large lakes and ocean shores; this energy occurs intermittently, being strong in some seasons or not manifesting at all for some period of times. Tides occur along some ocean shores and are intermittent in nature.

Due to these intermittent-fluctuating and local features, special engineered systems must be devised to harvest and convert the renewable energies into more useful forms. Moreover, energy storage systems are applied to smooth the fluctuation in the primary source and to make the energy available, when possible, at all times.

Recall that in Chapter 2 the outlook for primary energy source availability on earth was analyzed, among which renewables are a part. In this chapter, the renewable energy features are analyzed in more detail, and the systems used to harvest and convert these energies are presented. In general, the aim of renewable energy systems is ultimately to convert these energies into commodities such as electric energy, thermal energy, chemical energy (stored in the form of fuels),

İ. Dinçer and C. Zamfirescu, *Sustainable Energy Systems and Applications*,
DOI 10.1007/978-0-387-95861-3_9,

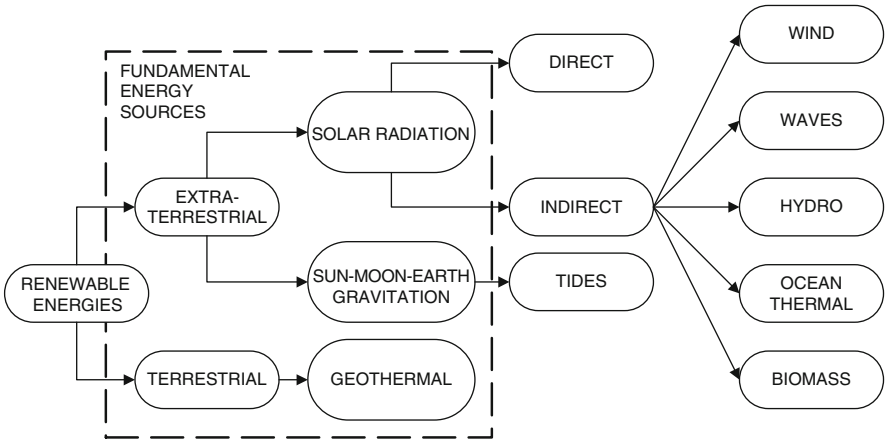

Fig. 9.1 Classification of renewable energies

potential energy (e.g., hydro energy), mechanical energy (e.g., compressed air energy), or biochemical energy (e.g., foods). Each kind of energy is discussed in detail in this chapter, together with the associated systems to convert, store, and use it.

9.2 Solar Energy

Figure 2.3 in Chapter 2 shows that from the total energy of the extraterrestrial solar radiation incident on earth's troposphere, 43% is direct beam radiation, 22% is hydro energy, 0.21% is wind energy, 0.02% is consumed by photosynthesis, and some minute percent is consumed by wave energy; the rest is dissipated into the atmosphere in other ways or reflected back in the extraterrestrial space. Therefore, the largest percent of solar radiation available for conversion on earth is direct beam radiation. This section analyzes especially direct beam radiation and its conversion into electricity and heat. However, some issues regarding diffuse radiation are also considered as they are important in solar energy conversion in many instances.

The basic conversion paths for converting direct solar radiation into other useful forms through engineered systems and devices are illustrated in Fig. 9.2. In principle, direct solar radiation can be converted using special "engineered" devices directly into electrical energy, thermal energy, chemical energy, biochemical energy, or it can be used "unconverted" as photonic energy. In the last form, solar energy is used as light—as the visible spectrum of solar radiation illuminates the earth's surface during the day.

When converted directly to electrical energy (e.g., through photovoltaic panels or other devices) solar energy can be transmitted to the electric grid, can be directly consumed, or can be stored (either as electric charge or by other mean of storing electric energy in other forms, viz. electric batteries, etc., see Chapter 11), or it can

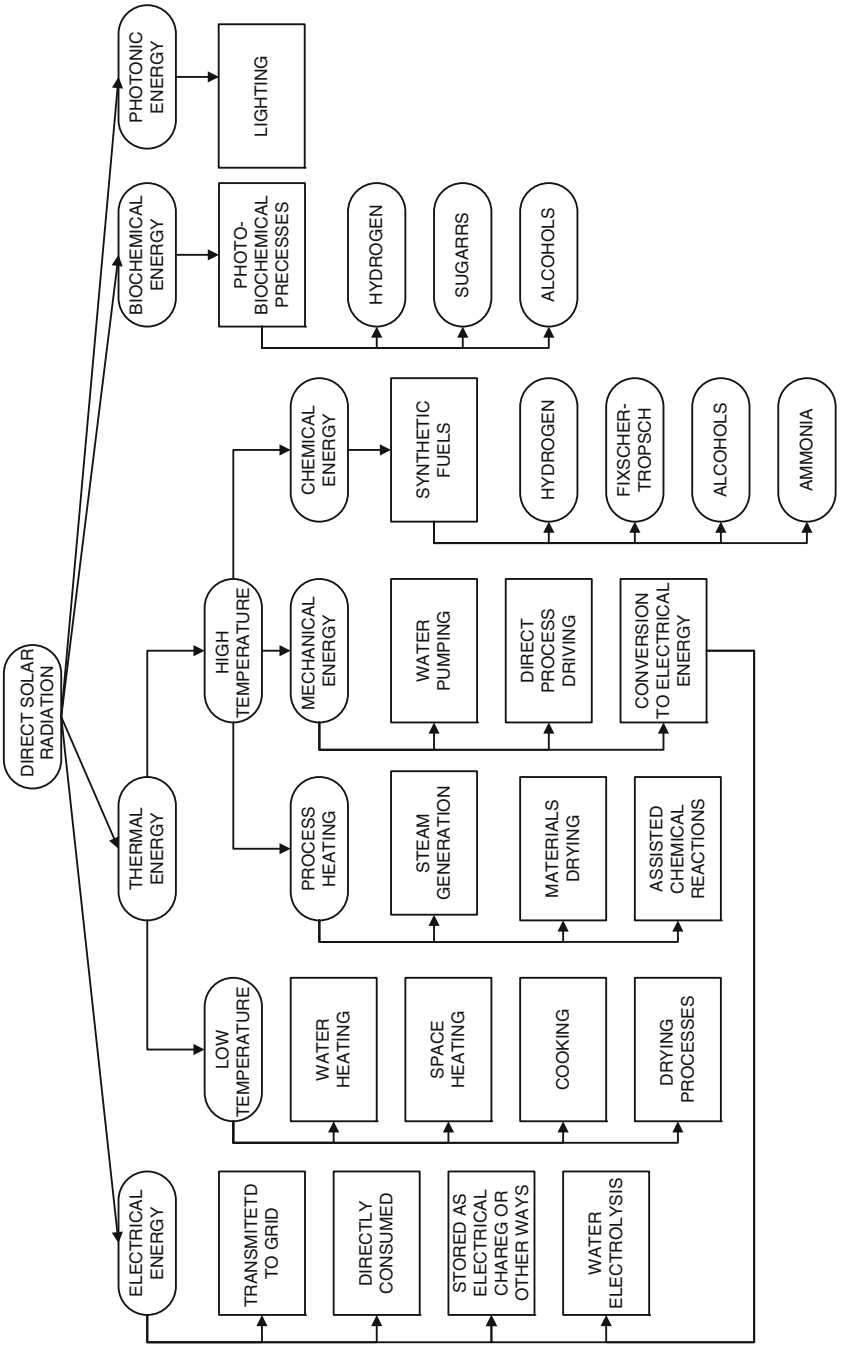

Fig. 9.2 Conversion paths of direct solar radiation with engineered systems

be converted into hydrogen through water electrolysis (see Chapter 13). When converted into thermal energy, low-, intermediate-, high-, or very high-temperature heat can be obtained (starting from the ambient temperature up to around 1,800°C). The low-temperature heat then can be used for water and space heating, for cooking, steam generation, process drying (like food drying, crop drying, paper pulp drying, etc.). Very high-temperature heat—obtained from concentrated solar radiation—can be used for process heating (including processes like thermally driven refrigeration, industrial processes, chemical processes, high-temperature materials drying, etc.). Also, the high-temperature heat can be converted into mechanical energy through solar-driven heat engines. This mechanical energy (as in the form of shaft turning) can be used for water pumping or direct driving of processes. Also, the mechanical energy can be converted into electrical energy through appropriate DC or AC electric generators.

Another path is to convert the high-temperature heat from concentrated solar radiation to chemical energy. This is a convenient form to store the solar energy. In this approach, chemical fuels are synthesized. Envisaged fuels are hydrogen (discussed in detail in Chapter 13), various Fischer–Tropsch fuels (formed from carbon dioxide/monoxide and hydrogen), alcohols, and ammonia. The primary materials for manufacturing synthetic fuels are taken from water (hydrogen), air (nitrogen), fossil fuels (carbon, hydrogen), and biomass (carbon, hydrogen).

The direct radiation can be used for driving photo-biochemical processes through special engineered devices and systems that mimic photosynthesis (so-called artificial photosynthesis, see Chapter 13) or other processes involving micro-organisms stimulated by light. Such processes lead to production of hydrogen, methane, some sugars, and alcohols, which can be further used as fuels. Of course, biochemical conversion of solar radiation also occurs naturally in living systems like green plants, or indirectly in animals that consume plants but use solar radiation for heating.

9.2.1 Thermodynamic Limits of Solar Energy Conversion

On average, the direct solar radiation illuminating the earth's surface, which consists of a flux of photons covering a spectrum of energies from infrared to ultraviolet, delivers 1.6 to 2.8 MWh annually for each square meter of the earth's surface. At the outer shell of the terrestrial atmosphere, the intensity of solar radiation, called the solar constant (see also Chapter 2), is taken on average as $I_{SC} = 1{,}353$ to 1,367 W/m^2, with a fluctuation of about 7% annually. Through photothermal solar radiation conversion, there is a process of conversion of solar radiation (which carries photonic energy) into high-temperature heat followed by conversion of the heat into mechanical energy (or shaft work). Because the mechanical energy may be converted into electrical energy, photothermal solar radiation conversion can be viewed as a means to generate either mechanical or electrical power. Photovoltaic solar radiation conversion results in the direct production of electric energy from solar energy

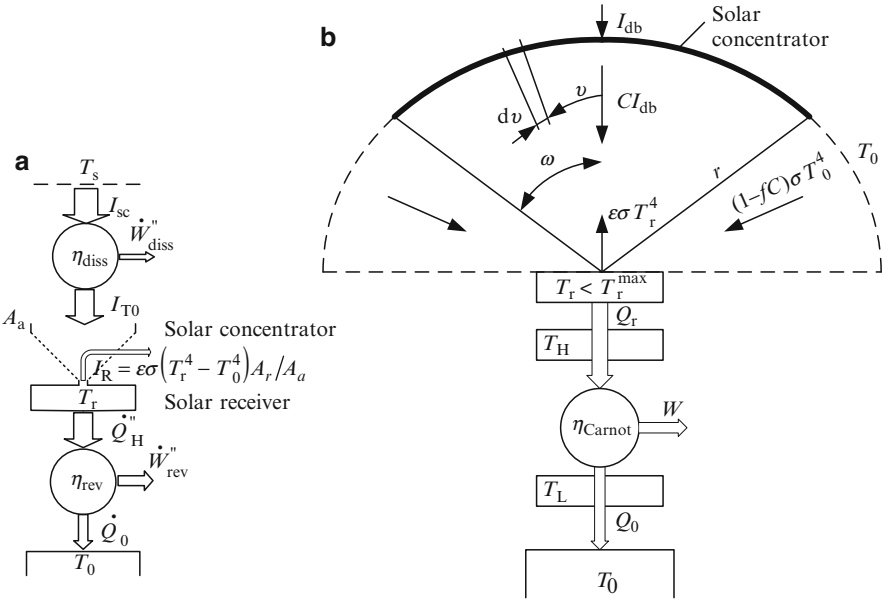

Fig. 9.3 Thermodynamic models for photothermal solar radiation conversion into work. (**a**) Model for exergy of insolation; (**b**) model accounting for solar concentration and heat transfer

using the photoelectric effect. It is important to have a theoretical model for converting solar radiation into work (electricity) and for determining the efficiency of this process.

9.2.1.1 Efficiency of Photothermal Solar Radiation Conversion into Work

A theoretical model for photothermal solar energy conversion can include a solar concentrator that generates heat from concentrated solar radiation and drives a Carnot heat engine operating between a high-temperature reservoir and the ambient temperature T_0. One can also consider in the model the existence of a temperature difference at the sink and the source owing to heat transfer. Thermodynamic modeling of the photothermal solar energy conversion is demonstrated in Fig. 9.3.

The model represented in Fig. 9.3a demonstrates the process of solar radiation conversion into work, which is affected by three factors: the sun, the terrestrial atmosphere, and the environment that exists at the terrestrial surface where the heat engine is located. The engineered system that generates work is simply made from a solar collector coupled to a heat engine directly. We assume first that there is no thermal resistance at the sink and source of the heat engine; this assumption will be relaxed thereafter. Between the sun and the collector is the terrestrial atmosphere. The atmosphere is responsible for ad hoc dissipation of the incident photonic radiation work and heat through various mechanisms such as scattering, absorption,

heating, evaporation, moving of air masses, and so on. The atmospheric dissipation can be modeled like a heat engine working between the outer shell of the atmosphere and the collector surface and operating as a "brake" with efficiency η_{diss}. The working fluid of such a heat engine is the so-called photonic gas, which is a representation of the photonic radiation. It is shown by many researchers, for example Bejan (2006), that such "equivalent" heat engine modeling makes sense thermodynamically, since photonic radiation can be viewed as thermal radiation, with both having the same electromagnetic nature and wave/particle behavior. If one denotes T_{S} as the temperature of the sun and T_{r} as the temperature of the solar receiver (see Fig. 9.3), then the efficiency of the "atmospheric brake" is

$$\eta_{\text{diss}} = \frac{\dot{W}''_{\text{diss}}}{I_{\text{SC}}} = \frac{I_{\text{SC}} - I_{\text{T0}}}{I_{\text{SC}}} = \varphi\left(1 - \frac{T_{\text{r}}}{T_{\text{S}}}\right), \quad \varphi \leq 1. \tag{9.1}$$

In the above equation, the parameter $\varphi \leq 1$ accounts for the Carnot abatement of the dissipater (its efficiency must be smaller or at most equal to that of a Carnot heat engine operating between the same temperatures). I_{SC} denotes the solar constant, which is the intensity of solar radiation on W/m^2 of terrestrial surface; $I_{\text{T0}} \leq I_{\text{SC}}$ represents the intensity of solar radiation incident on the solar collector; $\dot{W}''_{\text{diss}}$ is the atmospheric dissipation rate per unit of terrestrial surface. The solar collector has two components: a solar concentrator that reduces the area of the hot spot (using lenses or mirrors) from a large aperture area A_{a} to a small receiver area A_{r}. The receiver is, due to heating, at a higher temperature than that of ambient ($T_{\text{r}} > T_0$) and thus it loses heat through radiation accounting for (see the figure) $I_{\text{R}} = \varepsilon\sigma\left(T_{\text{r}}^4 - T_0^4\right)A_{\text{r}}/A_{\text{a}}$. The heat losses can be minimized by making $A_{\text{a}} \gg A_{\text{r}}$ and $\varepsilon \to 0$, where ε represents the emissivity factor of the solar receiver and $\sigma = 5.67 \times 10^{-8}\,\text{W/m}^2\,\text{K}^4$ is the Stefan–Boltzmann constant. Ideally, heat losses through radiation could be reduced to zero (even though this is not physically achievable in practice); in this case, the energy balance on the receiver reads $\dot{Q}''_{\text{H}} = I_{\text{T0}}$, which means that all the concentrated solar radiation that falls on the receiver is transformed into heat and delivered to the heat engine at the temperature T_{r}. The generated work by the reversible heat engine operating between T_{r} and T_0 represents the mechanical energy obtained through photothermal solar radiation conversion, and it is in these conditions that $\dot{W}''_{\text{rev}} = I_{\text{T0}}(1 - T_0/T_{\text{r}})$. The receiver temperature can be obtained by solving Eq. (9.1) for T_{r}, and one obtains

$$\dot{W}''_{\text{rev}} = I_{\text{T0}}\left[1 - \frac{T_0}{T_{\text{S}}} \times \frac{\varphi I_{\text{SC}}}{I_{\text{T0}} - (1-\varphi)I_{\text{SC}}}\right]. \tag{9.2}$$

The aim of this theoretical development is to find the maximum work generation from photothermal solar radiation conversion; therefore, one asks what is the maximum value of the $\dot{W}''_{\text{rev}}$. The answer can be found by considering what happens if the atmosphere is completely clear and the dissipation tends to zero. In this case $\varphi \to 1$ and the collector captures an incident radiation of the order of the solar

constant $I_{T0} \cong I_{SC}$. Since in this situation the work generated from solar radiation reaches the maximum possible (upper bound), Zamfirescu and Dincer (2008a) proposed the following equation:

$$\dot{E}x'' = I_{T0}\left(1 - \frac{T_0}{T_S} \times \frac{I_{SC}}{I_{T0}}\right), \quad I_{T0} \cong I_{SC} \tag{9.3}$$

to be adopted as the exergy content of the incident solar radiation (insolation). It can be observed that in the condition where $I_{T0} = I_{SC}$, the exergy of solar radiation becomes

$$\dot{E}x'' = I_{T0}\left(1 - \frac{T_0}{T_S}\right), \tag{9.4}$$

which was derived by many authors in various approaches (see Bejan 2006).

One may now find more realistic estimates of the amount of work that can be generated through photothermal conversion of solar radiation by accounting for some irreversibilities. After determining this amount of work, one can estimate the energy and exergy efficiencies of the conversion process. The model presented in Fig. 9.3b accounts for the optical process of concentration of the incident solar radiation, for radiation losses and for temperature drops at the source and sink of a heat engine driven by solar heat at high temperature T_r and connected with the environment at $T_0 \ll T_r$. The solar concentrator, which can be a mirror or a system of lenses, is shown abstractly in the figure as a hemisphere extending over a solid angle $\Omega_S < 2\pi$ above the solar receiver. Recall that according to definition a solid angle is the ratio between the area of a sphere segment and the square of the radius, measured in steradians (sr); therefore, the solid angle of a hemisphere is 2π. If the concentrator is used, the small hot spot of the solar receiver sees the sun on a larger solid angle $\Omega_C > \Omega_S$ without the concentrator (denoted in this case with Ω_S). The ratio between the two solid angles (with and without concentration) defines the concentration ratio $C = \Omega_C/\Omega_S \geq 1$. From the geometry shown in Fig. 9.3b, we can see that $\Omega_C = \pi \sin^2\omega$. If one denotes R_S as the radius of the solar disk and R_0 as the radius of a sphere centered on the earth and touching the sun, then the solid angle under which the receivers see the sun without a concentrator becomes $\Omega_s = \pi(R_s/R_0)^2$. Thus the concentration ratio is

$$C = \left(\frac{R_0}{R_S}\sin\omega\right)^2. \tag{9.5}$$

Note that the maximum concentration is obtained when the planar angle ω becomes $\pi/2$, that is when the receiver sees the sun under the whole hemisphere. In this case, the concentration ratio becomes $C_{max} = (R_0/R_S)^2 \cong 46{,}300$; if this situation occurs, then the solar receiver may be in thermodynamic equilibrium with the solar disk, that is $T_r = T_S$.

The radiation impacting the solar concentrator (the direct beam radiation, I_{db}) is smaller than the solar constant; thus one can simply write $I_{\mathrm{db}} = \zeta I_{\mathrm{SC}}, \zeta \leq 1$. This radiation is concentrated, thus

$$I_{\mathrm{r,db}} = C\zeta I_{\mathrm{SC}}, \tag{9.6}$$

where $I_{\mathrm{r,db}} = CI_{\mathrm{db}}$ is the concentrated solar radiation falling on the receiver. The aperture factor under which the receiver sees the environment that is the rest of the hemisphere (see Zamfirescu et al. 2009) is $1 - \sin^2\omega$; therefore, the environment at temperature T_0 emits radiation incident on the receiver according to

$$I_{\mathrm{r},0} = \left(1 - \sin^2\omega\right)\sigma T_0 = \left(1 - \tilde{C}\right)\sigma T_0, \tag{9.7}$$

where $\tilde{C} = C/C_{\max}$ and one observes from Eq. (9.5) that $\sin^2\omega = \tilde{C}$.

The receiver itself should be a gray body with emissivity ε that emits radiation over the whole hemisphere according to

$$I_{\mathrm{r,e}} = \varepsilon\sigma T_{\mathrm{r}}^4. \tag{9.8}$$

The energy balance on the receiver, accounting for the incoming and outgoing energy rate, states that $\alpha\left(I_{\mathrm{r,db}} + I_{\mathrm{r},0}\right) = I_{\mathrm{r,e}} + Q_{\mathrm{r}}$, where α is the receiver's absorptivity (namely what percent of the incoming radiation is absorbed) and Q_{r} is the heat delivered by the receiver to the heat engine (see Fig. 9.3b). Denoting the ratio $\chi = \varepsilon/\alpha$ as the "selective gray body factor," one obtains, using Eqs. (9.6) to (9.8), the following expression for the generated heat:

$$Q_{\mathrm{r}} = \alpha\left[(\zeta C)I_{\mathrm{SC}}C_{\max} + \left(1 - \tilde{C}\right)\sigma T_0^4 - \sigma\left(\chi T_{\mathrm{r}}^4\right)\right]. \tag{9.9}$$

The heat engine receives the heat flux Q_{r} at a lower temperature $T_{\mathrm{H}} < T_{\mathrm{r}}$ and discharges a heat fluid Q_{L} into the ambient air at $T_{\mathrm{L}} > T_0$ to generate the mechanical work $W = Q_{\mathrm{r}} - Q_{\mathrm{L}}$. Assuming linear heat transfer irreversibilities at the sink and the source, $Q_{\mathrm{r}} = U_{\mathrm{H}}(T_{\mathrm{r}} - T_{\mathrm{H}})$ and $Q_{\mathrm{L}} = U_{\mathrm{L}}(T_{\mathrm{L}} - T_0)$, one can obtain the following expression:

$$\frac{W}{\left(\zeta\tilde{C}\right)I_{\mathrm{SC}}\alpha C_{\max}} = \left(1 + \frac{1 - \tilde{C}}{\zeta\tilde{C}}\theta_0^4 - \frac{\chi}{\zeta\tilde{C}}\theta_{\mathrm{r}}^4\right)$$

$$\left\{1 - \theta_0\left[\theta_{\mathrm{r}} - \theta_{\mathrm{U}}\left(\zeta\tilde{C}\right)\alpha\left(1 + \frac{1 - \tilde{C}}{\zeta\tilde{C}}\theta_0^4 - \frac{\chi}{\zeta\tilde{C}}\theta_{\mathrm{r}}^4\right)\right]^{-1}\right\}. \tag{9.10}$$

From the above expression, the following dimensionless temperatures are used:

$$\left.\begin{aligned} \theta_0 &= \frac{T_0}{T_S} \\ \theta_r &= \frac{T_r}{T_S} \\ \theta_U &= \frac{\sigma T_S^3}{U}; \quad \text{where} \quad U = \frac{(U_H U_L)}{(U_H + U_L)} \end{aligned}\right\}. \tag{9.11}$$

Note that the ratio W/C, which represents the amount of work generated by the photothermal energy converter per unit of square meter of the earth's surface illuminated by the solar radiation, can be maximized, according to Eq. (9.10), if (1) the maximum concentration is achieved ($\tilde{C} \to 1$); (2) the emitted radiation by the receiver is negligible with respect to the absorbed radiation ($\chi \to 0$); (3) the receiver absorbs all radiation ($\alpha \to 1$); and (4) the receiver is in thermodynamic equilibrium with the sun ($\theta_r \to 1$). In these conditions, the work generated per unit of surface (W/C) according to Eq. (9.10) coincides with that given above in Eq. (9.4).

The energy and exergy efficiencies based on the produced work (W/C) and the concentrated radiation incident on the receiver $C\zeta I_{sc}$ are defined by

$$\left.\begin{aligned} \eta &= \frac{W/C}{\zeta I_{SC}} \\ \psi &= \frac{W/C}{\zeta I_{SC}(1 - T_0/T_S)} \end{aligned}\right\}. \tag{9.12}$$

Using Eq. (9.10), the energy and exergy efficiencies become

$$\left.\begin{aligned} \eta &= \alpha\left(1 + \frac{1-\tilde{C}}{\zeta\tilde{C}}\theta_0^4 - \frac{\chi}{\zeta\tilde{C}}\theta_r^4\right)\left(1 - \frac{\theta_0}{\theta_r - Q_r/(UT_S)}\right) \\ \psi &= \alpha\left(1 + \frac{1-\tilde{C}}{\zeta\tilde{C}}\theta_0^4 - \frac{\chi}{\zeta\tilde{C}}\theta_r^4\right)\left(1 - \frac{\theta_0}{\theta_r - Q_r/(UT_S)}\right)/(1 - \theta_0) \end{aligned}\right\}. \tag{9.13}$$

Note that these conversion efficiencies are functions of the following parameters:

- Climatologic parameters such as average environment temperature (θ_0) and direct beam radiation intensity (ζ)
- Optical parameters of the solar collector such as concentration ratio (C), hemispherical absorptivity of the solar receiver (α), ratio of hemispherical emissivity, and absorptivity of solar receiver (χ)
- Heat engine parameters such as the geometric mean of heat transfer resistance at the sink and the source (U)

Some theoretical idealizations can be applied to the efficiency equations (9.13). For example, one can assume that the receiver is a black body ($\alpha = 1, \chi = 1$), the sky is perfectly clean and does not dissipate solar radiation at all ($\zeta = 1$), and there

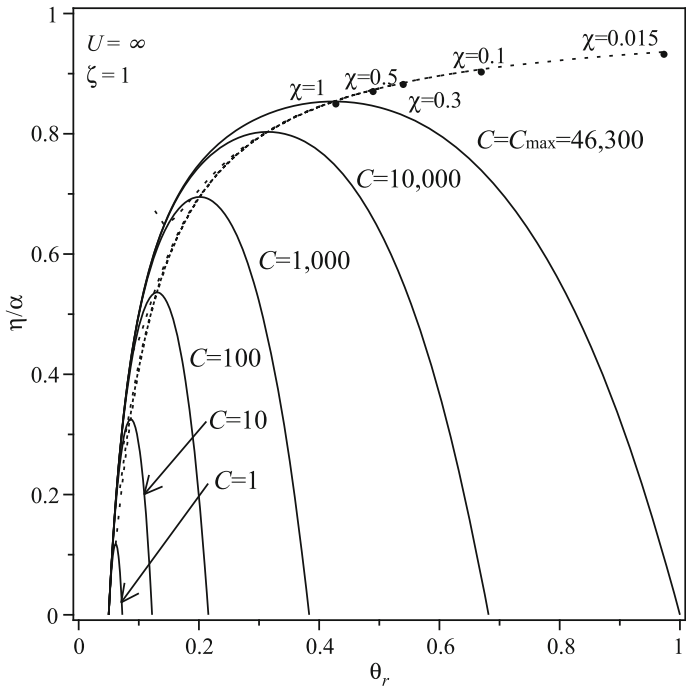

Fig. 9.4 Photothermal solar energy conversion efficiency for $\theta_0 = 0.05$ [modified from Zamfirescu et al. (2009)]

is no heat transfer resistance at the sink and source of the reversible heat engine ($U = \infty$). In these conditions, the energy efficiency becomes

$$\eta = \left[1 + \left(\frac{1}{\tilde{C}} - 1\right)\theta_0^4 - \frac{1}{\tilde{C}}\theta_r^4\right]\left(1 - \frac{\theta_0}{\theta_r}\right). \tag{9.14}$$

If in Eq. (9.14) one assumes maximum concentration of solar radiation ($\tilde{C} = 1$), then one can determine at which θ_r one obtains the maximum efficiency. Assuming $T_0 = 288$ K, that is, $\theta_0 = 0.05$ one obtains a known result, namely $\eta_{max} = 0.853$ for $\theta_r = 0.42$ or $T_r = 2{,}443$ K. This is a known result revised, for example, in Bejan (2006), and it represents the upper limit of the efficiency of a solar-driven reversible heat engine operating with maximum concentration under a clear sky, with no heat losses and no temperature differences due to heat transfer at the sink and the source. Better efficiency can be obtained if the receiver is more selective ($\chi < 1$). The maximum efficiency in such case can be calculated from Eq. (9.13): $\eta_{max} = 0.91$ for $\chi = 0.1$ or $\eta_{max} = 0.93$ for $\chi = 0.015$. More results based on Eq. (9.13) are seen in Fig. 9.4. It can be observed that the efficiency always has a maximum at a certain receiver temperature (given dimensionless as θ_r).

The maximum energy and exergy efficiency (divided by absorptivity of the receiver α) are indicated in Fig. 9.5 assuming infinite heat transfer conductance at

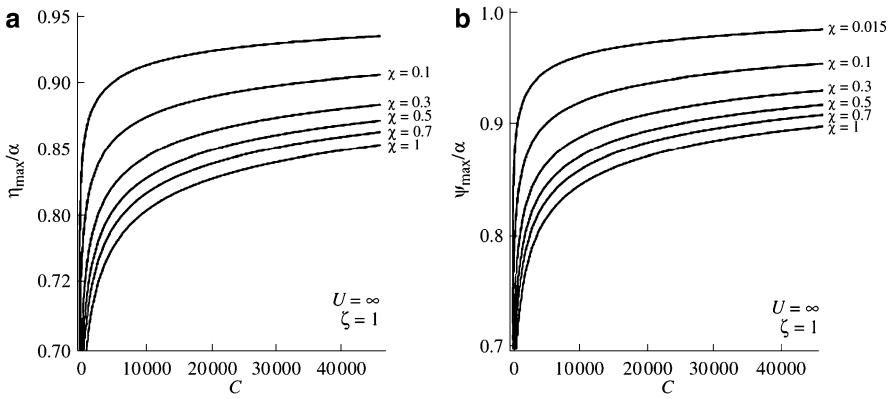

Fig. 9.5 Maximum energy (**a**) and exergy (**b**) efficiency for $\theta_0 = 0.05$, assuming infinite heat transfer conductance at the source and the sink [modified from Zamfirescu et al. (2009)]

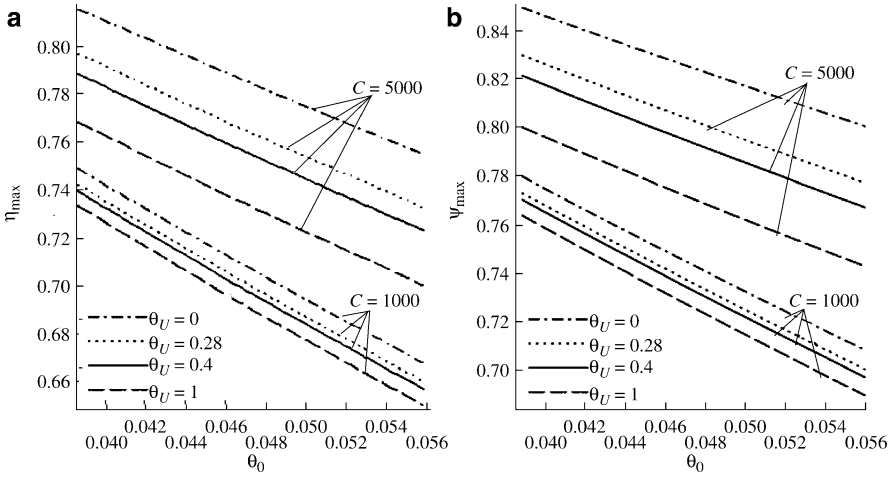

Fig. 9.6 Maximum energy (**a**) and exergy (**b**) efficiency of photothermal solar energy conversion as a function of ambient temperature, for various heat transfer conductances and concentration ratios [modified from Zamfirescu et al. (2009)]

the source and sink sides of the reversible heat engine. Figure 9.6 indicates the influence of heat transfer conductances involved in Eq. (9.13). The heat transfer conductances are given in the form of θ_U according to Eq. (9.11).

9.2.1.2 Efficiency of Photoelectric Energy Conversion of Solar Radiation into Work

Photoelectric energy conversion involves dislocation of electric charges in a substance caused by the energy of photons. When a photon is absorbed by a semiconductor, it promotes an electron in a high energy state and thus generates one electron–hole

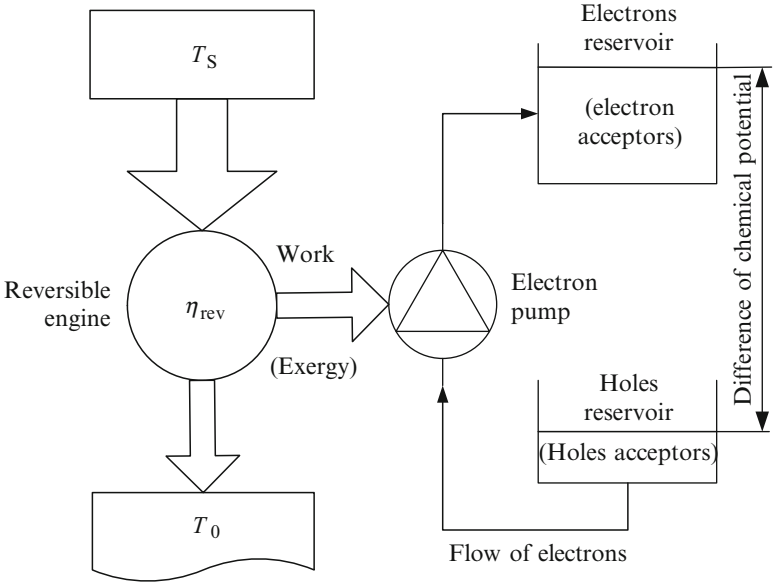

Fig. 9.7 Thermodynamic model for photoelectric solar energy conversion

pair that generates a voltage across the semiconductor junction. The same basic process happens at the molecular level where photons dislocate electrons, which causes transfer of charge between two molecules (one called the donor and the other the acceptor). The photoelectric conversion process can be modeled as in Fig. 9.7.

In the above model, there is an engine operating between two thermal reservoirs. This engine is similar to a heat engine. It operates with solar radiation, which in fact contains thermal radiation. The engine is in contact with the radiation of the sun at temperature T_S and rejects radiation in the ambient air (sensed in the form of heat) at temperature T_0. The work generated by this engine, assumed reversible, is given by the Carnot factor $1 - T_0/T_S$ as a proportion of the energy input; this work is used to drive an electron pump that takes electrons from a reservoir (hole reservoir) at low chemical potential and discharges them in a reservoir of high chemical potential. Other devices (not shown), external to this system, may take electrons from the high potential reservoir and discharge them at the low potential reservoir. When the two processes—moving electrons up and down—run at the same rate, then the overall system operates at steady state.

According to Markvart and Landsberg (2002) the electrochemical potential difference is given by the following equations:

$$\left.\begin{aligned} \Delta\mu &= e\Delta\Upsilon, \text{ in photovoltaic cells} \\ \Delta\mu &= kT\ln\left(\frac{pq}{p_0q_0}\right), \text{ in photochemical reactions} \\ \Delta\mu &= e\Delta\Upsilon + k_BT\ln\left(\frac{pq}{p_0q_0}\right), \text{ in photosynthesis} \end{aligned}\right\}, \tag{9.15}$$

where $e = 1.602 \times 10^{-19}$ C is the elementary electric charge, $\Delta\Upsilon$ is the light-induced electrostatic potential difference, p is the probability that an electron occupies the excited state, q is the probability that a hole occupies the donor state, and the index 0 indicates the probability of recombination of electrons and holes. Note that for all three conversion devices considered in Eq. (9.15)—photovoltaic cells, photochemical reactions, and photosynthesis systems—the processes require "dislocated" electrons; therefore, all these processes are photo/electric driven and the model shown in Fig. 9.7 is valid for all. By definition, the electrochemical potential combines the potential energy stored in chemical form and the electrostatic field. Thus electrochemical potential is the sum of the chemical and electric potentials, that is, $\mu_{ec} = \mu_{ch} + \mu_{el}$, where $\mu_{el} = nF\Delta V = e(nN_A\Delta V) = e\Delta\Upsilon$, where n is the number of electron transfer per mol of reaction product, $F = eN_A$ is the constant of Faraday, N_A is the Avogadro number, ΔV is the local electrostatic potential, and $\Delta\Upsilon$ is the electrostatic potential associated with 1 mol of reaction product. Thus in Eq. (9.15) the variation of potential is electrostatic by its nature for the photovoltaic case, is chemical for the photochemical case, and is electrochemical for the photosynthesis case. Thus the most general form of potential involved in photo/electric radiation conversion is "electrochemical potential."

The energy transmitted to a process in the form of work can be quantified by Gibbs energy variation, which at an infinitesimal scale is $dG = \sum d(\mu_i n_i) - s\,dT + v\,dP$, where μ_i is the chemical potential of specie "i" whose number of mols is n_i. In photonic driven processes (photovoltaic, photochemical, photosynthesis) the processes evolve at constant pressure and temperature, thus $dG = \sum d(\mu_i n_i)$. If a reaction occurs (stimulated by light), then the Gibbs energy of the reaction will be $\Delta G = \sum \Delta(\mu_i n_i) = \Delta\mu_{el}$. The Gibbs free energy of the reaction affects the reaction equilibrium whose equilibrium constant is $K_{eq} = \exp(-\Delta G/RT) = \exp(-\Delta\mu_{el}/RT)$, where R is the universal gas constant and T is the process temperature. Further, the equilibrium constant is related to the reaction rate of the forward (k_f) and backward (k_b) reactions through the following equation: $k_f = k_b K_{eq} = k_b \exp(-\Delta\mu_{el}/RT)$; thus the reaction rate is a function of electrochemical potential variation (induced by the photonic energy), $k_f = k_f(\Delta\mu_{el})$. Moreover, the reaction product generation rate is proportional with the reaction rate $\dot{n}_{prod} = \text{const} \cdot k_f$, where $\dot{n}_{prod}$ is given in mol per second; thus $\dot{n}_{prod} = \dot{n}_{prod}(\Delta\mu_{el})$.

The energy rate developed/consumed by the reaction is given by $\dot{W} = \dot{n}_{prod} \times \Delta\mu$. This energy is supplied to the system from the exterior (in our case it originates from photonic energy). Figure 9.8 illustrates qualitatively the typical dependence of the reaction rate with electrochemical potential. Note that the variation indicated in the figure is typical of any electrochemical-driven reaction, regardless of the driving energy sources from photons or an electric generator or something else. In essence, this diagram says that if the reaction rate (and implicitly the rate of production or the current) increases, the electrochemical potential must decrease. When the electrochemical potential is nil, the rate of reaction is at a maximum, as is denoted on the figure with $k_{f,sc}$; the index "f,sc" is borrowed from photovoltaics where it has the meaning "short circuit" (i.e., the current is at a maximum but the difference in chemical potential is nil).

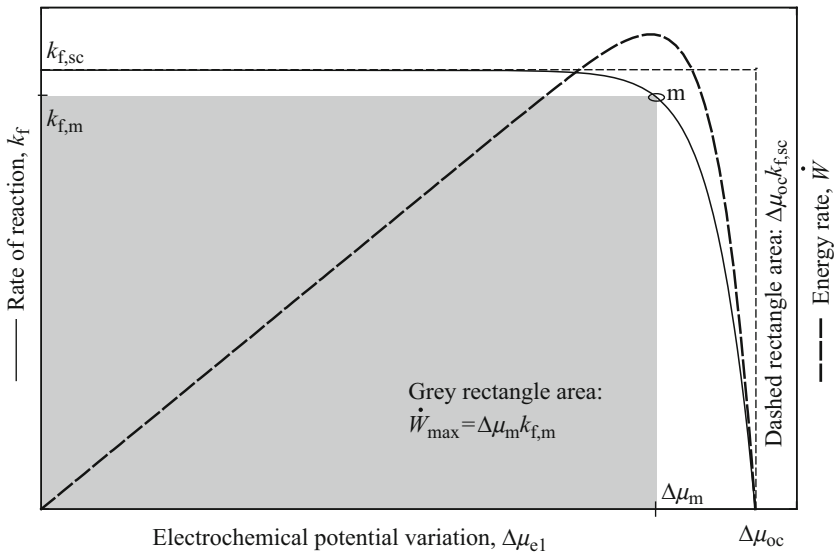

Fig. 9.8 Rate of reaction and reaction energy rate variation of electrochemical potential

This is a consequence of the limitation of the power supplied to the reaction ($\dot{W}$ is quasi-constant and bounded). In contrast, if the reaction rate decreases, necessarily the electrochemical potential increases. At the limit, when the reaction rate is nil (there is no current and no chemical production) the maximum potential is obtained, as indicated on the figure with $\Delta\mu_{oc}$ (the index "oc" is borrowed this time from "open circuit" used in photovoltaics). Figure 9.8 also shows qualitatively (with dashed line) the energy rate calculated as the product $\dot{W} = \dot{n}_{prod} \times \Delta\mu$. This curve has a maximum at $\Delta\mu_m$ with the $\dot{W}_{max} = \Delta\mu_m \times k_{f,m} \times$ const.

Observe here the analogy between the qualitative results for the photo/electric solar energy conversion indicated in Fig. 9.8 and the results for photothermal solar energy conversion shown in Fig. 9.4. Both show a maximum of the developed work. The analogue variables are the temperature and electrochemical potential on the abscissa, and the heat flux and the reaction rate (equivalent with molar production rate or current) on the ordinate. Quantitative calculation and plots will be shown later in this section regarding the photovoltaic power conversion. The analytical treatment is general (that is valid for photovoltaics, photochemical and photosynthesis) and the aim to determine the maximum efficiency of the process.

In Fig. 9.8, the maximum work generated by the conversion process is given by the area of the gray rectangle. The area of the dashed rectangle is $\Delta\mu_{oc} \times k_{f,sc}$, and it is similar to an energy rate that never can be developed by the process. It is useful to define the ratio of the "filling factor" as the ratio of the areas of the gray rectangle over the dashed rectangle.

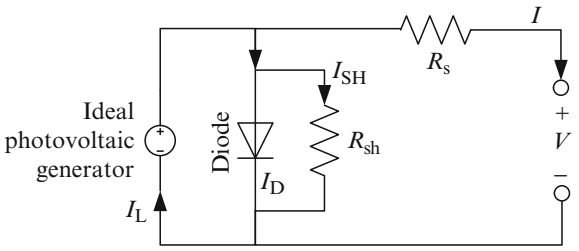

Fig. 9.9 Equivalent electrical circuit of a PV cell

The magnitude of the filling factor is useful in determining the maximum energy rate generation from the open circuit potential and the short circuit reaction rate, which are determinable quantities. The maximum energy rate generation becomes

$$\dot{W}_{\max} = \text{const} \cdot \Delta\mu_{\text{m}} \times k_{\text{f,m}} = \text{const} \cdot \text{FF} \times \Delta\mu_{\text{oc}} \times k_{\text{f,sc}}. \tag{9.16}$$

Therefore, the energy and exergy efficiency of photo/electric solar energy conversion are

$$\left.\begin{aligned} \eta &= \frac{\text{const} \cdot \text{FF} \times \Delta\mu_{\text{oc}} \times k_{\text{f,sc}}}{I_{\text{SC}} \times A} \\ \psi &= \frac{\text{const} \cdot \text{FF} \times \Delta\mu_{\text{oc}} \times k_{\text{f,sc}}}{I_{\text{SC}}(1 - T_0/T_{\text{S}}) \times A} \end{aligned}\right\}, \tag{9.17}$$

where A is the area exposed to solar radiation and $I_{\text{SC}}(1 - T_0/T_{\text{S}})$ represents the reversible work per unit of area (the exergy) that drives the process according to the model illustrated in Fig. 9.7. It is instructive to apply the general equation [Eq. (9.17)] for the case of photovoltaic systems. Their particular form in this case becomes

$$\left.\begin{aligned} \eta &= \frac{\text{FF} \times V_{\text{oc}} \times I_{\text{sc}}}{I_{\text{rated}} \times A} \\ \psi &= \frac{\text{FF} \times V_{\text{oc}} \times I_{\text{sc}}}{I_{\text{rated}}(1 - T_0/T_{\text{S}}) \times A} \end{aligned}\right\}, \tag{9.18}$$

where I_{rated} represents the solar irradiance under ratio conditions; typically for PV cells $I_{\text{rated}} = 1{,}000\ \text{W/m}^2$.

Three factors must be determined in order to calculate Eq. (9.18): the filling factor, the open circuit voltage, and the short circuit current. For this reason, one has to develop the current–voltage diagram of the PV (photovoltaic cell). The equivalent electric circuit of a PV cell is presented in Fig. 9.9. It consists of a source of photovoltaic current in parallel with a diode and a shunt resistor (R_{sh}). In series with the external load is the internal resistor (R_{s}). The photovoltaic current I_{L} splits into three currents such that $I_{\text{L}} = I + I_{\text{D}} + I_{\text{sh}}$.

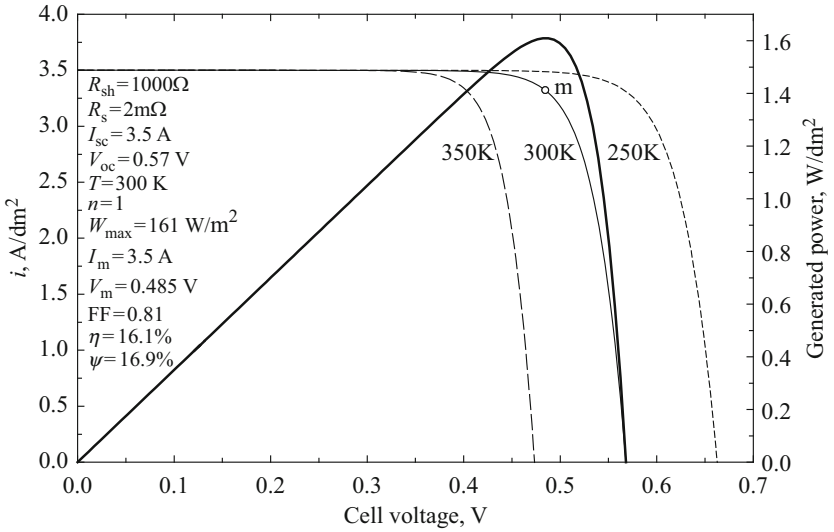

Fig. 9.10 Current density vs. voltage and power density vs. voltage of a typical PV cell

The Shockley equation gives the current through the diode as a function of the voltage and the temperature; using the Shockley equation one obtains

$$I = I_L - I_0\left\{\exp\left[\frac{e(V + IR_s)}{nk_BT}\right] - 1\right\} - \frac{V + IR_s}{R_{SH}}, \tag{9.19}$$

where I_0 is the reverse saturation current of the diode, e is the elementary electrical charge, n is the diode ideality factor (unity for the ideal diode), k_B is the Boltzmann constant, and T is the temperature.

When operating in an open circuit, the voltage on the load becomes $V = V_{oc} = I_0R_{sh}$, where the residual current depends on the temperature according to $I_0 = [k_BT/(eR_s)]\ln(I_L/I_0 - 1)$. When it operates in a short circuit, the voltage on the cell vanishes, thus $I_{sc} \cong I_L$.

Figure 9.10 reports the calculated results for a typical PV cell showing the current density and the power density in correlation with the cell voltage. The filling factor is 81%. The cell is rated under a solar irradiance of 1,000 W/m^2. In these conditions, the cell efficiencies are 16.1% (energy based) and 16.9% (exergy based) for standard temperature. Typical PV cells reach 10% to 15% energy efficiency; the advanced ones can reach 25% while some recently developed cells achieve 40%.

9.2.1.3 Solar Exergy Maps

The efficiency of the solar radiation conversion and the power generated per square meter of collector surface depend on the intensity of the solar radiation and the local temperature. These parameters vary with geographical location, the time of day,

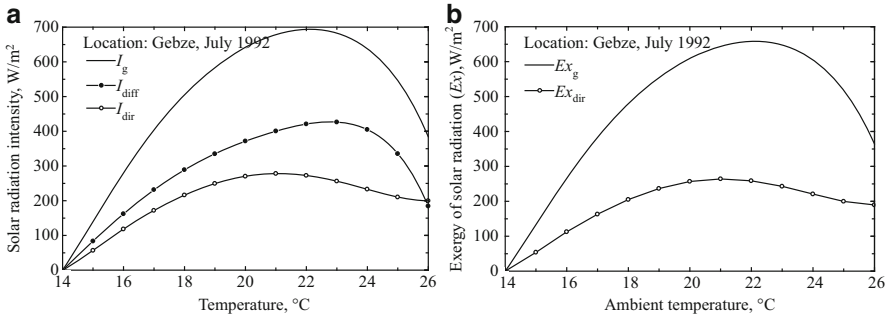

Fig. 9.11 Solar radiation intensity and exergy at Gebze, Turkey, correlated with ambient temperature [data from Dincer et al. (1996a)]

and the season. Information about the direct beam radiation and diffuse radiation is required for many reasons including design of solar collectors, design of buildings, design of heating, ventilation and air conditioning systems, snow melt calculations in hilly areas, climate prediction, and so on. Thus, both diffuse and global radiations are recorded at many meteorological stations and other institutions around the globe and are centralized in databases. Here through global radiation one notes the sum of direct beam radiation (coming directly from sun) and diffuse radiation (reflected on the surface by other bodies, including the clouds). Thus, $I_g = I_{dir} + I_{diff}$, where indices g, dir, and diff stand for global, direct, and diffuse radiation, all expressed in watts per square meter of the earth's surface.

It is important to determine the thermodynamic limits of solar radiation conversion at geographic locations and for each season such that the opportunity of installing solar power generation capacities can be judged on a rational basis. Thus exergy of solar radiation can be calculated for each geographic location. Moreover, it has been observed that the intensity of solar radiation can be correlated with local temperature variation. For example, Dincer et al. (1996a) show polynomial correlations between local temperature and global and diffuse radiation in Gebze, Turkey (approx. 40°N, 29°E). Using these correlations, one can predict the exergy content of solar radiation in Gebze, as shown in Fig. 9.11. For the case presented, which corresponds to the average values recorded for July 1992, one can observe that the diffuse radiation was quite high.

The exergy of the solar radiation, meaning the maximum expected work that can be generated by converting solar energy in July 1992 in Gebze, calculated with Eq. (9.4), was around 650 W/m^2. If only direct beam radiation is used for conversion, then the corresponding exergy is around 300 W/m^2 at maximum. If the solar concentrator would be tracing the sun, assuming a tilt angle of 45°, the maximum expected exergy becomes $\sqrt{2} \times 300 \cong 425$ W/m^2, or around 900 W/m^2 is the global radiation is used in exergy calculation.

Solar exergy maps were developed by Joshi et al. (2009a) including several geographic locations in the United States and India. The direct beam radiation intensity on a tilted surface (tracking the sun) was used for calculation of the exergy

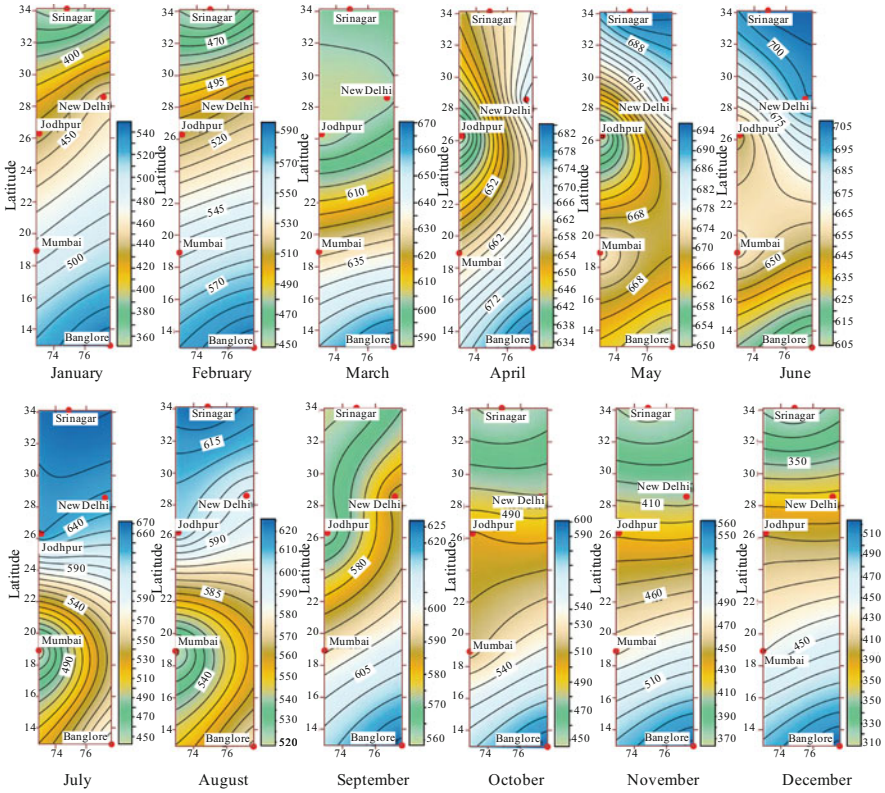

Fig. 9.12 Solar exergy maps for Indian cities (horizontal axis: the longitude) [modified from Joshi et al. (2009a)]

according to Eq. (9.4); diffusion radiation was not considered in the development of the solar exergy maps. Figure 9.12 shows the solar exergy maps for India as developed by Joshi et al. (2009a).

The solar energy conversion is more complete when cogeneration of electricity (work) and heat is applied. This can be done with various systems. For example, if a solar-driven heat engine is used, the heat ejected by the heat engine can be recovered at a temperature level that makes convenient the use of the associated thermal energy for some purpose. If a photovoltaic panel is employed to generate electricity from solar radiation, special arrangements can be designed to recover also some of the heat that is generated (on the panel surface) by the incident solar radiation.

One can define an exergy efficiency of power and heat cogeneration from solar radiation. The efficiency must be reported with respect to the exergy of the incident radiation. The corresponding formula is given as follows:

$$\psi = \frac{\dot{W} + \dot{E}x_{\text{th}}}{\dot{E}x}, \tag{9.20}$$

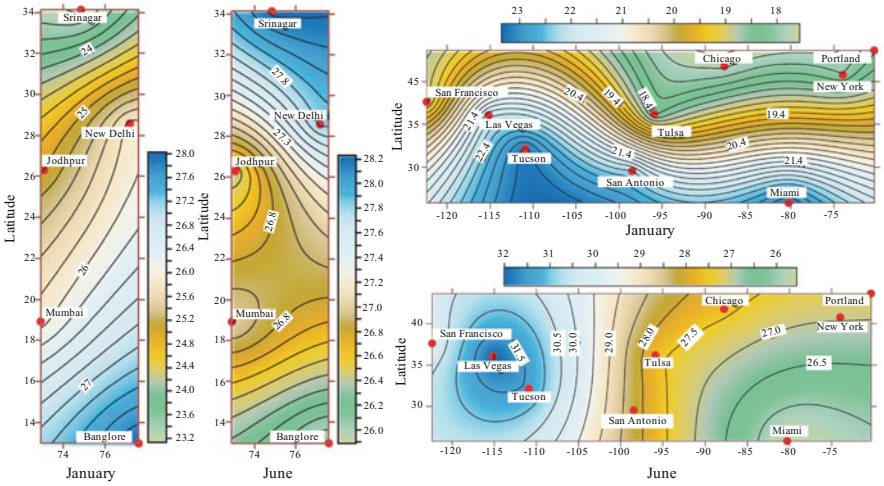

Fig. 9.13 Exergy efficiency maps for power and heat cogeneration developed for India and the U.S. (horizontal axis: the longitude) [modified from Joshi et al. (2009a)]

where $\dot{E}x$ is the exergy of the insolation (incident solar radiation), $\dot{W}$ is the generated power, and $\dot{E}x_{\text{th}}$ is the exergy associated with the generated thermal energy. The exergy of the solar radiation can be calculated as indicated by Eq. (9.4). The generated power depends on the efficiency of the conversion system. As shown above, the thermodynamic limit of photothermal solar energy conversion efficiency is ~84% for black body receivers and goes toward 90% for selective gray body receivers. If photo/electric conversion is applied, then the generated power depends on the filling factor of the specific process; with photovoltaics $\dot{W} = \text{FF} \times V_{\text{oc}} \times I_{\text{sc}}$.

Normally, the expected efficiency of photovoltaics is 10% to 15% as mentioned above. The exergy of the generated thermal energy also depends on the process. If one assumes that the solar energy converter heats a heat transfer fluid and increases its exergy from $\dot{E}x_{\text{in}}$ at inlet to $\dot{E}x_{\text{out}}$ at outlet, then the thermal exergy generated by the system would be $\dot{E}x_{th} = \dot{E}x_{\text{out}} - \dot{E}x_{\text{in}}$. In the case that the temperature of the heat transfer fluid does not change very much during the energy transfer process, then the thermal exergy can be calculated with $\dot{E}x_{\text{th}} = \dot{Q} \times (1 - T_0/\bar{T}_{\text{th}})$, where $\bar{T}_{\text{th}}$ is the average temperature at which the generated heat is made available, $\dot{Q} = \dot{H}_{\text{out}} - \dot{H}_{\text{in}}$ is the generated heat flux, and $\dot{H}$ is the enthalpy rate of the heat transfer fluid.

Solar exergy efficiency maps were developed by Joshi et al. (2009a) for India and the U.S. assuming the typical efficiency of a photovoltaic–thermal system (to be introduced later) that cogenerates power and heat. These maps are shown in Fig. 9.13. The heat generated is at a low-temperature level (under 100°C) and the corresponding exergy efficiencies calculated with Eq. (9.20) are in the range of 20% to 30%. Maps indicating solar exergy and exergy efficiency of the solar radiation conversion are useful for installing and designing solar energy systems because they indicate in a concise way the thermodynamic limits of solar energy conversion

for each geographic location and season. For example, the maps above show that Tucson is a better place than Portland for solar energy harvesting since one expects about 5% more conversion efficiency.

9.2.2 Solar Thermal Energy

As stated above, the thermodynamic limits of solar radiation conversion are important and must be known when any solar energy project is started. These limits are upper bound estimates. When the actual application is determined, various kinds of irreversibilities can be accounted for in the analysis, and accurate estimation of the conversion efficiency of each system can be obtained. We will analyze here and in the subsequent section various types of solar energy conversion systems. First, we focus in those systems that generate thermal energy from solar radiation; next the systems that generate electricity will be discussed; other systems (cogeneration, hydrogen generation) also will be briefly analyzed.

In principle, two kinds of systems exist for conversion of solar radiation into heat: nonconcentrating and concentrating solar radiation system. The systems that do not concentrate solar radiation operate at lower temperature (typically below 100°C) and are used in general for water heating or space heating or drying (see Fig. 9.2). They are mainly based on solar panel and solar pond designs. The solar concentrator uses optics (mirrors and lenses) to generate high-temperature heat on small area spots.

9.2.2.1 Passive Solar Heating

Solar passive heating is a technique of using solar thermal energy through designs that use few or no mechanical systems (i.e., no pumps, or fans, or evacuated tube collectors, or other advanced technologies). Passive solar energy mainly involves special arrangements of building facades and windows. Solar passive technology also may include solar stills (which are simple arrangements that produce water distillation through the greenhouse effect) or solar ponds, which will be introduced in the subsequent paragraphs.

Simple arrangements like south-facing widows allow a good transmittance of photonic energy inside the building; the light is then reflected and partially absorbed by the walls and eventually it reaches windows from the inside where it is partially reflected back and partly refracted toward the outside. Thus there is a positive accumulation of solar energy inside the building, during the daytime. The construction materials, such as internal walls, the building shell, and so on, store the thermal energy accumulated during the day and enable a temporal phase shift between solar radiation availability and heat utilization. The windows' glassing shows high transmittance for short waves (2–3 μm) and is relatively opaque to long infrared waves that are emitted by the building elements; thus, infrared radiation has a good chance to dissipate inside the building, and this is a form of passive solar heat.

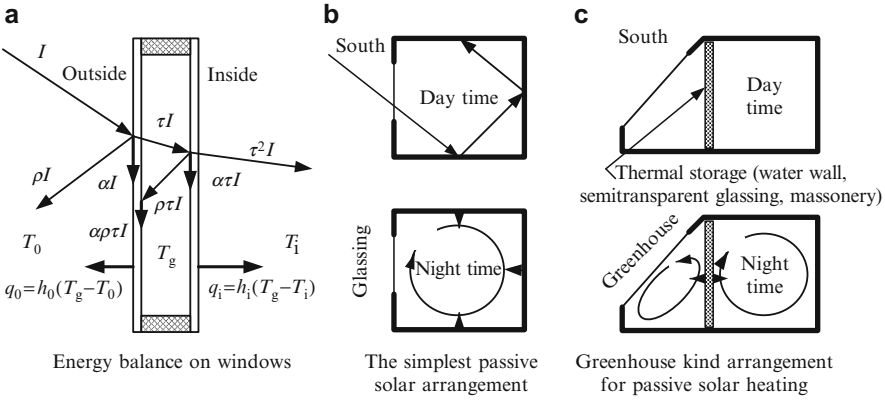

Fig. 9.14 Solar passive heating arrangements

The energy balance in double windows is suggested schematically in Fig. 9.14(a). Basically, the incident irradiation I (in W/m^2) is reflected by the exterior glassing outside (ρI, where ρ is the reflectivity), partly absorbed (αI), and partly transmitted (τI). The transmitted rays fall on the inner glassing where they are again reflected ($\rho\alpha I$) toward the outer glassing, partly absorbed in the glassing ($\alpha\tau I$), and partly transmitted toward the inside ($\tau^2 I$). The two types of glassing are heated by the absorbed radiation—the outer glassing with $\alpha(1+\rho\tau)I$ and the inner with $\alpha\tau I$—and thus they are at a higher temperature than both the outside air and the inside air. Therefore, heat transfer occurs between the glassing and the inner and outer spaces.

Assuming an average glassing temperature T_g, then the heat transfer toward the outside, per unit of glassing area, is $q_0 = h_0(T_g - T_0)$, and toward the inside is $q_i = h_i(T_g - T_i)$. Note that the absorption coefficient in single glassing can be up to 30%, allowing thus for rather high temperatures on their surface. The transmittance for perpendicular incidence can reach 90% for simple glassing, and 65% to 80% for two-pane glassing. The energy balance on the double glassing can be solved for the average temperature of the panes; it is $T_g = T_0 + T_i + 12/\bar{h}(\alpha I + \alpha\rho\tau I + \alpha\tau I)$, where $\bar{h}$ is the average heat transfer coefficient $\bar{h} = 0.5\,(h_0 + h_i)$.

Figure 9.14b,c suggests some possible passive solar heating arrangements that use no mechanical means and no solar collectors. The simplest arrangement is that of a south-facing window. During the daytime, solar rays heat the room and also the masonry back wall, floor, and ceiling, which accumulate heat during the day. In the nighttime, the air from the room is heated by the walls, which are at a slightly higher temperature. Natural heat convection currents are formed in the room during the night as indicated in the figure. One advanced design is shown in Fig. 9.14c, which uses a greenhouse and thermal storage. The greenhouse has a southward glassing with a tilted surface to capture more solar radiation. In between the room and the greenhouse a thermal storage device in the form of a wall is placed. This can be a masonry wall, or a water wall (that is, a water reservoir shaped as a wall), or semitransparent glassing materials with good thermal storage behavior. During the

daytime, the greenhouse temperature increases and the accumulated heat is stored in the wall. During the nighttime, the accumulated heat is discharged in both directions, toward the room and toward the greenhouse, with a preference for the room direction because of slightly larger temperature gradients.

9.2.2.2 Solar Ponds and Other Solar Thermal Storage Systems

The use of thermal energy storage is essential for solar thermal systems because in this way one can compensate for the solar energy intermittence and fluctuation in intensity. Several classes of storage may be required for a single installation depending on the scale, kind, and application (see Dincer and Dost 1996). For example, heating and hot water applications can use thermal storage in water itself, phase change materials, soil, rock, and other solids.

A variety of solids are also used; rock particles of 20 to 50 mm in size are most prevalent. Well-designed packed rock beds have several desirable characteristics for energy storage. The heat transfer coefficient between the air and the solid is high, the cost of the storage material is low, the conductivity of the bed is low when air flow is not present, and a large heat transfer area can be achieved at low cost by reducing the size of the particles. Chapter 11 reviews thermal storage system in detail. The particularity of solar thermal energy consists in its high range of temperature levels. Thermal storage at very high temperature is required by many thermal applications including heat-to-power conversion or synthetic fuel production. Thermal storage in oil–rock systems (in which the energy is stored in a mixture of oil and rock in a tank) for hot water and heat-recovery applications are examples of medium-temperature applications, while those in molten nitrate salt systems use high temperatures.

Solar ponds are passive solar systems that do these two functions in one single device. The principle of the solar pond is to create, with the help of solar heating, a salinity concentration gradient in a pool of salt water. Figure 9.15 introduces the operating principle of the solar pond. Basically, the solar pond is a pool of salt water placed in a position such that it is well illuminated by the solar radiation. Mostly, the solar radiation comes from the southerly direction during the day if the device is located in the Northern Hemisphere (note that the representation in the figure reflects the situation from the Northern Hemisphere; if placed in the Southern Hemisphere, the solar rays will come mostly from the north). The solar pond has three working zones (or layers). At the upper level is placed the convective zone of thickness X_1, as indicated in the figure. It follows the nonconvective zone until the depth X_2, and at the bottom of the pool is the heat storage zone.

Figure 9.15 shows details for each operating layer of the solar pond. The upper convective zone is fed with fresh water of a density close to the density of fresh water in the upper part to maintain the cleanliness of the pond and replenish lost water due to superficial evaporation process. As suggested in the figure, a part of the solar radiation incident on the surface is lost by reflection, while some other part

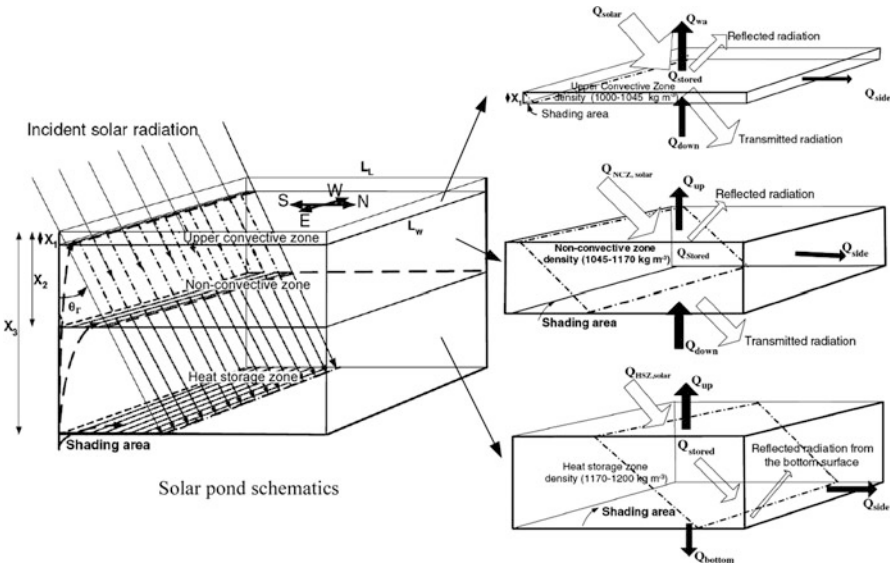

Fig. 9.15 Illustration of the operating principle of a solar pond with details of the three specific working zones [modified from Karakilcik et al. (2006)]

(Q_{wa}) is transmitted to the surrounding air through heat convection and water evaporation. The remaining, major part of the incident solar radiation is transmitted to the nonconvective layer.

This nonconvective layer plays the role of thermal insulation. It is composed of salty water layers whose brine density gradually increases up to about 1,170 kg/m^3. This layer allows an extensive amount of solar radiation to penetrate into the storage zone while inhibiting the propagation of long-wave solar radiation from escaping because water is opaque to infrared radiation.

The third layer is the heat storage zone with relatively uniform density, at the highest value within the pond. A considerable part of the solar energy is absorbed and stored in this region. This layer has the highest temperature; hence, the strongest thermal interactions occur between this zone and the adjacent insulated bottom-wall and insulated side-walls.

The relative thickness of each of the zones of a solar pond is about 7% for the convective layer, 40% for the insulating layer, and 53% for the heat storage layer. The heat stored in the lower layer can be recovered by a pumping system that continuously draws brine at a higher temperature and returns it at a lower temperature. The average temperature gradient between the upper and lower layers of the pond varies from about 8° to 10°C in the colder months to 25° to 30°C in the hotter months. The bottom layer can reach 50° to 80°C during the summer. Figure 9.16 shows the calculated results for the conversion efficiencies of a typical solar pond and their variation from the winter to the summer season. Each zone of the pond has an associated energy efficiency, as indicated in the following Eq. (9.21) by the subscripts

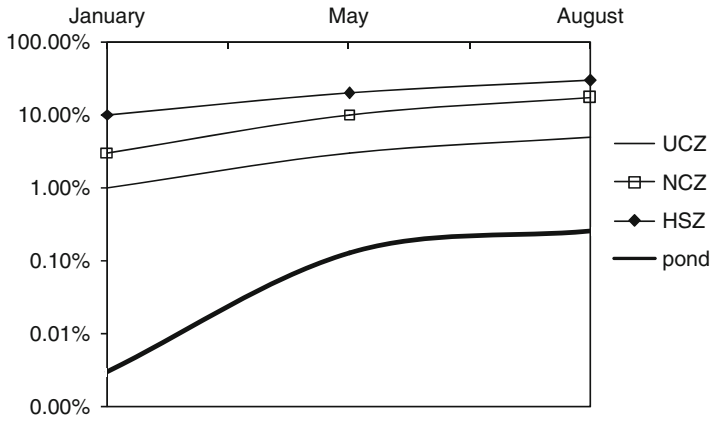

Fig. 9.16 Characteristic conversion efficiencies of a solar pond and its subsystems [data from Karakilcik et al. (2006)]

UCZ, NCZ, HSZ representing the upper convective zone, the nonconvective zone, and the heat storage zone, respectively:

$$\left.\begin{aligned} \eta_{\mathrm{UCZ}} &= \frac{Q_{\mathrm{NCZ}}}{Q_{\mathrm{solar}}} \\ \eta_{\mathrm{NCZ}} &= \frac{Q_{\mathrm{HSZ}}}{Q_{\mathrm{NCZ}}} \\ \eta_{\mathrm{HSZ}} &= \frac{Q_{\mathrm{stored}}}{Q_{\mathrm{HSZ}}} \\ \eta_{\mathrm{pond}} = \eta_{\mathrm{UCZ}}\eta_{\mathrm{NCZ}}\eta_{\mathrm{HSZ}} &= \frac{Q_{\mathrm{stored}}}{Q_{\mathrm{solar}}} \end{aligned}\right\}, \tag{9.21}$$

where η_{pond} is the overall energy efficiency of the solar pond.

The energy efficiency of the pond is very low, a fact that makes solar ponds economically justifiable only when the investment cost is low. Mostly, the efficiency of the pond is degraded by the losses in the upper convective layer.

9.2.2.3 Solar Thermal Collectors

Here we discuss all types of solar collectors used to convert solar energy into heat from a low temperature to a very high temperature. The usual thermal collectors employed for water heating do not concentrate the solar radiation. The types that concentrate the solar radiation are used mostly for electricity generation through heat engines. However, recent trends are to use concentrated solar radiation for process heating. A classification of solar thermal collectors is shown in Fig. 9.17.

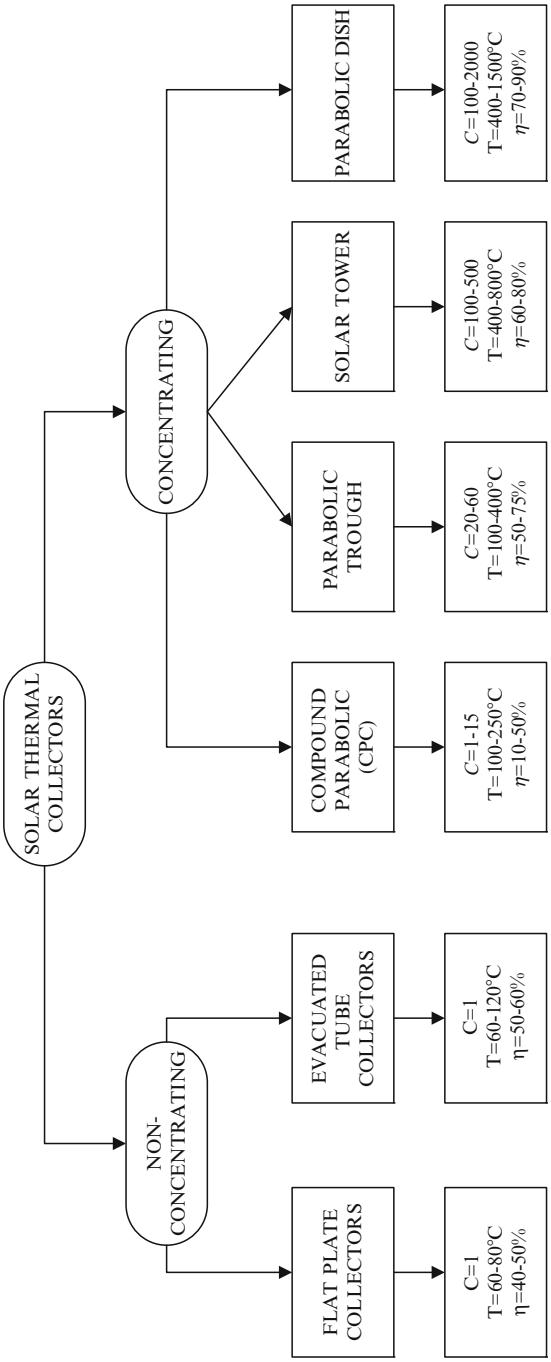

Fig. 9.17 Solar thermal collectors

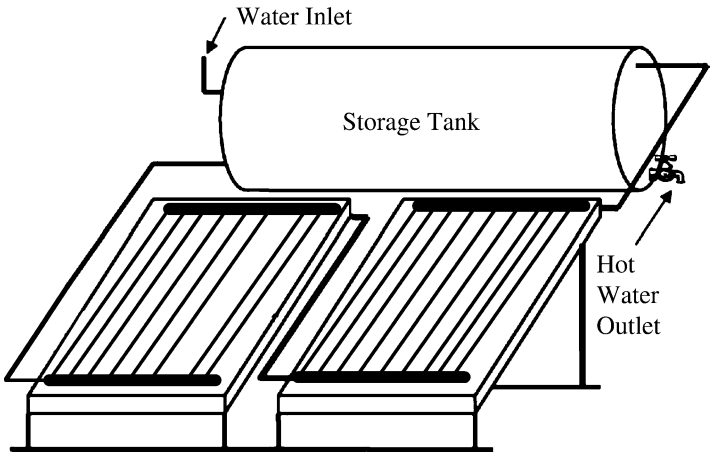

Fig. 9.18 Water heater system with flat plate solar collectors

Flat plate collectors are simply made from a number of tubes assembled in a flat box with glassing and a black back-plate. Water is circulated through the tubes that are exposed to incident solar radiation as indicated in Fig. 9.18. Flat-type solar collectors have good efficiency when used for water heating at temperatures higher than the ambient temperature up to 25°C. If the temperature is higher, the collector efficiency decreases due to heat losses through heat transfer by convection to the environment. For higher temperature applications, the use of evacuated tube collectors becomes more efficient than simple glass collectors. Evacuated tube collectors use vacuum to reduce heat losses by convection. They consist of a tube-in-tube assembly, where the outer tube is of transparent glass and is a vacuum. The inner tube is circulated by a heat transfer fluid or a two-phase working fluid having the role of transmitting the solar thermal energy. In the two-phase fluid case, the system works like a heat pipe.

Operation at higher temperature necessitates concentration of the solar radiation. Compound parabolic collectors are so-called nonimaging collectors that are able to concentrate solar radiation up to 15 times. The term *nonimaging* refers to the type of optics; that is, the concentrator does not form an image of the sun on the solar receiver. The compound parabolic collectors do not necessitate solar tracking, because their geometry is such that the solar rays are reflected on a hot spot regardless of the sun's position. For temperatures higher than about 200°C, the nonimaging concentrator shows major heat losses, and thus the preferred concentrators are of the imaging type. The imaging concentrators use optical systems to create an image of the sun on a small hot spot (the solar receiver). Imaging concentrators can concentrate the radiation on a line or on a spherical point. The imaging concentrators must track the sun in order to be able to focus the sun on the receiver. Parabolic collectors are those that concentrate the solar radiation along a line.

A solar tower consists of a field of mirrors, called heliostats, that track the sun and concentrate the radiation on a receiver placed on a tower. The receiver normally is of the line type made on an assembly of tubes. Other geometry variations are

Table 9.1 Characteristics of some solar collectors

Collector	Acurex 3001	M.A.N. M480	Luz LS-1	Luz LS-2	Luz LS-2	Luz LS-3
Year	1981	1984	1984	1985	1988	1989
Area (m^2)	34	80	128	235	235	545
Aperture (m)	1.8	2.4	2.5	5	5	5.7
Length (m)	20	38	50	48	48	99
Receiver diameter (mm)	51	58	42	7	7	7
Concentration ratio	36:1	41:1	61:1	71:1	71:1	82:1
Optical efficiency	0.77	0.77	0.734	0.737	0.764	0.8
Receiver absorptivity	0.96	0.96	0.94	0.94	0.99	0.96
Mirror reflectivity	0.93	0.93	0.94	0.94	0.94	0.94
Receiver emittance	0.27	0.17	0.3	0.24	0.19	0.19
Operating temperature (°C)	295	307	307	349	390	390

Data from Zamfirescu et al. (2008)

possible for the receiver of the solar tower; one can say that the concentration type in the case of the solar tower is somewhere in between line-type concentration and point-type concentration. The highest temperatures are obtained with solar dishes that use paraboloidal mirrors to focus the solar radiation on a point. Actually, the focal point has an elliptic shape.

The main characteristics and the performance of some parabolic systems constructed and tested in the 1980s are listed in Table 9.1. Regarding point concentrators, there have been a number of small-scale designs tried in the last decades, as summarized by Zamfirescu et al. (2008). The Omnium-G concentrator has a 6-m-diameter paneled dish that provides 7 to 12 kW of thermal power under 1,000 W/m^2 insolation. The "test bed" concentrator had an 11-m paneled dish and provided 76 kW thermal power. The Lajet concentrator comprises 24 1.5-m-diameter dishes and delivers 33 kW of thermal power. The Advanco concentrator provides 74 kW thermal power using a 10.6-m-diameter paneled dish. General Electric's Parabolic Dish Concentrator 1 used a 12-m paneled dish to provide 72.5 kW of heat. Power Kinetics had a 9-m square-shaped paneled concentrator that delivered 28 kW to a boiler under 0.88 to 0.94 kW/m^2 insolation. The Acurex Parabolic Dish Concentrator 2 used an 11-m paneled dish providing 800 W of concentrated solar heat per square meter of aperture. Boeing created a solar point concentrator equipped with 0.6 × 0.7 m mirror panels with an optical efficiency of up to 0.8, which provides a concentration ratio of 3,000. The ENTCH Fresnel Concentrator Lens used panels of 0.67 × 1.2 m and could only provide an optical efficiency of 0.68 at a concentration ratio of 1,500. Currently, the largest single-dish power system is Australia's Big Dish with an aperture of 20 m, which produces 200 kW of thermal power feeding a 500°C boiler.

Apart from the dish concentrator (of paraboloidal surface), another established system for solar thermal power generation is the Fresnel mirror formed from an assembly of plain or curved surface mirrors suspended from a frame structure. The individual mirrors point toward a single focal point where the solar receiver is placed. For tracing the sun, the whole assembly rotates around the azimuth and zenith angles. A similar option is represented by Fresnel lenses that use the light refraction phenomenon to focus the incident radiation.

Although line and point concentrators have been around, there is a cost and technological gap that needs to be closed in order to exploit their high efficiencies. The performance factors of a dish system can be greatly degraded with changes in geometry, and therefore accuracy and rigidity are important for their design. The optical efficiency of the solar concentrator, concentration ratio, and the intercept factor, which will be defined rigorously in the subsequent paragraphs, are important factors defining the system performance. Some cost estimations were compiled in Zamfirescu et al. (2008). On average, for an optical efficiency of 0.90 to 0.93, a concentration ratio of 2,000 to 5,000, an intercept factor of 0.98, and a lifetime of 30 years, a low-cost price estimate is \$200 to \$350 per m^2. Another cost estimate is based on the Acurex concentrator having an optical efficiency of 0.86 and a concentration ratio of 1,900 costing \$330 per m^2 for a production scale of 100,000 units/year.

Back-silvered glass is the standard design for the mirrors having 94% reflectivity. The reflector can be a single layer, which is more efficient and more expensive, or it can be broken into components, which is cheaper but less efficient. Another option is the stretched membrane mirror of which manufacture involves a vacuum process. Singular element stretched membrane mirrors have demonstrated optical efficiencies of 0.915, which is lower than that of the best glass-metal mirrors, but at a lower cost.

Two methods of tracking the sun are used with line and point concentrators. In the first method, sensors provide optical feedback of the sun's position to allow for variable tracking. In the second method, the system is preprogrammed to follow the sun based on the local longitude, latitude, and time. Line focus concentrators in general track the sun in one direction, namely along the polar axis. The second axis alignment is adjusted daily or weekly. The azimuth tacking is applied to point-focus concentrators because it allows for constant two-axis tacking.

In the design of the concentrating solar collector there is a trade-off between optics and heat losses. The solar collector efficiency represents the ratio between the heat absorbed by the solar receiver $\dot{Q}_\mathrm{r}$ and the incident solar radiation I_{T0}, normal on the collector's aperture of area A_a. Thus the thermal efficiency of the solar collector is $\eta_{\mathrm{coll}} = \dot{Q}_\mathrm{r}/(I_{\mathrm{T0}}A_\mathrm{a})$. The solar collector can be divided into two subsystems. The first is the optical subsystem, having the role to concentrate the solar radiation on the small spot receiver. The efficiency of the optical subsystem, called optical efficiency, can be defined as the intensity of the concentrated light over the intensity of the incident light. Because of optical losses due to reflectivity, transmissivity, optical error, and shading, $I_\mathrm{r}A_\mathrm{r} < I_{\mathrm{T0}}A_a$; thus the ratio between the two is the optical efficiency $\eta_{\mathrm{opt}} = (I_\mathrm{r}A_\mathrm{r})/(I_{\mathrm{T0}}A_a)$. The second subsystem is the thermal one, which converts the incident concentrated light radiation into heat. Several thermal radiation and heat convection losses are characteristic of this subsystem. The efficiency of this subsystem is known as thermal efficiency. The receiver's absorbance, emittance, and heat transfer coefficient by convection affect mostly the thermal efficiency, which is defined as the ratio of the absorbed heat and the concentrated solar radiation $(I_\mathrm{r}A_\mathrm{r})$, written as $\eta_{\mathrm{th}} = \dot{Q}_\mathrm{r}/(I_\mathrm{r}A_\mathrm{r})$. Thus, one can say

that the solar collector efficiency is given by $\eta_{\text{coll}} = \eta_{\text{opt}} \times \eta_{\text{th}}$. The energy balance on the solar receiver reads

$$I_{\text{r}} A_{\text{r}} = \dot{Q}_{\text{r}} + U A_{\text{r}} (T_{\text{r}} - T_0), \tag{9.22}$$

where U is the linearized heat loss coefficient of the receiver, assumed at the temperature T_{r}, higher than that of the environment T_0. If one divides Eq. (9.22) with $(I_{\text{T0}} A_a)$, the collector efficiency is obtained as follows (note that $C = A_{\text{a}}/A_{\text{r}}$ is the concentration ratio):

$$\eta_{\text{coll}} = \eta_{\text{opt}} \times \left[1 - \frac{U(T_{\text{r}} - T_0)}{C I_{\text{T0}} \eta_{\text{opt}}} \right], \tag{9.23}$$

which identifies that

$$\eta_{\text{th}} = 1 - \frac{U(T_{\text{r}} - T_0)}{C I_{\text{T0}} \eta_{\text{opt}}}. \tag{9.24}$$

Equations (9.22) to (9.24) are general and apply to all types of solar collectors classified in Fig. 9.17. We will detail next the optics point concentrator, as it is very instructive. For a point concentrator, the optical efficiency is large when most of the concentrated radiation is captured by the solar receiver surface placed in the vicinity of the focal point, that is, when the hot spot exposed to the radiation has a large area. However, a large hot spot area means large heat losses through radiation or possibly through convection.

The optics of a paraboloidal dish solar concentrator including the definition of the main parameters like the rim angle, aperture, parabola equation, and the focal distance is described in Fig. 9.19a, which illustrates the profile of a paraboloidal mirror targeting the sun. The image of the solar disk is incident on every point of the mirror surface under an angle of about 32 min (~0.54°) and is specularly reflected toward the focal point under the same angle. In the focal plane, the solar disk image will be deformed, depending on the location of any particular point on the mirror. The points from the rim circle produce mostly deformed images; this maximum deformation is indicated with D_{FP} in the figure. The minimal deformation corresponds to the central point of the mirror (note that this point is generally shaded). The mirror's reflectivity, shading, glazing transmissivity, absorptivity, and other parameters affect the quality of the optical image formed in the focal plane. The relevant parameters for optical modeling of the solar dish are defined in Table 9.2. Based on the definition of the optical efficiency (above) and the definitions presented in Table 9.2,

$$\eta_{\text{opt}} = \zeta \rho \gamma \tau \alpha. \tag{9.25}$$

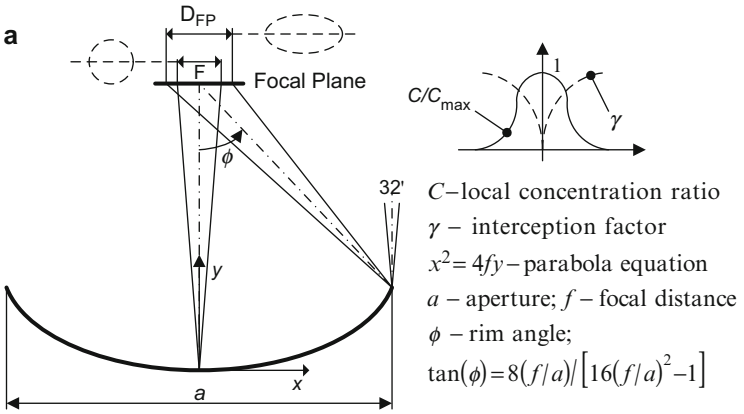

Optical parameters of solar concentrator

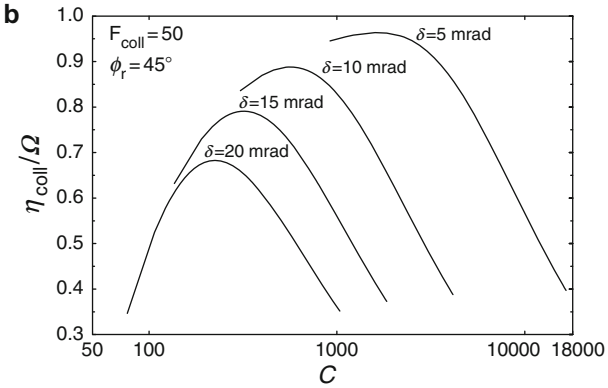

Point focus collector efficiency

Fig. 9.19 Optical model and efficiency of a point-focus solar collector with a rim angle $\phi_r = 45°$, as a function of the concentration ratio and optical errors δ [modified from Zamfirescu et al. (2008)]

For design calculation, the values of shading, reflectivity, transmissivity, and absorptivity are assumed to be average values. The statistical dispersion of their values, however, is taken into account through several kinds of optical errors. Thus, we will express the optical efficiency by two factors. The first factor is the optical factor introduced here as follows:

$$\Omega = \zeta \rho \tau \alpha. \tag{9.26}$$

The optical factor is calculated with averaged values for the reflectivity, transmissivity, and absorptivity, and it has values in the range of 0.75 to 0.85 depending

Table 9.2 Relevant optical parameters characterizing the optics of a solar dish concentrator

Name	Definition	Remarks
Shading factor	$\zeta = \frac{A_u}{A_a}$	It represents the ratio between unshaded mirror area and aperture area.
Reflectivity	$\rho = \frac{I_\rho}{I_{T0}}$	The reflected solar radiation intensity over the incident radiation intensity. Reflectivity accounts for imperfect specular reflection.
Intercept factor	$\gamma = \frac{\int_0^{A_{ab}} I \, dA}{I_\rho A_u}$	Not all concentrated radiation falls on the absorber surface. There is a practice to reduce the absorber surface in order to minimize the heat transfer. Thus, one accepts that some concentrated radiation is lost. The intercept factor represents the ratio between the radiation power falling on the absorber and the power associated to the radiation reflected toward the focal point.
Transmissivity	$\tau = \frac{I_\tau A_{ab}}{\gamma I_\rho A_u}$	In the case when the absorber is covered by glazing (a practice intended to reduce the heat loss via convection), a part of the incident (concentrated) radiation is lost due to transmission through glazing. The transmissivity represents the ratio between transmitted power through glazing and the radiation power incident on glazing.
Absorptivity	$a = \frac{I_c}{I_\tau}$	It represents the ratio between the absorbed heat flux and the power associated with the radiation incident on the absorber.

on the quality of the optics. The second factor is the intercept γ, which accounts also for statistical dispersion of the reflectivity and other optical errors (see Table 9.2). Note that

$$\eta_{opt} = \Omega\gamma. \tag{9.27}$$

Figure 9.19a also presents (qualitatively) the variation of the intercept factor in the focal plane, in the vicinity of the focal point (see the upper right corner). The intercept factor is nil in the focal point because no surface area can be associated with one single point; therefore, no radiation is "intercepted." The parameter x in the plot $\gamma(x)$ is the radial coordinate originating in the focal point. In measure with increasing x, the amount of intercepted light increases over a disk centered at the focal point; thus, the intercept factor increases and eventually reaches the unity value. The derivative of the $\gamma(x)$ represents the local concentration ratio that obviously has a maximum right at the focal point. The geometric concentration ratio is related to the optical system geometry, optical errors, and the intercept factor through the fact that γ is a function of A_r.

There are several kinds of optical errors that affect the quality of the solar image projected on the receiver's surface. All of the optical errors cited in the following discussion represent statistical means relative to the entire area of the solar concentrator. A first, unavoidable error is caused by the nonuniform angular distribution of solar radiation beam, δ_{sun}. Even though this is a small contribution to the overall optical error, it cannot be neglected; it has a typical value of one fourth of the solar angle, namely 2.3 mrad. Other errors are the slope error of the concentrator δ_{slope}

(typically 2–3 mrad), the specularity δ_ω (typically 0.5–1 mrad), and the pointing error δ_p, meaning the receiver is not placed exactly at the focal point. These individual angular errors produce an overall optical error accounted for by $\delta^2 = \delta_{sun}^2 + \delta_{slope}^2 + \delta_\omega^2 + \delta_p^2$.

Using the above derivations, it can be shown that the collector efficiency can be analytically expressed as $\eta_{coll}\Omega = \gamma(1 - F_{coll}/C\gamma)$, where $F_{coll} = U(T_r - T_0)/(I_{T0}\zeta\rho\tau\alpha)$ is a collector factor depending on the solar absorber temperature (assumed at the average), the insolation, and optical properties. Figure 9.19b illustrates the variation of collector efficiency (expressed as $\eta_{coll}\Omega$) with the concentration ratio for several optical errors δ. It is clearly observed that the efficiency increases with the quality of the surface (smaller δ), which occurs each time there is an optimal concentration ratio for which the collector efficiency is maximum. The existence of this maximum can be explained intuitively:

- If the concentration ratio is too low, then the concentrated radiation is low, and the heat absorbed by the receiver is low.
- If the concentration ratio is too high, then the receiver temperature and thus the heat losses to the ambient air are higher; thus, the heat absorbed by the receiver is also low.

In general, the optical factor is high (0.8–0.95), which indicates that the point-focus solar concentrators can reach an efficiency over 70%.

9.2.2.4 Solar Thermal Applications

The applications of solar thermal energy are classified in Fig. 9.2 into three categories, namely, heating, production of mechanical energy, and conversion to chemical energy. Many processes require heat as input. Some examples are suggested in Fig. 9.2 (water heating, space heating, cooking, drying, etc.) but the list is long (e.g., it may include solar refrigeration, various industrial processes, and many others). An important application is conversion of thermal energy into work using heat engines. This application is discussed largely in Section 9.2.3.2 regarding the conversion of solar energy into chemical energy; hydrogen production appears to be very important for the sustainable development. Various paths to produce hydrogen from solar thermal energy are analyzed in Chapter 13.

Illustrative Example: Drying Food Products with Solar Thermal Energy

In this example, the efficiency of a solar dryer for food products comprising an air heater driven by solar energy and a drying chamber is analyzed. The example is taken from Tiris et al. (1995). Drying is a method of preservation of food products. The system is presented schematically in Fig. 9.20. The air is taken from outside and circulated by a blower over a valve and electrical heater, a flowmeter, followed by a solar air heater and a drying chamber. The flow rate and pressure drop over the air heater are measured with appropriate instruments. The drying chamber includes a rack with food products among which warmed air is circulated.

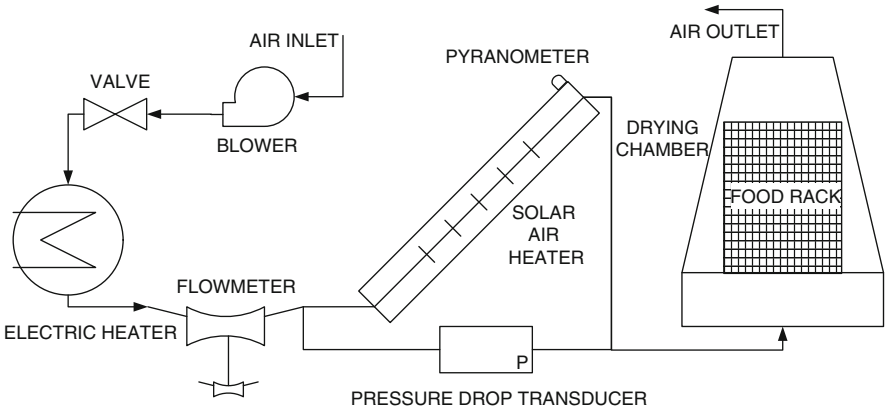

Fig. 9.20 Solar food drying system [modified from Tiris et al. (1995)]

The air dryer is a parallel-piped–shaped box that includes helical-type aluminum wires painted in black and functioning as an absorbent surface for solar radiation and an extended surface to enhance the heat transfer to the air. During the experiments, the air-solar collector has been tilted at 30° pointing in a southerly direction. The collector glassing has been made from polyester combined with transparent glass wool, conferring elasticity, durability, acoustic dumping, and high transmittance. The valve in the diagram has the role of air flow regulation, while the electric resistance was used to pretest the solar drying process and to preselect the air entrance temperature in the solar heater. A star-type pyranometer has been used to measure the solar radiation on the tilt surface. The wind speed and the air humidity were also recorded. Several kinds of foods were dried in this system in a series of experiments by Tiris et al. (1995). The moisture contents and weight changes of the test samples were determined based on measurements.

The efficiency of the solar air heater was calculated with $\eta_{\mathrm{SAH}} = \left(\dot{m}c_{\mathrm{p}}\right)_{\mathrm{air}}(T_{\mathrm{out}} - T_{\mathrm{in}})/I_{\mathrm{T0}}$. The process efficiency is based on absolute air humidity determinations in the drying chamber. Namely, the efficiency of the process is calculated by $\eta_{\mathrm{dry}} = (x_{\mathrm{out}} - x_{\mathrm{in}})/(x'' - x_{\mathrm{in}})$, where x'' is the saturation humidity of the air at inlet; note that because the air takes humidity from the products, it is always the case that $x_{\mathrm{out}} > x_{\mathrm{in}}$.

The results indicate that the collector efficiency η_{SAH} was around 40% to 80% while the drying process efficiency varied in time during the process depending on the type of food product. Initially, the process efficiency is higher, and while the process evolves the efficiency diminishes. For a mass velocity of the air of 0.055 kg/m^{2}s, the results were correlated according to Fig. 9.21. The beans show the best efficiency, which at the beginning of the process is about 90% and decreases to around 35% after 35 hours of drying. The efficiency varies by process, starting in the range 20% to 90%, the lowest value being for chili peppers. At the end of the process, the efficiencies are in the range of 7% to 30%. The average

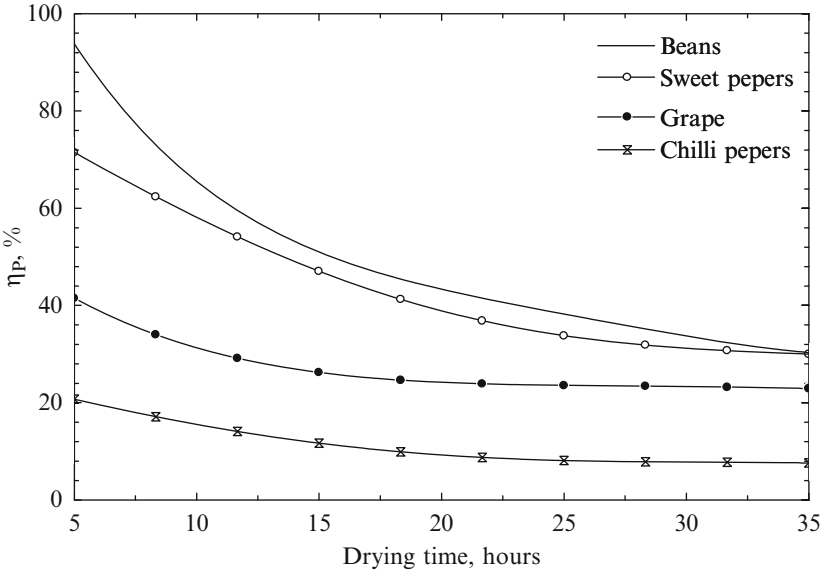

Fig. 9.21 Process efficiency of solar dryer for food products [data from Tiris et al. (1995)]

process efficiency is in the range 30% to 80%, and higher air flow rates are recommended for obtaining higher efficiencies.

Illustrative Example: Solar Refrigeration

In this example, it is shown how absorption refrigeration systems save energy when driven by solar radiation during the summer. On a summer day there is high solar radiation, and at the same time there is a peak demand of air conditioning. However, due to a higher ambient temperature, power generation during the summer is lower. Thus, an absorption-driven refrigeration system has a better chance to have higher thermal-to-cooling efficiency than an electrically driven vapor compression system. A system using an absorption machine operating with a mixture of R22 and DMETEG (DiMethyl Ether Tetra Ethylene Glycol) is exemplified here based on the results by Dincer et al. (1996b). The system has been designed to provide 4.65 kW of cooling load at −5°C and operates at a condensation pressure of 16 bar and an evaporation pressure of 4.8 bar. The solar collector is thermally connected with the vapor generator of the absorption machine, which operates at 80° to 100°C. The coefficient of performance (COP) of the system is defined in the usual manner as

$$\mathrm{COP} = \dot{Q}_e / \left(A_c I_{T0} + \dot{W}_p\right),$$

where $\dot{Q}_e$ is the evaporator capacity (see Fig. 9.22a), I_{T0} is the insolation on tilted surface (in W/m^2), A_c is the collector area (in m^2); one also has $A_c I_{T0} \dot{Q}_g$, where $\dot{Q}_g$ is the vapor generator capacity. The results show COP is in the range of 0.3 to 0.6 and correlated with the generator temperature and the temperature difference between the absorber and the evaporator ($T_a - T_e$) and are presented in Fig. 9.22b.

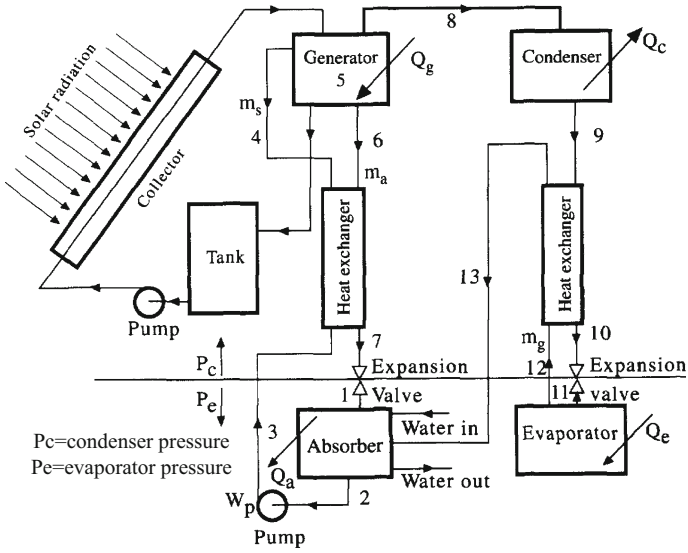

(a) The system

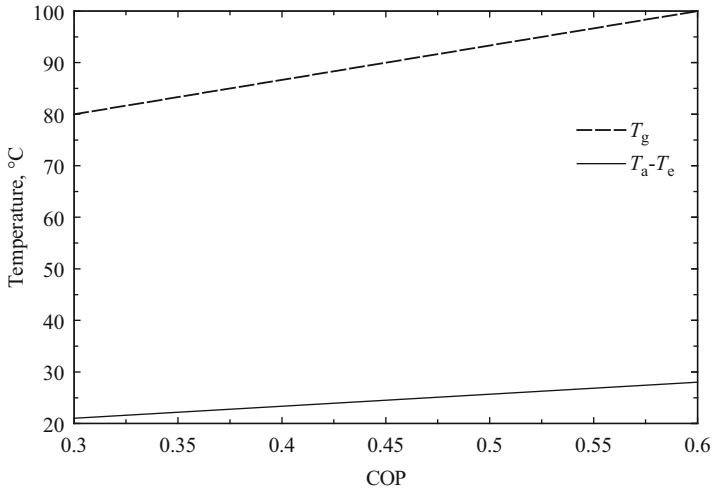

(b) The COP correlated with system temperatures

Fig. 9.22 Solar absorption refrigeration system operating with R22-DMETEG [modified from Dincer et al. (1996b)]

9.2.3 Solar Electricity

The classification of solar conversion systems from Fig. 9.2 suggests two major paths to generate electric power from solar energy: photovoltaics (where electricity is obtained by direct conversion of solar energy) and conversion of solar thermal

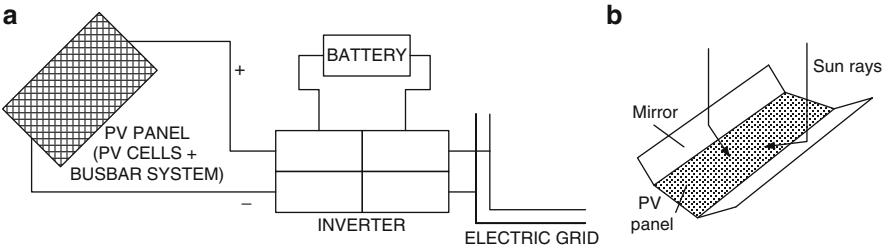

Fig. 9.23 (**a**) Simplified PV system diagram and (**b**) a V-trough concentrator

energy into mechanical energy followed by conversion of mechanical energy into electrical energy. There also may be some additional ways to generate solar electricity, namely by producing synthetic fuels with solar thermal energy and then converting the fuels into electrical energy by combusting them either in mechanical systems connected with heat engines or in fuel cell systems. However, one may argue that this path is rather a means of storage of solar energy for longer durations, because it has the quality to decouple the energy production from energy demand. We will focus in the next two sections on the photovoltaic system and solar-driven heat engines dedicated to generating electricity as the sole product.

9.2.3.1 Photovoltaic Systems

Photovoltaic systems comprise a number of elements such as photovoltaic panels, a tracking system (in some cases), an inverter (grid connection system), and an electrical storage system (batteries, reversible fuel cells together with hydrogen storage tank, or fuel cell/water electrolyzer system), such as indicated in a simplified manner in Fig. 9.23a. The most important component of these is the PV panel. The elemental component of a PV panel is the PV cell, which is a p–n semiconductor junction exposed to solar radiation. As already discussed above, the photons incident on the p–n junction dislocate electric charges in the form of electron–hole pairs. The many semiconductor junctions (PV cells) that constitute the PV panel are connected to a busbar system to form a series of parallel networks of sources. On the surface of the panel there is a "competition" for space occupation between the PC cells and the busbar system. On the one hand, one needs to install as many PV cells as possible per square meter of panel to have a higher number of electric generators; on the other hand, one needs to allocate as much space as possible to the busbar system in order to reduce the internal resistance of the panel. Thus, the efficiency of the PV panel can be written as the product of the PV cell efficiency and the efficiency of the busbar.

The efficiency of the PV cell itself (the semiconductor junction) is mostly affected by the filling factor. The operating temperature also affects the cell efficiency. Silicon-based and Ga-As-based semiconductors are currently the most used in PV panels because their price and efficiency are well balanced. Table 9.3 gives the efficiency of some PV cells for air mass zero and the beginning of

Table 9.3 Characteristics of the main types of PC cells

Cell type	Mass (kg/m^2)	Cost (k/m^2$)	Cost (k$/kg)	Efficiency (%) 28°C	58°C	η_{cell} at 100°C	$\eta_{cell,conc}$ at 100°C[a]
Si (200 μm)	0.55	11.0	20	13.5	11.9	9.7	17.0
High η Si (100 μm)	0.28	14.0	50	16.0	14.2	11.6	20.3
Double junction (100 μm)	0.83	116.2	140	22.0	20.7	18.8	32.9
Triple junction	0.85	127.5	150	25.0	23.3	20.9	36.6
Quadruple junction	0.86	133.3	155	28.8	26.8	24.1	42.2

η given with respect to 1,350 W/m^2 incident normal radiation
Data from Joshi et al. (2009b)
[a]At $C = 1.75$

life conditions at three temperatures: 28°C, 58°C, and 100°C. Note that higher operation temperatures on PV cells can be due to the solar radiation concentration.

For a concentration ratio of 1.75 the cell temperature becomes about 100°C. Note that the efficiency of the PV cell decreases with increasing temperature and increasing light concentration. However, the overall effect of light concentration is an increased efficiency of the cell, where the efficiency of the panel is given by

$$\eta_{cell,conc} = \eta_{cell} \times C, \tag{9.28}$$

where $\eta_{cell,conc}$ is the efficiency of the cell subjected to concentrated radiation. In Table 9.3, both the η_{cell} and $\eta_{cell,conc}$ for the 100°C operation temperature case are indicated. Note that a concentration as small as 1.75 can be easily obtained by adding side mirrors (known as V-trough concentrators) to the PV panel. The principle of V-trough concentrators is illustrated in Fig. 9.23b.

For each PV cell type Table 9.3 shows the weight per unit of the panel surface assembled with the respective cells and the cost per unit of panel weight. Currently, intensive research efforts are being pursued for development of PV cells with a quadruple semiconductor junction on a wafer. Table 9.4 lists the efficiencies of the components involved in a photovoltaic installation. For electricity storage, two cases can be considered: electricity storage in batteries and in reversible fuel cells. In the last case the storage medium is hydrogen (and possibly oxygen). The efficiency of the storage is defined as the energy retrieved per energy stored. In the reversible fuel cell system the efficiency is about 56% (energy) and 52% (exergy) for hydrogen/oxygen generation from water electrolysis during the storage phase and about 60% for the electricity retrieved during fuel cell operation of the storage system. Thus the storage efficiency is about 25% (energy) and 23% (exergy). If batteries are used for storage, approximately the same efficiency is expected.

The efficiency of a grid-connected system is represented by the product of the efficiency of the PV panel, the inverter efficiency, and the efficiency of other system

Table 9.4 Average energy and exergy efficiencies of the components of a photovoltaic plant

Component	Energy efficiency	Exergy efficiency
Photovoltaic panel	Monthly power generation as delivered to the grid per incident solar radiation per unit of area	Monthly power generation as delivered to the grid per incident solar exergy per unit of area
	11.2–12.4%	9.8–11.5%
Charge regulators	D.C. power output over D.C. power input	D.C. power output over D.C. power input
	85–90%	85–90%
Inverter	A.C. power delivered to the grid per D.C. power input	A.C. power delivered to the grid per D.C. power input
	85–90%	85–90%
Electricity storage (battery, reversible fuel cell)	Energy retrieved per energy stored (Note: in reversible fuel cells hydrogen is the storage medium)	Exergy retrieved per exergy stored
	25%	23%

Data from Joshi et al. (2009b)

components (η_{other}) such as electrical cables and resistors. Note that a grid-connected system may not require electricity storage systems. Thus, the grid-connected system without storage has an efficiency of

$$\eta_{\text{PV,GC}} = \eta_{\text{panel}} \times \eta_{\text{inverter}} \times \eta_{\text{other}}. \tag{9.29}$$

The annual average of a typical grid-connected PV system (without storage) is about 6%, while the inverter's annual average efficiency is 75%, and that of PV panel itself about 7% to 8%. If the system comprises electricity storage (the case in which it is not necessary for the system to be grid connected), the annual efficiency is about 3%.

Calculation of energy and exergy efficiency of the PV cells is based on Eq. (9.18); however, when PV cells are used within a PV panel, the arrangement is such that the cells necessarily heat up while they are exposed to heat transfer toward a colder environment. Thus the generated exergy by the panel is on one side electrical ($\dot{E}x_{\text{el}} = \text{FF} \times V_{\text{oc}} \times I_{\text{sc}}$) and on another side thermal, namely $\dot{E}x_{\text{th}} = (1 - T_0/T_{\text{cell}}) \times (UA)_{\text{cell}} \times (T_{\text{cell}} - T_0)$; this thermal exergy is lost. Thus the exergy efficiency of the PV cell is

$$\begin{aligned}\psi_{\text{PV}} &= \frac{\dot{E}x_{\text{el}} - \dot{E}x_{\text{th}}}{\dot{E}x_{\text{solar}}} \\ &= \frac{\text{FF} \times V_{\text{oc}} \times I_{\text{sc}} + (1 - T_0/T_{\text{cell}}) \times (UA)_{\text{cell}} \times (T_{\text{cell}} - T_0)}{(1 - T_0/T_{\text{S}}) I_{\text{T0}}},\end{aligned} \tag{9.30}$$

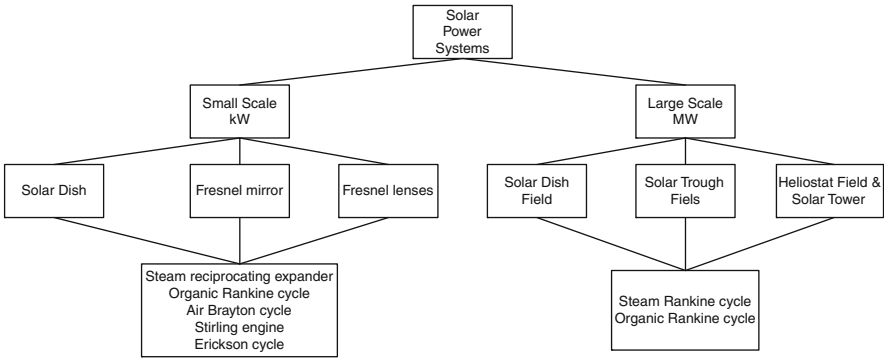

Fig. 9.24 Solar heat engines for power generation [modified from Zamfirescu et al. (2008)]

where I_{T0} is the global solar radiation on a tilted surface, while I_{sc} represents the short circuit current of the PV cell. The quantity $(UA)_{cell}$ represents the product of the superficial heat transfer coefficient between the panel and surroundings and the heat transfer area associated with the panel. Because of the associated heat losses, the exergy efficiency of the solar panel is lower than the energy efficiency by about 2%.

9.2.3.2 Solar-Driven Heat Engines for Power Generation

Solar-driven heat engine systems for power generation consist of solar-concentrating collectors that generate high-temperature heat to drive heat engines (e.g., Rankine or Brayton cycles). The heat engine produces shaft work that in turn drives an electrical generator. Such systems can be connected to the grid or they can work independently, such as the case in which electrical energy storage is applied to compensate for the intermittence of the solar source. In larger systems, a field of collectors is used to capture the solar energy, which is transmitted by means of a heat transfer fluid or a solar-produced synthetic fuel to a centralized power plant. In small-scale systems every individual unit is equipped with a low-power heat engine, usually placed in the focal point of a solar concentrator, close to the solar receiver. Small-scale systems are mainly based on paraboloidal dish solar-concentrating collectors.

In Fig. 9.24, a classification of solar power plant systems that use heat engines driven by solar thermal energy is suggested. The systems were classified into two categories: small-scale production capacities (of the order of kW) and large-scale ones from a few MW to hundreds of MW installed capacity. The type of solar concentrator and the type of heat engine for each category are indicated.

Low-power generation systems that normally use Rankine power generators operated with organic fluids (e.g., toluene), known also as organic Rankine cycles (ORC), are believed to be the most effective. Ammonia–water, ammonia, and other refrigerants are also working fluids worth considering in Rankine engines of low capacity that can use low-cost refrigeration compressors of the scroll or screw

type in reverse, namely as expanders. This feature increases the marketability of independent low-power solar-driven generators.

Other heat engine options are Stirling engines, which operate at very high pressures, of the order of 200 bar, and temperatures in the range of 700° to 800°C working with helium or hydrogen. Moreover, hydrogen is highly flammable, which imposes severe safety issues. A drawback with these systems is that hydrogen and helium leak easily, which raises maintenance problems. However, Stirling systems are very compact and reach high engine efficiency, which is around 40%, according to the review by Zamfirescu et al. (2008), leading to overall electricity production efficiency of 22% to 23% for 10 h/day operation and installed capacity of 10 to 25 kW. One of the main drawbacks of using Stirling engines in solar applications is the long warm-up time needed, which is at odds with the reality of solar energy's fluctuating nature.

Open-air Brayton cycle engines mounted at the dish focal point were also used in some applications (see Zamfirescu et al. 2008). They operate efficiently at higher receiver temperatures than what are usual for Stirling and Rankine cycles, that is, over 1,000°C where Brayton engines may attain over 26% efficiency. These cycles operate with air at once passing and they use internal heat recovery through heat exchanger between the incoming and outgoing flows.

Regarding large-scale solar technology, significant progress has been made with nine power-generating stations totaling 354 MW power-generating capacity that were built in California's Mojave Desert by the 1980s. These systems use parabolic trough collectors to collect heat and generate steam for a Rankine cycle. On average, large-scale solar trough steam power plants obtain 120 to 175 W of electric power per square meter of solar collector at a 350°C steam temperature.

Most of the large-scale solar plants are hybridized with natural gas or coal combustion. Figure 9.25 presents a significant example of a hybridized power plant. The net capacity of such systems, known as integrated solar combined cycle systems, is at least 10% for a capital cost of $3–5 million per installed MW.

The second representative large-scale power plant technology is based on solar tower concentrators. Dish-based systems are more cost competitive than parabolic troughs, mainly due to their better performance. Table 9.5 presents the main performance parameters of three kinds of nonhybridized large-scale solar power generation systems. The levelized electricity cost (see definition below) decreases with the installed performance.

Solar power plants entail lower maintenance costs than do fossil fuel power plants. The levelized cost of generated electricity is therefore affected mainly by the investment cost. According to the definition, the levelized electricity cost (LEC) is calculated based on the capital cost (CC), the maintenance cost (MC), and the lifetime (LT) according to the following basic equation:

$$\mathrm{LEC} = (\mathrm{CC} + \mathrm{MC})/(\mathrm{LT} \times \eta_{\mathrm{e}} \times \bar{I}_{\mathrm{T0}}), \tag{9.31}$$

where η_{e} is the solar to electrical energy conversion efficiency and $\bar{I}_{T0}$ is the global solar radiation averaged over the lifetime of the system.

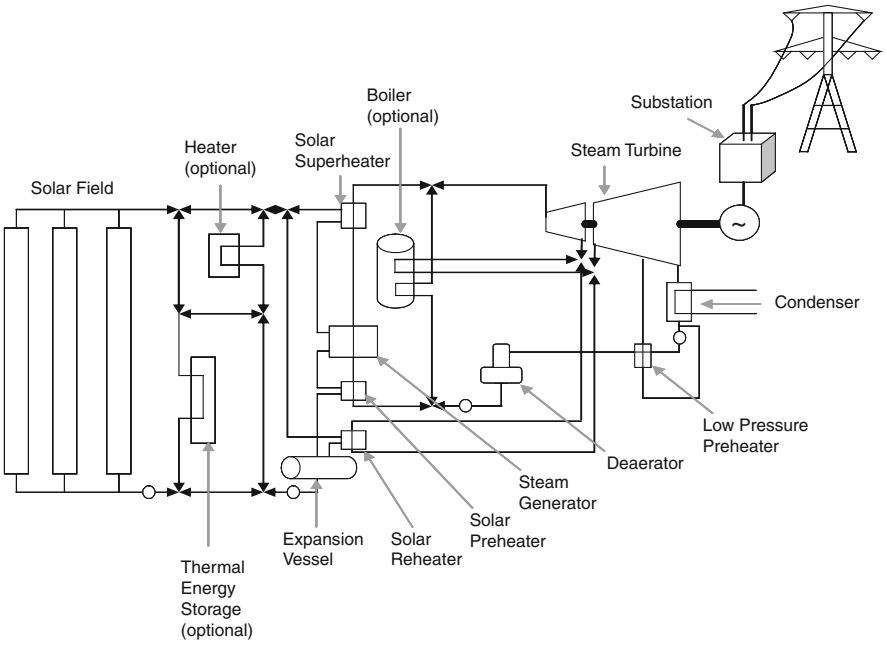

Fig. 9.25 Schematic of a hybrid solar trough power plant [modified from Zamfirescu et al. (2008)]

Table 9.5 Summary of performance of large-scale systems

Technology	Parabolic trough + oil	Solar tower system	Solar dish field
Mean net efficiency	14%	14%	20%
Specific power generation (kW h/m^2 year)	308	316.5	340
Levelized capital costs (\$/kW h_e year)	2.39	4.22	2–4
Operation and maintenance (¢/kW h)	4.96	6.05	4–6
Levelized electricity cost (LEC) (\$/kW h_e)	0.248–0.295	0.240–0.310	0.2–0.4

Data from Zamfirescu et al. (2008)

9.2.3.3 Solar Electric Storage

All large-scale systems are equipped with solar energy storage facilities. Solar power plants use typically high-temperature thermal storage in molten salt. Solar dish fields with centralized power generation are believed to be the most viable solution for the future because they provide the highest efficiency among all other systems. Chemical storage has been also applied in a test, using either the ammonia decomposition/synthesis loop or the sulfur trioxide $2SO_3 + 196.4\,\text{kJ/mol} \leftrightarrow 2SO_2 + O_2$, chemical loop for thermochemical storage or the loop based on ammonium hydrogen sulfate $NH_4HSO_4 + 132\,\text{kJ/mol} \leftrightarrow NH_3 + H_2SO_4$. In Chapter 11 we provide more information about thermal energy systems applicable to solar energy.

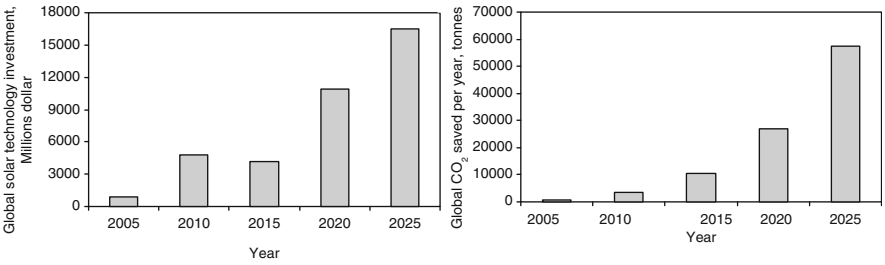

Fig. 9.26 Predictions of solar-electric technology investment and the resulting CO_2 mitigation [data from Zamfirescu et al. (2008)]

9.2.3.4 Solar Electric Applications

Obviously, solar electric power generation can be applied to a broad range of applications. Solar generators can operate either stand-alone or as grid-connected systems for electricity generation. One remarkable application is to use solar electricity to drive electrolysers for hydrogen generation. This application is discussed in detail in Chapter 13.

Water irrigation systems with electricity generated by PV panels to drive pumps became familiar in recent decades. Other applications of PV electricity are for highway signaling, remote located traffic indicators, and many other remote systems or aerospace applications. Thermoelectric concentrated solar generators are of medium to large scale. Low-scale concentrated power system (CSP) using heat engines appear to be an emerging technology that is not yet commercially available. Concentrated solar power generators were also found to be an attractive option for satellites and space missions, in which they operate outside the terrestrial atmosphere.

Two important advantages of solar electricity are reducing pollution and mitigating the release of CO_2. It is predicted that solar electric systems will proliferate in future years. The carbon dioxide mitigation can be estimated based on the installed electric power production capacity that replaces fossil fuel power plants. Zamfirescu et al. (2008) reported a correlation between the predicted evolution of investments in solar electric power technology and the carbon dioxide saved per annum (Fig. 9.26).

9.2.4 Solar to Biochemical Energy Conversion

Another route to solar energy conversion, indicated in the general classification form in Fig. 9.2, is the solar-biochemical one. In this case, special organisms are able to conduct light-stimulating enzymatic processes that convert biological matter from various substrates into biochemical energy present in various organic

molecules such as glucose, sucrose, carbohydrates, and fibers. Some of the bacteria generate combustible gases like hydrogen, ammonia, or methane. Green leaf plants perform the photosynthesis reaction, which mainly leads to fiber formation and the growth of the plants. Plants themselves are the source of the biomass, which, as already mentioned, is one of the renewable energy sources on the earth. Conversion of solar energy through hydrogen via the biological route is explained in detail in Chapter 13, where some general aspects regarding photo-bio-chemical energy conversion are also discussed.

9.2.5 Solar Multigeneration Systems

One principal characteristic of solar radiation is that it embeds two kinds of useful energies in it: light (or photonic radiation) and heat (or thermal radiation. It is known that the infrared spectrum of the solar radiation is viewed as a form of heat. When solar radiation is used to generate electricity, a part of the harvested energy is lost and converted into heat. It makes good sense to generate electricity and heat from solar radiation. In this way, much better solar energy utilization is achieved than with systems that generate only electricity or heat.

Moreover, it is possible to generate more products than heat and electricity from solar radiation with only one system. Electricity, high-temperature heat, low-temperature heat, refrigeration, hydrogen, oxygen, synthetic fuels, and chemicals can be generated simultaneously or in various combinations using solar energy. In Chapter 12 we discuss integrated multigeneration systems, which use various kinds of primary energy sources including solar. Two kinds of solar multigeneration systems have received much attention in recent years, namely photovoltaic/thermal systems and concentrated solar heating and power systems. Both of these are known as solar cogeneration systems. We discuss in this section only the solar cogeneration systems and refer the reader to Chapter 12 for some examples of solar multi-generation systems.

9.2.5.1 Photovoltaic–Thermal Systems

If exposed to a low solar concentration ratio, the temperature of a PV panel increases, as mentioned above. In this case, the PV cell efficiency decreases, but the overall panel efficiency increases. There is a limit to the operating temperature of the PC cells, which, depending on the construction, is in the range of about 60° to 100°C. Lowering the PV panel temperature is a means of increasing the efficiency. If cooling is applied with the help of a heat transfer fluid to a PV panel, its temperature can be maintained between 40° and 80°C (depending on the solar radiation intensity and on whether concentration systems are applied). The heat recovered from PV panel cooling is thus a good level of temperature to be used in a multitude of applications. Consequently, PV/T (photovoltaic–thermal) systems

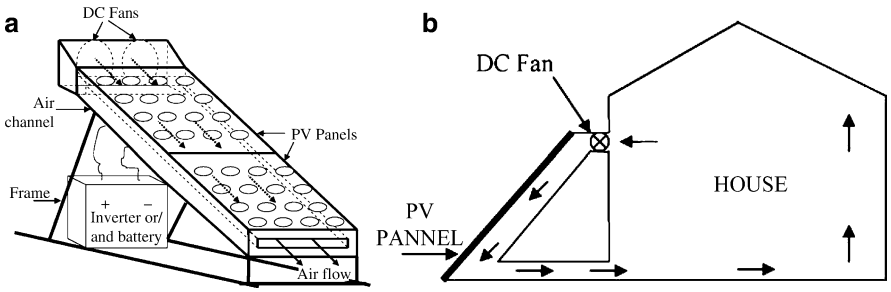

Fig. 9.27 Typical arrangement of PV/T systems using air as the heat transfer fluid (**a**) and their application in space heating (**b**) [modified from Joshi et al. (2009b)]

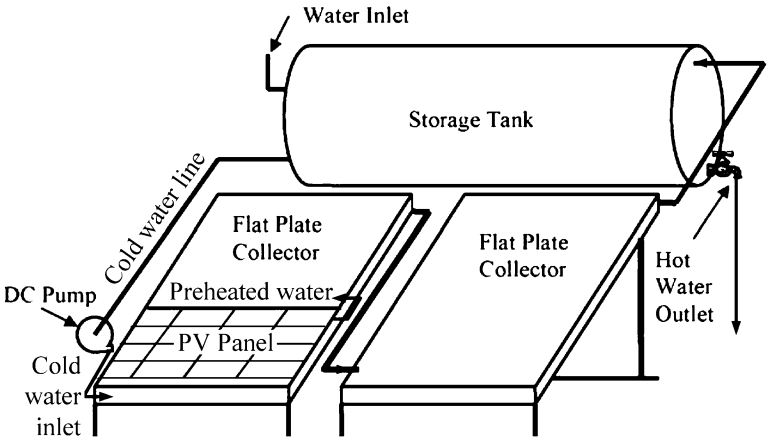

Fig. 9.28 Hot water production with PV/T systems [modified from Joshi et al. (2009b)]

make sense for both increasing the efficiency of power generation and increasing the efficiency of solar resource utilization.

Water, glycol–water, and air are typical heat transfer fluids used in PV/T systems. Hot water can be used for space heating, sanitary water heating, greenhouse heating, solar drying, solar stills, and other purposes. A typical PV/T arrangement that uses air as the heat transfer fluid is illustrated in Fig. 9.27a. The warmed air produced by such a system is at a sufficient temperature for supplying a crop drying facility or for heating a living space as in the arrangement suggested in Fig. 9.27b. When water is used as the cooling medium, arrangements can be made to combine PV technology with a flat plate solar thermal collector. Thus, water at its lower temperature can flow underneath a PV panel so that, through heat transfer, it cools the panel and improves its efficiency. Water is preheated in this way and then passed through flat plate solar thermal collectors for further heating. The diagram of a system as such, used for space and water heating in a residence, is suggested in Fig. 9.28.

The energy and exergy efficiency of the cogeneration system are usually defined as useful electricity and heat generated, expressed in energy or exergy units, respectively, over the consumed solar resource (again in energy exergy units). Thus the energy efficiency can be considered the resource utilization efficiency as, according to its definition, this efficiency is equivalent to the sum of the electrical and thermal efficiencies: $\eta_{cog} = \eta_e + \eta_{th}$. It is also possible to define the energy efficiency of the cogeneration system considering that the electricity is a more valuable product than the heat (Joshi et al. 2009b).

Assume that one disposes of some amount of thermal energy. A good power plant can convert this heat into electricity with $\eta_{PP} = 30$–40% energy efficiency. Thus, in order to generate a quantity of electricity W_e, the amount of heat generated is $Q_e = W_e/\eta_{PP}$. In a cogeneration system, the useful output can be expressed as the sum of the equivalent thermal energy used to generate electricity (Q_e) and the thermal energy that is used as heat (Q_{th}). Thus, the amount of useful heat is ($Q_e + Q_{th}$). By dividing this heat by the total solar energy used we obtain

$$\eta_{cog} = \frac{Q_e + Q_{th}}{I_{T0}} = \frac{W_e/\eta_{PP}}{I_{T0}} + \frac{Q_{th}}{I_{T0}} = \frac{\eta_e}{\eta_{PP}} + \eta_{th}. \tag{9.32}$$

Note that in the above equation the energy quantities are expressed per unit of irradiated surface and I_{T0} is the global solar radiation on the tilted surface. According to general practice (see Joshi et al. 2009b), it is customary to assume the electricity generation efficiency $\eta_{PP} = 38\%$. Thus, a typical air-based PV/T system, which may have a thermal efficiency of 40% and a PV electric efficiency of 8%, corresponds to a solar energy utilization efficiency of 8% + 40% = 48% if the electricity and heat production are directly added, or, if Eq. (9.30) is applied, the cogeneration energy efficiency becomes $8\%/0.48 + 40\% = 57\%$ which is more meaningful.

Solar stills use thermal energy from solar radiation to force water evaporation in a closed environment with the purpose of purifying or distilling brackish water with high salinity. Solar stills can be in this case coupled with a PV panel in order to run the necessary pumps within a PV/T kind of arrangement.

The exergy efficiency of the PV/T systems is substantially higher than that of simple PV systems because of their ability to recover and use the heat generated by the panel. The exergy efficiency of a PV cell that makes part of a PV/T assembly can be estimated by

$$\begin{aligned}\psi_{cog} &= \frac{\dot{E}x_e + \dot{E}x_{th}}{\dot{E}x_{solar}} \\ &= \frac{FF \times V_{oc} \times I_{sc} + (1 - T_0/T_{cell}) \times (UA)_{cell} \times (T_{cell} - T_0)}{(1 - T_0/T_S) I_{T0}}.\end{aligned} \tag{9.33}$$

Table 9.6 System parameters for the experimental PV/T system

Parameter	Value
PV module efficiency	15%
Short circuit current of PV module	4.8 A
Area of the module	139 cm^2
Number of modules per panel (series connected)	36
Open circuit voltage of the panel	21.7 V
Heat loss coefficient from glassing	2.8 W/m^2 K
Heat loss coefficient from channel bottom	0.62 W/m^2 K
Average air velocity in PV/T duct	2 m/s
Tilt angle (New Delhi)	28°

Data from Joshi et al. (2009c)

Exergy efficiency of air-cooled PV/T system is about 30% higher than that of the system wasting the heat generated by the PV panel. Based on the data from Joshi et al. (2009b), it can be estimated that if water is used as the heat transfer fluid, then the solar energy utilization efficiency becomes 25% higher than that of air-cooled PV/T, which means as much as double with respect to PV-only systems. The efficiency of the PV/T panel can be increased even more if a V-concentrator is applied, which leads to an increase of PV/TR efficiency of up to 30% with respect to settings without the concentrator.

Illustrative Example: PV/T System

An experimental PV/T system built and tested at IIT Delhi by Joshi et al. (2009c) is presented here to demonstrate the performance achievement and the system parameters. The experimental setting is similar to that described graphically in Fig. 9.27a; basically, it heats air by flowing it underneath the PV panel, using for this purpose a fan that consumes the electrical energy generated by the panel itself. The calculation of the efficiency of the system takes into account that a part of the generated power is internally consumed.

In Table 9.6, the general constructive parameters of the system are presented. Its panel is made from modules connected in series. The air channel underneath the panel is thermally insulated for better transmission of the thermal energy into the air. The system measures the temperature, air velocity, light intensity, and electric current/voltage probes every hour. The obtained readings for one typical summer day are presented in Fig. 9.29. It can be observed that the temperature difference between the warm PV cell and the exterior temperature is significant, varying from 9°C in the morning to 17°C at noon and to 4°C in the evening. This amount of temperature difference shows that there is a rather good potential to recover thermal energy from the air.

The energy and exergy efficiencies obtained with the PV/T system are presented in Fig. 9.30. For facilitating data interpretation, the variation of the global solar radiation is superimposed on the same figure. In the morning, when the solar radiation starts to grow in intensity and the panel surface temperature is reduced, the electrical efficiency of the system is high (10.5%). At noon, when the solar

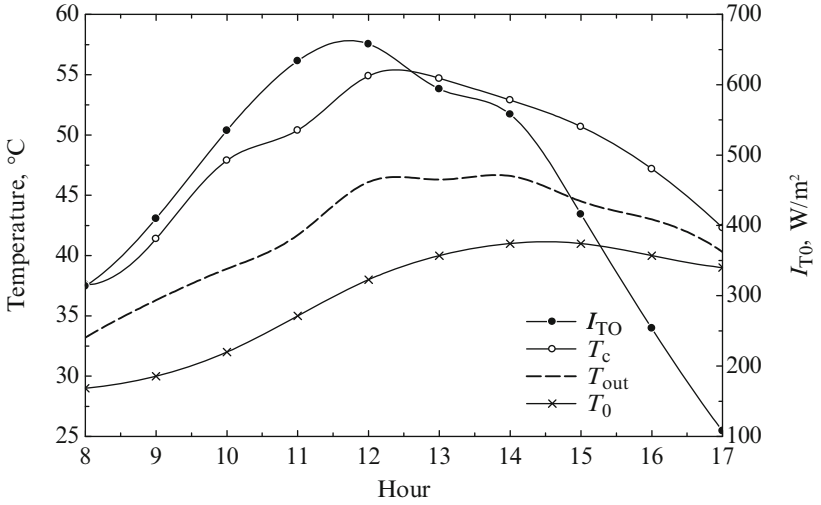

Fig. 9.29 Recorded experimental data for the PV/T system by Joshi et al. (2009c) for a typical summer day in New Delhi [data from Joshi et al. (2009c)]

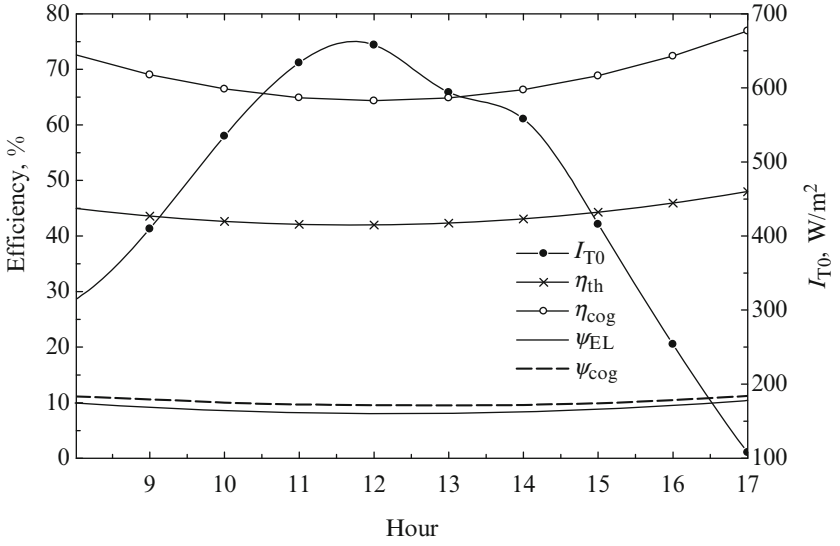

Fig. 9.30 Experimentally determined efficiencies of the PV/T system by Joshi et al. (2009c) [data from Joshi et al. (2009c)]

radiation reaches its highest value, and so does the panel's temperature, the electrical efficiency of the system is the lowest. We can conclude that the degradation of the electricity output due to the increase in cell temperature is more important than the increase in power generation due to the higher solar radiation intensity at noon.

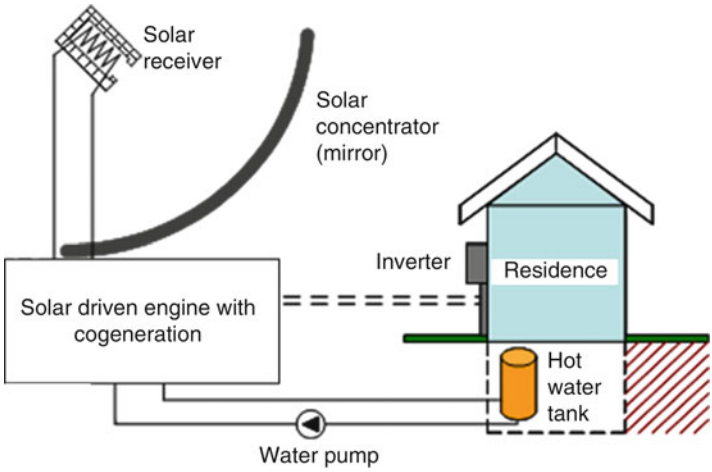

Fig. 9.31 Heat engine system for solar power and heating generation [modified from Zamfirescu et al. (2009)]

The beneficial effect of the continuous cooling of the panel with air can be observed in the early afternoon, when the radiation level is still high but the temperature of the panel stabilizes and so does the electrical efficiency.

The data from Joshi et al. (2009c) have been used here to calculate the exergy efficiencies plotted in Fig. 9.30. The exergy efficiency of the system has been calculated using the energy efficiency data and the Carnot factor associated with the solar radiation, which is $(1 - T_0/T_{\text{sun}})$, where for solar temperature we assumed here 5,777 K. The overall system efficiency has been calculated from energy efficiency data for electrical and thermal generation, according to Eq. (9.32). For calculating the exergy efficiency at heat generation the air output temperature has been used to determine the associated Carnot factor.

As observed on the figure, the system reached maximum cogeneration energy efficiency during the evening (75%) and maximum cogeneration exergy efficiency during the morning (11%). The average thermal efficiency is 44%, and the average electric energy efficiency is 9.5%.

9.2.5.2 Solar Heat Engines for Cogeneration

Solar energy is an excellent resource to supply high-temperature thermal energy to heat engine systems for cogeneration of power and heating. Figure 9.31 shows the schematics of such a system applied for a residence. During the daytime the heat engine generates power and heat at a higher rate than consumption. The additional power is either stored in batteries or delivered to the grid. The excess thermal energy is stored as hot water in an insulated tank. Thus the energy consumption is levelized such that the needs of heating and power during the night are partly or totally covered by the storage.

The heat engine is connected thermally at the low-temperature side with the water stream (or other heat transfer fluid, e.g., glycol, air, etc.), which recovers the heat that otherwise would be ejected by the heat engine at the rate $\dot{Q}_{\mathrm{HR}}$ while generating electric energy at the rate $\dot{W}_{\mathrm{E}}$. The solar concentrator continuously tracks the sun, which irradiates solar energy at the intensity I_{T0} on the aperture area A_{a}. The electric and thermal efficiencies of the system are written as

$$\left.\begin{aligned}\eta_{\mathrm{th}} &= \frac{\dot{Q}_{\mathrm{HR}}}{I_{\mathrm{T0}} A_{\mathrm{a}}} \\ \eta_{\mathrm{e}} &= \frac{\dot{W}_{\mathrm{E}}}{I_{\mathrm{T0}} A_{\mathrm{a}}}\end{aligned}\right\}, \tag{9.34}$$

while the cogeneration efficiency can be calculated with Eq. (9.32) and the cogeneration exergy efficiency with $\psi_{\mathrm{cog}} = \left(\dot{E}x_{\mathrm{e}} + \dot{E}x_{\mathrm{th}}\right)/\dot{E}x_{\mathrm{solar}}$.

One relevant advantage of such cogeneration system comes from the opportunity to recover the rejected heat by the heat engine with minimal losses. The design of the system offers the possibility of applying good thermal insulation around it. In fact, the system may have a point or line focus solar concentrator, characterized by reduced thermal and optical losses (of 5–20% in total). Furthermore, the heat engine can be enclosed in an insulated box, forcing it to deliver the ejected heat only to the heat transfer fluid. Thus at the level of the heat engine a very small amount of heat is lost (it can be lower than 1%). Next, the storage of hot water is made at a reasonably low temperature (say 30°C to 95°C), a fact that facilitates the application of good, inexpensive thermal insulation for reducing the heat leakage (it may be another 1% to 2% from the solar heat). Thus, the solar energy utilization in such a system for heat and power cogeneration can be over 80%.

Two implementations are possible for solar-driven cogeneration engine, depending on the temperature level at which the thermal energy is needed. These two possibilities are explained schematically in Fig. 9.32. The case (a) is the same as discussed above, which corresponds with the cogeneration system presented in Fig. 9.31. This is the case when low-temperature heat is needed (say 80°C to 200°C). In this case, it is advantageous to generate high-temperature concentrated solar heat and let the heat engine operate between T_{H} and $T_{\mathrm{HR}} < T_{\mathrm{H}}$.

If the thermal process served by the system requires high temperature, the system from Fig. 9.32b becomes the logical option. In this case, the concentrated solar heat is stored at the highest temperature. A part of the generated heat is delivered to the process, while the other part is supplied to a heat engine that operates between T_{HR} and the ambient temperature T_0. This option is particularly useful when a fuel is synthesized through a thermochemical process (viz., hydrogen). Chapters 12 and 13 discuss in detail the topics of multigeneration and hydrogen.

One important advantage of the solar cogeneration system (in particular those using heat engines) consists of the possibility of mitigating pollution and carbon dioxide emissions. The mitigation potential can be quantified if one introduces the parameter $\mathcal{M}_{\mathrm{CO_2}}$—the CO_2 mitigation—expressed in kg CO_2 mitigated per kWh

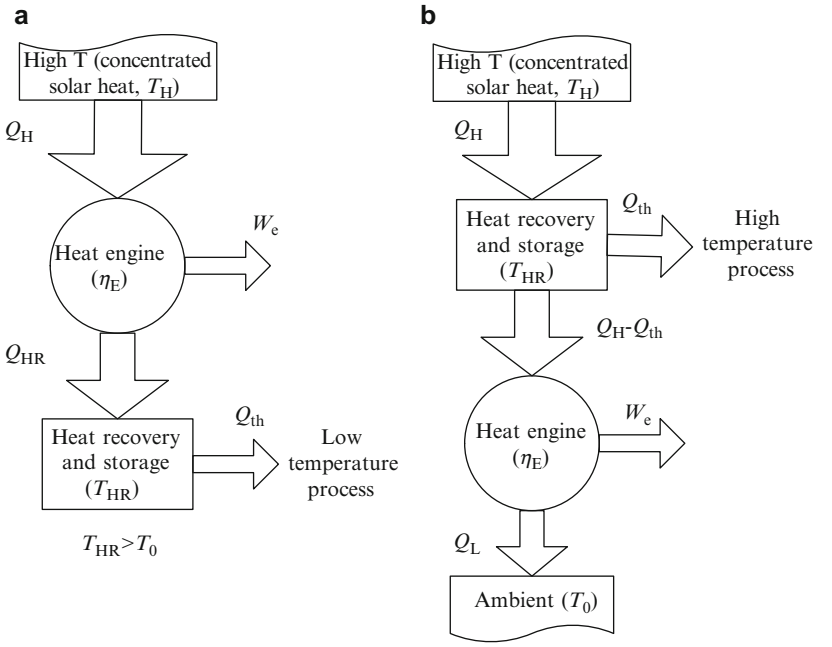

Fig. 9.32 General thermodynamic representation of heat engine systems for solar power and heat cogeneration. (**a**) Low-temperature heat; (**b**) high-temperature heat

of heat and power cogeneration. One can also denote $\mathcal{M}_W$ as the CO_2 mitigation due to avoiding electricity generation from fossil fuels (given in kg CO_2/kW $h_{electric}$) and $\mathcal{M}_Q$ as the CO_2 mitigation due to avoidance of conventional CO_2-emitting heating technologies (e.g., gas/coal combustion, electrical heat pumps). The dimensionless parameter $\tilde{\mathcal{M}}$ is defined as $\tilde{\mathcal{M}} = \mathcal{M}_Q/\mathcal{M}_W$. Note that the parameter $\tilde{\mathcal{M}}$ can vary from 0.5 if methane combustion is used, to 1 if direct electrical heating is used. With this notation the carbon dioxide mitigation $\mathcal{M}_{CO_2}$ can be calculated as

$$\mathcal{M}_{CO_2} = \mathcal{M}_W \frac{\dot{W}_e + \dot{Q}_{th}\tilde{\mathcal{M}}}{I_{T0}A_a} = \mathcal{M}_W\left(\eta_e + \eta_{th}\tilde{\mathcal{M}}\right). \tag{9.35}$$

It is shown in Zamfirescu et al. (2009) that heat engines used for power and low-temperature heat generation can mitigate at least three times more carbon dioxide than those without cogeneration. A typical figure for low-capacity solar cogeneration systems with heat engine is around 0.3 kg CO_2 mitigated per kWh of cogenerated power and heat. Note that some states and Canadian provinces started to adopt various carbon tax systems. British Columbia has already implemented a tax of $10 per ton of CO_2, expected to rise to $30 by 2012. By assuming a carbon tax of $30 per ton of emitted CO_2 in the atmosphere and a grid sell-back contract with the electrical utility at $0.80/kWh, Zamfirescu et al. (2009) showed that

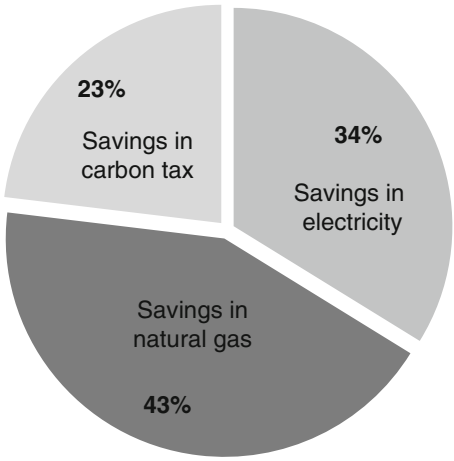

Fig. 9.33 Relative portions of financial savings from solar plant factors [data from Zamfirescu et al. (2009)]

low-capacity solar heat engines for power and heat cogeneration applied to typical Ontarian individual residences can have a payback period of 6 to 8 years. They also determined how much of the cost savings generated by the solar cogeneration system come from the reduction of electrical consumption, the reduction of natural gas (that without the system would be used for heating), and the carbon tax. These findings are summarized in Fig. 9.33, which shows that the largest part of the savings comes from solar heating.

9.3 Wind Energy

Wind energy is a significant renewable energy resource that has shown rapid growth in recent years. The cost of wind energy has come down enough that wind energy farms are now constructed in many locations around the world. Germany, Denmark, and Spain are three of the leading countries in installing wind energy capacities. Wind energy can be regarded as a meteorological variable signifying the energy content of the wind. The parameter that is important for meteorological modeling of wind is the wind velocity. In meteorology, an atmospheric boundary is considered for predicting the local or regional winds by simulation. Other meteorological variables such as temperature, pressure, and humidity of the atmosphere are also important in the occurrence of wind. Such information together with measured velocity data are necessary for determining locations where wind energy farms can be installed and for estimating their capacity and efficiency.

Wind is in fact a form of mechanical energy. It has to be harvested by appropriate engineered devices and converted into other useful energies such as electric energy. The major technical problem with a wind energy conversion system is the fluctuating

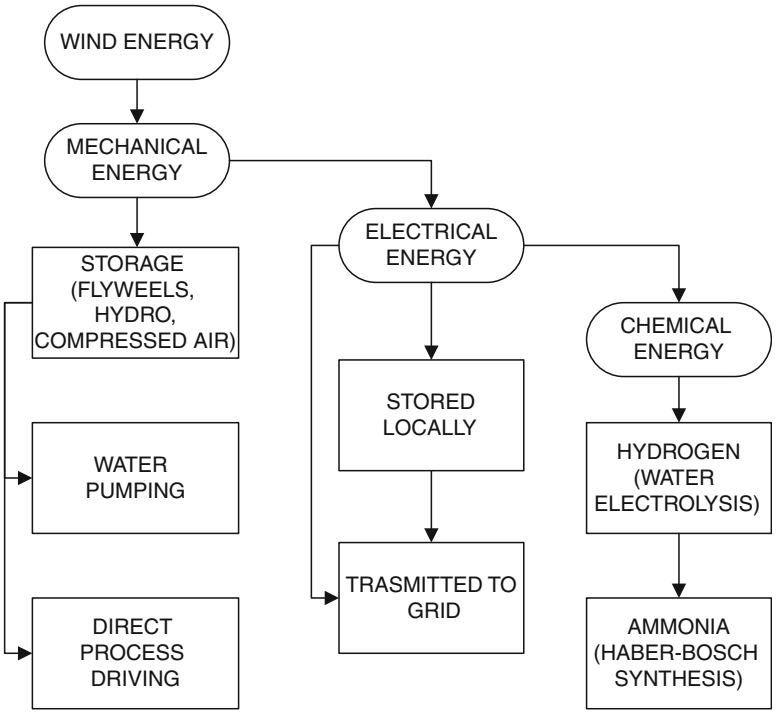

Fig. 9.34 Conversion paths of wind energy

and intermittent nature of wind. The harvesting system (typically a wind turbine) must react fast to the presence of wind or to a change in its direction and intensity. It is important to be able to store the mechanical energy harvested from wing. Several wind energy storage methods are possible, where the mechanical energy resulting from wind is stored in various forms: kinetic (flywheels), electrochemical (batteries), chemical (hydrogen), and thermomechanical (compressed air). Nevertheless, the most used systems are electrical generators actuated by wind energy and having local storage capacities in batteries and possibly being equipped with grid-connecting systems. Wind turbine efficiency reaches about 35% to 50% with the current technology.

The common conversion paths of wind energy are illustrated in Fig. 9.34. The harvested wind energy is normally converted in the shaft rotation of the wind turbine. The mechanical energy can then be used directly. For smooth generation, the mechanical energy can be stored in devices that are able to retrieve it in mechanical form, such as flywheels, hydrostorage, or compressed air. A typical direct use of wind energy is water pumping; others may be grain milling and wood cutting.

The shaft rotating mechanical energy can be converted by appropriate electric generators into electrical energy. The electrical energy can be stored locally or transmitted to the grid or further used for hydrogen generation through water

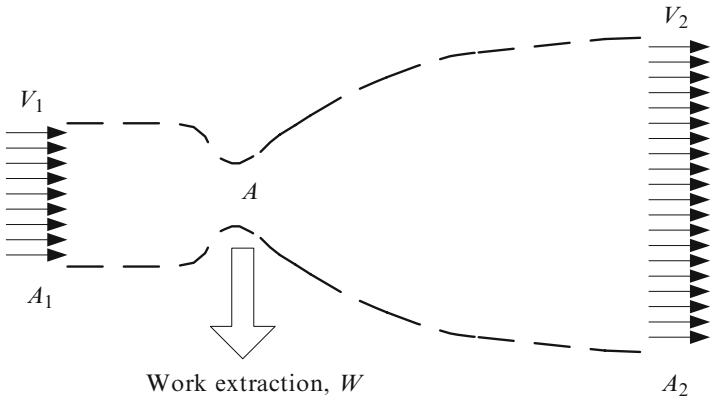

Fig. 9.35 Thermodynamic model for wind energy conversion

photosynthesis. Furthermore, hydrogen can be converted to ammonia through the well-known Haber–Bosch process; this process requires additional consumption of electricity.

9.3.1 Thermodynamic Limits of Wind Energy Conversion

As has been discussed, wind energy is an indirect form of solar energy. Therefore, from the thermodynamic viewpoint one can contemplate wind energy as a heat engine supplied with high-temperature solar thermal radiation at the source and ejecting lower-temperature heat in the terrestrial environment while generating the work necessary to move large masses of air.

9.3.1.1 Maximum Work Generation from Wind Energy

For thermodynamic analysis, a theoretical boundary can be drawn around the turbine for delimiting a control volume as indicated in Fig. 9.35. Outside this boundary, there is no significant modification of the velocity of air. In contrast, inside the control volume the air feels the presence of the turbine; thus, the turbine accelerates or decelerates according to the laws of energy conservation and applicable constraints. Basically, the upstream area of the control volume (A_1) is much smaller than the downstream area (A_2). Thus the velocity at the upstream (V_1) is much higher than the velocity downstream (V_2).

The geometry of the thermodynamic domain is similar to that of a nozzle that extracts work W from the wind. The average velocity of the wind is denoted by $\bar{V} = (V_1 + V_2)/2$, and the mass flow rate of air is approximated with $\dot{m} = \rho A \bar{V}$.

Thus, the rate of variation of wind momentum is $\dot{m} \times (V_2 - V_1) = \rho A\bar{V} \times (V_2 - V_1)$. Therefore, according to the second law of dynamics, the force exerted on the rotor is $F = -\rho A\bar{V}(V_2 - V_1)$. Based on the force and the average velocity, the work extracted by the rotor is $W = \rho A\bar{V}(V_2 - V_1) \times \bar{V}$. This work also can be calculated based on the kinetic energy variation of the air that is, $W = 0.5\rho A\bar{V}\left(V_1^2 - V_2^2\right)$. The equality of the two expressions for W results in $\bar{V} = (V_1 + V_2)/2$ which in fact justifies the definition of the average velocity as the arithmetic mean. Using the notation $\alpha = V_2/V_1$, one can obtain the work extraction as

$$W = \rho \frac{AV_1^3}{4}\left[(1+\alpha)\left(1-\alpha^2\right)\right], \tag{9.36}$$

where the quantities ρ, A, and V_1 should be assumed constant for the analysis; thus, for a given wind velocity, outside temperature and pressure (which fix the air density), and a given wind turbine area, the generated work is a function of the velocity ratio only, $W = W(\alpha)$. It is simple to show that the maximum work is obtained at $\alpha = 1/3$, which corresponds to

$$W_{\max} = \frac{8}{27}\rho \frac{AV_1^3}{4}. \tag{9.37}$$

9.3.1.2 Energy Efficiency and Wind Energy Maps

The energy efficiency of mechanical work production from wind energy must equal the useful shaft work generated per wind energy, both given per unit of turbine surface area. The wind energy is the kinetic energy (0.5). Thus the theoretical maximum energy efficiency of the wind energy conversion is

$$\eta_{\max} = \frac{(8/27)\rho(AV_1^3/4)}{(1/2)\rho AV_1^3} = \frac{16}{27} = 59.3\%. \tag{9.38}$$

Looking back to Eq. (9.36), the quantity between the square brackets defines the so-called power coefficient of the rotor efficiency given by

$$C_p = \left[(1+\alpha)\left(1-\alpha^2\right)\right]/2. \tag{9.39}$$

The turbine efficiency becomes

$$\eta = C_p. \tag{9.40}$$

As shown above, the maximum value of $C_{p,\max}$ is 0.593; however, the efficiency found in practice is in the range of 35% to 45%. With Eqs. (9.36) and (9.39) the work extraction reduces to

$$W = \rho C_p \frac{AV_1^3}{2}. \tag{9.41}$$

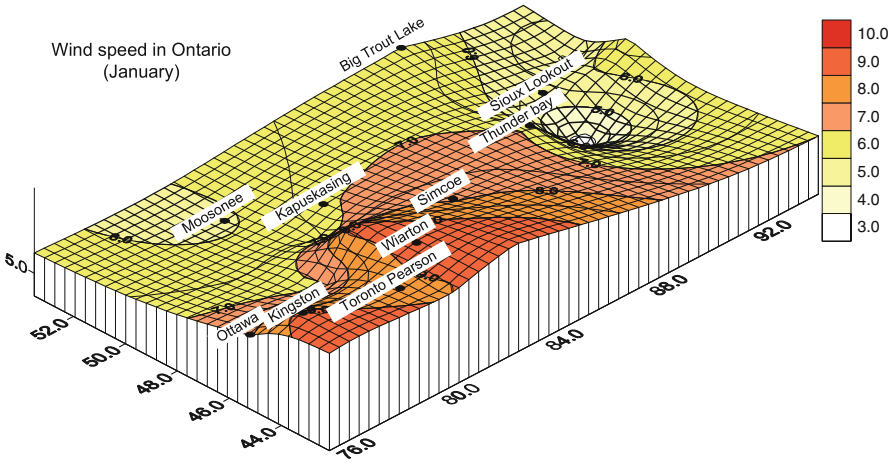

Fig. 9.36 Average wind speed distribution at a 30-m altitude in Ontario during January 3 (longitude, latitude, and amplitude are on the axes) [modified from Sahin et al. (2006)]

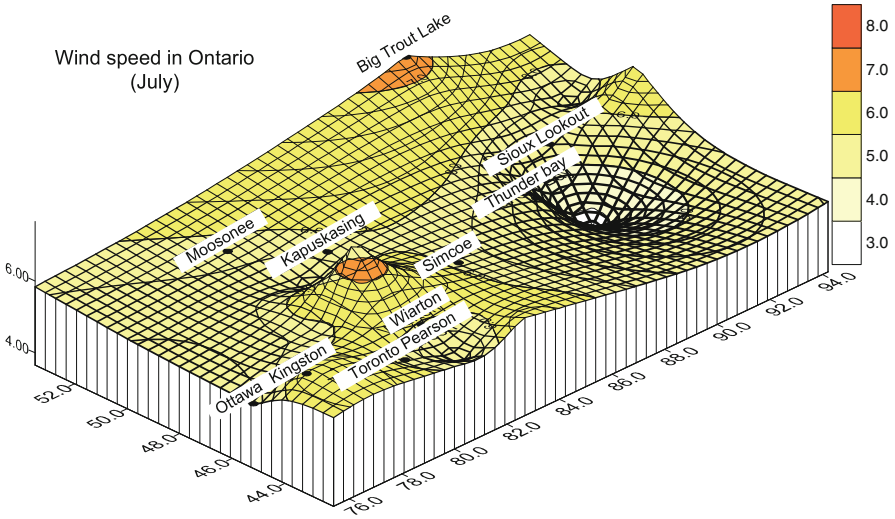

Fig. 9.37 Average wind speed distribution at a 30-m altitude in Ontario during July (longitude, latitude, and amplitude are on the axes) [modified from Sahin et al. (2006)]

Note also that during a period of time (e.g., day, month, season) the wind velocity (V_1) varies. Figures 9.36 and 9.37 exemplify wind velocity variation in Ontario during a winter month (January) and during a summer month (July), respectively.

The wind speed magnitude indicated in the maps is for a height of 30 m above ground, which is the average installation height of wind turbine rotors. In January low speeds are observed in the east and north parts of Ontario. The monthly

maximum average wind speed observed in southwestern Ontario is 9 to 10 m/s. The monthly minimum average value appears to be in Atikokan and it is below the typical wind turbine "cut-in wind speed," and as a result there is no electricity generation. In wind turbine technology, the cut-in wind speed is the minimum wind speed at which a typical wind turbine generator starts supplying electricity. Normally, the wind turbine turns the generator at increased speed when the wind velocity starts to grow. However, the generator does not produce enough voltage to supply the downstream equipment (inverter, battery, grid) unless the rotation speed passes a certain threshold.

This threshold is the cut-in speed and has values in a range, depending on the type of wind turbine and its construction; normally the cut-in wind speed is higher than 3 to 4 m/s. Wind speeds for July (Fig. 9.37) exhibit different clusters as a result of high heating during this month, which creates unstable surface conditions. The highest wind speed for this month is the lowest of the maximum of the other months. When the wind speed is too high it can damage the wind turbine; thus, if a certain higher wind limit is passed, the generator is disconnected from the turbine shaft so that the load is released and the turbine is protected against possible damage created by too high a stress; in this condition, the turbine does not generate velocity. Typically, this threshold wind speed, called the cut-off value, is about 20 to 25 m/s.

Another issue in wind energy conversion relates to the variation of the wind speed at a certain location during a year. The annual probability distribution of the wind velocity affects the total energy generated at a specific location during a year. The so-called Weibull probability distribution can be used to model the occurrence of wind velocity based on two parameters k and c, according to $h(V) = k/c(V/c)^{k-1} \exp\left[-(V/c)^k\right]$; for parameter $k = 2$, this probability distribution function is the Rayleigh distribution, which becomes

$$h(V) = \frac{2V}{c^2} \exp\left[-\left(\frac{V}{c}\right)^2\right]. \tag{9.42}$$

The Rayleigh distribution for annual variation of wind velocity is exemplified in the plot from Fig. 9.38 for the case $c = 7$ m/s; in the plot, the annual probability of occurrence of wind velocity is correlated with the cube of velocity. Two vertical lines are shown at a cut-in speed (V_{ci}) assumed to be 3 m/s and a cut-out speed (V_{co}) assumed to be 20 m/s. Outside the region delimited by V_{ci} and V_{co} the wind turbine does not operate. The hatched area from the plot, which correspond with the wind turbine operation domain, can be calculated with the integral

$$\int_{V_{ci}}^{V_{co}} h(V) d(V^3) = 100\% \times V_{RMC}^3, \tag{9.43}$$

where V_{RMC} denotes the so-called root mean cube wind velocity. Observe that Eq. (9.43) expresses the equality between the hatched area and the gray area from Fig. 9.38. The gray area defines the root mean cube wind velocity as an average

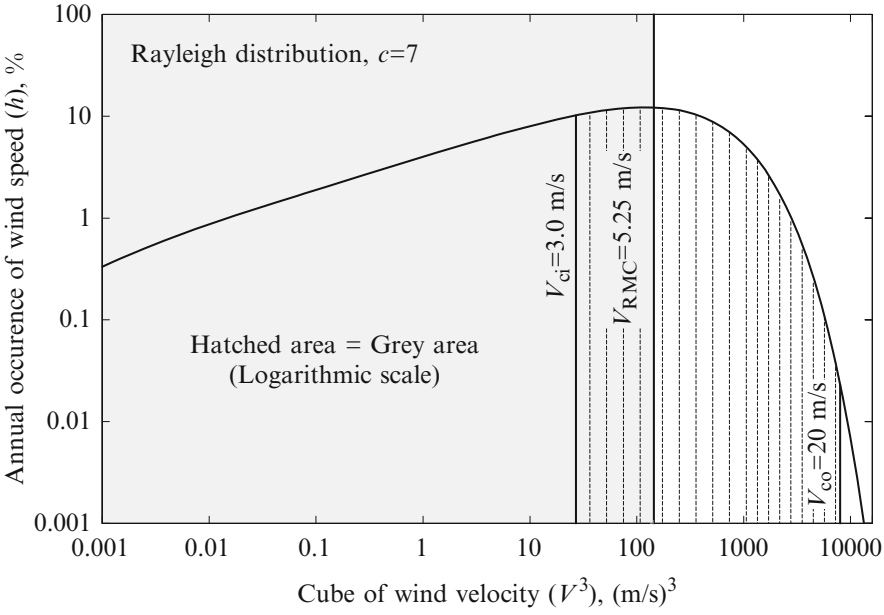

Fig. 9.38 Definition of the root mean cube wind velocity

velocity that has 100% occurrence and generates the same amount of wind energy as the probable velocity profile described by the adopted probability distribution function. Thus the generated mechanical energy by the turbine operating at a constant rate throughout the year, can be written as

$$W = \frac{1}{2}\rho C_{\mathrm{p}} A V_{\mathrm{RMC}}^3, \tag{9.44}$$

where

$$V_{\mathrm{RMC}}^3 = \int_{V_{\mathrm{ci}}}^{V_{\mathrm{co}}} h(V)\,\mathrm{d}(V^3). \tag{9.45}$$

When a wind turbine is to be selected for a location, it is important to know what is the average wind velocity in that location, because the turbine energy efficiency is specified by the manufacturer at a rated value that corresponds to a rated wind velocity (V_{r}). If the wind velocity is different from the turbine rating value, then a capacity factor can be used (as indicated by the manufacturer) to determine the generated power in the actual condition. The capacity factor is defined as the percentage of the nominal power that the wind turbine generates in actual wind conditions. In this case, the energy efficiency of the wind turbine becomes

$$\eta(V) = C_{\mathrm{f}}(V), \tag{9.46}$$

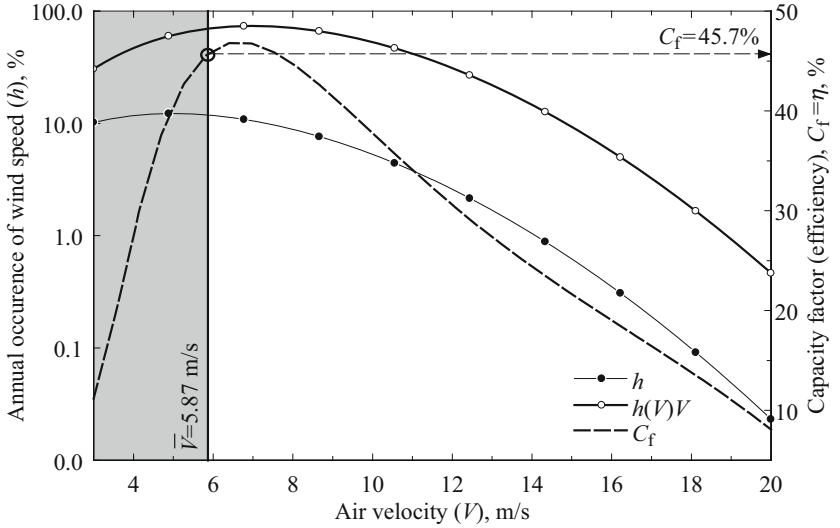

Fig. 9.39 Case study showing the capacity factor and annual wind speed occurrence probability as a function of air velocity

where $C_f(V)$ is the capacity factor expressed as a function of the actual wind velocity. The capacity factor is small at low and high velocities and has typically a maximum value at the design point.

Figure 9.39 exemplifies a typical variation of the wind capacity factor; on the same plot is superimposed an assumed annual occurrence of wind speed. It is possible to calculate the average wind velocity based on velocity occurrence, where in this case, the average velocity is defined as the velocity that occurs 100%; in other word the area between $h(V) \times V$ curve is equal to the gray area shown in the figure. Therefore,

$$\bar{V} = \int_{V_{ci}}^{V_{co}} h(V) V dV. \tag{9.47}$$

For the numerical example shown in the figure, the average wind velocity is $\bar{V} = 5.87$ m/s, which gives an average capacity factor of $C_f = 45.7\%$. In general, the average turbine efficiency is given by

$$\bar{\eta} = C_f(\bar{V}). \tag{9.48}$$

The average power generation of a wind turbine, placed in a certain location, becomes

$$\bar{W} = \frac{1}{2} \rho A C_f(\bar{V}) V_{RMC}^3. \tag{9.49}$$

Another effect, the wind chill, can influence some measures, as shown in Sahin et al. (2006), such as the efficiency of wind turbine generators. Faster cold wind makes the air feel colder than when wind is not present, because it removes heat from our bodies faster due to intensified heat transfer by convection. Wind chill is a measure of this effect and is defined as the hypothetical air temperature in calm conditions (air speed, $V = 0$) that would cause the same heat flux from the skin as occurs for the actual air speed and temperature. Wind chill temperature (see Sahin et al. 2006) can be estimated as

$$T_{\text{wch}} = 21.68 + 1.12T_0 - 38.58V^{0.16} + (0.83T_0 + 14.76)V^{0.16}, \tag{9.50}$$

where T is temperature in °C, the indices "wch" and "a" denote wind chill and surrounding air, and V is the wind speed in km/h.

Thus, a rigorous application of Eq. (9.49) implies the estimation of the air density at the wind chill temperature. The air density depends on the atmospheric pressure and temperature (a simple calculation of the air density can be based on the ideal gas law $\rho = \rho_{\text{ref}} \times T_{\text{ref}}/T_0 \times P_0/P_{\text{ref}}$, where the index 0 represents the actual environment, ref is the reference environment, T is the temperature in K, and P is the pressure. Due to expansion, air suffers additional cooling between upstream (1) and downstream (2) states. Thus the average air density is $\bar{\rho} = (\rho_1 + \rho_2)/2$, where $\rho_{1,2}$ are calculated with $(T_{1,2}, P_{1,2})$ and $T_{1,2}$ are the wind chill temperature calculated with Eq. (9.50). Thus, a more accurate energy efficiency expression accounting for wind chill temperature is

$$\bar{\eta} = C_{\text{f}}(\bar{V})\bar{\rho}/\rho_0, \tag{9.51}$$

where the index 0 indicates the surrounding temperature. Estimations by Sahin et al. (2006) for wind speeds in Ontario show that the energy conversion of wind energy can be up to 2% higher than the turbine capacity factor.

Using data representing the geographical and temporal distribution of velocity, air temperature, air pressure, and air humidity, it is possible to make accurate estimations of air density, wind chill temperature, average monthly or seasonal air velocities, and average seasonal root mean cube velocity. With these data, monthly or seasonal energy efficiency of wind energy conversion can be estimated at each geographic location. Sahin et al. (2006) provided monthly energy maps for Ontario. Two samples of these maps are shown in Fig. 9.40.

Since the average wind speed is below the cut-in wind speed in the month of January in Atikokan, the station energy efficiency is zero. At low wind speeds, efficiencies are high, but this does not mean that at these values the wind turbine is more efficient than rated for that wind speed. Rather, it means that the generated electricity is low and the potential of wind energy is low at these wind speeds. As a result, the ratio between generated electricity and potential energy is high. In July, the spatial distributions for energy efficiencies exhibit three clusters, and the general contour values are 40% to 50%.

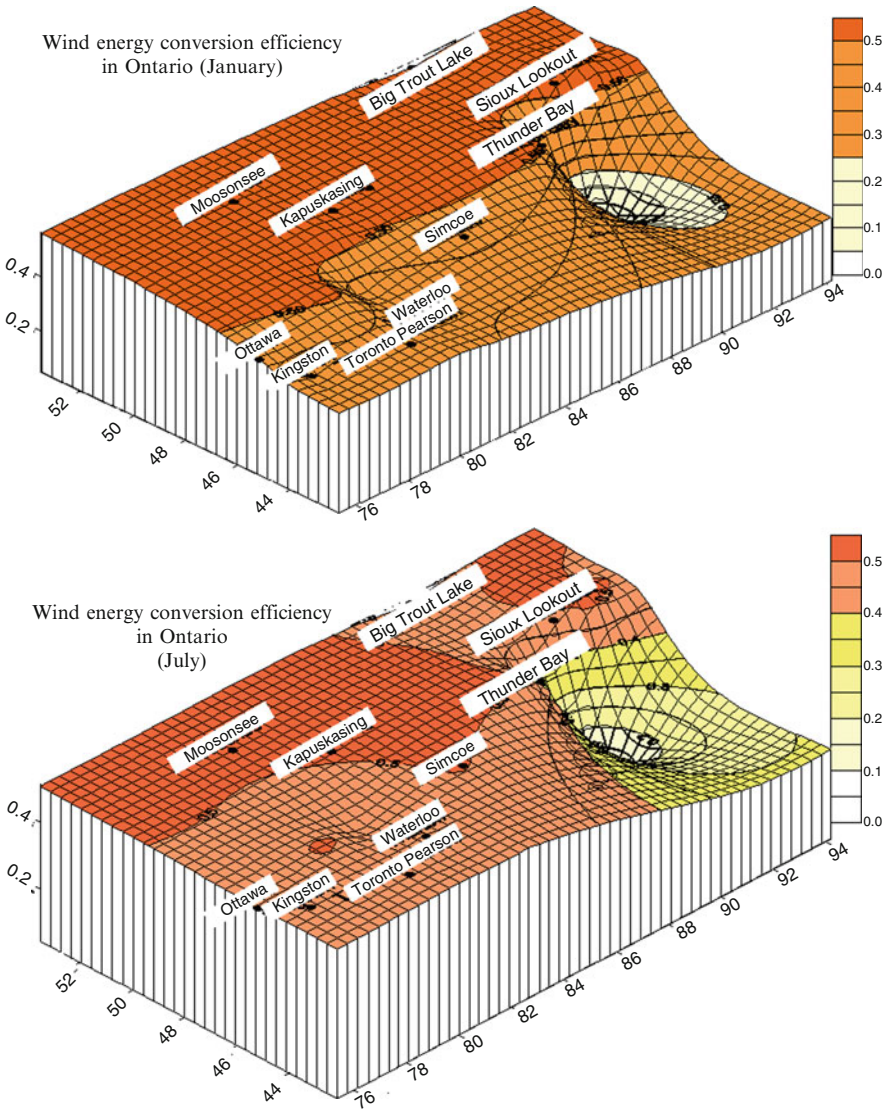

Fig. 9.40 Energy map for Ontario in January (longitude, latitude, and amplitude are on the axes) [modified from Sahin et al. (2006)]

9.3.1.3 Exergy Efficiency and Wind Exergy Maps

Exergy analysis is a useful tool for determining the thermodynamic limits and the irreversibilities of wind energy conversion. One important parameter affecting exergy analysis is the temperature of the surroundings. In the case of wind turbine, the wind chill temperature should be used as a reference state (see Sahin et al. 2006).

The exergy efficiency of a wind turbine is defined as the work produced per exergy associated with the wind. The work generated by the turbine can be calculated, as discussed above, as $W = 0.5C_f(\bar{V})\bar{\rho}AV^3_{RMC}$. The exergy associated with the wind surrounding the turbine must comprise the kinetic energy of the wind (which is a form of exergy) and the thermomechanic exergy of the wind. The thermomechanic exergy of the wind must be calculated with respect to wind chill temperature, because this is the temperature of the medium in the vicinity of the turbine. The wind has a higher exergy upstream (Ex_1) than downstream (Ex_2). Thus the exergy that enters the system is the difference ($Ex = Ex_1 - Ex_2$). Using appropriate expressions for thermomechanical and kinetic energy results in

$$\begin{aligned} Ex = {} & W + \bar{\rho}A\bar{V} \\ & \times \left\{ \bar{C}_p(T_1 - T_2) - T_0 \left[\bar{C}_p \ln\left(\frac{T_2}{T_1}\right) - R \ln\left(\frac{P_2}{P_1}\right) - \bar{C}_p\left(1 - \frac{\bar{T}}{T_0}\right) \right] \right\}, \end{aligned} \tag{9.52}$$

where $\bar{\rho}A\bar{V}$ is the mass flow rate of air, $T_{1,2}$ are the wind chill temperatures upstream and downstream of the turbine, T_0 is the temperature of the surroundings, $\bar{T}$ is the arithmetic mean of temperatures $T_{1,2}$, the pressures $P_{1,2}$ are at upstream and downstream, respectively, $\bar{C}_p$ is the specific heat, and R is the universal gas constant. The first term within the curly brackets represents the enthalpy difference, the second term is the entropy difference and the irreversibility due to heat transfer between the stream of air and the surroundings; basically, the expression between the curly brackets is the specific thermomechanical exergy consumed by the system. The exergy efficiency becomes

$$\psi = \frac{W}{Ex}. \tag{9.53}$$

Wind exergy maps were developed for Sahin et al. (2006) that correspond to the wind energy maps. These maps indicate the exergy efficiency of wind energy conversion temporally and geographically. The maps for January and July are reproduced in Fig. 9.41. The contours for exergy efficiency are seen to be lower than those for energy efficiency for all regions. The average exergy efficiency value is around 40%. In July, there is an area of high energy efficiency in northwest Ontario, but exergy analysis evaluates the lowest efficiencies in this area. The dominant efficiency in July is seen to be ~40%, except for the eastern regions of Ontario.

When comparing the results from Figs. 9.40 (energy efficiency) and 9.41 (exergy efficiency), large relative differences in energy efficiency values are observed, especially at low wind speeds. In contrast, the relative differences between energy and exergy efficiencies at high wind speeds are smaller. But these values are higher than 10% at all stations. These differences are large and should not be ignored in energy planning and management. However, for July the relative differences between the two types of efficiency are relatively low. Exergy efficiencies are lower than energy efficiencies for each station for every month considered.

Recall that the energy and exergy maps show the maximum conversion efficiency at specific geographic locations. This information is useful in selecting the wind

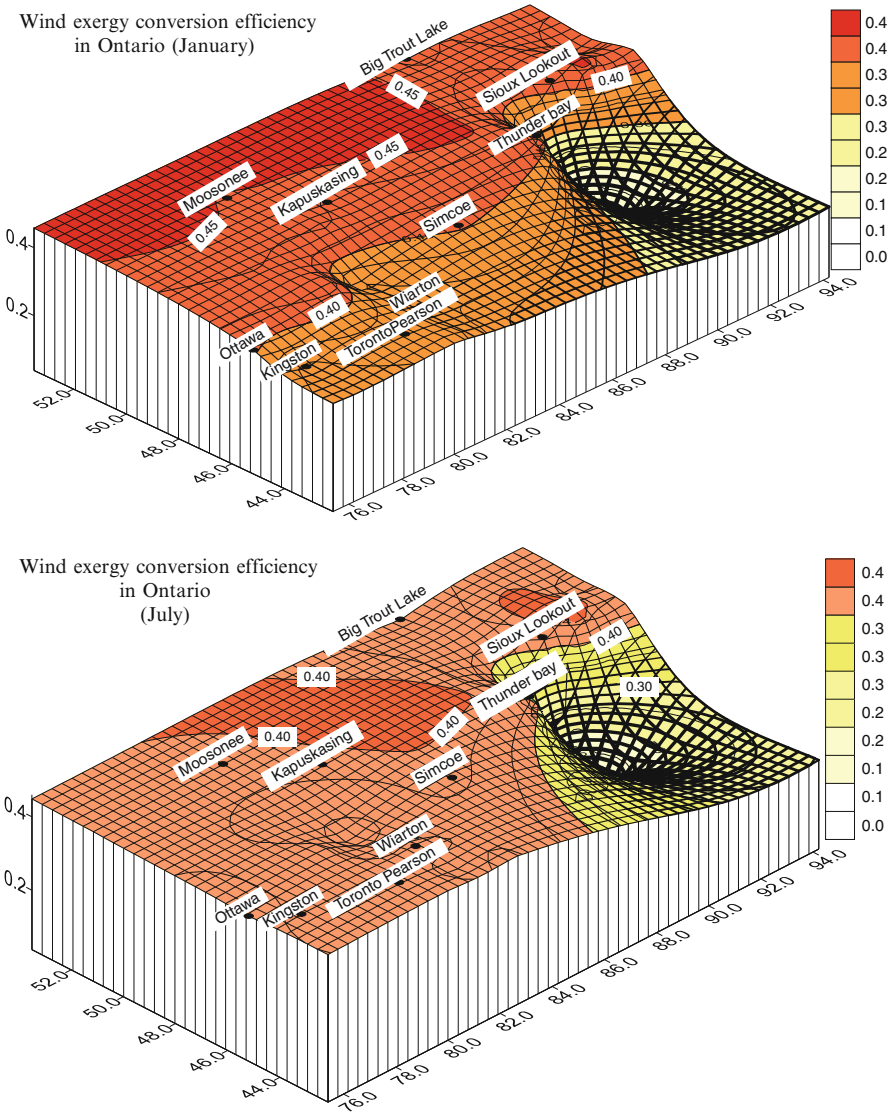

Fig. 9.41 Exergy map for Ontario in January (longitude, latitude, and amplitude are on the axes) [modified from Sahin et al. (2006)]

farm sites. However, lower efficiencies are obtained in practice due to additional losses of the actual systems.

9.3.2 Types of Wind Turbines

Basically there are two categories of wind turbine design: horizontal axis wind turbines (HAWT) and vertical axis wind turbines (VAWT). The horizontal axis wind turbines have emerged as the dominant technology. They place the rotor axis

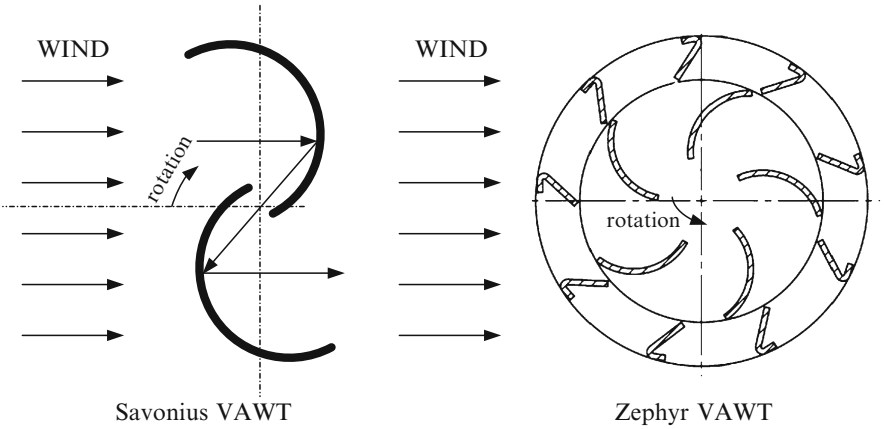

Fig. 9.42 Operating principles of the Savonius and Zephyr wind turbines

horizontal and in line with the wind direction. The common designs have the generator and the blade fixed on a rotating structure at the top of a tower. The mechanical system also comprises a gear box that multiplies the rotation of the blades. The HAWT achieves higher efficiency than the VAWT, but the VAWT operates well in fluctuating wind amplitudes provided that its direction remains quasi-constant.

One important feature of the VAWT is that it does not need to be pointed in the direction of the wind. Thus VAWT installation is appropriate where the wind changes direction very frequently. Another feature of VAWT is that it allows placing the generator and gear box lower, close to the support system of the turbine.

The HAWT construction can differ in the number of blades (generally two or three blades are used). The HAWT uses airfoils to generate lift under the wind action and rotate the propeller. The operation of some VAWT designs is based also on the aerodynamic lift principle, but there are designs that use form drag and aerodynamic friction to operate. Drag-type turbines are designed such that the form drag generates a torque; a typical drag turbine is the Savonius, used mostly in rural areas. The operating principle of the Savonius wind turbine is illustrated schematically in Fig. 9.42. The generated torque is due to the difference in pressure between the concave and convex surfaces of the blades and by reaction forces of the deflected wind coming from behind the convex surface. The efficiency of Savonius turbine is over 30%.

A more elaborated design of the VAWT, the Zephyr, is presented also in Fig. 9.42. It is designed to perform well in low wind speeds and high turbulence conditions. For this reason, several Zephyr wind turbines can be installed close to each other to form a compact wind farm. The power coefficient of the Zephyr wind turbine is rather low (0.11), but the turbine has a good utilization factor, a low cut-in speed, and a high cut-off speed, which make it competitive in urban areas. This kind of turbine was developed at the University of Ontario Institute of Technology; see Pope et al. (2010).

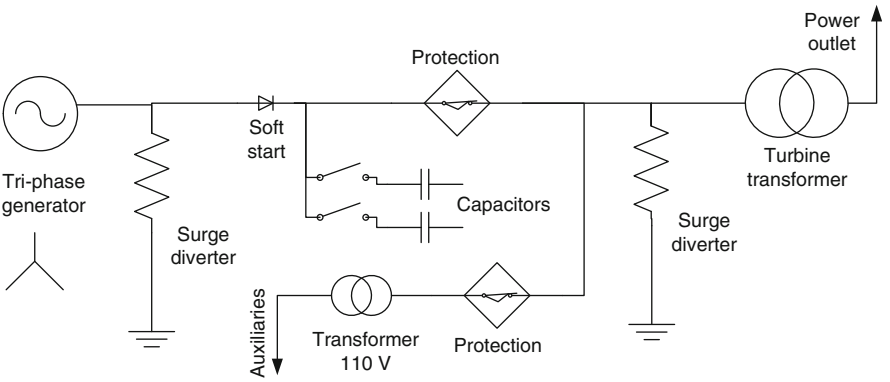

Fig. 9.43 Simplified electric diagram of a wind power generation unit

Common models of lifting VAWT turbines are the triangular (delta) Darrieus turbine, the Giromill turbine, and the Darrieus–Troposkien turbine. The triangular Darrieus turbine has straight blade geometry. The Giromill turbine is a low-load system with straight, vertical blades with an adjustable angle of attack to fit the best working conditions. The Darrieus–Troposkien turbine is the most used turbine for electric power generation. The blades of this turbine are airfoils assuming a Troposkien shape (which is a name derived from Greek meaning "the shape of a spinning rope"). Basically, the airfoil is a flexible blade connected in the vertical axis at two points (lower and upper) and while rotating approximates by revolution the shape of an ellipsoid. The blades can be made from light materials such as aluminum, fiberglass, steel, or wood.

9.3.3 Wind Power Plants

Apart from the wind turbine itself, wind power plants comprise several other important subsystems such as yaw control, speed multiplier (gear box), voltage-frequency and rotation controllers, voltage raising and lowering transformers (having the role of matching the generation, transmission, and distribution voltages at normal consumption levels), and protection systems for overcurrent, overspeed, overvoltage, atmospheric outbreaks, and other anomalous forms of operation. All these subsystems are sustained by a robust mechanical structure.

Figure 9.43 illustrates a simplified electric diagram of a wind power generation unit, its main components, and their functions. The system is equipped with general protection circuits, breakers, and overcurrent and reverse current protection. When a wind power generator is connected to the grid, it is possible that, during a low wind period, the generated voltage is lower than the grid voltage. If this situation occurs, the protection systems (see the figure) temporarily disconnect the system from the grid. Also if there is an overcurrent caused by too large a load, then the

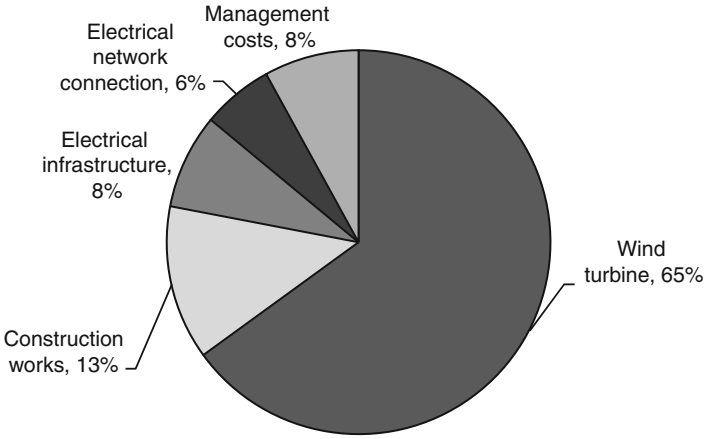

Fig. 9.44 Breakdown of costs for a typical 10-MW power plant [modified from Burton et al. (2001)]

thermal protection will disconnect the generator. The capacitors are used to correct the power factor of the generator and allow a soft start. The capacitors work together with a thyristor unit to soften the starting process of the generator. A small transformer is used to supply the auxiliary equipments. The system has a main transformer that allows connection of the unit to the grid. Local energy storage can be applied in batteries case in which the system will include an inverter. Moreover, it is possible to couple several turbines to the main transformer, when it applies, rather than equipping each turbine with its own grid connection transformer.

The electrical system and electrical infrastructure of a wind power plan may account for 13% to 15% of the total installation costs. A breakdown of various costs for installing a 10-MW wind power unit is shown in Fig. 9.44. The electrical infrastructure is costly because it involves extensive work for grounding and lightning protection. The damage produced by lightning to the wind farms and individual units is considerable. In Germany, statistics show that lightning produces damage annually to 8% of the installed wind turbines, while in Sweden this is 6% and in Denmark 4% (see Burton et al. 2001).

The noise generated by wind power plants is also a major concern. The blades, the gearbox, the generator, the generator hub, the tower, and the auxiliary system all generate significant amounts of noise during operation. The noise of a wind power plant operating 350 m away can be 10% higher than the typical rural night time background noise.

Considerable efforts were deployed in recent years to develop techniques for reducing noise from wind turbines by improving their design and installation. With the current technology, the noise level of the main power plant components ranges from 40 to 98 dB(A). Nevertheless, protection against noise increases the capital cost of the power plant. By the year 2004, the investment cost was around 50 cents per installed watt and 6 cents per generated kWh.

By expanding the wind power generation capacities in recent years, the cost of installed kW and the cost of generated kWh were reduced significantly. The investment cost is presently about 30% higher than that of natural gas power plants, while the generation cost is about 3.5 cents/kWh.

9.3.4 Hydrogen Production from Wind Electricity

Production of hydrogen by water electrolysis driven by wind-generated electricity is viewed as one promising method for promoting sustainable energy systems. The technology is mature, though the capital costs need to be reduced. Although wind energy can be considered a nonpolluting resource (renewable), the quantity of construction materials consumed per unit of hydrogen produced with wind electricity can be much higher than that for the more traditional approach of hydrogen production from natural gas.

Taking into account greenhouse gas (GHG) emissions from the construction and operation stages of wind-to-hydrogen generation plants, and their lifetimes and capacities, the indirect GHG emissions per unit of produced energy can be calculated and compared with figures specific to conventional systems. The conventional systems are characterized by significant pollution during operation, while wind-to-hydrogen systems have embedded emissions in the construction materials. A life cycle study by Granovskii et al. (2006) indicates that hydrogen obtained from natural gas reforming (including hydrogen compression to 350 bar) leads to life cycle emissions of 86 g CO_2 per MJ of energy with respect to the produced hydrogen HHV (higher heating value). In the case of using wind power, the amount of carbon dioxide for whole lifecycle is estimated to be 8 g CO_2 per MJ (including wind-electrically-driven compression of H_2 to 350 bar).

Hydrogen production from wind energy is also discussed in Chapter 13.

9.4 Geothermal Energy

Geothermal energy is a form of thermal energy that is available in some regions of the earth's surface at temperature levels in the range of about 35° to 500°C, even though most of the geothermal places provide temperature levels up to 250°C. Geothermal heat is used either for process heating or is converted into electricity through appropriate heat engines. A large palette of heat-consuming processes can be supplied by geothermal energy including space and water-heating applications, industrial processes, supplying various procedures in agriculture and food industry, and so on. Figure 9.45 illustrates the global utilization of geothermal heat.

It can be observed from the graph that most of the geothermal applications are the ground source heat pump systems. In recent years, there has been substantial development in geothermal energy, in which there is interest in a ground source

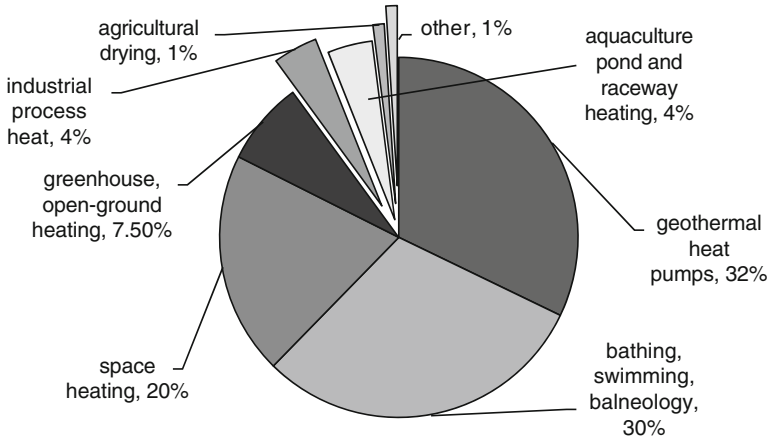

Fig. 9.45 Global utilization of geothermal energy for heating applications [data from Lund (2005)]

Table 9.7 Some historical milestones in geothermal development in Canada

Date	Milestone
1886	In Banff, Alberta, hot springs were piped to hotels and spas.
1975	Drilling to assess high-temperature geothermal resources for electricity generation in British Columbia.
1976–1986	Ten-year federal research program assesses geothermal energy resources, technologies, and opportunities for Canada.
1990	Hydro Ontario funds a program to install geothermal heat pumps in 6,749 residences.
1990s	Government take a greater interest in using renewable energy, including geothermal, as a way to decrease greenhouse gases and other emissions.
2004	Western GeoPower Corp. applies for government approval to build a $340 million, 100-MW geothermal power plant at Meager Creek, northwest of Whistler, British Columbia.
	Manitoba announces program to provide loans of $15,000 toward installation of geothermal heat pump systems.

heat pump, hydrogen production from geothermal energy, and installing electrical plants supplied by geothermal heat. Some historical milestones regarding geothermal development in Canada are listed in Table 9.7.

9.4.1 Thermodynamic Limits of Geothermal Energy Conversion

Because it is a source of heat, the limit of geothermal energy conversion is governed by the Carnot factor. Thus, it is important to assess the range of the Carnot factor for geothermal reservoirs. Additionally, it is useful to analyze relevant irreversibilities specific to geothermal energy conversion. Thus, one can obtain a general picture of the thermodynamic limits of geothermal energy conversion into work.

We will analyze, as a first step, the temperature level of the geothermal sources and the nature of the geothermal fluid. The average increase in temperature with depth, called the geothermal gradient, is about 0.03°C/m, that is, 30°C/km for a few kilometers near the earth's surface. Values as low as about 10°C/km are found in the ancient continental crust, and very high values (>100°C/km) are found in areas of active volcanism. Heat from the earth's depths is transported to the surface in three possible ways that characterize the type of geothermal field: hot water, wet steam, and dry steam. Hot water fields contain reservoirs of water with temperatures between 60° and 100°C, and are most suitable for space heating and agricultural applications. For hot water fields to be commercially viable, they must contain a large amount of water with a temperature of at least 60°C and lie within 2,000 m of the surface. Wet steam fields contain water under pressure and usually measure 100°C. These are the most common commercially exploitable fields. When the water is brought to the surface, some of the water flashes into steam, and the steam can drive turbines that produce electrical power. Dry steam fields are geologically similar to wet steam fields, except that superheated steam is extracted from the aquifer. Dry steam fields are relatively uncommon. Because superheated water explosively transforms into steam when exposed to the atmosphere, it is much safer and generally more economical to use geothermal energy to generate electricity, which is much more easily transported. The geothermal reservoirs can be categorized into three kinds according to the temperature level (Fig. 9.46).

Not only is the temperature level important when estimating the geothermal energy conversion, but also the pressure of the geothermal fluid. The exergy of a geothermal fluid (brine, steam, etc.), can be calculated based on specific thermo-mechanical exergy according to

$$\mathrm{ex} = h(T,P) - h_0 - T_0[s(T,P) - s_0], \tag{9.54}$$

where T, P represent the temperature and the pressure at which the geothermal fluid is made available to the energy conversion system (power generator). The enthalpy part shown in Eq. (9.54) represents the energy content of the stream, $e = h(T,P) - h_0$. Index 0 denotes the reference state. Thus the energy and exergy efficiencies of the geothermal generator can be expressed by

$$\left.\begin{aligned} \eta &= \frac{\dot{W}}{\dot{m} \times e} \\ \psi &= \frac{\dot{W}}{\dot{m} \times ex} \end{aligned}\right\}, \tag{9.55}$$

where $\dot{W}$ represents the generated work rate and $\dot{m}$ is the mass flow rate of the geothermal fluid.

In order to obtain an estimate of the conversion limit, one has to consider an ideal thermodynamic cycle to which the geothermal energy is transferred to generate work. Since the geothermal fluid is generally brine, it appears logical to assume that during the heat transfer process the brine exchanges sensible heat. Thus the temperature of the brine decreases to T_0.

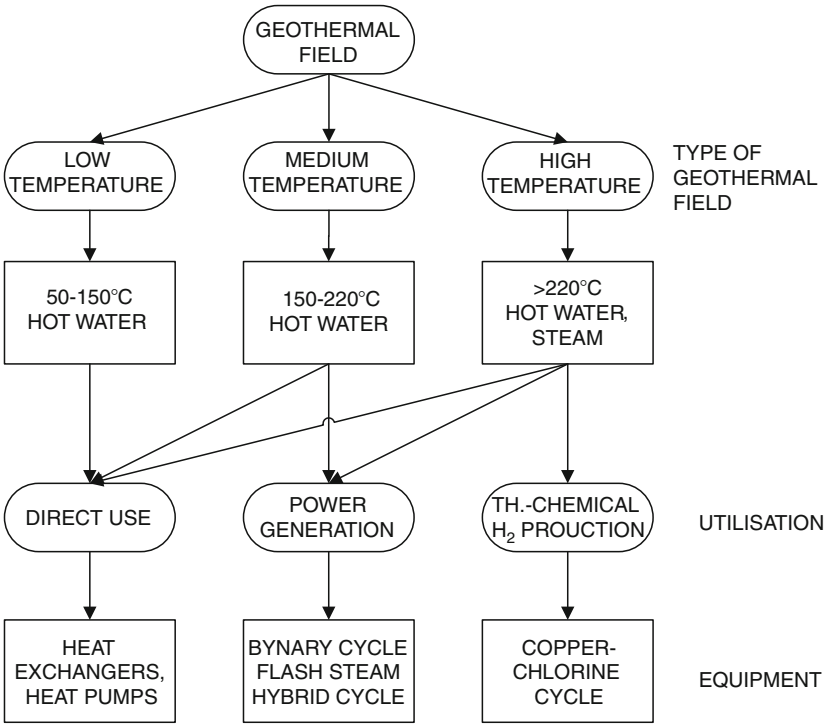

Fig. 9.46 Classification of geothermal fields and utilization of geothermal energy

Figure 9.47 suggests a thermodynamic cycle where the geothermal fluid delivers sensible heat within a cooling process through which it reaches equilibrium with the environment at (T_0, P_0). We assume the process as a straight line Ts in the diagram. The thermodynamic cycle that generates maximum work is in this case triangle shaped; the maximum generated work is indicated with the triangular gray area. The efficiency is $\eta = (T - T_0)/(T + T_0)$. In Table 9.8, figures for maximum conversion efficiency from low-, medium-, and high-temperature geothermal sources when sensible heat is extracted from the geothermal fluid are given. Note that in some cases the geothermal fluid is steam. One can assume in such cases that steam is condensed through an isothermal process, after which the entropy reaches s_0. This process is followed by an isentropic expansion to (T_0, P_0). This is an idealization; such processes cannot occur in an actual system, but it is informative to know the conversion efficiency in this case (which is the upper bound). Since this is a Carnot cycle, the efficiency is $\eta = (T - T_0)/T$; this efficiency is also reported in the table.

This analysis shows that the efficiency of geothermal energy conversion system must be much lower than 17% to 44% due to irreversibilities. Note that the energy efficiency of geothermal steam plants ranges from 10% to 17%. The energy efficiency of binary cycle plants ranges from 2.8% to 5.5%. These percentages are lower than in the case of steam power plants because binary plants are typically used for lower-temperature geothermal resources.

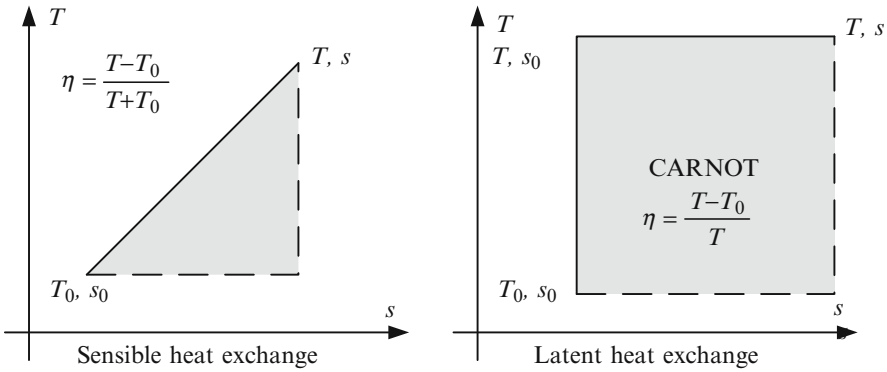

Fig. 9.47 Thermodynamic cycles for maximum work extraction from geothermal energy

Table 9.8 Thermodynamic limits of geothermal energy conversion

Geothermal source	Temperature (°C)	Sensible heat exchange (%)	Latent heat exchange (%)
Low temperature	150	17	29
Medium temperature	220	24	39
High temperature	500	44	61

The quality of a geothermal reservoir can be appreciated in terms of the exergy content of the brine. In this respect, Lee (2001) introduced the so-called specific exergy index (SExI):

$$\mathrm{SExI} = \frac{h_{\mathrm{brine}} - 273.16 s_{\mathrm{brine}}}{1{,}192}, \tag{9.56}$$

which is a straight line on an *h*-*s* plot of the Mollier diagram. Straight lines of SExI = 0.5 and SExI = 0.05 therefore can be drawn in this diagram and used as a map for classifying geothermal resources by taking into account the following criteria:

- SExI < 0.05 for low-quality geothermal resources
- $0.05 \leq$ SExI < 0.5 for medium-quality geothermal resources
- SExI ≥ 0.5 for high-quality geothermal resources

Here, the demarcation limits for these indexes are exergies of saturated water and dry saturated steam at 1 bar absolute.

9.4.2 Geothermal Power Plants

Many thermodynamic cycles were developed for geothermal power generation. The selection of the cycle depends on the kind of geothermal fluid, its flow rate, and the level of temperature. The possible geothermal fluid can be dry steam,

low-pressure brine, or high-pressure brine. The geothermal reservoir may or may not require reinjection of the fluid after its use in the power plant. The power plant design must be such that it extracts as much exergy as possible from the geothermal fluid. Figure 9.48 presents a classification of geothermal power plants.

When geothermal heat is available in the form of dry steam, then it can be converted into work by steam turbines. There are two methods: steam is created after expansion and it is condensed and reinjected into the geothermal well, or steam is simply released into the atmosphere. Figure 9.49 presents power plants diagrams with dry steam expansion and with or without reinjection.

Some geothermal reservoirs eject steam at high or lower pressure, which can be expanded in a turbine to generate power. Depending on the type of geothermal well, reinjection of the geothermal fluid may or may not be needed.

For example, if a geothermal site generates dry steam, a turbine can be used to generate power as indicated in Fig. 9.49. In the case when the steam pressure is considered low, or if there is no need to recycle the geothermal fluid, then after expansion down to atmospheric pressure, the steam can be released to the atmosphere (Fig. 9.49a). However, if the steam pressure and temperature are high enough, the amount of power generated allows for driving a recirculation pump and still generating a satisfactory yield by the turbine. In this case (Fig. 4.49b) the steam can be expanded in a vacuum, condensed, and the produced water pressurized in a pumping station and reinjected. Note that the reinjection pressure must be very high—a couple hundred bar. The reinjection is needed in many instances to keep the geothermal resources at steady production. If the geothermal reservoir is a hot rocky layer, then the water injected through one well is boiled, and it is extracted as steam through another well.

Geothermal sources generating low-pressure steam that needs to be reinjected can be coupled to an organic Rankine cycle (ORC) generator as shown in Fig. 9.50. These cycles are also known as binary cycles because sometimes they operate with binary mixtures of refrigerants (e.g., ammonia–water). The dry steam extracted from the geothermal well at point 9 is condensed (9–10) and subcooled (10–11) before water is reinjected at point 12. The heat released by the geothermal brine is then transmitted to a working fluid (toluene in the exemplary case). The working fluid is boiled and expanded as saturated toluene vapors at point 1. After expansion, internal heat is recovered in the heat exchanger (2–3/5–6), and then condensation (3–4), pressurization of the saturated liquid (4–5), preheating (5–6 and 6–7), and boiling (7–1) take place.

The calculation procedure of the cycle is presented in Table 9.9 based on EES (engineering equation solver) code, which includes all equations (energy and mass balance) needed to solve the problem and the calculated state parameters in Table 9.10. The energy and exergy efficiencies are calculated by

$$\left.\begin{aligned}\eta &= \frac{(h_1 - h_2) - (h_5 - h_4) - (h_{12} - h_{11})}{h_1 - h_6}\\ \psi &= \frac{(h_1 - h_2) - (h_5 - h_4) - (h_{12} - h_{11})}{h_9 - h_{11} - T_0(s_9 - s_{11})}\end{aligned}\right\}. \tag{9.57}$$

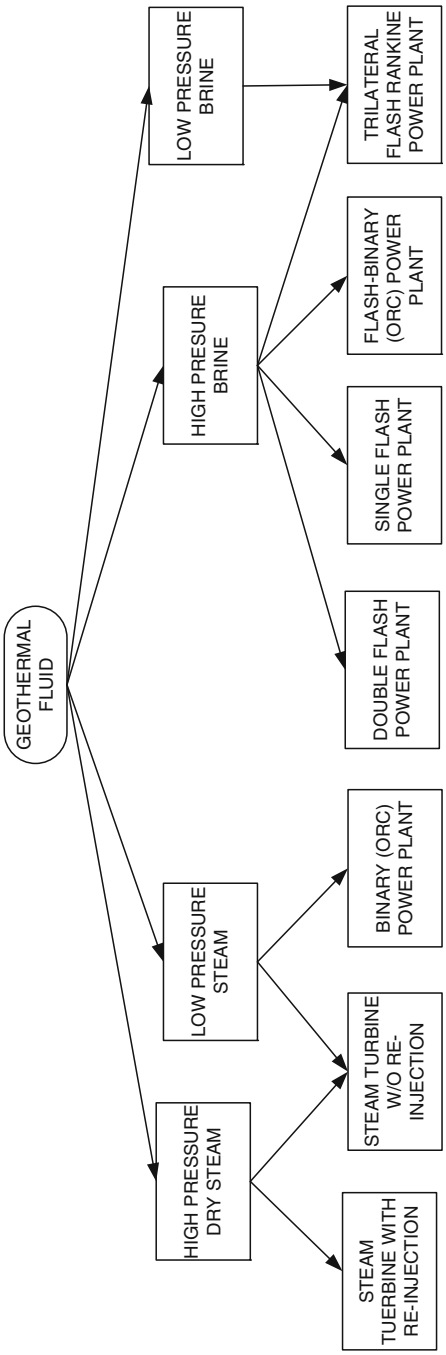

Fig. 9.48 Geothermal power plants categorized based on the kind of geothermal fluid. ORC, organic Rankine cyc

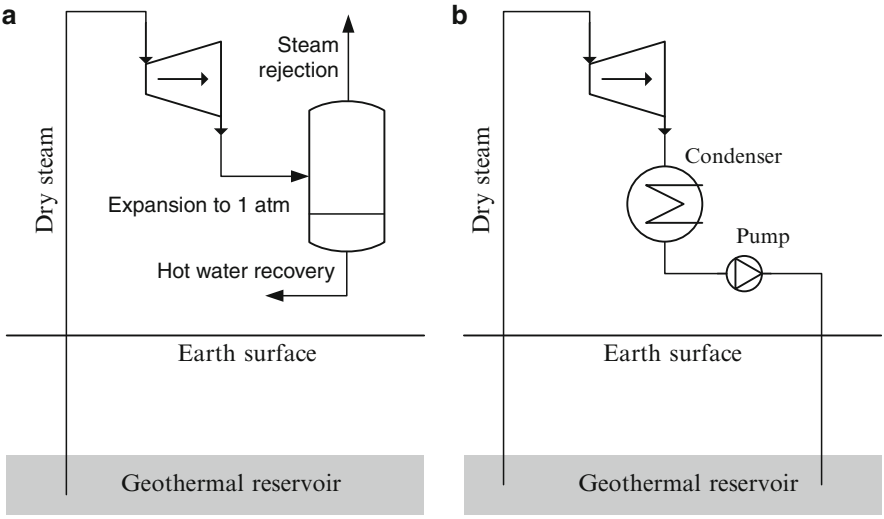

Fig. 9.49 Dry power plants with direct expansion

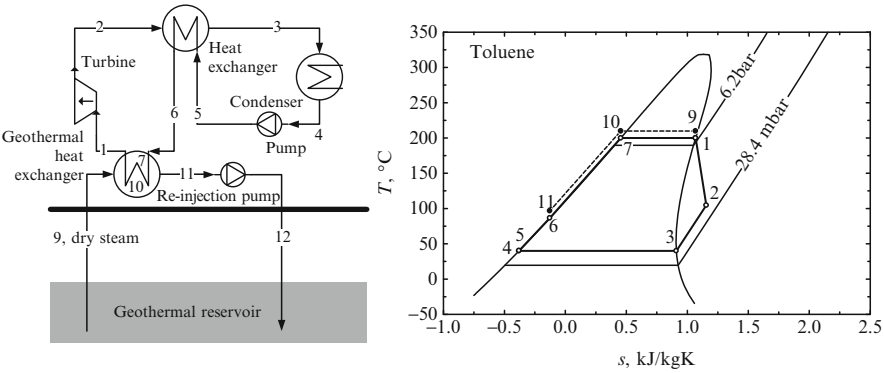

Fig. 9.50 Geothermal binary cycle power plant driven by dry steam

The energy efficiency of this cycle is 24%, the exergy efficiency is 15%, and the Carnot efficiency, calculated with the maximum temperature of the geothermal brine, is 38%.

If the pressure of the geothermal brine is high enough, then steam-flash power plant cycles can be an effective solution for power generation. Figure 9.51 presents two types of flash power plants, namely single flash and double flash. In these systems, the high-pressure geothermal brine is flashed at an intermediate pressure through an isenthalpic process (1–2). Thus, saturated vapors flash from the liquid and they are directed toward the turbine. There they are expanded to low pressure and then condensed using the ambient air as a heat sink. After condensation, the resulting water is reinjected into the well. Note also that the steam resulting from

Table 9.9 Energy and mass balance equations for modeling the system from Fig. 9.50

State	Equations	State	Equations
1	$T[1] = 200$; $x[1] = 1$ $s[1] = s$(Toluene, $T[1]$, $x[1]$) $P[1] = P$(Toluene, $T[1]$, $x[1]$) $h[1] = h$(Toluene, $T[1]$, $x[1]$)	6	$h[2] - h[3] = h[6] - h[5]$ $P[6] = P[1]$ $T[6] = T$(Toluene, $P[6]$, $h[6]$) $s[6] = s$(Toluene, $P[6]$, $h[6]$)
2	$s_{2s} = s[1]$; $P[2] = P[3]$;$\eta_T = 0.8$ $h_{2s} = h$(Toluene, $P[2]$, s_{2s}) $\eta_T \times (h[1] - h2s) = h[1] - h[2]$ $T[2] = T$(Toluene, $P[2]$, $h[2]$) $s[2] = s$(Toluene, $P[2]$, $h[2]$)	7	$h[7] = h$(Toluene, $P[7]$, $x[7]$) $P[7] = P[1]$; $x[7] = 0$; $T[7] = T[1]$ $s[7] = s$(Toluene, $T[7]$, $x[7]$)
3	$T[3] = 40$; $x[3] = 1$ $P[3] = P$(Toluene, $T[3]$, $x[3]$) $h[3] = h$(Toluene, $T[3]$, $x[3]$) $s[3] = s$(Toluene, $T[3]$, $x[3]$)	9	$T[9] = T[1] + 10$; $x[9] = 1$ $P[9] = P$(Steam, T[9], $x[9]$) $h[9] = h$(Steam, T[9], $x[9]$) $s[9] = s$(Steam, T[9], $x[9]$)
4	$T[4] = T[3]$; $x[4] = 0$; $P[4] = P[3]$ $h[4] = h$(Toluene, $T[4]$, $x[4]$) $s[4] = s$(Toluene, $T[4]$,$x[4]$)	10	$T[10] = T[9]$; $x[10] = 0$ $P[10] = P$(Steam, $T[10]$, $x[10]$) $h[10] = h$(Steam, $T[10]$, $x[10]$) $s[10] = s$(Steam, $T[10]$, $x[10]$)
5	$P[5] = P[1]$; $s_{5s} = s[4]$; $\eta_P = 0.9$ $h_{5s} =$ enthalpy (Toluene, $P = P[5]$, $s = s_{5s}$) $\eta_P \times (h[5] - h[4]) = h_{5s} - h[4]$ $T[5] = T$(Toluene, $P[5]$, $h[5]$) $s[5] = s$(Toluene, $P[5]$, $h[5]$)	11	$T[11] = T[6] + 10$; $P[11] = P[10]$ $h[11] = h$(Steam, $T[11]$, $P[11]$) $s[11] = s$(Steam, $T[11]$, P[11]) $\dot{m}_w \times (h[9] - h[11]) = h[1] - h[6]$

h enthalpy; P pressure; s entropy; T temperature; x quality
$\eta_{T,P}$ = efficiency (turbine, pump); $\dot{m}_w$ = water mass flow rate

Table 9.10 Calculated results for the system from Fig. 9.50

State	s (kJ/kg K)	T (°C)	P (bar)	h (kJ/kg)
1	1.068	200	7.475	485.7
2	1.156	104.6	0.07907	356.7
3	0.9104	40	0.07907	271.8
4	−0.3799	40	0.07907	−132.3
5	−0.3796	40.23	7.475	−131.4
6	−0.1271	86.65	7.475	−46.42
7	0.4545	200	7.475	195.5
9	6.357	210	19.06	2,798
10	2.425	210	19.06	897.7
11	1.267	96.65	19.06	406.3

flashing can be used for processes other than power generation. For instance, it can be used to produce refrigeration using ejectors in a refrigeration cycle. The double-flash cycle can be applied if the moisture content of the expanded steam is too high; this is done by expanding in two stages.

Another effective option for geothermal fields that generate high-pressure brine is the flash-binary power plant. This kind of power plant couples a flash cycle that operates with the geothermal brine as the working fluid with a bottoming organic Rankine cycle as illustrated in Fig. 9.52. After the flashing process the steam is

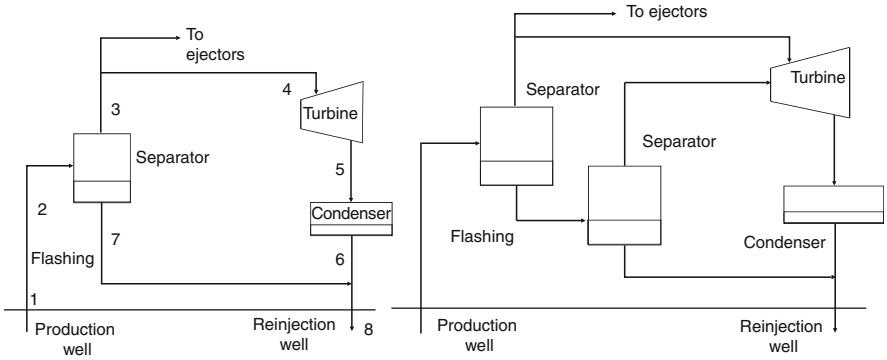

(a) Single flash power plant (b) Double flash power plant

Fig. 9.51 Types of steam-flash power plants: (**a**) single flash and (**b**) double flash

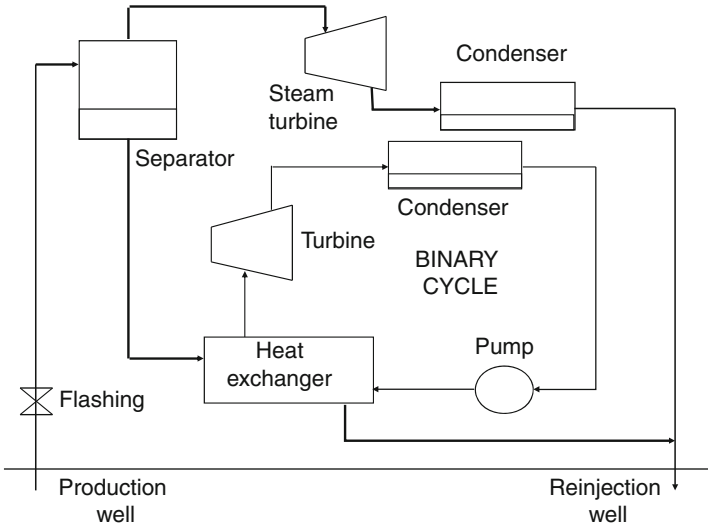

Fig. 9.52 Flash–binary power plant

expanded in a turbine, while the resulted liquid is passed through a heat exchanger that preheats and boils the working fluid of the bottoming cycle. The system will have two independent condensers. It is important to match the temperature profiles in the heat exchanger so that the available exergy could be exploited to a maximum for the benefit of an improved system performance.

Let us compare the temperature profiles in the boiler of a steam power plant with those of a binary plant operating with ammonia–water. The geothermal brine comes at the same temperature and flow rate in both cases. As observed in Fig. 9.53a, due to the necessity of having a pinch point at A, much of the flue gas exergy is wasted since it is exhausted at a rather high temperature.

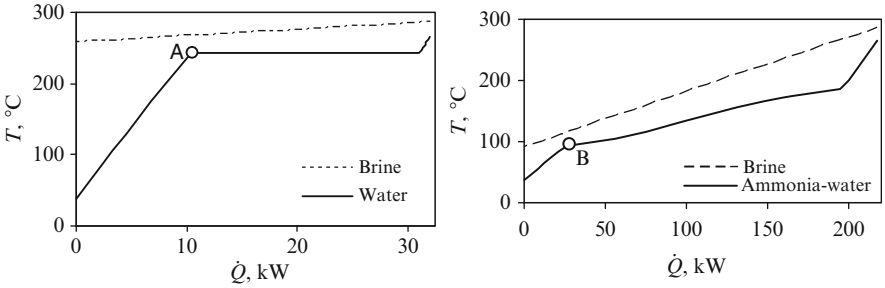

Fig. 9.53 (**a**) Temperature profiles in boiler for steam cycles and (**b**) ammonia–water cycle

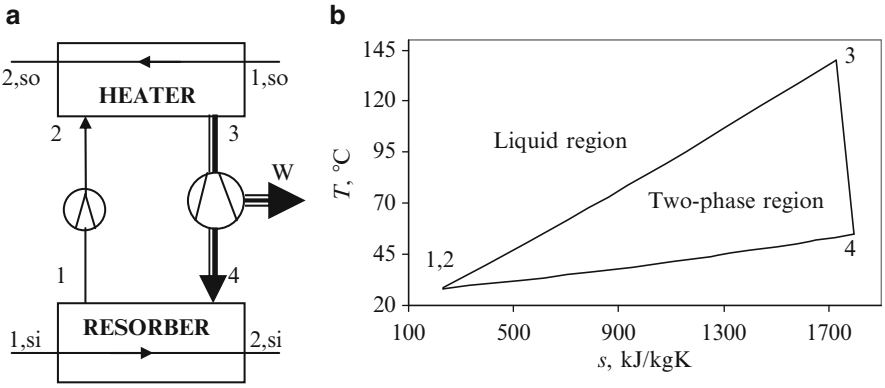

Fig. 9.54 Ammonia–water trilateral flash Rankine cycle: (**a**) the system diagram; (**b**) the thermodynamic cycle [modified from Zamfirescu and Dincer (2008b)]

If we consider the heat recovery from the same source but this time using an ammonia–water mixture with 70% ammonia concentration instead of water, the calculated temperature profiles look like the ones presented in Fig. 9.53b. The same pinch point temperature of 25°C has been considered in the two cases. The pinch point is denoted "B" in the second case.

As it can be seen from the comparative analysis of Fig. 9.53a,b, more of the brine exergy is used in the second case because the brine leaves the heat exchanger at a lower temperature. Therefore, the produced vapors in the second case have much higher enthalpy to be converted into work for power generation purposes.

Figure 9.54 illustrates another cycle that is shown to be effective for geothermal power generation when the geothermal well produces hot brine (indicated on the figure with "so", source). The cycle operates with ammonia water and comprises four elements corresponding to four processes, namely a pump, two heat exchangers (resorber and liquid heater), and an expander. In the state denoted with #1, there is a saturated ammonia water solution in liquid phase. This solution is pumped at high pressure, and it results in a subcooled liquid at #2. The liquid is then heated using the heat source stream up to the moment when it reaches the saturation in state #3.

Table 9.11 Performance comparison of geothermal power plants for 150°C brine temperature

	ORC cycles				NH_3–H_2O cycles	
Parameter	R141b	R123	R245ca	R21	Kalina	TFC
η (%)	10	9	9	9	3	8
ψ (%)	13	16	16	13	13	30

Data from Zamfirescu and Dincer (2008b)

The saturated liquid is flashed (expanded) in the volumetric expander that produces work at its shaft and a liquid–vapor mixture at its outlet, in state #4. In the resorber, cooling is applied to the two-phase mixture using the heat sink stream (indicated on the figure with "si", sink). As a consequence, a combined process of condensation and absorption occurs that eventually results in releasing a saturated liquid in state #1. Another implementation of the ammonia–water Rankine cycle is the Kalina cycle, where the ammonia–water mixture is heated in three phases: initially the subcooled liquid is preheated up to the pinch point where it becomes saturated, the fluid is then boiled and its temperature further increases, and in the last phase the vapors are superheated. The superheated vapors are expanded in a turbine and then condensed in a so-called distillation and condensation subsystem. This subsystem includes an absorber, a vapor–liquid separator, and a condenser.

Several thermodynamic cycles are compared in Table 9.11 in terms of energy and exergy efficiency assuming that the brine inlet temperature is 150°C. It can be noted that the trilateral flash Rankine cycle shows the best exergy efficiency, which is about two times higher than that of other options, which means that this cycle better recovers the exergy of the geothermal brine.

9.4.3 Thermal Applications

Geothermal energy is commonly used for a number of thermal applications such as ground source heat pumps and process heating. The domestic hot water requirement is one important parameter for the summer season. It increases on hot days when the demand for air conditioning is also high. Because of the increase in the domestic hot water requirement, pump energy consumption in total energy input increases. During the winter there is a need for space heating. Thus, a ground source heat pump can use the earth as either the source or the sink to operate both during winter and summer and to produce, as a function of the process, air conditioning, hot water, and space heating.

Basically, during the summer a ground–air heat exchanger can be used to generate air conditioning. In this case, a heat transfer fluid (water) is circulated through tubes embedded in the earth and water is cooled to a temperature of 4° to 10°C. Cold water is passed through a heat exchanger to cool the air and generate an air conditioning effect. Ground tube heat exchangers can be used for various process cooling applications. An example is cooling of electronics in shelters as studied in Vargas et al. (2005) where air is circulated directly through tubes buried in the ground that operate as a heat sink exchanger.

The ground can play the role of heat source for a heat pump that is used either for hot water or for space heating or process heating. In this case, the evaporation of the working fluid occurs at the temperature of the earth at the level of the buried heat exchanger. The thermodynamic cycle can be the typical vapor compression one. The condenser of the heat pump ejects useful heat at a temperature level convenient for space or water heating. Some other processes such as drying also can be driven with geothermal heat pumps.

9.4.4 Geothermal-Based Hydrogen Production

Geothermal energy appears to be an attractive renewable energy option for the production of hydrogen. In countries with abundant geothermal sources, certainly geothermal-based hydrogen production may become a major potential. It is the natural heat of the earth that is present in the earth's core, mantle, and crust. Also, an environmentally advantageous energy source that produces far less air pollution than fossil-fuel sources and the life of a geothermal resource may be prolonged by reinjecting the waste fluid, which is the most common method of disposal.

Although only approximately 200° to 250°C of thermal input in the hydrogen production process coupled with a geothermal source is possible today, this may change within the next decades. One should note that the technologies of hydrogen production and utilization can easily be integrated with geothermal sources and stand-alone energy systems. Using geothermal resources to produce the hydrogen would reduce the costs even further.

Geothermal-based hydrogen production offers potential advantages over other sources for a growing hydrogen economy. These advantages do not ensure that geothermal-based hydrogen will be the only option, but it will compete with other hydrogen production options. In some countries, geothermal energy is considered a primary energy source of producing hydrogen since it provides reliable energy supply in an environmentally benign manner.

Remarkable research efforts are being deployed to develop hydrogen production methods from geothermal energy. In Chapter 13, the most relevant of these are analyzed in detail.

9.4.5 District Energy

District heating and electricity can be supplied from geothermal energy. It makes sense to generate electricity from geothermal heat, using heat engines, and the heat ejected by the heat engine is further used for space heating or producing hot water, though most of the district applications using geothermal energy are for heating.

Here we present a case study analysis of the Salihli Geothermal District Heating System (SGDHS), which has a maximal yield of 87 L/s at an average reservoir

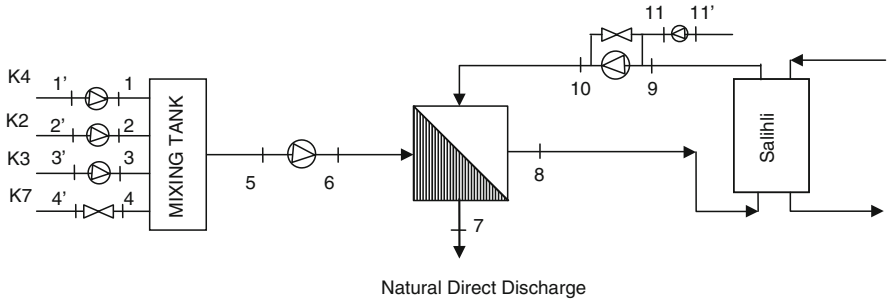

Fig. 9.55 Salihli Geothermal District Heating System [modified from Özgener et al. (2005)]

temperature of 95°C, with a minimal capacity of 838 MW (Özgener et al. 2005). The SGDHS was originally designed for about 20,000 residences. Of these, 2,400 residences are heated by geothermal energy as of February 2004. The outdoor and indoor design temperatures for the system are 4°C and 22°C, respectively.

Figure 9.55 illustrates a schematic of the SGDHS where two hospitals and office buildings heated by geothermal energy were also included. The SGDHS consists mainly of three cycles: (a) energy production cycle (geothermal well loop and geothermal heating center loop), (b) energy distribution cycle (district heating distribution network), and (c) energy consumption cycle (building substations). At the beginning of 2004, there were seven wells ranging in depth from 70 to 262 m in the SGDHS. Of these, five wells were in operation at the date studied and two wells (K5 and K6) were out of operation. Four wells (designated as K2, K3, K4, and K7) and one well (K1) are production and balneology wells, respectively.

The well head temperatures of the production wells vary from 56° to 115°C, while the volumetric flow rates of the wells range from 2 to 20 L/s. The geothermal fluid is basically sent to two primary plate–type heat exchangers and is cooled to about 45°C, as its heat is transferred to secondary fluid. The geothermal fluid (point 7) is discharged via natural direct discharge, with no recharge to Salihli geothermal field production, but reinjection studies are expected to be completed in the near future. The temperatures obtained during the operation of the SGDHS are, on average, 98°C/45°C for the district heating distribution network and 62°C/42°C for the building circuit.

By using the control valves for flow rate and temperature at the building's main station, the needed amount of water is sent to each housing unit and the heat balance of the system is achieved. Geothermal fluid, collected from the four production wells at an average well heat temperature of 95.5°C, is pumped to the inlet of the heat exchanger mixing tank and later to a main collector (from four production wells) with a total mass flow rate of about 47.62 kg/s. Geothermal fluid of intermingling molecules of different species through molecular diffusion was neglected in this study. As a result, not only irreversibility of the mixing tank was assumed to be equal to zero, but also heat losses from the tank and main collector pipe line (5–6) through the mixing process were ignored.

Taking into account the four productive wells when this study was conducted and using Eq. (9.56), the specific exergy index (SExI) is found to be 0.049, which is very close to the limit of the medium-quality geothermal resources. The energy and exergy efficiencies of the SGDHS are determined to be 55.5% and 59.4%, respectively. Here, the exergy efficiency is higher due to the recirculation and heat-recovery processes. The main parameters of this district heating system are listed in Table 9.12.

The highest exergy loss of 20.44% occurs from the natural direct discharge in this study. The second largest exergy destruction occurs from the heat exchanger with 17.90% (about 459 kW) of the total exergy input. This is followed by the total exergy destruction associated with the pumps, amounting to some 57 kW, which accounts for 2.22% of the exergy input to the system.

9.5 Hydro Energy

Hydro energy is derived from solar energy. The difference in elevation of the water level—upstream and downstream of a dam—represents an accumulation of potential energy that eventually can be transformed into mechanical work and thus into electricity. There are a number of water turbines and waterwheels that can generate rotation work when exposed to water flow. It is a worldwide potential method for electric power production and it has gained significance since many rural properties are near rivers with water streams and small water heads that can be used as the primary energy.

Energy is commonly used for stationary machine drivers, generation of electricity, and water storage in elevated reservoirs. Small electric power plants can still be used with waterwheels or, depending on the flow or the available head, with turbines. One important characteristic of a hydropower plant is the head, which represents the difference in elevation of the water level. Based on this, the hydro-energy plants are classified into two categories:

- Low-head power plants: head = 5–20 m
- High-head power plants: head = 20–1,000 m

As a function of the heat and the volumetric flow rate of water, specific turbines or water wheels can be selected. The known hydro-turbines are Pelton, Francis, Michel-Banki, Kaplan, Deriaz (where these are the name of their inventors); also some water pumps can work efficiently in reverse, as turbines.

The conversion of hydro energy into work is governed by the Bernoulli equation, which is a particular form of energy conservation equation. Accordingly, the thermodynamic limit of hydro-energy conversion into work is given by

$$W = \dot{V}\left(0.5\rho v^2 + \rho g \Delta z + P\right), \tag{9.58}$$

where $\dot{V}$ is the volumetric water flow rate, ρ the water density, v the water velocity, Δz the elevation difference, and P the water pressure.

Table 9.12 SGDHS data and energetic, exergetic, and thermodynamics parameters

Item no.	Component	Exergy destruction rate (kW)	Utilized power (kW)	Installed capacity (kW)	P (kW)	Relative irreversibility (%)	Energy efficiency, η (%)	Exergy efficiency, ψ (%)
1	Heat exchanger	458.46	10,226.83	43,961.38	1,524	44.09	–	76.87
2	K4 well pump	21.46	24.75	55	3.29	2.06	65–80	13.29
3	K2 well pump	12.74	20.25	45	7.51	1.22	65–80	37.09
4	K3 well pump	5.23	20.25	45	15.02	0.50	65–80	74.17
5	K7 well pump	–	–	–	–	–	–	–
6	Salihli booster pump	7.3	55	675	47.7	0.70	65–80	86.72
7	Salihli circulation pump	10.28	112.5	537	102.22	0.98	65–80	90.86
8	Heat exchangers and pumps	515.47	10,468.52	45,520.58	1,524	–	–	–
9	Overall system[a]	1,039.67	1,524	45,520.58	1,524	–	55.5	59.44

[a]Based on the exergy (or energy) input to thermal water and water
Data from Özgener et al. (2005)

The thermodynamic limit given by Eq. (9.58) is never reached in practice due to friction in ducts and irreversibilities in the turbine. Thus the efficiency of hydro-energy conversion is commonly 80% with respect to water head $\rho g \Delta z$. The water wheels are the least efficient devices to convert water energy due to losses because of friction, turbidity, and incomplete filling of the buckets. The water pushes the shovels tangentially around the wheel. The water does not exert thrust action or shock on the shovels as is the case with turbines. The advantage of water wheels is that they can operate in dirty water or water with suspension of solids.

The Pelton machine is a turbine of free flow (action). The potential energy of the water becomes kinetic energy through injectors and control of the needles that direct and adjust the water jet on the shovels of the motive wheel. They work under approximate atmospheric pressure with a typical head in the range of 400 to 2,000 m. Compared with the Francis turbine, the Pelton head has a better efficiency curve.

The Francis turbine is used in small hydroelectric power plants with a head in the range of 3 to 600 m while the flow rate of water is in the range of hundreds of dm^3/s. This turbine is very sensitive to cavitation and works well only close to the design point. Its operation becomes unstable at generated power lower than nominal with more than 40%.

The Michel–Banki turbine works with radial thrust. The range of power goes up to 800 kW per unit and the flow rate varies from 25 to 700 dm^3/s with the head in the range of 1 to 200 m. The number of slats installed around the rotor varies from 26 to 30, according to the wheel circumference, whose diameter is 200 to 600 mm. This multicell turbine can be operated at one or two thirds of its capacity (in the presence of low or average flows) or at full capacity (in the presence of design flows). The turbine can be operated even at 20% of its full power.

The Kaplan turbine is a hydraulic propeller turbine adapted to low heads from 0.8 to ~5 m. In addition, this turbine has the advantage of maintaining its electro-mechanical parts out of the water. This feature facilitates routine inspection and maintenance and adds safety in case of floods.

The Deriaz turbine was developed in the 1960s and can reach a capacity of up to 200 MW with flow rates in a broad range (from 1.5 to 250 m^3/s) and with heads of 5 to 1,000 m. The runner diameter may be up to 7,000 mm with six to eight runner blades. Diagonal turbines operate very economically as either turbines or pumps. The thrusting water follows an approximately conic surface around the runner.

The use of water pumps in reverse, as turbines, for small hydroelectric power plants has become quite popular because of the appreciable reduction in facility costs. These pumps, usually of small capacity, have been used for many years in industrial applications to recover energy that would otherwise be lost. They present the following advantages:

- They cost less because they are mass produced for other purposes (such as water pumps for buildings and residences).
- Their acquisition time is minimal because they have a wide variety of commercial standards and are available in hardware stores and similar shops.

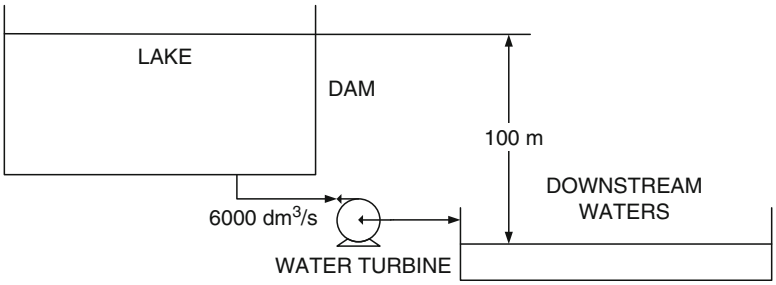

Fig. 9.56 Hydropower setting for the example in the text

However, there are a few disadvantages: slightly reduced efficiency compared with the same head height used for water pumping, and, sensitiveness to the cavitation and operating range.

Example

A typical hydropower setting is illustrated in Fig. 9.56 and has $\Delta z = 100\,\text{m}$ level difference between the lake's surface and downstream waters. On the water stream with a volume flow of $\dot{V} = 6{,}000\,\text{dm}^3/\text{s}$ a turbine coupled to an electric generator that produces $\dot{W} = 4.5$ MW power is installed with $\eta_g = 95\%$ efficiency. We want to calculate the efficiency of the water turbine itself, the overall efficiency, and the power generated by the turbine.

The energy rate supplied to the turbine-generator system is $\dot{E} = \rho \dot{V} \times g \times \Delta z$; assuming density of water of 1 kg/dm^3, the energy rate is $\dot{E} = 5.886$ MW. Thus, the overall conversion efficiency is $\eta = \dot{W}/\dot{E} = 4.5/5.886 = 76\%$. One can assume that the overall conversion efficiency is the product between the turbine and the generator efficiencies $\eta = \eta_t \times \eta_g$; thus, the turbine efficiency is $\eta_t = \eta/\eta_g = 0.76/0.95 = 80\%$. Thus the mechanical power generated by the shaft rotation of the turbine is $\dot{W}_{\text{shaft}} = \eta_t \times \dot{E} = 0.8 \times 5.886 = 4.71$ MW.

9.6 Biomass Energy

Biomass was discussed as a renewable resource in Chapter 2. Basically, any kind of fossilized living species is a form of biomass. It is one of the oldest energy sources on earth and may become one of the most significant large-scale energy sources in the future. Biomass originates from the photosynthesis portion of the solar energy distribution and includes all plant life (terrestrial and marine), all subsequent species in the food chain, and eventually all organic waste. Biomass resources come in a large variety of wood forms, crop forms, and waste forms. The basic characteristic of biomass is its chemical composition in such forms as sugar, starch, cellulose, hemicellulose, lignin, resins, and tannins.

Bioenergy (or biomass energy) can be defined as the energy extracted from biomass for conversion into a useful form for commercial heat, electricity, and transportation fuel applications. The simplest route to biomass energy conversion is

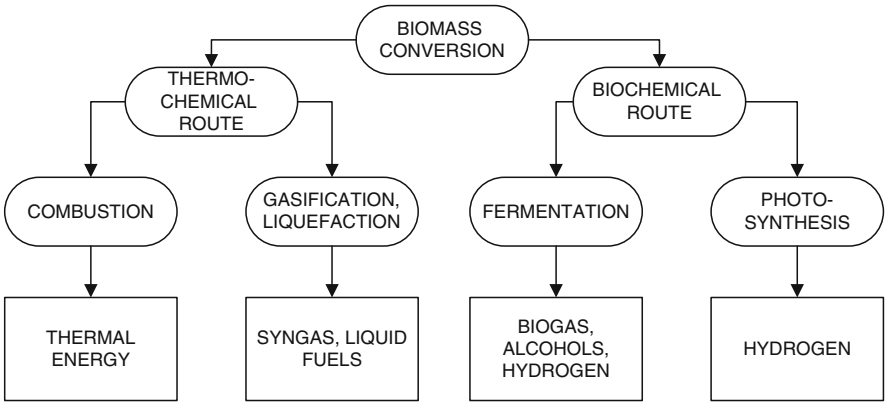

Fig. 9.57 Routes to biomass energy conversion

by combustion to generate heat. The high-temperature heat can be further converted into work through heat engines. Other biomass conversion routes are illustrated in Fig. 9.57. Combustion is a thermochemical process, as is the gasification. Gasification converts the biomass into a gaseous fuel. Liquefaction produces a liquid fuel. Another route of biomass energy conversion is biochemical. In this case, the fermentation process (anaerobic or aerobic digestion) can lead to biogas, alcohol, and hydrogen generation. Also, the photosynthesis process conducted by some phototrophic organisms can eventually produce hydrogen.

Because energy crop fuel contains almost no sulfur and has significantly less nitrogen than fossil fuels [reductions in pollutants causing acid rain (SO_2) and smog (NO_x)], its use will improve the air quality. An additional environmental benefit is in water quality, as energy crop fuel contains less mercury than coal or even none. Also, energy crop farms using environmentally proactive designs will create water quality filtration zones, uptaking and sequestering pollutants, such as phosphorus from soils that leach into water bodies.

Biomass generates about the same amount of CO_2 as do fossil fuels (when burned), but from a chemical balance point of view, every time a new plant grows, CO_2 is actually removed from the atmosphere. The net emission of CO_2 will be zero as long as plants continue to be replenished for biomass energy purposes. If the biomass is converted through gasification or pyrolysis, the net balance can even result in removal of CO_2. Energy crops such as fast-growing trees and grasses are called biomass feedstocks. The use of biomass feedstocks can help increase profits for the agricultural industry.

9.6.1 Thermodynamic Limits of Biomass Energy Conversion

The general model of biomass energy conversion into work can consist of an adiabatic combustor and a reversible heat engine. Figure 9.58 illustrates the biomass energy conversion system for maximum work generation. The biomass

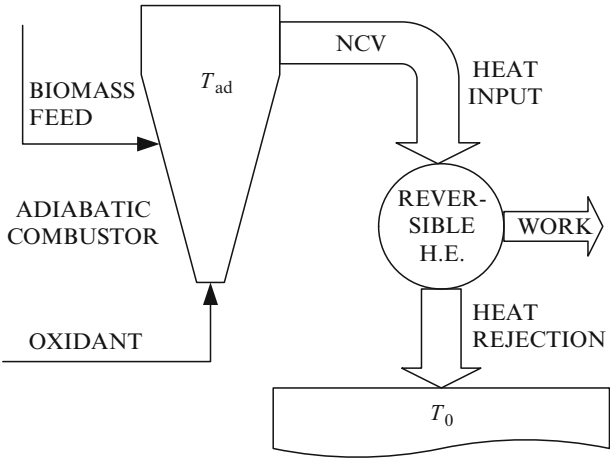

Fig. 9.58 Thermodynamic model for biomass energy conversion into work. *H.E.* heat engine

combusts in an adiabatic combustor that operates at the highest possible temperature (adiabatic flame temperature, T_{ad}). The heat generated in this process is the net calorific value of the biomass (NCV). This heat is further used to drive a reversible heat engine that generates useful work while it is in contact with the environment at the low-temperature side.

The work generated by this system is thus $\dot{W} = \text{NCV} \times (1 - T_0/T_{ad})$, and thus the efficiency of the biomass conversion process is given by the adiabatic flame temperature only $\eta = 1 - T_0/T_{ad}$. Therefore, determining the thermodynamic limit of biomass energy conversion is equivalent to determining the adiabatic flame temperature for the biomass. Thus, we will analyze the biomass composition and the way in which this affects the net calorific value of biomass and the corresponding adiabatic flame temperature.

The biomass contains various biochemicals (amino acids, fiber, cellulose, sugars, glucose, and many other). Some living micro-organisms and enzymes may be found in biomass. The most abundant chemical elements in biomass are carbon, hydrogen, oxygen, nitrogen, and sulfur. Other elements are also present, including metal atoms. When biomass is combusted, the metal atoms and other elements form ash.

Some biomass modeling equations were presented in Chapter 6. We repeat them here and we expand the theory. The general chemical model of biomass is written as $C_{X_C}H_{X_H}O_{X_O}N_{X_N}S_{X_S}\text{ash}_{X_{ash}}(H_2O)_{X_w}$, where X_i is the number of constituents of species "i." If the moisture (water) is eliminated by some drying process, then the chemical representation of the dry biomass becomes $C_{X_C}H_{X_H}O_{X_O}N_{X_N}S_{X_S}\text{ash}_{X_{ash}}$. The molecular mass of dry biomass can be calculated with

$$M = 12 \times X_C + X_H + 16 \times X_O + 14 \times X_N + 32 \times X_S + M_{ash}X_{ash}. \qquad (9.59)$$

On a dry basis, the mass concentration of each major chemical element constituent is $w_C = 12 \times \frac{X_C}{M}$; $w_H = \frac{X_H}{M}$; $w_O = 16 \times \frac{X_O}{M}$; $w_N = 14 \times \frac{X_N}{M}$; $w_S = 32 \times \frac{X_S}{M}$; $w_{ash} = M_{ash} \times \frac{X_{ash}}{M}$, where $w_{ash} = 0.5$–12% dry basis. The moisture content of biomass typically has a moisture concentration in the range of $w_w = 0$–50% that can be expressed on a wet basis as

$$M_{wet} = M + X_w \times 18. \tag{9.60}$$

Thus,

$$w_w = \frac{18X_w}{M + X_w \times 18}. \tag{9.61}$$

If the mass concentration of the moisture is known, then the molar concentration can be determined by

$$X_w = \frac{w_w M}{18(1 - w_w)}. \tag{9.62}$$

Equations (9.61) and (9.62) are useful for biomass combustion calculations and for determining its calorific and exergetic content. Thus, the gross calorific value of biomass can be calculated with

$$\begin{aligned} \mathrm{GCV} = {} & 34.91w_C + 117.83w_H + 10.05w_S - 1.51w_N - 1.034w_O \\ & - 2.11w_{ash} \end{aligned} \tag{9.63}$$

(see Van Loo and Koopejan 2008). The net calorific value is calculated under the constraint that water in the exhaust gases is in the vapor phase and all exhaust gases are at the same temperature as the biomass at the feed (standard temperature). The net calorific value can be calculated with

$$\mathrm{NCV} = \mathrm{GCV}(1 - w_w) - 2.444w_w - 2.444w_H \times 8.936(1 - w_w). \tag{9.64}$$

Szargut (2005) gives an equation for the chemical exergy of biomass (where the contribution of the sulfur to the combustion process is ignored):

$$e^{ch}_{x,Bmass} = \mathrm{NCV} \times \left(1.0347 + 0.014\frac{X_H}{X_C} + 0.0968\frac{X_O}{X_C} + 0.0493\frac{X_N}{X_C}\right). \tag{9.65}$$

The stoichiometric equation for complete biomass combustion with pure oxygen is as follows:

$$\begin{aligned} & C_{X_C}H_{X_H}O_{X_O}N_{X_N}S_{X_S}\mathrm{ash}_{X_{ash}}(H_2O)_{X_w} + X_{O_2}O_2 \\ & \quad \rightarrow X_C CO_2 + X_{H_2O}H_2O + X_N/2N_2 + X_S SO_2 + X_{ash}\mathrm{ash}, \end{aligned} \tag{9.66}$$

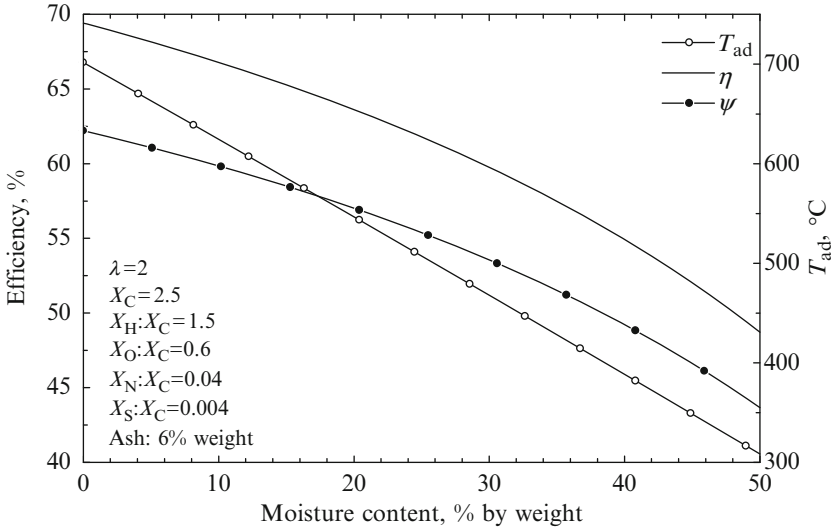

Fig. 9.59 Variation of adiabatic flame temperature, energy and exergy efficiency of biomass conversion with the moisture content

where $X_{O_2} = 2X_C + X_H/2 + 2X_S - X_O$; $X_{H_2O} = X_H/2 + X_w$. The corresponding energy balance is written as

$$h_{BMAF} = h_{BM} - X_{ash}h_{ash} = X_C h_{CO_2} + X_{H_2O}h_{H_2O} + X_S h_{SO_2} + NCV, \tag{9.67}$$

where h_{BM} is the formation enthalpy of biomass with respect to chemical elements and h_{BMAF} is the same for the ash-free biomass.

The general chemical equation of biomass combustion with enriched oxygen and flue gas recirculation is $C_{X_C}H_{X_H}O_{X_O}N_{X_N}S_{X_S}ash_{X_{ash}}(H_2O)_{X_w} + \lambda X_{O_2}[\zeta(O_2 + 3.76N_2) + (\zeta - 1)O_2] \rightarrow Prod + X_{ash}$ ash, where $\lambda \geq 1$ is the excess oxygen; 3.76 is the concentration of nitrogen in fresh air, $\zeta = 0 - 1$ is the fraction of fresh air, and "Prod" are the reaction products in the form of flue gas. Assuming complete combustion, then $Prod = X_C CO_2 + X_{H_2O}H_2O + X_S SO_2 + X_{N_2}N_2 + (\lambda - 1)X_{O_2}O_2$, where the stochiometric coefficients for nitrogen is $X_{N_2} = X_N/2 + 3.76\lambda\zeta X_{O_2}$.

Using Eqs. (9.59) to (9.67), it is easy to obtain the plot on Fig. 9.59 illustrating the variation of adiabatic flame temperature and conversion efficiency of a typical biomass with the moisture content. The energy and exergy efficiencies are calculated based on the useful work generated and the energy/exergy input (see Fig. 9.58) as

$$\left.\begin{aligned} \eta &= 1 - \frac{T_0}{T_{ad}} \\ \psi &= \frac{NCV}{ex^{ch}} \times \left(1 - \frac{T_0}{T_{ad}}\right) \end{aligned}\right\}. \tag{9.68}$$

Table 9.13 Characteristics of some biomass resources

Biomass type	Moisture content (% wb)	Bulk density (kg wb/m^3)	T_{ad} (°C)	GCV (MJ/kg db)	NCV (MJ/kg wb)	ex^{ch} (MJ/kg wb)
Wood pellets	10	600	1,140	19.8	16.4	18.3
Woodchips	30–50	250–450	530–840	19.8	8–12.2	8.9–13.6
Sawdust	50	240	530	19.8	8	8.9
Bark	50	320	540	20.2	8.2	9.2
Grass	18	200	1,020	18.4	13.7	15.3
Cereals	15	175	1,065	18.7	14.5	16.2
Straw	15	120	1,065	18.7	14.5	16.2
Olive kernels	53–63	650–1,130	370–530	21–23	6.5–8.5	7.1–9.0

db dry basis; *wb* wet basis in percent by weight

The maximum conversion efficiencies are obtained with dry biomass (moisture content 0%) and excess oxidant (air) as low as the stoichiometric one ($\lambda = 1$). In these conditions, the adiabatic flame temperature as well as the maximum biomass energy conversion efficiencies reach values around $T_{ad} = 1{,}280 - 1{,}300°C$, $\eta \cong 80\%$, and $\psi \cong 72\%$. Table 9.13 lists the characteristics of some biomass resources.

9.6.2 Conversion of Biomass in Biofuels

Biomass can be converted to a gaseous fuel by the two routes that were suggested in Fig. 9.57, namely the thermochemical and biochemical conversion routes. Through the thermochemical conversion route biosyngas is obtained, while by biochemical conversion one can generate either biogas or hydrogen.

The first step in thermochemical conversion of biomass is pyrolysis. Biomass pyrolysis refers to a process in which biomass is exposed to high temperatures in the absence of air, causing the biomass to decompose. The end product of pyrolysis is a mixture of solids (char), liquids (oxygenated oils), and gases (CH_4, CO, and CO_2). Flash pyrolysis gives high oil yields, but because of the technical effort needed to process pyrolytic oils, this energy-generating system does not seem very promising at the present stage of development. However, pyrolysis as a first stage in a two-stage gasification plant for straw and other agricultural feedstocks that pose technical difficulties in gasification does deserve consideration.

There are several widely used process designs for biomass gasification: (1) staged reformation with a fluidized-bed gasifier, (2) staged reformation with a screw auger gasifier, (3) entrained flow reformation, and (4) partial oxidation. In staged steam reformation with a fluidized-bed reactor, the biomass is first pyrolyzed in the absence of O_2. Then the pyrolysis vapors are reformed to synthesis gas with steam, providing added H_2 as well as the proper amount of O_2 and process heat that comes from burning the char. With a screw auger reactor, moisture (and O_2) is introduced at the pyrolysis stage, and process heat comes from burning some of the gas produced in the latter. In entrained flow reformation, external steam and air are introduced in a single-stage gasification reactor. Partial oxidation gasification uses

pure O_2 with no steam, to provide the proper amount of O_2. Using air instead of O_2, as in small modular uses, yields produced gas (including NO) rather than synthesis gas. A workable gasification process requires development of some technology, such as feed processing and handling, gasification performance improvement, syngas cleanup and conditioning, development of sensors, instruments and controls, process integration, and materials used for the systems.

The typical biochemical route to biomass gasification leads to biogas generation. Biogas, also termed methane or gobar gas, comprises a mixture of gases. It is a fuel of high caloric value resulting from anaerobic fermentation of organic matter called biomass. Composition of this gas varies with the type of organic material used. The caloric power of biogas depends on the amount of methane in its composition, which could reach 20 to 25 MJ/m^3. Biogas can be used for stove heating, water heaters, flowtorches, motors, and other equipment. Biogas contains typically 60% to 70% methane and 30% to 40% carbon dioxide with traces of nitrogen, ammonia, hydrogen, and hydrogen sulfide.

Several biodigester models are available. In a basic one, the digester is a reservoir built of bricks or concrete below ground level. A wall divides the biodigester into two semicylindrical parts for the purpose of retaining and providing circulation for the biomass loaded in a biofertilization process. The biodigester is loaded through the charge box, serving as a pre-fermenter. The load is typically a slurry containing biomass mixed with water. The charge box communicates with the digester through a pipe going down to the bottom. The output of the biofertilizer is through another pipe at a level that ensures that the amount of biomass entering the biodigester is the same as that leaving it in biofertilizer form. It should also have a discharge box, tank, or dam to pump and/or deliver the biofertilizer directly to the consumer. For a production capacity of 5 to 6 m^3 biogas per day, the biodigester has 3-m diameter and 3-m height, consumes 250 L of biomass per day, and has a retention time of about 50 days. The biodigester is usually buried because underground temperatures are higher and more constant. The process is affected by the material temperature (commonly 30–35°C), biodigestion acidity (i.e., pH: preferably 6–8), nutrients (e.g., N_2) and their concentration, and the concentration of solids (commonly 7–9%).

The type of biomass used in the biodigester can be diverse, including residues from industrialization of fruits, meats, cereals, and alcohol. Urban garbage can also be used as feedstock for biodigesters and transformed thus into sources of energy. The specific production of biogas is presented in Table 9.14 for various kinds of feedstock.

Similar to the case of biomass conversion into gas, its conversion into liquid fuels can be done through thermochemical or biochemical routes. Through liquefaction one obtains fuel oil. Liquefaction can be done by exposing a mixture of liquid water and solid biomass to high pressures and high temperature. The pressure is commonly of the order of 200 bar (that is close to the critical pressure of water). The biochemical route occurs through fermentation and leads to production of alcohols. In general, through biofuels, liquid fuels are obtained from biomass (biodiesel, bioethanol, biomethanol, biogasoline, etc.). However, the term *biofuel*

Table 9.14 Specific biogas production for several kinds of vegetable and manure feedstock

Feedstock	Production (m^3 gas per ton of feedstock)	Feedstock	Production (m^3 gas per ton of feedstock)
Bean straws	380	Rice straws	300
Sunflower leaves	300	Wheat straws	300
Soy straws	300	Linen stem	360
Potato leaves	270	Dry tree leaves	250
Grapevine leaves	270	Birds	55
Bovines	40	Equines	48
Suidae	64	Oviparous	70

is general, referring to any kind of fuel derived from biomass, be it gas (biogas, hydrogen, carbon monoxide), liquid, or solid (the biomass itself is a solid fuel). Thus, in general, biofuels include wood, wood waste, wood liquors, peat, railroad ties, wood sludge, spent sulfite liquors, agricultural waste, straw, tires, fish oils, tall oil, sludge waste, waste alcohol, municipal solid waste, landfill gases, other waste, and ethanol blended into motor gasoline.

Hydrogen can be also generated from biomass through several methods. These are discussed in detail in Chapter 13.

9.6.3 Electricity Generation

Several alternatives are available for generation of electric power from biomass. The simplest possibility to do this is by direct combustion of biomass to fire a steam generator that drives a turbine. Biomass combustion facilities also can be coupled with organic Rankine cycles, which are characterized by good turbine efficiency at low installed capacities. A basic biomass combustion facility coupled with a steam power plant is shown in Fig. 9.60.

In this system, biomass is first dried using the flue gas heat generated by the combustion process itself. Next, the dried biomass is combusted and the hot flue gas used to generate steam for a steam Rankine cycle power generator. Figure 9.61 shows an improved power generation system that generates electricity and steam from biomass energy. This system uses biomass gasification to generate clean synthesis gas that is fed into a solid oxide fuel cell (SOFC) system. The reaction products generated by SOFC are further combusted and the combustion heat used for air preheating and steam generation. Steam is partly used by the gasification process, and partly is supplied to users as a form of cogenerated heat. The remaining heat of the flue gases is used to dry the biomass prior to gasification.

Colpan et al. (2010a) analyzed and compared the efficiency and environmental impact of the power generation systems shown in Fig. 9.60 (conventional system) and Fig. 9.61 (advanced system with biomass gasification). Note that HRSG in the

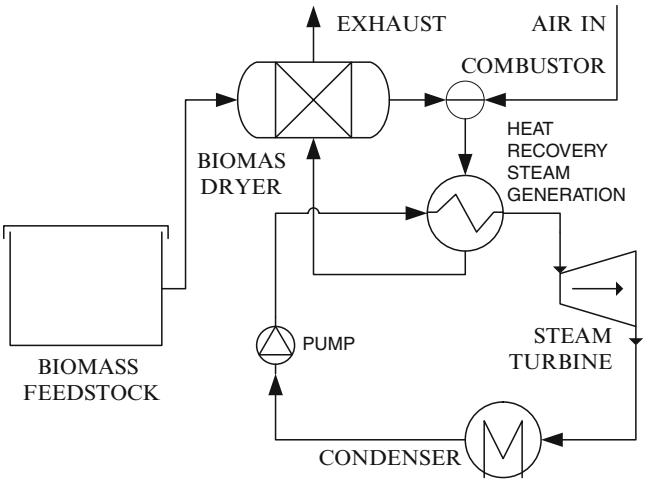

Fig. 9.60 Conventional biomass-fueled power generation system

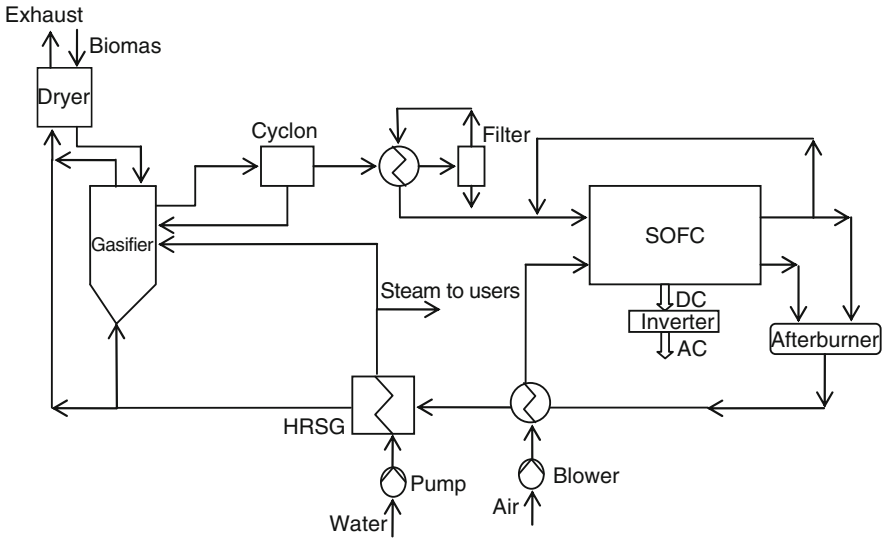

Fig. 9.61 Advanced power generation system with biomass gasifier and SOFC [modified from Colpan et al. (2010a)]

figure means heat recovery steam generator. The environmental impact of these systems can be assessed by calculating the specific greenhouse gas emissions, which are defined as the ratio of the GHG emissions from the system to the net power output of the system. From the viewpoint of energy and environment, the lower the ratio, the more environmentally friendly the system; the ratio is given as $\dot{m}_{\mathrm{GHG}}/\dot{W}_{\mathrm{net}}$. Assuming the case study data summarized in Table 9.15, the results

Table 9.15 Case study parameters for conventional and advanced biomass power generation

Environmental temperature	25°C
Type of biomass	Wood
Ultimate analysis of biomass (%wt dry basis)	50% C, 6% H, 44% O
Moisture content in biomass (%wt)	30%
Exhaust gas temperature	127°C
Conventional system (Fig. 9.60)	
Conditions of the steam entering the steam turbine	20 bar (saturated)
Pressure of the condenser	1 bar
Isentropic efficiency of the steam turbine	80%
Isentropic efficiency of the pump	80%
Electricity generator efficiency	98%
Advanced system (Fig. 9.61)	
Moisture content in biomass entering the gasifier (%wt)	20%
Temperature of syngas exiting the gasifier	900°C
Temperature of steam entering the gasifier	300°C
Molar ratio of steam to dry biomass	0.5
Number of cells per SOFC stack	50
Temperature of syngas entering the SOFC	850°C
Temperature of air entering the SOFC	850°C
Pressure of the SOFC	1 atm
Cell voltage	0.7 V
Reynolds number at the fuel channel inlet	1.2
Excess air coefficient	7
Active cell area	10×10 cm^2
Number of repeat elements per single cell	18
Flow configuration	Co-flow
Manufacturing type	Electrolyte supported
Thickness of the air channel	0.1 cm
Thickness of the fuel channel	0.1 cm
Thickness of the interconnect	0.3 cm
Thickness of the anode	0.005 cm
Thickness of the electrolyte	0.015 cm
Thickness of the cathode	0.005 cm
Pressure ratio of the blowers	1.18
Isentropic efficiency of the blowers	0.53
Pressure ratio of the pump	1.2
Isentropic efficiency of the pump	0.8
Inverter efficiency	0.95

Data from Colpan et al. (2010a)

presented in Fig. 9.62 are obtained. For the advanced system, the syngas composition is first calculated as 2.08% CH_4, 42.75% H_2, 25.80% CO, 9.44% CO_2, and 19.93% H_2O. The average current density of the cell is 0.253 A/cm^2 for the cell operating voltage of 0.7 V. It is found that the fuel utilization of the SOFC is 82%.

As shown in Fig. 9.62, the electrical and exergetic efficiencies of the conventional system are 8.3% and 7.2%, respectively, whereas the electrical and exergetic efficiencies of the advanced system are 44.9% and 41.1%, respectively. The environmental impact of the systems studied is compared calculating the specific GHG emissions from these systems. It is found that the conventional system has higher GHG emissions compared to the advanced system. As shown in Fig. 9.62,

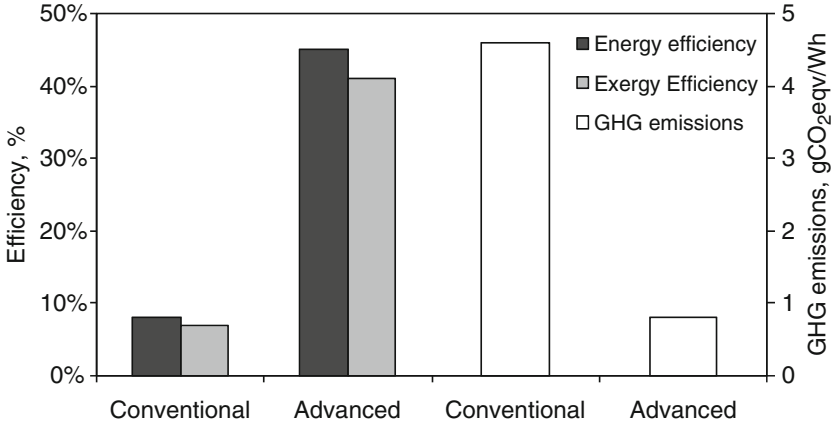

Fig. 9.62 Efficiency and GHG emission for conventional and advanced biomass power generation systems analyzed above [data from Colpan et al. (2010a)]

the specific GHG emissions are 4.564 g CO_2 eq/Wh and 0.847 g CO_2 eq/Wh for the conventional and the advanced system, respectively.

Figure 9.63 suggests an improved system that uses several thermodynamic cycles to generate power and heat through biomass gasification. The gasifier module converts biomass to a clean gas for power and steam generation with a combined system including a Brayton cycle, a steam expansion turbine, and a solid oxide fuel cell. In this system, biomass is gasified first and used in a gas turbine and a fuel cell system that operate in parallel. The uncombusted gases are directed toward a low-pressure combustor where additional combustion is applied at low pressure. The flue gases are used to generate high-pressure superheated steam that is expanded in a steam turbine. The resulting low pressure steam can be used for some heating applications. Another part of the high pressure steam is used for the gasification process.

The combined heat and power generation (via biomass gasification techniques connected to gas-fired engines or gas turbines) can achieve significantly higher electrical efficiencies, between 22% and 37%, than those of biomass combustion technologies with steam generation and steam turbine, 15% to 18%. If the gas produced is used in fuel cells for power generation, an even higher overall electrical efficiency can be attained, in the range of 25% to 50%, even in small-scale biomass gasification plants and under partial-load operation.

Due to the improved electrical efficiency of the energy conversion via gasification, the potential reduction in CO_2 is greater than with combustion. The formation of NO_x compounds can also be largely prevented, and the removal of pollutants is easier for various substances. The NO_x advantage, however, may be partly lost if the gas is subsequently used in gas-fired engines or gas turbines. Significantly, lower emissions of NO_x, CO, and hydrocarbons can be expected when the gas produced is used in fuel cells rather than in gas-fired engines or gas turbines.

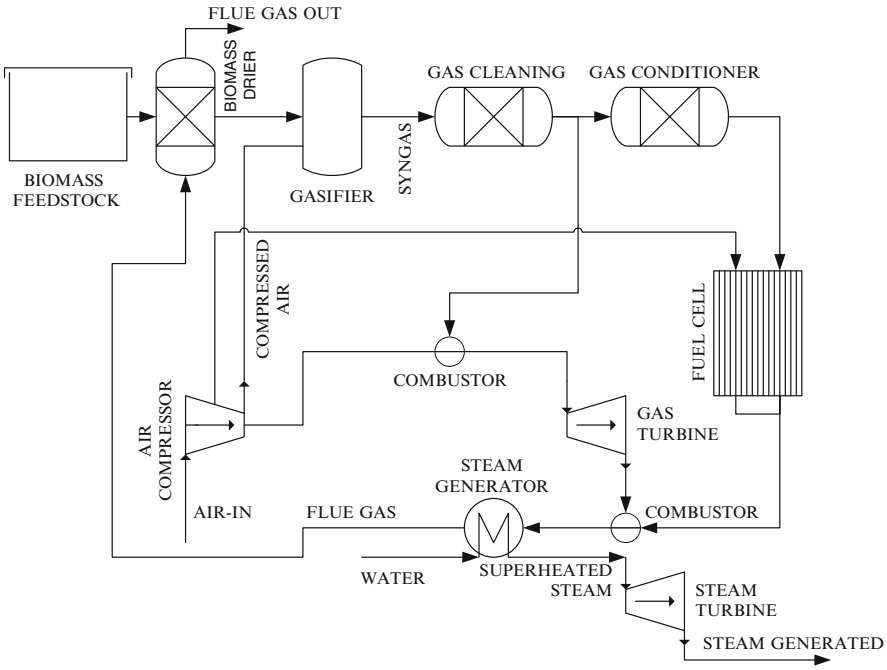

Fig. 9.63 System for electric power generation from biomass

When biomass is converted to biogas, then electric power generators based on internal combustion engines can be used for power production. It is also possible to couple biogas production facilities with micropower plants comprising gas turbines cascaded with reciprocating internal combustion engine. For micropower plants, alcohol and gasoline motors can be made to operate with methane without affecting their operational integrity. This adaptation is made by installing a cylinder of biogas in place of using conventional fuel. For gas flow regulation, a reducer is placed close to the motor.

It is interesting to introduce here the concept of biorefinery, which is an integrated hybrid system with multigeneration. The two technological platforms for biomass conversion, the biochemical and thermochemical ones, can be combined into the general concept of biorefinery. This is a facility that processes biomass to generate multiple products such as biodiesel, bioethanol, other liquid fuels, electric power, heat, hydrogen, and valuable bioproducts or biochemicals. The concept of biorefinery is illustrated schematically in Fig. 9.64.

The upper branch comprises thermochemical processes (see the figure), including gasification, gas separation, hydrogen production, Fischer–Tropsch synthesis to produce biodiesel, and heat recovery to produce steam, process heat and electricity. The lower branch comprises mostly biochemical processes including lignin separation from biomass. Lignin is a valuable commercial product that can be used in many chemical processes such as water formulation of dyes, production of humic acid and vanillin, an agent for leather tanning, and polyurethane foam.

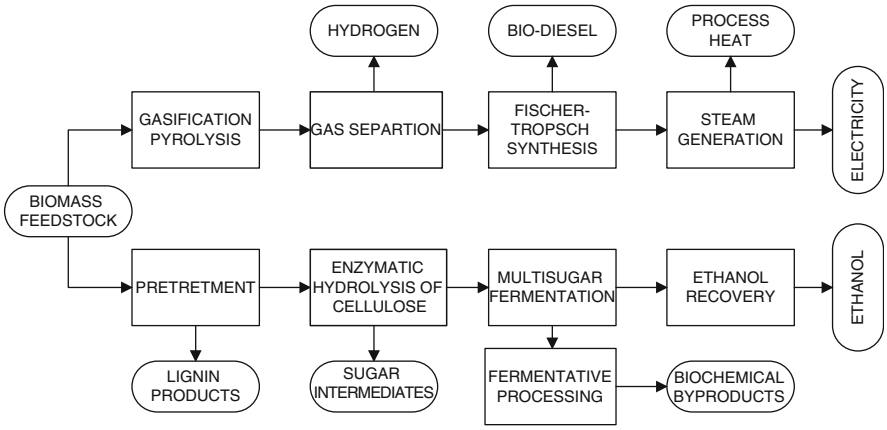

Fig. 9.64 Conceptual diagram of an integrated biorefinery

Through further enzymatic hydrolysis of cellulose one can produce a large variety of sugar intermediates. Further fermentative processes lead to production of ethanol and other biochemical by-products.

9.7 Ocean Thermal Energy

The temperature gradient of the ocean's depth results in a temperature difference just large enough over reasonable depths to extract thermal energy at low efficiency. This is called ocean thermal energy conversion (OTEC). Ammonia–water Rankine and Kalina cycles were proposed for OTEC. In arctic regions the difference in the temperature between water and cold atmospheric air can reach 40°C; in such locations there is potential for OTEC that operates between the surface water (heat source) and the atmospheric air (heat sink).

An OTEC system configuration is illustrated in Fig. 9.65. The system is basically a Rankine cycle operating with ammonia as the working fluid. The system can be installed on a floating platform or on a ship. It uses the surface water as the source. Normally, the water at the ocean surface is at a higher temperature than the water at the ocean's depths. The surface water is circulated with pumps through a heat exchanger that acts as a boiler for ammonia. Water from the deep ocean at 4°C is pumped to the surface, and used as the heat sink in an ammonia condenser.

Basically, the ocean surface in tropical oceans is warmed by the solar radiation to a depth of about 50 m. At depths of 1,000 m or more, the temperature is quasi-constant at 4°C. Therefore, all year round in tropical oceans there is a quasi-constant temperature difference between the surface and the deep water of 20° to 25°C. The thermodynamic limit for OTEC as expressed by the Carnot factor is 6% to 10%.

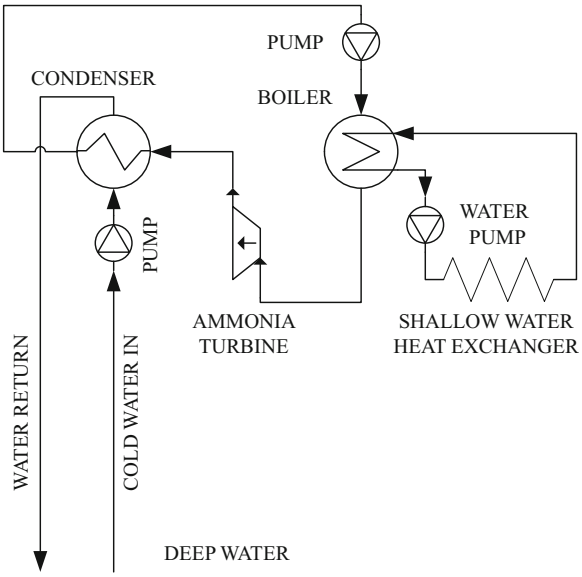

Fig. 9.65 Ocean thermal energy conversion system working with ammonia

Experimental tests and calculations show that at least 3% to 5% conversion is achievable (see comments in Zamfirescu and Dincer 2008b and Avery et al. 1985). Ammonia Rankine or Kalina cycles are the preferred solution for OTEC because the turbine shaft of the Rankine or Kalina power plant is connected with an electric generator to generate electricity. In general, it is difficult to transport the electricity generated by an OTEC plant ship since it is supposed to operate far from the shores. Thus, transporting the energy in chemicals is a better option. One cited option is to produce hydrogen from OTEC. This can be done through ocean water electrolysis. According to past studies [e.g., Avery et al. (1985)] building OTEC plant ships that generate hydrogen, transporting it to shore, and converting it into electricity are economically feasible in units of 150 to 400 MW electrical energy each.

It is suggested that hydrogen can be transported to shore either in the compressed phase, as cryogenic liquid, or by incorporating it into ammonia or methanol, which are substances relatively easy to manufacture onboard the plant ship. Calculations by Avery et al. (1985) show that when energy is transported in the form of ammonia or methanol, the overall electricity cost ends up to be about the same; however, the end-user cost is about four times higher if energy is transported in the form of liquefied hydrogen.

If the energy generated by OTEC is transported to shores in the form of ammonia or methanol and thereafter converted back to electricity, then the overall power production efficiency is about the same for both cases. However, if the OTEC energy is transported in the form of liquefied hydrogen, then the overall cost of electricity is estimated to be four times higher.

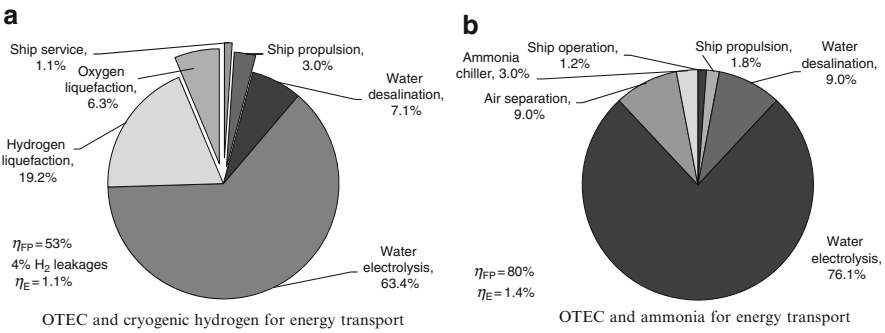

Fig. 9.66 Energy breakthroughs at OTEC using cryogenic hydrogen (**a**) or ammonia (**b**) as energy carriers [data from Avery et al. (1985)]

Figure 9.66 compares the energy breakthroughs at OTEC using cryogenic hydrogen or ammonia. The efficiency of OTEC electricity generation onboard the ship is assumed conservatively at 3%. The fuel conversion efficiency is defined as the energy in produced fuel with respect to HHV divided by the electrical energy input consumed by the fuel-generating plant. This efficiency is denoted by η_{FP}. In the case of a cryogenic hydrogen carrier, from the total of 100% electrical power input, the hydrogen production and transport facility loses (see Figure 9.66) 7.1% for water desalination, 63.4% for water electrolysis, 19.2% for hydrogen liquefaction, 6.3% for oxygen liquefaction (whereas the oxygen is to be used on the shore to produce electricity in fuel cells with improved efficiency), and 4% for hydrogen leaks during transport. At electricity production on the shore, hydrogen and oxygen are recombined in fuel cell systems cascaded with gas turbines and the Rankine cycle, operating at an assumed efficiency of 70%. Thus the hydrogen production efficiency (including the transport) is evaluated at 53%, while the overall OTEC electric power production on the shore is generated with the estimated efficiency of 1.1%.

In the case of ammonia as the carrier, the Haber–Bosch process is used for synthesis onboard. The electrolysis of water consumes 76% of the OTEC electricity generated onboard, air separation (needed to produce nitrogen) consumes 9% of the OTEC electricity, and water desalination consumes 9%. The ammonia synthesis reaction is exothermic; thus, it allows for the opportunity of heat recovery within the process. The ammonia production and transport efficiency is 80% and the overall electricity generation efficiency on the shore is 1.4%. For electricity generation, ammonia used in fuel cells is assumed to be 60% efficient.

9.8 Tidal and Wave Energy

Apart from being an immensely large thermal energy storage system (which is an indirect form of solar energy storage), oceans are at the same time huge reservoirs of mechanical energy. This mechanical energy manifests in the form of tides, ocean

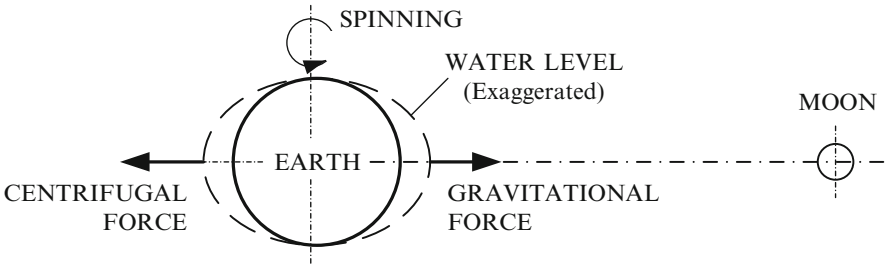

Fig. 9.67 Explaining the formation of tides

currents, and ocean waves. The kinetic energy resulting from the moon's (in addition to the sun's smaller) gravitational pull on the oceans under the earth's rotation produces a diurnal tidal effect. The formation of tides is explained in Fig. 9.67. Basically two bulges of water are formed at the equatorial belt due to the combined action of gravitational and centrifugal forces. Tidal energy shows good potential for electric energy generation. Their associated energy can be converted into electricity by two methods:

- Generation of a difference in water level through impoundment. When tides come into the shore, they can be trapped in reservoirs behind the dams. Then when the tide drops, the water behind the dam can be let out just like in a regular hydroelectric power plant. Since the tidal water level difference is rather small, Kaplan turbines are mostly used to generate power.
- Momentum transfer between the currents generated by tides and a conversion device such as water turbine. Ocean current-harvesting systems are used to rotate propellers that are coupled to electric generators.

Tidal impoundment (barrage) system can have three methods of operation depending on the phase when the tide generates power: ebb generation, flood generation, and two-way generation. When ebb generation is applied, the basin is filled during the flood tide. During the night additional water can be pumped into the basin as a means of energy storage during the off-peak hours. When the tide ebbs low enough, water is discharged over turbine systems that generate power. In flood generation, the dam gates are closed such that the water level increases on the ocean side until it reaches the maximum. Then water is allowed to flow through the turbine systems and to charge the basin while generating power. In two-way generation, electricity is generated both in the flood and the ebb phases of the tide. In Table 9.16 are listed some of the main tidal power generation systems and their principal characteristics. The world's largest tidal power generation site is in France at La Rance, with an installed capacity of 240 MW that operates with 24 reversible turbines and a hydrostatic head of 5 m.

Ocean water currents are generated by the action of tides, the earth's spinning, the heat cycle of tropical solar energy, and superficial winds. The water current's energy can be extracted through current turbines submerged in water. Basically, water current turbines are similar to wind turbines, with the difference that the

Table 9.16 Some of the major tidal impoundment sites

Location	Head (m)	Mean power (MW)	Production (GW h/year)
Minas–Cobequid, North America	10.7	19,900	175,000
White Sea, Russia	5.65	14,400	126,000
Mount Saint Michel, France	8.4	9,700	85,100
San Jose, Argentina	5.9	5,970	51,500
Shepody, North America	9.8	520	22,100
Severn, UK	9.8	1,680	15,000

Data from O'Rourke et al. (2010)

density and the viscosity of water are 100 and 1,000 times higher, respectively, than that of air. Therefore, there are some differences in operating conditions of water current turbines versus wind turbines. Similarly as for wind turbines, water current turbines are made in horizontal axis or vertical axis construction. The thrust generated by water current turbines is much higher than that specific to wind turbines; therefore, their construction material must be more massive and resistant.

Surface winds, tides, and ocean currents contribute to the formation of ocean waves. The energy of waves can be collected with floating bodies that execute elliptic movement under the action of gravity and wave motion. The wave energy can be measured in terms of wave power per meter of wave front. The highest wave power on the globe appears to be in southern Argentine across the Strait of Magellan where wave power density can reach 97 kW/m. Also along the south-western coast of South America, the wave power density is over 50 kW/m and often over 70 kW/m. In southwestern Australian coasts the wave power reaches 78 kW/m. In the Northern Hemisphere, the highest wave intensity is found along the coast of western Ireland and the UK with magnitudes around 70 kW/m. The southern coast of Alaska records wave power density of up to 65 to 67 kW/m. The wave power density on other coastal regions varies from about 10 kW/m to 50 kW/m. This impressive amount of energy can be converted into electricity with relatively simple mechanical systems that can be classified into two kinds: buoy and turbine type.

The principle of operation schematic of a buoy-type wave energy converter is shown in Fig. 9.68 and operates based on hydraulic-pneumatic systems. The buoy oscillates according to the wave movement at the ocean's surface. It transmits the reciprocating movement to a double effect hydraulic pump that is anchored rigidly on the ocean bottom. The pump generates a pressure difference between two pneumatic-hydraulic cylinders. A hydraulic motor generates shaft work by discharging the high-pressure liquid into a low-pressure reservoir. The shaft work turns an electric generator that produces electricity.

The energy of waves is correlated with the energy of surface winds. Two issues are important in determining the interrelation between the wave height and the wind characteristics, namely the wind–water fetch (i.e., the length over which the superficial wind contacts the water) and the duration of the wind. For example, if the wind blows constantly for 30 hours at 30 km/h and contacts the water over a length of 1,200 km, the wave height can reach 20 m (see Da Rosa 2009). The power density of the wave in deep ocean water can be approximated with

$$\dot{W} = 0.5v\rho g h^2, \tag{9.69}$$

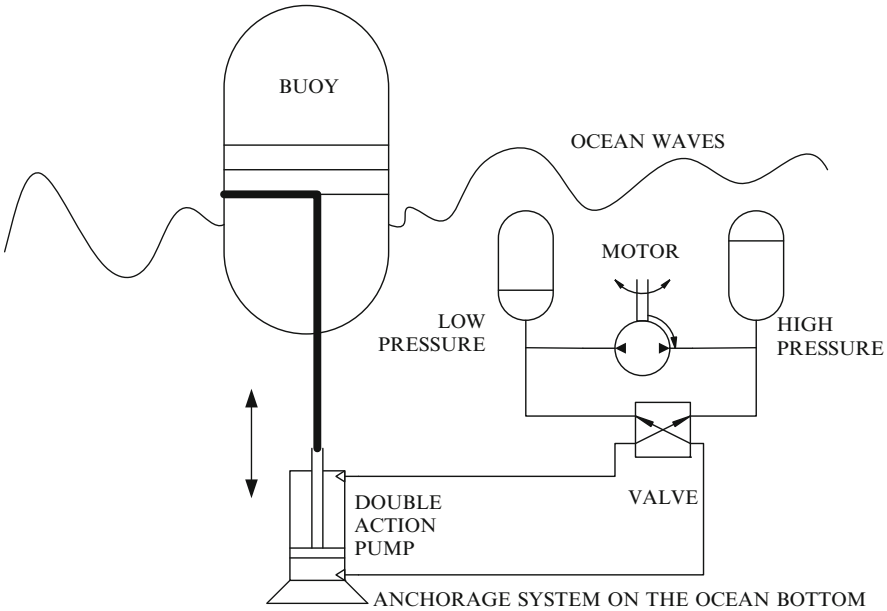

Fig. 9.68 Principle of operation of buoy-type ocean wave energy conversion system

while in shallow waters it is about half of this; in Eq. (9.69) v is the eave speed, ρ is the water density, $g = 9.81\ \text{m/s}^2$ is the gravity acceleration, and h is the height of the wave. Thus, a 10-m wave propagating with 1 m/s carries a power density of 49 kW/m.

If the waves are high, arrangements can be made in such a way that a difference of level can be created constantly through impoundment. Thus, the top of the wave carries waters over the impoundment constantly filling a small basin at a higher water level. The water-level difference is turned into shaft work by a Kaplan turbine system.

9.9 Concluding Remarks

In this chapter, renewable energy sources and the related energy conversion technologies were introduced for specific sources and applications. The renewable energy sources were classified into fundamental sources and energies derived from solar radiation (wind, waves, hydro, ocean thermal, and biomass energy). Solar energy, wind, geothermal, hydropower, biomass energy, and ocean energy were analyzed. The thermodynamic limits of renewable energy conversion into work were derived. Determining the energy and exergy efficiency of the processes was emphasized. The available technologies for converting renewable energies into work, heat, synthetic fuels, and hydrogen were analyzed. It appears that integrated hybrid systems show the potential for better renewable resource utilization and generating multiproducts.

Nomenclature

C	Concentration ratio
COP	Coefficient of performance
C_p	Power coefficient (−), specific heat (J/kg K)
e	Elementary electric charge (C)
$\dot{E}x$	Exergy rate (W)
FF	Filling factor
GCV	Gross calorific value (MJ/kg)
h	Specific enthalpy (J/kg) or (J/mol)
I	Irradiation (W/m^2), current intensity (A)
k_B	Boltzmann constant
LEC	Levelized electricity cost
M	Molecular mass (kg/kmol)
NCV	Net calorific value (MJ/kg)
Q	Heat (J)
R	Radius (m), resistance (Ω)
T	Temperature (K)
U	Heat transfer coefficient (W/m^2 K)
V	Voltage (V), velocity (m/s)
W	Work (J)
w	Moisture content

Greek Letters

α	Absorptivity
γ	Intercept factor
ε	Emissivity
η	Energy efficiency
μ	Chemical potential
ϕ	Subunitary factor
χ	Factor
ψ	Exergy efficiency
ρ	Reflectivity (−); density (kg/m^3)
ζ	Shading factor
σ	Stefan–Boltzmann constant (W/m^2 K^4)
τ	Transmissivity
θ	Dimensionless temperature
Ω	Solid angle
φ	Angle

Subscripts

0	Reference state
cog	Cogeneration
coll	Collector
db	Direct beam
e	Emitted or electric
diss	Dissipation
max	Maximum
oc	Open circuit
opt	Optical
PV	Photovoltaic
r	Receiver
rev	Reversible
S	Sun
SC	Solar constant
sc	Short circuit
T0	Tilted surface
th	Thermal

Superscripts

$(\dot{})$	Rate (per unit of time)
$()''$	Per unit of surface
$(\tilde{})$	Dimensionless

References

Avery W.H., Richards D., Dugger G.L. 1985. Hydrogen generation by OTEC electrolysis, and economical energy transfer to world markets via ammonia and methanol. *International Journal of Hydrogen Energy* 10:727–736.

Bejan A. 2006. Advanced Engineering Thermodynamics. Wiley, New York.

Burton T., Sharpe D., Jenkins N., Bossanyi E. 2001. Wind Energy Handbook. John Wiley and Sons, West Sussex.

Colpan C.O., Hamdullahpur F., Dincer I. 2010a. Solid oxide fuel cell and biomass gasification systems for better efficiency and environmental impact. Eighteenth World Hydrogen Energy Conference WHEC 16–21 May 2010, Essen, Germany.

Colpan C.O., Hamdullahpur F., Dincer I., Yoo Y. 2010b. Effect of gasification agent on the performance of solid oxide fuel cell and biomass gasification systems. *International Journal of Hydrogen Energy* 35:5001–5009.

Da Rosa A.V. 2009. Fundamentals of Renewable Energy Processes, 2nd ed. Elsevier, Burlington, MA.
Dincer I., Dilmac S., Ture I.E., Edin M. 1996a. A simple technique for estimating solar radiation parameters and its application for Gebze. *Energy Conversion and Management* 37:183–198.
Dincer I., Dost S. 1996. A perspective on energy storage systems for solar energy applications. *International Journal of Energy Research* 20:547–557.
Dincer I., Edin M., Ture E. 1996b. Investigation of thermal performance of a solar powered absorption refrigeration system. *Energy Conversion and Management* 37:51–58.
Granovskii M., Dincer I., Rosen M.A. 2006. Economic aspects of greenhouse gas emissions reduction by utilisation of wind and solar energies to produce electricity and hydrogen. IEEE EIC Climate Change Conference, pp. 1–5.
Joshi A.S., Dincer I., Reddy B.V. 2009a. Development of new solar exergy maps. *International Journal of Energy Research* 33:709–718.
Joshi A.S., Dincer I., Reddy B.V. 2009b. Performance analysis of photovoltaic systems: A review. *Renewable and Sustainable Energy Reviews* 13:1884–1897.
Joshi A.S., Tiwari A., Tiwari G.N., Dincer I., Reddy B.V. 2009c. Performance evaluation of a hybrid photovoltaic thermal (PV/T) (glass-to-glass) system. *International Journal of Thermal Sciences* 48:154–164.
Karakilcik M., Dincer I., Rosen M.A. 2006. Performance investigation of a solar pond. *Applied Thermal Engineering* 26:727–735.
Lee, K.C. 2001. Classification of geothermal resources by exergy. *Geothermics* 30:431–442.
Lund J.W. 2005. 100 years of geothermal power product. Proceedings Thirtieth Workshop on Geothermal Reservoir Engineering, Stanford University, Stanford, California, January 31–February 2, SGP-TR-176. Internet source http://iga.igg.cnr.it/index.php (accessed on September 15, 2009).
Markvart T., Landsberg P.T. 2002. Thermodynamics and reciprocity of solar energy conversion. *Physica E* 14:71–77.
O'Rourke F., Boyle F., Reynolds A. 2010. Tidal energy update 2009. *Applied Energy* 87:398–409.
Özgener L., Hepbasli A., Dincer I. 2005. Energy and exergy analysis of Salihli geothermal district heating system in Manisa, Turkey. *International Journal of Energy Research* 29:393–408.
Pope K., Dincer I., Naterer G.F. 2010. Energy and exergy efficiency comparison of horizontal and vertical axis wind turbines. *Renewable Energy* 35:2102–2113.
Sahin A.D., Dincer I., Rosen M.A. 2006. New spatio-temporal wind exergy maps. *Journal of Energy Resource Technology* 128:194–202.
Szargut J. 2005. Exergy Method. Technical and Ecological Applications. WIT Press, Boston.
Tiris G., Tiris M., Dincer I. 1995. Investigation of the thermal efficiencies of a solar drier. *Energy Conversion and Management* 36:205–212.
Van Loo S., Koopejan J. 2008. The Handbook of Biomass Combustion and Co-Firing. Earthscan, Sterling, VA.
Vargas J.V.C., Ordonez J.C., Zamfirescu C., Bejan A., Campos M.C. 2005. Optimization of the ground cooling of electronic packages. *Heat Transfer Engineering* 26:8–20.
Zamfirescu C., Dincer I. 2008a. How much work one can extract from incident solar radiation? *Journal of Applied Physics* 105/044911:1–5.
Zamfirescu C., Dincer I. 2008b. Thermodynamic analysis of a novel ammonia–water trilateral Rankine cycle. *Thermochimica Acta* 477:7–15.
Zamfirescu C., Dincer I., Verrelli T., Wagar W.R. 2008. Residential solar power generation systems for better environment. Proceedings of Global Conference on Global Warming, July 6–10, Istanbul, paper #805.
Zamfirescu C., Dincer I., Verrelli T., Wagar W.R. 2009. Environmental impact and cost analysis of residential systems for concentrated solar power and heat production. Proceeding of Global Conference on Global Warming, July 5–9, Istanbul, paper #531.

Study Questions/Problems

9.1 Explain and classify the renewable energies.
9.2 Describe the conversion paths of solar energy.
9.3 What is the thermodynamic limit of solar energy conversion with a blackbody receiver?
9.4 Define the exergy of solar radiation.
9.5 Define the concentration ratio.
9.6 Explain the existence of an optimum receiver temperature.
9.7 Calculate the optimum receiver temperature using Eq. (9.10) under reasonable assumptions.
9.8 Explain the concept of electric potential, chemical potential, and electrochemical potential and the differences among them.
9.9 Define the filling factor.
9.10 Comment on the utility of solar energy maps with respect to solar energy maps.
9.11 Describe the principle of operation of solar ponds.
9.12 Elaborate a calculation procedure of a flat plate solar collector for determining its efficiency.
9.13 Explain thermal and optical efficiency of solar concentrators and the difference between them.
9.14 Consider the system from Fig. 9.22a. Make reasonable assumption and calculate the cycle and its efficiency according to the first and second law of thermodynamics.
9.15 Explain the routes for solar-biochemical conversion.
9.16 Define the cogeneration efficiency of PV/T systems.
9.17 Consider the system described in Table 9.6. Make reasonable assumptions and calculate its efficiency under maximum solar radiation intensity.
9.18 Explain the wind-chill effect on the energy and exergy efficiency of wind turbines.
9.19 Comment on the role of wind exergy maps.
9.20 Describe the global utilization of geothermal energy.
9.21 Explain the thermodynamic limits of geothermal energy conversion.
9.22 Consider the system from Fig. 9.50. Make reasonable assumptions and calculate the cycle and determine its efficiency.
9.23 Consider the system from Fig. 9.52. Make reasonable assumptions and calculate the cycle and determine its efficiency.
9.24 Explain the advantage of ammonia–water in geothermal systems.
9.25 Using the ammonia–water diagram from Appendix B (Diagram B.5, p. 799), try to calculate the heat transfer process illustrated graphically in Fig. 9.53b.
9.26 Calculate the trilateral flash Rankine cycle with ammonia–water in EES or using the ammonia enthalpy diagrams.
9.27 A typical hydropower setting has a$\Delta z = 250\,\mathrm{m}$ level difference between the lake's surface and downstream waters. On the water stream with a volume

flow of $\dot{V} = 10{,}000\,\mathrm{dm}^3/\mathrm{s}$ a turbine coupled to an electric generator is installed that produces $\dot{W} = 9\,\mathrm{MW}$ power with $\eta_g = 99\%$ efficiency. Calculate the efficiency of the water turbine itself, the overall efficiency, and the power generated by the turbine.

9.28 Calculate the adiabatic flame temperature for a biomass having $X_C = 2$, hydrogen per carbon of 2, oxygen per carbon of 0.1, nitrogen per carbon of 0.4, sulfur per carbon of 0.1, and 20% moisture by weight.

9.29 For the above case, determine the maximum energy and exergy efficiency of combustion.

9.30 Consider the system from Fig. 9.63. Under reasonable assumptions calculate the cycle and determine its efficiency.

Chapter 10
District Energy Systems

10.1 Introduction

During the past decade, increasing local and global problems regarding energy, the environment, and the economy have created one of the biggest challenges for human beings to combat through sustainable solutions. District energy systems (DESs) for distributed heating and/or cooling, known also as district heating and cooling (DHC) systems, appear to be part of the solutions. In some situations, for example in the case of a major power plant, it may appear economically attractive to build a pipe network that distributes the ejected heat among a number of residential/commercial/industrial users covering a territory around the central power plant. Cogeneration, geothermal, or solar energy systems are the most suitable for being coupled to DHC. Steam, hot or cold water, or ice slurry can be used as heat-conveying fluids. The opportunity of using a DES must be judged first on an economic basis by comparison of the life-cycle cost (LCC) with the cost of other competing systems, such as electrically driven heat pumps at the user's location. There also are some ecological benefits because CO_2 or other emissions can be reduced and controlled better from a central plant rather than from distributed locations. In general, one recognizes that district heating (DH) as well as district cooling (DC) may be advantageous whenever a central source can be made available to distribute heat and/or cold to residential, commercial, or industrial consumers.

Most of the Rankine cycle–based power plants in operation nowadays eject an enormous amount of condensation heat into a cooling tower or a lake, even though it is obvious that by using the ejected heat to some purpose the overall efficiency is greatly augmented. If instead of ejecting it, the heat is distributed to a number of users over a territory around the power plant, one has a district heating system. Up to the present, this philosophy of design has been applied in a limited fashion in many European and North American countries, where the planned economy and political will allowed for large capital investments in network infrastructure.

Basically, DESs convert the primary energy in a commodity (heating and/or cooling) that can be bought or sold. The energy distributed by a DES can provide space heating, air conditioning, refrigeration, domestic hot water, and industrial

İ. Dinçer and C. Zamfirescu, *Sustainable Energy Systems and Applications*,
DOI 10.1007/978-0-387-95861-3_10,

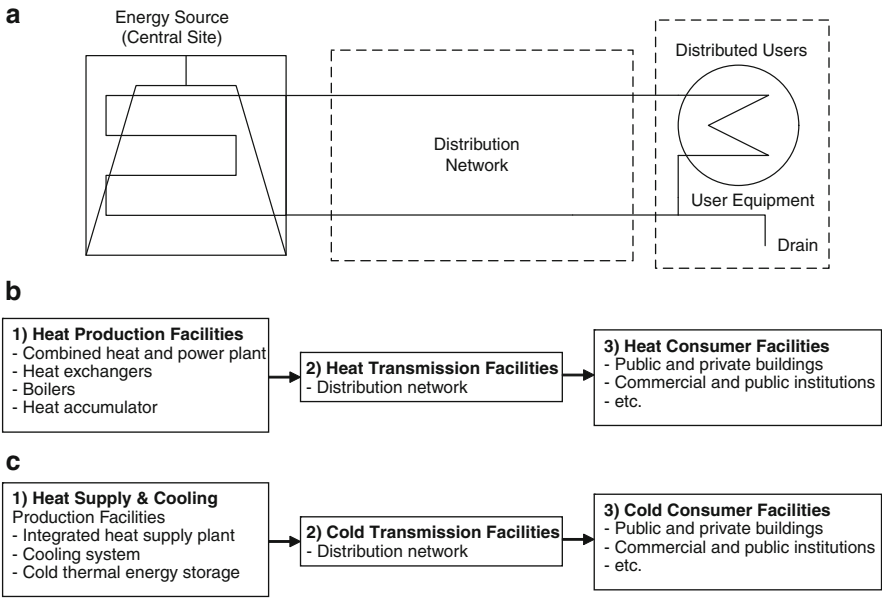

Fig. 10.1 (**a**) A general layout of a district energy system and basic flowcharts for (**b**) district heating and (**c**) district cooling applications

process heating and cooling, and often cogenerates electricity locally. Even more recently, there has been an attempt to look at the hydrogen production options in a combined or integrated form.

There can be a large number of central sources suitable for DHC: fossil fuels (coal, natural gas, oil, or other petroleum products) and nuclear-based power plants with cogeneration of electric power and heat, geothermal energy exploitation facilities, solar collector fields, city waste incinerators, and any combination of these. Typically, the carrier fluids are steam or hot or cold water and the more recently developed ice slurry, which is a mixture of water, ice particles, and antifreeze. The chilled water or the ice slurry can be produced by heat-driven absorption chillers (e.g., lithium bromide or ammonia–water), steam turbo-chillers, or steam ejectors, or mechanically driven vapor compression chillers.

The overall layout of a DES consisting of a central heat/cold production, a distribution network, and user equipment at consumers' locations is illustrated in Fig. 10.1a. The fluid carrying the thermal energy can be completely recirculated in a closed loop, or partially or totally drained (e.g., in the case of steam) at the users' locations. Figure 10.1b illustrates a district heating system layout. In this case, at the heat production site, there can be a combined heat and power (CHP) plant, a fuel boiler, a thermal storage system, or a combination of these. The primary source can be fossil fuel or biomass, nuclear, geothermal, or solar energy. Through the heat transmission network, hot water or steam may circulate, depending on the design option. At the user's site, various heat exchangers can be used to

Table 10.1 Some technical aspects of DES

Land use	Specific thermal load (MW/ha)	DES desirability
Downtown, skyscrapers	>0.70	Very favorable
Downtown, multistoried buildings	0.51–0.70	Favorable
City center; multifamily apartments, commercial building settings	0.20–0.50	Possible
Two-family residential building	0.12–0.20	Questionable
Single-family residence	<0.12	Unfeasible

Data from (Karlsson 1982)

serve for space heating, water heating, or industrial process heating. Figure 10.1c presents the general district cooling system layout. In this case, at the central site, a primary thermal energy (in general, in the form of a hot source) is converted into cold thermal energy. This can be done through an absorption chiller. An alternative is to use an electrically driven chiller. The central production site can also be equipped with a cold thermal energy storage system that has the advantage of allowing for cooling load levelizing (this is a better match for cold production and demand) during the day, week, or season.

In general, the most expensive component of a DES is the piping network made from a combination of field-insulated and preinsulated pipes either embedded in a concrete tunnel or buried in the ground, or a combination of the two. Its capital cost may range between 50% and 75% of the total. The user's equipment is assumed to be the least expensive, and can be formed from simple heat exchangers and distribution/regulating valves.

The fact that the distribution network is relatively expensive makes DHC systems most attractive in major cities, high-density building clusters, tall buildings with high thermal (heat or cold) load, and industrial parks. In Table 10.1, we quantify the desirability of a DES as a function of the land use and the specific thermal load. When cooling and heating is required simultaneously (e.g., in the case of industrial processes or if a refrigerated storage facility that requires cooling is in the vicinity of building settings that require heating), this can be economically advantageous because a central large capacity heat pump can generate both cooling and heating at a lower cost than individual on-site units.

The DHC systems are expected to provide other environmental and economic benefits:

- Reduced local/regional air pollution
- Increased opportunities to use ozone-friendly cooling and heating technologies
- Infrastructure upgrades and development that provide new jobs
- Enhanced opportunities for electric peak reduction through chilled water or ice storage
- Increased feasibility of thermal energy storage at the central location for better energy management
- Better part-load capability and efficiency (multiple units can be used to adjust to variable demand)
- Increased fuel flexibility

- Better energy security
- Better energy efficiency, lower operating and maintenance costs, specifically in large facilities
- Concentration of specialized personnel at the central plant location for better economics
- Better building economics by not needing on-site personnel for boiler or chiller surveillance
- Possibility of expansion to accommodate future growth (of network and central plant)
- Reducing the costs related to metering of the distributed energy
- Better noise and environment pollution control; CO_2 sequestration facilitated at the central location

The DHC's potential can be realized through policies and measures to increase awareness and knowledge of these systems; recognize the environmental benefits of district energy in air quality regulation; encourage investment; and facilitate the increased use of district energy in government, public, commercial, industrial, and residential buildings.

During the past few decades, there have been various key initiatives taken by major energy organizations (e.g., the International Energy Agency [IEA], the U.S. Department of Energy, Natural Resources Canada, etc.) on the implementation of DHC systems all over the world as one of the most significant ways to (1) maximize the efficiency of the electricity generation process by providing a means to use the waste heat, saving energy while also displacing the need for further heat-generating plants; (2) share heat loads, thereby using plants more effectively and efficiently; (3) achieve fuel flexibility and provide opportunities for the introduction of renewable sources of energy as well as cogeneration and industrial waste heat.

Furthermore, the IEA has developed a strategic document (IEA 2004) as an implementing agreement on DHC, including the integration of CHP, focusing on the following:

- Integration of energy-efficient and renewable energy systems for limited emissions of greenhouse gases
- Community system integration and optimization, use of waste thermal energy, renewable energy and CHP, for a better environment and sustainability
- Reliability, robustness, and energy security for effective maintenance and management of buildings
- Advanced technologies for an improved system integration, including information systems and controls
- Dissemination and deployment for rapid changes to foster energy efficiency and sustainability

Here, we present the historical development of DES, and we discuss some technical, economical, environmental, and sustainability aspects of these systems, their performance evaluation tools in terms of energy and exergy efficiencies, and LCC and life-cycle savings. The use of LCC or life-cycle savings criteria for

evaluating the feasibility of DHC versus other competing systems is discussed. Several design aspects of the DHC system are introduced. Some case studies and several numerical examples are also presented to highlight the importance of exergy use as a potential tool for system analysis, design, and improvement.

10.2 Distributed Energy Systems Description

The central energy source and the distribution network are two capital intensive components of the DES. It is important to understand the role and structure of these two subsystems, their development, the status of the present technology, and their future role as related to environment and sustainability. First, we briefly follow the historical dissemination and evolution of DES in the world; thereafter, we comment on the importance of cogeneration as central source for distributed energy systems. In this section, flow diagrams of DHC networks, piping layouts, and other technological and design issues are discussed.

10.2.1 Historical Development and Perspectives of District Energy Systems

The development of district heating systems traces back to antiquity when the Roman Empire developed thermaes (public baths) supplied by centrally heated water. Probably, the oldest DH system that is in operation today is the one created in the early fourteenth century in Chaudes-Aigues Cantal, a village in France. This system distributed warm water through wooden pipes and is still in use today. The first commercial DH system was created by Birdsill Holly in Lockport, New York, in 1877 (Dincer and Hepbasli 2010). In this system, the boiler is used as the central heat source and the system supplies a loop consisting of steam pipes, radiators, and even condensate return lines. At first, the system attracted a dozen customers. Only 3 years later, it served several factories as well as residential customers and had extended to a ~5-km loop.

The largest commercial district heating system in the United States that has operated continuously since 1882 is installed in New York (ConEd 2008). In addition to providing space and water heating, steam from the system is used in restaurants for food preparation, as process heat in laundries and dry cleaners, as well as in power absorption chillers for air conditioning.

The city of Paris operates a geothermal district heating system that delivers hot water at ~65°C, while the city of Vienna has a district heating system totaling a capacity of over 5 GWh/year. In Germany the district heating system has a market share of about 14%; the former Soviet Union, during the Communist era, developed most of its coal power plants as cogeneration units to supply heating to neighboring buildings (Skagestad and Mildenstein 2002).

The roots of district cooling (DC) systems go back to the nineteenth century. A DC system was initially introduced as a scheme to distribute clean, cool air to houses through underground pipes. Probably the first known DC system began operations at Denver's Colorado Automatic Refrigerator Company in late 1889. In the 1930s, large DC systems were created for Rockefeller Center in New York City and for the U.S. Capitol buildings in Washington, DC. So far few European cities have adopted DC systems for applications (National Academy of Sciences 1985).

It is believed that district energy in Canada began in London, Ontario, in 1880. The London system was built in the form of a group of systems serving the university, hospital, and government complexes. The University of Toronto is known to have developed a DH system in 1911 that served the needs of the university. The first commercial DH system in Canada was established in 1924 in the city of Winnipeg's commercial core. Canada boasts the site of one of the northernmost DESs in North America: Fort McPherson, located in the North West Territories. The Canadian District Energy Association (CDEA) was created in 1993 in recognition of the fact that the emerging Canadian district energy industry needed to create a common voice to promote DHC applications. It aims to exchange and share information and experience with its stakeholders. It has also been instrumental in helping to provide a forum for the exchange of ideas and information, and in identifying and addressing key technical and policy issues to advance the use of district energy in Canada. As a recent application of a district energy system, the city of Toronto has been using cold deep water from the Lake Ontario and heating from fuel-based cogeneration plants; for further information, see Enwave (2005).

10.2.2 Cogeneration as a Key Part of District Energy Systems

Cogeneration, also referred to as CHP, is the simultaneous sequential production of electrical and thermal energy from a single fuel. During the past couple of decades, cogeneration has become an attractive and practical proposition for a wide range of thermal applications, including DHC. Some examples are the process industries (pharmaceuticals, paper and board, cement, food, textile, etc.); commercial, government, and public sector buildings (hotels, hospitals, swimming pools, universities, airports, offices, etc.); and DHC schemes. Figure 10.2 shows a comparison of both conventional power systems and cogeneration systems. The main drawback in the conventional system is the amount of intensive heat losses, resulting in some drastic drops in efficiency.

The key question is how to overcome this and make the system more efficient. The answer is clear: by cogeneration. In this regard, we minimize the heat losses, increase the efficiency, and provide the opportunity to supply heat to various applications and facilities. The overall thermal efficiency of the system is the percent of the fuel converted to electricity plus the percent of fuel converted to useful thermal energy. Typically, cogeneration systems have overall efficiencies ranging from 65% to 90%.

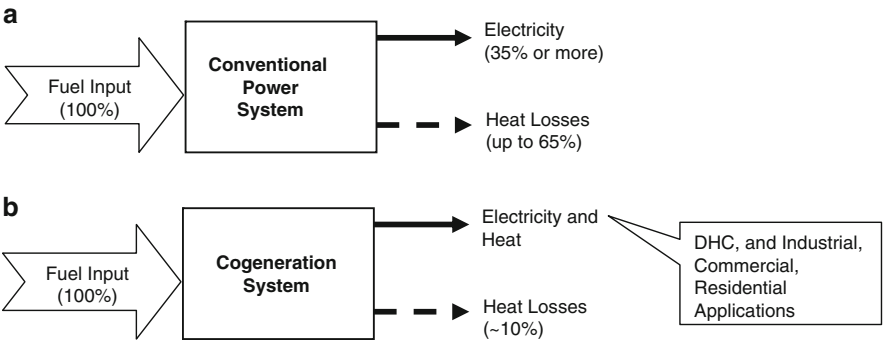

Fig. 10.2 Illustration of (**a**) a conventional power system and (**b**) a cogeneration system

The key point here is that the heat ejected from one process is used for another process, which makes the system more efficient, compared to the independent production of both electricity and thermal energy. Here, the thermal energy can be used in DH and/or DC applications. Heating applications basically include generation of steam or hot water. Cooling applications basically require the use of absorption chillers that convert heat to cooling. Numerous advanced technologies are available to achieve cogeneration, but the system requires an electricity generator and a heat recovery system for full functioning.

As mentioned above, cogeneration has been widely adopted in many European countries for use in industrial, commercial/institutional, and residential applications. It currently represents 10% of all European electricity production and over 30% of electricity production in Finland, Denmark, and the Netherlands. In Canada, however, cogeneration represents just over 6% of national electricity production (Strickland and Nyboer 2002). This relatively lower penetration is attributed to Canada's historically low energy prices and to electric utility policies for the provision of back-up power and the sale of surplus electricity. Despite these conditions, cogeneration has been adopted in some industrial applications, notably the pulp and paper and chemical products sectors, where a large demand for both heat and electricity exists. There are several classic technologies currently available for cogeneration, such as steam turbines, gas turbines, combined cycles (both steam and gas turbines, and reciprocating engines (gas and diesel). In addition, there has been increasing interest in using new technologies, namely, fuel cells, microturbines, and Stirling engines. Note that heat output from the system varies greatly depending on the system type. The output can range from high-pressure, high-temperature (e.g., 500–600°C) steam to hot water (e.g., 90°C). High-pressure, high-temperature steam is considered high-quality thermal output because it can meet most industrial process needs. Hot water is considered as low-quality thermal output because it can be used only for a limited number of DHC applications.

Cogeneration can be based on a wide variety of fuels, and individual installations may be designed to accept more than one fuel. While solid, liquid, or gaseous fossil

Table 10.2 Main characteristics and technical aspects of cogeneration systems

Technology	Fuel type	Capacity (MW_e)	Electrical efficiency (%)	Overall efficiency (%)	Average capital cost (US$/$kW_e$)	Average maintenance cost (US$/kWh)
Steam turbine	Any	0.5–500	7–20	60–80	900–1,800	0.0027
Gas turbine	Gaseous and liquid fuels	0.25–50 or more	25–42	65–87	400–850	0.004–0.009
Combined cycle	Gaseous and liquid fuels	3–300 or more	35–55	73–90	400–850	0.004–0.009
Reciprocating engines	Gaseous and liquid fuels	0.003–20	25–45	65–92	300–1,450	0.007–0.014
Microturbines	Gaseous and liquid fuels	–	15–30	60–85	600–850	<0.006–0.01
Fuel cells	Gaseous and liquid fuels	0.003–3 or more	35–50	80–90	–	–
Stirling engines	Gaseous and liquid fuels	0.003–1.5	~40	65–85	–	–

Data from UNEP (2005)

fuels dominate currently, cogeneration from biomass fuels is becoming increasingly important. Sometimes fuels are used that otherwise would constitute waste, such as refinery gases, landfill gas, agricultural waste, or forest residues. These substances increase the cost-efficiency of cogeneration (UNEP 2005). Table 10.2 lists cogeneration technologies and their fuel type, capacity, efficiency, average capital cost, and maintenance cost.

10.2.3 Technological Aspects

Many DHC systems do not include both DH and DC. For example, in Europe, where moderate summer temperatures prevail, most DESs provide heating capability only. DC has only recently become more widespread, with the most prevalent application being in North America, where summer temperatures can, over extended periods, reach extremes of 30° to 40°C.

In order to implement a DH, DC, or DHC system in a community, there are several factors that must be weighed in a feasibility study for determining whether or not a DH, DC, or DHC system is suitable. Some essential factors include energy, exergey, the environment, economics, social criteria, operating conditions, fuel availability, efficiency considerations, local benefits, viability of competing systems, local climatic conditions, users' characteristics, load density, total load requirements, characteristics of heating and cooling systems currently in place, the developer's perspectives, and local utility considerations.

Note that a DH or DC system differs fundamentally from a conventional system because, in the case of the latter, thermal energy is produced and distributed at the location of use. Examples of conventional systems include residential heating and

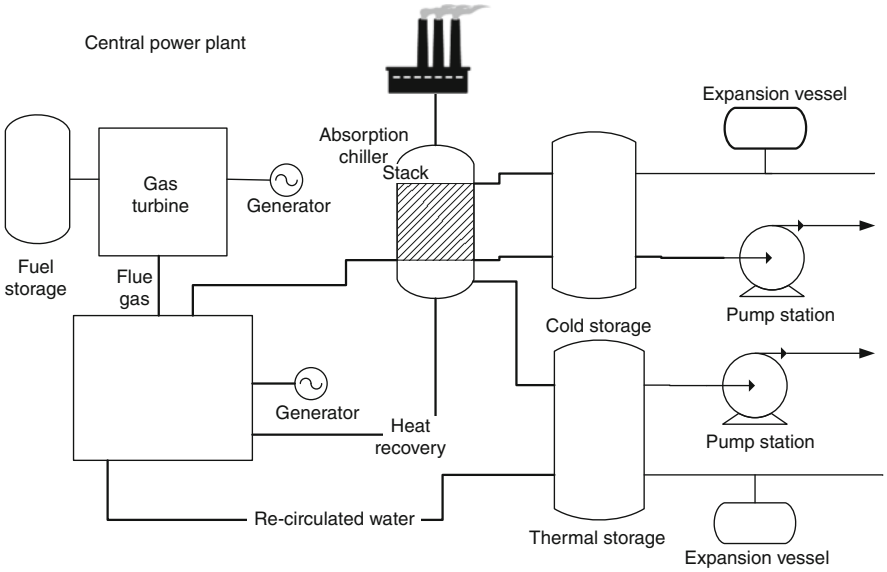

Fig. 10.3 Example of a hybrid gas turbine/steam Rankine cycle CHP facility

cooling with, respectively, furnaces and air conditioners; electric heating of offices; package boilers/chillers providing heating/cooling of apartment complexes; and a dedicated boiler plant providing heat to an industrial facility. The feasibility of a DHC system therefore must be compared to that of a convectional system.

A possible layout of a CHP central plant is shown in Fig. 10.3. In this example, the CHP unit is fueled with oil or natural gas and consists of a gas turbine engine cascaded with the steam boiler of a Rankine cycle. After being used to heat the steam cycle, the flue gas still possesses energy, which is directed toward the generator of an absorption chiller and then released into the atmosphere with possible prior filtering and CO_2 separation and sequestration. The refrigeration effect produced by the absorption chiller is carried by a selected heat transfer fluid (cold water or ice slurry) that supplies the cold distribution line. On this line, a cold storage facility can also be mounted, as illustrated in the figure. The pumping station and thermal expansion tanks equip also the central plant. The facility can be designed so that the heat ejected by the Rankine cycle could be upgraded with the heat ejected by the condenser of the absorption chiller and delivered to the heat distribution line. The heat distribution line itself can be equipped with a thermal storage tank based either on sensible heat storage (hot water) or on latent heat storage (in phase change materials). Both the gas turbine and steam turbine turn an electrical generator at their shaft, and the CHP site is equipped with all the needed electrical equipment to deliver power to the grid.

A number of issues must be addressed when designing a CHP plant that serves a DES. A decision must be made regarding the thermal carrier. Knowing the type of thermal energy carrier is compulsory for designing the heat exchangers for heat and

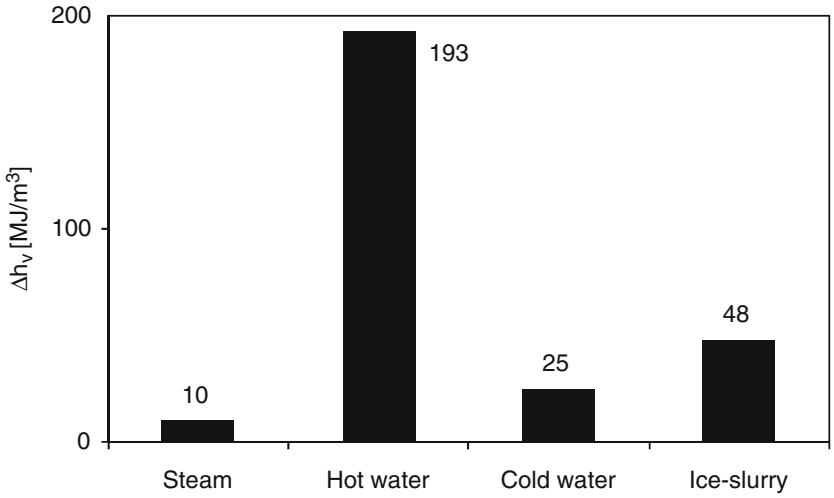

Fig. 10.4 Volumetric specific enthalpy variation of steam (at 8 bar from saturated vapor to 80°C subcooled liquid), hot water (from liquid saturated at 170°C and cooled to 120°C), cold water (from 4° to 10°C), and ice slurry (water–ethanol at 0°C, from 30% slurry to 0%)

cold recovery. The first thermophysical property that has to be analyzed is the heat capacity (or latent heat) of the carrier. In the case of heat, one must choose between steam and hot water. Here, the key question may be at what temperature the network should operate. There are several temperature thresholds as given below as a practical guide:

- Above 175°C supply temperature for high-temperature networks
- 120–175°C for average-temperature district heating
- Below 120°C for low-temperature district heating
- 4°C supply temperature for cold water at district cooling
- 0°C or slightly below if ice slurry is used for district cooling

Based on heat capacity (or latent heat) and the specific volume of the thermal carrier fluid, one can easily derive the specific volumetric enthalpy (measured in kJ/m^3) and compare this parameter to other options. Figure 10.4 shows the calculated value of specific volumetric enthalpy of high-temperature steam, water, and ice-slurry. Even though on a mass basis the enthalpy of steam is the highest, on a volumetric basis the steam enthalpy is the lowest among all options because of steam's high-specific volume. As a consequence, steam pipes have a higher diameter than water pipes and therefore are more costly. However, the condensate return pipe has a smaller diameter than the hot water return pipe, and this somehow compensates for the costs. Ice slurry's, specific volumetric enthalpy is about double that of chilled water because the latent heat of melting is stored in ice slurry. The ice-slurry properties can be calculated based on data taken from Bel et al. (1996).

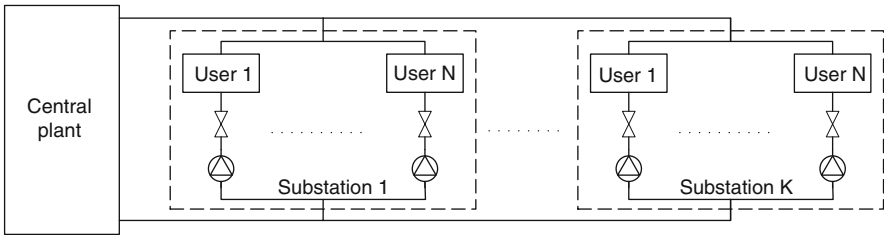

Fig. 10.5 Layout example of a primary and secondary distribution system

If cogeneration is not the adopted solution for a central power plant, heat could be produced using commercially available boilers fueled with coal, oil, or natural gas. Custom-made solutions can be devised for biomass combustion or city waste incinerators with heat recovery. Absorption refrigeration is the preferred method to produce cold water if heat is generated at the central plant. As an alternative, electrically- or heat engine–driven mechanical chillers can be adopted. In general, the chilled water is produced at 5°C and it returns at 7°C. The lower value of produced chilled water is 4°C (due to water density anomaly), and the maximum return temperature can go up to 10°C. Ice slurry can be generated either in mechanical ice scrapers or fluidized bed ice scrapers or in water turbo-refrigerators. Typically, the temperature of the ice slurry is slightly below 0°C.

Thermal and cold storage can be used at a central plant for better efficiency and adaptation to a variable load. With an appropriate thermal energy storage strategy, the capacity and the associated investment in heat or cold thermal energy generators can be reduced.

The layout of the distribution network can consist of a primary circuit that delivers the thermal carrier to a number of substations working in parallel. Each substation may include pumps for pressure head rebuilding, and it distributes the working fluid among a number of users connected in parallel. A typical network diagram is presented in Fig. 10.5.

Two flow control strategies are possible: (1) constant flow and variable temperature difference, or (2) variable flow and constant temperature difference. In the first approach, the flow rate is maintained constant and well balanced for all users. As a consequence of demand variation among users, the return temperature adjusts so that it meets the load. The variable flow/constant temperature control strategy is met to enhance the system efficiency by a better use of flow exergy. That is, if one keeps the temperature level constant, the specific exergy of the circulated streams is maintained constant, too, and the system efficiency is thus maximized. The flow rate can be adjusted either by flow-throttling with modulating valves or by using variable speed pumps.

At the user's location, it is preferable to design a temperature (or enthalpy) drop as large as possible so as to minimize the pumping power and reduce the diameter of distribution pipes (therefore their capital cost). Based on the current practice, the temperature drop for a district heating system is taken to be 22 K or

larger (ASHRAE 2008). The users' equipment (e.g., radiators) can be directly connected to the network, or indirectly via a heat exchanger. In the indirect connection, the heat exchanger transfers the heat from the distribution network to the users' equipment, creates a pressure separation between the district network and the building network (for safety reasons, it is preferred that the distribution network in buildings operates at low pressure), and separates the water quality treatment of the inner and outer networks.

10.3 Environmental Impact

Problems with energy supply and use are related not only to global warming but also to such environmental concerns as air pollution, acid precipitation, ozone depletion, forest destruction, and emission of radioactive substances. These issues must be taken into consideration simultaneously if humanity is to achieve a bright energy future with minimal environmental impact. Much evidence exists to suggest that the future will be negatively impacted if humans keep degrading the environment. One solution to both energy and environmental problems is to encourage much more use of DHC applications.

Numerous fuels are used at DHC plants, including various grades of oil and coal, natural gas, refuse, and other biofuels such as wood chips, peat, and straw. The combustion of such fuels may produce environmentally hazardous products of combustion, and thus flue gas cleaning devices and other emission reduction measures are often incorporated. Some measures are usually required under increasingly strict legislation, before approval to operate a facility is granted. Examples of pollution control equipment used at DHC plants include acid gas scrubbers. These systems typically utilize hydrated lime to react with the moisture, SO, and other acid gases in the flue gases discharged from the combustion system. With such systems, the lime–acid and gas–water vapor reaction products are efficiently collected by electrostatic precipitators as particulate matter. Bag filters are also utilized in many applications to capture the particulate matter as well as the acid gas scrubbing reaction products. Conventional oil/gas fired boilers utilizing low NO_x and burners to dramatically reduce NO_x emissions are also becoming more common. Flue gas recirculation to reduce NO_x emissions has also been proven to be effective. Other emission control or reduction techniques can be introduced with DHC systems, including optimization of combustion efficiency (i.e., reduces CO_2, CO, and hydrocarbon emissions) through the use of modern computerized combustion control systems, and utilization of higher quality and lower emission producing fuels. By addressing these issues, it is apparent that heating and cooling systems that minimize the quantity of fuel and electrical power required to meet the users' needs result in a reduced impact on the environment.

In addition, DHC systems that comprise several different types of thermal energy generation plants can optimize plant and system efficiency by utilizing, whenever possible, the thermal energy sources with the highest energy conversion

efficiencies for base and other partial load conditions. The sources with the poorer conversion efficiencies can then be utilized only to meet peak loads. Essentially, improved efficiency means the use of less fuel for the same amount of energy produced which in turn results in the conservation of fossil fuels, reduced emissions of pollutants, improved air quality, and reduced use of chlorofluorocarbon (CFC) refrigerants, if any, in DC applications.

The DHC systems are well suited to combine with electric power production facilities as cogeneration plants. The amalgamation of these two energy production/utilization schemes results in a substantial improvement in overall energy conversion efficiency since DH systems can effectively utilize the otherwise wasted heat associated with the electric power production process. A district system meeting much or all of its load requirements with waste heat from power generation facilities has a positive environmental impact, as fuel consumption within the community is reduced considerably. Conservation of fossil fuels and a reduction of combustion-related emissions are resultant direct benefits of such a DHC system.

The centralized nature of DHC energy production plants results in a reduced number of emission sources in a community. This introduces the potential for several direct benefits.

The higher operating efficiency afforded by larger, well-maintained facilities translates directly to reduced fuel consumption, which in turn results in the conservation of fossil fuels and reduced emissions. Higher operating efficiency of the combustion process (where parameters such as temperature, combustion air and fuel input levels, residence time, etc., are closely monitored) also impacts emission production in that the concentration of certain pollutants produced, particularly CO_2 and NO_x, is reduced.

Furthermore, measures to increase energy efficiency can reduce environmental impact by reducing energy losses. From an exergy viewpoint, such activities lead to increased exergy efficiency and reduced exergy losses (both waste exergy emissions and internal exergy consumption).

A deeper understanding of the relations between exergy and the environment may reveal the underlying fundamental patterns and forces affecting changes in the environment, and help researchers better address environmental damage.

The second law of thermodynamics is instrumental in providing insights into environmental impact. The most appropriate link between the second law and environmental impact has been suggested to be exergy, in part because it is a measure of the departure of the state of a system from that of the environment. The magnitude of the exergy of a system depends on the states of both the system and the environment. This departure is zero only when the system is in equilibrium with its environment.

In order to achieve the energy, economic, and environmental benefits that DHCs offer, the following integrated set of activities should instituted (Dincer 2000):

- *Research and development*. Research and development priorities should be set in close consultation with industry to reflect its needs. Most research is conducted through cost-shared agreements and falls within the short-to-medium term.

Partners in these activities should include a variety of stakeholders in the energy industry, such as private sector firms, utilities across the country, provincial governments, and other federal departments.

- *Technology assessment*. Appropriate technical data should be gathered in the lab and through field trials on factors such as cost benefit, reliability, environmental impact, safety, and opportunities for improvement. These data should also assist in the preparation of technology status overviews and strategic plans for further research and development.
- *Standards development*. The development of technical and safety standards is needed to encourage the acceptance of proven technologies in the marketplace. Standards development should be conducted in cooperation with national and international standards writing organizations, as well as other national and provincial regulatory bodies.
- *Technology transfer*. Research and development results should be disseminated through the sponsorship of technical workshops, seminars, and conferences, as well as through the development of training manuals and design tools, web tools, and the publication of technical reports.

Such activities also encourage potential users to consider the benefits of adopting DHC applications and using renewable energy resources. In support of developing near-term markets, a key technology transfer area is the acceleration of the use of cogeneration and DHC applications, particularly for better efficiency, cost-effectiveness, and the environment.

10.4 Role in Sustainable Development

Sustainable development requires a sustainable supply of clean and affordable energy resources that do not have negative societal impacts (Dincer and Rosen 2005). Supplies of such energy resources as fossil fuels and uranium are finite. Green energy resources, such as solar and wind, are generally considered renewable and therefore sustainable over the relatively long term.

Sustainability often leads local and national authorities to incorporate environmental considerations into energy planning. The need to satisfy basic human needs and aspirations, combined with the increasing world population, makes the need for successful implementation of sustainable development increasingly apparent. Here are the factors that are essential to achieve sustainable development in a society:

- Information about and public awareness of the benefits of sustainability investments
- Environmental education and training
- Appropriate energy and exergy strategies
- The availability of renewable energy sources and cleaner technologies
- A reasonable supply of financing
- Monitoring and evaluation tools

The key point here is to use renewable energy resources in DHC systems. As known, not all renewable energy resources are inherently clean in that they cause no burden on the environment in terms of waste emissions, resource extraction, or other environmental disruptions. Nevertheless, the use of DHC systems almost certainly can provide cleaner and more sustainable energy than can increased controls on conventional energy systems.

To seize these opportunities, it is essential to establish a DHC market and gradually build up the experience with cutting-edge technologies. The barriers and constraints to the diffusion of DHC use should be removed. The legal, administrative, and financing infrastructure should be established to facilitate planning and the application of geothermal energy projects. Government could/should play a useful role in promoting geothermal energy technologies through funding and incentives to encourage research and development as well as commercialization and implementation in both urban and rural areas.

Environmental concerns are significantly linked to sustainable development. Activities that continually degrade the environment are not sustainable. For example, the cumulative impact on the environment of such activities often leads over time to a variety of health, ecological, and other problems. Clearly, a strong relation exists between efficiency and environmental impact, since, for the same services or products, less resource utilization and pollution is normally associated with increased efficiency (Dincer 2002).

Improved energy efficiency leads to reduced energy losses. Most efficiency improvements produce direct environmental benefits in two ways. First, operating energy input requirements are reduced per unit output, and pollutants generated are correspondingly reduced. Second, consideration of the entire life cycle for energy resources and technologies suggests that improved efficiency reduces environmental impact during most stages of the life cycle.

In recent years, the increased acknowledgment of humankind's interdependence with the environment has been embraced in the concept of sustainable development. With energy constituting a basic necessity for maintaining and improving standards of living throughout the world, the widespread use of fossil fuels may have impacted the planet in ways far more significant than first thought. In addition to the manageable impacts of mining and drilling for fossil fuels and discharging wastes from processing and refining operations, the greenhouse gases created by burning these fuels are regarded as a major contributor to the global warming threat. Global warming and large-scale climate change have implications for food chain disruption, flooding, and severe weather events.

The use of renewable energy sources in DHC systems with cogeneration can help reduce environmental damage and achieve sustainability.

Sustainable development requires not just that sustainable energy resources be used, but that the resources be used efficiently. The authors and others feel that exergy methods can be used to evaluate and improve efficiency, and thus to improve sustainability. Since energy can never be "lost," as it is conserved according to the first law of thermodynamics, while exergy can be lost due to internal irreversibilities, this suggests that exergy losses, which represent potential not used,

particularly from the use of nonrenewable energy forms, should be minimized when striving for sustainable development. The next section discusses the exergy aspects of thermal systems and presents an efficiency analysis for performance improvement.

Furthermore, some environmental effects associated with emissions and resource depletion can be expressed based on physical principles in terms of an exergy-based indicator. It may be possible to generalize this indicator to cover a comprehensive range of environmental effects, and research in line with that objective is ongoing.

Although this book discusses the benefits of using thermodynamic principles, especially exergy, to assess the sustainability and environmental impact of energy systems, this area of work is relatively new. Further research is needed to provide a better understanding of the potential role of exergy in such a comprehensive perspective. This includes the need for research to (1) better define the role of exergy in environmental impact and design, (2) identify how exergy can be better used as an indicator of potential environmental impact, and (3) develop holistic exergy-based methods that simultaneously account for technical, economic, environmental, and other factors.

10.5 Thermodynamic Analysis

The analysis of any thermal system is based on thermodynamics because it allows for performance quantification, comparison with other systems, and design optimization. Using the exergy method, through thermodynamic analysis one can identify where and how a preliminary design can be improved to obtain a better final design. If an existent system is analyzed, the expected outcome of the exergy method is represented by the identification and quantification of losses (or irreversibilities). Measures may often be taken thereafter for improving the system's performance. In what follows, the main approaches regarding thermodynamic analysis and design optimization of DES are presented, and illustrative numerical examples are given.

We now analyze the energy fluxes through the DES component by component. With the help of Fig. 10.6, the energy fluxes at the central source of a distributed energy system for cooling, heating, and power (CHP) can be inventoried. The general "black-box" model of the central CHP plant is represented in Fig. 10.6a. There, the primary energy flux $\dot{E}_s$ that enters the "black-box" is indicated. The primary energy could be the energy carried by a specific fuel (coal, natural gas, petroleum, biomass) or any other forms of thermal energy (e.g., solar, geothermal, nuclear) (Fig. 10.6a).

In the figure, the input thermal energy flux is converted into electrical power, cold, and heat in the CHP plant. Each of these conversions has a certain associated efficiency. Therefore, one can define the conversion efficiency for electrical power, heat, and cooling, respectively, as

$$\eta_e = \frac{\dot{W}}{\dot{E}_s};\ \eta_h = \frac{\dot{Q}_h}{\dot{E}_s};\ \eta_c = \frac{\dot{Q}_c}{\dot{E}_s}. \tag{10.1}$$

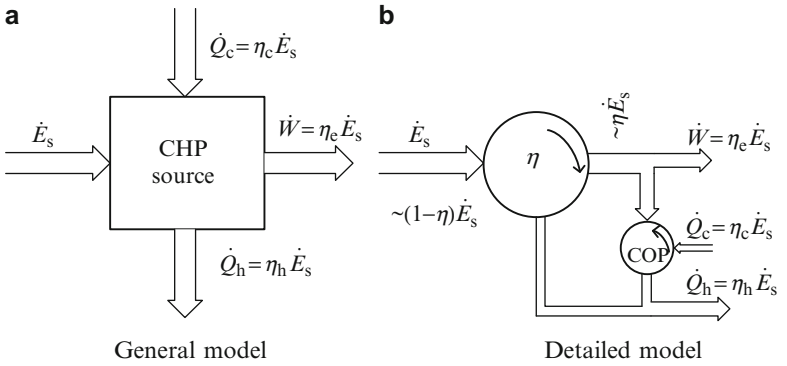

Fig. 10.6 Thermodynamic models of a cooling, heating, and power cogeneration system

The exergy efficiency counterparts of Eq. (10.1) is written noting the exergy of the primary energy flux $\dot{E}_s$ with $\dot{E}x_s$, and the temperature levels at which the heat and the cold are available with T_h and T_c, respectively. Thus, one has

$$\psi_e = \frac{\dot{W}}{\dot{E}x_s};\ \psi_h = \frac{\dot{Q}_h(1-(T_0/T_h))}{\dot{E}x_s};\ \psi_c = \frac{\dot{Q}_c(1-(T_0/T_c))}{\dot{E}x_s}, \tag{10.2}$$

where T_0 represents the environment temperature.

Figure 10.2b shows the main components of a typical CHP plant regardless of the primary fuel. The plant consists of two thermodynamic cycles. The first cycle converts with the efficiency η the primary energy flux $\dot{E}_s$ into electricity; this amounts to electrical power $\sim\eta\dot{E}_s$ as it is indicated in the figure. At the same time, the heat rejected by the cycle is $\sim(1-\eta)\dot{E}_s$. A part of the produced electrical energy is used to drive the compressor of a chiller having the role of producing cold water for the DHC system. One can design the chiller such that it discharges heat into the ambient air at the same temperature level as the power plant. Therefore, the heat ejected by the chiller $\dot{Q}_c(\mathrm{COP}+1)/\mathrm{COP}$ upgrades the heat ejected by the power plant $(1-\eta)\dot{E}_s$. Note that the chiller coefficient of performance is defined by "cold" delivered over work input $\mathrm{COP} = \dot{Q}_c/\dot{W}_c$.

A figure of merit f_s that quantifies the energy efficiency of the system can be introduced as the sum of the efficiencies for cooling, heating, and power generation. Note that the term f_s cannot signify energy efficiency because summation of heat and work does not have a clear physical sense, and it can have values even over unity. Similarly, the total exergy efficiency of the CHP system results as a summation of the particular components. Therefore,

$$\left.\begin{aligned} f_s &= \eta_e + \eta_h + \eta_c \\ \psi_s &= \psi_e + \psi_h + \psi_c \end{aligned}\right\}. \tag{10.3}$$

The energy balance over the heat distribution network, that is the second component of the DES, can be derived if one assimilates the network with two parallel pipes connecting the CHP side with the user's side, as illustrated in Fig. 10.7. The energy "introduced" into the distribution network is represented by the heat energy $\dot{Q}_{\mathrm{h}}$ and the pumping energy $\dot{W}_{\mathrm{p}}$. Some heat $\dot{Q}_{\mathrm{L}}$ is lost through the insulation. Analogously, some heat is gained through the insulation of cold distribution networks. On the user's side, the heat $\dot{Q}_{\mathrm{h,u}}$ is delivered (this is denoted with $\dot{Q}_{\mathrm{c,u}}$ for cooling).

The energy balance for the system shown in Fig. 10.7 is written as

$$\dot{Q}_{\mathrm{h}} + \dot{W}_{\mathrm{p}} = \dot{Q}_{\mathrm{h,u}} + \dot{Q}_{\mathrm{L}}, \tag{10.4}$$

where $\dot{Q}_{\mathrm{h,u}}$ represents the useful heat delivered to the users. The amount of energy consumed to convey this heat to the user's site includes the input heat energy at the central source side $\dot{Q}_{\mathrm{h}}$ and the pumping energy $\dot{W}_{\mathrm{p}}$. Therefore, the energy efficiency of the network can be defined by

$$\eta_{\mathrm{L,h}} = \frac{\dot{Q}_{\mathrm{h,u}}}{\dot{Q}_{\mathrm{h}} + \dot{W}_{\mathrm{p}}} = \frac{\dot{Q}_{\mathrm{h,u}}}{\dot{E}_{\mathrm{s}}(\eta_{\mathrm{h}} + f_{\mathrm{p}})} = \frac{1}{1 + \dot{Q}_{\mathrm{L}}/\dot{Q}_{\mathrm{h,u}}}, \tag{10.5}$$

where the second part of Eq. (10.5) was obtained by noting $f_{\mathrm{p}} = \dot{W}_{\mathrm{p}}/\dot{E}_{\mathrm{S}}$, and the third part by making use of Eq. (10.4).

For writing the exergy balance, it is useful to assume that the distribution network operates at an equivalent temperature $\overline{T}_{\mathrm{L}}$. Following this assumption, note that in the model represented in Fig. 10.7 the heat flux $\dot{Q}_{\mathrm{h}} = \dot{m}\,(h_1 - h_4)$ is "discharged" into the distribution line at the $\overline{T}_{\mathrm{L}}$. As a consequence, the corresponding entropy variation in the fluid stream is $\Delta\dot{S}_{\mathrm{h}} = \dot{m}\,(s_1 - s_4)$. It therefore results that the generated entropy in this process is $\Delta\dot{S}_{1-4} = \dot{Q}_{\mathrm{h}}/\overline{T}_{\mathrm{L}}$; from this the last relationship yields the definition of the equivalent line temperature:

$$\overline{T}_{\mathrm{L}} = \frac{h_1 - h_4}{s_1 - s_4}. \tag{10.6}$$

We now observe that according to the model proposed in Fig. 10.3, the useful heat $\dot{Q}_{\mathrm{h,u}}$ is delivered to be used at the network equivalent temperature $\overline{T}_{\mathrm{L}}$. Therefore, the exergy flux at the user's side is given by $\dot{Q}_{\mathrm{h,u}}(1 - (T_0/\overline{T}_{\mathrm{L}}))$ and then, accordingly, the network exergy efficiency is

$$\psi_{\mathrm{L,h}} = \frac{\dot{Q}_{\mathrm{h,u}}(1 - T_0/\overline{T}_{\mathrm{L}})}{\dot{Q}_{\mathrm{h}}(1 - T_0/\overline{T}_{\mathrm{L}}) + \dot{W}_{\mathrm{p}}}. \tag{10.7}$$

In an analogous manner with Eqs. (10.6) and (10.7), it is possible to define energy $\eta_{\mathrm{L,c}}$ and exergy $\psi_{\mathrm{L,c}}$ efficiency for a cold distribution line.

The last component of the DES system is the user. At the user's place, the delivered heat (or cold) serves some purpose (e.g., heating or cooling a space). For space heating purposes, it is customary to use radiators (static heating corps), while for space cooling fan coils are used. In a real situation, a part of the thermal energy that is delivered to the user's building is lost (e.g., heat losses through insulation or through the building envelope). Therefore, one can define energy and exergy efficiency at the user's side. In a general case, the heat received by the user from the distribution line can be used both for space heating and service water heating. If one denotes $\overline{T}^{\mathrm{s}}_{\mathrm{h,u}}$ the average temperature at the user's radiators or fan-coil units, and with $\overline{T}^{\mathrm{w}}_{\mathrm{h,u}}$ the temperature at the water heater, then the corresponding energy and exergy efficiencies are

$$\begin{aligned}\eta_{\mathrm{h,u}} &= \frac{\dot{Q}^{\mathrm{s}}_{\mathrm{h,u}} + \dot{Q}^{\mathrm{w}}_{\mathrm{h,u}}}{\dot{Q}_{\mathrm{h,u}}} \text{ and } \psi_{\mathrm{h,u}} \\ &= \frac{\dot{Q}^{\mathrm{s}}_{\mathrm{h,u}}\left(1 - \left(T_0 \Big/ \overline{T}^{\mathrm{s}}_{\mathrm{h,u}}\right)\right) + \dot{Q}^{\mathrm{w}}_{\mathrm{h,u}}\left(1 - \left(T_0 \Big/ \overline{T}^{\mathrm{w}}_{\mathrm{h,u}}\right)\right)}{\dot{Q}_{\mathrm{h,u}}\left(1 - \left(T_0 / \overline{T}_{\mathrm{L}}\right)\right)}, \text{ respectively.}\end{aligned} \tag{10.8}$$

In analogy, the energy and exergy efficiencies of the space cooling equipment are written as

$$\eta_{\mathrm{c,u}} = \frac{\dot{Q}^{\mathrm{s}}_{\mathrm{c,u}}}{\dot{Q}_{\mathrm{c,u}}} \text{ and } \psi_{\mathrm{c,u}} = \frac{\dot{Q}^{\mathrm{s}}_{\mathrm{c,u}}\left(1 - \left(T_0 \Big/ \overline{T}^{\mathrm{s}}_{\mathrm{c,u}}\right)\right)}{\dot{Q}_{\mathrm{c,u}}\left(1 - \left(T_0 / \overline{T}_{\mathrm{L}}\right)\right)}, \text{ respectively,} \tag{10.9}$$

where in Eqs. (10.7) to (10.9) the equivalent line temperature refers to either heat or cold distribution situations.

In general, during the cold season hot water is distributed, while during the hot season chilled water or ice slurry is distributed. However, a system may be useful that distributes simultaneously heating and cooling (e.g., for some industrial parks); in this case, two distribution networks must exist. Therefore, one may define the figure of merit quantifying the energy efficiency of DES in three forms, namely, for district heating (index DH), district cooling (index DC), and district heating and cooling (index DHC), respectively:

$$\left.\begin{aligned} f_{\mathrm{DH}} &= \eta_{\mathrm{e}} + \eta_{\mathrm{h}}\eta_{\mathrm{L,h}}\eta_{\mathrm{h,u}} \\ f_{\mathrm{DC}} &= \eta_{\mathrm{e}} + \eta_{\mathrm{c}}\eta_{\mathrm{L,c}}\eta_{\mathrm{c,u}} \\ f_{\mathrm{DHC}} &= \eta_{\mathrm{e}} + \eta_{\mathrm{h}}\eta_{\mathrm{L,h}}\eta_{\mathrm{h,u}} + \eta_{\mathrm{c}}\eta_{\mathrm{L,c}}\eta_{\mathrm{c,u}} \end{aligned}\right\}. \tag{10.10}$$

An analogue set of equations can be written for the exergy efficiency counterparts, in which the symbol f is replaced by ψ. Note that for calculating the electrical efficiency η_{e} the pumping power $\dot{W}_{\mathrm{p}}$ must be extracted from the power generated by the CHP plant in order to obtain the correct results.

Example 10.1

A geothermal district heating system (GDHS) is devised to provide heat to a large university campus. The harvested thermal energy is available at 90°C and at a flow rate of 120 kg/s. At the central station, a shell and tube heat exchanger that recirculates the water through the geothermal loop is placed while the reinjected water temperature is 75°C. The power consumption to run the pumps is 75 kW. The heat exchanger loses 2% of thermal energy through insulation. In the distribution network, hot water is circulated at a rate of 60 kg/s with the associated electricity consumption of 25 kW and has the maximum temperature of 85°C. The hot fluid reaches the user's location with 70°C temperature and leaves it with 60°C. An amount of 5% from the delivered heat at the user's location is lost due to imperfect insulation. Calculate the energy and exergy efficiency of the system and its components.

Solution. The rate of thermal energy harvested is $\dot{Q}_{\text{harv}} = \dot{m}c_{\text{p}}\Delta T = 120 \times 4$, $185 \times 15 = 7.5\,\text{MW}$.

The total electrical energy needed to drive the pumps of the system (wells $\dot{W}_{\text{w}}$ plus distribution network $\dot{W}_{\text{L}}$) is $\dot{W} = \dot{W}_{\text{w}} + W_{\text{L}} = 75 + 25 = 100\,\text{kW}$.

Therefore, the primary energy of the system is the sum $\dot{E}_{\text{s}} = \dot{Q}_{\text{harv}} + \dot{W} = 7.6\,\text{MW}$.

The heat loss through insulation is $2\% \times \dot{Q}_{\text{harv}} = 0.15\,\text{MW}$ and the thermal energy delivered to the network is $\dot{Q}_{\text{h}} = (100 - 2)\% \times \dot{Q}_{\text{harv}} = 7.35\,\text{MW}$.

The thermal energy efficiency of the source is therefore

$$\eta_{\text{h}} = \frac{\dot{Q}_{\text{h}}}{\dot{E}_{\text{S}}} = \frac{7.35}{7.60} = 0.98.$$

The exergy associated with the harvested heat having the average temperature $\overline{T}_{\text{harv}} = (75 + 90)/2 = 82.5°\text{C} = 355.65\,\text{K}$ is $\dot{E}x = (1 - (T_0/\overline{T}_{\text{harv}}))\dot{Q}_{\text{harv}} = (1 - (300/355.65))7.5 = 1.17\,\text{MW}$ and the exergy of the primary energy flux is $\dot{E}x_{\text{s}} = \dot{E}x + \dot{W} = 1.17 + 0.1 = 1.27\,\text{MW}$.

The exergy associated with the heat delivered by the geothermal facility to the distribution line is

$$\dot{E}x_{\text{h}} = \left(1 - \left(\frac{T_0}{\overline{T}_{\text{harv}}}\right)\right)\dot{Q}_{\text{h}} = \left(1 - \left(\frac{300}{355.65}\right)\right)7.35 = 1.15\,\text{MW}.$$

The exergy efficiency of the heat generating source of the district geothermal energy system is therefore $\psi_{\text{h}} = \dot{E}x_{\text{h}}/\dot{E}x_{\text{S}} = 0.98/1.15 = 0.85$.

The heat delivered to all users is calculated based on total flow rate, and the temperature difference at the user's location $\dot{Q}_{\text{h,u}} = \dot{m}c_{\text{p}}\Delta T = 60 \times 4185 \times (70 - 60) = 2.511\,\text{MW}$.

Therefore, the energy efficiency of the distribution network is $\eta_{\text{L,h}} = \dot{Q}_{\text{h,u}}/(Q_{\text{h}} + \dot{W}_{\text{L}}) = 2.511/(7.35 + 0.025) = 0.34$.

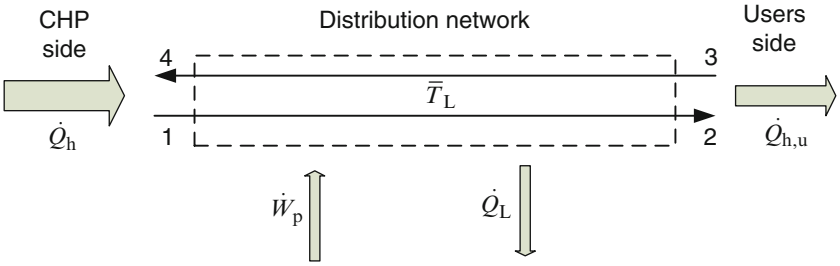

Fig. 10.7 Thermodynamic model of the distribution network

The temperature difference in the secondary circuit of the geothermal heat exchangers is calculated with $\Delta T_h = \dot{Q}_h/(\dot{m}c_p) = 7.35 \times 10^6/(60 \times 4,185) = 29.3°C$.

The temperature of water in the return pipes, with reference to Fig. 10.7, is $T_4 = T_1 - \Delta T_h = 85 - 29.3 = 55.7°C = 328.85\,K$; therefore the average temperature is $\overline{T} = (T_1 + T_4)/2 = 70.85°C = 344\,K$. One can estimate the density of water to be $\rho = 1{,}000\ kg/m^3$ and the enthalpy variation $\Delta h_{1-4} = h_1 - h_4 = c_p \Delta T_h = 4,185 \times 29.3 = 122.62\,kJ/kg$. Derived from the first and second law combination, the entropy variation on the lines is $\Delta s_{1-4} = s_1 - s_4 = (\Delta h_{1-4} - \Delta P_{1-4}/\rho)\ /\overline{T} = (122.62 - 3 \times 10^5/1{,}000/1{,}000)/344 = 0.357\,kJ/kg\,K$.

The equivalent line temperature results in $\overline{T}_L = (h_1 - h_4)/(s_1 - s_4) = 122.62/0.357 = 343.47\,K$.

The exergy associated with the heat and work received by the distribution network is $\dot{E}x_h = (1 - (T_0/\overline{T}_L))\dot{Q}_h + \dot{W}_L = (1 - (300/343.47)) \times 7.35 + 0.025 = 0.955\,MW$.

The exergy associated with the heat delivered by the distribution network is $\dot{E}x_{h,u} = (1 - (T_0/\overline{T}_L))\dot{Q}_{h,u} = (1 - (300/343.47)) \times 2.511 = 0.318\,MW$.

The exergy efficiency of the distribution line is therefore $\psi_{L,h} = \dot{E}x_{h,u}/\dot{E}x_h = 0.318/0.955 = 0.33$.

The heat delivered to the users for space and water heating is $\dot{Q}^s_{h,u} + \dot{Q}^w_{h,u} = (1 - 0.05)\dot{Q}_{h,u} = 0.95 \times 2.511 = 2.38\,MW$ and the efficiency of the user's installation is $\eta_{h,u} = \dfrac{\dot{Q}^s_{h,u} + \dot{Q}^w_{h,u}}{\dot{Q}_{h,u}} = \dfrac{2.38}{2.511} = 0.95$. Assuming the average temperature of water at the user's location $\overline{T}_{h,u} = (60 + 70)/2 = 65°C = 338.15\,K$ to be the same for both space and water heating, one obtains the exergy efficiency of the users' facility:

$$\psi_{h,u} = \frac{\left(\dot{Q}^s_{h,u} + \dot{Q}^w_{h,u}\right)\left(1 - \left(T_0/\overline{T}_{h,u}\right)\right)}{\dot{E}x_{h,u}} = \frac{2.38 \times (1 - (300/338.15))}{0.318} = 0.84.$$

The results of the system energy and exergy efficiencies are summarized below:

Location	η	ψ
Central plant	0.98	0.85
Network	0.34	0.33
User's site	0.95	0.84
Total	0.32	0.23

One may observe that most of the losses are network losses; therefore, to increase the system efficiency one has to provide better insulation of the hot water distribution lines.

10.6 Economic Analysis

Economic analysis of distributed energy systems is of fundamental importance because the thermodynamic analysis provides the information needed for the LCC. The LCC is useful for two reasons: (1) it allows for a feasibility study of the distributed energy system, by comparing it with other technical alternatives (e.g., using electrically driven heat pumps at distributed locations), and (2) it represents the objective function for optimization of the design (i.e., one has to minimize the LCC to obtain a better design). The fundamentals of economic analysis of sustainable energy systems are discussed in Chapter 18. In this section, the theory is applied for the particular case of DHC systems for deriving the LCC. The peculiarity of DESs is that they reduce or eliminate the costs associated with installation, maintenance, administration, repair, and operation of the on-site equipment for cooling and heating. These factors reflect in the relative weight of the components of LCC. Moreover, the costs associated with auxiliary equipment for local generation and the building space occupied by them can reach 20% to 30% of the total operating costs (ASHRAE 1999).

As a preliminary step for calculating the LCC of any system, the analysis period must be established. The analysis period is taken to be equal to the life-time of the system. In some cases, it may be useful to determine the total cost for the period of the loan that finances the investment. In order to determine the lifetime of a distributed energy system, the service lifetimes of the main system components must be estimated. In Table 10.3, typical service lifetimes of important components of DES are given. Table 10.4 gives the average costs of electrically driven residential heat pumps that are normally used in nondistributed energy systems (for the purpose of comparison with a nondistributed system).

The analysis results tabulated in Tables 10.3 and 10.4 show that most elements of the DES (e.g., piping/network, hot water or steam radiant heater, base-mounted pumps, and absorption chillers) have service lifetimes of over 20 years. In contrast, equipment specific to local heat and cold generation (heat pumps, electric radiant heaters, gas or electric water heaters) has a service lifetime of 10 to 15 years.

The LCC of the system can be expressed in constant currency, which is the present worth of money, and includes several components. Chapter 18 discusses the main parameters of economic analysis that we now apply to the DES case:

(a) *Capital cost*. The capital cost may be considered the most important component of the DES LCC because it is the highest. The capital cost is that part of the LCC that does not depend on the system outcome and it pays for the

Table 10.3 Service life-time of typical components of DES

Component	Lifetime (years)
Air-to-air heat pump (or air conditioner)	15
Water-cooled heat pump	15
Electric radiant heater	10
Hot water or steam radiant heater	25
Fan-coil unit	20
Piping/network	30
Thermal insulation	20
Fired boiler	25
Electric boiler	15
Gas or electric water heater	13
Electrically driven chiller	20
Absorption chiller	23
Pumps (base mounted)	20
Reciprocating engines	20
Steam turbines	30

Data from ASHRAE (1999)

Table 10.4 Specific costs of various components of district energy systems

Category	Specific cost	Remarks
Cooling plant	425–740, US$/kW	Includes building infrastructure, chillers, heat exchangers, pumping station, piping, controls
Heating plant	150–230, US$/kW	Includes boilers, building infrastructure, stacks, pumps, piping, controls
Gas turbine power plant	400–600, $/kW	Power plant + afferent infrastructure
Coal fires power plant with scrubber	1,300, $/kW	
Hydropower	1,500, $/kW	
Geothermal power plant	1,900, $/kW	
Solar thermal power plant	3,100, $/kW	
Solar photovoltaic	4,800, $/kW	
Advanced nuclear power plant	2,100, $/kW	
Fuel cell power plant	4,500, $/kW	
Distribution network	1,600–4,100, $/m	Direct buried chilled water pipes
	2,400–4,900, $/m	Direct buried preinsulated heating pipes
	1,600–3,200, $/m	Inaccessible tunnels
	11,500–49,000, $/m	Walkable tunnels
Radiators or fan-coil units	50–150, $/kW	

Data from ASHRAE (2008) and JcMiras (2008)

initial investment. The main component of the capital cost is the infrastructure, namely, the pipe network and associated work related to installing the pipelines. Depending on the economic scenario, it is possible to include in the capital cost of DES the equipment at the users' locations (e.g., fan coils, hot water radiant heaters, etc.). In any case, the lifetime cost is reimbursed by the substantial contribution of the users, who pay for the service. However,

an initial large investment is needed to install the DES system, and this investment comes from government subsidies, bonds, endowments, and loans. Therefore, the capital cost is divided into the down payment and the cost of loan. The main components of the capital costs are as follows:

- Cost of the pipes
- Cost of the insulation
- Cost of work associated with infrastructure development/installation
- Cost of the pumping station
- Heat exchanger costs (condensers, boilers, etc.)
- Cost of the chiller
- Testing and balancing
- Other costs

If one denotes the capital cost with C, and f_{Loan} is the fraction of the capital cost that is paid through a loan ($f_{\text{Loan}} < 1$), then the down payment is

$$C_{\text{Down}} = (1 - f_{\text{Loan}})C. \tag{10.11}$$

The rest of the capital C_{Loan} comes from the loan with the interest rate r_{Loan}, while the business represented by DES has to assume an associated discount rate r. For an accurate analysis, both rates must account for the average inflation I, that is, they are "converted" in the form of real rates with $r_{\text{real}} = (r_{\text{market}} - i)/(1 + i)$. The cost of the loan at rate r_{Loan} is discounted by the business rate r; therefore, with the notations for capital recovery factor introduced in Chapter 18, the cost of the loan is

$$C_{\text{Loan}} = \frac{(A/P, r_{\text{Loan}}, N_{\text{Loan}})}{(A/P, r, N_{\text{Loan}})} f_{\text{Loan}} C, \tag{10.12}$$

where N_{L} is the number of years for the loan repayment, which in general differs from the system's lifetime N. Now, the principal of the loan repayments is tax deductible; if one notes t the incremental income tax, then the total deduction for the loan cost is (according to Chapter 18)

$$D_{\text{Loan}} = t\left[\frac{(A/P, r_{\text{Loan}}, N_{\text{Loan}})}{(A/P, r, N_{\text{Loan}})} - \frac{(A/P, r_{\text{Loan}}, N_{\text{Loan}}) - r_{\text{Loan}}}{(1 + r_{\text{Loan}})(A/P, r'_{\text{Loan}}, N_{\text{Loan}})}\right] f_{\text{Loan}} C, \tag{10.13}$$

where $r'_{\text{Loan}} = (r - r_{\text{Loan}})/(1 + r_{\text{Loan}})$ is the effective loan interest rate.

Therefore, the present worth of the invested capital C_{P} is given by Eqs. (10.11) to (10.13), namely, the sum of the down payment and the loan cost from which the tax deduction is extracted:

$$C_{\text{P}} = C_{\text{Down}} + C_{\text{Loan}} - D_{\text{Loan}}. \tag{10.14}$$

(b) *Depreciation*. A DES is always viewed as a large investment of which the value depreciates over time. The depreciation is proportional with the capital cost and the incremental income tax. Depending on the law in place, the depreciation can be assessed based on "straight line" schedule,

$$D_{\text{Dep}} = t(P/A, r, N)\, C/N, \tag{10.15}$$

or based on the so-called sum-of-the-yearly-figures schedule

$$D_{\text{Dep}} = 2t[N - (P/A, r, N)]/[rN(N + 1)], \tag{10.16}$$

where one takes the years of depreciation equal to the lifetime of the system.

(c) *Tax credit*. Distributed energy systems are eligible for receiving tax credits because by improving efficiency they can contribute to CO_2 emission reduction, promoting clean energy alternatives and achieving a better environment. If one denotes with t_{cred} the tax credit, then the capital investment is reduced proportionally with the invested capital, namely,

$$D_{\text{cred}} = t_{\text{cred}} C. \tag{10.17}$$

(d) *Salvage value*. At the end of the lifetime, the system has a depreciated value known in economics as the *salvage value*. The salvage value for a DES can be thought of as the sum of worth of all equipment (pump, chillers, heat pumps, piping, etc.) that can be valorized by the end of the service time (or lifetime) of the system. The salvage value is proportional to the invested capital and is given by

$$D_{\text{salv}} = f_{\text{salv}}(P/F, r, N)C(1 - t_{\text{salv}}), \tag{10.18}$$

where r is the real discount rate of the business and t_{salv} is the tax perceived by the government when the salvage is valorized; this tax can be different from the income tax; the factor $(1 - t_{\text{salv}})$ represents the amount of money that the business earns after tax, on amount that discounts the capital investment.

(e) *Tax on property*. At least a part f_{prop} of the invested capital C is present in the form of property. For example, the business that owns and/or administers the DES is the proprietary owner of the equipment and the buildings that accommodate the business; the distribution lines may be in the property of the district. In this case, a tax on the property (denoted here with t_{prop}) has to be paid by the business; this tax is deductible. Therefore, the cost of the property tax is

$$C_{\text{prop}} = f_{\text{prop}} C t_{\text{prop}}(1 - t). \tag{10.19}$$

(f) *Other periodic and random costs*. Among the periodic costs paid during the lifetime of the DES are the costs related to operation, maintenance, and insurance.

These costs may be modeled as a fraction of the capital costs of the system, and are tax deductible:

$$C_{\text{omi}} = f_{\text{omi}} C(P/A, r, N)(1-t). \tag{10.20}$$

Furthermore, during the lifetime of the system some singular or random replacement, disposal, or overhauls may occur. Let us assume that $f_{\text{r,k}}C$ is a random cost occurring in the year k. In this condition, the present worth of this cost, including the tax deduction is

$$C_{\text{r,k}} = f_{\text{r,k}} C(P/F, r, k)(1-t). \tag{10.21}$$

(g) *Cost of operating energy*. The link between economic and thermodynamic analysis is made through the cost of the operating energy. Assuming the energy production occurs at a uniform rate, the cost paid on fuel for the first year (or first analysis period, e.g., the first month) is

$$C_{\text{oe},1} = \frac{Q_1}{\text{HHV}_\text{f}\eta} p_1, \tag{10.22}$$

where Q_1 is the amount of heat or cold energy (e.g., in MJ) delivered by the system in each period, HHV_f represents the heating value of the fuel (e.g., in MJ/kg), η is the energy efficiency, and p_1 is the fuel price for the first period per unit of mass (e.g., in \$/kg). An alternative to Eq. (10.22) that is more comprehensive is proposed here based on exergy efficiency:

$$C_{\text{oe},1} = \frac{E_1}{e_\text{f}\psi} p_1, \tag{10.23}$$

where E_1 is the amount of heat or cold energy (e.g., in MJ) delivered by the system in each period, e_f represents the specific exergy of the fuel (e.g., in MJ/kg), and ψ is the exergy efficiency. The cost introduced by Eq. (10.23) can be called the *cost of operating exergy*.

The total cost of the operating energy, or exergy, whichever one adopts for analysis, is discounted with the fuel effective rate that accounts for the real discount rate r of the business and the real fuel price escalation rate r_e; this is $r'_\text{e} = (r - r_\text{e})/(1 + r_\text{e})$. Moreover, the cost of fuel is tax deductible, thus

$$C_{\text{oe}} = C_{\text{oe},1} \frac{1-t}{(A/P, r'_\text{e}, N)}. \tag{10.24}$$

Summing up Eqs. (10.14) to (10.21) and (10.24), which includes the adopted alternative for the cost of the operating energy or exergy, one obtains the LCC as

$$C_{\text{Life}} = C_\text{P} + C_{\text{prop}} + C_{\text{omi}} + \sum C_{\text{r,k}} + C_{\text{oe}} - (D_{\text{Dep}} + D_{\text{cred}} + D_{\text{salv}}). \tag{10.25}$$

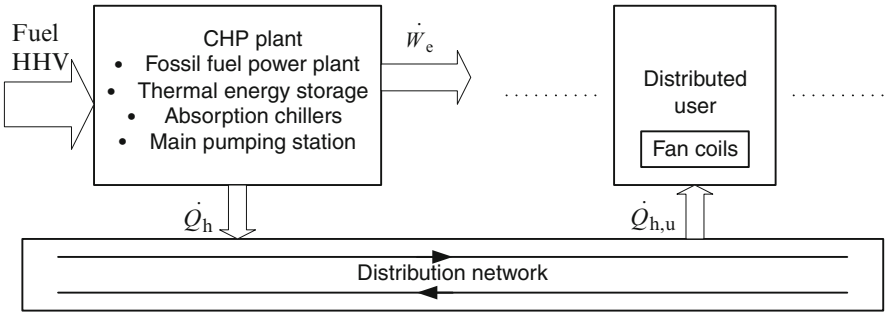

Fig. 10.8 A DES as studied in Example 10.2

Example 10.2

We now estimate the LCC of the DES illustrated in Fig. 10.8 that uses a CHP coal plant with scrubber and serves a territory of 1 km^2, using following input data:

- peak electrical power $P_e = 100$ MW$_e$
- load factor $l = 68\%$
- efficiency hth $= 30\%$ (thermodynamic cycle), hme $= 95\%$ (mechanical to electrical)
- price of coal for the first year $c_{coal} = \$2.5$/GJ and $r_e = 10\%$ price escalation rate
- heat losses at power plant $f = 5\%$
- absorption chillers' coefficient of performance (COP) $= 0.8$
- specific cost of cooling plant $c_c = \$500$/kW
- Cost of distribution line $c_L = \$4{,}000$/m
- Length of pipe network $L = 5$ km
- Fan coil unit cost $c_{fc} = \$100$/kW
- Number of years of service $N = 20$
- Inflation rate $i = 1\%$, market discount rate $r_m = 6\%$, market loan rate $r_{mL} = 5\%$
- Other financial parameters $f_{Loan} = 0.8$, $t = 40\%$, $t_{cred} = 2\%$, $f_{salv} = 10\%$, $t_{salv} = 20\%$, $f_{prop} = 50\%$, $t_{prop} = 25\%$, and $f_{omi} = 1\%$.

Solution

- Annual electrical energy production is $E_{ey} = 365\,\text{days} \times 100 \times 10^6\,\text{MW} \times 24 \times 3{,}600\,(\text{s/day}) \times 0.68 = 2.1\,\text{PJ}$.
- The power plant's coal-to-electrical efficiency is $\eta_{PP} = \eta_{th}\eta_{me} = 0.3 \times 0.95 = 0.285$.
- Annual consumption of primary energy (coal) is $E_{py} = E_{ey}/\eta_{PP} = 2.1\,\text{PJ}/0.285 = 7.4\,\text{PJ}$.
- Annual cost of coal fuel $c_{fy} = E_{py} \times c_{coal} = 7.5 \times 10^6\,\text{GJ} \times 2.5\$/\text{GJ} = \$18.75\,\text{million/year}$.
- Amount of annual rejected heat $Q_{0y} = (1 - \eta_{PP})E_{py} = 5.29\,\text{PJ}$.
- Recovered heat with 5% losses $Q_{hy} = (1 - \phi)Q_{0y} = 0.95 \times 5.29 = 5.02\,\text{PJ}$.
- Cold energy production, yearly $Q_{cy} = COP\,Q_{hy}(3\text{ summer months}/\text{year's }12\text{ months}) = 0.975\,\text{PJ}$.

- Needed total chiller capacity $\dot{Q}_c = (Q_{cy}/4 \text{ summer months}) \times (1/(30 \times 24 \times 3,600)) = 94\,\text{MW}$.
- Cost of chillers $C_c = \$500/\text{kW} \times 94,000\,\text{kW} = \$47$ million.
- Number of fan-coil units at the users' locations (assumed in average 1 kW/unit) $Q_{fcy} = 1,000\,\text{W} \times (365 \times 24 \times 3,600)\text{s} = 32\,\text{GJ}; N_{fc} = Q_{hy}/Q_{fcy} = 30,500$ units.
- Cost of the distribution network $C_L = L \times c_L = 5,000 \times 4,000 = \$20$ million.
- Cost of the coal fired power plant $C_P = c_P \times P_e = \$1,300,000/\text{MW} \times 100\,\text{MW} = \$130$ million.
- Total fan coil cost $C_{fc} = c_{fc} \times N_{fc} \times \dot{Q}_{fc} = \$3$ million.
- Capital cost as follows:
  - Central plant $C_{cp} = C_P + C_c = 130 + 47 = \$177$ million.
  - Distribution lines $C_L = \$20$ million.
  - User's $C_{fc} = \$3$ million.
  - Total CHP cost $C = \$200$ million.
- Down payment $C_{Down} = (1 - 0.8) \times 200 = \$40$ million.
- Cost of the loan $C_{Loan} = ((A/P, 0.04, 20)/(A/P, 0.05, 20)) \times 0.8 \times 200 = \$\ 147$ million.
- Tax deduction on loan using Eq. (10.13) and $r'_{Loan} = (5 - 4)/(1 + 4) = 0.2$, therefore $D_{Loan}0.4[(0.0736/0.08) - (0.0736 - 0.04)/(1.04 \times 0.2053)] \times 0.8 \times 200 = \$48.8$ million.
- Therefore, the total worth of capital is $C_P = C_{Down} + C_{Loan} - D_{Loan} = 40 + 147 - 48.8 = \$138.2$ million.
- The depreciation of the capital, assumed linear – Eq. (10.15) $D_{Dep} = 0.4 \times (P/A, 0.05, 20) \times 200/20 = \$50$ million.
- Tax credit $D_{Cred} = t_{cred} \times C = 0.02 \times 200 = \$4$ million.
- Salvage worth $D_{salv} = 0.1 \times (P/F, 0.05, 20) \times 200 \times (1 - 0.2) = \$42.4$million.
- Tax paid on property $C_{prop} = 0.5 \times 200 \times 0.25 \times (1 - 0.4) = \$15$ million.
- Cost of operation, maintenance, and insurance $C_{omi} = 0.01 \times 200 \times (P/A, 0.05, 20)(1 - 0.4) = \$5$ million.
- Total cost of fuel (coal) $C_{oe} = \$18.75\,\text{million} \times [(1 - 0.4)/(A/P, r'_e, 20)] = \$377.5$ million, where $r'_e = ((5 - 10)/101) = -0.045$ is the real discount rate for coal price.
- The LCC is

$$\begin{aligned} C_{Life} &= C_P + C_{prop} + C_{omi} + C_{oe} - (D_{Dep} + D_{cred} + D_{salv}) \\ &= 138.2 + 15 + 15 + 377.5 - (50 + 4 + 42.4) \\ &= 168.2 + 377.5 - 96.4 = \$450\,\text{million}. \end{aligned}$$

10.7 Case Studies

Here we present an efficiency analysis, accounting for both energy and exergy considerations, for two case studies: (1) a cogeneration-based DES, and (2) a geothermal district heating system (GDHS).

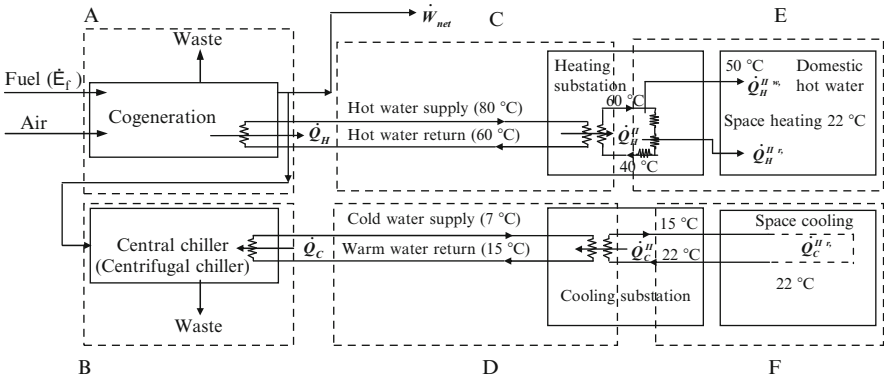

Fig. 10.9 Simplified diagram of the cogeneration-based DES at Edmonton Power [modified from Rosen et al. (2004, 2005)]

10.7.1 Case Study I

The system considered in this case study is a major cogeneration-based DHC project in downtown Edmonton, Alberta, Canada (Edmonton Power 1991, MacRae 1992), having (1) an initial supply capacity of 230 MW (thermal) for heating and 100 MW (thermal) for cooling; (2) the capacity to displace about 15 MW of electrical power used for electric chillers through DC; and (3) the potential to increase the efficiency of the Rossdale power plant that would cogenerate to provide the steam for the DHC system from about 30% to 70%. The design includes the potential to expand the supply capacity for heating to about 400 MW (thermal). The design incorporated central chillers and a DC network. Screw chillers were to be used originally and absorption chillers in the future. Central chillers are often favored because (1) the seasonal efficiency of the chillers can increase due to the ability to operate at peak efficiency more often in a central large plant, and (2) lower chiller condenser temperatures (e.g., 20°C) can be used if cooling water from the environment was available to the central plant, relative to the condenser temperatures of approximately 35°C needed for air-cooled building chillers. These two effects can lead to large central chillers having almost double the efficiencies of distributed small chillers.

There are two main stages in this case study as taken from Rosen et al. (2004, 2005). First, the design for cogeneration-based DHC (Edmonton Power 1991, MacRae 1992) is evaluated thermodynamically. Then, the design is modified by replacing the electric centrifugal chillers with heat-driven absorption chillers (first single- and then double-effect types) and reevaluated.

The cogeneration-based DES considered here (Fig. 10.9) includes a cogeneration plant for heat and electricity, and a central electric chiller that produces a chilled fluid. Hot water was produced to satisfy all heating requirements of the users, at a temperature and pressure of 120°C and 2 bar, respectively. The heat was

Table 10.5 Monthly heating and cooling load breakdown (in %) in the design area of Edmonton, Alberta

	Period 1 (winter)								Period 2 (summer)					
	Oct.	Nov.	Dec.	Jan.	Feb.	Mar.	Apr.	Total	May	June	July	Aug.	Sep.	Total
Heating	6.90	12.73	16.83	18.67	14.05	12.95	7.34	89.46	2.39	1.56	1.34	1.92	3.33	10.54
Cooling	0.0	0.0	0.0	0.0	0.0	0.0	0.0	0.0	10.62	22.06	32.00	26.80	8.52	100

Data from Edmonton Power (1991)

distributed to the users via heat exchangers, DH grids, and user's heat exchanger substations. A portion of the cogenerated electricity was used to drive a central centrifugal chiller, and the remaining electricity was used for other purposes (e.g., export, driving other electrical devices, etc.). The central chiller produces cold water at 7°C, which is distributed to users via DC grids. The system, which uses electric chillers, is divided into six subsections within three categories. On the left are production processes, including cogeneration of electricity and heat (A) and chilling (B). In the middle are district-energy transport processes, including DH (C) and DC (D). On the right are end-user processes, including user heating (E) and user cooling (F).

For the cogeneration-based DES using absorption chillers, the design was modified by replacing the electric chiller with single-effect absorption chillers. Hot water was produced at 120°C and 2 bar to satisfy all heating requirements of the users and to drive the central absorption chillers. A small portion of the cogenerated electricity was used to drive the absorption solution and refrigeration pumps, and the remaining electricity was used for purposes other than space cooling. This cogeneration-based DES was then further modified by replacing the electric centrifugal chillers with double-effect absorption chillers. The system was similar to the cogeneration-based DES using single-effect absorption chillers, except that higher quality heat (170°C and 8 bar) was produced to drive the double-effect absorption chillers.

For the analysis, the year was divided into two seasonal periods (see Table 10.5). Period 1 (October to April) has an environmental temperature of 0°C and was considered to be a winter period with only a heating demand. Period 2 (May to September) has an environmental temperature of 30°C and was considered to be a summer period with a cooling demand and a small heating demand for hot water heating. The small variations in plant efficiency that occur with changes in environmental temperature are ignored here.

The overall energy efficiency of the proposed cogeneration plant was 85%, the electrical efficiency (i.e., the efficiency of producing electricity via cogeneration) was 25%, and the heat production efficiency was 60%. Also, the total heating requirement of the buildings in the design region was $\dot{Q}_{\mathrm{H}} = 1,040\,\mathrm{GWh/year}$ for space and hot water heating, and the cooling requirement was $\dot{Q}_{\mathrm{C}} = 202\,\mathrm{GWh/year}$ for space cooling. The total fuel energy input rate can be evaluated for the cogeneration plant using electric chillers as $\dot{E}_{\mathrm{f}} = 1{,}040/0.6 = 1733\,\mathrm{GWh/year}$. Since 33 GWh/year of this cooling was provided through free cooling, the cooling requirement of the chilling plant was 169 GWh/year (Edmonton Power 1991).

The COP of the single-effect absorption chiller used here was taken to be 0.67, a typical representative value. Therefore, the annual heat required to drive the single-effect absorption machine was $\dot{Q}_{\text{gen}} = 169/0.67 = 252$ GWh/year. The total fuel energy input rate of the cogeneration plant can thus be evaluated as $\dot{E}_{\text{f}} = (1{,}040 + 252)/0.6 = 2{,}153$ GWh/year [for details, see Rosen et al. (2004, 2005)].

As mentioned above, steam was required at higher temperatures and pressures to drive the double-effect absorption chillers, and more electricity was curtailed as a higher quality of heat or more heat was produced. The overall energy efficiency of the proposed cogeneration plant was unchanged (85%) in period 2. Only the electrical and heat efficiencies are changed due to more heat being produced in this period, when the absorption chiller was in operation. Thus, the electrical efficiency (i.e., the efficiency of producing electricity via cogeneration) was 25% and 21% in periods 1 and 2, respectively, and the heat production efficiency was 60% and 64% in periods 1 and 2, respectively. The COP of the double-effect absorption chiller used here was taken to be 1.2, a typical representative value. Therefore, the annual heat required to drive the double-effect absorption machine was $\dot{Q}_{\text{gen}} = 169/1.2 = 141$ GWh/year. The total fuel energy input rate to the cogeneration plant can be evaluated as the sum of the fuel energy input rate to the plant in two periods. Thus, $\dot{E}_{\text{f}} = 1{,}942$ GWh/year [for details, see Rosen et al. (2004, 2005)].

The average supply and return temperatures, respectively, were taken as 80°C and 60°C for DH, and 7°C and 15°C for DC. The supply and return temperatures, respectively, were taken as 60°C and 40°C for the user heating substation, and 15°C and 22°C for the user cooling substation. Furthermore, the users' room temperature was considered constant throughout the year at 22°C for DH; the equivalent temperature was 70°C for the supply system and 50°C for the user substation, while for DC the equivalent temperature was 11°C for the supply system and 19°C for the user substation.

Table 10.6 shows that 89.46% and 10.54% of the total annual heat loads occur in periods 1 and 2, respectively. Since there was assumed to be no space heating demand in period 2, the 10.54% quantity was taken to be the heat needs for water heating (which was assumed constant throughout the year). Table 10.6 also presents the space cooling breakdown in period 2. Annual energy transfer rates for the cogeneration-based DES are shown in Table 10.7, with details distinguished where appropriate for the three chiller options considered. The data in Table 10.7 are used to calculate exergy efficiencies for the systems for each period and for the year.

Edmonton Power had annual free cooling of 33 GWh/year; the cooling requirement of the chilling plant was 169 GWh/year. The COP of the centrifugal chiller in the design was 4.5. Thus, the annual electricity supply rate to the chiller was $\dot{W}_{\text{ch}} = 169/4.5 = 38$ GWh/year. For the chilling operation, including free cooling and electrical cooling, COP = (169 + 33)/38 = 5.32. The net electricity output ($\dot{W}_{\text{net}}$) of the combined cogeneration/chiller portion of the system was $433 - 38 = 395$ GWh/year, where the electrical generation rate of the cogeneration plant was 433 GWh/year. Similarly, for the chilling operation, including free cooling and

Table 10.6 Annual energy transfer rates (in GWh/year) for the cogeneration-based DHC system in Edmonton, Alberta

Type of energy	Period 1, $T_0 = 0°C$	Period 2, $T_0 = 30°C$
District heating, $\dot{Q}_H$	$0.8946 \times 1{,}040 = 930$	$0.1054 \times 1{,}040 = 110$
Water heating, $\dot{Q}_H^{u,w}$	(22 GWh/yr/mo.) × 7 mo. = 154	$0.1054 \times 1{,}040 = 110$ (or 22 GWh/yr/mo.)
Space heating, $\dot{Q}_H^{u,s}$	$930 - 154 = 776$	0
Space cooling, $\dot{Q}_C$	0	$1.00 \times 202 = 202$
Electric chiller case		
Total electricity, $\dot{W}$	$0.8946 \times 433 = 388$	$0.1054 \times 433 = 45.6$
Input energy, $\dot{E}_f$	$0.8946 \times 1{,}733 = 1{,}551$	$0.1054 \times 1{,}733 = 183$
Single-effect absorption chiller case		
Heat to drive absorption chiller, $\dot{Q}_{gen}$	0	$1.00 \times 252 = 252$
Total electricity, $\dot{W}$	$0.8946 \times 433 = 388$	$25/60(110 + 252) = 151$
Input energy, $\dot{E}_f$	$0.8946 \times 1{,}733 = 1{,}551$	$(110 + 252)/0.6 = 603$
Double-effect absorption chiller case		
Heat to drive absorption chiller, $\dot{Q}_{gen}$	0	$1.00 \times 141 = 141$
Total electricity, $\dot{W}$	$0.8946 \times 433 = 388$	$(21/64)(110 + 141) = 82$
Input energy, $\dot{E}_f$	$0.8946 \times 1{,}733 = 1{,}551$	$(110 + 141)/0.64 = 391$

Data from Rosen et al. (2004, 2005)

single-effect absorption cooling, COP = 202/252 = 0.80, and for double-effect absorption cooling COP = 202/141 = 1.43. It should be noted that the work required to drive the solution and refrigeration pumps was very small relative to the heat input to the absorption chiller (often less than 0.1%); this work was thus ignored here.

Table 10.7 lists the energy and exergy efficiencies evaluated for the individual subsystems, several subsystems comprising selected combinations of the individual subsystems, and the overall system for cogeneration-based DES using electric chillers, single-effect absorption chillers, and double-effect absorption chillers. Overall energy efficiencies are seen to vary, for the three system alternatives considered, from 83% to 94%, respectively, and exergy efficiencies from 28% to 29%, respectively. Table 10.7 demonstrates that energy efficiencies do not provide meaningful and comparable results relative to exergy efficiencies when the energy products are in different forms. For example, the energy efficiency of the overall process using electric chillers is 94%, which could lead one to believe that the system is very efficient. The exergy efficiency of the overall process, however, is 28%, indicating that the process is far from ideal thermodynamically. The exergy efficiency is much lower than energy efficiency because the heat is being produced at a temperature (120°C) much higher than the temperatures actually needed (22°C for space heating and 40°C for hot-water heating). The low-exergy efficiency of the chillers is largely responsible for the low-exergy efficiency of the overall process. The exergy-based efficiencies in Table 10.7 are generally lower than the energy-based ones because the energy efficiencies utilize energy quantities that are in different forms, while the exergy efficiencies provide more meaningful and useful results by evaluating the performance and behavior of the systems using electrical

Table 10.7 System and subsystem efficiencies for the cogeneration-based DES, for several types of chillers

System	Efficiency (%)					
	Energy (η)			Exergy (ψ)		
	Centrifugal chiller	1-stage absorption chiller	2-stage absorption chiller	Centrifugal chiller	1-stage absorption chiller	2-stage absorption chiller
Individual subsystems						
Cogeneration	85	85	85	37	37	37
Chilling	450[a]	67[a]	120[a]	36	23	30
District heating (DH)	100	100	100	74	74	74
District cooling (DC)	100	100	100	58	58	58
User heating (UH)	100	100	100	54	54	54
User cooling (UC)	100	100	100	69	69	69
Combination subsystems[b]						
Cogeneration + chilling	94	83	88	35	35	35
District energy (DE)	100	100	100	73	73	73
User energy (UE)	100	100	100	53	53	53
Cogeneration + DH	85	85	85	34	35	34
Cogeneration + DH + UH	85	85	85	30	31	31
Chilling + DC	532[a]	80[a]	143[a]	21	14	18
Chilling + DC + UC	532[a]	80[a]	143[a]	14	9	12
DH + UH	100	100	100	40	40	40
DC + UC	100	100	100	41	41	41
Cogeneration + Chilling + DE	94	83	88	32	32	32
DE + UE	100	100	100	40	40	40
Overall process	94	83	88	28	29	29

Data from Rosen et al. (2004, 2005)

[a]These are coefficient of performance (COP) values when divided by 100

[b]DE = DH + DC and UE = UH + UC

equivalents for all energy forms. The results for cogeneration-based DESs using absorption chillers (single-effect and double-effect absorption chillers) and electric chillers are, in general, found to be similar [for details, see Rosen et al. (2004, 2005)].

For cogeneration-based district energy, where electricity, heating, and cooling are simultaneously produced, exergy analysis provides important insights into the performance and efficiency for an overall system and its separate components. This thermodynamic analysis technique provides more meaningful efficiencies than energy analysis, and pinpoints the locations and causes of inefficiencies more accurately. The present results indicate that the complex array of energy forms involved in cogeneration-based DESs make them difficult to assess and compare thermodynamically without exergy analysis. This difficulty is primarily attributable to the different nature and quality of the three product energy forms: electricity, heat, and cool. The results are expected to aid designers of such systems in development and optimization activities, and in selecting the proper type of system for different applications and situations.

10.7.2 Case Study II

Geothermal district heating has been given increasing attention in many countries during the last decade, and many successful geothermal district heating projects have been reported. In order for district heating to become a serious alternative to existing or future individual heating and/or cooling systems, it must provide significant benefits to both the community in which it is operated and the consumers who purchase energy from the system. Further, it must provide major societal benefits if federal, state, or local governments are to offer the financial and/or institutional support that are required for successful development (Bloomquist and Nimmons 2000).

The case here is the Izmir-Balcova GDHS, which is one example of a high-temperature district heating application in Turkey. The Balcova region is about 7 km from the center of the Izmir province, located in the western part of Turkey, and is endowed with considerably rich geothermal resources. The Izmir-Balcova geothermal field (IBGF) covers a total area of about 3.5 km^2 with an average thickness of the aquifer horizon of 150 m. In the district heating system investigated here, there are two systems, namely, the Izmir-Balcova GDHS and the Izmir-Narlidere GDHS. The design heating capacity of the Izmir-Balcova GDHS is equivalent to 7,500 residences. The Izmir-Narlidere GDHS was designed for 1,500-residence equivalence but has a sufficient infrastructure to allow a capacity growth to 5,000-residence equivalence. The outdoor and indoor design temperatures for the two systems are 0° and 22°C, respectively. Figure 10.10 is a schematic of the IBGF, where the Izmir-Balcova GDHS, the Izmir-Narlidere GDHS, and hotels and official buildings heated by geothermal energy are included. The Izmir-Balcova GDHS consists mainly of three cycles: (1) energy production cycle (geothermal well loop and geothermal heating center loop), (2) energy distribution

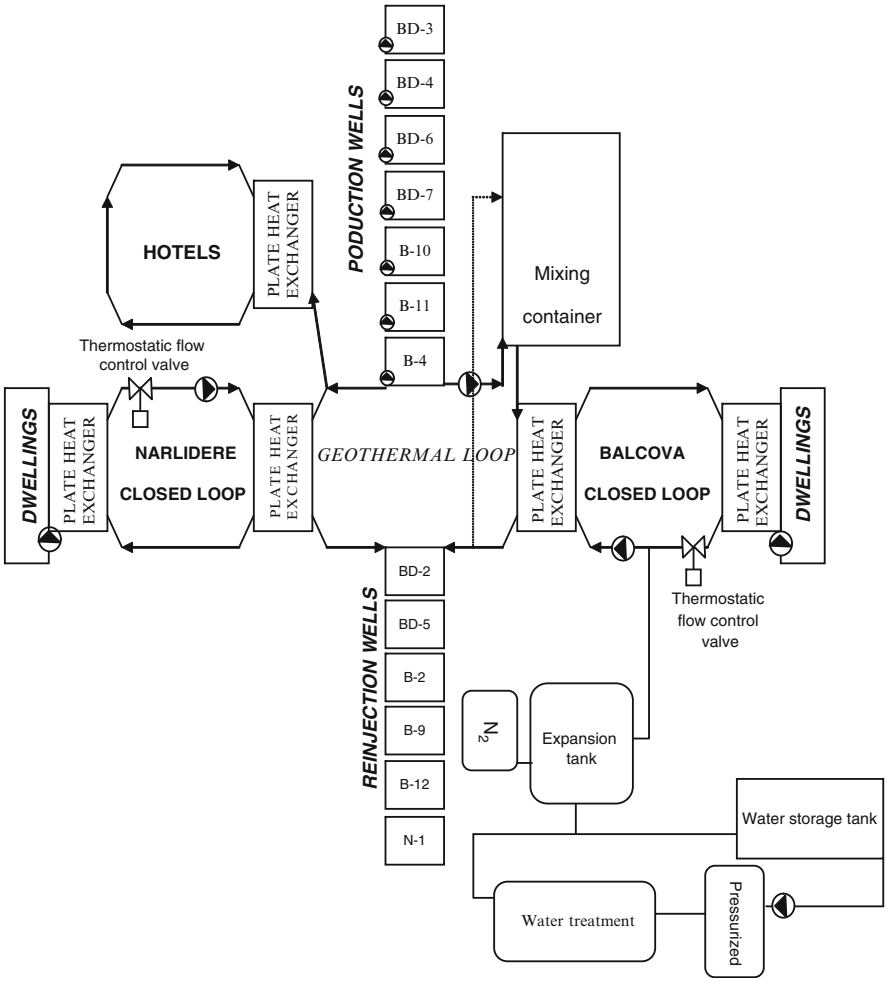

Fig. 10.10 A schematic of the Izmir-Balcova-Narlidere geothermal district heating system [modified from Ozgener et al. (2004)]

cycle (district heating distribution network), and (3) energy consumption cycle (building substations). As of the end of 2001, there are 14 wells ranging in depth from 48 to 1,100 m in the IBGF. Of these, seven and six wells are production and reinjection wells, respectively, while one well is out of operation. The well head temperatures of the production wells vary from 95° to 140°C, with an average value of 118°C, while the volumetric flow rates of the wells range from 30 to 150 m^3/h. Geothermal fluid, collected from the seven production wells at an average well head temperature of 118°C, is pumped to a mixing chamber, where it is mixed with the reinjection fluid at an average temperature of 60° to 62°C, cooling the mixture to 98° to 99°C. This geothermal fluid is then sent to two primary plate-type heat

exchangers and is cooled to about 60° to 62°C, as its heat is transferred to the secondary fluid. The geothermal fluid whose heat is taken at the geothermal center is reinjected into the reinjection wells, while the secondary fluid (clean hot water) is transferred to the heating circulation water of the building by the heat exchangers of the substations. The average conversion temperatures obtained during the operation of the Izmir-Balcova GDHS are, on average, 80°/57°C for the district heating distribution network and 65°/45°C for the building circuit. By using the control valves for flow rate and temperature at the building substations, the needed amount of water is sent to each housing unit and the heat balance of the system is achieved (Hepbasli and Canakci 2003).

In the following, we give the main relations for mass, energy, and exergy flows along with the energy and exergy efficiencies for the Izmir-Balcova GDHS [for further information, see Ozgener et al. (2004)].

The mass balance equation is written as follows:

$$\sum_{i=1}^{n} \dot{m}_{\mathrm{w,tot}} - \dot{m}_{\mathrm{r}} - \dot{m}_{\mathrm{d}} = 0, \tag{10.26}$$

where $\dot{m}_{\mathrm{w,tot}}$ is the total mass flow rate at the well head, $\dot{m}_{\mathrm{r}}$ is the flow rate of the reinjected thermal water, and $\dot{m}_{\mathrm{d}}$ is the mass flow rate of the natural direct discharge.

We define the energy efficiency as follows:

$$\eta_{\mathrm{system}} = \frac{\dot{E}_{\mathrm{useful,HE}}}{\dot{E}_{\mathrm{brine}}}. \tag{10.27}$$

The geothermal brine exergy input from the production field is calculated as follows:

$$\dot{E}x_{\mathrm{brine}} = \dot{m}_{\mathrm{w}}[(h_{\mathrm{brine}} - h_0) - T_0(s_{\mathrm{brine}} - s_0)]. \tag{10.28}$$

The exergy destructions in the heat exchanger, pump, and the system itself are calculated using:

$$\dot{E}x_{\mathrm{dest,HE}} = Ex_{\mathrm{in}} - \dot{E}x_{\mathrm{out}} = \dot{E}x_{\mathrm{dest}}, \tag{10.29}$$

$$\dot{E}x_{\mathrm{dest,pump}} = \dot{W}_{\mathrm{pump}} - (\dot{E}x_{\mathrm{out}} - \dot{E}x_{\mathrm{in}}), \text{ and} \tag{10.30}$$

$$\dot{E}x_{\mathrm{dest,system}} = \sum \dot{E}x_{\mathrm{dest,HE}} + \sum \dot{E}x_{\mathrm{dest,pump}}. \tag{10.31}$$

Here, we define the exergy efficiency as follows:

$$\psi_{\mathrm{sys}} = \frac{x_{\mathrm{useful,HE}}}{\dot{E}x_{\mathrm{brine}}} = 1 - \frac{x_{\mathrm{dest,sys}} + \dot{E}x_{\mathrm{reinjected}} + x_{\mathrm{naturally\ discharged}}}{\dot{E}x_{\mathrm{brine}}}. \tag{10.32}$$

In this study, the reference environment was taken to be the state of the environment at which the temperature and the atmospheric pressure are 13.1°C and 102.325 kPa, respectively, which were the values measured at the time when the GDHS data were obtained. For analysis purposes, the actual data were taken from the Balcova GDHS on January 1, 2003, and the respective thermodynamic properties were obtained based upon these data. It is important to note that the number of the wells in operation in the IBGF may vary depending on the heating days and operating strategy.

Using Eq. (10.26), the total geothermal reinjection fluid mass flow rate is 111.02 kg/s at an average temperature of 66.1°C and the production well total mass flow rate is 148.19 kg/s, and the natural direct discharge of the system is then calculated to be 37.17 kg/s on January 1, 2003. This clearly indicates that in the Balcova GDHS, there is a significant amount of hot water lost through leaks in the hot water distribution network.

The exergy destructions in the system particularly occurs in terms of the exergy of the fluid lost in the pumps, the heat exchanger losses, the exergy of the thermal water (geothermal fluid) reinjected, and the natural direct discharge of the system, accounting for 3.06%, 7.24%, 22.66%, and 24.1%, respectively, of the total exergy input to the Balcova GDHS. Both energy and exergy efficiencies of the overall Balcova GDHS are investigated for system performance analysis and improvement and are determined to be 37.60% and 42.94%, respectively.

In the GDHSs, the temperature difference between the geothermal resource and the supply temperature of the district heating distribution network plays a key role in terms of exergy loss. In fact, the district heating supply temperature is determined after the optimization calculation. In this calculation, it should be taken into account that increasing the supply temperature results in a reduction of investment costs for the distribution system and the electrical energy required for pumping stations, while it causes an increase of heat losses in the distribution network. Unless there is a specific reason, the district heating supply temperature should be higher in order to increase the exergy efficiency of the heat exchangers and hence the entire system. Besides this, in the design and operating condition of the primary heat exchangers, a temperature approach of about 3°C is desired. On the other hand, dropping the district heating supply temperature increases the amount of building heating equipment to be oversized. Oversizing does not mean only cost, but also more exergy production due to unnecessarily inflated pumping, pipe frictions, etc. In this regard, there is an optimum district flow rate and the minimum possible exergy loss (mainly due to pumping), of which determination is planned as future work to be conducted.

10.8 Concluding Remarks

This chapter presented some historical background on DESs along with cogeneration and GDHS applications, and discussed some technical, economic (especially life-cycle costing), environmental, and sustainability issues and performance

evaluations tools in terms of energy and exergy analyses for such DHC systems. Case studies have also been presented to highlight the importance of exergy use as a potential tool for system analysis, design, and improvement. The benefits have been demonstrated by using the principles of thermodynamics via exergy to evaluate energy systems and technologies as well as environmental impact. Thus, thermodynamic principles, particularly the concepts encompassing exergy, can be seen to have a significant role to play in evaluating energy and environmental technologies.

Nomenclature

$\dot{E}x$	Exergy rate, W
f	Figure of merit
h	Specific enthalpy, kJ/kg
$\dot{m}$	Mass flow rate, kg/s
$\dot{Q}$	Heat rate, W
s	Specific entropy, kJ/kg K
T	Temperature, K
$\dot{W}$	Work rate, W

Greek Letters

η	Energy efficiency
ψ	Exergy efficiency

Subscripts

0	Reference state
c	Cooling
c,u	Useful cooling
DC	District cooling
DH	District heating
DHC	District heating and cooling
e	Electrical
h	Heating
h,u	Useful heat
L	Line
S	Source or system

Superscripts

$\overline{()}$ Average value
s Radiators and fan coils
w Water heater

References

ASHRAE 1999. Handbook of Heating, Ventilating and Air Conditioning Applications, SI eds., American Society of HVAC&R, Atlanta, GA.

ASHRAE 2008. Handbook of Applications, SI eds., Chapter 11: Owning and operating costs. American Society of HVAC&R, Atlanta, GA.

Bel O., Hunyadi-Kiss I., Zweig S., Lallemand A. 1996. Thermal study of an ice slurry used as refrigerant in a cooling loop. International Institute of Refrigeration (IIR) Commissions B1, B2, E1, E2-Aarhus (Denmark).

Bloomquist R., Nimmons J. 2000. Geothermal district energy. In: Course on Heating with Geothermal Energy: Conventional and New Schemes, Lienau P.J. eds., WGC-2000 Short Courses, 8-10 June, Kazuno, Japan, pp. 85–136.

ConEd 2008. Consolidated Edison Company of New York. http://www.coned.com/ (accessed on November 6, 2008).

Dincer I. 2000. Renewable energy and sustainable development: a crucial review. *Renewable and Sustainable Energy Reviews* 4:157–175.

Dincer I. 2002. The role of exergy in energy policy making. *Energy Policy* 30:137–149.

Dincer I., Hepbasli A. 2010. District energy systems. In: Encyclopedia of Energy Engineering Technology, Capehart B.L. ed., Chapter 43. CRC Press, New York.

Dincer I., Rosen M.A. 2005. Thermodynamic aspects of renewables and sustainable development. *Renewable and Sustainable Energy Reviews* 9:169–189.

Edmonton Power 1991. City of Edmonton District Energy Development Phase. Section 2: Engineering Report.

Enwave 2005. History of District Energy. Internet source http://www.enwave.com/enwave/view.asp?/solutions/heating/history (accessed on November 6, 2008).

Hepbasli A, Canakci C. 2003. Geothermal district heating applications in Turkey: a case study of Izmir–Balcova. *Energy Conversion and Management* 44:1285–1301.

IEA 2004. Implementing agreement on district heating and cooling including the integration of CHP. Strategy Document. International Energy Agency, Paris.

JcMiras 2008. Estimated Capital Cost of Power Generating Plant Technologies. Internet source http://www.jcmiras.net/surge/p130.htm (accessed on November 7, 2008).

Karlsson T. 1982. Geothermal district heating the Iceland experience. UNU Geothermal training Programme. Iceland, Report 1982–4.

MacRae K.M. 1992. Realizing the Benefits of Community Integrated Energy Systems. Canadian Energy Research Institute, Calgary, Alberta.

National Academy of Sciences 1985. District Heating and Cooling in the United States: Prospects and Issues. Committee on District Heating and Cooling, National Research Council.

Ozgener L., Hepbasli A., Dincer I. 2004. Thermo-mechanical exergy analysis of Balcova geothermal district heating system in Izmir, Turkey. *ASME Journal of Energy Resources Technology* 126:293–301.

Rosen M.A., Le M.N., Dincer I. 2004. Thermodynamic assessment of an integrated system for cogeneration and district heating and cooling. *International Journal of Exergy* 1:94–110.

Rosen M.A., Le M.N., Dincer I. 2005. Efficiency analysis of a cogeneration and district energy system. *Applied Thermal Engineering* 25:147–159.
Skagestad B., Mildenstein P. 2002. District heating and cooling connection handbook. International Energy Agency.
Strickland C., Nyboer J. 2002. Cogeneration Potential in Canada–Phase II. Report for Natural Resources Canada.
UNEP 2005. Cogeneration, Energy Technology Fact Sheet, Division of Technology, Industry and Economics-Energy and Ozone Action Unit. Internet source http://www.uneptie.org/energy (accessed at November 6, 2008).

Study Questions/Problems

10.1 Define district energy systems and explain their benefit.
10.2 List some technical characteristics of district energy systems.
10.3 Explain the benefit of cogeneration with respect to power-only generation.
10.4 Consider the general system from Fig. 10.3. Make reasonable assumptions regarding the efficiency of each unit and then determine the efficiency of the overall system.
10.5 Describe how district energy systems benefit the environment.
10.6 Describe the role of district energy systems in sustainable development.
10.7 A GDHS provides heat from the harvested thermal energy that is available at 80°C and a flow rate of 200 kg/s. At the central station, the heat exchanger that recirculates the water through the geothermal loop is placed while the reinjected water temperature is 50°C. The power consumption to run the pumps is 150 kW. The heat exchanger loses 1% of thermal energy through insulation. In the distribution network, hot water is circulated at a rate of 80 kg/s with the associated electricity consumption of 35 kW and has the maximum temperature of 70°C. The hot fluid reaches the user's location with 65°C temperature and leaves it with 55°C. An amount of 7% of the delivered heat at the user's location is lost due to imperfect insulation. Calculate the energy and exergy efficiency of the system and its components.
10.8 Define the life-cycle cost in the context of distributed energy systems.
10.9 List and explain the main cost components of a distributed energy system.
10.10 What represents the capital cost and how it can be estimated?
10.11 Define "depreciation" and explain its calculation.
10.12 Define the "cost of operating energy" and explain its calculation.
10.13 Estimate the life-cycle cost of the district energy system illustrated in Fig. 10.8 that used a CHP coal plant with a scrubber and a served a territory of 2 km^2, for the following input data: peak electrical power $P_e = 200\ MW_e$; load factor $l = 75\%$; efficiency 25% (power cycle), 90% (mechanical to electrical); price of coal for the first year $c_{coal} = \$3.0/GJ$ and $r_e = 10\%$ price escalation rate; heat losses at power plant $f = 5\%$; absorption chillers' COP = 0.6; specific cost of cooling plant $c_c = \$600/kW$; cost of distribution line $c_L = \$4{,}100/m$; length of pipe network $L = 10$ km; fan coil unit

cost $c_{fc} = \$110/kW$; number of years of service $N = 30$; inflation rate $i = 1\%$, market discount rate $r_m = 6\%$, market loan rate $r_{mL} = 5\%$; other financial parameters $f_{Loan} = 0.8$, $t = 40\%$, $t_{cred} = 2\%$, $f_{salv} = 10\%$, $t_{salv} = 20\%$, $f_{prop} = 50\%$, $t_{prop} = 25\%$, $f_{omi} = 1\%$.

10.14 In order to assess the feasibility of the district energy system presented in Example 10.2, compare its life-cycle cost to a system that uses local heating and cooling through vapor compression heat pumps. Each heat pump unit has the capacity of 1 kW for both the cooling and the heating mode. The cost of a heat pump/air condition unit is \$800/kW. To make the two systems equivalent, the number of heat pump units is the same as the number of fan coils, that is 30,500 units. In the local heat pump case, there is no need of a heat and cold distribution network, therefore the capital investment is lower; however, the electricity/fuel consumption is larger.

10.15 Using the cost analysis presented in the text, perform a parametric study to determine the optimum diameter of a pipe if the flow rate and the length are imposed.

10.16 Conduct a parametric study to determine the optimal thickness of the insulation of a buried pipe.

Chapter 11
Energy Storage

11.1 Introduction

Any energy system includes at least two essential entities, namely, energy generators and energy consumers. Each of these elements has its associated characteristics, and it is not necessary that at all times the energy generated is the same as the energy consumed. Moreover, it is not necessary that the energy is generated at the same location where it is consumed. The *transmission grid* is a medium that interconnects the energy generators with the energy consumers. The multitude of generators connected to a transmission grid is called the "energy supply side," while the multitude of consumers is called the "energy demand side." Figure 11.1 shows the general layout of an energy system that apart from the energy supply and demand sides also includes the distribution grid and the energy storage facilities. The energy storage fills the temporal gap between energy supply and energy demand.

One notes the abstract level at which Fig. 11.1 describes the energy system; there is no reference to the nature of energy that flows through it. Moreover, the energy that is generated, transmitted, stored, and consumed can be of different forms because the energy grid can include energy converters that transform one form of energy into another. Furthermore, the energy at the supply side can occur in a variety of forms, and the grid can connect to a multitude of generators as well as to a multitude of consumers and to various kinds of energy storage systems.

Generally speaking, the energy supply cannot be constant because the energy reserves depend on the season, the time of day, and climacteric conditions. Think of solar energy: the sun is available only 8 to 10 h/day to produce useful heat, chemicals, and electricity. The storage of solar energy is critically important for matching the energy supply and demand profiles. In fact, storage is critically important for any intermittent source of energy. Figure 11.2 is a conceptual diagram of solar heating and powering of a house. On the roof, one mounts a thermal solar panel that heats water. The hot water is stored in a tank and used throughout the whole day. In parallel with this system, photovoltaic arrays are mounted that generate electrical energy. The panels are coupled to a local grid system that stores the electricity in batteries and makes it available to serve the electrical power needs

İ. Dinçer and C. Zamfirescu, *Sustainable Energy Systems and Applications*,
DOI 10.1007/978-0-387-95861-3_11, © Springer Science+Business Media, LLC 2011

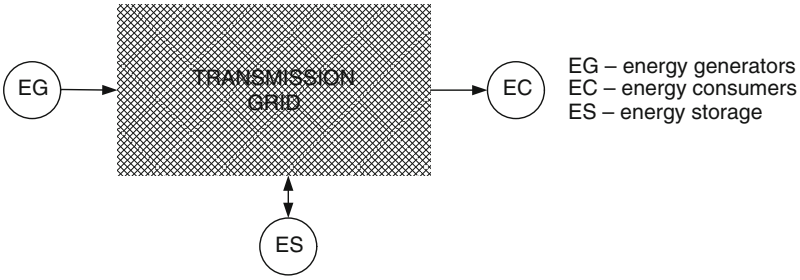

Fig. 11.1 The general layout of an energy system

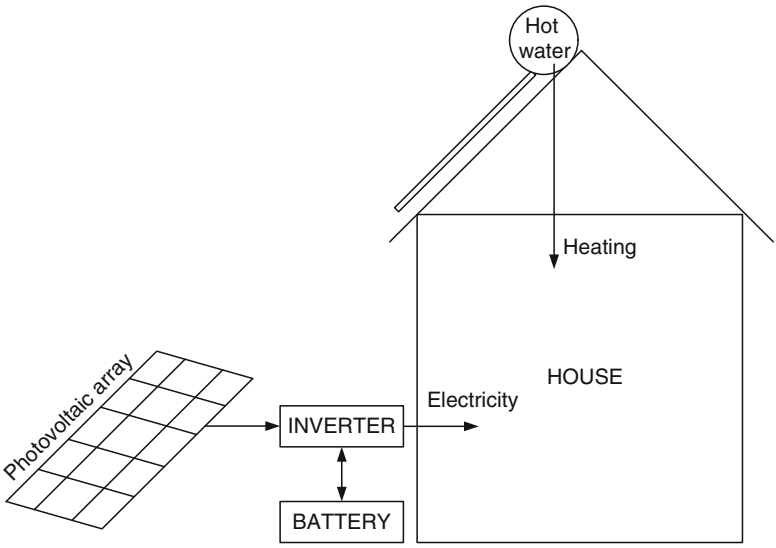

Fig. 11.2 Solar power and heating of a house

of the house for the whole day. The two systems that work in parallel represent a particular case of the general concept presented in Fig. 11.1. The generated, stored, and consumed energy is in the form of heat for one of the systems, and in the form of electricity for another one. The heat is stored as thermal energy (in hot water); however, the electricity is stored in the form of electrochemical energy in the battery. Many energy systems based on the general concept introduced in Fig. 11.1 can be contemplated, at smaller as well as larger scale.

For smaller scale, one can consider a laptop computer as an example. When an electrical supply plug is available, the user plugs the laptop in for charging the battery. At times when no electrical network is available, the computer is powered by the energy stored in the electrical battery. An example of a larger-scale energy system is the natural gas distribution system of a region. Such a system is represented schematically in Fig. 11.3. The natural gas in principle can be produced at a

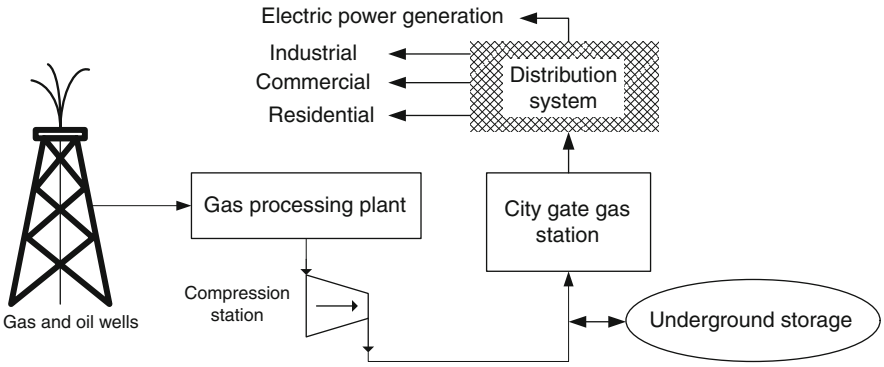

Fig. 11.3 General layout of a natural gas distribution system

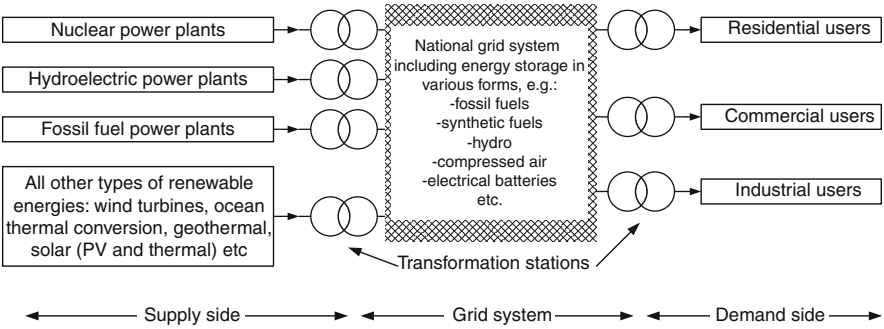

Fig. 11.4 General layout of a national electrical energy grid system

constant rate throughout the year, but natural gas consumption is higher in winter. Therefore, the supply is higher than the demand during the summer and the excess of supply is accumulated in large (in general underground) storage facilities. This is an example of seasonal storage. Note that the cost of natural gas is higher in winter because of the way in which the economy works. One can further observe that the natural gas network has at least the flow of following three entities: the material (i.e., the natural gas), the associated energy carried by the natural gas, and the economic currency associated with the natural gas business. It is therefore suggested that energy storage, in general, is a necessity and ultimately it can be viewed as a business.

The last example illustrated here represents the layout of a national electricity grid system. Such a system is shown in Fig. 11.4 and it consists of three major elements: the supply side, the demand side, and the grid system including energy transmission and storage facilities. The system is distributed over a territory and connects all possible sorts of electrical energy generation technologies placed at multiple locations. The grid receives, stores, and transmits the electrical energy. As suggested, the storage can be made in a multitude of ways including the seasonal

or shorter time storage of fossil fuels, production of synthetic fuels for storage, hydrostorage in accumulation lakes, and compressed air storage or electrical batteries stations; all of these are distributed over the territory. Also the system interacts with three categories of users at the demand side: residential, commercial, and industrial.

Thus, the energy storage systems are of major importance, as they play a key role in matching the energy supply and demand at all spatial scales and time frames (either for short term, that is, of seconds, or for long term, that is, seasonal). In what follows, we investigate the general thermodynamics of energy storage systems, and introduce and analyze the most relevant energy storage methods.

11.2 Energy Demand

Design of an energy storage system starts naturally with the analysis of the energy demand side (i.e., energy demand characteristics). In this respect, it is important to determine the variation of energy demand in time. This can be a periodic temporal profile, characterized by minima and maxima, and the profile can incorporate periods with no demand.

Depending on the scale of energy system (e.g., local, regional, and national) and on the peculiarity of the application (e.g., milk factory, building air conditioning, national electricity grid, etc.), the demand profile and its characteristics are different. Figure 11.5 illustrates three examples of daily demand profiles, namely, the

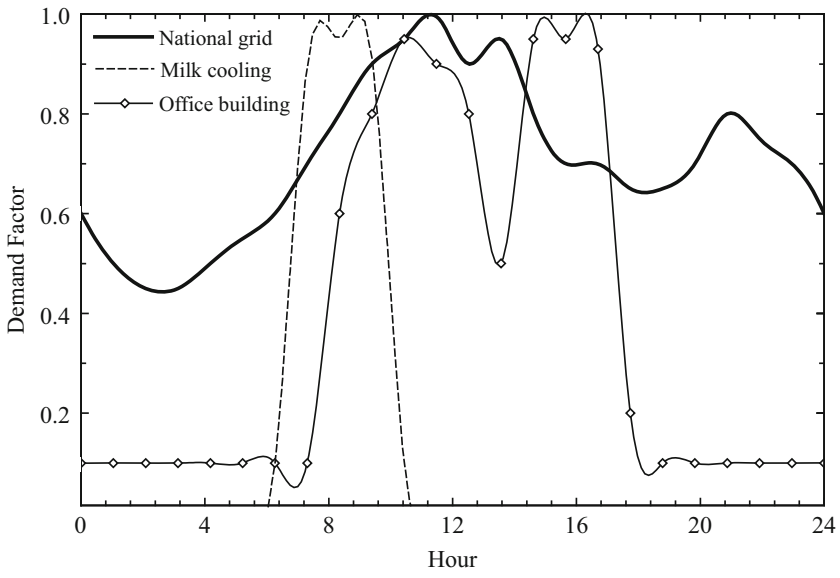

Fig. 11.5 Typical energy daily demand profiles for three cases

typical national grid system, electricity demand for a typical commercial building during a winter day, and the cooling demand of a milk factory for the pasteurization process; all three profiles are normalized with respect to their maxima. The ratio between the actual power demand and the maximum power demand is called demand factor, which according to the definition must be subunitary. The storage strategy and related devices must be adapted to the associated demand profiles. In analyzing the demand, statistical and forecast techniques can be applied to determine the maximum abatement of the demand from the typical situation, so that precautions can be taken.

Looking at Fig. 11.5, one can observe that the national grid demand has a demand factor of over 40% at all times (herewith, we denote the demand factor as the ratio between the actual demand and the maximum demand during the day). In contrast is the case of the milk factory, where the demand is nil for most of the day. Cooling is needed as part of the milk pasteurization process, which is performed immediately after the milk is collected by the milk factory. The processing occurs in the morning and is of short duration. Therefore, the pasteurization unit operates for very few hours per day. The third case illustrated in Fig. 11.5 lies in between the other two cases just discussed. This is the case of a commercial building that needs a base load of about 10% for its daily operation; however, there are two energy demand peeks during the day, one at the end of the morning and the other one in the afternoon.

11.3 Storable Energies

As mentioned in the introduction, the profile of the energy production system does not generally match the energy demand profile. Because of such a mismatch, energy storage is required. There are several known methods to store energy, and their main features are summarized in Table 11.1. Whatever the technology is, ultimately it has to process an energy form that is storable. The following kinds of energies are considered storable:

Table 11.1 Summary of energy storage technologies and their main characteristics

Device	Stored energy	η (%)
Flywheel	Kinetic	85–95
Pumped hydro storage	Potential	65–85
Compressed air	Thermomechanical	70–80
(Ultra/super) capacitors	Electrical charge	90–95
Electrical batteries	Electrochemical	85–95
Synthetic fuel storage (H_2, NH_3)	Chemical	~25
Biochemical storage	Chemical	~1
Thermochemical storage	Chemical	~30
Thermal energy storage (hot, cold)	Thermal	80–95

Note: η denotes energy efficiency, which is defined as the energy retrieved over energy transmitted to the storage device

Data from Dincer and Rosen (2002), Granowskii et al. (2008), Peters (2008), and Ter-Gazarian (1994)

- Mechanical energy in the forms of:
  - Kinetic energy—the energy of a mass that moves (rotates) fast
  - Potential energy—energy of a mass that is at high elevation in the gravitational field or is connected to an elastic spring displaced from its equilibrium position
- Thermomechanical energy—associated with the enthalpy of a gas (or fluid) that can be compressed (for storage) or expanded (for retrieval)
- Electrical charge energy—in the form of energy associated to the electrical field
- Electrochemical energy—stored in an electrolyte or in a reversible fuel cell (this is explained in the next section)
- Chemical energy that can be stored as follows:
  - By enthalpy of a reversible chemical reaction (thermochemical)
  - In a synthetic fuel that can be combusted (e.g., hydrogen)
  - In a biochemical "fuel" (e.g., glucose)
- Thermal energy—stored in the form of heat (either cold or hot)

In the next section, we discuss the energy storage technologies.

11.4 Energy Storage Methods

11.4.1 Electrical Charge Storage in Capacitors

Electrical charge can be stored in a device known as a capacitor. The simplest capacitor consists of two metallic plates between which a dielectric is interposed. A sketch of a simple capacitor is shown in Fig. 11.6a, while Fig. 11.6b illustrates the advanced ultracapacitor with high storage density. The electrical capacity of the plate capacitor can be defined by the following equation:

$$C = \frac{\varepsilon A}{d} = \frac{q}{V_c}, \tag{11.1}$$

where C is the electric capacity in farads, d is the distance between the parallel plates, A is the area of the plates, and ε is the electric permittivity of the material between the plates (the electric permittivity is a measure of how a material concentrates the lines of electric flux). On the right-hand side of the above equation, there is a second definition of the electrical capacity, which is more general, that is applied regardless of the geometrical configuration of the capacitor: the capacity is the electrical charge q (measured in coulombs) over the electrical potential V_c (measured in volts).

A capacitor can be charged or discharged in a electrical circuit that comprises the source (or the sink) of potential V, a combined electrical resistance R including the resistance of the transmission lines, the internal capacitor's resistance, and the internal source/sink resistance. For such a circuit the Kirchhoff law states

$$V_c = V - i(t)R, \tag{11.2}$$

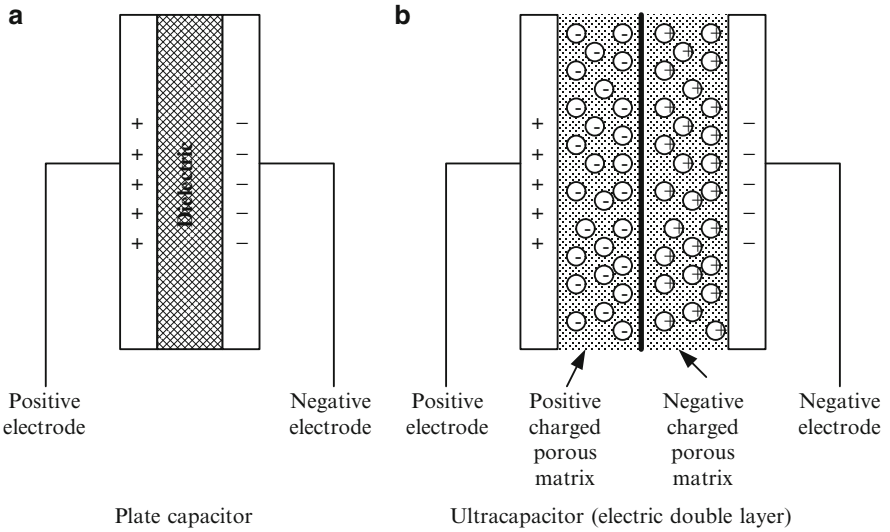

Fig. 11.6 Capacitors for energy storage of electrical charge

where $i(t)$ is the electric current that passes through the circuit at the time t. In the above expression, the voltage V in the charging and discharging line is constant; thus, by differentiation with respect to time, Eq. (11.2) becomes

$$\frac{\mathrm{d}V_\mathrm{c}}{\mathrm{d}t} = -R\frac{\mathrm{d}i(t)}{\mathrm{d}t}, \tag{11.3}$$

where one uses Eq. (11.1) to express $V_\mathrm{c} = q/C$ or $\mathrm{d}V_\mathrm{c}/\mathrm{d}t = 1/C(\mathrm{d}q/\mathrm{d}t)$; furthermore, one can determine the electric intensity, which is the same as the variation of electric charge with respect to time, $i(t) = \mathrm{d}q/\mathrm{d}t$; then Eq. (11.3) becomes

$$\frac{1}{C}i(t) + R\frac{\mathrm{d}i(t)}{\mathrm{d}t} = 0, \tag{11.4}$$

which can be integrated in time with the initial condition $i(t = 0) = I_0$ to give

$$i(t) = I_0 \exp\left(-\frac{t}{\tau}\right), \tag{11.5}$$

where $\tau = RC$ is known as the time constant of the circuit.

Note that the initial current I_0 is limited by the total resistance R; thus one has $I_0 = V/R$. Also note that the equation for charging and discharging of a capacitor is similar, and therefore the time constant at charging is the same as the time constant at discharging. However, during the charging process, the capacitor draws the maximum current I_0 at the beginning and nil current at the end of the process. Care must be taken in the design because at the discharging, the current intensity is

the reverse of that of the charging: that is, at the beginning of the discharging process the current intensity is nil, and at the end the current reaches its maximum value.

It is simple to show that the amount of energy stored in a condenser is proportional to the square of the voltage and is given by the following equation:

$$E = \frac{CV_c^2}{2}. \tag{11.6}$$

The efficiency of the charging process can be calculated by observing that the energy "injected" into the capacitor is proportional to the total electrical charge and the source voltage, $E_s = qV_s$; therefore, one can derive that

$$\eta = \frac{E}{E_s} = \frac{CV_c^2/2}{qV_s} = \frac{qV_c/2}{qV_s} = 0.5, \tag{11.7}$$

where one can reduce qV_c with qV_s because at the end of the charging process $V_c = V_s$.

The only way to increase the charging efficiency of the capacitor is by increasing the source voltage during charging such that the charging current is kept constant. Table 11.1 shows that capacitors can achieve very high storage efficiency of over 90% if the charging current is properly controlled. Figure 11.6b shows a second capacitor principle that provides another way of increasing the efficiency and the volumetric packing of the energy storage unit. Rather than storing the electrical field energy between the two parallel electrically charged surfaces, one can use a special porous substrate on each of the plates. The porous matrix that is deposited at each of the electrodes is very conductive, but the materials are chosen such that the interface between the two layers (left and right porous matrices in Fig. 11.6b) blocks very well any electrical current leakage. Therefore, a very strong electrical field is maintained between the two layers. The advantage of this type of capacitor comes from the fact that the layers and the electrodes are extremely thin. There is therefore a great opportunity for packing more storage capacity per unit of volume. The energy density of ultracapacitors ranges from 0.5 to 30 Wh/kg; at the upper range the energy storage density of these devices is comparable to that of lead–acid batteries. The capacitors are the fastest devices for storage and delivery of electrical energy; they can accumulate and deliver energy at a rate of a thousand times higher than that of electrical batteries, their specific power density being over 1,000 W/kg.

11.4.2 Electrochemical Energy Storage in Batteries

Storage of energy in electrical batteries is a mature technology that has also achieved a large diversity of implemented solutions. The storage of electrochemical energy requires the existence of a cell that comprises an electrolyte and two

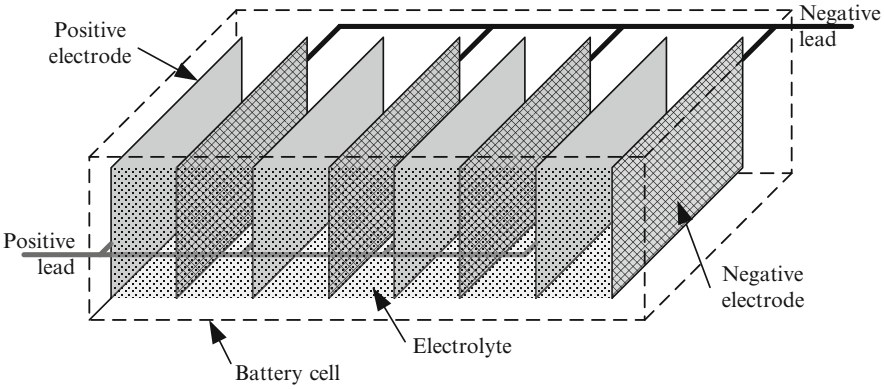

Fig. 11.7 The configuration of an electrical battery cell

Table 11.2 Electrochemical characteristics of various battery electrodes

Anode material	Standard potential (V)	Electrochemical equivalence (Ah/kg)	Cathode material	Standard potential (V)	Electrochemical equivalence (Ah/kg)
Pb	−0.13	0.26	PbO_2	1.455	224
Zn	−0.76	0.82	MnO_2	1.23	308
Cd	−0.4	0.48	Cl_2	1.36	755

Data from Ter-Gazarian (1994)

electrodes. In general, the current generated by a single cell is low, and in order to increase it one has to increase the surface of the electrodes. This is done by connecting a number of electrodes in parallel. The typical geometric configuration of a single battery cell is shown in Fig. 11.7. The voltage of the battery can be increased by connecting multiple cells in series.

Specific electrochemical reactions occur at each electrode of the cell, depending on the chosen electrolyte and the electrodes. Both electrodes are at a negative potential with respect to the electrolyte as they inject metal atoms into the electrolytic solution where they dissolve. Each atom that leaves the electrode leaves behind one or more electrons, which polarize the electrode with negative charge with respect to the electrolyte. A pair of electrodes, both of different metals, is inserted into the electrolyte. Each electrode is at a different negative potential (called standard potential) with respect to the electrolyte. The difference between the standard potential of the two electrodes gives the electromotive force of the elementary electrolytic cell. In Table 11.2, the standard potentials of various electrodes are summarized, both for the anode (the negative pole of the battery) and the cathode (the positive pole of the battery).Using Table 11.2, an example is given as follows:

- Consider a carbon–zinc battery having one electrode on Zn and the other on MnO_2.
- The cathode standard potential of MnO_2 is, from Table 11.2, +1.23 V.
- The anode potential for Zn is −0.76 V.
- The difference $+1.23 - (-0.76) = 1.99$ V represents the cell voltage.

Table 11.3 Main parameters of three important types of rechargeable batteries

Type	Voltage (V)	Specific energy		Specific power (W/kg)	Operating temperature (°C)
		Wh/kg	Wh/l		
Lithium–Ion	2.8	250–600	400–1,100	430	−55 to +85
Nickel–Cadmium	1.2	50	90	120	−20 to +45
Lead–Acid	2	35	85	180	−40 to +60

Data from Ter-Gazarian (1994)

- The electrochemical equivalence for Zn is, from the table, 820 Ah/kg.
- The electrochemical equivalent of MnO_2 is 308 Ah/kg.
- Therefore, the specific capacity of the battery is given by the sum 820 + 308 = 1,128 Ah/kg.
- The energy density of the battery can be obtained with the product 1,130 Ah/kg × 1.99 V, i.e., 2.25 kWh/kg.

Table 11.3 lists the main parameters of three important types of rechargeable batteries, namely, the voltage, the stored specific energy per mass and per volume and the specific power, and the operating temperature. Another important parameter, which is not included in the table, is represented by the voltage versus time characteristics. During the operation, the internal resistance of the battery increases in a manner that the voltage produced by the battery on a load decreases in time, until it reaches a cut-off value at which the device being powered does not function well.

11.4.3 Kinetic Energy Storage in Flywheels

The flywheel, a wheel of relatively large mass that stores rotational kinetic energy, has long been used to smooth out the shaft power output from one- or two-cycle (stroke) engines and to adjust for uneven loads. A flywheel can be designed to work both as a motor when driven by electric power and as a generator when driven by mechanical power. Flywheel systems for electrical energy storage have two properties in which they differ from the rechargeable batteries: (1) high-power mass density specified by the maximum charge (discharge) power per system mass, and (2) high life cycle.

If one denotes I as the moment of inertia of the flywheel, then it is defined by the following expression $I = \int_0^R r^2 \mathrm{d}m$, where r is the radial coordinate centered in the rotation center, dm is the infinitesimal mass rotating with the flywheel, and R is the radius of the flywheel. The kinetic energy stored in the rotating disk of radius R is

$$E = \frac{I\omega^2}{2}, \tag{11.8}$$

where ω is the angular velocity.

If one assumes that the flywheel is in the form of a ring, that is, all mass is concentrated at the rim, then the moment of inertia becomes $I = mR^2$ and the stored energy is

$$E = \frac{mR^2\omega^2}{2}. \tag{11.9}$$

The flywheel can be charged with kinetic energy by increasing its angular velocity. The increase of angular velocity produces, however, an increase of the tensile stress in the wheel material. The tensile stress in a rim is $\rho\omega^2R^2$, where ρ is the material density. The tensile stress is limited by the maximum value over which the failure of material occurs:

$$\sigma_{\max} = \rho\omega^2R^2. \tag{11.10}$$

Combining Eqs. (11.9) and (11.10), one can get the maximum volumetric energy density of the rim-kind flywheel:

$$E_{\mathrm{v}} = \frac{E}{V} = \frac{\sigma_{\max}}{2}, \tag{11.11}$$

where V is the volume of the flywheel.

The mass specific energy density can be derived from Eq. (11.11) as follows:

$$E_{\mathrm{m}} = \frac{E}{m} = \frac{E}{\rho V} = \frac{E_{\mathrm{v}}}{\rho} = \frac{\sigma_{\max}}{2\rho}. \tag{11.12}$$

The result from Eq. (11.12) is important; it shows that in order to pack as much as possible energy per unit of volume, one needs to have a material with low density (i.e., a light material) and with a high admissible (maximum) tensile stress; a heavy material will not be suitable, contrary to common intuition. In general, the energy density of a flywheel of arbitrary profile is given by an equation of the form

$$E_{\mathrm{m}} = \frac{K\sigma_{\max}}{\rho}, \tag{11.13}$$

where one can note that $K = 0.5$ for the rim-shaped flywheel. The challenge is to obtain a good shape characterized by a high shape factor K and a high admissible tensile stress $\sigma_{\max}$. For a flat disk, the shape factor is $K \cong 0.61$; a better K is obtained for a so-called constant stress disk, which has $K > 0.93$ (Ter-Gazarian 1994). The constant stress disk is made in such a way that the radial and axial stress components are equal at all points.

During the discharge time, it is not possible to retrieve all the energy of the flywheel, because the angular speed of the flywheel must be kept to a minimum value that is of the order of 20% from the maximum angular speed. Moreover, there

is a friction associated with the rotation of bearings and possible aerodynamic forces. Friction's influence can be quantified by a subunitary factor $\zeta(t)$, which depends on the duration of the storage: if the storage time is high, the factor is low. The retrieved energy per unit of mass is therefore

$$E_{\mathrm{r,m}} = \frac{\zeta(t)\left(1 - \left(\frac{\omega_{\min}}{\omega_{\max}}\right)^2\right) K\sigma_{\max}}{\rho}. \tag{11.14}$$

Therefore, the expected energy efficiency of the flywheel discharged immediately is given by

$$\eta = \frac{E_{\mathrm{r,m}}}{E_{\mathrm{m}}} = \zeta(t)\left(1 - \left(\frac{\omega_{\min}}{\omega_{\max}}\right)^2\right) \cong 0.98\,(1 - 0.2^2) \cong 0.94. \tag{11.15}$$

Note that because the stored energy is kinetic, the energy and exergy efficiencies are the same. In general, flywheels are used for short-term energy storage; they are discharged relatively immediately after charging. If discharging follows after 1 day, the friction factor drops and the efficiency of the flywheel falls below 50%.

11.4.4 Storing Gravitational Potential Energy Through Pumped Hydrostorage

Hydrostorage is very simple and is widely used in the power industry to store off-peak power for peak load periods. This technique utilizes a dam that has a sufficient hydrostatic head to drive a hydroelectric power plant. Water is pumped into the reservoir during off-peak periods and drawn out during peak periods. The basic requirement is a dam with a large quantity of water at its base, or two dams with a height difference between them. Hydrostorage is relatively efficient. The energy used to pump water upward is recovered in a storage cycle with about 65% to 75% efficiency. Hydrostorage is often ideal for solar power storage. The solar plant produces power at the maximum rate during the day and is on standby during the night, maintaining only system temperatures so that it is ready to turn out power the next day as soon as the collector subsystem reaches the operating temperature. Pumped storage is the only well-established energy storage concept that is available on a large scale. The concept is simple. Energy is stored during the evening hours by pumping the water from a lower body of water to an upper reservoir behind a conventional dam. During peak demand hours, the water flows down from the upper reservoir through a hydroelectric turbine back into the lower body of water. Because of the environmental concerns associated with large-scale hydroelectric facilities, however, it is doubtful that many conventional pumped hydro plants will be constructed in the future.

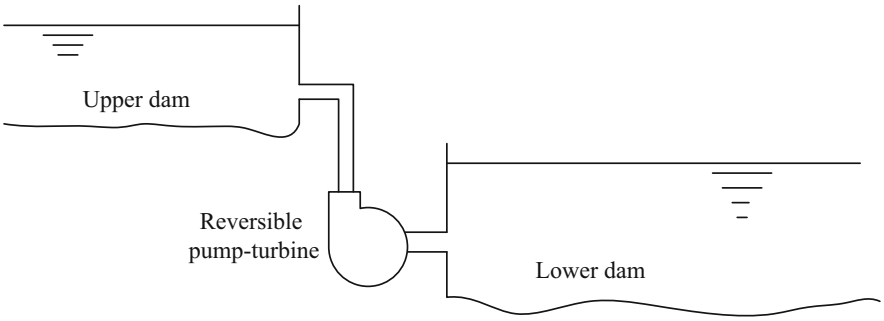

Fig. 11.8 Diagram of the principle of pumped hydrostorage

The diagram explaining the principle of pumped hydrostorage is shown in Fig. 11.8. The efficiency of this storage system, defined as the energy supplied to the user versus the energy supplied to the storage at charging time, can be derived as follows:

$$\eta = \frac{E_{\text{retrieved}}}{E_{\text{supplied}}} = \frac{E_{\text{retrieved}}}{E_{\text{potential}}} \frac{E_{\text{potential}}}{E_{\text{supplied}}} = \eta_{\text{charging}} \eta_{\text{discharging}}. \tag{11.16}$$

In general, the overall efficiency of pumped hydrostorage is of the order of 65% to 85%.

11.4.5 Thermomechanical Energy Storage in Compressed Air

Compressed air storage is a thermomechanical process in which energy is transmitted and retrieved, respectively, through mechanical work and heat. In a compressed air energy storage system, air is compressed during off-peak hours and stored in large underground reservoirs, which may be naturally occurring caverns, salt domes, abandoned mine shafts, depleted gas and oil fields, or man-made caverns. During peak hours, the air is released to drive a gas turbine generator. The technique used by such a system to compress air to store energy is relatively straightforward. In a conventional gas turbine, high-pressure hot gas is supplied, and about two thirds of the gross power output is used to drive the compressor. A compressed air system decouples the compressor and the turbine, and operates the former during off-peak hours to produce compressed air that is stored in natural caverns, old oil or gas wells, or porous rock formations. Such energy storage is advantageous when an appreciable part of the power load is carried by nuclear stations and where suitable spent salt caverns make it easy to build the compressed gas reservoirs.

Figure 11.9 presents the layout of a compressed air storage facility. Because air compression and expansion is necessarily accompanied by the release or absorption

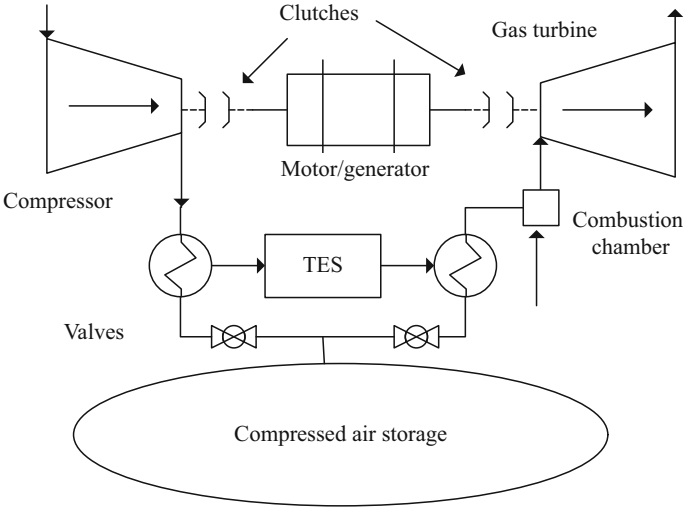

Fig. 11.9 Layout of a compressed air storage facility

of heat, a compressed air storage system can be coupled to the thermal energy storage (TES). The system shown above operates as follows:

- During charging time, which is preferred in winters when electricity generation is at higher efficiency and air is easier to be compressed, the motor is coupled with the compressor through the corresponding clutch.
- Air is compressed with intercoolers and the associated thermal energy is stored in a TES system, while the compressed air is stored in a large reservoir.
- During energy retrieval, the motor plays the role of electric generator and is coupled to the turbine.
- The thermal storage delivers heat to preheat the air before combustion.
- Combustion expands the exhaust gases in the turbine, which generates electricity.

Note that decoupling the turbine from the compressor makes it possible to deliver three times more work than in a regular Brayton cycle. Also, compression is facilitated when the ambient air is colder: compression work is 10% to 15% lower if the suction temperature is $-10°C$ (winter) instead of $+30°C$ (summer). The attractiveness of the compressed air storage comes from the possibility of storing the compressed air seasonally.

There is experience accumulated in designing large storage reservoirs in underground salt caverns. Such caverns can be mined by using aqueous solutions that dissolve salt and generate the desired shape of the reservoir. As a second option, large quantities of compressed air can be stored in aquifers, above the water level, if the geomorphological configuration is above the aquifer such that there is hard rock that impedes air leakages.

For defining the efficiency of the compressed air–gas turbine storage system, one has to take into consideration that the energy delivered by the system is in any situation higher than the energy consumed to compress the air. This approach will lead to efficiency higher than unity. Therefore, a fair definition of efficiency in the case of such energy storage systems is to consider the chemical energy stored in the fuel (either the higher or the lower heating value) as part of the input. Therefore, the total energy input is the sum of the energy consumed for air compression plus the fuel energy. The system efficiency becomes

$$\eta = \frac{E_{\text{generated}}}{E_{\text{compressed air}} + \text{LHV} \times m_{\text{fuel}}}. \tag{11.17}$$

The mass of fuel and the mass of stored air are correlated through the air–fuel ratio.

11.4.6 Chemical Energy Storage in Synthetic Fuels

There is a large number of technologies for producing synthetic fuels, of which the most representative is hydrogen fuel. Other materials that can be viewed as synthetic fuels are ammonia, ethanol, Fischer–Tropsch diesel, syngas, and methane. During low-demand periods, the primary energy can be used to produce a synthetic fuel that can be used to release energy during high demand periods. The energy release can be obtained either by fuel combustion in various internal combustion engines, or in fuel cells or hybrid energy systems. In an extended approach, liquid nitrogen can be viewed as a fuel since its energy of thermomechanical nature can be retrieved at a later time in special pneumatic turbines arrangements.

Production of hydrogen from renewable sources like wind and solar is a current area of development. Figure 11.10 shows possible paths for hydrogen production from primary energy sources including fossil fuels, nuclear, and renewable energies. Hydrogen is the primary element from which other synthetic fuels or chemicals can also be produced, but it is difficult to store. Many production and storage methods of hydrogen are detailed in other parts of this book. In this chapter, we emphasize only that the storage volumetric density of hydrogen is low with respect to other systems discussed above, and moreover, the storage duration is the lowest with respect to other synthetic fuels. The storage of hydrogen seasonally in large volumes becomes very expensive and is not applicable because of leakages and high compression costs or high costs associated with hydrogen liquefaction. These facts limit the volume and duration of storage. In general, it appears economical to store hydrogen for days or weeks. Hydrogen can be converted into ammonia with the expense of some additional energy, which in relative terms is reasonably low. Ammonia can be stored in bulk quantities seasonally or even for several years without sensible degradation and an associated cost, which is

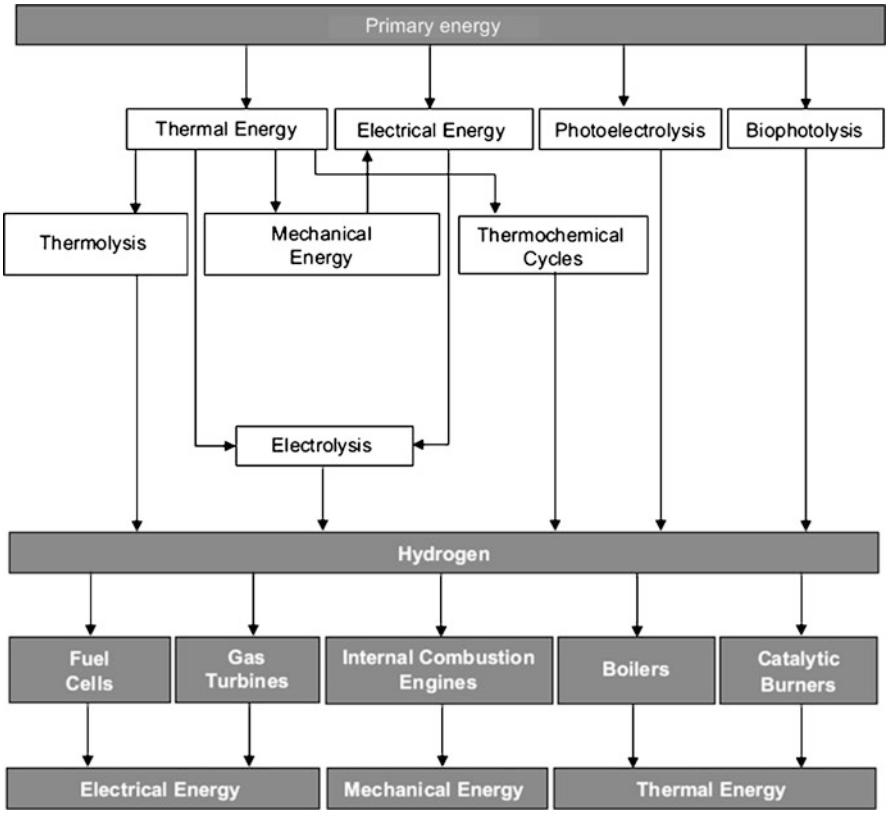

Fig. 11.10 Production and utilization paths of hydrogen from primary energy sources [modified from Yilanci et al. (2009)]

rather cheap. Ammonia can be synthesized from hydrogen and nitrogen in advanced Haber–Bosch plants that operate intensively with energy recovery. In general, one can say that storage of energy in synthetic fuels is characterized by the highest energy per unit of mass and the lowest power extraction per unit of mass because of the high mass associated with fuel production plus power generation facilities.

11.4.7 Thermochemical Energy Storage with Chemical Heat Pump Systems

These system are based on a discontinuously working solid-state absorption heat pump incorporating a storage function, of which the operating principle is as follows: two chambers are connected to each other. Chamber I is the energy accumulator containing the vapor absorbing salt (Na_2S), and chamber II is the

condenser/evaporator containing the working fluid (H_2O). The reversible chemical reaction, in the case of sodium sulfide and water used as a working pair, is given as follows:

$$Na_2S \cdot nH_2O + \text{Heat} \leftrightarrow Na_2S + nH_2O. \tag{11.18}$$

Another chemical reaction of interest is

$$CH_4 + H_2O + \text{Heat} \leftrightarrow CO + 3H_2, \tag{11.19}$$

which during off-peak hours is used to accumulate heat by driving the reaction toward the left, while during on-peak periods the reaction is driven toward the right to generate heat. The chemicals from the right-hand side of Eq. (11.19) do not react at low temperatures; therefore, they can be stored for long periods of time in ambient conditions. Only if the temperature rises above 850 K do the carbon monoxide and hydrogen react and dissipate heat. A system that uses the reaction (11.19) to upgrade the temperature of the CANDU nuclear power reactors has been proposed by Granowskii et al. (2008) in the context of using the reaction heat to drive a thermochemical water splitting cycle to produce hydrogen.

11.4.8 Thermal Energy Storage

Thermal energy storage (TES), both in the form of cold and heat storage, has attracted increasing interest for many applications such as space heating, hot water, cooling, and air conditioning. Most importantly, TES systems have the potential of increasing the efficiency of energy systems by shifting the level of operating temperatures during the cold and warm seasons. The power generation is more efficient in winter, when the thermal sink reservoir, that is, the environment, is at a lower temperature; therefore, the heat engine systems operate better. Using a seasonal TES system facilitates the increase of power generation efficiency. Shorter-term thermal storage also has positive impact on a large range of energy consuming or energy production systems. Like any other energy storage systems, TES is useful for correcting the mismatch between the supply and demand of energy. Thermal energy and its storage are discussed in detail in Section 11.6.

11.4.9 Comparison of Energy Storage Methods

For any specific application, it is important to decide on a rational basis which method of energy storage is best suited. As listed in Table 11.4, there are eight main forms of energy that are storable through various energy conversion and storage methods. These energies are electric, electrochemical, kinetic, gravitational,

Table 11.4 Comparison of energy storage methods

Stored energy	Term	Energy density (kWh/dm^3)	Specific energy (kWh/kg)	Recommended capacity
Electric	Very short (seconds)	10^{-2}	10^{-3}	Low (kW)
Electrochemical	Long (weeks)	10^{0}	10^{-1}	Low (kW)
Kinetic	Short (hours)	10^{-1}	10^{-1}	Low (kW)
Gravitational (hydro)	Very long (years)	10^{-3}	10^{-3}	Very high (GW)
Thermomechanical	Long (seasons)	10^{-3}	10^{-1}	High (MW)
Chemical (fuel[a])	Very long (years)	10	10	High (MW)
Thermochemical	Long (months)	10^{0}	10^{0}	High (MW)
Thermal energy	Long (seasons)	10^{-1}	10^{-1}	Low/high (kW/MW)

Data from Ter-Gazarian (1994)
[a]Except nuclear

thermomechanical, chemical, thermochemical, and thermal. One of the points of comparison among these methods is the term of storage, which can be either long or short.

The following main characteristics are important when comparing energy storage systems: the duration (term) of storage, the energy density (stored energy per unit of volume), the specific energy (defined as stored energy per unit of mass), and the recommended installed capacity (in units of energy discharge rate, i.e., power). One can observe from Table 11.4 that the electric, electrochemical, and kinetic energy storage have the shortest storage terms and the shortest recommended storage capacity. Therefore, these kinds of storage can be used for "buffer" applications, when low amounts of energy need to be stored for a short duration and also retrieved at a fast rate. It can also be observed that as the storage increases, the recommended installed capacity increases too, while the energy density and specific energy decrease. For example, hydro/gravitational energy is characterized by the longest storage term among all but also the lowest storage density and specific energy. Therefore, hydrostorage is recommended for very high installed capacity. The figures presented in Table 11.4 are only the orders of magnitude of storage density and specific energy for each of the systems.

11.5 Methods of Analysis of Energy Storage Systems

This section presents a general thermodynamic treatment of energy storage regardless of the nature of stored energy. In this respect, exergy is used to describe the stored energy as well as the associated losses at energy storage plus losses at energy transfer when charging and discharging the storage. Exergy is a comprehensive concept because in its general form it includes a thermomechanical component as well as other forms of energy such as electric, chemical, magnetic, kinetic, potential, and so on.

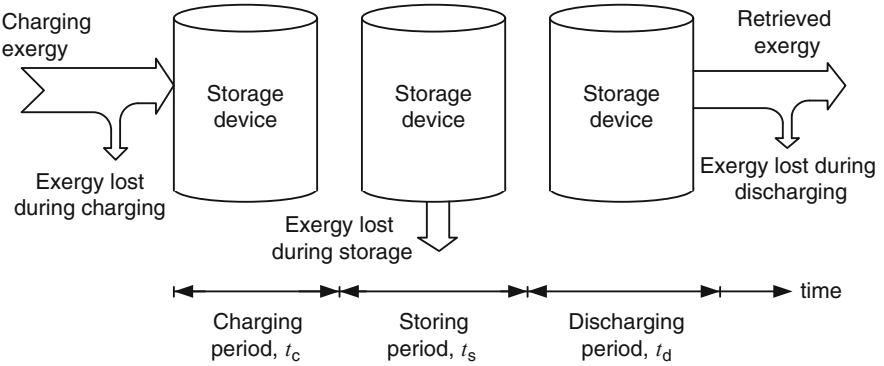

Fig. 11.11 General description of an energy storage process

Therefore, in the general treatment presented here, we quantify the flows of exergy. In the subsequent sections, particular situations when the flow of exergy is of one form only, say electrochemical (in the case of electrical batteries) or thermal (in the case of hot or cold thermal storage) or purely kinetic (in the case of flywheel), are demonstrated. The general description of an energy storage process is introduced in Fig. 11.11 and operates cyclically in three periods: charging, storing, and discharging. In the first period of time t_c, the storage device is charged (possibly up to its maximum capacity). During the charging process, a stream of exergy is "transmitted" toward the storage device. Any exergy transmission implies the existence of a difference of potential that generates the flow of exergy. For example, if the storage device is an electrical battery, then the flow of electricity is at any time higher than the voltage of the battery. Since the electrical current passes through a medium, one must consider the electrical resistance at charging. The resistance dissipates heat that is associated with the exergy lost during the charging process.

A similar example can be given for a thermal storage system, where a temperature difference must be created between the heat flux that charges the device and the temperature within the device. The temperature difference is associated necessarily with thermal resistance and exergy losses during charging.

An ideal storage device is insulated perfectly against any exergy losses that may occur during the storage time. However, if the storage time is long enough, exergy leakages out of the storage devices are unavoidable and must be taken into account. These are the exergy losses during the storage period t_s. During the discharging period t_d, the stored exergy is transmitted back to the grid or to the point of consumption. Consequently, there are exergy losses associated with the transmission process since the potential (electrical charge, voltage, temperature, water level, rotation speed, etc.) of the storage device always must be higher than that of the transmission line at discharge.

The process of exergy storage and retrieving is demonstrated in Fig. 11.12, which shows qualitatively the evolution of the exergy rate in time for all cycles.

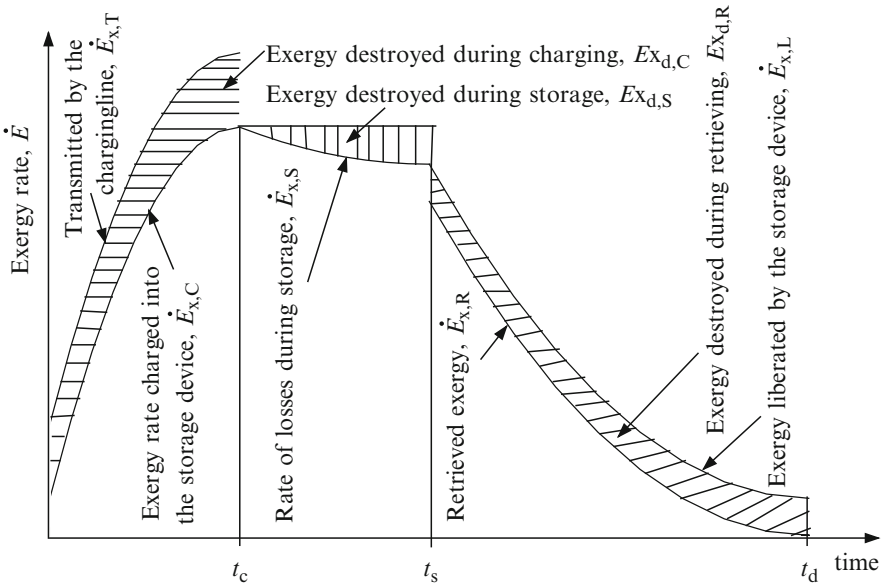

Fig. 11.12 Exergy cycle in a storage device

For the charging period, it is shown that the exergy rate delivered by the charging medium (or charging line or energy transmission system, whichever is the case) is always higher than that received by the storage device. The figure emphasizes the losses of exergy during the charging time, which is represented by the hatched area between the lines of "transmitted exergy by the charging line" and "exergy charged into the storage device." The accumulated exergy in the storage at the end of the charging time is measured by the area below the $\dot{E}_{x,C}$ line. Note that the lines represented in the figure represent the exergy rate, while the hatched areas represent the amounts of destroyed exergy. With reference to the notation shown in Fig. 11.6, the exergy balance for the process can be written as

$$\begin{cases} \int_0^{t_c} \dot{E}x_T \mathrm{d}t = \int_0^{t_c} \dot{E}x_C \mathrm{d}t + Ex_{d,C}, \\ \int_0^{t_c} \dot{E}x_C \mathrm{d}t = \int_{t_c}^{t_s} \dot{E}x_S \mathrm{d}t + Ex_{d,S}, \\ \int_{t_c}^{t_s} \dot{E}x_S \mathrm{d}t = \int_{t_s}^{t_d} \dot{E}x_L \mathrm{d}t, \\ \int_{t_s}^{t_d} \dot{E}x_L \mathrm{d}t = \int_{t_s}^{t_d} \dot{E}x_R \mathrm{d}t + Ex_{d,R}, \end{cases} \tag{11.20}$$

where $Ex_{inp} = \int_0^{t_c} \dot{E}x_T \mathrm{d}t$ and $Ex_{ret} = \int_{t_s}^{t_d} \dot{E}x_R \mathrm{d}t$ represent the exergy input into the system and exergy retrieved from the system, respectively. Therefore, one can

define the exergy efficiency of the storage system as the exergy retrieved over the exergy input, that is:

$$\psi = \frac{Ex_{\text{ret}}}{Ex_{\text{inp}}}. \tag{11.21}$$

Based on Eq. (11.20), one can express the retrieved exergy as $Ex_{\text{ret}} = Ex_{\text{inp}} - Ex_{d,\text{tot}}$, where $X_{\text{d,tot}}$ denotes the total exergy destruction, which is given as follows:

$$Ex_{d,\text{tot}} = Ex_{d,\text{C}} + Ex_{d,\text{S}} + Ex_{d,\text{R}}. \tag{11.22}$$

The exergy efficiency of the energy storage system is given by the following equation:

$$\psi = 1 - \frac{Ex_{d,\text{tot}}}{Ex_{\text{inp}}}. \tag{11.23}$$

Regarding the energy efficiency of the system, which is also a parameter of interest, one can reasonably assume for most systems that during the charging and discharging time there is no energy loss, but mainly the energy loss occurs during the storage time (e.g., heat losses through insulation in the case of thermal storage or electrical charge leakage through internal resistance at electricity storage in capacitors). In general, one can write the energy efficiency as

$$\eta = \frac{E_{\text{ret}}}{E_{\text{inp}}}, \tag{11.24}$$

where E_{ret} is the retrieved energy and E_{imp} is the input energy.

The energy storage strategy must be designed to correspond to the demand profile and the load profile of energy generators (supply side profile). For example, there is no reason to install a cooling capacity for the milk factory that meets the peak of cooling demand, since the duration of the demand is short. Rather, one can install a lower capacity that accumulates cold throughout the day and delivers it when needed. In general, there are three known storage strategies that can be applied in conjunction with the specific characteristics and profiles of the energy demand and supply side of the energy system.

If the energy demand profile extends partially over the operation cycle of the system, such that the energy is needed only for a shorter period of time than the process cycle, then the load shifting strategy can be applied. This strategy can also be favored by economic incentives and differentiated on- and off-peak energy tariffs. Figure 11.13a illustrates the load shifting energy storage strategy. In peak hours, the cost of energy is high; therefore, it is preferable not to consume it. At off-peak times, the price of energy is low but there is no demand. In such

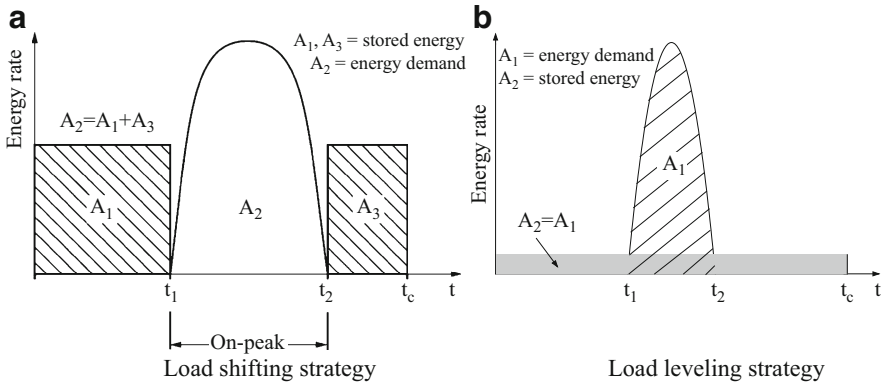

Fig. 11.13 Illustration of two "extreme" storage strategies: (**a**) load shifting strategy; (**b**) load leveling strategy

situations, the energy storage system can allow for load shifting between on- and off-peak hours. Energy is stored continuously during the off-peak hours. The energy demand, which is coincident with the on-peak period, is obtained by discharging the storage device rather than from direct generation. Many thermal storage systems are operated based on this strategy.

In load shifting, the energy generation system can operate discontinuously in an on–off manner. On the other extreme, there can be a situation where the energy is generated continuously but at a lower capacity. This can be the case exemplified above with regard to milk cooling. Whenever a process needs energy for a short duration with respect to the overall cycle, the load leveling energy storage strategy can be applied as illustrated in Fig. 11.13b.

In this case, the energy is generated at a lower rate. During the off-demand periods, the energy supply charges the storage. During the demand time, both the energy generators and the storage devices are joined to meet the demand. In between the two "extreme" storage strategies—load shifting and load leveling—one can have the "mixed" strategy of "partial storage," as illustrated in Fig. 11.14. This is a more general case, where the energy demand profile is almost uniform during a part of the operation cycle, but it has a peak period for another part.

In this case, the energy can be generated at a higher rate during the off-peak period to meet the demand and to charge the storage. During the peak period, the energy is generated at a lower rate and the storage device is discharged to compensate for the rest of the need. Regardless of the storage strategy, as a general rule, the power capacity of the storage must always be greater than the maximum deviation of the demand above or below the mean.

Subsequently, after determining the appropriate energy storage strategy, one has to design the storage device. The challenge is to design a storage facility so that the most energy possible is accumulated per unit of volume, and with minimum irreversibility at energy transmission in and out of the tank, during the charging and discharging periods, respectively.

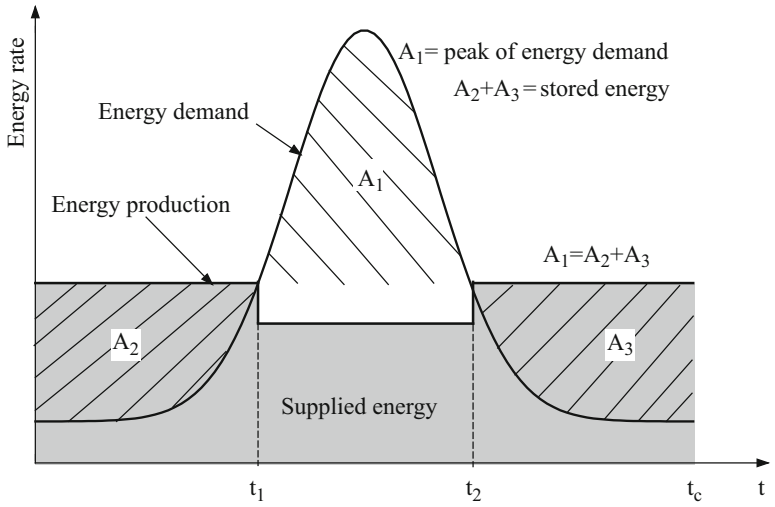

Fig. 11.14 Partial storage strategy

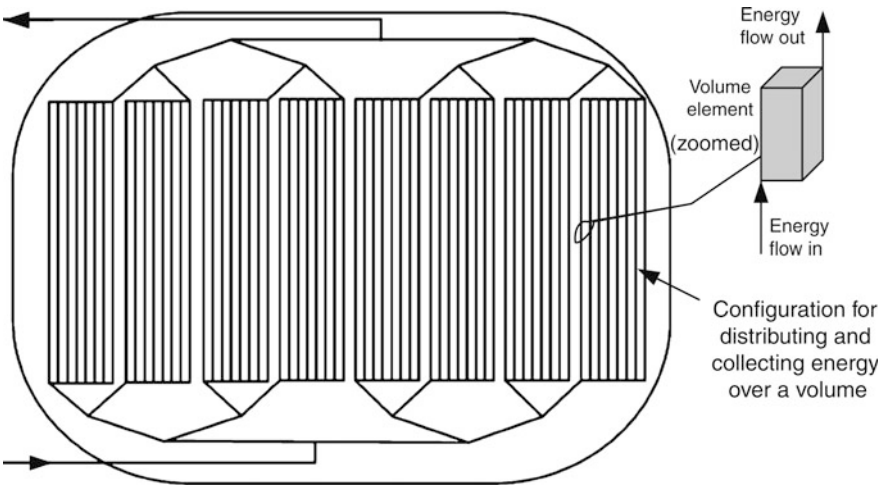

Fig. 11.15 Constructal configuration of an energy storage device

Furthermore, during the storage time, the device must act as a well-insulated thermodynamic system with a reduced irreversibility associated with energy leakage. The suggested general design concept of the storage device is shown in Fig. 11.15. The question mark on the figure indicates the geometrical configuration of the elemental cell, which represents the design's unknown. The constructal theory of Bejan (2000) states that any flow system must evolve in time such that it provides easier access to the currents. That is, regardless of the nature of the

energy that flows through our energy storage device, the system has to have a configuration that facilitates the optimal access to currents. In other words, in order to achieve a good design, the design must evolve in time from simple to complex and from smaller scale to larger scales.

Note the similarity between the elemental volume shown in Fig. 11.15 and the capacitor storage systems shown in Fig. 11.6. One can imagine that, conceptually, a storage device will link a multitude of simple capacitors in a distribution/collection network as shown in Fig. 11.15. The electrochemical battery system discussed above in association with Fig. 11.7 will eventually look similar to the system described conceptually in Fig. 11.15, where the positive and negative leads in the network distribute the electrical current during charging and discharging periods of the elementary electrolytic cells throughout the storage device's volume.

The role of the energy storage is twofold: (1) to distribute or collect the flow of energy over the storage volume, and (2) to store the energy in every bit of volume with reduced losses. Therefore, the storage device comprises two elements: (1) a distribution/collection network of energy streams spread over the volume, and (2) a multitude of optimized elemental volumes that store energy. In a subsequent section, we demonstrate the application of a constructal design concept for a cold storage tank. The method is general with respect to the nature of the energy flow. That is, it can be applied for any kind of storage, regardless of whether ice is accumulating on the tubes of a cold storage tank, or an electrical charge accumulates on the elemental plates of a capacitor, or a synthetic fuel is produced in a constructal chemical reactor. If, for example, one stores hydroenergy, the constructal design method can guide the conceptual design of the dam toward a shape/configuration that minimizes the material consumption while keeping the mechanical resistance high enough; note that the dam itself is a flow structure through which the strain and tension flow.

11.6 Thermal Energy

11.6.1 Thermal Energy Sources

There are mainly two types of TES systems: sensible (e.g., water and rock) and latent (e.g., water/ice and salt hydrates). The selection of a TES system mainly depends on the storage period required (e.g., diurnal or seasonal), economic viability, and operating conditions. Many research and development activities on energy have concentrated on efficient energy use and energy conservation, and TES appears to be one of the more attractive thermal technologies that have been developed. For example, the solar energy accumulated during the day can be stored and used for night use, and the ice accumulated during winter can be stored and used for space air conditioning in summer.

As thermal storage can use sensible or latent heat to store energy, one can use two types of balance equation expressing the amount of stored thermal energy:

$$Q = mc_{\mathrm{p}}\Delta T \quad \text{or} \quad Q = m\Delta h, \tag{11.25}$$

where Q is the amount of stored thermal energy, m is the mass of storage material, c_{p} is the specific heat, ΔT is the storage temperature variation at the end and beginning of the storage period, and Δh is the phase change enthalpy of the storage medium.

A TES system has a wide variety of applications, the majority of which relate to heating and cooling applications. TES provides a link and buffer between a heat source and a heat user. A common example of a TES system is the solar hot water storage system. The energy source is solar radiation and the heat user is the person demanding hot water. In this situation, storage is required because the energy supply rate is small compared with the instantaneous demand and because solar radiation is not always available when hot water is demanded. A thermal energy system can be used for both cooling and heating applications as we describe in detail in the subsequent subsections (see Dincer and Rosen 2002).

11.6.2 TES for Cooling and Heating

Summer air conditioning bills have two components: an electric demand charge and an electric usage charge. The usage and demand charges are often further divided into on- and off-peak periods. The peak operating period of electric air conditioning systems normally occurs during the high-cost demand and usage periods (i.e., the summer afternoon). TES systems are designed to shift the peak operating period of electric air conditioning systems to the less expensive nighttime periods. Cold TES-based air conditioning systems remove heat from an intermediate substance when the building does not need cooling, producing a cool reservoir that is stored until there is a need for cooling. The intermediate substance is normally water, ice, or eutectic salt solutions.

The most popular thermal storage medium is ice. The conversion of 1 kg of water to ice at 0°C requires the removal of 152 kJ of heat. Similarly, adding 152 kJ of heat to the ice at 0°C causes water to be formed. Ice TES operates in this fashion. At night, heat is removed from water to produce ice (i.e., charging of the storage occurs). During the day when the building requires cooling, heat is removed from the building and added to the ice (i.e., discharge occurs). The melted ice is reused during the next charging period. The advantage of this cooling scheme is that the main electrically driven device in cooling systems, namely, the compressor motor, is operated during low-electrical cost periods. Cooling TES systems are generally advantageous for new facilities that will have a large daytime cooling load and little or no cooling load at night. For retrofit situations, cooling TES is usually difficult to justify unless the cooling system is being replaced because of old age or inadequate capacity.

Heating TES using electricity entails operating resistance heaters at night when electricity rates are low, to produce heating capacity for use during the day. Electric resistance efficiencies (near 100% on an energy basis) combined with lower off-peak electric rates can produce heat at a fraction of the cost of conventional systems. Heat produced by electrical resistance heaters at night is stored in such storage media as earth materials or ceramic bricks in insulated containers. The production of heat at night takes advantage of electric off-peak rates, which are generally 33% to 75% less expensive than on-peak rates. When heat demand rises (e.g., for space heating), heat is recovered from the storage unit and transferred into the room.

The use of earth as a TES medium is usually restricted to new construction since the application requires that electric resistance grids be placed 0.5 to 1 m in the ground, beneath a structure. The need to place the grids under a building makes retrofit work extremely difficult for any facility without a basement or crawl space. For new construction applications, approximately 2 m of earth directly below the structure is used for the storage of heat produced by the grid. A rigid and waterproof insulating material is placed vertically around the perimeter of the building and extends approximately 4 ft below the earth grade level. The insulation ensures that heat stored in the ground is radiated mainly into the structure and not into the surrounding earth. The electric resistance grid is placed 0.5 to 1 m below the earth's surface and covered with about 2 inches of sand and earth materials.

Ceramic bricks provide an excellent heat storage medium for retrofit as well as new construction applications due to their modular sizes, ease of installation, and high heat-retention abilities. These units are normally manufactured in various sizes and transported to building sites. The construction of this type of TES normally consists of an insulated box, about the size of a conventional radiant hot water or steam heating unit, filled with ceramic bricks. The number of bricks in a module depends on the heat storage requirement. The unit also includes a small fan. The ceramic bricks contain electric resistance strip heaters in their holes. During charging, the strip heating units produce heat that is absorbed by the ceramic bricks. The insulation surrounding the bricks restricts heat losses from them. During the day, a conventional thermostat is used to control the fractional horsepower fan that circulates air from the room across the ceramic bricks to recover the stored heat and transports it into the room.

11.6.3 Benefits of a TES System

A TES system can contribute significantly to meeting society's needs for more efficient, environmentally benign energy use in building heating and cooling, aerospace power, and utility applications. The use of TES systems often results in some significant benefits:

- Reduced energy costs
- Reduced energy consumption
- Improved indoor air quality
- Increased flexibility of operation

- Reduced initial and maintenance costs
- Reduced equipment size
- More efficient and effective utilization of equipment
- Conservation of fossil fuels (by facilitating more efficient energy use and/or fuel substitution)
- Reduced pollutants and greenhouse gas emissions (e.g., CO_2)

Although TES is used in a wide variety of applications, all are designed to operate on a cyclical basis (usually daily, occasionally seasonally). The systems achieve benefits by fulfilling one or more of the following purposes:

- *Increase generation capacity*. Demand for heating, cooling, or power is seldom constant over time, and the excess generation available during low-demand periods can be used to charge a TES in order to increase the effective generation capacity during high-demand periods. This process allows a smaller production unit to be installed (or to add capacity without purchasing additional units) and results in a higher load factor for the units.
- *Enable better operation of cogeneration plants*. Combined heat and power, or cogeneration, plants are generally operated to meet the demands of the connected thermal load, which often results in an excess of electric generation during periods of low electric use. By incorporating TES, the plant need not be operated to follow a load. Rather it can be dispatched in more advantageous ways (within some constraints).
- *Shift energy purchases to low-cost periods*. This is the demand-side application of the first purpose listed above and allows energy consumers subject to time-of-day pricing to shift energy purchases from high- to low-cost periods.
- *Increase system reliability*. Any form of energy storage, from the uninterruptable power supply of a small personal computer to a large pumped storage project, normally increases system reliability.
- *Integration with other functions*. In applications where on-site water storage is needed for fire protection, it may be feasible to incorporate thermal storage into a common storage tank. Likewise, apparatus designed to solve power-quality problems may be adaptable to energy-storage purposes as well.

The most significant benefit of TES is reducing electric costs by using off-peak electricity to produce and store energy for daytime cooling. Indeed, TES is successfully operating in offices, hospitals, schools, universities, and airports in many countries, shifting energy consumption from periods of peak electricity rates to periods of lower rates. That benefit is accompanied by the additional benefit of lower demand charges.

11.6.4 Methods of Sensible and Latent TES

The media used for sensible or latent thermal storage are classified in Table 11.5. In Table 11.6, the features of the main thermal storage technologies are summarized. Thermal storage can be done for short (minutes) or long (seasonal) periods of time.

Table 11.5 Storage media for thermal energy

	Sensible	
Latent (short term)	Seasonal	Short term
Aromatics and fatty acids	Aquifers	Rock beds
Organic chemicals	Solar ponds	Earth beds
Inorganic materials (e.g., ice, water)	Earth beds	Water tanks

Table 11.6 Summary of sensible thermal storage technologies

Name of the technology	Description
Thermally stratified TES tanks	Can be used for cold as well as heat storage in vertical water tanks that present a at certain height a narrow band of high-temperature gradient. This region impedes convection between the top and bottom levels of the tank, separating thus the colder and the hotter ends. The mixing of hot and cold volumes of water is thus minimal.
Rock and water/rock	Rock is an inexpensive TES material from the standpoint of cost, but its volumetric thermal capacity is much less than that of water. Rock-bed and water storage types can both be utilized in many ways. For example, they may be used in conjunction with heat pumps to improve efficiency of heat recovery, or with more elaborate heat exchangers, or in conjunction with each other.
Aquifer thermal energy storage	The material in an aquifer is highly permeable to water, and the boundary layer consists of more impermeable materials such as clay or rock. Water from precipitation continuously seeps down to an aquifer and flows slowly through it until finally reaching a lake or the sea. Aquifers are often used as fresh water sources. Aquifers often have large volumes, often exceeding millions of cubic meters, and as they consist of about 25% of water they have a high-TES capacity. When heat extraction and charging performances are good, high heating and cooling powers can be achieved.
Solar ponds	A salinity gradient solar pond is an integral collection and storage device of solar energy. In the solar pond technology, salt is dissolved into the bottom layer, making it too heavy to rise to the surface, even when hot. The salt concentration increases with depth, thereby forming a salinity gradient. The sunlight that reaches the bottom of the pond remains entrapped there. The useful thermal energy is then withdrawn from the solar pond as hot brine.

The temperature at which the energy is held in part determines the potential application. Examples of TESs are storage of solar energy for nighttime and weekend use, of summer heat for winter space heating, and of ice from winter for space cooling in summer.

In terms of storage media, a wide variety of choices exist depending on the temperature range and application. For sensible heat storage, water is a common choice because, among its other positive attributes, it has one of the highest specific heats of any liquid at ambient temperatures. While the specific heat of water is not as high as that for many solids, it has the advantage of being a liquid that can easily be pumped to transport thermal energy. Being a liquid, water also allows good heat

Table 11.7 Summary of latent thermal storage technologies

Name of the technology	Description
Phase change material	Is applicable for both hot and cold storage and involves the use of a phase change material that releases heat by solidifying and stores heat by melting. There are a large number of storage materials for heating applications (e.g., naphthalene) or cooling (e.g., ice and eutectic salts).
Ice slurry	Refers to a mixture of ice crystals and liquid. The liquid in question is usually an antifreeze solution of water and a freezing point depressant such as ethylene glycol.
Ice on coil	This is an easy-to-operate, yet low-cost system that typically comes in two types: internal and external melt. Internal melt systems use a subcooled brine solution, most likely a refrigerant running in a vapor-compression refrigeration cycle, which runs through coils immersed in a tub of water. External melt systems employ the same procedure for freezing the water, but during discharge periods the ice is melted from outside the coils.
Encapsulated ice	The water is packed into capsules, which in turn are packed into a storage tank. A heat transfer fluid can then be run through the storage tank when heat extraction or input is desired. The simplicity in design in this case occurs where the capsules are mass-produced and used to fill any sized storage tank to meet any cooling load requirements.

transfer rates. Solids have the advantage of higher specific heat capacities, which allow for more compact storage units. For higher temperature applications, such as for preheating furnace air supplies, solids become the preferred sensible heat store. Usually, refractory materials are used as the storage material for high temperature. If the storage medium needs to be pumped, liquid metals are often used.

A TES system using latent heat changes has received a great deal of interest. The most common example of latent heat storage is the conversion of water into ice. Cooling systems incorporating ice storage have a distinct size advantage over equivalent-capacity chilled-water units because of the relatively large amount of energy that is stored through the phase change. Size is the major advantage of latent heat thermal storage. For aerospace applications, lithium fluoride salts are used to store heat in the zero-gravity environment of the space shuttle. Another interesting development is the use of phase change materials in wall paneling. These panels incorporate compounds that undergo solid-to-solid structural phase changes. With the right choice of material, the phase change occurs at ambient temperature. These materials act as high-density heat sinks/sources that resist changes in ambient room temperature (Table 11.7).

11.6.4.1 Analysis of TES Systems

The overall energy balance for a thermal energy system can be calculated as energy input minus energy recovered minus energy loss, which is equal to energy accumulation into the storage device. Using total enthalpies, $H_a = mh_a$—the enthalpy of the heat transfer fluid that charges the storage device—where m is the total mass of

heat transfer fluid circulated during the charging time, H_b is the enthalpy of the heat transfer fluid leaving the storage during charging, H_c and H_d are the enthalpies of the heat transfer fluid during discharging, and so the energy balance can be determined as follows:

$$(H_a - H_b) - [(H_c - H_d) + Q_{loss}] = \Delta E_{accumulated}. \tag{11.26}$$

Similarly, one can write the exergy balance equation as follows (see Dincer and Rosen 2007):

$$(Ex_a - Ex_b) - [(Ex_c - Ex_d) + Ex_{loss}] - I = \Delta Ex_{accumulated}, \tag{11.27}$$

where Ex_{loss} is exergy loss through thermal insulation, I is the exergy destroyed, and $\Delta Ex_{accumulated}$ is the exergy accumulated by the system.

The energy and exergy efficiencies defined in terms of retrieved output over the input during the charging period can be expressed as

$$\eta = \frac{H_c - H_d}{H_a - H_b} = 1 - \frac{Q_{loss}}{H_a - H_b} \tag{11.28}$$

and

$$\psi = \frac{Ex_c - Ex_d}{Ex_a - Ex_b} = 1 - \frac{Ex_{loss} + I}{Ex_a - Ex_b}. \tag{11.29}$$

Note that if the TES device is kept adiabatic ($Ex_{loss} = 0$), then the exergy efficiency becomes

$$\psi = 1 - \frac{I}{Ex_a - Ex_b}. \tag{11.30}$$

More detailed exergy analysis can be performed by studying separately the charging and discharging periods. Examples of detailed exergy analysis of thermal energy systems can be found in Dincer and Rosen (2002, 2007) and MacPhee and Dincer (2009). The exergy analysis identifies the methods of, and the amounts for, system improvements.

11.7 Case Studies: New Energy Storage Systems and Applications

Here are two case studies regarding the design of energy storage devices. The first study addresses sensible thermal storage in earth, and the second addresses cold storage in an advanced tree-shaped ice-on-tube tank. In both cases, we show that there is an optimal design configuration that satisfies the design requirements.

11.7.1 Energy and Exergy Efficiencies of a Sensible Heat Thermal Storage System

1. Consider two sensible TES systems, X and Y, in surrounding environments with a temperature of 25°C. Each one receives 104,650 kJ of heat from a stream of 500 kg of water, which is cooled from 80° to 30°C. Therefore, the heat input to the storage during the charging period for each storage unit is
$Q_{\mathrm{i}} = m_{\mathrm{i}} c_{\mathrm{p}} \Delta T = 500 \times 4.186 \times (80 - 30) = 104,650\,\mathrm{kJ}.$

For system X:
After 1 day, the heat of 94,185 kJ is recovered during the discharging period from storage system X by a stream of 4,500 kg of water being heated from 30° to 35°C. That is,
$Q_0 = m_0 c_{\mathrm{p}} \Delta T = 4,500 \times 4.186 \times (35 - 30) = 94,185\,\mathrm{kJ}.$
Therefore, the energy efficiency for TES system X becomes
$\eta_X = Q_{\mathrm{o}}/Q_{\mathrm{i}} = 94,185/104,650 = 0.90.$
The heat ejection to the surroundings during storage is
$Q_{\mathrm{r}} = Q_{\mathrm{i}} - Q_{\mathrm{o}} = 104,650 - 94,185 = 10,465\,\mathrm{kJ}.$

For system Y:
The heat recovered during discharging, the energy efficiency, and the heat rejection to the surrounding can be evaluated in a similar way. This system stores the heat for 90 days, after which an energy quantity of 94,185 kJ is recovered during the discharging period by heating a stream of 500 kg of water from 30° to 75°C, with the resulting energy efficiency of the storage cycle as follows:
$Q_0 = m_0 c_{\mathrm{p}} \Delta T = 500 \times 4.186 \times (75 - 30) = 94,185\,\mathrm{kJ}.$
Thus, the energy efficiency for TES system Y is found to be the same as for storage X:
$\eta_Y = Q_0/Q_{\mathrm{i}} = 94,185/104,650 = 0.90.$
The value of heat rejection to the surroundings during storage is
$Q_{\mathrm{r}} = Q_{\mathrm{i}} - Q_0 = 104,650 - 94,185 = 10,465\,\mathrm{kJ}.$
It is useful to mention that the ability of storing sensible heat in a given tank (or container) strongly depends at the same time on the value of ρc_{p} for the material. As a result, both storage systems have the same energy efficiency when calculated by considering the first law of thermodynamics, but storage system Y, which stores the heat for 90 days rather than 1 day, and which returns the heat at the much more useful temperature of 75°C rather than 35°C, gives a considerably higher performance. It is clear that a more perceptive measure of comparison than that provided by the energy efficiency of the storage cycle is needed if the true usefulness of a TES is to be assessed and a rational basis for the optimization of its economic value is to be established. Therefore, it is necessary to introduce the term *exergy efficiency*, which is a measure of the effectiveness of the TES system. Efficiency is simply defined as the percentage of the total energy stored in a system that can be recovered by ignoring the quality

(availability) of the recovered energy, and so cannot provide a measure of ideal performance, as mentioned earlier. It is obvious that the exergy efficiency definition provides a better measure.

2. Consider the aforementioned example of sensible TES systems X and Y. For the corresponding cases, an exergy analysis is conducted below. The exergy change during the charging period can be obtained as
$A_i = m_j c_p[(T_1 - T_2) - T_0(\ln(T_1/T_2))]$
$= 500 \times 4.186 \times [(353 - 303) - 298 \times (\ln(353/303))] = 9,386\,\text{kJ}.$

For system X:
The exergy change during the discharging period can be calculated as follows:
$A_0 = m_0 c_p[(T_1 - T_2) - T_0(\ln(T_1/T_2))]$
$= 4,500 \times 4.186 \times [(308 - 303) - 298 \times (\ln(308/303))] = 2,310\,\text{kJ}.$
Therefore, the exergy efficiency for storage X becomes
$\psi_X = A_0/A_i = 2,310.18/9,386.88 = 0.25.$

For system Y:
As mentioned earlier, heat is recovered from the storage after 90 days by a stream of 500 kg of water entering at 30°C and leaving at 75°C. The exergy change and efficiency of storage Y can be obtained as follows:
$A_0 = m_0 c_p[(T_1 - T_2) - T_0(\ln(T_1/T_2))]$
$= 500 \times 4.186 \times [(348 - 303) - 298 \times (\ln(348/303))] = 7,819\,\text{kJ}$
$\psi_Y = A_0/A_i = 7,819.52/9,386.88 = 0.83.$
As a result, it can be seen in the example that for both storage systems, the energy efficiencies are the same, 90%, despite having two different storage periods. This means that the first law of thermodynamics is not sufficient to distinguish these two TES systems running for two different storage periods. This requirement brings exergy to the forefront as a more capable tool. So, the distinction can easily be made between the two storage systems (X and Y) by using exergy analysis, resulting in two different exergy efficiencies: 25% for system X and 83% for system Y. This is due to the fact that Y has an advantage over X because of the higher temperature, and therefore greater availability of its recoverable heat. This example offers some practical illustrations of the abstract concepts discussed before and highlights the importance of understanding and considering the exergy, rather than the energy, as the exergy is a more effective and more efficient tool for the performance analysis of TES systems. Consequently, some intuitive advantages of exergy analysis can be listed as follows:

1. It provides a better accounting of the loss of availability of heat in TES systems using conservation of mass and energy principles together with the second law of thermodynamics for the goals of design and analysis.
2. It gives more meaningful and useful information than energy analysis regarding the efficiency, losses, and performance of TES systems.
3. It correctly reflects the thermodynamic and economic values of the operation of TES systems.
4. It is an efficient technique revealing whether or not and by how much it is possible to design more efficient TES systems by reducing the inefficiencies in the existing units.

11.7.2 Efficiency of a Cold Storage System

In this illustrative example, a TES system for cooling capacity is considered (for details, see Rosen et al. 2000). The system is designed in such a way that the chiller operates continuously during the design day and utilizes three operating modes:

- *Charging*. The charging mode is the normal operating mode during no-load periods. The chiller cools the antifreeze solution to approximately −4°C. The antifreeze solution flows through the storage module, causing the liquid water inside the encapsulated units to freeze. The temperature of the circulating fluid increases (to a limit of 0°C) and returns to the chiller to be cooled again. During charging, the building loop is isolated so that full flow is achieved through the storage module.
- *Chilling*. The chilling mode is the same as for a nonstorage (conventional) chiller system. In this mode, the storage module is already completely charged, and the entire building load is met directly by the chiller. The chiller operates at a warmer set point than for ice making, which results in an increased capacity and a higher coefficient of performance (COP). In this mode, there is no flow through the storage module, and ice is kept in reserve for use later in the day.
- *Chilling and discharging*. Chilling and discharging is the normal operating mode during daytime hours. The chiller and storage modules share the cooling load, normally in a series configuration. When the heat transfer fluid passes through the chiller last, the storage module precools the building-return fluid before it is cooled to the design supply temperature by the chiller. Systems are normally designed with the chiller downstream of the storage. This sequence gives a higher effective storage capacity since the exit temperature from the storage can be higher. The ice melting rate is controlled by modulating valves, which cause some flow to bypass the storage module, usually set so that the blended fluid temperature downstream of the storage is held constant throughout the discharge cycle.

The cooling load of a typical office building and data for the case of a full 24-hour cycle are considered. The TES module has nonadiabatic storage boundaries with a total thermal resistance of 1.98 m^2 K/W. Work interactions and kinetic and potential energy terms are considered negligibly small. The specific heat of the heat transfer fluid (a glycol-based antifreeze solution) is 3,224.0 J/kg K at −6.6°C and 3,600.8 J/kg K at 15.5°C, and the specific gravity is 1.13. The storage fluid (deionized water) has a freezing point of 0°C, a mass of 144,022 kg, and a density of 1,000 kg/m^3. The storage module has a volume of 181.8 m^3, with 144.0 m^3 occupied by the storage fluid, and a surface area A of 241.6 m^2. The reference environment conditions are 20°C and 1 atm.

The overall energy and exergy efficiencies are 99.5% and 50.9%, respectively. The hourly exergy efficiencies range from 80% to 94% and average 86% for the overall charging period, range from 53% to 66% and average 60% for the overall discharging period, and range from 99% to 100% for the overall storing period. The hourly energy efficiencies exceed 99% for all periods.

The energy efficiencies are high since they only account for heat gains from the environment, which are small. The exergy efficiencies are much lower since they account for the "usefulness" of the energy, which is related to the inlet and outlet temperatures and the mass flow rates of heat transfer fluid. In the example, the charging fluid being at −4°C, a much lower temperature than that of the environment, is a high-quality cold flow. The cold flow recovered during discharging, however, is of much lower quality as its temperature is now much closer to the environment temperature. Thus, the energy efficiencies, for each hour or for the entire cycle, are misleadingly high as they only account for energy recovery but neglect entirely the loss of quality of the flows. This quality loss is quantifiable with exergy analysis.

The energy efficiency for a TES merely represents the ratio of useful energy output to total energy input. However, the exergy efficiency incorporates the notion of increasing thermodynamic unavailability, as reflected by increasing entropy, in a process or subprocess. That is, since the irreversibilities in a TES process destroy some of the input exergy, TES exergy efficiencies are always lower than the corresponding energy efficiencies.

Another interesting observation stems from the fact that exergy efficiencies provide a measure of how nearly a process approaches ideality, while energy efficiencies do not. The energy efficiencies being over 99% here for the overall process and all subperiods implies that the TES system is nearly ideal, when this in fact is not the case. The overall exergy efficiency of approximately 51%, as well as the subprocess exergy efficiencies, points out that the TES system is far from ideal and that there exists a significant margin for efficiency improvement. In this example, the same cooling capacity could be delivered from the TES using about half of the input exergy if the TES was ideal. Thus, overall electrical use by the chillers could be greatly reduced while still maintaining the same cooling services. Such a reduction would reduce the necessary installed cooling power and electrical costs. There are two further implications of the results:

- The fact that the exergy efficiencies are less than 100% implies that a mismatch exists between the quality of the thermal energy delivered by the TES (and required by the cooling load) and the quality of the thermal energy input to the TES. This mismatch, which is detectable through the temperature of the thermal energy flows across the TES boundaries, is quantifiable with exergy analysis as the work potential is lost during the storage process. The exergy loss, therefore, correlates directly with an additional use of electricity by the chillers than would occur without the exergy loss. When exergy efficiencies are 100%, there is no loss in temperature during storage.
- The nonideal exergy efficiencies imply that excessively high-quality thermal energy is supplied to the TES, higher than is required by the cooling load. Thus, exergy analysis indicates that lower quality sources of thermal energy could be used to meet the cooling load. Although economic and other factors must be taken into account when selecting energy resources, the exergy-based results presented here can assist in identifying feasible energy sources that have other desired characteristics (e.g., environmentally benign or abundant).

It is clear that a more appropriate measure of comparison than that provided by the energy efficiency of the storage cycle is needed if the true usefulness of a TES is to be assessed and a rational basis for the optimization of its economic value is to be established. The efficiency is simply defined as the percentage of the total energy stored in a system that can be recovered by ignoring the quality (exergy) of the recovered energy, and so it cannot provide a measure of ideal performance. It is necessary to consider exergy efficiencies in order to have more comprehensive and useful efficiency measures for practical TES systems and to facilitate more rational comparisons of different systems. The results presented here suggest that exergy analysis would be useful in comparing different alternative thermal storage system configurations. In addition, exergy analysis could assist in the optimization of TES systems when combined with the assessments of other factors, such as resource-use reductions, decreases in environmental impact and emissions, and economics.

11.7.3 Fundamental Optimal Configuration for Underground Thermal Storage

Consider, as shown in Fig. 11.16a, a tube that is surrounded by an "infinite" solid medium at a constant temperature. The objective of the design is to maximize the heat transfer rate during charging and discharging periods, thus minimizing the irreversibility. According to Vargas et al. (2005), the energy balance and heat transfer equations can be written as follows:

$$\begin{cases} \dot{Q} = \dot{m} c_{\mathrm{p}} T_{\infty} (\theta_{\mathrm{in}} - \theta_{\mathrm{out}}), \\ \dot{Q} = U A_{\mathrm{L}} T_{\infty} \dfrac{\theta_{\mathrm{in}} - \theta_{\mathrm{out}}}{\ln(\theta_{\mathrm{in}} - 1/\theta_{\mathrm{out}} - 1)}, \end{cases} \tag{11.31}$$

where $\theta_{\mathrm{i}} = T_{\mathrm{i}}/T_{\infty}$ defines the dimensionless temperature.

The pressure drop across the tube and the associated pumping power are derived for a steady flow:

$$\begin{cases} \Delta P = 2f \dfrac{L}{D} \rho V^2, \\ \dot{W} = \dfrac{\dot{m} \Delta P}{\rho} = \text{fixed value}, \end{cases} \tag{11.32}$$

where f is the friction factor, and D and L are the pipe diameter and length, respectively.

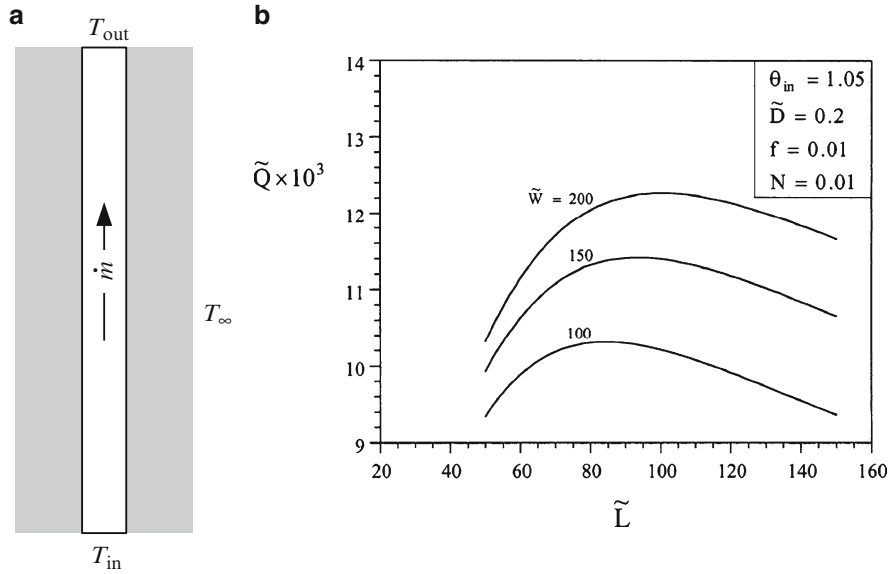

Heat transfer model Maximization of the extracted heat

Fig. 11.16 Optimal design parameters of earth to fluid heat storage devices: (**a**) heat transfer model and (**b**) maximization of the extracted heat [modified from Vargas et al. (2005)]

We introduce a reference length L_{ref} and a reference mass flow rate $\dot{m}_{ref}$, with the help of which one can express the pumping power $\dot{W}$ derived in Eq. (11.32) in the following dimensionless form:

$$\tilde{W} = \frac{\psi^3 32}{\pi^2} f \frac{\tilde{L}}{\tilde{D}^5}, \tag{11.33}$$

where $(\tilde{L}, \tilde{D}) = (L, D)/L_{ref}$ and $\psi = \dot{m}/\dot{m}_{ref}$.

With the notations $N = UL_{ref}^2/\dot{m}_{ref}c_p$, $B_1 = (32\pi f/\tilde{D}^2)^{0.5}$, $B_2 = (\pi^2\tilde{D}^5/32f)^{1/3}$, and $\tilde{Q} = \dot{Q}/(\dot{m}_{ref}c_pT_\infty)$, the expression that allows for the optimization of the tube length for obtaining a maximum heat transfer rate is given as follows:

$$\begin{cases} \theta_{out} = (\theta_{in} - 1)/\exp\left(NB_1\tilde{W}^{-\frac{1}{3}}\tilde{L}^{\frac{4}{3}}\right) + 1, \\ \tilde{Q} = B_2\left(\dfrac{\tilde{W}}{\tilde{L}}\right)^{\frac{1}{3}}(\theta_{in} - 1)\left[1 - \exp\left(-NB_1\tilde{W}^{-\frac{1}{3}}\tilde{L}^{\frac{4}{3}}\right)\right]. \end{cases} \tag{11.34}$$

The fact that an optimum tube length does exist is explained as follows:

- If the tube is small, then the heat transfer rate is small because in this case the heat transfer area tends to zero.
- If the tube is long, then the pressure drop is high; and in order to maintain the fixed pumping power imposed by Eq. (11.33), the mass flow rate must tend to zero; thus the heat transfer rate also tends to zero.

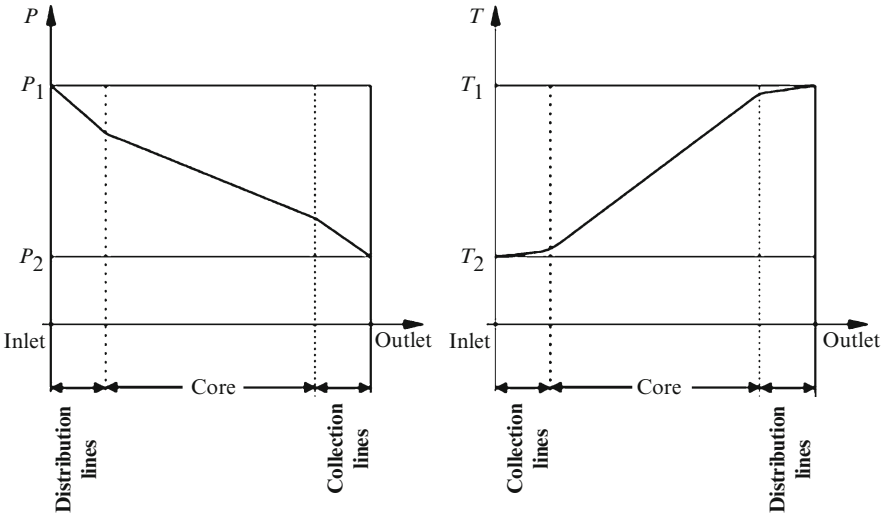

Fig. 11.17 Pressure and temperature distributions at charging of a thermal storage device

In between the two extremes, there is a tube length that maximizes the heat transfer rate. For fixed operating conditions $(\tilde{W}, \theta_{\text{in}}) = \text{fixed}$, one can obtain an analytical expression for the dimensionless optimal length, namely

$$\tilde{L}_{\text{opt}} = 1.89 N^{-(3/4)} \left(\frac{\tilde{D}^2}{32\pi f} \right)^{0.25} \tilde{W}^{0.25}. \tag{11.35}$$

The existence of the optimum length can be observed in Fig. 11.16b that shows the variation of the dimensionless heat transfer rate with the dimensionless tube length for several fixed pumping powers. This theoretical result is important because it demonstrates that when designing an energy storage device, the geometrical configuration plays a crucial role in reducing the irreversibilities and the associated charging and discharging rates. For the case discussed here, it turns out that the thermal storage device must comprise a bundle of tubes of optimized lengths. Additional optimization opportunities do exist when designing the distribution network that serves each tube. The thermal storage device acts as a multiscale heat exchanger tuning the charging and discharging periods to allow for the fastest and most uniform charging/discharging process possible. Conceptually, such a multiscale heat exchanger shows a temperature and pressure variation as indicated in Fig. 11.17.

The configuration of the storage device eventually looks like the tree-shaped geometry indicated in Fig. 11.15. The distribution lines spread the heat transfer fluid throughout the volume, to reach each elemental energy storage cell. The collection lines collect the "used" heat transfer fluid after it does its "job" to charge each element of storage. The design from the next examples focuses more on the geometric design including the distribution lines.

11.7.4 Constructal Tree-Shaped Cold Storage Device

In this example, taken from Zamfirescu and Bejan (2005), we illustrate the application of the constructal theory to design a cold storage device. In the beginning, the geometry of the cold storage is not known, but based on previous results of constructal design one may guess that it looks like a tree-shaped structure as the one illustrated in Fig. 11.15. We consider here the ice-on-tube storage case and impose the following constraints on the design:

$$\begin{cases} \dfrac{V_{\text{ice}}}{V_{\text{tank}}}, \text{ to be maximized,} \\ \text{Material of the tubes is fixed, } A = 2\pi \sum (r_i L_i), \\ \text{Fixed temperature drop, } T_2 - T_1 \le \Delta T_{\max}, \\ \text{Fixed pressure drop, } P_1 - P_2 \le \Delta P_{\max}, \\ \text{Fixed temperature drop between the ice and coolant inlet, } T_0 - T_1 = \Delta T_{0f}, \end{cases} \tag{11.36}$$

where 1 and 2 are the indexes of the inlet and outlet port of the cold storage system.

According to constructal design, the process of designing proceeds with optimization at the smallest design scales and continues with larger and more complex scales. The simplest elemental volume to imagine is in the form of a plate channel (the tube has narrow rectangular cross-section) illustrated in Fig. 11.18. The geometry and the temperature distribution are shown in Fig. 11.18a for the charging phase, and the configuration during the discharging (melting) phase is presented in Fig. 11.19b. The design challenge is to find the element shape (L/H) that maximizes the ice produced per unit volume during a given charging time, t_{ch}.

The energy conservation within the ice layer and the fluid requires that

$$\begin{cases} q = -h_{\text{LS}} \dfrac{\mathrm{d}m_{\text{ice}}}{\mathrm{d}t} = -k_{\text{ice}} \left(\dfrac{\mathrm{d}T}{\mathrm{d}y} \right)_{\delta} LW, \\ q = 4WHc_{\text{p,c}} \left(\dfrac{2\rho_{\text{c}} H \Delta P}{fL} \right)^{0.5} (T_{\text{e}} - T_{\text{i}}), \end{cases} \tag{11.37}$$

where h_{LS} is the latent heat of ice, k_{ice} is the thermal conductivity of ice, $m_{\text{ice}} = LW\delta_{\text{ice}}$ is the formed mass of ice, $c_{\text{p,c}}$ is the specific heat of coolant, and the mass flow rate of coolant is expressed as a function of the pressure drop ΔP with the help of the friction factor f, namely

$$\dot{m} = 4WH \left(\frac{2\rho_{\text{c}} H \Delta P}{fL} \right)^{0.5} \tag{11.38}$$

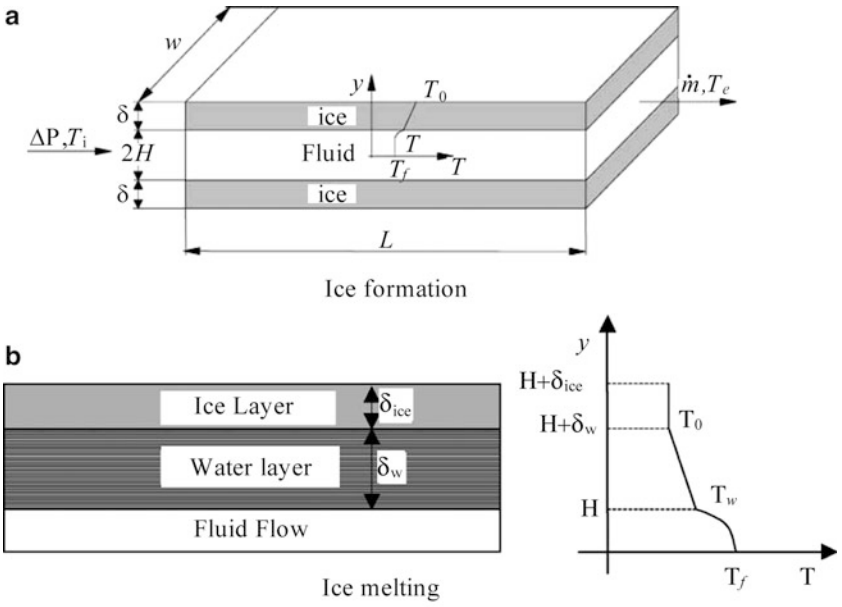

Fig. 11.18 Ice formation and melting in narrow tubes: (**a**) model for ice formation, and (**b**) model for ice melting [modified from Zamfirescu and Bejan (2005)]

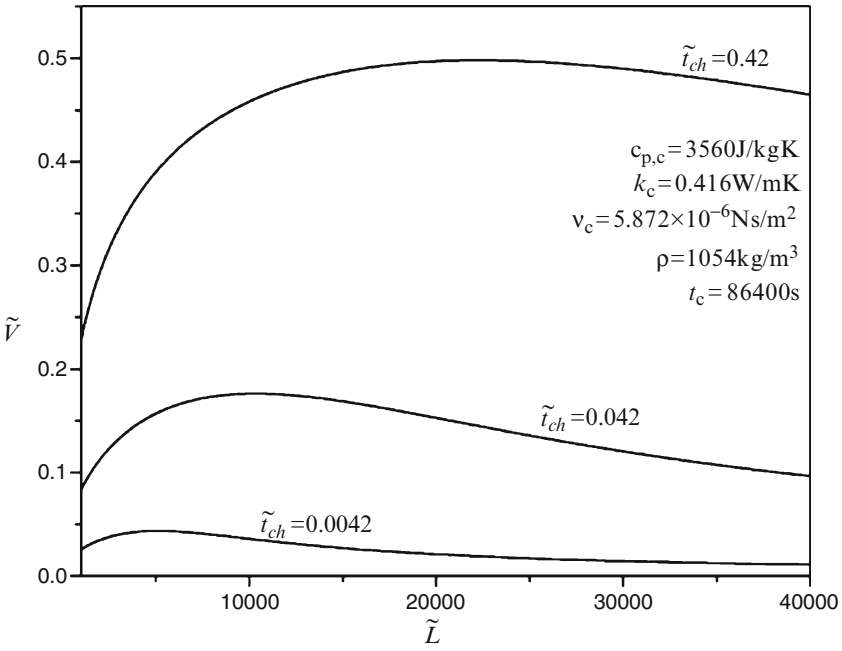

Fig. 11.19 Volumetric specific production of ice on narrow channel [modified from Zamfirescu and Bejan (2005)]

The condition at the ice–water interface is expressed in terms of continuity of the heat flux according to:

$$\left(\frac{\mathrm{d}T}{\mathrm{d}y}\right)_{\delta,\text{upper}} = \left(\frac{\mathrm{d}T}{\mathrm{d}y}\right)_{\delta,\text{lower}} = \frac{T_0 - T_\text{w}}{\delta}. \tag{11.39}$$

The heat transfer on the fluid side can be expressed based on the heat transfer coefficient h and the logarithmic temperature difference between the wall—assumed at the uniform temperature T_w—and the fluid with temperature T_i at the entrance and T_e at the exit:

$$q = 2hLW \frac{T_\text{e} - T_\text{i}}{\ln((T_\text{w} - T_\text{i})/(T_\text{w} - T_\text{e}))}. \tag{11.40}$$

Equations (11.37) to (11.39) form an algebraic system with an analytical solution for T_e, T_w, q with all other parameters having imposed values. One can study the influence of the ice layer thickness, because the system of equations has a solution of the form

$$q(\delta) = \frac{a_1}{a_2 + a_3\delta}, \tag{11.41}$$

where a_i are the coefficients depending on the thermodynamic properties and geometrical characteristics, which for brevity are not given here. By inserting the result from Eq. (11.41) in the interface condition Eq. (11.39), one can obtain the following first-order differential equation for ice thickness variation in time, $\delta(t)$:

$$\frac{\mathrm{d}\delta}{\mathrm{d}t} = \frac{1}{h_\text{LS}\rho_\text{ice}LW} \times \frac{a_1}{a_2 + a_3\delta}, \tag{11.42}$$

which can be integrated with the initial condition $\delta(0) = 0$ and has the following solution:

$$\begin{cases} \delta(t) = -C + \sqrt{C^2 + 2C_2(T_0 - T_\text{i})t}, \\ C = C_1\tilde{L}^{1.5}\dfrac{\exp\left(C_3\tilde{L}^{1.5}\right)}{\exp\left(C_3\tilde{L}^{1.5}\right) - 1}, \\ C_1 = \dfrac{k_\text{ice}}{2c_\text{p,c}}\sqrt{\dfrac{f}{2\rho_\text{c}\Delta P}}, \\ C_2 = \dfrac{2k_\text{ice}}{h_\text{LS}\rho_\text{ice}}, \\ C_3 = \dfrac{h}{2c_\text{p,c}}\sqrt{\dfrac{f}{2\rho_\text{c}\Delta P}}, \end{cases} \tag{11.43}$$

where $\tilde{L} = L/H$ is the aspect ratio of the channel.

The analytical solution expressed by Eq. (11.43) is plotted for proprieties of ice and coolant (ethylene–glycol–water at 30% concentration and at $-20°C$) is assumed to be constant. The volume of the element of storage, shown in Fig. 11.18a, is also assumed constant: $A = LH$, fixed. The plot shows the variation of the ice fraction per unit of volume $\tilde{V} = V_{\text{ice}}/V = \delta/(H + \delta)$ versus $\tilde{L}$ for three dimensionless charging times, $\tilde{t}_{\text{ch}} = t_{\text{ch}}/t_{\text{c}}$, where t_{ch} is the dimensional charging time of the storage and t_{c} is the storage cycle period.

If the element tube is long, then because of the constrained volume the height H must be short; therefore, due to the fixed pressure constraint, the mass flow rate of coolant is small, and the cooling rate is reduced and so is the ice production $\tilde{V}$. If the tube is short, the height is large and therefore the pressure drop constraint produces a large mass flow rate of coolant. Consequently, the temperature drop on the coolant side is reduced, which means again a reduced cooling rate and ice production. The conclusion is that there must be an optimal length of channel (or an optimal aspect ratio) that maximizes the ice production $\tilde{V}$; the existence of this optimum is demonstrated by the result shown in Fig. 11.19.

During the discharge process, the ice is melted in the vicinity of the channel in the manner suggested in Fig. 11.18b. The heat flux continuity condition at the ice–water interface can be written in a more general form than Eq. (11.39), namely

$$\pm\, k(T_0 - T_{\text{w}})\mathrm{d}t = h_{\text{LS}}\rho \mathrm{d}(\delta), \tag{11.44}$$

where (δ, k) denotes either $(\delta_{\text{ice}}, k_{\text{ice}})$ from Fig. 11.19a or $(\delta_{\text{w}}, k_{\text{w}})$ from Fig. 11.19b and the "+" sign refers to the charging while the "−" sign refers to the discharging periods, respectively. Equation (11.44) can be integrated in the limit of small δ when it is reasonable to assume that T_{w} remains constant. By integration, one can obtain the driving temperature differences between charging (index "ch") and discharging (index "dsch") periods as follows:

$$\begin{cases} (T_0 - T_{\text{w}})_{\text{ch}} = \dfrac{h_{\text{LS}}\rho_{\text{ice}}\delta_{\text{ice}}^2}{2k_{\text{ice}}t_{\text{ch}}}, \\ (T_{\text{w}} - T_0)_{\text{dsch}} = \dfrac{h_{\text{LS}}\rho_{\text{w}}\delta_{\text{W}}^2}{2k_{\text{w}}t_{\text{dsch}}}. \end{cases} \tag{11.45}$$

Equation (11.45) can be divided to obtain the first estimate of the ratio of driving temperature differences at charging and discharging of storage device, respectively. It becomes

$$\frac{(T_0 - T_{\text{w}})_{\text{ch}}}{(T_{\text{w}} - T_0)_{\text{dsch}}} = \frac{k_{\text{w}}\rho_{\text{ice}}t_{\text{dsch}}}{k_{\text{ice}}\rho_{\text{w}}t_{\text{ch}}}. \tag{11.46}$$

Equation (11.46) suggests the ways of tuning the charging and discharging times of the storage in accordance with an imposed storage strategy: the tuning can be done by adjusting the driving temperature differences. For example, if the

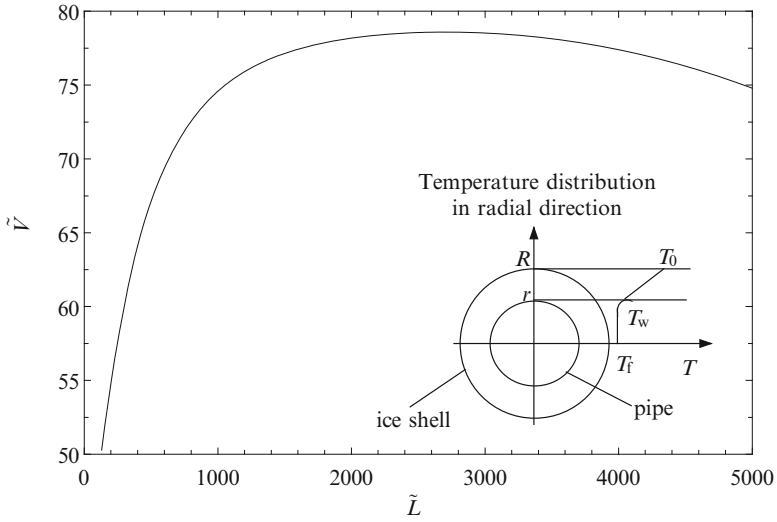

Fig. 11.20 Volumetric specific ice production on a single cylindrical tube [modified from Zamfirescu and Bejan (2005)]

temperature difference ratio between the charging and discharging processes is set to 0.56, the ratio of discharging and charging time periods becomes 2.

An increase of storage density can be obtained if instead of narrow channels one uses circular tubes, because circular cross sections transport the maximum amount of coolant per unit of volume. For the circular tube geometry, depicted in the corner of Fig. 11.20, the aspect ratio can be defined by $\tilde{L} = L/r$, where r is the tube radius and L is the tube length. The design constraint is $A = 2\pi rL$, which fixes both the amount of tube material and the amount of coolant. The objective of the design is to maximize the ice production per volume $\tilde{V} = 1 - (r/R)^2$, where R denotes the outer radius of the ice shell.

One can also constrain the flow at a given pressure difference, which translates mathematically into the following equation for the mass flow rate of coolant $\dot{m} = 4\pi\rho_c r^3/\Delta P(\rho_c f L)^{0.5}$. The energy balance can be written in the form equality of the following heat fluxes: (1) heat delivered by the coolant, (2) heat transferred by the wall to the coolant by convection, (3) heat transferred through the ice shell by conduction, and (4) heat flux at the water–ice interface. These fluxes can be written per unit of tube length q' as follows:

$$\begin{cases} q' = \dfrac{\pi r^2 c_{p,c}}{L(4\rho_c r/fL)^{0.5}(T_e - T_i)}, \\ q' = \dfrac{2\pi rh\,(T_e - T_i)}{\ln[(T_w - T_i)/(T_w - T_e)]}, \\ q' = \dfrac{2\pi k_{ice}(T_0 - T_w)}{\ln(R/r)}, \\ q' = 2\pi R\rho_{ice}h_{LS}\dfrac{dR}{dt}. \end{cases} \tag{11.47}$$

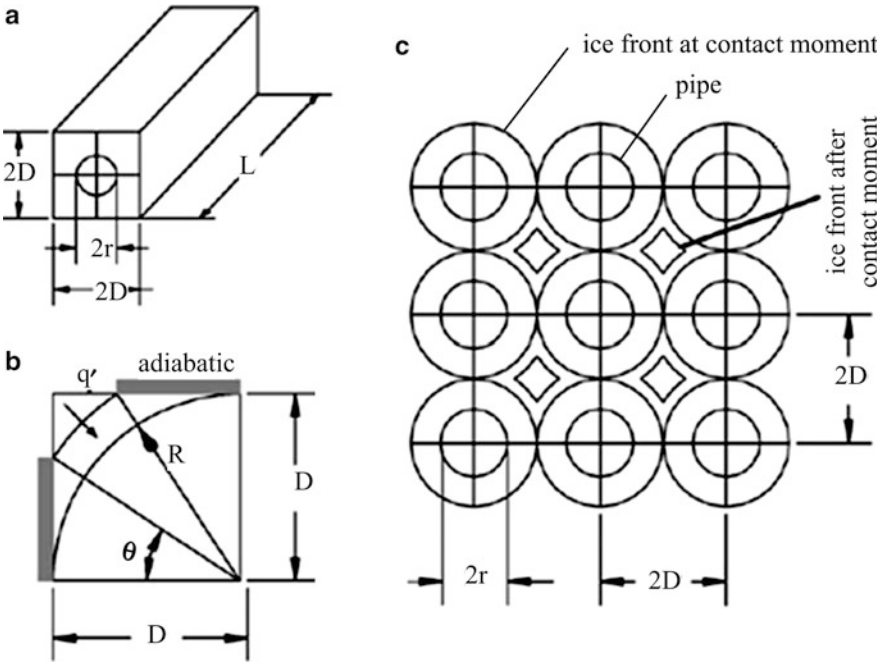

Fig. 11.21 Ice production on an array of cylindrical tubes: (**a**) ice element formed around a single tube, (**b**) detail of ice growing, and (**c**) tube array geometry [modified from Zamfirescu and Bejan (2005)]

For a differential algebraic system, Eq. (11.47) can be integrated by imposing the following initial condition: at $t = 0$ there is no ice shell, that is, $R = r$. Moreover, the radius of the shell at the end of the storage charging period, $t = t_{ch}$, is simply denoted as R.

After some mathematical manipulation, the system of four equations (11.47) reduces to one single algebraic equation that can be solved numerically to determine the volumetric specific ice fraction when all other parameters are known. The result is plotted in Fig. 11.20, which shows that there is an optimum aspect ratio $\tilde{L}$ of the tube that maximizes the ice production.

The maximum ice compactness in an ice-on-tube storage tank is obtained when the water freezes completely. Figure 11.21 shows the geometry of a tube array when water freezes around the tubes. There is a moment when neighboring ice shells touch each other, that is, when the ice shell diameter reaches a value equal to the distance between the tubes in the tube array, that is, $2D$. After this moment, the heat transfer at the ice–water interface starts to be constrained.

It is shown in Fig. 11.21b how the heat transfer area diminishes and adiabatic surfaces are formed between shells. Thus, the freezing process has two steps: In the first step, ice grows until the contact time t_{cnt}. In the second step, $t = t_{cnt} - t_{ch}$, the pocket of water entrapped between the shells freezes. The new

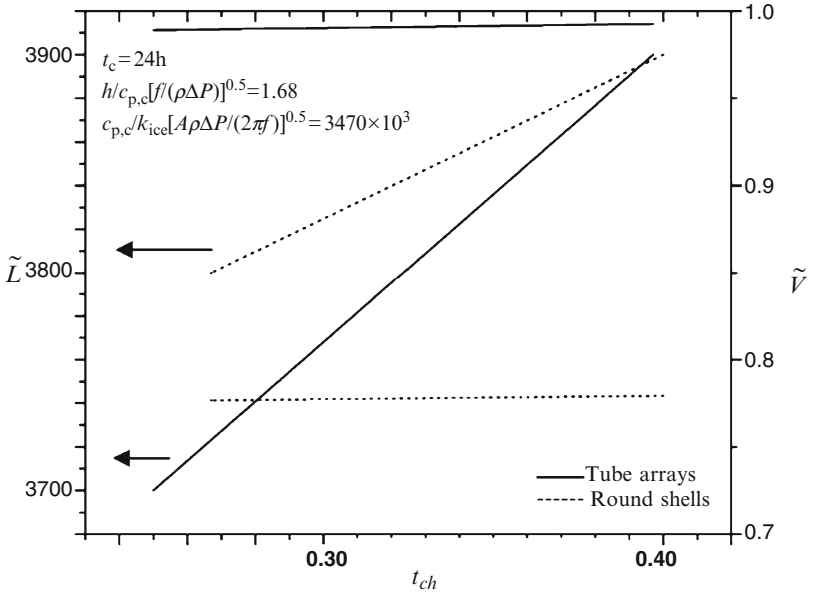

Fig. 11.22 Optimal geometrical configuration and the volumetric ice production on single cylindrical tubes and on cylindrical tube arrays [modified from Zamfirescu and Bejan (2005)]

design objective is to find the optimal aspect ratio $\tilde{L} = L/r$ of the element presented in Fig. 11.21c under the fixed tube material constraint $A = 2\pi RL$. For mathematical details regarding this design optimization, the reader is referred to the work by Zamfirescu and Bejan (2005). The result is shown in Fig. 11.22, which demonstrates that there is an optimal geometrical configuration of the storage device for any imposed charging time. On the same figure, the optimal aspect ratio for the ice-on-single-tubes configuration is presented. For the same charging time, the optimized single tubes are longer than the tube bank. From the figure, it is known that the compactness of tube array is 15% to 20%, which is higher than that of single tubes. Moreover, the volumetric ice production $\tilde{V}$ of the optimized configuration is less sensitive to the optimal geometry, which means that the design is robust: it can perform close to its maximum performance for a range of operating parameters, namely, $\tilde{t}_{ch}$ near the "design point."

11.8 Concluding Remarks

This chapter discussed the main energy storage methods and applications, and analyzed various issues regarding storage device design and optimization. We have also discussed the energy storage in various kinds of storable energies: electric field, electrochemical, thermochemical, chemical, thermal, and mechanical

(thermomechanical, kinetic, and potential). The specifics of all of them relate to different issues in physics, but eventually the aim is to pack as much energy as possible on a given volume and to be able to charge and discharge that volume at the desired times. In energy storage it is important to overcome the mismatch between energy supply and energy demand; thus, any energy storage analysis must start with the study of the supply and demand characteristics and must determine the proper storage strategy that fits the purpose. Ultimately, a design of the storage device must be elaborated so that it performs at the maximum efficiency possible. A constructal design approach can play a crucial role in identifying important design features and determining the best design and how the design configuration can be changed for better performance. Exergy analysis is a potential tool for determining the thermodynamic irreversibilities and identifying where/how the design of the device can be improved. Regardless of the nature of the stored energy, the design and analysis problems are similar.

Nomenclature

A	Area, m^2
C	Electric capacity, F
c_p	Specific heat, J/kg K
d	Distance, m
D	Diameter, m
E	Energy, J
Ex	Exergy, J
$\dot{E}x$	Exergy rate, W
d	Distance, m
f	Friction factor
H	Enthalpy, kJ or height, m
h	Specific enthalpy, J/kg, or heat transfer coefficient, W/m^2K
i	Electric current intensity, A
I	Maximum current intensity, A or moment of inertia, $kg{\cdot}m^2$
k	Thermal conductivity, W/mK
K	Flywheel constant
L	Length, m
LHV	Lower heating value, MJ/kg
m	Mass, kg
$\dot{m}$	Mass flow rate, kg/s
N	Number of heat transfer units
P	Pressure, bar
C	Electric capacity, F
q	Heat, kJ
$\dot{Q}$	Heat rate, W

R	Electric resistance, Ω
R, r	Radius, m
t	Time, m
T	Temperature, K
V	Volume, m^3, or velocity m/s or electric potential, V
W	Width, m or work, kJ
$\dot{W}$	Work rate, W
y	Coordinate, m

Greek Letters

δ	Thickness, m
ε	Electric permittivity, F/m
ξ	Friction factor
η	Energy efficiency
ψ	Exergy efficiency
ρ	Density, kg/m^3
σ	Tensile stress, N/m^2
τ	Time constant, s
θ	Dimensionless temperature
ω	Angular velocity, rad/s

Subscripts

∞	Surroundings
0	Initial
c	Charging or capacitor or coolant
ch	Charging
d	Destroyed
dsch	Discharging
e	Exterior
i	Interior
ice	Ice
in	Inner
inp	Input
L	Lateral
loss	Losses
LS	Melting
m	Per unit of mass
max	Maximum
opt	Optimal

out	Outer
R	Retrieved
ref	Reference
ret	Retrieved
s	System or storage or source
tot	Total
T	Total
w	Wall

References

Bejan A. 2000. Shape and Structure, from Engineering to Nature. Cambridge University Press, Cambridge, UK.

Dincer I., Rosen M.A. 2002. Thermal Energy Storage: Systems and Applications. John Wiley and Sons, West Sussex, UK.

Dincer I., Rosen M.A. 2007. Exergy, Environment and Sustainable Development. Elsevier, Oxford, UK.

Granowskii M. Dincer I., Rosen M.A., Pioro I. 2008. Thermodynamic analysis of the use a chemical heat pump to link a supercritical water-cooled nuclear reactor and a thermochemical water-splitting cycle for hydrogen production. *Journal of Power and Energy Systems* 2:756–767.

MacPhee D., Dincer I. 2009. Performance assessment of some ice TES systems. *International Journal of Thermal Sciences* 48:2288–2299.

Peters R. 2008. Storing renewable energy power. Pembia Institute for Appropriate Development, Drayton Valley, AB.

Rosen M.A., Dincer I., Pedinelli N. 2000. Thermodynamic performance of ice thermal energy storage systems. *ASME—Journal of Energy Resources Technology* 122:205–211.

Ter-Gazarian A. 1994. Energy Storage for Power Systems. Peter Peregrinus, Herts, UK.

Vargas J.V.C., Ordonez J.C., Zamfirescu C., Campos M.C., Bejan A. 2005. Optimal ground tube length for cooling of electronics shelters. *Heat Transfer Engineering* 26:8–20.

Yilanci A., Dincer I., Ozturk H.K. 2009. A review of solar-hydrogen/fuel cell hybrid energy systems for stationary applications. *Progress in Energy and Combustion Science* 35:231–244.

Zamfirescu C., Bejan A. 2005. Tree-shaped structures for cold storage. *International Journal of Refrigeration* 28:231–241.

Study Questions/Problems

11.1 Describe the role and the general layout of energy storage systems.

11.2 For an average house (three to four people), calculate the need for electrical energy storage in batteries if all electricity is supplied by photovoltaic cells.

11.3 Explain the features of energy demand.

11.4 List the main methods for energy storage.

11.5 Describe the principle of capacitors and the range of storage time in these devices.
11.6 Describe the principle of the flywheel and its optimal geometry.
11.7 Consider a system for compressed air storage from Fig. 11.9. Make reasonable assumptions and determine its efficiency.
11.8 Calculate the standard reaction heat for thermochemical energy storage according to the process described in Eq. (11.19).
11.9 Give a categorization of thermal energy storage systems.
11.10 Redo the analysis from Case Study 11.7.1 for a surrounding temperature of 35°C and cooling of water from 95° to 40°C.
11.11 Repeat the fundamental analysis from Section 11.7.3 and determine the maximum dimensionless heat transfer for a dimensionless tube length of 100, dimensionless fan power of 300, $\theta_{in} = 1.05$, $\tilde{D} = 0.25$, $f = 0.02$, and $N = 0.01$.
11.12 Repeat the fundamental analysis from Section 11.7.4 and determine the optimum dimensionless length of a charging time of 0.2 (dimensionless).

Chapter 12
Integrated Multigeneration Energy Systems

12.1 Introduction

Multigeneration, also called *polygeneration*, refers to energy systems that produce several useful outputs from one single or several kinds of primary energy input (viz. fuel). The purpose of multigeneration is to enhance the utilization of primary resources (fuels) and reduce the wasted energy. This is a method of improving the efficiency of energy generation processes for better sustainability. Less fuel is required to produce a given amount of electrical and thermal energy in a single unit than is needed to generate the same quantities of both types of energy with separate, conventional technologies (e.g., turbine-generator sets and steam boilers). Apart from generating "energy products" through a multigeneration system, one can also fabricate by-products with added value, such as carbon fibers and various chemicals.

Assume that one possesses a high-temperature thermal energy source (e.g., as obtained by fuel combustion or concentrated solar radiation). In a typical power generation application, the high-temperature heat is converted into work with heat engines. It is known from thermodynamics that only a part (limited by the Carnot factor) of the source heat can be converted into mechanical work, while the rest is wasted as low-temperature heat ejected into the environment. Therefore, the use of a primary energy source for generating one single product—power (or mechanical work)—is limited in terms of efficiency. The situation changes if the heat ejected by the heat engine is recovered and used for some purpose (e.g., space heating or water heating or industrial process heating). In such a case, the system cogenerates power and heat—two useful outputs from the primary energy (fuel) input. This is the simplest multigeneration system, known as cogeneration or a combined heat and power (CHP) system.

There are many possibilities for multigenerating valuable energy products from a single primary energy sources. Some examples are combined power and cooling; trigeneration of power cooling and heating; and multigeneration of hydrogen, oxygen, power, heating, cooling, and desalination. The multigeneration systems integrate several kinds of devices such as various kinds of heat engines, heat pumps, refrigeration units, and hydrogen production units, and desalination units. For example,

İ. Dinçer and C. Zamfirescu, *Sustainable Energy Systems and Applications*,
DOI 10.1007/978-0-387-95861-3_12,

gas turbines (GTs) can be integrated with solid oxide fuel cells to generate power and heating and enhance fuel utilization.

It is important to define the efficiency of multigeneration systems on a rational basis. But the difficulty comes from the fact that the outputs of the system are of several kinds. In order to determine the overall system output, it is not logical to simply add energies of different nature. For example, one cannot add electrical energy to thermal energy because their values are different: work is more valuable than heat. If heat and work are to be added, Carnot factors can be used for weighting the heat fluxes. Without recognizing the differences in these coproducts, as done by using associated exergy, possible improvements in the efficiency of cogeneration plants, or in their configuration within larger energy systems, can be missed; environmental benefits can also be wrongly interpreted. Furthermore, the attribution of costs and environmental emissions to the products of multigeneration systems is generally inappropriate when based on energy, as is commonly done, but it is appropriate, meaningful, and rational when it is based on exergy.

In this chapter, the theory of integrated multigeneration energy systems is reviewed with an emphasis on formulating the efficiency and the sustainability. The increase in efficiency and the corresponding decrease in fuel use by a multigeneration system, compared to other conventional processes for thermal, chemical, and electrical energy production, normally yield large reductions in greenhouse gas emissions. These reductions can be as large as 50% in some situations, while the same thermal and electrical services are provided. Several case studies are included.

12.2 System Integration

System integration in engineering entails combining several modules of subsystems into a larger system in which the subsystems work together to achieve better effectiveness or efficiency. There are many examples of system integration in energy technology:

- Cascading gas turbine cycles with bottoming Rankine cycles for improved efficiency of power generation
- Integrating a solid oxide fuel cell with gas turbine cycles for better fuel utilization and enhanced power production efficiency
- Using coal gasification coupled to gas turbine generators, again for better power generation efficiency
- Work recovery from the exhaust gas of vehicle engines to drive turbochargers and enhance the combustion process and fuel utilization for better propulsion efficiency

To elucidate the concept of integration, we present here a typical case from sustainable energy engineering, namely, the integration of a gas turbine cycle with solid oxide fuel cells (SOFCs). This topic has been extensively investigated as a mean of enhancing the thermodynamic efficiency of power production.

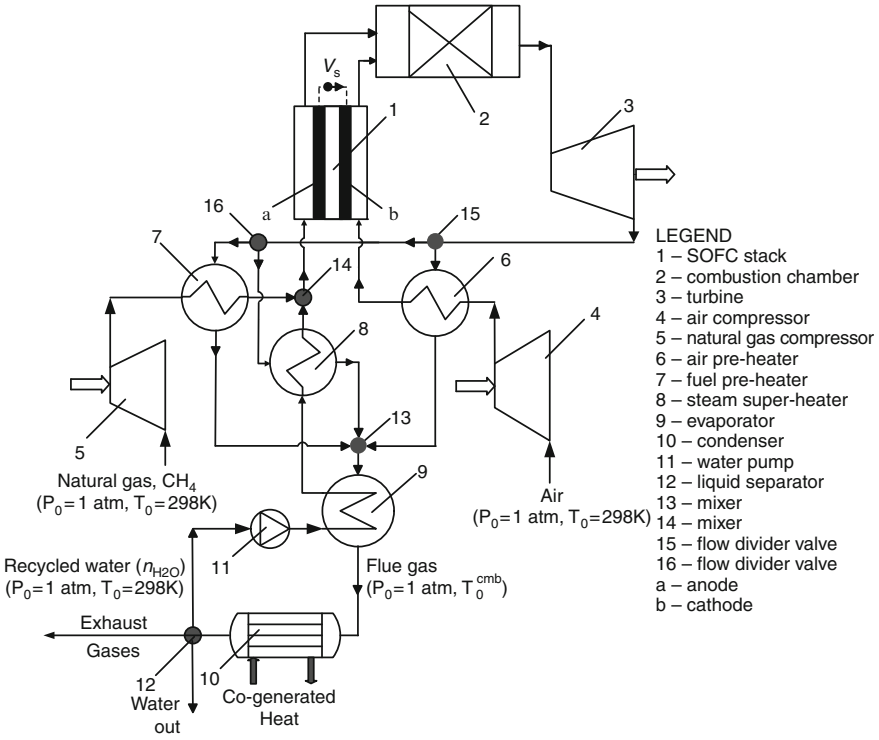

Fig. 12.1 Integrated SOFC–gas turbine cogeneration system with methane conversion [modified from Dincer et al. (2010)]

An interesting characteristic of SOFC is the application of yttrium-stabilized zirconia anodes that permit conversion on their surface of methane into synthesis gas (hydrogen and carbon monoxide). The synthesis gas is more efficient than natural gas (methane) as a fuel in gas turbines, and furthermore cascading SOFC with gas turbines allows for a very efficient fuel utilization. We present an integration scheme of gas turbines and SOFC for cogeneration of power and heat. The treated system is adapted from the one proposed by Granovskii et al. (2007, 2008) and Dincer et al. (2010) by modifying it to a cogeneration system. As mentioned in Dincer et al. (2010) SOFC–gas turbine cycles with cogeneration have the potential of achieving 66% utilization efficiency.

Figure 12.1 introduces the proposed system. As can be seen, the system generates three outputs: DC electric current by the fuel cell stack (label 1), shaft rotation power by the gas turbine (label 3), and low-temperature heat—used for heating purposes—by the steam condenser (label 10). Note that the figure shows the work inputs (in the compressors) and outputs (from the turbine) with block arrows. Looking at the integrated system diagram, one can observe that this is a kind of Brayton cycle, including two compressors (for air and natural gas) and a turbine; in between is interlaced the SOFC, which plays the role of an "active" preheater that

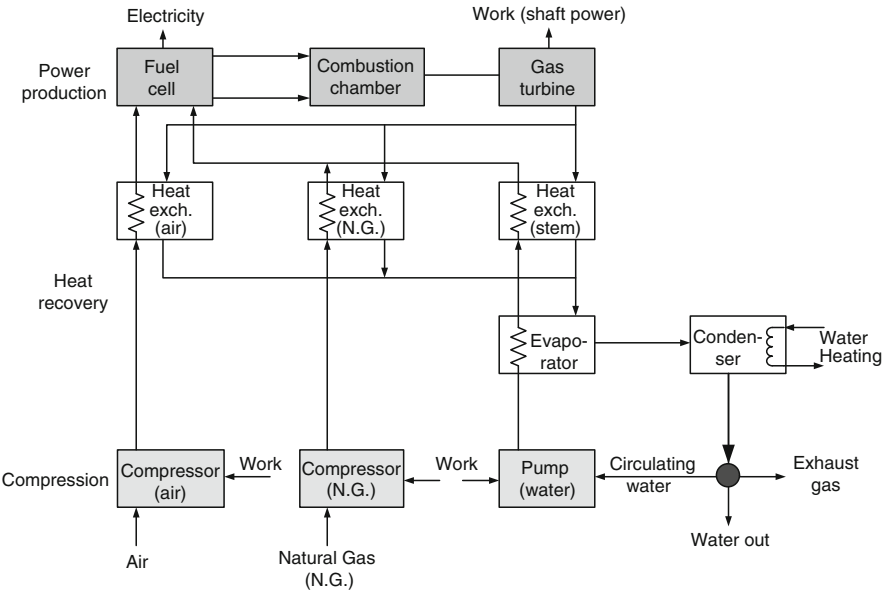

Fig. 12.2 Operational modules of the integrated SOFC–gas turbine system [modified from Dincer et al. (2010)]

generates electricity while consuming some of the energy of the primary fuel and is followed by a combustor, where the fuel energy is utilized fully. Water is recovered from exhaust gases by cooling and condensing. Part of the resulting heat is used internally in the steam evaporator (label 9) and steam super-heater (label 8) while the condenser rejects the heat in the exterior; this heat is recovered by a stream of water and represents the cogenerated (useful) heat.

The system can be divided in three operational modules as indicated in Fig. 12.2, namely: (1) the compression section (bottom); (2) the heat recovery section (middle); and (3) the power production section (top), which comprises the fuel cell stack and the gas turbine. Several assumptions for thermodynamic modeling of the system were considered, such as that the values of pressure and temperature (T_0, P_0) of the reference environment are taken as standard, the inlet temperature in the SOFC is taken as 1,073 K and the outlet as 1,273 K (based on the literature, these values are advantageous with regard to SOFC efficiency), and the gas turbine output temperature is taken as 1,123 K to provide at least a 50°C temperature difference at the heat exchanger inlets.

The isentropic efficiency of the turbine is assumed to be 93% and that of the compressors 85%, while the air composition is considered to be 21% oxygen and 79% nitrogen. Energy losses due to fluid friction are ignored; the water pump work is also ignored because it is significantly small with respect to produced power; the chemical reactions are assumed to be at equilibrium.

The modeling starts by analyzing the chemical reactions at the level of SOFC (which is regarded as a "black box"); these reactions are

$$\begin{cases} CH_4 + 2O_2 \rightarrow CO_2 + 2H_2O(g) - 802\,\text{kJ/mol} \\ CH_4 + H_2O \leftrightarrow CO + 3H_2 + 206\,\text{kJ/mol} \\ CO + H_2O \leftrightarrow CO_2 + H_2 + 41\,\text{kJ/mol} \end{cases}. \tag{12.1}$$

The chemical equilibrium equations for methane reforming at the fuel cell anode give the equilibrium constants that correspond to the methane steam reaction and the carbon monoxide steam reaction listed above. According to these chemical equations, the reaction constants become

$$\begin{cases} K_{CH_4} = \dfrac{\left[P_{H_2}^3 P_{CO}\right]}{\left[P_{CH_4} P_{H_2O}\right]}, \\ K_{CO} = \dfrac{\left[P_{H_2} P_{CO_2}\right]}{\left[P_{CO} P_{H_2O}\right]}, \end{cases} \tag{12.2}$$

where P is the partial pressure of the component.

Mass, molar, energy, entropy, and exergy balances are written for each component of the system. The SOFC stack exergy efficiency η_s is expressed as a percentage of the Gibbs free energy change, $W_e = -\eta_s \Delta G_1$, where ΔG_1 is the Gibbs free energy difference between the output and input flows, that is, $\Delta G_1 = G_1^{out} - G_1^{in}$. The Gibbs free energy of a component in a gaseous mixture can be written as $G_i = H - TS_i$ and $S_i = S_i^0 - R\,\ln(P_i)$, where H_i and S_i represent the molar enthalpy and entropy of a component at $P_0 = 1$ atm, and P_i denotes partial pressure, T the temperature, and R the universal gas constant. The thermal efficiency η_s is related to the open-circuit fuel cell voltage $V_s = W_e/(n_{O_2} n_e F)$, where n_{O_2} is the number of moles of oxygen that traverse the fuel cell electrolyte, n_e is the number of moles of electrons transmitted to a circuit chain per mole of oxygen, and F is the Faraday constant.

The output flows of the SOFC stack are the input flows to the combustion chamber. Anode exhaust and oxygen-depleted air from the SOFC enters the combustion chamber, and combustion products exit. Sufficient oxygen is provided for complete combustion of the CH_4, H_2, and CO from the SOFC stack. The temperature of the input flows is the same as that of the air and methane exiting the SOFC stack. An energy balance can be determined for the adiabatic combustion chamber ($\Delta H_2 = 0$). The exergy destroyed by each component is calculated with $Ex_{d,i} = T_0 \Delta S_i$, where i is the index of the component as indicated in Fig. 12.1.

By applying the general efficiency equations for utilization efficiency and for exergy efficiency, the cogeneration efficiencies of the overall system may be calculated; the particular forms of the efficiency equations are in this case

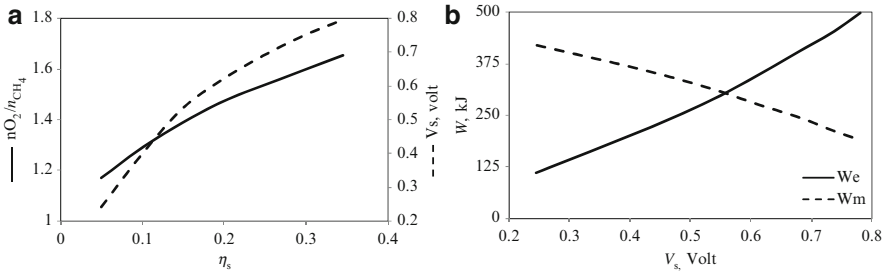

Fig. 12.3 The effect of the air/fuel ratio on fuel cell stack efficiency (**a**), and voltage and power output (**b**); W_e fuel cell power output; W_m net turbine power output, both per mol of fuel [data from Dincer et al. (2010)]

$$\begin{cases} \eta = \dfrac{\dot{W}_{FC} + \dot{W}_T + \dot{Q}_C}{\dot{m}_{CH_4} LHV_{CH_4}}, \\ \psi = \dfrac{\dot{W}_{FC} + \dot{W}_T + \dot{Q}_C(1 - T_0/T_C)}{\dot{m}_{CH_4} \dot{E}x^{ch}_{CH_4}}, \end{cases} \tag{12.3}$$

where $\dot{Q}_C$ is the heat recovered from the condenser. As mentioned above, the energy efficiency can be referred to the lower or higher heating value of the fuel depending on the case. In this analyzed case, the water is expelled out of the system both in liquid form and as steam; however, the portion that comes from methane–fuel utilization is expelled as steam; thus, the reference for utilization efficiency is the lower heating value (LHV) of methane.

For better overall efficiency, it is important to adjust the molar flux of air and fuel such that the operational-circuit fuel cell voltage is the highest. Figure 12.3 shows the results regarding the variation of the voltage and the power output of the fuel cell stack and the net turbine work correlated with the air (oxygen)/fuel ratio. To avoid carbon deposition on the anode surface, the molar ratio of methane to steam should exceed 1:2. Values of V_s greater than 0.7 V are therefore unsuitable for the system considered here.

Note that the maximum efficiency of an SOFC stack does not coincide with the maximum thermodynamic efficiency. The cost of SOFC stacks is a limiting factor, and their operation at higher work densities reduces the power generation cost for the overall system. This observation, along with the fact that the work output from the methane conversion catalyst is stable when the steam–methane ratio ranges between 2:1 and 3:1, suggests that the most beneficial SOFC operating conditions occur for V_s of 0.4 to 0.7 V. Then, the energy efficiency of the overall system is seen to be 70% to 80%, respectively.

For the numerical example assumed in Dincer et al. (2010), the operational cell voltage is taken to be 0.61 V and the fuel cell stack energy efficiency is 20%. In these conditions, the calculated exergy destructions for each component are depicted in Fig. 12.4. The exergy destruction in the condenser is small because of the reduced level of temperature (close to T_0) and is negligible with respect to that

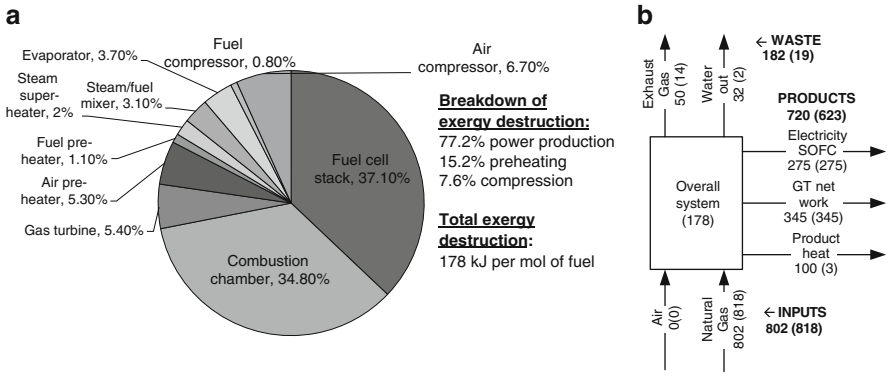

Fig. 12.4 The destruction of exergy in various components (**a**) and the overall outputs (**b**) of the SOFC/GT system [data from Dincer et al. (2010)]

of other components. Also, because the pump work is ignored, (as justified above), the exergy destruction in the pump is nil.

The efficiency of power production only of the integrated system can be estimated from the efficiency of the SOFC itself, which becomes $\eta = 275/802 = 34.2\%$ and $\psi = 275/818 = 33.6\%$.

12.3 Multigeneration

The above example of an integrated SOFC and gas turbine demonstrated that the power production efficiency increases because of the integration of two technologies. There we calculated the efficiencies of power production only. However, as mentioned, the system cogenerates useful heat. The overall efficiency of the system with cogeneration, calculated according to Eq. (12.3) is $\eta = 720/802 = 90\%$ (for fuel utilization) and $\psi = 623/818 = 76\%$ (for exergy conversion). Thus, the gain in efficiency due to cogeneration is about 56% in fuel utilization terms and about 43% in terms of exergy. This example demonstrates the important benefit of multiple energy system integration (viz. fuel cells and gas turbines) and multigeneration. Multigeneration can potentially generate even better efficiencies than cogeneration.

Figure 12.5 presents the general layout of an integrated multigeneration system, which shows that from a primary energy input several useful outputs are obtained. Basically, these systems could integrate various conversion technologies to produce commodities from a primary source of a single kind.

According to the definition, the efficiency of a multigeneration system can be expressed as the ratio of useful output(s) to the consumed primary energy at input. As mentioned above, the outputs can be of different kinds (electric power, heat, synthetic fuel, and others). Therefore, the energy outputs must be converted

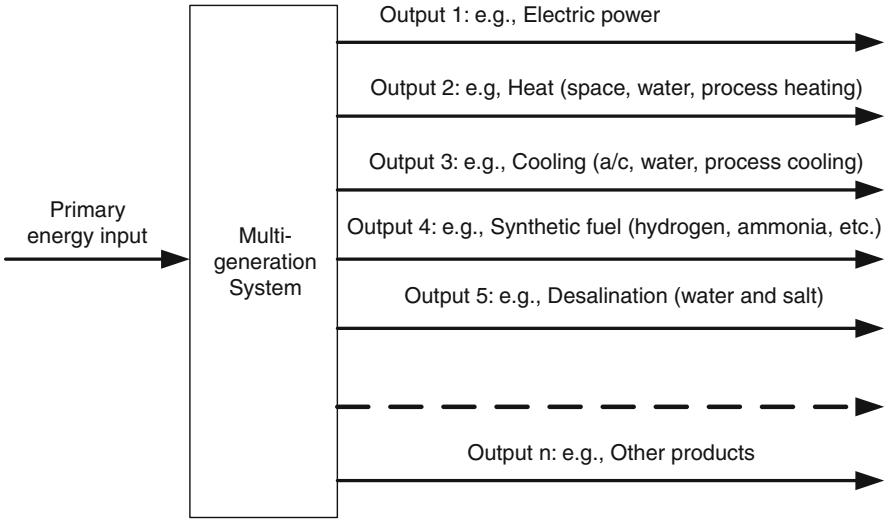

Fig. 12.5 General layout of an integrated multigeneration system

first into similar forms of energy (e.g., work, heating value) and then summated. One can, for example, express the outputs and the inputs in terms of energy content. Thus, the energy-based efficiency is obtained. A fairer approach is to express each output and the input in terms of exergy. Adding exergies is more meaningful than energy contents because one operates with quantities of the same kinds, namely, mechanical work equivalents. Another possibility of quantifying the performance of multigeneration systems is to express each stream (outputs, inputs) through costing equivalents. One obtains thus an economic effectiveness showing the ratio between the product's price (output 1 to output n in Fig. 12.5) versus the fuel consumption cost. Furthermore, the ecological impact of the system can be calculated by considering the equivalent pollutant emissions (viz. greenhouse gases, etc.) per unit of primary energy consumption or per unit of total product.

With reference to Fig. 12.5, the typical expression for the system energy efficiency can be exemplified as follows:

$$\eta = \frac{W + Q_{\mathrm{H}} + Q_{\mathrm{C}} + \mathrm{HHV}_{\mathrm{SF}} + H_{\mathrm{salt}} + H_{\mathrm{OP}}}{\mathrm{HHV}_{\mathrm{PF}}}, \tag{12.4}$$

where the outputs are expressed in terms of energy, W is the work (or electric power), Q_{H} and Q_{C} are the energy in the form of heat used for heating and cooling, respectively, $\mathrm{HHV}_{\mathrm{SF}}$ is the caloric energy embedded in the synthetic fuel (based on its higher heating value), H_{salt} is the equivalent energy embedded in the produced salt, and H_{OP} is the energy in other products; the input is expressed with respect to the higher heating value of the consumed primary fuel (or primary energy source) as $\mathrm{HHV}_{\mathrm{PF}}$. Observe that the water produced by desalination is not included in Eq. (12.4) at the numerator; this is due to the fact that the equivalent energy

embedded in water is nil (water can neither be combusted nor reacted with the standard environment to generate energy).

Efficiency equations similar to Eq. (12.4) can be developed for each particular case. For example, in the case of cogeneration of electric power and heat, the energy efficiency expression is

$$\eta = \frac{W + Q_{\mathrm{H}}}{[m_{\mathrm{PF}}\mathrm{HHV}_{\mathrm{PF}}]}. \tag{12.5}$$

Note that Kanoglu and Dincer (2009) refer to Eqs. (12.4) and (12.5) as the "utilization efficiency" to differentiate it from the thermal efficiency, which is commonly used for a power plant with a single output, power. As also pointed out above, it is inappropriate to summate commodities that are different [like the addition of power and heating in Eq. (12.5)], although work and heat both have units of energy. The exergy efficiency of the general system from Fig. 12.5 is given according to general exergy analysis methodology (Dincer and Rosen 2007) by

$$\psi = \frac{W + Ex_{\mathrm{H}} + Ex_{\mathrm{C}} + m_{\mathrm{SF}}ex^{\mathrm{ch}}_{\mathrm{SF}} + m_{\mathrm{salt}}ex^{\mathrm{ch}}_{\mathrm{salt}} + Ex_{\mathrm{OP}}}{m_{\mathrm{PF}}ex^{\mathrm{ch}}_{\mathrm{PF}}}, \tag{12.6}$$

where $Ex_{\mathrm{H,C}}$ are the exergy equivalent of heat and cooling produced ($Q_{\mathrm{H,C}}$), m_{SF} is the quantity of produces synthetic fuel having the exergy $ex^{\mathrm{ch}}_{\mathrm{SF}}$, $m_{\mathrm{salt}}ex^{\mathrm{ch}}_{\mathrm{salt}}$ is the exergy content associated with salt resulting from desalination, and Ex_{OP} is the exergy associated with other products; the consumed primary fuel is m_{PF} having the specific chemical exergy $ex^{\mathrm{ch}}_{\mathrm{PF}}$. The exergy associated with the generated heating and cooling $Ex_{\mathrm{H,C}}$ is expressed with the help of Carnot factor; in general, assuming a variable heat transfer process, this exergy is

$$Ex_{\mathrm{H,C}} = \int \delta Q \left(1 - \frac{T_0}{T}\right). \tag{12.7}$$

Here, T is the temperature at which heat is transferred. This relation is of little practical value unless the functional relationship between the rate of heat transfer ($Q_{\mathrm{H,C}}$), heat flux, and temperature T is known. In many cases, heat is utilized by transferring it from the working fluid exiting the heat or cooling producing device (e.g., turbine, internal combustion engine, heat pump, refrigeration evaporator) to a secondary fluid, in a heat exchanger. Therefore, the exergy rate of heating or cooling $\dot{E}x_{\mathrm{H,C}}$ can be expressed as exergy variation in working fluid (or heat transfer fluid, depending on the case):

$$\dot{E}x_{\mathrm{H,C}} = \dot{m}_{\mathrm{WF}}(\Delta h - T_0\ \Delta s)|_{\mathrm{WF}}, \tag{12.8}$$

where index WF stands for "working fluid" and h and s represent the specific enthalpy and entropy, while $\dot{m}$ is the mass flow rate.

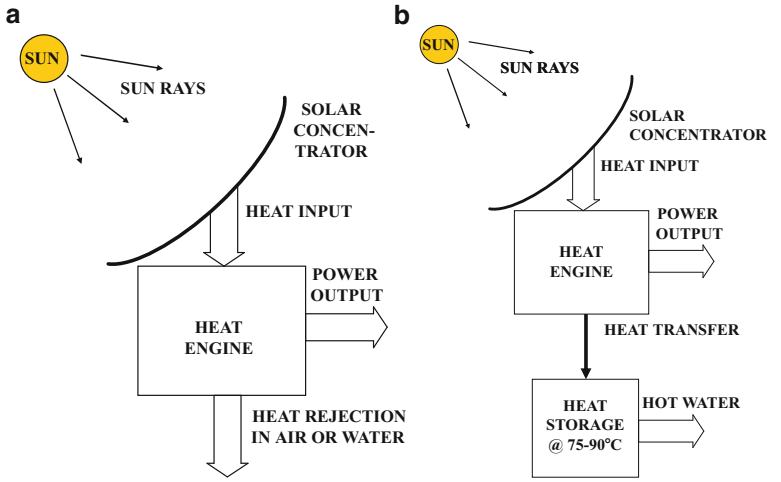

Fig. 12.6 Concentrated solar energy systems: (**a**) solar power and (**b**) solar power and hot water

In order to better illustrate the application of Eqs. (12.4) and (12.6) for energy and exergy efficiency of multigeneration system, we analyze now a number of relevant examples. We start with the system presented in Fig. 12.6a, which represents a concentrated solar power system, where concentrated solar radiation is used to drive a heat engine.

The energy efficiency of system (a) is given by $\eta = W/I_{\text{sun}}$, where W is the electric power output and I_{sun} is the total direct bean radiation input. The exergy associated with I_{T_0} is the exergy of solar radiation and is $I_{\text{sun}}(1 - T_0/T_{\text{sun}})$, where T_{sun} is the temperature of the solar radiation. Therefore, the exergy efficiency of system (a) is $\psi = W/[I_{\text{sun}}(1 - T_0/T_{\text{sun}})]$. The typical values for the practical system are 20% for η and 21% for ψ. Now, if the rejected heat by the heat engine is recovered and used to heat water, as illustrated in Fig. 12.6b, the corresponding energy and exergy efficiency are, respectively, $\eta = (W + Q_{\text{H}})/I_{\text{sun}}$ and $\psi = (W + Ex_{\text{H}})/[I_{\text{sun}}(1 - T_0/T_{\text{sun}})]$, where Ex_{H} can be estimated with Eq. (12.7) or (12.8); in the case that the temperature variation at the heat engine sink is nil or negligible, the exergy associated with heat exchange is given by

$$Ex_{\text{H}} = Q_{\text{H}}\left(1 - \frac{T_0}{T_{\text{H}}}\right). \tag{12.9}$$

Example

In order to illustrate the application of Eq. (12.8), let us consider a particular heat engine for the cogeneration system illustrated in Fig. 12.6b. A simple cogeneration heat engine can be a steam power plant with steam extraction. This is presented in Fig. 12.7; this heat engine can be supplied with "primary fuels" other than solar radiation (e.g., coal). Therefore, the energy associated with the primary energy source is either I_{sun} for the solar concentrator system or, more generally, is

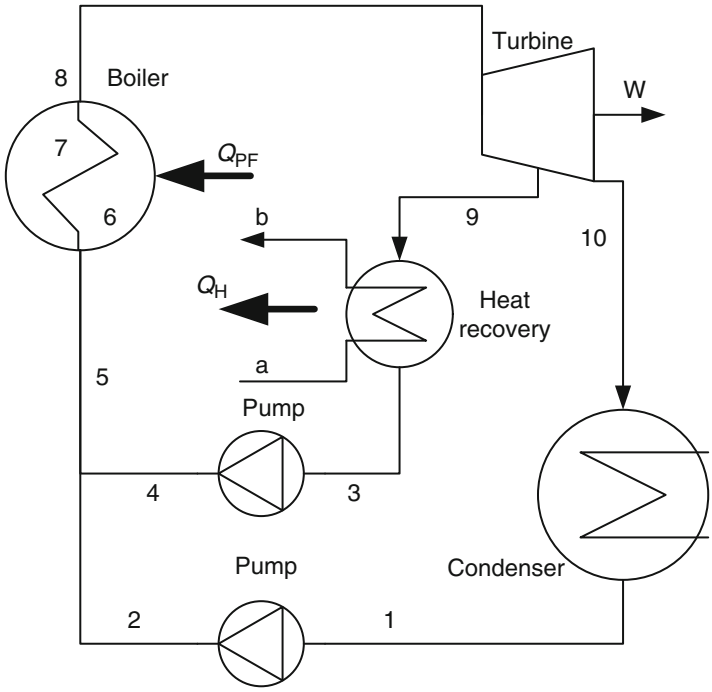

Fig. 12.7 Steam heat engine with cogeneration

$m_{PF}HHV_{PF}$, where m_{PF} is the quantity of fuel consumed per unit of energy output; this energy and the useful product energies can be expressed also as a rate, for example, $\dot{m}_{PF}HHV_{PF}, \dot{E}x_H$. For the numerical example considered here, we assume that the power plant operates with steam that boils at 300°C and is superheated up to 450°C in a solar collector. The condensation is at 40°C, and the condenser for heat recovery operates at 80°C.

At states 1 and 3 of the cogeneration heat engine, one assumes saturated liquid. Moreover, one assumes that 50% of the expanded flow is extracted from the turbine in state 9 and used for heat cogeneration. Engineering Equation Solver (EES) is used to estimate the thermodynamic properties of the steam (though simple steam tables could be used for cycle calculation). The calculation of the thermodynamic cycle is done with the purpose of determining pressure, temperature, entropy, enthalpy, and specific exergy, all in state point, and eventually calculating the overall efficiency. The calculation proceeds by writing energy and mass balance equations for each component and relevant equations for each state as follows:

- Flow fraction is $f = 0.5$; the flow division fraction is defined based on mass balance equations, namely, $\dot{m}_8 = \dot{m}_9 + \dot{m}_{10}$; $\dot{m}_5 = \dot{m}_4 + \dot{m}_2$; $\dot{m}_{10} = \dot{m}_1 = \dot{m}_2$; $\dot{m}_9 = \dot{m}_3 = \dot{m}_4$. The flow division is defined as $f = \dot{m}_4/\dot{m}_5 = \dot{m}_9/\dot{m}_8$.
- State 1: $T_1 = 40°C$, $x_1 = 0$, and $f = 0.5$, one evaluates the specific enthalpy to $h_1 = 167.5$ kJ/kg, total flow enthalpy $h_{t1} = 83.75$ kJ/kg of stream 5–8, pressure $P_1 = 74$ mbar, and specific entropy $s_1 = 572$ J/kg K.

- State 2: Pressure is the same as in state 6 (saturated liquid at 300°C), $P_2 = P_6 = 86$ bar, isentropic efficiency of the pump is assumed $\eta_{P1} = 0.8$ and defined by the equation $\eta_{P1} \times (h_{2s} - h_1) = h_2 - h_1$, where $h_{2s} = h(P_2, s_1) = 176.1$ kJ/kg is the specific enthalpy for isentropic pressurization; thus, $h_2 = 174.4$ kJ/kg and $s_2 = 567$ J/kg K.
- State 3: It is assumed that condensation is at 80°C, thus $T_3 = 80°C$ and $x_3 = 0$; the specific enthalpy is $h_3 = 334.9$ kJ/kg and the total enthalpy $h_{t3} = (1 - f)\, h_3 = 167.5$ kJ; the pressure of saturated liquid is $P_3 = 0.474$ bar and specific entropy $s_3 = 1{,}075$ J/kg K.
- State 4: This is a pressurized liquid state at $P_4 = P_6 = 86$ bar. The pump efficiency is $\eta_{P2} = 0.8$ and the pump equation is $\eta_{P2} \times (h_{4s} - h_3) = h_4 - h_3$, which is solved for h_4 for known isentropic process enthalpy $h_{4s} = 343.7$ kJ/kg, thus $h_4 = 341.9$ kJ/kg and $h_{t4} = 171$ kJ.
- State 5: We have the energy balance $h_5 = h_{t5} = h_{t4} + h_{t2} = 258.2$ kJ/kg while $P_5 = P_6$, $T_5 = T(h_5, P_5) = 60°C$, and $s_5 = 826$ J/kg K.
- State 6: We have saturated liquid ($x_6 = 0$) at $T_6 = 300°C$ and $h_6 = h_{t6}$ 1,344 kJ/kg.
- State 7: Saturated vapor is at $x_7 = 1$, $P_7 = P_6$, $h_7 = 2{,}749$ kJ/kg, and $s_7 = 5{,}704$ J/kg K.
- State 8: Superheated vapor is at $P_8 = P_6$, $T_8 = 450°C$, $h_8 = h_{t8} = 3{,}263$ kJ/kg, and specific entropy $s_8 = 6{,}513$ J/kg K.
- State 9: Expansion to intermediate pressure $P_9 = P_3$; turbine's isentropic efficiency is assumed $\eta_T = 0.8$, and turbine equation is $\eta_T \times (h_8 - h_{9s}) = h_8 - h_9$, where $h_{9s} = h(P_9, s_8) = 2{,}255$ kJ/kg and $h_9 = 2{,}457$ kJ/kg; the total enthalpy is $h_{t9} = 1{,}228$ kJ; the specific entropy is $s_9 = 7{,}084$ J/kg K.
- State 10: Expansion at lowest pressure $P_{10} = P_1$, assuming $\eta_T = 0.8$ and $\eta_T \times (h_8 - h_{10s}) = h_8 - h_{10}$; thus, $h_{10} = 2{,}275$ kJ/kg and $h_{t10} = 1{,}138$ kJ.
- All calculations are done for a main flow rate of 1 kg/s. The electric power generation efficiency is given by $\eta_E = \dot{W}_{net}/\dot{Q}_{PF}$, where $\dot{W}_{net} = \dot{W}_T - \dot{W}_{P1} - \dot{W}_{P2}$.
- Using the total enthalpies, one can determine the work generated and consumed by the turbine and pumps, respectively, and also the energy consumed by the primary fuel. One obtains $\eta_E = 30\%$.
- For the system with cogeneration, the fuel utilization efficiency is given by $\eta_{cog} = \left(\dot{W}_{net} + \dot{Q}_H\right)/\dot{Q}_{PF}$, for which one obtains 65%.
- The exergy efficiency is based on the exergy input in the system, which can be calculated with $\dot{E}x_{PF} = h_8 - h_5 - T_0(s_8 - s_5) = 1{,}310$ kJ.
- Thus, the exergy efficiency of electric power generation is $\psi_E = \dot{W}_{net}/\dot{Q}_{PF} = 68\%$; also, the exergy efficiency of the cogeneration system is calculated accounting for the cogenerated heat exergy, $\dot{E}x_H = (1 - f) \times [h_9 - h_3 - T_0(s_9 - s_3)] = 165.6$ kJ. The cogeneration exergy efficiency becomes $\psi_{cog} = \left(\dot{W}_{net} + \dot{E}x_H\right)/\dot{E}x_{PF} = 80\%$.

The heat recovered from the heat engine is indicated in the figure with Q_H and can be expressed based on the enthalpy of the stream a–b, that is $\dot{Q}_H = \dot{m}_{ab}(h_b - h_a)$; then, the cogeneration energy efficiency is

$$\eta = \frac{\left[\dot{W} + \dot{m}_{ab}(h_b - h_a)\right]}{\dot{m}_{PF}\mathrm{HHV}_{PF}} \tag{12.10}$$

and the exergy efficiency becomes

$$\psi = \frac{\dot{W} + \dot{m}_{ab}[h_b - h_a - T_0(s_b - s_a)]}{\dot{m}_{PF}Ex_{PF}}, \tag{12.11}$$

where the term $h_b - h_a + T_0(s_b - s_a)$ represents the specific exergy of the heat transfer fluid, ex_{HT}. This term can be rearranged as $ex_{HT} = (h_b - h_a)\{1 - T_0/[(h_b - h_a)/(s_b - s_a)]\}$.

If the temperature at which heat transfer occurs is constant, that is, $T_a = T_b = T_H$, then one can express the entropy variation simply as $s_b - s_a = (h_b - h_a)/T_H$. The case when the heat is transferred to a phase-change material is a good example of a situation when heat transfer occurs at a constant temperature. In such cases, the Carnot factor $(1 - T_0/T_H)$ can be within the expression of exergy efficiency. Therefore, the exergy efficiency becomes

$$\psi = \frac{\dot{W} + \dot{m}_{ab}(h_b - h_a)(1 - T_0/T_H)}{\dot{m}_{PF}Ex_{PF}}. \tag{12.12}$$

Typically, for the system from Fig. 12.6b, the cogeneration efficiency values are 60% to 80% for energy and about 30% to 35% for exergy. If sources other than solar radiation are used, the energy-based efficiency (or utilization efficiency) can be even higher, up to 90% to 98%. The high utilization efficiency is obtained by insulating the system well, so that all produced thermal energy is recovered and used. In a solar concentrating system, perfect insulation is not possible, and various losses such as optical and thermal radiation impede obtaining utilization efficiencies higher than about 80% to 85%. For systems using fuel combustion, it is possible to devise better insulation so that less primary energy is lost. Typical efficiency figures for various heat engines with cogeneration are shown in Table 12.1. It is assumed that the cogenerated heat is used for water heating, where the stream of water at the inlet (state *a* in Fig. 12.7) is assumed to be 50°C and at the outlet (state *b*) 90°C.

Other typical systems for cogeneration of heat and power are suggested Fig. 12.8. For systems (a) and (b), Eqs. (12.10) and (12.11) can be applied to determine the utilization and exergy efficiencies, respectively. In the case of a

Table 12.1 Typical efficiencies of various cogeneration systems

Efficiency	Concentrated solar (%)	Steam engine (%)	Gas power plant (%)	Diesel engine (%)	Geothermal plant (%)
Utilization	70–80	48	47	78	16
Exergy	30–35	23	23	48	44

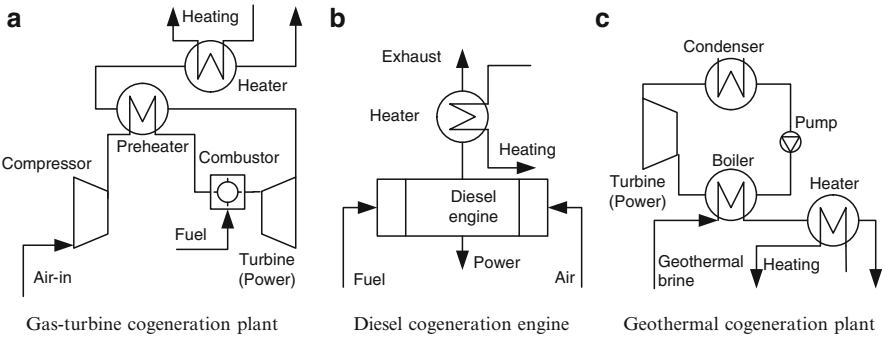

Fig. 12.8 Some typical cogeneration systems

geothermal system, the energy and exergy content of the primary source, which is geothermal brine, can be calculated by assuming that the brine is cooled down to the ambient temperature. Denoting (h_0, s_0) the specific enthalpy and entropy of the brine at environmental temperature T_0, the associated primary energy and exergy become

$$\begin{cases} \dot{Q}_{\text{geo}} = \dot{m}_{\text{geo}}\left(h_{\text{geo}} - h_0\right), \\ \dot{E}x_{\text{geo}} = \dot{m}_{\text{geo}}\left[h_{\text{geo}} - h_0 - T_0\left(s_{\text{geo}} - s_0\right)\right], \end{cases} \tag{12.13}$$

where subscript "geo" stands for "geothermal" and h_{geo}, s_{geo} are the specific enthalpy and entropy, respectively, of the hot geothermal brine.

Some multigeneration systems are suggested here by expanding the concentrated solar cogeneration plant from Fig. 12.6b. Thus, Fig. 12.9a shows a system with tri-generation, where the outputs are power, hot water, and space heating. Heat storage can be applied in order to store solar energy in the form of thermal energy for overnight heating.

The system from Fig. 12.9b is an extension of the tri-generation system to multigeneration. In this case, the system produces power heating and cooling, where cooling is used for air conditioning and other purposes (like food preservation) and heating is used for space and water. Such a system thus generates five useful outputs. The exergy efficiency can be written as

$$\psi = \frac{\dot{W} + \dot{Q}_{\text{HW}}(1 - T_0/\bar{T}_{\text{HW}}) + \dot{Q}_{\text{SH}}(1 - T_0/\bar{T}_{\text{SH}}) + \dot{Q}_{\text{C}}(1 - T_0/\bar{T}_{\text{C}}) + \dot{Q}_{\text{AC}}(1 - T_0/\bar{T}_{\text{AC}})}{I_{\text{sun}}(1 - T_0/T_{\text{sun}})}, \tag{12.14}$$

where indices HW, SH, C, and AC mean hot water, space heating, cooling, and air conditioning, respectively. The average process temperature $\bar{T}$ has been used to express the Carnot factors used for expressing the exergy of heat fluxes. This approximation is valid if the temperature does not vary much. With the system in Fig. 12.9b, one can achieve 35% exergy efficiency while utilization efficiency can

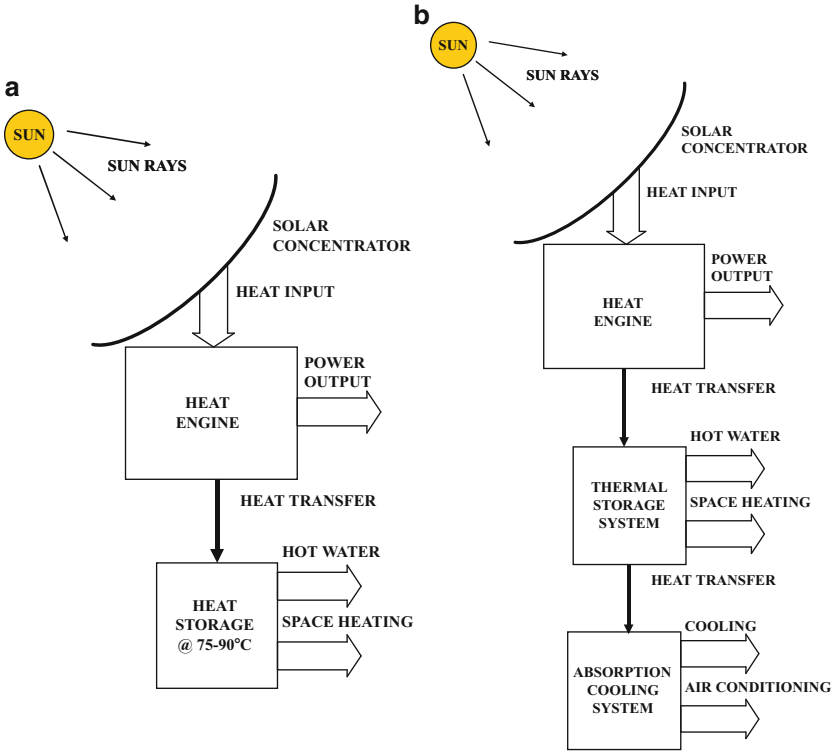

Fig. 12.9 Examples of tri- and multigeneration hybrid concentrated solar power systems

reach, in principle, 90%. The system integrates several components such as the heat engine, heat recovery heat exchangers, thermal storage system, and an absorption refrigeration system.

The system suggested in Fig. 12.10 integrates a solar-driven heat engine with an electrolyzer that produces hydrogen and oxygen from water and an absorption refrigeration system that generates cooling from heat recovery from the heat engine; in addition, there is a thermal storage system and a heat recovery system that delivers heating as useful product for heating water and some other needs. The energy efficiency of the system from Fig. 12.10a is

$$\eta = \frac{\left(\dot{W} + \dot{m}_{\mathrm{H_2}}\mathrm{HHV}_{\mathrm{H_2}} + \dot{Q}_{\mathrm{HW}} + \dot{Q}_{\mathrm{SH}} + \dot{Q}_{\mathrm{C}} + \dot{Q}_{\mathrm{AC}}\right)}{I_{\mathrm{sun}}}. \tag{12.15}$$

In Eq. (12.15), the term $\dot{m}_{\mathrm{H_2}}$ denotes the production rate of hydrogen. A part of the produced electricity is used to drive the electrolyzer, which produces hydrogen and oxygen from water during the day. In the nighttime, the stored hydrogen can be used in a fuel cell to generate electricity. Thus, one can have a continuous production of electricity for 24 hours.

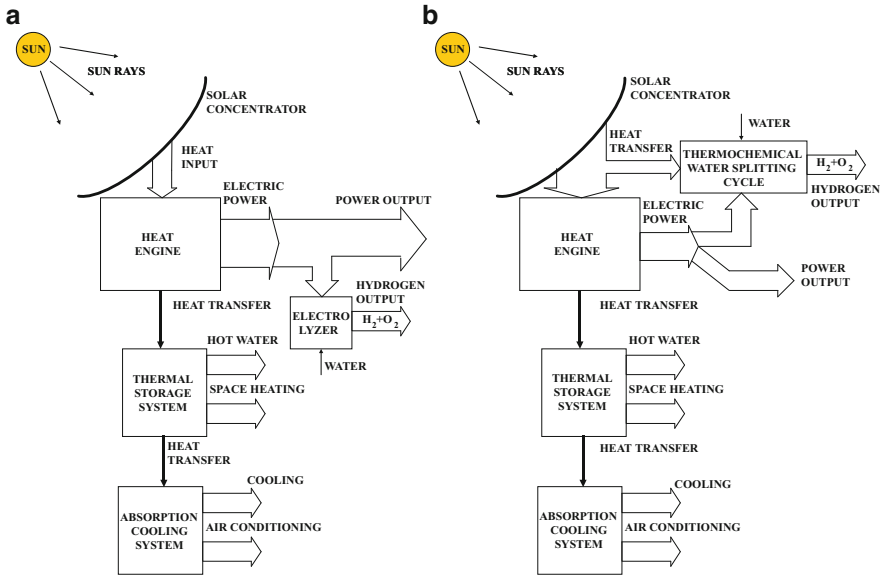

Fig. 12.10 Solar-driven multigeneration hybrid systems with hydrogen production (**a**) by electrolysis and (**b**) by thermochemical water splitting

An alternative to the system from Fig. 12.10a is presented in Fig. 12.10b, where the electrolyzer is replaced by a thermochemical water splitting plant. The thermochemical water splitting process consumes less primary thermal energy than the electrolyzer because it does not require any electricity or it requires much less electricity. Therefore, the generation of electricity to drive the water splitting process (or at least substantially reduce the required electricity for it) is avoided with the benefit of improving energy utilization and exergy efficiency. Rough calculations indicate that the integrated system based on thermochemical water splitting can be at least 5% more efficient in exergy terms than the one based on the electrolyzer.

An additional example is illustrated in Fig. 12.11, which shows two integrated multigeneration systems for power, heating, cooling, and desalination. The products are nine in number: electric power, hydrogen, oxygen, drinking water, salt, hot water, space heating, process cooling (e.g., food refrigeration), and air conditioning. The inputs are two: solar energy (which drives the process) and brine. Two implementations of the system are suggested: (a) using the electrolyzer and (b) using the thermochemical water splitting process. The multigeneration exergy efficiency of these systems is given by

$$\psi = \frac{\dot{W} + \dot{Q}_{\mathrm{HW}}(1 - T_0/\bar{T}_{\mathrm{HW}}) + \dot{Q}_{\mathrm{SH}}(1 - T_0/\bar{T}_{\mathrm{SH}}) + \dot{Q}_{\mathrm{C}}(1 - T_0/\bar{T}_{\mathrm{C}}) + \dot{Q}_{\mathrm{AC}}(1 - T_0/\bar{T}_{\mathrm{AC}}) + \dot{E}_{\mathrm{S}}}{I_{\mathrm{sun}}(1 - T_0/T_{\mathrm{sun}})}, \tag{12.16}$$

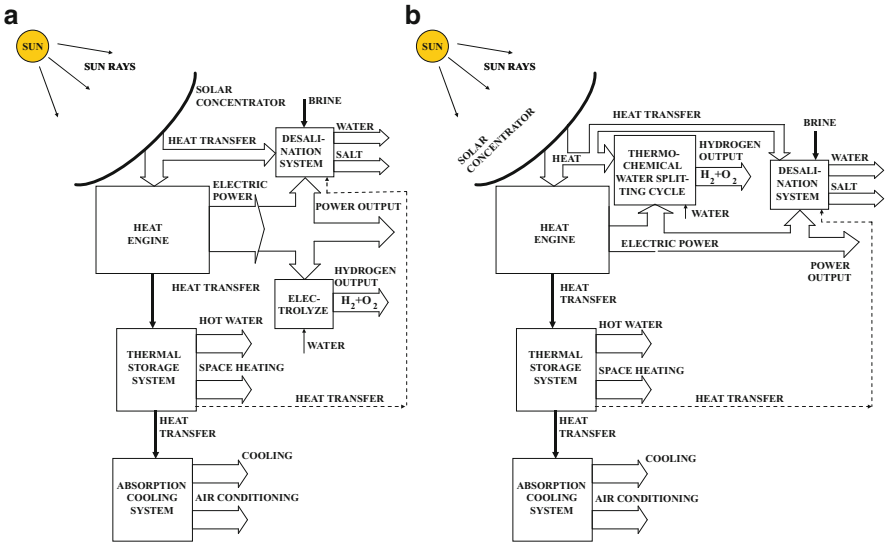

Fig. 12.11 Hybrid solar multigeneration systems with hydrogen production and desalination using high temperature electrolysis (**a**) and thermochemical water splitting process (**b**)

where the meaning of the indexes are the same as above, and "S" stands for "salt." The process (b) uses high-temperature heat to drive water splitting, desalination, and the heat engine; thus, this system generates less electricity than system (a), which uses high-temperature heat only for the heat engine and for desalination. Using Eq. (12.16), the multigeneration exergy efficiency of system (a) is theoretically estimated to be 45%, while that of system (b) is estimated to be 50%.

12.4 Hybridization

The examples above refer to integrated multigeneration systems that are able to generate multiple products from a primary energy source of a single kind. There is also potentially more benefit if the system is engineered to produce outputs from multiple kind sources. Thus, systems can be devised to generate power from wind and solar simultaneously, or generate power and heat from geothermal and solar source, or from biomass combustion and solar source. A typical case entails solar electric generation systems that integrate concentrated solar collector technology with advanced Rankine generators and with natural gas steam generators for backup power. Such systems are called hybrid.

Hybridization of conversion systems involves coupling various technologies together to extract useful energy system from sources that are fundamentally different, with the purpose of obtaining better utilization factors and better effectiveness than that of the integrated systems that use one single kind of primary energy. Obviously, hybrid systems can be devised to generate multiple products.

We demonstrate in this section the benefit of hybridization through an illustrative example that integrates solar and geothermal energy to generate absorption cooling. Absorption cooling systems (ACSs) have become suitable for producing an inexpensive heat energy source over 65°C. Therefore, geothermal and solar energy have a wide range of application potentials for cooling. In the example presented here, the Bigadic geothermal field is selected; this site is located about 38 km south of Balikesir Province, situated in the western part of Turkey. The well head temperature is 98°C, and the geothermal fluid temperature, entering the heat exchangers constructed under each house, changes between 65° and 80°C depending on the operating condition in the system. The ACS utilizes a solution of lithium bromide (LiBr) and water under a vacuum as the working fluid. The absorption cycle is energized by hot water at 85° to 95°C. In the system, the LiBr–water solution temperature is increased to 85° to 95°C by using solar energy.

The following assumptions are made in energy and exergy analyses for the LiBr–water refrigerant system:

- Heat and pressure losses in all the heat exchangers and the pipelines are negligible.
- The reference state temperature and pressure for the system is chosen as 25°C and 101 kPa.
- The temperature of the solution entering the throttle valve is checked by using the EES program to avoid crystallization.
- The solution in the generator and the absorber are assumed to be in equilibrium at their respective temperatures and pressures.
- Water at the condenser and evaporator exit is in a saturated state.
- The strong solution of the refrigerant leaving the absorber and the weak solution of the refrigerant leaving the generator are saturated.

The energy balances for the condenser, evaporator, absorber, generator, and heat exchanger are given (per unit of mass basis) in the following equations (Fig. 12.12):

For the condenser,

$$Q_{\text{con}} = m_{\text{water}}(h_8 - h_9) = m_{\text{con}}(h_{19} - h_{18}). \tag{12.17}$$

For the evaporator,

$$Q_{\text{ev}} = m_{\text{water}}(h_{11} - h_{10}) = m_{\text{ev}}(h_{16} - h_{17}). \tag{12.18}$$

For the absorber,

$$Q_{\text{abs}} = m_{\text{water}} \cdot h_{11} + m_{\text{WS}} \cdot h_7 - m_{\text{SS}} \cdot h_1 = m_{\text{abs}}(h_{15} - h_{14}). \tag{12.19}$$

For the generator,

$$Q_{\text{gen}} = m_{\text{WS}} \cdot h_5 + m_{\text{water}} \cdot h_8 - m_{\text{SS}} \cdot h_4 = m_{\text{gen}}(h_{20} - h_{21}). \tag{12.20}$$

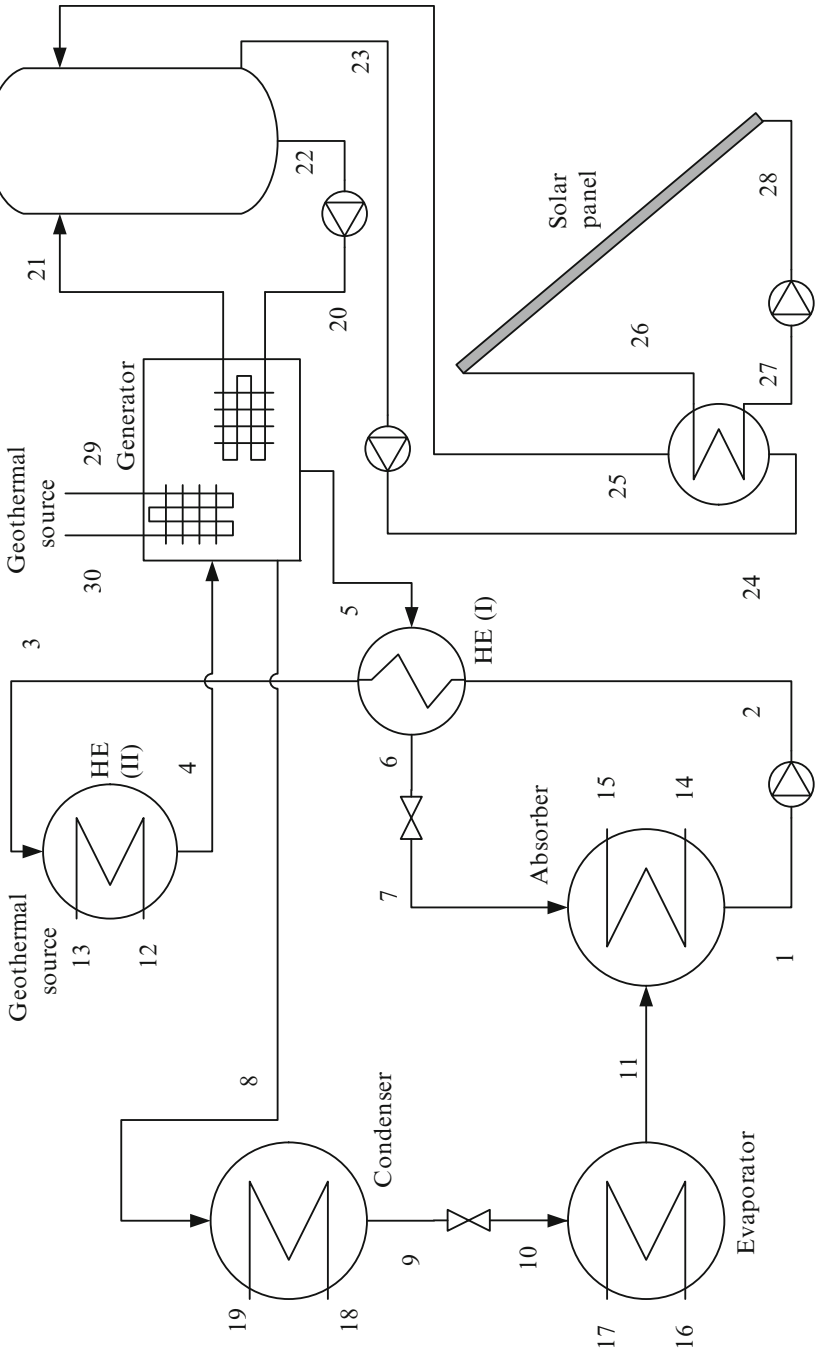

Fig. 12.12 Hybrid solar and geothermal-driven absorption cooling system [modified from Coskun et al. (2010)]. *HE* heat exchanger

For the heat exchanger,

$$Q_{\text{geo}} = m_{\text{SS}}(h_4 - h_3). \tag{12.21}$$

Collector efficiency is a major indicator in the conversion process of solar energy to thermal energy. To find the converted energy in the solar collector, collector efficiency should be determined for each possible condition. It is known that many parameters affect the energetic and exergetic efficiencies of thermal collectors. Some of them can be expressed as the intensity of the solar irradiance, outdoor temperature, and input–output feed water temperature. The evacuated vacuum tube type collectors should be utilized effectively to achieve a higher water temperature. Thermal collector efficiency changes with the intensity of the solar irradiance (I), outdoor temperature (T_0), and input–output feed water temperature (T_{in}, T_{out}).The formulation of the energy efficiency characteristic is given in the following equation:

$$\eta_{\text{coll}} = 0.83 - 2.19 \times \frac{(T_{\text{in}} + T_{\text{out}})/2 - T_0}{I}. \tag{12.22}$$

Coskun et al. (2010) introduced the *geothermal–solar energy fraction* (GSEnF), a parameter expressed as the fraction of the geothermal energy to solar energy utilized in the system:

$$GSEnF = \frac{E_{\text{geo}}}{E_{\text{solar}}}, \tag{12.23}$$

where E_{solar} and E_{geo} represent the solar and geothermal energy inputs for cooling. Geothermal energy input throughout the daytime varies between 20% and 8% of total energy input for 2° to 18°C evaporator temperature variation. The GSEnF varies between 0.08 and 0.24 for investigated system. It decreases with increasing evaporator temperature. In addition, GSEnF also decreases with decreasing absorber temperature. The analysis results show that GSEnF gives the same value (0.10) for a 14°C evaporator temperature, although the absorber temperature varies.

Another parameter, the geothermal–solar exergy fraction (GSExF), is expressed as the fraction of the geothermal exergy to solar exergy utilized in the system:

$$GSExF = \frac{Ex_{\text{geo}}}{Ex_{\text{solar}}}, \tag{12.24}$$

where Ex_{solar} and Ex_{geo} represent the solar and geothermal exergy inputs for cooling. The GSExF is investigated for different working conditions, and the results are given in Fig. 12.13. Exergy input from geothermal sources is very low level and it varies between 0.1% and 1% of total exergy input. The percentage solar energy input rate increases with evaporator temperature. As can be seen in the figure, it decreases with increasing evaporator temperature.

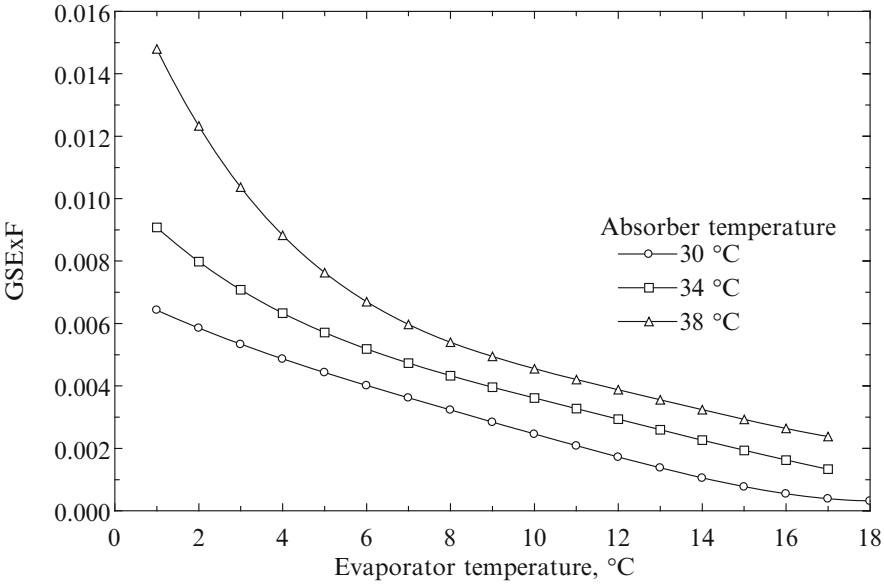

Fig. 12.13 GSExF versus evaporator temperature for different operating conditions [modified from Coskun et al. (2010)]

12.5 Economic Aspects of Multigeneration Systems

Multigeneration systems can be found in many applications, starting with residential settings (where they can be used for generation of power, heating, and cooling, for example) and ending with industrial parks or agricultural farms. Their successful integration within a larger process requires detailed information regarding the energy consuming technologies to be desired and the availability of primary energy resources. It is important that all technical information regarding energy demand be organized in a working model that allows for the effective design of the multigeneration system. Walker (1984) provided a general method for the analysis and design of integrated energy systems; the primary application is in agricultural settings, but the method is more general and can be used to design an integrated multigeneration energy system for any kind of application.

Design engineers must address logistical, environmental, and economic problems with regard to the integration of energy systems in agricultural, industrial, commercial, and residential settings. When analyzing the integration of multigeneration energy system in a given setting, one first has to study the involved technological processes, which for an industrial or agricultural setting can be classified into three categories: material transformation, material transport, and material storage. Residential and commercial settings are different, even though their energy needs consist mainly of electric power, space heating, hot water, air conditioning, and cooling (e.g., for water cooling, ice making, or food preservation). These needs are present also in industrial and agricultural settings;

in the above three category classifications, they can be assimilated to the material transformation category. With any phase of the process there are associated costs. Three main categories of costs are identified in Walker (1984): land, labor, physical energy costs. Depending on the case, there also may be other costs relevant to the analyses. For multigeneration systems, specific costs eventually can be assigned for any kind of output. In the cost assignment process, one must account for all categories of costs involved.

In the multigeneration example suggested in Fig. 12.11, the value of the drinking water is not accounted for in the utilization and exergy efficiency equations; it cannot be! This is because water has no energy value. Moreover, for the same reasons, in the systems that generate hydrogen and oxygen from water, the water itself cannot be considered in energy/exergy efficiency or as an input. However, water, even in abundance, is not free. This reasoning leads to the conclusion that the performance of multigeneration energy systems must be evaluated from the economic point of view, in addition to the performance defined through thermodynamics. The "economic effectiveness" of an integrated multigeneration system can be estimated by the following equation:

$$Ee = \frac{\sum_i C_{\mathrm{o},i}}{C_{\mathrm{PF}} + \sum_j C_{\mathrm{m},j}}, \tag{12.25}$$

where $C_{\mathrm{o},i}$ is the monetary cost of the output i, C_{PF} is the monetary cost of the primary fuel, and $\sum_j C_{\mathrm{m},j}$ is the total cost of materials input in the process. The cost of products in the numerator of Eq. (12.25) can include only the benefit part and exclude the part used for amortization of the investment in the multigeneration equipment.

For a simple cogeneration system, the economic effectiveness includes the costs associated with electric and thermal energy and the cost of fuel. If the system is more complicated, advanced economic calculations must be performed to determine the economic effectiveness. The problem becomes more complicated if economic incentives that help financing are available. Cogeneration (CHP) projects are generally recognized by governments and other financing bodies as drivers toward better sustainability and a healthier environment; therefore, at present there is relevant experience in financing those projects.

Through financing, both the capital cost and the price of products (like the kWh of power or thermal energy) can be made more favorable so that the economic effectiveness of the cogeneration system is increased. Hamrin (2005) describes the financing system of cogeneration projects in California. There, the Public Utility Regulatory Policy Act established in 1978 has been prolific in encouraging cogeneration, which increased in the market from virtually nil to a multimillion dollar business in about 10 years. Several types of financing were used both in the United States and in the European Community (See Fee 2005):

- Innovative vendor financing such as financial savings guarantees, package financing, shared savings contracts, and vendor-backed equipment leasing

- Third-party financing
- Energy project or utility financing

The legal framework regarding the encouragement of cogeneration (CHP) plants differs from country to country. Some countries allow the installer of the CHP system to sell back electricity to the grid at a favorable price so that the producer can make a profit; other countries do not encourage this kind of business. Here are some financing examples from various countries, as taken from Fee (2005), that reflect the situation:

- *Canada*: Only Alberta offers the right to sell back to the grid; Ontario and British Columbia implemented policies of "encouraging" sales to the grid. The tariffs for electricity sold to the grid in Alberta are established at the provincial level only. In Ontario, the power utility can affiliate with local energy producers and buy the electricity produced by them.
- *United States*: Energy auto-producers have the right to sell electricity to the grid at a fixed tariff and the grid has an obligation to buy. The rates are set by the state's public utility commission. Some states give local producers the right to sell electricity to third parties while other states do not.
- *Sweden*: Energy auto-producers have the right to sell electricity to the grid at a fixed tariff and the grid has an obligation to buy. The profit is equally shared between the seller and the buyer.
- *Austria*: Auto-producers have the right to sell to the grid only where the power is in surplus to their own use. The tariff is aligned with the State Power Board's wholesale tariff in a range of 80% to 100% of the energy charge of the wholesale tariff.

The usual practice regarding the financing of cogeneration systems is by either purchasing the equipment or by leasing it for a period of 3 to 7 years (Kolanowski 2008). An important factor in financing multigeneration projects is represented by the reduction of greenhouse gas emissions that these systems are capable of with respect to other systems. The expected reduction in CO_2 emissions as a result of using tri-generation and cogeneration plants is 170 Mt/year in 2015, while in 2030 the expected reduction is 950 Mt/year (International Energy Agency 2008).

The cost-effectiveness of any multigeneration system is directly related to the amount of power it can produce for a given amount of other products such as process heat and cold. For tri-generation systems, one can define the electrical to thermal energy ratio (R_{ET}) as an important performance assessment parameter.

Illustrative Example: Hybrid Solar–Natural Gas System

Let us consider a hybrid solar–natural gas system that is intented to provide heating to a residence, such as a house. The residence is connected to the natural gas network. During the daytime, it uses concentrated solar power to generate steam and reform methane to hydrogen. Thus, during the day, the supply of heat is obtained by combusting hydrogen combined with natural gas. The energy harvested from the sun diminishes the consumption of natural gas. During the nighttime,

when no hydrogen is generated, the heating is obtained by the combustion of natural gas only. Natural gas can be converted to hydrogen by adding steam according to the overall reaction $CH_4 + 2H_2O \rightarrow CO_2 + 4H_2$, which needs 48.3 MJ/kmol of hydrogen.

Assume that the solar collector has a 10 m^2 aperture area; if 5 kWh/m^2 day is the the average solar radiation, then the incident radiation is 50 kWh/day. Assuming 10% losses through optics and heat transfer, the amount of harvested heat is 45 kWh/day or 162 MJ. Thus, one can produce 162/48.3 = 3.35 kmol hydrogen per day, which is 6.7 kg. This hydrogen comes from about 0.7 kmol of natural gas or the equivalent of 0.5 GJ, which costs about $5. The total thermal effect generated by combustion of 6.7 kg of hydrogen is about 950 MJ. Thus, the cost of heating becomes $5/950 MJ = $5.3/GJ. If the same heat is generated by combusting natural gas only, the cost is the same as that of natural gas, which is taken as $10/GJ. Therefore, the savings resulting from using the hybridized solar–natural gas system is 47%.

12.6 Case Studies

12.6.1 Power, Hydrogen, and Oxygen Multigeneration Using Nuclear Energy

This example, which is based on Zamfirescu et al. (2010), examines the multigeneration of power, hydrogen, and oxygen as a way of upgrading the exergy efficiency of nuclear reactors. The tri-generation exergy efficiency can be calculated in this case with the following equation:

$$\psi = \frac{\dot{W} + \dot{m}_{H_2}\left(ex_{H_2}^{ch} + ex_{H_2}^{P}\right) + \dot{m}_{O_2}\left(ex_{H_2}^{ch} + ex_{H_2}^{P}\right)}{\dot{m}_U ex_U^{ch}}, \tag{12.26}$$

where superscript ch indicates chemical exergy and exponent P indicates thermomechanical exergy due to pressurizing the product gases for storage.

Consuming the electrical energy produced by the nuclear power plant for water electrolysis and hydrogen cogeneration would not augment the overall exergy efficiency; therefore, this is not the appropriate option for multigeneration. In contrast, recent advances in thermochemical water splitting at intermediate temperatures would enhance the exergy efficiency by recovering heat from a nuclear plant to drive a Cu–Cl system for water splitting and hydrogen and oxygen generation (see Naterer 2008 and Naterer et al. 2009; also detailed in other chapters of this book). Thermochemical water splitting cycles are a promising alternative to electrolysis because they require little or no electricity. If the electricity generation efficiency (about 25% for typical power plants, including average grid loses) and

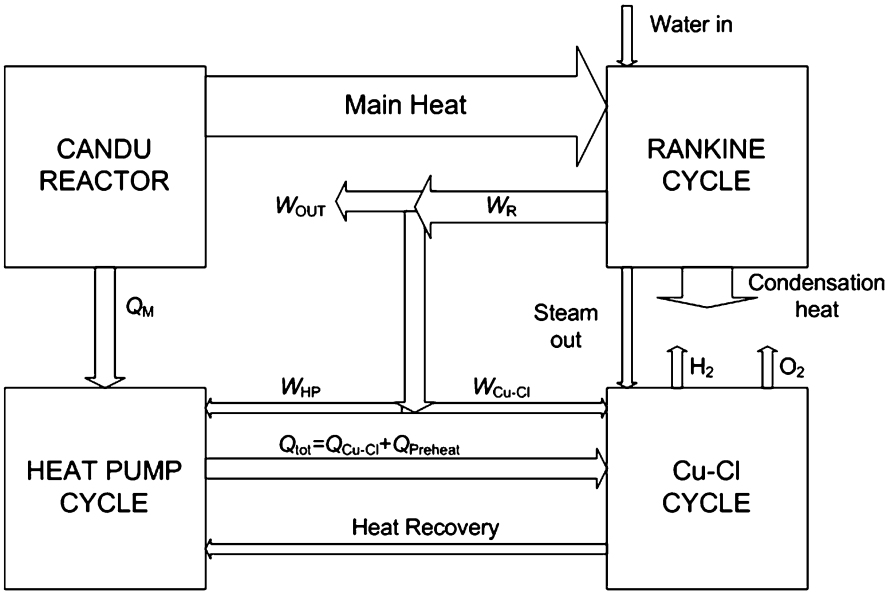

Fig. 12.14 Nuclear reactor multigeneration system for power, H_2 and O_2. *W* work; *Q* heat. Indices: *M* moderator; *R* Rankine; *tot* total; *Cu–Cl* reaction heat [modified from Zamfirescu et al. (2010)]

electrolyzer efficiency (typically about 80% grid-to-hydrogen) are multiplied, the overall efficiency of electrolysis becomes about 20%.

The system configuration presented here utilizes waste heat from a CANDU nuclear reactor, at ~80°C from the moderator vessel, to drive various processes in the Cu–Cl cycle for hydrogen production. Figure 12.14 presents a system that couples a heat pump, Cu–Cl cycle, and a nuclear power plant with the aim to enhance the exergy efficiency of the power plant alone, via multigeneration of hydrogen, oxygen, and power.

The original power plant is a typical nuclear CANDU reactor and represents the reference case. Mainly, a CANDU power plant comprises the nuclear reactor with its moderator circuit, which ejects the moderator heat to the environment and, with the coupled steam generator, produces steam to be expanded in the multi-pressure Rankine power plant. For safety reasons, CANDU power plants are placed in the vicinity of large lakes, which can provide a cooling sink for the condenser. However, the heat from the moderator is at a temperature too high (>60°C) to be ejected into a lake without affecting the ecosystem. With the technology available in the past decade, this temperature is not sufficient to justify the conversion of the moderator heat into work through a heat engine. The practical solution that ensures also the safety of the reactor is to use cooling towers. The proposed method for making use of the heat ejected by the moderator is by coupling the CANDU

Table 12.2 Case study results for the integrated multigeneration for nuclear power, H_2, and O_2

Item	Value (MJ/kmol H_2)	Remarks
Exergy of produced hydrogen	236	At 70°C and 1 bar, as delivered by Cu–Cl plant
Exergy of stored hydrogen	240	Stored in metal hydrides at 14 bar and 20°C
Compression of H_2	7	Electrical power is spent; ideal compression process
Exergy of produced oxygen	2	At 70°C and 1 bar, as delivered by Cu–Cl plant
Exergy of compressed oxygen	122	Stored in cylinders at 200 bar and 20°C
Compression of O_2	107	Electrical power is spent; ideal compression process
Electricity supplied to Cu–Cl plant	140	Spent from the power plant electricity generation
Heat supplied to Cu–Cl plant	179	Comes from the Cu–Cl cycle analysis
Heat extracted from the moderator	188	Comes from heat pump analysis, where QM = 105% $Q_{reaction}$
Generated nuclear heat	3,760	Assumes that all moderator heat is used and this is 5% from generated nuclear heat
Generated power	1,316	Assumed 35% power plant efficiency
Power consumed by heat pump	35.8	Assumed COP = 5
Total consumed power	290	Compressing gases, running the heat pump and Cu–Cl plant
Net power generated	1,026	Total generation minus consumption
Total useful exergy	1,388	See Eq. (12.1)
Carnot factor for nuclear energy	0.52	T_0 is assumed as 26°C and the nuclear reaction temperature T_N = 350°C
Consumed exergy	1,950	Based on specific exergy of nuclear fuel
Exergy efficiency with multigeneration	71%	Calculated with Eq. (12.18)

Data from Zamfirescu et al. (2010)
COP coefficient of performance

power plant moderator with the water splitting cycle through the system, as shown here in Fig. 12.14. The three system components are as follows:

1. Rankine cycle (i.e., the power plant that is coupled to the nuclear reactor): low pressure superheated steam is extracted from the Rankine cycle and expanded to 1 bar pressure in the Cu–Cl plant.
2. Heat pump cycle: upgrades the temperature of waste heat from the moderator vessel and consumes electricity, indicated by $W_{HP.}$
3. Cu–Cl cycle: supplied with electricity by the Rankine generator to drive the electrochemical reaction and compress/store the produced hydrogen and oxygen. The total heat received by the Cu–Cl plant from the heat pump comprises the heat needed to supply the chemical reactions (indicated by $Q_{Cu–Cl}$) and the heat used for reactant preheating.

The predicted results of this case study and the relevant assumptions and comments are presented in Table 12.2. The calculations are scaled for 1 kmol of produced and stored hydrogen. The exergy efficiency of the multigeneration plant

(which recovers and uses the moderator's heat) is improved by 4%, with respect to exergy efficiency of the original power plant (which rejects the moderator heat to the environment), that is, 71% vs. 67%.

The assumptions and calculations for the case study represent the approximate estimates. They represent the first evaluation of the newly proposed multigeneration plant and encourage detailed studies for further confirmation. Based on these results, more improvement in exergy efficiency can be obtained if additional waste heat is recovered to generate electricity.

12.6.2 Integration of SOFC and Rankine Cycles for Tri-Generation

This case study is based on the work of Al-Sulaiman et al. (2010), who proposed and analyzed an integrated tri-generation system comprising a solid oxide fuel cell (SOFC) coupled with a Rankine cycle for producing power, heating, and cooling. The proposed system consists of an SOFC, an organic Rankine cycle (ORC), a heating process, and a single-effect absorption chiller, as shown in Fig. 12.13. The waste heat from the SOFC is used to heat the organic fluid in the ORC. Consecutively, the waste heat from the ORC is used for heating and cooling. The waste heat from the ORC is used to produce steam in the heating process, using a heat exchanger, and to produce cooling, using a single-effect absorption chiller. To have an efficient ORC, the working fluid in the ORC should have a high critical temperature so that usable waste heat can be gained. One of the typical organic fluid types used to operate the ORC is *n*-octane, which has a relatively high critical temperature, 569 K. Hence, it is selected as the working fuel of the ORC.

The assumptions for steady-state modeling of the cycle include the following: efficiency of the ORC turbine and pump of 80% (both), effectiveness of the ORC boiler of 80% and of the solution heat exchanger of the absorption refrigerator of 70%, electric generator efficiency of 95%, dc–ac inverter efficiency of the SOFC of 95%, fuel utilization factor in the SOFC of 85%, and inlet stream temperature of the SOFC of 1,000 K.

Here, the fuel cell is modeled using steady-state gas concentration, Nernst voltage, and the loss voltage, which include ohmic, activation, and polarization losses. Referenced equations are provided in the Al-Sulaiman et al. (2010) study for all voltage components to eventually determine the cell voltage as the difference $V_C = V_N - V_{loss}$. It is assumed that the overall chemical reaction in the fuel cell evolves at equilibrium; based on this assumptions, the molar concentration of the components of the output streams are calculated.

As can be observed in Fig. 12.15, in addition to natural gas, the tri-generation system uses wood as the primary fuel. This should not be considered a variation from the definition of the multigeneration systems that normally use a single kind of primary fuel. Rather, in this case, wood, being a biomass, has the role of

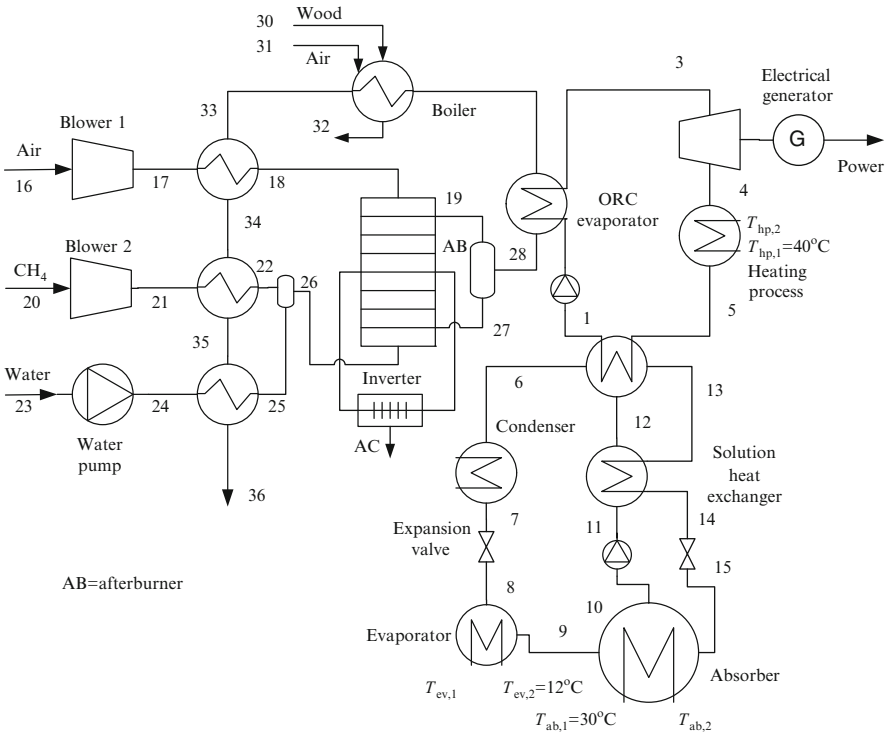

Fig. 12.15 Integrated tri-generation system with SOFC, ORC, and absorption chiller [modified from Al-Sulaiman et al. (2010)]

diminishing the greenhouse gas emissions per unit of useful product. Moreover, burning wood in an externally fired boiler (states 29–33 in Fig. 12.15) is a cheap and well-known technology. Therefore, one considers as the total input exergy in the plant the sum of the exergy consumed from natural gas and from wood: $\dot{E}x_{PF} = \dot{m}_{CH_4} ex^{ch}_{CH_4} + \dot{m}_{wood} ex^{ch}_{wood}$. The tri-generation exergy efficiency becomes

$$\psi = \frac{\dot{W}_{net} + (T_0/T_{ev} - 1)\dot{Q}_{ev} + \left(1 - T_0/\bar{T}_{hp}\right)}{\dot{E}x_{PF}}, \tag{12.27}$$

where $\dot{W}_{net} = \eta_{inv}\dot{W}_{SOFC} + \eta_{gen}\dot{W}_T - (\dot{W}_{blow,1} + \dot{W}_{blow,2} + \dot{W}_{pmp,w} + \dot{W}_{pmp,ORC})/\eta_{mot}$, T_{ev} is the temperature of the cooling at the evaporator level of the refrigerator, and $\bar{T}_{hp}$ is the average temperature for process heating. Here, one assumes that the plant heats a water stream that enters the heat exchanger at 40°C. The current density, the inlet flow temperature in the SOFC, the pressure inlet of the turbine, and the inlet temperature of the ORC pump are important parameters to be studied.

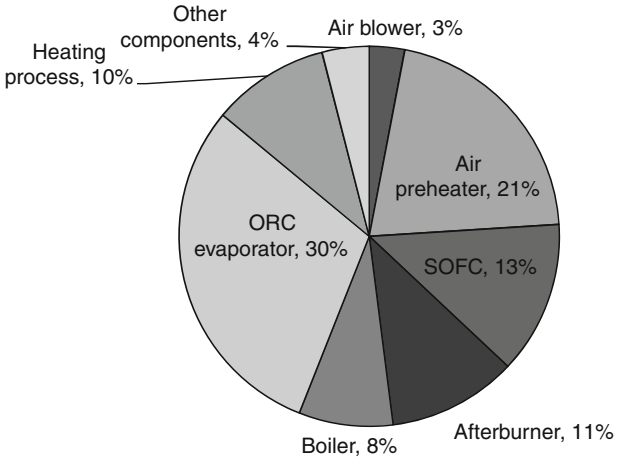

Fig. 12.16 Exergy destruction in percentage for different plant components at 0.75 A/cm^2, 16 bar ORC high pressure, 1,000 K at SOFC inlet, and $T_1 = 345$ K [data from Al-Sulaiman et al. (2010)]

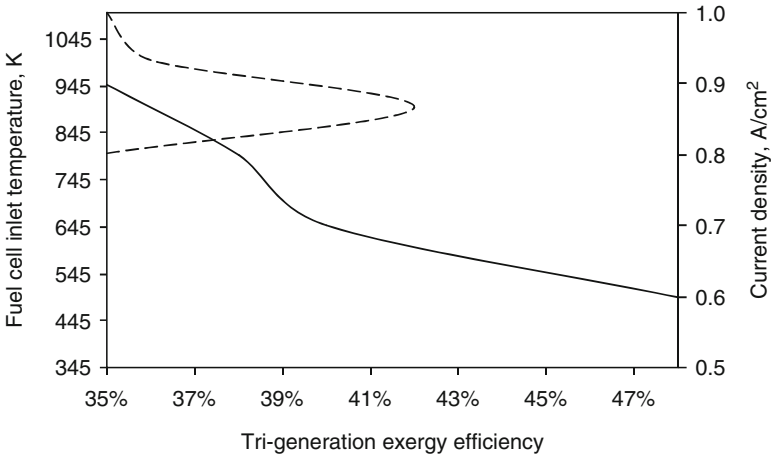

Fig. 12.17 The effect of fuel cell inlet temperature and current density on the overall tri-generation exergy efficiency [data from Al-Sulaiman et al. (2010)]

The calculated exergy efficiency of the tri-generation system varies between 35% and 45% depending on the fuel cell current density (0.6–0.9 A/cm^2) and the inlet flow temperature in the SOFC (800–1,100 K). For an average current density of 0.75 A/cm^2, the exergy destruction rate in percents of the total are given in Fig. 12.16.

The parameters that most affect the overall exergy efficiency are the current density and the fuel cell inlet temperature. The correlation between exergy efficiency and these parameters can be seen from the plot shown in Fig. 12.17.

According to Al-Sulaiman et al. (2010), the gain in the exergy efficiency when tri-generation is used compared with only a power cycle is from 3% to 25%, depending on the operating condition.

12.6.3 Tri-Generation System with Combined Brayton and Absorption Cycles

This case study presents a tri-generation system comprising two Brayton cycles and an LiBr/H_2O absorption refrigeration cycle. One of the Brayton cycles works as a refrigerator and is applied for compressor inlet air cooling. The second Brayton cycle is a gas turbine power generator. A heat recovery steam generator (HRSG) for process heat is used in addition to absorption refrigeration for cold production. This system is shown in Fig. 12.18.

The power cycle labeled 1–2–3–4 consists of a compressor, a combustion chamber, and a turbine, and the reverse Brayton refrigeration cycle 1–6–7–8 consists of a cooling coil and an expansion device. A common compressor is used by both the cycles, where the working fluid is divided between the two cycles. A portion of the compressed air $\alpha\dot{m}$ 1 at pressure P_6 is extracted, cooled in a heat exchanger to T_7, and then expanded to the atmospheric pressure at T_8. The hot ambient air at T_0 mixes with the cold stream at T_8 before entering the compressor. Owing to the mixing of cold air at T_8 with that at T_0, the temperature at the compressor inlet drops. The expanded gas in the turbine at label 4 is utilized in the HRSG to generate process heat.

The water vapor mixture that enters the evaporator at label 11 is boiled and exits the evaporator in a saturated state at label 12. The saturated steam at label 12 enters the absorber, where it mixes with a solution leaving the generator that is weak in refrigerant and strong in absorbent at label 18, generating heat that has to be dissipated to increase the efficiency of mixing process.

For thermodynamic modeling, mass, energy, and entropy balances are written for each component of the system. In the mixing chamber it is assumed that a 2% pressure drop takes place. The compression process is assumed polytropic. An equation similar to that in the cases above is applied to calculate the tri-generation exergy efficiency. Additionally, the fuel utilization efficiency is calculated as:

$$\eta = \frac{\dot{W}_{\text{net}} + \dot{Q}_{\text{hp}} + \dot{Q}_{\text{C}}}{\dot{m}_{\text{PF}}\text{HHV}_{\text{PF}}}, \tag{12.28}$$

where PF stands for primary fuel, in this case natural gas, and hp stands for process heating. Also the electrical to thermal energy ratio can be calculated as

$$R_{\text{ET}} = \frac{\dot{W}_{\text{net}}}{\dot{Q}_{\text{hp}} + \dot{Q}_{\text{C}}}. \tag{12.29}$$

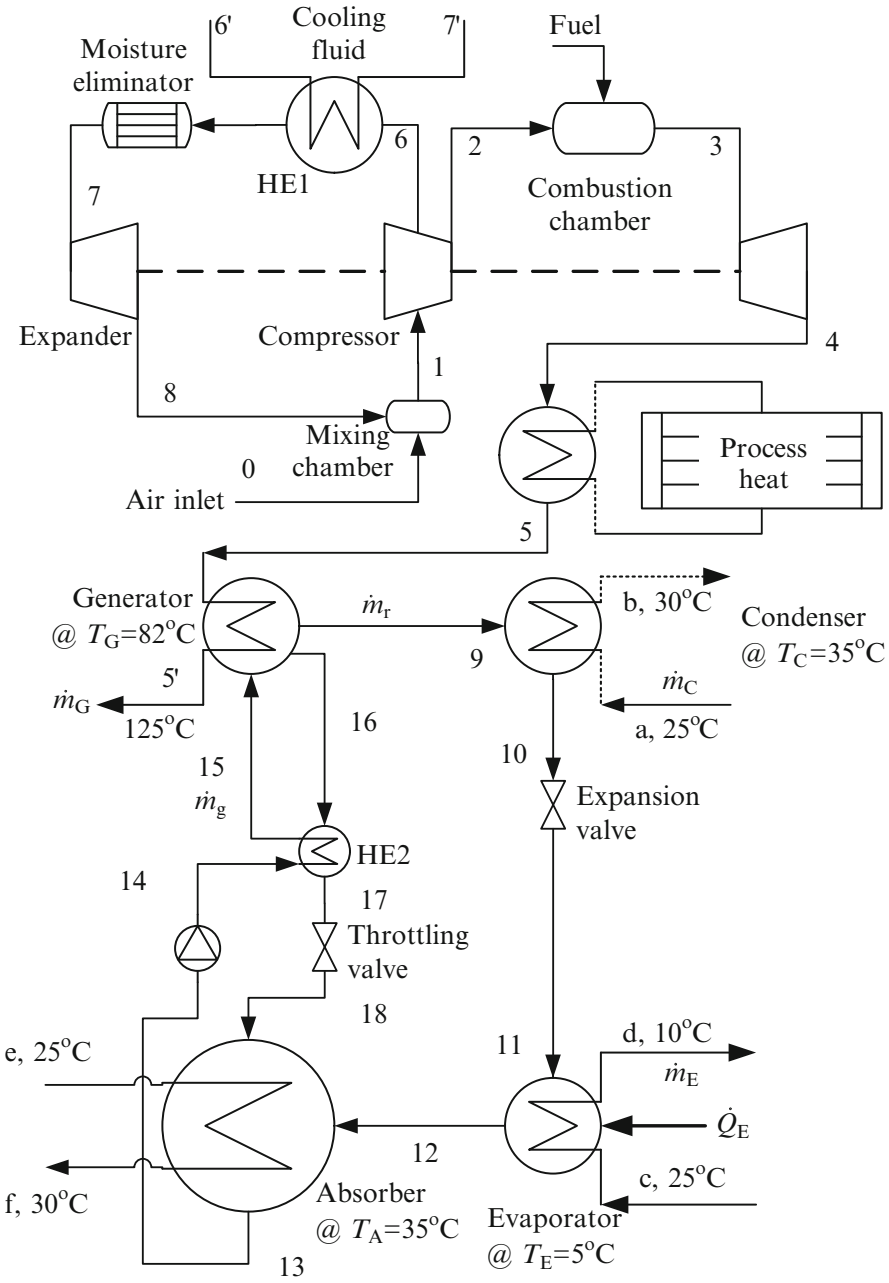

Fig. 12.18 Combined Brayton/absorption cycle tri-generation system with inlet air cooling [modified from Khaliq et al. (2009a)]. *HE* heat exchanger

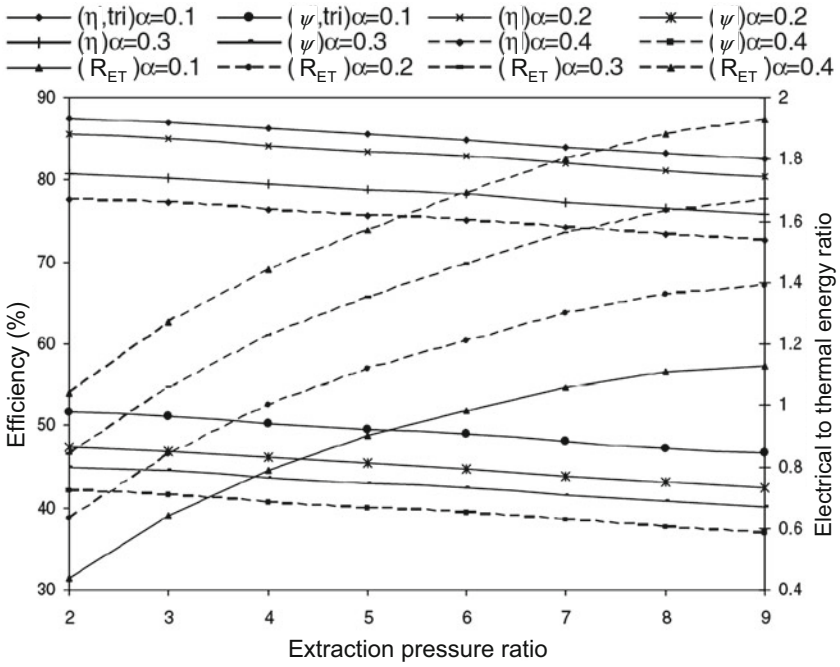

Fig. 12.19 Performance of the tri-generation system expressed as efficiency (utilization and exergy) and electrical-to-thermal ratio as a function of air extraction pressure ratio and α, the air mass flow extraction rate [modified from Khaliq et al. (2009a)]

For the numerical calculation, the inlet air has been assumed at 310 K with 60% relative humidity, the gas turbine pressure ratio has been taken to be 10 with 1,473 K inlet temperature and a fixed specific heat ratio of the combustion gases $\gamma = 1.33$, while for the air compressor process $\gamma = 1.4$. The temperature difference in the heat exchanger is assumed to be 5 K and the pinch point 25 K. With this assumption, the tri-generation efficiency in terms of fuel utilization and exergy, and R_{ET} are reported as a function of the air extraction pressure ratio in the air compressor (defined as P_6/P_1). It can be observed in Fig. 12.19 that the exergy efficiency can reach 50%, while the fuel utilization efficiency approaches 90%.

The performed thermodynamic analysis demonstrates that the utilization and exergy efficiencies increase while the electrical to thermal energy ratio decreases with the extracted mass rate (inlet air cooling). Moreover, the electrical to thermal energy ratio and exergy efficiency are sensitive to process heat pressure, and the process heat pressure should be high for better performance based on the first and second laws of thermodynamics. Regarding the exergy destruction, 21% irreversibility occurs in the combustion chamber, 17% in HRSG, 13.5% in the generator of the absorption refrigeration system, and 12% in the components.

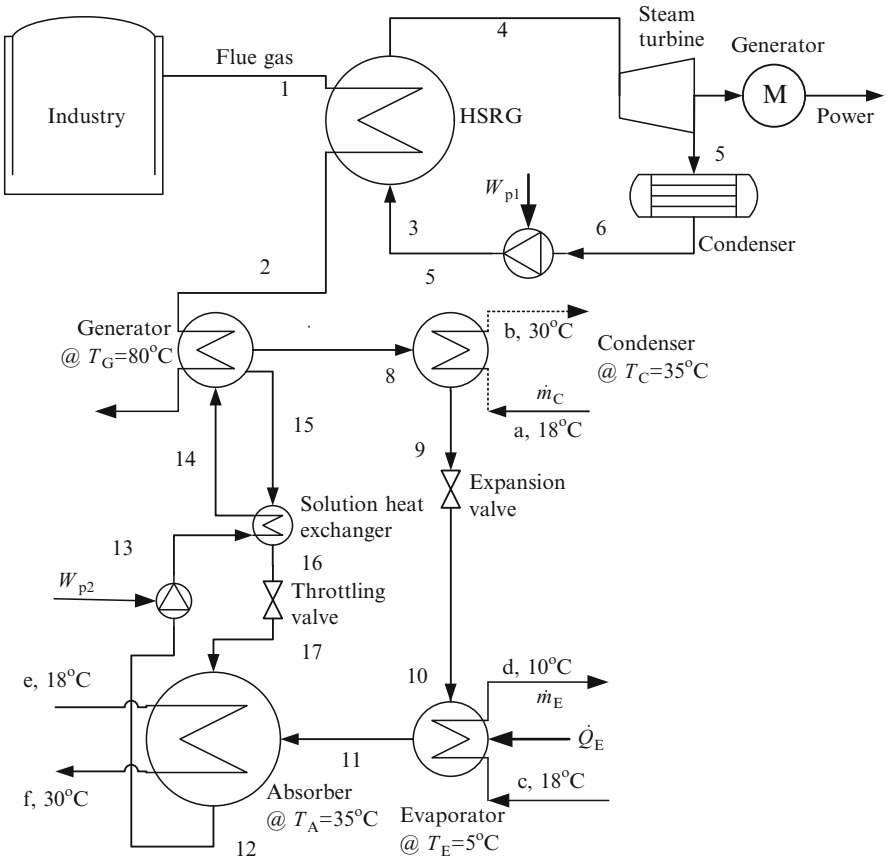

Fig. 12.20 Power and cooling system with combined Rankine and absorption cycles [modified from Khaliq et al. (2009b)]

12.6.4 Integrated Rankine and Absorption Cycles for Power and Refrigeration

This example, based on the work of Khaliq et al. (2009b), is a system for tri-generation that is driven by industrial waste heat available in the temperature range 425–525°C. The system is presented in Fig. 12.20. The waste heat is transferred to the boiler of a steam Rankine cycle, which generates power at its turbine (ST in Fig. 12.20). Further, the hot stream is sent to the generator of an absorption refrigeration machine operating with LiBr/H_2O; the generator is driven with 80°C temperature heat. The cooling effect is obtained at the evaporator of the refrigeration machine.

The thermodynamic analysis indicates that the exergy efficiency is defined in this case with $\psi = \left[\dot{W}_{\text{net}} + \dot{Q}_{\text{C}}(T_0/T_{\text{C}} - 1)\right]/\dot{E}_{\text{PF}}$, where the exergy rate of the primary fuel consumption $\dot{E}_{\text{PF}}$ is calculated as follows:

$$\dot{E}_{\text{PF}} = \dot{m}_{\text{PF}}\{h(T_1) - h(T_0) - T_0[s(T_1) - s(T_0)]\}. \tag{12.30}$$

The nature of the fluid transferring heat from industry and its associated specific exergy are important. For the range of temperature considered, this fluid is assumed to be a gas. Khaliq et al. (2009b) calculated the efficiency of the cogeneration system for three gases, namely, air, combustion gas with 16.5% oxygen, and combustion gas with 7.5% oxygen. The power-to-cold ratio, defined similarly to the electrical-to–thermal energy ratio—Eq. (12.21)—as the ratio between power output and cooling heat flux output, varies from 2 to 8 for the range of temperature considered. Here, the effect of the considered hot gas stream is minimal. Its effect is also reduced (on the order of 2%) on the value of utilization efficiency, but it is more important on the exergy efficiency, which shows 8% to 10% variation. The highest exergy efficiency is obtained with air and the lowest with the combustion gas with 7.5% oxygen. The exergy efficiency ranges between 35% and 52% depending on the inlet gas temperature. Also the effect of the pinch point in the HRSG has been studied: it is shown that the exergy efficiency varies from 45% to 52% if the pinch point is reduced from 50° to 10°C.

12.6.5 Tri-Generation with Integrated Absorption Refrigeration with Ammonia Turbine

In this case study, an innovative system of generation of power, heating, and cooling that is based on a modified ammonia–water absorption refrigeration cycle that has an integrated power turbine is presented. The cycle is illustrated in Fig. 12.21. It is assumed that the heat source is recovered from an industrial process, and, as in the above example, a combustion gas transfers the heat from the industrial process to the tri-generation unit.

Thermodynamic modeling at steady state has been applied to quantify the system performance. The results shown here are based on the work of Khaliq et al. (2009c). Note that the modified ammonia–water cycle, which incorporates an ammonia turbine, was first proposed by Hasan et al. (2002). The turbine is applied after the ammonia rectification, which is usually done in the ammonia–-water absorption cycle. Here, after the rectifier, the resulting high-purity and high-pressure ammonia is superheated. Thereafter, ammonia is expanded in a turbine that operates in two phases. That is, at the turbine outlet one finds an ammonia liquid–vapor at low temperature.

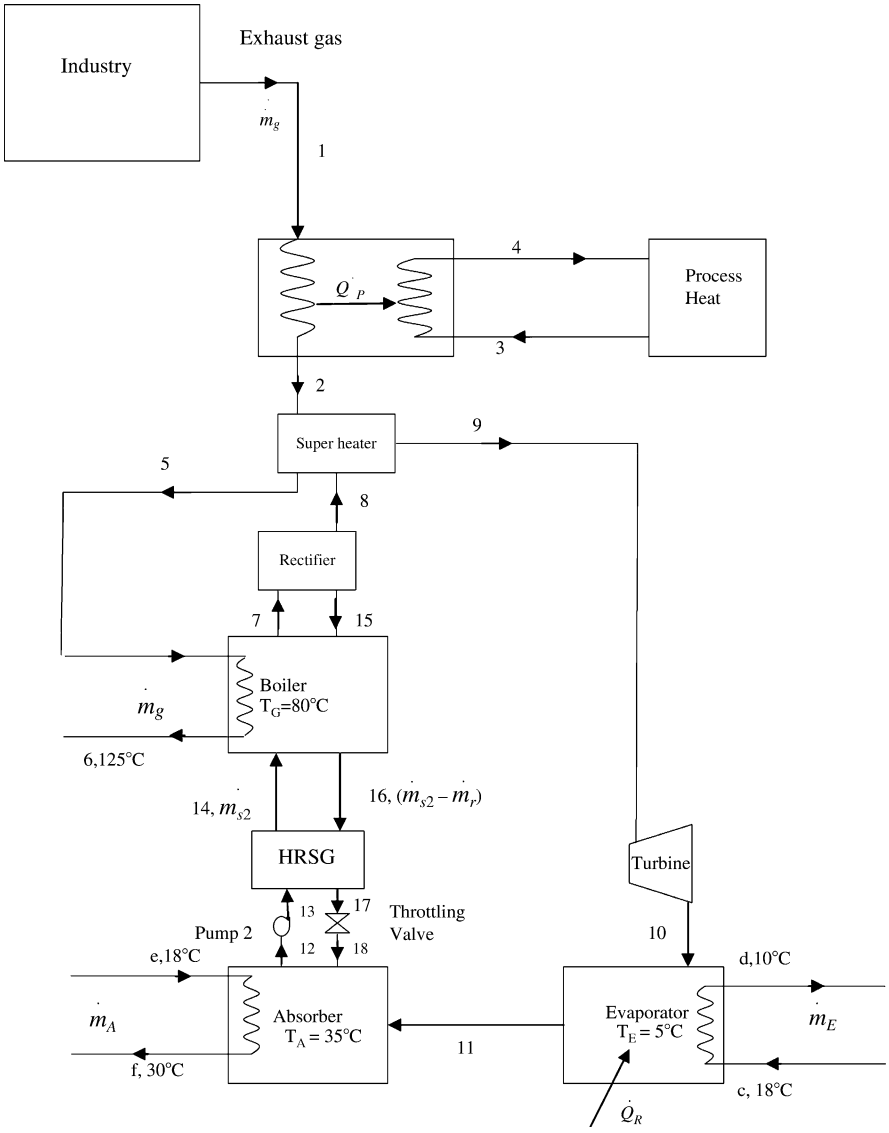

Fig. 12.21 Waste heat recovery driven tri-generation system with ammonia–water [modified from Khaliq et al. (2009c)]

The results show the utilization and exergy efficiency plus the electrical-to–thermal energy ratio as a function of waste heat temperature. The figure ranges between 80% to 85% and 34% to 42% for exergy and utilization efficiency, respectively. The electrical to thermal energy ratio varies from 10 to 20. The considered range of source temperature for the analysis is 375° to 475°C. The process heat is assumed to be used for steam generation (see Fig. 12.21).

The process steam pressure is important because it has an effect on the exergy efficiency of the system. The higher the pressure, the higher the exergy efficiency of the system for a given pinch point. For pressure varying from 10 to 20 bar, the exergy efficiency increases by 10% while the energy efficiency is practically not affected. For the same range of pressures, the electrical-to–thermal energy ratio increases from 8% to 18%.

12.7 Concluding Remarks

This chapter introduced the concept of integrated multigeneration energy systems for practical applications. In a multigeneration energy system, several useful outputs are obtained by using the same input. Such systems offer a wide range of advantages, namely, better efficiency, better cost-effectiveness, better resource use, better environment, and hence better sustainability. Several case studies were presented to highlight the importance of hybrid and integrated multigeneration systems for practical applications.

Nomenclature

C	Specific cost, any currency
Ee	Economic effectiveness
ex	Specific exergy, kJ/kg
Ex	Exergy, kJ
G	Gibbs free energy, kJ/mol
GSEnF	Geothermal-solar energy fraction
h	Specific enthalpy, kJ/kg
HHV	Higher heating value, MJ/kg
H	Enthalpy, kJ
I	Solar irradiance, W
K	Equilibrium constant, Eq. (12.16)
LHV	Lower heating value, MJ/kg
m	Mass, kg
$\dot{m}$	Mass flow rate, kg/s
P	Pressure, bar
Q	Heat, kJ
R	Universal gas constant, J/kmol.K
R_{ET}	Thermal energy ratio
s	Specific entropy, kJ/kg K
S	Entropy, kJ/kgK
T	Temperature, K
V	Voltage, V
W	Work, kJ

Greek Letters

γ	Specific heat ratio
Δ	Difference
η	Utilization efficiency
ψ	Exergy efficiency

Subscripts

0	Reference state
abs	absorber
AC	Air conditioning
blow	Blower
C	Cooling or condenser
con	Condenser
d	destroyed
e	Electric
ev	Evaporator
FC	Fuel cell
gen	Generator
geo	Geothermal
H	Heating
hp	Heating process
HW	Hot water
i	index
inv	Inverter
j	Index
m	Material
mot	Motor
N	Nernst
o	Output
OP	Other product
PF	Primary fuel
pmp	Pump
S	Salt or stack
SF	Synthetic fuel
SH	Space heating
SS	Strong solution
T	Turbine
WF	Working fluid
WS	Weak solution
U	Uranium

Superscripts

ch Chemical
P Thermomechanical
($\dot{}$) Rate (per unit of time)
($\bar{}$) Average value

References

Al-Sulaiman F.A., Dincer I., Hamdullahpur F. 2010. Exergy analysis of an integrated solid oxide fuel cell and organic Rankine cycle for cooling, heating and power production. *Journal of Power Sources* 195:2346–2354.

Coskun C., Oktay Z., Dincer I. 2010. Investigation of a Hybrid Solar and Geothermal Driven Absorption Cooling System for District Energy Systems. Second International Conference on Nuclear and Renewable Energy Resources, Ankara, 4–7 July.

Dincer I., Rosen M.A. 2007. Exergy: Energy, Environment and Sustainable Development. Elsevier, Oxford, UK.

Dincer I., Rosen M.A., Zamfirescu C. 2010. Exergetic performance analysis of a gas turbine cycle integrated with solid oxide fuel cells. *Journal of Energy Resources Technology* 131/032011:1–11.

Fee D.A. 2005. Third party financing. In: Combined Production of Heat and Power (Cogeneration), Sirchis J., ed. Elsevier Science Publishing Co., Essex, UK.

Granovskii M., Dincer I., Rosen M.A. 2007. Performance comparison of two combined SOFC–gas turbine systems. *Journal of Power Sources* 165:307–314.

Granovskii M., Dincer I., Rosen M.A. 2008. Exergy analysis of a gas turbine cycle with steam generation for methane conversion within solid oxide fuel cells. *Journal of Fuel Cell Science and Technology* 5/031105:1–9.

Hamrin J. 2005. The history and status of financing cogeneration projects in California with prospects for the future. In: Combined Production of Heat and Power (Cogeneration), Sirchis J., ed., Elsevier Science Publishing Co., Essex, UK.

Hasan A.A., Goswami D.Y., Vijayaraghavan S. 2002. First and second law analysis of a new power and refrigeration thermodynamic cycle using a solar heat source. *Solar Energy* 73:385–393.

International Energy Agency. 2008. Combined Heat and Power: Evaluating the Benefits of Greater Global Investment.

Kanoglu M., Dincer I. 2009. Performance assessment of cogeneration plants. *Energy Conversion and Management* 50:76–81.

Khaliq A., Choudhary K., Dincer I. 2009a. Exergy analysis of a gas turbine trigeneration system using the Brayton refrigeration cycle for inlet air cooling. Proceedings of IMechE Part A. *Journal of Power and Energy* 224:449–461.

Khaliq A., Kumar R., Dincer I. 2009b. Exergy analysis of an industrial waste heat recovery based cogeneration cycle for combined production of power and refrigeration. *Journal of Energy Resources Technology* 131/022402:1–9.

Khaliq A., Kumar R., Dincer I. 2009c. Performance analysis of an industrial waste heat-based. *International Journal of Energy Research* 33:737–744.

Kolanowski B.F. 2008. Small-Scale Cogeneration Handbook: CRC Press, Lilburn CA.

Naterer G.F. 2008. Second law viability of upgrading industrial waste heat for thermochemical hydrogen production. *International Journal of Hydrogen Energy* 33:6037–6045.

Naterer G.F., Suppiah S., Lewis M., Gabriel K., Dincer I., Rosen M.A., Fowler M., Rizvi G., Easton E.B., Ikeda B.M., Kaye M.H., Lu L., Pioro I., Spekkens P., Tremaine P., Mostaghimi J., Avsec J., Jiang J. 2009. Recent Canadian advances in nuclear-based hydrogen production and the thermochemical Cu–Cl cycle. *International Journal of Hydrogen Energy* 34:2901–2917.

Walker L.P. 1984. A method for formulating and evaluating integrated energy systems in agriculture. *Energy in Agriculture* 3:1–27.

Zamfirescu C., Naterer G.F., Dincer I. 2010. Upgrading of waste heat for combined power and hydrogen production with nuclear reactors. *Journal of Engineering for Gas Turbines and Power* 132/102911:1–9.

Study Questions/Problems

12.1 Define the concept of system integration and its benefits. Give practical examples.

12.2 Consider the system from Fig. 12.1. With reasonable assumptions similar to those presented in the chapter, calculate the system efficiency and all state point parameters.

12.3 Explain the concept of multigeneration and its benefits.

12.4 Calculate the system from Fig. 12.7 if the maximum temperature of the working fluid is 400°C and the minimum is 20°C.

12.5 Calculate the efficiency of the system from Fig. 12.8a that operates with biogas. Make reasonable assumptions.

12.6 Explain the concept of hybridization and its benefits.

12.7 Repeat the calculation for the hybrid system from Fig. 12.12 assuming 5% more solar energy input.

12.8 Devise a hybrid system for biomass and concentrated solar power generation.

12.9 Consider the system from Fig. 12.14; make reasonable assumptions for the efficiency of each component and determine the energy and exergy of the overall system.

12.10 Calculate the cycle from Fig. 12.18 under reasonable assumptions.

Chapter 13
Hydrogen and Fuel Cell Systems

13.1 Introduction

The *hydrogen economy* emerged as a potential response to two major problems that mankind faces today, namely, its dependence on fossil fuels and the high level of pollution associated with the fossil fuel combustion process. Indeed, the exploitable and proved fossil fuel reserves are limited. As a consequence of population growth and industrial development of the Asiatic continent (with countries like China and India counting over one billion people each), the rate of fossil fuel exploitation increases constantly together with their costs and the associated pollution levels.

The necessity to shift to an alternative energy–based economy is obvious. Such an economy is based on renewable energy sources such as solar (which includes biomass energy), hydro, wind, tides and currents, ocean thermal, and geothermal. It was mentioned in Chapter 9 that energies are available temporally, incidentally, or locally. For example, solar energy is available during the day; wind energy is available with more intensity in some seasons or days and is not present in others; geothermal energy can be found only in certain locations on the globe. Therefore, with alternative energies there is, most of the times, a mismatch between availability and demand. Moreover, these energies are difficult to store and transport.

The idea of a hydrogen economy was introduced at a scientific conference held in March 1974 in Miami, Florida, titled "The Hydrogen Economy Miami Energy (THEME) Conference," at which the International Association for Hydrogen Energy (IAHE) was established. Today, after 37 years of information dissemination and advances in hydrogen economy technologies, the world's most developed countries (the United States, Japan, and countries in the European Union) and many other countries invest extensively in shifting toward a hydrogen-based economy.

This chapter discusses hydrogen fuel and fuel cell systems. The issues regarding production, storage, and distribution of hydrogen are discussed, along with hydrogen utilization for power generation with fuel cells. The primary focus is on renewable-based hydrogen production through solar, wind, hydro, geothermal, biomass, and other options, and the opportunities and challenges are discussed with several case studies, examples, and applications from various systems.

İ. Dinçer and C. Zamfirescu, *Sustainable Energy Systems and Applications*,
DOI 10.1007/978-0-387-95861-3_13,

Hydrogen production methods from fossil fuels are also discussed and compared with renewable energy-based technologies. Efficiency evaluation, environmental impact, and sustainability assessment are also discussed.

13.2 Hydrogen

Hydrogen is the simplest chemical element with atomic number $Z = 1$, and it is the most abundant chemical element in the universe. As a consequence of its simplicity, hydrogen can lose valence electrons easily, and therefore it is very reactive. Thus, hydrogen cannot be found as an individual element on earth, but rather is embedded in other materials. Water is the most abundant resource of hydrogen on earth; also, hydrogen is part of most fossil fuels and biomass. In nature, hydrogen can also be found in the form of hydrogen sulfide (H_2S), which is abundant in some springs, geothermal sites, and the seas. Regarding its properties, hydrogen has a high caloric value, the lowest molecular weight, the highest thermal conductivity among all gases, and the lowest viscosity. Table 13.1 summarizes the main thermophysical properties of hydrogen.

The heating value of hydrogen is much higher than that of conventional fuels if taken as per unit of weight. However, hydrogen cannot be kept in a condensed phase with current technology. Mostly, hydrogen is stored in the form of compressed gas or as cryogenic liquid. In any of these storage conditions, the heating value of hydrogen per unit of volume is the lowest of all the conventional fuels. Nevertheless, the efficiency of power generation systems fueled with hydrogen is much higher than that obtained with conventional fuel, and this fact compensates for the low storage density problem of hydrogen. Furthermore, hydrogen combustion is completely clean, producing only water vapor in the exhaust gas. Heat recovery can be applied intensively to hydrogen combustion to obtain liquid water, which can be recycled to produce hydrogen again via various methods for extracting hydrogen from water, including electrolysis and thermochemical splitting. Therefore, hydrogen can be viewed as an energy storage medium or energy carrier. The major problem with hydrogen as a fuel is the difficulty of storing it in its pure form and the enormous costs of a hydrogen infrastructure, which must be put in place in order to implement a hydrogen energy–based economy. It is arguably believed that the storage and distribution problem is well balanced by the benefits brought by the hydrogen economy.

Table 13.1 Thermophysical properties of hydrogen

Property	MP	BP	T_c	P_c	Flammability	IT	AFT	Flame velocity	LHV
Value	14.01 K	20.3 K	32.97	12.9 bar	4.1–75%	850 K	2,400 K	2.75 m/s	120 MJ/kg

MP melting point; *BP* normal boiling point; *IT* ignition temperature; *AFT* adiabatic flame temperature

13.3 Hydrogen Economy

Utilization of any kind of energy resources leads unavoidably to some environmental impact. Increasing the efficiency throughout the whole chain from energy supply to end use is a way to alleviate concerns regarding emissions and their negative environmental impact. Higher efficiency means less resource utilization and associated pollution.

Using hydrogen as an energy carrier can help in reducing environmental damage and in achieving sustainability. If hydrogen is produced from clean and renewable energy sources, the environmental impact is reduced because fossil fuel resources are not consumed and hydrogen combustion emissions do not contribute to global warming or generate substantial waste. At the hydrogen utilization phase, the associated processes (e.g., combustion) are more efficient than with traditional fuels. For example, fuel cell technologies can provide more efficient, effective, and environmentally benign and sustainable alternatives to conventional energy technologies, particularly fossil fuel–driven ones. Hydrogen energy systems are a key component of sustainable development for four main reasons:

- They are compatible with renewable energy sources and carriers for future energy security, economic growth, and sustainable development.
- The variety of hydrogen and fuel cell technologies provide a flexible array of options for their use in various applications with reduced environmental impact and increased efficiency.
- Hydrogen cannot be depleted since the basic source is water. In contrast, fossil fuel and uranium resources are diminished by extraction and consumption.
- These technologies favor system decentralization and local and individual solutions that are somewhat independent of the national network, thus enhancing the flexibility of the system and providing economic and environmental benefits to small isolated populations.

Even if hydrogen is produced from fossil fuel sources, which normally cause a burden on the environment, it is almost certain that hydrogen technologies can provide a cleaner and more sustainable energy system than increased controls on conventional energy systems because hydrogen

- can be extracted from widely available materials such as water, natural gas (NG), petroleum, coal, and biomass; in addition, if sustainable energy sources are used for its production (e.g., renewable energy, nuclear energy, energy recovered from waste heat) its fabrication process becomes low-polluting;
- can be used in stationary and mobile applications without damaging emissions, especially by using fuel cells;
- can be made available everywhere, can substitute for oil and gas, and can be burned without changing the climate.

Hydrogen is only a secondary energy source (a “storage carrier”) and must be produced from a primary energy source. For physical reasons, there will

always be losses from these conversion processes, and therefore in any case the costs of hydrogen must be higher than the costs of the energy used to produce hydrogen. This simple physical reason complicates the decision about priorities and time scales for the introduction of hydrogen. It is the same simple methodology leading to a higher CO_2-mitigation effect while using the input energy carrier for the production of hydrogen directly.

The scientific and technical challenges for a hydrogen economy are as follows:

- Reduction of the cost of hydrogen production to a level comparable to the energy cost of petroleum
- Development of a CO_2-free route for the mass production of sustainable hydrogen at a competitive cost
- Development of a safe and efficient national infrastructure for hydrogen delivery and distribution
- Development of viable hydrogen storage systems for both vehicular and stationary applications
- Dramatic reduction in costs and significant improvement in the durability of fuel cell systems

The advantages of hydrogen versus fossil fuels are as follows:

- Liquid hydrogen is the best transportation fuel when compared to liquid fuels, such as gasoline, jet fuel, and alcohols, and gaseous hydrogen is the best gaseous transportation fuel.
- While hydrogen can be converted to useful energy forms (thermal, mechanical, and electrical) at the user end generally through five different processes, fossil fuels can be converted generally only through one process: flame combustion. Thus, hydrogen is the most versatile fuel.
- Hydrogen has the highest utilization efficiency when it comes to conversion to useful energy forms (thermal, mechanical, and electrical) at the user end. Roughly, hydrogen is 30% to 40% more efficient than fossil fuels. Thus, hydrogen saves primary energy resources. It could also be termed as the most energy conserving fuel.
- When fire hazards and toxicity are taken into account, hydrogen is the safest fuel.

13.4 Hydrogen Production Methods

Hydrogen can be extracted from a large variety of material resources such as water, fossil hydrocarbons, biomass, hydrogen sulfide, boron hydrides, and others. In order to extract and separate hydrogen from such material resources, one needs energy.

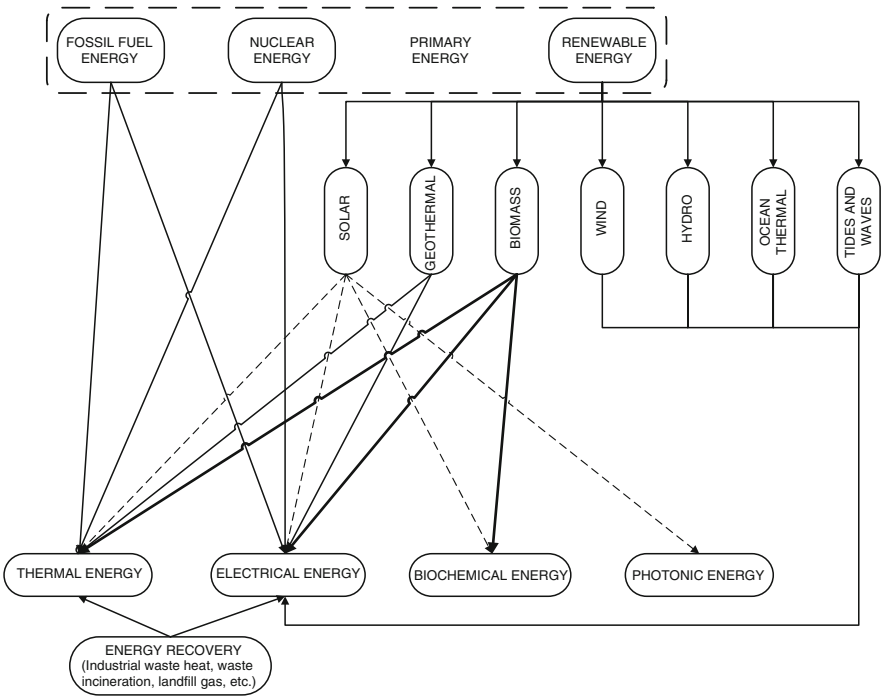

Fig. 13.1 Paths of generation of basic forms of energy from primary energy

The forms of energy that can drive a hydrogen production process can be classified into four categories: thermal, electrical, photonic, and biochemical. These kinds of energy can be obtained from primary energy (fossil, nuclear, and renewable) or from recovered energy through various paths, as suggested in Fig. 13.1. Electrical and thermal energy can be derived from fossil fuels, renewable energies (like solar, wind, geothermal, tidal, wave, ocean thermal, hydro, and biomass), nuclear energy, or recovered energy like industrial waste heat, municipal waste incineration, landfill gas, and others. Photonic energy comprises solar radiation only and it is, therefore, renewable. Biochemical energy is that stored in organic matter (in the form of carbohydrates, glucose, and sugars), and it can be manipulated by certain microorganisms that can extract hydrogen from various substrates. In Table 13.2, the main hydrogen production methods are described and the material and energy resources specific to each are listed.

Currently, 18% of hydrogen production globally sources from coal, 30% from petroleum, 40% from natural gas, and 12% from other sources of which an important share is represented by water electrolysis (Das and Veziroglu 2008). The sales have increased by 5% to 6% per annum in recent years, with the most H_2 use in the fertilizer industry (50%) and the petroleum industry (37%).

Table 13.2 General hydrogen production methods

Method	Description	Material resources	Energy supply
Water electrolysis	Water decomposition into oxygen and hydrogen by passing a direct current that drives electrochemical reactions	Water	Electrical
High-temperature steam electrolysis	Steam decomposition by using direct current assisted by thermal energy to drive electrochemical reactions to split water molecule	Steam	Electrical + thermal
Photoelectrochemical water splitting	Uses electric and photonic energy to electrolyze water and generate H_2 and O_2	Water	Photonic + electric
Photocatalysis	Uses photonic energy and catalysts to decompose water molecule	Water	Photonic
Biophotolysis	Uses a reversible reducible cofactor and photometabolically active microbes to generate hydrogen from water; viz. photosynthesis	Water	Photonic + biochemical
Anaerobic digestion (anaerobic fermentation)	Uses biological energy manipulated by microbes to extract hydrogen from biodegradable materials in the absence of oxygen	Biomass	Biochemical
Thermolysis	Uses thermal energy to decompose water molecule at very high temperature (~2,500°C)	Water	Thermal
Thermochemical water splitting	Thermally driven chemical reactions performed in a loop with the overall result of water splitting	Water	Thermal
Thermocatalytic cracking	Uses thermal energy to break the carbon– hydrogen bonds of hydrocarbons and eventually generate hydrogen	Fossil fuels	Thermal
Gasification	Converts solid carbonaceous materials (fossil or biofuels, wastes, etc.) into carbon monoxide and hydrogen by reacting them with O_2 and/or steam	Water + fossil fuels + biomass	Thermal
Reforming	Reacts carbon-based liquid or gaseous fuels with steam at high temperature to produce carbon dioxide and hydrogen	Water + fossil or biofuels	Thermal

13.4.1 Electricity-Driven Hydrogen Production Methods

13.4.1.1 Water Electrolysis

Electrolysis of water is a basic method to produce hydrogen through redox reactions in water by using a direct current. The overall reaction is water decomposition: $H_2O \rightarrow H_2 + 0.5O_2$. Therefore, water electrolysis is an electrically driven method to generate hydrogen, even though electrolysis can be assisted by some additional thermal energy, as is discussed in this section. The typical process involves a liquid electrolyte, such as an aqueous solution containing sulfate anions SO_4^{2-}; also, there are available solid polymer electrolytes in the form of proton conducting membranes, such as NAFION (a brand name of Du Pont de Nemours) or other kinds, or oxygen ions conduction membranes. The electrical circuit is closed by external conductors that are connected to the direct current electricity source. The contact between the external conductors and the electrolyte is made through electrodes that normally are plated with precious metals, such as platinum, that have the role of accelerating the electrochemical reactions.

The electrode connected to the negative polarity of the direct current source is called the "anode," which is where the water oxidation reaction takes place, releasing oxygen as follows:

$$2H_2O(l) \rightarrow O_2(g) + 4H^+(aq) + 4e^- \quad \text{at } E^0_{ox} = -1.23\,V. \tag{13.1}$$

The electrode connected to the positive polarity of the source is called the "cathode," which is where the proton reduction reaction occurs, releasing hydrogen as follows:

$$4H^+(aq) + 4e^- \rightarrow 2H_2(g) \quad \text{at } E^0_{red} = 0.0\,V. \tag{13.2}$$

The potentials E^0_{ox} and E^0_{red} are called standard potentials because they correspond to operation at 25°C and standard pressure in pure water. Figure 13.2 presents the conceptual design of an electrolytic cell for water electrolysis. In the electrolytic bath, an ionic medium is maintained by adding some salts or other chemicals that maintain an appropriate pH that helps the transport of ions through it. Within the electrolyte some combination of hydroxyl and protons may occur, and the reverse, water ionization forming hydroxyl and protons according to $H_2O \rightarrow H^+ + OH^-$ without affecting the overall water splitting reaction.

The Gibbs free energy of the water decomposition equation can be calculated with $\Delta G = \Delta H - T\Delta S$, where $\Delta H = H_{prod} - H_{react}$ is the total molar enthalpy difference between products and reactants, thus $\Delta H = h_{H_2} + 0.5h_{O_2} - h_{H_2O}$, where h is the specific molar enthalpy of chemicals and includes the formation enthalpy and the thermomechanical enthalpy; one can assume ideal gas behavior of hydrogen and oxygen and thus their enthalpy as a function of temperature only; moreover, the enthalpy of liquids (like water liquid) is practically independent

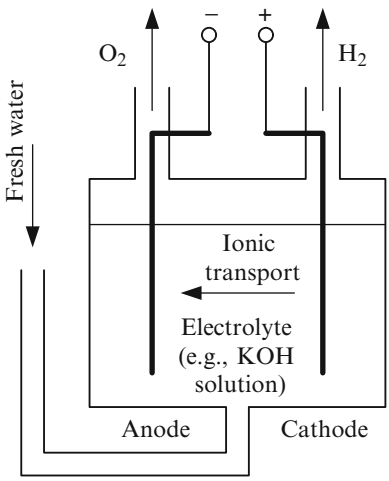

Fig. 13.2 Simplified design of an electrolysis cell

of pressure; if water is present in the form of steam, then again, the ideal gas law applies. The reaction's entropy is calculated similarly, with the only difference being that the entropy is a function of both temperature and pressure: $s(T,P) = s^0(T) - R\ln(P/P^0)$, where R is the universal gas constant and $s^0(T)$ is the entropy at standard pressure P^0.

The Faraday constant relates the Gibbs energy of the reaction with the (ideal/minimum) electric potential that must be applied to the electrodes in order to dissociate the water molecule. The Faraday constant is defined by

$$F = eN_{\mathrm{A}} = -\frac{\Delta G}{n\Delta E_{\mathrm{EL}}} = 96485.3\,\mathrm{C/mol}, \tag{13.3}$$

where $e = 1.602 \times 10^{-19}\,\mathrm{C}$ is the electron's charge, $N_{\mathrm{A}} = 6.022 \times 10^{23}\,\mathrm{mol}^{-1}$ is the Avogadro number, n is the number of moles of electrons per mol of decomposed water, and $\Delta E_{\mathrm{EL}} = E_{\mathrm{red}} - E_{\mathrm{ox}}$ is the difference of potential between the electrodes. The above equation can be solved for ΔE_{EL}:

$$\Delta E_{\mathrm{EL}} = -\frac{\Delta G(T,P)}{nF} = \left[-\frac{\Delta H(T)}{nF}\right] - \left[-T\frac{\Delta S(T,P)}{nF}\right], \tag{13.4}$$

which by rearranging it further becomes

$$\Delta E_{\mathrm{TOT}} = \Delta E_{\mathrm{EL}} + \Delta E_{\mathrm{TH}}, \tag{13.5}$$

where

$$\Delta E_{\mathrm{TOT}} = -\frac{\Delta H(T,P)}{nF} \tag{13.6}$$

is the total equivalent electric potential difference that must be applied to the electrolytic cell and

$$\Delta E_{\mathrm{TH}} = -\frac{T\Delta S(T,P)}{nF} \tag{13.7}$$

is the equivalent potential difference that must be applied to the cell in order to generate the thermal energy Q_{TH} needed to drive the reaction. Note that the portion of energy Q_{TH} can be given either in the form of heat, accounting for $Q_{\mathrm{TH}} = -T\Delta S(T,P)$, or as electricity that is converted through the joule effect into heat, by applying a difference of potential at the electrodes as indicated by Eq. (13.7). The total energy needed to drive the reaction $\Delta H(T,P)$ can be given totally through electricity by applying the difference of potential ΔE_{TOT} to the electrodes, or partially as electricity through ΔE_{EL} corresponding to energy $\Delta G(T,P)$ transmitted to the reaction and Q_{TH} as the thermal counterpart.

There are three possibilities to conduct the electrolysis for splitting the H_2O molecule:

- Cold electrolysis of liquid water at or close to the ambient temperature: in this case, the minimal potential difference between the electrodes is given by Eq. (13.5) calculated for standard conditions, $\Delta E_{\mathrm{TOT}}(T_0,P_0)$; alkaline and proton exchange membrane (PEM) electrolyzer cells can be used.
- High-pressure electrolysis; in this case, the electric potential difference is calculated with $\Delta E_{\mathrm{TOT}}(T,P)$. Here, $(T,P)>(T_0,P_0)$. The high-pressure electrolysis is attractive because it facilitates hydrogen and oxygen compression and storage. In order to increase the efficiency of the process, both temperature and pressure must be increased; moreover, the water is given in pressurized liquid form. It is thermodynamically efficient to pressurize water rather than to compress hydrogen and oxygen products. However, there is a design trade-off in the sense that too high an operating pressure leads to reduced efficiency and higher cost.
- High-temperature steam electrolysis (HTSE) in solid oxide electrolysis cells (SOECs): in this case, water is converted to steam with the expense of thermal energy. Moreover, the electrochemical bath is heated, directly (through steam) or indirectly (through heat transfer) so that the electric energy needed by the process is only $\Delta E_{\mathrm{EL}}(T,P_0)$. The remaining energy is supplied thermally as Q_{TH}.

When the efficiency of electricity generation (which is normally $\eta_{\mathrm{E}} = 20$–30%) is accounted for, the electrolysis energy efficiency assuming no losses becomes

$$\eta_{\mathrm{EL}} = \frac{\Delta H}{(\Delta H/\eta_{\mathrm{E}})} = \eta_{\mathrm{E}}, \tag{13.8}$$

where $\Delta E_{\mathrm{TOT}}/\eta_{\mathrm{E}}$ represents the heat input needed to generate the total electricity to drive the electrolysis; in that case that the process is driven only electrically. If HTSE is considered, then

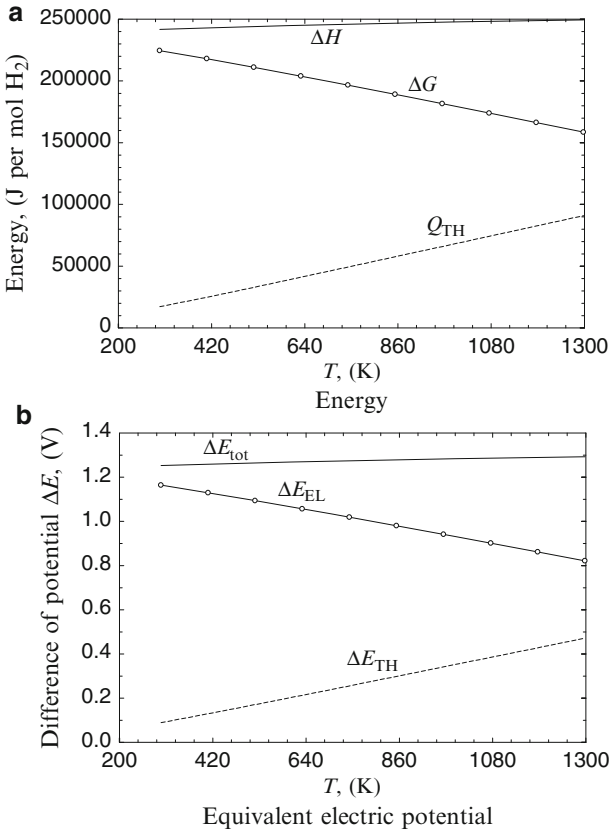

Fig. 13.3 The energy and the equivalent electric potential needed to drive the water electrolysis process for a range of temperatures and standard pressure

$$\eta_{EL} = \frac{\Delta G + Q_{TH}}{\Delta G/\eta_E + Q_{TH}} = \eta_E \times \frac{\Delta G + Q_{TH}}{\Delta G + \eta_E Q_{TH}} > \eta_E, \tag{13.9}$$

where $\Delta G/\eta_E$ is the amount of thermal energy needed to generate the electricity amount equivalent to ΔG. It can be observed in Eq. (13.9) that the factor $(\Delta G + Q_{TH})/(\Delta G + \eta_E Q_{TH}) > 1$; thus, $\eta_{EL} > \eta_E$, which demonstrates that the theoretical efficiency of HTSE is necessarily higher than the theoretical efficiency of liquid water electrolysis.

The ideal/minimal energy needed to drive the water electrolysis process can be calculated as $\Delta H(T)$, $\Delta S(T,P)$, and Q_{TH} using the thermodynamic properties of water, hydrogen, and oxygen. These energy components are presented in Fig. 13.3a) and their corresponding electric potential equivalents in Fig. 13.3b). Many energy losses occur in electrolyzers due to various reasons such as over-potentials, ohmic losses. Consequently, the energy required to drive the electrolysis process is much higher than that calculated with $\Delta H(T)$.

The energy efficiency, defined as the energy retrieved in molar HHV of hydrogen, is divided into the total energy consumed to drive the process ΔH_{in},

$$\eta_{EL} = \frac{HHV_{H_2}}{\Delta H_{in}}, \tag{13.10}$$

and the corresponding exergy efficiency then becomes

$$\psi_{EL} = \frac{ex^{ch}_{H_2} + 0.5ex^{ch}_{O_2}}{Ex_{in}}. \tag{13.11}$$

η_{EL} and ψ_{EL} are of the order of 55% and 50%, respectively, for liquid water electrolysis; note that the chemical exergy of oxygen is very much smaller than that of hydrogen; also note that Eq. (13.11) is written for 1 mol of hydrogen produced. For HTSE, the energy efficiency achieves 80% while the exergy efficiency achieves 60%.

The total efficiency of the electrolysis, considering the electricity generation process, becomes the product $\eta^{TOT}_{EL} = \eta_{EL}\eta_E$ and $\psi^{TOT}_{EL} = \psi_{EL}\psi_E$. Based on these considerations, the hydrogen generation efficiency through water electrolysis is 15% (energy) and 10% (exergy). The corresponding figures for high-temperature electrolysis become 24% (energy) and 12% (exergy). Note also that high-temperature electrolysis is very favorable at 1,000 to 1,200 K and does not require expensive catalysts because the reaction rate is naturally accelerated at high temperature. Applications of HTSE are discussed below as electrothermal methods for hydrogen production.

Basically, any electricity generation process can be connected to a water electrolyzer to generate hydrogen using electricity only. All sorts of renewable energy, nuclear energy, and fossil energy plus energy recovered from other processes can then be used to generate electricity. Therefore, specific methods were developed to produce hydrogen through electricity from all these various routes.

13.4.1.2 Solar–Electrical Routes for Hydrogen Production

Solar radiation is a source of high-quality energy that can be converted through two major methods to electric energy, that is, either directly, through various kinds of photovoltaic (PV) systems, or indirectly, by first concentrating thermal radiation to generate high-temperature heat and then converting the heat into mechanical energy through a heat engine, which further is converted into electric energy by power generators. The solar-generated electric energy can be further used to drive electrolysis, which produces hydrogen, as suggested in Fig. 13.4.

There is one additional electricity-based method that makes use of solar radiation to generate electricity; this is photoelectrolysis, which is conducted in an electrochemical cell. The electrochemical cell represents a compact device that

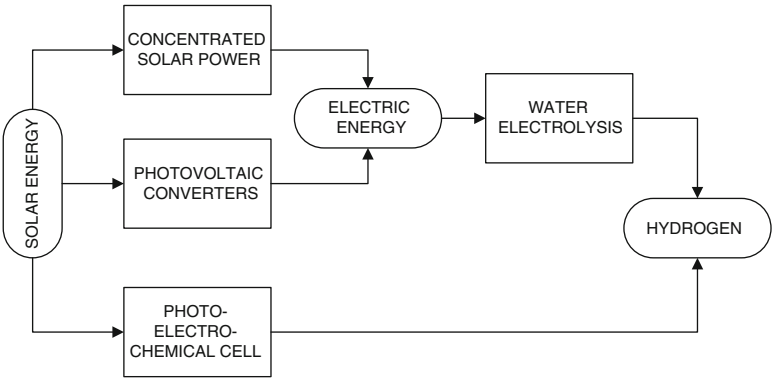

Fig. 13.4 Two major routes for solar-electrical hydrogen production

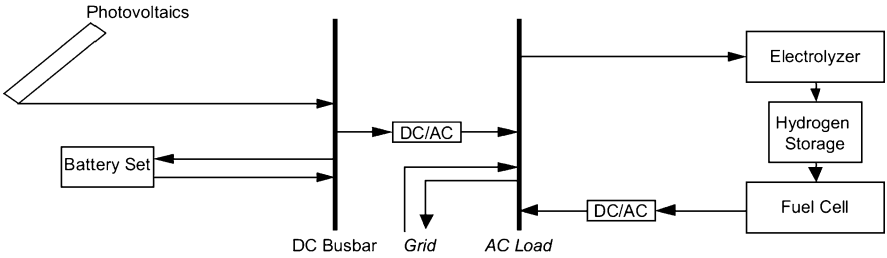

Fig. 13.5 System for PV-driven water electrolysis [modified from Yilanci et al. (2009)]

combines the photovoltaic cell with an electrolyzer. Several interesting concepts were developed for generating electricity from solar energy; they are reviewed in detail in Chapter 9, where we analyze solar energy. Here, we discuss some relevant methods using solar energy for water electrolysis, without entering into the details of solar electric power generation, and we discuss the photoelectrochemical cell (PEC).

Photovoltaic-driven water electrolysis is a reference system that can be assembled with off-the-shelf components. Such system is described schematically in Fig. 13.5. It comprises PV panels, a DC bus bar, a AC grid, an accumulator battery set, an electrolyzer, and hydrogen storage canisters. The cost of PV-generated electricity is in continuous decline; for example, in 1998 the average cost was $12 per installed watt and in 2008 it was $8. This technology is currently a $10 billion business, growing by 30% per annum. This fact shows an encouraging trend for PV hydrogen production cost. The efficiency of the solar cell can range from 12% to 15% for the silicon solar cell. However, it is as high as 25% to 30% for a GaAs solar cell. The total efficiency of solar radiant energy transformed to chemical hydrogen energy is nearly 16% (Yilanci et al. 2009). The exergy efficiency of the PV-electrolyzer system is calculated as the product of exergy efficiency of the PV system ψ_{PV} and the exergy efficiency of the electrolyzer ψ_{EL} is

Table 13.3 Efficiencies of the solar-H_2 generator components from Pamukkale University

Components	Energy efficiency (%)	Exergy efficiency (%)
PVs	11.2–12.4	9.8–11.5
Charge regulators	85–90	85–90
Batteries	80–85	80–85
First inverter	85–90	85–90
Electrolyzer	56	52
Hydrogen tanks	100	100
Fuel cells	30–44	24.5–38
Second inverter	85–90	85–90

Data from Yilanci et al (2009)

$$\psi = \psi_{\mathrm{PV}}\psi_{\mathrm{EL}} = \frac{V_{\mathrm{m}}I_{\mathrm{m}} - \left(1 - \frac{T_0}{T_{\mathrm{cell}}}\right)hA(T_{\mathrm{cell}} - T_0)}{\dot{E}x_{\mathrm{solar}}} \times \frac{\dot{E}x_{\mathrm{H_2}} + \dot{E}x_{\mathrm{O_2}}}{V_{\mathrm{m}}I_{\mathrm{m}}}, \qquad (13.12)$$

where $V_{\mathrm{m}}I_{\mathrm{m}}$ is the electrical power accounting for all electrical losses of the PV panel, associated electronics, and electrical lines. This power is the same as that retrieved at the input of the electrolyzer. The quantity $hA(T_{\mathrm{cell}} - T_0)$ represents the heat losses between the PV panel and the ambient air due to heat transfer; some exergy losses are associated with this heat as indicated in the numerator of the above equation.

Illustrative Example: PV-Electrolyzer System

This example is a hybrid PV-based hydrogen production system, based on the principle introduced in Fig. 13.5, which was installed in February 2007 in the Clean Energy Center (CEC) on the campus of Pamukkale University in Denizli, Turkey, and is equipped with 5-kWe PV panels. For the purposes of our example, one-half of the photovoltaic modules are on a fixed tilt, and the other half are mounted on solar trackers. The fixed tilt (45° south) photovoltaic modules are located on the roof of the building. Each tracker consists of ten modules with nominal power of 1.25 kWp.

A line feed deionizer was selected to supply the quality of water needed for the electrolyzer. A basic particle water filter was also used before the deionizer. A PEM-type electrolyzer was used in the system. A metal hydride (MH) storage tank was used for hydrogen. The downside is that the hydrogen produced for MH storage must be of very high purity. Six OVONIC 85G250B storage tanks were chosen. The system includes also a fuel cell to generate electricity from the produced hydrogen and is connected to the grid. Table 13.3 lists the efficiencies of the individual system components. Average hydrogen production of the system for a week is 4.43 kg.

As for the solar concentrators, there were many test performed in the last 50 years to develop such electric generators. In a typical configuration (see Chapter 9), a parabolic mirror concentrates the solar radiation in the focal point, where it generates high-temperature heat. This heat is captured and used to drive

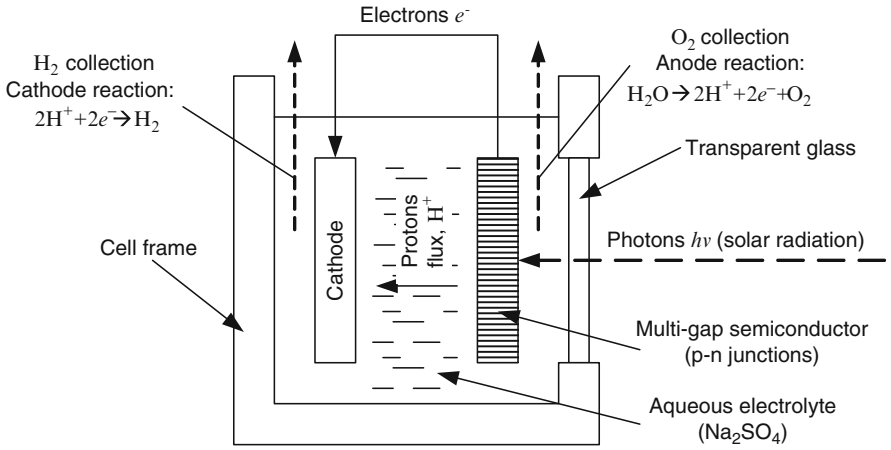

Fig. 13.6 Sketch illustrating the operating principle of the photoelectrochemical cell

a heat engine that turns an electric generator. The typical efficiency of these electric power generating devices is 20% to 25%. When coupled with a water electrolyzer, the total solar-to-hydrogen efficiency becomes on the order of 10% to 15%.

Another electric-solar method for hydrogen production is photoelectrochemical water splitting. In this method, the photonic energy carried by solar radiation is used to generate an electric current that in turn drives the water electrolysis. This method is also called photoelectrolysis. It uses the so-called photoelectrochemical (PEC) cell, which may comprise photosensitive semiconductors immersed in an aqueous electrolyte and counter electrodes.

Figure 13.6 presents a possible configuration of the PEC cell, which was first proposed by Fujishima and Honda (1972). The semiconductor operates similarly to a photovoltaic cell, and it uses the photons with energy greater than the semiconductor band gap to generate electron-hole pairs that are split by the electric field that traverses the electrolyte. The water splitting reaction through the PEC cell becomes

$$H_2O \xrightarrow{hv} H_2(g) + 0.5O_2(g), \tag{13.13}$$

where hv represents the photonic energy consumed for driving the process.

One remarkable advantage of the PEC cell is that it actually integrates solar energy absorption and water electrolysis into a single unit. Thus, the device does not require a separate solar power generator (e.g., a PV cell) and electrolyzer, and it is consequently more compact. The technology is in the course of development, and it achieved in the laboratory about 18% efficiency (Licht et al. 2001). The lifetime of a PEC cell was shown to be short because water corrodes the electrolyte. Many kinds of photosensitive semiconductor electrodes were investigated, one of the most promising being titanium dioxide (TiO_2); the other kinds are strontium titanate, carbonate oxides, NaOH oxides, tantalum oxynitride, other niobates and titanates, and cadmium sulfide.

Table 13.4 Some projects of geothermal hydrogen production

Location	Geothermal capacity (MW)	Electrolyzer capacity (MW)	H_2 production (ton/day)
Hawaii	3.0	2.6	0.5
Hawaii	2.4	1.9	0.3
Portugal	250	234	N/A

Data from Balta et al. (2009)

13.4.1.3 Hydrogen Production Through Electric Renewable Energy Other Than Solar

It is noted in Fig. 13.1 that energy sources such as hydro, wind, biomass, geothermal, ocean thermal, tides, and waves, and the energy recovered from human activity (industrial heat waste, municipal waste, landfill gas, etc.) can all be converted ultimately to electric energy. This energy can be further used for water electrolysis to produce hydrogen.

Biomass can be converted to electricity by either combustion or heat transfer to a power cycle (e.g., steam engine, organic Rankine cycle, or other engine). It is also possible to convert biomass into biogas or biofuel that further can generate electricity through internal combustion engine generator sets. Again Chapter 9 detailed the methods of electricity generation from biomass. The efficiency of electricity generation in this case ranges from 10% to 15% for a steam engine to 50% to 60% for a combined fuel cell/gas turbine cycle with gasification and heat recovery. Therefore, hydrogen efficiency production with biomass–electricity is of the order of 5% to 30%.

Geothermal energy can be used to generate electricity through various kinds of flash cycles and organic Rankine cycles. Depending on the level of temperature of the geothermal source, the energy efficiency of the electricity generation process may vary between 5% and 25%; correspondingly, if a geothermal generator is coupled with an electrolyzer, the expected hydrogen production efficiency is expected to be in the range of 3% to 12%. Some recent projects demonstrating geothermal hydrogen production are described briefly in Table 13.4.

Hydroelectric power generation is an established technology that uses the potential energy of water to generate electricity. The main components of the hydropower plants are a dam/retaining wall, a water turbine, and an electrical generator. A dam or retaining wall is built along the width of a river so that the water level can rise on one side of the wall. On the other side of the dam/retaining wall, water turbines coupled with electricity generators are installed. The potential energy of water is then used to run turbines, and then turbines run generators and produce electricity. Water turbines are available in a large variety and depending upon the different water head the flow rate turbines can be selected. A Pelton wheel and Francis turbines are generally used for high water heads, and the Kaplan turbines can be used for low water heads. Some intermediate water head turbines that can be used for both high and low water heads are the Michel Banki and Deriaz turbines. The electricity produced is then supplied to the grid from where

it is distributed to its users. Mini-hydropower stations can also be built to fulfill the electricity demand of a community that is situated near small rivers and where the water head is not enough for large hydropower plants. Hydro energy is used essentially to produce electricity, and then the electricity can be used for hydrogen production via electrolysis. Hydropower plants are more eco-friendly than the thermal power plants, as they cause less harm to the environment, but as they require large civil structures and community relocation for those who live near the river, they sometimes face substantial public resistance. Because of the high efficiency of hydroelectric power generation (90%), the expected hydro-to-hydrogen efficiency is around 45%.

Wind mills and horizontal-axis and vertical-axis turbines are used to convert the kinetic energy of the wind into electricity. It is one of the more cost-effective forms of renewable energy in today's technology. The electricity produced by wind energy can be supplied to the grid. The technology is beneficial for the locations, where the wind velocity is high, for example, the coastal and subcoastal areas. For better functioning of a wind energy system, the knowledge of the natural geographical variation in wind speed is important so as to smooth out fluctuations. Similar to the limitations of solar energy, wind energy generation is also affected by the intermittent nature of wind speed. Similar to hydro energy, wind energy also essentially is used to produce electricity first, and then the electricity can be used for hydrogen production. However, the problem with wind energy resides in its fluctuating availability. Fortunately, one of the remarkable features of electrolyzers is that they can adapt fast enough to fluctuations in the supplied voltage so that they are suitable to couple with wind turbines. Taking into account the low-capacity factor (~25%), the expected efficiency of wind-electricity-hydrogen production is ~10%.

Some other renewable sources are tidal, wave, and ocean thermal technologies that can produce electricity or can help reduce the electrical load of a power plant. Tidal energy utilizes the power of tide to produce electricity, whereas wave energy systems use the waves formed in an ocean or sea. Oscillators are placed in the sea and they oscillate when waves come in contact with them. This oscillatory motion is utilized to generate electricity. The ocean thermal technology uses the temperature difference between the upper and the deep lower level of ocean water. This thermal difference is utilized to generate electricity.

Several human activities waste large amounts of energy; this energy is lost either in the form of heat, some form of biochemical energy as in landfill gas case, or chemical energy waste that can be incinerated to obtain heat. Heat recovered can be applied in such situations, and depending on the temperature level of the heat source, it is possible to generate electricity with a certain efficiency. There are heat engines that operate at a low-temperature differential, as well as many kinds of power plant technologies that use higher—combustion level—temperature. Landfill gas can be supplied to internal combustion engine-driven generators to obtain electric power and therefore hydrogen.

One important aim of producing hydrogen from renewable sources is leveling electricity production. Many renewable sources like wind, solar, hydro, tides, or

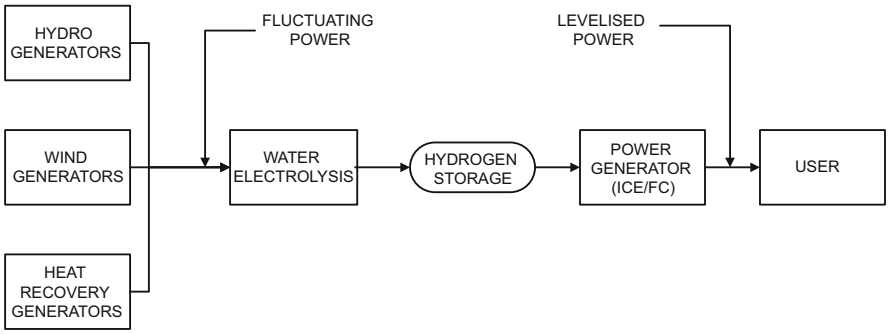

Fig. 13.7 General concept for H_2 generation from renewables for levelized power production

industrial heat recovery are fluctuating in nature or intermittent. A design like the one shown in Fig. 13.7 suggests how, through hydrogen, the power production is levelized. Power generators from various renewable sources can work either separately or in parallel to drive water electrolysis, although with a fluctuating electric capacity. Hydrogen is produced from these sources and accumulated in tankers. The hydrogen may further supply a power generator (e.g., fuel cell, internal combustion engine, etc.) to generate electricity at a levelized rate according to the demand.

13.4.1.4 Fossil Fuel–Based Electricity for Water Electrolysis

The combustion of coal, petroleum, and natural gas is widely used nowadays for electricity production. There is a large number of technologies available to generate electricity from such basic fuel sources. We exclude from our discussion the integrated gasification/gas turbine cycles and fuel cells because such methods already generate hydrogen through thermochemical means, and it does not appear logical to drive an electrolyzer to produce hydrogen in this case. The conventional fossil fuel–based power plants are the steam turbine (Rankine), gas turbine, and diesel engine power plants.

The lowest efficiency is attained by coal power plants, up to 30%, but a combined cycle (topping-bottoming) can reach 50%. Therefore, the expected hydrogen production efficiency from this source is 15% to 25%. This efficiency is degraded if carbon dioxide capture is applied to the power generation plant.

13.4.1.5 Nuclear Power Coupled with Water Electrolyzer

There are two main ways to couple nuclear reactors with water electrolysis stations. In the first and simpler way, all electrical production of a nuclear power plant can be used to drive water electrolysis and to generate hydrogen, as illustrated in Fig. 13.8a. The efficiency of the power plant is indicated in the figure with

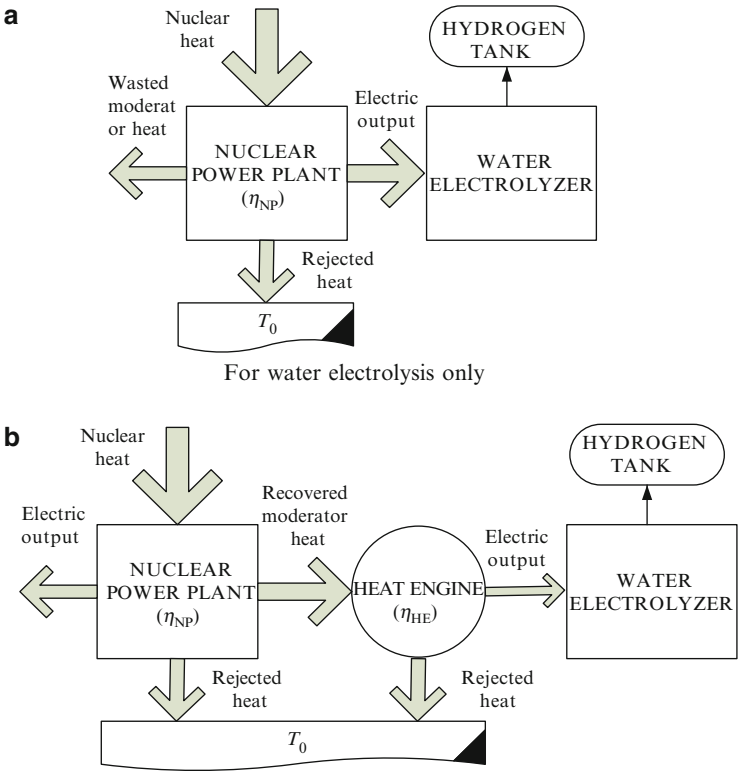

Fig. 13.8 Ways to couple water electrolysis to nuclear reactors for (**a**) dedicated hydrogen production systems or (**b**) cogeneration systems of electricity and hydrogen

the notation η_{NP}. The advantage of such a system comes from the possibility of operating at the design load without direct interference with the grid, which can be congested in some periods of time. Another important advantage of nuclear/water electrolysis is that there is no need to modify the reactor. Such systems were applied on nuclear submarines to generate oxygen (for maintaining life) and hydrogen. It is possible to adapt the system to the existent nuclear power plants to generate off-peak electricity.

The generation of hydrogen during off-peak hours at nuclear plants allows for constant load operation at the highest efficiency and lowest electricity production cost. Also, grid congestion that decreases the reliability and efficiency of the electrical grid is avoided. Recall that the maximum expected efficiency of the water electrolysis process is 80% even though studies show less than 55%. Coupled with current light water reactors or advanced light water reactors (ALWRs), the expected thermal-to-hydrogen efficiency is 27%; coupled with a modular helium reactor (MHR) or an advanced gas reactor (AGR), the expected efficiency is ~35%.

The second way to couple nuclear reactors with a water electrolysis system is suggested in Fig. 13.8b. In this case the moderator heat is recovered with

specially designed heat exchangers and supplied to a heat engine able to operate with a low temperature differential. Examples of low differential heat engines are the organic Rankine cycles (ORC) and the Kalina cycle. The efficiency of these cycles is indicated in the figure with η_{HE}. Thus the efficiency of hydrogen generation becomes $\eta_{H_2} = (1 - \eta_{\mathrm{NP}}) \times \eta_{\mathrm{HE}} \times \eta_{\mathrm{EL}}$, where the subscript EL stands for electrolyzer.

13.4.2 Thermally-Driven Hydrogen Production Methods

13.4.2.1 Water Thermolysis

As indicated in Table 13.2, the hydrogen production methods driven by thermal energy are thermolysis, thermochemical water splitting (TCWS), reforming and gasification, and thermal cracking. All these processes are presented here as well as their coupling with various primary energy and energy recovery sources.

The single-step thermal dissociation of water is known as water thermolysis and can be given as

$$\mathrm{H_2O} \overset{\text{heat}}{\rightarrow} \mathrm{H_2} + 0.5\mathrm{O_2}. \tag{13.14}$$

The reaction requires a high-temperature heat source at above 2,500 K to have a reasonable degree of dissociation, and by the need for an effective technique for separating H_2 and O_2 to avoid ending up with an explosive mixture. Kogan (1998) tested semipermeable membranes based on ZrO_2 and other high-temperature materials at up to 2,500 K. The very high temperature required by the process (e.g., 3,000 K for 64% dissociation at 1 bar) poses severe material problems and can lead to significant reradiation from the reactor, thereby lowering the absorption efficiency.

13.4.2.2 Thermochemical Water Splitting

Thermochemical water splitting (TCWS) involves a series of chemical reactions performed in a loop with the general effect of water decomposition into hydrogen and oxygen. One major advantage of a thermochemical cycle is that it normally does not require catalysis to drive the chemical reactions. All chemicals involved in the process are recycled except water, which is the material source from which hydrogen is derived. Water-splitting thermochemical cycles are attractive for the following reasons: (a) there is no need for hydrogen–oxygen separation membranes; (b) the temperature of the required thermal energy source is in a reasonable range (600–1,200 K); (c) there is no or very little requirement for electrical energy to drive the process. If no electricity is needed to drive thermochemical cycles, then an only thermally driven hydrogen production method is possible. If electricity and heat are both needed to drive the thermochemical water process, the associated

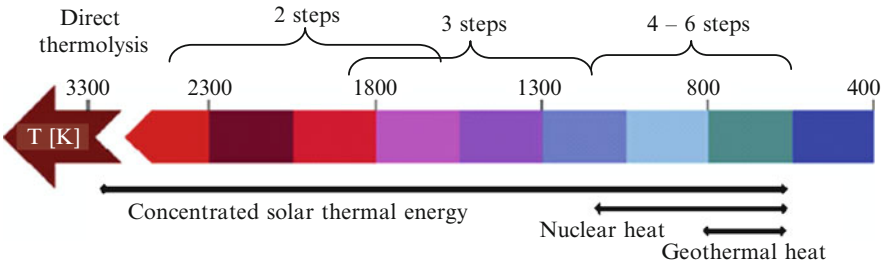

Fig. 13.9 Correlation between number of chemical steps (cycles) of thermochemical water splitting systems with process temperature [modified from Balta et al. (2009)]

cycle is called a hybrid. Some relevant hybrid thermochemical cycles are reviewed in a subsequent section. Here, we refer only to the thermal-only driven methods.

Balta et al. (2009) noted an interesting finding: the number of chemical reactions involved by the thermochemical water splitting cycles is smaller as the process temperature increases. They correlated the number of cycles with the temperature as indicated in Fig. 13.9. The plot also suggests that concentrated solar energy is suitable for all thermochemical methods.

Abanades et al. (2006) compiled a database with 280 thermochemical cycles referenced in the literature. From those, we will analyze in the subsequent paragraph only two, which are probably the most promising thermal-only cycles. Other hybrid cycles (electro-thermal) will be discussed in Section 13.4.3.1. Various sustainable sources of high temperature heat can be considered to drive these cycles. Nuclear heat probably can be used up to 1,000 K, geothermal heat is available up to 800 K, biomass combustion and concentrated solar radiation may generate heat up to about 1500 K.

The sulfur–iodine (S–I) cycle operates at a maximum temperature of 1000 K to 1075 K, which is needed to drive the oxygen-evolving reaction. The S–I cycle has been fully demonstrated in both Japan and the United States, and has been shown to be technically viable. However, the commercial viability has yet to be demonstrated. The equipment cost of an S–I plant with 790 tons/day of hydrogen production capacity is $125 million. Membrane technology was developed to enhance the separation efficiency for this cycle. The maximum attainable one-pass S-I conversion rate was reported to exceed 90% with membrane technology, whereas the equilibrium rate is about 20%.

The first reaction of this cycle is the sulfuric acid decomposition to release water; this reaction is thermally driven, noncatalytic, and conducted at 300° to 500°C:

$$H_2SO_4(aq) \xrightarrow{\text{heat @ } 300-500^\circ C} H_2O(g) + SO_3(g). \tag{13.15}$$

The resulting steam is separated from $SO_3(g)$ and by further heating up to 800° to 900°C the sulfur trioxide is decomposed thermally to release oxygen:

$$SO_3(g) \xrightarrow{\text{heat @ } 800-900^\circ C} SO_2(g) + 0.5O_2(g). \tag{13.16}$$

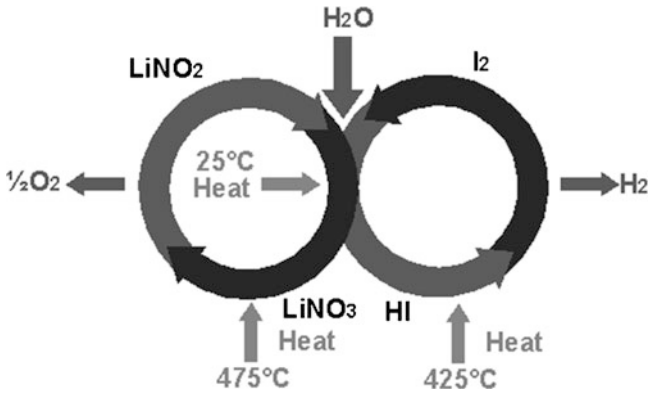

Fig. 13.10 The $LiNO_3$ water splitting process [modified from Balta et al. (2009)]

The so-called Bunsen reaction follows, which combines the sulfur dioxide $SO_2(g)$ separated from oxygen with iodine and water. The reaction is exothermic and occurs at low temperatures, spontaneously, to produce sulfuric acid:

$$SO_2(g) + I_2(g) + 2H_2O(l) \rightarrow 2HI(g) + H_2SO_4(aq). \tag{13.17}$$

The hydrogen iodine is further decomposed thermally at 425° to 450°C and generates hydrogen:

$$2HI(g) \xrightarrow{\text{heat @ } 425-450^\circ C} H_2(g) + I_2(g). \tag{13.18}$$

One major advantage of the S–I cycle consists of the fact that there are no side reactions occurring during the process, and the separation of chemicals is relatively straightforward. The drawback of the process is that it occurs at a rather high temperature. Thus, a relatively lower number of sustainable thermal energy sources is available to drive this process. Among such possible sources are nuclear heat from high-temperature gas-cooled reactors, concentrated solar thermal heat, and biomass combustion heat. Note that the S–I cycle has a hybrid version also in which the hydrogen evolving reaction is conducted electrochemically.

An interesting process, but less well developed, is the $LiNO_3$ cycle for water splitting. This thermally driven cycle evolves completely at lower temperatures. The highest temperature required is 475°C for the $LiNO_3$ decomposition reaction that releases oxygen. Also, the hydrogen iodine decomposition reaction is evolving at 425° to 450°C. The cycle is represented schematically in Fig. 13.10.

The first reaction occurs at a temperature close to the ambient and is endothermic:

$$LiNO_2(g) + I_2(g) + H_2O(l) \xrightarrow{\text{heat @ } 40^\circ C} LiNO_3(g) + 2HI(g). \tag{13.19}$$

The other two reactions are also endothermic evolving at higher temperature and releasing hydrogen and oxygen:

$$\left.\begin{aligned} 2\mathrm{HI(g)} &\xrightarrow{\text{heat @425–450°C}} \mathrm{I_2(g) + H_2(g)} \\ \mathrm{LiNO_3} &\xrightarrow{\text{heat @475°C}} \mathrm{LiNO_2(g) + 0.5O_2(g)} \end{aligned}\right\}. \tag{13.20}$$

13.4.2.3 Reforming and Gasification

When water is the primary source, the thermochemical processes for hydrogen production are called thermochemical cycles, suggesting that the involved chemicals, except water, are recycled. If other chemicals like hydrocarbons, fossil fuels, biomass, and alcohols are used as hydrogen sources, the thermochemical processes do not occur cyclically. For example, the process of steam methane reforming can be categorized as thermochemical, and no chemicals are recycled, but they are rather completely transformed; overall, methane and steam enter into the reaction, and it results in hydrogen and carbon monoxide.

We turn now to reforming and gasification processes for hydrogen production. The terminological distinction between reforming and gasification addresses the nature of the consumed fuel by the conversion process. When a solid fuel like coal or biomass or solid waste is converted to hydrogen gas or synthesis gas (hydrogen + carbon monoxide), the process is called gasification. When a fluid fuel (gas or liquid: alcohols, natural gas, petroleum) is converted to synthesis gas, this process called reforming.

The steam-reforming/gasification method requires additional steps for shifting CO and for separating CO_2, whereas the thermal cracking accomplishes the removal and separation of carbon in a single step. The schematic of the gasification process is represented in Fig. 13.11. The steam-reforming of natural gas, oil, and other hydrocarbons, and the steam-gasification of coal and other solid carbonaceous materials (e.g., biomass) can be expressed by the simplified net reaction:

$$C_x\mathrm{H}_y + x\mathrm{H_2O} \xrightarrow{\text{high temperature heat}} \left(\frac{y}{2} + x\right)\mathrm{H_2} + x\mathrm{CO}. \tag{13.21}$$

Depending on the reaction kinetics and on the presence of impurities in the raw materials, other compounds may also be formed during the conversion. Among the other possible reactions occurring concurrently at various rates are: $\mathrm{CH_4 + H_2O \rightarrow CO + 3H_2 - 206\,kJ/mol}$, $\mathrm{CH_4 + 2H_2O \rightarrow CO_2 + 4H_2 - 165\,kJ/mol}$, $\mathrm{C + H_2O \rightarrow CO + H_2 - 131\,kJ/mol}$, $\mathrm{C + H_2 \rightarrow CH_4 - 75\,kJ/mol}$, and $\mathrm{C + CO_2 \rightarrow 2CO - 172\,kJ/mol}$. The carbon monoxide content present in the product of the reforming/gasification process can be shifted to H_2 via the catalytic water–gas shift reaction ($\mathrm{CO + H_2O \rightarrow H_2 + CO_2}$), and the carbon dioxide can be separated from H_2 using various methods as discussed in Chapter 14.

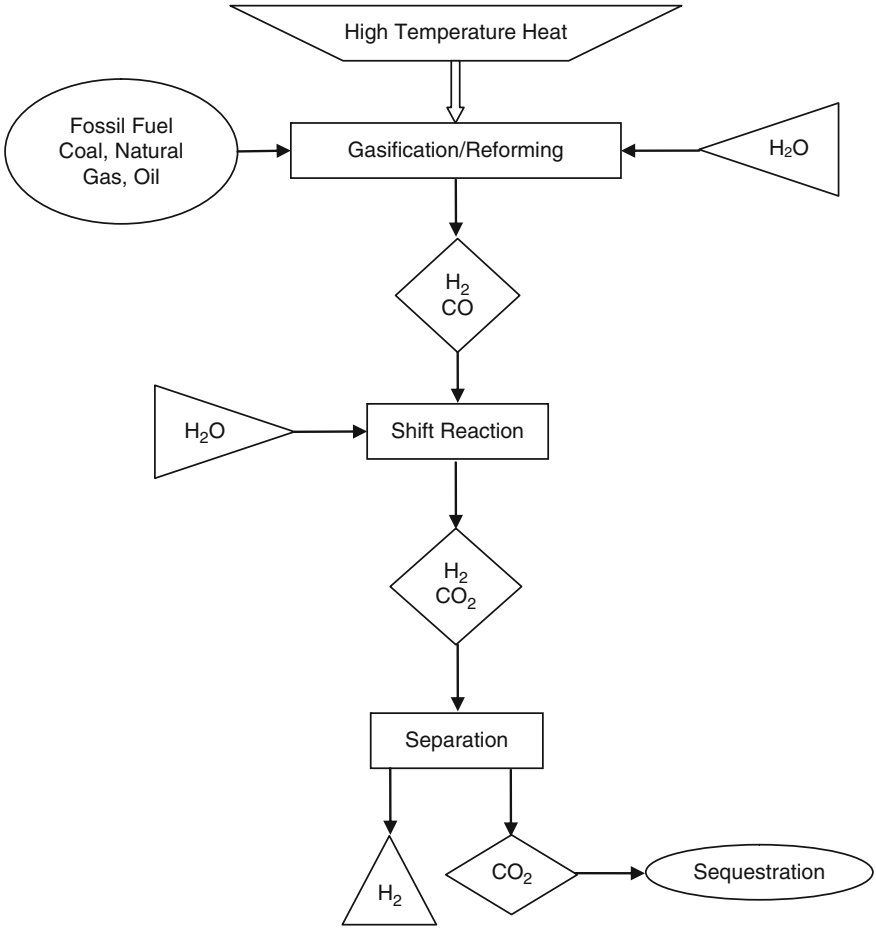

Fig. 13.11 Schematic diagram of the gasification/reforming process

The gasification agents are described in Table 13.5. Gasifiers and reformers are in general large equipment that operate at high temperature and are exposed to ambient conditions. Consequently, one of the energy losses characteristic of such equipment is the heat leaks through the exterior. If T_w is the temperature of the gasifier, the lost heat can be simply calculated with $Q_{lost} = U_w A(T_w - T_0)$, where T_0 is the ambient temperature and U_w is the heat transfer coefficient at the wall, which can be determined with an appropriate equation that considers a combined heat transfer through convection and radiation. One recommended equation for the heat transfer coefficient is that by Isachenko et al. (2004):

$$U_w = 1.9468(T_w - T_0)^{1/2}(2.8633V_{wind} + 1)^{1/2} + 5.75 \times 10^{-8}\varepsilon_{ins}\frac{T_w^4 - T_0^4}{T_w - T_0}, \quad (13.22)$$

Table 13.5 Gasification agents

Agent	Process temperature	Remarks
Oxygen	1,000–1,400°C	Syngas heating value is high: 10–15 MJ/m^3; oxygen handling is expensive and implies safety issues
Air	900–1,100°C	Syngas has low heating value (4–6 MJ/m^3) because it contains up to 60% N_2 and other contaminants like tars and hydrocarbons; it is the cheapest method and most used
Steam	800–1,200°C	The heating value of product gas is 8–10 MJ/m^3 with around 45% H2, 25% of CO and a large quantity of steam (~18%); presence of steam creates problems with corrosion
Supercritical water	400–800°C	Operates at high pressures, around 30 MPa; this process can suppress the formation of tar and char; drying of fuel (like biomass) can be avoided

where ε_{ins} is the thermal emissivity of the insulation and V_{wind} is the average velocity of the wind in m/s. The temperature of the wall is calculated based on the average temperature of the gasification process T, and the thermal conductivity of the wall insulation, k_{ins}, assumed to be of thickness δ:

$$U_{\text{w}}(T_{\text{w}} - T_0) = \frac{k_{\text{ins}}}{\delta}(T - T_{\text{w}}). \tag{13.23}$$

The main parameters affecting the gasification process are listed in Table 13.6. Different gasifiers are employed in the gasification process: fixed bed, moveable bed, and fluidized bed. The process could be either auto-thermal or all-thermal depending on how this heat is provided. In the case of auto-thermal gasification, the necessary heat is generated directly by partial oxidation in the gasifier itself.

13.4.2.4 Thermocatalytic Cracking

Hydrogen can also be produced from hydrocarbons by using thermal cracking processes. The thermal cracking process normally necessitates catalysts, as opposed to thermochemical hydrogen production, which does not. Thermal cracking can be conducted either as an oxidative or nonoxidative process. The nonoxidative process of thermal cracking of hydrocarbons to produce hydrogen can be represented by the simplified net reaction:

$$\text{C}_x\text{H}_y \rightarrow x\text{C(s)} + \frac{y}{2}\text{H}_2\text{(g)}, \tag{13.24}$$

where C(s) represents carbon that is precipitated as a powder or granulate matter.

The thermal cracking reaction produces a carbon-rich condensed phase and a hydrogen-rich gas phase. The carbonaceous solid product can be used as a material

Table 13.6 Parameters influencing the gasification process

Parameter	Description	Effects
Equivalent ratio	The oxygen supplied over the stoichiometric oxygen	Higher oxidant delivered through increased air rate dilutes the product gas and reduces the efficiency; too low air rate does not suffice for partial oxidation, which reduces gas production
Steam-fuel ratio	$\mathrm{SBR} = \frac{\dot{m}_{\mathrm{steam}} + \dot{m}_{\mathrm{moist}}}{\dot{m}_{\mathrm{fuel}}(1 - \mathrm{moist}_{\%})}$	Influences the required energy input and product gas composition; low SBR leads to more methane and solid carbon formation; high SBR means more syngas produced
Process temperature	Process temperature is not constant; gasifier temperature is considered that which occurs after the pyrolysis zone	Lower temperatures lead to more solid carbon and methane in the product gas; in general, optimal values are 800–900°C; above these hydrogen yield reduces
Process pressure	Gasification occurs at constant pressure in the gasifier	Chemical equilibrium indicates that gasification is favored by low pressures and high temperatures; however, no substantial gain is obtained if the process runs in a vacuum

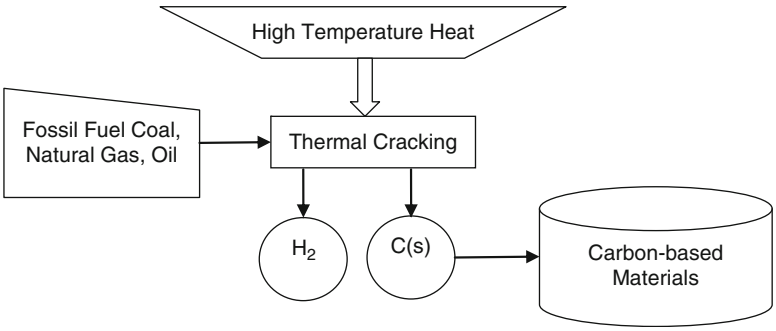

Fig. 13.12 Schematic diagram of solar cracking

commodity or reducing agent. The process of thermal cracking is illustrated schematically in Fig. 13.12. Thermal cracking may be the preferred option for natural gas and other hydrocarbons with a high H_2/C ratio. Oxidative thermal cracking can be implemented as cyclic redox reactions on metals. An efficient two-step thermocatalytic cycle uses metal oxide redox reactions. The first step is the endothermic reduction:

$$\mathrm{M}_x\mathrm{O}_y \xrightarrow{\text{high temperature heat}} x\mathrm{M} + \frac{y}{2}\mathrm{O}_2. \tag{13.25}$$

The second step is the exothermic oxidation:

$$xM + yH_2O \rightarrow M_xO_y + yH_2, \tag{13.26}$$

where M denotes a metal and M_xO_y the corresponding metal oxide. The first, endothermic step is of thermal dissociation of the metal oxide to lower-valence metal oxide. The second process is exothermic hydrolysis of the metal to form H_2 and to reform the initial metal oxide. The net reaction is of water splitting ($H_2O = H_2 + 1/2O_2$), but since H_2 and O_2 are formed in different reactors (reduction and oxidation reactors), the need for high-temperature gas separation is thereby eliminated.

A very well known redox process for hydrogen production is the so-called steam–iron process:

$$\left.\begin{aligned} 2Fe_3O_4 + H_2O &\rightarrow 3Fe_2O_3 + H_2 \\ 3Fe_2O_3 + CO &\rightarrow 2Fe_3O_4 + CO_2 \end{aligned}\right\}, \tag{13.27}$$

which normally evolves at very high temperature (~1,000°C). The carbon monoxide is consumed in this process. Sources of carbon monoxide can be found in metal processing plants. Note that the thermal cracking process can also be electrically driven in plasma produced by electric arcs.

13.4.2.5 Biomass-Thermal Routes for Hydrogen Production

Biomass having moisture content lower than 35% can also be used as primary energy to extract hydrogen from steam. If the moisture content is too high, either the biomass must be dried before gasification or supercritical steam gasification can be applied. Supercritical steam gasification is a process that uses steam at supercritical pressure and temperature, and it is adapted to convert biomass to hydrogen regardless of its moisture content. Wood sawdust, sugar cane, and bagasse are some general forms of biomass that can be used to produce hydrogen.

Abuadala et al. (2010) analyzed a hydrogen production system based on steam gasification of biomass that uses wood sawdust and 4.5 kg/s of steam at 500 K. They found that the hydrogen yield reaches 80 to 130 gH_2/kg biomass with 50% molar concentration in the product gas, which reaches a heating value of 15 to 20 MJ/m^3. The biomass is introduced to a gasifier at an operating temperature range of 1,000 to 1,500 K. The global reaction of the biomass gasification process to produce hydrogen is as follows:

$$\alpha C_lH_mO_n + \gamma H_2O \xrightarrow{\text{heat}} aH_2 + bCO + cCO_2 + dCH_4 + eC + f\,\text{Tar}, \tag{13.28}$$

where $\alpha C_lH_mO_n$ is the general chemical representation of the biomass. The formation of tars is undesirable because of the negative effect on the pipes, ducts, and

Table 13.7 Energy and exergy efficiency of biomass gasification process

Case	Energy efficiency	Exergy efficiency
Only hydrogen is considered as output	$\eta = \frac{\mathrm{HHV}_{\mathrm{H_2}}}{n_\mathrm{b}\mathrm{HHV}_\mathrm{b} + n_\mathrm{s}\Delta h_\mathrm{s}}$	$\psi = \frac{\mathrm{ex}^{\mathrm{ch}}_{\mathrm{H_2}}}{n_\mathrm{b}\mathrm{ex}^{\mathrm{ch}}_\mathrm{b} + n_\mathrm{s}\mathrm{ex}_\mathrm{s}}$
All product gas (PG) is considered as output	$\eta = \frac{\mathrm{HHV}_{\mathrm{PG}}}{n_\mathrm{b}\mathrm{HHV}_\mathrm{b} + n_\mathrm{s}\Delta h_\mathrm{s}}$	$\psi = \frac{\mathrm{ex}^{\mathrm{ch}}_{\mathrm{PG}}}{n_\mathrm{b}\mathrm{ex}^{\mathrm{ch}}_\mathrm{b} + n_\mathrm{s}\mathrm{ex}_\mathrm{s}}$
The product gas (PG), tar (T), and char (C) are all considered as useful outputs	$\eta = \frac{\mathrm{HHV}_{\mathrm{PG}} + n_\mathrm{T}\mathrm{HHV}_\mathrm{T} + n_\mathrm{C}\mathrm{HHV}_\mathrm{C}}{n_\mathrm{b}\mathrm{HHV}_\mathrm{b} + n_\mathrm{s}\Delta h_\mathrm{s}}$	$\psi = \frac{\mathrm{ex}^{\mathrm{ch}}_{\mathrm{PG}} + n_\mathrm{T}\mathrm{ex}^{\mathrm{ch}}_\mathrm{T} + n_\mathrm{C}\mathrm{ex}^{\mathrm{ch}}_\mathrm{T}}{n_\mathrm{b}\mathrm{ex}^{\mathrm{ch}}_\mathrm{b} + n_\mathrm{s}\mathrm{ex}_\mathrm{s}}$

Table 13.8 Indicative parameters and H_2 yields of biomass gasifiers

Biomass	T (°C)	Steam-biomass ratio	H_2 yield (%)
Pine and eucalyptus	880	0.8	41
Pine sawdust	750	0.5	40
Mixed sawdust	750	0.51	62.5
Mixed sawdust	800	4.7	57.4
Mixed sawdust	800	1.4	48.8
Mixed sawdust	800	1.1	46
General biomass	777	1.5	59

Source: Abuadala et al. (2010)

equipment by slugging and fouling. Tar formation can be diminished by proper controls and by using various catalysts.

Assuming that the inputs in the steam gasifier are the energy embedded in steam and in the fed biomass, the energy and exergy efficiencies can be defined as in Table 13.7. In the efficiency expressions, n represents the number of mols of biomass (index b), steam (index s), tars (index T), and char (index C) needed to generate 1 mol of product. For the first row in the table, the product is considered to be hydrogen only; for the other two cases, the number of mols corresponds to the generation of 1 mol of product gas. The enthalpy difference Δh_s is calculated based on the molar specific enthalpy of the steam at gasifier inlet conditions and the enthalpy of the water at the reference state, $\Delta h_\mathrm{s} = h_\mathrm{s} - h_0$. The thermomechanical exergy of the steam is given by $ex_\mathrm{s} = \Delta h_\mathrm{s} - T_0(s_\mathrm{s} - s_0)$, where s_s is the specific molar entropy of steam. The notation $\mathrm{ex}^{\mathrm{ch}}$ stands for the specific molar chemical exergy; the HHV are the respective molar higher heating values. Table 13.8 indicates the H_2 yield and operating parameters of typical gasifiers.

Illustrative Example: Biomass Gasification for Hydrogen Production

This example entails steam biomass gasification for hydrogen production according to the results by Abuadala et al. (2010), in a gasifier with 80 cm outside diameter and 50 cm height, insulated with a material with $k_\mathrm{ins}/\delta = 12\,\mathrm{W/m^2\,K}$ and $\varepsilon_\mathrm{ins} = 0.01$, exposed to an average wind condition of 2 m/s and fed with sawdust wood biomass at a rate in the range of 10 to 32 kg/s. Steam is fed at 500 K, while the temperature of the gasifier is kept in the range of 1,000 to 1,500 K. For modeling purposes, the chemical formula of tars is assimilated to that of benzene.

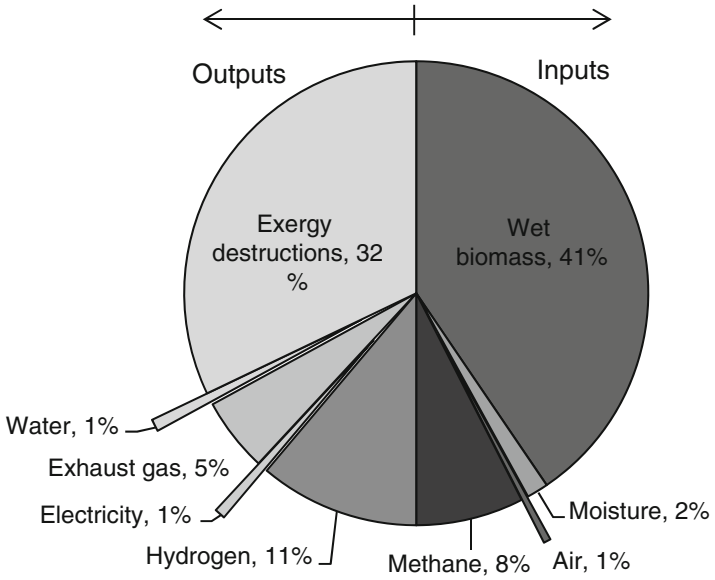

Fig. 13.13 Typical exergy balance on a biomass gasifier [data from Cohce et al. (2010)]

At these conditions, the simulations performed by Abuadala et al. (2010) with Engineering Equation Solver (EES) software indicate the variation of the product gas concentration with the biomass feed rate in the range of 50% to 60%. It is interesting to note that the hydrogen concentration behaves in an opposite manner to the carbon monoxide concentration. These results indicated that only 7% to 11% of the fed biomass is converted to hydrogen. If the steam feed rate is increased in the same conditions (from 4.5 to 6.3 kg/s), the hydrogen concentration in the product gas increases by about 4%, which indicates the beneficial effect of adding steam. It has been found that the rise of the gasification temperature from 1,000 to 1,500 K led to the decrease of hydrogen concentration by 2%.

The order of magnitude of energy inputs and outputs in a gasification process is indicated in Fig. 13.13, which is constructed based on the results of Cohce et al. (2010) that simulated palm oil gasification with ASPEN Plus software. Note also that a biomass gasifier is a complex system involving many types of equipment such as heat exchangers, particle–gas separators (cyclones), gas–gas separation devices (membranes), gas turbines, compressors, pumps, blowers, biomass feeders, and so on. Figure 13.14 illustrates the biomass gasifier as programed in ASPEN Plus software.

13.4.2.6 Hydrogen Extraction from Hydrogen Sulfide

Hydrogen sulfide, with chemical formula H_2S, embeds 76 g of hydrogen per liter at standard atmospheric conditions, which is about 1,000 times more than the mass

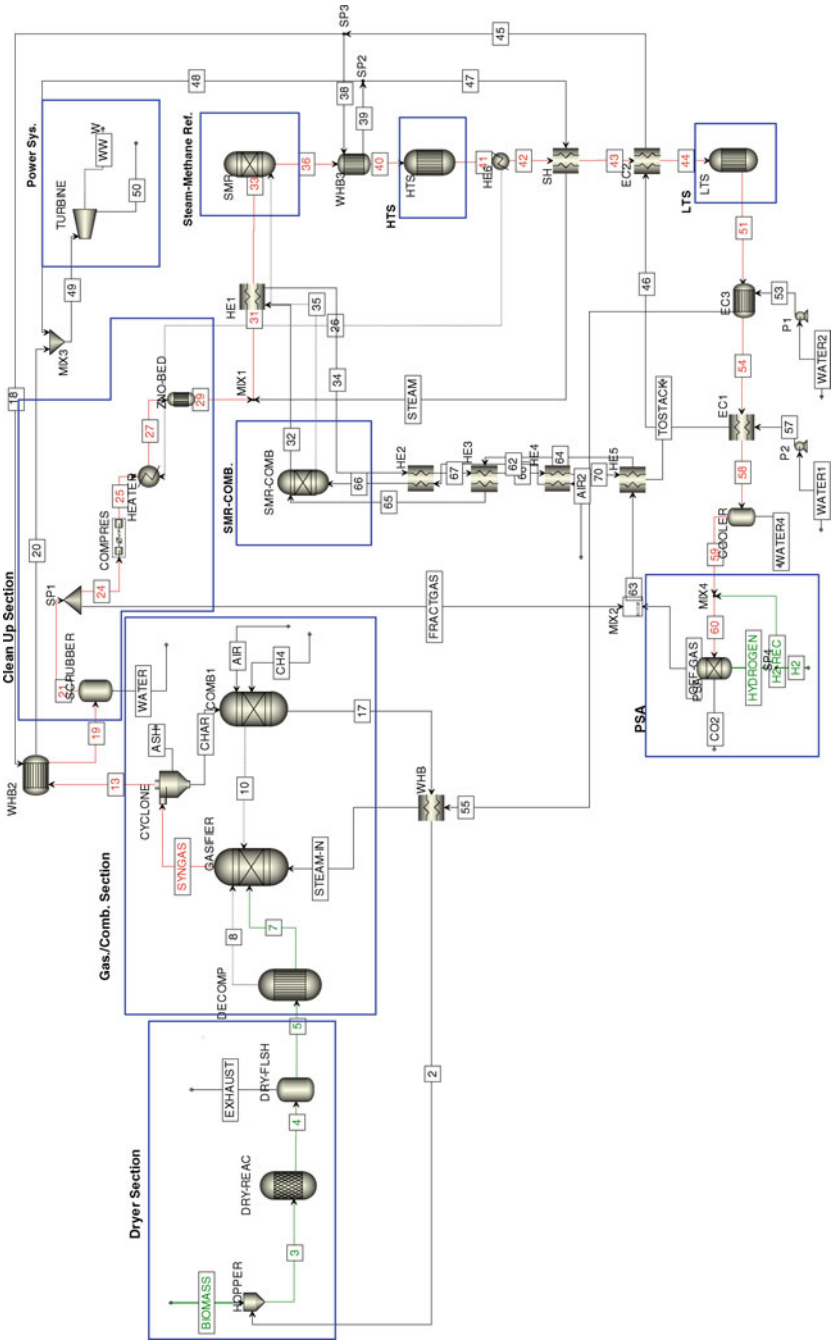

Fig. 13.14 ASPEN Plus diagram of a biomass gasifier [modified from Cohce et al. (2010)]

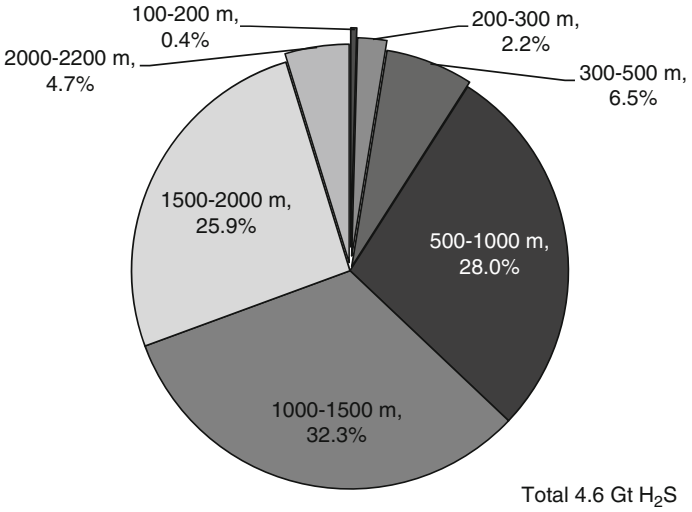

Fig. 13.15 Hydrogen sulfide distribution in Black Sea deep sea waters [data from Midilli et al. (2007)]

of pure hydrogen per unit of volume in the same conditions. Hydrogen sulfide occurs naturally in various environments, such as regions with volcanic activities, hot springs, well water, oil wells, and in certain lakes and seas.

Thus, hydrogen sulfide can be seen as a natural resource from which hydrogen and sulfur can be extracted. A recent study by Midilli et al. (2007) demonstrates that deep waters of the Black Sea have a resource of 4.6 billion tons of H_2S, which offer the potential of extracting 270 million tons of hydrogen; in energy terms, this amount is equivalent to 851 millions tons of natural petroleum (or 7×10^9 barrels). Exploited properly, this resource can be made renewable, since the bacterial activity could in principle be maintained. Extraction of hydrogen from hydrogen sulfide can be made via thermal cracking at high temperatures or by special membrane technology.

The Black Sea is unique in the sense that most microbial activity that it hosts (90%) is anaerobic. This facilitates the proliferation of sulfur-reducing bacteria, which generate hydrogen sulfide. It has been observed that the anaerobic activity is more intense in deep water (at depths of over 150 m), where the concentration of H_2S increases steadily; close to the sea bottom at 1,000 to 2,000 m depth the concentration reaches 8 to 8.5 ml/l (Midilli et al. 2007). The hydrogen sulfide distribution in the Black Sea depths is presented as percentages in Fig. 13.15, which is constructed based on the data published in Midilli et al. (2007). Hydrogen sulfide can be extracted from (sea) waters through various methods, including distillation, and further cracked.

Cracking of hydrogen sulfide generates hydrogen and sulfur according to the decomposition reaction $H_2S \rightarrow H_2 + 0.5S_2$. The thermal cracking of the hydrogen sulfide molecule occurs at about 900 to 1,200 K. Other methods of decomposition include plasma cracking (see Gutsol and Fridman 2008), and photochemical and electrochemical methods. However, presently there is no commercially available

method to produce hydrogen from H_2S. The available laboratory methods known to date and the potential to develop a commercial process were analyzed by Zaman and Chakma (1995).

One of the cited possibilities is to use catalytic separation membranes made from a combination of glass and alumina, which allow permeation of hydrogen from the H_2S decomposition reactor. The membrane is doped with catalysts. Among tested catalysts, those based on molybdenum (MoS_2) showed excellent yield; other catalysts are based on WS_2, NiW, NiMo, and alumina (Zaman and Chakma 1995). Two-step thermochemical cycle extracting hydrogen from H_2S with the help of metals of various valences were also investigated; they operate as follows (see Zaman and Chakma 1995):

$$\left.\begin{aligned} &M + zH_2S \rightarrow MS_z + zH_2 \\ &MS_z \rightarrow M + zS \end{aligned}\right\}, \tag{13.29}$$

where M represents a metal; some encouraging results were obtained with transition metals such as vanadium. Other thermochemical cycles for hydrogen sulfide decomposition can operate with iodine or carbon monoxide:

$$\left.\begin{aligned} &\text{Iodine cycle: } H_2S + I_2 \rightarrow 2HI + S; \quad 2HI \rightarrow H_2 + I_2 \\ &\text{Carbon monoxide cycle: } H_2S + CO \rightarrow COS + H_2; \quad COS \rightarrow CO + S \end{aligned}\right\}. \tag{13.30}$$

All these processes are still in the development phase as they entail several technical problems with controlling the reactions, improving yields and reaction rates, and diminishing the formation of nondesired products. For example, as cited in Zaman and Chakma (1995), the thermochemical cycle operating with carbon monoxide, though very attractive because its hydrogen releasing reaction evolves at very low temperature (373–473 K), is difficult to cycle because of the formation of CS_2 in a concurrent reaction, namely $2COS \rightarrow CO_2 + CS_2$.

13.4.2.7 Solar–Thermal Hydrogen Production

Concentrated solar energy, being a source of high-temperature heat, can be used to drive many thermal methods of disassociating water into hydrogen and oxygen or extracting it from other materials like hydrocarbons or hydrogen sulfide. Figure 13.16 shows the main paths to produce hydrogen from solar energy using thermal methods. Among these, one notes that solar gasification/reforming of fossil fuels can be accompanied by carbon dioxide capture and sequestration.

The sulfur–iodine TCWS cycle also can be driven by high-temperature steam generated by solar concentrators. Considerable work has been done on solar-driven thermal cracking via redox reactions, where at the focal point a solar concentrator is placed as the chemical reactor. Solar energy also can be applied to extract hydrogen from fossil fuels. For coal and other solid carbonaceous materials, the

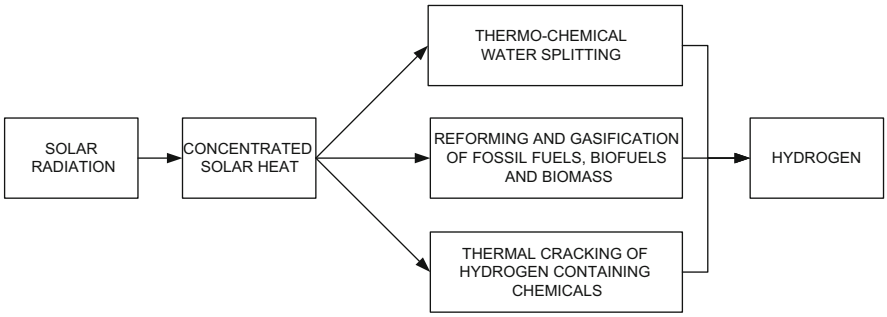

Fig. 13.16 Solar thermal paths for hydrogen production

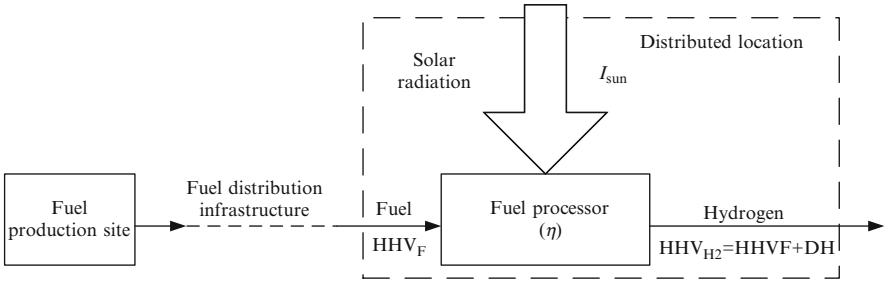

Fig. 13.17 Solar reforming of fuels or hydrogen carriers to generate hydrogen at distributed locations

solar gasification via steam methane reforming reaction has the additional benefit of converting a solid fuel traditionally used to generate electricity in Rankine cycles into a cleaner fluid fuel—cleaner only when using solar process heat—that can be used in highly efficient fuel cells. In addition, liquid and gaseous fuels and biofuels can be reformed to generate hydrogen using solar energy. In such a system, a fossil fuel, hydrocarbon (e.g., propane, butane), biofuel, or a hydrogen carrier (e.g., ammonia, ammonia borane) can be converted to hydrogen under the proper exposure to high-temperature solar heat. The principle of this kind of solar hydrogen generation technique is presented in Fig. 13.17.

By considering a unitary production of transformed energy from the reformation process, say 1 MJ, the usage costs of reforming fuels in addition to an on-site CO_2 mitigation factor can be compared to the direct use of the fuels. For direct decomposition of the fuel, such as the ammonia reformation case, the development of a cost index is simple. First, some parameters must be defined:

$$\varepsilon = \frac{\mathrm{HHV}_{\mathrm{H}_2}}{\mathrm{HHV}_{\mathrm{F}}}, \tag{13.31}$$

where $\mathrm{HHV}_{\mathrm{H}_2}$ is the higher heating value of the reformed fuel, in this case hydrogen, and $\mathrm{HHV}_{\mathrm{F}}$ is the higher heating value of the original fuel. Next, the

molar ratio of product fuel to reactant fuel must be determined from the chemical equation:

$$\mathrm{MR}_{i/\mathrm{H}_2} = \mathrm{kmol}_i/\mathrm{kmol}_{\mathrm{H}_2}. \tag{13.32}$$

The cost index for the reformation is now shown, where the value of the index is between 0 and 1, clearly showing the cost reduction for reformed fuel:

$$\mathrm{CI} = \frac{1}{\varepsilon}(\mathrm{MR}_{i/\mathrm{H}_2}). \tag{13.33}$$

It also should be noted that in terms of the equilibrium reactions, water may be recycled in the system, but by analyzing the stoichiometric reaction, we can see that water is consumed in the process. First, the molar ratio of water to the final fuel product must be determined from the chemical equation:

$$\mathrm{MR}_{\mathrm{w}/\mathrm{H}_2} = \mathrm{kmol}_{\mathrm{w}}/\,\mathrm{kmol}_{\mathrm{H}_2}, \tag{13.34}$$

where the subscript w indicates water. Cost parameters must also be added on a per unit mass basis for the consumption of the original fuel as well as water: $C_{\mathrm{i}} = \$/(\mathrm{kg\ initial\ fuel})$, and $C_{\mathrm{w}} = \$/(\mathrm{kg\ water})$. The cost index for steam reformed fuels, such as methane or propane, then becomes

$$\mathrm{CI} = \frac{1}{\varepsilon}\left(\mathrm{MR}_{i/f} + \mathrm{MR}_{w/f}\frac{\mathrm{MM}_{\mathrm{H_2O}} \cdot C_w}{\mathrm{MM}_i \cdot C_i}\right). \tag{13.35}$$

For carbon-based fuels that may be reformed, and for every quantity of initial fuel used, the same amount of CO_2 is released during the reformation process as would be released during combustion. However, the solar energy that is added to the system results in a diluted release of CO_2. As such, a CO_2 mitigation index is defined as follows. This time, there must be a direct comparison of the reformation reaction to the combustion reaction. The first molar ratio is the ratio of CO_2 released upon combustion of the initial fuel to the amount of initial fuel burned: $\mathrm{MR}_{\mathrm{CO_2}/i} = \mathrm{kmol}_{\mathrm{CO_2}}/\mathrm{kmol}_i$. The second molar ratio is the ratio of CO_2 released upon reformation of the fuel to the amount of final fuel produced: $\mathrm{MR}_{\mathrm{CO_2}/\mathrm{H_2}} = \mathrm{kmol}_{\mathrm{CO_2}}/\mathrm{kmol}_{\mathrm{H_2}}$. It follows that the CO_2 mitigation index shown below is once again a value between 0 and 1, where for example an index of 0.85 represents a mitigation of 15%:

$$\mathrm{CO_2}I = \frac{1}{\varepsilon}\left(\frac{\mathrm{MR}_{\mathrm{CO_2}/\mathrm{H_2}}}{\mathrm{MR}_{\mathrm{CO_2}/i}}\right). \tag{13.36}$$

The above analysis is meant to quantify in terms of cost and carbon mitigation the benefits of distributed hydrogen production through fuel/carriers reforming.

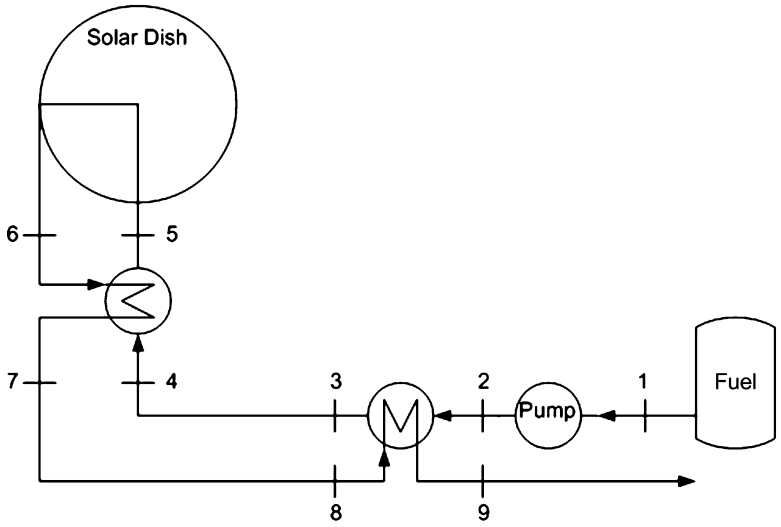

Fig. 13.18 Simplified diagram of a solar-driven fuel reforming system for hydrogen production

The system, shown in Fig. 13.18, comprises a number of stages: 1–2, pumping; 2–3, first preheating; 3–4, fuel pipeline transport; 4–5, second preheating; 5–6, solar-driven fuel reforming; 6–7, heat recovery; 7–8, reformate pipeline transport; 8–9, second stage of heat recovery.

13.4.2.8 Nuclear–Thermal Routes for Hydrogen Production

Using nuclear energy as the primary energy source for hydrogen production is attractive because (1) the greenhouse gas emissions associated with nuclear energy production are much lower than those with conventional fossil fuel combustion, and (2) nuclear energy is adaptable to large-scale hydrogen production. Progress has been made in nuclear-based hydrogen production in recent years as evidenced by many research studies published in the literature.

The typical utilization of nuclear reactors has been for electricity generation with steam power plants. Studies indicate that more benefits can be obtained if in addition to electricity a sustainable fuel such as hydrogen is produced. The efficiency of power generation normally increases with increasing temperature of the working medium, which, in the case of the nuclear energy utilization, leads to increased nuclear reactor coolant temperatures and pressures. However, increases in the power generation efficiency of nuclear power plants are mainly limited by the permissible temperatures in nuclear reactors and the corresponding temperatures and pressures of the coolants. Coolant parameters are limited by the corrosion rates of materials and nuclear reactor safety constraints.

Table 13.9 Progress in high-temperature reactor design for hydrogen production

Reactor type	Progress description
Advanced gas reactor (AGR)	– Commercially available in the UK; 14 units in operation with 1,500 MW thermal each – Coolant temperature 650°C to be upgraded to 750°C – Subcritical carbon dioxide coolant at 43 bar to be upgraded at supercritical pressures
High-temperature gas-cooled reactor	– Developed by Japan Atomic Energy Research Institute (JAERI) – Prototype power 30 MW cooled with helium at maximum 950°C – Adaptable to drive the S-I thermochemical water splitting cycle – Advantageous concept for efficient, economic, and safe nuclear energy
Secure transportable autonomous reactor (STAR-H_2)	– Not available yet commercially; based on proven technology from Russian submarine propulsion – Demonstrated liquid lead coolant at 500°C to be upgraded to 800°C – 400 MW thermal capacity in compact units transportable by rail
Modular helium reactor (MHR)	– Based on demonstrated German and the U.S. technologies – Helium coolant at 850°C at 70 bar, upgradable to 1,000°C – Meets the requirements for hydrogen production – Proposed as a basis for a nuclear energy source
Sodium-cooled fast reactor (SFR)	– Demonstrated technology in Russia, the U.S., and France – Sodium coolant at 500°C upgradable to 550°C – Closed fuel cycle with efficient management of actinides and conversion of fertile uranium
Molten-salt-cooled advanced high-temperature reactor	– Only in design phase; not yet built – High-temperature (750–1,000°C) heat – Molten fluoride salts coolant and a pool configuration – Efficient low-cost thermochemical H_2 and electricity – Coated-particle graphite-matrix fuel
Supercritical water cooled CANDU reactor	– Coolant (supercritical water) pressure of about 25 MPa – Coolant temperature 625°C – Expected power generation efficiency 45%

Many studies address nuclear reactor modifications and the progress needed to meet the requirements for producing cheap electricity and high-temperature heat by efficiently coupling the heat with a hydrogen production plant. The envisaged reactor technologies and the progress in their development are listed in Table 13.9. With respect to the process heat temperature level that these technologies offer, gas-cooled reactors, molten-salt-cooled reactors, and heavy-metal-cooled reactors appear to be the most promising technologies for hydrogen production. The various nuclear reactor technologies combined with thermally driven hydrogen production processes adaptable to nuclear reactors complement but do not compete with heat in shaping the future nuclear-based hydrogen generation capability. Table 13.10 lists the envisaged thermally driven hydrogen production methods that can be integrated with nuclear reactors.

Table 13.10 Envisaged hydrogen production methods coupled with nuclear reactors

H_2 production method	Description and remarks
Thermochemical cycles	Best candidate is the S–I cycle. It allows for centralized, base-load production of hydrogen and the utilization of waste heat from nuclear power plant provided that suitable temperature level upgrade methods are elaborated. Potential efficiency of the overall process can be higher than 40%. The technology is proven at lab scale but requires development to achieve commercialization phase.
Nuclear coal gasification	European research led by Germany since 1999. Requires temperatures higher than 700°C. The gasification technology is mature, and coupling with nuclear reactors can show overall efficiency over 60%. The main advantage: carbon dioxide emissions are reduced as compared to auto-thermal processes.
Nuclear steam reforming of fossil fuels using membranes	Chemical reactions, the required heat for reactions, fuel savings, and CO_2 emission reductions were investigated for natural gas and petroleum. The process temperature can be reduced to 550°C. High efficiency (>60%) and lower CO_2 emissions are achievable.

13.4.2.9 Fossil Fuel–Based Thermally Driven Hydrogen Production

When hydrogen is produced from fossil fuels via thermal methods, the energy associated with fuel combustion is used to drive the conversion process in which the hydrogen atoms are extracted from steam and/or from the fuel itself. For example, by adding oxygen in a steam methane reformer, the reaction becomes exothermic:

$$4CH_4 + 2H_2O + O_2 \rightarrow 10H_2 + 4CO, \tag{13.37}$$

which can generate syngas at 1,200 to 1,400 K and 72.2 kJ/mol of hydrogen. This reaction can be conducted at higher pressure—up to 100 bar—producing thus compressed hydrogen. The water gas shift reaction can be subsequently applied so that the overall reaction of auto-thermal methane conversion is $4CH_4 + 6H_2O + O_2 \rightarrow 14H_2 + 4CO_2$, which delivers hydrogen at 500 K and an exothermic reaction heat of 20.8 kJ/mol of hydrogen.

The auto-thermal fossil fuel reforming or gasification process is one of the most well known and widely applied hydrogen processes in industry. With natural gas as the starting fuel, 4 mol of carbon dioxide are released in the atmosphere for each 14 mol of hydrogen produced. In principle, the hydrogen production from fossil fuels can be assisted by carbon dioxide sequestration. This is a path toward cleaner hydrogen production and is called fossil fuel decarbonization (see Muradov and Veziroglu 2008); sometimes the process of decarbonization of fossil fuel to generate hydrogen and possibly to produce electricity is called precombustion, meaning that the decarbonization of the fossil fuel is done prior to the combustion process; what is combusted is the produced carbon-free fuel—the hydrogen.

An alternative to auto-thermal fossil fuel conversion to hydrogen, which emits carbon dioxide, is the process of thermal cracking of the hydrocarbons, which is not supposed to emit any CO_2 but rather to generate carbon. Thermal cracking is a process of decomposition. It can be successfully applied to the hydrocarbons with the smallest molecular mass for which more desirable products are formed. Thermal decomposition of methane, $CH_4 \rightarrow C(s) + 2H_2$, is an endothermic reaction with the associated heat of 75.6 kJ/mol. Methane can be decomposed through catalytic or noncatalytic processes that can be conducted thermally or under the influence of plasma. The advantage of the method comes from the fact that the resulting carbon powder can be viewed as a by-product. Carbon is very much needed by industry to construct carbon fibers and nano-materials.

13.4.3 Electrothermally-Driven Hybrid Hydrogen Production

The processes studied in Section 13.4.2 are categorized as thermally driven because the energy needed to generate hydrogen is in the form of high-temperature heat. When implemented in practice, such processes need electricity to run pumps, compressors, conveyers, fans, and so on. Thus, in a practical implementation, most of the hydrogen production methods are electrothermally driven. Another aspect to mention is that the thermally driven methods require very high temperature heat. In contrast, the electrochemical processes do not require high temperature. Because the sustainable high-temperature sources are limited mainly to solar and nuclear, it is desirable to devise hybrid methods that are driven electrically/electrochemically and thermally. Some thermochemical cycles are hybrid and can operate at temperatures below 550°C as compared to the S–I cycle, which runs at close to 1,000°C. Another process of interest is the high-temperature electrolysis in which part of the energy needed by the process is transferred thermally and part is transferred electrically. In this section, the major electrothermal processes and systems for hydrogen production are discussed.

13.4.3.1 Hybrid Thermochemical Water Splitting Cycles

Apart from thermally driven TCWS cycles, mentioned above, three other TCWS cycles—called hybrid—draw special attention because they operate at lower temperatures. Hybrid cycles use thermal and electrical energies to conduct certain endothermic and electrochemical reactions. As a consequence of their lower operating temperatures, other sustainable thermal sources in addition to solar, high-temperature nuclear, and biomass combustion can be used to drive the involved processes. The additional heat sources are nuclear reactors of the present generation operating at 250° to 650°C and entailing geothermal and waste heat recovery. Figure 13.19 presents in a schematic manner the operation of the Mg–Cl cycle (a) and the H_2SO_4 cycle (b)—both being driven electrothermally. The flux of

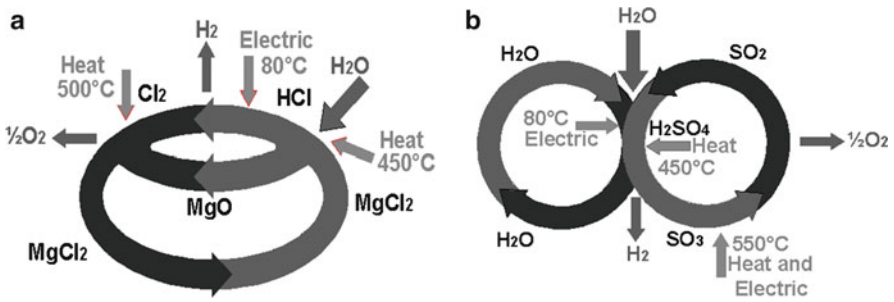

Fig. 13.19 Low-temperature thermochemical water splitting cycles: (**a**) Mg–Cl cycle, and (**b**) H_2SO_4 cycle [modified from Balta et al. (2009)]

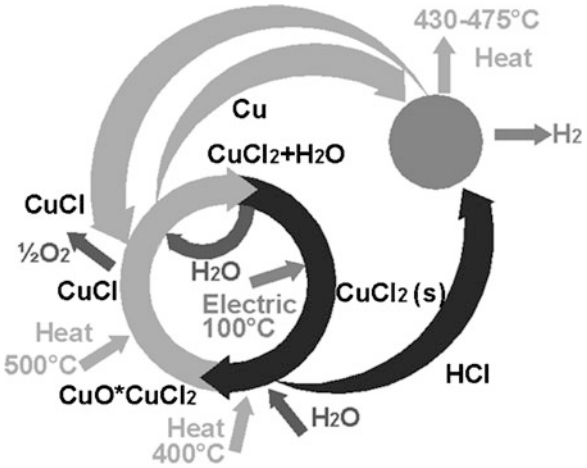

Fig. 13.20 The Cu-Cl thermochemical water splitting cycle [modified from Balta et al. (2009)]

the recycled chemicals is shown as well as the energy inputs and temperature level; a distinction is made between electrical and thermal energy inputs.

Recently, a group of institutions led by the University of Ontario Institute of Technology, the Atomic Energy of Canada (AECL) Limited, and the Argonne National Laboratory in the U.S., with other participants, is developing a pilot scale prototype of the Cu-Cl TCWS plant. The maximum temperature level required from the heat source is about 550°C, which is needed to drive the oxygen generation reaction. There are several variants of the Cu–Cl cycle; the one that is most studied is called the "five-steps" version. The five-step Cu–Cl cycle comprises three thermally driven chemical reactions, one electrochemical reaction, and one physical step of drying. According to the study by Orhan et al. (2009a), the energy efficiency of hydrogen production by a Cu-Cl plant is close to 60%, while the energy efficiency is about 11%. The processes involved in the five-step cycle are indicated in Fig. 13.20.

The copper chlorine cycle for TCWS has advantages over the other cycles regarding hydrogen generation from low-grade temperature sources, especially those sources that can be considered sustainable thermal energy. These categories include nuclear heat, industrial heat, heat recovered from power plants, concentrated solar heat, heat resulting from municipal waste incineration, geothermal heat, and other sources. The current stage of development of this cycle is reviewed in Naterer et al. (2009).

Among the topics under investigation are kinetics of the hydrogen production reaction, development of the electrochemical step for copper particulate generation, drying of the aqueous cupric chloride, transport processes in hydrolysis reactor, modeling the molten salt reactor for oxygen production, scale-up study and economic analysis of the plant, thermochemical data compilation for the involved materials (see Zamfirescu et al. 2010a), development of appropriate materials, linkage of nuclear and other sustainable thermal sources, and the hydrogen plant.

The process diagram of the Cu-Cl TCWS cycle is shown in Fig. 13.21. Low-pressure superheated steam is extracted from a steam turbine and supplied to the Cu–Cl cycle, which decomposes water into hydrogen and oxygen. The superheated steam fed in line 0 is expanded with work recovery to 1 bar of pressure, where it is assumed that saturated or nearly saturated steam exists. The saturated steam is superheated to 400°C at the state labeled 2 on the figure using a heat pump (details are given later). The extracted amount of steam is replaced by supplying an equal amount of water back into the cycle.

Liquid water at 20°C is supplied into the cycle and then boiled and superheated to 400°C. This process induces a number of losses. The steam is injected into a fluidized bed reactor CR_1, where it chemically reacts with copper (II) chloride ($CuCl_2$) under heat addition Q_{CR1} (endothermic reaction). This step dissociates the water molecule and forms hydrochloric acid (HCl). An additional compound is formed, which is a metallic solution of copper oxide and copper dichloride. This chemical reaction and others in the Cu–Cl cycle are summarized in Table 13.11, which gives the reactor, reaction, temperature, and heat per kmol of hydrogen produced. Hydrogen is a product of the fifth chemical reactor (CR_5), involving the exothermic combination of particulate copper with HCl at 450°C.

In the second reactor (CR_2), oxygen is produced by thermal dissociation of copper oxide at about 500°C. Step 3, called the copper production step, is driven electrochemically. The third reactor (CR_3) is an electrochemical cell containing an aqueous solution of copper chloride. The reaction heat is shown in Fig. 13.21, with W_{CR_3} designating the electrical power.

The copper precipitate is removed from CR_3 and transferred to CR_5. In reactor CR_4, there is no chemical reaction, but rather water is removed (by drying) from the aqueous solution of $CuCl_2$ that was produced by electrolysis. Table 13.12 shows the substances circulated within the Cu–Cl cycle, together with their state and temperature. The entire Cu–Cl cycle operates at atmospheric pressure. Therefore, the products (hydrogen and oxygen) must be compressed for storage. To facilitate compression, the products are cooled first with heat recovery. A blower (indicated

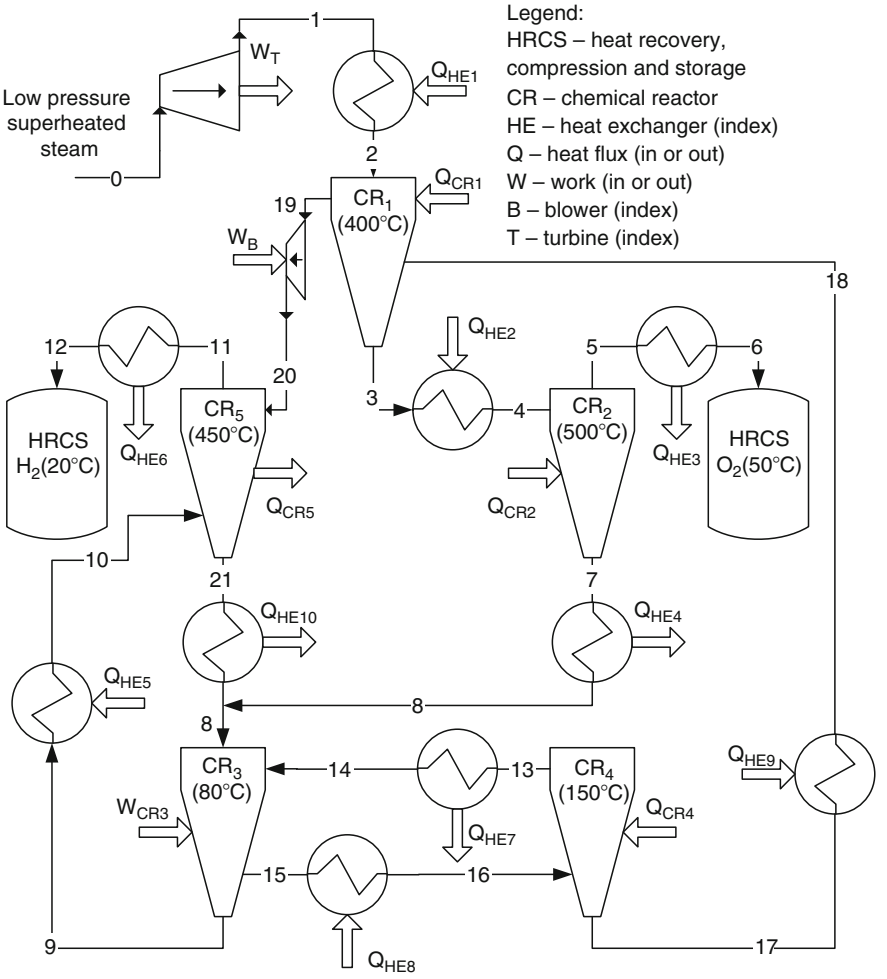

Fig. 13.21 The five-step Cu–Cl water splitting cycle [modified from Zamfirescu et al. (2010b)]

by W_B in Fig. 13.21) is necessary to extract the HCl from CR_1 and to deliver it to CR_5. During this process, the circulated HCl is slightly heated.

On Fig. 13.21, one notes that in the Cu-Cl plant there are four chemical reactors that comprise the hydrolysis reactor CR_1; the oxygen producing reactor CR_2; the hydrogen producing reactor CR_5; the copper electrolyzer CR_3. With CR_4 one indicates the dryer of aqueous $CuCl_2$, which does not actually perform any chemical reaction, but rather conducts a physical process of drying. For the design of these reactors, it is important to have a good understanding of the reaction kinetics and equilibrium, and to determine the optimum parameters that enhance the yields and production rates. We briefly address here some relevant results regarding the chemical reactors.

Table 13.11 Process steps of the Cu–Cl cycle

Step	Reaction	T (°C)	Q (MJ/ kmol H_2)	G (kcal)	H (kcal)
1	$2CuCl_2(s) + H_2O(g) \rightarrow CuO \cdot CuCl_2(s) + 2HCl(g)$ (endothermic)	400	105.3	9.5	27.9
2	$CuO \cdot CuCl_2(s) \rightarrow 2CuCl(l) + 0.5O_2(g)$ (endothermic)	500	110.5	−0.71	30.9
3	$4CuCl(s) + H_2O(l) \rightarrow 2CuCl_2 \cdot H_2O(aq) + 2Cu(s)$	80	140.4		
	(i) $4CuCl(s) + 4Cl^- \rightarrow 4CuCl_2^-$			8.27	0.062
	(ii) $4CuCl_2^- \rightarrow 2CuCl_2 + 2Cu + 4Cl^-$ (electrochemical)			14.5	2.93
4	$CuCl_2 \cdot H_2O(aq) \rightarrow CuCl_2(s) + H_2O(g)$ (drying only)	150	18.3	6.0	19.9
5	$2Cu(s) + HCl(g) \rightarrow 2CuCl(l) + H_2(g)$ (exothermic)	450	−55.5	0.23	−11.2

Data from Zamfirescu et al. (2010b)

Table 13.12 Substances circulated within Cu–Cl cycle

Line	Substance	State	T, °C	Remarks
0	Steam	Superheated	>100	$P > 1$ bar
1	Steam	Saturated	100	$P = 1$ bar
2	Steam	Superheated	400	–
3	$CuO{\cdot}CuCl_2$	Solid	400	Metallic solution, powder
4	$CuO{\cdot}CuCl_2$	Solid	500	Metallic solution, powder
5	O_2	Gas	500	–
6	O_2	Gas	80	–
7	CuCl	Liquid	500	Liquid metal
8	CuCl	Solid	80	Precipitated, particulate
9	Cu	Solid	80	Particulate, powder
10	Cu	Solid	450	Particulate, powder
11	H_2	Gas	450	–
12	H_2	Gas	80	–
13	Steam	Superheated	150	Pressure 1 bar
14	Water	Liquid	80	Pressure 1 bar
15	$CuCl_2$	Slurry	80	Aqueous solution
16	$CuCl_2$	Slurry	150	Aqueous solution
17	$CuCl_2$	Solid	150	Metallic powder
18	$CuCl_2$	Solid	400	Metallic powder
19	HCl	Gas	400	Acid
20	HCl	Gas	430	Slightly compressed
21	CuCl	Solid	450	Particulate

Data from Zamfirescu et al. (2010b)

Hydrogen is generated through an exothermic reaction that combines particulate copper with gaseous hydrochloric acid at about 400°C. The kinetics of this reaction, in the context of reactor design has been studied parametrically by Zamfirescu et al. (2010e). The involved reaction is $Cu(s) + HCl(g) \rightarrow CuCl(l) + 0.5H_2(g)$.

The suggested residence time of copper particles varies between 10 and 100 seconds, depending on the operating conditions, while the conversion varies between 55% and 85%.

The noncatalytic gas–solid reaction that occurs in the hydrolysis reactor CR_1, where $CuCl_2$ reacts with steam to obtain hydrochloric acid and copper oxychloride, assumes the following:

- The reactor is a fluidized bed comprising two regions: bubble and emulsion.
- The temperature gradient within the bed reactor is negligible.
- Only one reaction occurs: cupric chloride particles react with superheated steam.
- The reaction takes place in the emulsion phase.
- The conversion of particles at the inlet of the reactor is zero.
- The hydrolysis reaction is first-order.

The results by Haseli et al. (2009) indicate that the gas conversion ranges from 20% to 50% and the solid conversion ranges between 30% and 60% with a recommended interface velocity of 0.4 to 0.8 m/s. The optimum temperature in this reactor is around 500° to 550°C. According to Orhan et al. (2009b) the exegy efficiency of the hydrochloric acid production reactor is around 65% at about 400°C. The oxygen production reactor has been analyzed by Orhan et al. (2009c). It has been found that at 500°C the exergy destruction in this reactor is around 5,300 kJ/kmol of hydrogen. The exergy destruction of the electrochemical step for copper production is, according to the calculations by Orhan et al. (2008b), 140 MJ/kmol hydrogen at 45°C.

The coupling between the Cu–Cl cycle and a sustainable energy source must consider necessarily various opportunities for heat recovery and heat upgrading. Depending on the temperature level of the temperature sources, one can either upgrade the temperature via heat pumps or use internal heat recovery within the cycle. Granovskii et al. (2008a) proposed a chemical heat pump based on the reversible steam methane conversion reaction, and Zamfirescu et al. (2010b,f) analyzed some vapor compression heat pumps.

The thermodynamic calculations of heat requirements and heat ejection from the Cu–Cl cycle lead to the determination of the *T*–*H* in Fig. 13.22, where *H* is total enthalpy. This diagram shows the required heat inputs and outputs and their associated temperature levels. The continuous line refers to heat input streams, and the dashed line refers to heat outputs. The streams requiring heat are identified with the line 1–2–3–4–5–6–7–8 and those releasing heat with 9–10–11–12–13.

It is desirable to apply heat recovery as much as possible and upgrade the temperature of the ejected heat so that it reaches the temperature level needed for heat input. The heat released by stream 9–10–11–12 should be received by a heat pump that, at the expense of additional power, upgrades the temperature and enthalpy content and delivers a hot stream to the Cu–Cl cycle that matches the profile 3–4–5–6–7–8. The work required to operate such a heat pump can come from a sustainable heat source available at an intermediate temperature T_m, which drives a heat engine operating between T_m and the ambient air at T_0. This heat engine also delivers power to the Cu–Cl cycle.

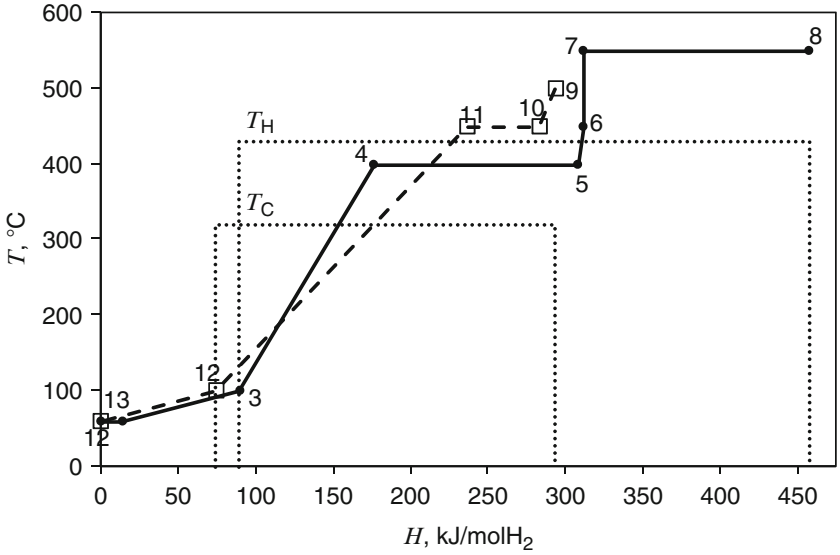

Fig. 13.22 T-H diagram of heat inputs and outputs associated with the Cu–Cl cycle [modified from Zamfirescu et al. (2010b)]

It is useful to transpose the *T–H* presented in Fig. 13.22 in *T–S* coordinates, where *S* is the stream entropy expressed in kJ/K and mol H_2. The streams are thermodynamic systems that interact with the exterior by heat transfer only. Consequently, for any stream, $\delta Q = \mathrm{d}H$, thus,

$$\mathrm{d}S = \int \frac{\delta Q}{T} = \int \frac{\mathrm{d}H}{T}. \tag{13.38}$$

The area embraced by the lines 1–2–3–4–5–6–7–8 and that indicated by "Heat Source" in Fig. 13.23 represent the ideal/minimum work needed by the heat pump to upgrade the temperature of the heat source and deliver useful heat to the Cu–Cl cycle. The area embraced by the lines 9–10–11–12–13 and that indicated with "Heat Sink" in Fig. 13.23 represent the ideal/maximum work that can be obtained from the heat recovered by the Cu–Cl cycle. The engineering challenge regarding the integration of the Cu-Cl plant with the thermal energy source T_m consists of finding suitable working fluids and processes that allow for the construction of a heat pump and heat engine cycle operating like the one presented in Fig. 13.23.

One original idea is to use the CuCl as working fluid in a vapor compression heat pump that recovers heat from the hydrogen production reactor and other hot stream, upgrades the temperature level, and delivers the heat to the oxygen production reactor. Zamfirescu et al. (2010f) proposed such a system, as shown in Fig. 13.24.

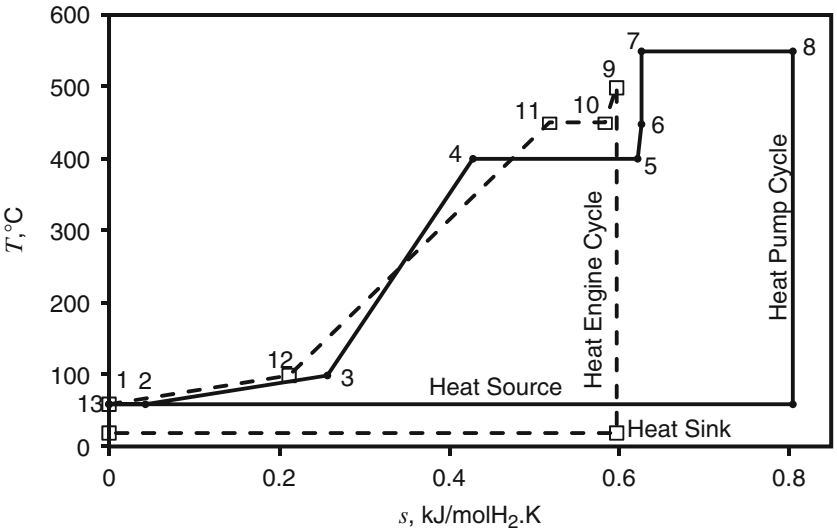

Fig. 13.23 T-S diagram of ideal power and heat pump cycles coupled to the Cu-Cl plant [modified from Zamfirescu et al. (2010b)]

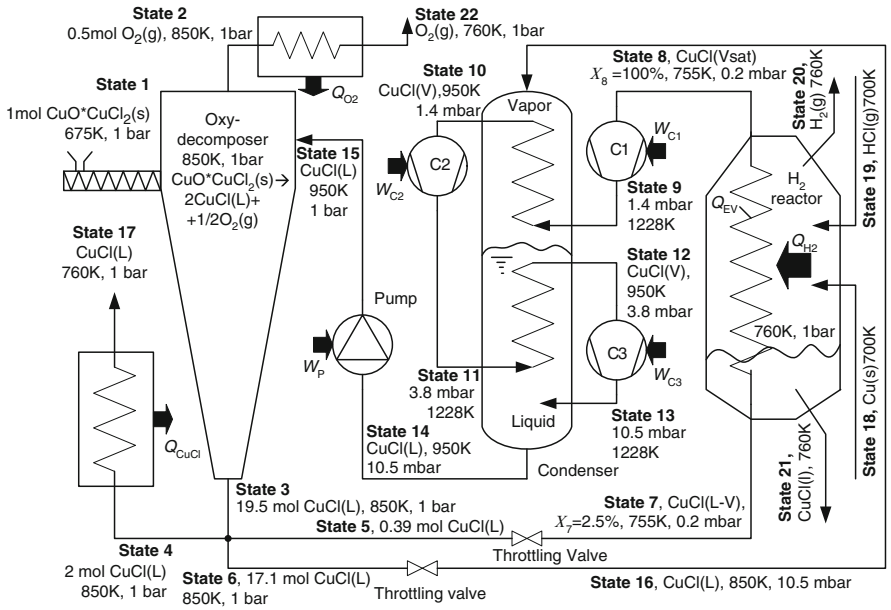

Fig. 13.24 Heat pump with CuCl vapor compression for internal temperature level upgrading within the Cu-Cl water splitting cycle [modified from Zamfirescu et al. (2010f)]; *g* gas; *L* liquid; *V* vapor; *Vsat* saturated vapor; *X* vapor quality; *W* work; *Q* heat; *C* compressor

The copper oxychloride is fed at state 1 into the oxy-decomposer at 675 K. The temperatures, pressures, and other parameters indicated in Fig. 13.24 correspond to the reference case. Inside the reactor, the particulate $CuO \cdot CuCl_2$ is heated by direct contact with molten cuprous chloride, which is injected at state 15 at 950 K. The molten salt delivers its sensible heat and cools down to the average reactor temperature, which is assumed to be 850 K for the reference case considered in this study.

The heat delivered by the hot stream at state 15 makes copper oxychloride decompose thermally and release oxygen, while forming molten cuprous chloride (CuCl). At the top of the reactor, oxygen gas is expelled at state 2, while at the bottom, molten CuCl is collected and drained out at state 3. The molten CuCl product is split into three parts at the reactor exit (state 3): one part (state 4) is sent for further processing within the plant (quantitatively, state 4 flows 2 mol of CuCl for 1 mol of copper oxychloride); and the remaining two parts (streams in states 5 and 6) are further processed thermomechanically within the heat pump.

The stream in state 5 is expanded through a throttling valve in a vacuum, down to 0.2 mbar and reaches a two-phase state at state 7 at a saturation temperature of 755 K. This stream is further heated and reaches 100% saturated vapor at state 8. The vapor is then compressed in three stages with intercooling in order to reduce compression work. The final pressure is 10.5 mbar, for which the corresponding saturation temperature is 950 K. A design of the condenser that embeds a direct contact heat exchanger is indicated in the figure. The condenser consists of a vessel that incorporates two coils, where superheated vapors are cooled after stages 1 and 2 of compression. During the operation, at the bottom of the condenser, saturated CuCl is collected. The superheated vapor at the final stage of compression—state 13—is injected into this liquid, and thus cooled by direct contact and condensed. The condensation heat is transferred to an additional stream of molten CuCl. This stream flows as follows:

- From state 6, the liquid is throttled and its pressure is reduced from 1 bar to 10.5 mbar, wherein the CuCl is still in a subcooled thermodynamic state; therefore, the liquid temperature does not change sensibly during the throttling (state 16).
- The subcooled liquid (state 16) is injected into the condenser at the top.
- Inside the condenser, the enthalpy of stream at state 16 is increased such that it takes all condensation heat of the vapor stream at state 9.
- The saturated liquid collected at the bottom of the condenser (state 14 at 950 K) incorporates all condensation heat.

Furthermore, the pressure of stream at state 14 is increased up to atmospheric pressure and then the heated flow is injected into the oxy-decomposer at state 15. The CuCl stream is one of the products of the oxy-decomposer, and therefore injecting this substance in excess does not affect the chemical species present in the oxy-decomposer, even though it may affect the chemical equilibrium. However, because oxygen is drawn constantly out of the reactor, there is a tendency to shift the equilibrium toward the right, which compensates the tendency of shifting toward the left due to excess CuCl present in the reactor.

Figure 13.24 shows the heat and mechanical power fluxes associated with various components. The heat flux Q_{O_2} rejected by the heat exchanger cools the oxygen from state 2 to state 16. The heat flux Q_{CuCl} of cooling the molten cuprous chloride from state 4 to state 17 can be recovered and used internally to provide heat to the heat pump's evaporator. A part of the evaporation heat, Q_{EV}, can be supplied by these two sources. Additional sources of heat to deliver to the evaporator can be found within the water splitting plant. For example, the hydrogen production reaction, which combines particulate copper with gaseous hydrochloric acid, is exothermic and rejects heat at over 725 K. This reactor can operate also at 760 K, and the rejected heat is recovered and used to drive the heat pump. Figure 13.24 suggests that the evaporator coils of the CuCl heat pump can be embedded in the hydrogen production reactor. For the proposed settings, the heat flux received by the evaporator is the summation of heat fluxes recovered from the hydrogen production reactor and from the heat exchangers for oxygen and CuCl(L) product cooling ($Q_{EV} = Q_{H_2} + Q_{O_2} + Q_{CuCl}$).

The theoretical calculations indicate that the coefficient of performance (COP) of the heat pump is much higher than 2.5, being possible to reach the value of 10. The explanation of such a high COP is that the working fluid is rather easy to compress, and the temperature lift of the heat pump is reasonable. The work needed to drive the heat pump is about 10 to 15 kJ/mol of H_2.

The capital cost of Cu-Cl plant, as estimated by Orhan et al. (2008a) is roughly $10–50 million for a capacity range of 1 to 10 tons of hydrogen per day. The cost of produced hydrogen by such a large-scale plant must account for many production cost components apart from the direct production costs such as taxation, depreciation, insurance, rent, overhead, administrative expenses, distribution and marketing expenses, research and development costs, financial allocations, and gross-earning expenses. A rough estimation of the contribution of individual costs in the hydrogen product price is shown in Fig. 13.25. Table 13.13 compares the hydrogen production costs with other methods.

13.4.3.2 Solar-Driven Electrothermal Systems

Solar energy can be converted into high-temperature heat and electricity to supply electrothermal processes for hydrogen production. Figure 13.26 suggests two possible routes to do this. The first route entails simultaneous generation of electricity (through photovoltaic panels) and high-temperature heat from concentrated solar radiation.

Both the high-temperature heat and the electricity are then used to fuel a hybrid process for hydrogen production, such as the thermochemical copper chlorine cycle of HTSE. The second route proposes to concentrate solar radiation first and then obtain high-temperature heat, which is supplied to the hybrid process for hydrogen production. The process rejects heat—such as that associated with high-temperature products that must be cooled—which can be recovered and used to run a heat engine to generate electricity for the hybrid process. Solar energy converted in high-temperature heat is suitable for all kinds of hybrid processes.

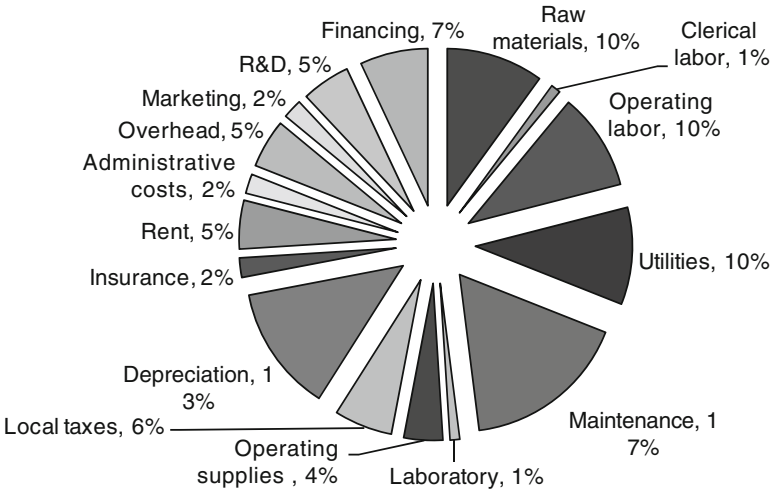

Fig. 13.25 Various contributions to the total product cost of a Cu-Cl water splitting plant for hydrogen production [data from Orhan et al. (2008a)]

Table 13.13 Comparison of Cu-Cl hydrogen cost with other methods for 10 tons of hydrogen per day

Cost item ($/GJ)	Cu-Cl plant	Off-peak electrolysis	Steam–methane reforming
Capital cost	7.7	3.2	3.1
Energy charge	0.5	1.0	0.8
Carbon charge	0	0	1.6
Hydrogen cost	2.71	2.41	2.67

Data from adapted from Orhan et al. (2008a)

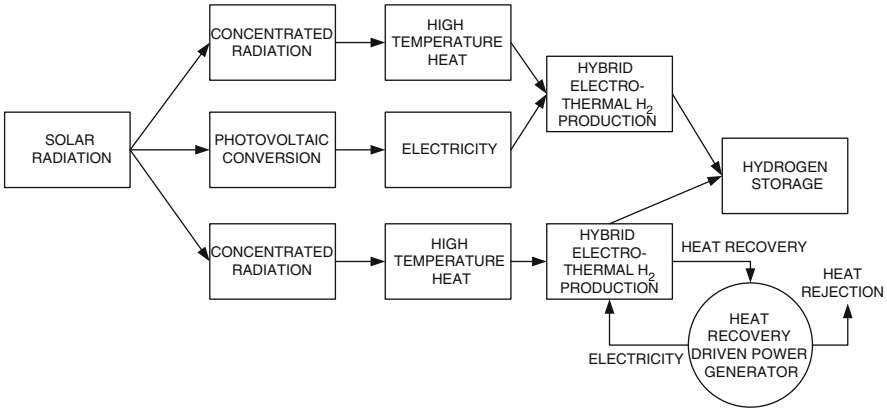

Fig. 13.26 Routes for supplying electrothermal H_2 production processes with solar energy

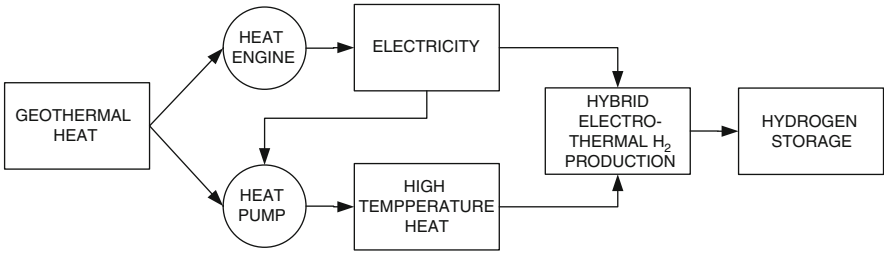

Fig. 13.27 Geothermal hydrogen production through electrothermal methods

13.4.3.3 Geothermal Electrothermal Hydrogen Production

The temperature range of geothermal heat is narrower than that of solar, with typical temperatures of about 50°C to 450°C. Few geothermal sources reach temperature over 500°C. Thus, most of the geothermal sources available need to be coupled to heat pumps to upgrade the temperature to a suitable level for hybrid processes for hydrogen production. Figure 13.27 shows a system for driving a hybrid electrothermal process for hydrogen production with geothermal energy.

In this approach, the geothermal heat is used to supply a heat engine that converts heat into electricity. The generated electricity is used partially to "fuel" the hybrid process for hydrogen production and partly is supplied to a high-temperature heat pump. The role of the heat pump is to lift the temperature level of the geothermal source. Therefore, the heat pump is supplied with heat from the geothermal source and delivers high-temperature heat to the hybrid process.

The configuration of the geothermal hydrogen production system intimately depends upon the available temperature range. Say, for example, it is very high temperature (500°C); it can be used to provide heat directly in hybrid thermochemical cycles for water splitting, and there is no need for temperature level upgrading. If it is moderate temperature range, then electricity and heat upgrading can be applied, or if the level of temperature is too low, hybrid thermochemical cycles may not be applicable; rather in this condition geothermal energy can be used to drive cold water electrolysis process.

Figure 13.28 suggests a possible diagram of a geothermal-driven steam electrolysis system operating at very high temperature that uses the opportunity of heat recovery from the hot product streams. The heating of water is done in three stages, whereas at low temperatures regular materials are used for heat exchangers. At intermediate temperatures water is boiled, and at high temperature water is superheated in heat exchangers that make use of expensive materials with appropriate thermal behavior and durability. The temperature that steam has to reach before entering in the electrolyzer should be higher than 1,000°C. The geothermal energy is converted into electricity and used to drive the electrolysis. The same arrangement can be used for other thermal energy sources.

Depending on the geothermal source characteristic, the efficiency of electric power generation varies greatly, with typical values of energy efficiency between

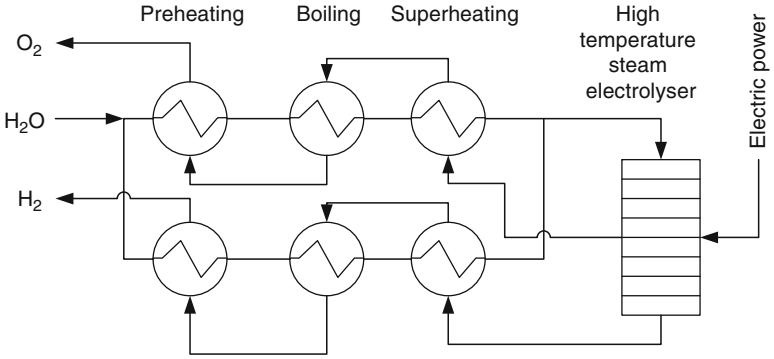

Fig. 13.28 Arrangement for high-temperature steam electrolysis

5% and 50%. Assuming 80% energy efficiency of the HTSE systems, the expected energy of geothermal hydrogen production may be in the range of 4% to 40%. Geothermal-based hydrogen production can also be implemented by coupling thermochemical cycles with geothermal heat, power generators, and heat pumps for temperature upgrading.

13.4.3.4 Biomass-Based Electrothermal Systems

Another option to generate good-purity hydrogen by using biomass energy is by coupling a biomass combustion facility with an HTSE system. A possible implementation is shown in Fig. 13.29. The system uses an SOEC and two biomass furnaces. The SOEC is basically the reverse of a solid oxide fuel cell (SOFC), which contains a solid electrolyte permeable to oxygen ions. Various types of solid oxide electrolytes were tested, but the technology is in development. The electrolyte can be formed on a porous support made of calcium-stabilized zirconia ZrO_2 (CSZ), whose porosity may be about 35%. Other approaches use yttrium-stabilized zirconia (YSZ), containing about 10% molar Y_2O_3. The operation range of SOEC is of about 900° to 1,100°C, respectively.

The main furnace (line 14–15–16–17 in Fig. 13.29) is supplied with wet biomass and operates at a relatively low exhaust gas temperature. The function of the main furnace is to generate heat to drive a steam power plant and to dry some biomass. The well-dried biomass is fed in a second furnace, of smaller capacity, that, with dry biomass, can generate exhaust gases with very high temperature (around 1,000 K). The hot exhaust gases transfer heat to the SOEC, which generates hydrogen and oxygen.

The oxygen generated by SOEC is used to enhance the combustion efficiency in the high-temperature furnace. Because the heat needed for the water splitting reaction is supplied completely via heat transfer, it is said that the SOEC operates above the "thermo-neutral point." At 1,000°C and 20% H_2 conversion, the SOEC efficiency η_{Cell} can be estimated conservatively at 80%. A possible, highly efficient,

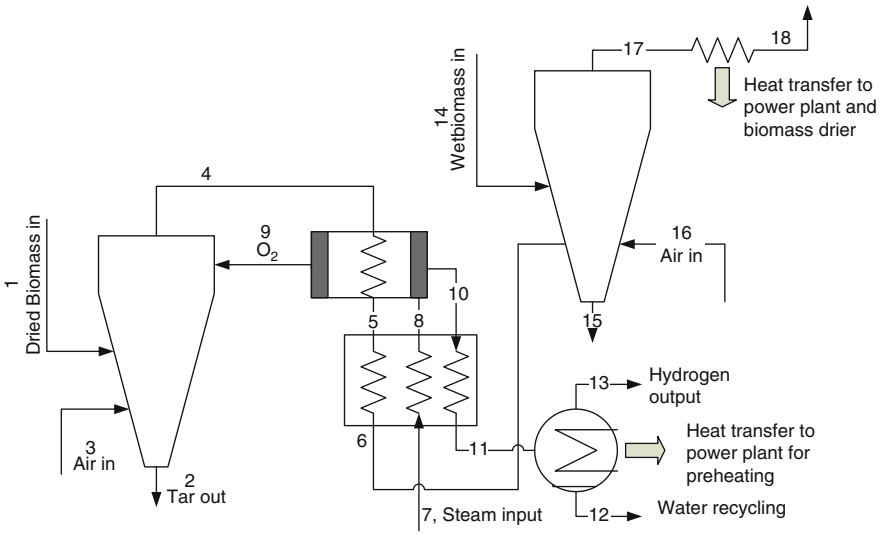

Fig. 13.29 Biomass-driven high-temperature steam electrolysis system

steam Rankine cycle driven by the low-temperature furnace is shown in Fig. 13.30. The cycle allows for the extraction of process steam and is designed especially for coupling to the above steam electrolysis system.

Another possible system is the biomass-driven hybrid thermochemical water splitting to generate hydrogen. Figure 13.31 shows a possible design. In this system, a low-grade (wet) biomass is used and there is no need for drying because the temperature required of the exhaust gases is slightly below 700°C to supply the thermochemical cycle. The kind of thermochemical cycle considered here is the Cu-Cl one. There is also enough heat in the exhaust gases to supply a steam power plant that produces the required amount of electricity.

The steam power plant is detailed in Fig. 13.32. The steam cycle features a two-phase steam expander at line 7–8 that helps increase the exergy efficiency by allowing for a perfect match of temperature profiles of the exhaust gas and the working fluid (steam). The required heat inputs and outputs in the Cu–Cl cycle can be calculated from energy balances and it results in the temperature-total enthalpy in Fig. 13.33.

Illustrative Example: Comparison of Two Water Splitting Systems

The biomass-driven HTSE system and the biomass-driven TCWS system introduced above were compared with respect to energy and exergy efficiencies and biomass utilization. It was assumed that heat losses from the system are 0.5% from the reaction heats. The results were obtained by Zamfirescu et al. (2010d) based on standard thermodynamic analysis conducted according to the first and second laws of thermodynamics.

Since the required temperature level is available anyway for the flue gas produced by biomass combustion, internal heat recovery within the Cu-Cl plant is applied. The plot in Fig. 13.33 shows with dashed lines the temperature level and

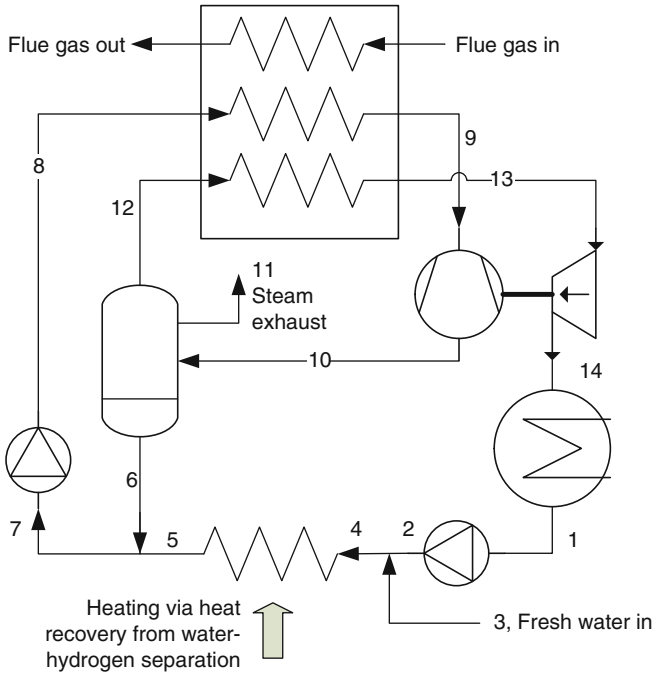

Fig. 13.30 Efficient Rankine cycle with steam extraction used in conjunction with the high-temperature steam electrolysis system shown in Fig. 13.29

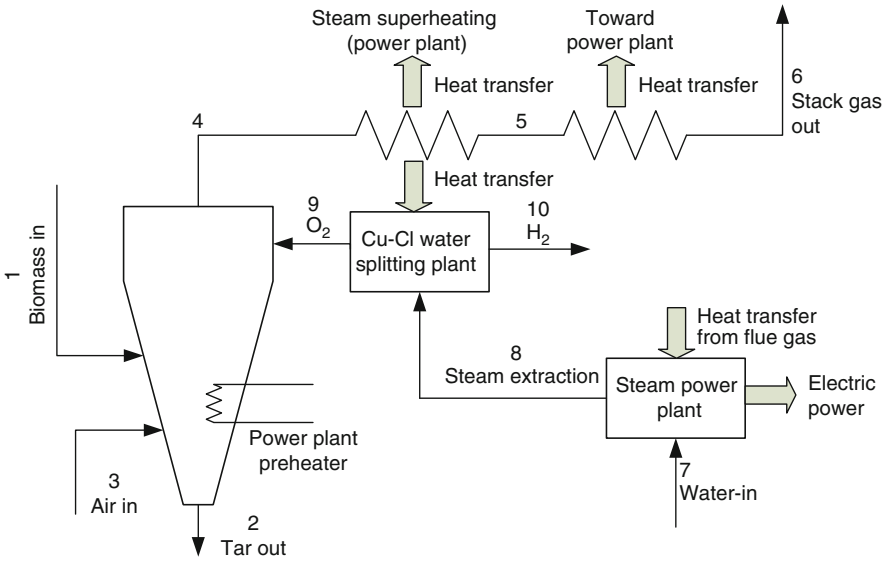

Fig. 13.31 Biomass-driven thermochemical water splitting system

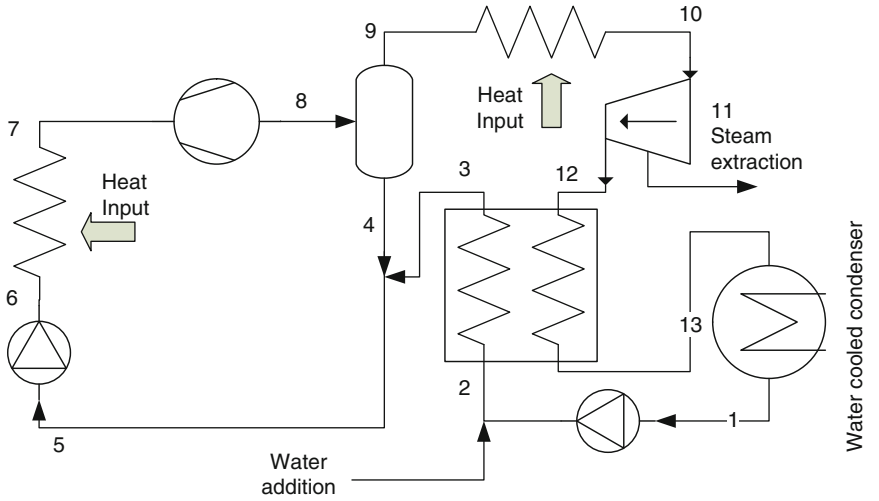

Fig. 13.32 Steam power plant coupled with the biomass-driven thermochemical water splitting system suggested in Fig. 13.31

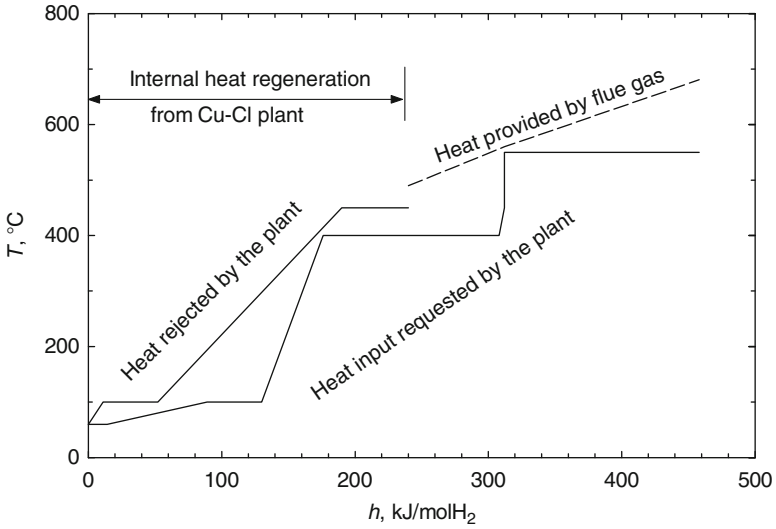

Fig. 13.33 Heat input and heat rejected by the Cu-Cl plant per 1 mol of H_2

enthalpy range of the flue gas delivering heat to the Cu-Cl plant. The highest temperature of the flue gas is 680°C. Figure 13.34 shows the energy and exergy efficiencies as a function of biomass moisture content. The definitions of these efficiencies are shown on the same figure.

The last result indicates in Fig. 13.35 the biomass utilization as a function of technology and biomass quality. *N* represents the number of mols of biomass

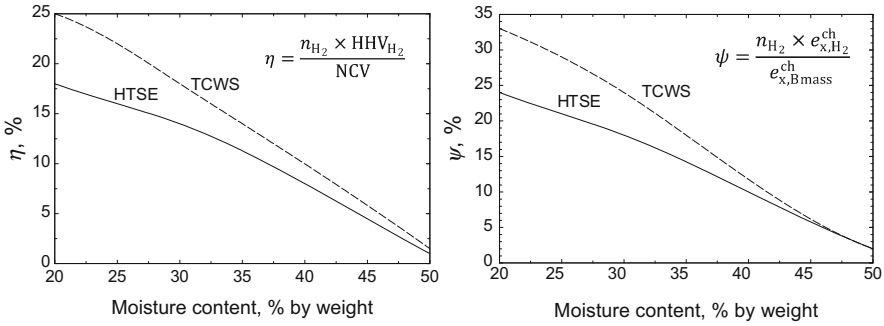

Fig. 13.34 Energy (η) and exergy (ψ) efficiencies of HTSE and TCWS driven by biomass energy [data from Zamfirescu et al. (2010d)]

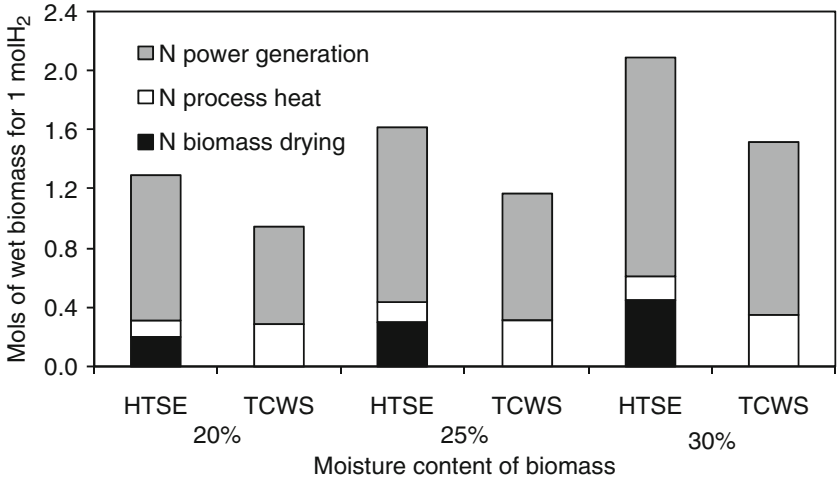

Fig. 13.35 Biomass utilization at hydrogen production via HTSE and TCWS [data from Zamfirescu et al. (2010d)]

used per mol of hydrogen produced. The result demonstrates that the TCWS consumes less biomass than HTSE because (1) the requirement of electrical energy is reduced and (2) there is no need to dry the biomass before utilization. The conclusion is that TCWS appears more attractive than HTSE.

13.4.3.5 Energy Recovery Routes for Electrothermal Hydrogen Production

Energy recovery can be applied in various instances to generate high-grade or low-grade temperature heat. Municipal waste incineration and landfill gas combustion are typical examples of high-temperature heat recovery obtained from human

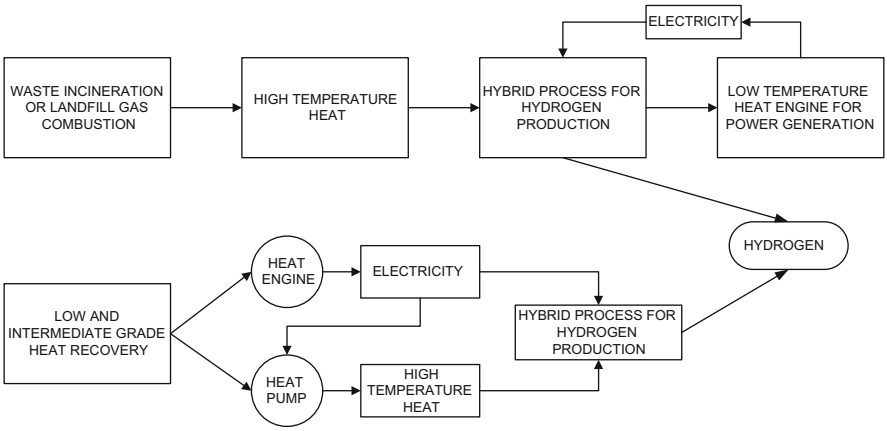

Fig. 13.36 Routes to hybrid hydrogen production processes driven by energy recovery

activity. Also, various industries eject a large amount of heat into the surroundings. In general, such heat comes at a lower grade, typically from 60°C to 150°C, or at intermediate temperatures that are up to 400°C.

Figure 13.36 presents some possible routes to generate hydrogen through hybrid processes starting from energy recovery. The recovered energy is present or it is eventually converted into heat at high, intermediate, or low grade. The high-temperature heat can be directly used to feed hybrid processes; in this case, the heat ejected by the processes can be used to drive electricity generation through heat engine power generation, which is fed back to the hybrid process. Additional heat possibly can be obtained from the high-temperature heat by using appropriate power cycles. In the case when low or intermediate heat is recovered, heat engine generators and heat pumps may be used simultaneously to obtain electricity and higher temperature heat appropriate for the process. It may be economically advantageous to drive a hybrid process in this way instead of producing electricity only and conducting water electrolysis. The economic advantage of the system depends on the temperature level of the heat source. If the level is too low, upgrading the temperature is not beneficial.

13.4.3.6 Fossil Fuel–Based Electrothermal Systems

Fossil fuels can be used to generate high-temperature heat and electricity to supply hybrid processes for hydrogen production. Figure 13.37 illustrates some ways to do this. Electrothermal plasma methods are emerging technologies for hydrogen generation. In this approach, fossil fuel feedstock is supplied to a plasma reactor. The plasma process can be of two kinds: (1) steam–hydrocarbon reforming and (2) plasma hydrocarbon decomposition. In the first kind, preheated fuel and superheated steam are fed into the reactor. In the second kind, only hydrocarbon is fed.

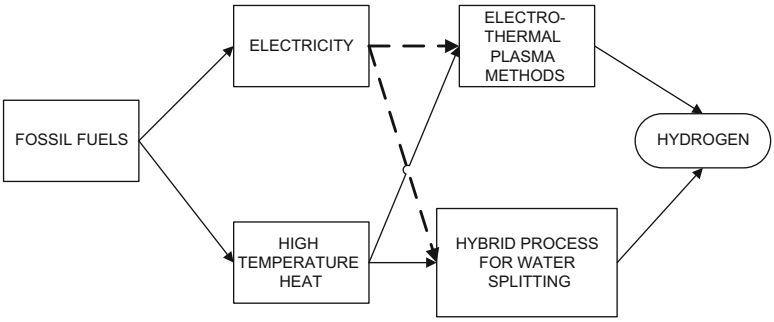

Fig. 13.37 Thermoelectrical routes for hydrogen production supplied by fossil fuel energy

The feedstock is subjected to a high-voltage electric arc that increases the process temperature up to 5,000°C, enough to dissociate chemicals and generate hydrogen. For plasma steam reforming, the resulted syngas contains 50% to 75% hydrogen and the rest is mostly CO.

If steam is not fed in the plasma process, carbon is separated from the hydrocarbon material. The advantage of the plasma decomposition is its high electrical efficiency (80–90%) and hydrogen purity (98% or more). One of the major technical problems with plasma reactors comes from the carbon deposits on the electrodes, which often must be replaced.

The second route shown in Fig. 13.37 involves electricity and high-temperature heat generation from fossil fuels, followed by a hybrid process for water splitting. In the preferable arrangement, high-temperature combustion heat is used to supply the process, while heat recovery can be applied to generate electricity. The involved hybrid processes can be the HTSE and the hybrid thermochemical water splitting cycles. Therefore, in this route, fossil fuels are used only to generate thermal and electric energy to drive the process, while the feedstock of hydrogen is the water.

13.4.3.7 Nuclear Electrothermal Routes for Hydrogen Production

The HTSE can be coupled with nuclear reactors. The required temperature level for the process is 500° to 1,200°C. SOEC can obtain an electrical-to-hydrogen efficiency of over 90%, provided that the process temperature is higher than 1,000°C. The estimated overall efficiency in conjunction with Advanced Light Water Reactor (ALWR) is around 30%. The efficiency is over 45% with Modular Helium Reactor (MHR) and Advanced Gas Reactor (AGR). The technology requires more research and development before it can become commercially available.

Much attention is paid to the development of heat-upgrading solutions of nuclear heat generated by reactors of the current generation so that one can raise the efficiency of the hydrogen-generation process. Most nuclear reactors generate heat at two levels: high temperature (which is transferred by the reactor coolant) and low temperature (which is ejected through the moderator fluid). Typically, the

Table 13.14 Heat-upgrading solution of nuclear heat to drive hydrogen production

Method	Description
Chemical heat pumps	Heat pumps operating based on the reversible steam methane reaction can deliver heat up to about 650°C with a source at around 500°C. Magnesium oxide/steam-based chemical heat pumps, operating according to the reversible reaction $MgO(s) + H_2O(g) \leftrightarrow Mg(OH)_2$ can upgrade the heat source temperature from about 250°C to 550°C. Ammonia/salt chemical heat pumps based on reversible reactions, such as $MnSO_4 \cdot 6NH_3 \leftrightarrow MnSO_4 \cdot 2NH_3 + 4NH_3$, can upgrade the heat source temperature from about 80°C to 260°C. In principle, several kinds of chemical heat pumps can be cascaded to upgrade the low-level temperature heat ejected by the moderator of the nuclear power plant reactors and to obtain heat at over 600°C, which eventually can drive a thermochemical water splitting cycle.
Vapor compression heat pumps	Novel working fluids were investigated by Zamfirescu and Dincer (2009a), Zamfirescu et al. (2009a), and Zamfirescu et al. (2010f). Siloxane-base can upgrade the source temperature with about 100°C and deliver heat at maximum 400°C, showing a heat pump COP higher than 6; special thermodynamic cycles are proposed operating in the dense gas region and two-phase vapor compression. Biphenyl-based heat pump shows potential to upgrade heat source temperature from about 250°C to 450°C with COP higher than 2.5. Titanium tetra-iodide-based heat pumps are an attractive technical solution to upgrade the source temperature from 350°C to 650°C with a COP higher than 3. A cascaded cyclohexane-biphenyl heat pump upgrades the heat recovered from moderator at 80°C and delivers variable temperature heat between 250°C and 600°C, showing a COP around 5.
Reversed Brayton cycle heat pumps	Several reversed Brayton cycle-based heat pumps were suggested and analyzed by Marmier and Füterer (2008) operating with helium and/or CO_2 at 70 bar and able to upgrade the nuclear heat temperature from 400°C to 850°–1,000°C. Internal work recovery between the turbine and compressor is applied to enhance the COP.

moderator heat comes at temperatures in the range of 40° to 80°C and the process heat at temperatures of 250°C up to 650°C.

It is justifiable in view of financial efforts and safety issues not to change the nuclear reactor design but rather to adapt the external cooling loop in such a way that it can be coupled thermally with hydrogen production facilities. Two possibilities can be envisaged for coupling the current nuclear reactors to hydrogen production facilities, without requiring reactor modifications. The first is to recover the heat ejected by the moderator fluid and use this thermal energy for hydrogen generation. In this case, the reactor cogenerates hydrogen and electricity. The second possibility is to dedicate the reactor to hydrogen production only. In this case, the reactor coolant transfers the thermal energy to the hydrogen production facility. In both described situations, heat pumps may be necessary to upgrade the source temperature to a higher level, appropriate for driving the hydrogen production process via thermochemical cycles. Some possible heat-upgrading solution with heat pumps are described in Table 13.14.

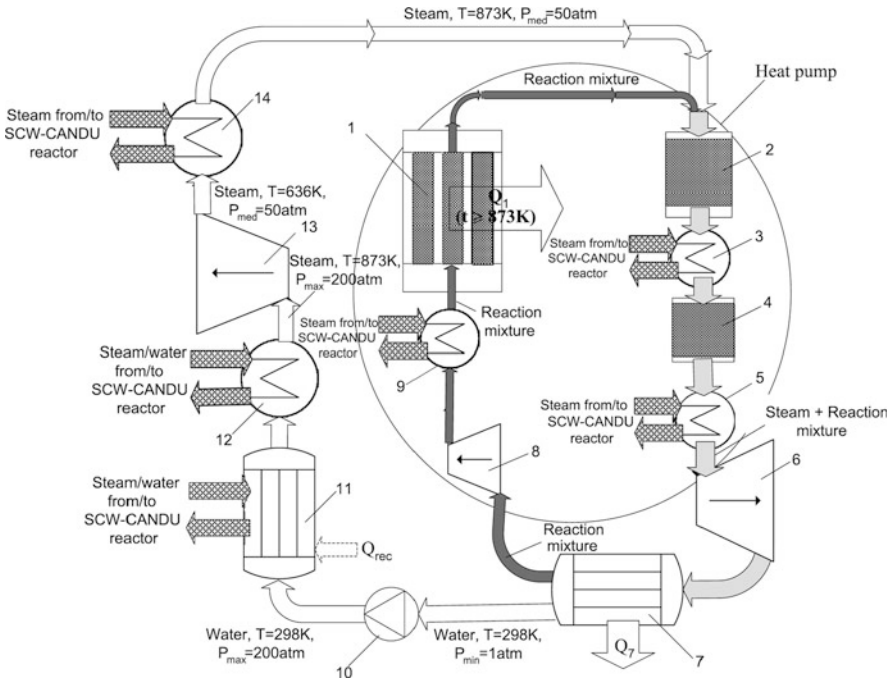

Fig. 13.38 Chemical heat pump coupling a thermochemical water splitting cycle with the SCW-CANDU nuclear reactor [modified from Granovskii et al. (2008a)]

Case Study: Chemical Heat Pump Integrated with the SCW-CANDU Reactor

This case study presents the solution proposed by Granovskii et al. (2008a) to couple a Cu-Cl TCWS plant with a supercritical water-cooled CANDU reactor for hydrogen generation. The proposed heat pump is of the chemical type, performing cyclically the reversible methane–steam reaction. This is a known process that is used largely for hydrogen production, according to $CH_4 + H_2O + Q \rightarrow CO + 3H_2$ which is favored at low pressure. The reverse reaction is favored at high pressures, and it can deliver heat at higher temperatures according to $CO + 3H_2 \rightarrow CH_4 + H_2O + Q$. The system studied by Granovskii et al. (2008a) to conduct cyclically these reactions is presented in Fig. 13.38.

The high-temperature heat is generated in the methanator (1), where the methane synthesis reaction is conducted at higher pressure. The heat absorbing reaction occurs as slightly lower pressure in two stages in reactors 2 and 4. The heat is transmitted to the heat pump through a heat exchanger 3 inserted between the two steam–methane conversion stages. The reaction products are expanded in turbine 6 after reheating using nuclear heat in the heat exchanger 5.

The water is condensed in the condenser 7 and the noncondensed gases, containing reaction products are recompressed by compressor 8, reheated at point 9, and delivered to the high-temperature reactor 1 to close the heat pump cycle. In the Rankine power cycle, water is pressurized up to 200 atm, then boiled at point 11 and

superheated at point 12 prior to the first stage of steam expansion in the turbine system at point 13. Reheating of intermediate pressure steam is applied at point 14. Within the chemical heat pump loop the reversible water gas shift reaction occurs rapidly and concurrently with the other reactions according to $CO + H_2O \leftrightarrow H_2 + CO_2$. The calculated hydrogen generation efficiency with a nuclear and chemical heat pump and a copper chloride TCWS plant is calculated to be between 45% and 50%.

13.4.4 Photonic Energy-Driven Hydrogen Production Methods

Solar radiation is in essence a source of photonic energy. It is known that photonic energy is proportional to the frequency of the radiation and given by hv, where h is the Planck constant and v is the frequency. Photons can be used by various living or "non-living" processes to dislocate electrons by their interaction with matter. While electrons are dislocated, the obtained electrical charge can be used either to generate electricity (viz. photovoltaic effect) or to manipulate the valence electrons of chemical species in order to conduct chemical reactions. These kinds of reactions, called photochemical or electrophotochemical depending upon the context, can lead to hydrogen generation. The following methods of hydrogen production, discussed here, are light-driven: photoelectrochemical water splitting, photocatalytic water splitting, and biophotolysis.

13.4.4.1 Photocatalytic Water Splitting

Photocatalytic water splitting uses various kinds of supramolecular complexes capable of capturing photons from incident solar radiation and that release energy to dislocate electrons that in turn either reduce water to hydrogen or oxidize water to produce oxygen; when reduction and oxidation reactions are coupled, a complete water splitting process is performed. The supramolecular catalysts possess active centers and photosensitive centers. The photoreduction and photo-oxidation of water molecule occur as follows:

$$\left.\begin{array}{l}\text{Photoreduction: } 2H_2O + 2e^- \xrightarrow{hv} H_2 + 2OH^- \\ \text{Photo}-\text{oxidation: } 2H_2O \xrightarrow{hv} 4H^+ + 4e^- + O_2(g)\end{array}\right\}. \tag{13.39}$$

It is a major technological challenge to maintain photoelectrons for a sufficiently long duration at the supramolecular level. A recently declassified proprietary technology developed by Brewer and Elvington (2006) demonstrated at laboratory scale the water photoreduction reaction, with nonsacrificial supramolecular complexes capable of generating multiple electrons and maintaining them at the active center for a long enough duration. In this process, water is exposed to an

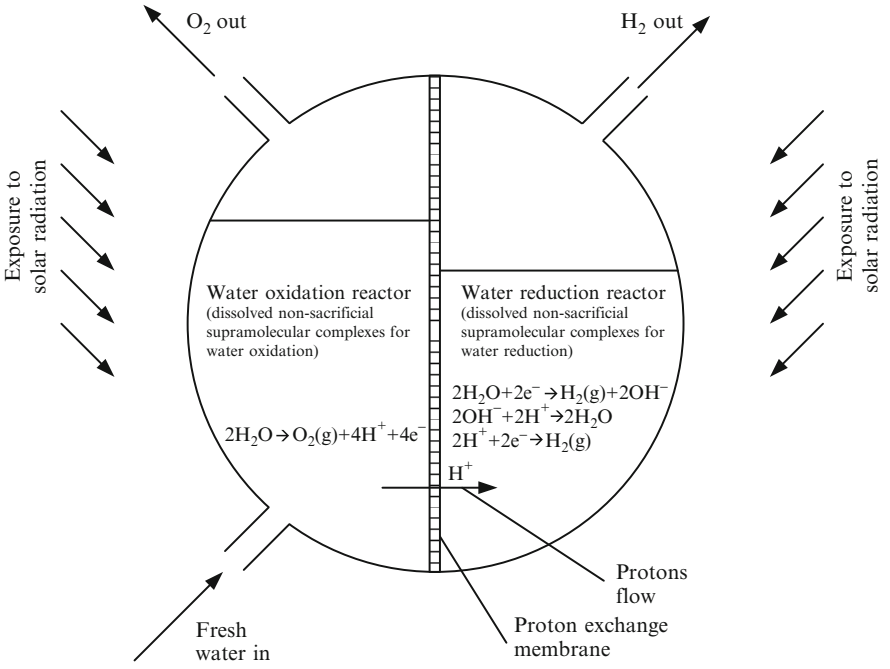

Fig. 13.39 Conceptual design of a photochemical water splitting reactor [modified from Zamfirescu et al. (2010c)]

electrically charged supramolecular complex that reduces water to hydrogen at the active center. Simultaneously, the supramolecular complex is exposed to solar radiation, during which the incident photons dislocate multiple electrons. Electrons propagate along a molecular chain within nanoseconds and "recharge" the supramolecular complex with electrons. The supramolecular complex can be placed on a support or dissolved in water.

A possible conceptual design of a photocatalytic water splitting system is proposed in Fig. 13.39 and consists of a vessel comprising two photochemical reactors separated by a PEM. Both reactors are exposed to solar radiation. On the left side, the water photo-oxidation reactor is located, in which selected supramolecular photocatalysts are dissolved at a proper quantity to generate electrical charges that oxidize water and generate oxygen gas and protons. Fresh water is continuously supplied to this reactor, while the photocatalysts remain in solution. The flow rate of fresh water is adjusted such that the water level in the vessel remains constant. The protons released by the photochemical oxidation reaction are driven by a concentration gradient and they cross the proton exchange membrane. In the water reduction reactor, selected supramolecular complexes for photocatalytic reduction of water to hydrogen are dissolved in the proper concentration. The water from this reactor is not consumed in a steady-state operation because the only overall reaction is that of proton reduction to form hydrogen gas. Above the

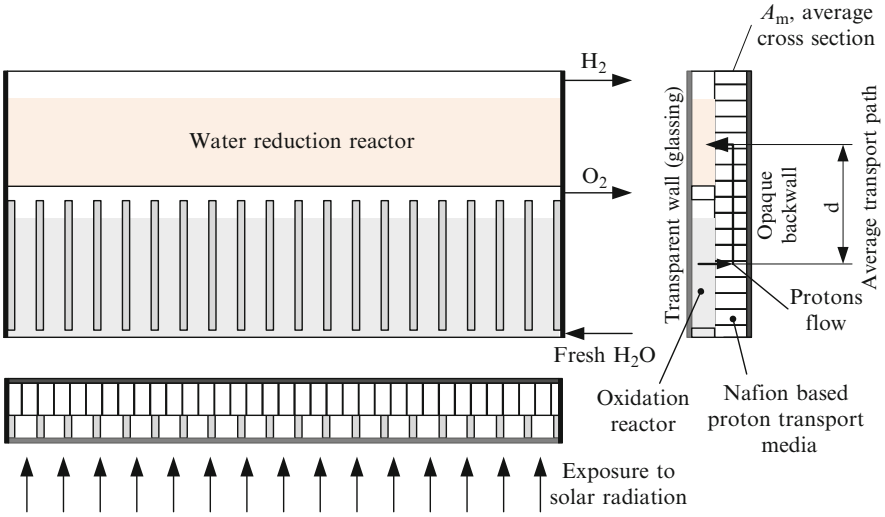

Fig. 13.40 Possible implementation of the reactor as a flat-plate type [modified from Zamfirescu et al. (2010c)]

liquid level, the product gases (oxygen and hydrogen) are continuously extracted with the use of external fans, which maintain low pressure in the system. In order to avoid water migration through the proton exchange membrane, the pressure is maintained at about the same level on both sides.

In a practical implementation, the photochemical reactor can be constructed with a flat-plate–type geometry. Figure 13.40 suggests a possible practical construction. The system possesses a transparent glassing divided in two sections: below is the water oxidation reactor and above the water reduction reactor. The PEM is placed behind the glassing in the lower reactor. In the lower part, there are a number of vertical channels on both sides, which support the proton exchange membrane.

A water distribution channel and an oxygen collection channel are placed below and above the water oxidation reactor. The space above the water reduction reactor is free of liquid and hydrogen is collected from one of the sides. A flat-plate–type photochemical reactor, as illustrated in Fig. 13.40, can be mounted on a tilted position to capture 4 to 7 kWh of incident solar radiation per day.

There are many catalysts based on complex organic molecules and rare metal active centers that are capable of splitting water, photocatalytically. A brief summary of past results is given here based on Zamfirescu et al. (2010c). Ruthenium-based complexes based on 4-picoline and 2,2′-bipyridine were synthesized; they promote photochemical water oxidation. Bipyridine is a key chemical compound that can be linked to a ruthenium metal active center to have the role of photosensitizer, which dislocates electrons each time when the active center is hit by photons of appropriate energy. Bipyridine is derived from pyridine C_5H_5N, which is an aromatic heterocyclic organic compound. Bipyridine comprises two pyridine rings. It has the chemical formula $(C_5H_4N)_2$. A typical photosensitizer embeds a ruthenium atom in three bipyridine molecules, and it is known as $[Ru(bpy)_3]^{2+}$.

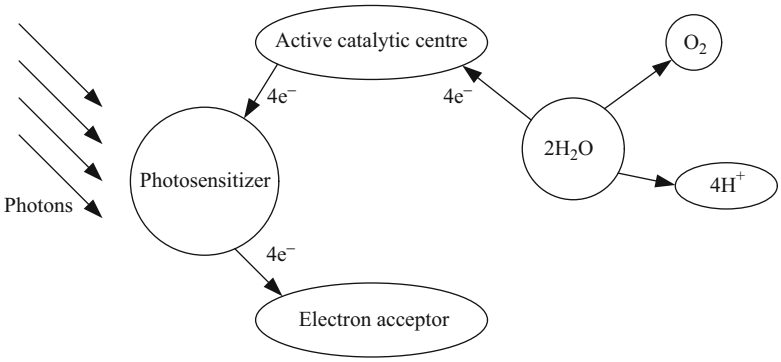

Fig. 13.41 Mechanism of photocatalytic water oxidation [modified from Zamfirescu et al. (2010c)]

The mechanism of photocatalytic water oxidation is demonstrated in Fig. 13.41. When the ruthenium atom is photoexcited, it enters into a metastable state (it increases its valence by one), characterized by the ability to lose one valence electron. The valence electron is transferred to an adjacent molecule that serves the role of electron acceptor. After losing one valence electron, the ruthenium atom takes one electron from the active catalytic center (typically a metal), which is now activated. The active center is then capable of accepting electrons from adjacent water molecules and oxidizing them. Therefore, at the active center, an oxygen molecule and four protons are formed for each oxidizing cycle, which consumes two water molecules. The crucial issue with the operation of this oxidation mechanism is the nature of the electron acceptor. The majority of electron acceptors developed in the past are consumed in the reaction, so one must continuously supply the process with fresh electron acceptors and remove the ones that are consumed. Many types of electron acceptors are known: $[Co(NH_3)_5Cl]Cl_2$, $Na_2S_2O_8$, $K_2S_2O_8$, $AgNO_3$, S_2O_8 or $[Co(NH_3)_5Cl]^{2+}$. For example, if the persulfate $S_2O_8{}^{2-}$ is used as an electron donor, the photoexcitation yields

$$2[Ru(bpy)_3]^{2+} + S_2O_8{}^{2-} \xrightarrow{h\nu} 2[Ru(bpy)_3]^{3+} + 2SO_4{}^{2-}. \tag{13.40}$$

The persulfate is consumed as it transforms in sulfate ($SO_4{}^{2-}$). Once the photosensitizer is excited, it is able to react with the water molecule at the active center (RuO_2):

$$4[Ru(bpy)_3]^{3+} + 2H_2O \xrightarrow{RuO_2} 4[Ru(bpy)_3]^{2+} + O_2 + 4H^+. \tag{13.41}$$

As observed in reaction (13.41), the photosensitizer takes one electron from the catalyst (RuO_2), which then during four catalytic cycle charges with a charge of +4e, becomes able to split the water molecule. In general, the catalyst is in the form of a colloidal suspension in water.

Table 13.15 Preparation and performance characteristics of the selected water oxidation reaction

Parameter	Characteristics	Remarks
Photosensitizer	Tris(2,2′-bipyridil) ruthenium-II; $[Ru(bpy)_3]^{2+}$	6.8×10^{-4} mol/dm^3
Catalyst	Colloidal $RuO_2 \cdot 2H_2O$	4.8×10^{-5} mol(RuO_2)/dm^3
Electron acceptor	Nonsacrificial Fe-III in the form of $NH_4Fe(SO_2) \cdot 12H_2O$	0.1 mol (Fe-III)/dm^3
Ionic strength fixer	$NaSO_4$	0.1 mol/dm^3
Illumination	Filtered light with λ>400 nm	3,333 W/dm^3
pH	pH adjuster H_2SO_4	1.9 (optimized)
O_2 yield rate	At quantum efficiency of 48%	0.043 μmol/dm^3 s

Data from Christensen et al. (1985)

There is a limited number of recyclable electron acceptors. A possible acceptor is methylviologen (MV^{2+}), a chemical molecule based on the bipyridine structure. However, coupling ruthenium–bipyridine systems with methylviologen as a reversible electron acceptor, in order to oxidize water, is improbable because the oxidation process is slower than the electrical charge lifetime in the system. Another recyclable (nonsacrificial) electron acceptor is mercury-II. Oxygen generation with mercury-II as an electron acceptor show, that upon irradiation of water containing $[Ru(bpy)_3]^{2+}$ at pH 3 and 0.01 mol/dm^3 $Hg(NO_3)_2$ and colloidal RuO_2 of 3.2×10^{-5} mol/dm^3, the rate of oxygen production was about $(1.3 \pm 0.3) \times 10 - 9$ mol/dm^3 min. However, the quantum efficiency of oxygen production was rather low, that is, 0.25%.

An interesting photo-oxidation system has been proposed by Christensen et al. (1985), which is based on iron-III as nonsacrificial electron acceptor. This was demonstrated experimentally with a quantum efficiency of oxygen production of about 48%. The system is based on reaction (13.41), where the recycling of the photosensitizer is performed:

$$\begin{cases} 4[Ru(bpy)_3]^{2+} \xrightarrow{h\nu} 4[Ru(bpy)_3]^{3+} \\ 4[Ru(bpy)_3]^{3+} + 4Fe^{2+} \rightarrow 4[Ru(bpy)_3]^{2+} + 4Fe^{3+} \\ 4[Ru(bpy)_3]^{2+} + 4Fe^{3+} \xrightarrow{h\nu} 4[Ru(bpy)_3]^{3+} + 4Fe^{2+} \end{cases} \tag{13.42}$$

In the first reaction of set (13.42), the ruthenium atom increases its valence under the influence of photonic radiation. Furthermore, the ruthenium atom recharges the electron acceptor Fe^{2+} by giving one electron to it. Next time, when the ruthenium atom is hit by the photonic radiation, it takes an electron from the active center (RuO_2) and gives it to the electron acceptor. In this mechanism, the electron acceptor is recycled. The preparation and performance characteristics of reactions (13.41) and (13.42) are listed in Table 13.15. The proton production rate is four times higher than the oxygen yield rate. Based on the data reported in Table 13.15, this is 0.172 μmol(H^+)/dm^3 s. The rate of fresh water to be added to the system is

Table 13.16 Preparation and performance characteristics of the selected water reduction reaction

Parameter	Characteristics	Remarks
Molecular device	$[\{(bpy)_2Ru(dpp)\}_2RhBr_2](PF_6)_5$ dissolved in CH_3CN	65 μmol/dm^3
Electron donor	*N*,*N*-dimethylaniline (DMA)	1.5 mol/dm^3
Illumination	Monochrome light with $\lambda = 470$ nm and $\lambda = 520$ nm	400 W/dm^3
pH	pH adjuster CF3SO$_3$H	9.1 (optimized)
H_2 yield rate	Maximum achieved during 3 tests at $\lambda = 470$ nm	0.085 μmol/dm^3 s
H_2 yield rate	Maximum achieved during 3 tests at $\lambda = 520$ nm	0.024 μmol/dm^3 s
H_2 yield rate	Averaged for solar radiation	0.054 μmol/dm^3 s

Data from Brewer and Elvington (2006)

double the moles of produced oxygen. According to reaction (13.22), it is then 0.086 μmol/dm^3 s.

For photocatalytic water reduction, the method by Brewer and Elvington (2006) attracts much attention because of its ability to generate multiple photoelectrons with specially designed molecular complexes. With a 5-W monochromatic LED array, the yield of hydrogen was a maximum 10.9 μmol in 4 hours for a wavelength of 470 nm (blue light). Brewer and Elvington measured the produced hydrogen, both in the gas phase (above the reactor) with a chromatograph, and dissolved in liquid, which was calculated using Henry's law, with the reported solubility of hydrogen in various solvents.

In total, Brewer and Elvington investigated seven molecular complexes, of which four have been dissolved in water and three in a solution of acetonitrile (CH_3CN). The molecular compound that showed the maximum yield was $[\{(bpy)_2Ru(dpp)\}_2RhCl_2](PF_6)_5$ in a basic aqueous solution of pH 9.1. This molecular complex has two 2,2′-bipyridine (bpy) branches that embed one ruthenium (Ru) atom each. The Ru atom is the light absorber (LA), and it transfers one electron each time it is hit by a photon. Table 13.16 show the parameters of a selected water reduction system based on Brewer and Elvington's work.

Bipyridine has the role of a terminal ligand (TL) that possesses the quality of long-lived metal-to-ligand charge transfer excited states. This facilitates the presence of an electrical charge in the system for enough time to react with the water molecule (as mentioned also above). The complex (dpp) represents 2,3-bis (2-pyridil)pyrazine, which has the role of a bridging ligand that transfers the electrical charge to an electron collector, which is a metal atom, in this case rhodium (Rh). This molecular complex is unique and shows effectively the water reduction to hydrogen. The two-branch complex with Ru light-absorbing atoms can collect up to four electrons and convert trivalent Rh to monovalent Rh, which further reduces the water molecule. This feature is unprecedented and allows for multielectron photochemistry.

The following issues affect the design of the photocatalytic water splitting device:

- The volume (and therefore the content of chemicals) of the reactors must be adjusted so that the two reactors can be coupled by the interface condition. The flow rate of protons produced in the oxidation reactor must be the same as

Table 13.17 Main geometric design parameters of the water splitting device

Design parameter	Equation	Value	Remarks
Volume ratio of reactors	$\frac{V_{H_2} \times \dot{n}'''_{H_2}}{V_{O_2} \times \dot{n}'''_{O_2}} = \frac{2}{1}$	$\frac{V_{H_2}}{V_{O_2}} = 1.6$	$\dot{n}'''$, mols produced per second and volume
Area ratio of exposed surfaces to solar radiation	$\frac{V_{H_2} \times I_{H_2}}{V_{O_2} \times I_{O_2}} = \frac{I_{T0} A_{H_2}}{I_{T0} A_{O_2}}$	$\frac{A_{H_2}}{A_{O_2}} = 0.2$	$I_{H_2} = 400\,\text{W/dm}^3$ $I_{O_2} = 3{,}333\,\text{W/dm}^3$ I_{T0}, solar radiation incident
Porous media configuration	$\dot{n}_{H_2} = \frac{150 A_m}{\delta} = 0.054 V_{H_2}$	$\frac{A_m}{\delta} \cong 70 \dot{n}_{H_2}$	$\frac{A_m}{\delta}$, in mm^2/dm^2 $\dot{n}_{H_2}$, in μmol H_2 produced per second

Data from Zamfirescu et al. (2010c)

the flow rate of protons crossing the membrane, and the same as the number of reduced protons in the water reduction reactor.

- The surfaces exposed to solar radiation of each reactor must be calculated so that the reaction conditions for the illumination are met.
- The parameters of two fans must be specified (flow rate per capacity of reactor) to ensure that the oxygen and hydrogen are swept out at the rate corresponding to the reaction.
- A mass flow controller for dosing fresh water must be programmed to deliver the required water in the oxidation reactor and thus maintain the desired pH.

Based on the above issues, the main parameters characterizing the design geometry are listed in Table 13.17.

The overall result, however, is hydrogen and oxygen generation, without the consumption of any chemicals except the electron donor DMA, which is converted into DMA^+ in the photocatalytic water reduction reactor. Recycling of the DMA^+ to DMA can be implemented, possibly, through an electron conducting media between the two reactors. In this way, iron-2 could be converted faster to iron-3 in the water oxidation reactor simultaneously with conversion of DMA^+ to DMA in the water reduction reactors. In fact, in such a setup Fe^{2+} donates one electron to DMA^+. This hypothetical electron transfer process remains to be proved experimentally.

13.4.4.2 Biophotolysis for Hydrogen Production

Another light-driven process is biophotolysis, which is a photonic-driven biochemical hydrogen production process from water. The photosynthesis process used by green plants to convert solar radiation into biochemical energy can be adapted to some extent for hydrogen generation and stands at the base of biophotolysis. Production of hydrogen through biophotolysis can be classified as direct or indirect types and photofermentation type (Kotay and Das 2008).

In biophotolysis, some microorganisms sensitive to light are used as biological converters in a specially designed photobioreactor. The most suitable microorganisms

are microalgae because they exhibit hydrogen evolution and can be cultured in closed systems that can permit hydrogen capture. Microalgal strains can be cultured that exhibit high hydrogen yields. One remarkable advantage of biophotolysis is to produce hydrogen from water in an aqueous environment at standard temperature and pressure. Biophotolysis is not yet developed for commercial use but is demonstrated at laboratory scale. According to Das and Veziroglu (2008), the energy efficiency of the method potentially can reach 10%.

Water molecule can be split through biophotolysis under the action of Cyanobacteria, also known as green microalgae (*Chlamydomonas reinhardtii*) under special conditions. These microorganisms generate and manipulate nitrogenase and hydrogenase enzymes in such a way that they may generate hydrogen and oxygen from water. The bacteria that were found to be hydrogen productive are mainly anabaena variabilis PK84, anabaena cylindica, anabaena AMC 414, gloebacted PCC742, synechococcus PCC602, and aphanocapsa montana; also, the microalgae chlamydomonas reinhardrii cc124 and cc1036 proved to be hydrogen productive. The general reactions producing hydrogen from water with the help of photoactivated enzymes can be written as follows (Das and Veziroglu 2008):

$$\left.\begin{aligned} 12H_2O + 6CO_2 &\xrightarrow{hv} C_6H_{12}O_6 + 6O_2 \\ C_6H_{12}O_6 + 12H_2O &\xrightarrow{hv} 6CO_2 + 12H_2 \end{aligned}\right\}. \tag{13.43}$$

13.4.5 Biochemical Methods for Hydrogen Production

Biochemical energy is stored in organic matter in the form of glucose, cellulose, sucrose, and other complex chemicals containing, for example, adenosine triphosphate, and it can be manipulated by microorganisms to extract hydrogen in the absence or presence of oxygen. When oxygen is completely absent or is present in very reduced quantities, the biochemical conversion of organic matter to various forms of biochemical energy is called anaerobic digestion.

Anaerobic digestion is attractive as hydrogen production method for two important reasons: (a) it can generate hydrogen from organic waste, and (b) it stabilizes waste that otherwise may become a source of uncontrolled microbial growth with the potential danger of contamination of biological species. Moreover, the digester hardware is simple and the system is appropriate for mass production. Two types of bacteria are used in anaerobic digestion: mesophilic (which is active at temperatures of 35–40°C) and thermophilic (which is active at 55–60°C). Note that hydrogen production is also possible by aerobic digestion, but this process is less productive and consequently less developed at the present time, and thus is not discussed here.

Experiments were done in both batch and flow reactors, generating hydrogen from various biomass substrates, including sucrose, and maintaining an appropriate

control of the hydrogen-generating and hydrogen-consuming bacteria present in the reactor. The production rate is about 1.5 mol hydrogen per mol of sucrose in the substrate. *Clostridium* bacteria positively affect the hydrogen production rate under certain conditions. One major problem regarding reaction control in anaerobic digestion reactors is the inhibition of methanogens, which represent hydrogen-consuming bacteria. One possibility to eliminate these bacteria, which normally are present in the organic substrate, is to heat the substrate for a short time at about 100°C, which kills all bacterial populations. Further, the biomass is seeded with hydrogen-producing bacteria such as *Clostridium* and *Bacillus* species.

One of the possible chemical reactions favored by the enzymes generated by hydrogen bacteria (viz. hydrogenase) is acetic acid fermentation from sucrose:

$$C_{12}H_{22}O_{11} + 2H_2O \rightarrow 4CH_3COOH + 4CO_2 + 8H_2. \tag{13.44}$$

In an organic substrate, both nitrogenase and hydrogenase enzymes contribute to hydrogen production by reducing free protons according to the following general reactions:

$$\left.\begin{array}{l}\text{Nitrogenase: } N_2 + 8H^+ + 8e^- + 16ATP \rightarrow 2NH_3 + H_2 + 16ADP + 16Pi \\ \text{Hydrogenase: } 8H^+ + 8e^- + 16ATP \rightarrow 4H_2 + 16ADP + 16Pi\end{array}\right\}, \tag{13.45}$$

where ATP is adenosine triphosphate, ADP is adenosine diphosphate, and Pi is inorganic phosphate which is cleaved from the ATP molecule according to the reaction ATP → ADP + Pi, which releases free energy of about 30.5 kJ/mol; this biochemical energy is used to drive the reaction.

Koutrouli et al. (2009) studied hydrogen production from water-diluted (1:4) olive oil using anaerobic digestion. The retention time in the bioreactor was 7.5 to 30 hours as compared to that typical for methane formation from the same substrate, namely, 10 to 20 days. The results show a thermophilic bacteria production rate 1.5 times higher than that of mesophilic ones, and it is at maximum 320 mol of hydrogen per ton of olive pulp.

Another study, Das and Veziroglu (2008), found a hydrogen yield of 7 mol H_2 per mol of glucose. The major challenge with aerobic digestion for hydrogen production is the reduced production rate per unit of capital investment in the facility. Remarkable energy conversion efficiency is observed at anaerobic digestion of molasses (which is a by-product of sugar processing), namely 28%. Based on the data compiled by Das and Veziroglu (2008) and Kalinci et al. (2009), the cost per unit of energy content in produced hydrogen via anaerobic digestion is compared with other technologies and with biophotolysis as shown in Fig. 13.42. In this comparison, for anaerobic digestion it has been assumed that the process is "biological water gas shift reaction." This process is a relatively new method for hydrogen production driven by bacteria that perform in anaerobic conditions, and in the absence of light the water gas shift reaction generates hydrogen. The production cost of hydrogen by this method, as reported by Kalinci et al. (2009), is about $24/GJ.

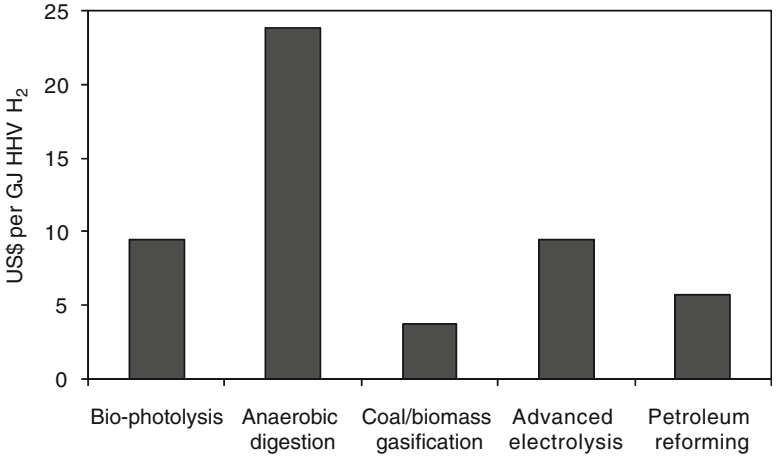

Fig. 13.42 Cost comparison between biochemical routes and some common methods of hydrogen production

13.4.6 Hybrid Methods for Hydrogen Production

All sorts of methods for hydrogen production can be combined in a complex system aiming to generate hydrogen more effectively. Section 13.4.3 described the electrothermal methods for hydrogen production. It is possible to combine electric, thermal, and photobiochemical methods for better productivity. At the same time, all kinds of primary energy sources (renewables, fossil, nuclear) and recovered energy can be used in various combinations to drive the processes.

Hydrogen can also be produced by combining renewable technologies, for example, photovoltaic and wind. These technologies are not competing with each other; rather, they are complementing and supporting each other. On the one hand, the wind technology can be beneficial for periods without sunshine, on the other hand, solar photovoltaic technology can compensate when there is no wind during the daytime. This symbiotic behavior of the two technologies ensures a better and continuous supply of electricity to the electrolyzer to produce hydrogen. The access power produced by the system can be stored in batteries and can be used in adverse conditions. Another example of coupling two technologies is solar thermal and geothermal.

The hot water from geothermal sources can further heated to the desirable temperature (approximately 550°C) by using solar concentrating collectors and then by using a high-temperature electrolyzer to produce hydrogen. One of the advantages of hybrid renewable technology assisted with fossil fuel and nuclear energy is that it ensures a continuous supply of input energy, which when using these technologies individually sometimes can be challenging. The performance of such hybrid systems can be better than the performance of systems that use the two technologies separately.

Illustrative Example: Hybrid Artificial Photosynthesis System

Here is an example of a hydrogen production method that combines photovoltaic electricity generation with electrolysis and artificial photosynthesis. Note that there are many other hybrid systems for hydrogen production; this example is only meant to illustrate the general idea. As a matter of fact, sustainable development requires not only that sustainable energy resources be used, but also that the resources should be used efficiently. Artificial photosynthesis is a concept that not only produces hydrogen (and food), but also improves the environment by removing carbon dioxide and adding oxygen to the environment. This concept is a replica of the photosynthesis of plants and algae. The two reactions involved in photosynthesis, as described before, are the light reaction and the dark reaction:

- *Light reaction*

Light energy is absorbed by special cell membranes and transferred to chlorophylls. Electrochemical reactions generate vital "energy-rich" biological compounds. Oxygen is produced as a by-product of this process and is released to the atmosphere. This is actually nature's own photovoltaic energy conversion system (photosystem), in which the trapped light energy is first converted into electrically stored energy in cell membranes. The light phase requires the cooperation of membrane-bound photochemical assemblies (also called photosystems). Each photosystem operates in series to photochemically "charge" the membrane.

- *Dark reaction*

The products of the light phase, that is, the energy-rich biological compounds, are used within cells for the formation of carbohydrate (sugars) from carbon dioxide, via a series of biochemical intermediates in the presence of some enzymes (catalysts). This process is central to the progressive chemical "assembly" of sugar molecules from carbon dioxide and water. This is the only point at which continued water consumption is absolutely required for carbohydrate formation, and it represents only a tiny fraction of the water supplied conventionally in plant growth. So, the overall reaction of natural photosynthesis, including the carbon fixation process, can be given as $CO_2 + H_2O + \text{Sunlight} = O_2 + \text{Carbohydrate}$.

Artificial photosynthesis is a means of achieving the aims of clean power generation and dry food production as shown in Fig. 13.43, which is a schematic diagram of artificial photosynthesis. The upper half shows the light reaction and the bottom half shows the dark reaction of the photosynthesis.

The main steps in the natural photosynthesis processes of plants and bacteria provide the models and inspiration for a totally biomimetic, industrial-scale technological approach to achieve the following specific goals:

- Electricity generation using photovoltaic systems. The power generated can directly be supplied to the national grid.
- "Dry agriculture," employing enzyme bed reactor systems to fix carbon dioxide from the air or other convenient sources, powered by hydrogen and bioelectric transducers drawing power from the national grid. These produce carbohydrates

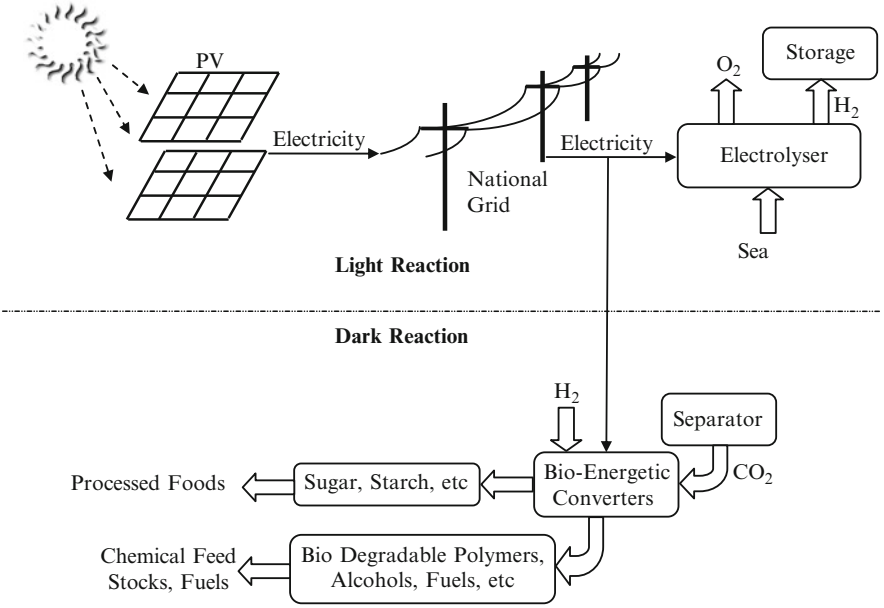

Fig. 13.43 Schematic of artificial photosynthesis concept [modified from Collings and Critchley (2005)]. *PV* photovoltaic cells

(food), liquid fuels, chemical feed stocks, and polymers for fiber production. Water usage is at or near the absolute chemical minimum and thousands of times lower than in conventional agriculture.

- Hydrogen production from seawater or other suitable water sources. Electrode systems employing catalytic surfaces modeled on the relevant high-efficiency active sites in photosynthetic organisms achieve the electrolytic decomposition of water (into hydrogen and oxygen).

The economical comparison between competing energy systems should be based on the effective costs of the services these fuels provide. The effective costs include the utilization energy, the cost of fuel, and the costs associated with fuel consumption that are not included in its price (so-called external costs). External costs include the costs of the physical damage done to humans, fauna, flora, and the environment due to harmful emissions, oil spills and leaks, and coal strip mining, as well as governmental expenditures for pollution abatement and expenditures for military protection of oil supplies. In economic considerations, it is also important to compare the future costs of hydrogen (which will be considerably lower than they are today because of the assumed market and technology development) with the future costs, both internal and external, of fossil fuels (which unavoidably will be higher than today's prices due to depletion, international conflicts, and environmental impact).

13.5 Hydrogen Storage

It is very difficult to store hydrogen in a satisfactorily dense phase so that the packed energy density is similar to that of common fuels used today for vehicles. Based on a higher heating value, 324 g of hydrogen have the same content as 1 kg of gasoline. The corresponding volume of 1 kg of gasoline is about 1.3 L; if 324 g of hydrogen is stored as gas under standard temperatures and pressure conditions, the occupied volume is 3,932 L. At the normal boiling point (20.3 K), under atmospheric pressure the density of the cryogenic liquid hydrogen is 70.77 kg/m^3; the volume of 324 g of liquid hydrogen is 4.6 L, which is 3.5 times larger than that of gasoline with the same energy content. Under the standard temperature (298.15 K) and 400 bar pressure, the hydrogen gas density is 25.98 kg/m^3 and the gas volume becomes 12.5 L or 9.6 times more than the gasoline volume with the same energy content. The following potential storage methods are considered for hydrogen:

- Compressed gas at standard temperature and very high pressure
- Cryogenic liquid at standard pressure and 20 K
- Physical binding of hydrogen molecule in a solid material matrix
- Chemical binding to synthesize a denser chemical that can later release hydrogen

For storage in any of these methods, hydrogen must be purified to an acceptable degree; for compressed storage 4-ppm impurities are acceptable, while for cryogenic storage 1 ppm is recommended.

For compressed storage, the current target is to develop commercial systems capable of storing hydrogen at 700 bar, at which 5 kg of hydrogen occupy 125 L. Such systems were built and tested for vehicles, but the common storage pressure used today is 300 bar. The adiabatic compression work can be easily calculated under the reasonable assumption of ideal gas behavior of hydrogen:

$$W|_{s=\mathrm{ct}} = \frac{\gamma}{\gamma - 1} RT_1 \left[\left(\frac{P_2}{P_1} \right)^{\frac{\gamma}{\gamma - 1}} - 1 \right], \tag{13.46}$$

where $\gamma = C_\mathrm{p}/C_\mathrm{v}$. The isentropic efficiency depends on the compression ratio; typical values are 70% to 80% for small compression ratios of the order of 3 to 4 and 50% to 60% for larger compression ratios of 100. For compressing hydrogen at 350 bar, the expected energy consumed is around 10 MJ/kg.

Liquefaction of hydrogen implies its cooling to a cryogenic temperature; this is a well-documented process, and there are mature technologies in industry for obtaining cryogenic hydrogen. But some problems occur in this process:

- It is not possible to obtain a refrigeration effect with hydrogen at a temperature over 190 K because of the "positive" Joule–Thomson coefficient of hydrogen; therefore, liquid nitrogen is used in the first stage of cooling to get hydrogen below 190 K.
- There are two configurations of the hydrogen molecule at ambient temperature: ortho- and para-hydrogen. At cryogenic conditions, all hydrogen converts to the

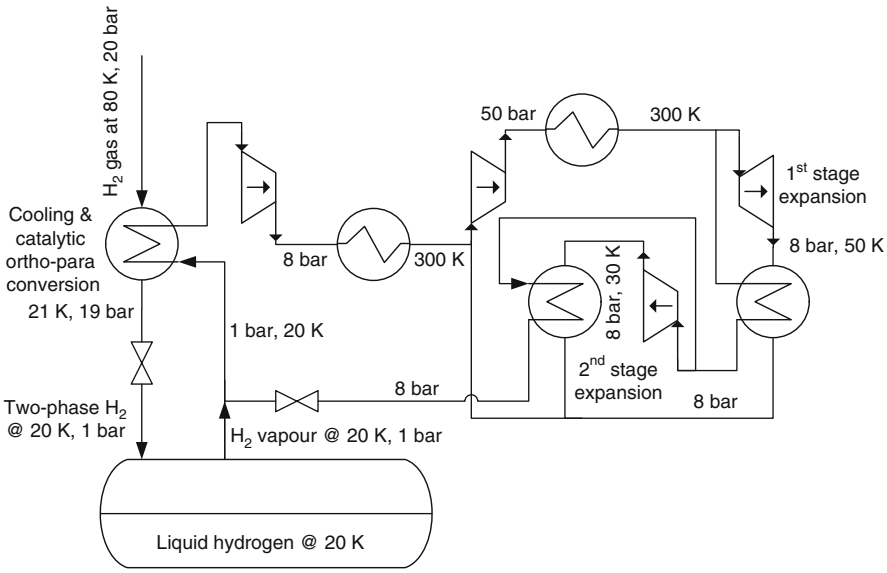

Fig. 13.44 Simplified diagram of the Claude hydrogen liquefaction process

para configuration. This process is slow, and for an acceptable rate of hydrogen production it must be accelerated by using catalysts. Catalysts (iron-oxide) are normally integrated in the heat exchanger that cools the hydrogen.

- The ortho-para conversion heat of 530 kJ/kg at 20 K adds to the latent heat of condensation, which is about 450 kJ/kg; therefore, an important amount of heat must be extracted at the proper rate in order to obtain liquid hydrogen.
- The evaporation heat of liquid hydrogen (para configuration) is rather low; therefore, the storage tank must be extremely well insulated.

Liquefaction of hydrogen requires expensive materials (e.g., chrome-based) that are suitable for very low temperatures; all the equipment must be placed in a vacuum box and must be thermally very well insulated. In the first stage, liquid nitrogen is used to cool hydrogen down to 80 K. Further cooling of hydrogen from 80 to 20 K is obtained by a special double-stage Brayton refrigeration cycle operating with hydrogen gas. This cycle recycles the hydrogen evaporated from the cryogenic tank; it is drawn, in a simplified way, in Fig. 13.44. After compression to about 20 bar, hydrogen is cooled, down to 80 K. This cooling (not shown in the figure) is done in three stages: cooling with water to 300 K, cooling with a vapor compression refrigeration plant down to ~250 K, and cooling with liquid nitrogen down to 80 K. With further cooling with a cryogenic cooler, the main stream temperature is decreased to 21 K; the throttling process generates colder two-phase liquid–vapor hydrogen introduced in the cryogenic hydrogen tank.

Above the liquid level, hydrogen vapors are always generated because of heat penetrations. They are extracted from the tank at 20 K and 1 bar and used for cooling the main stream of hydrogen down to 21 K; further, the vapor is compressed

in two stages with intercooling, in the first stage, from 1 bar to about 8 bar, and in the second stage from 8 to 50 bar. A part of the compressed hydrogen is expanded to intermediate pressure (8 bar) and reaches 50 K.

The cold stream at 50 K is used to cool the remaining stream prior to the second stage of expansion; before the second stage of expansion, the flow is divided into two streams. Note that the second stage of expansion occurs also from 50 to 8 bar, with the difference being that the flow is much colder prior to expansion. Consequently, the temperature at the end of the second stage of expansion reaches around 30 K. The remaining stream is cooled further down to a little above 30 K prior to the final expansion process that occurs in a throttling valve, after which the temperature of the hydrogen stream reaches 30 K.

Cryogenic hydrogen is normally stored in double-wall stainless steel vessels with vacuum between the walls. The typical evaporation losses due to heat penetration with current storage tank technology vary between 0.3% and 5% per day. The energy associated with the liquefaction process is estimated to be an average of 50 MJ/kg of hydrogen, which adds substantially to the hydrogen cost. It is, therefore, important to reduce the greenhouse gas emissions associated with hydrogen liquefaction. This can be done by using renewable energies to drive the liquefaction process. Kanoglu et al. (2007) studied the ways of using geothermal energy for hydrogen liquefaction. They suggested that the best way of doing this is by using one part of the geothermal energy to drive an absorption cycle that precools the hydrogen gas, and another part of the geothermal energy to generate electricity that drives the liquefaction plant.

There are two processes that can be applied for storing hydrogen in a solid matrix: physisorption (absorption of molecular hydrogen by a solid structure) and chemisorption (dissociation of the hydrogen molecule and bonding of the protons with the metal lattice). Many metal-hydride–based methods were developed for both physisorption and chemisorption of hydrogen. In general, they require some thermal energy at the discharging phase, and some cooling should be applied to enhance the efficiency of the hydrogen charging process.

Some chemical elements such as sodium, lithium, magnesium, and boron can create hydrides (called "chemical hydrides") that store hydrogen more densely than is possible in metal hydrides via physisorption and chemisorption. Decomposition of chemical hydrides is irreversible. Therefore, sophisticated processes must be put in place to recycle the chemical compounds after the hydrogen is released. Two processes are possible for hydrogen evolution from chemical hydrides, namely, thermal decomposition and hydrolysis. Examples of simple chemical hydrides are NaH, LiH, CaH_2, MgH_2, and various boron hydrides with the general formula MBH_4, where M represents a metal from the series Na, K, and Li. A general representation of chemical hydride hydrolysis is $MH_n + nH_2O \rightarrow nH_2 + M(OH)_n$. During hydrolysis, the chemical hydrides release heat. An example, is the hydrolysis of sodium borohydride, which occurs as follows:

$$NaBH_4 + 2H_2O \rightarrow NaBO_2 + 3H_2, \tag{13.47}$$

and which releases heat of 67 kJ/mol of hydrogen. Note that sodium borohydride is nonflammable and nonexplosive and allows hydrogen generation as in Eq. (13.47) at about 80°C over ruthenium or platinum catalysts.

Ay et al. (2006) investigated hydrogen release from sodium boron hydride, which is produced from sodium tetraborate ($Na_2B_4O_7$), which is decomposed at 400° to 500°C under hydrogen atmosphere, endothermically. They found that the release of hydrogen from the formed sodium borohydride can occur under atmospheric pressure and temperature in the range of 25° to 40°C. The reaction of sodium borohydride synthesis, according to Ay et al. (2006), is as follows

$$Na_2B_4O_7(s) + 16Na(s) + 7SiO_2(s) + 8H_2 \rightarrow 4NaBH_4(s) + 7NaSiO_3(s). \quad (13.48)$$

Note that sodium tetraborate (known also as borax) is naturally found as a mineral; the largest borax reserves are in Turkey; other countries having significant borax reserves are the United States, Chile, China, and Romania.

One interesting possibility for storing hydrogen in solid form is to first produce ammonia from it, and then absorb the ammonia gas in metal amines. This solution has been investigated by Sørensen et al. (2008), who found that up to six molecules of ammonia can be bound weakly by magnesium chloride to form $Mg(NH_3)_6Cl_2$, which embeds 109 g/L of hydrogen and 92 g/kg of magnesium ammine; recall that liquid hydrogen density is 71 g/L. The release of ammonia can be obtained by thermal desorption, and the process is reversible; that is, by applying proper cooling, ammonia is absorbed back in the form of ammine.

To completely release the ammonia according to the formula $Mg(NH_3)_6Cl_2 \rightarrow 6NH_3 + MgCl_2$, the associated desorption heat needed is 218 kJ/mol; further, 1 mol of ammonia generates 1.5 mol of hydrogen according to the decomposition reaction $NH_3 \rightarrow 1.5H_2 + 0.5N_2$, which needs at least 68 kJ/mol of ammonia; thus, in order to release 1 mol of hydrogen from the metal amine, the thermal energy must be higher than 191 kJ. This energy can be provided by a heat recovery process or by solar energy (if applicable) or by combustion of the released hydrogen itself. In the last case, accounting for the higher molar heating value of hydrogen of 284 kJ/mol, the remaining energy after the hydrogen that is extracted from the ammine is 93 kJ/mol of hydrogen, a value that reflects the price of generating hydrogen from salt. Nevertheless, metal amines are an attractive solution for hydrogen storage, but one must account for the diminishing of the calorific value due to hydrogen extraction, or alternatively, this method of storage should be applied where some combustion heat can be recovered to drive the ammonia cracking reaction itself.

Hydrogen storage in the form of ammonia has been recognized as an attractive possibility. In this solution, hydrogen can be converted to ammonia by the well-established Haber–Bosch process. The advantages of ammonia as a hydrogen source and storage medium are analyzed in Chapter 7. Storing hydrogen chemically in the form of urea is also an attractive solution, as urea is very stable, can be stored for a very long time, and can be safely transported. Urea is a particulate material delivered in small-size prills. It can be combusted as it has a low calorific value comparable to that of wood, that is, about 10 MJ/kg. The average price of urea is $0.30 per kg.

Urea can be synthesized from biomass or other renewable energy sources so that the result can be a CO_2-free fuel. Urea, with the chemical formula $CO(NH_2)_2$, is extensively produced in industry and is used as fertilizer. It is considered a nontoxic substance, and several car manufacturers use it in their passenger vehicles for NO_x exhaust reduction. Currently, urea is synthesized from natural gas or petroleum and is then reformed to produce hydrogen. The hydrogen, therefore, is combined with nitrogen (taken from air) to obtain ammonia, which is eventually combined with CO_2 to produce urea. It is simple to produce urea starting only from biomass sources. Another path to synthesize urea is via hydrogen production from renewable sources (e.g., water electrolysis, thermochemical or photocatalytic water splitting, etc.). The hydrogen is then combined with nitrogen to generate ammonia and with CO_2 to produce urea.

Carbon dioxide can be recovered from cement factories or power plants, taken from biomass combustion, or extracted from atmospheric air. In any of these cases, the produced urea is either a zero carbon or low carbon hydrogen source. To extract hydrogen from urea is relatively straightforward as discussed in the next illustrative example. A case study demonstrating the benefits of gasoline–urea or diesel–urea co-fueling is demonstrated in Chapter 6.

Ammonia-based compounds, as shown in the above example of urea, have a good capability of hydrogen storage and release. One of the most promising ammonia-based storage methods is ammonia borane with the chemical formula NH_3BH_3, which contains 120 g of hydrogen per liter in a weight concentration of 19% (Karkamkar et al. 2007). Ammonia borane releases hydrogen by thermal cracking according to the following reaction evolving at successively higher temperatures:

$$\left.\begin{aligned} 2NH_3BH_3 &\xrightarrow{<120^\circ} C(NH_2BH_2)_2 + 2H_2 \\ (NH_2BH_2)_2 &\xrightarrow{\sim 150^\circ} C(NHBH)_2 + 2H_2 \\ (NHBH)_2 &\xrightarrow{>500^\circ} CBN + 2H_2 \end{aligned}\right\}. \tag{13.49}$$

Therefore, one molecule of ammonia borane can release three molecules of hydrogen if heated at over 500°C. An interesting factor is that ammonia borane can release hydrogen at temperatures lower than 120°C; if properly conducted, the decomposition reaction can release hydrogen even at room temperature. Releasing hydrogen at a low temperature is a crucial characteristic for storage systems used for the cold start-up of engines.

Figure 13.45 presents the hydrogen storage density that is possible with various technologies. The storage density is presented in two different ways. On the horizontal axis, it is the volumetric storage density in kg of hydrogen per unit of volume of storage facility. On the vertical axis, the energy embedded in the quantity of hydrogen that can be released by the storage is presented; this amount is given per unit of mass (kg) of the storage facility (tank). The ammonia-boron compound with the chemical formula NH_4BH_4 appears to be the densest hydrogen storage.

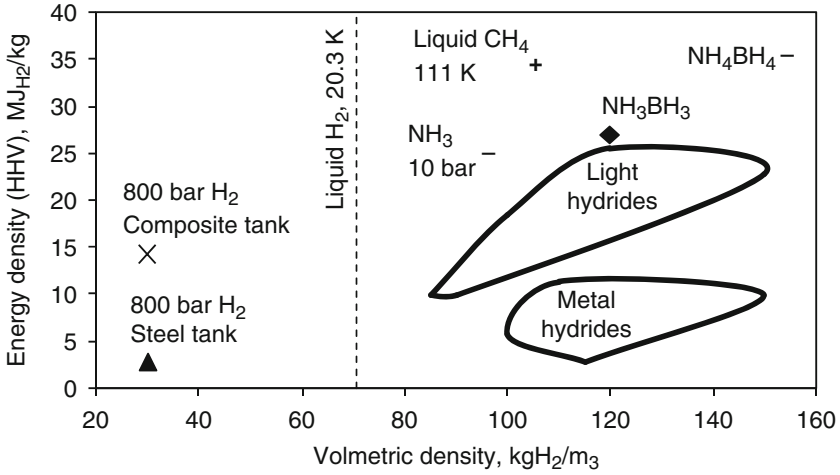

Fig. 13.45 Density of hydrogen storage with various technologies [data from Kanoglu et al. (2007), Ay et al. (2006), Sørensen et al. (2008), Karkamkar et al. (2007)]

13.6 Hydrogen Transportation and Distribution

It is interesting to estimate the total cost of hydrogen, including its production, distribution, and storage. Depending on the production method, the hydrogen costs vary from $1/kg at coal gasification to $9.50/kg using solar energy for electricity generation that in turn is used for water electrolysis (see also Zamfirescu and Dincer 2009b). After production, hydrogen is stored at the manufacturer's location for a certain period prior to delivery. Liquefaction adds at least 30% to the hydrogen price per kg, and on top of that one must add the energy consumed to keep the storage tank at cryogenic temperatures during the storage time.

The minimum cost penalty for hydrogen storage (when hydrogen is stored for 1–3 days) is CN$0.30/kg for compressed H_2 and CN$0.70/kg for liquefied H_2. Hydrogen distribution to the consumption points is also expensive. If one assumes, for example, that the hydrogen transport is made in pressurized containers at 345 bar, the transported energy content is 8 GJ/m_3, that is, a four times smaller amount than for gasoline (32 GJ/m^3). The high explosion risk of hydrogen raises the price even more because of the required safety measures. Due to these factors, the estimated minimum cost of hydrogen distribution is ~$1/kg H_2. Thus, if one considers the production, storage, and distribution costs, the minimum expected hydrogen price at delivery point should be ~CN$2.50/kg if produced from coal, and ~CN$11/kg if produced from solar energy-driven water electrolysis. Chapter 7 showed that the storage and distribution of hydrogen in the form of ammonia is more advantageous than its storage and distribution as cryogenic or compressed gas.

13.7 Hydrogen Utilization

Hydrogen is a basic chemical that is used in many industrial processes in the chemical industry, glass production, oil refining, and metallurgical processes. The projected hydrogen economy is based on hydrogen use as fuel and energy carrier medium. In industry, the use of hydrogen is mostly as a reactant, for ammonia production, methanol production, and petroleum processing. In the electronics industry, hydrogen is used for silicon tetrachloride reduction to silicon, which is needed for semiconductor processing. In the metallurgical industry, hydrogen is used to remove oxygen in annealing, sintering, and furnace brazing. In nuclear power reactors, water dissociates under neutron flux, and hydrogen is used to scavenge the oxygen and impede the possible corrosion that it can produce. The aerospace industry makes significant use of hydrogen as fuel; liquid hydrogen and liquid oxygen propel most rockets. Very promising applications of hydrogen are the fuel cells that can produce clean electricity, without greenhouse gas (GHG) emission at the utilization side. Moreover, hydrogen is proposed as a fuel for internal combustion engines for improved efficiency and to lower the emissions.

Forty million tons of hydrogen are produced worldwide per year for refinery and industrial uses. In Canada, a country highly engaged in hydrogen economy development, hydrogen is utilized in large quantities as a feedstock for various chemical processes in industries and refineries. According to the Canadian Hydrogen Association (CHA), Canada produces more than 3 Mton of hydrogen per annum (CHA 2010). In the past, hydrogen was used in Canada for four main purposes: oil refining, ammonia production, methanol production, and process gas in the metallurgical sector. Presently, there is significant use of hydrogen in Canada for upgrading heavy oil from the oil sand sites of Alberta. Based on statistical data compiled by Taylor (1983) and the CHA (2010), the present, past, and predicted future hydrogen utilization in Canada is shown in Fig. 13.46. In the past, the oil refining sector and ammonia production accounted for 40% of Canadian hydrogen utilization. At present, it is observed that the sectors of oil refining and heavy oil upgrading increased their share of utilization to 46%. It is predicted that by 2025 their share will reach 62%.

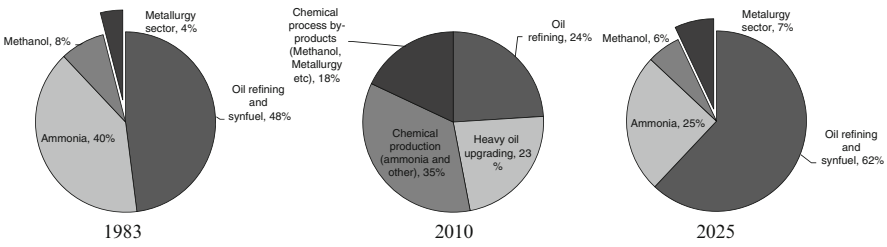

Fig. 13.46 Evolution of hydrogen utilization in Canada [data from Taylor (1983) and CHA (2010)]

Hydrogen utilization for ammonia production decreased in Canada by 5% in 20 years, and it is predicted to decrease by another 10% in the next 15 years. It appears that by 2025 methanol production will consume 6% of produced hydrogen, while 7% of hydrogen will be used in metallurgy.

13.8 Fuel Cells

A fuel cell is a device that conducts the electrochemical reaction between hydrogen and oxygen to produce water and generate electricity. Fuels other than hydrogen can also be used in some special configurations. The primary application of such devices is in sustainable power generation. The basic structure of a fuel cell is represented in Fig. 13.47. It comprises an electrolytic bath and two electrodes. Fuel cells were developed starting in 1838–1839 with phosphoric acid as the electrolyte, and continued in the second half of the nineteenth century. In the twentieth century, various research programs led by the National Aeronautics and Space Administration (NASA) and other spatial agencies further developed fuel cells. Several kinds of fuel cells are available today with both liquid and solid electrolytes.

Hydrogen is fed at the anode of the fuel cell, where it enters in contact with a porous media electrode that is permeable to protons and has a positive charge. Because of the positive charge of the electrode, the valence electrons of the hydrogen molecule are dislocated, and thus the molecule breaks apart, forming two protons, according to the following anodic reaction:

$$H_2(g) \rightarrow 2H^+(aq) + 2e^-. \tag{13.50}$$

The electrode is continuously depleted from electrons by an external circuit that establishes a current of electrons through the electrical load. Since the electrons flow from the anode to the cathode as shown in Fig. 13.47, for the exterior circuit the anode

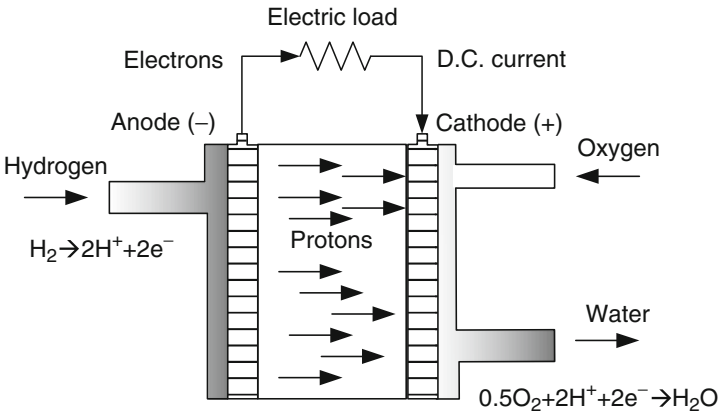

Fig. 13.47 Schematic illustration of the basic fuel cell principle

appears to be the negative electrode, and the cathode is the positive one. The protons that traverse the porous anode are submerged in an electrolytic solution subjected to a coulomb electric field that drives them from the anode to the cathode. The protons permeate through the cathode, which being at a positive charge allows for the more complex reaction of water formation. During this process, the oxygen molecule that is fed through the oxidant stream at the cathode side (see Fig. 13.47) receives additional electrons that interfere with its valence electrons; consequently, the oxygen molecule is split apart and each of the resulting ions becomes able to react with two protons and form two water molecules; the cathodic reaction can be written as follows:

$$2H^{+}(aq) + 0.5O_2 + 2e^{-} \rightarrow H_2O. \tag{13.51}$$

The above reaction generates energy in the form of heat and electricity. Both these forms of energy are very important commodities for humankind. Conducting the water formation reaction in a fuel cell presents some advantages with respect to direct combustion, namely:

- One can cogenerate electricity and heat more easily.
- The temperature level of the cogenerated heat can be adjusted to correspond to the fuel cell and the application.
- The reaction products are much cleaner than in the case of combustion (no or extremely little NO_x is formed).
- The process is flameless and in general considered safer than combustion.

Several kinds of fuel cell have been developed, from which at least two—proton exchange membrane and SOFCs—have achieved technological maturity. Most of the commercially available fuel cells operate with hydrogen as the fuel. However, due to the fact that the hydrogen's density is extremely low, the fuel cell vehicle technology faces a difficult technical problem, namely, to accommodate a large fuel tank while keeping enough free/useful space onboard. As a consequence, fuel cell vehicle makers are struggled to reduce the size of the fuel cell system while maximizing its power generation capacity. As already mentioned above, it is also possible to use fuels other than hydrogen. This can be done either through specialized fuel cells, or by reforming, directly or indirectly, various fuels to hydrogen.

13.9 Fuel Cell Types and Classification

The main types of fuel cells are classified as in Fig. 13.48, and they comprise three main categories based on the level of the operating temperature: low-, intermediate-, and high-temperature fuel cells. The chemical reactions and electrolyte type are explained for each type of fuel cell in Fig. 13.48. Another way to categorize the fuel cell is by the nature of ions that transverse the electrolyte. There are two possibilities: either protons (H^{+}) or oxygen ions (O^{2-}) migrate from one electrode to the other. If protons migrate, then the water formation reaction occurs

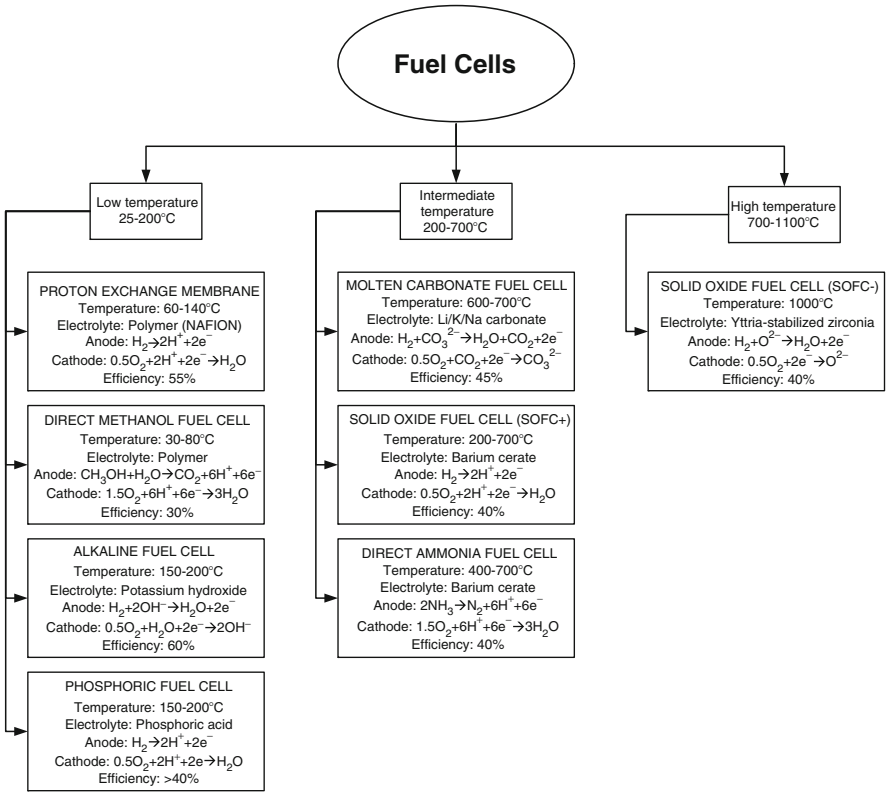

Fig. 13.48 Classification of fuel cells according to their operating temperature

at the cathode side. Conversely, if the oxygen ions transverse the electrolyte solution, this implies that the water molecule forms at the anode. Looking at the fuel cell types in Fig. 13.48, we see that PEM, direct methanol, and SOFC+ systems have proton conducting electrolytes; also, alkaline, molten carbonate, and SOFC− systems have oxygen ions permeating electrolytes.

The photon exchange membrane (PEM) fuel cell is the most frequently used low-capacity and vehicular power generation system. It has a solid polymer membrane electrolyte from a material known as NAFION. A PEM-based system includes several auxiliary pieces of equipment: an air compressor, heat exchangers, and a rather large and complicated water management subsystem. Note that the NAFION membrane must be continuously humidified with water in order to keep its proton conducting property. Even though PEM systems have a relatively compact stack, they are rather voluminous, and on top of this, their cost is high because they include expensive metal catalysts (platinum) at the electrodes, and their lifetime is relatively short.

Solid-oxide fuels cells (SOFCs) with oxygen ions conducting electrolytes (denoted SOFC− or SOFC-O^{2-}) are characterized by stacks of relatively large

size and operate at a very high temperature. Their electrolyte is a solid layer of Yttria-Stabilized Zirconia (YSZ). They may feature a less voluminous and more cost-effective overall system than PEM systems. This fact is due to their high operating temperature, which leads to some important advantages: (a) they are inexpensive and have a long lifetime because no noble metal catalysts are needed for the electrodes, (b) internal reforming of alternative fuels (e.g., methane, syngas, methanol, ammonia) to hydrogen is facilitated so that SOFCs can use a smaller fuel tank, (c) the exhaust gases possess high exergy that can be converted into additional power and low-temperature heating.

One major drawback of SOFC− systems that probably impededs their expansion on low capacity and vehicular applications is represented by their rather long start-up time. It has been suggested that this drawback can be solved by using an SOFC-PEM combination. During start-up, the electricity of an SOFC-PEM system is generated only by the PEM, which has a reasonably short start-up time. At steady operation, when both cells operate, the heat generated by the SOFC is used for reforming the fuel to be delivered downstream to the PEM.

However, as has already been demonstrated, the design of such a system entails a large number of auxiliary components and thus is rather costly, has a short lifetime, and requires a voluminous amount of solution with respect to the generated power. As mentioned above, in SOFC−systems the oxygen ions (O^{2-}) traverse the electrolyte from cathode to anode, where they react with the supplied hydrogen to produce steam and release the reaction heat. During this process, at the anode, the hydrogen is consumed and the steam is generated, and thus the hydrogen's partial pressure decreases.

As a consequence of the low partial pressure of hydrogen, the reaction kinetics are degraded and the only solution to compensate for this effect is to supply hydrogen in excess. The excess hydrogen then must be consumed. This can be done in multiple ways. One common method is to combust the excess hydrogen in an afterburner, and the released heat is recovered or converted into work by a gas turbine. Thus, certain amounts of NO_x are formed during the combustion of hydrogen with air.

Recent advances in SOFC technology have led to the development of intermediate-temperature proton-conducting membranes. These are electrolytic membranes based on oxides of a metal such as barium. Therefore, these fuel cells are solid oxide. The proton-conducting solid oxide membranes have the important advantage of letting the protons migrate from anode to cathode. As a consequence, the water formation reaction occurs at the cathode. This type of fuel cell is known as a proton-conducting SOFC, commonly denoted as SOFC+ (or SOFC-H^+) to distinguish it from the traditional ion-conducting SOFC.

Complete hydrogen utilization is therefore possible (in principle) in SOFC+ systems with direct implication in increasing the system's simplicity and compactness by eliminating the need for the afterburner. Moreover, because all the hydrogen is reacted electrochemically at the fuel cell cathode, practically no NO_x is formed, and thus the fuel cell emission consists only of steam and nitrogen; thus, it is clean. The SOFC-H^+ technology has the potential to replace or complement PEM-FC systems in vehicular applications because it will be inexpensive and

compact, with high power generated per unit of volume, and it may operate at intermediate temperature (e.g., even 300°C), a fact that makes it possible to achieve an acceptable start-up time.

At present, certain efforts are being devoted worldwide to developing proton-conducting membranes. In this respect, barium cerate ($BaCeO_3$)-based materials are identified as excellent solid oxide electrolytes because of their high proton-conducting capability over a wide range of temperatures (300–1,000°C). By letting the protons diffuse through the electrolyte and letting the water-formation reaction occur at the cathode, the electromotive force and conversion efficiency of the fuel cell is significantly increased with respect to the SOFC system.

It is speculated that the governing mechanism of proton conduction is based on the hopping of protons between adjacent oxygen ions that are bound to the atomic structure of the solid oxide electrolytic membrane. The protons, being extremely small, necessitate reduced activation energy as compared to the case of oxygen ion transport through the most advanced SOFC—membranes such as those based on YSZ or doped ceria systems.

Moreover, the electronic conduction of barium cerate materials is much lower than that of doped ceria under operating conditions, and this explains the superior electromotive force, power output, and efficiency obtained with the SOFC+ systems. It also has been shown that proton conduction is enhanced at lower temperatures, such as 300°C. The main problem with barium cerate is the difficulty to sinter it in the form of a solid membrane. One option appears to be doping the barium cerate with samarium (Sm), which allows for sintering thin membranes with a thickness as low as 50 μm and high-power densities in the range of 1,300 to 3,400 W/m^2.

Phosphoric acid fuel cells uses platinum-coated porous carbon electrodes and a phosphoric acid electrolyte in the liquid state and kept in a silicon-carbide matrix. The efficiency of this kind of fuel cell is around 40%. The level of temperature required to produce steam is high, and so the fuel cell can be used for cogeneration purposes. As compared with PEM-FC, the phosphoric acid fuel cell is more voluminous for the same generated power.

The alkaline fuel cell potentially can reach an efficiency close to 70%. The electrolyte is an aqueous alkaline solution of potassium hydroxide (KOH) that is embedded in a porous matrix. If air is supplied as the oxidant, the small concentration of carbon dioxide in the intake air is large enough to convert some of the electrolyte (KOH) to potassium carbonate (K_2CO_3). In order to lengthen the electrolyte life, air is purified from CO_2 with various techniques such as scrubbers or other techniques of carbon dioxide removal (see Chapter 14). In some designs, the liquid electrolyte is replaceable so that after a period of operation, when the fuel cell is gradually poisoned, it can be renewed.

Molten carbonate fuel cells (MCFCs) operate at the upper limit of the intermediate temperature defined in Fig. 14.48 for fuel cells (around 650°C), and it can use fuels other than hydrogen. The fuels are reformed internally to hydrogen using

the high-temperature heat ejected by the cell. The reformation process occurs at the anode. These cells are very efficient, reaching a fuel-to-electricity energy efficiency of around 60%. The MCFCs can be coupled with other thermodynamic cycles that can convert the high enthalpy of steam and nonreacted fuel and carbon dioxide to additional power. Moreover, the MCFCs can be used in cogeneration systems, in which the fuel utilization efficiency can go over 85%. The electrodes do not need to be coated with expensive catalysts; simple carbon-based, inexpensive electrodes operate very well at the high temperature specific to these cells. The electrolyte is a carbonate (e.g., of lithium or potassium) that is suspended in an alumina-based porous matrix. The durability of the fuel cell is low because the electrolyte is highly corrosive.

The direct methanol fuel cell is a low-temperature, proton-conducting, polymer-based membrane fuel cell that is fueled directly with methanol diluted in water at its anode. The methanol is supplied in a proportion of 1:1 molar for the stoichiometric reaction. Direct methanol fuel cells are used for supplying low-power electronics since they are compact and store energy at high density; however, the rate of energy discharge (that is, the power density) is rather low.

Direct ammonia fuel cells have been recently developed as a variant of SOFC+ using ammonia as the fuel, as reviewed in Zamfirescu and Dincer (2009b,c). The high operating temperature of SOFC+ allows for ammonia decomposition at the anode, releasing hydrogen. The protons are formed at the anode and migrate through the solid electrolyte toward the cathode, where the water formation reaction occurs. The reaction products are nitrogen gas and steam. In general the hydrogen utilization is very high, as this characteristic is typical of SOFC+ systems. The energy efficiency of the duel cell stack may reach 55%.

Fuel cells can also be classified according to other criteria:

- Cell and stack design
  - Planar (flat-planar, radial-planar)
  - Tubular (microtubular, tubular)
  - Segmented-in-series (or integrated-planar)
  - Monolithic design
- Type of support
  - Self-supporting (anode-supported, cathode-supported, electrolyte-supported)
  - External-supporting (interconnect-supported, porous substrate supported)
- Flow configuration
  - Co-flow
  - Cross-flow
  - Counter-flow
- Fuel reforming type
  - External reforming
  - Direct internal reforming
  - Indirect internal reforming

13.10 Fuel Cell Systems and Applications

Fuel cells have many applications, notably in stationary, mobile, automotive, backup, auxiliary, and portable power generation, transportation technologies, specialty vehicles, small and large distributed generation, district power and heating, various military and space applications, and systems for pure oxygen production. Fuel cell applications can be roughly classified into four categories: power generation; transportation; specialty applications (military, aerospace, medical); and multigeneration applications (Fig. 13.49). In multigeneration applications, the fuel cell system generates multiproducts like power, heating, oxygen, and water.

When used for any application, a fuel cell stack must operate within a more complex system that has the function of supplying fuel and oxidant at appropriate pressure and temperature, recovering heat and work internally (when possible), and expelling heat, water, and reaction products. In many cases, the fuel cell stack must be insulated and maintained at an optimum operating temperature. Also, the balance of the plant has the role of ensuring the start-up and shut-down operations and regulating the system to operate at partial load and full load. In what follows, we present some typical fuel cell systems, including the fuel cell stack and the balance of the plant.

A typical PEM fuel cell power plant (including the fuel cell stack and the balance of the plant) is presented in Fig. 13.50. The diagram comprises a hydrogen tank,

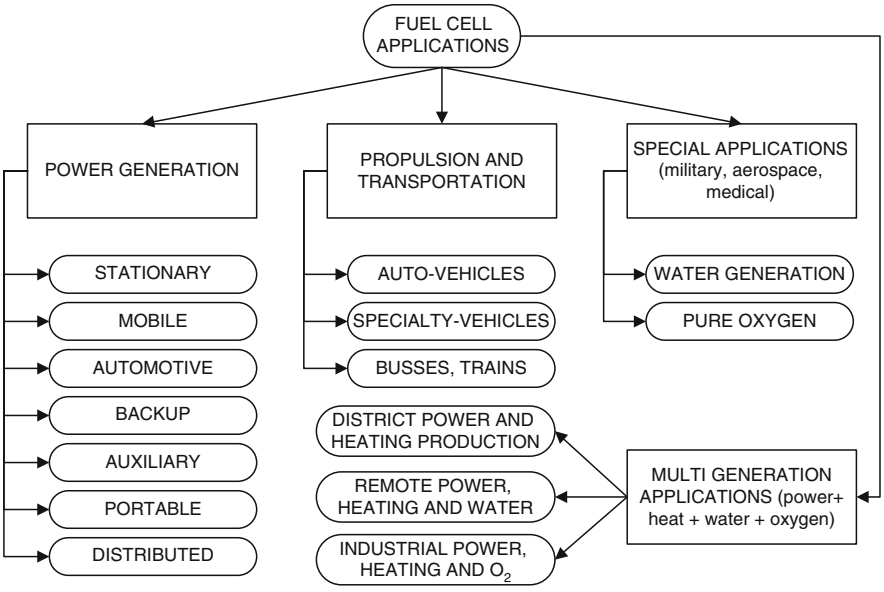

Fig. 13.49 Classification of fuel cell applications

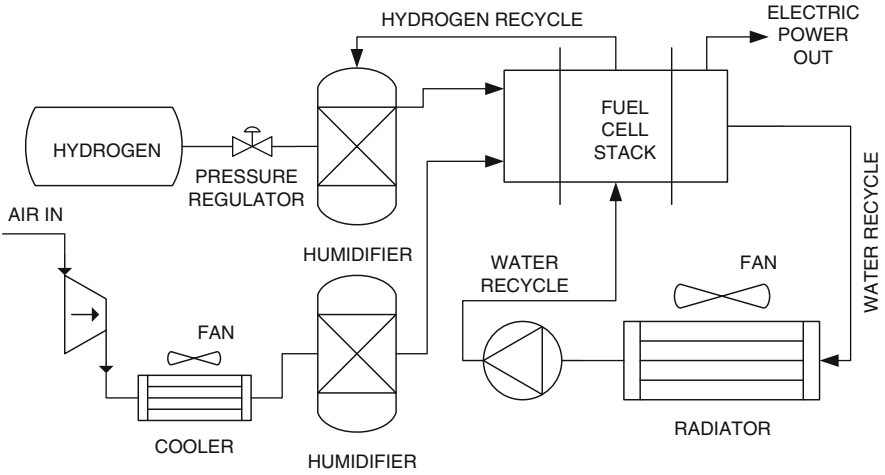

Fig. 13.50 Simplified diagram of a PEM fuel cell power plant

pressure regulator, humidifiers, fuel cell stack, radiator, cooler, air compressor, and water recycle pump.

Both the hydrogen gas and oxygen gas must be humidified before entering the fuel cell stack because the NAFION membrane works only under humid conditions. The system normally operates at temperatures under 100°C and pressures slightly above the atmosphere. In these conditions, the formed water is in a liquid state. The system continuously generates water when it runs. A part of the water is maintained in the system for hydration purpose. The other part can be expelled (e.g., by spraying it out) or stored. However, storing water may raise problems when the system is applied to an auto-vehicle. The most important feature of the PEM-FC power plant is its fast start-up. Some electric power must be stored in a common accumulator battery as is needed for running the air compressor and the pump at start-up.

Figure 13.51 shows an SOFC+-based system for power generation, which comprises the SOFC+ stack, a turbocharger, four compact heat exchangers, a hydrogen fuel tank, and a pressure regulating device. Hydrogen is provided at state point 11 of the diagram. After the pressure regulator, the hydrogen supplies the power generation system at point 12, and then is preheated in two steps through points 12–13 and 13–14.

Air taken from the surroundings at point 1 is compressed in the turbocharger, delivered to the air-preheater at point 2, and then to the fuel cell stack at point 3. The exhaust of the fuel cell, consisting of oxygen-depleted air and steam, is directed toward the turbine inlet at point 4 and expanded with work recovery up to state point 5. The hot exhaust at point 5 is used to preheat the two reactants: air (point 7–8) and hydrogen (points 6–8 and 8–9), and then either released to the ambient air or used for heat recovery in an additional heat exchanger (point 9–10).

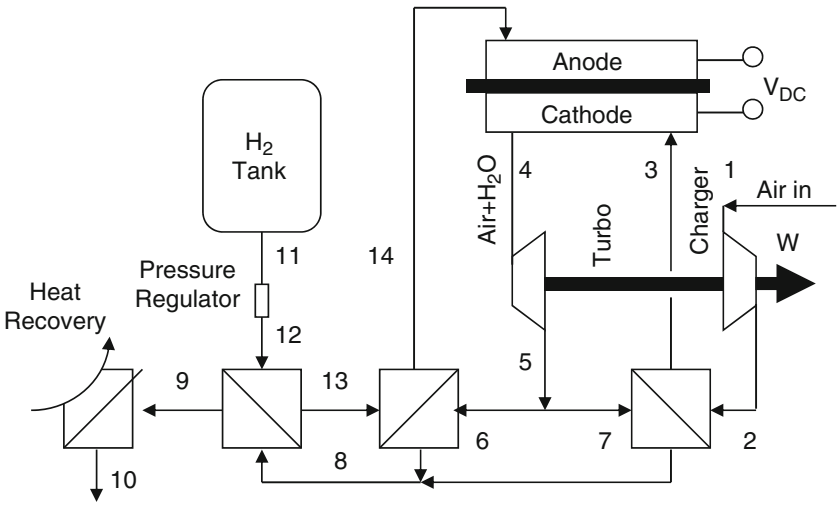

Fig. 13.51 Fuel cell power plant based on proton conducting SOFC+ technology [modified from Zamfirescu and Dincer (2009c)]

The conceptual design is made so that the two reacting streams, prior to being supplied to the fuel cell stack, are preheated to the same temperature in an equal number of two steps. In fact, the air temperature at point 2 is the same as the hydrogen temperature at point 13, and the air temperature at point 3 is the same as the hydrogen temperature at point 14.

Fuel cells that operate at a higher temperature—like molten carbonate and SOFCs—in general must be coupled with gas turbines in order to achieve satisfactory fuel utilization. Moreover, high-temperature heat is commonly recovered from the reaction product of these kinds of fuel cells and used for reforming of some high-density fuels such as compressed natural gas, alcohols, and others, to hydrogen. An example is given in Fig. 13.52, consisting of an MCFC with reformed natural gas. This is a simplified diagram of a system installed recently by the natural gas provider Embridge Inc. in Toronto, Ontario. The system is connected to the high-pressure natural gas network at point 1.

The high-pressure gas is first preheated (point 1–2) and then expanded to generate about 1 MW electric power from a 6,000 m^3/h gas flow rate. After expansion, a part of the low-pressure gas is sent to the distribution network to be used for water/space heating in residences. The other part (point 5) is mixed with water (point 6), preheated (point 7–8) and reformed (point 8–9) and supplied to the MCFC (point 10). The resulting uncombusted anodic gases are further combusted with additional air (point 16) in a catalytic burner (point 11–12) that delivers its produced heat to the reformation process. The CO_2-rich combustion gases (point 12) are mixed with air (point 15) and fueled to the MCFC cathode (point 17). The heat carried by the cathode gas is recovered (point 18–19) and used to preheat the high-pressure fuel. Fresh ambient air is used for combustion and fuel cell

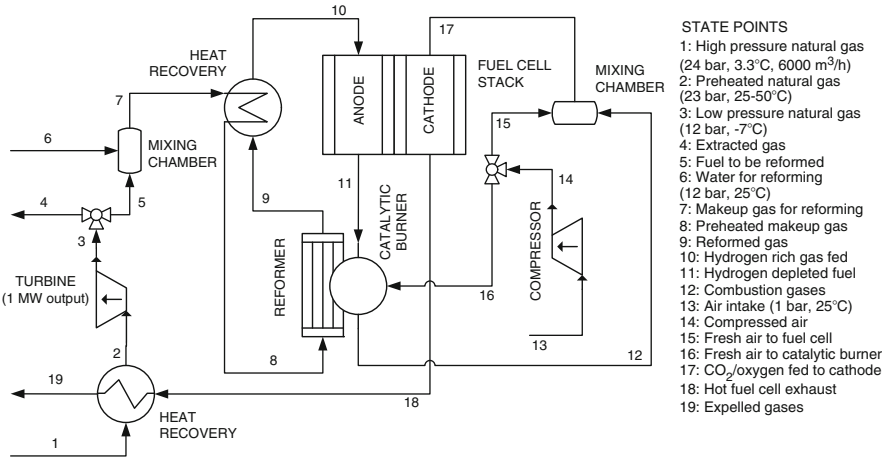

Fig. 13.52 Natural gas fueled system with molten carbonate fuel cell

processing as it is compressed first (point 13–14) and then split (point 15+16). The energy (η) and exergy (ψ) efficiencies of this system, as calculated by Rashidi et al. (2009), are 60% and 50%, respectively. The efficiencies are defined as:

$$\left.\begin{aligned}\eta &= \frac{W_{\mathrm{FC}} + W_{\mathrm{T}} - W_{\mathrm{C}}}{\mathrm{LHV}} \\ \psi &= \frac{W_{\mathrm{FC}} + W_{\mathrm{T}} - W_{\mathrm{C}}}{ex_1^{\mathrm{ch}} + ex_1^{\mathrm{thm}} + n_6 ex_6^{\mathrm{thm}}}\end{aligned}\right\}, \tag{13.52}$$

where W represent the work per mol of fuel consumed, indices FC, T, and C mean fuel cell, turbine and compressor, respectively, indices 1 and 6 represent the respective state points indicated in Fig. 13.52, ex is molar exergy, the exponents "ch" and "thm" mean chemical and thermomechanical, respectively, and n_6 is the number of mols of water mixed with 1 mol of fuel.

The SOFC systems have the great advantage of operating at very high temperature, which facilitates steam-assisted reforming of the primary fuel to hydrogen, without the need for expensive catalysts. It was explained above that owing to hydrogen consumption in the anode, its partial pressure decreases, which affects negatively the chemical equilibrium and reaction rate. Thus, hydrogen is fed in excess and is only partially consumed in the fuel cell. One method to improve fuel utilization in the fuel cell is by recycling the product gases as illustrated in Fig. 13.53. Recirculation from ${n_1}^{\mathrm{CH_4}}$ mols of fuel fed results in $(\zeta - 1)$ $({n_2}^{\mathrm{CH_4}} + n^{\mathrm{CO}} + n^{\mathrm{H_2}})$ mol of unused fuel, where $\zeta {n_2}^{\mathrm{CH_4}} < {n_1}^{\mathrm{CH_4}}$.

If product gas recirculation is not applied, then the quantity of noncombustible gases for the system producing the same electric output would be higher $\zeta({n_2}^{\mathrm{CH_4}} + n^{\mathrm{CO}} + n^{\mathrm{H_2}})$. The system with recirculation still requires an additional

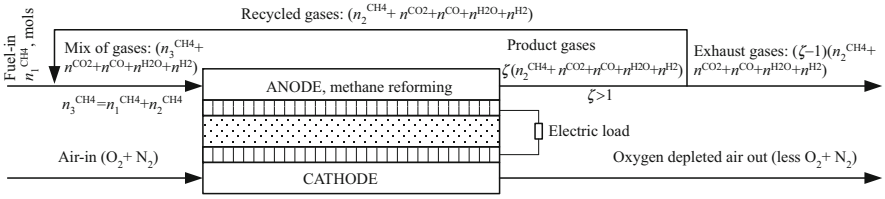

Fig. 13.53 Product gas recycling in a SOFC system for steam reforming and better fuel utilization

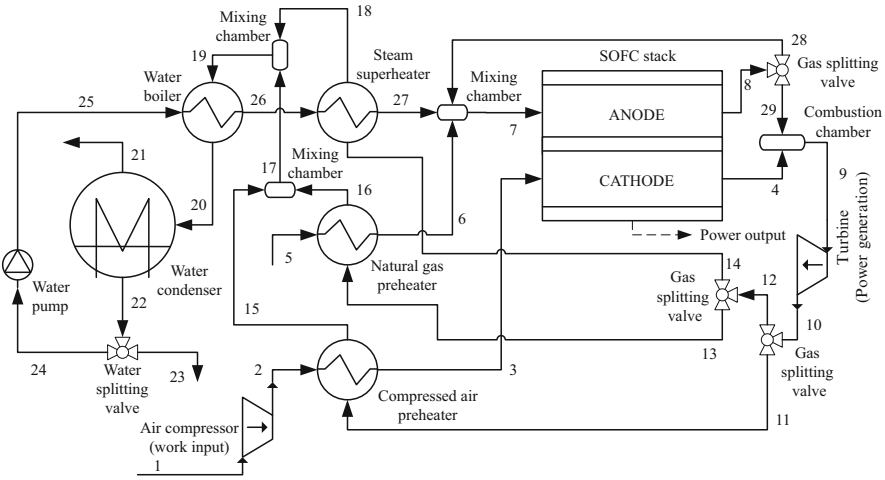

Fig. 13.54 SOFC/gas turbine power generator with natural gas fuel

afterburner or other system to consume the remaining fuel, but it is a fact that the fuel utilization within the fuel cell is better. Another factor is that steam is needed for reforming the primary hydrocarbon fuel (in the above example, the methane). Through recirculation of product gases, steam is provided to the fuel feed side. Depending on the operating parameter, it is possible that this steam is sufficient for obtaining enough fuel reformation. However, in many practical situations, the steam provided by product gas recirculation is not sufficient. Additional steam then can be provided through water condensation from exhaust gases, followed by water reheating and steam generation. A complete diagram of an SOFC system is presented in Fig. 13.54.

The system use natural gas from municipal distribution lines (assumed at 6–8 bar) which is reformed with steam recovered from the product gas. Air from the ambient is aspired by the air compressor at point 1 and discharged at high pressure at point 2 with further preheating (point 2–3); preheated air is fed in fuel cell at point 3. The oxygen-depleted air is discharged at the cathode side at point 4. Natural gas enters at point 5 and is preheated (point 5–6) and mixed with

superheated steam recycled from the fuel cell stack (point 28) and extracted from the exhaust gases (point 27). The make-up gas consisting of natural gas, steam, uncombusted gases (hydrogen, methane, carbon monoxide) enters at the fuel cell anode at point 7. The product gas exhaust at the anode at point 8 is split into two streams: stream 28 (recycled) and stream 29 directed toward the combustion chamber, where it combusts with oxygen-depleted air from the cathode (point 4), producing hot exhaust gas at point 9.

The exhaust gas at high temperature and pressure at point 9 is expanded with work generation in the gas turbine and retrieved downstream at point 10, where it is split in three streams that are to be used for heat recovery (streams 11, 13, and 14). The enthalpy of these gases is used for preheating air, preheating natural gas, and superheating steam. After this, all three streams are mixed at point 19 and their enthalpy is used for steam generation from recovered water in the water boiler. Colder exhaust gases at point 20 (assumed completely combusted) are further cooled in the water condenser, which condensates water while releasing the non-condensable gases at point 21. The resulting water is partially drained (point 23) (or used for other purposes), and partially recycled at point 24. The recycled water is first pressurized (point 24–25), and then boiled (point 25–26), and the resulting steam is superheated (point 26–27).

Note the essential difference with the MCFC system presented in Fig. 13.52, where the natural gas reforming is done indirectly (outside of the fuel cell stack) because of the lower temperature of the process heat. In that case, more water is needed for the process, and this water is provided from exterior sources. In the SOFC system all water needed by the system is separated from the combustion gases and recycled within the system; there is no need for additional water supply. Consequently, the exergy efficiency of the SOFC system has the potential to be higher than in the MCFC system. The energy and exergy efficiencies can be defined for the SOFC system as follows:

$$\left.\begin{aligned} \eta &= \frac{W_{\mathrm{FC}} + W_{\mathrm{T}} - W_{\mathrm{C}} - \mathrm{W_P}}{\mathrm{LHV}} \\ \psi &= \frac{W_{\mathrm{FC}} + W_{\mathrm{T}} - W_{\mathrm{C}} - W_{\mathrm{P}}}{ex_{\mathrm{NG}}^{\mathrm{ch}} + ex_{\mathrm{NG}}^{\mathrm{thrm}}} \end{aligned}\right\}, \tag{13.53}$$

where the generated work W is given per molar unit of natural gas consumption, indices FC, T, C, P, and NG represent fuel cell, turbine, compressor, pump, and compressed natural gas, respectively, and ex is the molar chemical exergy, and the exponents "ch" and "thrm" mean chemical and thermomechanical, respectively. Granovskii et al. (2008b) calculated the energy and exergy efficiency of an SOFC system like that presented in Fig. 13.57 and showed that depending on the operating condition they can achieve 73% to 85% (energy-based) and 72% to 85% (exergy-based).

13.11 Integrated Fuel Cell Systems

Fuel cell systems can be integrated with other cycles, as discussed above, to obtain better fuel utilization efficiency. This is especially the case for fuel cells with oxygen ion-conducting electrolytes, where water is formed at the anode and reduces hydrogen concentration. PEM fuel cell systems do not suffer from this operating deficiency, and, therefore, they can obtain excellent fuel efficiency by themselves; there is no need for a downstream afterburner or other fuel-consuming system.

The need for integration of fuel cell systems with other systems stems from other reasons in addition to that of achieving better fuel utilization. These reasons can be, for example, using fuel other than hydrogen and applying direct and indirect reforming, whichever is the case, or applying heat recovery for cogeneration of power and heat or for driving a bottoming cycle for additional power generation. In addition, fuel cells can be integrated in systems with purposes other than power generation. An example is an oxygen production system as shown in Fig. 13.55. This system combines a fuel cell system with a water/steam electrolyzer system. In this approach, a high-efficiency SOFC power plant is used to drive steam electrolysis. The SOFC system exhaust contains steam at very high temperature along with other combustion products (mainly nitrogen and carbon dioxide). A steam recovery unit cools the exhaust gases, condensates steam, separates water, boils it, and superheats the steam using heat recovery from the gases extensively.

Noncondensable gases are expelled at colder temperature. Thus, high-temperature steam, carrying high enthalpy, is fed into a solid oxide electrolyzer that operates around its thermal neutral point. Consequently, the electrolysis process needs less electricity per mol of water split. The electricity is supplied by the SOFC generator. The hydrogen produced by electrolysis is fed back to the SOFC system in combination with methane. The system is highly effective and can generate hydrogen at a pressure higher than the ambient—at 2 to 6 bar. Having pressurized hydrogen as the output, any further compression as oxygen must be stored at 200 bar or more.

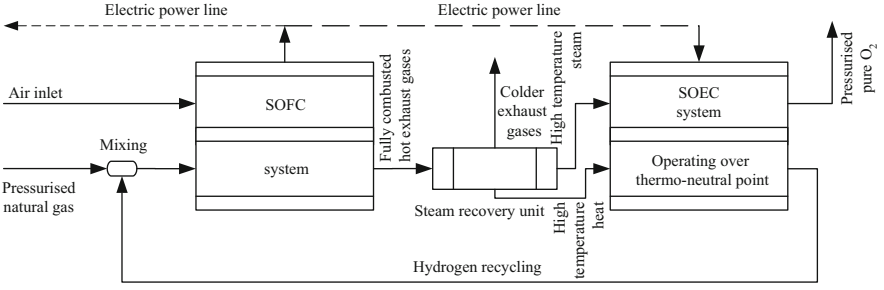

Fig. 13.55 Integrated system with SOFC and SOEC for pure pressurized oxygen production

Illustrative Example: An SOEC System

Let's assume that for the oxygen-producing system above, the energy efficiency of the SOFC is 90% and that of the electrolyzer subsystem, operating above its thermal neutral point, is 95%. We need to calculate the natural gas energy (with respect to LHV) to generate 1 mol of oxygen assuming that the system operates at 1 bar pressure.

The calculation can be made backward from the output to the input. To generate 1 mol of oxygen, we need 2 mol of water and we generate 2 mol of hydrogen. The total energy needed to operate the SOFC at, say, 800°C is simply calculated with EES software assuming that 2 mol of steam is fed at 950°C: $\Delta H = 2h_{H_2O}|_{950°C} - (2h_{H_2} + h_{O_2})|_{800°C} = -483.6\,\text{kJ/mol}$ of oxygen. The associated entropy change is calculated similarly, but, in addition, we assume complete conversion, that is in the inlet stream the steam concentration is 1 as well as in the outlet streams—since the products are not mixed, the hydrogen as well as the oxygen concentration is also 1; thus, we obtain $\Delta S = -100.1\,\text{J}$ and $\Delta G = \Delta H + (800 + 273.15)\Delta S = 591\,\text{kJ}$, both per mol of oxygen produced. Accounting for the SOEC efficiency, the electrical energy needed to drive the electrolysis is $E = -\Delta G/0.95 = 591/0.95 = 622.1\,\text{kJ/mol}\,O_2$. The thermal energy is $Q = -(800 + 273.15)\Delta S/0.95 = 113\,\text{kJ/mol}\,O_2$. The 2 mol of steam deliver to the electrochemical reaction a quantity of heat $Q_1 = 2c_p(950 - 800) = 4.4\,\text{kJ}$ while the rest of $Q_2 = Q - Q_1 = 108.6\,\text{kJ}$ is provided by the heat recovery unit driven by the exhaust gases produced by the SOFC subsystem. It is fair to assume 10% losses in the heat recovery unit; therefore, the heat generated by the SOFC is $Q_g = Q/0.9 = 125.6\,\text{kJ}$. In order to generate the needed electricity, the SOFC must be supplied with 2.29 mol of hydrogen at 800°C and additionally 53.4 kJ of heat is generated per mol of hydrogen consumed. In order to generate 125.6 kJ of heat, the number of mols of supplied hydrogen becomes 4.7; the generated electricity is 1,150 kJ, from which only 622.1 kJ are used to generate 1 mol of oxygen while the rest, 527 kJ, is available as electricity. This calculation suggests that the oxygen-generation system may be used for cogeneration of electricity and oxygen. Note that 2 mol of hydrogen from the total of 4.7 are recycled internally; thus, the consumption of hydrogen is 2.7 mol, which comes from reforming 1.35 mol of methane.

Another integrated fuel cell system, this time operating at intermediate temperature with a SOFC+ device and gas turbine, is presented in Fig. 13.56. This system operates with ammonia and cogenerates refrigeration and electric power. The cooling effect is produced in the ammonia storage tank, which features a cooling coil (point 10) and is thermally insulated. When ammonia vapor is drawn out of the tank (point 1), it removes enthalpy. Some liquid thus evaporates and generates refrigeration.

At start-up, ammonia can be heated electrically through the heating element (point 2). At steady operation, heating is applied in steps (2–3) and (3–4) up to about 700°C, the temperature at which ammonia is fed into the fuel cell. There, ammonia is decomposed catalytically at the anode and hydrogen is consumed.

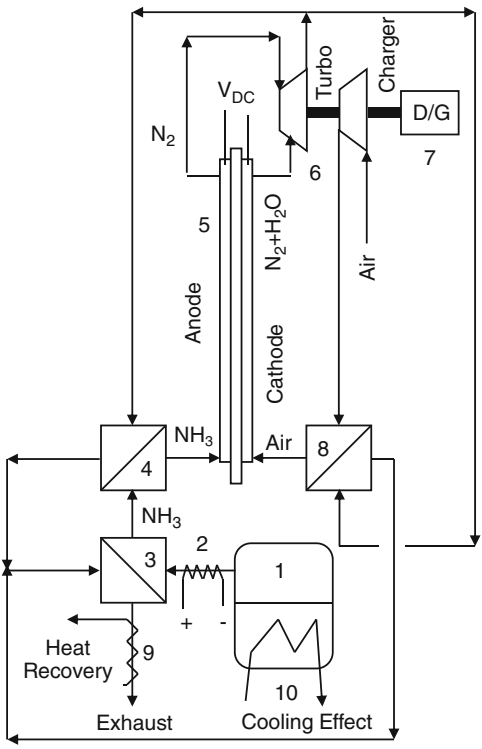

Fig. 13.56 Integrated fuel cell system with SOFC+ and gas turbine for power and cooling. *D*/*G* drive generator; *VDC* direct current voltage

Steam is formed at the cathode and expanded at point 6 together with the resulting nitrogen to generate power for air compression. The element (point 7) is an electric drive-generator that during the start-up drives the air compressor, while during the steady operation of the system it generates some electricity. Heat recovery can be applied to the exhaust gases. The system emits only benign gases such as steam and nitrogen.

Alkaline fuel cells also need improved fuel utilization, which can be done in principle by recirculation of the exhaust gases. However, their operating temperature is ~200°C, which means a low enthalpy of the reaction products. Moreover, the electrodes of the alkaline fuel cells are sensitive to poisoning, especially if the pressure is increased. Consequently, it is not appropriate to recycle the products or to expand them in a gas turbine. An alternative is to couple alkaline fuel cell systems with an organic Rankine cycle operating at the bottoming side. Figure 13.57 illustrates the concept: the exhaust gases from the alkaline fuel cell are combusted externally at constant pressure, and the combustion heat from the exhaust gases is recovered through a heat exchanger. The heat is further transferred to a Rankine cycle, which generates additional power. Preferably, for low- to medium-capacity application, the Rankine cycle should run with an organic fluid.

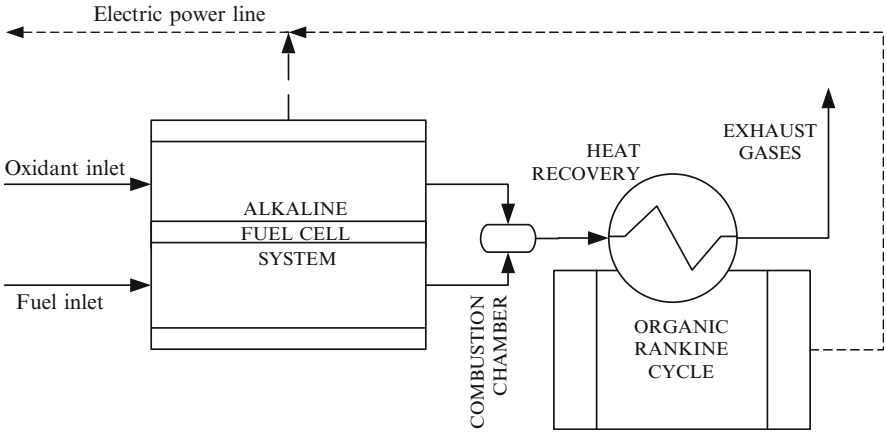

Fig. 13.57 Alkaline fuel cell system with a bottoming Rankine cycle for better fuel utilization

13.12 Fuel Cells: Analysis and Modeling

There are a number of fundamental equations from electrochemistry that must be applied for any fuel cell modeling attempt. In addition, first law and second law analyses together with molar balances can be written for the fuel cell itself and for each subsystem. Reaction kinetics and chemical equilibrium are important factors in fuel cell modeling and analysis. Fluid mechanics and heat transfer problems occur when analyzing and designing fuel cell stacks. Optimization of geometry and of the operating parameters is required for the fuel cell stack and the overall system. In brief, the analysis and modeling of fuel cells and fuel cell systems are complex problems, but they are very important for the optimized design of such systems. In this section, we discuss various factors in fuel cell analysis and modeling.

13.12.1 Classification of Fuel Cell Models

A classification of fuel cell models is presented in Fig. 13.58. It is difficult to classify models of fuel cells. In principle, one can categorize the model based on the modeling level, the number of spatial dimensions taken into consideration, the process time consideration, and the modeled processes taken into account. Modeling can be done at the cell level (which is the deepest analysis) and at the stack level (which accounts for flow distribution, channeling, flow collection, temperature distribution, spatial component concentration, etc.). Also, modeling can be done at the system level, where the fuel cell stack is integrated into a larger system. General thermodynamic analysis through conservation laws and specific equations must be applied at the system level.

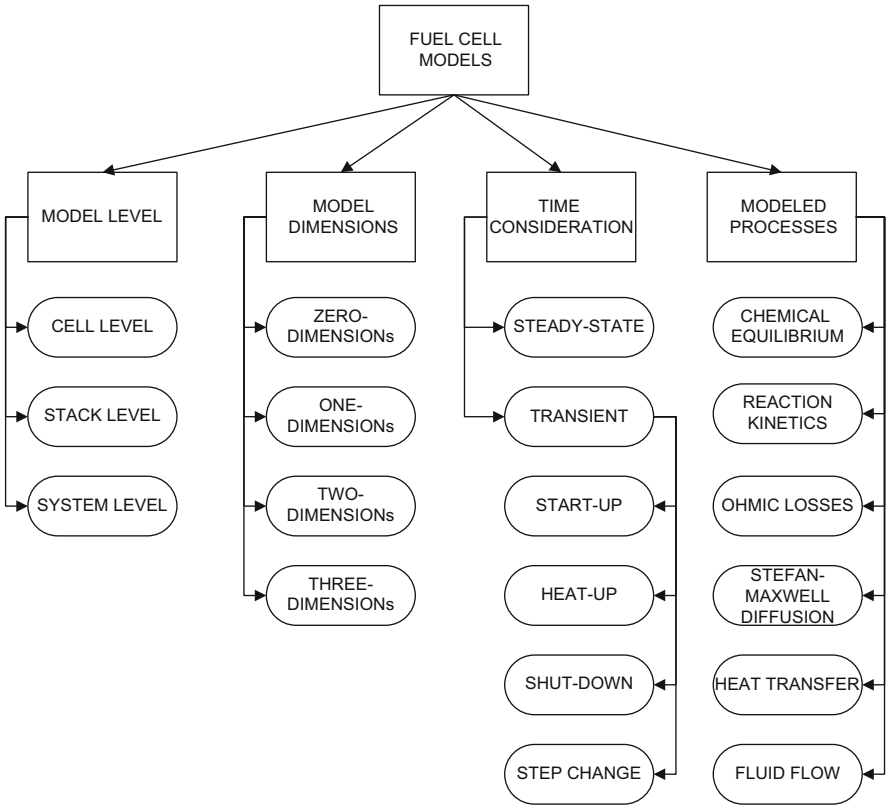

Fig. 13.58 Classification of fuel cell models

The zero-dimension models consider the fuel cell as a black box, characterized by unique parameters such as temperature, generated voltage, current density, inlet and outlet flow rates, and concentrations. A one-dimensional approach can be applied to planar fuel cell or to tubular configurations with axial symmetry. Parameter variation is considered only in one relevant direction (that is across electrolyte) while the other directions are neglected. In two-dimensional modeling, one of the considered directions is across the electrolyte, and the other direction is parallel with the stream flow directions in the channel (which in general is the direction along which one observes relevant gradients of important quantities).

Models can be either steady state or transient. Most of the published models in the literature refer to steady-state operation because it affects the design. However, operation at start-up, heat-up, shut-down, and step-change events must be analyzed, too. Thus, transient models are applied for these situations.

Models can also be categorized by the function of the physical–chemical processes. In general, reaction heat must be taken into the account in modeling, as well as the Gibbs free energy and the entropy of the overall reaction. Moreover, chemical equilibrium should be included in the models. Other aspects to be studied

are reaction kinetics, electric charge distribution, ohmic losses of various kinds, diffusion of chemical species and of ionic species (Stefan-Maxwell-Knudsen), heat transfer, and fluid flow in channels.

Fuel cell models can also be classified as macro- and micromodels. In macromodels, porous media models are applied to electrodes, which are assumed to be electron-conducting media. The electrode/electrolyte interface is the place where electrochemical reactions occur. In micromodels, electrodes are considered porous structures made of electron-conducting and ion-conducting particles. The micromodels predict the electrochemical characteristics at the electrodes.

13.12.2 Fundamental Equations and Definitions

A number of parameters and fundamental equations are very important for fuel cell modeling. These are reviewed in this section. The first equation introduced here is the Nernst equation. This equation was proposed by the German scientist Walther Nernst and can be understood if one reconsiders the Gibbs energy of water formation based on Eq. (13.4). The water formation reaction is $H_2 + 0.5O_2 \rightarrow H_2O$; we assume here all the reactants and the product in the gas phase. The total electric potential generated at the electrodes of the fuel cell comes from the Gibbs free energy of the reaction, and it is given by $\Delta H - T\Delta S = -nF\Delta E_{EL}$, where $n = 2$. Treating all chemicals as ideal gases, we find that the enthalpies do not depend on pressure $H(T,P) = H(T)$. Therefore, the reaction enthalpy can be calculated as if the reaction occurs at the reference pressure $P_0 = 1.01325$ bar. Note that $\Delta H = \Delta H^0(T)$. The reaction entropy is given as the difference between the molar entropy of the products and of the reactants $\Delta S = S_{\text{Products}} - S_{\text{Reactants}}$; thus, $\Delta S(T,P) = S_{H_2O}(T,P_{H_2O}) - S_{H_2}(T,P_{H_2}) - 0.5S_{O_2}(T,P_{O_2})$, where P_{H_2O}, P_{H_2}, and P_{O_2} are the partial pressure of the species. Recall that the entropy variation of ideal gases in isothermal transformation is $S(P) - S(P_0) = -R\ln(P/P_0)$. Thus, $\Delta S(T,P) = S_{H_2O}(T,P) - S_{H_2}(T,P) - 0.5S_{O_2}(T,P) - R\left[\ln\left(\frac{P_{H_2O}}{P_0}\right) - \ln\left(\frac{P_{H_2}}{P_0}\right) - \ln\left(\frac{P_{O_2}}{P_0}\right)^{0.5}\right]$. Finally,

$$\Delta S = \Delta S^0(T) - R\ln\left(\frac{P_{H_2O}}{P_{H_2}P_{O_2}^{0.5}}P_0^{0.5}\right). \tag{13.54}$$

Thus, the maximum electric potential retrieved at the electrodes is

$$-nF\Delta E_{EL} = \Delta H^0(T) - T\Delta S^0(T) - RT\ln\left(\frac{P_{H_2O}}{P_{H_2}P_{O_2}^{0.5}}P_0^{0.5}\right). \tag{13.55}$$

Expression (13.55) can be rearranged as

$$\Delta E_{\mathrm{EL}} = -\frac{\Delta H^{\,0}(T) - T\Delta S^{\,0}(T)}{nF} - \left(\frac{RT}{nF}\right)\ln\left(\frac{P_{\mathrm{H_2O}}}{P_{\mathrm{H_2}} P_{\mathrm{O_2}}^{\,0.5}} P_{\,0}^{\,0.5}\right), \tag{13.56}$$

where the quantity $-[\Delta H^{\,0}(T) - T\Delta S^{\,0}(T)]/nF = \Delta E_{\mathrm{EL}}^{\,0}$ is the standard cell potential (also called reversible cell voltage) at the given temperature (and standard pressure).

This quantity is fixed. We observe that the maximum cell potential is obtained if the second term in Eq. (13.56) is nil. This is possible if the argument of the logarithm is 1; if $P_{\mathrm{H_2O}} = P_{\mathrm{H_2}}$ and $P_{\mathrm{O_2}} = P_0$, this fact is accomplished; however, this is not possible in practical implementations because of various losses. Therefore, always $\Delta E_{\mathrm{EL}} < \Delta E_{\mathrm{EL}}^{0}$. Several definitions follow:

- *Air utilization ratio*: the number of mols of oxygen utilization with respect to the quantity fed at the fuel cell inlet $U_{\mathrm{a}} = n_{\mathrm{O_2,utilized}}/n_{\mathrm{O_2,inlet}}$.
- *Fuel utilization ratio*: similar to air utilization, it is $U_{\mathrm{f}} = n_{\mathrm{H_2,utilized}}/n_{\mathrm{H_2inlet}}$.
- *Excess air coefficient*: amount of oxygen at the inlet vs. stoichiometric oxygen: $\lambda_{\mathrm{a}} = U_{\mathrm{f}}/U_{\mathrm{a}}$.
- *Electric current through fuel cell*: $I = n \times n_{\mathrm{H_2}} \times F$, where n is the number of mols of electrons per reaction and $F = 96{,}485.3$ A/mol is the constant of Faraday.
- *Open circuit cell voltage*: $V_{\mathrm{oc}} = \Delta E_{\mathrm{EL}}^{\,0} - V_{\mathrm{ohm}} - V_{\mathrm{act}} - V_{\mathrm{conc}}$, where V means voltage and the indices ohm, act, and conc represent ohmic, activation, and concentration losses. This voltage exists between electrodes if there is no load connected. The actual load voltage is $V < V_{\mathrm{oc}}$.
- *Electric power output of the cell*: $W = VI$, where V is the actual voltage on the load.
- *Cell energy efficiency*: $\eta_{\mathrm{cell}} = W/(n_{\mathrm{H_2,inlet}} \times \mathrm{LHV})$.
- *Cell exergy efficiency*: $\psi_{\mathrm{cell}} = W/(n_{\mathrm{H_2,inlet}} \times ex^{\mathrm{ch}})$.
- *Current density:* the current per unit area of the electrolyte in the direction normal to ionic flow $i = I/A$.
- *Area-specific ohmic resistance*: the ohmic resistance of the electrolyte, and it has two different components: $\mathrm{ASR} = \mathrm{ASR_{contact}} + \mathrm{ASR_{bulk}}$, where $\mathrm{ASR_{contact}}$ represents the contact resistance per unit of area and $\mathrm{ASR_{bulk}}$ represents the summation of the resistivities of the materials traversed by ions and electrons (copper wires/leads, electrolyte, etc.), given as per unit of area of electrolyte.
- *Ohmic polarization*: $V_{\mathrm{ohm}} = \mathrm{ASR} \times i$, the total ohmic voltage losses.
- *Concentration polarization*: the partial pressure of the reactants decreases while they diffuse through the porous layers of the electrodes; this creates an additional voltage loss called the concentration polarization. The V_{conc} can be estimated with complicated empirical equations as reviewed in Colpan et al. (2008).
- *Activation polarization*: any reaction needs some energy to be activated; in the fuel cell case, the activation energy is transmitted to the ions electrically;

this is sensed as a loss of electric potential, according to the comments in Colpan et al. (2008):

$$V_{\text{act}} = \frac{RT}{F}\left[\sinh^{-1}\left(\frac{i}{2i_{\text{o,a}}}\right) + \sinh^{-1}\left(\frac{i}{2i_{\text{o,c}}}\right)\right], \tag{13.57}$$

where $i_{\text{o,a}}$ and $i_{\text{o,c}}$ are exchange current densities at the anode and cathode, respectively; these are the currents that exist at the electrode level even when the load is not connected; the cathode and anode exchange currents balance each other so that the total effect is nil, when the load is not connected.

In a detailed modeling of the fuel cell, the conservation laws take the form of partial differential equations. Since in fuel cells one works with several chemical species, the conservation equation of species becomes important; this equation is

$$\left[\frac{\partial C}{\partial t} + \nabla \cdot (\boldsymbol{u} \cdot C) = \nabla \cdot (D \nabla C) + \dot{S}\right]_k, \tag{13.58}$$

where t is time, C is the concentration, $\boldsymbol{u}$ is the velocity vector of the species k, and $\dot{S}$ is the source term that takes into account the rate of apparition or disparition of chemicals.

One important characteristic for the design and analysis of fuel cells is the voltage– current density curve, which Fig. 13.59 illustrates for a typical fuel cell. This kind of curve is determined from experimental measurements. Advanced modeling can roughly predict the curve. Once the curve is available, it is possible to use it for fuel cell optimization purpose. On the abscissa is the current density. If the current density is nil, that is, the circuit is open, then the voltage read at the fuel cell electrodes is the open circuit voltage V_{oc}. The diagram illustrates also the standard cell potential ΔE^{0}_{EL} and the ΔE_{EL}.

At low current density, in the region indicated with "A," the voltage losses are dominated by the activation polarization effects. In the region where the cell voltage decreases quasi-linearly, indicated with "Ω," the ohmic polarization is the dominant effect. In the region "C," the concentration losses become dominant. The actual power density delivered by the fuel cell is obtained by $W = Vi$; therefore, it can be calculated from the $V - i$ diagram. It can be observed that at low current density (no load) the power tends to zero (because $i \to 0$); similarly, at high current density there is a limiting value over which the power tends to zero (because $V \to 0$). The polarization losses become very high in region C. For a current density higher than i_{Limiting}, the fuel cell cannot generate power anymore because of the dissipative effects that can be observed in the form of heat, $Q = -T\Delta S$, and increase dramatically at high current density (see the thermal power density curve in Fig. 13.59). At a certain current density, the power delivered by the fuel cell represents a maximum.

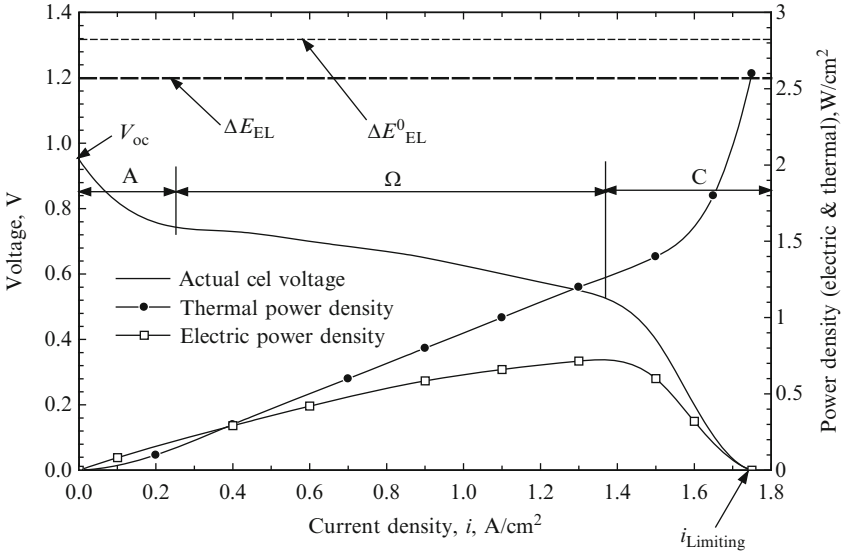

Fig. 13.59 Voltage-current density curve of a typical fuel cell

Table 13.18 Equations for fuel cell modeling

Parameter	Equation
Stoichiometric oxygen consumption	$\dot{m}_{O_2 s} = 0.0000000829 i_{opt}$, kg/s
Number of moles of stoichiometric oxygen	$\dot{n}_{O_2 s} = \dot{m}_{O_2 s}/\mu_{O_2 s}$, kmol/s
Number of moles of stoichiometric air	$\dot{n}_{Air,s} = \dot{n}_{O_2 s}/c_{O_2}$, kmol/s
Mass flow rate of stoichiometric air	$\dot{m}_{Air,s} = \dot{n}_{Air,s}\mu_{Air}$, kg/s
Mass flow rate of air	$\dot{m}_{Air} = \dot{m}_{Air,s}\lambda$, kg/s
Water consumption	$\dot{m}_{H_2O} = 0.0000000934\, i_{opt}$, kg/s
Hydrogen consumption	$\dot{m}_{H_2} = 0.0000000105 \cdot i_{opt}$, kg/s
Molar flow rate of hydrogen	$\dot{n}_{H_2} = \dot{m}_{H_2}/2$, kmol/s

Data from Zamfirescu and Dincer (2009c)

13.12.3 Case Study: Design Optimization of a Fuel Cell System

We consider here the SOFC+ system introduced above in Fig. 13.51. The aim of this case study is to develop an optimal design of the system for maximum power generation per unit of cell volume and maximum efficiency. The study is based on the work of Zamfirescu and Dincer (2009c). Since the fuel cell considered here is of the proton exchange type, some basic modeling equations relating the current density to hydrogen and oxygen consumption and water formation can be employed as summarized in Table 13.18. The stack is assumed to operate at the optimal current density i_{opt} and its corresponding maximum power density, W_{max}.

All of the supplied hydrogen is assumed to be consumed by the reaction. The current generated is proportional to the mass exchange surface of the stack

Table 13.19 Summary of the parameters used in the modeling

Parameter	Value
T_1	25°C
P_1	1.01325 bar
v_{N_2}	0.775 kmol/kmol
e_{ch,N_2}	631.51 kJ/kmol
v_{O_2}	0.206 kmol/kmol
e_{ch,O_2}	3,914.26 kJ/kmol
v_{H_2O}	0.018 kmol/kmol
e_{ch,H_2O}	9,953.35 kJ/kmol
v_{CO_2}	0.0003 kmol/kmol
e_{ch,CO_2}	20,108.5 kJ/kmol
v_{Ar}	0.0007 kmol/kmol
$e_{ch,Ar}$	17,998.14 kJ/kmol
e_{ch,H_2}	236,100 kJ/kmol
P_2	5 bar
η_{cmp}	0.75
η_T	0.85
P_{11}	14 bar
P_{12}	5.3 bar
US_{Loss}	0.05 W/K

(total membrane surface). The cell voltage is calculated with $V_C = W/i_{opt}$, the cell efficiency with $\eta_C = V_C/1.25$, where the reversible cell voltage is 1.25 V, the heat generated with $Q_C = W_m(1/\eta_C - 1)$, and lastly the heat loss through the stack's insulation (see Fig. 13.51) with $Q_L = US_L(\bar{T}_e - T_1)$.

In order to perform the calculations, a series of modeling parameters are assumed to have constant values, as summarized in Table 13.19. These parameters and their values are set based on some relevant engineering data for fuel cell systems. They refer to the ambient temperature and pressure, intake air composition, turbocharger efficiency and its operating pressure, hydrogen storage pressure, characteristics of the stack's thermal insulation, and chemical exergies.

The heat balance at the level of the fuel cell states that the heat generated by the electrochemical reaction Q_C upgrades the enthalpy of the input streams of hydrogen (point 14) and of air (point 3) (referring to Fig. 13.51), and the energy balance for the stack can be written as

$$\dot{m}_{14}h_{14} + \dot{m}_3h_3 + \dot{Q}_C = \dot{m}_4h_4 + \dot{Q}_L. \tag{13.59}$$

Two streams at equal temperature enter the stack, (points 3 and 14), and one stream of oxygen depleted air exits at point 4. Taking into account the above-mentioned design criterion as $T_{14} = T_3$, one may assume an average electrolyte temperature as

$$\bar{T}_e = \frac{2T_3 + T_4}{3}. \tag{13.60}$$

The pressure is evaluated starting from the assumed compressor discharge pressure P_2 and by approximating the pressure losses in the heat exchangers so that the exhaust discharges at the atmospheric pressure. It is also assumed that the flow is turbulent and fully developed. Here, compact plate heat exchangers are used. The pressure drop calculations entail a rough estimation of the friction coefficient; their corresponding values range between 0.1 and 0.5 bar.

The air composition at state 4 is calculated based on the air composition in the surroundings (through states 1, 2, and 3) and the amount of oxygen consumed and water generated, which are

$$\left.\begin{aligned} \dot{m}_{4,\mathrm{O_2}} &= \dot{m}_{3,\mathrm{O_2}} - \dot{m}_{\mathrm{O_2 s}} \\ \dot{m}_{4,\mathrm{H_2O}} &= \dot{m}_{3,\mathrm{H_2O}} + \dot{m}_{\mathrm{H_2O}} \end{aligned}\right\}. \tag{13.61}$$

Based on Eq. (13.61), the mass concentration of each air component at state 4 can be calculated:

$$c_i = \frac{\dot{m}_i}{\dot{m}_4}, \quad i = \mathrm{N_2,O_2,H_2O,CO_2,Ar}. \tag{13.62}$$

The enthalpy, entropy, and exergy values of each state point are calculated by assuming the turbine and compressor isentropic efficiencies as listed in Table 13.19, and hence, assuming that the heat losses from the heat exchangers are negligible as compared to the heat losses at the level of the fuel cell stack (which is in fact the component where the heat is generated and, therefore, the maximum temperature on the system occurs). The system performance is quantified here by two parameters, namely, the energy efficiency as

$$\eta = \frac{\dot{W}_\mathrm{C} + \dot{W}_\mathrm{T} - \dot{W}_\mathrm{Cmp}}{\dot{m}_{11}\mathrm{HHV}} \tag{13.63}$$

and the volumetric power density as

$$\dot{W}''' = \frac{\dot{W}_\mathrm{C} + \dot{W}_\mathrm{T} - \dot{W}_\mathrm{Cmp}}{\vartheta_\mathrm{C} + \vartheta_\mathrm{hx}}, \tag{13.64}$$

where ϑ_C is the stack volume and ϑ_hx represents the volume of the heat exchangers used to preheat the reactants between states 2 and 3 for air and 12–13–14 for hydrogen (see Fig. 13.50).

The volume of the fuel cell stack ϑ_C can be estimated based on the electrolyte membrane thickness, the number of cells, and the thickness of the thermal insulation. Here, we first consider a fixed fuel cell stack volume ϑ_C in the subsequent analysis and vary the volume occupied by the heat exchangers ϑ_hx. The total volume of the heat exchangers can be simply estimated based on their total energy (heat) capacities:

$$\dot{Q}_\mathrm{hx} = \dot{Q}_{2-3} + \dot{Q}_{12-13} + \dot{Q}_{13-14} \tag{13.65}$$

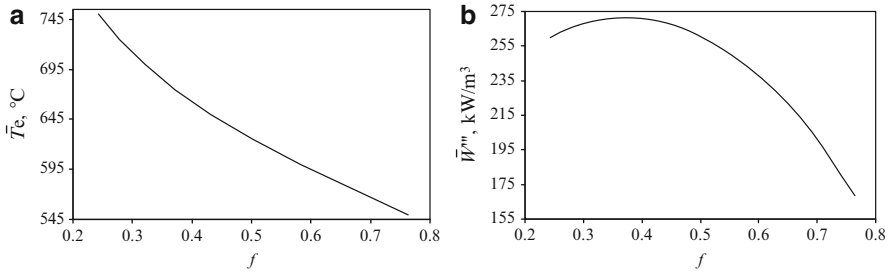

Fig. 13.60 The effect of the system's configuration f on the operating parameters and performance; (**a**) variation of the electrolyte temperature; (**b**) variation of the power density [data from Zamfirescu and Dincer (2009c)]

and a compactness factor φ is introduced to represent the power density of the heat exchanger as

$$\vartheta_{hx} = \frac{\dot{Q}_{hx}}{\phi}. \tag{13.66}$$

Here, the typical values of φ for compact plate-type heat exchangers are expected to range from 100 to 400 kW/m^3, respectively. In the present analysis, we consider 300 kW/m^3 as a common figure and an air stoichiometry of 3, and perform the calculations according to the scheme presented above. As already mentioned, the results regarding the system power density and system efficiency are correlated to the volumetric fraction f, occupied by the fuel cell stack with respect to the overall system volume as follows:

$$f = \frac{\vartheta_C}{\vartheta_C + \vartheta_{hx}}. \tag{13.67}$$

This helps determine the amount of heat exchanger capacity and volume required for better design, analysis, and optimization. In this regard, the results of our calculations are presented in Fig. 13.60, in terms of variation of the average electrolyte temperature (a) and the power density (b) with f. As the volumetric fraction f increases, both the volume and capacity of the heat exchangers for reactant streams heating decrease. Therefore, the hydrogen and air streams need to be less heated and this reduces the electrolyte temperature as clearly seen in Fig. 13.60a. As shown in Fig. 13.60b, one can observe that there is a maximum value of the power density between these two extreme cases. The first extreme occurs when f is low. Then, the fuel cell operates at high temperature and generates high power; however, the overall system volume is large, due to the large heat exchanger volumes that occupy the fraction $1 - f$ from the overall system.

The combination high-power/high-system volume leads to a low power density. In the second case, one ends up with a large f, and thus the heat exchangers having

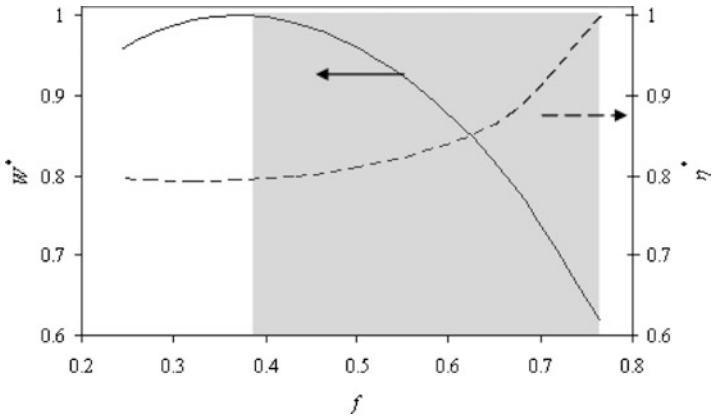

Fig. 13.61 Variation of the system's power density and energy efficiency with the volumetric fraction occupied by the stack. The quantities are normalized with respect to their maxima [data from Zamfirescu and Dincer (2009c)]

smaller size (capacity) makes the fuel cell operate at low temperature and hence to generate low power. The combination low-power/low-system volume leads to a low power density. As demonstrated by the results obtained in Fig. 13.60b, in between the two extreme situations is found an optimum f that maximizes the power density.

The design problem as illustrated in Fig. 13.60b can be reformulated as an optimization problem under constraints as follows: find the optimum system configuration that maximizes the power generated per unit of system volume; the system configuration is defined by the parameter f, and the volume of the system, consisting of the stack and heat exchangers, is fixed:

$$\max\{\dot{W}'''(f), \vartheta = \vartheta_C + \vartheta_{hx}, \text{fixed}\}. \tag{13.68}$$

The result of the optimization can be better contemplated in Fig. 13.61, where both the power density and energy efficiency are plotted on the same graph against the volume fraction f. In order to plot the two curves on the same graph, they were normalized with their maximal values. Therefore, one plots the quantities $W^* = \dot{W}'''/\dot{W}'''_{max}$ and $\eta^* = \eta/\eta_{max}$ against f. As can be seen in Fig. 13.62, the system's geometrical configuration, as defined by f, affects the performance of the system in terms of both energy efficiency and power density. As mentioned before, these two parameters are important especially in hydrogen-fueled vehicles; the designers have struggled with the problem of fitting a large hydrogen storage tank onboard and with the problem of maximizing the driving range (Fig. 13.61).

The results shown in Fig. 13.62 suggest that there are two design options for such fuel cell systems. The first option is to design the system for maximum efficiency. In this case, the system configuration is such that f is large, that is, the fuel cell stack is large with respect to the other system components (the heat exchangers).

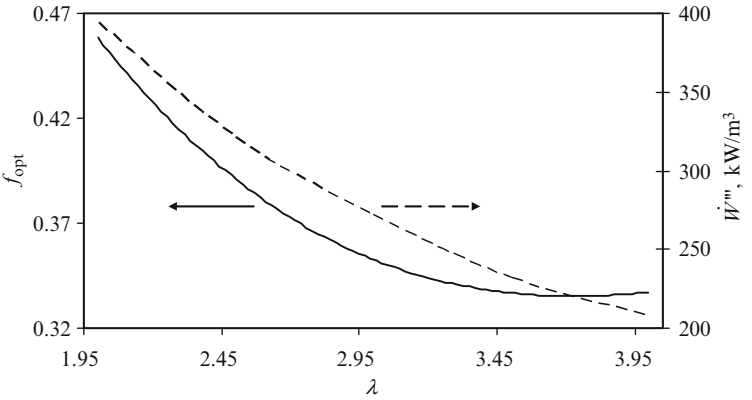

Fig. 13.62 Optimal volume fraction occupied by the stack and the maximum power density as a function of the air stoichiometry [data from Zamfirescu and Dincer (2009c)]

For obtaining the maximum efficiency, the stack occupies about 75% from the system volume (f is 0.75), as can be seen in Fig. 13.62. The second option is to design the system for maximum power per unit of volume, that is, for more compactness. In this case, the system configuration is such that the stack occupies about 40% of the system's volume while the rest of the system is occupied by the heat exchangers. It can also be said that if a system is designed for maximum power generation, it loses efficiency by about 20% of its maximum efficiency. This is expected to reduce the driving range by the same percent.

In addition, if the system is designed for a maximum energy efficiency to get a maximum driving range with a vehicle, the power density of the system is reduced by about 40% with regard to the system for a maximum power density. Therefore, if this option is chosen, one may end up with less useful space onboard for the system. This is even clearer in Fig. 13.62 as the gray-shaded area for the range of the design parameter f. It apparently ranges in between the two extreme points, that is, 0.35 and 0.75. It is not feasible to go beyond this range. So, one can consider this as the optimum configuration domain for design.

Furthermore, the minimum threshold of f depends on the adjustment of air stoichiometry. Small air stoichiometry means large f and high power density, while large λ means small f and low power density. These aspects can be contemplated from the results presented in Fig. 13.62. As shown here, the system power density reaches about 400 kW/m^3 for an air stoichiometry of 2.

The exergy efficiency is generally defined as the useful exergy output divided by the exergy input:

$$\psi = \frac{\dot{W}_c + \dot{W}_T - \dot{W}_{cmp}}{\dot{m}_{11}\mathrm{ex}_{11} + \dot{m}_1\mathrm{ex}_1}. \tag{13.69}$$

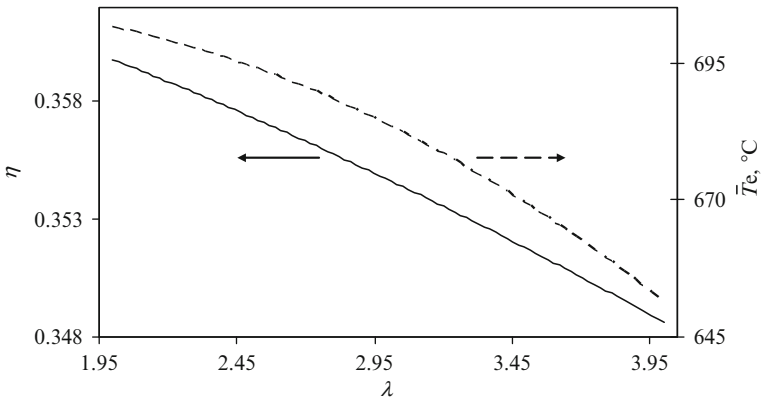

Fig. 13.63 The energy efficiency and the cell's average temperature of the optimized system as a function of the air stoichiometry [data from Zamfirescu and Dincer (2009c)]

Moreover, if the exhaust heat is recovered, the corresponding heat exergy results in

$$\dot{E}_{9-10} = \dot{Q}_{9-10}\left(1 - \frac{T_1}{\bar{T}_{9-10}}\right) \tag{13.70}$$

and therefore, the system effectiveness, including heat recovery, then becomes

$$\psi_{\text{hr}} = \frac{\dot{W}_{\text{c}} + \dot{W}_{\text{T}} - \dot{W}_{\text{cmp}} + \dot{E}_{9-10}}{\dot{m}_{11}\text{ex}_{11} + \dot{m}_1\text{ex}_1}. \tag{13.71}$$

The energy and exergy efficiencies of the system optimized for a maximum power density are studied for a range of air stoichiometry values. The results are presented in Fig. 13.63, which correlates both energy efficiency and electrolyte temperature with λ. As can be seen, the efficiency of the optimized system is less affected by varying the air stoichiometry while the stack temperature is affected more drastically. This remains the same if the exergy efficiency is considered instead of energy efficiency. The energy efficiency is thus about 35%; also, the exergy efficiency has been calculated; this is according to Eq. (13.69) around 40% while the exergy efficiency of the system with heat recovery, calculated according to Eq. (13.71), is 61% to 74%, depending upon the chosen excess air ratio.

In brief, it is shown that there is an optimal allocation of volumes for the various components of the fuel cell system that leads to power maximization per unit of system volume. If more volume is allocated to the heat exchangers, the temperature of the preheated gases increases and so does the average cell temperature. Therefore, the cell power density increases. However, the overall volume of the system is large because of the volume occupied by the heat exchangers; thus, a decrease in the system power density is induced. If the volume allocated to the heat exchangers

is small, the average cell temperature decreases, and so does the power density of the stack; the combination of low power and small system volume means low power density. The optimal design configuration, as defined by the volumetric fraction occupied by the stack from the whole system volume, is found in between the two above-stated extreme situations.

13.13 Case Study: Environmental Impact, Efficiency, and Sustainability Assessment

Here, we investigate three important parameters to compare the renewable energy-based hydrogen production options and other conventional methods.

As discussed earlier, electricity is one of the energy inputs for hydrogen production; therefore, its generation cost, efficiency, and environmental impact become important parameters for environmentally benign and cost-effective hydrogen production. Table 13.20 shows these parameters along with the efficiency of the hydrogen production system using the electrolyzer unit and the environmental impact reduction factor.

The efficiency of hydrogen production is calculated by multiplying the efficiencies of electricity production and the electrolyzer unit, whereas environmental impact reduction factor can be given as

$$\mathrm{EIRF} = \frac{\mathrm{gCO_{2\,coal}} - \mathrm{gCO_2}}{\mathrm{gCO_{2\,coal}}}, \tag{13.72}$$

where the numerator denotes the difference in carbon dioxide ejection into the environment by conventional (coal-based) and nonconventional methods and the denominator denotes the carbon dioxide ejection into the environment by coal-based electricity generation. There is no carbon dioxide produced during the electrolysis of water, but it is produced during electricity production. Hence, the environmental impact reduction factor (EIRF) is calculated by using the carbon dioxide emission from different sources for electricity production only.

The value of EIRF is between 0 and 1: where 1 is the best technology and 0 is the worst for which the environmental impact is lowest and highest, respectively. Table 13.20 shows that the conventional technologies like coal and gas are more economical for per kWh of electricity generation, but they pollute the environment more. However, the price of per kWh of electricity generation for coal and gas is lower than that for the renewable energy sources. Therefore, one can say that renewable energy sources are either cost-effective (for example, wind, biomass, and geothermal) or are less polluting of the environment.

Further, the electricity generation efficiency of the different technologies is given in the same table, and it is clear that some renewable sources (e.g., wind and hydro), if not more efficient, are competitive with the conventional

Table 13.20 Mean price of electricity generation, efficiencies of electricity and hydrogen generation, average greenhouse gas emissions expressed as CO_2 equivalent and environmental impact reduction factor for individual energy generation technologies

		Efficiency			
Energy sources	US$/kWh	Electricity (%)	Hydrogen production[a] (%)	gCO_2/kW h	EIRF
Photovoltaic	0.24	4–22	2–12	90	0.91
Wind	0.07	24–54%	13–28	25	0.98
Hydro	0.05	>90	47	41	0.96
Geothermal	0.07	10–20	5–11	170	0.83
Coal	0.042	32–45	17–23	1,004	0.00
Gas	0.048	45–53%	23–28	543	0.46

[a]Hydrogen production considered here is by using electrolyzer unit only
Data from Evans et al. (2009)

technologies (coal, gas, etc.) The efficiency of hydrogen production is greatly affected by the efficiency of electricity production. One can see from the above table that by using photovoltaic, wind, and geothermal, the hydrogen production efficiency can be 2–12%, 13–28%, and 5–11%, whereas for hydro it is the highest, that is, 47% and for coal and gas it remains between 17–23% and 23–28%, respectively. However, for the EIRF coal is the most polluting (0.00 for coal is taken as base case) and gas is the second highest (0.46). Wind, hydro, photovoltaic, and geothermal energies are said to be more environmentally benign and sustainable sources, as the EIRF is quite high, that is 0.98, 0.96, 0.91, and 0.83, respectively.

Evans et al. (2009) present sustainability indicators for some renewable technologies; wind, hydro, photovoltaic, and geothermal are ranked 1 to 4 based on the indicators as shown in Table 13.21, with 1 being the best technology for that indicator. The average and range were considered together, where values were quantifiable, as there was often significant overlap between the values. Some impact categories, such as availability and limitations as well as social impacts, that are unable to be quantified were assessed qualitatively. In the case of limitations, hydro was chosen as the least limited, due to its ability to provide base load power, a number of suitable sites worldwide, and the flexibility of operation. Wind was considered the second best for similar reasons. Geothermal is slightly more limited worldwide, with fewer suitable locations. Solar is considered the most limited, since excess power during the daylight hours is not yet able to be stored sufficiently to provide adequate power during periods with no sunshine(nights and on cloudy days). As far as social impact was concerned, wind was allocated the least negative social impact, due to its benign nature. Solar was second, as careful management during manufacturing and proper site selection mitigate its potential negative impacts, and geothermal was third due to increased seismic activity and pollution potential. Hydro had the largest impact, primarily due to the large number of people and animals displaced during dam inundation. The ranking in Table 13.21 suggests that electricity production from wind is the most sustainable followed by hydropower, and solar and geothermal were found to rank the lowest of the four noncombustion renewable energy technologies. This ranking was provided for

Table 13.21 Sustainability indicators for some renewable energy sources

	Photovoltaic	Wind	Hydro	Geothermal
Price	4	3	1	2
CO_2 emission	3	1	2	4
Availability and limitations	4	2	1	3
Efficiency	4	2	1	3
Land use	1	3	4	2
Water consumption	2	1	3	4
Social impact	2	1	4	3
Total	20	13	16	21

Data from Evans et al. (2009)

global international conditions, while each technology can be significantly geographically affected. For a specific geographical location, some of the listed sustainability indicators may become more important than others.

Sustainable development requires not only that the sustainable energy resources be used, but also that they should be used efficiently. Exergy analysis is essential to improve efficiency, which allows society to maximize the benefits it derives from its resources while minimizing the negative impact (such as environmental damage). Exergy efficiency gives an idea not only of the amount (quantity) of useful energy that can be completely utilized in useful work, but also of the quality of the energy. The part of energy that is not going to be utilized for useful work is called exergy destruction. Exergy analysis gives a realistic analysis of a system for its possible feasibility, and the exergy destruction gives the scope for improvement in the existing system. Another way to understand the scope for improvement or the performance of a system is through the sustainability index, which indicates how sustainable a system is in actual practice.

The exergy efficiency of a system can be defined in terms of exergy efficiency of the different units involved in that particular system, for example, a photovoltaic-based solar hydrogen system involves PV panels, a charge regulator, an inverter, and an electrolyzer. Recall that the relation between exergy efficiency (ψ) and the sustainability index (SI) can be given as (Dincer and Rosen 2007)

$$\psi = 1 - \frac{1}{\mathrm{SI}}, \quad \text{where SI} = \frac{1}{D_\mathrm{P}} \tag{13.73}$$

and D_P is the depletion factor/number defined as the ratio of the exergy destruction rate to the input exergy rate to the system and can be given as

$$D_\mathrm{P} = \frac{\dot{E}x_\mathrm{D}}{\dot{E}x_\mathrm{in}}. \tag{13.74}$$

The exergy efficiency of the system is calculated as a minimum of 3.68% to a maximum of 4.84%. Similarly, the energy efficiency of the system is also calculated as a minimum of 4.53% to a maximum of 5.62% for comparison purposes.

Table 13.22 Exergy efficiency and sustainability index for some H_2 production methods

Hydrogen production methods	Exergy efficiency (%)	Sustainability index
• Electrolysis		
Low-temperature (353 K)	58–64	2.38–2.78
Medium-temperature (473 K)	79	4.76
High-temperature (1,173 K)	86	7.14
• Photoelectrolysis	35[a]	1.54
• Steam gasification of petroleum coke	17	1.20
• Steam gasification of coal	46	1.85
• Decomposition of natural gas	32	1.47
• Steam reforming of natural gas	46	1.85
• Thermolysis	3.39	1.04
• Hybrid thermolysis + electrolysis	4.44	1.05
• Thermochemical cycle (e.g., Cu–Cl cycle)	33–65	1.49–2.86

[a]Maximum theoretical efficiency according to Dincer (2002)

Slightly higher values for energy efficiency can be seen, as the first law analysis does not incorporate losses due to irreversibility.

The sustainability index for the PV array varies between 1.11 and 1.13, for both charge regulator and inverter, between 6.67 and 10 for the electrolyzer unit is 2.08, whereas the sustainability index of the entire system is between 1.04 and 1.05. A higher sustainability index shows better sustainability of the process/unit. It should be noted here that despite the higher exergy efficiency of the electrolyzer, charge regulator, and inverter units, the system exergy efficiency remains low, mainly because of the low PV exergy efficiency. There is a need to improve the PV array efficiency in order to have a better sustainability index and hence better sustainability.

The exergy efficiency and sustainability index of the different hydrogen production methods discussed earlier are listed in Table 13.22. It is evident that the electrolysis process has better exergy efficiency, and subsequently the sustainability index is also high. For a temperature range of 353 to 1,173 K, the exergy efficiency range of the electrolysis process is 58% to 86% and the sustainability index range is (MS PAGE NO 620) 2.38 to 7.14. The biophotolysis range is the lowest of all, as the conversion efficiency of plants is very low. The sustainability index for photoelectrolysis is 1.54 for the maximum theoretical efficiency of 35%.

Exergy efficiency of steam gasification of petroleum coke and coal is 17% and 46% and the sustainability index is 1.2 and 1.85, respectively. Exergy efficiency of decomposition (also known as cracking) and steam reforming of natural gas is 46% and 32% and their sustainability index is 1.47 and 1.85. High-temperature thermolysis has a relatively low exergy efficiency (3.39%) and sustainability index (1.04). However, its performance can be improved by coupling thermolysis with electrolysis (also known as the hybrid thermolysis and electrolysis process). In this case, exergy efficiency is 4.44% and the sustainability index is 1.05. Thermochemical cycles, such as the Cu–Cl cycle, have a reasonably good exergy efficiency range (33–65%), and its sustainability range is 1.49–2.86.

13.14 Concluding Remarks

In this chapter, potential technologies for hydrogen production were thoroughly reviewed. It was explained why hydrogen is important for sustainable energy development: it is the cleanest energy carrier that can be produced from any kind of energy source such as water or other abundant materials. There are many hydrogen production methods. They were categorized here based on the energy source they use, such as electric, thermal, biochemical, and photonic-based methods. Each of these kinds of energy can be obtained from primary energy such as nuclear, fossil fuel, renewable sources, or recovered energy.

Various solar hydrogen production methods have been studied. Water electrolysis using photovoltaic cells is the most mature method for producing hydrogen. Photoelectrolysis is still at an early stage of development, and material cost and practical issues have yet to be solved. The photobiological processes are also still at a very early stage of development and thus far only low conversion efficiencies have been attained. High-temperature processes need further material development that focuses on high-temperature membranes and heat exchangers for solar–thermal processes. Therefore, the world's solar hydrogen utilization systems consist mainly of photovoltaic-hydrogen systems for transportation and stationary applications. Eco-friendly hydrogen production via solar energy is very important to save the environment as it does not emit any greenhouse gases during operation. At present, it is a challenging task for researchers and scientists, as the exergy efficiency of the PV array is low, and hence the overall exergy efficiency of a solar hydrogen system is low. The geothermal-based hydrogen production is another suitable alternative that uses the renewable energy of the geothermal water/steam to produce hydrogen using a high-temperature electrolyzer. Environmentally benign and sustainable hydrogen production via artificial photosynthesis is also discussed. The EIRF and SI have been evaluated and studied for different energy sources, and it can be concluded that renewable energy sources are environmentally benign as they have a higher value for the EIRF. In the end, a case study showing energy and exergy efficiencies of a hydrogen production system are discussed in brief, as is the sustainability index of some processes. The variation ranges of exergy efficiency and sustainability index for various hydrogen production methods are summarized in the form of a table. It can be concluded that the hydrogen systems with high sustainability index are desirable to ensure high exergy efficiency, which in turn ensures high exergy output for the maximum benefit for society.

Hydrogen is difficult to store and distribute, but technologies evolve and in the future they will become commercially available. The utilization of hydrogen is predicted to grow, with a large share of the petrochemical industry and of agriculture, where it is used as fertilizer. The use of hydrogen as fuel is expanding constantly. Fuel cells are the main systems that utilize hydrogen fuel for power production. They have high efficiency, a fact that justifies efforts for their improvement and commercialization. Here, fuel cells were classified and their basic modeling and optimization issue were presented with some examples.

Nomenclature

C	Cost, $ or concentration
CI	Cost index
e	Elementary charge, C
E	Energy, kJ
EIRF	Environmental impact reduction factor
ex	Specific exergy, kJ/kg
Ex	Exergy, kJ
D_p	Depletion factor
f	Volume fraction
F	Faraday constant, As/mol
G	Gibbs free energy, kJ/mol
h	Specific enthalpy, kJ/kg or heat transfer coefficient, W/m^{2}K
H	Enthalpy, kJ/kg
HHV	Higher heating value, MJ/kg
I	Solar irradiance, W, or current intensity, A
k	Thermal conductivity, W/mK
LHV	Lower heating value, MJ/kg
m	Mass, kg
MR	Mols ratio
n	Number of mols
N_A	Number of Avogadro
P	Pressure, bar
Q	Heat, kJ
R	Universal gas constant, J/molK
s	Specific entropy, kJ/kgK
S	Entropy, kJ/K
SI	Sustainability index
T	Temperature, K
U	Overall heat transfer coefficient, W/m^{2}K
V	Voltage, V
W	Work, kJ

Greek Letters

δ	Thickness, m
γ	Specific heat ratio
Δ	Difference

λ Excess ratio
ϕ Compactness factor, kW/m^3
η Utilization efficiency
ψ Exergy efficiency
υ System volume, m^3

Subscripts

0 Reference state
C Condenser
Cmp Compresser
E Electrical
EL Electrolysis
FC Fuel cell
gen Generator
geo Geothermal
H Heating
hx Heat exchanger
hr Heat recovery
in Inlet
ins Insulation
m Material or mean
N Nernst
o Output
oc Open circuit
ohm Ohmic
ox Oxidation
OP Other product
PF Primary fuel
pmp Pump
red Reduction
S Salt
sc Short circuit
SF Synthetic fuel
SH Space heating
TH Thermal
TOT Total
W Wall
WF Working fluid

Superscripts

ch	Chemical
thrm	Thermomechanical
$\dot{(\ )}$	Rate (per unit of time)
$\bar{(\ )}$	Average value

References

Abanades S., Charvin P., Flamant G., Neveu P. 2006. Screening of water-splitting thermochemical cycles potentially attractive for hydrogen production by concentrated solar energy. *Energy* 31:2805–2822.

Abuadala A., Dincer I., Naterer G.F. 2010. Exergy analysis of hydrogen production from biomass gasification. *International Journal of Hydrogen Energy* 35:4981–4990.

Ay M., Midilli A., Dincer I. 2006. Investigation of hydrogen production from boron compounds for PEM fuel cells. *Journal of Power Sources* 157:104–113.

Balta M.T., Dincer I., Hepbasli A. 2009. Thermodynamic assessment of geothermal energy use in hydrogen production. *International Journal of Hydrogen Energy* 34:2925–2939.

Brewer K.J., Elvington M. 2006. Supramolecular complexes as photocatalysts for the production of hydrogen from water. US Patent 7,122,172 B2.

CHA 2010. Hydrogen systems. The Canadian opportunity for greenhouse gas reduction and economic growth through the deployment of hydrogen technologies and infrastructures. Canadian Hydrogen Association. Internet source http://www.h2.ca (accessed on September 1, 2010).

Christensen P.A., Erbs W., Harriman A. 1985. Photo-oxydation of water in non-sacrificial systems. *Journal of Chemical Society, Faraday Transactions* 81:575–580.

Cohce M.K., Dincer I., Rosen M.A. 2010. Thermodynamic analysis of hydrogen production from biomass gasification. *International Journal of Hydrogen Energy* 35:4970–4980.

Collings A.F., Critchley C. 2005. Artificial Photosynthesis from Basic Biology to Industrial Application. Wiley-VCH Verlag GmbH & Co, Weinheim, Germany.

Colpan C.O., Dincer I., Hamdullahpur F. 2008. A review on macro-level modeling of planar solid oxide fuel cells. *International Journal of Energy Rresearch* 32:336–355.

Das D., Veziroglu T.N. 2008. Advances in biological hydrogen production processes. *International Journal of Hydrogen Energy* 33:6046–6057.

Dincer I. 2002. Technical, environmental and exergetic aspects of hydrogen energy systems. *International Journal of Hydrogen Energy* 27:265–285.

Dincer I., Rosen M.A. 2007. Exergy: Energy, Environment and Sustainable Development. Elsevier, Oxford, UK.

Evans A., Strezov V., Evans T.J. 2009. Assessment of sustainability indicators for renewable energy technologies. *Renewable and Sustainable Energy Reviews* 13:1082–1088.

Fujishima A., Honda K. 1972. Electrochemical photolysis of water at a semiconductor electrode. *Nature* 238: 37–38.

Granovskii M., Dincer I., Rosen M.A., Pioro I. 2008a. Performance assessment of a combined system to link a supercritical water-cooled nuclear reactor and a thermochemical water splitting cycle for hydrogen production. *Energy Conversion and Management* 49:1873–1881.

Granovskii M., Dincer I., Rosen M.A. 2008b. Exergy analysis of a gas turbine cycle with steam generation for methane conversion within solid oxide fuel cells. *Journal of Fuel Cell Science and Technology* 5/031005:1–9.

Gutsol A.F., Fridman A. 2008. Hydrogen production from hydrogen sulfide. Patent #WO 137936.

Haseli Y., Naterer G.F., Dincer I. 2009. Fluid-particle mass transport of cupric chloride hydrolysis in a fluidized bed. *International Journal of Heat and Mass Transfer* 52:2507–2515.

Isachenko V.P., Osipova V.A., Sukomel A.S. 2004. Heat transfer. In: Solid Fuels Combustion and Gasification Modeling, Simulation, and Equipment Operation, de Souza-Santos M.L., eds., Marcel Dekker, New York.

Kalinci Y., Hepbasli A. Dincer I. 2009. Biomass-based hydrogen production: A review and analysis. *International Journal of Hydrogen Energy* 34:8799–8817.

Kanoglu M. Dincer I., Rosen M.A. 2007. Geothermal energy use in hydrogen liquefaction. *International Journal of Hydrogen Energy* 32:4250–4257.

Karkamkar A., Ardahl C., Autrey T. 2007. Recent developments on hydrogen release from ammonia borane. *Mater Matters* 2:6–9.

Kogan A. 1998. Direct solar thermal splitting of water and onsite separation of the products. II. Experimental feasibility study. *International Journal of Hydrogen Energy* 23:89–98.

Kotay S.M., Das D. 2008. Biohydrogen as a renewable energy resource—prospects and potentials. *International Journal of Hydrogen Energy* 33:258–63.

Koutrouli E.K., Kalfas H., Gavala H.N., Skiadas I.V., Stamatelatou K., Lyberatos G. 2009. Hydrogen and methane production through two-stage mesophilic anaerobic digestion of olive pulp. *Bioresource Technology* 100:3718–3723.

Licht S., Wang B., Mukerji S., Soga T., Umeno M., Tributsch H. 2001. Over 18% solar energy conversion to generation of hydrogen fuel; theory and experiment for efficient solar water splitting. *International Journal of Hydrogen Energy* 26:653–659.

Marmier A., Füterer M.A. 2008. Nuclear powered heat pumps for near-term process heat applications. *Nuclear Engineering and Design* 238:2272–2284.

Midilli A., Murat Ay, Kale A., Veziroglu T.N. 2007. A parametric investigation on hydrogen energy potential based on H_2S Black Sea deep waters. *International Journal of Hydrogen Energy* 32:117–124.

Muradov N.Z., Veziroglu T.N. 2008. "Green" path from fossil-based to hydrogen economy: An overview of carbon neutral technologies. *International Journal of Hydrogen Energy* 33:6804–6839.

Naterer G.F., Suppiah S., Lewis M., Gabriel K., Dincer I., Rosen M.A., Fowler M., Rizvi G., Easton E.B., Ikeda B.M., Kaye M.H., Lu L., Pioro I., Spekkens P., Tremaine P., Mostaghimi J., Avsec J., Jiang J. 2009. Recent Canadian advances in nuclear-based hydrogen production and the thermochemical Cu–Cl cycle. *International Journal of Hydrogen Energy* 34:2901–2917.

Orhan M.F., Dincer I., Naterer G.F. 2008a. Cost analysis of a thermo-chemical Cu–Cl pilot plant for nuclear-based hydrogen production. *International Journal of Hydrogen Energy* 33:6006–6020.

Orhan M.F., Dincer I., Rosen M.A. 2008b. Thermodynamic analysis of the copper production step in a copper–chlorine cycle for hydrogen production. *Thermochimica Acta* 480:22–29.

Orhan M.F., Dincer I., Rosen M.A. 2009a. Efficiency analysis of a hybrid copper–chlorine (Cu–Cl) cycle for nuclear-based hydrogen production. *Chemical Engineering Journal* 155:132–137.

Orhan M.F., Dincer I., Rosen M.A. 2009b. Energy and exergy analyses of the fluidized bed of a copper–chlorine cycle for nuclear-based hydrogen production via thermo-chemical water decomposition. *Chemical Engineering Research and Design* 87:684–694.

Orhan M.F., Dincer I., Rosen M.A. 2009c. The oxygen production step of a copper–chlorine thermo-chemical water decomposition cycle for hydrogen production: Energy and exergy analyses. *Chemical Engineering Science* 64:860–869.

Rashidi R., Berg P., Dincer I. 2009. Performance investigation of a combined MCFC system. *International Journal of Hydrogen Energy* 34:4395–4405.

Sørensen R.Z., Hummelshøj J.S., Klerke A., Reves J.B., Vegge T., Nørskov J.K., Christensen C.H. 2008. Indirect, reversible high density hydrogen storage in compact metal ammines. *Journal of American Chemical Society* 130:8660–8668.

Taylor J.B. 1983. Hydrogen energy prospects in Canada. *International Journal of Hydrogen Energy* 1/2:1–7.

Yilanci A., Dincer I., Ozturk H.K. 2009. A review on solar-hydrogen/fuel cell hybrid energy systems for stationary applications. *Progress in Energy and Combustion Science* 35:231–244.

Zaman J., Chakma A. 1995. Production of hydrogen and sulphur from hydrogen sulfide. *Fuel Processing Technology* 41:159–198.

Zamfirescu C., Dincer I. 2009a. Performance investigation of high-temperature heat pumps with various BZT working fluids. *Thermochimica Acta* 488:66–77.

Zamfirescu C., Dincer I. 2009b. Ammonia as a green fuel and hydrogen source for vehicular applications. *Fuel Processing Technology* 90:729–737.

Zamfirescu C., Dincer I. 2009c. Thermodynamic performance analysis and optimization of a SOFC-H^+ system. *Thermochimica Acta* 486:32–40.

Zamfirescu C., Dincer I., Naterer G.F. 2009a. Performance evaluation of organic and titanium based working fluids for high temperature heat pumps. *Thermochimica Acta* 496:18–25.

Zamfirescu C., Dincer I., Naterer G.F. 2010a. Thermophysical properties of copper compounds in copper–chlorine thermochemical water splitting cycles. *International Journal of Hydrogen Energy* 35:4839–4852.

Zamfirescu C., Dincer I., Naterer G.F. 2010b. Upgrading of waste heat for combined power and hydrogen production with nuclear reactors. *Journal of Engineering for Gas Turbines and Power* 132/102911:1–9.

Zamfirescu C., Dincer I., Naterer G.F. 2010c. Design and analysis of a photocatalytic hydrogen production system with mixed-metal photoinitiated electron collection. International Conference on Hydrogen Production (ICH_2P), Istanbul, June 16-18.

Zamfirescu C., Dincer I., Naterer G.F. 2010d. Biomass-based heat driven water splitting using copper-chlorine cycle. Eightieth World Hydrogen Energy Conference (WHEC 2010) Essen, Germany, May 16-20.

Zamfirescu C., Naterer G.F., Dincer I. 2010e. Kinetics study of the copper/hydrochloric acid reaction for thermochemical hydrogen production. *International Journal of Hydrogen Energy* 35:4853–4860.

Zamfirescu C., Naterer G.F., Dincer I. 2010f. Novel CuCl vapor compression heat pump integrated with a water splitting plant. *Thermochimica Acta* 512:40–48.

Study Questions/Problems

13.1 What characteristics of hydrogen make it attractive for energy economy?
13.2 Describe the idea of hydrogen economy.
13.3 Categorize the methods for hydrogen production.
13.4 Calculate the reaction enthalpy and the Gibbs energy of water decomposition reaction at 25°, 1,000°, and 2,500°C and compare the results.
13.5 Calculate the energy efficiency of the system in Fig. 13.5 using the data from Table 13.3.
13.6 Explain the concept of thermochemical water splitting.
13.7 Calculate the reaction heat for Eq. (13.15).
13.8 Describe the S–I cycle.
13.9 What is the difference between fuel reforming and gasification?

13.10 Calculate the reaction heats for Eq. (13.27) at 1,000°C.
13.11 Describe the nuclear–thermal routes for hydrogen production.
13.12 What are the envisaged hydrogen production methods coupled with nuclear reactors?
13.13 Calculate the reaction heats for Eq. (13.37) at 1,100°C.
13.14 Making reasonable assumptions, calculate the copper chlorine hydrogen production cycle in Fig. 13.21.
13.15 Making reasonable assumptions, calculate the biomass-driven high-temperature electrolysis cycle in Fig. 13.29.
13.16 Explain the principle of photocatalytic water splitting.
13.17 Calculate the reaction enthalpy for Eq. (13.43) at standard temperature.
13.18 Calculate the work needed to compress 1 kg of hydrogen from 1 bar pressure to 800 bar according to the process described by Eq. (13.46).
13.19 Calculate the simplified Claude cycle in Fig. 13.44 under reasonable assumptions.
13.20 Comment on the storage density of various hydrogen storage methods according to Fig. 13.45.
13.21 Comment on the potential of ammonia borane for hydrogen storage. Investigate the sufficiency of natural reserves of boron.
13.22 Compare the hydrogen utilization in Canada in 1983 with respect to 2010.
13.23 Describe the fuel cell principle.
13.24 Is the fuel cell operation benefited by high pressure and low temperature or by low pressure and high temperature?
13.25 Present a classification of fuel cell types.
13.26 Present a classification of fuel cell applications.
13.27 Calculate the system in Fig. 13.50 under reasonable assumptions.
13.28 Calculate the system in Fig. 13.51 under reasonable assumptions.
13.29 Calculate the system in Fig. 13.52 under reasonable assumptions.
13.30 Calculate the system in Fig. 13.54 under reasonable assumptions.
13.31 Calculate the system in Fig. 13.56 under reasonable assumptions.
13.32 Present a classification of fuel cell modeling techniques.
13.33 Explain the equation of Nernst.
13.34 Describe the type of energy losses in fuel cells.

Chapter 14
Carbon Dioxide Technologies

14.1 Introduction

Besides being a greenhouse gas and a major component of the carbon cycle in nature, carbon dioxide (CO_2, CAS 124-38-9) is a substance of major industrial importance. It has a stable linear molecule in which each atom of oxygen is linked with two strong covalent bonds to the atom of carbon. The number of industrial processes using carbon dioxide is very large; it is used for welding; plastics; synthetic fuel processing; oil, gas, and coal-bed methane recovery; refrigerant; heat transfer fluid (e.g., in refrigeration applications and for gas-cooled nuclear reactors); cryogenic cooling (e.g., dry ice); working fluid in power and heat pump cycles, beverage and food processing and preservation; pharmaceutical and processing industry; pneumatic systems; fighting; fire; powder processing; spray painting and coating; polymerization; separation technologies; crystallization processes; dyeing and dry cleaning of textiles; chemical extractions; various chemical reactions; and so on.

The total amount of CO_2 used in industry is equivalent to about 2% of the CO_2 emitted globally by power plants into the atmosphere. Therefore, capturing the CO_2 emitted by power plants could be economically attractive, as the captured carbon dioxide can be sold back to industry. Nevertheless, capturing carbon dioxide emissions from industrial processes (e.g., power generation sector, and cement and steel manufacturing, which are major pollutants), even if it is costly, is beneficial to the environment.

This chapter reviews those carbon dioxide technologies that have a link to sustainable energy applications.

14.2 Thermophysical Properties of Carbon Dioxide

There are many interesting properties of carbon dioxide that make it very attractive for a large range of applications. Its main thermophysical constants are compiled in Table 14.1. The critical point temperature is at 31.13°C at a pressure that can be

İ. Dinçer and C. Zamfirescu, *Sustainable Energy Systems and Applications*,
DOI 10.1007/978-0-387-95861-3_14,

Table 14.1 Main thermophysical constants of carbon dioxide

Molecular weight (g/mol)	Critical point			Triple point			Sublimation	
	T_c (K)	P_c (bar)	v_c (cm^3/mol)	T_t (K)	P_t (bar)	Δh_{fus} (kJ/kg)	T_s (K)	Δh_{sub} (kJ/kg)
44.01	304.13	73.75	94	216.59	5.18	204.95	194.68	571

Table 14.2 Coefficients for vapour-pressure equations (14.1–14.3) and fluid density (14.4)

i	a_i	b_i	$c_{i,L}$	$c_{i,V}$	$d_{i,L}$	$d_{i,V}$
1	−7.0602087	1.0	1.9245108	−1.7074879	0.34	0.34
2	1.9391218	1.5	−0.62385555	−0.8227467	0.5	0.5
3	−1.6463597	2.0	−0.32731127	−4.6008549	5/3	1.0
4	−3.2995634	4.0	0.39245142	−10.111178	11/6	7/3
5	N/A	N/A	N/A	−29.742252	N/A	14/3

considered moderate (73.75 bar); thus, supercritical carbon dioxide can be easily obtained. The supercritical carbon dioxide is very important in separation technologies where it is used as a solvent and carrier agent. By expansion over the transcritical region the carbon dioxide is transformed suddenly into gas, thus facilitating the separation from products that are in the form of solid or liquid particles.

There is no liquid state for carbon dioxide below 5.18 bar (which is the pressure of the triple point); therefore, at the standard pressure CO_2 is either a gas or a solid. Its sublimation temperature at standard pressure is −78.47°C. At these conditions, the carbon dioxide exists in the form of carbonic ice (or dry ice), which has many applications in food processing (making ice cream, flash-freezing foods) and in industry (e.g., for blast cleaning).

The experimental data for the critical region of carbon dioxide are exceptionally accurate, which means that these data are considered a benchmark for testing general thermodynamic models of critical-point–related phenomena. There were many equations of state for carbon dioxide developed between 1960 and 1996, as reviewed in Span and Wagner (1996). The melting pressure has been correlated with the temperature by Span and Wagner according to a simple quadratic equation:

$$\frac{P}{P_t} = 1 + a_1\tau + a_2\tau^2, \tag{14.1}$$

where $\tau = T/T_t - 1, T > T_t$. $T_t = 216.592\,\mathrm{K}$ is the triple-point temperature, $P_t = 0.51795\,\mathrm{MPa}$ is the triple-point pressure, and $a_1 = 1944.539$ and $a_2 = 2055.4593$ are two dimensionless constants (Table 14.2).

The melting curve can be observed in the *P–T* diagram shown in Fig. 14.1 as a curve that separates the solid and liquid regions. In the plot, the sublimation curve and the sublimation point at standard pressure are also indicated: this is the point of formation/sublimation of dry ice. The available experimental data for the sublimation

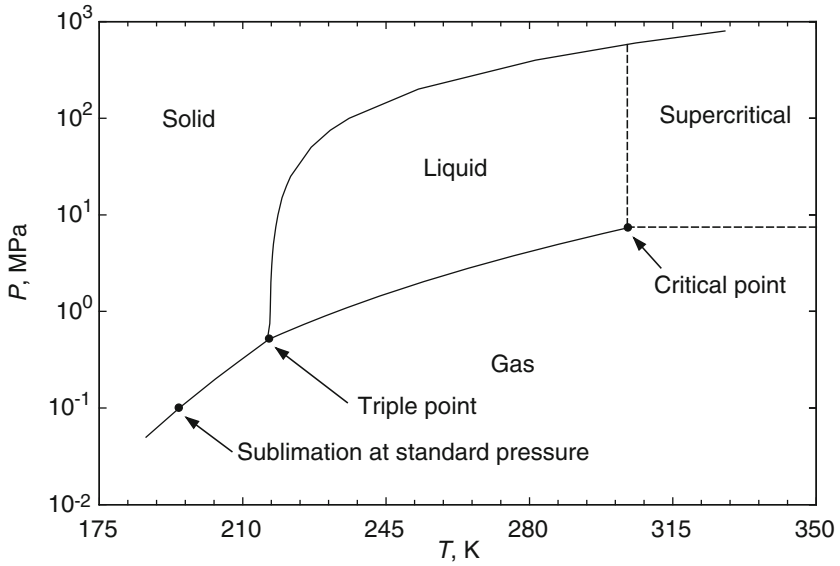

Fig. 14.1 The *P–T* diagram of carbon dioxide

pressure of carbon dioxide are exceptionally good and can be correlated with the following equation from Span and Wagner (1996):

$$\frac{P}{P_t} = \exp\left[\left(a_1\tau + a_2\tau^{1.9} + a_3\tau^{2.9}\right)/(1-\tau)\right], \tag{14.2}$$

where $\tau = 1 - T/T_t, T<T_t$, and $a_1 = -14.740846$, $a_2 = 2.4327015$, $a_3 = -5.3061778$.

The vapor-pressure line, which is the line separating the gas and liquid phases between the triple point and the critical point, in the *P–T* diagram from Fig. 14.1, is described by the vapor-pressure equation given also by Span and Wagner (1996), namely:

$$\frac{P}{P_c} = \exp\left[\left(\sum_{i=1}^{4} a_i\tau^{b_i}\right)/(1-\tau)\right], \tag{14.3}$$

where $\tau = 1 - (T/T_c), T_t < T < T_c$, and $(T,P)_c$ are the critical temperature and pressure, respectively.

The density data of saturated liquid and saturated vapor have been regressed by Span and Wagner (1996) with the following correlation:

$$\frac{\rho_{L,V}}{\rho_c} = \exp\left(\sum_{i=1}^{4} c_{i,L,V}\tau^{d_{i,L,V}}\right), \tag{14.4}$$

where index L stands for liquid and index V stands for vapor.

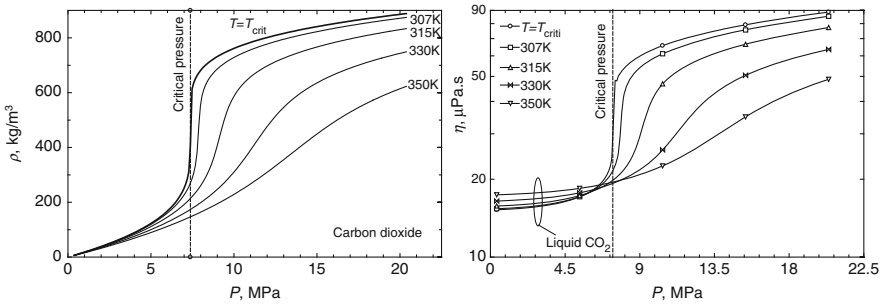

Fig. 14.2 Density variation with pressure across the transcritical region of carbon dioxide

The density variation along supercritical isotherms is presented in Fig. 14.2 for a range of pressures from subcritical to supercritical states. The Engineering Equation Solver (EES) (Klein 2010), which implements the Span and Wagner (1996) equation of state, has been used to calculate the data plotted in Fig. 14.2. A large density variation across the transcritical region where a small change in pressure produces important variation in density can be observed.

Moreover, if liquid carbon dioxide is compressed isothermally up to the supercritical pressure, one can observe a large variation in the dynamic viscosity over the transcritical region. These large variations in density and viscosity across the supercritical region make carbon dioxide an excellent agent for chemical separation technologies. Vesovic et al. (1990) developed a state-of-the-art equation for the transport properties of carbon dioxide: dynamic viscosity and thermal conductivity. These equations are employed here to calculate the viscosity plotted in Fig. 14.2 as well as the thermal conductivity shown in Fig. 14.3.

The surface tension of carbon dioxide, which is an important property that characterizes the fluid behavior at the interface with gas or solids, can be calculated with the equation developed by Somayajulu (1988):

$$\sigma\left[\mathrm{g}/\mathrm{s}^2\right] = a\tau^{5/4} + b\tau^{9/4} + c\tau^{13/4}, \tag{14.5}$$

where $\tau = (T_c - T)/T_c$, $a = 75.9675$, $b = -5.0913$, $c = 3.9907$. This equation is particularly relevant for carbon dioxide because it covers all liquid domains, from the triple point to the critical point.

The temperature–entropy diagram of carbon dioxide is presented in Fig. 14.4 as calculated with EES (Klein 2010) software. The critical isotherm is the boldface line to emphasize the delimitation between the supercritical fluid region and the gaseous region. It can be observed that in the range of common temperatures and pressures that meet in industrial practice, carbon dioxide is mostly in the supercritical fluid state. The melting line, which is indicated in Fig. 14.4, has been determined by calculating first the melting pressure for each temperature with Eq. (14.1) and then the associated entropy as a function of pressure and temperature.

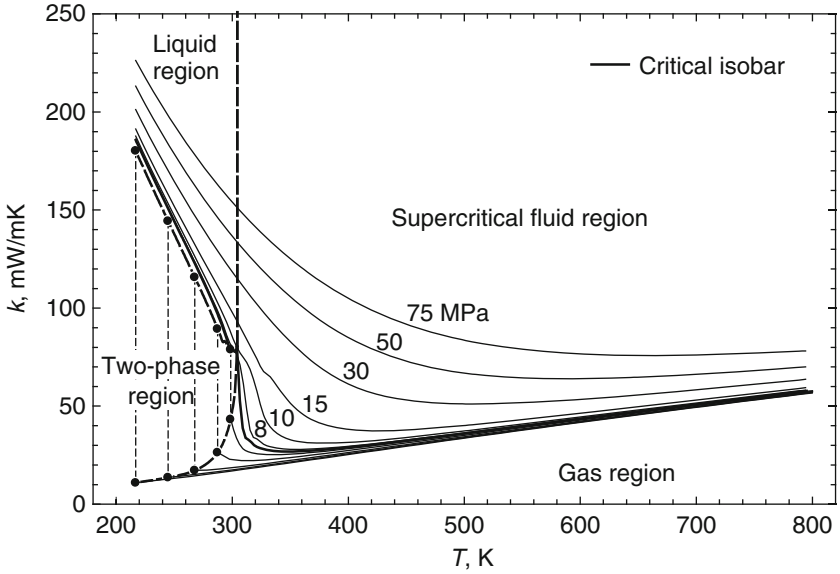

Fig. 14.3 Thermal conductivity of carbon dioxide

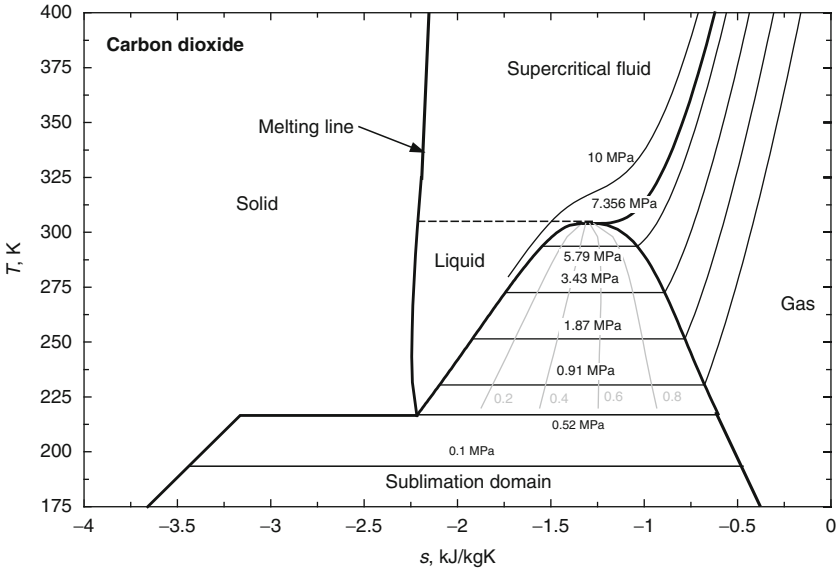

Fig. 14.4 *T–s* diagram of carbon dioxide

Separation of chemicals through supercritical CO_2 extraction technology involves mixing of chemicals with carbon dioxide, which transports the useful products and—by depressurization is converted sharply in gas—separating the

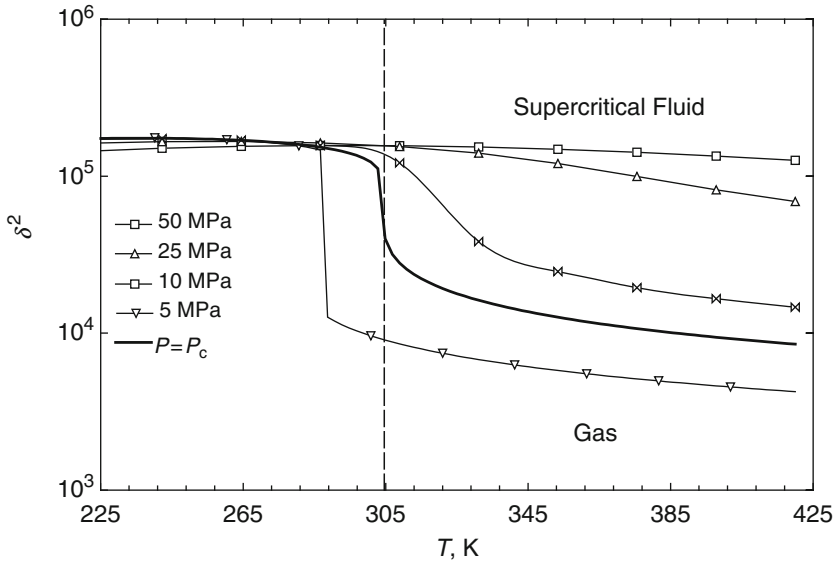

Fig. 14.5 The solubility strength of carbon dioxide

products that remain in solid (powder) or liquid phase. Of major importance in these technologies is the solubility of carbon dioxide, which, for extraction/separation purposes, must be high. In precipitation processes, the solubility of carbon dioxide is desired to be low to facilitate the process.

The solubility of supercritical carbon dioxide acting as a solvent can be adjusted from liquid-like values to gas-like values. The strength of the solvent can be quantified by the solubility parameter δ, which represents the square root of the cohesive energy density of the fluid introduced in Desimone and Tumas (2003) as

$$\delta^2 \cong \left(\frac{\partial u}{\partial v}\right)_T = T\left(\frac{\partial P}{\partial T}\right)_v - P, \tag{14.6}$$

where u is the specific internal energy of the fluid and v is the specific volume. An illustration of the solubility parameter for carbon dioxide, calculated based on (14.6) and employing the Span and Wagner (1996) equation of state, is presented in Fig. 14.5, which demonstrates the variation with one order of magnitude of this parameter in the supercritical and transcritical regions.

14.3 Technologies Using CO_2 as Heat Transfer Medium, Refrigerant, or Working Fluid

There are a number of already mature technologies that exploit the qualities of carbon dioxide as a heat transfer medium or working fluid. Here we mention first dry ice, which, because of its property of being "dry," finds many industrial

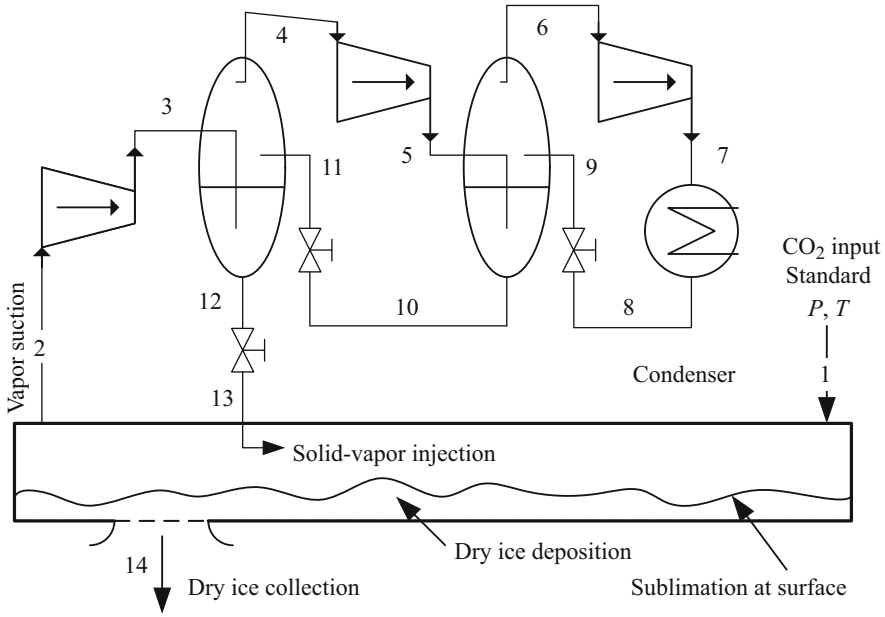

Fig. 14.6 Typical layout of a dry ice production plant

applications such as food preservation by chilling, food processing (e.g., ice cream), process technology, and machining (blast cleaning). Carbon dioxide in the liquid phase is an excellent heat transfer fluid for cooling. Such a technology is used for commercial refrigeration systems where a central refrigeration plant cools liquid CO_2, which in turn is used to transport the cold to refrigerated displays or cabinets. Carbon dioxide can be used also as a heat transfer fluid in advanced gas-cooled reactors. Furthermore, CO_2 can be used as working fluid in supercritical power cycles and heat pumps. In this section, we review some relevant technologies using carbon dioxide as either a heat transfer medium or working fluid.

Dry ice production technology is shown in Fig. 14.6, which illustrates the typical layout of such a plant. In general, dry ice plants are coupled with ammonia plants that produce ammonia either from coal or natural gas or other petroleum products (e.g., naphtha). During the process, large quantities of carbon dioxide are separated and collected. Carbon dioxide has several downstream uses such as production of urea, production of dry ice, production of liquid CO_2 to be used in various industries, or the carbon dioxide is stored in the supercritical state.

The collected carbon dioxide is cooled as close as possible to the environment temperature (say, down to standard temperature and pressure) and enters the plant at state 1. There the carbon dioxide is blown over the surface of the dry ice deposit, which has the temperature corresponding to the sublimation point at standard pressure, which is 198.68 K. During this process, the stream of carbon dioxide cools down by direct contact with the dry ice and by mixing with the gas that sublimated;

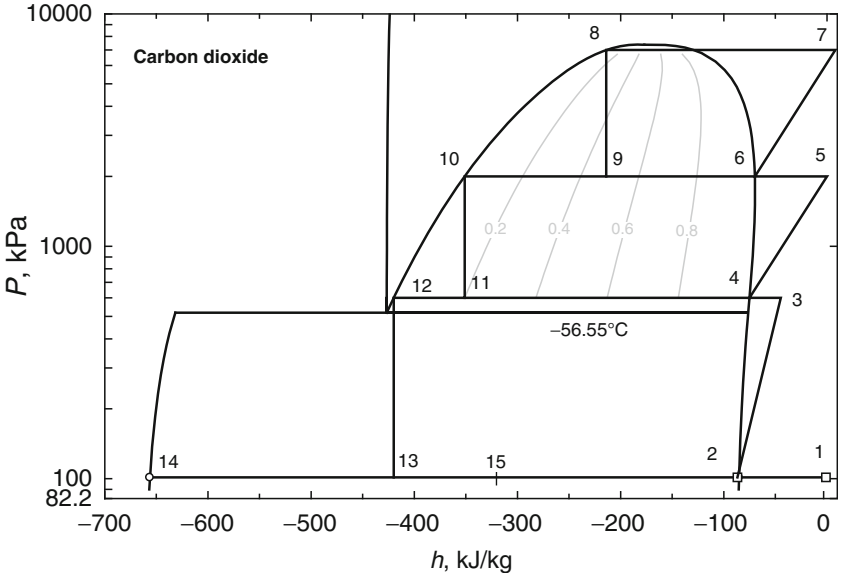

Fig. 14.7 The process of dry ice production in a *P–h* diagram

eventually the CO_2 reaches the thermodynamic equilibrium with the dry ice such that at state 2 the vapors are at saturation. Further, the vapors are compressed in three stages: 2–3, 4–5, and 6–7. After each compression stage, the superheated vapors are cooled by direct contact with cold CO_2 liquid, which is at the same pressure and saturation temperature. The direct contact cooling is made in three liquid–vapor separators. At the discharge of the last phase, the pressure reaches about 70 bar, which corresponds to a condensation temperature of about 29°C. The condensed liquid at state 8 is then throttled and injected at state 9 into the higher pressure liquid–vapor separator. The liquid collected at the bottom of this separator at state 10 is further throttled and injected at state 11 in the lower pressure liquid separator where it helps cool the superheated vapors discharged by the first-stage compressor. Further, the liquid accumulated at the bottom of the lower pressure separator is collected at state 12 and expanded to standard pressure at state 13. During this process, vapors are formed, and due to important cooling effects the remaining liquid solidifies completely, forming dry ice flocks that deposit due to gravitational separation at the bottom of a closed collection tray. The tray is provided with appropriate mechanical systems to move the deposited dry ice and compact it further into large blocks or pellets. Moreover, the tray is designed so that it allows heat and mass transfer at the dry ice surface with the fresh CO_2 stream that must be cooled prior to compression.

The *P–h* diagram of the dry ice manufacturing process is shown in Fig. 14.7. Mass balance and energy balance equations can be written for each system component to perform thermodynamic analysis. The dry ice collection tray system also has the role of cooling the carbon dioxide intake stream.

The mass balance for the dry ice tray is written as

$$\dot{m}_1 + \dot{m}_{13} - \dot{m}_2 - \dot{m}_{14} = 0, \tag{14.7}$$

where one also note that at steady-state operation (see Fig. 14.6) the mass flow rate of carbon dioxide that enters the compression system must be the same as the expanded quantity, that is $\dot{m}_{13} = \dot{m}_2$. Therefore, $\dot{m}_{14} = \dot{m}_1$. On the other hand, the energy equation is

$$\dot{m}_1 h_1 + \dot{m}_{13} h_{13} - \dot{m}_2 h_2 - \dot{m}_{14} h_{14} = 0, \tag{14.8}$$

from which one can determine the vapor fraction in the tray, denoted here with x_{15}:

$$x_{15} = \frac{\dot{m}_2}{\dot{m}_1 + \dot{m}_2} = \frac{h_1 - h_{14}}{h_2 - h_{13} + h_1 - h_{14}}. \tag{14.9}$$

The fraction of produced ice becomes $y_s = 1 - x_{15}$, and the consumed compression work to produce this quantity is

$$w_{comp} = h_3 - h_2 + h_5 - h_4 + h_7 - h_6. \tag{14.10}$$

If the quantity y_s of produced ice is fully used for refrigeration purposes, its enthalpy varies from h_{14} to h_1. Therefore, the total refrigeration effect is given by

$$q_{ref} = y_s(h_1 - h_{14}). \tag{14.11}$$

One can define a coefficient of performance (COP) for the dry ice production system, in a similar manner as for mechanical refrigeration systems. This can be

$$\text{COP} = q_{ref}/w_{comp}. \tag{14.12}$$

In Table 14.3, we present, as an example, calculated state parameters for the system presented in Fig. 14.6. It has been assumed that the isentropic efficiency of all compressors is 0.7. In these conditions, the calculated ice fraction is 35%, which means that the system produces 34 kg of ice per 100 kg of CO_2 compressed by the three-stage compression station. The associated COP of the system is 1.13. A practical indicator is 1 MJ of electricity per kg of dry ice.

Note that apart from being a refrigerant or to serve for abrasive blasting in manufacturing processes, dry ice can be considered an excellent medium for carbon dioxide storage, sequestration, or transportation. The dry ice density is around 1,500 kg/m^3.

We illustrate in the next paragraph how carbon dioxide can be used as working fluid or coolant in refrigeration and power cycles. In Fig. 14.8, a supercritical carbon dioxide cycle is shown where the working fluid is pumped up to 200 bar

Table 14.3 Calculated state parameters for the dry ice plant from Fig. 14.6

State	h (kJ/kg)	P (kPa)	T (°C)	s (kJ/kg K)	x
1	−0.9383	101.3	25	−0.002199	Superheated
2	−86.86	101.3	−78.47	−0.5428	1
3	−44.86	600	−19.45	−0.4917	Superheated
4	−75.13	600	−53.12	−0.6198	1
5	−0.05486	2,000	45.07	−0.5464	Superheated
6	−69.93	2,000	−19.5	−0.7929	1
7	8.172	7,000	90.29	−0.7268	Superheated
8	−213.9	7,000	28.68	−1.433	0
9	−213.9	2,000	−19.5	−1.361	0.4882
10	−351.3	2,000	−19.5	−1.902	0
11	−351.3	600	−53.12	−1.875	0.1993
12	−420	600	−53.12	−2.187	0
13	−420	101.3	−78.47	−2.225	0.4166
14	−657.9	101.3	−78.47	−3.426	0

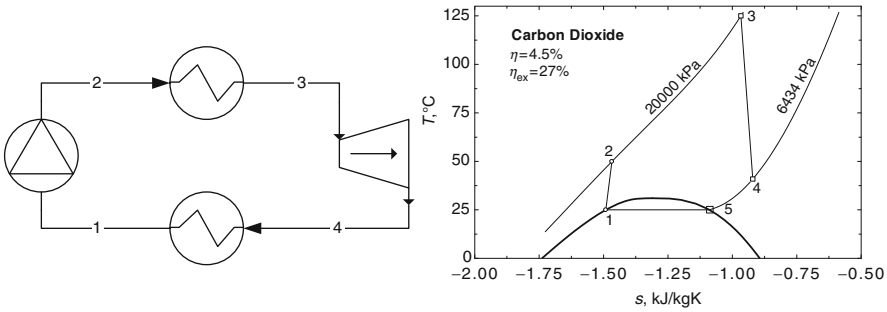

Fig. 14.8 Supercritical CO_2 power cycle

and heated to 125°C before expansion at points 3→4. The calculated efficiency by assuming turbine's isentropic efficiency of 70% is 4.5%, while the exergy efficiency is defined as

$$\psi = \frac{h_3 - h_4 - h_2 + h_1}{(h_3 - h_2) - T_0(s_3 - s_2)}, \tag{14.13}$$

where T_0 is the reference temperature (27%). This kind of cycle has practically no pinch point; therefore, one can better use the temperature of a sensible thermal energy source; the profile of temperatures at the heat source (the hot fluid and working fluid temperature) can be matched with each other to minimize the overall temperature difference.

Supercritical carbon dioxide also has excellent heat transfer properties that allow for better and more compact heat exchangers with respect to those for common working fluids. The fact that the operation of power and refrigeration (heat pump)

cycles with transcritical or supercritical carbon dioxide works at high pressure represents an advantage with respect to the specific volumetric enthalpy of the working fluid, which is higher at elevated pressures. Therefore, the circulated flow rates are smaller, and as a consequence the compressors or expanders are more compact. Obviously, supercritical CO_2 technology requires materials that resist at high pressures in conjunction with moderate temperatures. Such materials do exist and the associated manufacturing technology, too. For example, it is preferred that the CO_2 heat exchangers are made with microchannels extruded in aluminum plates; such heat exchangers are characterized by high power per unit of volume and mass.

The cycle presented in Fig. 14.8, which is a special kind of Rankine cycle, can be inverted, and in this way a carbon dioxide heat pump or a carbon dioxide refrigerator is obtained. Since 1990, there has been a renewed interest in carbon dioxide as a natural refrigerant. A number of conferences were initiated by Gustav Lorentzen as a consequence of his seminal work in this area (Lorentzen 1994).

14.4 Supercritical Carbon Dioxide Technologies in Process Industries

There are many processes in the industry for the separation of materials. Think for example of a chemical reactor in which the reactants are introduced to perform the desired chemical reaction and obtain the resulting products. However, no chemical reaction can achieve completeness since the chemical kinetic reactions evolve until equilibrium is reached in the reactor. Therefore, at the reactor outlet one finds, in general, a mixture of products with unreacted reactants plus other chemical species. Commonly, downstream of the reactor the separation of the product and the reactants occurs, such that pure products exit eventually out of the process while the reactants are recycled. Several kinds of separation technologies are available, such as cyclones, separation by condensation or distillation, separation by freezing or cryogenics, separation by solvents, crystallization, osmosis, and others. Separation technologies are crucial for many kinds of chemical and physical processes in the industry. An example from the food industry is the extraction (separation) of caffeine from coffee beans, which can be done by distillation, crystallization, or reverse osmosis; all these processes may involve the use of other chemicals that in some instances are considered harmful to health. In recent years, technologies for separating caffeine using supercritical carbon dioxide have been developed; they have the benefit of being a nonharmful process and cost-effective. Supercritical CO_2 is also used in textile dyeing in a process in which carbon dioxide it used to dissolve the dye and to transport it to the textile material; after impregnation, the pressure is sharply reduced to atmospheric values, and the supercritical carbon dioxide transforms into gas and is collected and recompressed. Other uses of supercritical CO_2 include polymerization and drug processing. Here we present some relevant technologies that use supercritical CO_2 for the separation of materials.

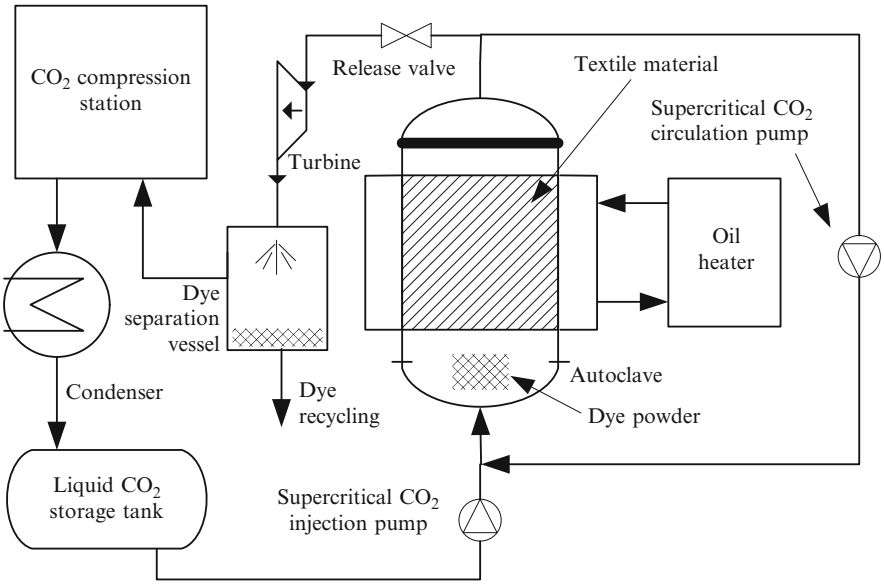

Fig. 14.9 System for textile dyeing using supercritical carbon dioxide as dye solvent

The system shown in Fig. 14.9 illustrates the use of supercritical CO_2 for textile dyeing. Dyeing requires a dye, which is in general a powder-like chemical, and a solvent that dissolves the dye and transports it to the surface where it is applied. Chemical or physical reactions, or both, occur when the dye is in contact with the material to be covered. The solvent must be removed by a process such as drying so that the dye remains firmly on the material. In the textile industry the most used solvent is water. Water is needed in large quantities to transport the dye, and large quantities of heat are needed to release the water through evaporation and drying of the product. Supercritical carbon dioxide technology has been developed in recent years (see, e.g., Fernandez Tumas Cid et al. 2004). The advantages of the supercritical carbon dioxide over other common dyeing systems can be summarized as follows:

- Supercritical CO_2 is an excellent solvent to dissolve the dye, and its solubility can even be adjusted by regulating the operating pressure and temperature.
- Supercritical CO_2 has high diffusivity and low viscosity; therefore, it easily transports the dissolved dye to the material where it is applied; this results in faster diffusion of dye and a shorter dyeing process.
- After the fixation time period, the supercritical carbon dioxide is quickly removed by expanding it to an ambient pressure, a process during which the CO_2 transforms into gas and separates easily from the residual dye.
- The carbon dioxide can be recycled by recompression and condensation, and stored as pressurized liquid at standard temperature.

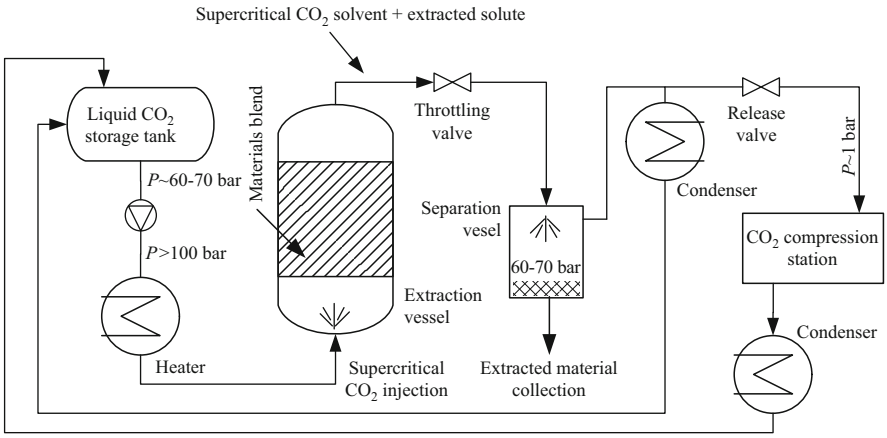

Fig. 14.10 Extraction–separation process with supercritical CO_2

In the above concept, the textiles are placed in an autoclave that can operate at temperatures up to about 150°C and pressures up to 200 to 300 bar. At the bottom of the autoclave is placed a basket with powder dye. The autoclave is heated with oil circulated in a double mantel. Supercritical CO_2 is injected at the bottom of the autoclave with the help of a pump. While passing over the powder dye basket, the supercritical liquid-like CO_2 dissolves the dye and transport it to the deposition place—that is, the textile material. The solvent–solute fluid is recirculated with a pump in a loop for a certain time such that the paint can penetrate the textile pores and fix on the surface. When the process is ready, the release valve (see above) is open and the carbon dioxide carrying the dissolved dye is expanded to ambient pressure with work recovery in a turbine. At ambient pressure the carbon dioxide converts in the gas phase while the dye converts back in the powder phase. In the separation vessel, the dye is separated from the gaseous CO_2, which is then recompressed by a compression station (up to about 70 bar) and then condensed and collected and stored in pressurized liquid form for the next use.

A general setup for the supercritical extraction and separation process that can be applied to a variety of cases is shown in Fig. 14.10. In the extraction vessel, a blend of materials from which one component must be extracted and separated is placed. The carbon dioxide, which is stored in the pressurized liquid phase at ambient temperature, is compressed to supercritical pressure and injected at the bottom of the extraction vessel. While diffusing through the material bed, the supercritical carbon dioxide dissolves the desired component. As discussed above, the solubility strength can be adjusted by modifying the operating pressure and temperature. At the top of the extraction vessel exits the supercritical fluid carrying the extracted component. Next, this mixture is expanded sharply such that CO_2 converts in the gaseous phase and separates from the other components, which remain either in solid (powder) or liquid (droplets) phase. The extracted material is collected at the bottom of the extraction vessel, which operates usually at a pressure of 60–70 bar, a

Table 14.4 Extraction efficiency of metals from dry soil using supercritical CO_2 and a ligand

Metal	80 bar	120 bar	160 bar	200 bar
Cu	8	29	46	55
Cd	6	21	41	49
Pb	2	6	11	21
Zn	5	28	50	55

Data from Kersh et al. (2000)

pressure at which the CO_2 can be condensed at ambient temperature. Therefore, for recycling of CO_2, condensation is applied and the resulting liquid is returned in the liquid tank. When the process ends, the CO_2 is expanded to atmospheric pressure and removed from the loop by suction in the compression station and further compression and condensation.

A concrete example of supercritical extraction and separation can be that of poisonous metal removal from flue gases or soil. Municipal incinerators burn various waste materials through a process resulting in flue gas being expelled in the atmosphere. Because of the nature of the combusted materials, the concentration of metal atoms in flue gas is high. Similarly, the concentration of poisonous materials in soil is elevated in landfills. It is possible and effective to use supercritical carbon dioxide in combination with various chemical ligands to extract metals from flue gas or soil (see, e.g., Kersh et al. 2000). Such metals are present in the form of ions like Cu^{2+}, Pb^{2+}, Cr^{2+}, Cd^{2+}, and Zn^{2+}. In the technology developed by Kersh et al. (2000), the solvating strength of supercritical CO_2 is combined with the chemical reactivity of metal ions and the selectivity feature of organic ligands to develop an effective method for extraction of the desired species. The extraction efficiency can be defined as

$$\eta_{\text{ext}} = m_{\text{ext}}/m_{\text{inp}}, \tag{14.14}$$

signifying the mass of the metal extracted with respect to the mass of the metal present in the input material. Table 14.4 lists the extraction efficiency obtained by Kersh et al. (2000) for metal extraction from dry soil using Cyanex 302 as the ligand for a duration of the process of 40 minutes at 45°C.

14.5 Technologies for Carbon Dioxide Capture from Flue Gas

Many technological processes depend on the combustion of fuels or the incineration of materials. Combustion of fuels produces a primary source of heat at high temperature, which can be used either directly as heat or can be converted into electricity by power plants. In any of these situations, combustion leads to carbon dioxide emission as a product of the combustion of any carbonaceous material.

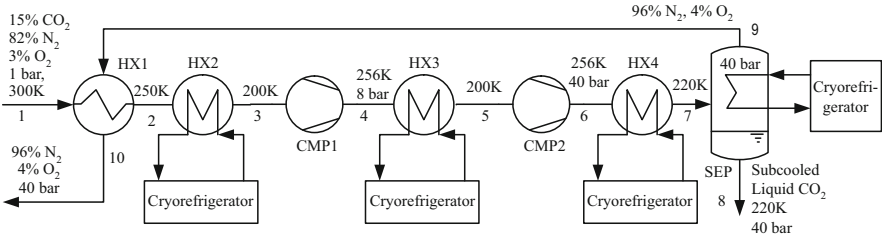

Fig. 14.11 Cryogenic separation of carbon dioxide from flue gas (*HX* heat exchanger; *CMP* compressor; *SEP* separator)

The flue gas emitted into the atmosphere is a major source of pollution and, due to the high concentration of carbon dioxide, is a contributor to global warming.

There is obvious interest in capturing carbon dioxide from flue gases in view of further compression or sequestration (storage) in a condensed phase. In this section, we present the main methods of carbon dioxide capturing from flue gases. A process that operates combustion without any emission of carbon dioxide is usually denoted as a "zero emission process." One can thus have zero emission power plants, zero emission H_2 production from CH_4, and so on. A review of carbon capture technologies can be found in Aaron and Tsouris (2005). Flue gas contains mainly nitrogen (about 80%) followed by carbon dioxide (8–15%), steam (~6%), oxygen (2–4%), and other gases present at the level of parts per million (ppm): SO_x (200–2,000 ppm), NO_x (50–70 ppm), CO (70–110 ppm). NO_x is reduced with ammonia and converted to nitrogen and steam, SO_x can be removed by dry alkaline adsorption before particulate matter elimination, or sodium bicarbonate can be added to the flue gas to release sodium carbonate, steam, and carbon dioxide; further, sodium carbonate reacts with SO_2 in the presence of carbon dioxide and forms solid sodium sulfate that precipitates. Alternatively, limestone ($CaCO_3$) and water can be injected into flue gas to form calcium sulfite ($CaSO_3$), which is further oxidized to form gypsum ($CaSO_4$). In the paragraphs that follow we assume that the flue gas has been treated to eliminate particulate matter and all other components, and the remaining gas comprises only nitrogen, oxygen, and carbon dioxide.

We first discuss the carbon dioxide separation process by cryogenic distillation. A possible process for cryogenic distillation (also called cryogenic separation) of carbon dioxide from flue gas is shown in Fig. 14.11. The process starts with the intake of flue gas with the composition of 15% CO_2, 82% N_2, and 3% O_2, which is representative of many practical situations. In the first step, the flue gas stream is cooled from the ambient temperature (300 K) to 250 K using a cold stream of 96% nitrogen and 4% oxygen, which results from the process itself. Note that the partial pressure of carbon dioxide in the flue gas is 15 kPa in accordance with its concentration.

The flue gas is further cooled to 200 K using a cryorefrigerator (which can work in principle with carbonic ice). The cold stream at state 3 is compressed up to 8 bar at state 4 where the partial pressure of CO_2 reaches ~1.25 bar. Further, the stream is cooled again to 200 K, a temperature at which the carbon dioxide almost reaches

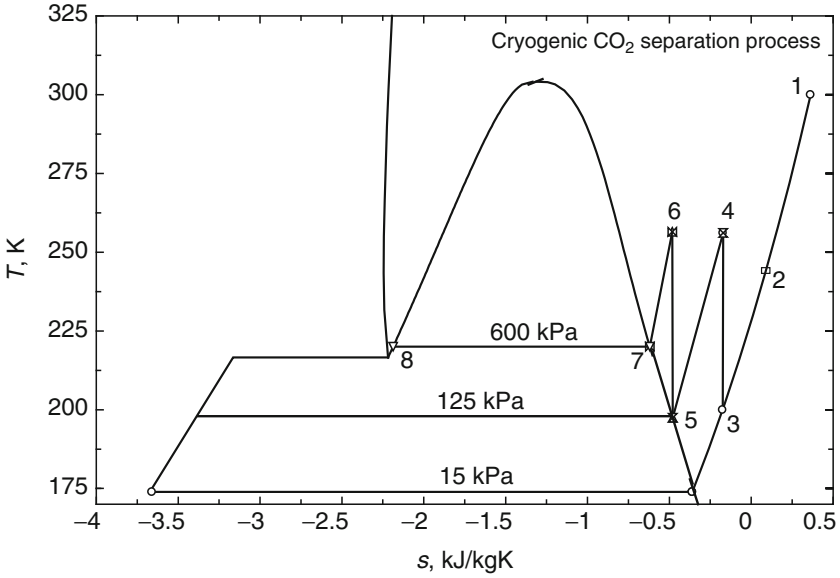

Fig. 14.12 The process of cryogenic CO_2 separation represented in a *T*–*s* diagram

saturation. In the second stage of compression, the pressure is raised to 40 bar, for which the partial pressure of CO_2 is 6 bar, which is slightly above the triple point. It follows the cooling of the stream down to 220 K, where the carbon dioxide vapor reaches the saturation at state 7. The flue gas stream is discharged into a liquid gas separator that is continuously cooled by a cooling coil coupled with a cryorefrigerator. Consequently, the CO_2 condenses at state 8 and is collected at the bottom of the separator vessel. The remaining gases (nitrogen and oxygen) are extracted at the top of the vessel; the composition in the return gas line becomes 96% nitrogen and 4% oxygen. The return gas is cold; it has a temperature of 220 K and enough enthalpy to cool the intake flue gas in the heat exchanger HX1 from 300 to 250 K. The expelled gas being at high pressure can be expanded in a turbine after heating it at a higher temperature. The liquid carbon dioxide collected at state 8 is subcooled; it can be further pumped to about 70 bar and its coldness used for any useful cooling; after pressurizing, this stream can be heated up to ~25°C and remains in a subcooled liquid state. The diagram of the process is presented in Fig. 14.12, in which the indicated pressures are the partial pressures of carbon dioxide at various state points.

Cryogenic separation of CO_2 is attractive because it produces high-purity liquid (>99.9%) ready for transport and sequestration. As it requires cryogenic cooling and gas compression, the process is expensive, namely, according to Gottlicher and Pruschek (1997), around $30 per ton. About one fourth of the primary energy of a power plant must be consumed to separate cryogenically the carbon dioxide from flue gas, and store it in liquid or dry ice form.

Another mature technology for separating carbon dioxide from flue gas uses selective diffusion of chemicals through membranes. A variety of materials are

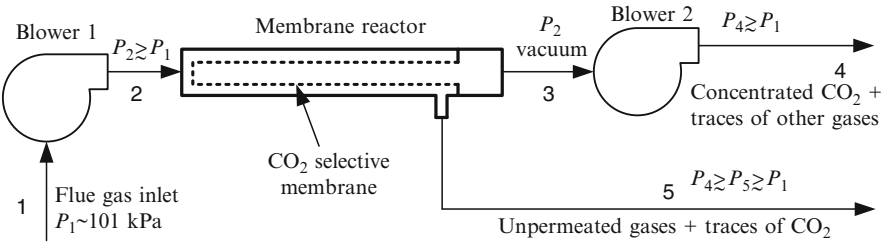

Fig. 14.13 Arrangement for CO_2 separation from flue gas through membranes

used as carbon dioxide membranes, depending on the application, such as metallic materials, ceramics, polymers, and inorganic chemicals. What is important is the degree of selectivity of the membrane to the chemical species to be separated. A typical arrangement for membrane CO_2 separation from flue gas is shown in Fig. 14.13. The flue gas is circulated by a blower that increases its pressure to compensate for a pressure drop across the reactor. The membrane reactor is a basic mass exchanger possessing a selective membrane that is permeable to carbon dioxide. On the other side of the membrane, the carbon dioxide is collected and the pressure is maintained low (typically at 10% from the pressure upstream of the reactor). In general, the partial pressure of carbon dioxide upstream is about 15 kPa while at the feed side it is 10 kPa. The difference between the partial pressures generates the driving force of carbon dioxide diffusion through the membrane. The unpermeated gases contain traces of CO_2, and the permeated one contains traces of other gases too.

In a single-stage separation, the carbon dioxide can be concentrated from 15% at the feed to about 45% at the outlet. The membrane reactors can be cascaded. In such an arrangement, the second stage accepts carbon dioxide of 45%, which is concentrated to about 90%. The great advantage of the membrane reactor is that it can operate, depending on the type of membrane, either at ambient temperature or at high temperature; therefore, the method of membrane separation offers large freedom for implementation. Moreover, compared with cryogenic distillation and other methods that need mechanical work for sustaining compression process, the energy penalty at membrane separation is much lower.

In the oil industry, the membrane separation of carbon dioxide from light hydrocarbon is an established technology. An important breakthrough in the membrane technology happened in the middle of the twentieth century when polymer membranes were invented. Two mechanisms of diffusion are possible within polymer membranes: solution diffusion and absorption diffusion. These mechanisms confer selectivity to molecule transport; the polymeric membranes are "impregnated" with chemicals that allow mass transport of the desired species (in this case carbon dioxide) and do not facilitate the transport of other species. The mechanism of transport is more likely dissolution of carbon dioxide into a solvent that is entrapped in the polymeric matrix of the membrane and further released after permeation.

The metallic membranes have a simpler mass transfer mechanism than do polymeric membranes. They basically act as sieves that filter smaller molecules.

In recent years, however, metallic membranes were developed that are impregnated with solvents that allow for a better membrane selectivity and operation at higher temperatures. In general, metallic membranes operate at temperatures over 350°C as opposed to polymeric membranes operating at ambient temperature conditions.

Membrane reactors comprise a membrane module (which is the active part) that does the separation. The membrane module can be of the spiral wood type, plate and frame type, capillary or background type, or cartridge type. Fouling and pore clogging is a common phenomenon with membranes; therefore, maintenance must be applied regarding membrane cleaning or replacing. The smaller the membrane's pores, the higher are the chances of clogging, and the membrane permeation is better. The permeation of a membrane, which, for first-modeling approximation can be assimilated to a capillary tube, is proportional with the volumetric flow rate, which, for the established laminar flow in the capillary, is

$$\dot{V}_{\text{mem}} = \frac{\pi}{128} \frac{\Delta P d^4}{\eta \delta}, \tag{14.15}$$

where ΔP is the pressure difference driving the flow over the membrane, d is the pore diameter, η is the viscosity, and δ is the membrane thickness.

As can be seen, if the pore diameter is reduced, that is, if the membrane is made more selective, the permeability decreases for the same pressure differential. The membrane design strategy implies the determination of the pore size in the first design phase. Once the pore diameter is known, the membrane thickness must be established. There is a design trade-off, so that for an imposed permeation one can select the membrane thickness in a range from thin to thick. If the membrane is thin, the pressure drop across it is reduced, but from a structural point of view the membrane is fragile. In this situation, the operating cost of the membrane reactor is reasonable, but its lifetime is short. On the other hand, a thick membrane is structurally strong, but the associated operating cost is high because of the large associated pressure drop. Another design factor is membrane selectivity. A thicker membrane is more selective, because the residence time of the molecules that diffuse through the pores is higher. In brief, a better selective membrane has a larger associated pressure drop and associated operating costs, while a thinner membrane operates at a lower cost but poorer selectivity.

It is interesting to note that the carbon dioxide molecule is smaller than the nitrogen and oxygen molecules; in angstroms, the radii of these molecules are 3.3 for CO_2, 3.5 for O_2, and 3.6 for N_2. From Eq. (14.15) under the approximation that the area of the membrane (A) is about the same as the area of one pore times the number of pores, it results that the mass flux through the membrane, defined as the mass flow per unit area ($j = \rho \dot{V}/A$), is

$$j \sim \frac{\Delta P d^2}{v \delta}. \tag{14.16}$$

At the same time the mass flow through the membrane can be expressed as a summation of mass flow of each component, that is, $j = \sum j_i$, where the mass flux of any component depends on the diffusivity, which, according to Cen and Lichtenthaler (1995) can be expressed by Fick's law, namely,

$$j_i = -D_i \rho \frac{\mathrm{d}C}{\mathrm{d}\delta}, \tag{14.17}$$

an expression that can be integrated across the membrane thickness, where at the feed the solute concentration is C_F and at the outlet the permeate concentration is C_P. Therefore,

$$j_i = \frac{\rho}{\delta} \int_{C_\mathrm{P}}^{C_\mathrm{F}} D_i \mathrm{d}C. \tag{14.18}$$

The purpose of the design is to maximize the mass flux of the selected component (e.g., the carbon dioxide, $j_{\mathrm{CO_2}}$) while minimizing the mass flux of the other diffusing elements. The permeability of the membrane can be defined, then, as $\alpha_i = j_i / \sum j_i$. One example of a membrane designed to separate carbon dioxide from flue gas, applied after all water has been condensed and the gas is at a temperature close to that of the ambient, is shown here based on a recent research by Yave et al. (2010). A nanostructure membrane has been devised based on a polymer impregnated with polyethylene glycol dimethyl ether. The selectivity of the membrane separating carbon dioxide from nitrogen is defined by the ratio $\alpha_{\mathrm{CO_2/N_2}} = \alpha_{\mathrm{CO_2}} / \alpha_{\mathrm{N_2}}$. It is reported that on average, the selectivity of carbon dioxide is about 40; this means that the carbon dioxide is ~40 times more permeable than nitrogen.

The porous electrodes—similar to membranes—can be used to separate CO_2 from physical sorbents under the influence of the electrical field. This is a method of electrical desorption (see Aaron and Tsouris 2005) for separating the carbon dioxide and the proposed carrier quinone ($C_6H_4O_2$). Figure 14.14 proposes a device to conduct electrical desorption. A membrane permeable to carbon dioxide is placed at the low-pressure side (right side of the figure). At the permeate side, quinone, found in the liquid state, is circulated by a pump. The membrane must be made from an electrical conductive material because it must act as an electrode polarized at "minus" electrical charge. Quinone polarizes and captures a molecule of carbon dioxide, becoming an ionic liquid, $C_6H_4O_2CO_2^{2-}$. The carbon dioxide carrying quinone is pressurized at high pressures (possible about 70 bar) and enters another membrane reactor that has its membrane connected at positive polarity. Quinone releases the carbon dioxide molecule, which diffuses through the membrane and is collected at the other side. The high pressure of the collected carbon dioxide allows for condensation at ambient temperatures, and therefore it facilitates the storage in liquid or in a supercritical state.

Absorption of carbon dioxide in sorbents is the most established carbon dioxide separation technology to date. In this technology, a liquid sorbent is used to scrub the carbon dioxide from flue gas. The solvent is selective: it dissolves only carbon dioxide but not nitrogen, oxygen, or other gases present in the flue gas.

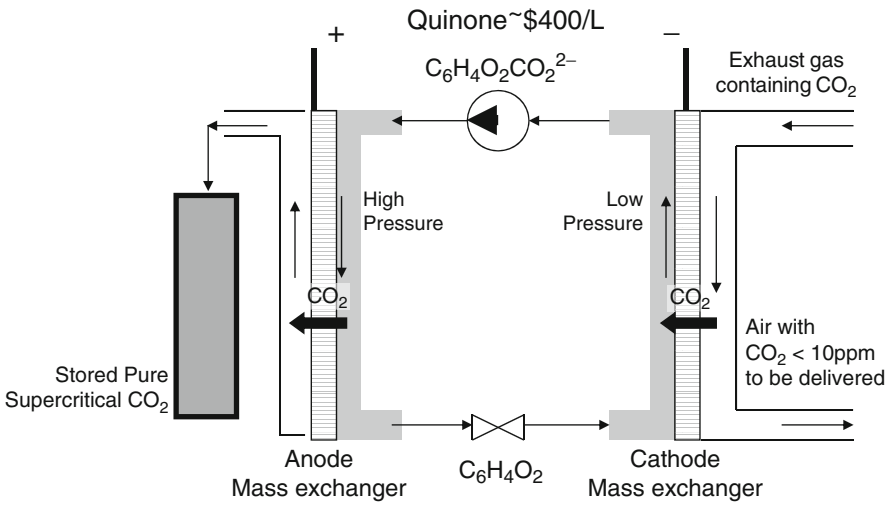

Fig. 14.14 Electrical desorption for carbon dioxide separation

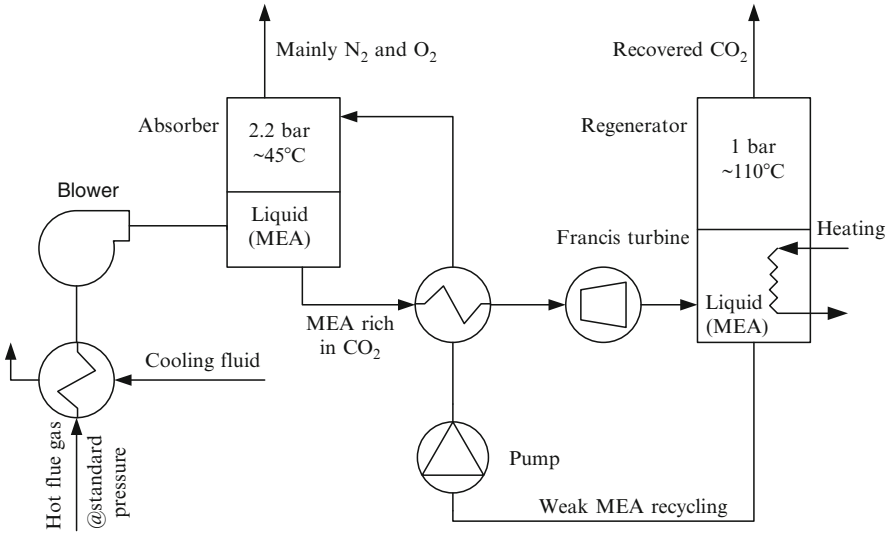

Fig. 14.15 Typical carbon dioxide absorption system

After absorption, the carbon dioxide is stripped out of the solution by swinging the pressure and temperature, while the liquid solvent is recycled.

A typical solvent for carbon dioxide absorption is monoethanolamine (MEA), which operates at pressures slightly higher than the standard (~2.5 bar) in the absorption phase and at standard pressure for the regeneration phase. The MEA process is presented in Fig. 14.15. In this process, the flue gases must be cleaned

first to remove water content and other contaminants like particulate matter and SO_x and NO_x. Then, the remaining hot flue gases are cooled down to about 45°C and pressurized with the help of a blower up to 2.5 bar; these are the optimal temperature and pressure for the absorption process. At these conditions most of the carbon dioxide is absorbed in liquid MEA, which is withdrawn at the bottom of the absorber. At the top of the absorber, the remaining gases—having almost zero carbon dioxide content—are expelled into the atmosphere. The MEA rich in carbon dioxide is heated to about 110°C, which is the typical temperature for CO_2 release. Thereafter, the hot liquid can be expanded to standard pressure to recover some work. The rich liquid is injected into the regenerator, which is continuously heated so that it releases gaseous carbon dioxide, which is collected at the top of the regenerator. Due to the carbon dioxide release, the MEA solution is regenerated and it can be pumped back to high pressures for a new absorption cycle. The actual system diagram is more complicated because it must include flash condensers and reboilers that are used to make the regeneration process more efficient. MEA is applicable for low concentrations of carbon dioxide in flue cases (lower than 15% concentration). Other solvents do exist for these conditions and some of them can absorb 20% more than MEA. In the case when the concentration of carbon dioxide in flue gas is higher, solid sorbents like those based on lithium or calcium are recommended. If the absorption is made with solid sorbents, then the regeneration temperature is extremely high (higher than 800°C).

The method of adsorption of carbon dioxide in pores of solid materials has also been applied to remove CO_2 from flue gas (see Aaron and Tsouris 2005). Carbon dioxide can be adsorbed by porous coal beds or zeolites. To make the adsorption process cyclically, three basic methods are available: pressure swing adsorption (PSA), temperature swing adsorption (TSA), and electrical swing adsorption (ESA). In temperature swing adsorption, the process of carbon dioxide adsorption and release is controlled by temperature, while in PSA it is controlled by pressure swing.

14.6 Transportation and Sequestration Technologies for Carbon Dioxide

Once the carbon dioxide is captured from a process, it has to be stored in some form. Storage of carbon dioxide is a sustainable alternative to emitting it into the atmosphere where it acts as greenhouse gas. The general term for carbon dioxide storage when this is done with the purpose of avoiding emitting it into the atmosphere is "sequestration." The storage can be short term or very long term (e.g., ocean deep sequestration has a time range of more than 100 years). Another factor regarding sequestration is carbon dioxide transport. Transport is needed to move the carbon dioxide from capturing sites to sequestration sites. In this section, we discuss and analyze some methods for carbon dioxide transportation and sequestration.

If ammonia water is sprayed over flue gas at a temperature around 60°C, the process of ammonia carbonation occurs (see Fig. 14.16). Through this process,

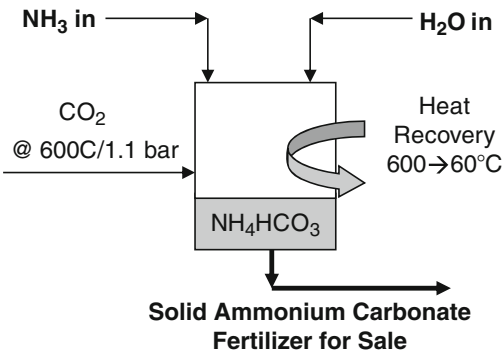

Fig. 14.16 Diagram for carbon dioxide sequestration through ammonia carbonation

Table 14.5 Thermodynamic values for the ammonia carbonation reaction (14.19)

Chemical	h^0 (kJ/mol)	s^0 (J/mol K)	g^0 (kJ/mol)
CO_2 (g)	−393.4	213.8	−457.2
NH_3 (g)	−45.9	192.7	−103.4
H_2O (l)	−285.8	69.9	−306.6
NH_4HCO_3 (s)	−849.4	120	−885.2
Reaction (14.19)	$\Delta_f H^0$	$\Delta_f S^0$	$\Delta_f G^0$
Formation quantities	−124.1	−356.4	−17.9

Exponent 0 indicates standard state; index f indicates formation

solid ammonium carbonate is formed, which is a good fertilizer that can be sold as a by-product of the main process. The residence time for the involved reactants is about 7 hours.

The chemical reaction for ammonia carbonation is

$$CO_2\ (g) + NH_3\ (g) + H_2O\ (l) \rightarrow\ NH_4HCO_3\ (s), \tag{14.19}$$

where the product precipitates in the chemical reactor. The reaction is exothermic and therefore allows for heat recovery to some degree. The method can be used for simultaneous capturing and sequestration of CO_2 from flue gases. Basically, the flue gas is scrubbed through an ammonia water solution. According to Li et al. (2003), the efficiency of carbon dioxide removal from flue gas and simultaneous sequestration in ammonium bicarbonate is around 40%. The removal efficiency is defined in this case by

$$\eta_{\text{res}} = \frac{C_\text{i} - C_\text{o}}{C_\text{i}(1 - C_\text{o})}, \tag{14.20}$$

where C_i, C_o are the CO_2 concentration in input and output streams, respectively. The reaction enthalpy (h), entropy (s), and free energy ($g = h - Ts$) for Eq. (14.19) are given in Table 14.5 for standard conditions. In the same table are shown the calculated values for enthalpy, entropy, and Gibbs free energy formation.

Table 14.6 Volumetric content of carbon dioxide for various means of transportation

Means of transport	Supercritical fluid	Refrigerated liquid	Dry ice	Urea	Ammonium bicarbonate
Symbol	sc CO_2	liq CO_2	CO_2 ice	$(NH_2)_2CO$	NH_4HCO_3
Characteristics	70 bar, 25°C	20 bar, −40°C	1 bar, −78°C	Standard T and P	Standard T and P
Density of CO_2 content	743 kg CO_2/m^3	1,030 kg CO_2/m^3	1,500 kg CO_2/m^3	952 kg CO_2/m^3	883 kg CO_2/m^3
Storage facilities	Cylinders, pipelines	Insulated, pressurized tanks	Insulated containers	Tanks of ~50 m^3	Tightly insulated at $T < 27$°C

The constant of equilibrium of the reaction (14.19) can be estimated by $\ln(K) = -\Delta_f G^0/RT$, where $R = 8.314$ J/mol.K is the universal gas constant and T is the process temperature. For standard conditions, the calculated reaction constant is $K = 1635$ and the Gibbs free energy of formation is negative, which indicate that the reaction is favored. Ammonium bicarbonate can be sold at ~$70 per ton with the condition that the energy penalty for capturing and sequestration of carbon dioxide, according to the U.S. Department of Energy (see also Li et al. 2003), should not be higher than $10 per ton.

Another possibility to sequestrate carbon dioxide is in the form of dry ice, stored in large thermally insulated facilities. Seifritz (1993) shows that carbon dioxide can be stored for 800 years in the form of dry ice; in this time interval, the mass that sublimates is half the initial mass. The storage density in this case is 1.55 kg of carbon dioxide per cubic meter. Carbon dioxide can be transported in the form of dry ice, or in a pressurized and refrigerated liquid form, from production places to sequestration points. Several safety issues must be addressed regarding the carbon dioxide transportation in these ways. Assume, for example, that liquid CO_2 is transported in a tank or pipeline. If leakage occurs, the expansion of carbon dioxide to atmospheric pressure generates a dry ice bank and cold CO_2 vapors. The continuous sublimation of dry ice generates more vapors for a longer time. Carbon dioxide is heavier than air; therefore, locally its concentration in the atmosphere can go up to a level that affects human or animal life. These factors as such were analyzed recently by Mazzoldi et al. (2008), who found that because carbon dioxide is heavier than air, in the case of leakage during transport its concentration increases locally up to levels that affect human or animal life. Transportation of carbon dioxide can be done either in the form of dry ice or in refrigerated liquid form, or as supercritical fluid, or in the form of urea or ammonium carbonate. The transportation density in kg of carbon dioxide per cubic meter is listed in Table 14.6. By far, urea is the most convenient way of storing carbon dioxide at standard pressure and temperature; by adding water and heat, urea can be converted back to carbon dioxide and ammonia, while ammonia can be recycled.

Another sequestration method is there fertilizing oceans with urea, though there is a debate in the literature regarding the possible side effects of urea in the ocean

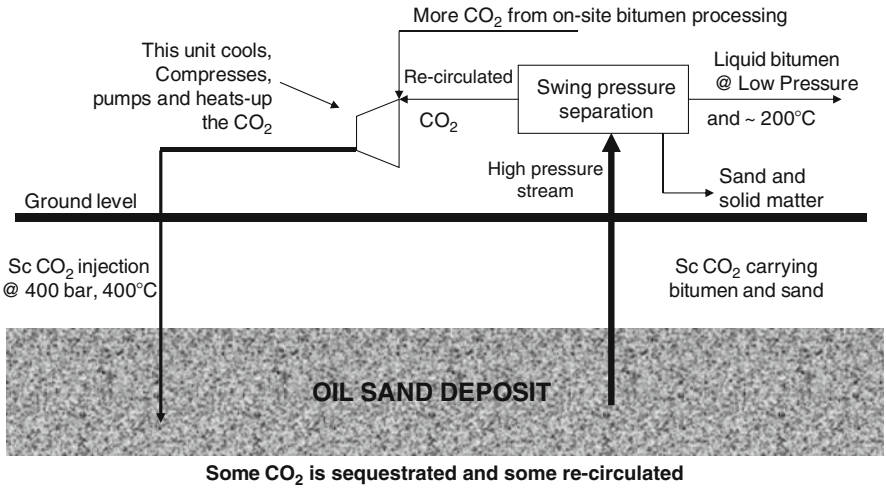

Fig. 14.17 Carbon dioxide sequestration in oil sands

(see Gilbert et al. 2008). It is interesting to note that the ocean is the major carbon dioxide reservoir on the planet, and CO_2 stores 20 times more than the atmosphere does. It is estimated that the ocean has accumulated one third of the anthropogenic carbon dioxide emissions in the last 250 years (Secretariat 2006 of the Convention on Biological Diversity 2009). Carbon dioxide can be directly injected into the ocean deep in two ways:

- As large dry ice blocks that sink and dissolve in deep ocean
- As supercritical CO_2 that is injected through pipes into deep ocean

Once present in deep-sea formations, where the pressure is many hundreds of bars, the carbon dioxide reacts with sea water and basalt and forms hydrates (e.g., $CO_2 \cdot 6H_2O$) and clathrates, compounds denser than seawater, which stay stable on the seabed.

Another possible way of carbon dioxide sequestration is discussed in conjunction with Fig. 14.17, which suggests a possible arrangement for extraction of bitumen from oil sands. Carbon dioxide is injected at supercritical pressure and temperature into the oil sand, where due to high temperature it dissolves bitumen. A mixture of liquid bitumen and sand is carried out at the surface, where through swing pressure separation liquid bitumen is extracted while the resulting carbon dioxide in gas phase is recirculated. When the bitumen has been extracted completely, the carbon dioxide remains sequestrated into the former oil sand deposit. The carbon dioxide can be sequestrated in a supercritical state in saline formations or oil and gas fields. Moreover, with the purpose of enhancing resource recovery, carbon dioxide is injected and remains sequestrated; examples are enhanced oil and gas recovery or enhanced coal methane bed recovery. It is also possible to sequestrate carbon dioxide in cement, at the bottom of the ocean (as compressed liquid).

Carbon dioxide can also be injected in exhausted oil wells and other geological structures like saline aquifers. In hydrocarbon extraction industry, carbon dioxide has been used for many decades for enhanced recovery, such as enhanced natural gas (EGR) and oil recovery (EOR), or enhanced coal bed methane recovery. In these techniques, the carbon dioxide is injected into the coal bed or oil/gas well and "presses" the useful products (oil, gas, coal bed methane depending on the case) out of the reservoir. After the extraction process is completed, the injected carbon dioxide remains sequestrated in the reservoir.

14.7 Case Study

We consider here a process for clean hydrogen production from natural gas where the resulting carbon dioxide is converted to dry ice. The resulting dry ice can be considered either a by-product or a means of carbon dioxide sequestration. Posada and Manousiouthakis (2006) proposed a process in which the many products of methane reaction with steam are separated by phase equilibrium (i.e., through sequential distillation), and eventually the system generates compressed hydrogen and dry ice. In general, hydrogen production from natural gas, through the steam–methane reaction, needs separation of hydrogen from other gases such as unreacted methane, steam, carbon dioxide, and carbon monoxide. In common implementations, this is done through membranes or through pressure swing absorption processes. Once separated, the hydrogen gas and carbon dioxide gas are compressed for storage. The system proposed here for analysis is based on the high-pressure steam–methane reaction process and cryogenic separation of gases. A part of the resulting hydrogen is combusted in a solid oxide fuel cell to produce the electricity and heat needed to sustain the process.

The core of the system is the steam–methane reactor, which operates at high temperature and takes at the inlet high-pressure steam and methane as reactants, while delivering a mixture of gases. The chemical reaction and pressure and temperature conditions of the steam–methane reactor (SMR) are similar to the ones determined by Posada and Manousiouthakis (2006). For our case, we assume the following overall chemical reaction in the SMR:

$$0.261\,CH_4 + 0.478\,H_2O + 0.045\,CO \rightarrow H_2 + 0.216\,CO_2 + 0.045\,CO, \quad (14.21)$$

for which we assumed that the methane is supplied at 811 K, the steam at 1,200 K, and the products are delivered at 1,010 K. The heat of the endothermic reaction for this case is calculated to be 60.814 kJ/mol of hydrogen produced. Additionally, based on common experience with SMR systems, we assumed that the methane must be supplied to the reaction in excess with 20% molar. The SMR system is presented in Fig. 14.18. Water is supplied in excess at 1,200 K that is at high enthalpy, with the purpose of delivering in this way the necessary reaction heat to SMR.

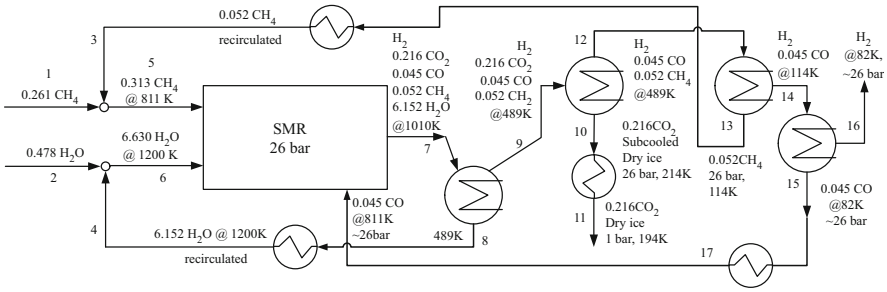

Fig. 14.18 Operating parameters of the steam–methane reactor (modified from Posada and Manousiouthakis 2006)

The goal is to conceive an overall system that sustains and delivers the reactants at the SMR in the desired pressure and temperature conditions and separates the gases from the output stream to recycle the steam and methane and to eventually produce hydrogen and dry ice. Stream 7 is cooled down to 489 K, a temperature at which the water vapor, having the partial pressure of 21.39 bar, is condensed and subcooled in state 8; further, the recycled water is heated again to 1,200 K. The cooling to be applied to heat exchanger 7–8–9 is 52.15 kJ/mol of hydrogen produced. The heating to be applied to heat exchanger 8–4 is 391 kJ/mol H_2. The partial pressure of carbon dioxide in stream 9 is 4.28 bar for which the sublimation temperature is, according to Eq. (14.2), 214 K. The heat to be extracted by the heat exchanger 9–10–12 is 47 kJ/mol of produced hydrogen. The dry ice separates at the bottom of the heat exchanger and is further compacted and cooled down to 194 K in the heat exchanger 10–11, while at the same time the pressure is released to 1 bar. The heat removed by the heat exchanger 10–11 is 4.7 kJ/mol of hydrogen. The partial pressure of methane in the remaining stream of gases at point 12 is 1.23 bar, while that of carbon monoxide is 1.067 bar; the corresponding saturation temperatures for these pressures are 114.1 K for methane and 82.08 K for carbon monoxide. Methane is further separated by condensation in the heat exchanger 12–13–14 and removed in subcooled liquid form at 114 K and ~26 bar at state 13; the heat to be removed is 3.4 kJ/mol of hydrogen produced. The collected liquid methane is then heated to 811 K in the heat exchanger 13–3 and recycled to the SMR; the heat to be added is 2.1 kJ/mol H_2.

Further, the carbon monoxide is separated by cooling the remaining stream to 82 K, because its corresponding saturation temperature in stream 14 is 82.52 K at a partial pressure of 1.12 bar. The carbon monoxide is reheated to 811 K and injected back into the SMR. A fraction x of the produced hydrogen is used in a system, such as the one suggested in Fig. 14.19, which generates the power and heat needed to sustain the hydrogen and dry ice production process (Fig. 14.18). After heating the hydrogen to about 900 K, the high-pressure/high-enthalpy stream is expanded to produce useful work. Further, the hydrogen is supplied as fuel to a high-temperature solid oxide fuel cell (SOFC), where it reacts with air at a pressure of about 4 bar. The remaining uncombusted fuel is further combusted in a combustion chamber and

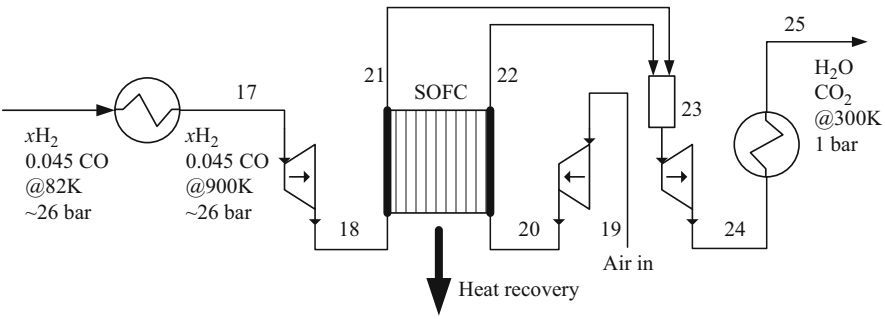

Fig. 14.19 Heat and work production system to sustain the H_2/dry ice production process

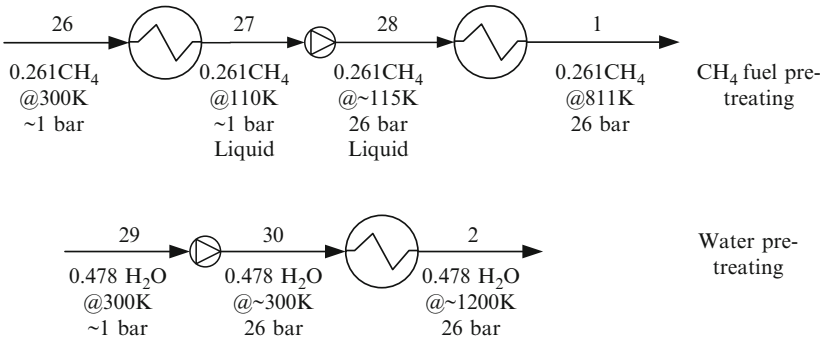

Fig. 14.20 Preheating and pressurizing systems for water and methane

expanded in turbine 23–24 for additional work. The resulting gas mixture, containing mainly water vapor and slight carbon dioxide, is cooled until water completely condensates, such that water can be recovered and reintroduced in the process.

The heat and work generated by the system described in Fig. 14.19 is partially used to preheat and pressurize the primary fuel (methane) and the water (Fig. 14.20). In this respect, methane present in the form of gas at the intake is cooled to cryogenic temperatures and liquefied; then it is pressurized to the operating pressure of SMR and preheated to 811 K. Water is first pressurized by pumping and then preheated to 1,200 K, which is the temperature at which water must be introduced in the SMR. The efficiency of the system can be quantified in terms of higher heating value of produced hydrogen per that of methane consumed, and it is given by

$$\eta = \frac{(1-x)\mathrm{HHV}_{\mathrm{H_2}}}{0.261\mathrm{HHV}_{\mathrm{CH_4}}} = 1.6(1-x). \tag{14.22}$$

Equation (14.22) imposes the constraint that $x>0.375$, which means that the fraction of hydrogen from the total produced, which must be used to maintain the process, must be higher than 0.375. The estimated fraction x for a practical

system is higher than 0.6, for which it corresponds to an efficiency of the proposed environmentally benign system for hydrogen and dry ice production of 60%.

14.8 Concluding Remarks

In this chapter, carbon dioxide technologies, which are important with respect to sustainable development, were discussed. Carbon dioxide is a stable chemical that is obtained as a product of most of the combustion processes. Due to its interesting features, carbon dioxide can be used in a multitude of roles, such as refrigerant, heat transfer fluid, cold storage medium (dry ice), working fluid in supercritical Rankine cycles, and active agent in separation technologies. There is no need to "manufacture" carbon dioxide for industrial needs; rather it can be separated from flue gas and purified. Carbon dioxide separation from flue gas avoids emission of CO_2 into the atmosphere, thus reducing its impact on global warming. Various methods of carbon dioxide sequestration (or long-term storage), which is an important process for sustainable development, were also discussed.

Nomenclature

A	Area, m^2
C	Concentration
COP	Coefficient of performance
d	Diameter, m
D	Diffusion coefficient, m^2/s
g	Specific Gibbs energy, kJ/kg
j	Mass velocity, $kg/s.m^2$
K	Equilibrium constant
m	Mass, kg
$\dot{m}$	Mass flow rate, kg/s
h	Specific enthalpy, kJ/kg
HHV	Higher heating value, MJ/kg
R	Universal gas constant, J/kmol.K
P	Pressure, Pa
q	Mass specific heat, kJ/kg
s	Specific entropy, kJ/kg.K
S	Entropy, kJ/K
T	Temperature, K
v	Specific volume, m^3/kg
$\dot{V}$	Volume flow rate, m^3/s
w	Specific work, kJ/kg
x	Vapor quality or hydrogen fraction
y	Ice fraction

Greek Letters

α Membrane permeability
δ Solubility parameter, $N^{0.5}/m$ or thickness, m
η Efficiency or dynamic viscosity, Ns/m^2
ν Kinematic viscosity, m^2/s
ψ Exergetic efficiency
ρ Density, kg/m^3
σ Surface tension, g/s^2
τ Reduced temperature

Subscripts

0	Reference state
c	Critical
comp	Compression
ex	Exergy
ext	Extracted
F	Feed
i	Input
inp	Input
L	Liquid
L,V	Liquid–vapor
mem	Membrane
o	Output
p	Permeate
ref	Refrigeration
res	Removal
sub	Sublimation
V	Vapor
t	Triple

References

Aaron D., Tsouris C. 2005. Separation of CO_2 from flue gas. *Separation Science and Technology* 40:321–348.

Cen Y., Lichtenthaler R.N. 1995. Vapor permeation. In: Membrane Separation Technology; Principles and Applications, Chapter 3. Noble R.D., Stern S.A. eds., Elsevier, Syracuse, NY.

Desimone J.M., Tumas W. 2003. Green Chemistry Using Liquid and Supercritical Carbon Dioxide. Oxford University Press, Oxford, UK.

Fernandez Tumas Cid M.V., Van der Kraan M., Veugelers W.J.T., Woerlee G.F., Witkamp G.J. 2004. Kinetics study of a dichlorotriazine reactive dye in supercritical carbon dioxide. *Journal of Supercritical Fluids* 32:147–152.

Gilbert P.M., Azanza R., Burford M., Furuya K., Abal E., Al-Azri A. et al. 2008. Ocean urea fertilization for carbon credits poses high ecological risks. *Marine Pollution Bulletin* 56:1049–1056.
Gottlicher G., Pruschek R. 1997. Comparison of CO_2 removal systems for fossil-fuelled power plant processes. *Energy Conversion and Management* 38:S173–S178.
Kersh C., Van Roosmalen M.J.E., Woerlee G.F., Witkamp G.J. 2000. Extraction of heavy metals from fly ash and sand with ligands and supercritical carbon dioxide. *Industrial and Engineering Chemistry Research* 39:4670–4672.
Klein S.A. 2010. Engineering Equation Solver (Academic Commercial v.8.629).
Li X., Hagman E., Tsouris C., Lee J.W. 2003. Removal of carbon dioxide from flue gas by ammonia carbonation in gas phase. *Energy and Fuels* 17:69–74.
Lorentzen G. 1994. Revival of carbon dioxide as a refrigerant. *Internal Journal of Refrigeration* 17:292–302.
Mazzoldi A., Hill T., Colls, J.J. 2008. CO_2 transportation for carbon storage: sublimation of carbon dioxide from a dry ice bank. *International Journal of Greenhouse Gas Control* 2:210–218.
Posada A., Manousiouthakis V. 2006. Hydrogen and dry ice production through phase equilibrium separation and methane reforming. *Journal of Power Sources* 156:480–488.
Secretariat 2006 of the Convention on Biological Diversity. 2009. Scientific Synthesis of the Impacts of Ocean Fertilization on Marine Biodiversity. Montreal, Technical Series No. 45.
Seifritz W. 1993. The terrestrial storage of CO_2-dry ice. *Energy Conversion and Management* 34:1121–1141.
Somayajulu G.R. 1988. A generalized equation for surface tension from the triple point to the critical point. *International Journal of Thermophysics* 9:559–566.
Span R., Wagner W. 1996. A new equation of state for carbon dioxide covering the fluid region from the triple-point temperature to 1100K at pressures up to 800 MPa. *Journal of Physical and Chemical Reference Data* 25:6.
Vesovic V., Wakeham A., Olchowy G.A., Sengres J.V., Watson J.T.R., Millar J. 1990. The transport properties of carbon dioxide. *Journal of Physical and Chemical Reference Data* 19:763–808.
Yave W., Anja C., Peinemann K.-W. 2010. Nanostructured membrane material designed for carbon dioxide separation. *Journal of Membrane Science* 350:124–129.

Study Questions/Problems

14.1 Present a classification of carbon dioxide technologies.
14.2 What feature makes carbon dioxide an excellent working fluid and process separation medium?
14.3 What is supercritical carbon dioxide?
14.4 What is dry ice and how it is obtained?
14.5 Define the solubility strength.
14.6 Calculate the cycle from Fig. 14.6 such that you obtain the diagram from Fig. 14.7.
14.7 Calculate a supercritical power cycle with carbon dioxide operating at 120 bar and with 200°C maximum temperature in the cycle. Take the isentropic efficiency of the turbine 0.8.
14.8 Calculate the process illustrated in Fig. 14.11 such that you obtain the diagram from Fig. 14.12.
14.9 Calculate the cycle represented in Fig. 14.18.

Chapter 15
Life-Cycle Assessment

15.1 Introduction

Development of sustainable energy systems implies comprehensive analyses that go beyond thermodynamics. The environmental impact, resource depletion, cost, and societal impact must be accounted for in addition to the efficiency and effectiveness defined according to the first and second laws of thermodynamics. The method of life-cycle assessment (LCA) is commonly used to analyze the life cycle of a system from cradle to grave. This method is defined by International Standards Organization norm ISO 14040 as the "compilation and evaluation of the inputs, outputs, and potential environmental impacts of a product system throughout its life cycle." In general, LCA, when applied to energy systems, defines, on a case-by-case base, an integrated efficiency of the whole process by considering final outputs over the lifetime and initial material inputs and the associated energy and exergy flows. This kind of cradle-to-grave analysis is extremely important for policy elaboration and decision making for sustainable development. Sustainability often leads authorities to incorporate environmental considerations into planning. The need to satisfy basic human needs and aspirations, combined with the increasing world population, is a driver toward successful implementation of sustainable development. LCA is a key tool for identifying the best paths leading to sustainable development.

The LCA methodology and its scientific background are incorporated in a number of international standards promulgated by the ISO:

- ISO International Standard 14040, 1997E: principles and framework
- ISO International Standard 14041, 1998E: goal and scope definition and inventory analysis
- ISO International Standard 14042, 2000E: life-cycle impact assessment
- ISO International Standard 14043, 2000E: life-cycle interpretation

The phases that are analyzed in an LCA project include extraction of resources, production of materials, production of parts and of the product (system) itself, the period of product service, and management after the product is discarded (considering partial recycling, final disposal, and other factors). The associated costs

İ. Dinçer and C. Zamfirescu, *Sustainable Energy Systems and Applications*,
DOI 10.1007/978-0-387-95861-3_15,

and environmental burdens (pollution, extraction of resources, and type of land use) are evaluated for all life-cycle phases and the overall process.

Comparative LCA studies are possible and desirable to compare and select among various products or technologies. In the case of a comparative LCA study, the function provided by the products (technologies) is quantified and confer the basis for comparisons. For example, one can assess and compare various technologies for biomass-based electricity production. The product in this case is the kWh of generated electricity.

Guinee (2004) states that the driving force of the economy is the consumption of products. The LCA offers the opportunity to adjust economic policy in a rational manner, so that indirect environmental management for better sustainability is achieved in addition to economic benefits. The method of LCA can be applied, in the context of sustainable energy, for analyzing a particular technology for the entire life-cycle, comparing various technologies, selecting a technology among several competitors, and designing better energy products and technologies.

One of the prime specificities of the LCA of energy systems is the necessity of performing thermodynamic analysis of the mass, energy, and exergy balance throughout the product's life cycle. Dincer and Rosen (2007) discuss and exemplify the use of exergy in life-cycle analysis by introducing the concept of "exergetic life-cycle analysis," which is presented in this chapter. The exergy analysis is often interlaced with cost analysis, as, for example, with the method of "exergy–cost–energy–mass" developed by Rosen and Dincer (2003).

The ability to track and document shifts in environmental impacts can help engineers as well as decision and policy makers to fully characterize the environmental trade-offs associated with product or process alternatives. Performing an LCA allows one to do the following:

- Quantify environmental releases to air, water, and land in relation to each life-cycle stage and/or major contributing process
- Evaluate systematically the environmental consequences associated with a given product or process
- Assess the human and ecological effects of material and energy consumption and environmental releases to the local community, region, and world
- Compare the health and ecological impacts of alternative products and processes
- Identify impacts related to specific environmental areas of concern
- Analyze the environmental trade-offs associated with one or more specific products/processes to help gain stakeholder (region, community, etc.) acceptance for a planned action.

In this chapter, we discuss the application of LCA to sustainable energy systems and exemplify the use of LCA through a number of relevant case studies, such as LCA of hydrogen–fuel cell and gasoline vehicles, exergetic LCA of

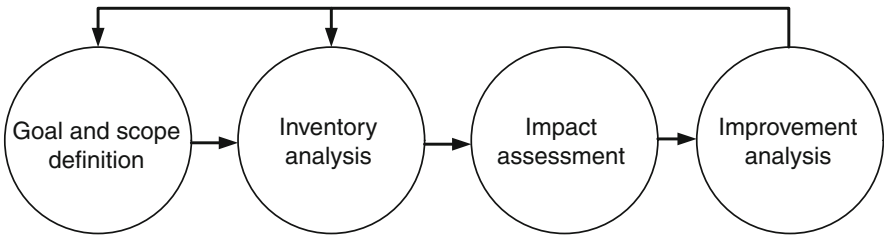

Fig. 15.1 Stages of LCA and their interactions

hydrogen production from renewables, LCA of nuclear-based hydrogen production using thermochemical water decomposition, and greenhouse gas emission assessment of hydrogen and kerosene-fueled aircraft propulsion.

15.2 General Description of LCA Methodology

An LCA involves, in general, four main stages that are illustrated in Fig. 15.1: goal and scope definition of the study, inventory analysis, impact assessment, and improvement assessment. Inventory of material and energy fluxes is at the base of LCA methodology. The rational way in which such an inventory can be done (the guideline) is described in the *Handbook on Life Cycle Assessment*, by Guinee (2004) and in the book by Rubin and Davidson (2001). In general, LCA projects include phases of analysis, design, management, organization, and assignment. There are available a number of procedures that help in elaborating the inventory analysis, such as flow diagram, data collection, estimation, and validation methods. After the inventory analysis is done, an impact assessment should be conducted.

There are several kinds of impact categories: depletion of resources (abiotic or biotic), land use (competition, biodiversity loss, and life support function loss), climate change, desiccation, stratospheric ozone depletion, human- and ecotoxicity, acidification, photo-oxidant formation, eutrophication, waste heat generation, noise and odor (in water and air), and ionizing radiation. Toxicity pertains to aquatic (marine and freshwater) and terrestrial ecosystems. Eutrophication represents the excessive increase of chemical nutrients in the ecosystem, which causes productivity augmentation. This creates an unbalance in the ecosystem because other biological species may occur and experience an increase in number with respect to other species that can be depleted.

An important part of the LCA methodology is the interpretation of results, which includes various checks (such as consistency and completeness checks) and perturbation/sensitivity/uncertainty analyses. The LCA can be conducted in several ways, as it may be treated as an organizational process. In all cases, an LCA project should go according to the following steps: description procedures, definition of goal and scope, inventory analysis, impact assessment, and interpretation and final conclusions.

The inventory analysis is the core of the LCA study, as it provides support for assessment and interpretation. As a first step of the inventory analysis, one must define the system boundary by identifying the flows of matter, pollution, energy, and currency that interact with the system. Elaboration of a flow diagram is recommended in this phase. One must address data collection, compilation, evaluation, validation, and data quality estimation. The result of inventory analysis is the inventory table showing the inputs and outputs of materials and nonmaterial (e.g., energy and currency) flows exchanged by the delimited system with the environment. A subsequent result of the inventory analysis is the flow diagram, which demonstrates the modeled processes and their interrelationships.

Once inventory analysis is performed, the data interpretation follows. The first step of interpretation is data validation. The basic tool for data validation is material balance (specified, depending on the case, on kg or molar basis). On the top of the material balance is the energy balance and cross-comparison of the data with other sources. In the case of missing data, one can use appropriate modeling and interpolation tools. If estimation is not possible, one can decide that certain flows are not considered for the analysis. This approach is known as "cut-off." This practice of cut-off can affect substantially the results of the LCA; however, such results can be considered valuable as first estimates.

According to Rubin and Davidson (2001), one can categorize environmental impact as (1) depletion of natural resources, (2) effects on human health, (3) effects on the ecosystem, and (4) impairment of human welfare. Natural resources can be categorized as renewable or nonrenewable. The resources that are nonrenewable, such as fossil fuels and minerals, concern us the most. However, the impact of renewable resource depletion is also very important and difficult to quantify. For example, the environmental impact of deforestation produced by excessive consumption of wood can be assessed qualitatively rather than quantitatively.

The most important environmental impact is represented by the direct effects on human health. A list of toxic products emitted by industry is compiled by the United States Environmental Protection Agency (EPA) under the title Toxic Release Inventory (TRI). The toxic substances can be inhaled in the human body as gases or airborne particles or ingested as contaminated water or food. The toxic substances and pollutants can also affect plants and animals in all types of environments. The impacts of category (4) refer to factors that affect humans, such as climate change, haze, industrial smog, corrosion of structures, noise, unpleasant odors, and others.

Table 15.1 presents the main quantifiable environmental impact categories and their descriptions. The first quantifiable impact is called abiotic resource depletion, which is expressed, as proposed in Guinee (2004), with reference to the antimony resource. For each kind of resource, an abiotic depletion potential (ADP) is assigned, which is expressed in kg of antimony equivalent for kg of resource. Table 15.2 lists the ADP of some important resources.

In an LCA, the abiotic resource depletion is calculated by

$$\mathrm{AD} = \sum_i \mathrm{ADP}_i \times m_i, \tag{15.1}$$

Table 15.1 Quantification of environmental impact

Impact category	Unit	Definition
Depletion of abiotic resources	kg antimony equivalent	Abiotic resources include all nonliving resources (coal, oil, iron ore, renewable energies, etc.). See Eqs. (15.1) and (15.2)
Climate change	GWP (CO_2 equivalent)	Kilogram of CO_2 equivalent. See Chapter 3 for more detailed definition
Ozone depletion	ODP (CFC11 equivalent)	ODP, the ozone depletion potential, is a time-dependent parameter characterizing the potential of a substance to deplete the stratospheric ozone layer; it represents the amount of a substance that depletes the ozone layer relative to CFC11 (trichlorofluoromethane)
Photo-oxidant formation	kg of ethylene equivalent	Depends on photochemical ozone creation potential expressed with respect to the reference substance, ethylene; see Eq. (15.4)
Toxicity	kg DCB equivalent	Human toxicity and ecotoxicity produced in air, freshwater, seawater, or terrestrial; it is quantified with respect to the toxicity of DCB
Acidification	kg SO_2 equivalent	Expressed in SO_2 equivalent emitted in Switzerland; there are three acidification factors: ammonia, NO_x, and SO_2; see Eq. (15.5)
Eutrophication	kg PO_4 equivalent	Covers all potential impacts of high levels of nutrients, the most important of which are nitrogen (N) and phosphorus (P)

DCB 1,4-dichlorobenzene; *GWP* global warming potential

Table 15.2 Abiotic depletion potential of some natural resources

Resource	Aluminum	Bismuth	Cadmium	Copper	Gold	Helium	Iridium	Lead	Mercury
ADP	10^{-8}	0.0731	0.33	0.002	89.5	148	32.3	0.013	0.495
Resource	Neon	Osmium	Platinum	Rhodium	Silver	Tin	Uranium	Xenon	Zinc
ADP	0.325	14.4	1.29	32.3	1.84	0.033	0.003	17,500	10^{-3}

ADP abiotic depletion potential in kg antimony equivalent
Data from Guinee (2004)

where index i represents the specific resource of the ADP and the depleted mass m. For fossil fuels, ADP is calculated accounting for the fact that fossil fuels are both materials and energy carriers. The assigned value of ADP for fossil fuels is $ADP_f = 4.81 \times 10^{-4}$. For a specific fuel, the ADP is given by

$$ADP_{fuel} = ADP_f \times HHV. \tag{15.2}$$

Here, the values calculated by Guinee (2004) for various fossil fuels are 0.0187 for natural gas, 0.02 for petroleum, 0.014 for hardcoal, and 0.0067 for softcoal.

The toxicity potential of a substance emitted in the environment is given relative to 1,4-dichlorobenzene. The environment in which the substance is emitted affects the value of the toxicity potential. Five kinds of environments are commonly considered: air, fresh water, sea water, agricultural soil, and industrial soil. Using the toxicity potential, the total toxicity is calculated by a double summation:

$$T = \sum_i \sum_e \left(\mathrm{TP}_{e,i} \times m_{e,i}\right), \tag{15.3}$$

where $\mathrm{TP}_{e,i}$ represents the toxicity potential on the environment e caused by the pollutant i. The values for $\mathrm{TP}_{e,i}$ are listed in literature sources, such as Guinee (2004) for each category of substance. The toxicity potential of a substance depends also on the factor that generates the pollution. There are two main kinds of toxicities: human toxicity and ecotoxicity. Ecotoxicity covers the impact of toxic substances on aquatic, terrestrial, and sediment ecosystems, whereas human toxicity refers to the impact of toxic substances present in the environment on human health.

The generation of oxidative compounds under the influence of solar radiation is denoted as photo-oxidant formation. One typical photo-oxidant is the ozone formed in the stratosphere. Some air pollutants can accelerate or decelerate the production of photo-oxidants. The photo-oxidant formation potential is expressed with respect to the reference substance ethylene using the following equation:

$$\mathrm{PO} = \sum_i \mathrm{POCP}_i \times m_i, \tag{15.4}$$

where POCP_i is the photochemical ozone creation potential of the substance i, present in quantity m_i. Values for POCP are listed in Guinee (2004) and vary from 0.009 for 1,1,1-trichlorethane to 1.27 for 1,2,3-trimethyl benzene.

The acidification potential is expressed with respect to sulfur dioxide equivalent emitted in Switzerland. The substances present in the terrestrial atmosphere that generate acidification of soils are ammonia, sulfur dioxide, and $\mathrm{NO_x}$. The maximum acidification potential corresponds to ammonia, which is 1.6, while that of $\mathrm{NO_x}$ is 0.5 (see Guinee 2004). The equation to calculate the acidification impact based on the acidification potential (ACP) is

$$A = \sum_i \mathrm{ACP}_i \times m_i. \tag{15.5}$$

The impact factors most relevant to sustainable energy systems are mainly the global warming potential (GWP) and acidification. Any energy system based on fossil fuel combustion emits carbon dioxide, nitrogen oxides ($\mathrm{NO_x}$), and volatile organic compounds (VOCs). Other energy systems, including those based on renewable resources, can have associated $\mathrm{CO_2}$, VOCs, and $\mathrm{NO_x}$ emissions indirectly—for example, those generated during hardware manufacturing. A general picture illustrating the environmental impact of energy systems is illustrated in Fig. 15.2, which refers to power generation and transportation sectors. The LCA in these sectors can take into account the greenhouse gas emissions sourcing from carbon dioxide, methane, nitrous oxide ($\mathrm{N_2O}$), and sulfur hexafluoride ($\mathrm{SF_6}$) with sufficient approximation. Considering the GWP of these substances (GWP = 1 for $\mathrm{CO_2}$, 21 for $\mathrm{CH_4}$, 310 for $\mathrm{N_2O}$, and 24,900 for $\mathrm{SF_6}$) and the emitted amounts for the

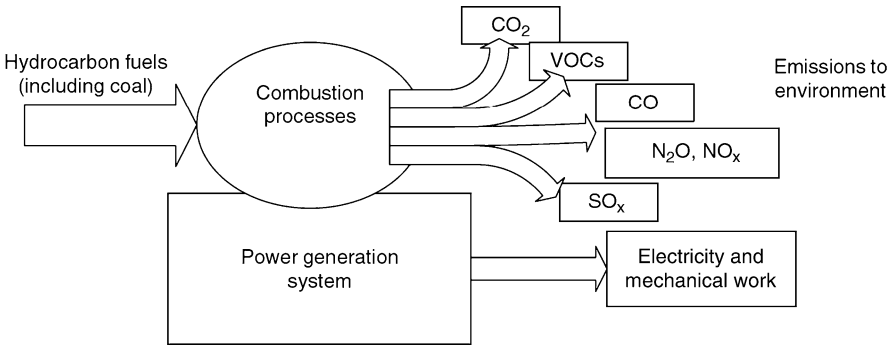

Fig. 15.2 Environmental impact of energy systems [modified from Dincer and Rosen (2007)]

entire life-cycle, the greenhouse gas equivalent effect can be calculated as a weighted sum:

$$\mathrm{GW} = \sum_i \mathrm{GWP}_i \times m_i. \tag{15.6}$$

Moreover, the major airborne pollutants produced by power generation and transportation sectors are carbon monoxide, nitrogen oxides (NO_x), sulfur oxides (SO_x), and VOCs. Thus, an air pollution indicator (AP) can be defined as the weighted sum:

$$\mathrm{AP} = \sum_i \mathrm{APP}_i \times m_i, \tag{15.7}$$

where APP_i is the air pollution potential of the pollutant i, and has the values of 0.017, 0.64, 1, and 1.3 for CO, VOCs, NO_x and SO_x, respectively.

The LCA of energy systems must include the estimation of efficiency and effectiveness for the whole life cycle. Better efficiency of systems lead to less resource consumption and less pollution, which ultimately means reduced environmental damage. Such parameters as life-cycle efficiency and effectiveness are useful for comparing various technological alternatives. As mentioned above, exergy analysis plays a major role.

15.3 Exergetic Life-Cycle Analysis

The extension of LCA methodology to include exergy analysis for the whole life cycle of systems has been proposed by Dincer and Rosen (2007). When considering exergy in LCA, the inventory analysis phase has to account more carefully for mass and energy flows into, out of, and through all the stages of the life cycle; next, the energy flow is associated with an exergy flow; eventually, a life-cycle efficiency based on energy and exergy is defined and studied.

One can consider that the life cycle of the analyzed product comprises a number of technological steps. For the *i*th technological cycle, the exergy consumption rate can be determined, for example, by considering only the exergy of the consumed fuels to drive the associated processes. The fuel exergy is consumed for the generation of the final product ($\dot{E}x_{\text{dir}}$), covering the necessary energy to drive the process ($\Delta\dot{E}x_{\text{dir}}$), and for fueling indirect processes such as extraction of material, construction of the hardware/equipment, installation, operation, maintenance, and decommissioning ($\Delta\dot{E}x_{\text{ind}}$); therefore, for the *i*th technological cycle, one can write the following expression giving the corresponding life-cycle fossil fuel exergy consumption rate:

$$\dot{E}x^{i}_{\text{LFC}} = \dot{E}x^{i}_{\text{dir}} + \Delta\dot{E}x^{i}_{\text{dir}} + \Delta\dot{E}x^{i}_{\text{ind}}. \tag{15.8}$$

A typical example explaining the nature of exergy losses by the direct use of fuel is the hydrogen production from steam reforming, which occurs based on the endothermic reaction $CH_4 + H_2O \rightarrow 4H_2 + CO_2 - 165$ kJ. The direct exergy input $\dot{E}x^{i}_{\text{dir}}$ is in this case the exergy embedded in the amount of methane that is converted into hydrogen. The heat necessary to drive the endothermic reaction, however, is generated by the combustion of additional methane according to the reaction $CH_4 + O_2 \rightarrow CO_2 + H_2O + 803$ kJ; the exergy associated with the combusted methane represents the amount $\Delta\dot{E}x^{i}_{\text{dir}}$ included in Eq. (15.8).

In many practical situations, the energy that drives a process is electricity or a synthetic fuel (hydrogen, ethanol, etc.) that is produced starting from fossil fuel by various processes (e.g., electricity generation by fossil fuel combustion, etc.). Production of any kind of such energy carriers from fossil fuels has typical exergy efficiency ψ, which is known. Based on ψ, one can simply determine the exergy embedded in the consumed fossil fuel to drive the process with

$$\Delta\dot{E}x^{i}_{\text{dir}} = \frac{\dot{E}x^{i}}{\psi}, \tag{15.9}$$

where $\dot{E}x^{i}$ is the exergy consumed by the *i*th technological step.

The indirect exergy must be calculated such that one accounts not only for the chemical exergy of the material but also for the economic value. A typical example (see Dincer and Rosen 2007) is the comparative use of limestone and natural gas as material inputs. Natural gas has a high exergy content to its reactivity in the environment (chemical exergy), whereas limestone (as well as many other construction materials) has very little chemical exergy. An exergy content equivalent "EEQ" of materials can be introduced such that the indirect exergy can be expressed with

$$\Delta\dot{E}x^{i}_{\text{ind}} = \frac{\text{EOP} + \sum \text{EEQ}}{\text{LFT}}, \tag{15.10}$$

where EOP is the fossil fuel exergy associated with the manufacturing of materials, equipment, devices, construction work, maintenance, and decommissioning; LFT is

the lifetime that can be associated with the devices performing the technological step; and EEQ is the sum of the total exergy equivalents of construction materials and devices. Some examples of quantifying EEQ are given in this chapter.

Life-cycle efficiency can be defined with the following general formula:

$$\psi = \frac{\dot{E}x^{\text{products}}}{\dot{E}x^{\text{LFC}}}, \tag{15.11}$$

where $\dot{E}x^{\text{products}}$ is the total exergy retrieved in the products and $\dot{E}x^{\text{LFC}}$ is the exergy consumed for the whole life cycle.

Together with exergy, the life-cycle cost, energy, and mass (material) balances can be considered. Rosen and Dincer (2003) developed the exergy–cost–energy–-mass analysis methodology (EXCEM), which is applicable to LCA. The basic rationale underlying an EXCEM analysis is that an understanding of the performance of a system requires an examination of each category of flows, such as mass, energy, exergy, and cost flows, through which the analyzed system interacts with the exterior. For each of these categories (mass, energy, exergy, and cost), one can write a general balance equation in the form of

$$\text{Input} + \text{Generation} = \text{Accumulation} + \text{Output} + \text{Consumption}, \tag{15.12}$$

where input and output refer, respectively, to quantities entering and exiting through system boundaries; generation and consumption refer, respectively, to quantities produced and consumed within the system; and accumulation refers to a change of the quantity within the system.

Various energy technologies are generally distinguished by (1) the source of the energy consumed, (2) the efficiency of the energy produced per unit of primary energy consumed, and (3) capital investments made per unit of energy produced. To account for these factors, we can utilize a quantity called the capital investment efficiency factor, γ, as a measure of economic efficiency, which has been proposed by Granovskii et al. (2006a,b, 2007b) in the context of analysis of hydrogen production technologies. This indicator is proportional to the relationship between gain and investment and is expressed as

$$\gamma = \frac{\dot{E}x}{\dot{E}x_{\text{ind}}}\left(\alpha - \frac{1}{\psi^{\text{LFC}}}\right), \tag{15.13}$$

where $\dot{E}x$ is the exergy retrieved in the product and $\dot{E}x_{\text{ind}}$ is the indirect exergy rate that is proportional to the capital investment in a technology; α is the ratio of the unitary costs of product and the consumed primary energy for the production of one unit of product; ψ^{LFC} is the life-cycle exergy efficiency.

We illustrate here the use of the capital investment efficiency factor for the case of hydrogen production technologies. The most frequent source of hydrogen production is natural gas. The alternatives to natural gas are many, but we consider in Fig. 15.3 only wind and solar as the primary energy to generate electricity for water electrolysis.

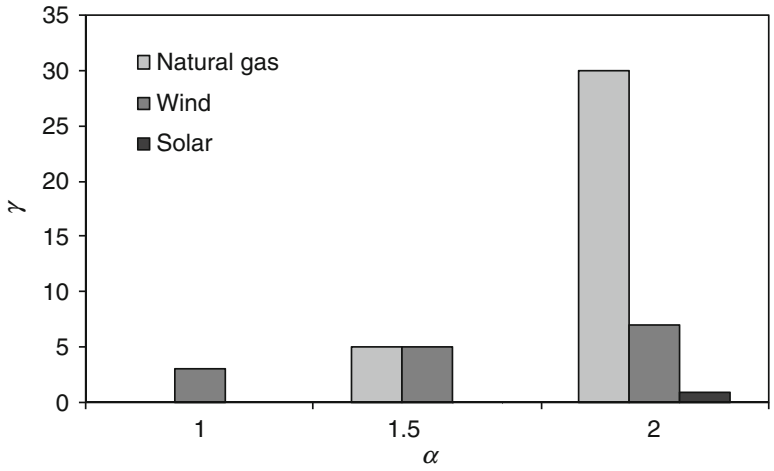

Fig. 15.3 Capital investment efficiency factor for H_2 production [modified from Granovskii et al. (2007a)]

Figure 15.3 shows the variation of γ with respect to α [data from Dincer and Rosen (2007)]. It has been assumed that ψ^{LFC} is 0.72 for hydrogen production from natural gas, 0.75 for hydrogen production driven by solar energy, and 3.32 for hydrogen production using wind energy. Note that, according to Dincer and Rosen (2007), there are no direct costs associated with primary energy consumption when wind is used to drive hydrogen production process; as a result, $\psi^{\mathrm{LFC}} > 1$. It follows from Fig. 15.3, at $\alpha = 2$, that the capital investment efficiency factor for hydrogen production via natural gas is about five times higher than that via wind energy. This situation can be altered by reducing the construction material requirements of wind per unit of electricity generated.

In order to allow for different technologies (products) to be compared when various kinds of indicators are available (e.g., technical, economical, and environmental), a normalization procedure is proposed by Granovskii et al. (2006b) and Dincer et al. (2010). Normalized indicators can include technology costs, greenhouse gases (GHGs), and AP (air pollution) emissions. They can be defined using the reciprocal of the individual indicators ($1/\mathrm{Ind}_i$) as

$$N\,\mathrm{Ind}_i = \frac{1/\mathrm{Ind}_i}{(1/\mathrm{Ind}_i)_{\max}}, \tag{15.14}$$

where the denominator represents the maximum value of the reciprocal of the considered indicator. Once the normalized individual indicators (N $\mathrm{Ind_i}$) are calculated, a generalized indicator can be determined, represented by the product of the normalized indicators. The generalized indicator is thus written as

$$N\ \mathrm{Ind} = \Pi_i (N\ \mathrm{Ind})_i. \tag{15.15}$$

The general indicators provide a measure of how far a given technology is from the "ideal."

15.4 Case Studies

15.4.1 Comparative LCA of Hydrogen–Fuel Cell vs. Gasoline Vehicles

Hydrogen appears to be one of the most effective solutions for power generation in stationary and mobile applications. In the utilization phase, hydrogen can be supplied to fuel cells that produce clean electricity, the only emission being water vapor. It is very important to assess the environmental impact and the sustainability of hydrogen and fuel cell system from the perspective of the whole life cycle. In this respect, the environmental impact is assessed for the hydrogen production phase as well as its distribution; also in the utilization phase, one has to consider the environmental impact of fuel cell system construction, which involves expensive materials, depletion of some resources, and pollution associated with the manufacturing process. In this case study, the application of LCA methodology is exemplified in quantifying the environmental and energy impacts of hydrogen–fuel cell vehicles as compared with conventional gasoline vehicles. It is assumed that hydrogen is derived from natural gas. The vehicle is based on PEM (proton exchange membrane) fuel cell technology. Assessing such systems over their entire life cycle is essential for obtaining relevant information on energy consumption and emissions and for determining competitive advantages. The gasoline vehicle used for comparison uses a conventional internal combustion engine (ICE). Moreover, it is assumed that the gasoline is derived from the processing of crude oil according to the typical chain involving oil extraction, oil distribution to refineries, fractional distillation, gasoline distribution, and temporary storage.

15.4.1.1 Inventory Analysis

The life-cycle flow diagram of a vehicle (either conventional gasoline or hydrogen–fuel cell) is illustrated in Fig. 15.4. The life-cycle diagram has two branches, starting with resource extractions for construction materials (left) and primary energy sources (right). The extracted materials are processed and the vehicle is manufactured. The distribution phase follows.

Together with the vehicle distribution network, there is also the vehicle maintenance network comprising workshops and spare parts manufacturers and distributors. On the second branch, the primary energy sources are processed for fuel production; further, there is the fuel distribution network. After the vehicle use phase, scraping and recycling are done, where the recycled materials are fed back into the vehicle manufacturing process.

The boundaries of the system, which have to be established for the inventory analysis, are set such that the secondary effects are not considered. Here, "secondary effects" means the emissions and energy involved in the construction of the plants that process fuels and materials and manufacture the vehicle. For clarification,

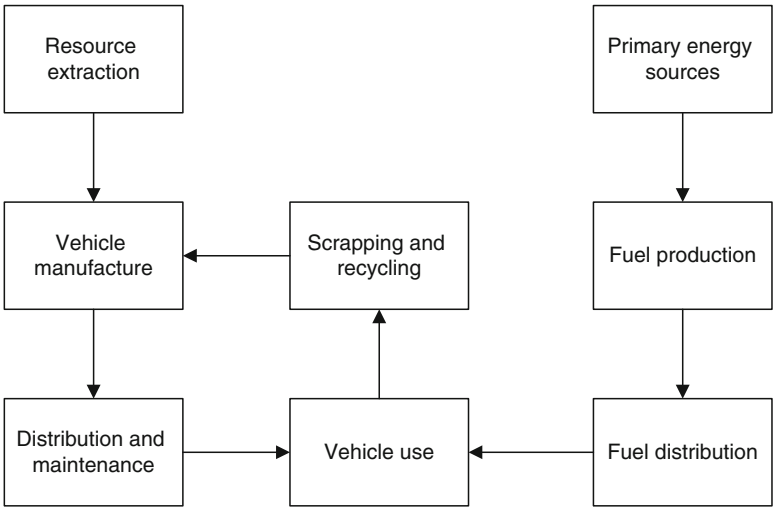

Fig. 15.4 The life-cycle phases of a vehicle

consider hydrogen production by natural gas reforming. In this case, the energy consumed to produce materials (concrete, steel, etc.) embodied in the hydrogen plant itself is considered secondary and is not accounted for in the inventory analysis. Moreover, the inventory analysis is limited to common passenger vehicles. The results shown in this case study are derived from the paper by Dincer (2007).

In order to elaborate the inventory analysis, both branches shown in the flow diagram (Fig. 15.4) are considered; these branches are called further "vehicle cycle" and "fuel cycle" (left/right, respectively). The characteristics of the two cycles are described in Table 15.3. Here, both energy consumption and GHG emissions during the fuel cycle of hydrogen are higher when compared with gasoline fuel cycle. The fuel production stage of the hydrogen cycle is the major contributor to total energy consumption and GHG emissions. The other significant contribution to energy consumption and GHG emissions during the hydrogen cycle comes from the fuel distribution stage, which includes primary energy for the generation of the electric power that is used for compressing hydrogen.

Figure 15.5 presents compactly the inventory analysis of fuel and vehicle cycles as expressed in terms of the primary energy consumed. For the fuel cycle, the results are given as energy consumed for unit of energy embedded in the fuel with respect to the lower heating value (LHV). For the vehicle cycle, the results are presented in GJ of energy consumed to produce one single vehicle. In order to develop the plots shown in this figure, an inventory table has been elaborated (data not shown here, for simplicity) that quantifies material consumption and the associated energy for each involved subphase and process.

It can be observed from Fig. 15.5a that most energy consumption for the fuel cycle comes from fuel production. The energy for hydrogen production is about 3.5 times higher than that of gasoline. Also for hydrogen distribution, one needs

Table 15.3 Characteristics of vehicles and fuel cycles

Vehicle cycle		Fuel cycle	
Material production	Vehicle incorporates ~890 kg of ferrous metals, 100 kg of different types of plastics, roughly 80 kg of aluminum, and about 200 kg of other materials; PEM fuel cells include polymer membrane, platinum catalyst, graphite, etc.	Fuel sources extraction	Quantified in this stage are the energy consumption and GHG emissions during the extraction of natural gas and crude oil per unit of energy embedded in final products (hydrogen or gasoline)
Vehicle assembly	The energy and GHG emissions associated with manufacturing are typically estimated as a linear function of vehicle mass	Feedstock production	Energy consumption and GHG emissions during the production of natural gas for hydrogen and crude oil for gasoline are quantified
Distribution/ maintenance	The energy needed and GHG emissions during the transport of a vehicle from the assembly line to the dealership are quantified per unit of curb mass of vehicle	Feedstock transport	Crude oil and natural gas as the raw materials for gasoline and hydrogen have to be transported to the refineries (assumed centralized plants) and reforming plants (assumed decentralized plants); energy consumption and GHG emissions during the transport of raw materials are counted in this stage
Vehicle use	Lifetime of typical vehicle assumed 300,000 km Maintenance and repair during the lifetime is considered; fuel usage of PEM fuel cell/hydrogen is 0.65 MJ/km and of ICE/gasoline vehicles is 2.73 MJ/km	Fuel production	Energy consumption and GHG emissions during refining of crude oil and steam reforming of natural gas are quantified in this stage
Scrapping and recycling	The disposal energy is the sum of energy needed to move the bulk from the dismantler to a shredder and the shredding energy; one also considers the energy related to recycling of materials	Fuel distribution	Gasoline: from refineries to terminals by ship or pipeline, transfer to road tankers, to service stations, and finally to vehicle tank Hydrogen: natural gas is transported through pipeline or road tankers to decentralized refueling stations, where it is produced through steam reforming; it includes primary energy and GHG emissions associated with compression

Data from Dincer (2007)

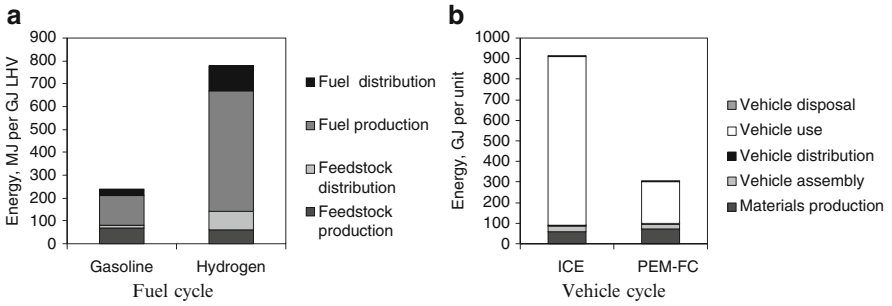

Fig. 15.5 Energy inventory analysis for fuel and vehicle cycles

approximately four times more energy than for gasoline. Thus, regarding the fuel cycle, the gasoline is—energy-wise—clearly superior to hydrogen. However, if one looks at the vehicle cycle (Fig. 15.5b), it is observed that the ICE vehicle is four times more energy consuming than the proton exchange membrane fuel cell (PEMFC) vehicle at the vehicle utilization stage. Overall, per unit of vehicle, the PEMFC consumes three times less energy during the life-cycle.

15.4.1.2 Impact Analysis

The inventory analysis, presented above in terms of specific energy consumption during the life cycle, facilitates the impact analysis. Here, one determines the GHG emissions during various segments of the life cycles for the two vehicles compared here (Fig. 15.6).

The largest contributor to GHG emissions for the ICE vehicle is the usage stage. The energy consumption of the ICE vehicle is about three times higher than that of the PEMFC vehicle. Moreover, GHG emissions during the vehicle cycle of PEMFC vehicles are around 8% of the GHG emissions of the ICE vehicle, which clearly indicates the environmental friendliness of PEMFC vehicles.

15.4.1.3 Improvement Assessment

The results of the LCA can be summarized as indicated in Fig. 15.7, which shows both the energy consumption and GHG emission for the life cycle of the two vehicles. The figures are presented in percents of the total. This is calculated as follows:

- The energy consumption for all life-cycle phases is summated to determine the total life-cycle energy consumption in both cases for one vehicle.
- The life-cycle energy consumption for one gasoline vehicle is considered as the reference value and is assigned to 100%.

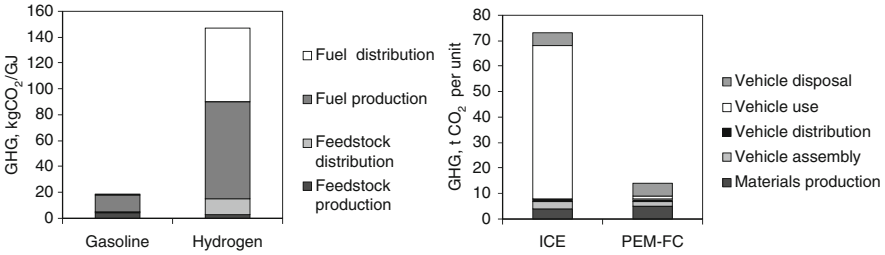

(a) Fuel cycle (b) Vehicle cycle

Fig. 15.6 Impact analysis presented in the form of GHG emissions for fuel and vehicle cycles

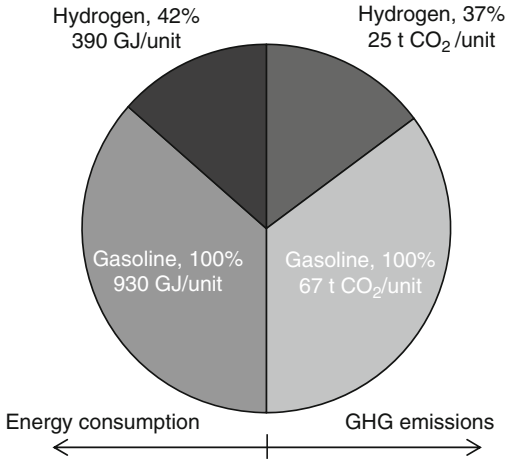

Fig. 15.7 Improvement assessment of hydrogen vehicle with respect to gasoline reference

- The life-cycle energy consumption of the hydrogen vehicle is divided by that of the reference gasoline vehicle to determine the energy reduction in percents.
- Similarly, the GHG emissions for the two cases are determined by adding the contribution of each phase.
- The GHG emissions of the gasoline vehicle are assigned to 100%.
- The percent of the life cycle of the GHG emission for the hydrogen vehicle case with respect to the gasoline reference case is calculated by dividing the GHG emissions associated with the hydrogen vehicle into that of the gasoline vehicle.

Figure 15.7 presents the improvement assessment of the transportation sectors, restricted for this case study to passenger cars. By comparing the reference gasoline vehicle case, which is the technology presently in use, with the hydrogen vehicle, which represents a technology in the course of implementation, one can comparatively assess the life-cycle improvement. Indeed, by using the hydrogen vehicle, even if the hydrogen is derived from a fossil fuel as natural gas, there is an improvement with respect to the reference case in at least two important directions: (a) the primary energy consumption is reduced to 42%, and (b) the associated life-cycle GHG emissions are

reduced to 35%. Of course, the analysis can be extended by including the effects of other pollutants and of other effects such as material resource depletion. However, as this preliminary analysis indicates, implementing hydrogen–fuel cell vehicles represents an important step toward sustainable transportation.

15.4.2 Comparative Life-Cycle Assessment of Conventional and Alternative Vehicles

In this case study, one exemplifies the use of LCA methodology in the automotive industry. This example is extracted from Granovskii et al. (2006b,c) and Dincer et al. (2010). One component of sustainability requires the design of environmentally benign vehicles characterized by little or no atmospheric pollution during operation. Note also that the conventional gasoline vehicles generate about 350 g of GHG per km; in a country like Canada, these figures lead to 70 million tons of GHG emissions per year due to vehicle use.

There are many opportunities to improve vehicles for better sustainability, such as advanced power train systems, fuel processing, and power conversion technologies utilizing various fuels or electricity stored in batteries for vehicle propulsion. Appropriate assessment of the environmental impact and energy consumption throughout the overall hydrogen production and utilization life cycle, in comparison with that of the gasoline vehicle, is critical for making proper decisions about the hydrogen vehicle's competitiveness.

In this LCA study, six kinds of vehicles are compared:

1. Conventional vehicle equipped with gasoline-fueled ICE
2. Hybrid vehicle equipped with lower capacity gasoline-fueled ICE, electrical drive/generator, and rechargeable electrical battery
3. Electric vehicle comprising high-capacity electrical battery and electrical drive/generator
4. Hydrogen–fuel cell vehicle with hydrogen storage on-board in a high-pressure tank
5. Hydrogen internal combustion vehicle equipped with ICE and high-pressure H_2 tank
6. Ammonia-fueled vehicle that uses ammonia as a hydrogen source (ammonia is stored as pressurized liquid in a tank; it is decomposed thermo-catalytically to generate pure hydrogen, which in turn is used to fuel an ICE)

Six vehicles were selected from manufacturer catalogs that represent the six options described above. For options 1 to 5, the five vehicles are, respectively, Toyota Corolla, Toyota Primus Hybrid, Toyota RAV4EV all-electric, Honda FCX, and Ford Focus H_2ICE. For the analysis, the necessary technical data for vehicles 1 to 5 were taken from manufacturers' published data sheets. For option 6, a thermodynamic model was elaborated to predict the operation of Ford Focus H_2ICE (vehicle 5); in this case, the primary fuel stored on-board is ammonia, which is converted to hydrogen

Table 15.4 Main characteristics of inventoried vehicles

Vehicle	Engine type	Fuel consumption (MJ per 100 km)	Fuel type	Driving range (km)	Battery life cycle cost (USk$)	Curb mass (kg)
Conventional	ICE	237	Gasoline	540	0.1	1,134
Hybrid	ICE + electric	138	Gasoline	930	1.02	1,311
Electric	Electric	67	Electricity	164	30.8	1,588
Fuel cell	Electric	129	Hydrogen	355	0.1	1,678
H_2–ICE	ICE	200	Hydrogen	300	0.1	1,500
NH_3–H_2–ICE	ICE	175	Ammonia	430	0.1	1,500

Data from Dincer et al. (2010)

(as already mentioned) by thermo-catalytic cracking using heat recovered from the exhaust gases. Moreover, it is assumed that the vehicle engine operates with hydrogen delivered at the same parameters as for the original Ford design specifications.

15.4.2.1 Inventory Analysis

The main characteristics of the selected vehicles are compiled in Table 15.4; the life cycle of the vehicle is assumed to be 10 years for all cases. The curb mass of each vehicle is also reported. We assume that the ammonia-fueled vehicle has the same curb mass as the H_2–ICE vehicle from which it originates. The justification for this assumption comes from the fact that the ammonia and hydrogen vehicles have system components of similar weight, because the car frame is the same, the engine is the same, and the supercharger of the hydrogen vehicle likely has a similar weight as the ammonia decomposition and separation unit of the ammonia-fueled vehicle. Table 15.5 presents the materials for the batteries and the fuel cell stack and the vehicle energy inventory for the entire life-cycle. Other common materials, mainly steel, are considered for the inventory analysis, which includes ICE engines.

The inventory includes analyses regarding the fuel-processing stages (for both the gasoline and hydrogen case). This part of the inventory is based on the results published in the reference source (Granovskii et al. 2006c), which lead to the conclusion that for producing 1 MW equivalent of fuel one has to consume 0.273 MW for the hydrogen (from natural gas) case and 0.173 MW for the gasoline case. Therefore, hydrogen production efficiency from natural gas is 78% while that of gasoline from crude oil is 85%. Also, the case of hydrogen production from wind energy and photovoltaic panels is considered in the present analysis, according to the results already presented above. All this information is applied to the particular case of the six vehicles considered here.

15.4.2.2 Impact Assessment

The life-cycle GHG emissions for 1 MJ of mechanical work generated at the vehicle shaft are calculated based on the results of Granovskii et al. (2006c),

Table 15.5 Materials for battery and fuel cell stack and vehicle life-cycle energy inventory

Component	Mass (kg)	Remarks
Battery (hybrid vehicle)	53	1.8 kWh capacity; 1.96 MJ electricity; and 8.35 MJ petroleum per kg
Battery (electric vehicle)	430	27 kWh capacity; 1.96 MJ electricity; and 8.35 MJ petroleum per kg
PEMFC stack		
Electrode	4.44	Contains platinum, ruthenium, carbon paper
Membrane	5.64	Nafion
Bipolar plate	53	Contains polypropylene, carbon fibers, carbon powder
End plate	2.8	Aluminum alloy
Current collectors	1.14	Aluminum alloy
Tie rod	2.05	Steel
Vehicle energy inventory		Energy consumption (GJ/unit)
Vehicle type		ICEPEMFC
Materials production		5055
Vehicle assembly		2524
Vehicle distribution		2.12.1
Vehicle use		819195
Disposal		0.300.3

Data from Hussain et al. (2007) and Dincer et al. (2010)

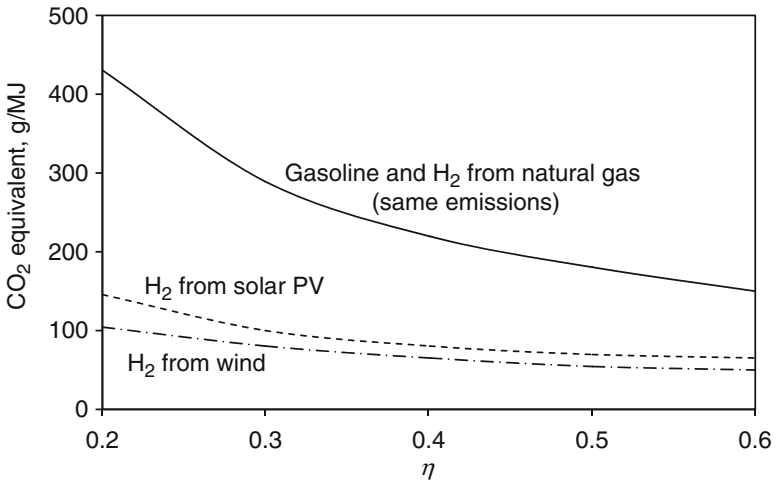

Fig. 15.8 GHG emissions for entire life cycle, during fuel processing and utilization

which are presented in Fig. 15.8. The emissions are correlated with the vehicle efficiency. Taking into account that the efficiency of the hydrogen vehicle is high (>40%) and that of the gasoline vehicle is low (~20%), these results show that the gasoline vehicle emits the most during its lifetime.

The result from Fig. 15.8 is further used to calculate the GHG emission for the exact cases of the six vehicles. In this respect, the actual shaft work is considered for each particular vehicle. In addition to the GHG, for the assessment of

Table 15.6 Environmental impact for the life-cycle of several types of vehicles

Vehicle	Impact calculation equations	GW (kg CO_2 equivalent/ 100 km)	AP (g/ 100 km)
Conventional	$AP = m_{curb}AP_m$; $GW = m_{curb}GWP_m$	1.5	3.6
Hybrid	$AP = (m_{curb} - m_{bat})$ $AP_m + m_{bat}AP_{bat}$; $GW = (m_{curb} - m_{bat})$ $AP_m + m_{bat}GWP_{bat}$	1.7	4.2
Electric	$AP = (m_{curb} - m_{bat})$ $AP_m + m_{bat}AP_{bat}$; $GW = (m_{curb} - m_{bat})$ $AP_m + m_{bat}GWP_{bat}$	2.0	6.2
Fuel cell	$AP = (m_{curb} - m_{fc})$ $AP_m + m_{fc}AP_{fc}$; $GW = (m_{curb} - m_{fc})$ $AP_m + m_{fc}GWP_{fc}$	4.1	17.8
H_2–ICE	$AP = m_{curb}AP_m$; $GW = m_{curb}GWP_m$	1.5	4.0
NH_3–H_2–ICE	$AP = m_{curb}AP_m$; $GW = m_{curb}GWP_m$	1.4	3.0

Data from Dincer et al. (2010)

environmental impact, the air pollution (AP) indicator is calculated and both the AP and GHG are correlated with the curb mass of the car. Thus, the AP and GWP are estimated first for 1 kg curb mass of vehicle. The formulas used for the calculation and the amounts of GHG and AP are presented in Table 15.6.

Regarding electricity production for the electric car case, three scenarios are considered here:

- Scenario 1: electricity is produced from renewable energy sources and nuclear energy
- Scenario 2: 50% of the electricity is produced from renewable energy sources and 50% from natural gas at an efficiency of 40%
- Scenario 3: electricity is produced from natural gas at an efficiency of 40%

Each of the electricity-generation scenarios is characterized by its GHG and AP figures. For scenario 1, the emissions are the least; as reported in Dincer et al. (2010), they are 5.1 g CO_2 equivalent and 20 mg AP equivalent per MJ of electricity produced. Scenario 3 is the most polluted, with 150 g CO_2 and 573 mg AP. The life-cycle environmental emissions, quantified through GWP and AP, are indicated in Table 15.7 for each vehicle type and electricity-generation scenario. Using other vehicle parameters such as cost, range, and fuel cost, together with GWP and AP, normalized indicators were obtained for all cases. The normalized indicators are obtained according to Eq. (15.12) for each scenario. For example, in the case of scenario 1, the hydrogen–fuel cell vehicle has the maximum vehicle cost with a cost indicator of 0.154; the conventional vehicle has the minimum cost with a cost indicator of 1. For each case, a general indicator is obtained using Eq. (15.13);

Table 15.7 Normalized performance, economic, and environmental indicators

				Normalized indicators					
Vehicle	Scenario	GWP (kg/100 km)	AP (mg/100 km)	Cost	Range	Fuel cost	GWP	AP	General
Conventional	1	21	60	1	0.581	0.307	0.098	0.126	0.096
	2			1	0.581	0.307	0.098	0.283	0.2
	3			1	0.581	0.307	0.098	0.283	0.2
Hybrid	1	13	37	0.733	1	0.528	0.105	0.204	0.362
	2			0.733	1	0.528	0.105	0.459	0.755
	3			0.733	1	0.528	0.105	0.459	0.755
Electric	1	2.3	7	0.212	0.177	1	0.610	1	1
	2	7.2	26	0.216	0.177	1	0.194	0.649	0.195
	3	12	45	0.212	0.177	1	0.117	0.379	0.067
Fuel cell	1	14.2	31	0.154	0.382	0.523	0.098	0.247	0.033
	2	14.7	32	0.154	0.382	0.523	0.095	0.525	0.063
	3	15.2	34	0.154	0.382	0.523	0.092	0.497	0.058
H_2–ICE	1	11.5	18	0.255	0.322	0.110	0.122	0.420	0.020
	2			0.255	0.322	0.110	0.122	0.940	0.042
	3			0.255	0.322	0.110	0.122	0.940	0.042
NH_3–H_2–ICE	1	1.4	17	0.382	0.462	0.140	1	0.440	0.475
	2			0.382	0.462	0.140	1	1	1
	3			0.382	0.462	0.140	1	1	1

Data from Dincer et al. (2010)

furthermore, the general indicator is normalized by dividing it by the maximum value for each scenario. The normalized general indicator is shown in the last column of Table 15.7.

The results indicate that hybrid and electric cars are competitive if nuclear and renewable energies account for about 50% of the energy used to generate electricity. If fossil fuels (in this case natural gas) are used for more than 50% of the energy to generate electricity, the hybrid car has significant advantages over the other five. For electricity-generation scenarios 2 and 3, however, the ammonia-fueled vehicle becomes the most advantageous option, based on the normalized general indicator values.

15.4.3 Comparative LCA of Hydrogen Production from Renewable Sources

Exergy efficiency, economic effectiveness, and environmental impact of producing hydrogen using wind and solar energy in place of fossil fuels are evaluated here using exergetic comparative LCA. The product is hydrogen fuel, and its assumed use is only to fuel hydrogen–fuel cell vehicles as a substitute for gasoline. The use of hydrogen as a fuel for fuel cell vehicles can lead to significant reductions in air pollution and greenhouse gas emissions.

The utilization of hydrogen in fuel cell vehicles can be considered as ecologically benign, regarding direct vehicle emissions. The emissions of pollutants occur during hydrogen production. In a gasoline-fueled vehicle, the combustion process

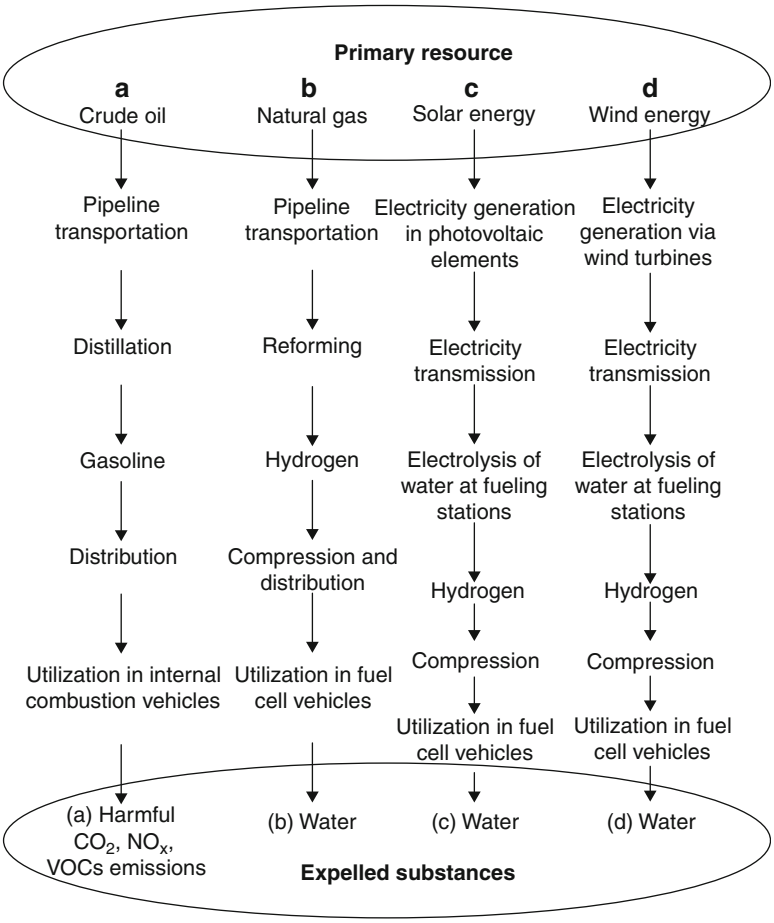

Fig. 15.9 Principal technological phases considered in the comparative LCA of transportation fuels: (**a**) crude oil/gasoline; (**b**) natural gas/H_2; (**c**) solar energy/H_2; (**d**) wind energy/H_2

generates steam, carbon dioxide, and heat, and the heat is partially converted into mechanical work for propulsion. Because combustion of gasoline in ICE occurs at about 1,300°C, formation of nitrogen oxides is promoted. Evaporation of gasoline and incomplete combustion lead to emissions of VOCs and carbon monoxide. Thus, air pollution and greenhouse gas emissions are associated with gasoline production and its utilization in ICE vehicles.

Adequate evaluation of environmental impact and energy use throughout the overall production and utilization life cycle, that is, application of the comparative LCA method, is critical for the proper evaluation of technologies. The present case study aims to examine the efficiency, cost-effectiveness, environmental impact, and sustainability aspects of the processes for comparison purposes. The principal technological phases considered in the comparative LCA are presented in Fig. 15.9.

As it can be seen, for two cases the considered primary energy source is a fossil fuel, while for the other two cases it is a renewable energy (wind and solar). Life-cycle exergy efficiencies, capital investment effectiveness factors, and environmental impacts are then examined.

15.4.3.1 Inventory Analysis

The comparative LCA study starts with the inventory analysis of each phase of the life cycle. The analysis is done for all four cases considered for comparison. In cases (a) and (b), the primary fossil fuel (crude oil and natural gas, respectively) is transported first from the extraction sites to the production site. At the production site, crude oil is refined to gasoline and natural gas is reformed to hydrogen. For cases (c) and (d), there is no transportation of primary resource, but rather electricity is generated locally.

We first discuss crude oil and natural gas transport, from the perspective of inventory analysis. Both crude oil and natural gas are transported in pipelines with an assumed lifetime of 80 years, whereas the pumps and compressors that serve for oil and natural gas transport, respectively, have an assumed lifetime of 20 years. In order to evaluate the exergy embodied in the oil and natural gas pipelines, both are assumed to have a 1,000-km length. The analysis starts by considering the typical characteristics of the pipelines, which are given as follows:

- Crude oil: 40 cm diameter, exergy rate of input flow 90 GW, mass of pipeline 64 kt, embodied exergy 2.3 PJ in pipeline and 4.2 in pumps
- Natural gas: 80 cm diameter, 6.9 GJ exergy rate of input flow, mass of pipeline 126 kt, embodied exergy 4.5 PJ in pipeline and 1.5 PJ in compressors

In addition, one assumes 0.65 isothermal efficiency of compressors and pumps, and an 80-year lifetime of the pipelines and a 20-year lifetime of the compressors and pumps. It is also assumed that the exergy associated with installation, maintenance, and operation of the equipment is the same as the embodied exergy to produce it. The energy needed to drive the fuel transportation to pipelines is produced by a gas turbine power plant with an exergy efficiency of 33%. Based on this efficiency, one can determine the indirect and direct exergy consumption rate, which is, for transportation of a fuel quantity with an exergy rate equivalent to 1 MW,

- 95.3 kW (direct) and 13 kW (indirect) for natural gas pipeline
- 16.2 kW (direct) and 2.2 kW (indirect) for crude oil pipeline

One observes that the indirect exergy rate is much smaller than the direct one; thus, for the purpose of this study, the indirect exergy consumption rate is ignored.

We discuss now alternative (d) from Fig. 15.9, that is, production of hydrogen from wind energy. This production system has two components: a wind turbine electric power generator and an electrolyzer. Granovskii et al. (2007a) used the typical material consumption figures for a 6-MW wind turbine to determine the

Table 15.8 Material requirements and associated exergy for 6-MW wind power generation

Materials	Quantity (tonnes)	Embodied exergy (GJ/t)	Exergy equivalent per second of lifetime (MJ/s)
Concrete	7,647	1.46	0.216
Copper	5.275	136	0.0119
Fiberglass	497	13.5	0.122
Carbon steel	1,888	35.8	0.545
Stainless steel	226	55	0.101

Data from Granovskii et al. (2007a)

Table 15.9 Devices and associated exergy for 1.231-kW photovoltaic system

Devices	Embodied exergy (GJ/unit)	Exergy equivalent (GJ/unit)	Percent distribution of embodied energy in solar cells (%)			
Inverters	41.6	116	Encapsulation	79	Busbar	2
Electric components and wiring	3.02	49	Substrate	5	Back reflector	2
Solar cells	123.1	716	Deposition	9	Grid	2

Data from Granovskii et al. (2006c) and Granovskii et al. (2007a)

exergies associated with its construction. These exergies and the materials are listed in Table 15.8. Also the assumed exergy efficiency for electrolysis is 72% and the indirect exergy is 6.6% of the wind power generation. Accounting for 7% electricity loss during transmission, the efficiency of hydrogen production is 66.9%.

Regarding hydrogen production from solar energy, a system of photovoltaic panels and an electrolyzer are considered. Thin-film amorphous silicon technology is assumed for the photovoltaic system. Table 15.9 presents the equipment and associated exergy for a unit producing 1.231-kW photovoltaic electricity and having a 30-year lifetime. The resulting operation exergy per second of lifetime is 82.1 J and the indirect exergy rate is 1.01 kW. The combined system of solar panel and electrolyzer produces 807 W of hydrogen energy.

Another process for inventory analysis, common to scenarios (b), (c), and (d) from Fig. 15.9, is hydrogen compression, which is needed for short-term storage (storage of hydrogen is discussed in Chapters 4 and 13). In order to compress one mole of hydrogen isothermally, the consumed exergy, assuming ideal gas behavior, is given as follows:

$$\Delta Ex_{\text{dir}}^{\text{cmp}} = \frac{RT_0}{\eta_{\text{cmp}}\eta_{\text{el}}^{\text{ng}}} \ln\left(\frac{P_{\max}}{P_{\min}}\right), \tag{15.16}$$

where T_0 is the standard reference temperature, R is the universal gas constant, P is the pressure of hydrogen before (min) and after (max) compression, η_{cmp} is the isothermal compression efficiency assumed to be 0.65, and $\eta_{\text{el}}^{\text{ng}}$ is the efficiency of electricity generation from natural gas, which is taken to be an average value of

Table 15.10 Process phases considered for environmental assessment

Phase	Gasoline	Natural gas	Wind and solar
1	Crude oil pipeline transportation and distillation	Pipeline transportation and reforming	Electricity generation
2	Gasoline delivery to fueling stations	Hydrogen compression from 20 to 350 bar	Water electrolysis
3	Gasoline utilization in ICE engines	Hydrogen delivery to fueling stations	Hydrogen compression

40% (assuming a gas turbine generator). The minimum pressure is taken to be 1 atm if the process of production is electrolysis, and 20 atm if hydrogen is produced by natural gas reforming. The pressure of compressed hydrogen is assumed to be 350 atm.

Regarding the fuel distribution, this is a common step for all the production strategies (a–d) considered here. However, what differentiates the options is that, in the case of solar and wind energies, the transmitted energy is in the form of electricity. The distribution of compressed hydrogen after its production via natural gas reforming is similar to that for liquid gasoline, but compressed hydrogen is characterized by a lower volumetric energy capacity and higher material requirements for a hydrogen tank. The direct exergy for fuel distribution of 1 MJ equivalent fuel (hydrogen or gasoline) is as follows:

- Hydrogen from natural gas: 0.119 MW (compression) and 0.025 MW (distribution)
- Hydrogen from wind: 0.238 MW (electricity consumed for distribution and compression)
- Hydrogen from solar: 0.238 MW (electricity consumed for distribution and compression)
- Gasoline fuel: 0.0025 MW (distribution only; compression is not needed).

15.4.3.2 Comparative Impact Assessment

The following categories of environmental impact from via pollution are most relevant for the studied technologies: (a) greenhouse gases comprising carbon dioxide (CO_2 as the major product of combustion processes), methane (CH_4 occurring mainly as a result of incomplete combustion), and nitrous oxide (N_2O); (b) airborne pollutants comprising carbon monoxide (CO), nitrogen oxides (NO_x), and VOCs. The greenhouse gas emission and equivalent air pollution are calculated by considering three phases of emissions for each of the parallel technologies, which are illustrated in Table 15.10. For the same phase, the air pollutants (CO, NO_x, and VOCs) were calculated as a pre-unit of MJ of the produced hydrogen or gasoline (whichever is the case) with respect to the LHV.

Figure 15.10a shows the equivalent greenhouse gas emissions in grams per MJ shaft energy LHV. Observe that the total GHG emissions are low for wind and solar

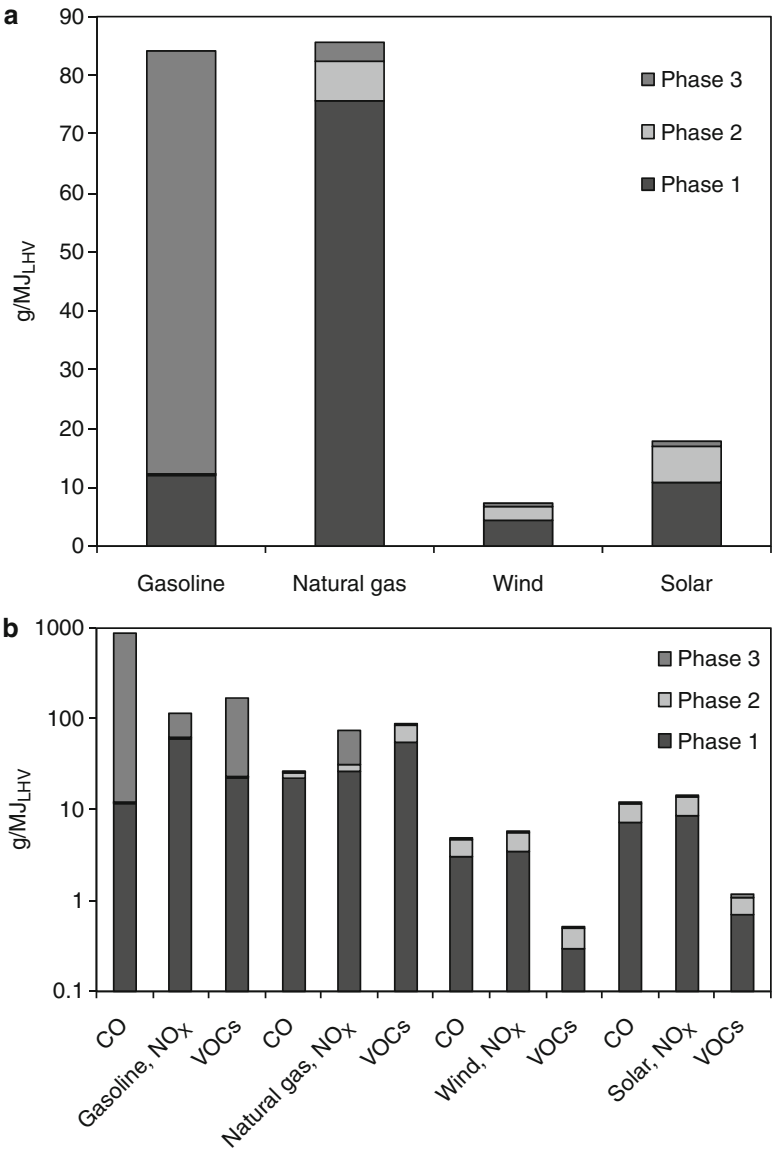

Fig. 15.10 Pollution associated with technological processes [data from Granovskii et al. (2007a)]: (**a**) greenhouse gas emissions and (**b**) air pollutant emissions

technologies as compared to natural gas reformed by hydrogen and gasoline fuel. In Fig. 15.10b, the calculated air pollution components (CO, NO_x, and VOCs) for all considered phases of the life cycle are shown.

The emission data are further compiled to obtain the graphical representations in Fig. 15.11, which show the improvement in air pollution due to alternative

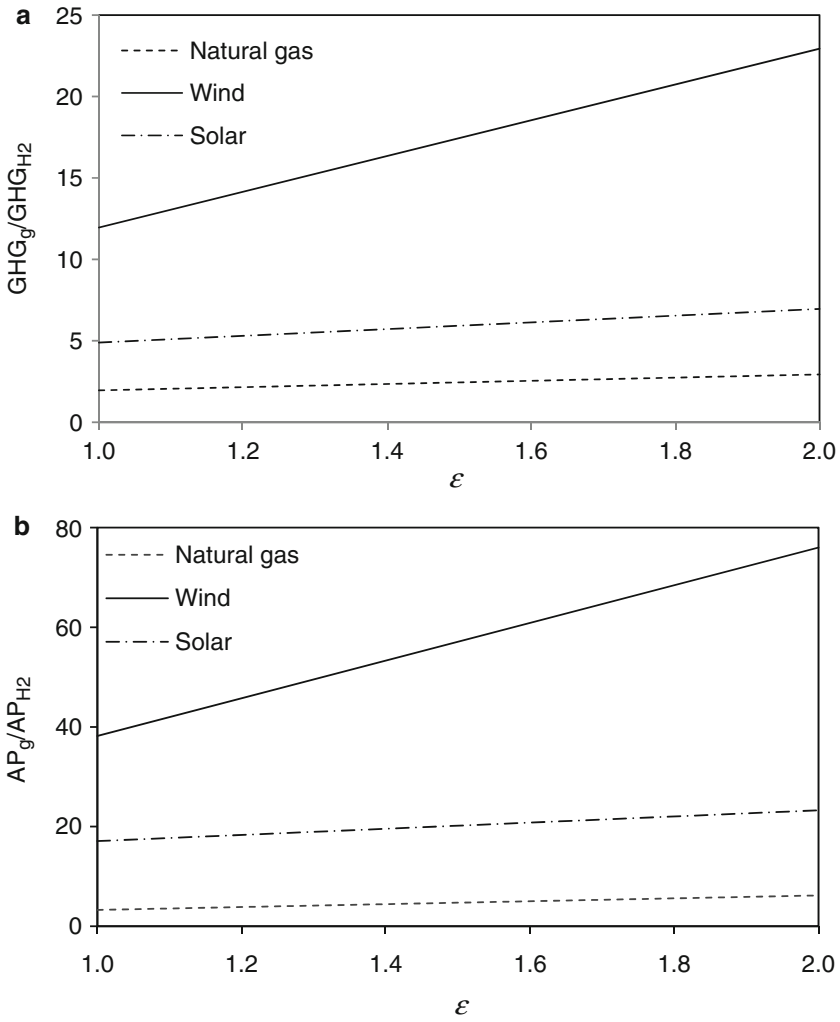

Fig. 15.11 Reduction of air pollution via alternative hydrogen technology, given with respect to gasoline-fuel reference case [data from Granovskii et al. (2007a)]: (**a**) greenhouse gas emissions and (**b**) air pollutant emissions

hydrogen technologies with respect to the gasoline-fuel reference case. In Fig. 15.11a, the ratio between the life-cycle GHG emissions for the gasoline case and the alternative technology case (hydrogen from natural gas, wind, and solar energy) is plotted against the reference case. In Fig. 15.11b, the analogous ratio for the equivalent air pollution factor (AP) calculated with Eq. (15.7) is shown. One observes that the application of wind-hydrogen technology leads to the greatest reduction in air pollution.

Table 15.11 Life-cycle exergy efficiency and resource utilization to produce 1 MW of chemical exergy in the form of fuel

Energy carrier	$\sum \Delta \dot{E}x_{\text{dir}}$ (MW)	$\dot{E}x_{\text{LFC}}$ (MW)	ψ^{LFC}
(a) Gasoline fuel	0.171	1.171	0.85
(b) H_2 from natural gas	0.535	1.535	0.65
(c) H_2 from solar	0.238	1.338	0.64
(d) H_2 from wind	0.238	0.539	1.86

The other renewable solution—solar energy—is also attractive, but its associated pollution reduction is much lower than those of wind energy, because construction of photovoltaic cells is an intensive energetic process characterized by air pollution.

15.4.3.3 Exergetic Life-Cycle Assessment

The life-cycle exergy of the overall process is calculated using Eq. (15.9) where the input is the overall life-cycle fossil fuel and mineral exergy consumption rates to produce hydrogen and gasoline, respectively. Table 15.11 reports the LCA results. Observe that the life-cycle exergy efficiency of hydrogen production from wind energy reaches 1.86, which is a supra-unitary value, which means that the consumed fuel exergy (including the equivalent embodied materials and equipment exergy) is lower than the exergy in the produced hydrogen. The wind exergy is considered free and is not included as input.

However, the exergy efficiency of a wind power plant, which is a parameter used for the design of a power generation system, refers to the wind exergy as input. The life-cycle exergy efficiency for the case when solar radiation is the primary source also accounts for the fact that the solar energy is "free"; in this case the life-cycle efficiency is still less than 1 because valuable materials are required for PV cell manufacturing, and thus the indirect exergy consumption becomes very high.

One can add a last step to the life cycle, namely the utilization of hydrogen as fuel. Two kinds of engines are considered for propulsion of vehicles, namely, ICE and PEMFC. The exergy efficiency of ICE ranges from 20% to 30% while that of PEMFC is much higher: 40% to 60%. Thus, one can define the life-cycle exergy efficiency of fuel consumption on a vehicle as

$$\psi_{\text{VLC}} = \psi_{\text{LFC}} \times \psi_{\text{ENG}}, \tag{15.17}$$

where ψ_{ENG} is the exergy efficiency of the engine. We denote ε as the ratio of exergy efficiency of the hydrogen-powered fuel cell engine and the efficiency of gasoline-powered ICE. The mechanical energy developed at the engine shaft for a unit of exergy of primary energy can be calculated for the two cases: hydrogen PEMFC (W_{H_2}) and gasoline ICE (W_{g}). The ratio, $W_{\text{H}_2}/W_{\text{g}}$, calculated for a range of ε is presented in Fig. 15.12, which shows that the efficiency of a fuel cell vehicle operating on hydrogen from natural gas must be at least 25% to 30% greater than

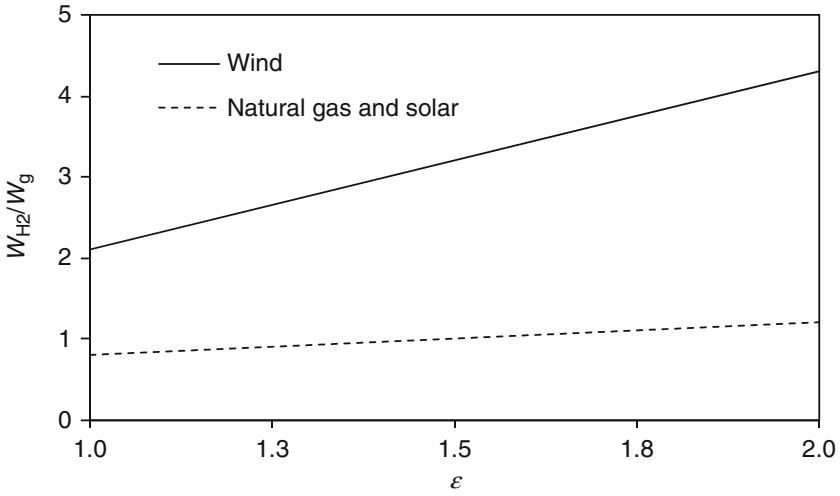

Fig. 15.12 Shaft work developed by hydrogen engine vs. gasoline engines for the same amount of exergy embedded in the primary energy source

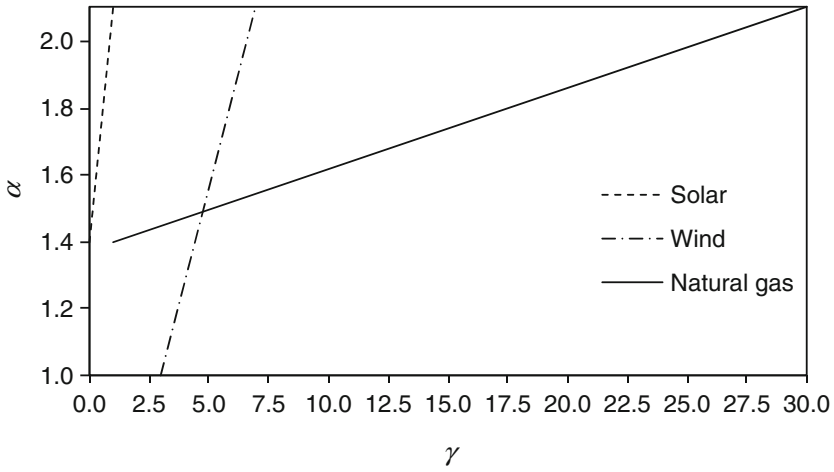

Fig. 15.13 Cost ratio (α) for a given investment effectiveness factor (γ) for alternative technologies

that of an internal combustion gasoline engine. The application of hydrogen from wind energy in a fuel cell vehicle is extremely efficient with respect to fossil and mineral resources utilization.

The exergy analysis allows the calculation of the capital investment effectiveness factor (γ) according to Eq. (15.13). For the particular case studied here, the parameter α appearing in Eq. (15.13) is taken as the ratio of hydrogen and natural

unitary cost (i.e., cost per unit of embedded energy). Figure 15.13 correlates the cost ratio (α) with the investment effectiveness factor (γ) for the three alternative technologies considered here.

The assumed life-cycle exergy efficiencies for calculating γ were 0.72 for hydrogen production via natural gas, 3.32 for hydrogen generation with wind energy, and 0.75 for hydrogen production using solar energy. Since the current cost per unit of energy of hydrogen is about two times that of natural gas, the capital investment effectiveness in hydrogen–natural gas solution is close to 30 while that for solar technology is about 6 (that is, 5 times less). This situation can be altered by reducing the requirements of construction materials of wind power plants per unit of electricity generated. It appears that fossil fuel technologies for hydrogen production from natural gas and gasoline from crude oil are complement with renewable ones.

The use of wind power to produce hydrogen via electrolysis, and its application in a fuel cell vehicle, exhibits the lowest fossil fuel consumption rate. However, the economic attractiveness (capital investment effectiveness factor) of renewable technologies depends significantly on the ratio of costs for hydrogen and natural gas.

"Renewable" hydrogen appears to provide a potential long-term solution to environmentally related problems. Depending on the ratio of efficiencies of fuel cell (hydrogen powered) and ICE (gasoline powered) vehicles, substitution of gasoline with "renewable" hydrogen leads to a reduction of GHG emissions of up to 23 times for hydrogen from wind and 8 times for hydrogen from solar energy, and a reduction of air pollution emissions of up to 76 times for hydrogen from wind and 32 times for hydrogen from solar energy.

15.4.4 LCA of Nuclear-Based Hydrogen Production by Thermochemical Water Splitting

The application of LCA is exemplified here for the production of hydrogen via a CuCl thermochemical water splitting cycle driven by thermal energy that is derived from nuclear reactors. Hydrogen, when used for power generation, does not emit any pollutants, and thus is totally benign to the environment. However, the true environmental benefit of hydrogen can be determined by considering the environmental impacts of the hydrogen production processes. A series of copper- and chlorine-based compounds are used in the thermochemical water splitting cycle to drive a series of reactions that have the overall effect of water splitting in hydrogen and oxygen. The CuCl thermochemical water splitting cycle is detailed elsewhere in this book. For the purpose of LCA analysis, this cycle is briefly explained in Lubis et al. (2008, 2010), which is the reference work for the case study presented here. The nuclear reactor to drive the water splitting process in this case study is the supercritical water cooled reactor (SCWR). The SCWR is somewhat different from other reactor technologies in its reliance on heavy water to achieve a nuclear reaction with uranium fuel. The amount of uranium fuel for 1 MWth (megawatt thermal) heat is

$$m = \frac{Q}{B_d}, \tag{15.18}$$

where B_d is the discharge burn-up (assumed 480 MWh per kg uranium).

The entire life cycle of nuclear-based thermochemical hydrogen production is considered, allowing environmental issues to be quantified and related specifically to the part of the life cycle that is responsible for them.

15.4.4.1 Inventory Analysis

The emissions from the overall system are the sum of the emissions from the advanced nuclear power plant and the thermochemical hydrogen production plant. It is assumed that the nuclear plant is rated at 2,060 MWth and that the entire thermal output of the nuclear plant is dedicated to producing hydrogen. The thermochemical plant is assumed to have a hydrogen production capacity of 5,200 kg/h of H_2 and a 30-year operational life. Calculations are based on 1 hour of operation of the entire plant. The environmental emissions from the nuclear plant are mainly from the nuclear fuel cycle and the plant construction and installation stages.

The environmental impacts of the thermochemical hydrogen production plant can be estimated based on the energy used for chemicals in the process, the use of raw materials, and the fabrication and installation of the plant. The energy required to operate the thermochemical plant is provided by the nuclear power plant, and it has been accounted for in its assessment. It is determined that 514,800 kg of CuCl and 189,600 kg of HCl are required to produce 5,200 kg of hydrogen. The CuCl has a density of 3,700 kg/m^3 and the volume of the pressure vessel is 72 m^3. Then, HCl has a density of 1,191 kg/m^3 and a pressure vessel volume of 403 m^3. No loss of CuCl and HCl is assumed over the lifetime of the plant. Since calculations here are based on 1 hour of operation of the plant, the inventory of CuCl and HCl required on an hourly basis can be thought of as being the above values divided by the number of hours in 30 years. The inventory of water is 40 tons, which has a density of 15 kg/m^3 and a pressure vessel volume of 4,454 m^3.

Overall, the inputs for producing 5,200 kg of hydrogen are 4.29 kg uranium and 163 tons of heavy water; the thermal output of the nuclear reactor is 7.43 TJ. The total emissions of the system are the sum of the emissions from the advanced nuclear plant and the thermochemical hydrogen production plant. Table 15.12 gives the inventory analysis for 1 hour of operation of the nuclear-driven hydrogen production plant.

15.4.4.2 Impact and Improvement Assessments

The environmental impact and improvement assessment are two consecutive stages of LCA. We discuss first the environmental impact, which estimates the actual environmental burden produced by the analyzed product/technology.

Table 15.12 Inventory analysis for 1 hour of operation of a nuclear-driven hydrogen production plant

Phase	Process	Description	Economic inflows	Economic outflows	Environmental resources
Uranium fuel processing	Mining	Mining of uranium ore	158 MJ Electricity 37 MJ Fuel	4.29 kg Uranium in ore	Land 0.7 m^2 Water 0.009 m^3
	Milling	Milling the ore	176 MJ Electricity 359 MJ Heat	4.29 kg Milled uranium	Land 3.22 m^2 Water 1.96 m^3
	Conversion	Producing UF_6	136 MJ Electricity 49.3 GJ Coal 712 MJ Natural gas	4.29 kg Uranium in form of UF_6	Water 2.84 m^3
	Enrichment	Enriching up to 3.5% ^{235}U isotope	28.4 GJ Electricity 407 MJ Coal 7.21 MJ Gasoline	4.9 kg Uranium in form of enriched ^{235}U	Water 8.32 m^3
	Fabrication	Uranium fuel elements	163 MJ Electricity 463 MJ Coal 124 MJ Natural gas	4.9 kg Uranium in fuel elements	Water 0.53 m^3
	Heavy water	Production of D_2O	3.9 PJ Electricity	163 t	N/A
Construction	Nuclear plant	Construction and decommissioning of nuclear plant	199 kg Concrete 0.15 kg Copper 0.25 kg Lead 0.11 kg Aluminum 0.8 kg PVC 19 kg Spurce 50 kg Steel 0.07 kg Titanium	1 Nuclear power plant	N/A
	Water splitting plant		0.08 kg Aluminum 152 kg Concrete 1.2 kg Copper 0.19 kg Lead	1 Hydrogen production plant	N/A

(continued)

Table 15.12 (continued)

Phase	Process	Description	Economic inflows	Economic outflows	Environmental resources
			0.6 kg PVC 14 kg Spruce 3.9 kg Steel 0.06 kg Titanium		
Operation	Nuclear plant	For production of 7,430 GJ heat in the nuclear reactor	0.03 kg Aluminum 0.27 kg Copper 0.073 kg Lead 0.98 kg Steel 0.002 kg Titanium	Nuclear heat 7,430 GJ	Heavy water 163 t
	Water splitting plant	For production of 5,200 kg/day hydrogen	1.9 kg CuCl 0.7 kg HCl 1.6 t Water 0.13 g Aluminum 1 kg Copper 0.28 g Lead 1 g PVC 3.9 g Steel 17 mg Titanium	Hydrogen 5,208 kg	N/A

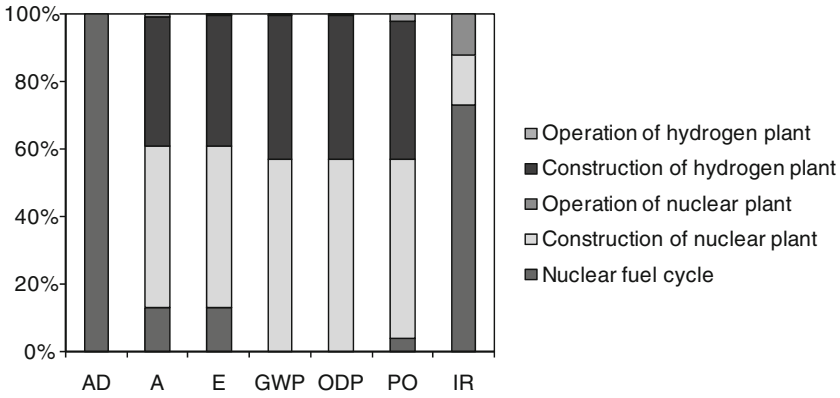

Fig. 15.14 Percentage contributions to environmental impact from main processes of nuclear-driven hydrogen production [data from Lubis et al. (2010)]

The improvement assessment aims to offer a number of alternatives to reduce the environmental impact of the studied process. The environmental impacts are assessed based on the emission determined by the inventory analysis phase, considering each category, according to the definitions in Table 15.1 and Eqs. (15.1) to (15.5). The authors of the study, Lubis et al. (2010), used the GaBi (2010) database to determine and quantify the environmental emissions. The results of the impact assessment are summarized in Table 15.12 (second column) and Fig. 15.14.

A number of possible improvements of the life cycle have been identified for reducing the environmental impacts associated with nuclear-based hydrogen production via thermochemical water decomposition using the copper–chlorine thermochemical cycle. The proposed improvements are as follows:

- Changing the quantity of materials for the construction of the thermochemical plant
- Changing the inventory requirements of chemicals and raw materials in a thermochemical plant
- Reducing nuclear plant emissions. The actual emissions can be 50% higher due to the increased plant complexity. In contrast, a higher burn-up and more efficient utilization of nuclear fuel would lower the emissions from ore processing.

The improvement assessment is presented compactly in columns 3 to 6 of Table 15.13. The LCA indicates that most of the environmental impacts are associated with the nuclear plant and construction of the hydrogen plant. In fact, over 95% of the GWP is released from the nuclear plant and the construction of the hydrogen plant, while 99% of the total acidification potential is contributed during the deployment of the nuclear fuel cycle and construction of the nuclear plant and the hydrogen plant. This LCA highlights the fact that the nuclear plant and construction of the hydrogen plant contribute significantly to the environmental impacts of the overall system. Improvement analysis suggests the development of more sustainable processes in the nuclear plant and construction of a hydrogen production plant.

Table 15.13 Impact and improvement assessments of nuclear-driven hydrogen production

		Improvement assessment			
Category	Impact assessed	Materials doubled	Chemical inventory doubled	Nuclear emissions doubled	Nuclear emissions halved
AD (g antimony equivalent)	1.88×10^{-7}	1.88×10^{-7}	1.88×10^{-7}	3.75×10^{-7}	9.39×10^{-8}
A (g SO_2 equivalent)	1.531×10^{-4}	2.1×10^{-4}	1.546×10^{-4}	2.478×10^{-4}	1.057×10^{-4}
E (kg PO_4 equivalent)	1.071×10^{-4}	1.473×10^{-4}	1.078×10^{-4}	1.73×10^{-4}	0.74×10^{-4}
GW (g CO_2 equivalent)	2.5144×10^{-3}	3.5843×10^{-3}	2.5235×10^{-3}	3.9496×10^{-3}	1.7967×10^{-3}
ODP (g CFC 11 equivalent)	7.161×10^{-7}	1.020×10^{-6}	7.18×10^{-7}	1.125×10^{-6}	5.113×10^{-7}
PO (kg ethylene equivalent)	1.425×10^{-4}	2.02×10^{-4}	1.437×10^{-4}	2.243×10^{-4}	1.015×10^{-4}
IR (DALY)	2.387×10^{-5}	2.659×10^{-5}	2.387×10^{-5}	4.503×10^{-5}	1.329×10^{-5}

AD abiotic resource depletion; *A* acidification; *E* eutrophication; *GW* global warming indicator; *PO* photo-oxidant formation indicator; *IR* ionizing radiation impact (measured in DALY = disability adjusted life years)

In summary, LCA is a method of system analysis from cradle to grave that is essential for the evaluation of sustainable energy systems and improvement of the design for better efficiency, reduced environmental impact, better economic outcome, and other goals. The analysis considers all phases of a product (system and technology) life cycle, starting with extraction of resources, manufacturing of materials and parts, assembly, use, maintenance, and disposal. In order to pursue an LCA project for all phases of the life cycle, an inventory analysis is developed. Data regarding material and energy consumption, cost, and environmental emission are compiled in an inventory table. Material and energy balances can be determined for the purpose of data validation. With an inventory table, it is possible to perform an environmental assessment and to quantify the overall life-cycle impact of the product/technology. Several technologies can be compared with regard to environmental impact, cost, efficiency (effectiveness), and other criteria. For an energy system, it is important to include exergy in the analysis and to determine the exergetic life-cycle efficiency and overall exergy balance. The improvement assessment is the final stage of an LCA project, in which various scenarios for improvement of the life-cycle performance of the product/technology are proposed and quantified. Normalized indicators can be developed with the purpose of quantifying various effects in an integrated manner. For example, a normalized general indicator can account for environmental impact, cost, and technical performance. LCA represents a valuable tool for policy and planning, offering a rational basis for decision making.

15.5 Concluding Remarks

The LCA represents a valuable tool for policy and planning offering a rational basis for decision making. This chapter presented the LCA methodology, which is comprised of a number of ISO standards. Exergetic-based LCA is an extension of the traditional LCA by including exergy flows, which give more insight regarding life-cycle losses and help in identifying ways of improving of the involved processes. Quantitative and qualitative methods to characterize the environmental impact of involved processes were described. The application of the LCA method was exemplified through four case studies. Some specific conclusions can be drawn as follows:

- In order to pursue an LCA project, an inventory analysis is developed first. Data regarding material, energy, and, if needed, exergy consumption, cost, and environmental emission are compiled in an inventory table. The acquired data can be validated in several ways, one of them being based on material and energy balances. Determining such balances requires a clear specification of the system boundaries.
- Developing an inventory table facilitates performing an environmental assessment and quantifying the overall life-cycle impact of the product/technology.
- Several technologies can be compared with respect to environmental impact, cost, efficiency (effectiveness), and other criteria. For energy systems, it is important to include exergy in the analysis and to determine the exergetic life-cycle efficiency and overall exergy balance.
- The improvement assessment is the final stage of an LCA project where various scenarios for improvement of the life-cycle performance of the product/technology are proposed and quantified.
- Normalized indicators can be developed with the purpose of quantifying various effects in an integrated manner. For example, a normalized general indicator can account for environmental impact, cost, and technical performance.

Nomenclature

A	Acidification indicator, kg SO_2 equivalent
ACP	Acidification potential, kg SO_2 equivalent per kg
AD	Abiotic depletion, kg antimony equivalent
ADP	Abiotic depletion potential, antimony equivalent per kg
AP	Air pollution indicator, kg NO_x equivalent
APP	Air pollution potential, kg NO_x equivalent per kg
Bd	Discharge burn-up, MJ/kg
EEQ	Total exergy equivalents
EOP	Exergy associated with manufacturing

Ex	Exergy, MJ
GW	Global warming indicator, kg CO_2 equivalent
GWP	Global warming potential, kg CO_2 equivalent per kg
HHV	Higher heating value, MJ/kg
LFT	Life-cycle time
LHV	Lower heating value, MJ/kg
m	Mass, kg
NInd	Normalized indicator
ODP	Ozone depletion potential
P	Pressure, Pa
PO	Photo-oxidant formation indicator, kg ethylene equivalent
POCP	Photochemical ozone creation potential, kg ethylene equivalent per kg
Q	Heat, MJ
R	Universal gas constant, J/mol·K
T	Toxicity indicator, kg DCB equivalent
TP	Toxicity potential, kg DCB equivalent per kg
W	Shaft work, MJ

Greek Letters

α	Cost ratio
γ	Capital investment efficiency factor
ψ	Exergy efficiency
η	Energy efficiency

Subscripts

cmp	Compression
dir	Direct
e	Environment
el	Electric
ENG	Engine
f	Fossil fuel
g	Gasoline
i	Index
ind	Indirect
LFC	Life-cycle
max	Maximum
min	Minimum
VLC	Vehicle life-cycle

Superscripts

$(\dot{})$	Rate (per unit of time)
i	Index
LFC	Life-cycle
ng	Natural gas

References

Dincer I. 2007. Environmental and sustainability aspects of hydrogen and fuel cell systems. *International Journal of Energy Research* 31:29–55.

Dincer I., Rosen M.A. 2007. Exergy: Energy, Environment and Sustainable Development. Elsevier, Oxford, UK.

Dincer I., Rosen M.A., Zamfirescu C. 2010. Economic and environmental comparison of conventional, hybrid, electric and hydrogen fuel cell vehicles. In: Electric and Hybrid Vehicles: Power Sources, Models, Sustainability, Infrastructure and Market, Pistoia G., eds., Elsevier, Oxford, UK.

GaBi 2010. LCA software databases, http://www.gabi-software.com/gabi/databases1/. Internet source (accessed on January 20, 2010).

Granovskii M., Dincer I., Rosen M.A. 2006a. Environmental and economic aspects of hydrogen production and utilization in fuel cell vehicles. *Journal of Power Sources* 157:411–421.

Granovskii M., Dincer I., Rosen M.A. 2006b. Economic and environmental comparison of conventional, hybrid, electric and hydrogen fuel cell vehicles. *Journal of Power Sources* 159:1186–1193.

Granovskii M., Dincer I., Rosen M.A. 2006c. Life cycle assessment of hydrogen fuel cell and gasoline vehicles. *International Journal of Hydrogen Energy* 31:337–352.

Granovskii M., Dincer I., Rosen M.A. 2007a. Exergetic life cycle assessment of hydrogen production from renewables. *Journal of Power Sources* 167:461–471.

Granovskii M., Dincer I., Rosen M.A. 2007b. Greenhouse gas emissions reduction by use of wind and solar energies for hydrogen and electricity production: economic factors. *International Journal of Hydrogen Energy* 32:927–931.

Guinee J.B. 2004. Handbook on Life Cycle Assessment. Operational Guide to the ISO Standards. Kluwer Academic Publishing, New York.

Hussain M.M., Dincer I., Li X. 2007. A preliminary life cycle assessment of PEM fuel cell powered automobiles. *Applied Thermal Engineering* 27:2294–2299.

ISO International Standard 14040. 1997E. Environmental management – Life cycle assessment – Principles and framework. International Organisation for Standardisation (ISO), Geneva.

ISO International Standard 14041. 1998E. Environmental management – Life cycle assessment – Goal and scope definition and Inventory analysis. International Organisation for Standardisation (ISO), Geneva.

ISO International Standard 14042. 2000E. Environmental management – Life cycle assessment – Life cycle Impact assessment. International Organisation for Standardisation (ISO), Geneva.

ISO International Standard 14043. 2000E. Environmental management – Life cycle assessment – Life cycle Interpretation. International Organisation for Standardisation (ISO), Geneva.

Lubis L.I., Dincer I., Rosen M.A. 2008. Life cycle assessment of nuclear-based hydrogen production using thermochemical water decomposition: extension of previous work and future needs. Canadian Nuclear Society 29th Annual Conference 2:686–697.

Lubis L.I., Dincer I., Rosen M.A. 2010. Life cycle assessment of hydrogen production using nuclear energy: an application based on thermochemical water splitting. *Journal of Energy Resources Technology* 132:021004/1-6.

Rosen M.A., Dincer I. 2003. Exergy–cost–energy–mass analysis of thermal systems and processes. *Energy Conversion and Management* 44:1633–1651.

Rubin E.S., Davidson C.I. 2001. Introduction to Engineering and the Environment. McGraw-Hill, New York.

Study Questions/Problems

15.1 Define the method of life-cycle assessment and explain its applications.
15.2 What represents comparative LCA?
15.3 What represents exergetic LCA?
15.4 Describe the stages of LCA methodology.
15.5 What are the parameters used to quantify the environmental impact in an LCA?
15.6 Explain the notion of abiotic resource depletion potential.
15.7 Comment on the environmental impact of energy systems.
15.8 Explain how an exergetic life-cycle assessment can be performed.
15.9 Define the capital investment efficiency factor.
15.10 What is the use of normalized indicators?
15.11 Perform a comparative life-cycle assessment between electric vehicles and compressed air vehicles of proximity.

Chapter 16
Industrial Ecology

16.1 Introduction

Industrial ecology is an approach to sustainable development that combines the sciences of environment, ecology, and engineering technology. The word *industrial* indicates that the approach focuses on manufacturing processes of a complex of products, which eventually can be interrelated. The significance of the term *ecology* is twofold: first, that man-designed industrial systems can mimic natural ecosystems (bio-mimetics of natural cycles); second, that minimization of the environmental impact of the designed process is an important goal.

The industrial ecology approach was proposed in a paper by Frosch and Gallopoulos (1989) that raised the question, Can our industrial system behave like an ecosystem? That is, can the wastes (or outputs) from one industrial process become the inputs for another industrial process? The answer is yes. Thus, in principle, an industrial park can be designed so that it minimizes the use of primary resources and of overall wastes while recycling or reusing the intermediate materials. One can say that industrial ecology is a method of designing industrial systems so that they produce less damage to the environment. The approach seeks a reasonable balance between industrial profit and environmental stewardship and thereby can contribute to sustainable development.

White (1994) defines industrial ecology as "the study of the flows of materials and energy in industrial and consumer activities, of the effects of these flows on the environment, and of the influences of economic, political, regulatory, and social factors on the flow, use, and transformation of resources." Since industrial ecology aims to design and analyze fluxes of energy and matter, industrial ecology methods can beneficially incorporate exergy to provide more powerful tools. Exergy analysis pinpoints significant losses in the processes, or nonrecoverable losses of the exergy associated with primary energy sources. An attempt to develop exergy analysis from an industrial ecology perspective as conducted by Dincer and Rosen (2007) will be discussed later in this chapter.

One typical example is application of the industrial ecology concept to the design of industrial parks. Thermodynamic and economic analyses must be complemented in this case with ecology and waste management studies, societal impact

İ. Dinçer and C. Zamfirescu, *Sustainable Energy Systems and Applications*,
DOI 10.1007/978-0-387-95861-3_16,

analysis, and creating the legal and economic framework that enables companies to act for the benefit of the overall system. In brief, industrial ecology is concerned with shifting industrial processes from linear (open loop) systems, in which resource and capital investments move through the system to become waste, to closed loop systems, in which wastes become the inputs for new processes.

According to the above conception, modern industrial technologies should be designed like ecosystems where (1) input mass and energy flows are minimized and (2) energy supply is provided by renewable energy sources. Minimization of fossil fuel energy consumption in industrial processes implies eliminating output waste energy flows or the emission of wastes that are in equilibrium with the conditions (pressure, temperature, composition) of the environment. Figure 16.1 shows three situations illustrating a gradual minimization of input and output material and energy streams. Case 1 (the reference case) entails three technologies or manufacturing processes that evolve within the same industrial park. One step toward implementing industrial ecology is shown in case 2 (reduced waste) where the waste from technology 1 is taken as input to technology 2; thus the inputs and outputs (wastes) from the overall process are reduced.

In the third case, all three processes are coupled in a loop, and there is no material input or waste output. The only requirement for the process to run is the energy. In a completely sustainable scenario, the input energy should be in the form of renewable energy.

16.2 Relevant Natural and Industrial Cycles

Industrial ecology is concerned with the design of industrial systems in an ecological manner. All fluxes of materials and energy must be inventoried and integrated with the biogeochemical cycles of nature. One of the main goals of industrial ecology design is accounting for the natural cycles of substances. Moreover, the natural cycles are seen as an inspiration for designing material cycles in industry. There are five biogeochemical cycles of nature—water, nitrogen, carbon, sulfur, and phosphorus—which we briefly review here.

The water (or hydrologic) cycle is driven by solar energy as water evaporates or ice sublimates and the generated vapor rises in the atmosphere where it eventually condenses and generates rain. There are several mechanisms involved in the hydrologic cycle: evaporation, transpiration, sublimation, cloud formation, precipitation, canopy interception, infiltration, runoff, subsurface flow, and advection. The residence time of water in the atmosphere is 9 days, in rivers up to 6 months, and in the oceans up to 3,000 years.

It is obvious that the impact of human activities on the amount of water circulated on the earth is not considerable. However, industrialization has drastically changed in some cases the local water balances (e.g., installation of large water dams for hydroelectricity, expelling into the atmosphere water vapor from combustion exhausts). Moreover, the global warming effect, which is a

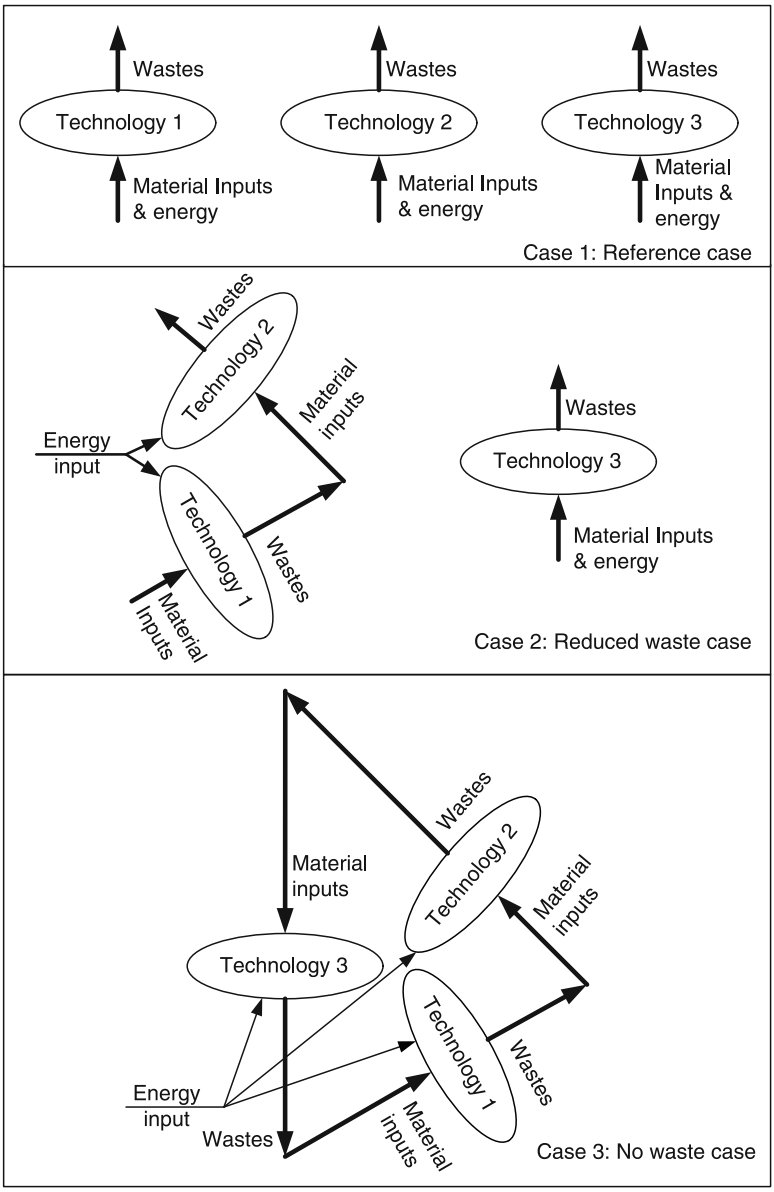

Fig. 16.1 Illustrating the industrial ecology concept

consequence of the industrial activity of humans, accelerates the hydrologic cycle. The water cycle is relevant in industrial ecology because of its indirect effect of circulating other chemicals through the atmosphere, waters, and soil. For example, the flow of water beneath the earth is one of the most important means of transportation of other chemicals. Phosphorus is transported from land to lakes

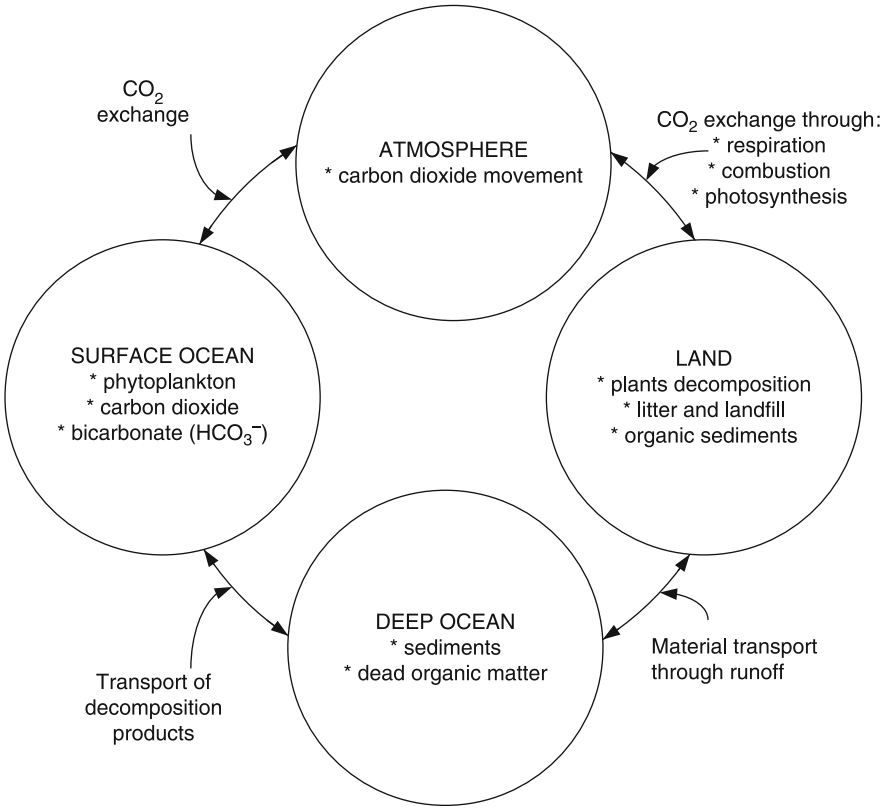

Fig. 16.2 The carbon cycle in nature

or oceans mainly through runoff. After erosion and dissolving processes, salt is transported from the land to the seas. Underground water and runoff are important in circulating nitrogen from soil to water bodies.

The carbon cycle is next in importance after the hydrologic cycle. The carbon itself can be transported by water in the form of eroded solid materials or various kind of particulate matter (including that originating from human activity). Figure 16.2 illustrates the carbon cycle in nature. The carbon dioxide emissions in the atmosphere increased by ~6% per annum since 1900 due to fossil fuel combustion in the industrial era. Presently, about 8 Gt are emitted each year. However, the contribution of the fossil fuel combustion process is a small percent of the total carbon circulation. The soil contains about two times more carbon than does the atmosphere. The ocean assimilates ~50 Gt annually, from which 90% is returned to the superficial water layer, where it is partially assimilated by phytoplankton and partially released back to the atmosphere. In the oceans, 95% of the sequestrated carbon is present in the form of bicarbonate. The anthropogenic CO_2 released in the atmosphere in the industrial era produced an increase of the troposphere temperature

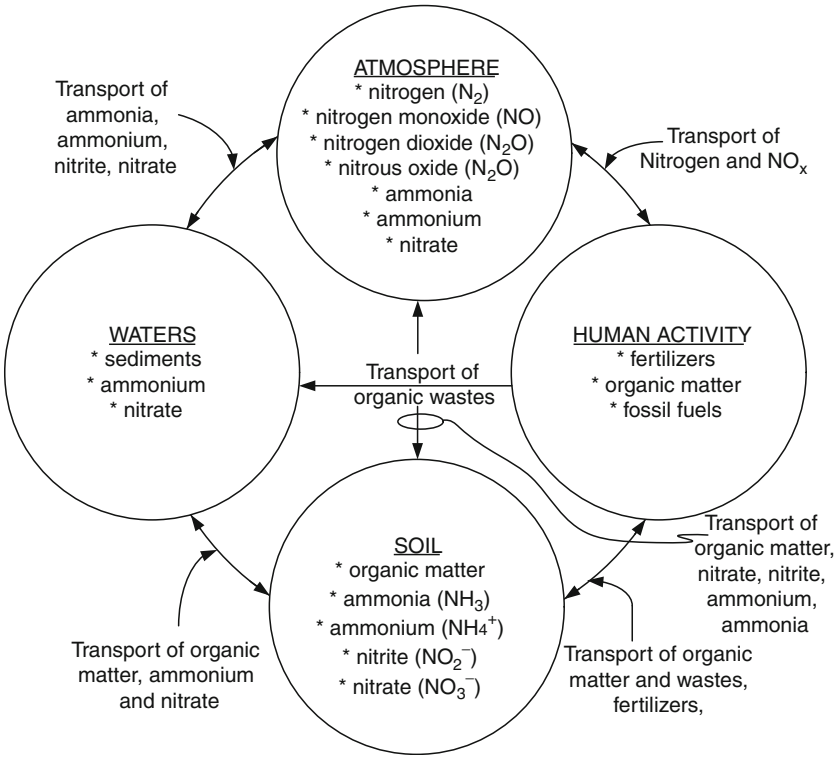

Fig. 16.3 Nitrogen cycle in nature and human activity

by 2° to 3°C (on average). This increase raises major concern due to the rapid global warming that intensifies the hydrologic cycle. Thus any industrial process must be designed or retrofitted for minimum CO_2 release into the atmosphere.

The global nitrogen cycle is illustrated in Fig. 16.3, along with the major interaction of this natural cycle with human activity. The principal forms in which nitrogen is present in the global ecosystem are the nitrogen molecule with three (strong) covalent bonds (N_2), ammonia (NH_3), ammonium (NH_4^+), nitrous oxide (N_2O), nitrate (NO_3^-), and nitrite (NO_2^-). The earth's reservoir of nitrogen is the atmosphere, which comprises a volumetric percentage of 78.1% nitrogen.

Nitrogen is an element present in all life systems as a constituent of amino and nucleic acids, proteins, chlorophyll, and animal excretions. However, nitrogen cannot be used in its molecular form by life systems because its molecule is very stable: it has three strong covalent bonds. The activation energy for nitrogen cracking, which is equivalent to the energy needed for breaking the triple covalent bond of the nitrogen molecule ($N{\equiv}N \rightarrow 2N^{3+} + 6e^-$), namely 460 kJ/mol, appears to be insurmountable, so that this energy is higher than the formation energy of other stable molecules such as carbon dioxide (−393.5 kJ/mol) or water (−241.82 kJ/mol).

Microbes and bacteria have the ability to fix nitrogen (i.e., to convert the stable molecule of atmospheric nitrogen into reactive compounds) thanks to nitrogenase, which is the most complex enzyme capable of breaking the nitrogen molecule and generating ammonia. Therefore, nitrogenase performs a crucial step in the global nitrogen cycle, namely that of transforming nitrogen captured from the atmosphere by living organisms, through specific respiration mechanisms, and converting it into ammonia. Further, ammonia is easily manipulated by biological cells by converting it into ammonium and other compounds such as nitrate and nitrite, and synthesizing more complex chemicals such as urea. Other natural ways to fix nitrogen is through lightning; when lightning occurs, the released energy is sufficient to transform amounts of atmospheric N_2 into NO_x, which can be further converted by living species to nitrates, which are more soluble and more easily manipulated compounds. However, lightning is responsible for a minute portion of natural nitrogen fixation compared with the enzymatic process that fixes the overwhelming majority.

The opposite of the nitrogen fixation process is the process of denitrification, which converts nitrites and nitrates into mainly nitrogen molecules and some amounts of NO_x and nitrous oxide (N_2O) that are released back into the atmosphere. Recall that nitrous oxide has a greenhouse effect 200 times stronger than that of CO_2. Nitrogen is returned into the atmosphere also in the form of ammonia; the NH_3 is stable in the atmosphere and dissolves in water, through which it is redeposited on the soil through rain. According to Tsunogai and Igeuki (1968), the residence time of ammonia in the atmosphere is ~30 days, which is much shorter than that of other atmospheric gases.

Humans intervene to a major extent in the natural nitrogen cycle, mainly through the use of artificial fertilizers and the combustion of fossil fuels. Starting in the second half of the twentieth century, production of ammonia through the Haber–Bosch process became economically efficient and expanded rapidly so that in 2008 the global ammonia synthesis surpassed 130 Mt. Through the Haber–Bosch process, the nitrogen molecule is cracked by heating at temperatures over 850 K and then combined with hydrogen by catalysts at elevated pressures. The process uses either natural gas or coal as the primary energy input and materials from which hydrogen is synthesized as a first step. Nitrogen is extracted from the atmosphere through air separation methods. Basically, Haber–Bosch is the artificial path invented by humans to fix the atmospheric nitrogen. All nitrogen fixed through artificial ammonia synthesis is used as fertilizers (80%) or as building blocks for other synthetic chemicals (20%). Another artificial path of nitrogen fixation is combustion processes, which generates NO_x in an annual estimated amount, according to Smil (2002), of ~25 Mt nitrogen.

The high pace of artificial nitrogen fixation is not compensated through artificial denitrification. Therefore, the role of the denitrification process (converting the nitrogen reactive compounds into stable atmospheric nitrogen) is left in the hands of nature. Whether natural mechanisms of denitrification can keep pace with artificial fixation is an open question. The industrial ecology approach can play a major role in balancing artificial fixation with natural and artificial denitrification so that the environment is affected minimally by human activity.

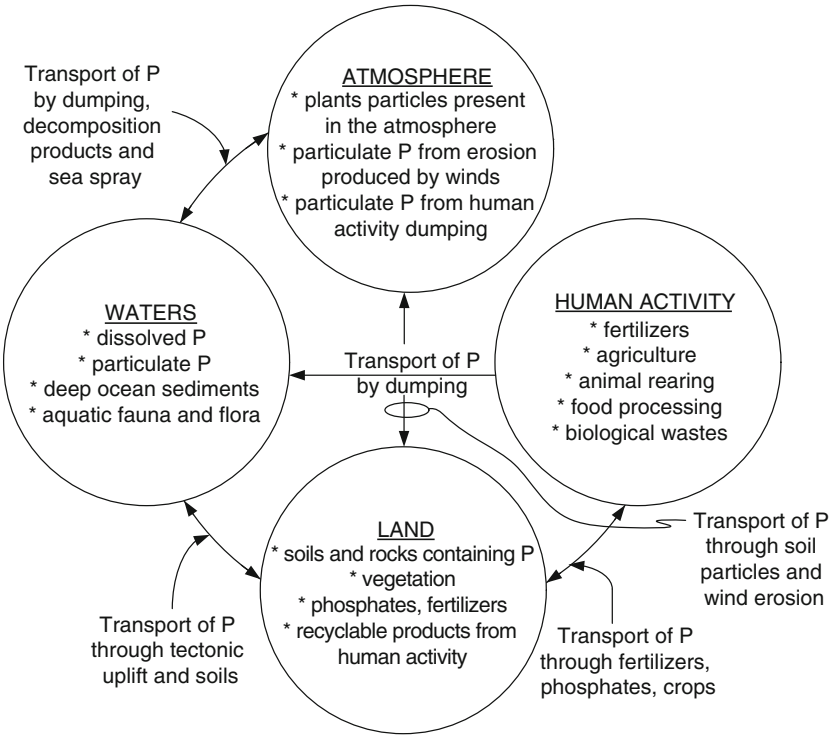

Fig. 16.4 The phosphorus cycle in nature and human activity

The phosphorus (P) cycle in nature is affected by human activity that manipulates phosphorus through fertilizers and biological wastes. With respect to the nitrogen cycle, there is no direct interaction between human activity and the transport of phosphorus in the atmosphere, as seen in Fig. 16.4. The biological wastes, fertilizers, and phosphates resulting from human activity are dumped mainly on land; some of the phosphorus dumping reaches water. In the land, the phosphorus is present in soils, rocks, phosphates (fertilizers), and other products resulting from human (industrial, agricultural, etc.) activity. Tectonic uplift and soils transport phosphorus between soil and water, while winds, through erosion, transport phosphorus from land into the atmosphere. In waters, the phosphorus is present in dissolved or particulate forms, in various sediments from deep oceans, and as a constituent of aquatic fauna and flora.

Figure 16.5 presents the distribution of phosphorus, globally, as a consequence of the natural cycle and of manmade activities. The largest storage of phosphorus is in soils (40 Gt) and the smallest results from weathering of rocks and materials containing P.

Phosphorus is recycled rapidly in the biosphere because life systems are capable of harvesting it in diluted form and concentrating it up to 1,000 times. For example, according to Smil (2002), the marine phytomass processes 1 Gt of phosphorus

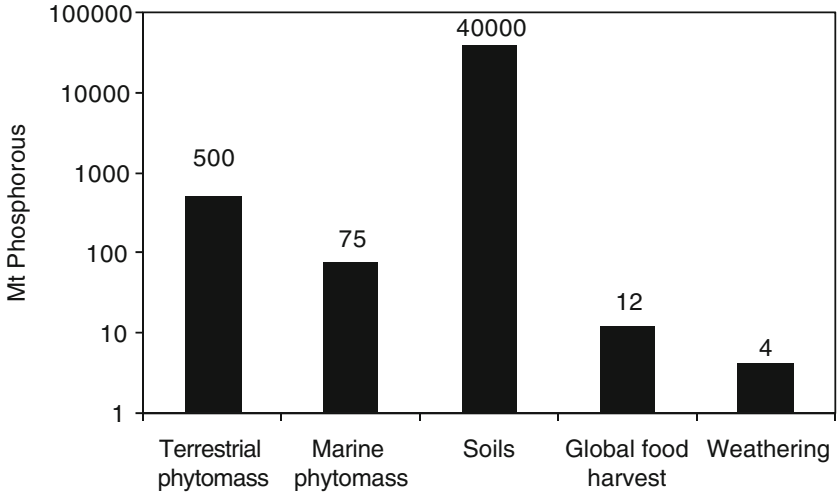

Fig. 16.5 Distribution of phosphorus storage [data from Smil (2002)]

annually and the terrestrial phytomass processes up to 100 Mt/year. Nevertheless, phosphorus is one of the most important elements for life systems, because it is present in adenosine triphosphate (ATP) and in nucleic acids. Phosphorus is present in nature in larger amounts as calcium phosphates. In human activity, phosphorus is present mainly in the form of fertilizers.

Sulfur is also an important element for life systems due to its role in linking amino acids and forming proteins. Sulfur is transported through the ecosystem mainly in the form of the following chemicals: sulfate (SO_4^{2-}), sulfur dioxide (SO_2), hydrogen sulfide (H_2S), dimethyl sulfide (C_2H_6S), and carbonyl sulfide (COS).

The residence time of sulfur in the atmosphere, as embedded in various chemicals, is very short (from minutes to a maximum of 3 to 4 days); thus sulfur cannot be transported far. Therefore, the natural cycle of sulfur manifests regionally rather than locally (Fig. 16.6).

The main mechanisms of sulfur transport are by sea spray, volcanic eruptions, airborne dust and precipitations, and biogenic and anthropogenic emissions. In Fig. 16.7 are illustrated the annual rates of various transport mechanisms of sulfur through the ecosystem. The plot is constructed based on data from Smil (2002). The anthropogenic emissions of sulfur (93%) originate from the combustion of fossil fuels, while 7% come from smelting of metallic sulfides (Smil 2002). From Fig. 16.7, it can be deduced that the rate of anthropogenic sulfur emissions represents roughly 23% from all sulfur transport mechanisms occurring in the ecosystems.

Here, we also illustrate some examples of material cycles that occur in industrial activity. It will become evident that industrial cycles present similarly to natural cycles. Both are subjected to the general laws of physics that state, for example, that energy is never destroyed, mass is conserved, and if no nuclear reactions take place,

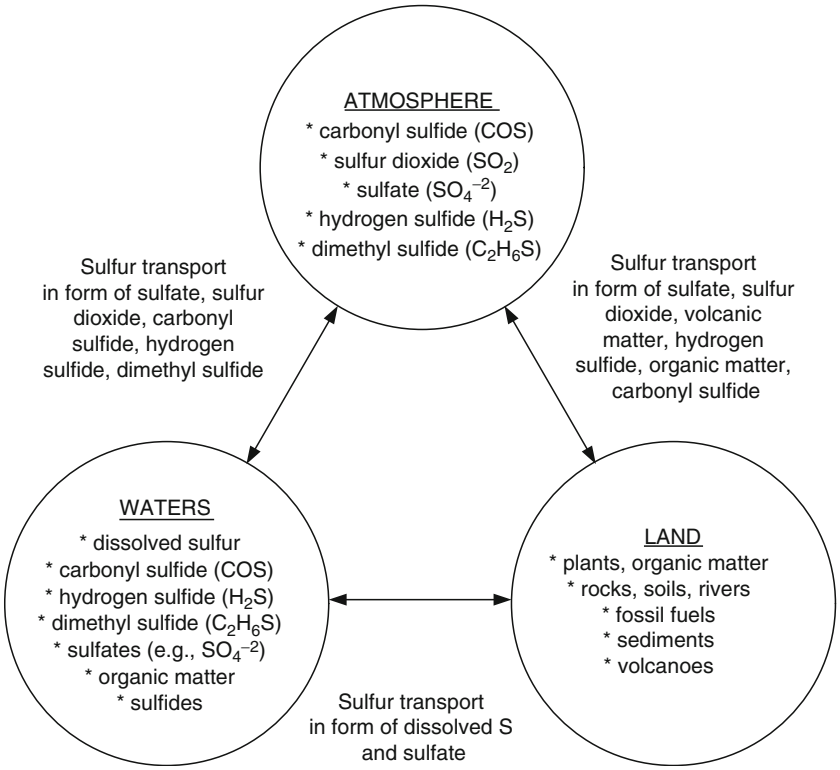

Fig. 16.6 The sulfur cycle in nature

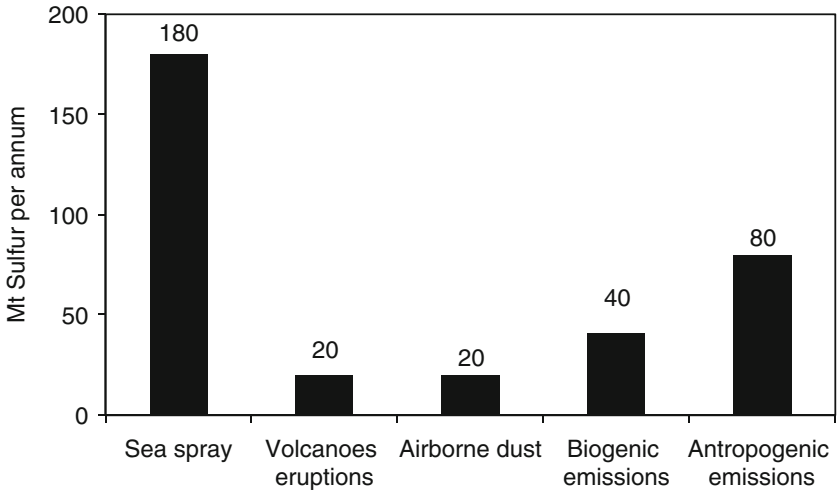

Fig. 16.7 The annual rates of sulfur transport through the ecosystem

the chemical elements are conserved. In the first few examples, the cycle of platinum group materials (PGMs) is illustrated for European countries.

Platinum group metals consist mainly of platinum (Pt), palladium (Pd), and rhodium (Rh) and are found in many industrial materials starting with catalysts, electrical appliances, jewels, dental prostheses, glass-based materials, and others. European countries obtain their primary sources of PGM from four countries: the United States, Canada, Russia, and South Africa. Due to the high values of the PGMs, these metals are highly recycled. The high cost explains the fact that industrial ecology for PGM processing is currently in effect, mainly in the form of material recycling, reprocessing, and reuse. The data from Saurat and Bringezu (2008) have been used to build the European flow diagram of PGM as illustrated in Fig. 16.8. From 100% of extracted PGM (by mass) only 80% arrives in Europe, while the rest is wasted during the preliminary processing in the countries of origin. There are high greenhouse gas (GHG) emissions associated with the extraction and preprocessing of PGMs, amounting, as indicated in Fig. 16.8, to ~60,000% of the extraction.

Europe uses, recycles, and reprocesses the PGMs extensively; thus, ~2,500 t of GHGs are emitted into the atmosphere per ton of metal. There are four major sectors in which PGMs are used in Europe: the auto industry (which consumes 62% of imports to produce catalysts), jewelry manufacturing with 5.3%, industrial catalysts with 4.7%, and manufacturing of electric, electronics, and other products with ~8% of the import. The intense recycling of PGMs in Europe makes possible the reuse of ~16% of the metals by weight of the amount imported.

Similar material cycles exist for regular metals used in industry (e.g., iron-based metals). Figure 16.9 illustrates a generic lifecycle diagram that is valid for any industrial metal. After resource extraction comes primary production and metal use. Then, the old scrap and dumped scrap can be partially recovered, reprocessed, and recycled. Thus, one reduces the wastes and the consumption of primary resources. At the same time, the associated pollution (e.g., GHG emissions) is also reduced. The opportunity to recycle and reprocess metals was extensively used in the past; thus, metal cycles are representative examples of an industrial ecology application. Among metal cycles, much attention is paid to the rare/expensive metal, such as the PGMs discussed above. Another example of rare metal cycles, which illustrate the application of the industrial ecology concept is the tungsten cycle. Tungsten is a strategic metal that is used in construction machinery and equipment, electronic equipment, lamps for electronics and for lighting, and dies. Figure 16.10 illustrates the tungsten cycle in the United States. Being an extremely valuable material, the tungsten cycle includes a thorough waste management system that interacts with production, fabrication, and use phases (see Harper 2008).

Figure 16.11 exemplifies the material flow and recycling of plastic materials for product packaging. Plastic sources from secondary products of fossil fuel refineries are used to make two main substances that are constitutive blocks of packing materials: ethylene and styrene. The first is prime matter for polyethylene production, while the second is used for making expanded polystyrene. Plastic materials are recovered from the products through waste management systems, and then recycled and reused for new packaging. Eventually, unrecoverable plastics are expelled in landfill.

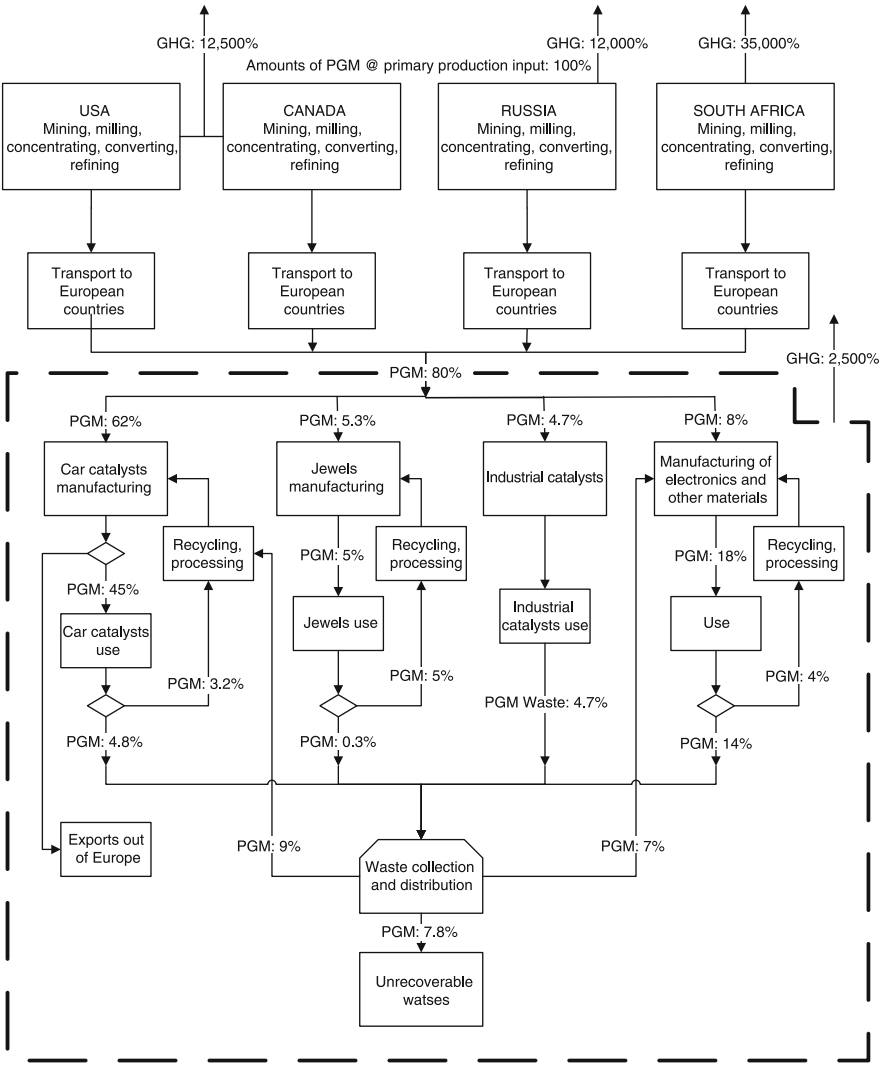

Fig. 16.8 Platinum Group Metals (PGMs) flow in European countries [data from Saurat and Bringezu (2008)]

16.3 Methods of Analysis in Industrial Ecology

There are a number of established analysis methods in industrial ecology that can be applied for a defined system and over a defined period of time. We discuss in this section some of the main analysis methods: material flow analysis (MFA) and the energy and exergy analyses.

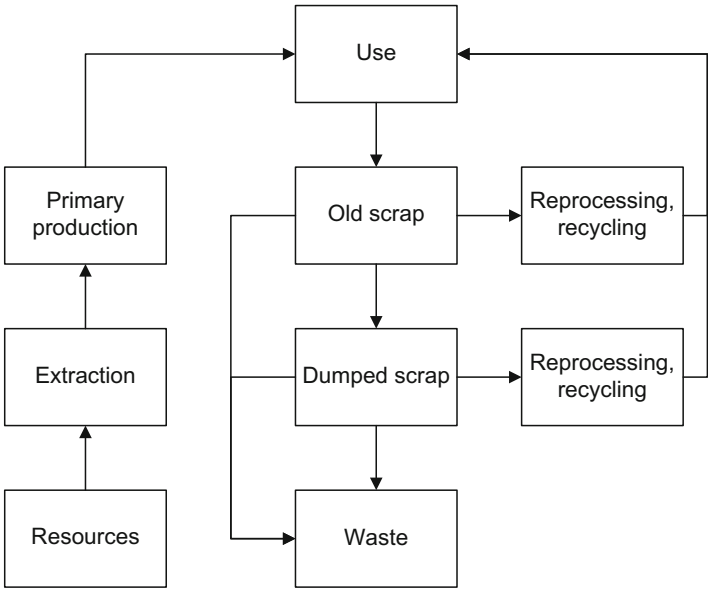

Fig 16.9 Generic diagram for industrial metal life cycle

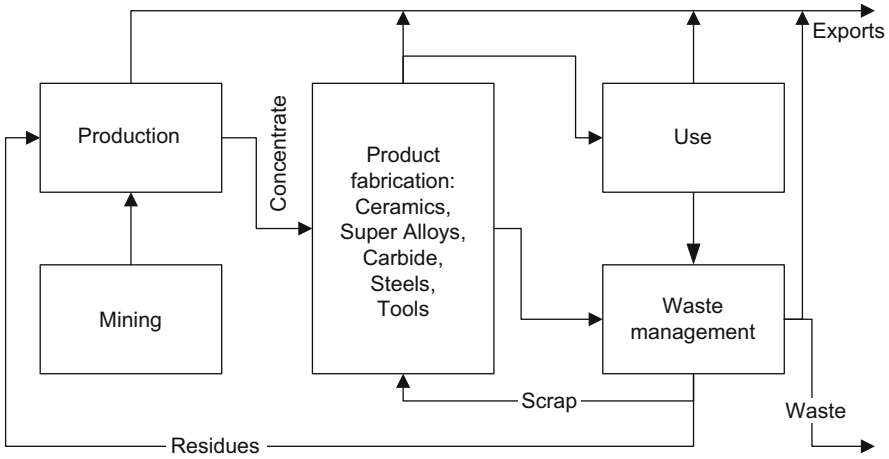

Fig. 16.10 The tungsten cycle in the United States

MFA accounts for inputs and outputs of materials, quantified in physical units, associated with various processes such as resource extraction or harvesting, chemical processing and manufacturing, consumption and use, recycling and reuse, and material disposal. MFA is not supposed to account for energy flows; it is restricted to substance flows. The substances can be categorized in various ways, such as primary resources, intermediate materials and emissions, input materials, products,

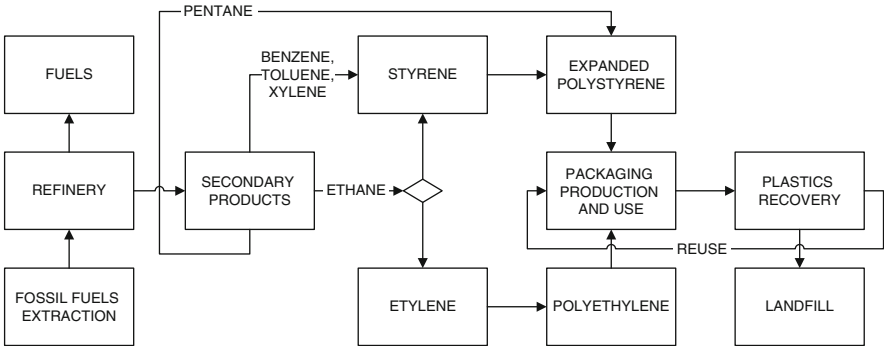

Fig. 16.11 Plastic material flow and recycling for product packaging

and polluting emissions. The methodological principle used for MFA is mass balancing.

When studying the environmental impact, two kinds of MFA are possible, as reported by Bringezu and Moriguchi (2002):

- Analysis within certain companies, sectors of activity, or geopolitical regions of the environmental impact per unit of flow of substances, materials, or products
- Analysis for various substances, materials, or products of the environmental concern related to the throughput of companies, sectors of activity, or geopolitical regions

The results of MFA are of major importance for many subsequent analyses such as energy, economic, or environmental ones. For example, the study of the flow of carbon within an industrial system is important because it is related to GHG emissions. Moreover, the MFA is the basis for defining and deriving various kinds of indicators that quantify the environmental impact or other impacts.

The following steps are recommended for performing an MFA in a systematic manner:

- Defining the system and its spatial–temporal boundaries
- Identifying and categorizing the flows of materials
- Analyzing through mass balance and stoichiometric calculations
- Defining and determining of environmental and other impact coefficients per unit of flow
- Evaluating the results

Another analysis method equivalent to MFA is known as physical input–output accounting. Basically through this method one accounts for all physical flows between the economy and the environment and for all involved material flows. In this method of analysis the processes under study are represented through the associated material inputs and outputs. Further details on this method can be found in Strassert (2002).

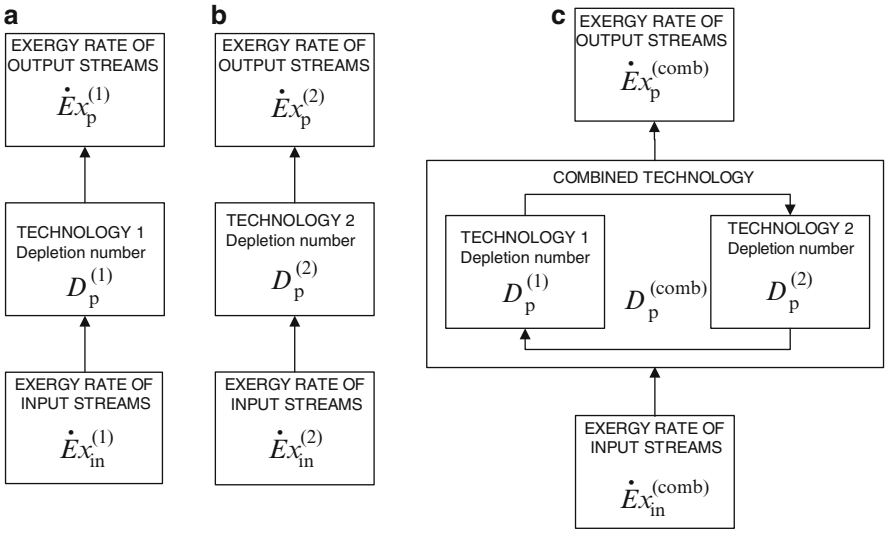

Fig. 16.12 Depletion number of separate and combined technologies

Energy and exergy analyses are thermodynamic methods discussed in Chapter 1 that in principle can be applied to any system. Energy balance accounts for any involved energy flow associated with streams of matter and those associated with any form of energy transport, such as heat, mechanical work, electricity, and fuel.

Exergy as a method of analysis in industrial ecology is useful because it accounts for waste exergy emissions and exergy destructions. Reducing entropy generation leads to a decline in exergy destruction (losses) $\dot{E}x_D$ due to reducing the irreversibility of the processes constituting an industrial system. The exergy efficiency of any process or system generally can be written as

$$\psi = 1 - D_p, \tag{16.1}$$

where D_p is the *depletion number* introduced in Chapter 5 and defined according to Dincer and Rosen (2007) by

$$D_p = \frac{\dot{E}x_D}{\dot{E}x_{in}}, \tag{16.2}$$

where $\dot{E}x_D$ represents the exergy destruction rate and $\dot{E}x_{in}$ the total exergy consumption by the system.

Assume that the analyzed system is from the domain of industrial ecology, that is, it comprises a number of combined technologies and industrial fluxes that operate as a whole. In this case, the exergy efficiency of the integrated system can be evaluated on the basis of the depletion number of each independent component. In an abstract manner, the exergy efficiency of industrial ecology systems is illustrated in Fig. 16.12.

For combined technologies, the depletion number $D_{\mathrm{p}}^{(\mathrm{comb})}$ is lower than for separate technologies $D_{\mathrm{p}}^{(\mathrm{sep})}$, which is expressed as

$$D_{\mathrm{p}}^{(\mathrm{comb})} = \frac{\dot{E}x_{\mathrm{p1}}^{\mathrm{comb}}}{\dot{E}x_{\mathrm{p1}}^{\mathrm{comb}} + \dot{E}x_{\mathrm{p2}}^{\mathrm{comb}}} D_{\mathrm{p}}^{(1)} + \frac{\dot{E}x_{\mathrm{p2}}^{\mathrm{comb}}}{\dot{E}x_{\mathrm{p1}}^{\mathrm{comb}} + \dot{E}x_{\mathrm{p2}}^{\mathrm{comb}}} D_{\mathrm{p}}^{(2)}, \tag{16.3}$$

where $\dot{E}x_{\mathrm{p1}}^{\mathrm{comb}}$ and $\dot{E}x_{\mathrm{p2}}^{\mathrm{comb}}$ are the rates of output exergy flows for products 1 and 2, respectively.

The application of exergy methods to industrial ecology analysis can be done by calculating the exergy flows of every stream of matter and energy and associating depletion numbers with every independent technology or process. Further, the depletion number of the separate and combined technologies is calculated and compared in order to quantify the benefit of technology integration from both an energetic and ecologic point of view.

16.4 Case Study

Here is an example of integration from energy technology—a system combining power generation and hydrogen production technologies. The system comprises the following technologies: gas turbine, solid oxide fuel cell (SOFC), membrane reactor (MR), and hydrogen generator. It is taken from Dincer and Rosen (2007). Both SOFCs and MRs utilize high-temperature oxygen ion-conductive membranes that permit the separation of oxygen from air. The membranes are applicable as electrolytes in SOFCs. In the case presented here, the chemical exergy of methane fuel is transformed into electrical work through an intermediate stage involving its conversion to hydrogen and carbon monoxide and electrochemical oxidation with oxygen. In a membrane reactor, the membrane conducts both oxygen ions and electrons in opposite directions; such membranes are consequently often called mixed conducting membranes. In this case study the electrical work is not generated, but oxygen is separated from air, and fuel combustion proceeds in an atmosphere of oxygen, which improves the quality/efficiency of combustion.

Several advanced materials must be included in the discussed technologies:

- Ceramic materials including zirconium oxides for membranes that operate at over 500 K
- Noble metal catalysis for electrodes resistant to high temperatures of over 1,000 K
- Catalysts for generation of hydrogen from methane through a reforming process directly at the surface of the electrodes

The process diagram is shown in Fig. 16.13 and operates as follows. The initial stream of natural gas, after heating in device 14 (in order to achieve, after compression, the temperature of combustion products) and compression in device 15, is

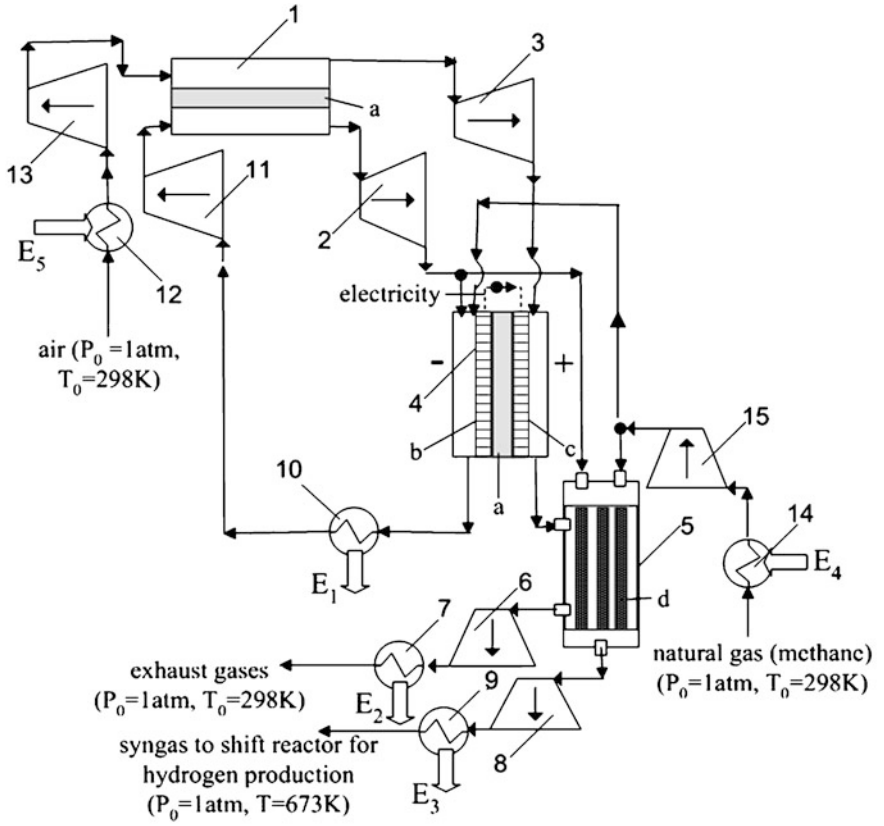

Fig. 16.13 Example of combining hydrogen and power generation technologies [modified from Dincer and Rosen (2007)]: 1, MR; 2, 3, 6, 8, turbines; 11, 13, 15, compressors; 4, SOFC; 5, methane converter; 7, 9, 10, 12, 14, heat exchangers; (**a**) oxygen conductive membranes; (**b, c**) anode and cathode of SOFC stack; (**d**) reactor

divided into two flows. The first is mixed with combustion products (carbon dioxide and steam) and directed to the anodes of the SOFC stack (device 4), where two processes occur simultaneously: conversion of methane into a mixture of carbon monoxide and hydrogen on the surface of the anodes, and electrochemical oxidation of the resultant mixture with oxygen. The oxygen reduction is accompanied by electricity generation in the SOFCs. The gaseous mixture from the anodes (conversion and combustion products) is cooled in a heat exchanger (device 10), compressed in device 11, and directed to the MR (device 1), where the remainder of the conversion products combust in oxygen, and then expand in a turbine (device 2).

The combustion products are then divided into two flows. The first is mixed with the initial flow of methane and directed to the SOFC stack, while the other is mixed with the second flow of methane and enters the catalytic methane converter (device 5). After methane conversion to hydrogen and carbon monoxide in device 5, the gaseous

mixture is expanded in a turbine (device 8), cooled in a heat exchanger (device 9), and directed to the shift reactor, where the remainder of the carbon monoxide and steam is converted to hydrogen.

Air is heated in device 12, compressed in device 13, and directed to the MR (device 1), where some quantity of oxygen is transferred through the oxygen ion-conductive membrane and combusted with fuel. The air heating in device 12 is required in order to achieve, after compression, the temperature of the fuel flow, which is directed, like air, to the MR. The temperature of air reaches its maximum at the MR (device 1) outlet, at which point it is expanded in the turbine (device 3) and directed to the cathodes of the SOFCs (device 4). In the SOFCs, the oxygen concentration in the air decreases, and the air is heated and enters the space between pipes in the catalytic converter (device 5). In device 5, heat is transferred from the air to the reaction mixture in the pipes. The mixture is then expanded in the turbine (device 6) and cooled in the heat exchanger (device 7).

The power generation design combines a traditional gas turbine cycle—which consists of compressors (devices 11 and 13), a combustion chamber (which is represented by the MR, device 1), and turbines (devices 2 and 3)—with the SOFC stack (device 4) and the methane converter (device 5). Heat exchangers are conditionally divided into the heat releasing (devices 7, 9, and 10) and heat receiving (devices 12 and 14) types. Mechanical work is produced in the turbines and consumed in the compressors. The work is transformed into electrical energy, which is also directly generated in the SOFC stack. The endothermic process of methane conversion to hydrogen (via a synthesis gas) in device 5 is implemented into the power generation cycle.

Table 16.1 gives the general parameters used in this analysis, which is done through the exergy method, making a number of assumptions, such as:

- All gases follow the ideal gas law.
- Mechanical friction is negligible throughout the system.
- Thermochemical equilibrium is achieved at the output of the SOFC and the methane converter.
- The combustion process is complete in the membrane reactor.

The exergy balance for the system can be expressed as

$$\Delta \dot{E}x = \dot{E}x_{\text{in}} - \dot{E}x_{\text{out}} = \sum \dot{W}_i + \Delta \dot{E}x_{\text{T}} + \sum \dot{E}x_{\text{D}_i}, \tag{16.4}$$

where $\Delta \dot{E}x$ is the rate of exergy change in the system, $\dot{E}x_{\text{in}}$ is the sum of the exergy rates of the input flows of methane and air, $\dot{E}x_{\text{in}}$ is the sum of the exergy rates of the output flows of conversion products (synthesis gas) directed to a shift converter and exhaust gases, $\sum \dot{W}_{\text{i}}$ is the sum of powers generated in the turbines and in SOFCs, and consumed in the compressors, $\Delta \dot{E}x_{\text{T}}$ is the sum of thermal exergy rates released in heat exchangers 7, 9, and 10 and consumed in 4 and 12, and $\sum \dot{E}x_{\text{D}_i}$ is the sum of the exergy loss rates in the devices of the system. Table 16.2 presents the calculated destroyed exergy for all system components.

Table 16.1 Assumed parameters for the system discussed in Fig. 16.13

Parameter	Value
Isentropic efficiency of turbines η_t	0.9
Isentropic efficiency of compressors η_{cmp}	0.8
Operational circuit voltage of the SOFC stack, V	0.8
Maximum pressure in the gas turbine cycle P_{max}, bar	10
Minimum pressure in the gas turbine cycle P_{min}, bar	1.01325
Maximum temperature in the cycle (at the MR outlet) T_{max}, K	1,500
Temperature of fuel at the inlet of the SOFC stack T_s, K	1,300
Temperature of fuel and air at the outlet of the SOFC stack T_s, K	1,300
Ratio of methane combusted in the power generation cycle to the methane converted	1.0:0.7
Molar ratio of combustion products after MR to the combusted CH_4	6
Ratio of amounts of combustion products directed to SOFC and methane converter	1:1
Standard temperature T_0, K	300
Standard pressure P_0, bar	1.01325
Air composition, volume percentage	21% O_2, 79% N_2

Table 16.2 The destroyed exergy in relevant components of the system from Fig. 16.13

Device	1	2	3	4	5	6	8	11	13	14
Destroyed exergy, kJ/mol	28	3	5	30	17	3	0.3	5	23	1

The data are calculated per mole of combusted methane, which has the standard chemical exergy of $Ex^0_{CH_4} = 831.7\,\text{kJ/mol}$. The system consumes 1.7 mol of methane to generate two useful products: synthesis gas (hydrogen and carbon monoxide) and electricity. Therefore, the depletion number of the combined system is calculated in this case by

$$D_p^{(comb)} = \frac{\sum Ex_{D_i}}{1.7 Ex^0_{CH_4}} = 0.14. \tag{16.5}$$

For 1 mol of methane consumed, the system produces 0.7 mol of syngas. From this proportion and the chemical exergy of hydrogen and carbon monoxide, one can calculate the exergy associated with the syngas, which is $Ex^0_{SG} = 656\,\text{kJ/mol}$. Individual efficiencies of technologies were estimated based on the known performance parameters derived from other studies (see Dincer and Rosen 2007) and are given as follows:

- For technology 1: gas turbine steam power cycle $\psi^{(1)} = 0.5$ and $D_p^{(1)} = 0.5$
- For technology 2: methane conversion $\psi^{(2)} = 0.8$ and $D_p^{(2)} = 0.2$

Therefore, the depletion number for separated technologies can be calculated by

$$D_{\mathrm{p}}^{(\mathrm{sep})} = \frac{W}{W + \mathrm{Ex}_{\mathrm{SG}}^{0}} D_{\mathrm{p}}^{(1)} + \frac{\mathrm{Ex}_{\mathrm{SG}}^{0}}{W + \mathrm{Ex}_{\mathrm{SG}}^{0}} D_{\mathrm{p}}^{(2)} = 0.33. \tag{16.6}$$

As observed by comparing the depletion numbers of separate and combined technologies, in the latter case (which corresponds to the industrial ecology approach) the depletion number is reduced by more than two times. The ratio between the depletion numbers in the two cases quantifies the amount of environment pollution and primary resource reduction that can be obtained.

Further, one can calculate how much higher must be the efficiencies of the separate technologies in order to equalize the combined technology performance. This can be done by equating $D_{\mathrm{p}}^{(\mathrm{comb})}$ with $D_{\mathrm{p}}^{(\mathrm{sep})}$. For example, one can keep $D_{\mathrm{p}}^{(2)} = 0.2$ as a constant value and determine $D_{\mathrm{p}}^{(1)} = 0.061$, which means that the exergy efficiency of gas turbine steam power cycle must be 0.94, which is not possible; the conclusion is that the separated technology approach can never reach the efficiency of the combined approach.

16.5 Concluding Remarks

The industrial ecology approach suggests designing industrial systems in an analogy with ecosystems, that is, with systems that can be observed from nature. Basically, as in nature, the wastes of one living species are used by other species as food or as natural biogeochemical cycles circulate chemicals in a closed loop, the industrial activities can minimize the resource consumption and waste production by using a combined approach of various technologies. Important ways of implementing industrial ecology include the appropriate combination of separate technologies in order to match the waste outputs of one with the inputs of the other, and the introduction of processes that reduce nonrenewable energy consumption. MFA is the basis of every industrial ecology design activity. This analysis must be complemented with thermo-energetic studies that account for the fluxes of energy and exergy.

Exergy analysis can help in designing industrial systems that follow the principles of industrial ecology, and in the evaluation of the efficiencies and losses for such activities. One such evaluation measure is the depletion number, which relates the exergy destruction and exergy input for a system. The example illustrated here compared the depletion numbers for separate and combined technologies as a means of assessing the effectiveness of the technology integration. The conducted analysis confirms that integrated energy systems, developed via an appropriate combination of technologies, represent an important opportunity for increasing the utilization efficiency of natural resources and thereby achieving the aims of industrial ecology.

Nomenclature

D_p	Depletion factor
$\dot{E}x$	Exergy rate, kW
$\dot{E}x_d$	Exergy destruction rate, kW
W	Work, kJ
$\dot{W}$	Work rate, kW

Greek Letter

ψ	Exergy efficiency

Subscripts

D	Destruction
in	Input
out	Output
SG	Syngas

Superscripts

(comb)	Combined
(sep)	Separated

References

Bringezu S., Moriguchi Y. 2002. Material flow analysis. In: A Handbook of Industrial Ecology, Ayres R.U., Ayres L.W., eds., Edward Elgar, Northampton, MA.

Dincer I., Rosen M.A. 2007. Exergy and industrial ecology. In: Exergy—Energy, Environment and Sustainable Development. Elsevier, Oxford, UK, pp. 417-423.

Frosch R.A., Gallopoulos N.E. 1989. Strategies for manufacturing. *Scientific American* 261:94–102.

Harper E.M. 2008. A product-level approach to historical material flow analysis. Tungsten as a case study. *Journal of Industrial Ecology* 12:768–783.
Saurat M., Bringezu S. 2008. Platinum group metal flows of Europe, Part I: Global supply, use in industry and shifting of environmental impacts. *Journal of Industrial Ecology* 12:754–767.
Smil V. 2002. Global biogeochemical cycles. In: A Handbook of Industrial Ecology, Ayres R.U., Ayres L.W., eds., Edward Elgar, Northampton, MA.
Strassert G. 2002. Physical input-output accounting. In: A Handbook of Industrial Ecology, Ayres R.U., Ayres L.W., eds., Edward Elgar, Northampton, MA.
Tsunogai S., Igeuki K. 1968. Ammonia in the atmosphere. *Geochemical Journal* 2:157–166.
White R. 1994. Preface. In: The Greening of Industrial Ecosystems, Allenby B.R., Richards D.J., eds., National Academy Press, Washington, DC.

Study Questions/Problems

16.1 Explain the concept of industrial ecology and its application.
16.2 Describe the natural carbon dioxide cycle.
16.3 Describe the nitrogen cycle and quantify the anthropogenic influence on it.
16.4 Describe the phosphorus cycle in nature.
16.5 Describe the sulfur cycle and the anthropogenic influence on it.
16.6 Explain the general industrial metal life cycle.
16.7 Explain plastic materials flow and recycling for product packaging.
16.8 Define the depletion number and comment on its usefulness.
16.9 Comment on the benefit of combining technologies.
16.10 What is the relationship between depletion number and exergy efficiency?
16.11 What is the effect of depletion number on resource sustainability?
16.12 Are the depletion numbers for renewable energy systems zero? Explain.
16.13 Obtain a published article on industrial ecology. Using the data provided in the article, try to duplicate the results. Compare your results to those in the original article.

Chapter 17
Sectorial Energy and Exergy Utilization

17.1 Introduction

Thermodynamic analysis based on energy and exergy balance can be applied at macroscales such as sector of activity, geopolitical region, country, group of countries, or the world. An energy balance can be determined by accounting for all primary energy flows, all useful forms of energy, and the energy losses in the conversion processes. Such analysis gives important insights regarding the way in which the primary energy resources are used; it helps identify the ways and places for improvement, and it is a necessary tool for macroeconomical planning.

In a world with finite natural resources and large energy demands, it is important to understand the mechanisms that degrade energy and resources and to develop systematic approaches for improving systems in terms of such factors as efficiency, cost, environmental impact, and so on. The application of thermodynamic analysis at a macroscale is illustrated in Fig. 17.1. As a first step, the thermodynamic system subjected to analysis must be delimited. For example, the thermodynamic system can be a sector of activity, such as industrial, commercial, transportation, agricultural, utility, and so on.

The boundary of such system cannot be delimited physically; rather, the fluxes of energy/exergy in and out of the system under consideration can be inventoried. For the analysis to be done, a period of time must be specified, for example, one year or one season. The energy consumed by the system subjected to analysis can be determined based on the primary energy (or fuel sources) consumed over the specified period of time. The consumption of primary energy sources can be found from regional or national statistics. At any macrolevel (sector of activity, geopolitical region, country, etc.) statistics regarding the energy consumption by type (coal, natural gas, petroleum, etc.) and other useful information are issued regularly. For each fuel source, the higher or lower heating value can be used to convert the quantitative consumption (e.g., quantity by mass, mol, or volume) into energy or exergy terms. The useful energy or exergy is made available, depending on the case, in the form of work, heat, electric power, chemicals (e.g., synthetic fuels, electric batteries), or other forms. The difference between useful and consumed energy or exergy represents the energy loss or exergy destruction, respectively. Such energy/exergy balances can be determined for

İ. Dinçer and C. Zamfirescu, *Sustainable Energy Systems and Applications*,
DOI 10.1007/978-0-387-95861-3_17,

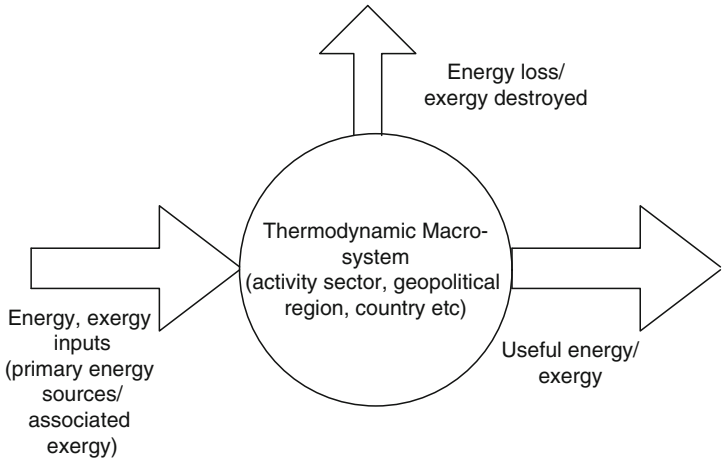

Fig. 17.1 Thermodynamic analysis at a macroscale based on energy and exergy

any category of processes specific to the analyzed system. Based on inputs, outputs, and losses, energy and exergy efficiencies at a macroscale can be defined, in an analogue manner, to that commonly considered for any thermodynamic system.

Extensive efforts have been pursued in the last 40 years to perform sectorial energy analysis in many countries. The capstone work of Reistad (1975) referred to the U.S. economy and was followed by many relevant studies such as those of Dincer (1997), Dincer and Al-Rashed (2002), Dincer et al. (2004a,b, 2005), Jaber et al. (2008) for OECD countries, Rosen (1992), Dincer et al. (1997) for Canada, Ji and Chen (2006) for China, Kondo (2009) for Japan, Ayres et al. (2003) for the U.S., Koroneos and Nanaki (2008), Xydis et al. (2009) for Greece, Oladiran and Meyer (2007) for South Africa, Saidur et al. (2007) for Malaysia, and Utlu and Hepbasli (2004, 2006, 2007a, 2009) for Turkey. Synthesis work and studies regarding the elaboration of the methodology for thermodynamic analysis at the sectorial level are those of Dincer and Rosen (2007), Hepbasli (2005), and Utlu and Hepbasli (2007b).

In this chapter, we introduce the methodology of thermodynamic analysis at the sectorial level and emphasize its specificity for various sectors such as industrial, commercial, residential, transportation, agricultural, and utility. The methodology is illustrated with a case study at the end of the chapter. The impact of sectorial analysis on sustainable development is emphasized.

17.2 Thermodynamic Modeling at the Sectorial Level

The use of exergy in thermodynamic analysis at a macroscale is of the utmost importance. Consider, for example, petroleum oil and wood. Commonly, the first is perceived as fuel and the second as a construction material. Yet oil can be converted

Table 17.1 Quality factors associated with some energy forms

Energy form	Quality factor
Mechanical energy	1
Electrical energy	1
Nuclear energy	0.95
Sunlight	0.9–0.95
Steam at 600°C	0.6
District heating at 90°C	0.2–0.3
Heating at room temperature	<0.2
Thermal radiation from earth	0

Data from Dincer and Rosen (2007)

into a plastic material to be used for various purposes, including in construction, and wood can be burned as fuel. At the sectorial level, it is important to quantify the material fluxes and the associated exergy. As for any material, a specific chemical exergy can be determined. Exergy is a measure that has the quality of unifying the thermodynamic analysis. If one knows the energy carried by material flows crossing the system boundary, the corresponding exergy can be determined through a quality factor. For example, if the flux of energy flows in the form of heat, the quality factor is given by Carnot efficiency $1 - T_0/T_f$, where T_0 is the environment temperature and T_f is the temperature associated with the energy flux. If the flow of energy is in the form of electricity or work, the quality factor is 1. Quality factors associated with various energy fluxes are presented in Table 17.1.

The exergy associated with each flow of energy can be obtained simply by multiplying the energy quantity with the quality factor. For fuels, one uses the chemical exergy that is related to the higher or lower heating value. The procedure to determine the chemical exergy of fuels is described in detail in Chapter 6. Simply, a factor can be used to correlate the chemical exergy with the higher heating value (see Dincer and Rosen 2007). For better accuracy, the exergy can be correlated with the lower heating value based on a regressed linear approximation. An example of a correlation for hydrocarbon-based fuels is given by Brzustowski and Brena (1986) as shown in Table 17.2. Fuels such as gasoline, kerosene, fuel oil, and diesel are not included. According to Reistad (1975), their chemical exergy can be calculated, in a simplified manner, as 99% of their higher heating values.

In general, five kinds of useful energy flows can be considered as products: heating, cooling, work production, electric energy production, and kinetic energy generation. Table 17.3 defines the energy and exergy efficiency for the five considered cases. For each of the corresponding conversion processes, both energetic and exergetic efficiencies can be defined as follows:

- Energy efficiency η is given by the energy in products over the total energy input.
- Exergy efficiency ψ is defined as the exergy in products over the total exergy input.

The analysis made for each sector of activity that takes place in a specific geopolitical region can be compiled into a sectorial energy/exergy flow diagram.

Table 17.2 Simplified correlations for exergy of fuels

Fuel	Exergy, MJ/kmol
Methane, ethane, propane, *N*-butane, *N*-pentane, *N*-decane, *N*-pentadecane, *N*-heptadecane, *N*-eicosane	1.0660 × LHV − 27.39
Ethene, propene, butene, pentene, heptene, octene, nonene, decene,	1.0651 × LHV − 49.17
Ethyne, propyne, butyne, pentyne, hexyne, heptyne, octyne, nonyne, decyne	1.0651 × LHV − 72.95
Methanol, ethanol, propanol, buthanol, penthanol, hexanol, heptanol, octanol, nonanol, decanol	1.0651 × LHV + 1.60
Benzene, methylbenzene, ethylbenzene, *N*-propylbenzene, *N*-butylbenzene, *N*-hexylbenzene, *N*-heptylbenzene, *N*-octylbenzene	1.0648 × LHV − 76.77
Natural gas, coal gas, continuous reformer gas, cyclic reformer gas, commercial propane, pure propane, commercial butane, pure normal butane, low calorific value refinery gas	1.0641 × LHV − 21.78

LHV lower heating value
Data from Brzustowski and Brena (1986)

Table 17.3 Energy and exergy efficiency of typical sectorial processes

Process	Energy efficiency	Exergy efficiency	Definitions
Electric heating	$\eta = Q/W$	$\psi = (1 - T_0/T_p)Q/W$	Q, process heat; W, electric energy
Fuel heating	$\eta = q/\text{HHV}$	$\psi = (1 - T_0/T_p)q/ex^{ch}$	q, specific heat consumption by weight or mol; ex^{ch}, specific chemical exergy of fuel consumed
Mechanical cooling	$\eta = Q/W$	$\psi = (1 - T_0/T_p)Q/W$	Q, process cooling in energy units; W, electric energy
Absorption/fuel cooling	$\eta = q/\text{HHV}$	$\psi = (1 - T_0/T_p)q/ex^{ch}$	Fuel is combusted to heat the vapor generator of the absorption machine
Absorption/solar cooling	$\eta = q''/I_T$	$\psi = (1 - T_0/T_p)q/ex^{s}$	I_T, intensity of solar radiation; ex^{s}, exergy of solar radiation; quality factor of 0.9–0.95
Work production, renewable energy	$\eta = W/W_{inp}$	$\psi = \eta$	Primary energy source: solar, wind, hydro, electric power; W_{inp}, input work
Work production, fuel combustion	$\eta = w/\text{HHV}$	$\psi = w/ex^{ch}$	w, specific work production per weight or mol of fuel consumed; ex^{ch}, fuel's chemical exergy
Kinetic energy production	$\eta = ke/\text{HHV}$	$\psi = ke/ex^{ch}$	ke, kinetic energy per unit of fuel consumption; occurs in turbojet engines and rockets

An example of such a diagram is presented in Fig. 17.2, in which a particular system, a utility, generates electricity and delivers it to the grid. All other sectors are connected to the grid and also to the stream of primary energy/exergy fuel sources. In each sector, specific products and wastes are generated. Note that for each sector there are specific processes that transform the energy input into useful products. For example, in the residential sector one can have space heating, water heating, cooking, electrical appliances, lighting, refrigeration and air conditioning, dish

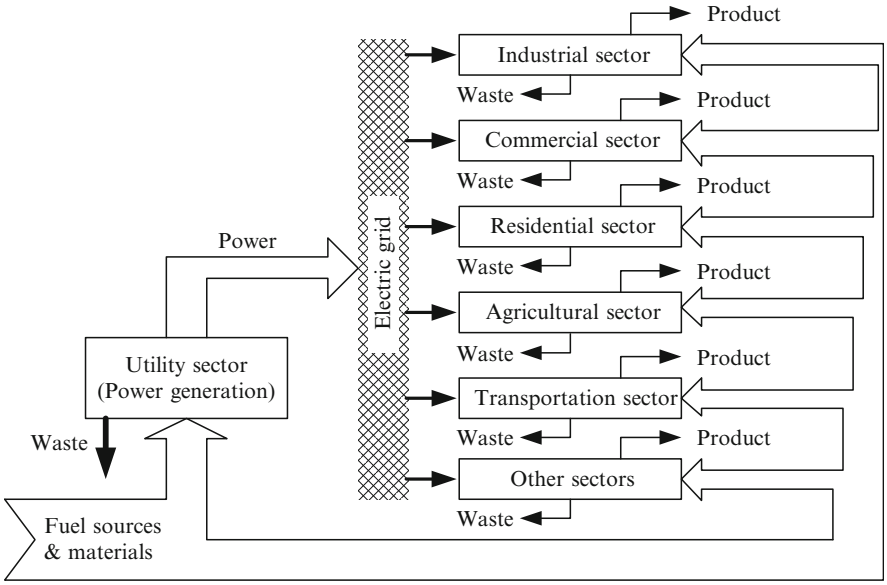

Fig. 17.2 Energy/exergy flows at the sectorial level of a geopolitical region

washing and ironing, television and computer, washing machine, vacuum cleaner, and others.

The waste from each sector includes pollutants like carbon dioxide emissions or other emissions, tars, residual, radioactive waste, and other kinds of wastes. Energy and exergy efficiency for all analyzed sectors (complete geopolitical regions) also can be derived by considering the overall energy and exergy output as a summation of those for each sector.

17.3 Residential, Commercial, and Public Sectors

The residential and commercial sectors present various similarities. There is a relevant difference between the residential and commercial sectors in developing and developed countries. For example, the total population of developing countries makes up 80% of the total world population, but the energy consumption in those sectors represents only 30% of the commercial/residential global energy (Utlu and Hepbasli 2007a).

In most countries, one third of the energy consumption is attributed to the commercial and residential sectors. The main subcomponents of the commercial and residential sectors relevant to energy/exergy sectorial analysis are presented in Fig. 17.3 (there, HVAC&R represents heating, ventilation, air conditioning and refrigeration, and LPG means liquefied petroleum gas). Energy is used in these sectors for space and water heating, cooking, and running various kinds of electrical

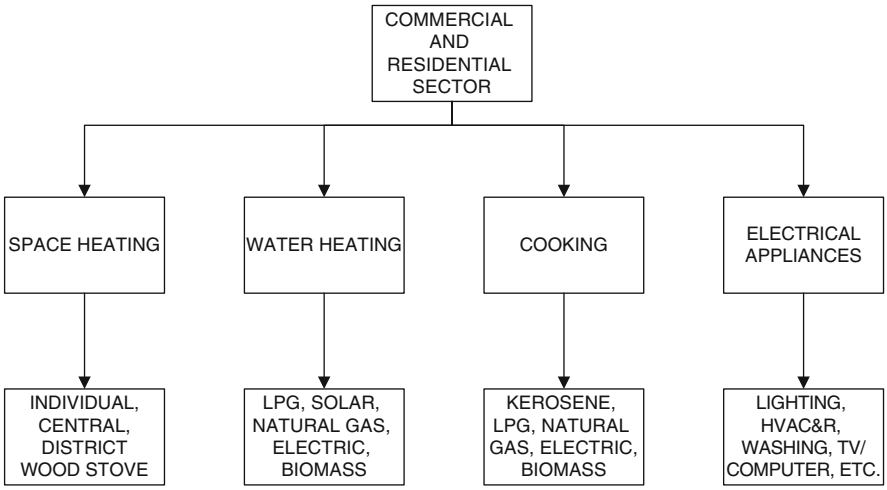

Fig. 17.3 Subsystems of commercial and residential sectors for sectorial analysis

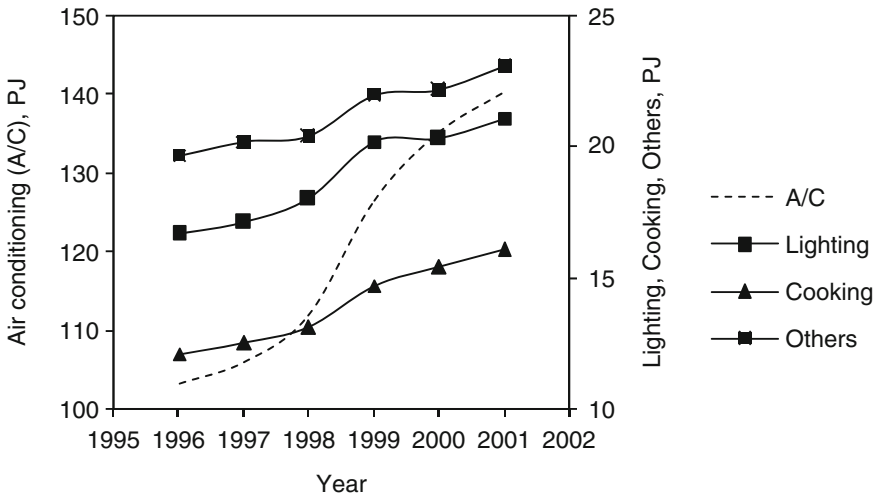

Fig. 17.4 Consumption of electric energy in residential sector of Saudi Arabia

appliances. A large variety of primary fuel sources are employed, including solar, biomass, LPG, natural gas, and grid electricity. The magnitude of energy flows varies with geographical region, especially for space heating, which is directly affected by climate and the local practices regarding building construction, insulation, and the efficiency of the heating equipment.

Some examples of energy consumption in the residential, commercial, and public sectors are given here. Figure 17.4 presents the historical data of energy consumption in the residential sector of Saudi Arabia, and Fig. 17.5 shows historical

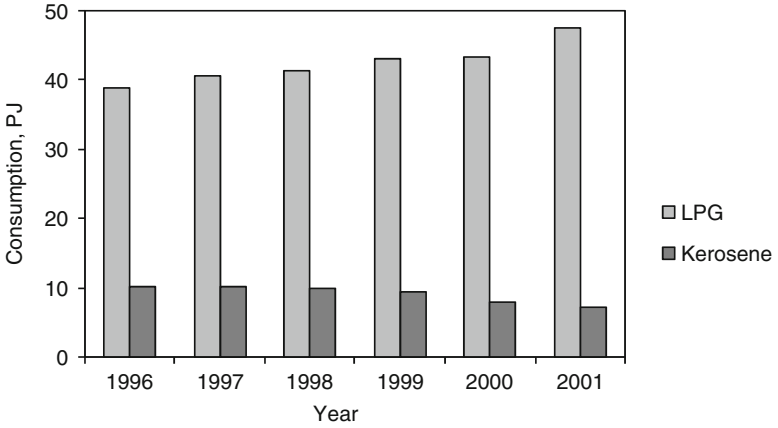

Fig. 17.5 Primary fuel consumption for cooking in Saudi Arabia

data regarding fuel consumption for cooking. These plots were based on published data from Dincer et al. (2004a,b). It can be observed from the plot that the most significant consumption comes from air conditioning units.

About 40% to 50% of the energy input in a residence or commercial setting is consumed for space heating in most countries. Exergy efficiency for space heating can be calculated, according to Utlu and Hepbasli (2007a), based on the process temperature for heating T_p, the first law efficiency,

$$\eta = Q_p/\text{HHV}, \tag{17.1}$$

and the quality factor

$$\zeta = \text{HHV}/ex^{ch}, \tag{17.2}$$

with the following equation:

$$\psi = \eta\zeta\left[1 - \frac{T_0}{T_p - T_0}\ln\left(\frac{T_p}{T_0}\right)\right]. \tag{17.3}$$

Based on Eq. (17.3), the energy and exergy efficiencies in the residential and commercial sectors, as derived by Utlu and Hepbasli (2007a), are summarized in Table 17.4 as a function of the standard temperature. For these ranges of standard temperature, the efficiency varies as follows:

- For space heating from 40% to 98% energy and 3% to 30% exergy depending on heating type
- For water heating from 30% to 99% energy and 1% to 15% exergy efficiencies
- For cooking, exergy efficiency varies from 5% to 30%

Table 17.4 Equations for energy and exergy efficiency in the residential and commercial sectors

Subsystem	Primary fuel	η, %	ψ, %
Space heating	Coal stove	$0.0031T^2 - 0.294T + 7.1358$	$-1.8T + 90$
	Coal district heating	$0.0024T^2 - 0.2695T + 7.847$	$-1.4035T + 84.2105$
	Fuel oil	$0.0035T^2 + 0.338T + 8.2491$	$-2T + 100$
	Natural gas	$-0.0006T^2 - 0.236T + 10.3912$	$-0.0352T^2 - 0.2772T + 99.17$
	Wood	$0.0027T^2 - 0.2599T + 6.343$	$-1.6T + 80$
	Dried dung	$0.0044T^2 - 0.3746T + 7.9279$	$-2.6316T + 100$
	Electricity	$0.0018T^2 - 0.3004T + 13.5446$	$-T + 100$
	Geothermal	$0.017T^2 - 1.3973T + 29.0186$	$-2.2222T + 100$
	LPG	$-0.0013T^2 - 0.1805T + 9.5487$	$-0.401T^2 + 0.1679T + 97.8575$
Water heating	Natural gas	$0.032T^2 - 0.3583T + 10.4324$	$-1.6667T + 100$
	Wood	$0.0046T^2 - 0.4229T + 9.3169$	$2.7778T + 100$
	LPG	$0.0027T^2 - 0.3207T + 9.695$	$-0.00115T^2 - 1.5068T + 100.709$
	Electricity	$-0.0018T^2 - 0.3004T + 13.5446$	$-0.0246T^2 - 0.014T + 97.6012$
	Fuel oil	$0.0029T^2 - 0.333T + 9.6948$	$-1.6667T + 100$
	Dried dung	$0.0047T^2 - 0.3848T + 7.77666$	$-2.8571T + 100$
	Geothermal	$0.0151T^2 - 1.1715T + 23.0135$	$-2.5T + 100$
	Solar	$0.0031T^2 - 0.3541T + 10.3976$	$-1.6667 + 100$
Cooking	LPG	$0.0018T^2 - 0.2884T + 15.8494$	$0.0023T^2 - 0.5139T + 51.4203$
	Natural gas	$0.0028T^2 - 0.3365T + 17.2219$	$0.0023T^2 - 0.5139T + 51.4203$
	Wood	$0.0007T^2 - 0.1483T + 7.9588$	$-0.247T + 29.6339$
	Electricity	$0.0033T^2 - 0.5272T + 28.9694$	$-0.0042T^2 - 0.9484T + 94.9347$
	Dried dung	$0.0008T^2 - 0.1418T + 6.9878$	$-0.2602T + 26.0183$

Electric appliances	Refrigeration	$0.0466T^2 - 2.0118T + 30.4948$	$0.0155T^2 - 0.1087T + 6.2757$
	Air conditioning	$-0.0019T^2 + 0.4080T + 197.8795$	$0.012T^2 - 0.6867T + 3.4641$
	Drying clothes	$-1.3333T + 100$	$0.0038T^2 - 0.5754T + 21.5424$
	Dish machine	$-2.0T + 100$	$-0.2941T + 14.7059$
	Ironing	$-0.6667T + 100$	$-0.2317T + 34.7518$
	Washing machine	70	70
	Vacuum cleaner	70	70
	Computer	75	75
	Television	75	75
	Lighting	9.8	8.7
	Others	64	64

Note: $T = T_0$ is the standard temperature in degrees Celsius, which is taken to vary in the range of 0–25°C; the temperature for space heating is assumed to be 50°C

Data from Utlu and Hepbasli (2007a)

- For electric appliances the energy efficiency varies from 10% to 99% while the coefficient of performance of refrigeration equipment and heat pumps varies from 1 to 2
- The exergy efficiency of electric appliance varies from 1% to 21% for most equipment; for ironing, computer, television, and vacuum cleaners it ranges from 30% to 75%

The exergy efficiency for cooking is correlated with the energy efficiency through the Carnot factor:

$$\psi = \eta\left(1 - \frac{T_0}{T_p}\right), \tag{17.4}$$

where T_p is the process temperature for cooking, which is taken as an average value.

The electrical appliances include lighting, refrigeration and air conditioning, dishwashers and irons, television and computer, washing machine and vacuum cleaner, and others (e.g., hair driers, entertainment, etc.). For washing machines and vacuum cleaners, the energy and exergy efficiency are the same because these devices convert electricity into mechanical work.

Basically, in these machines, there are only electromechanical losses, which have overall values typically of 30%. Computers and television units are also electric equipment with typical losses of 25%. The dishwasher and the iron use electrical energy to generate heat (and some mechanical work, in the case of the dishwasher). The exergy destroyed is mainly that caused by electrical energy conversion into heat. Equation (17.4) can be used for calculating exergy efficiency based on energy efficiency.

The coefficient of performance (COP) for refrigeration, air conditioning, and heat pump units can be calculated with the usual equation $\mathrm{COP} = Q_{\mathrm{output}}/W_{\mathrm{input}}$ for which the associated exergy efficiency can be written as

$$\psi = \mathrm{COP} \times \left(\frac{T_0}{T_p} - 1\right). \tag{17.5}$$

The efficiency of lighting in commercial and residential applications is considered to be 5% for incandescent bulbs and 20% for fluorescents; the corresponding exergy efficiencies are 4.5% and 18.5%, respectively. With respect to the situation in countries, Kondo (2009) showed that the exergy efficiency in Canada is the best (15%) among the analyzed cases, including Brazil (12%), Saudi Arabia (9%), Turkey (9%), and Japan (6%). For Saudi Arabia, the efficiencies in the residential sector were calculated based on the following figures given in Dincer et al. (2004b):

- For air conditioning, the average COP is 1 and the exergetic COP is 3.4%.
- For lighting, the efficiency is 25% for energy and 24.3% for exergy.
- For electric cooking, there are 80% energy and 22.5% exergy efficiencies.
- For fuel cooking, the overall efficiency is 65% for energy and 15.8% for exergy.

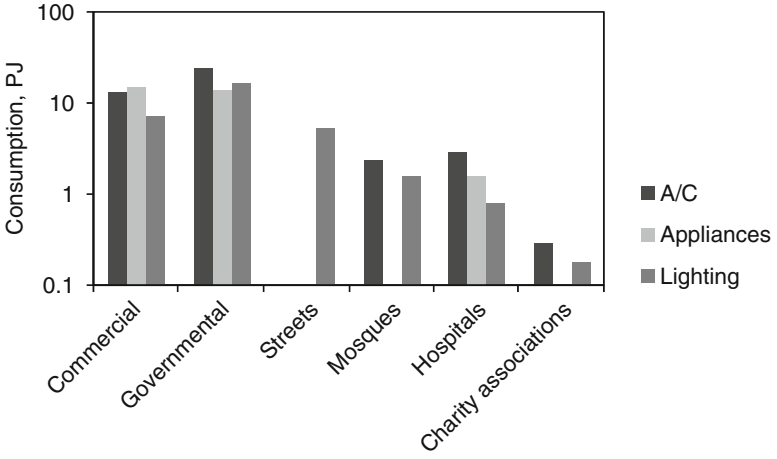

Fig. 17.6 Electric power consumption in the public and private sectors of Saudi Arabia

In Saudi Arabia, about 38% of the electrical energy used in the public and private sectors is for air conditioning, 42% is for appliances, and 20% is for lighting. The public and private sectors comprise six subsectors: commercial, governmental, streets, mosques, hospitals, and charity associations. Figure 17.6 shows the electric power consumption by subsectors of the public and private sectors of Saudi Arabia. The governmental sector consumes the most energy, followed by the commercial sector. For the street subsector, only lighting consumes electric energy. In edifices like that of mosques and charity associations, there are no electric appliances in operation.

17.4 Industrial Sector

The industrial sector comprises many subsectors of which the most important are iron–steel, other metallurgical subsectors, nonmetal material subsectors, chemical–petrochemical industry, fertilizer subsectors, petrochemical feedstock subsectors, cement, sugar, and other industries. Figure 17.7 illustrates the main subsectors of the industrial sector together with their principal attributes, and Table 17.5 illustrates the typical exergy and energy efficiency for various relevant industrial processes. Figure 17.8 presents the exergy and energy consumption of the industrial subsectors of Turkey. Both charts represent percents of energy/exergy consumption per sectors. About 83% of primary energy in Turkey for the industrial sector is from fuels and 17% is from electricity.

Industrial heating can be categorized by temperature level: low ($\leq 120^{\circ}$C), medium (121–399°C), and high ($\geq 400^{\circ}$C). The typical efficiencies for process heating, as a function of the temperature level, can be easily derived from energy

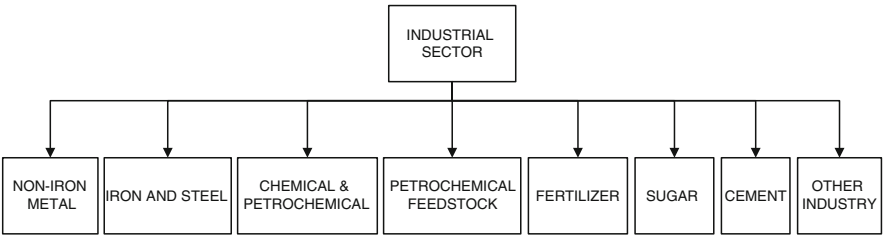

Fig. 17.7 Main subsectors of the industrial sector and their principal attributes

Table 17.5 Typical energy and exergy efficiency of some industrial processes

Process	High-pressure steam boiler	Steam-heated reboiler	Fuel combustion based tobacco drier	Coal gasification	Petroleum refining	Blast furnace
η, %	90	100	40	55	90	76
ψ, %	50	40	4	46	10	46

Data from Utlu and Hepbasli (2007b)

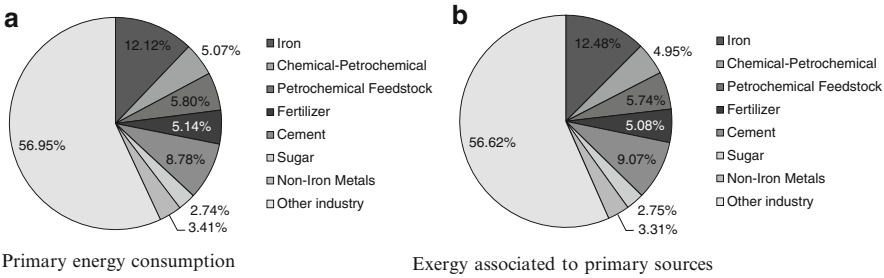

Fig. 17.8 Energy and exergy consumption from primary sources (**a**), and the exergy associated with it (**b**) in Turkey [data from Utlu and Hepbasli (2007b)]

and exergy balances. For low-temperature electric heating, the heat losses through good-quality insulation are below 0.1% of the useful energy; therefore; they can be ignored. This means that the efficiency of low-temperature electric heating according to the first law of thermodynamics is 100%. For fuel heating, the energy efficiency is lower because the combustor, which operates at higher temperatures, loses more heat; typically, the energy efficiency is 65%.

For medium-temperature electric heating, about 10% of heat losses are considered; that is, the energy efficiency of the process is ~90% while the fuel heating efficiency is 60%. For high-temperature electric heating, the considered efficiency is 70% while for fuel heating it is 50%. The exergy efficiency of electrical heating ranges from 7% at low to 54% at high temperature. Exergy efficiency of fuel-based heating ranges from 3.5% at low and 40% at high temperature. Table 17.6 gives the energy and exergy efficiencies of process heating for each industrial subsector

Table 17.6 Exergy and energy efficiency of process heating in industrial subsectors

		Electric heating		Fuel heating	
Subsector	T, °C	η, %	ψ, %	η, %	ψ, %
Iron and steel	45	100	6.3	65.0	4.1
	985	70.0	53.4	50.0	38.1
Chemical and petrochemical	45	100	5.4	65	3.5
	140	90	25.2	60	16.8
	495	70	42.8	50	30.6
Petrochemical feedstock	60	100	9.7	65	6.3
	230	90	36.4	60	24.2
	495	70	42.8	50	30.6
Fertilizer	60	100	9.7	65	6.3
	350	90	46.9	60	31.3
	900	70	52.2	50	37.3
Cement	40	100	5.4	65	3.5
	140	90	25.2	60	16.8
	590	70	45.7	50	32.6
Sugar	80	100	16.3	65	10.6
	315	90	44.4	60	29.6
	400	70	39.0	50	27.9
Non-iron metals	60	100	10.8	65	7.0
	130	90	23.4	60	15.8
	400	70	39.0	50	27.9
Mining and quarrying	31	91.7	28.0	0.9	0.5
	160	N/A	N/A	9.0	5.0
	1,480	8.3	4.2	90.1	45.2
Other industry	60	100	9.7	65	6.3
	130	90	23.8	60	15.8
	400	70	39	50	27.9

Data from Dincer et al. (2004a,b), Utlu and Hepbasli (2007b), Oladiran and Meyer (2007), Utlu and Hepbasli (2009)

categorized as fuel-based heating and electrical heating. The data presented in Table 17.6 are based on the actual situation in Turkey; however, the results are relatively general: much variation of figures from country to country is not expected.

The number of industrial subsectors may vary. For example, apart from those considered in Fig. 17.7, one can have manufacturing industries (e.g., aerospace, automotive, pharmaceuticals, shipbuilding, and marine) and resource industries (nuclear, oil and gas, mining and quarrying, etc.). In Saudi Arabia, the industrial sector comprises the four most significant subsectors—oil and gas, chemical and petrochemical, iron and steel, and cement—which account for more than 80% of the total sector energy use; these subsectors were chosen for the analysis to represent the overall industrial sector.

The energy used to generate heat for industrial production processes in Saudi Arabia accounts for 68% of the total energy consumption, and mechanical drives account for 17%. The remaining 15% is divided among lighting, air conditioning, and others. Figure 17.9 shows the exergy and energy efficiencies of the industrial subsectors of Saudi Arabia calculated based on the assumption that heating and mechanical power generation is the most representative use of energy. This

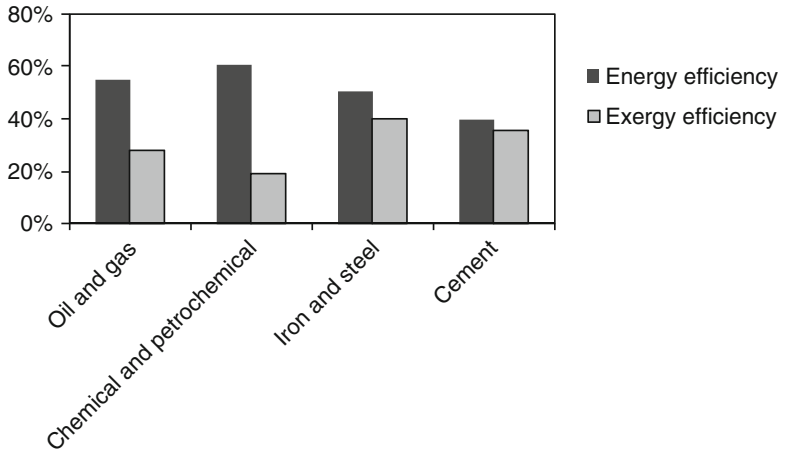

Fig. 17.9 Overall energy and exergy efficiencies in industrial sector of Saudi Arabia [data from Dincer (1997), Dincer and Al-Rashed (2002), and Dincer et al. (2004a, b)]

simplification is considered valid since these processes account for 85% of the energy consumption in the industrial sector. The data published in past works by Dincer (1997), Dincer and Al-Rashed (2002), and Dincer et al. (2004a,b) have been used for drawing the plot in Fig. 17.9. Interestingly, the energy efficiency in the oil and gas and chemical and petrochemical sectors is the highest, while the exergy efficiency in these sectors is the lowest. The highest exergy efficiency in the iron and steel sector is about 40%.

17.5 Agricultural Sector

Farming depends on the supply of water and on climate. Diesel and electricity are used in this sector as the primary energy sources. The devices that are assumed to be representative of the agricultural sector are tractors and pumps, which cover more than 80% of the total energy consumption. Mean energy and exergy efficiencies are calculated by multiplying the energy used in each end use by the corresponding efficiency for that end use as follows:

$$\left(\frac{\eta}{\psi}\right)_{\text{mean}} = \frac{(\eta/\psi)_{\text{tractor}} \times (\text{Consumption}_{\text{tractor}}) + (\eta/\psi)_{\text{pump}} \times (\text{Consumption}_{\text{pump}})}{(\text{Consumption}_{\text{total}})}. \tag{17.6}$$

According to the study by Dincer et al. (2005), the efficiency of diesel-running tractors used in the agricultural sector can be taken to be 75% under part load conditions; the electrically driven pumps for irrigations are assumed to be 70%

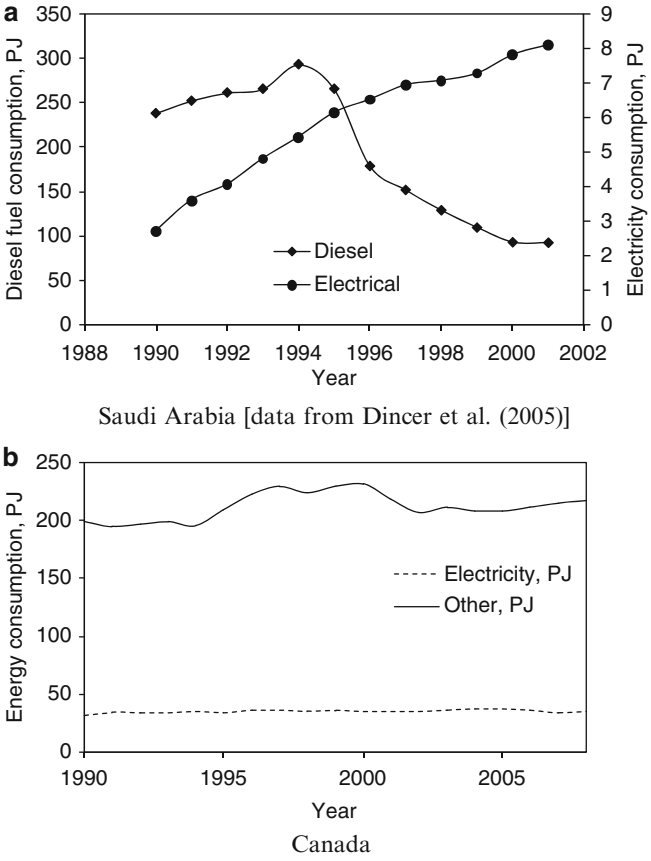

Fig. 17.10 Primary energy consumption in the agricultural sector of Saudi Arabia (**a**) and Canada (**b**)

efficient. Figure 17.10 compares the evolution of the energy consumption in the agricultural sector in Saudi Arabia between 1990 and 2001 with that of Canada for which the data are available until 2008. It can be seen that in this particular situation, the electrical energy consumption increases almost steadily over time in Saudi Arabia while it was almost constant in Canada. In fact, through adequate policy measures in Saudi Arabia, diesel fuel consumption decreased at the same time that electricity consumption increased. For Canada, the plot shows electrical energy consumption and energy consumption from other sources, which obviously include diesel fuel. The efficiency of diesel tractors has been assumed to be 75%, the same as for the sectorial analysis of Saudi Arabia. The energy consumption from other sources plotted in Fig. 17.10 is assimilated to that of fuel utilization in agricultural equipment.

The overall energy and exergy of the agricultural sector of Saudi Arabia have been calculated by Dincer et al. (2005) for a range of years, and the results are presented in Fig. 17.11a. The dead state temperature for the calculation has been chosen to be

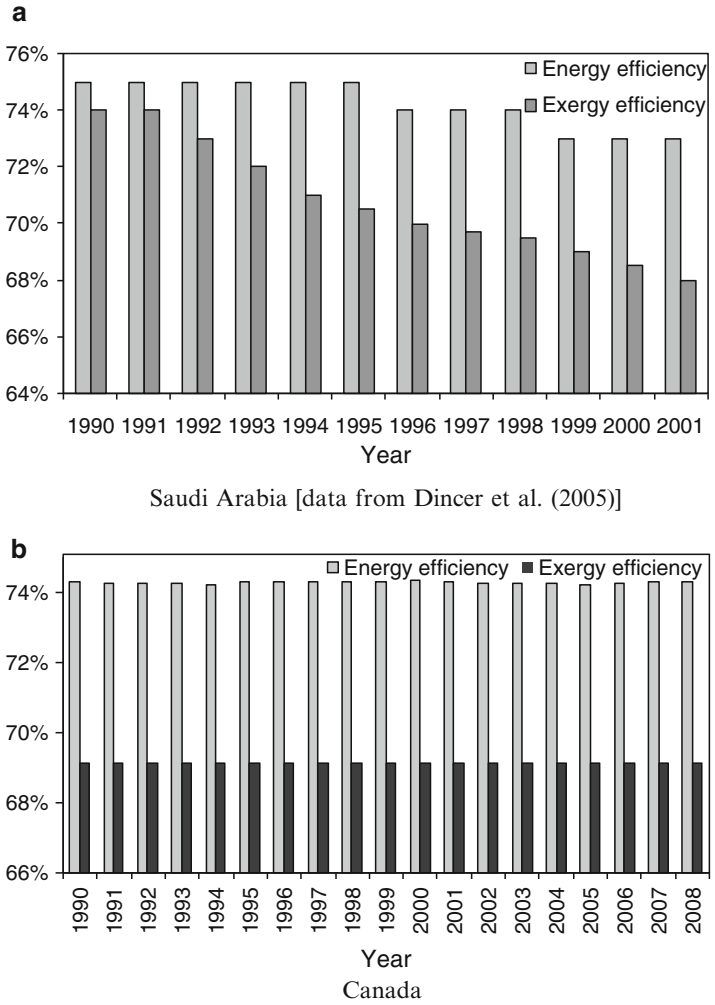

Fig. 17.11 Energy and exergy efficiency history in agricultural sector of Saudi Arabia (**a**) and Canada (**b**)

25°C. As observed, the exergy efficiencies appear to be slightly less than the energy efficiencies due to irreversibilities, mainly caused by mechanical work losses in tractors and pumps. In order to minimize the irreversibilities in the tractors, it is necessary to increase the work output for the same energy input supplied from the fuel combustion, and in the pumps the main source is the pressure drop, which should be eliminated. As a result, it appears that the efficient use of the tractors and pumps in the agricultural sector is crucial for better efficiency. For comparison, the energy and exergy efficiency in the agricultural sector of Canada were estimated following the same procedure and plotted in Fig. 17.11b. It can be observed that the corresponding

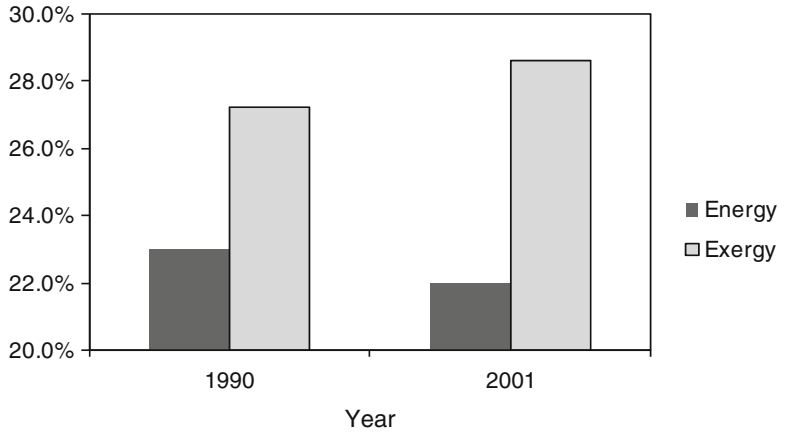

Fig. 17.12 Efficiencies of the agricultural sector of Saudi Arabia in 1990 vs. 2001

figures were about constant for two decades, as opposed to the large variation specific to Saudi Arabia.

For the agricultural sector, mean energy and exergy efficiencies are calculated by multiplying the energy used in each device type by the corresponding device efficiency. Then these values are added to obtain the overall efficiency of the agricultural sector. Figure 17.12 compares the efficiencies in the agriculture sector at the level of years 1990 and 2001. It is observed that the exergy efficiency increased but the energy efficiency decreased. The increase of exergy efficiency demonstrates better energy utilization in that sector.

17.6 Transportation Sector

The transportation sector comprises subsectors, namely, roadway, railway, seaway, airway, and off-road transport for fuel and electricity consumption. The sector consumes, as its main energy input, various types of fuels such as gasoline, compressed natural gas, fuel oil, kerosene, diesel oil, and hard coal. The use of coal in transportation sector is indirect, in that coal is liquefied to obtain synthetic fuels in the liquid phase. Electricity is also used to some extent for transportation, such as for railways and metropolitan public transit. In the future, hydrogen will make up a larger share of transportation fuels. Among all transportation means, road transport is expected to evolve the fastest in the coming decades and to offer the most exergetic improvement among all transportation ways. For example, according to Utlu and Hepbasli (2006), in Turkey, it is expected that the exergy utilization efficiency in the transportation sector will increase from about 24% (at present) to 29% (in 2020).

Various geopolitical factors affect the configuration of the transportation sector. For example, Jordan is a small country in which there have been important population shifts in recent decades from rural to urban areas (the urban population

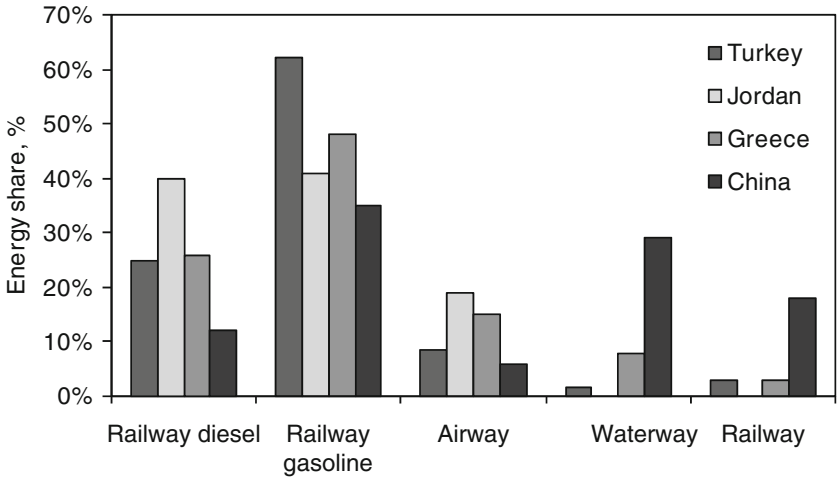

Fig. 17.13 Energy shares of the modes of transportation in four countries [data from Utlu and Hepbasli (2006), Jaber et al. (2008), Koroneos and Nanaki (2008), Ji and Chen (2006)]

now accounts for 82% of the country's population). Due to the size of the country and urbanization, rail transport is undeveloped, while the main means of transportation are via the roadway and the airway. In contrast, Turkey is a country 85 times larger than Jordan, for which all modes of transportation are well represented, even though road transport dominates. Regarding the efficiency of the transportation subsectors, the Greek and Chinese situations can be given as examples: road transportation is the most efficient in Greece, while waterway transportation is the most efficient in China. Interestingly, China still uses some steam locomotives, which account for 13%, of the total railway transport; diesel locomotives account for 77%, while electric trains account for 10%. The energy share for the four modes of transportation is presented in Fig. 17.13 for four countries for comparison purposes.

The chart in Fig. 17.14a shows the overall energy and exergy efficiency of 13 countries. Figure 17.9b exemplifies the changes in energy and exergy efficiencies of the transportation sector of Saudi Arabia across the span of a decade, from 1990 to 2001. Both energy and exergy efficiencies of the transportation sector of this country increased during that period. Note that the operating load efficiency of transportation vehicles is 12% less than the rated load because they function at partial load. Also note that the transportation sector of Saudi Arabia is represented by three subsectors, each using specific fuel sources: roadway, using gasoline and diesel; airway, using jet kerosene and air fuel; and waterway, using ship fuel and diesel.

17.7 Electric Utility Sector

The electric utility sector is responsible for production, distribution, and marketing of electric power. Depending on the country, the utility sector is comprised of private or/and governmental organizations. The electric utility sector does not

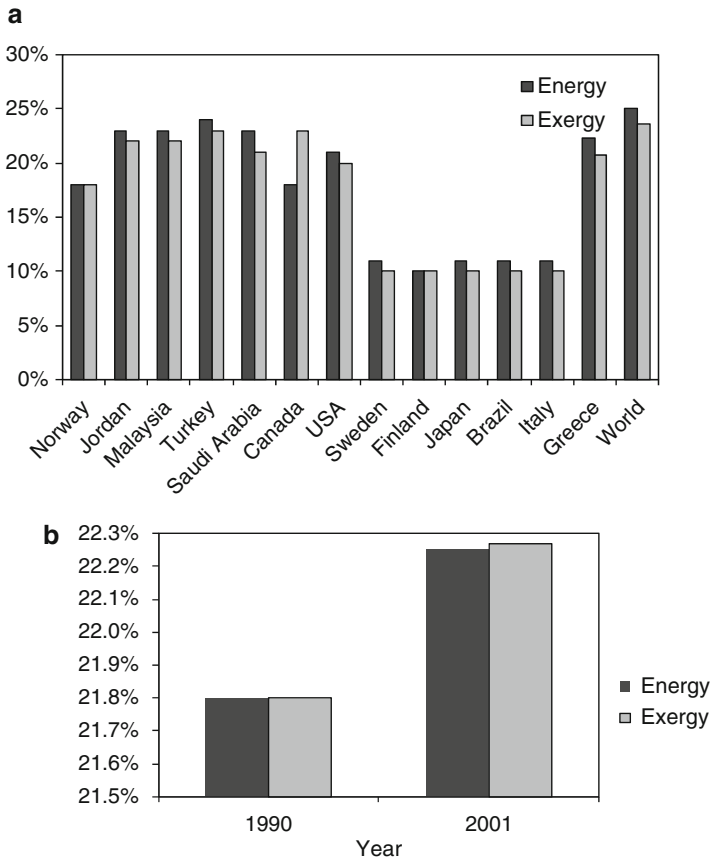

Fig. 17.14 Energy and exergy efficiency in transportation sector for 13 countries and the world (**a**) and evolution of efficiencies over the span of a decade in Saudi Arabia (**b**) [data from Jaber et al. (2008), Utlu and Hepbasli (2006), Koroneos and Nanaki (2008), and Rosen (1992)]

include the electricity produced by industrial establishments for their own use. The electric utility sector also includes electrical power generated by desalination plants. Desalination plants produce electricity as a by-product with high a efficiency, that is, about 46% as compared to the average efficiency of a power station, which is 28% (see Dincer and Rosen 2007). Countries with desert regions such as Saudi Arabia use water desalination to produce drinkable water. In Saudi Arabia, the overall efficiency of the utility sector, calculated by Dincer and Rosen (2007), is 31.75%.

Figure 17.15 exemplifies the trends of energy generation in the utility sector of Saudi Arabia, which shows the peculiarity of a high production share for the desalination plants. The main electricity generation sources are fossil fuels (diesel, crude oil, natural gas, fuel oil) and the electricity that comes as a by-product of desalination plants.

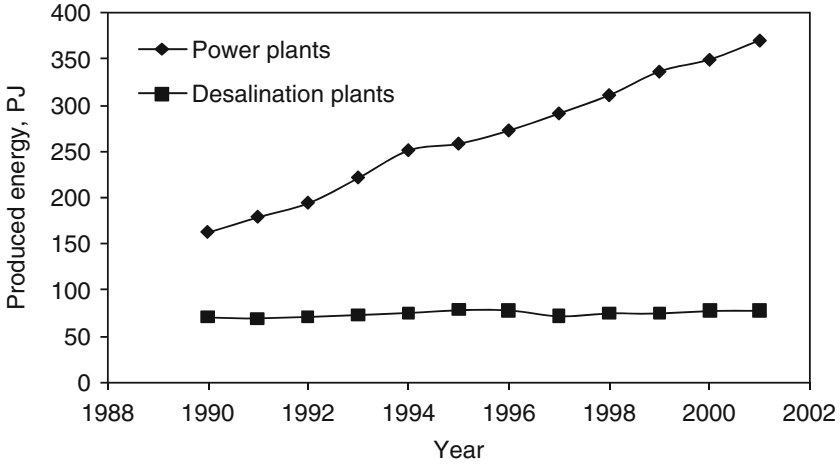

Fig. 17.15 Trends of energy generation in the utility sector of Saudi Arabia [data from Dincer and Rosen (2007)]

17.8 Case Study: Sectorial Exergy Utilization in Canada

Canada's gross domestic product (GDP) $1.34 trillion, ranking tenth in the world and amounting to $39,700 per capita. The Canadian economy is divided into a number of sectors that reflect the national energy use, namely, residential, commercial, institutional (or the public administration sector), agricultural, industrial, and transportation. The industrial sector includes a number of subsectors such as mining, oil and gas extraction, pulp and paper, iron and steel, smelting, refining and nonferrous industries, cement, petroleum refining, chemicals, manufacturing, forestry, and construction. The Canadian transportation sector includes airlines, the domestic marine subsector, the pipeline transport subsector, and road transport and urban transit. These sectors are supplied with energy from various primary sources, including fossil fuels (coal, coke, coke oven gas, natural gas, natural gas liquids, and crude oil), nuclear energy, hydro-energy, and other renewables that make up a small fraction of the energy used. Statistics Canada collects and reports data regarding national energy consumption by sectors, types, and regions. The 2008 report analyzes Canada's sectorial energy and exergy utilization (Statistics Canada 2008).

For 2008, the amounts of primary energy in peta joules (PJ) consumed by Canada are reported in Table 17.7, as are the assumptions considered for calculating the exergy factors that relate to the energy and exergy amounts (there, NCV means net calorific value). Biomass energy is ignored in the analysis because it amounts to only 0.5 PJ of production, according to Statistics Canada (2008). Also, of the primary electricity sources only hydro and nuclear are considered, while other forms of renewables and other forms of energy such as solar, wind, tidal, and waves are ignored because they are insignificant compared with hydro and nuclear.

Table 17.7 Energy and exergy production of Canada (primary sources) for 2008

Primary source	Energy production, PJ	Exergy factor		Exergy production, PJ	Export, %
		PJ/PJ	Assumptions		
Coal, coke, coke oven gas	1,896	0.5	7 MJ/kg specific exergy; 15 MJ/kg average NCV	948	3
Natural gas	7,005	1.02	1.066–27.39/LHV[a]	7,145	18
Natural gas liquids	670	1.05	35% propane, 26% butane, 39% ethane[a]	703	1
Crude oil	10,282	1.14	Assimilated to heavy naphtha	11,721	19
Hydro[b]	1,698	1	Mechanical energy	1,698	3
Nuclear[c]	1,130	0.95	Table 17.1	1,073	2
Secondary sources	2,715[d]	0.6	Assumed mostly steam	1,629	1
Total	25,396	N/A	N/A	24,917	47

[a]Assumed 80% efficiency of hydroelectricity production
[b]Assumed 30% efficiency of nuclear power generation
[c]Taken from Table 17.2
[d]Thermal sources resulting from heat recovery from industry that is used from electricity generation

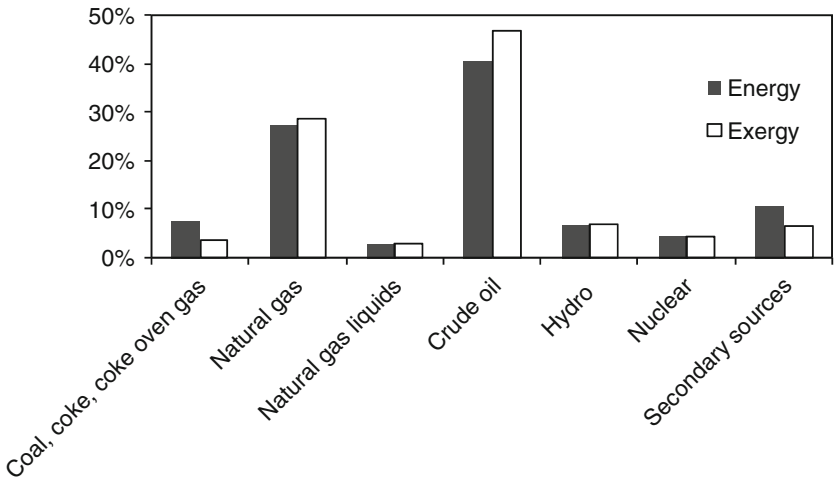

Fig. 17.16 Canadian energy and exergy supply in 2008 (in percents from total) [data from Statistics Canada (2008)]

The secondary energy sources are those recovered from industry or other activities and are in the form of thermal energy.

The secondary sources were assimilated with steam for the purpose of this analysis. The energy and exergy supply is presented in percents in Fig. 17.16. The total energy supply of Canada is partly exported and partly used for domestic needs. Table 17.7 shows that in 2008 Canada exported 47% of its primary energy sources. The remaining 53% was used for satisfying domestic energy needs.

After extracting the exports, the energy and exergy production in Canada is presented in Fig. 17.17 for each type of energy source. The total supply of energy

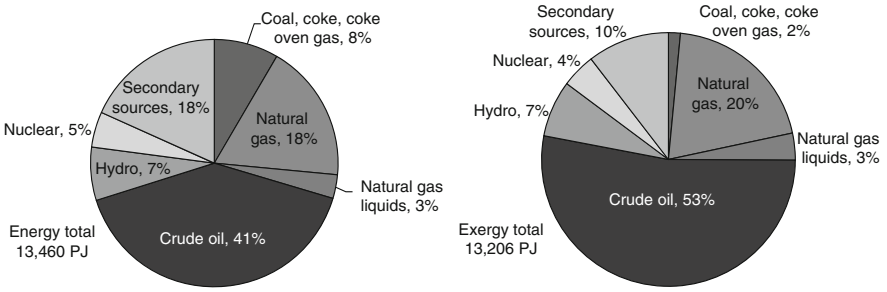

Fig. 17.17 Energy and exergy supply for domestic use in Canada [data from Statistics Canada (2008)]

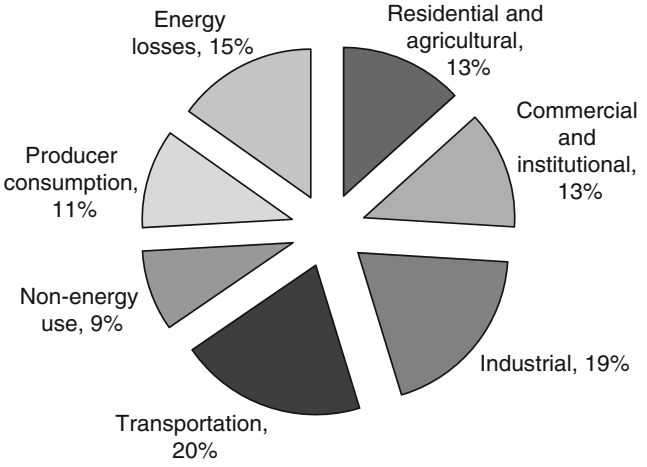

Fig. 17.18 Energy demand in Canada 2008 [data from Statistics Canada (2008)]

for domestic use is 12,500 PJ and that of exergy is 12,630 PJ. It is interesting to note that crude oil represents 41% in energy terms and 53% in exergy measures. Also coal, coke, and coke oven gas represent an 8% energy share, while in exergy terms their share is only 2%. Moreover, natural gas has similar shares in energy and exergy terms—18% and 20%, respectively. These facts demonstrate that the quality of the energy resource, in terms of conversion, is well taken into account by exergy. That is, the exergy content of coal is low, and that of oil is high. For natural gas, the energy and energy content are about the same.

The energy demand of Canada is shared among various economic sectors according to the proportions presented in Fig. 17.18. There, through producer consumption, we see the amount of energy consumed by the producers of energy such as refineries and power plants, which must use a small part of the produced energy for their own needs. From the figure we see that the energy losses are 15%, which means that the energy utilization efficiency in Canada is about 85%.

Table 17.8 Efficiency of electricity generation in Canada, year 2008 (overall)[a]

	Input, PJ			Efficiency	
Energy source	Energy	Exergy	Electrical output	Energy, %	Exergy, %
Nuclear	1,130	1,073	339	30	32
Hydro	1,698	1,698	1,358	80	80
Secondary	2,715	1,629	543	20	33
Coal	1,260	630	378	30	60
Fuel oil	60.5	62.5	23	38	37
Diesel	8	8.3	3.2	40	38
Natural gas	249	254	112	45	44
Natural gas liquids	32	33.6	8	25	24
Biomass	95	66	19	20	29
Overall	7,247	5,454	2,783	38	51

[a]Rough estimates based on data from Statistics Canada (2008)

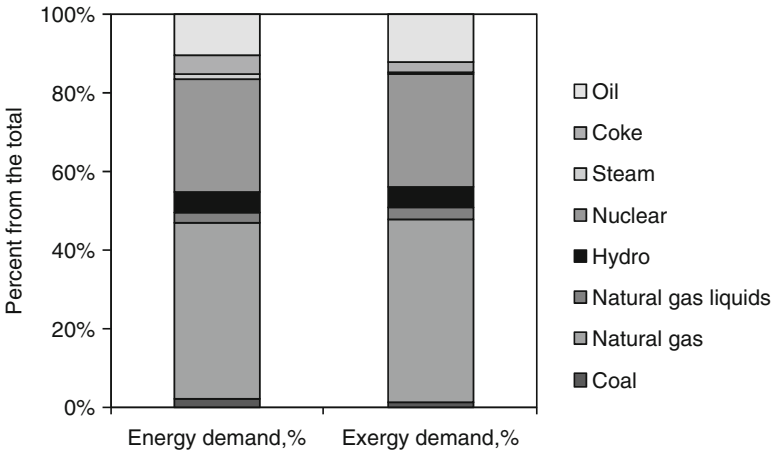

Fig. 17.19 Energy and exergy demand in Canadian industry from various sources

The estimation of electricity production efficiency for domestic use in Canada (by utility and industry together) is presented in Table 17.8. The energy and exergy input is listed for each fuel type as well as the generated electricity. The overall energy efficiency at electricity generation is 38% energy-wise and the exergy efficiency is 51%. It is remarkable that the largest share of electricity production is due to hydropower, which operates at high efficiency. Figure 17.19 analyzes the energy and exergy demand in the Canadian industrial sector. The bar plot is presented in percents of the total energy/exergy demand. The largest demand in industry is the natural gas nuclear electricity. Figure 17.20 analyzes further the industrial sector, showing the percent use of fuels (per type) for each major subsector. The energy is used in each industrial subsector for two major purposes: work generation (including electricity production at industrial sites) and heat generation.

Regarding heat generation, we considered three levels of heat needed by industry, namely, low-temperature heat (Carnot factor 0.25), intermediate-temperature heat

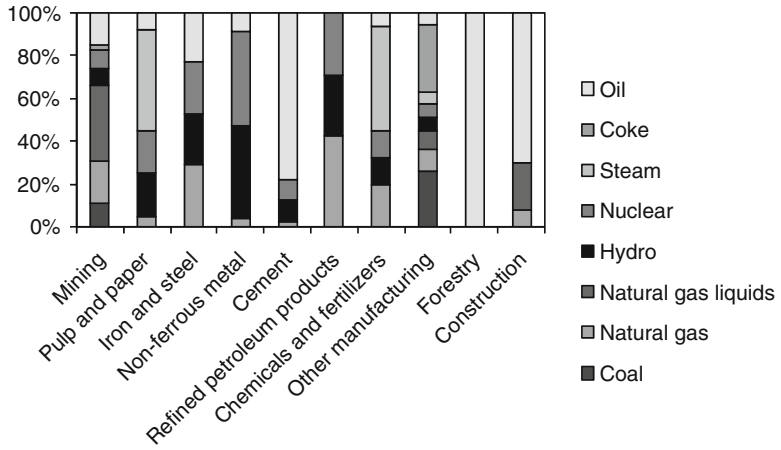

Fig. 17.20 Energy utilization in industrial subsectors of Canada (in percents)

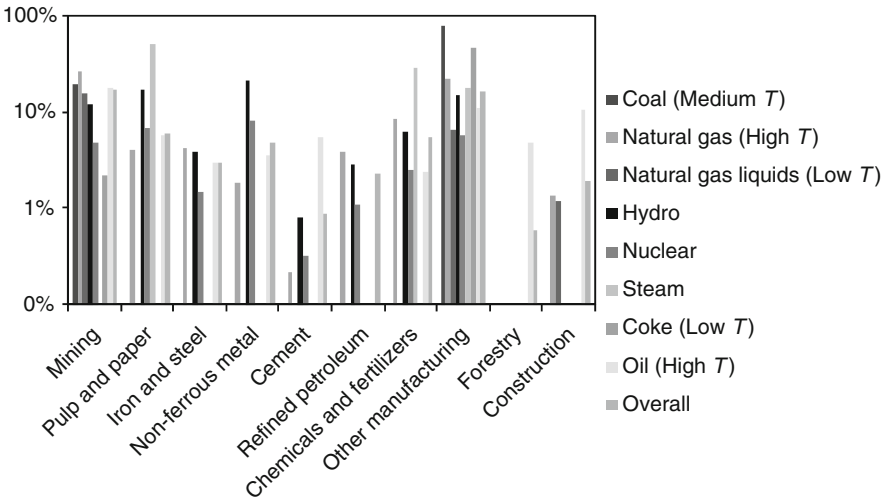

Fig. 17.21 Exergy efficiency in industrial subsectors for specific energy supply

(Carnot factor 0.5), and high-temperature heat (Carnot Factor 0.75). Some of the energy resources are used only for electricity production, for example, hydro and nuclear. Steam is associated with a Carnot factor of 0.6.

Figure 17.21 shows the calculated exergy efficiency of industrial subsectors as a function of the type of energy supply. For this plot, it has been assumed that natural gas liquids and coke are used in industry to heat low-temperature processes; coal is used mostly in medium-temperature and natural gas and oil in high-temperature processes.

The overall exergy efficiency for each subsector, obtained by weighting, is reported in Fig. 17.22. The results show that the mining and manufacturing sectors are the

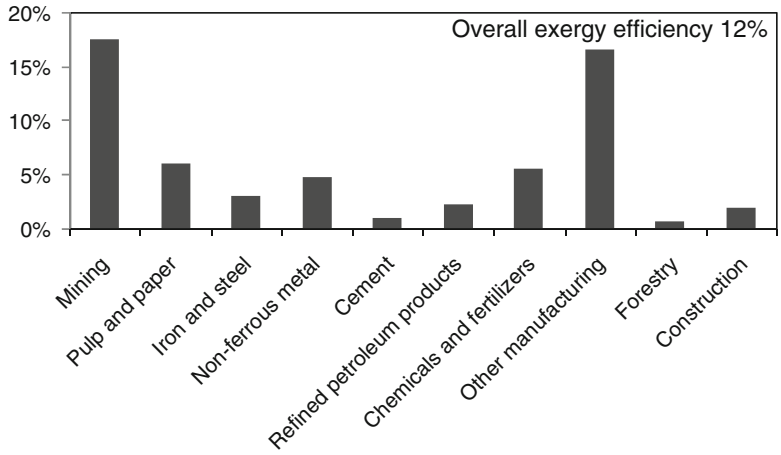

Fig. 17.22 Exergy efficiency in industrial subsectors

most exergy efficient while the cement sector and forestry are the least efficient. The calculated overall exergy efficiency of the industrial sector of Canada is 12%.

For transportation sector analysis, it is considered that the main product of this sector is the propulsion work of vehicles or to circulate fluids in pipelines. The Canadian transportation sector include railways (4% energy consumption), airlines (10%), marine transport (1%), road transport and urban transit (14%), and the rest (61%) being retail pump sales. The energy efficiency of petroleum-based vehicles is on average 25%, while vehicles of large capacity such as ships and large diesel trucks may reach 35% efficiency; electric vehicles are 65% efficient (with respect to the primary energy). Based on the nature of energy consumption of the transportation sector, one may argue that 7% of vehicles are 40% efficient, 1% are 80% efficient (e.g., electric street cars), and 93% of vehicles are 25% efficient. Thus, the calculated energy efficiency of the transportation sector is 26%. The exergy efficiency is calculated by using the exergy factors presented in Table 17.7, and the result is 29%.

The agricultural sector consumes fuels mainly to run tractors and electricity mainly to run irrigation pumps. The demand in Canadian agriculture is 84% fuels and 16% electricity. Assuming as above 75% efficient tractors and 90% efficient pumps, the energy efficiency of the agricultural sector is 77% and the exergy efficiency is 50%.

The residential sector consumes 42% electricity and 58% fuels for heating at low temperature (Carnot factor of ~25%). The energy efficiency becomes 64%, while the exergy efficiency is 23%. The public sector uses ~58.6% fuels for low-temperature heating, 0.4% steam, and 41% primary electricity. Thus, one calculated 84% energy efficiency and 41% exergy efficiency. The commercial sector consumes 36.8% primary electricity, 0.2% steam, and 63% fuels for heating. Thus, one has 85% energy efficiency and 36% exergy efficiency. Finally, the sectorial analysis concludes with the energy and exergy efficiency of the Canadian economy and its activity sectors. This result is illustrated in Fig. 17.23a. The estimated overall energy efficiency of the Canadian economy is 42% and that of exergy efficiency is 38%.

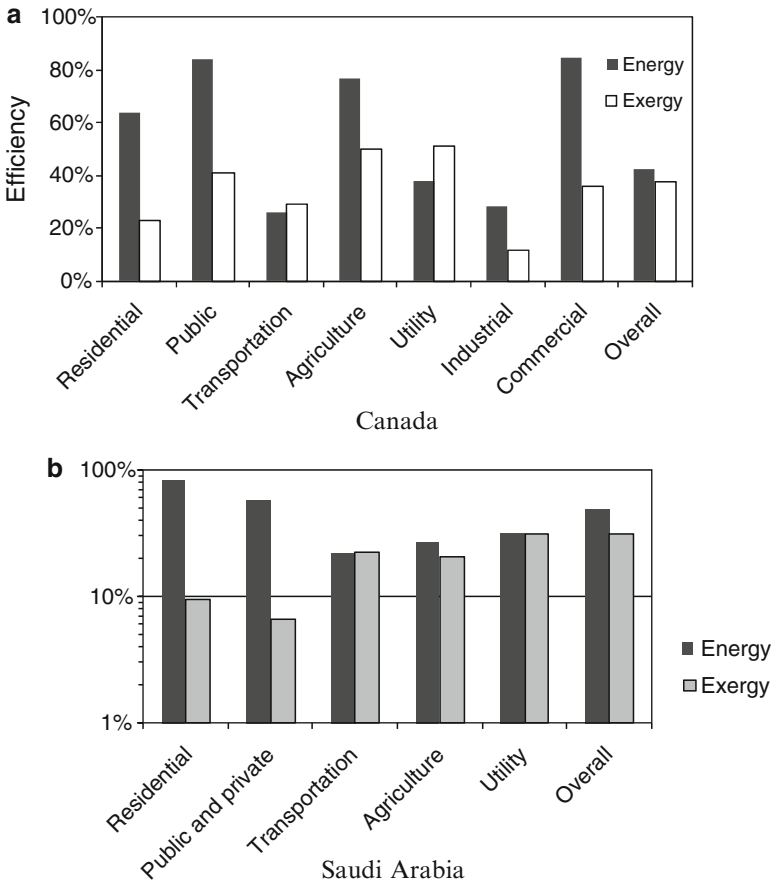

Fig. 17.23 Energy and exergy efficiency of Canadian (**a**) economy and its sectors and those of Saudi Arabia (**b**) [for case (**b**) data from Dincer and Rosen (2007)]

Figure 17.23 also compares the results of the Canadian sectoral energy analysis with a similar one for Saudi Arabia. The overall energy efficiency of Saudi Arabia is 51% energy-wise and 31% exergy-wise.

17.9 Concluding Remarks

The assessment of overall energy and exergy utilization in a macrosystem in the form of a sector of activity for a geopolitical region or a country provides useful information that can help achieve energy savings through efficiency and conservation measures. Sectorial analysis through energy and exergy can also help in establishing standards to facilitate better energy planning in the entire macrosystem and its sectors, including subsectors. The case study presented demonstrates that the

methodology is simple to apply, using thermodynamic analysis through the first and second laws, and addresses the general concepts of thermodynamic system, mass and energy conservation, material flows balance, and exergy balance equations.

Nomenclature

COP	Coefficient of performance
ex	Specific exergy, kJ/kg
HHV	Higher heating value, MJ/kg or MJ/kmol
I_T	Solar radiation, W/m^2
ke	Specific kinetic energy, kJ/kg
LHV	Lower heating value, MJ/kg
q	Heat per unit of mass, kJ/kg or mol, kJ/mol or surface ($''$), kW/m^2
Q	Heat, J
T	Temperature, K
w	Specific work, J/kg
W	Work, J

Greek Letters

η	Energy efficiency
ψ	Exergy efficiency
ζ	Quality factor

Subscripts

0	Reference state
inp	Input
p	Process

Superscripts

ch	Chemical
s	Solar
$''$	Per unit of surface

References

Ayres R.U., Ayres L.W., Warr B. 2003. Exergy, power and work in the US economy, 1900–1998. *Energy* 28:219–273.

Brzustowski T.A., Brena A. 1986. Second-law analysis of energy processes part IV: the exergy of hydrocarbon fuels. *Transactions of the Canadian Society of Mechanical Engineers* 10:121–128.

Dincer I. 1997. Energy and GDP analysis of OECD countries. *Energy Conservation and Management* 38:685–696.

Dincer I., Al-Rashed B. 2002. Energy analysis of Saudi Arabia. *International Journal of Energy Research* 26:263–278.

Dincer I., Dost S., Li X. 1997. Energy reality and future projections in Canada. *Energy Sources* 19:233–243.

Dincer I., Hussain M.M., Al-Zaharnah I. 2004a. Energy and exergy use in public and private sector of Saudi Arabia. *Energy Policy* 32:1615–1624.

Dincer I., Hussain M.M., Al-Zaharnah I. 2004b. Energy and exergy use in residential sector of Saudi Arabia. *Energy Sources* 26:1239–1252.

Dincer I., Hussain M.M., Al-Zaharnah I. 2005. Energy and exergy utilization in agricultural sector of Saudi Arabia. *Energy Policy* 33:1461–1467.

Dincer I., Rosen M.A. 2007. Exergy: Energy, Environment and Sustainable Development. Elsevier, Oxford, UK.

Hepbasli A. 2005. Modeling of sectoral energy and exergy utilization. *Energy Sources* 27:903–912.

Jaber J.O., Al-Ghandoor A., Sawalha S.A. 2008. Energy analysis and exergy utilization in the transportation sector of Jordan. *Energy Policy* 36:2985–2990.

Ji X., Chen G.Q. 2006. Exergy analysis of energy utilization in the transportation sector in China. *Energy Policy* 34:1709–1719.

Kondo K. 2009. Energy and exergy utilization efficiencies in the Japanese residential/commercial sectors. *Energy Policy* 37:3475–3483.

Koroneos C.J., Nanaki E.A. 2008. Energy and exergy utilization assessment of the Greek transport sector. *Resources, Conservation and Recycling* 52:700–706.

Oladiran M.T., Meyer J.P. 2007. Energy and exergy analyses of energy consumptions in the industrial sector in South Africa. *Applied Energy* 84:1056–1067.

Reistad G.M. 1975. Available energy conversion and utilization in the United States. *Journal of Engineering for Power* 97:429–434.

Rosen M.A. 1992. Evaluation of energy utilization efficiency in Canada using energy and exergy analyses. *Energy* 17:339–350.

Saidur R., Sattar M.A., Masjuki H.H., Abdessalam H., Shahruan B.S. 2007. Energy and exergy analysis at the utility and commercial sectors of Malaysia. *Energy Policy* 35:1956–1966.

Statistics Canada 2008. Report on energy supply and demand in Canada. Catalogue 57-003-X.

Utlu Z., Hepbasli A. 2004. Turkey's sectoral energy and exergy analysis between 1999 and 2000. *International Journal of Energy Research* 28:1117–1196.

Utlu Z., Hepbasli A. 2006. Assessment of the energy utilization efficiency in the Turkish transportation sector between 2000 and 2020 using energy and exergy analysis method. *Energy Policy* 34:1611–1618.

Utlu Z., Hepbasli A. 2007a. Parametrical investigation of the effect of dead (reference) state on energy and exergy utilization efficiencies of residential-commercial sectors: A review and an application. *Renewable and Sustainable Energy Reviews* 11:603–634.

Utlu Z., Hepbasli A. 2007b. A review and assessment of the energy utilization efficiency in the Turkish industrial sector using energy and exergy analysis method. *Renewable and Sustainable Energy Reviews* 11:1438–1459.

Utlu Z., Hepbasli A. 2009. Exergoeconomic aspects of sectoral energy utilization for Turkish industrial sector and their impact on energy policies. *Energy Policy* 37:577–587.

Xydis G., Koroneos C., Polyzakis A. 2009. Energy and exergy analysis of the Greek hotel sector: An application. *Energy and Buildings* 41:402–406.

Study Questions/Problems

17.1 Why should sectorial exergy utilization accompany sectorial energy utilization studies?
17.2 Explain the thermodynamic analysis at macroscale based on energy and exergy.
17.3 How is thermodynamic modeling performed at the sectorial level?
17.4 What are the quality factors associated with some energy forms?
17.5 Comment on the features of energy/exergy flows at the sectorial level of a geopolitical region.
17.6 What are the main subsystems of the commercial and residential sectors?
17.7 What are the main subsectors of the industrial sector and their principal attributes?
17.8 Taking an example from Turkey, explain the quantitative differences between energy and exergy utilization from primary sources.
17.9 How one can calculate the exergy efficiency of the agricultural sector?
17.10 Comment on the differences between energy and exergy efficiencies of the agricultural sector of Canada and Saudi Arabia.
17.11 Comment on energy shares of means of transportation in Turkey, Jordan, Greece, and China.
17.12 Similar to the case study presented in the chapter, try to perform a sectorial energy and exergy analysis of a country or geopolitical region.

Chapter 18
Economic Analysis

18.1 Introduction

The future of any energy resource depends on the state of the art of the technology to harvest, convert, and transport it and hence on economic and political factors. The political factors include rules and regulations. The relationships among factors have been studied and characterized during the past century in the context of power plant engineering and regulated utilities. Between energy engineering and economics there is obviously a trade-off because a design achieving high energy generation efficiency is costly and this leads to a high price per unit of energy. On the other extreme, a low-cost design features low efficiency, and hence the cost of energy is high because one needs to spend large amounts of primary energy resources. Somewhere in between a technical–economical optimum of the design can be found.

One of the roles of engineering economics is to establish technical–economical criteria for design optimization. For example, such criteria can be minimum life-cycle cost, maximum life-cycle savings (LCS), minimum levelized energy cost, and so on. Even though these concepts are well developed in the context of classic power plant engineering (Drbal et al. 1996), there are only a few texts that discuss and give instructive examples of the technical–economical peculiarities of recently established sustainable energy systems.

The key factor to be considered here is the additional costs involved in clean emission enforcement. These costs may include the CO_2 separation and sequestration system, the carbon tax, tax deductions on renewable energy development and associated power generation, incentives and bonds issued by governments to help initial investments in renewable energy generation, and others. These factors as such can change the economic picture in general and accelerate the march of societies toward a globally spread sustainable energy practice.

Apart from their use in system design and optimization, engineering economics establishes the criteria for choosing among options. For example, life-cycle cost can be used to decide which of two or more alternative energy systems attaining the same purpose is preferable. These systems can be based on fossil fuel or on renewable sources or a combination of sources.

İ. Dinçer and C. Zamfirescu, *Sustainable Energy Systems and Applications*,
DOI 10.1007/978-0-387-95861-3_18,

If several equivalent energy systems are studied during the same period of time (or if the systems have a similar lifetime), normally the system with the lowest life-cycle cost is to be preferred. If the studied alternatives each have a different lifetime, the system featuring the lowest levelized energy cost should be selected.

Economics is crucial in guiding the engineering decisions in the implementation of various sustainable energy systems and technologies. The goal is to make such systems and technologies more cost-effective and hence more economical.

Politics, influences the economic decisions about renewable energy. Boyle (2004) summarized the main political factors through which governments may influence the promotion of sustainable energy technologies. These are related first to legislation and regulations that specify standards and codes for renewable energy. For example, in Greece and Israel there are requirements that new buildings have solar collectors for water heating. Most countries rely, however, on various financial incentives that modify the life-cycle cost or savings so that sustainable energy sources are promoted by making them economically attractive. Some examples are given below:

- Exemption from taxes
- Capital grants
- Auction to supply contracts for renewable energy
- Renewable obligations (electricity suppliers must purchase a specific proportion of renewable energy)
- Feed-in tariffs (fixed premium prices for electricity from renewables)

The U.S. Energy Policy Act of EPACT (2008) states that the Department of Energy shall seek, to the extent that is economically feasible and technically practicable, to increase the total amount of renewable energy that the federal government consumes during the following fiscal years:

(a) Not less than 3% in fiscal years 2007 through 2009
(b) Not less than 5% in fiscal years 2010 through 2012
(c) Not less than 7.5% in fiscal year 2013 and each fiscal year thereafter

The U.S. implements this policy by offering Renewable Energy Certificates (RECs) to eligible economic actors and agencies that generate, buy, or sell any form of renewable energy. An REC represents an allowance given in equivalent of 1 MWh unit, especially to new projects to reduce the initial costs and hence to promote the development of renewable energy trade. The European Union proceeds somewhat similarly, but its target is to achieve a 12% share for renewable energy of the total energy consumption by 2010 (EC 2001).

Other books discuss the topic of sustainable energy systems and include chapters on economic analysis and optimization. Rabl (1985) discusses solar concentrators. Rubin and Davidson (2001) discuss the fundamentals of engineering economics and its applications for life-cycle cost analysis and compare technology options for environment control and policy. Boyle (2004) and Tiwari and Ghosal (2007) discuss renewable energy. Tester et al. (2005) discuss sustainable energy economics (including nuclear).

In contrast, this chapter discusses finance issues such as the rate of discounting the future, worth analysis, loan payments and taxation, the current prediction of fuel price escalation and consumer price index (CPI) evolution up to 2050, life-cycle cost analysis and optimization for renewable energy sources, homeowner or non-utility energy generators and utility electrical energy generators, and cogeneration and district energy systems.

The work by Fuller and Petersen (1995), which describes the life-cycle cost methodology and criteria established by the U.S. Federal Energy Management Program (FEMP) for economic evaluation of (renewable) energy and water conservation projects, has been consulted for updated information on fuel price and electrical energy escalation rates. Their report is accompanied by a yearly supplement that offers price indexes and discount factors for life-cycle cost analysis. The last issue of the supplement is by Rushing and Lippiatt (2008) and includes fossil fuel and electrical energy escalation prices, as predicted up to 2038.

Another important reference is ASHRAE (2007), which presents a chapter on owning and operating costs that includes information about the life-cycle cost of heating, ventilating, air conditioning and refrigeration systems, and district energy systems. The costs are categorized as incidental (initial cost, replacement cost, salvage value) or periodic (e.g., loan, insurance, tax, etc.). The operating costs are differentiated into fuel, utility and water costs and in-house labor, materials, maintenance services, and other maintenance allowances. This source offers valuable tabulated data of the life-cycle costs of residential, commercial, and industrial energy conversion systems.

This chapter discusses some fundamental aspects of engineering economic analysis and its applications to various practical cases, where the role of economics is critical. Several problems are presented to explain and illustrate the concepts and definitions. The criteria that can be used for life-cycle cost analysis, design selection, and optimization are also explained.

18.2 Elements of Financing and Engineering Economics

This section introduces some relevant financing and economics concepts in, such as discount rate, inflation, present and future worth of capital, levelizing, financing through loans, taxation, depreciation, and salvage. These concepts constitute the fundamental building blocks of life-cycle cost analysis and technical–economical system optimization.

18.2.1 Rate of Discounting the Future

The most basic concept in economics is *capital*, which refers to items of extensive value. Even though the term has several other meanings, we refer here only to *financial capital*, which represents a value owned by legal entities that can be saved, traded, and useful when retrieved.

When traded, financial capital can be liquidated as *money* because by its nature money is used as a medium of exchange. It is important to note that the market value of capital is not based on the historical accumulation of money invested but on the perception by the market of its expected revenues and of the risk entailed. The revenue may come from the investment of financial capital in the form of money. Since money can be invested, it augments the capital, and thus the future worth of money always increases. Said another way, the present worth of money (or of a capital measured by money) is always smaller than the future worth. In economics, one says that the present worth is discounted with respect to the future worth.

By definition, the *rate of discounting the future* (or the discount rate) represents the incremental growth of worth during a period of time. If one denotes the discount rate with r, the future worth with F, and the present worth with P, then the incremental growth of worth, $1 + r$, is $1 + r = F/P$, and therefore the discount rate for one time period is

$$r = \frac{F}{P - 1}. \tag{18.1}$$

In general, the unit of time period in economics is 1 year. However, it is common that the discount rate stays constant along several time intervals n; hence, $r = F_k/P_k - 1, k = 1 \ldots n$. In this situation, the present worth in the second period, P_2, is the same as the future worth after the first period, F_1. Moreover, the present worth in the third period, P_3, is equal to the future worth after the second period, F_2, and, in general one can write $P_k = F_{k-1}$, $k = 2 \ldots n$. Taking the product of (F_k/P_k) for $k = 1 \ldots N$ and reducing any P_k with F_{k-1}, one eventually obtains $(1 + r)^N = F_N/P_1$; hence,

$$r = \left(\frac{F_N}{P_1}\right)^{1/N} - 1 \tag{18.2}$$

represents the discount rate that models the present worth P_1 growth after n times intervals.

Application of the discount rate for more than one period is known as *compounding*. Through compounding one obtains the ratio between the future and present worth, which is an equivalent form of Eq. (18.2), such as

$$\frac{F_N}{P_1} = (1 + r)^N, \tag{18.3}$$

which is called *compound amount factor* and denoted with the consecrated notation $(F/P, r, N)$, where N is the number of periods (e.g., years), F the future worth after N periods, P is the present worth, and r is the discount rate (see Fraser et al. 2006).

The converse of Eq. (18.3) is known as the *present worth factor* and it facilitates the calculation of the present worth, which is a value gain after a number N of time

periods during which the present value is incrementally augmented. Hence, the present worth factor, denoted $(P/F, r, N)$, is

$$\frac{P_1}{F_N} = (1+r)^{-N}. \tag{18.4}$$

The present and future worth are general notions because they refer to values. For example, they apply to money that increases its present value due to the productivity of capital, but as well these concepts apply to any commodity (e.g., oil). It is interesting to note that taxes that increase in time at a constant rate can be modeled on the same equation Eq. (18.2), as can be seen in the next example.

Example 18.1

An industry consumes oil at a constant rate per day for heating purposes. The period under consideration is from 2010 to 2050. It is known that about 0.3 tonne of CO_2 is produced per GJ of combusted oil. Estimate the total tax paid for CO_2 emission in constant dollars in 2008. Calculate the rate of increase in the CO_2 tax if one assumes that between 2010 and 2050 this rate is constant. The following equation gives the tax on CO_2 emission in 2008 dollars of constant currency (amended for inflation) per tonne for any year between 2007 and 2050:

$$t_{CO_2} = (3.2y - 6,422.4)\frac{\text{US\$}_{2008}}{\text{tonne}CO_2},$$

where y is the year and US$2008 represent the U.S. dollars at their 2008 value.

Solution

- The tax on CO_2 per GJ of energy produced from oil combustion is $t_{CO_2} = (3.2y - 6,422.4)\,(\text{US\$}_{2008}/\text{tonne}CO_2) \times 0.3\,(\text{tonne}CO_2/\text{GJ})$.
- The above equation becomes $t_{CO_2} = 0.96y - 1,926.72\,(\text{US\$}_{2008}/\text{GJ})$.
- The total tax on CO_2 emission paid per GJ of combusted oil between 2007 and the year y is then $t_{CO_2,2007}(y) = \int_{2007}^{y}(0.96y - 1,926.72)\text{d}y$, which solves to

$$t_{CO_2,2007}(y) = 0.48y^2 - 1,926.72y + 1,933,463\frac{\text{US\$}_{2008}}{\text{GJ}}.$$

- Thus, the total tax paid between 2010 and 2050 is

$$t_{CO_2,\text{tot}} = t_{CO_2,2007}(2050) - t_{CO_2,2007}(2010) = 883\frac{\text{US\$}_{2008}}{\text{GJ}}.$$

- The tax in 2010 is, according to above equation, $t_{CO_2,2010} = \text{US\$}13.8/\text{GJ}$; if one assumes a constant rate of tax increase, the future value in year N is $F_N = (1+r)^N t_{CO_2,2010}$; therefore, for a fixed rate of emission during 2010 and 2050 the total tax paid is the summation

$$t_{CO_2,\text{tot}} = \sum_{k=1}^{N} F_k = t_{CO_2,2010}\sum_{k=1}^{N}(1+r)^k,$$

which is a geometric progression with ratio $a = 1 + r$ and has the known sum of

$$\sum_{k=1}^{N} a^k = a\left(\frac{1-a^N}{1-a}\right),$$

where $N = 40$ years; therefore, one equates

$$13.8a\left(\frac{1-a^{40}}{1-a}\right) = 883$$

and solves it for a; the result is $a = 1.022$ or $r = 2.2\%$.

- Written according to Eq. (18.3) the tax in year N is given with respect to the present tax in 2008 by $F_N = 1.022^N t_{CO_2,2008}$.
- Note that in the constant rate of increase approach, the tax in the year 2050 is $t_{CO_2,2050} = F_{40} = 1.022^{40} \times 13.8 = \text{US}_{2008}\$33/\text{GJ}$, which is different from that predicted by the equation given in the problem statement, $t_{CO_2,2050} = \text{US}\$_{2008}138/\text{GJ}$.

Example 18.2

What is the value after 5 years of a deposit of $1,000 in a bank savings account with 6% compounding yearly?

Solution

- The interest rate of 6% is in fact the rate of discounting the future; hence $r = 0.06$.
- The present worth is $P_1 = \$1{,}000$ and the number of compounding periods $N = 5$.
- The compound amount factor calculated with Eq. (18.3) is $(F/P, 0.06, 5) = 1.06^5 = 1.338$.
- Therefore, the future worth of the deposit is $F_5 = (F/P, 0.06, 5)P_1 = 1.338 \times \$1{,}000 = \$1{,}338$.

Example 18.3

A homeowner assumes that his water heater needs to be replaced after 15 years at a cost of $2,000. What amount must he deposit today with 4% interest so that he can buy the replacement boiler after 15 years? How much should the interest rate be if he deposits $1,000?

Solution

- The future value $F_{15} = \$2{,}000$ is discounted by the rate $r = 0.04$ for $N = 15$ years.
- The present worth factor is, according to Eq. (18.4), $(P/F,0.04,15) = 1.04^{-15} = 0.555$.
- The homeowner has to deposit $P_1 = (P/F, 0.04, 15)F_{15} = 0.555 \times 2{,}000 = \$1{,}110$.
- If the homeowner deposits $P_1 = \$1{,}000$, then the discount rate for 15 compounding periods is given by Eq. (18.2), $r = (F_{15}/P_1)^{1/15} - 1 = 2^{1/15} - 1 = 4.73\%$; thus the interest rate must be 4.73%.

In the examples given above, we used the term *interest rate* without defining it since it is assumed that the reader is familiar with it (this term is commonly used for bank-related business). The important aspect here is to observe that the rate of discounting the future is a consequence of the productivity of capital, and therefore, for the case of bank savings, the discount rate is the same as the interest rate. However, the discount rate is a more general concept, as can be deduced from Example 18.1, where the discount rate is taken to be the same as the growth rate of the carbon tax.

It is clear that the higher the discount rate, the lower the present worth. However, the choice of the discount rate is not clear because different investments yield different returns. Similarly, regulators have the dilemma of determining what taxation rate to impose (which, as exemplified above, acts similarly to a discount rate) because imposing a high tax or too low a tax may lead to unwanted economic consequences. It is useful here to discuss some examples of how to choose a discount rate for some relevant situations.

First, consider a homeowner who has enough money in his savings account to purchase a solar water heater. Instead of buying the water heater, he could leave the money in his savings account. If he does buy the water heater, he forgoes the interest that he could otherwise earn from the savings account. Hence, his discount rate is the interest rate of his savings account. If he had no savings, he would have to borrow money for the water heater. In that case, his discount rate would be the interest of his loan. Loan interest rates are generally higher than the rates for savings account.

The situation is more complex if there are several investment alternatives. For example, a homeowner might invest his money in real estate, stocks, or bonds, each with a different rate of return and a different risk. Industrial and commercial investors usually have a range of investment opportunities. In such cases, the appropriate discount rate for the analysis of a sustainable energy investment is the rate of return for investments of comparable risk that would be made if the money were not spent on a sustainable energy system.

When a project is examined from the point of view of society, the discount rate should be based on the rate of return for society as whole. This rate is called the social discount rate. It is the subject of much controversy, entailing as it does delicate problems such as intergenerational equity. A high discount rate de-emphasizes the importance of future costs or benefits; in other words, it favors the present generation over future generations.

18.2.2 Inflation Rate

Another factor regarding the discount rate is the volatile value of money, which can inflate or deflate. Inflation refers to increase over time in the average *price* of goods and services. The term *price* refers to the assignment of a monetary value to a good or service. Any price is given in a specific currency that represents a unit of trade, which is a measure of money.

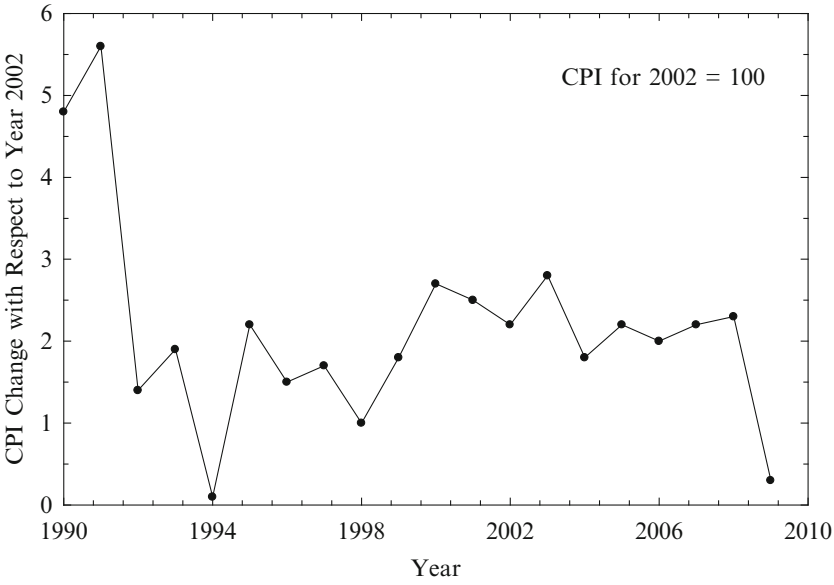

Fig. 18.1 Variation of the Canadian CPI in the period 2004–2008 [data from StatCan (2010)]

Deflation is the opposite of inflation, representing a decrease over time in the average purchasing power of money. Inflation and deflation phenomena come in succession; that is, after a period of inflation may come a period of deflation, depending on the march of the economy as a whole. These phenomena can be quantified by accounting for the relative variation of currency.

The rate of discount of any kind of business is affected by inflation and deflation because they modify the cash flows associated with any economic (and engineering) project conducted over a period of time. It is important therefore to quantify these effects and their impact on the discount rate.

Inflation and deflation can be quantified through the CPI that represents the average price of a basket of goods in a given period, divided by the price of the same basket in a base period. Since it refers to price, the CPI is always given with respect to a specific currency. In Canada, for example, the year 2002 is taken as the reference year for CPI estimation (the CPI value is set to 100 for year 2002). In Fig. 18.1, the variation of the CPI in Canada for the period 1990–2008 is shown. One can clearly observe how a period of inflation (CPI growth) is followed by a period of deflation (CPI decrease).

The CPI provides a means to differentiate between the real worth and the nominal worth of a currency. The *real worth of a currency* (RW) represents the worth of that currency in the reference period taken by convention for computing the CPI. The *nominal worth of currency* (NW) refers to the actual worth at the

current date or at any other specified period different from the reference period for the CPI. The CPI is therefore defined by

$$\mathrm{CPI}_N = \frac{\mathrm{NW}_N}{\mathrm{RW}}, \tag{18.5}$$

where the subscript N indicates that the CPI and the nominal worth correspond to the year N after (or before) the reference period. On the other hand, the nominal worth can be viewed as a future worth of currency in the reference period that inflated (or deflated) with the discount rate i; therefore, the equation becomes

$$\mathrm{NW}_N = \mathrm{RW}\left(\frac{F}{P}, i, N\right), \tag{18.6}$$

which introduces the *inflation rate* that represents the discount rate i of nominal currency with respect to real currency. Solving simultaneously Eq. (18.5) and Eq. (18.6) for CPI_N, one obtains

$$\mathrm{CPI}_N = \left(\frac{F}{P}, i, N\right), \tag{18.7}$$

an equation that can be further solved for the inflation rate i to get

$$i = \mathrm{CPI}_N^{1/N} - 1. \tag{18.8}$$

Observe from Eq. (18.8) that if a deflation occurs with respect to reference period for CPI, that is, if CPI is subunitary, and then the inflation rate is negative, indicating thus a deflation period. Hence, the inflation rate is a universal indicator that models both the periods of inflation (positive i) and deflation (negative i).

The U.S. Department of Energy predicts that the implied long-term (up to year 2040) average inflation that may be included in economic analysis of energy projects is 1.8% (see Rushing and Lippiatt 2008). The predicted yearly variation of the U.S. dollar inflation rate up to 2018 is presented in Fig. 18.2, with reference to year 2007.

18.2.3 Real Rate

It is important to account for inflation when adopting a discount rate in any engineering project that extends over a predictable period in future. Assume that for a given period of time the inflation rate is i and the discount rate is r. Then, due to the productivity of capital, the future worth increases by $(1 + r)$ times, while due to inflation it decreases by $(1 + i)$ times. Hence, the future worth F of a present worth P is

$$F = \frac{1+r}{1+i}P. \tag{18.9}$$

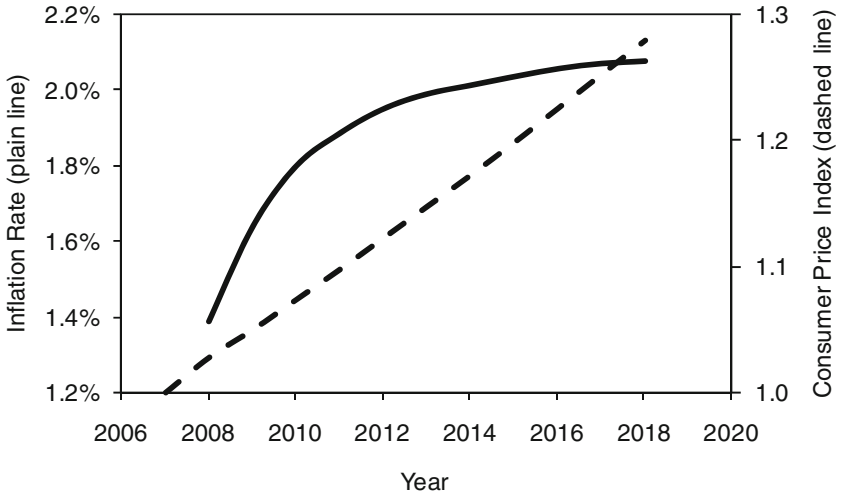

Fig. 18.2 Predicted inflation rate and CPI of the U.S. currency with respect to reference year 2007 [data from Sahr (2008)]

Equations (18.1) and (18.9) introduce the *real rate* of discount, namely,

$$r_{\mathrm{r}} = \frac{1+r}{1+i} - 1, \tag{18.10}$$

where one has to distinguish the term r as the *market discount rate*, that is, a discount rate given in nominal currency, which does not account for inflation.

In engineering economics, it is recommended to pursue the analysis in *constant currency* (or real currency) that represents the currency amended for the inflation. Therefore, in calculation of the present worth and compound amount factors and other economic indicators, the real discount rate must be used and not the market discount rate. This is illustrated in the following example.

Example 18.4

A loan of \$1,000 is made at an interest rate of 15% when the inflation rate is 12%, and it is repaid in one installment after 2 years. Calculate the amount repaid. What is the difference between this result and the result obtained if inflation is ignored?

Solution

- The real rate is given by Eq. (18.10), $r_{\mathrm{r}} = 1.15/1.12 - 1 = 2.67\%$.
- The compound amount factor is $(F/P, r, N) = (1 + r_{\mathrm{r}})^2 = 1.054$.
- The amount paid after 2 years is $F_2 = 1.054 \times 1,000 = \$1,054$.
- If inflation is ignored, the compound amount factor is $(F/P, r, N) = (1 + r)^2 = 1.322$.
- Therefore, the future worth is $F_{2i} = 1.322 \times 1,000 = \$1,322$.
- Hence, due to the effect of inflation, one pays $F_{2i} - F_2 = 1,322 - 1,054 = \$268$ less.

One important comment regarding the real rate is that it may be considered as relatively constant over a long period of time. For example, as mentioned in Rabl (1985), the real rate was 2.2% for 25 years, from 1955 to 1980, despite large fluctuations in the inflation rate. However, the inflation rate must be accounted for if tax deduction and depreciation claims are to be taken. This factor which is relevant when dealing with long-term loans, is analyzed later.

18.2.4 Price Escalation

The inflation rate is calculated based on the average price of a basket of goods and services. However, some commodities, such as fuel and electricity, display a real growth so that their price escalates more than the average price represented by inflation. Observe in Fig. 18.1 the major impact that the energy market (and implicitly fuels) has on inflation. As a consequence, for a more accurate economic analysis, the price escalation of fossil fuels and electrical energy must be accounted for. This analysis is similar to the one presented above for inflation.

If one denotes the market price escalation rate of a commodity with r_{pe}, then the real escalation rate r_{per} accounting for inflation is calculated with Eq. (18.10), which is equivalent with

$$r_{\text{per}} = \frac{r_{\text{pe}} - i}{1 + i}. \tag{18.11}$$

Now, assume that an economic activity runs at a real discount rate r_{r} consuming a commodity with a real price escalation rate r_{per}. The future worth is therefore

$$F = \frac{1 + r_{\text{r}}}{1 + r_{\text{per}}} P. \tag{18.12}$$

Consequently, the real equivalent discount rate accounting for price escalation is

$$r_{\text{e}} = \frac{r_{\text{r}} - r_{\text{per}}}{1 + r_{\text{per}}}. \tag{18.13}$$

Example 18.5

From Example 18.1, calculate the total cost spent per GJ of combusted oil between 2010 and 2050. If the fuel consumption is 10 MWh per day, what are the total costs in 2008 dollars? What is the ratio between the CO_2 tax and the oil price? Calculate the rate of oil price increase in the assumption that this rate is constant. It is given that the cost of oil by 2010 is \$6/GJ; it increases quasi-linearly to ~\$8/GJ by 2015, and one can approximate a further linear increase to \$18/GJ by 2050. What is the market growth rate of the oil price taxed for CO_2 emission if the average inflation rate is 1.5%? If the real discount rate is 10%, calculate the equivalent discount rate that accounts for the oil price escalation.

Solution

- We assume that the oil price escalation occurs in two linear steps, from 2010 to 2015 and from 2015 to 2050. Thus, the cost of oil per GJ is obtained by linear interpolation

$$c_{\text{oil}} = \begin{cases} \frac{2}{5}y - 798, & y \in [2010, 2015] \\ \frac{2}{7}y - 567.7, & y \in [2016,\ 2050] \end{cases},$$

  where y is the year.
- By integrating the above expression from year 2010 until year y one obtains the total cost of GJ in the following form:

$$C_{\text{oil},2010}(y) = \begin{cases} \frac{1}{5}y^2 - 798y + 795,960, & y \in [2010,\ 2015] \\ \frac{1}{3}y^2 - 567.714y + 563,946, & y \in [2016,\ 2050] \end{cases}.$$

- The total cost of GJ on oil consumed up to 2050 is therefore $c_{\text{tot}} = \$490$. Since the associated CO_2 emission tax in the same period is \$883, the total cost of 1 GJ of oil combusted at a constant rate in the period 2010 to 2050 is \$1,373.
- At 10 MWh per day, the amount for a period of 40 years is

$$\begin{aligned} C_{\text{tot}} &= 40 \times 365 \times 10\text{MWh} \times 36\left(\frac{\text{GJ}}{\text{MWh}}\right) \times 1,373\left(\frac{\text{US\$}_{2008}}{\text{GJ}}\right) \\ &= \text{US\$}_{\ 2008}7,216,488,000. \end{aligned}$$

- The amount paid for the CO_2 tax in this period is

$$\begin{aligned} t_{\text{CO}_2} &= 40 \times 365 \times 10\,\text{MWh} \times 36\left(\frac{\text{GJ}}{\text{MWh}}\right) \times 883\left(\frac{\text{US\$}_{2008}}{\text{GJ}}\right) \\ &= \text{US\$}_{\ 2008}4,641,048,000. \end{aligned}$$

- Note that in the scenario proposed by the present example, the amount paid on the CO_2 tax is larger than the real cost of oil; from the total cost of combusted oil 883/1,373 = 64% represents the carbon tax.
- For calculating the rate of oil price increase r_{o}, one proceeds similarly as in the previous example. The total cost spent on oil is therefore

$$c_{\text{tot}} = c_{\text{oil}(2010)} \sum_{k=1}^{N} (1 + r_{\text{o}})^k,$$

  where $C_{\text{oil}(2010)} = \$20{,}086/\text{GJ}$.

- With the notation $a_0 = 1 + r_0$ and for $c_{tot} = US\$_{2008}490/GJ$,

$$490 = 6a_0\left(\frac{1 - a_0^{40}}{1 - a_0}\right),$$

  which gives $a_0 = 1.032$ and $r_o = 3.2\%$.
- Note that for a fixed oil increase rate the predicted oil price by 2050 comes to $c_{oil\,(2050)} = F_{2050} = (1 + r_o)^{40} c_{oil(2010)} = US\$_{2008}21.1/GJ$, which is slightly higher than the value of $US\$_{2008}18/GJ$ predicted with the equation given in the problem statement.
- The price growth rate of oil taxed for emission is given by solving $1,373 = 6a_0(1 - a_0{}^{40})/(1 - a_0)$ for a_0, which results in the price growth rate of oil, including carbon tax $r_{ot} = 7.26\%$.
- Conversely, one can estimate the total cost of GJ for oil plus tax in 2050 based on 2010 present value that is $2/5 \times 2010 - 768 = US\$_{2008}36$ for oil plus $0.96 \times 2010 - 1,926.72 = US\$_{2008}2.88$ for the carbon tax. In total, the present value in 2010 for oil is $36 + 2.88 = 38.88US\$_{2008}/GJ$.
- The future worth for 2050 is therefore $38.88 \times (1 + r_{ot})^{40} = 642US\$_{2008}/GJ$.
- With an average inflation rate $i = 1.5\%$, the market rate of taxed oil price escalation results from Eq. (18.10), which is solved for r knowing that $r_r = r_{ot} = 7.26\%$.
- Hence, $r = (1 + r_{ot})(1 + i) - 1 = 1.0726 \times 1.015 - 1 = 23.3\%$.
- With a real rate $r_r = 10\%$, the equivalent discount rate, including fuel price escalation, is given by Eq. (18.13), where $r_{per} = r_{ot} = 7.26\%$, thus $r_e = 2.55\%$.
- Note that in the assumed scenario, businesses must have high real discount rate (over 7.5%) so that the equivalent discount rate, including inflation, is positive. In the negative discount rate case, the future worth of money decreases, thus the business does not make sense.

Figure 18.3 gives the price range of biofuels in GJ equivalent for two cases: the average price of 2006 and the predicted price for 2030.

For example, if an investor makes an equity investment in an oil field by 2010, he or she would like to seal it and exploit it some decades later, let's say by 2050. If he sells the oil in 2010, the estimated real value is \$6/GJ, while if he sells it by 2050 the oil price estimate reaches \$18/GJ in real terms (see Fig. 18.2). Thus, the discount rate for 40 years is $r = (18/6)^{1/40} - 1 = 2.8\%$.

Due to the predicted oil price escalation, businesses that consume oil have to support a substantial increase of expenses in future years. This is why conversion to nonconventional energy might be an attractive alternative. If biofuels are used instead of oil, the fuel expense reduces in relative terms according to the estimation presented in Fig. 18.3. Moreover, because biofuels are a renewable energy source, no tax on CO_2 emission has to be paid.

For example, based on bioethanol data from Fig. 18.3, the fuel reduces its value—one says that it *discounts*—from \$20.5 in 2006 to \$13.4 in 2030. Viewed from a consumer's point of view, the discount rate for 24 years is in this case $r = (20.5/13.4)^{1/24} - 1 = 1.8\%$. From the same figure, in the case of biodiesel, the

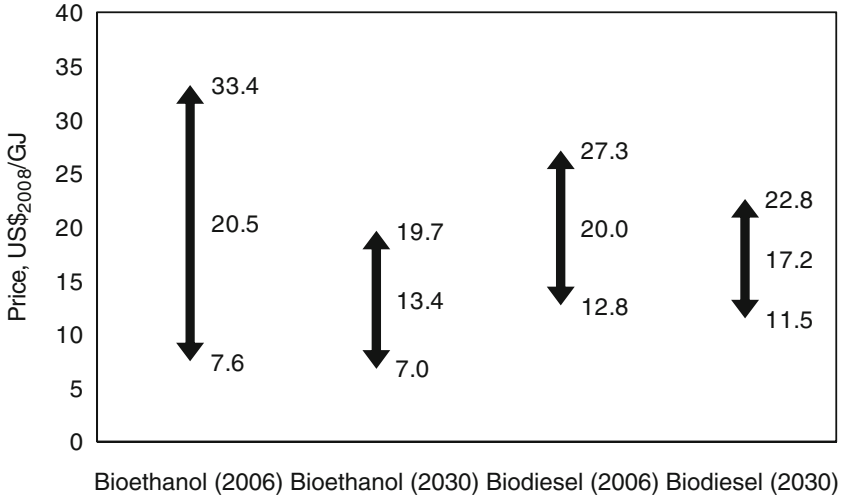

Fig. 18.3 Recent (averaged) and future (2030 predicted) price of biofuels [data from IEA (2006)]

discount rate is $r = (20/17.2)^{1/24} - 1 = 0.6\%$. This figure suggests that those who base their fuel dependence on bioethanol will benefit with a three times higher discount rate than for businesses using biodiesel.

Example 18.6

In Example 18.5, calculate the present worth of savings if the bank average interest rate on long-term deposits is 8% per annum and the respective industry makes oil provisions for 5-year periods.

Solution

- The amount of oil stored for 5 years in energy units is

$$E_{5\text{years}} = 5 \times 365 \times 10\,\text{MWh} \times 36\left(\frac{\text{GJ}}{\text{MWh}}\right) = 657,000\,\text{GJ}.$$

- The total cost of oil paid eight times during the 40-year period is

$$C_{\text{oil,tot}} = E_{5\text{years}} \sum_{y=1}^{8} c_{\text{oil}\,(2005+5y)} = \text{US\$}_{\,2008}60,445,126.$$

- According to Example 18.5, the tax paid on continuous CO_2 emission during the whole period is 883 US$$_{2008}$/GJ of combusted oil, which makes US $$_{2008}$4,641,048,000.
- The total cost in the present situation is then $F_{40} = \text{US\$}_{2008}4,701,493,126$.
- From Example 18.5 the former cost is $F_{40,\text{ex5}} = \text{US\$}_{2008}7,216,488,000$.

- Hence, the savings after 40 years is $S_{40} = F_{40,ex5} - F_{40} =$ US $\$_{2008}$2,514,994,874.
- Thus, according to Eq. (18.4), for 40 years the present worth factor is $(P/F, 0.08, 40) = 0.046$.
- The present worth is $S_{40} \times (P/F, 0.08, 40) =$ US$\$_{2008}$2,514,994,874 $\times$ 0.046 = US$\$_{2008}$115,689,764.

Example 18.7

An old heat engine–driven electrical generator runs with oil fuel with 10% efficiency. Calculate the discount rate that is obtained if the generator is replaced with a bioethanol fuel cell with 65% efficiency. One assumes that the capital is available as equity investment. The reference period is 2010–2030.

Solution

- Assuming a constant oil consumption rate, one estimates the pay on the carbon tax between 2010 and 2030 according to Example 18.1; the result is $0.48 \times (2030^2 - 2010^2) - 1{,}926.72 \times (2030 - 2010) =$ US$\$_{2008}$249.6 per GJ oil combusted.
- Since the efficiency is 10%, one has to pay \$249.6/0.1 = \$2,496 per GJ.
- From Fig. 18.3 the average cost of the GJ of bioethanol is \$20.5 in 2006 and \$13.4 in 2030. Based on these readings, we approximate the cost variation linearly with $c(y) = 614.3 - 0.296y$ US$\$_{2008}$/GJ.
- Integrating the bioethanol costs between 2006 and year y, the cost per GJ equivalent of fuel $C(y) = 641.3y - 0.148y^2 - 690{,}890.5$.
- The expenses on bioethanol fuel between 2010 and 2030 are therefore $C_{tot} = C(2030) - C(2010) =$ US$\$_{2008}$867.6/GJ.
- Since efficiency of the fuel cell is 65%, \$20,081,335 has to be paid per GJ.
- The savings after 20 years of operation are $S_{20} = 2{,}496 - 1{,}335 =$ US $\$_{2008}$1,161/GJ.
- In the present worth with a 6% discount, the savings are $(P/F, 0.06, 20) \times 1{,}161 =$ US$\$_{2008}$362.
- The actual fuel cell cost is ~ US$\$_{2008}$4,000/kW and for 20 years this produces 630 GJ; this is the cost of US$\$_{2008}$7/GJ; in conclusion, the initial investment in fuel cells can be largely paid from savings.

18.2.5 Levelizing

It is customary in economics to express costs and revenues that occur once or at irregular intervals as equivalent equal payments at regular intervals. This is beneficial in many situations: comparing the levelized cost of economic activities that extend over different period, establishing the rate on energy or electricity, computing loan rates, and so on.

This practice is known as *levelizing*. To introduce this notion, let us consider the example of a natural gas provider. Due to shortage, the natural gas cost increases at the rate r every year. If A is the levelized annual payment (which is the same every

year in future worth), the corresponding present value in the kth year, according to Eq. (18.4), is $P_k = A(1 + r)^{-k}$. Therefore, the total payment over the N years expressed in the present worth is

$$P = \sum_{k=1}^{N} A(1+r)^{-k}. \tag{18.14a}$$

This is a geometric progression for which the formula is known as

$$P = \frac{A[1-(1+r)^{-N}]}{r}. \tag{18.14b}$$

The ratio P/A derived from Eq. (18.14b) is known in economics as the *present worth factor*, denoted with

$$\left(\frac{P}{A}, r, N\right) = \frac{1-(1+r)^{-N}}{r} \tag{18.15}$$

and its inverse A/P is called the *capital recovery factor:*

$$\left(\frac{A}{P}, r, N\right) = \frac{r}{1-(1+r)^{-N}}. \tag{18.16}$$

In Eq. (18.16), when $r \to 0$, the capital recovery factor tends to $1/N$.

Example 18.8

It is given that the electrical energy cost increases at a rate of 1% yearly. A capital C is invested at present in a field of solar panels that produce electricity that is sold at an annually levelized cost A. What is the levelized cost per unit of invested capital so that the capital is recovered after $N = 20$ years?

Solution

- We consider the rate of electricity cost increase as a discount rate r, and the invested capital C as the present worth.
- Thus, the levelized electricity cost (LEC) calculated with $r = 1\%$ is

$$\text{LEC} = \left(\frac{A}{P}, r, N\right) C \to \frac{\text{LEC}}{C} = 0.055.$$

- Note: at a 1% discount rate, the yearly levelized cost for 20 years is 5.5% from the invested capital.

Example 18.9

A geothermal energy system that produces constant revenue at a rate r needs an overhaul after the kth year of operation with cost C. The lifetime of the system is $N > k$. The value of the cost to be paid in year k is saved from the annual revenue in

levelized tranches during the lifetime of the system. What is the levelized cost of the overhaul?

Solution

- The present worth of the overhaul is $P = (P/F, r, k)C$.
- This present worth is levelized over the lifetime of the system using the capital recovery factor; thus the levelized cost is $A = (A/P, r, N)P$.
- Using the formula for P, one then obtains $A = (A/P, r, N)(P/F, r, k)C$.
- Therefore, the levelized cost A over N years of a future payment C made in year $k < N$ is given by the formula

$$A = \frac{r(1+r)^{-k}C}{1-(1+r)^{-N}}. \tag{18.17}$$

Example 18.10

A renewable energy system saves the amount S at the end of its lifetime of N years. The equity invested capital (meaning that no loan is made for initial investment) is C, and the discount rate is r. What is the levelized benefit from the produced energy?

Solution

- The present worth of the savings S obtained at rate r after the lifetime N is $P = (P/F, r, N)S$.
- The levelized savings is then $A_s = (A/P, r, N)P$, which is given by Eq. (18.17) if one replaces C with S and k with N.
- The levelized capital cost for the same discount rate is $A_c = (A/P, r, N)C$.
- Therefore, the levelized benefit is $A_b = A_s - A_c$

$$A_b = \frac{r(1+r)^{-N}S}{1-(1+r)^{-N}} - \frac{rC}{1-(1+r)^{-N}}.$$

Example 18.11

A company runs a business having the present worth of its financial capital of \$1 million. The real rate of discount $r_r = 4\%$, which means that the present worth is discounted with respect to the future worth after 1 year such that $P = (1 + r_r)^{-1}F$. Due to the electricity price escalation, the future worth of the capital is diminished with respect to the present worth at an annual rate of $r_{per} = 2\%$. Calculate the present worth after $N = 10$ years. What is the benefit obtained after N years?

Solution

- According to the problem statement, if there is no electricity price escalation, after 1 year, due to the discount rate, the worth is $(1 + r_r)P$.
- However, this amount is reduced due to escalating expenses on electricity. Therefore, the future worth after 1 year is $F = [(1 + r_r)/(1 + r_{per})]P$.

- Then, the levelized worth obtained in year k can be related to the present worth with the expression $A = [(1 + r_r)/(1 + r_{per})]^k P_k$.
- Therefore, the present worth after N years of benefit is the summation of the present worth for each year:

$$P = \sum_{k=1}^{N} P_k = A \sum_{k=1}^{N} \left(\frac{1 + r_{per}}{1 + r_r} \right)^k . \tag{18.18}$$

- This is a geometric progression with ratio $a = (1 + r_{per})/(1 + r_r) = 0.981$ having the sum

$$\frac{P}{A} = \frac{a(1 - a^N)}{1 - a} = 9.01.$$

- For the present worth of \$1 million, the levelized return is $A = \$0.111$ million/year for 10 years.
- Therefore, the future worth after 10 years is $F = NA = \$1.11$ million and the benefit is \$0.11 million.

Note that if in Eq. (18.15) one uses the real escalation rate r_e defined by Eq. (18.13), then the levelized amount can be expressed with the help of the present worth factor using r_e as the real rate:

$$P = \left(\frac{P}{A}, r_e, N \right) A. \tag{18.19}$$

The total present worth P can be levelized also in amounts A_r based on the business discount rate r_r over the same number of years:

$$P = \left(\frac{P}{A}, r_d, N \right) A_d. \tag{18.20}$$

Solving simultaneously Eqs. (18.19) and (18.20) for A_d/A one obtains

$$\frac{A_d}{A} = \frac{(P/A, r_e, N)}{(P/A, r_r, N)}. \tag{18.21}$$

The factor A_d/A represents the *levelizing factor* (LF) and can be expressed also using the capital recovery factors for rate r_e and r_r:

$$\mathrm{LF} = \frac{(A/P, r_r, N)}{(A/P, r_e, N)}. \tag{18.22}$$

The factor given by Eq. (18.20) is useful for calculating the levelized amounts at the business real discount rate r_r for the case when due to reasons such as escalating prices the returns (or expenses) come at another rate r_e.

Example 18.12

Owing to the fact that fuel price increases at the real rate of $r_{per} = 4\%$ per year, a business decides to replace the gas cooker with a solar cooker with the capital cost C that is 7.44 times higher than the total costs paid on fuel for the first year. The real discount rate is $r_r = 10\%$ per annum. Calculate in how many years the benefit returns if the capital is recovered in equal yearly payments.

Solution

- If one denotes the fuel cost in the first year with C_{f1}, then, according to the problem statement we have $C_{f1} = C/7.44$.
- If the oil cooker would be used, from Eq. (18.15) where A is replaced with the fuel cost for the first year (C_{f1}), then the present worth of fuel value after N years is $P_{oil} = (P/A, r', N)C_{f1}$.
- The equivalent discount rate r_e is calculated with Eq. (18.13), $r_e = 5.77\%$.
- If the solar heater is used, the capital invested has to be balanced by the present worth of the oil consumed in the case when the oil cooker would be in operation, thus $C = P_{oil}$.
- Therefore, one has $C = (P/A, r_e, N)C_{f1} = (P/A, r_e, N)C/7.44$, which becomes $(P/A, r_e, N) = 7.44$ with $r_e = 5.77\%$.
- Using Eq. (18.15), $1 - (1 + 1.0577^{-N}) = 7.44 \times 0.0577$, which solves for $N = 10$.

Example 18.13

It is given that the main providers sell electricity with a discount rate $r_{d1} = 1\%$ while the price escalates with a real rate $r_{per} = 4\%$ for the next $N = 20$ years, due to a fossil fuel shortage. In this context, a competing company analyzes the opportunity of investment in wind energy. To be economically attractive, the company intends to sell electrical energy with a levelized price lower with $f = 10\%$ with respect to conventional energy providers and a discount rate of $r_{d2} = 6\%$ in the same time interval of 20 years. What is the ratio between invested capital C in wind energy and the electricity price in the first year p_1?

- The *LEC* practiced by the main providers during the specified period is $LEC_1 = LF_1 p_1$ where the levelizing factor is calculated using Eq. (18.22) for $r_d = r_{d1} = 1\%$ and r_e is calculated according to Eq. (18.13) for $r_{per} = 4\%$ and $r_r = r_{d1} = 1\%$. The result is $LF_1 = 1.529$.
- The invested capital C is to be discounted with the real rate $r_{d2} = 6\%$ in $N = 20$ years, thus the levelized capital discount rate is $A = (A/P, r_{d2}, N)C = 0.0872C$.
- The capital is recovered by selling electricity at the levelized cost LEC_2 that balances the rate for discounting the capital, $LEC_2 = A = 0.0872C$.
- According to the problem statement (above), $LEC_2 = (1 - f/100)LEC_1$.
- Therefore, $0.0872C = (1 - f/100)LF_1 p_1$; thus,

$$\frac{C}{p_1} = \left(1 - \frac{10}{100}\right)\frac{1.529}{0.0872} = 15.78.$$

- Consequently, if one succeeds in reducing the capital investment such that it is less than 16 times the conventional electricity price for the first year, the business becomes competitive.

18.2.6 Taxation

The picture of economic analysis of any energy project is affected by the laws regarding taxation. In any society (or economic context), taxation is practiced for purposes such as (1) infrastructure works, education, health services, army, justice, and other basic social services administered by governments, (2) redistribution of revenue toward undeveloped regions or industrial/social sectors, and (3) reprising certain activities, such as carbon emissions. This section presents the general means to compute taxes as a part of the life-cycle cost of any energy system.

Income tax: In order to introduce the general taxation method, assume that at the end of the fiscal year an entity reports the total obtained as the taxable income I_t during that year. The income tax required by the law is a fraction t of the taxable income. Therefore, the considered entity has to pay the amount $T = I_t \times t$, where t is the tax rate. In order to determine the taxable income, a deduction D can be subtracted from the total income I, therefore $I_t = I - D$. Relevant to life-cycle analysis is the fact that some of the expenses (e.g., loans interest) are tax deductible. Assume that the amount C_t is tax deductible from the inventory of a project's life-cycle cost. Then, the amount $D_t = t \times C_t$ represents the tax deduction and can be extracted from the life-cycle cost.

Tax credit: If the economic entity deploys a certain category of business (e.g., generates energy from renewable sources), it might be eligible for a tax credit. In this case, the income tax that the entity has to pay is reduced with an amount proportional to the investment in the tax credit activity. Let us note with C the investment in a tax creditable activity. Then, the deduction received due to the tax credit is $D_{\text{cred}} = t_{\text{cred}} \times C$, where t_{cred} is the tax on the credit. In some countries, the tax credit on renewable energy can go up to 40% (see Rabl 1985). The amount D_{cred} should be extracted from the initial cost of the project.

Property tax: Assume that a property is owned by an economic entity such as a business, a society, or an individual. In this case, a tax on the property (denoted here with t_{prop}) has to be paid to the regulating authority. However, this tax is deductible from the income tax. If C_{prop} is the capital value of the property and t the income tax, then the tax paid on the property is

$$T_{\text{prop}} = C_{\text{prop}} \times t_{\text{prop}} \times (1 - t). \tag{18.23}$$

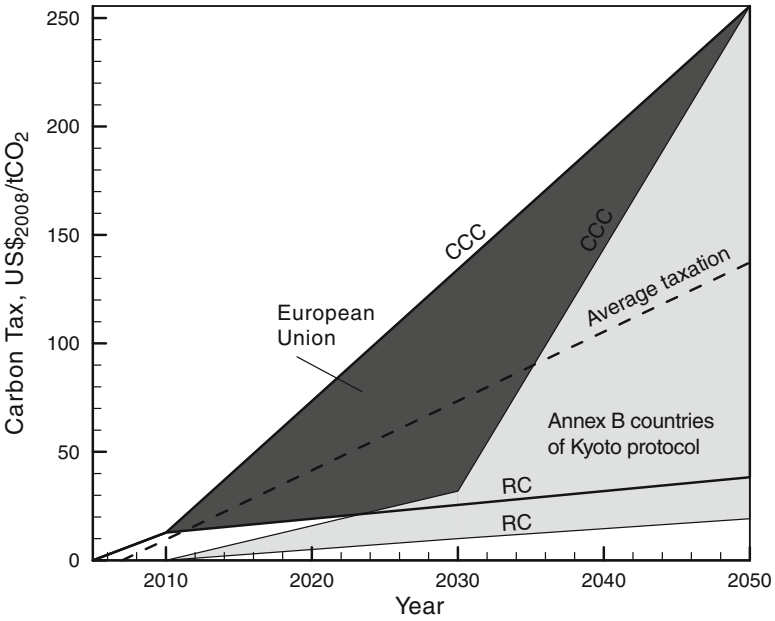

Fig. 18.4 Estimated tax on CO_2 emission in 2008 US$ for the European Union and Kyoto protocol countries

Carbon tax: It is certain that most governments will impose (some already do) a tax on CO_2 emission so that the investment and consumption decisions of the economic agents could be modified for the benefit of a better environment. For example, in the European Union (EU 2006) a carbon value of €10/tCO_2 is assumed in 2010 that increases, according to the predictions, to €110/tCO_2 by 2050. In this report, the geopolitical context, CO_2 emission profile, oil, gas, and coal production profiles, H_2-technology development, population growth, predicted energy demand, and other factors are accounted to propose for three scenarios for energy technology development up to 2050.

In the reference case (RC) scenario, a minimum degree of political initiative is assumed in all countries toward sustainable development. In the second scenario, the carbon constraint case (CCC), severe political limits in CO_2 emissions are assumed up to 2050. In the third scenario, the H_2-case, it is assumed that a firm political decision is made in most countries to develop a hydrogen economy, and therefore major breakthroughs are possible.

There are two predicted limits of taxation: the upper limit corresponds to CCC and the lower to RC as indicated in Fig. 18.4. The European Union promises the highest tax on CO_2 emissions in the years to come. By the end of 2050, in the CCC the tax reaches \$250/tCO_2 in 2008 currency, while for the reference case scenario this tax is estimated to be \$38/tCO_2. For the non–Annex B countries of the Kyoto protocol (United Nations 1998), the tax policy is expected to be in rapport with the European Union. These countries start imposing carbon tax by ~2010,

which will increase up to \$19/tCO_2 by 2050 in the RC. For the CCC scenario, the increase suggested in (EU 2006) can be approximated by two slopes, namely from zero to \$32 per tonne of CO_2 emission from 2010 until 2030, and a further increase to \$255/tCO_2 by 2050.

Thus, in the CCC scenario, all country signatories of the Kyoto protocol may reach the amount of \$255 per tonne of CO_2 emitted. For the estimation presented in Fig. 18.4, we indicate the average taxation with a dashed line. This curve can be approximated by

$$t_{CO_2} = 3.2y - 6,422.4\left(\frac{\text{US\$}_{2008}}{\text{tonne}CO_2}\right), \tag{18.24}$$

where y is the year between 2007 and 2050.

Depreciation is a tax deduction due to the fact that, according to law, the worth of some categories of goods depreciates over time. Say that a good has a capital value C_i at time zero; after a period of time, its worth depreciates by the amount C_Dep; then the current worth becomes $C_\text{i} - C_\text{Dep}$. Since from the point of view of depreciation the capital is a property and its worth diminishes over time, then for each year a tax deduction can be claimed for depreciation. Depending on the law in place, the depreciation can be assessed based on a "straight line" schedule:

$$D_\text{Dep} = \frac{t(P/A, r, N)C}{N} \tag{18.25}$$

or based on the so-called sum-of-the-yearly-digits schedule:

$$D_\text{Dep} = \frac{2t[N - (P/A, r, N)]}{rN(N+1)}, \tag{18.26}$$

where one takes the years of depreciation equal to the lifetime of the system, N, and r as the real discount rate. In the above two formulas, the present worth factors were used in order to assess the deduction on depreciation D_Dep.

Tax on salvage: At the end of the lifetime, the system has a depreciated value known in economics as the *salvage value*. The tax perceived by the government when salvage is valorized, t_salv, is in general different from the income tax. Therefore, the factor $(1 - t_\text{salv})$ represents the amount of money that the business earns after tax, the amount that discounts the capital investment. Hence, the deduction on the salvage value is proportional to the invested capital and given by

$$D_\text{salv} = f_\text{salv}\left(\frac{P}{F}, r, N\right)C(1 - t_\text{salv}), \tag{18.27}$$

where r is the real discount rate.

18.2.7 Loans

Loans are paid in regular installments over a period of time N_{Loan} and with a real interest rate r_{Loan}, defined by the loan agreement. The cost of the loan is discounted by the business rate real discount rate r_{r}; therefore, using the capital recovery factor the cost of loan whose present value is C, is

$$C_{\text{Loan}} = \frac{(A/P, r_{\text{Loan}}, N_{\text{Loan}})}{(A/P, r_{\text{r}}, N_{\text{Loan}})} C, \tag{18.28}$$

where N is the period over which the business runs (it can be the lifetime of an energy system).

Loan payments are composed of two parts: the principal, which represents the part of the loan that pays for reducing the loan balance, and the interest, which is the other part (the revenue obtained by the bank). In any year k, $i_k + p_k = A$, where A represents the annual payment while i and p are the interest and principal. The interest in year $k + 1$ is smaller than the interest in year k because less loan is left to be paid; the difference is given by the interest rate, $r_{\text{Loan}} = (i_k - i_{k+1})/p_k$, where $p_k = A - i_k$. Thus, $i_{k+1} = (1 + r_{\text{Loan}})i_k - r_{\text{Loan}}\text{A}$, a recursion that has the following solution, as can be demonstrated by mathematical induction:

$$\frac{i_k}{A} = 1 - (1 + r_{\text{Loan}})^{k-1-N}. \tag{18.29}$$

The interest can be expressed in the present worth such that the total amount of the tax deduction on the loan interest can be determined. The final expression for the tax deduction on loans is given as given below (see Rabl 1985):

$$D_{\text{Loan}} = t\left[\frac{(A/P, r_{\text{Loan}}, N_{\text{Loan}})}{(A/P, r, N_{\text{Loan}})} - \frac{(A/P, r_{\text{Loan}}, N_{\text{Loan}}) - r_{\text{Loan}}}{(1 + r_{\text{Loan}})(A/P, r'_{\text{Loan}}, N_{\text{Loan}})}\right] C, \tag{18.30}$$

where $r'_{\text{Loan}} = (r - r_{\text{Loan}})/(1 + r_{\text{Loan}})$ is the effective loan interest rate, and t is the income tax.

18.3 Technical and Economic Criteria for Sustainable Energy Systems

The basis of financing and economics presented in the above section allows for defining a number of criteria that can be used for technical and economic evaluation of a sustainable energy system. Furthermore, through these criteria, it is possible to perform system design optimization, or one may use them for system selection

among various options. We introduce the following criteria: life-cycle cost, life-cycle savings, internal rate of return, cost of saved energy, and payback period.

Life-cycle cost: This represents the total cost of the system and it is divided into two parts: initial cost and periodic costs. The initial costs are mainly owing (or capital costs), while the periodic costs include operating and maintenance costs. We show here how to calculate the life-cycle cost of an energy system, in general. The calculation goes as follows:

1. Estimate the total capital cost C (or initial costs) by inventorying all materials, manufacturing, works, permissions, etc.
2. Negotiate a loan: establish how much is the down payment and how much is the loan (denote with f_{Loan}), the portion of the capital that is paid with a loan. Agree on the number of years for the loan N_{Loan} and the real interest rate. The down payment is

$$C_{\text{Down}} = (1 - f_{\text{Loan}})C.$$

3. Determine the real discount rate r_{r} of the energy business. Then, the cost of the loan in the present worth is

$$C_{\text{Loan}} = \frac{(A/P, r_{\text{Loan}}, N_{\text{Loan}})}{(A/P, r, N_{\text{Loan}})} \times f_{\text{Loan}} \times C.$$

4. The associated tax deduction on loan payments is calculated according to Eq. (18.30).
5. Calculate the tax credit, $D_{\text{cred}} = t_{\text{cred}} \times C$.
6. Calculate the depreciation $D_{\text{Dep}} = t(P/A, r, N)C/N$; in the case of a homeowner, the law does not accept depreciation.
7. Calculate the salvage value $D_{\text{salv}} = f_{\text{salv}}(P/F, r, N)C(1 - t_{\text{salv}})$; in the case of homeowner, the tax on salvage is zero.
8. To calculate the tax on property, one has to determine first the value of the property, that is a fraction f_{prop} of the initial cost $C_{\text{prop}} = f_{\text{prop}} \times C \times t_{\text{prop}} \times (1 - t)$.
9. The cost of operation and maintenance is tax deductible (except for homeowners); the operation and maintenance costs are a fraction of the capital cost; hence, $C_{\text{o\&m}} = f_{\text{o\&m}} \times C \times (P/A, r_{\text{r}}, N) \times (1 - t)$.
10. The cost of fuel $C_{\text{f}} = (P_{\text{e1}}/\eta) \times (P/A, r_{\text{e}}, N) \times (1 - t)$, where P_{e1} represents the amount spent on fuel in the first year, r_{e} represents the real discount rate, including the fuel price escalation rate, η represents the conversion efficiency of the fuel consuming energy system (this augments the fuel consumption and therefore operating costs). Note that the cost of fuel is not deductible for homeowners. If the system does not consume fuel (e.g., solar heaters, etc.), then the cost of fuel is not part of the life-cycle cost. However, one may want to add the equivalent fuel cost that a system based on fossil fuels needs to achieve

the same useful output as a renewable energy system under study. As shown later this is a way to compare and select among options.

The life-cycle cost is therefore the sum of the individual cost minus the sum of deductions:

$$\begin{aligned}\mathrm{LCC} = &\left(C_{\mathrm{Down}} + C_{\mathrm{Loan}} + C_{\mathrm{prop}} + C_{\mathrm{o\&m}} + C_{\mathrm{f}}\right)\\ &- \left(D_{\mathrm{cred}} + D_{\mathrm{Dep}} + D_{\mathrm{salv}}\right).\end{aligned} \tag{18.31}$$

The life-cycle cost can be levelized over the lifetime using the capital recovery factor, so that investments having different lifetimes can be compared. The levelized life-cycle cost is therefore

$$\overline{\mathrm{LCC}} = \mathrm{LCC} \times \left(\frac{A}{P}, r_{\mathrm{r}}, N\right). \tag{18.32}$$

Life-cycle savings (LCS): The LCS is defined as the difference between the cost savings on conventional fuel and the capital cost of the renewable energy system that is supposed to replace (or compete with) the energy system based on fossil fuel.

To derive an expression for the LCS, let us consider that the quantity of energy produced by the renewable energy system, whatever its form (work, heat, electricity, chemical energy), is denoted with E. The fossil fuel system generates the same amount of energy over the same period with a given efficiency η. If the price of the fuel per unit of energy content in the first year is p_1, and it escalates with a fixed rate such that the equivalent discount rate is r_{e} during the life-cycle of N years, and if the discount rate that defines the future worth of money is r, then the levelized cost spent on fuel each year is $A = p_1 E/h$. This means that the LCS is

$$\left(\frac{P}{A}, r_{\mathrm{e}}, N\right)\frac{p_1 E}{\eta} - C. \tag{18.33}$$

The *internal rate of return* represents that rate of return for which the LCS is zero. Hence, in Eq. (18.33) one sets LCS $= 0$ and solves for r_{e}. Further, assuming that the real price escalation of fuel r_{per} is known, Eq. (18.13) is solved for the real rate of the business, r_{r}. The internal rate of return is useful for comparing investments when the discount rate cannot be evaluated. If the real internal rate of return is higher than the average real rate of return on similar investments, then the business is profitable.

Cost of saved energy: Assume a renewable energy system that has the life-cycle cost C_{Life} and produces the amount of energy E every year. The same energy can be obtained by converting fuel with a conversion efficiency η. Then, the cost of fuel in the first year is

$$p_1 = \left(\frac{A}{P}, r_{\mathrm{r}}, N\right) \times C_{\mathrm{Life}} \times \frac{\eta}{E}. \tag{18.34}$$

One can compare this cost with the price of fuel in that year to determine if the renewable energy system is beneficial or not.

Payback period: The last criterion discussed here is the payback period defined as the ratio of capital cost over annual savings. In other words, the investment in the system is paid by the savings, at the end of the payback period.

$$\mathrm{NP} = \frac{C}{E \times p_1/\eta}, \tag{18.35}$$

where C is the invested capital, E is the energy produced per year, p_1 is the price of energy in the first year, and η is the conversion efficiency. The payback period may be misleading because it does not account for price escalation, discount rate, and tax deduction. However, it is easy to compute the criterion that can be used for first-hand evaluation.

18.4 Concluding Remarks

In this chapter we discussed the main economic and financing elements relevant to life-cycle cost analysis of energy systems as well as its engineering economics. Several example problems were presented to explain and illustrate the concepts and definitions for analysis. The criteria that can be used for life-cycle cost analysis, design selection, and optimization were also explained.

Nomenclature

A	Levelized annual payment
A/P	Capital recovery factor
c	Specific cost, currency per unit of product
C	Cost, currency
CPI	Consumer price index
D	Depreciation
E	Energy, MJ
F	Future worth
i	Inflation rate
N	Number of years
NP	Payback period, years
NW	Nominal worth of currency
LCC	Life-cycle cost
LCS	Life-cycle savings
LEC	Levelized electricity cost

LF	Levelizing factor
p	Cost of saved energy, currency
P	Present worth, currency
r	Rate of discounting the future
RW	Real worth of currency, currency
t	Taxation, currency per unit of product
T	Tax, currency
y	Year

Greek Letter

η	Energy efficiency

Subscripts

cred	Credit
Dep	Depreciation
Down	Down payment
e	Equivalent
k	Index
N	Number of time periods
pe	Price escalation
per	Real price escalation
prop	Property
r	Real
salv	Salvation
tot	Total

References

ASHRAE 2007. Owing and operating costs. ASHRAE handbook of HVAC applications. Chapter 36, Ammerican Society of HVAC & R, Atlanta, GA.

Boyle G. 2004. Renewable Energy. Power a Sustainable Future, 2nd ed., Oxford University Press, Oxford, UK.

Drbal L.F., Boston P., Westra K.L., Ericson R.B. 1996. Power Plant Engineering. Springer Science + Business Media, New York.

EC 2001. Green paper – Towards a European strategy for the security of energy supply. European Commission paper #769.
EPACT 2008. Renewable energy requirement guidance for EPACT 2005 and Executive Order 13423. US Department of Energy EERE.
EU 2006. World Energy technology Outlook – 2050. WETO-H_2. European Commission.
Fraser N.M., Jewkes E.M., Bernhardt I., Tajima M. 2006. Engineering Economics in Canada, 3rd ed., Pearson Prentice Hall, Toronto, ON.
Fuller S.K., Petersen S.R. 1995. Life-Cycle Costing Manual for Federal Energy Management Program. NIST Handbook 135.
IEA 2006. Medium Term Oil Market Report. International Energy Agency. July.
Rabl A. 1985. Active Solar Collectors and Their Applications. Oxford University Press, Oxford, UK.
Rubin E.S., Davidson C.I. 2001. Introduction to Engineering and the Environment. McGraw-Hill, New York.
Rushing A.S., Lippiatt B.C. 2008. Energy price indices and discount factors for life-cycle cost analysis. U.S. Department of Commerce and National Institute of Standards and Technology report NISTIR 85-3273-23 Rev. 5/08.
Sahr R.C. 2008. Consumer price index conversion factors. Internet source http://oregonstate.edu/cla/polisci/faculty/sahr-robert (accessed on June 3, 2008).
StatCan 2010. Statistics Canada. Internet source http://www.statcan.ca (accessed on February 28, 2008).
Tiwari G.N., Ghosal M.K. 2007. Fundamentals of Renewable Energy Sources. Alpha Science International Ltd, New Delhi.
Tester J.W., Drake E.M., Driscoll M.J., Golay M.W., Peters W.A. 2005. Sustainable Energy. Choosing Among Options. MIT Press, Cambridge, MA.
United Nations 1998. Kyoto Protocol to the United Nations Framework Convention on Climate Change. United Nations.

Study Questions/Problems

18.1 Why is economic analysis important in sustainable energy engineering?
18.2 Define the rate for discounting the future and comment on its usefulness.
18.3 An industry consumes oil at a constant rate per day for heating purposes. The period under consideration is from 2000 to 2020. It is known that about 0.4 tonne of CO_2 is produced per GJ for combusted oil. Estimate the total tax paid for CO_2 emission in constant dollars for 2010. Calculate the rate of increase in the CO_2 tax if one assumes that between 2000 and 2020 this rate is constant. The following equation gives the tax on CO_2 emission in US $2010 constant currency (amended for inflation) per tonne for any year between 2000 and 2020: $t_{CO_2} = (3y - 6,420)\text{US\$}_{2010}/\text{tonne}CO_2$.
18.4 What is the value after 5 years of a deposit of $10,000 in a bank savings account with 7% interest compounded yearly?
18.5 A water heater needs to be replaced after 20 years of operation at a cost of $1,000. What amount must be deposited today with 1% interest so that one can buy the replacement boiler after 20 years? How much should the interest rate be on a deposit of $500?
18.6 Define the inflation rate and its relation to the consumer price index.

18.7 A loan of $2,000 is made at an interest rate of 7% when the inflation rate is 10% and paid in one installment after 1 year. Calculate the amount paid. What is the difference between this result and the result obtained if the inflation is ignored?

18.8 Explain the importance of price escalation in economic analysis.

18.9 What is cost levelizing and what is its importance?

18.10 Electrical energy costs increase at a rate of 0.5% yearly. An amount of capital C is invested today in a field of solar panels that produce electricity that is sold at an annually levelized cost A. What is the levelized cost per unit of invested capital so that the capital is recovered after $N = 10$ years?

18.11 Fuel price increases at the real rate of $r_{\text{per}} = 1\%$ per year. In these conditions a gas cooker is replaced with a solar cooker with the capital cost C that is ten times larger than the total cost paid on fuel for the first year. The real discount rate is $r_{\text{r}} = 7\%$ per annum. Calculate in how many years the benefit returns if the capital is recovered in equal yearly payments.

18.12 What is depreciation and what is its impact in economic calculations?

18.13 Define the life-cycle cost and explain how life-cycle cost analysis is performed.

18.14 What is life-cycle savings and what is the difference between life-cycle cost and life-cycle savings with regard to the manner in which the economic analysis is performed?

Appendix A
Conversion Factors

Table A.1 Conversion factors for commonly used quantities

Quantity	SI to English	English to SI
Area	1 m^2 = 10.764 ft^2 = 1,550.0 $in.^2$	1 ft^2 = 0.00929 m^2
		1 in^2 = 6.452 × 10^{-4} m^2
Density	1 kg/m^3 = 0.06243 lb_m/ft^3	1 lb_m/ft^3 = 16.018 kg/m^3
		1 slug/ft^3 = 515.379 kg/m^3
Energy	1 J = 9.4787 × 10^{-4} Btu	1 Btu = 1,055.056 J
		1 cal = 4.1868 J
		1 lb_f ft = 1.3558 J
		1 hp h = 2.685 × 10^6 J
Energy per unit mass	1 J/kg = 4.2995 × 10^{-4} Btu/lb_m	1 Btu/lb_m = 2,326 J/kg
Force	1 N = 0.22481 lb_f	1 lb_f = 4.448 N
		1 pdl = 0.1382 N
Gravitation	g = 9.80665 m/s^2	g = 32.17405 ft/s^2
Heat flux	1 W/m^2 = 0.3171 Btu/h ft^2	1 Btu/h ft^2 = 3.1525 W/m^2
		1 kcal/h m^2 = 1.163 W/m^2
		1 cal/s cm^2 = 41,870.0 W/m^2
Heat generation (volume)	1 W/m^3 = 0.09665 Btu/h ft^3	1 Btu/h ft^3 = 10.343 W/m^3
Heat transfer coefficient	1 W/m^2 K = 0.1761 Btu/h $ft^{2\circ}$F	1 Btu/h $ft^{2\circ}$F = 5.678 W/m^2 K
		1 kcal/h $m^{2\circ}$C = 1.163 W/m^2 K
		1 cal/s $m^{2\circ}$C = 41,870.0 W/m^2 K
Heat transfer rate	1 W = 3.4123 Btu/h	1 Btu/h = 0.2931 W
Length	1 m = 3.2808 ft = 39.370 in.	1 ft = 0.3048 m
		1 in. = 2.54 cm = 0.0254 m
	1 km = 0.621371 miles	1 miles = 1.609344 km
		1 yd = 0.9144 m
Mass	1 kg = 2.2046 lb_m	1 lb_m = 0.4536 kg
	1 ton (metric) = 1,000 kg	1 slug = 14.594 kg
	1 grain = 6.47989 × 10^{-5} kg	
Mass flow rate	1 kg/s = 7,936.6 lb_m/h = 2.2046 lb_m/s	1 lb_m/h = 0.000126 kg/s
		1 lb_m/s = 0.4536 kg/s

(continued)

İ. Dinçer and C. Zamfirescu, *Sustainable Energy Systems and Applications*,
DOI 10.1007/978-0-387-95861-3, © Springer Science+Business Media, LLC 2011

Table A.1 (continued)

Quantity	SI to English	English to SI
Power	1 W = 1 J/s = 3.4123 Btu/h =0.737562 lb_f ft/s	1 Btu/h = 0.2931 W 1 Btu/s = 1,055.1 W
	1 hp (metric) = 0.735499 kW	1 lb_f ft/s = 1.3558 W
	1 ton of refrig. = 3.516 85 kW	1 hp^{UK} = 745.7 W
Pressure and stress (Pa = N/m^2)	1 Pa = 0.020886 lb_f/ft^2 = 1.4504×10^{-4} $lb_f/in.^2$ = 4.015×10^{-3} in water = 2.953×10^{-4} in Hg	1 lb_f/ft^2 = 47.88 Pa 1 $lb_f/in.^2$ = 1 psi = 6,894.8 Pa 1 standard atm. = 1.0133×10^5 Pa 1 bar = 1×10^5 Pa
Specific heat	1 J/kg K = 2.3886×10^{-4} $Btu/lb_m°F$	1 $Btu/lb_m°F$ = 4,187 J/kg K
Surface tension	1 N/m = 0.06852 lb_f/ft	1 lb_f/ft = 14.594 N/m 1 dyn/cm = 1×10^{-3} N/m
Temperature	T(K) = T(°C) + 273.15 = T(°R)/1.8 = [T (°F) + 459.67]/1.8	T(°R) = 1.8T(K) = T(°F) + 459.67 = 1.8T(°C) + 32
	T(°C) = [T(°F) − 32]/1.8	T(°R) = 1.8[T(K) − 273.15] + 32
Temperature difference	1 K = 1°C = 1.8°R = 1.8°F	1°R = 1°F = 1 K/1.8 = 1°C/1.8
Thermal conductivity	1 W/m K = 0.57782 Btu/h ft°F	1 Btu/h ft°F = 1.731 W/m K 1 kcal/h m°C = 1.163 W/m K 1 cal/s cm°C = 418.7 W/m K
Thermal diffusivity	1 m^2/s = 10.7639 ft^2/s	1 ft^2/s = 0.0929 m^2/s 1 ft^2/h = 2.581×10^{-5} m^2/s
Thermal resistance	1 K/W = 0.52750°F h/Btu	1°F h/Btu = 1.8958 K/W
Velocity	1 m/s = 3.2808 ft/s	1 ft/s = 0.3048 m/s
	1 km/s = 0.62137 miles/h	1 ft/min = 5.08×10^{-3} m/s
Viscosity (dynamic) (kg/m s = N s/m^2)	1 kg/m s = 0.672 lb_m/ft s = 2,419.1 lb_m/fh h	1 lb_m/ft s = 1.4881 kg/m s 1 lb_m/ft h = 4.133×10^{-4} kg/m s 1 cP = 10^{-2} P = 1×10^{-3} kg/m s
Viscosity (kinematic)	1 m^2/s = 10.7639 ft^2/s = 1×10^4 stokes	1 ft^2/s = 0.0929 m^2/s 1 ft^2/h = 2.581×10^{-5} m^2/s 1 stoke = 1 cm^2/s
Volume	1 m^3 = 35.3134 ft^3 1 L = 1 dm^3 = 0.001 m^3	1 ft^3 = 0.02832 m^3 1 $in.^3$ = 1.6387×10^{-5} m^3 1 gal^{US} = 0.003785 m^3 1 gal^{UK} = 0.004546 m^3
Volumetric flow rate	1 m^3/s = 35.3134 ft^3/s = 1.2713×10^5 ft^3/h	1 ft^3/s = 2.8317×10^{-2} m^3/s 1 ft^3/min = 4.72×10^{-4} m^3/s 1 ft^3/h = 7.8658×10^{-6} m^3/s 1 gal^{US}/min = 6.309×10^{-5} m^3/s

Appendix B
Thermophysical Properties

Table B.1 Thermophysical properties of pure water at atmospheric pressure

T (°C)	ρ (kg/m^3)	μ (Pa s)	c_p (J/kg K)	k (W/mK)	Pr	β (K^{-1})	c (m/s)	σ (N/m)
5	1,000	0.001519	4,200	0.5576	11.44	0.00001135	1,426	0.07494
10	999.7	0.001307	4,188	0.5674	9.642	0.00008743	1,448	0.07422
15	999.1	0.001138	4,184	0.5769	8.253	0.0001523	1,467	0.07348
20	998.2	0.001002	4,183	0.5861	7.152	0.000209	1,483	0.07273
25	997.1	0.0008905	4,183	0.5948	6.263	0.0002594	1,497	0.07197
30	995.7	0.0007977	4,183	0.603	5.534	0.0003051	1,509	0.07119
35	994	0.0007196	4,183	0.6107	4.929	0.000347	1,520	0.0704
40	992.2	0.0006533	4,182	0.6178	4.422	0.0003859	1,528	0.06959
45	990.2	0.0005963	4,182	0.6244	3.994	0.0004225	1,534	0.06877
50	988	0.0005471	4,181	0.6305	3.628	0.0004572	1,537	0.06794
55	985.7	0.0005042	4,182	0.636	3.315	0.0004903	1,538	0.0671
60	983.2	0.0004666	4,183	0.641	3.045	0.0005221	1,537	0.06624
65	980.6	0.0004334	4,184	0.6455	2.81	0.0005528	1,534	0.06536
70	977.8	0.000404	4,187	0.6495	2.605	0.0005827	1,529	0.06448
75	974.9	0.0003779	4,190	0.653	2.425	0.0006118	1,523	0.06358
80	971.8	0.0003545	4,194	0.6562	2.266	0.0006402	1,514	0.06267
85	968.6	0.0003335	4,199	0.6589	2.125	0.0006682	1,504	0.06175
90	965.3	0.0003145	4,204	0.6613	2	0.0006958	1,491	0.06081
95	961.9	0.0002974	4,210	0.6634	1.888	0.000723	1,475	0.05987
100	0.5896	0.00001227	2,042	0.02506	0.9996	0.002881	472.8	0.05891

T temperature; ρ density; μ dynamic viscosity; c_p specific heat; k thermal conductivity; Pr Prandtl number; β volume expansion coefficient; c sound speed; σ superficial tension; $\omega = 0.3443 =$ accentric factor

Critical parameters: $T_c = 373.984°C$, $P_c = 220.64$ bar, $v_c = 3.106$ dm^3/kg

Triple point parameters: $T_t = 0.01°C$, $P_t = 611.732$ Pa

Table B.2 Properties of air at atmospheric pressure

T (°C)	ρ (g/dm^3)	μ (μPa s)	c_p (J/kg K)	k (mW/m K)	Pr	β (K^{-1})	c (m/s)	γ
−200	47.61	5.201	1,002	6.667	0.7821	0.01367	171.6	1.401
−170	33.77	7.311	1,002	9.668	0.7581	0.009695	203.7	1.401
−140	26.16	9.296	1,002	12.53	0.7435	0.00751	231.4	1.401
−110	21.35	11.16	1,003	15.26	0.7332	0.006129	256.2	1.401
−80	18.03	12.93	1,003	17.87	0.7251	0.005177	278.8	1.401
−50	15.61	14.6	1,003	20.37	0.7186	0.004481	299.6	1.401
−20	13.76	16.19	1,003	22.77	0.7131	0.00395	319.1	1.401
10	12.3	17.7	1,004	25.09	0.7086	0.003532	337.4	1.4
40	11.12	19.15	1,006	27.32	0.7049	0.003193	354.7	1.4
70	10.15	20.54	1,008	29.49	0.702	0.002914	371.2	1.398
100	9.334	21.88	1,011	31.6	0.6999	0.00268	386.8	1.397
130	8.639	23.18	1,014	33.64	0.6985	0.00248	401.8	1.395
160	8.041	24.43	1,018	35.64	0.6978	0.002309	416.2	1.393
190	7.52	25.64	1,023	37.59	0.6977	0.002159	429.9	1.39
220	7.063	26.82	1,028	39.5	0.6982	0.002028	443.2	1.387
250	6.658	27.96	1,034	41.37	0.6991	0.001912	456	1.384
280	6.296	29.07	1,041	43.2	0.7004	0.001808	468.3	1.381
310	5.973	30.16	1,047	45.0	0.7019	0.001715	480.3	1.378
340	5.68	31.22	1,054	46.77	0.7038	0.001631	491.9	1.374
370	5.415	32.26	1,061	48.51	0.7058	0.001555	503.1	1.371
400	5.174	33.28	1,069	50.23	0.7079	0.001486	514.1	1.367
430	4.953	34.27	1,076	51.92	0.7101	0.001422	524.7	1.364
760	3.371	44.21	1,147	69.34	0.7314	0.0009679	629	1.334
790	3.276	45.04	1,153	70.84	0.7328	0.0009406	637.5	1.332
820	3.186	45.86	1,158	72.33	0.7341	0.0009148	646	1.33
850	3.101	46.67	1,163	73.82	0.7353	0.0008904	654.3	1.328
880	3.02	47.48	1,168	75.29	0.7364	0.0008672	662.6	1.326
910	2.944	48.28	1,172	76.75	0.7374	0.0008452	670.7	1.324
940	2.871	49.07	1,177	78.21	0.7383	0.0008243	678.8	1.323
970	2.802	49.85	1,181	79.65	0.7391	0.0008044	686.7	1.321
1,000	2.736	50.63	1,185	81.09	0.7398	0.0007855	694.5	1.32

T temperature; ρ density; μ dynamic viscosity; c_p specific heat; k thermal conductivity; Pr Prandtl number; β volume expansion coefficient; c sound speed; γ adiabatic expansion coefficient; $\omega = -0.009278$ = accentric factor
Critical parameters: $T_c = 132.531$ K, $P_c = 37.86$ bar, $v_c = 2.917$ dm^3/kg

Table B.3 Standard chemical exergy of some elements

Element	B	C	Ca	Cl_2	Cu	F_2	Fe	H_2	I_2	K	Mg	Mo
ex^{ch}, kJ/mol	628.1	410.27	729.1	123.7	132.6	505.8	374.3	236.12	175.7	336.7	626.9	731.3
Element	N_2	Na	Ni	O_2	P	Pb	Pt	Pu	S	Si	Ti	U
ex^{ch}, kJ/mol	0.67	336.7	242.6	3.92	861.3	249.2	141.2	1,100	609.3	855.0	907.2	1,196.6

Source: Rivero R., Garfias M., Standard chemical exergy of elements updated. *Energy* 31:3310–3326

Table B.4 Formation enthalpy, entropy, Gibbs energy, and chemical exergy of some substances

Substance name	Chemical formula	M	$\Delta_f H^0$	$\Delta_f S^0$	$\Delta_f G^0$	ex^{ch}
Acetone	C_3H_6O	59	−217.14	295.6	−152.69	1,788
Acetylene	C_2H_2	26	228.19	200.9	210.67	1,267
Ammonia	NH_3	17	−46.14	99.5	−16.5	337.9
n-Butane	C_4H_{10}	58	−125.78	309.90	−16.529	2,805
Calcium carbonate	$CaCO_3$	100.1	−1,207	91.7	−1,128	17.52
Carbon monoxide	CO	28	−110.53	197.6	−137.17	275.06
Carbon dioxide	CO_2	44	−393.49	213.8	−394.35	198.38
Copper oxychloride	Cu_2OCl_2	214	−384.65	154.35	−369.7	21.08
Cupric oxide	CuO	79	−156.06	42.59	−128.29	6.27
Copper(II) chloride	$CuCl_2$	134	−218.0	108.07	−173.83	82.47
Cuprous chloride	CuCl	100	−136.82	87.45	−119.44	75.00
Ethanol	C_2H_5OH	47	−234.94	280.60	−167.71	1,363
Iron(III) oxide	Fe_2O_3	159.7	−824.20	205.1	−742.22	12.26
Lithium bromide	LiBr	86.85	−351.14	74.01	−341.83	101.37
Magnetite	Fe_3O_4	231.5	−1,118	146.1	−1,015	115.61
Methane	CH_4	16	−74.60	186.40	−50.53	831.98
Nitrogen dioxide	NO_2	46	34.19	240.20	52.31	56.56
Nitrous oxide	N_2O	44	81.59	220.00	103.71	106.34
n-Octane	C_8H_{18}	131	−208.74	5.734	16.25	7,549
Propane	C_3H_2	44	−104.67	130.7	−24.29	2,151
Sodium chloride	NaCl	58.44	−411.24	223.1	−384.20	14.353
Sulfur dioxide	SO_2	64	−296.79	248.2	−300.0	313.10
Uranium hexafluoride	UF_6	352	−2,198	227.8	−2,069	644.96
Water	H_2O	18	−285.81	69.94	−237.12	0.750

M molecular mass (kg/kmol)
$\Delta_f H^0$ formation enthalpy (kJ/mol)
Formation entropy: $\Delta_f S^0 = s^0 - \sum_{\text{elements}} v s^0_{f,\text{element}}$ (J/mol K), where v is the number of moles of the element in chemical equation of formation of the substance
Gibbs free energy of formation: $\Delta_f G^0 = \Delta_f H^0 - T_0 \Delta_f S^0$ (kJ/mol)
Chemical exergy: $\text{ex}^{ch} = \Delta_f G^0 + \sum_{\text{elements}} v \times \text{ex}^{ch}_{\text{element}}$ (kJ/mol)
Reference temperature: $T_0 = 298.15$ K
Reference pressure: $P_0 = 1$ bar; superscript 0 in above notations refers to standard pressure

Table B.5 Some general thermodynamic properties of selected substances

Substance	R_g	TPT	TPP	ΔH_{fus}	NBP	ΔH_{boil}	P_c	T_c	v_c	Z_c	ω	a	b
Hydrogen	4,124	13.96	73.59	454.5	20.37	448.7	12.96	33.15	0.0336	3.135	−0.2187	26,785	0.0165
Parahydrogen	4,124	13.8	70.41	432.5	20.27	446.6	12.86	32.94	0.0327	3.228	−0.2186	26,670	0.0165
Oxygen	259.8	54.36	1.463	243	90.19	213.2	50.43	154.6	0.00217	3.661	0.0222	149,769	0.0198
Nitrogen	296.8	63.15	125.2	215.5	77.36	199.2	33.96	126.2	0.00280	3.936	0.0372	148,225	0.0240
Helium	2,077	1	1	1	4.222	20.7	2.275	5.195	0.01196	3.967	−0.385	3,751	0.0147
Neon	412	24.56	432	88.16	27.11	85.77	26.8	44.49	0.00188	3.62	−0.037	23,345	0.0107
Argon	208.1	83.81	688.9	172.2	87.3	169.4	48.63	150.7	0.00161	4.002	−0.002	147,587	0.0200
xenon	63.32	161.4	827.6	96.72	164.9	95.87	58.4	289.7	0.001	3.142	0.0036	454,364	0.0320
Fluorine	218.8	53.48	2.413	196.3	85.03	175.2	52.4	144.4	0.00163	3.691	0.0504	125,813	0.0178
Ammonia	488.2	195.5	61.02	1,486	239.8	1,369	113.3	405.4	0.00516	3.381	0.2558	458,377	0.0231
Hydrogen sulfide	244	187.7	231.9	574.7	212.9	546.6	89.63	373.4	0.00298	3.401	0.0961	491,620	0.0269
Krypton	99.21	115.8	732	108.8	119.8	107.5	55.1	209.4	0.00121	3.101	−0.002	251,616	0.0245
Methane	518.3	90.69	117	544.2	111.7	510.8	45.99	190.6	0.00734	2.923	0.0114	249,574	0.0268
Methanol	259.5	175.6	0.0018	1,314	338.2	1,103	81.04	513.4	0.00581	2.828	0.5646	1.028E+06	0.0409
Ethane	276.5	90.37	0.0114	595.7	184.6	489.4	48.72	305.3	0.00451	3.838	0.0995	604,771	0.0405
Ethanol	180.5	159.1	0.00002	1,017	351.4	848.8	61.48	513.9	0.00611	2.466	0.6442	1.358E+06	0.0540
n-Octane	72.79	216.4	0.01399	411.5	398.6	302.4	24.97	569.3	0.00390	4.249	0.3928	4.103E+06	0.1475
Isobutane	143	113.6	0.00021	482.9	261.5	365.5	36.4	407.8	0.0049	3.271	0.1853	1.444E+06	0.0724
Propane	188.6	85.48	N/A	1	231.1	425.3	42.47	369.8	0.00505	3.245	0.1524	1.017E+06	0.0563
Isopentane	115.2	112.7	N/A	N/A	301	342.5	33.7	460.4	0.00446	3.524	0.2266	1.988E+06	0.0883
n-Butane	143	134.9	0.00693	494	272.6	384.7	37.96	425.1	0.00373	4.29	0.2	1.505E+06	0.0724
n-Decane	58.44	243.5	0.01452	392.6	447.4	276.3	21.03	617.7	0.00379	4.519	0.4903	5.735E+06	0.19
n-Dodecane	48.81	263.6	0.00631	381.5	489.5	256.3	18.17	658.1	0.00514	3.436	0.574	7.534E+06	0.2343
Isobutane	143	113.6	0.00021	482.9	261.5	365.5	36.4	407.8	0.0049	3.271	0.185	1.444E+06	0.0724
Isopropanol	138.4	0	N/A	N/A	355.6	663.1	47.62	508.3	0.00363	4.062	0.668	1.715E+06	0.0690
Ethylene	296.4	104	1.226	568.2	169.3	482.2	50.4	282.3	0.00484	3.43	0.086	499,944	0.0362
Cyclohexane	98.79	279.5	52.49	402.4	353.9	356	40.75	553.6	0.00375	3.571	0.2091	2.378E+06	0.0878
n-Heptane	82.98	182.6	0.00176	441.1	371.5	316.9	27.27	540.1	0.00556	2.956	0.3479	3.382E+06	0.1281

Table B.5 (continued)

Substance	R_g	TPT	TPP	ΔH_{fus}	NBP	ΔH_{boil}	P_c	T_c	v_c	Z_c	ω	a	b
n-Hexane	96.49	177.8	0.0035	618.8	342.4	329.9	30.58	507.9	0.00400	3.998	0.3117	2.666E+06	0.1074
n-Nonane	64.83	219.7	0.0046	410.3	424.2	288.4	22.81	594.6	0.00482	3.5	0.4468	4.898E+06	0.1686
n-Pentane	115.2	143.5	0.00012	466.1	309	358	33.64	469.7	0.00540	2.977	0.2499	2.073E+06	0.0903
Propylene	197.6	87.95	N/A	N/A	225.4	439.2	46.65	365.6	0.00458	3.38	0.1407	905,579	0.0506
R22	96.15	115.7	0.004715	301.9	232.3	232.5	49.89	369.3	0.00203	3.503	0.2208	864,055	0.0478
R134a	81.49	168.9	3.545	263.7	247.1	217	40.59	374.2	0.00170	4.408	0.3269	1.09E+06	0.0596
R290	188.6	85.48	1	1	231.1	425.3	42.47	369.8	0.00505	3.245	0.1524	1.0E+06	0.0563
R404a	85.19	−555	1	1	226.6	199.7	37.35	345.3	0.00193	4.065	0.275	1.0E+06	0.0598
R218	44.22	125.5	0.02119	141.1	236.5	105.1	26.4	345	0.00169	3.417	0.3201	1.4E+06	0.0845
R245fa	62.03	171.1	0.1303	258.5	288.3	196	36.51	427.2	0.00203	3.561	0.379	1.5E+06	0.0756
R507a	84.1	−555	1	1	226.1	196.3	37.14	343.9	0.00199	3.903	0.2793	1.0E+06	0.0599
R508b	87.16	−555	1	1	184.9	163	39.25	287.1	0.0017	3.735	0.2272	664,053	0.047

R_g real gas constant (J/kg K); *TPT* triple point temperature (K); *TPP* triple point pressure (bar); ΔH_{fus} fusion heat at triple point (kJ/kg); *NBP* normal boiling point (K); ΔH_{boil} boiling enthalpy at normal boiling point; *P* pressure (bar); *T* temperature (K); *v* specific volume (m^3/kg); Z compressibility factor; *subscript "c"* critical point; ω accentric factor; *a*, *b* constants in Peng–Robinson equation of state

Table B.6 Thermophysical properties of ammonia at saturation

T	P	σ	ρ_L	c_{pL}	k_L	μ_L	Pr_L	β_L	v_V	c_{pV}	k_V	μ_V	Pr_V	β_V	γ
−77.6	0.061	44.78	733.6	3.95	821.2	564.1	2.713	1.514	15.68	2.062	19.64	6.84	0.7182	5.23	1.325
−65	0.1563	41.51	719.3	4.162	774.8	430.6	2.312	1.586	6.478	2.102	19.82	7.162	0.7597	4.99	1.328
−55	0.3013	38.95	707.8	4.332	739.3	357.5	2.095	1.63	3.498	2.147	20.07	7.433	0.7951	4.86	1.331
−45	0.5447	36.42	696	4.387	704.6	303	1.887	1.717	2.008	2.205	20.43	7.715	0.8328	4.77	1.336
−35	0.9307	33.93	683.9	4.439	670.8	261.2	1.728	1.804	1.215	2.277	20.88	8.004	0.8729	4.72	1.343
−25	1.515	31.46	671.4	4.489	638	228.3	1.606	1.896	0.7695	2.365	21.44	8.3	0.9154	4.716	1.352
−15	2.362	29.04	658.6	4.538	605.9	201.7	1.511	1.995	0.5068	2.47	22.12	8.599	0.9603	4.757	1.364
−5	3.549	26.65	645.4	4.589	574.7	179.8	1.436	2.079	0.3452	2.595	22.92	8.902	1.008	4.846	1.379
5	5.16	24.29	631.8	4.643	544.3	161.4	1.377	2.199	0.2421	2.74	23.85	9.209	1.058	4.989	1.399
15	7.288	21.98	617.6	4.705	514.7	145.6	1.331	2.338	0.1741	2.908	24.92	9.519	1.111	5.193	1.424
25	10.03	19.71	602.9	4.781	485.7	131.8	1.297	2.499	0.1279	3.104	26.16	9.834	1.167	5.466	1.456
35	13.51	17.49	587.5	4.873	457.4	119.6	1.275	2.688	0.0956	3.333	27.58	10.16	1.228	5.826	1.497
45	17.82	15.32	571.3	4.993	429.6	108.8	1.264	3.006	0.0726	3.604	29.21	10.5	1.295	6.295	1.549
55	23.1	13.2	554.1	5.143	402.3	98.99	1.265	3.335	0.0557	3.93	31.11	10.86	1.372	6.912	1.615
65	29.48	11.14	535.8	5.34	375.4	90.06	1.281	3.768	0.0432	4.334	33.33	11.25	1.463	7.738	1.702
75	37.09	9.154	516.1	5.608	348.6	81.83	1.316	4.359	0.0336	4.851	35.97	11.7	1.578	8.876	1.819
85	46.09	7.24	494.5	5.987	322	74.18	1.379	5.21	0.0262	5.55	39.21	12.23	1.732	10.52	1.983
95	56.65	5.414	470.2	6.56	294.6	66.84	1.489	6.525	0.0203	6.56	43.31	12.9	1.954	13.05	2.227
105	68.95	3.695	442.1	7.52	266.1	59.7	1.687	8.801	0.0156	8.168	48.83	13.82	2.312	17.35	2.622
115	83.22	2.113	407.4	9.492	235	52.35	2.114	13.67	0.0116	11.14	56.96	15.22	2.977	26.03	3.358
125	99.7	0.7327	357.8	16.29	196.6	43.8	3.629	31.43	0.0082	18.25	71.25	17.84	4.57	50.81	5.121
127.5	104.2	0.437	338.7	21.71	183.4	40.94	4.848	46.11	0.0074	21.75	76.35	18.82	5.363	65.59	6.022
130	108.9	0.1754	310.5	34.41	165.1	37.05	7.72	81.46	0.0065	26.74	84.63	20.44	6.457	90.37	7.258
132.2	113.1	0.0017	248.5	64.71	129.5	29.55	14.77	168.7	0.0055	32.93	97.33	22.96	7.77	127.8	8.808

T temperature (°C); P pressure (bar); σ surface tension (mN/m); ρ density (kg/m^3); c_p specific heat (kJ/kg K); k thermal conductivity (mW/m K); μ dynamic viscosity (μPa s); Pr Prandtl number; β volumetric expansion coefficient (mK^{-1}); v specific volume (m^3/kg); γ isentropic expansion coefficient of saturated vapor; indices: L liquid; V vapor

Table B.7 Thermophysical properties of water at saturation

T	P	σ	ρ_L	c_{pL}	k_L	μ_L	Pr_L	β_L	v_V	c_{pV}	k_V	μ_V	Pr_V	β_V	γ
0.01	0.00612	75.64	1,000	4.23	547.5	1,792	13.84	N/A	206.0	1.87	17.07	9.216	1.008	3.672	1.33
10	0.0123	74.22	999.7	4.19	567.4	1,307	9.645	0.0872	106.3	1.87	17.62	9.461	1.006	3.548	1.33
20	0.0234	72.73	998.2	4.18	586	1,002	7.154	0.209	57.78	1.88	18.22	9.727	1.004	3.435	1.33
30	0.0425	71.19	995.6	4.18	602.9	797.7	5.535	0.305	32.9	1.89	18.88	10.01	1.003	3.332	1.33
40	0.0738	69.59	992.2	4.18	617.8	653.3	4.423	0.386	19.53	1.90	19.59	10.31	1.002	3.239	1.33
50	0.1234	67.94	988	4.18	630.4	547.1	3.629	0.457	12.04	1.92	20.36	10.62	1.001	3.156	1.33
60	0.1993	66.24	983.2	4.18	640.9	466.6	3.045	0.522	7.674	1.94	21.18	10.93	1	3.082	1.33
70	0.3118	64.48	977.7	4.19	649.5	404	2.605	0.583	5.045	1.96	22.06	11.26	0.9995	3.017	1.33
80	0.4737	62.67	971.8	4.19	656.2	354.5	2.266	0.64	3.409	1.98	23	11.59	0.9993	2.962	1.33
90	0.7012	60.81	965.3	4.20	661.3	314.5	2	0.696	2.362	2.01	24	11.93	0.9994	2.917	1.34
100	1.013	58.91	958.4	4.22	665.1	281.9	1.787	0.75	1.674	2.04	25.08	12.27	1	2.882	1.34
110	1.432	56.96	951	4.23	667.6	254.8	1.615	0.804	1.211	2.08	26.22	12.61	1.001	2.857	1.34
120	1.985	54.96	943.2	4.25	669.1	232.1	1.474	0.858	0.892	2.12	27.44	12.96	1.004	2.843	1.35
130	2.7	52.93	934.9	4.27	669.7	213	1.357	0.912	0.669	2.17	28.73	13.3	1.007	2.84	1.36
140	3.612	50.85	926.2	4.29	669.4	196.6	1.259	0.968	0.509	2.23	30.09	13.65	1.012	2.849	1.36
150	4.757	48.74	917.1	4.31	668.3	182.5	1.178	1.026	0.393	2.30	31.54	13.99	1.02	2.872	1.37
160	6.177	46.59	907.5	4.34	666.4	170.3	1.109	1.087	0.3071	2.37	33.06	14.34	1.029	2.908	1.39
170	7.915	44.4	897.5	4.37	663.7	159.6	1.051	1.152	0.243	2.46	34.66	14.68	1.042	2.959	1.40
180	10.02	42.19	887.1	4.40	660.2	150.2	1.002	1.221	0.194	2.56	36.34	15.03	1.057	3.027	1.42
190	12.54	39.94	876.1	4.44	655.9	141.8	0.9607	1.296	0.156	2.67	38.09	15.37	1.077	3.114	1.44
200	15.54	37.67	864.7	4.49	650.7	134.4	0.9269	1.377	0.127	2.80	39.93	15.71	1.1	3.221	1.46
210	19.06	35.38	852.8	4.54	644.7	127.7	0.8994	1.467	0.104	2.94	41.85	16.06	1.129	3.351	1.48
220	23.18	33.06	840.3	4.60	637.6	121.6	0.8777	1.567	0.086	3.11	43.86	16.41	1.162	3.508	1.52
230	27.95	30.73	827.3	4.67	629.5	116	0.8615	1.679	0.071	3.30	45.96	16.76	1.203	3.697	1.55
240	33.45	28.39	813.5	4.76	620.3	110.9	0.8508	1.807	0.06	3.51	48.15	17.12	1.25	3.923	1.59
250	39.74	26.04	799.1	4.86	609.8	106.2	0.8455	1.954	0.050	3.77	50.46	17.49	1.306	4.195	1.64
260	46.89	23.68	783.8	4.97	598	101.7	0.846	2.126	0.042	4.06	52.9	17.88	1.373	4.523	1.70

(continued)

Table B.7 (continued)

T	P	σ	ρ_L	c_{pL}	k_L	μ_L	Pr_L	β_L	v_V	c_{pV}	k_V	μ_V	Pr_V	β_V	γ
270	55	21.33	767.7	5.11	584.5	97.55	0.853	2.33	0.036	4.41	55.49	18.28	1.453	4.923	1.77
280	64.13	18.99	750.5	5.28	569.4	93.56	0.8673	2.576	0.031	4.83	58.28	18.7	1.549	5.415	1.86
290	74.38	16.66	732.2	5.48	552.3	89.71	0.8908	2.88	0.026	5.33	61.31	19.15	1.666	6.032	1.97
300	85.84	14.35	712.4	5.74	533.1	85.95	0.9262	3.266	0.022	5.97	64.67	19.65	1.813	6.822	2.11
310	98.61	12.08	691	6.08	511.3	82.22	0.9782	3.773	0.018	6.78	68.45	20.21	2.001	7.861	2.29
320	112.8	9.858	667.4	6.54	486.8	78.46	1.054	4.47	0.015	7.87	72.84	20.84	2.251	9.278	2.54
330	128.5	7.697	641	7.2	458.8	74.57	1.17	5.489	0.013	9.41	78.1	21.6	2.603	11.31	2.91
340	145.9	5.62	610.8	8.24	426.9	70.45	1.359	7.116	0.011	11.8	84.68	22.55	3.137	14.43	3.47
350	165.2	3.66	574.7	10.1	389.7	65.88	1.711	10.1	0.0088	15.9	93.48	23.81	4.058	19.77	4.47
360	186.6	1.872	528.1	14.7	344.4	60.39	2.574	17.11	0.007	25.2	106.6	25.71	6.085	30.79	6.74
370	210.3	0.3846	453.1	41.7	280.7	52.25	7.765	45.88	0.0050	70.4	132.6	29.57	15.7	64.53	18.0
373.9	220.4	0.0004	349.4	N/A	210.8	41.95	277.1	87.51	0.0034	340.1	180	37	69.91	104.5	84.5

T temperature (°C); P pressure (bar); σ surface tension (mN/m); ρ density (kg/m^3); c_p specific heat (kJ/kg K); k thermal conductivity (mW/m K); μ dynamic viscosity (μPa s); Pr Prandtl number; β volumetric expansion coefficient (mK^{-1}); v specific volume (m^3/kg); γ isentropic expansion coefficient of saturated vapor; indices: L liquid; V vapor

Table B.8 Thermophysical properties of carbon dioxide at saturation

T	P	σ	ρ_L	c_{pL}	k_L	μ_L	Pr_L	β_L	v_V	c_{pV}	k_V	μ_V	Pr_V	β_V	γ
−56.6	5.18	15.7767	1,178.5	1.953	180.4	256.7	2.78	N/A	0.0727	0.90	10.97	10.95	0.90	6.11	1.44
−50	6.82	14.3248	1,154.6	14.29	171.8	229.3	19.07	3.27	0.0558	0.95	11.51	11.31	0.93	6.30	1.46
−45	8.32	13.2367	1,135.9	1.989	165.3	210.7	2.54	3.36	0.0460	0.98	11.94	11.58	0.95	6.50	1.48
−40	10.05	12.1654	1,116.5	2.011	158.9	193.8	2.45	N/A	0.0383	1.03	12.41	11.87	0.98	6.74	1.51
−35	12.02	11.1118	1,096.4	4.99	152.5	178.3	5.83	N/A	0.0320	1.07	12.90	12.16	1.01	7.04	1.54
−30	14.28	10.0769	1,075.7	2.377	146.3	164.2	2.67	3.93	0.0270	1.13	13.42	12.46	1.05	7.41	1.57
−25	16.83	9.0619	1,054.2	2.114	140	151.3	2.28	4.38	0.0228	1.19	13.99	12.78	1.09	7.87	1.62
−20	19.70	8.0682	1,031.7	2.165	133.8	139.3	2.25	4.74	0.0193	1.27	14.60	13.12	1.14	8.44	1.67
−15	22.91	7.0974	1,008.0	2.227	127.6	128.3	2.24	5.18	0.0165	1.36	15.27	13.47	1.20	9.15	1.73
−10	26.49	6.1514	982.9	2.306	121.4	118	2.24	5.73	0.0140	1.47	16.01	13.86	1.27	10.06	1.81
−5	30.46	5.2326	956.2	2.406	115.1	108.4	2.27	6.44	0.0120	1.61	16.84	14.30	1.37	11.23	1.92
0	34.85	4.3440	927.4	2.539	108.7	99.39	2.32	7.37	0.0102	1.79	17.77	14.79	1.49	12.79	2.05
5	39.69	3.4893	896.0	2.72	102.2	90.81	2.42	8.67	0.0087	2.03	18.86	15.36	1.65	14.95	2.23
10	45.02	2.6737	861.1	2.985	95.46	82.55	2.58	10.59	0.0074	2.37	20.14	16.06	1.89	18.12	2.49
15	50.87	1.9043	821.2	3.405	88.32	74.43	2.87	13.71	0.0062	2.89	21.74	16.95	2.25	23.17	2.88
20	57.29	1.1924	773.4	4.159	80.48	66.15	3.42	19.52	0.0051	3.77	23.83	18.19	2.87	32.32	3.51
25	64.34	0.5584	711.8	5.903	71.43	57.23	4.73	33.72	0.0041	5.54	26.94	20.16	4.14	53.05	4.69
30	72.14	0.0582	602.4	13.83	57.69	44.68	10.71	102.99	0.0029	10.16	33.86	25.03	7.51	128.22	6.80
30.9	73.64	0.0025	521.3	18.05	49.07	37.25	13.71	141.42	0.0024	11.77	39.21	29.16	8.75	163.45	5.80

T temperature (°C); P pressure (bar); σ surface tension (mN/m); ρ density (kg/m^3); c_p specific heat (kJ/kg K); k thermal conductivity (mW/m K); μ dynamic viscosity (μPa s); Pr Prandtl number; β volumetric expansion coefficient (mK^{-1}); v specific volume (m^3/kg); γ isentropic expansion coefficient of saturated vapor; indices: L liquid; V vapor

Table B.9 Thermophysical properties of hydrogen at saturation

T	P	σ	ρ_L	c_{pL}	k_L	μ_L	Pr_L	β_L	v_V	c_{pV}	k_V	μ_V	Pr_V	β_V	γ
14	0.08	2.977	77.0	6.992	74.36	24.30	2.29	10.58	7.6332	10.56	14.51	1.24	0.90	74.32	1.69
15	0.13	2.819	76.1	7.335	81.62	21.68	1.95	11.26	4.7044	10.69	15.21	1.27	0.89	70.67	1.70
16	0.21	2.656	75.3	7.717	87.55	19.39	1.71	12.01	3.0742	10.85	15.94	1.31	0.89	67.82	1.72
17	0.32	2.490	74.3	8.132	92.26	17.40	1.53	12.87	2.1066	11.03	16.69	1.34	0.89	65.69	1.74
18	0.47	2.321	73.4	8.574	95.85	15.69	1.40	13.85	1.4996	11.25	17.49	1.37	0.88	64.23	1.77
15	0.13	2.819	76.1	7.335	81.62	21.68	1.95	11.26	4.7044	10.69	15.21	1.27	0.89	70.67	1.70
20	0.91	1.977	71.3	9.563	100.1	12.97	1.24	16.18	0.8288	11.85	19.21	1.44	0.89	63.20	1.84
21	1.22	1.804	70.1	10.13	101	11.92	1.20	17.60	0.6370	12.25	20.15	1.48	0.90	63.63	1.89
22	1.59	1.630	68.9	10.76	101.1	11.02	1.17	19.26	0.4981	12.75	21.16	1.51	0.91	64.74	1.95
23	2.04	1.458	67.6	11.48	100.7	10.26	1.17	21.23	0.3951	13.36	22.25	1.54	0.93	66.61	2.03
24	2.58	1.286	66.2	12.31	99.8	9.61	1.18	23.60	0.3171	14.12	23.43	1.68	1.01	69.39	2.12
25	3.21	1.117	64.7	13.28	98.51	9.03	1.22	26.55	0.2569	15.07	24.72	1.73	1.05	73.32	2.23
26	3.94	0.952	63.1	14.46	96.94	8.51	1.27	30.30	0.2098	16.29	26.14	1.78	1.11	78.77	2.37
27	4.78	0.790	61.3	15.95	95.2	8.00	1.34	35.28	0.1722	17.90	27.73	1.85	1.19	86.38	2.56
28	5.74	0.634	59.3	17.91	93.4	7.49	1.44	42.19	0.1418	20.09	29.53	1.92	1.31	97.27	2.82
29	6.82	0.484	57.1	20.69	91.64	6.95	1.57	52.50	0.1168	23.24	31.62	2.01	1.47	113.61	3.19
30	8.04	0.343	54.5	25.02	90.02	6.35	1.76	69.50	0.0957	28.15	34.11	2.11	1.74	140.12	3.76
31	9.42	0.213	51.4	32.99	88.65	5.65	2.10	102.69	0.0775	36.81	37.28	2.26	2.23	189.42	4.75
32	10.96	0.097	47.1	53.14	87.64	4.84	2.93	193.05	0.0606	55.68	42.11	2.50	3.31	308.86	6.89
33.1	12.88	0.0017	35.3	200	1,000	N/A	N/A	981.45	0.0367	131.74	59.93	3.41	7.50	1,036.71	15.44

T temperature (K); P pressure (bar); σ surface tension (mN/m); ρ density (kg/m^3); c_p specific heat (kJ/kg K); k thermal conductivity (mW/m K); μ dynamic viscosity (μPa s); Pr Prandtl number; β volumetric expansion coefficient (mK^{-1}); v specific volume (m^3/kg); γ isentropic expansion coefficient of saturated vapor; indices: L liquid; V vapor

Table B.10 Thermophysical properties of oxygen at saturation

T	P	σ	ρ_L	c_{pL}	k_L	μ_L	Pr_L	β_L	v_V	c_{pV}	k_V	μ_V	Pr_V	β_V	γ
55	N/A	22.30	1,303.5	1.455	201	747.53	5.41	N/A	80.029	0.93	4.48	4.15	0.86	18.28	1.39
60	0.01	20.98	1,283.1	126.4	194.3	582.46	379.02	3.49	21.463	0.95	4.98	4.55	0.86	16.87	1.39
65	0.02	19.66	1,260.7	1.65	187.2	460.77	4.06	3.58	7.2177	0.96	5.49	4.96	0.87	15.70	1.38
70	0.06	18.348	1,237.9	1.657	180.1	373.97	3.44	3.70	2.8933	0.97	5.99	5.36	0.87	14.70	1.38
75	0.15	17.039	1,214.9	9.855	172.9	310.37	17.69	3.83	1.3306	0.98	6.50	5.75	0.86	13.84	1.39
80	0.30	15.739	1,191.4	1.66	165.8	262.53	2.63	N/A	0.6819	0.97	7.03	6.15	0.85	13.13	1.40
85	0.57	14.450	1,167.5	1.669	158.6	225.61	2.37	4.15	0.3809	0.97	7.56	6.54	0.84	12.58	1.41
90	0.99	13.176	1,142.9	1.683	151.3	196.38	2.18	4.36	0.2281	0.97	8.12	6.94	0.83	12.22	1.43
95	1.63	11.919	1,117.7	1.704	144	172.66	2.04	4.59	0.1445	0.98	8.70	7.33	0.83	12.03	1.46
100	2.54	10.6829	1,091.5	1.731	136.7	152.96	1.94	4.88	0.0959	1.00	9.31	7.73	0.83	12.04	1.49
105	3.79	9.4707	1,064.4	1.765	129.3	136.23	1.86	5.21	0.0661	1.04	9.96	8.13	0.85	12.26	1.52
110	5.43	8.2861	1,035.9	1.808	121.9	121.74	1.81	5.62	0.0470	1.09	10.66	8.55	0.88	12.71	1.57
115	7.56	7.1328	1,006.0	1.861	114.4	108.97	1.77	6.13	0.0342	1.16	11.42	8.98	0.92	13.42	1.62
120	10.22	6.0154	974.2	1.927	106.9	97.53	1.76	6.76	0.0254	1.26	12.26	9.43	0.97	14.49	1.70
125	13.51	4.9387	939.7	2.013	99.43	87.09	1.76	N/A	0.0192	1.38	13.19	9.91	1.04	16.05	1.80
130	17.49	3.9088	902.6	2.152	92.02	77.59	1.81	9.52	0.0146	1.56	14.26	10.44	1.14	18.36	1.95
135	22.25	2.9333	861.0	2.35	84.54	68.69	1.91	11.69	0.0112	1.81	15.50	11.06	1.29	21.96	2.17
140	27.88	2.0224	813.1	2.682	76.97	60.20	2.10	15.40	0.0086	2.22	17.04	11.82	1.54	28.07	2.52
145	34.48	1.192	755.0	3.337	69.11	51.85	2.50	23.04	0.0065	3.00	19.09	12.88	2.02	40.28	3.17
150	42.19	0.472	675.5	5.225	60.16	42.90	3.73	46.63	0.0047	4.95	22.39	14.71	3.26	74.61	4.73
154	49.31	0.036	547.4	15.42	48.04	32.13	10.31	N/A	0.0031	10.63	29.63	19.14	6.86	218.2	8.44

T temperature (K); P pressure (bar); σ surface tension (mN/m); ρ density (kg/m^3); c_p specific heat (kJ/kg K); k thermal conductivity (mW/m K); μ dynamic viscosity (μPa s); Pr Prandtl number; β volumetric expansion coefficient (mK^{-1}); v specific volume (m^3/kg); γ isentropic expansion coefficient of saturated vapor; indices: L liquid; V vapor

Table B.11 Thermophysical properties of nitrogen at saturation

T	P	σ	ρ_L	c_{pL}	k_L	μ_L	Pr_L	β_L	v_V	c_{pV}	k_V	μ_V	Pr_V	β_V	γ
64	0.15	11.9581	863.7	2.002	171.5	297.50	3.47	4.78	1.2869	1.06	5.71	4.44	0.82	16.13	1.41
65	0.17	11.7169	859.6	1.994	169.5	282.08	3.32	4.82	1.0950	1.06	5.82	4.51	0.82	15.95	1.41
70	0.39	10.5262	838.5	2.005	159.5	220.26	2.77	5.11	0.5274	1.08	6.35	4.88	0.83	15.24	1.43
75	0.76	9.3624	816.7	27.05	149.5	176.75	31.99	N/A	0.2825	1.11	6.91	5.26	0.84	14.82	1.44
80	1.37	8.2276	793.9	2.054	139.5	145.11	2.14	N/A	0.1642	1.14	7.49	5.65	0.86	14.69	1.47
85	2.29	7.1240	770.1	2.094	129.6	121.31	1.96	N/A	0.1018	1.19	8.11	6.06	0.89	14.89	1.51
90	3.60	6.0544	745.0	2.147	119.6	102.83	1.85	6.94	0.0663	1.26	8.79	6.48	0.93	15.46	1.56
95	5.41	5.0222	718.3	7.073	109.7	88.02	5.68	N/A	0.0449	1.35	9.55	6.94	0.98	16.54	1.64
100	7.78	4.0318	689.4	2.301	99.71	75.77	1.75	9.15	0.0313	1.55	10.44	7.43	1.10	18.14	1.67
105	10.83	3.0892	659.0	2.432	90.15	65.72	1.77	10.21	0.0222	1.44	11.49	7.98	1.00	18.19	1.80
110	14.66	2.2025	625.6	2.736	80.72	56.96	1.93	12.90	0.0160	1.16	12.80	8.63	0.78	20.83	3.96
115	19.37	1.3844	583.8	3.211	70.45	48.23	2.20	18.78	0.0115	2.02	14.51	9.44	1.32	31.69	3.57
120	25.11	0.6578	527.5	4.351	59.19	39.02	2.87	33.00	0.0080	3.74	16.98	10.62	2.34	56.88	4.00
125	32.07	0.0829	430.2	11.79	44.96	27.35	7.17	136.45	0.0049	9.65	22.52	13.33	5.71	187.71	N/A
126	33.65	0.0083	378.6	20.16	38.93	22.77	11.79	266.83	0.0039	13.27	26.63	15.37	7.66	308.90	8.52

T temperature (K); P pressure (bar); σ surface tension (mN/m); ρ density (kg/m^3); c_p specific heat (kJ/kg K); k thermal conductivity (mW/m K); μ dynamic viscosity (μPa s); Pr Prandtl number; β volumetric expansion coefficient (mK^{-1}); v specific volume (m^3/kg); γ isentropic expansion coefficient of saturated vapor; indices: L liquid; V vapor

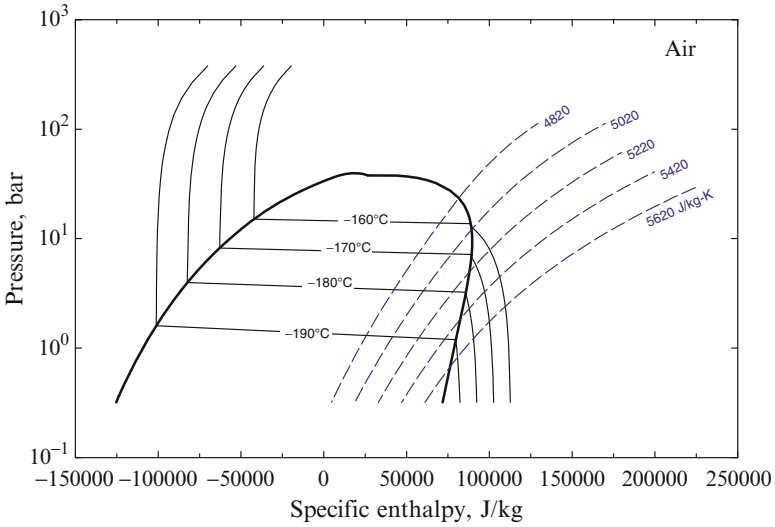

Diagram B.1 Pressure–specific enthalpy diagram of air

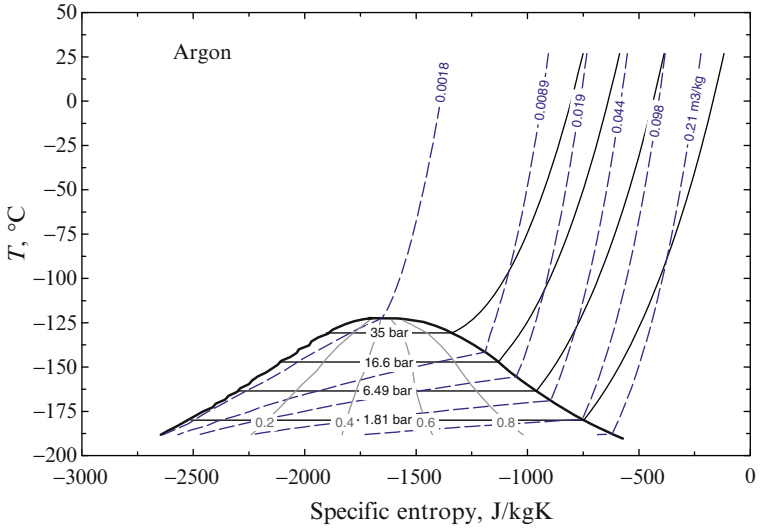

Diagram B.2 Temperature–specific entropy diagram of argon

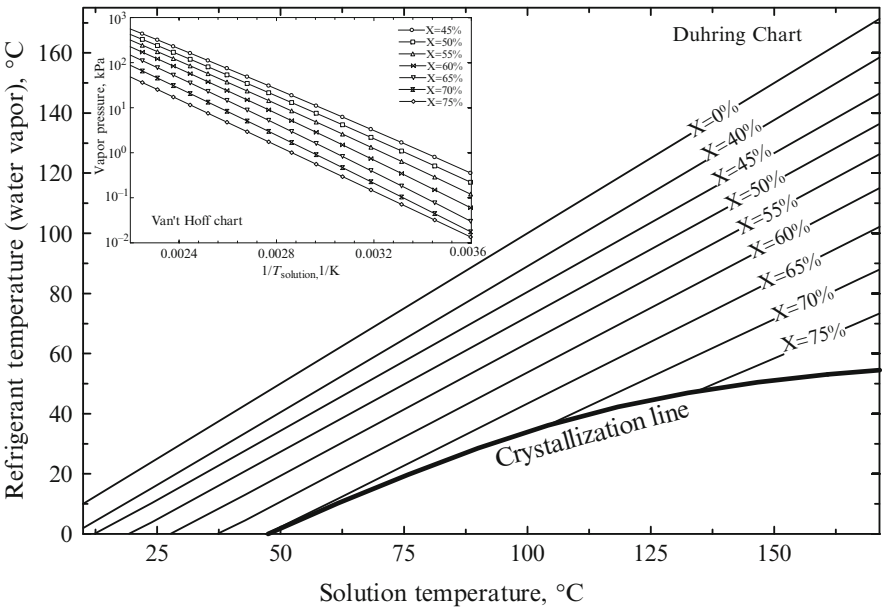

Diagram B.3 Durhing chart for lithium bromide/water solution

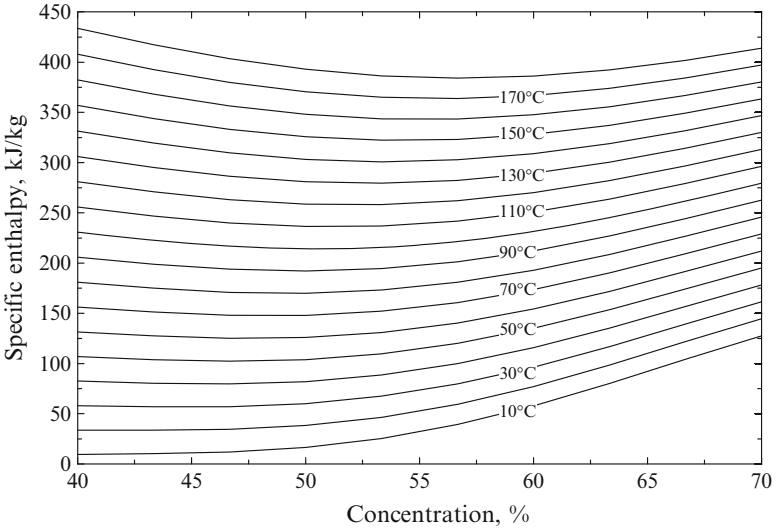

Diagram B.4 Specific enthalpy–concentration diagram for LiBr–water

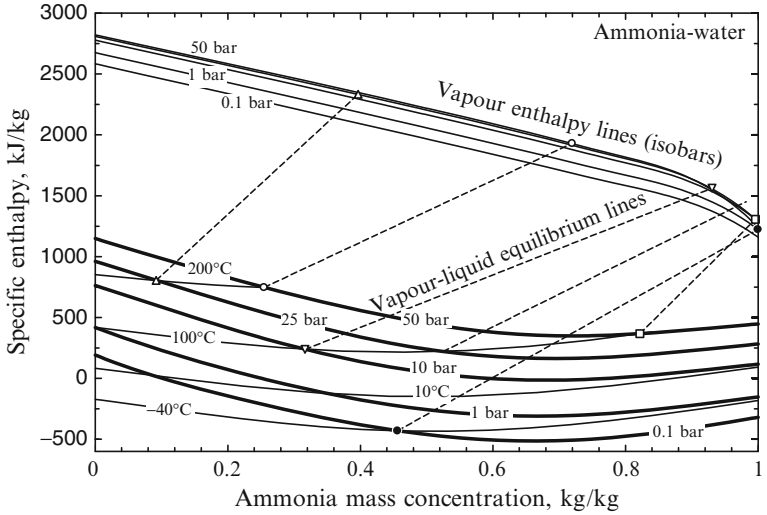

Diagram B.5 Specific enthalpy–concentration diagram of ammonia–water

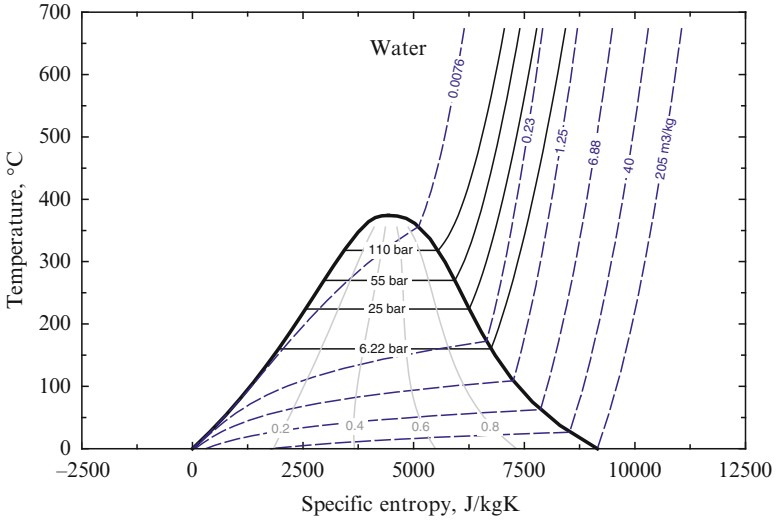

Diagram B.6 Temperature–specific entropy diagram of water

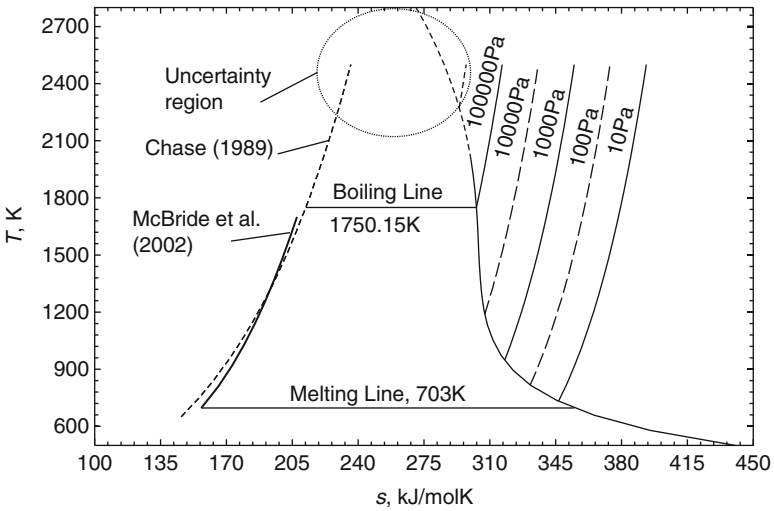

Diagram B.7 Temperature–specific molar entropy diagram of CuCl

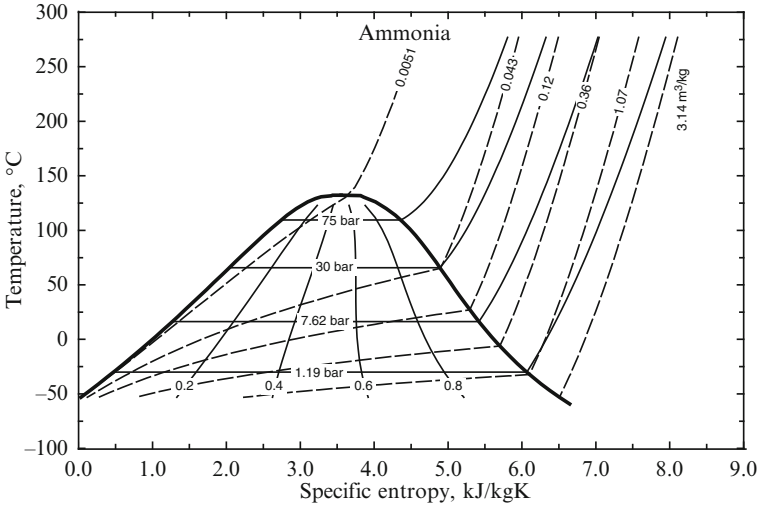

Diagram B.8 Temperature–specific entropy diagram of ammonia

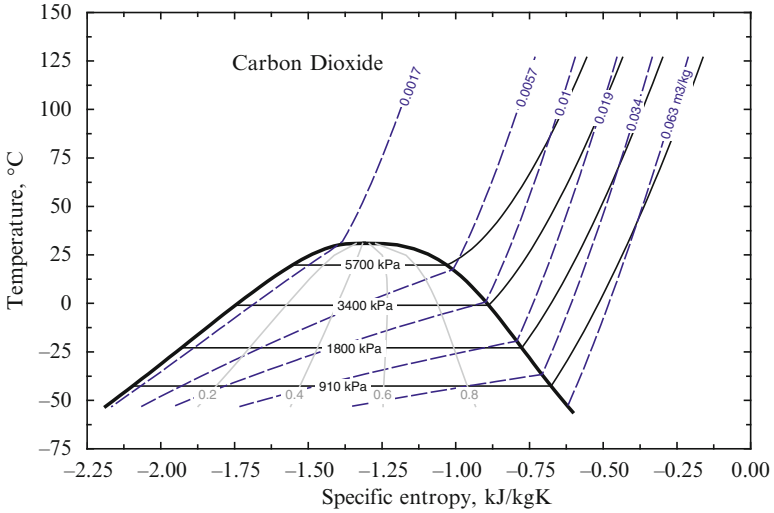

Diagram B.9 Temperature–specific entropy diagram of carbon dioxide

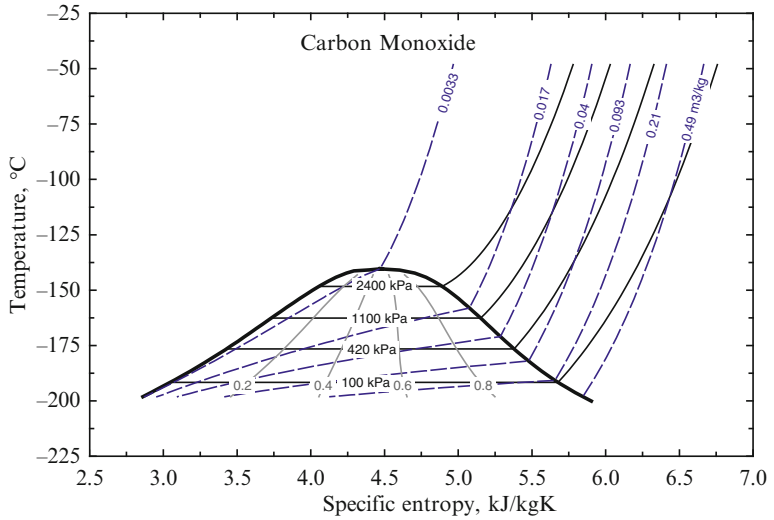

Diagram B.10 Temperature–specific entropy diagram of carbon monoxide

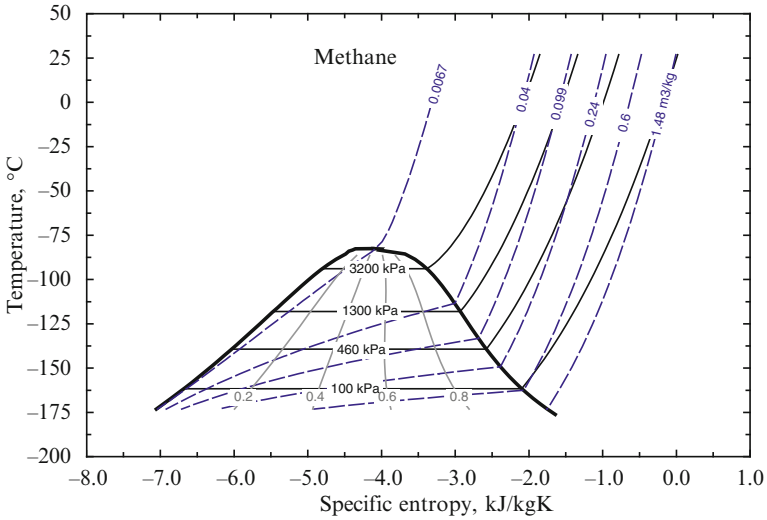

Diagram B.11 Temperature–specific entropy diagram of methane

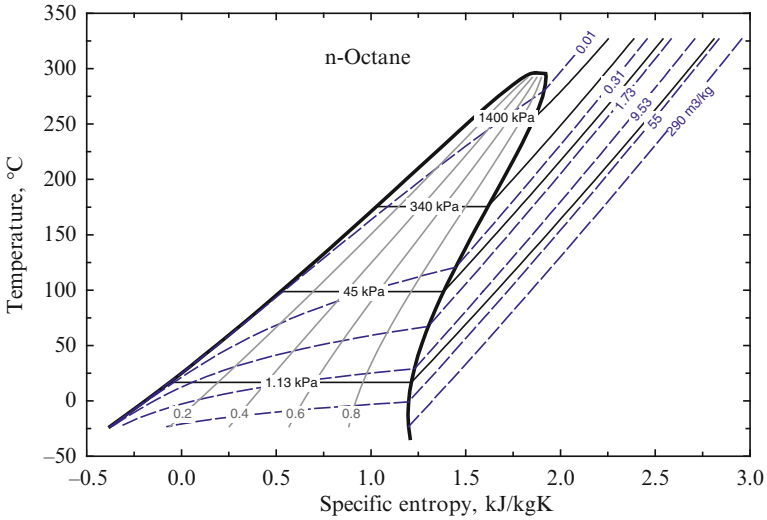

Diagram B.12 Temperature–specific entropy diagram of *n*-octane

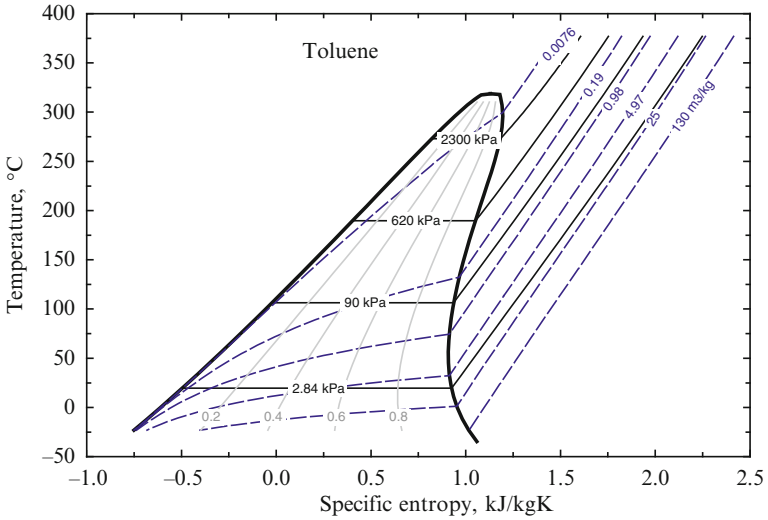

Diagram B.13 Temperature–specific entropy diagram of toluene

Index

F